International Conference on

Quark Nuclear Physics

QNP2002

Jülich, Germany
2002

edited by
Ch. Elster, J. Speth and Th. Walcher

Società Italiana di Fisica

Springer

Quark Nuclear Physics
QNP2002

Società Italiana
di Fisica

Springer

Refereed and selected contributions from

International Conference on Quark Nuclear Physics

QNP2002

June 9–14, 2002

Jülich, Germany

edited by

Ch. Elster, J. Speth and Th. Walcher

Prof. Charlotte Elster
Prof. Josef Speth
Institut für Kernphysik
Forschungszentrum Jülich
52425 Jülich, Germany

Prof. Thomas Walcher
Institut für Kernphysik
Universität Mainz
J.-J.-Becher-Weg 45
55099 Mainz, Germany

The articles in this book originally appeared in the journal
The European Physical Journal A – Hadrons and Nuclei
Volume 18, Numbers 2-3
ISSN 1434-6001
© SIF, Springer-Verlag 2003

Cataloging-in-Publication Data applied for

Bibliographic information published by Die Deutsche Bibliothek Die Deutsche Bibliothek lists this publication in the Deutsche Nationalbibliografie; detailed bibliographic data is available in the Internet at http://dnb.ddb.de

ISBN 978-3-642-05843-1 ISBN 978-3-662-09712-0 (eBook)
DOI 10.1007/978-3-662-09712-0

This work is subject to copyright. All rights reserved, whether the whole or part of the material is concerned, specifically the rights of translation, reprinting, reuse of illustrations, recitation, broadcasting, reproduction on microfilm or in any other way, and storage in data banks. Duplication of this publication or parts thereof is permitted only under the provisions of the German Copyright Law of September 9, 1965, in its current version, and permission for use must always be obtained from Springer-Verlag Berlin Heidelberg GmbH. Violations are liable for prosecution under the German Copyright Law.
springeronline.com

© Springer-Verlag Berlin Heidelberg 2004
Originally published by Springer-Verlag Berlin Heidelberg New York in 2004

The use of general descriptive names, registered names, trademarks, etc. in this publication does not imply, even in the absence of a specific statement, that such names are exempt from the relevant protective laws and regulations and therefore free for general use.

Typesetting and Cover design: SIF Production Office, Bologna, Italy

Printed on acid-free paper SPIN: 10974940 – 5 4 3 2 1 0

The European Physical Journal A

Volume 18 • Number 2-3 • October-November • 2003

■ Preface

167 A.P. Szczepaniak
A possible interpretation of the $\pi_1(1400)$ exotic meson

■ Structure and Spectroscopy of Hadrons

129 K.S. Kumar
Status and plans for neutral weak form factors measurements

135 U. Thoma
Scalar mesons and the search for the 0^{++} glueball

141 C.N. Papanicolas
Nucleon deformation
A status report

147 K.R. Schubert
CP violation in B-meson decays

155 R.F. Wagenbrunn et al.
Relativistic study of nucleon electroweak properties in a constituent-quark model

159 S. Baunack and the A4 Collaboration
Parity-violating electron scattering at MAMI
Strangeness in the nucleon

163 V. Credé
Baryon spectroscopy with the CB-ELSA detector at ELSA

171 E. Doroshkevich et al.
Study of baryon and search for dibaryon resonances by the $pp \to pp\pi^+\pi^-$ reaction

177 J. Ritman
Antiproton physics at GSI: Studying the physics of hadronic matter

181 T. Reichelt et al.
The Jefferson Laboratory E93-038 Collaboration
Measurement of the neutron electric form factor via recoil polarimetry

185 C. García-Recio et al.
$S = -1$ meson-baryon scattering in coupled-channel unitarized Chiral Perturbation Theory

189 B. Metsch et al.
The spectrum and strong decays of baryons in a relativistic quark model

193 D. Merten et al.
Electromagnetic properties of baryons in a relativistic quark model

197 F.P. Sassen et al.
t-dependence of pion production in $\pi^- p \to \pi^0\pi^0 n$

■ QCD-Inspired Quark Models of Hadrons and Nuclei

201 D.O. Riska
Nuclear forces and currents in large-N_C QCD

207 V.Yu. Grishina et al.
Polarization observables in high-energy deuteron photo-disintegration within the Quark-Gluon Strings Model

211 C.G. Strouthos
Phase diagram of the three-dimensional NJL model

215 A.E. Dorokhov and I.O. Cherednikov
Nonperturbative contribution to the quark form factor within the instanton model

219 S. Leupold
Determination of vector meson properties by matching resonance saturation to a constituent quark model

223 G. Martens et al.
Chromofields of strings and baryons

■ Effective Theories

227 B.R. Holstein
Effective effective interactions

231 P. Maris et al.
Facets of confinement and dynamical chiral symmetry breaking

237 H. Merkel
Experimental tests of Chiral Perturbation Theory

■ Lattice Gauge Theories

241 A.W. Thomas et al.
Recent developments in quark nuclear physics

247 D.B. Leinweber et al.
FLIC fermions and hadron phenomenology

253 K. Jansen
Lattice calculations

257 C. Michael
Beyond the quark model of hadrons from lattice QCD

261 R. Alkofer et al.
Infrared exponents and the running coupling of Landau gauge QCD and their relation to confinement

265 F. Frömel et al.
Spectral functions of quarks in quark matter

269 W. Detmold et al.
Moments of isovector quark distributions in lattice QCD

■ Soft and Hard Hadronic Processes

273 A.R. Dzierba
Mapping gluonic excitations and confinement
The GlueX/Hall D project at Jefferson Lab

277 T. Johansson
Meson production at CELSIUS

Erratum

In the table of contents, the following papers:

487 Ulf-G. Meißner
Some recent results in baryon chiral perturbation theory

491 A. Rusetsky
Including virtual photons in strong interactions

495 B. Moussallam
Electromagnetic corrections in the anomaly sector and the π^0 lifetime

499 E. Epelbaum et al.
Quark mass dependence of the nuclear forces

503 V. Bernard et al.
Moments of polarized parton distribution functions

507 A. Wirzba et al.
In-medium chiral perturbation theory

511 G. Krein
Chiral-symmetry restoration in clustered hadronic matter

have been listed by mistake under the section "Medium Modifications of Hadrons". They should have been listed instead under the section "Effective Theories" after

237 H. Merkel
Experimental tests of Chiral Perturbation Theory

We sincerely apologize to our authors and readers for the unpleasant inconvenience.

283 T. Nagae
Progress in hypernuclear physics

289 V.R. Brown et al.
Parity non-conservation in proton-proton elastic scattering

293 K. Hatanaka et al.
pd scattering at 250 MeV and three-nucleon forces

297 E. Doroshkevich et al.
Experiments on the search for the NN-decoupled NNπ-resonance d$'$

301 I.R. Afnan and A.D. Lahiff
The Bethe-Salpeter equation and the Low Energy Theorems for πN scattering

305 A.M. Gasparyan et al.
Exclusive and semi-inclusive strangeness and charm production in πN and NN reactions

309 T.S. Belozerova and V.K. Henner
Coupled-channel analysis of isoscalar f_0-mesons in $\bar{N}N$ annihilation and $\pi\pi$ scattering

313 A.Yu. Illarionov et al.
Probing the deuteron structure at small N-N distances by cumulative pion production

317 Yu.N. Uzikov et al.
Short-range NN properties in the processes pd $\rightarrow$ dp and pd $\rightarrow$ (pp)n

321 I. Seluzhenkov et al.
Charge "asymmetry" from the isospin symmetry in pp $\rightarrow$ pp$\pi^+\pi^-$

323 W. Oelert
Hadronic threshold reactions

327 S.D. Bass
Manifestations of anomalous glue: Light-mass exotic mesons and $g_{\eta' NN}$

331 I. Fröhlich et al.
Exclusive η production in pp reactions

335 P. Moskal et al.
Eta physics at threshold

339 P. Fedorets and V. Kleber
Investigation of the $a_0^+(980)$-resonance with ANKE

343 E. Oset et al.
Chiral dynamics in the pp $\rightarrow$ d$K^+\bar{K}^0$ and pp $\rightarrow$ d$\pi^+\eta$ reactions

347 W. Schroeder
Hyperon production in proton-proton collisions at the time-of-flight spectrometer COSY-TOF

351 P. Kowina et al.
Associated strangeness production at threshold

355 P. Winter et al.
First close-to-threshold measurement of the analysing power A_y in the reaction $\vec{p}p \rightarrow pp\eta$

359 C. Hanhart
Aspects of a_0^0-f_0 mixing in the reaction pn $\rightarrow$ dX

363 H. Toki et al.
Surface pion condensation in finite nuclei

367 S. Abdel-Samad et al.
Study of $p + d \rightarrow {}^3A + \pi$ reactions in the Δ-resonance region

■ Soft and Hard Electroweak Processes

371 R.A. Schumacher
Strangeness production and other recent results from Hall B at Jefferson Lab

377 G. van der Steenhoven
The (spin) structure of the nucleon

383 B. Foster
HERA results on the structure of the proton

389 M. Garçon
An introduction to the Generalized Parton Distributions

395 J.-C. Peng
Flavor structure of the nucleon sea

401 P. Pedroni
Helicity dependence of the γN interaction and the GDH sum rule

405 S. Schadmand
Photon-induced reactions

409 F. Ronchetti
Deuteron photodisintegration at high energy

413 H. Xiang
Measurement of π^- and π^+ photoproduction in deuterium at large momentum transfer for E = 1.7–5.6 GeV

417 J.G. Messchendorp
$\pi\pi$ correlations in $\gamma + A$ reactions

421 S. Schneider et al.
ηN final-state interaction in incoherent photoproduction of η-mesons from the deuteron

425 J.W. Martin
Prospects for measurements of parity-violating photoproduction of $\pi^{\pm}$

429 M. Vanderhaeghen
Generalized parton distributions

433 S.M. Eliseev
Deep inelastic scattering of leptons on nuclei: Hadron formation, cumulative particles production

437 I.P. Ivanov et al.
High-density QCD and saturation of nuclear partons

441 J. Stewart
Measurement of the polarized parton distribution functions at HERMES

445 A. Szczurek and J. Speth
Perturbative versus nonperturbative effects at medium energies in the $\gamma\gamma \to \pi^+\pi^-$ reaction

449 A.I. Signal and F.G. Cao
Parton symmetries and the NuTeV anomaly

■ Medium Modifications of Hadrons

453 J. Wambach
Hadrons in dense and hot matter

459 R. Rapp
Hadrons in hot and dense matter

463 M. Ericson and G. Chanfray
Scalar and pseudoscalar QCD susceptibilities in nuclei

467 W. Cassing
Transport analysis of in-medium hadron effects in pA and AA collisions

471 M. Beyer
Few-body correlations in the QCD phase diagram

475 A. Sibirtsev
Hadrons with charmed quarks in matter

479 M.J. Vicente Vacas
Experimental signals of σ-mesons in nuclei and chiral symmetry

483 E.F. Lütz et al.
Naturalness of nonlinear σ, ω self-couplings in relativistic mean-field models for neutron stars

487 Ulf-G. Meißner
Some recent results in baryon chiral perturbation theory

491 A. Rusetsky
Including virtual photons in strong interactions

495 B. Moussallam
Electromagnetic corrections in the anomaly sector and the π^0 lifetime

499 E. Epelbaum et al.
Quark mass dependence of the nuclear forces

503 V. Bernard et al.
Moments of polarized parton distribution functions

507 A. Wirzba et al.
In-medium chiral perturbation theory

511 G. Krein
Chiral-symmetry restoration in clustered hadronic matter

■ Matter under Extreme Conditions and Quark-Gluon Plasma

515 B.V. Jacak
Exploring superdense matter at RHIC

521 J.P. Wessels
Electron-positron pairs as a probe for hadrons in dense matter

527 A.H. Mueller
Saturation in small-x and heavy-ion physics

531 T. Barnes
Charmonium cross-sections and the QGP

537 Z. Rudy et al.
Properties of hot residual nuclei produced in pA reactions

■ Heavy-Quark Physics

541 M. Jezabek
Heavy-quark physics
Recent developments and old problems

543 Ulf-G. Meißner and S. Gardner
Chiral dynamics and B $\rightarrow 3\pi$ decay

547 D. Blaschke et al.
Mott effect and J/ψ dissociation at the quark-hadron phase transition

551 P. Urban
Gluonic penguin contribution to $B \to \pi\pi$ decays

555 H. Rohdjeß et al.
Cross-sections and spin observables in proton-proton elastic scattering: Results from EDDA at COSY

559 H. Weigel
Flavor symmetry breaking and strangeness in the nucleon

563 K.K. Seth
Experimental review of charmonium spectroscopy

567 R.G. Milner
Summary talk

■ Editorial

The Publishing Policy of the European Physical Journal A

DOI 10.1140/epja/i2003-10142-y

Preface

The *International Conference on Quark Nuclear Physics 2002 (QNP2002)* was held in the Forschungszentrum Jülich from June 9 to 14, 2002. It was organized by the Institute of Nuclear Physics (IKP) at the Forschungszentrum Jülich, together with the Universities of Bonn und Mainz.

This meeting takes place every two years, and was the successor to QNP2000 which was held in Adelaide. QNP2002 brought together about 200 scientists from 25 countries who met for their scientific work in the Forschungszentrum, but spent their free time in the medieval city of Aachen, the former capital of Charles the Great.

The particular feature of this conference is that it provides a comprehensive overview of the attempts in understanding hadrons and nuclei, including dense matter, in terms of their fundamental constituents, the quarks and the gluons. One of the basic themes of the program was that fact that we do have an underlying theory of strongly interacting particles, namely the QCD. For that reason, the experimental topics covered during the meeting ranged from precision measurements with hadronic and electromagnetic probes to ultra-relativistic heavy-ion reactions. Correspondingly, the theoretical topics spanned an equally wide range, including perturbative and lattice QCD calculations as well as effective theories and QCD motivated quark models. In the morning sessions invited reviews were given. In the afternoon twelve topical parallel sessions, directed by conveners, summarized the newest research results.

The conferences was sponsored by the Deutsche Forschungsgemeinschaft (DFG), the Wilhelm and Else Heraeus Foundation, the Bundesministerium für Bildung und Wissenschaft (BMBF), the Thomas Jefferson National Accelerator Facility (TJNAF), the Brookhaven National Laboratory (BNL), the Mainz Microtron Facility (MAMI), the University of Bonn, Ohio University, and the Forschungszentrum Jülich (FZJ).

We would like to thank all the sponsors, the members of the Advisory Committee and the Program Committee for their contributions to make the conference a very successful one.

Much of the organizational work was done by our conference secretary, Roswitha Bley, who carried out this demanding task in a professional way. We also want to thank the staff of the Tagungsbüro of the Forschungszentrum Jülich, who were responsible for the organization of hotels, the companion program and the outstanding conference dinner in Aachen's historical Aula Carolina.

Charlotte Elster
Josef Speth
Thomas Walcher

Editors

Eur. Phys. J. A **18**, 129–133 (2003)
DOI 10.1140/epja/i2002-10288-0

THE EUROPEAN PHYSICAL JOURNAL A

Status and plans for neutral weak form factors measurements

K.S. Kumar[a]

Department of Physics, University of Massachusetts, Amherst, MA 01002, USA

Received: 30 September 2002 /
Published online: 22 October 2003 – © Società Italiana di Fisica / Springer-Verlag 2003

Abstract. We report on a mature experimental program to measure the parity-violating asymmetry in the elastic scattering of longitudinally polarized electrons from unpolarized ^{1}H, ^{2}H and ^{4}He targets. The focus is the measurement of the nucleon neutral weak form factors at intermediate four-momentum transfer $(0.1 < Q^2 < 1)$ $(\mathrm{GeV}/c)^2$ which provide information about the impact of virtual strange quarks on the charge and current distributions inside nucleons. We report on recent technical progress in the design and scope of the experimental techniques. The physics implications of the published measurements are discussed and the current status and anticipated results from experiments under construction are summarized.

PACS. 12.15.Mm Neutral Currents – 14.20.Dh Protons and Neutrons

1 Introduction

In analogy to the charge current weak interactions like beta decay mediated by W-bosons, there is a corresponding neutral current weak interaction mediated by the Z^0-boson. One way to measure the weak neutral current amplitude between electrons and quarks is to measure the extent of parity violation in electron-quark electroweak interactions. If one scattered longitudinally polarized electrons off unpolarized protons and flipped the sign of the beam polarization, the fractional difference in the cross-section would be [1]:

$$A_{\mathrm{LR}} \equiv \frac{\sigma_{\mathrm{R}} - \sigma_{\mathrm{L}}}{\sigma_{\mathrm{R}} + \sigma_{\mathrm{L}}} \simeq \frac{|A_Z|}{|A_\gamma|} \simeq \frac{4\pi\alpha}{Q^2} \simeq 10^{-4} Q^2 . \qquad (1)$$

Since the observation of parity violation in deep inelastic electron-nucleon scattering at SLAC [2], the experimental techniques employed to measure these tiny left-right asymmetries have been steadily refined such that statistical errors approaching 0.01 parts per million (ppm) and systematic errors of a few parts per billion (ppb) are possible [3]. This has spawned an important series of experiments that is the focus of the review.

2 Physics motivation

Over the past decade, several experimental programs have focused on probing for the manifestations of strangeness in nucleon properties, such as mass, spin, momentum , magnetic moment and charge radius. A clean measurement of the contribution of strange quarks to any of these properties would be a dramatic proof of non-trivial dynamics of sea quarks inside nucleons, providing a new window into non-perturbative QCD.

There are some indications that the strange quarks might contribute to the mass (via π-proton scattering measurements) and the spin (via spin-dependent deep inelastic scattering measurements). While these experiments are sensitive to the strange scalar and axial vector matrix elements, parity-violating elastic electron scattering can access vector strangeness matrix elements sensitive to the the contribution of strange quarks to nucleon charge and magnetic-moment distributions [4,5].

Elastic electron nucleon electromagnetic scattering is well described by the Dirac and Pauli (or, equivalently, the Sachs electric and magnetic) form factors. One can introduce equivalent neutral weak form factors that would be accessible in parity-violating elastic electron scattering. If one assumes the validity of the standard model (weak isospin symmetry) and charge symmetry and that only three flavors are active, then one needs three elastic electroweak electron nucleon amplitudes to achieve flavor separation [6]. Thus, for a given value of Q^2, if the proton and neutron electromagnetic form factors are well measured, the measurement of the neutral weak form factors at the same value of Q^2 allows the extraction of the strange form factors.

The exact calculation of the strange form factors from QCD is currently impossible since it involves non-perturbative dynamics of sea quarks. Various model approaches are used, such as chiral perturbation theory, quark models, lattice gauge theory, Skyrme models and dispersion relations [7,8]. Most models attempt to model

[a] e-mail: kkumar@physics.umass.edu

Table 1. Strange form factor experiments.

Experiment	Target	θ_{electron}	Q^2	Status
SAMPLE	^{1}H	150°	0.1	published
HAPPEX	^{1}H	12.5°	0.47	published
SAMPLEII	^{2}H	150°	0.1	published
SAMPLEIII	^{2}H	150°	0.04	completed
A4	^{1}H	35°	0.23	2002
HAPPEX-H	^{1}H	6°	0.11	2003
HAPPEX-He	^{4}He	6°	0.11	2003
G0	^{1}H	10°	0.3–0.8	2003
A4	^{1}H	35°	0.1	2003
G0	^{1}H	110°	0.3–0.8	2004-7
G0	^{2}H	110°	0.3–0.8	2004-7
A4	^{1}H	145°	0.23	future
A4	^{1}H	145°	0.5	future

the low-Q^2 behaviour of the form factors:

$$\mu_s \equiv G_M^s(0); \qquad \rho_s \equiv \frac{\mathrm{d}G_E^s}{\mathrm{d}\tau}; \qquad \tau \equiv \frac{Q^2}{4M_p^2} \tag{2}$$

known as the strange magnetic moment and the strange radius.

These models agree on neither the signs or magnitude of the strange form factors. Nevertheless, some guidance can be obtained from the size of the magnetic moment of the Λ-baryon ($0.6\mu_N$) and the charge radius of the neutron ($\rho_n \sim 3$).

2.1 The experimental program

Experiments must therefore achieve a sensitivity signifincantly smaller than these values for the corresponding leading moments of the strange form factors. The full exploration further requires measurements over the range $0.1 < Q^2 < 1$ (GeV/c)^2, as well as forward- and backward-angle measurements off ^{1}H, ^{2}H and ^{4}He targets. In table 1, the past, current and future experiments measuring strange form factors are summarized in roughly chronological order.

3 Published measurements

3.1 SAMPLE

The SAMPLE experiment was carried out at the MIT-Bates Linear Accelerator, with the principal goal of measuring μ_s. This was accomplished by measuring the parity-violating amplitude in elastic electron proton scattering at backward angles at $Q^2 \sim 0.1$ (GeV/c)^2. The neutral current amplitude has two primary contributions, one from G_M^s and one from the axial form factor G_A. In order to separate these contributions, three separate physics runs were carried out: 200 MeV on a hydrogen target and 200 MeV and 125 MeV on a deuterium target.

Elastic events at backward angles were detected by the Čerenkov light produced as they pass through air. This detection technique can provide a very large solid angle on very thick targets. At 200 MeV, scattered electrons at backward angles from inelastic scattering did not have very high efficiency for producing Čerenkov light, thus avoiding spurious asymmetry contributions from unknown inelastic amplitudes. The Čerenkov light was collected into 10 shielded phototubes via concave mirrors from a total solid angle of 0.7 steradian.

Polarized electrons were produced by a Ti-Sapphire laser shining on a bulk GaAs crystal. The polarization of the beam was about 36%. The accelerator provided 25 μs long pulses at 600 Hz for a duty cycle of 1.5%. The electrons impinged on a 40 cm long liquid-hydrogen target with an average beam current ranging from 40 μA and 60 μA.

False asymmetries due to helicity correlations in the electron beam parameters were minimized using a linear regression technique. This was tested on the response of a luminosity monitor, which detected charge particles at 12°. These data showed that the cumulative asymmetry in the luminosity monitor was less than 0.2 ppm.

For the hydrogen target, at an incident beam energy of 200 MeV, the measured asymmetry is [9]

$$A_p = -4.92 \pm 0.61 \pm 0.73\,\text{ppm}, \tag{3}$$

while for the deuterium target with the same beam energy, the measured asymmetry is

$$A_d = -6.79 \pm 0.64 \pm 0.55\,\text{ppm}, \tag{4}$$

from which the following parameters are extracted at $Q^2 = 0.1$ (GeV/c)^2 [10]:

$$G_M^s = 0.14 \pm 0.29 \pm 0.31; G_A^e(T=1) = 0.22 \pm 0.45 \pm 0.39. \tag{5}$$

In order to improve the accuracy of the G_A result, SAMPLE has recently completed a third physics measurement, this time with a 125 MeV beam on a deuterium target. The contribution from G_A is further enhanced at this lower Q^2 and the result is expected to be released soon.

3.2 HAPPEX

The HAPPEX experiment was carried out in Hall A at JLab, where the emphasis was on the measurement of the electron-proton weak neutral current amplitude at forward angles, where both electric and magnetic form factors contribute. A CW beam of 3.3 GeV struck a 15 cm liquid-hydrogen target. Scattered electrons at $\theta_{\text{lab}} \sim 12.5°$ were detected by a pair of 5.5 msr precision spectrometers, whose optics provides a mass focus that spatially separate the elastic events from all inelastic events. This allowed the use of integrating flux counters, thus making high rates possible.

The integrating detector in each spectrometer consisted of a sandwich of five lead and lucite layers viewed by a single phototube. Separate low-rate runs which tracked

individual particles established that the backgrounds in the integrated signal were negligible. The polarized beam at JLab is exceptionally quiet, ideal for parity violation experiments. The beam jitter in intensity, position, angle and energy are small enough so that the impact of false asymmetries due to helicity-correlated beam motion can be studied to a sensitivity of 10 parts per billion within a few hours.

The beam polarization was 39% during the first half of data taking, while a strained GaAs photocathode provided 70% polarization during the second half of the experiment. The beam polarization was measured both with a conventional Moller polarimeter as well as a newly commissioned Compton polarimeter, which provided a non-invasive, continuous monitor of the beam polarization. The final combined result of all the data taking runs is [11]

$$A_{\mathrm{LR}} = -14.60 \pm 0.94(\mathrm{stat}) \pm 0.54(\mathrm{syst})\ \mathrm{ppm}. \quad (6)$$

Combining the above result with data on nucleon electromagnetic form factors allows the extraction of a linear combination of electric and magnetic strange form factors:

$$(G_E^s + 0.392 G_M^s)/(G_M^{p\gamma}/\mu_p) = 0.091 \pm 0.054 \pm 0.039. \quad (7)$$

The result is shown normalized to the proton magnetic form factor to underscore the sensitivity of the measurement. It implies that the linear combination of strange form factors that was probed is less than 10% of the proton electromagnetic form factor.

4 Experiments in progress

4.1 A4

The A4 experiment is taking place at MAMI, the Mainz Microtron and is measuring the weak neutral current amplitude in the elastic electron proton scattering at a scattering angle of $\theta_{\mathrm{lab}} \sim 35 \pm 5°$. Their first measurement is with an incident energy of 855 MeV, giving a Q^2 of 0.23 $(\mathrm{GeV}/c)^2$. The unique feature of the experiment is a large-acceptance lead fluoride (PbF_2) calorimeter.

A 20 μA 70% longitudinally polarized beam scatters off a 20 cm liquid-hydrogen target. Data are obtained in 20 ms time windows locked to the 50 Hz power line frequency. A water Čerenkov luminosity monitor detects charged particles between 4 and 11 degrees and is used to normalize the data and study the effects of spurious asymmetries. The beam polarization is measured by a Compton backscattered laser polarimeter.

The calorimeter is designed to detect elastic electrons at a rate of 10^7/s amongst a background rate of 10^8/s made up of inelastic electrons, soft pions and photons. The calorimeter is made up of an array of 15 radiation length long PbF_2 crystals with a front surface of 25 × 25 mm. Light from showers in the crystal array are summed, integrated over 20 ns, digitized and histogrammed in real time by custom-built fast electronics. The system was carefully monitored to ensure that there was minimal dead time and/or non-linearity.

The experiment has accumulated more than 600 hours of data in 2001 and 2002. They measure an asymmetry of $A_{\mathrm{phy}} = -7.90 \pm 1.10 \pm 0.85$ (ppm), while the standard model expectation is -5.7 ppm. This result is preliminary and more work on systamatic corrections, estimation of the neutron electromagnetic form factors as well as standard model radiative corrections are required before any information on strange form form factors can be extracted.

The A4 Collaboration plans to double their accumulated statistics at this kinematic point and then measure the neutral current amplitude at $Q^2 \sim 0.1$ $(\mathrm{GeV}/c)^2$, which is achieved in the same detector configuration with a reduced incident beam energy. They then plan to turn the calorimeter apparatus around by 180° to look at electrons scattered at backward angles. They plan to measure the asymmetry at $Q^2 \sim 0.23$ and 0.5 $(\mathrm{GeV}/c)^2$, which would complement the forward-angle measurements made by A4 and HAPPEX.

5 Experiments under construction

5.1 G0

The G0 experiment at JLab plans to make a complete set of forward- and backward-angle asymmetry measurements on hydrogen and deuterium in the range $0.16 < Q^2 < 0.95$ $(\mathrm{GeV}/c)^2$. It is based on a novel toroidal spectrometer which detects scattered events in the range $62° < \theta < 78°$. When the spectrometer is oriented in the forward direction, recoil protons are detected in this range, which corresponds to electrons scattering in the range $15° < \theta < 5°$. The entire range of Q^2 is thus obtained simultaneously, with an incident beam energy of 3 GeV.

The spectrometer would then be rotated by 180° and backward angle electrons will be detected. In this configuration, data would be taken at three different beam energies with both hydrogen and deuterium targets. In this way, the electric and magnetic strange form factors as well as the axial form factor would be each independently obtained at $Q^2 \sim 0.3, 0.5, 0.8$ $(\mathrm{GeV}/c)^2$.

The spectrometer is made up of eight superconducting coils in a common cryostat, with a diameter of 4 m and an operating current of 5 kA. The geometry provides line-of-sight sheilding of the detectors from the target. The total solid angle of 0.9 sr is accepted. Recoil protons and electrons are momentum-analyzed and detected by plastic scintillators that are placed on the focal surface to accept specific Q^2 values from the entire 20 cm target length.

For forward-angle events, time of flight is used to reject backgrounds. The high degree of segmentation keeps instantaneous rates below 1 MHz. The beam microstructure is reduced from 497 MHz by a factor of 16 to provide ∼ 32 ns timing windows. For backward-angle measurements, additional detectors are added at the entrance of the spectrometer to separate electrons from pions and protons.

Custom electronics have been developed to count particles at very high rates in each beam helicity window while rejecting backgrounds, with minimal dead time. Data are recorded by shift registers feeding scalers and

by time-to-digital converters. Kinematics corresponding to elastic scattering as well as the N-Δ transition will be employed.

Installation of the apparatus is nearing completion and the commissioning will take place in fall 2002. It is anticipated that the first physics run will begin in late 2003. Backward-angle measurements will take place between 2005-7.

5.2 HAPPEX-II

The HAPPEX Collaboration in Hall A at JLab is preparing for two new experiments, scheduled to begin in summer 2003. These experiments will detect scattered electrons at $\theta_{\rm lab} \sim 6°$, which is achieved by the HRS high-resolution spectrometers in conjunction with septum magnets. One experiment will measure the weak neutral current amplitude off hydrogen, while the other will make the measurement of ^{4}He, both employing an incident beam energy of 3.2 GeV.

For the hydrogen measurement, the physics asymmetry is 1.7 ppm and the goal is to measure it with a statistical error of 5% and a systematic error of 3%. The total rate into the two spectrometers is 125 MHz. The combination of small statistical error and high rate requires significant improvements in the monitoring and control of electron beam fluctuations, as well as an improved detector technology capable of handling a high radiation dose.

For the helium measurements, a dense gas target capable of holding 10 atmospheres of helium at a temperature of 20 K is being constructed. The spectrometer system in Hall A easily separates elastic events from the inelastic events that have lost more than 20 MeV. The physics asymmetry is about 15 ppm and will be measured to an accuracy of 3%. Significant improvement in reducing normalization errors from those of the HAPPEX measurement is required, most notably in the beam polarization measurement.

The hydrogen and helium measurements combine to form a powerful constraint on the leading moments of the strange form factors ρ_s and μ_s. One measures the combination $\rho_s + \mu_p\mu_s$ to an accuracy of ± 0.31, while the other measures ρ_s to an accuracy of ± 0.5. The helium measurement has the advantage that it only depends on the nucleon electric form factors.

6 Other applications

6.1 SLAC E158

The E158 experiment is taking place at the Stanford Linear Accelerator Center (SLAC), using the longitudinally polarized 50 GeV electron beam incident on a 1.5 m long liquid-hydrogen target. The goal of the experiment is to measure the weak neutral current amplitude for electron-electron (Moller) scattering to a precision of about 8%, from which the most precise determination of the weak mixing angle $\sin\theta_{\rm W}$ can be extracted at $Q^2 \ll M_Z^2$. The raw asymmetry is small, of the order of 130 ppb and the goal is to measure it to an accuracy of 10 ppb.

The electron beam is produced by a novel gradient-doped GaAs photocathode that produced a charge 6×10^{11} electrons per pulse, at a pulse length of 200 ns, repetition rate of 120 Hz and 80% polarization. The experiment requires unprecedented control and monitoring of the electron beam parameters. During recent data taking, the charge asymmetry was kept well below 1 part per million (ppm) and was verified by independent devices to within 5 ppb. The electron beam position was controlled to be within 20 nm on target and was verified to within 2 nm by redundant measurements.

The experiment has completed two data taking runs, each accumulating about one-quarter of the total approved statistics, for a cumulative error on the asymmetry of the order of 15 parts per billion. The expected error on the weak mixing angle $\sin^2\theta_{\rm W} \sim 0.0017$. It is anticipated that the remaining statistics will be collected in a final run in late 2003.

6.2 Qweak

A new experiment has been approved at JLab to measure the asymmetry in elastic scattering from hydrogen with an incident energy of 1.2 GeV and a Q^2 of 0.03 $({\rm GeV}/c)^2$. At these kinematics, the contribution of strange form factors is small and the asymmetry measures the weak charge of the proton, thus probing for physics beyond the standard model in a manner similar to SLAC E158. The experiment is in the early stages of design and aims at being ready to run in 2007

6.3 ^{208}Pb

Another approved experiment at JLab is the measurement of the asymmetry in elastic scattering from ^{208}Pb. The basic idea is that from electromagnetic scattering, the photon couples to the proton, whereas the Z couples predominantly to the neutron. While a detailed map of the ground-state neutron distribution is possible in principle, only one or two Q^2 points are practical in parity violation experiments. Nevertheless, a judicious choice of the kinematical point, it is possible to establish the difference between the proton and neutron average radius (the so-called neutron skin) at the 1% level.

The experiment will scatter 850 MeV electrons at 6°. The asymmetry is estimated to be about 0.7 ppm and the goal is to measure it to a relative accuracy of 3%.

7 Conclusion

The technique of parity-violating electron scattering has made giant strides over the past two decades. The HAPPEX experiment has set important limits on the size of strange form factors and the SAMPLE experiment has suggested that the proton axial current may be important.

New experiments that are about to come on line will clarify the picture. If axial current effects turn out to be small, the new measurements should set stringent limits on the size of the strange form factors or better still, establish their existence.

References

1. Ya.B. Zel'dovich, Zh. Eksp. Teor. Fiz. **36**, 964 (1959).
2. C.Y. Prescott *et al.*, Phys. Lett. B **84**, 524 (1979).
3. K.S. Kumar and P.A. Souder, Prog. Part. Nucl. Phys. **45**, S333 (2000).
4. D.B. Kaplan, A. Manohar, Nucl. Phys. B **310**, 527 (1988).
5. R.D. McKeown, Phys. Lett. B **219**, 140 (1989).
6. D.H. Beck, Phys. Rev. D **39**, 3248 (1989).
7. M.J. Musolf *et al.*, Phys. Rep. **239**, 1 (1994), and references therein.
8. D.H. Beck, B.R. Holstein, Int. J. Mod. Phys. E **10**, 1 (2001).
9. D. Spayde *et al.*, Phys. Rev. Lett. **84**, 1106 (2000).
10. R. Hasty *et al.*, Science **290**, 2117 (2000).
11. K.A. Aniol *et al.*, Phys. Lett. B **509**, 211 (2001).

Eur. Phys. J. A **18**, 135–140 (2003)
DOI 10.1140/epja/i2002-10307-2

THE EUROPEAN PHYSICAL JOURNAL A

Scalar mesons and the search for the 0^{++} glueball

U. Thoma[a]

Thomas Jefferson National Accelerator Facility, 12000 Jefferson Avenue, Newport News, VA 23606, USA

Received: 30 September 2002 /
Published online: 22 October 2003 – © Società Italiana di Fisica / Springer-Verlag 2003

Abstract. The possibility that gluonic excitations of hadronic matter or of the QCD vacuum may exist is perhaps one of the most fascinating topics in hadron spectroscopy. Glueballs are predicted by many models; in particular, present-day lattice gauge calculations require their existence. All these models agree that the lightest glueball should have scalar quantum numbers and a mass around 1.6 GeV, which corresponds to the mass region where the scalar $q\bar{q}$-mesons are expected. Therefore, mixing effects can complicate the search for the glueball. Experiments indeed show an overpopulation of states, for which many different interpretations exist. This reflects the complexity of the situation. New data from various experiments on scalar states give hints toward an interpretation of the scalar states. But still many questions remain.

PACS. 12.39.Mk Glueball and nonstandard multi-quark/gluon states – 12.38.-t Quantum chromodynamics – 14.70.Dj Gluons

1 Introduction

Quantum chromodynamics is believed to be the correct theory of strong interactions. The theoretical understanding of QCD is limited to two regimes: at high momentum transfer, where perturbative methods can be applied, and at very low energies in the realm of chiral perturbation theory. At medium energies, where perturbative methods fail, our present understanding is very limited. This is the energy regime of meson and baryon resonances, and one of the key issues is to identify the relevant degrees of freedom and the effective forces between them. This is strongly related to the question of whether gluonic degrees of freedom play a role in the hadronic spectrum. Do bound states of gluons (glueballs) or bound states of a $q\bar{q}$-pair and a gluon (hybrids) exist? Glueballs and hybrids are predicted by many models and by lattice gauge calculations; a whole spectrum of glueballs and hybrids is expected to exist. The lowest-mass glueball is predicted to have scalar quantum numbers and a recent lattice calculation [1] predicts a mass of about 1730 MeV. This corresponds to the mass region of the scalar $\bar{q}q$-mesons. So mixing between the pure scalar glueball and the nearby $q\bar{q}$ states can occur. A good understanding of all scalar states is therefore absolutely necessary, in order to identify the scalar glueball. There are some hints, how a glueball should reveal its existence, apart from the expected overpopulation of states. Glueballs are supposed to be produced preferentially in gluon-rich processes and should be suppressed in gluon-poor reactions: Radiative J/Ψ decays is, *e.g.*, such a gluon-rich process. The OZI rule suppresses decays of the $c\bar{c}$ system into light quarks and the $D\bar{D}$ threshold is far above the mass of the J/Ψ. Thus, the J/Ψ has the chance to decay into two gluons and a photon. The two gluons can interact with each other and must form glueballs —if they exist. Central production is another process in which glueballs should be produced abundantly. In central production two hadrons pass by each other "nearly untouched" and are scattered diffractively in the forward direction. No valence quarks are exchanged. The absence of valence quarks in the production process makes central production a good place to search for glueballs. In addition, $\bar{p}p$ annihilation is a gluon-rich environment; quark-antiquark pairs annihilate into gluons. These gluons can interact and can form a glueball. On the other hand, the situation is quite different in photon-photon collisions. Photons couple to the electric charges of the quarks and the production of glueballs should be suppressed. This reaction is often called "anti-glueball filter". Of course, this picture is rather naive. Glueballs couple to hadrons and glueballs can in general be produced in every reaction where hadrons occur. The reactions discussed above can provide only a rough hint toward the interpretation of the observed states.

2 The scalar resonances

For the tensor $J^{PC} = 2^{++}$-states a clear nonet consisting of the $K_2^*(1430)$, the $a_2(1320)$, the $f_2(1270)$ and the $f_2(1525)$ exists [2]. In contrast, the situation for the scalar states is rather unclear. Here the number of known states

[a] e-mail: uthoma@jlab.org

exceeds the number of expected states by far. Most people agree that the $K_0^*(1430)$ belongs to the scalar nonet, while all other states are controversially discussed. Possible candidates are $a_0(980)$, and $a_0(1450)$ for the isovector state, and for the two isoscalar nonet states five candidates exist: the $f_0(400\text{–}1200)$, $f_0(980)$, $f_0(1370)$, $f_0(1500)$, and the $f_0(1710)$, if its existence is established. The reasons for the uncertainties in the assignment of the scalar mesons to the $^3P_0$ $q\bar{q}$ nonet are manyfold: the scalar mesons couple strongly to their decay channels, their production rates are weak in many processes and the scalar glueball may play a role in the spectrum. In contrast to the scalar glueball, the tensor glueball is expected to have a mass well above the ground-state tensor mesons.

2.1 Possible interpretations

For the scalar states several very different interpretations exist, some of them will be discussed briefly in this section. The assignment given, *e.g.*, by the PDG [3] is based on the interpretation of $f_0(980)$, $a_0(980)$, and $f_0(400\text{–}1200)$ as non-$q\bar{q}$ states, with a possible interpretation of the $f_0(980)$, and the $a_0(980)$ as $K\bar{K}$-molecules, and of the $f_0(400\text{–}1200)$ as a background structure, which could, *e.g.*, be explained by t-channel exchanges [4]. Excluding these three states from the list of scalar resonances, three isoscalar states remain. The states $f_0(1370)$, $f_0(1500)$, and $f_0(1710)$ cannot possibly belong to the same nonet. Since the $f_0(1370)$ is dominantly a $u\bar{u} + d\bar{d}$ state (it decays only weakly into $K\bar{K}$), one would expect ideal mixing and an $s\bar{s}$ state at 1620 MeV. This state cannot be the $f_0(1500)$, which has a weak $K\bar{K}$ decay mode only. The expected mass is not too far from the $f_0(1710)$. This leads to an assignment in which the $f_0(1370)$ and $f_0(1710)$ belong to the $1\,^3P_0$ nonet, while there is no space for the $f_0(1500)$, which is then discussed as glueball candidate.

A distinctive property of glueballs is their decay. Being a flavor singlet, glueballs should decay with flavor symmetry: thus the decay into $\pi\pi$, $\eta\eta$, $\eta\eta'$ and $K\bar{K}$ should scale as $3:1:0:4$, after correcting for phase space. This decay pattern is inconsistent with the decay pattern of the $f_0(1500)$, but also with the decay pattern of all other scalar states [5]. So none of the observed states seems to be a pure glueball. This leads to the suggestion that the glueball mixes with the nearby $q\bar{q}$ states. Several authors suggested different mixing scenarios [6–8], which lead to a different distribution of glue over the f_0-states. The unproven assumption made in these mixing schemes is that $a_0(980)$, $f_0(980)$, and $f_0(400\text{–}1200)$ are non-$q\bar{q}$ states.

These assumptions are not made by Anisovich *et al.* [9], who believe 5 states to exist below 1.8 GeV. They develop from the $1\,^3P_0$ and $2\,^3P_0$ $q\bar{q}$ states and the scalar glueball. Through mixing the glueball strength distributes between the $f_0(1370)$, the $f_0(1500)$, and a broad underlying component. Of course, these mixing schemes can only be valid, if an $f_0(1710)$ exists.

A phenomenological analysis by Minkowski and Ochs [10] results in a different interpretation. Here the $a_0(980)$ and the $f_0(980)$ as well as the $f_0(1500)$ are interpreted as $q\bar{q}$ states. They claim that the $f_0(1370)$ is not a genuine resonance, but part of a broader object, which they call "red dragon". Both the $f_0(400\text{–}1200)$, and $f_0(1370)$ belong to this broad structure, that is interpreted as scalar glueball. As last interpretation, we discuss the results of a relativistic quark model which takes instanton-induced forces into account [11]. Within this model the spectrum of pseudoscalar mesons is reproduced properly; the η-η' mass splitting is described correctly. For the scalar sector the instanton interaction changes sign. Using the same parameters as for the pseudoscalar states, the model predicts a low-lying singlet state, which can be identified with the $f_0(980)$, and two octet states of higher mass. These can be identified with the $f_0(1500)$, the $a_0(1450)$, and the $K_0^*(1430)$. The $a_0(980)$ and $f_0(1370)$ remain unexplained. Other interpretations exist, but will not be discussed here. The different interpretations mentioned above raise important questions which must be answered, if we want to understand the spectrum of scalar states:

- What is the nature of the $a_0(980)$ and the $f_0(980)$?
- Is the existence of the $f_0(1370)$ and of the $f_0(1710)$ established?
- What are the production and decay properties of the scalar states ?

These questions will be discussed in the following.

Table 1. Branching ratios for radiative $\phi(1020)$ decays from CMD2, SND, and KLOE [12–14]. The CMD2 branching fraction given in the $\phi \to a_0\gamma$ column corresponds to $\phi \to \gamma\pi\eta$.

	$\phi \to f_0\gamma$	$\phi \to a_0\gamma$
CMD2	$(2.9 \pm 0.21 \pm 1.54)10^{-4}$	$(0.90 \pm 0.24 \pm 0.10)10^{-4}$
SND	$(3.5 \pm 0.3^{+1.3}_{-0.5})10^{-4}$	$(0.88 \pm 0.14 \pm 0.09)10^{-4}$
KLOE	$(4.47 \pm 0.21)10^{-4}$	$(0.74 \pm 0.07)10^{-4}$

2.2 The nature of the $a_0(980)$ and the $f_0(980)$

Data on ϕ decays into $\gamma\pi\pi$ and $\gamma\pi\eta$ have been taken by CMD2 [12], SND [13] and, more recently, by KLOE [14]. The results are given in table 1. The big difference in the branching ratio for $\phi \to \gamma f_0$ from KLOE and CMD2/SND is due to the introduction of the $\phi \to \gamma\sigma$-channel in the KLOE analysis, which leads to a strong destructive interference with the γf_0-contribution, thus increasing the $\phi \to \gamma f_0$ branching ratio. Of course, the reliability of this $\sigma\gamma$ contribution can be questioned.

The measured ϕ radiative decay rates are surprisingly large. Early predictions [15] assuming different structures for the $f_0(980)$, $q\bar{q}$, $K\bar{K}$ or four-quark were all well below the recent experimental value. Recently, the reaction was studied by Markushin [16]. It was found that kaonic loops play a decisive role and that, including these, rate and $\pi\pi$ invariant mass distributions are well reproduced. The $f_0(980)$-resonance corresponds to a T-matrix pole close

Table 2. Yield of light mesons per hadronic Z^0 decay; (from [22,23]).

π^0: $9.55 \pm 0.06 \pm 0.75$	η: $0.97 \pm 0.03 \pm 0.11$
η': $0.14 \pm 0.01 \pm 0.02$	$a_0^{\pm}(980)$: $0.27 \pm 0.04 \pm 0.10$
$f_0(980)$: $0.141 \pm 0.007 \pm 0.011$	$\phi(1020)$: $0.091 \pm 0.002 \pm 0.003$
$f_2(1270)$: $0.155 \pm 0.011 \pm 0.018$	

to the $K\bar{K}$ threshold; a good description of the data is achieved assuming that the pole is of dynamical origin and represents a molecular-like $K\bar{K}$ state. An underlying $q\bar{q}$ component is possible but not required. This seems to be in disagreement with the rate for $\phi \to \gamma a_0(980)$ being smaller than the rate for $\phi \to \gamma f_0(980)$ by a factor of ~ 4 or even ~ 6. This appears to be difficult to reproduce if both mesons are $K\bar{K}$ molecules. In this case their rates should be equal [15]. Other authors claim that the measured branching ratios favor a four-quark structure of these states, *e.g.* [17]. Oset, on the other hand, using a chiral unitary approach, finds that these states are generated dynamically [18].

We conclude that the predictions for the branching ratios differ significantly from one work to another; they cannot all be correct.

The same is also true for the two-photon widths [19] of the $f_0(980)$ and $a_0(980)$. These are quite often used to argue that these states are $K\bar{K}$-molecules [20]. But there exist also calculations which show that the f_0 and the a_0 are consistent with a $q\bar{q}$ nature [21].

At LEP, the inclusive production of mesons in the Z^0 decay has been studied [22]. In particular, the investigation of the $f_0(980)$ and $a_0(980)$ provides new insight into their internal structure. The OPAL Collaboration searched for these and other light-meson resonances in hadronic Z^0 decays. The total inclusive rates (table 2) for the η', the $f_0(980)$ and the $a_0(980)$ —which have very similar masses— are nearly identical (with the two charge modes of the $a_0(980)^{\pm}$ taken into account). This points to an identical internal structure of these states. This conclusion can be substantiated by further studies [23], which investigate the production characteristics of $f_0(980)$, $f_2(1270)$ and $\phi(1020)$. Their fragmentation functions have been measured as well as their production as a function of the event multiplicity and of the rapidity gap. In all these measurements the three states show an almost identical behavior, which is, in addition, in good agreement with the Lund string model of hadronization in which the $f_0(980)$ is treated as a conventional meson. This again supports the hypothesis that these states have the same nature. Results on ν_μ-charged current interactions hint in the same direction. The NOMAD Collaboration has studied the inclusive production of the $\rho(770)$, the $f_0(980)$, and the $f_2(1270)$ [24]. Also here the $f_0(980)$ shows the same behavior as the two $q\bar{q}$ states $\rho(770)$, and $f_2(1270)$.

From these experiments one can conclude that:

$\Rightarrow$ the $f_0(980)$ and $a_0(980)$ seem to be $q\bar{q}$ states.

This interpretation cannot be disproven by the data from radiative $\phi(1020)$ decays or by the measurement of their two-photon width.

If the $f_0(980)$ and $a_0(980)$ are $q\bar{q}$ states, the f_0 wave function can be written as

$$f_0(980) = \sin\varphi_s \cdot 1/\sqrt{2}(u\bar{u} + d\bar{d}) + \cos\varphi_s \cdot s\bar{s}.$$

Using the measured ratios

$$R_1 = \frac{J/\Psi \to \phi f_0(980)}{J/\Psi \to \omega f_0(980)},\ R_2 = \frac{f_0 \to \gamma\gamma}{a_0 \to \gamma\gamma},\ R_3 = \frac{f_0 \to K\bar{K}}{f_0 \to \pi\pi},$$

one can show that they are consistent with a mixing angle φ_s of about 35° [25]. The measured ratios R_i are therefore also in agreement with a $q\bar{q}$ nature of the $f_0(980)$.

2.3 The existence of an $f_0(1710)$

Radiative J/Ψ-decays

Three scalar resonances are observed at BES in radiative J/Ψ-decays into $2\pi^+2\pi^-$ [26]. The results of a partial wave analysis show a slowly rising instrumental background and 3 important contributions with scalar, pseudoscalar, and tensor quantum numbers. The scalar part contains three resonances, at 1500, 1740, and 2100 MeV, a pattern of states as already suggested in a reanalysis of MARKIII data [27]. The $f_0(1500)$, $f_0(1710)$, and the $f_0(2100)$ have a similar production and decay pattern. Neither a $f_0(1370)$ nor a "background" intensity is assigned to the scalar isoscalar partial wave. The mass and width given for the $f_0(1710)$ is $m = 1740^{+30}_{-25}$ MeV, $\Gamma = 120^{+50}_{-40}$ MeV [26]. Additional evidence for a scalar state has been found by the BES Collaboration in $J/\Psi \to \gamma K^+K^-$. Here a scalar contribution was observed around a mass of 1710 MeV [28].

Central production

Clear evidence for an $f_0(1710)$ was also found in central production. The WA102 experiment investigated several final states like $\pi\pi$, $\eta\eta$, $\eta\eta'$, $K\bar{K}$, and 4π to search for scalar states and especially for the $f_0(1710)$ [29]. The $f_0(1710)$ was observed in its decay into $\pi\pi$, $K\bar{K}$, and $\eta\eta$. For the other two channels upper limits have been derived. They find for the relative decay rates $\pi\pi : \eta\eta : \eta\eta' : K\bar{K} : 4\pi = 1 : 2.4 \pm 0.6 : < 0.8 : 5.0 \pm 0.7 :< 5.4$. Surprisingly, they do not observe a 4π-decay mode. This is in contradiction to the BES results, where this decay was clearly observed.

From the experiments discussed above, one can conclude that

$\Rightarrow$ An $f_0(1710)$ exists ($m \approx 1713$ MeV, $\Gamma \approx 125$ MeV [2]).

2.4 Production and decay properties

$\pi\pi$-scattering

Data on $\pi^- p_\uparrow \to \pi^+\pi^- n$ at 17.2 GeV/c (CERN-Cracow-Munich Collaboration) were analysed by Kaminski *et*

al. [30]. The phase of the $\pi\pi$-scattering amplitude rises slowly, then there is a sudden phase increase at 980 MeV indicating the presence of the $f_0(980)$. The modulus of the amplitude shows a dip at the mass of the $f_0(980)$: intensity is taken from $\pi\pi$ scattering to the $K\bar{K}$ inelastic channel. A second dip together with a phase motion is observed at 1500 MeV. This indicates evidence for two resonances, the $f_0(980)$, and the $f_0(1500)$.

D_s decays into three pions

D_s decays into three pions provide further insight into the spectrum of isoscalar scalar resonances. The comparatively large rate for three-pion production is surprising [31, 32]; consider the reaction $D_s^+ \to 2\pi^+\pi^-$. The quark content of the D_s^+ is $c\bar{s}$. In the decay, the c can undergo a transition to an s and the produced W^+ converts into a π^+. Hence a $s\bar{s}$ state is produced which decays into $\pi^+\pi^-$. This violates the OZI rule, and the OZI violation is strong. In the three-pion Dalitz plots the $f_0(980)$ is clearly seen [31, 32]. E687 finds in a partial wave analysis a second scalar state at 1470 MeV which we identify with the $f_0(1500)$. E791 finds a scalar state with a mass of about 1434 MeV and a width of about 173 MeV. The latter could in principle be produced by the $f_0(1370)$, and the $f_0(1500)$. For the time being we assume that the observed state is the $f_0(1500)$. We note two aspects: first, the two states $f_0(980)$, $f_0(1500)$ are produced in a similar way and —taking phase space into account— with similar couplings. Second, if produced by the process described above, both mesons do not respect the OZI rule. Then the wave functions of both, $f_0(980)$ and $f_0(1500)$, must contain $1/\sqrt{2}(u\bar{u} + d\bar{d})$ and $s\bar{s}$ components. In principle, the states can also be produced over a graph, where the $\bar{s}$- and c-quark of the D_s^+ annihilate into an W^+, which then converts into a $\bar{d}$- and an u-quark. Producing an $u\bar{u}$-pair out of the vacuum, the f_0 states might then also be produced via their $u\bar{u}$ component. In general, it is believed, that the process described first is the dominant one. This would hint to an $f_0(980)$ and $f_0(1500)$ which contain a $1/\sqrt{2}(u\bar{u} + d\bar{d})$ and a $s\bar{s}$ component.

Radiative J/Ψ decays

As discussed before in $J/\Psi \to 4\pi\gamma$ (BES) three peaks due to an $f_0(1500)$, an $f_0(1710)$, and an $f_0(2100)$ are observed.

$\bar{p}p$ in flight

In the $\bar{p}p \to \pi^0\eta\eta$ data of E760 at a CMS energy of 3 GeV /3.5 GeV, three peaks are observed at masses corresponding to the same three scalar states [33]. The data were not decomposed in partial waves, so the peaks could have $J^{PC} = 0^{++}$ or 2^{++}. If the states have $J^{PC} = 2^{++}$, their decay into $\eta\eta$ would be suppressed by the angular-momentum barrier. The fact that they are so clearly seen might suggest that they have indeed scalar quantum numbers.

Table 3. Partial widths Γ_i (in MeV) of $f_0(1370)$ and $f_0(1500)$ (from [35]), $\Gamma_{tot}(f_0(1370)) = 275 \pm 55$ MeV, $\Gamma_{tot}(f_0(1500)) = 130 \pm 30$ MeV. σ is used as an shortcut for the $\pi\pi$-S wave.

	$\sigma\sigma$	$\rho\rho$	$\pi(1300)\pi$	$a_1\pi$
	$\pi\pi$	$\eta\eta$	$\eta\eta'$	$K\bar{K}$
$f_0(1370)$	120.5 ± 45.2	62.2 ± 28.8	41.6 ± 22.0	14.1 ± 7.2
	21.7 ± 9.9	0.41 ± 0.27		(7.9 ± 2.7) to (21.2 ± 7.2)
$f_0(1500)$	18.6 ± 12.5	8.9 ± 8.2	35.5 ± 29.2	8.6 ± 6.6
	44.1 ± 15.3	3.4 ± 1.2	2.9 ± 1.0	8.1 ± 2.8

In the Crystal Barrel data $\bar{p}p \to \pi^0\eta\eta$ at an antiproton momentum of 1.94 GeV/c the $f_0(1500)$ and an $f_J(2100)$ were clearly observed while no $f_0(1710)$ was needed to describe the data.

From the discussed data sets one can conclude that

$\Rightarrow$ $f_0(980)$, $f_0(1500)$, $f_0(1710)$ and $f_0(2100)$ show very similar production and decay characteristics.

The $f_0(980)$ and the $f_0(1500)$ have both been observed in $\pi\pi$ scattering and probably also in D_s decays, where the $f_0(980)$ is clearly observed, while the parameters for a second scalar state found by E687 and E791 differ significantly. Future data, taken, *e.g.*, by the BarBar experiment, might help to clarify the situation. The $f_0(1500)$, the $f_0(1710)$ and the $f_0(2100)$ have all been observed in radiative J/Ψ decays.

The $f_0(1370)$

One of the scalar particles is obviously missing on this list, the $f_0(1370)$. The $f_0(1370)$ has not been observed in radiative J/Ψ decays, there is no clear evidence for its existence in D_s decays and in $\bar{p}p$ annihilation in flight. On the other hand, there exists evidence for this particle in $\pi\pi$ scattering [2], in $\bar{p}p$ annihilation at rest, and in central production. The evidence in the two latter reactions will be discussed using recent results of the Crystal Barrel and the WA102 experiment.

$\bar{p}p$ at rest (data from Crystal Barrel)

The decays of the $f_0(1370)$, and the $f_0(1500)$ into two pseudoscalar mesons have been measured by the Crystal Barrel (CB) experiment and are summarized in [5]. In order to gain additional information on the two states, their decays into 4π have been investigated by analysing four different 5π final states: $\bar{p}p \to 5\pi^0$, $\bar{p}n \to \pi^-4\pi^0$, $\bar{p}p \to \pi^+\pi^-3\pi^0$ and $\bar{p}n \to \pi^+2\pi^-2\pi^0$ [34,35]. The data demand two scalar states, the $f_0(1370)$ with $m = 1395 \pm 40\,\mathrm{MeV}/c^2$, $\Gamma = 275 \pm 55\,\mathrm{MeV}/c^2$ and the $f_0(1500)$ with mass and width compatible with previous findings. Using the determined 4π branching ratios together with the known ratios

into two pseudoscalar mesons the partial widths of the two states can be determined, assuming that all decay modes of the particles are known These are given in table 3.

Central production (data from WA102)

Not only the Crystal Barrel, but also the WA102 experiment has investigated the decay of scalar resonances into two pseudoscalar particles and into 4π [36]. The relative decay rates found by WA102 for the $f_0(1370)$, the $f_0(1500)$, and the $f_0(1710)$ are as follows [29]:

	$\pi\pi$	$K\bar{K}$	$\eta\eta$	$\eta\eta'$	4π
$f_0(1370)$	1	0.46 ± 0.19	0.16 ± 0.07	–	34.0^{+22}_{-9}
$f_0(1500)$	1	0.33 ± 0.07	0.18 ± 0.03	0.096 ± 0.026	1.36 ± 0.15
$f_0(1710)$	1	5.0 ± 0.7	2.4 ± 0.6	<0.18	<5.4

In the following the 4π decays will be discussed in more detail. The partial wave analysis decomposes the observed structures into several scalar resonances, the $f_0(1370)$, $f_0(1500)$, and a new $f_0(2000)$. We note that the partial wave analysis finds that the $f_0(1370)$ decays into $\rho\rho$ but not into $\sigma\sigma$, while the $f_0(1500)$ shows both decay modes. This is in contradiction to the Crystal Barrel results, where a strong $\sigma\sigma$ decay mode of the $f_0(1370)$ was found (table 3). WA102 gives an upper limit for the $\sigma\sigma$ decay modes, which is $< 25\%$ of its $\rho\rho$ decay mode. In addition, WA102 did not observe a decay into $a_1\pi$ or $\pi(1300)\pi$ for the states, which is again in disagreement with the Crystal Barrel experiment.

The results of the two experiments can be compared qualitatively. One finds that the $4\pi/2\pi$ rates for the $f_0(1500)$ are in good agreement in both experiments (WA102: 1.36 ± 0.15, CB: 1.62 ± 0.7). WA102 finds a $\rho\rho/\sigma\sigma$ ratio for the $f_0(1500)$ of about 3, Crystal Barrel finds, adding up all decay modes which include a ρ, a very similar value: $(\rho\rho + a_1\pi + \pi(1300)\pi)/\sigma\sigma \approx 2.9$. So one could argue that the results are consistent, if one ignores the different isobar decomposition in the 4π decay modes. This is no longer the fact for the $f_0(1370)$. Here the $4\pi/2\pi$ rate differs substantially: WA102 finds 34^{+22}_{-9} and CB: 11 ± 3.2. A further disagreement is the $\sigma\sigma/\rho\rho$ rate; while WA102 gives an upper limit for $\sigma\sigma$, Crystal Barrel finds that $\sigma\sigma$ is the strongest decay mode of this particle. It should be noted that it is impossible to describe the $4\pi^0$-invariant mass of the $5\pi^0$ and $\pi^-4\pi^0$ Crystal Barrel data by the $f_0(1500)$ alone. This difference is so far not understood, but may be related to processes like, *e.g.*, t-channel exchange [37]. Such effects are not included in the analyses and should have a different influence on central production and in $\bar{p}p$ annihilation.

$\gamma\gamma$-collisions

As mentioned in the beginning, the observation or non-observation of states in $\gamma\gamma$-collisions may give hints concerning the nature of the states. While there is evidence for a $\gamma\gamma$-coupling of the $f_0(400\text{–}1200)$, $f_0(980)$, and maybe also of the $f_0(1370)$ [2], the L3 experiment investigated $\gamma\gamma \to K_sK_s$ to search for the $f_J(1710)$. In the mass region around 1700 MeV a dominant contribution from a 2^{++} wave, but also some evidence for a 0^{++} contribution of $24\pm16\%$ at 84%CL was found [38]. If the existence of an $f_0(1710)$ in $\gamma\gamma$-collisions could be confirmed, this would be rather interesting. It discriminates between models, where the state has a big or small gluonic contribution. This result would indicate, that the gluonic component (if there is one) of the $f_0(1710)$ is smaller than that of the $f_0(1500)$, which was so far not observed in $\gamma\gamma$-collisions.

Table 4. Observation (√) or non-observation (–) of the scalar states in different reactions. First three reactions: "gluon-rich processes"; last one: "anti-glueball filter".

	$f_0(400\text{–}1200)$	$f_0(980)$	$f_0(1370)$	$f_0(1500)$	$f_0(1710)$
$\bar{p}p$	√	√	√	√	?
$J/\Psi \to \gamma X$	–	–	–	√	√
$pp \to p_f X p_s$	–	√	√	√	√
$\gamma\gamma$	√	√	√ ?	–	(√) ?

3 Conclusions

Table 4 summarizes the production properties of the scalar states. The $f_0(1500)$ is the only state which is produced in all "gluon rich" processes, but was so far not observed in $\gamma\gamma$-collisions, if the L3 result is confirmed. Otherwise, the $f_0(1710)$ would be the second candidate. If a scalar glueball exists and mixes with the $q\bar{q}$ states, this would support a mixing scenario, where the $f_0(1500)$ has a sizable gluonic component. On the other hand, the results from OPAL (and NOMAD) show that the most probable interpretation of the $a_0(980)$ and the $f_0(980)$ is that of $q\bar{q}$ states. This questions the validity of the glueball-meson mixing schemes [6–8]. Not only the $1\,^3P_0$ but also the $2\,^3P_0$ must then be included in the mixing scenario as done in the analysis by Anisovich *et al.* [9].

The $f_0(400\text{–}1200)$ and the $f_0(1370)$ should be produced in radiative J/Ψ decays, if they are indeed part of the scalar glueballs as claimed by Minkowski and Ochs [10]. That is not the case; this makes the interpretation of the scalar background as glueball unlikely.

Not understood at present is why the $f_0(1370)$ is not observed in J/Ψ decays, where it should not only be produced if it is a glueball but also if it is a $q\bar{q}$ state. The same is true for its non-observation in $\bar{p}p$ annihilation in flight and probably also in D_s decays. From this observation one could argue that the $f_0(1370)$ is a non-$q\bar{q}$ state [37].

The scalar states are an exciting topic; not all of them can be $q\bar{q}$ states. But we certainly have to admit that so far not everything is understood. The question, whether a scalar glueball exists and how the glue is distributed over the observed states, still remains without a generally accepted answer [39,40].

The author acknowledges an Emmy Noether grant from the Deutsche Forschungsgemeinschaft. The Southeastern Universities Research Association (SURA) operates the Thomas Jefferson National Accelerator Facility for the United States Department of Energy under contract DE-AC05-84ER40150.

References

1. C.J. Morningstar, M. Peardon, Phys. Rev. D **60**, 034509 (1999).
2. K. Hagiwara *et al.*, Phys. Rev. D **66**, 010001 (2002).
3. C. Caso *et al.*, Eur. Phys. J. C **3**, 1 (1998).
4. B.S. Zou, D.V. Bugg, Phys. Rev. D **50**, 591 (1994).
5. C. Amsler, Rev. Mod. Phys. **70**, 1293 (1998).
6. C. Amsler, F.E. Close, Phys. Lett. B **353**, 385 (1995); Phys. Rev. D **53**, 295 (1996).
7. F.E. Close, A. Kirk, Phys. Lett. B **483**, 345 (2000).
8. W. Lee, D. Weingarten, Phys. Rev. D **61**, 014015 (2000).
9. A.V. Anisovich *et al.*, Z. Phys. A **357**, 123 (1997); Phys. Lett. B **395**, 123 (1997).
10. P. Minkowski, W. Ochs, Eur. Phys. J. C **9**, 283 (1999).
11. E. Klempt *et al.*, Phys. Lett. B **361**, 160 (1995).
12. R.R. Akhmetshin *et al.*, Phys. Lett. B **462**, 380 (1999).
13. M.N. Achasov *et al.*, Phys. Lett. B **485**, 349 (2000), Phys. Lett. B **479**, 53 (2000).
14. A. Aloisio *et al.*, Phys. Lett. B **536**, 209 (2002); **537**, 21 (2002).
15. F.E. Close *et al.*, Nucl. Phys. B **389**, 513 (1993)
16. V.E. Markushin, Eur. Phys. J. A **8**, 389 (2000).
17. N.N. Achasov *et al.*, Nucl. Phys. B **315**, 465 (1989).
18. E. Marco *et al.*, Phys. Lett. B **470**, 20 (1999).
19. M. Boglione, M.R. Pennington, Eur. Phys. J. C **9**, 11 (1999).
20. F.E. Close, A. Kirk, Phys. Lett. B **397**, 333 (1997).
21. A.V. Anisovich *et al.*, Phys. Lett. B **456**, 80 (1999).
22. A. Bohrer, Phys. Rep. **291**, 107 (1997).
23. K. Ackerstaff *et al.*, Eur. Phys. J. C **4**, 19 (1998).
24. P. Astier *et al.*, Nucl. Phys. B **601**, 3 (2001).
25. W. Ochs, *Hadron'2001*, AIP Conf. Proc. **619** (2002), hep-ph/0111309.
26. J.Z. Bai *et al.*, Phys. Lett. B **472**, 378 (2000).
27. D.V. Bugg *et al.*, Phys. Lett. B **353**, 207 (1995).
28. Z.J. Guo, *Hadron'2001*, AIP Conf. Proc. **619** (2002).
29. D. Barberis *et al.*, Phys. Lett. B **479**, 59 (2000).
30. R. Kaminski *et al.*, Z. Phys. C **74**, 79 (1997).
31. P.L. Frabetti *et al.*, Phys. Lett. B **407**, 97 (1997).
32. E.M. Aitala *et al.*, Phys. Rev. Lett. **86**, 765 (2001).
33. T.A. Armstrong *et al.*, Phys. Lett. B **307**, 394 (1993).
34. A. Abele *et al.*, Eur. Phys. J. C **19**, 667 (2001).
35. A. Abele *et al.*, Eur. Phys. J. C **21**, 261 (2001).
36. D. Barberis *et al.*, Phys. Lett. B **471**, 440 (2000); **474**, 423 (2000); Nucl. Phys. B **389**, 513 (1993).
37. E. Klempt, Acta Phys. Polon. B **31**, 2587 (2000).
38. S. Braccini, *IHEP Conference, Osaka, July 2000.*
39. E. Klempt, hep-ex/0101031.
40. C. Amsler, Phys. Lett. B **541**, 22 (2002).

Eur. Phys. J. A **18**, 141–145 (2003)
DOI 10.1140/epja/i2002-10289-y

THE EUROPEAN PHYSICAL JOURNAL A

Nucleon deformation

A status report

C.N. Papanicolas[a]

University of Athens and Institute of Accelerating Systems and Applications, Athens, Greece

Received: 30 September 2002 /
Published online: 22 October 2003 – © Società Italiana di Fisica / Springer-Verlag 2003

Abstract. The conjectured deformation of hadrons and its experimental verification offer a particularly fertile ground for understanding the intricate dynamics of their constituents and QCD at the confiment scale. The detailed study of the $N \to \Delta$ transition is viewed as the preferred method of experimental investigation of this central issue in hadronic physics. A brief overview of the field is presented, followed by a presentation of the most recent results from Bates $N \to \Delta$ program. The new Bates/OOPS data at $Q^2 = 0.127(\mathrm{GeV}/c)^2$ yield $R_{SM} = (-6.27 \pm 0.32_{\mathrm{stat+sys}} \pm 0.10_{\mathrm{model}})\%$ and $R_{EM} = (-2.00 \pm 0.40_{\mathrm{stat+sys}} \pm 0.27_{\mathrm{model}})\%$ and they exclude a spherical nucleon and/or Δ. The magnitude and the origin of the deformation is the focus of the ongoing and planned investigations.

PACS. 13.60.Le Meson production – 13.88.+e Polarization in interactions and scattering – 13.40.Gp Electromagnetic form factors – 14.20.Gk Baryon resonances with $S = 0$

1 Introduction

QCD inspired models [1–3] and recent lattice calculations [4,5] strongly suggest that the shapes of hadrons are expected to deviate from spherical symmetry. While the possibility of nucleon deformation was raised more than 20 years ago [6], it is only recently that results of exclusive experiments of high precision are able to confirm the deviation from spherical shape. The origin of deformation is attributed to different mechanisms in the various nucleon models, suggesting that the deviation from spherical symmetry is the result of several mechanisms. In "QCD-inspired" constituent quark models, it arises from the intra-quark effective color-magnetic tensor forces [1], while in chiral bag models [2] most of the deformation can be attributed to the asymmetric coupling of the meson cloud to the spin of the nucleon. Our current understanding of the nucleon indicates that most of the deformation at long distances (low momenta) is driven by the pionic cloud, while at short distances (high momenta) it is generated by intra-quark forces.

The vanishing of the static quadrupole moment of the nucleon due to its $J = \frac{1}{2}$ spin, precludes accesss to the most direct observable of deformation. As a result, the presence of resonant quadrupole amplitudes in the $N \to \Delta$ transition has emerged as the definitive experimental signature of deviation from the simplistic spherical models of the nucleon and/or the delta. This is easily understood in the spherical quark model of the nucleon, where the $N \to \Delta$ excitation is a pure $M1$ ($M_{1+}^{3/2}$) transition. The resonant quadrupole multipoles $E2$ ($E_{1+}^{3/2}$) and $C2$ ($S_{1+}^{3/2}$) contain the pertinent information, as they arise from D state admixtures in the wave functions —a case reminiscent of the deformation of the deuteron. In pion production the amplitudes are denoted by $M_{l\pm}^I$, $E_{l\pm}^I$, $S_{1\pm}^I$ and $L_{l\pm}^I$, indicating their character (magnetic, electric, scalar or longitudinal), their isospin I and their total angular momentum ($J = l \pm 1/2$).

Experimental and theoretical results are routinely quoted in terms of the Electric- and Scalar(Coulomb)-to-Magnetic-Ratios of amplitudes defined as $R_{EM} = \Re(E_{1+}/M_{1+})$ and $R_{SM} = \Re(S_{1+}/M_{1+})$, respectively. QCD-inspired models predict values of R_{SM} in the range from -0.1% to -8%, at low momentum transfers, $Q^2 \leq 1.0\ (\mathrm{GeV}/c)^2$. However, the isolation of the resonant R_{EM} and R_{SM} is complicated by the presence of the nonresonant "background processes" which are coherent with the resonant excitation of the $\Delta(1232)$. These interfering processes (such as the pion pole, Born terms, tails of higher resonances) need to be constrained in order to isolate the resonant contributions to R_{EM} and R_{SM} which contain the physics of interest. As a result, R_{EM} and R_{SM} are invariably extracted with model error which is often poorly known and rarely quoted.

[a] Invited plenary talk; e-mail: cnp@cc.uoa.gr

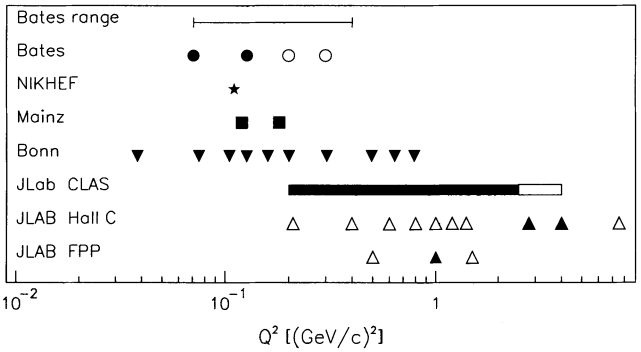

Fig. 1. Recently performed (filled symbols) and planned (open symbols) $N \to \Delta$ experiments at different laboratories for different Q^2. CLAS has a continuous coverage for $Q^2 > 0.35$ (GeV/c)^2.

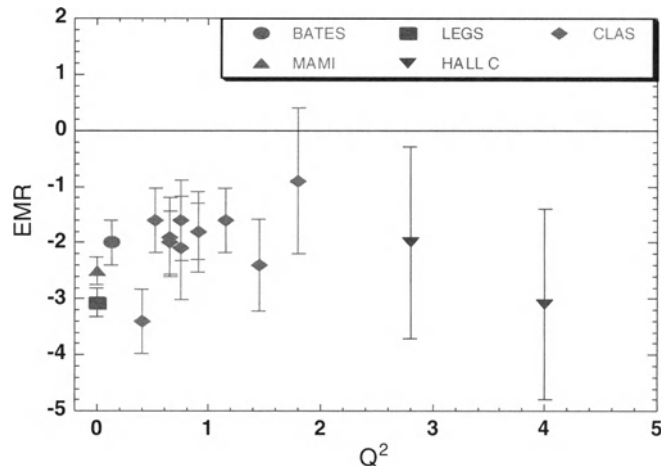

Fig. 2. Experimentally derived R_{EM} values.

2 Experimental landscape

Precision measurements with polarized tagged photons performed at Mainz and Brookhaven (LEGS) have converged at the level of asymmetries resulting in a resonant $R_{EM} = \mathrm{Im}E_{1+}^{3/2}/\mathrm{Im}M_{1+}^{3/2}$ of $(-3.0 \pm 0.3)\%$ [7] and $(-2.5 \pm 0.3)\%$ [8]. A number of theoretical calculations are in good agreement with the experimentally derived R_{EM}. However, important discrepancies still persist in the measurements of the two labs in the detailed angular and energy distributions.

The situation in electron scattering investigations is rapidly changing. Results are reported from several groups which are consistent and converging [9]. Figure 1 shows performed and programmed experiments exploring the issue of deformation through $N \to \Delta$ experiments at several laboratories [10–17]. The high-Q^2 range can only be reached by Jefferson, whereas Bonn, Mainz, and Bates are better suited to explore medium and low Q^2. Recent measurements at Bates [10,11,18], Bonn [15,14], and Mainz [13,12] demonstrate that observables sensitive to the R_{SM} can be obtained with the required high experimental precision.

The coincident $p(e, e'\pi)$ cross-section in the one-photon-exchange approximation can be written as [19]

$$\frac{\mathrm{d}\sigma}{\mathrm{d}\omega \mathrm{d}\Omega_e \mathrm{d}\Omega_\pi^{\mathrm{cm}}} = \Gamma_\mathrm{v}\ \sigma_\mathrm{h}(\theta, \phi)\,, \tag{1}$$

$$\sigma_\mathrm{h}(\theta, \phi) = \sigma_\mathrm{T} + \varepsilon\sigma_\mathrm{L} + \sqrt{2\varepsilon(1+\varepsilon)}\sigma_\mathrm{TL}\cos\phi + \varepsilon\sigma_\mathrm{TT}\cos 2\phi + hp_\mathrm{e}\sqrt{2\varepsilon(1-\varepsilon)}\sigma_{\mathrm{TL}'}\,,$$

where Γ_v is the virtual photon flux, $h = \pm 1$ is the electron helicity, p_e is the magnitude of the longitudinal electron polarization, ε is the virtual photon polarization, θ and ϕ are the pion CM polar and azimuthal angles relative to the momentum transfer $\boldsymbol{q}$, and σ_L, σ_T, σ_TL, and σ_TT are the longitudinal, transverse, transverse-longitudinal, and transverse-transverse interference cross-sections, respectively [19].

The resonant quadrupole multipoles ($E_{1+}^{3/2}$) and ($S_{1+}^{3/2}$) which are small are investigated in the interference responses σ_LT and σ_TT, where the small amplitudes are exposed by interfering with the dominant $M1$ amplitude. From these responses R_{SM} and R_{EM} are extracted through one of the following two approaches: a) In the Truncated Multipole Expansion (TME) approximation, most or all of the nonresonant multipoles are neglected (*e.g.*, see [14–16]) assuming that at resonance only the resonant terms contribute significantly. b) A phenomenological reaction framework with adjustable quadrupole amplitudes is used to perform a model extraction (*e.g.*, see [16, 11]). It is assumed that the reaction is controlled at the level of precision required for the disentanglement of the background from the resonance.

The TL and the TL′ (transverse-longitudinal) response functions are the real and imaginary parts of the same combination of multipole amplitudes. In the TME approximation they can be written as [19]

$$\begin{aligned} \sigma_\mathrm{TL}(\theta) &= -\sin\theta \mathrm{Re}[A_\mathrm{TL} + B_\mathrm{TL}\cos\theta]\,, \\ \sigma_{\mathrm{TL}'}(\theta) &= \sin\theta \mathrm{Im}[A_\mathrm{TL} + B_\mathrm{TL}\cos\theta]\,, \\ A_\mathrm{TL} &\approx -L_{0+}^* M_{1+}\,, \\ B_\mathrm{TL} &\approx -6L_{1+}^* M_{1+}\,. \end{aligned} \tag{2}$$

The two responses are particularly valuable because σ_LT is most sensitive to the presence of resonant quadrupole amplitudes, while σ'_LT is particularly sensitive to the background contributions, thus providing information on the two key experimental issues being explored.

The importance of background is clearly seen in the W behavior of the responses [11] and the nonvanishing recoil polarization P_n [10,12]. New precise results of R_{EM} have recently been published from CLAS (Jefferson) [17] and been reported by Bonn [14]. It will be interesting to ascertain whether the R_{EM} at the low and intermediate Q^2 values studied assumes positive values or it stays negative (as at the precisely known photon point [7,8]). We should also point out that the transverse background contributions at finite Q^2 are even less understood than the scalar ones.

Figures 2 and 3 offer a recent compilation of the current status of R_{EM} and R_{SM} as a function of Q^2. It can be observed that both R_{EM} and R_{SM} are small and negative in the region where they have been measured. At

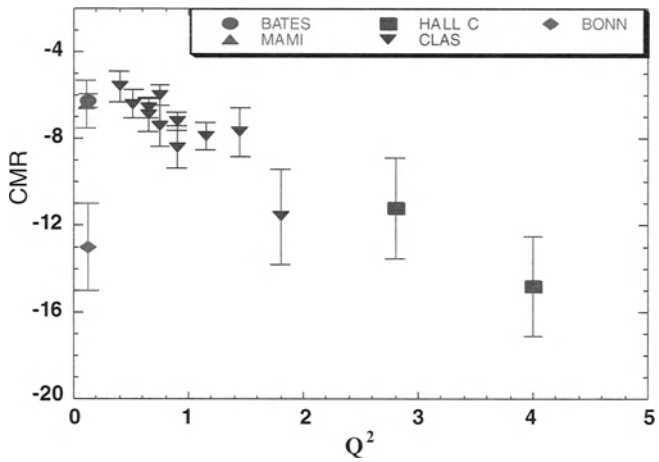

Fig. 3. Experimentally derived R_{SM} values.

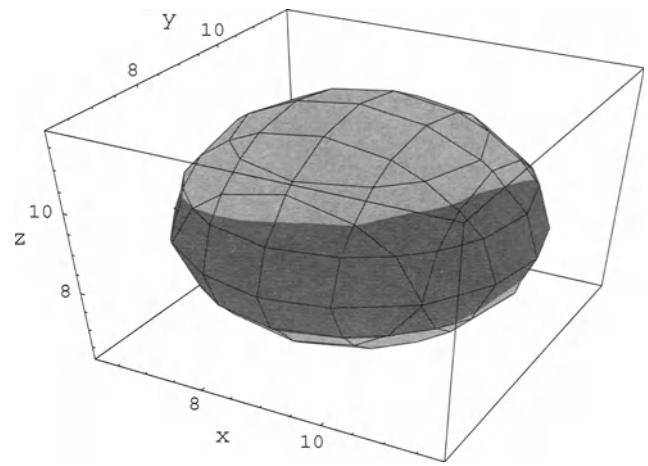

Fig. 4. The shape of the Δ in lattice gauge calculation [4] which predicts an oblate shape.

asymptotic values of Q^2, helicity conservation [20] requires that $R_{EM} \to 1.0$ and that $R_{CM} \to$ constant. Clearly, this regime has not been reached.

3 Theoretical developments

While direct links to QCD only very recently appear to be within reach, QCD-inspired models have provided since the very beginning schemes for both guiding the experimental programs and for interpreting their results. The very fertile and strong interplay between theory and experiment is a key feature of the field. Nucleon models are continuously being refined providing valuable guidance as to the magnitude of the resonant amplitudes. The overwhelming majority of nucleon models have a definite prediction for the value of R_{EM} and often of the Q^2 evolution of R_{EM} and R_{SM}.

The development of phenomenological reaction models, which in addition to the resonant amplitudes can calculate in a consistent fashion the contribution of the background, has been crucial to the development of the field. They provide predictions for the responses and the cross-sections which allows the interpretation of experimental data in a meaningful and consistent way. Prominent in this category are the models of RPI [21], MAID [22] SL [2] and the DMT [23]; they offer a rich and yet flexible phenomenology that allows for the extraction from the data of the amplitudes of interest (albeit model dependent). Deficiencies of the models that emerge as a result of the comparison with the data are rectified by re-adjustments of the parameters and/or by modifying the phenomenology. This results in an improved understanding of the underlying physics and gradual reduction of the model error.

Important is the $H(e,e'p)\gamma$ channel which has not been exploited experimentally yet. The new dispersion theory [24] of the Mainz group, taken in conjunction with the previous work of Vanderhaegen *et al.* [25] allows to addresses the physics of "deformation" and of nucleon polarizabilities in the region above pion threshold simultaneously.

The prediction of the DMT [3,23] and of SL [2] that most of the responses and the R_{EM} and R_{SM} exhibit a distinct structure at very low Q^2 values (below 0.10 GeV^2/c^2) which arises as manifestation of the mesonic degrees of freedom is most intriguing. We may thus have for the first time a clear signature of the manifestation of the pion cloud at low Q^2 which paves the way for the experimental exploration of this effect.

Finally, it is very exciting that remarkable progress in recent years both in the theoretical understanding but also in computational techniques and computing power has allowed the first results with direct connection to QCD to emerge. Recent results from chiral perturbation theory [26] or lattice gauge theory calculations [4] are clearly indicating that we can expect to establish for the first time contact between QCD theory and experiment in immediate future. It is remarkable that very recently lattice gauge calculations, both in quenched and unquenched approximations, have yielded R_{EM} and R_{SM} values with acceptable uncertainties and within the range of the experimental results [4]. They have also measured on the lattice and shown for the first time the shape of hadrons; in fig. 4 the calculated shape of the Δ is shown, which is found to be oblate, consistent with the experimental findings.

4 The Bates γ^*N $\to$ Δ program

The Bates $\gamma^* N \to \Delta$ from its very inception back in 1997 relies on a major instrumentation initiative, the Out-Of-Plane Spectrometer (OOPS) system. The OOPS facility is now fully developed and commissioned. It exceeds all design requirements [27,28]. It was explicitly designed to take advantage of the ϕ-dependence of the cross-section which acts as lever arm for isolating the interference responses. It also allows access to the fifth response, which requires both polarized beam and out-of-plane detection. The so-called "+" configuration, schematically depicted in fig. 5, has been mostly employed in recent runs. The four spectrometers measure the coincidence cross-section

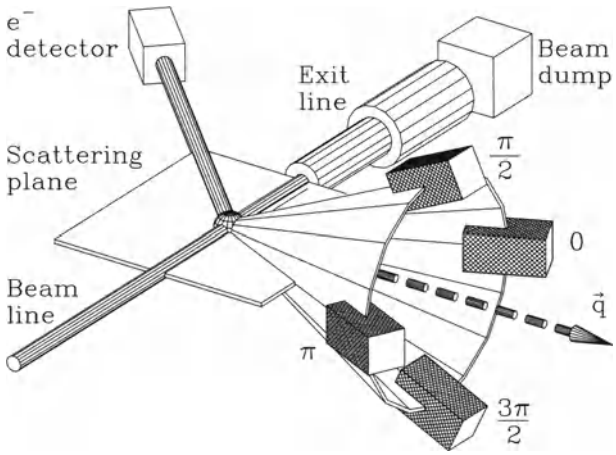

Fig. 5. A schematic diagram of the "+" configuation of the Bates OOPS spectrometer.

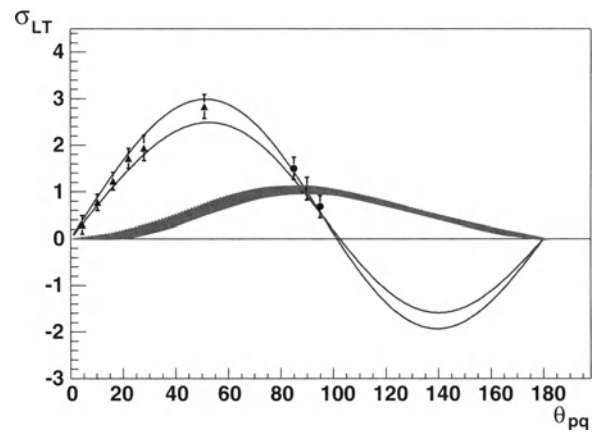

Fig. 6. The nucleon is deformed: The $\sigma_{\rm LT}$ response measured by the OOPS Collaboration at $W = 1232$ GeV. The shaded band represents the allowed uncertainty for a spherical nucleon (both $N(938)$ and $\Delta(1232)$). The band ecompassing the data represents the uncertainly allowed by all of our data analyzed simultaneously (see the discussion in the text).

at four different azimuthal angles but at the same θ^*_{pq} simultaneously thus allowing the extraction of the interference responses with minimal systematic uncertainty.

The first $\gamma^* N \to \Delta$ measurements [10,11,29] resulted in the precise determination of the cross-section in "parallel kinematics", σ_0, of the LT-asymmetry, $A_{\rm LT}$, and response $\sigma_{\rm LT}$ and the measurement of the induced proton polarization P_n. P_n is proportional to the $\sigma^n_{\rm LT}$ response and it would be identically zero in the absence of background. It was found [10] to be $-0.397 \pm 0.055 \pm 0.009$ which established the importance of the background contributions. Recent FPP measurements at Mainz [13] of higher statistical precision and which measured all three polarization responses, both confirmed the above measurement but in addition were able to determine the magnitude of the R_{SM}, the point shown in fig. 3.

The coincident cross-section in parallel kinematics was measured from $W = 1155$ to $W = 1320$ MeV; however, it was the precise $R_{\rm LT}$ results that amply demonstrated the sensitivity of the data to the "deformation" [11]. All available models fail dramatically to predict the behavior of the data unless nonzero resonant quadrupole amplitudes are introduced. Reasonable agreement is achieved when the parameters of the models are adjusted allowing for their determination either through a variant of the $M1$ dominance TME fit or through model extraction. By adjusting the relevant parameters in the models of MAID [22], of RPI [21] and of SL [2], values for R_{SM} and R_{SM} have been derived [11]. The dynamical Models of SL [2] and DMT [3] provide acceptable description, while the RPI [21] model could not account for all the measured responses simultaneously.

The first out-of-plane $N \to \Delta$ measurements [30] were performed for proton or pion detection. In addition to measuring the $\sigma_{\rm LT}$ response at a larger angle, the data allowed for the extraction of the helicity asymmetry $A_{\rm h}$ and the $R_{\rm LT}{}'$ response. $A_{\rm h}$ has analogous significance to P_n in isolating the background contributions, as they both are an imaginary part of a LT interference.

The year 2000/2001 was marked by major technical achievements for the OOPS program which led to production runs for the VCS and $N \to \Delta$ experiments. A 950 MeV beam energy, with currents up to 7 μA and a duty-factor in excess of 50% was used in conjunction with the completed and commissioned 4-OOPS cluster.

The TT response which is sensitive to the electric-quadrupole amplitude, and of which little is known at nonzero Q^2 was isolated for the first time [18]. The response functions $\sigma_{\rm T}$ and $\sigma_{\rm TT}$ contain the term $\Re[E^*_{1+}M_{1+}]$ but also the dominant term $|M_{1+}|^2$. The influence of the dominant $|M_{1+}|^2$ term can be diminished by measuring the following combination of the $\sigma_{\rm T}$ and $\sigma_{\rm TT}$ responses:

$$\begin{aligned}\sigma_{00}(\theta^*_{pq}) = \sigma_{\rm T}(\theta^*_{pq}) + \sigma_{\rm TT}(\theta^*_{pq}) - \sigma_{\rm T}(0) = \\ 2\Re[E^*_{0+}(3E_{1+} + M_{1+} - M_{1-})](1 - \cos\theta^*_{pq}) \\ -12\Re[E^*_{1+}(M_{1+} - M_{1-})]\sin^2\theta^*_{pq}\,. \qquad (3)\end{aligned}$$

The term of interest $\Re[E^*_{1+}M_{1+}]$ is enhanced by a factor of twelve (12)! while the leading term ($|M_{1+}|^2$) is eliminated. The cross-sections needed to derive this quantity were measured; as a result, we expect to extract a most precise measurement of R_{EM} at $Q^2 = 0.126$ GeV^2. The sensitivity to the EMR is maximized at the measured kinematics as shown in fig. 7.

A very recent combined analysis of all the available OOPS data has been performed by Sparveris [18]. The data base at $Q^2 = 0.126$ is quite rich allowing for a "model independent" extraction of the R_{EM} and R_{SM} values. This analysis which has yielded the results in fig. 6 and fig. 7 demonstrated beyond any doubt that both the R_{EM} and R_{SM} yield incompatible results with a spherical nucleon. Based on this same analysis, we have derived [18] $R_{SM} = (-6.27 \pm 0.32_{\rm stat+sys})\%$ and $R_{EM} = (-2.00 \pm 0.40_{\rm stat+sys})\%$. We assign model uncertainties of 0.10% and 0.27% to R_{SM} and R_{EM}, respectively. This

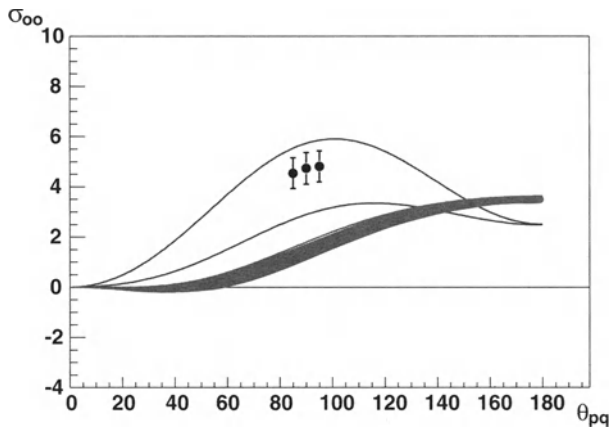

Fig. 7. The measured σ_{00} exhibits high sensitivity to R_{EM} allowing the exclusion of a "spherical nucleon". See text. The error bands have the same meaning as in fig. 6.

is to contrasted with the similar analysis of then available data which resulted in [11] in model uncertainties of 2.5% and 2.0% to R_{SM} and R_{EM}, respectively. The derived results are consistent with the interpretation of Buchmann [31] and coworkers suggesting a prolate nucleon and an oblate Δ.

During the same running period we were able to access the low-momentum branch of the recoiling protons by tuning the OOPS spectrometers to very low-momentum detection. We thus accessed $\theta^*_{pq} = 151°$ and at $\theta^*_{pq} = 180°$ for an $\sigma_{\rm LT}$ measurement. The high duty cycle extracted beam also provided a significant advantage for studies of the π^+ channel dramatically reducing the experimental background. The $p(e,e'\pi^+)n$ reaction was measured at $W = 1232\,\mathrm{MeV}$, $Q^2 = 0.127\,\mathrm{GeV}^2$ and $\theta^*_\pi = 44.5°$. All three unpolarized response functions could be determined. In addition, we measured the cross-section in parallel kinematics. These results are currently in the final stages of analysis.

5 Future prospects

A new level of sophistication and precision is emerging from the experimental programs in pursuit of the issue of hadron deformation through the $N \to \Delta$ transition. It is apparent that in the next few years the definitive signature will be established and we can hope to achieve firm contact with QCD. Of immediate concern is the role of the pion cloud at low momentum transfers and the quantification of model error in the extracted quantities.

I want to thank the organizers for their invitation to this exciting conference and Prof. S. Stiliaris, C. Alexandrou and N. Sparveris for contributing significantly to this paper. I am indebted to the Bates community and to the OOPS Collaboration and to Drs S. Kamalov, L.Tiator for many useful suggestions. This work was supported in part by E.U. RTN HPRN-CT-2000-00130 and Athens University.

References

1. N. Isgur, G. Karl, R. Koniuk Phys. Rev. D **25**, 2394 (1982); S. Capstick, G. Karl, Phys. Rev. D **41**, 2767 (1990).
2. T. Sato, T.-S.H. Lee, Phys. Rev. C **54**, 2660 (1996); Phys. Rev. C **63**, 055201 (2001).
3. S.S. Kamalov, Shin Nan Yang, Phys. Rev. Lett. **83**, 4494 (1999).
4. C. Alexandrou *et al.* hep-lat/0206026; nucl-th/0212005 and private communication.
5. D.B. Leinweber, T. Draper, R.M. Woloshyn Phys. Rev. D **48**, 2230 (1993).
6. S.L. Glashow, Physica A **96**, 27 (1979).
7. G. Blanpied *et al.*, Phys. Rev. Lett. **79**, 4337 (1997).
8. R. Beck *et al.*, Phys. Rev. Lett. **78**, 606 (1997); Phys. Rev. C **61**, 35204 (2000).
9. D. Drechsel, L. Tiator (Editors), *Nstar2001, Proceedings of the Workshop on the Physics of Excited Nucleons*, (World Scientific, 2001).
10. G.A. Warren *et al.*, Phys. Rev. C **58**, 3722 (1998).
11. C. Mertz *et al.*, Phys. Rev. Lett. **86**, 2963 (2001).
12. H. Schmieden, in ref. [9].
13. Th. Pospischil *et al.*, Phys. Rev. Lett. **86**, 2959 (2001).
14. R.W. Gothe, in ref. [9].
15. F. Kalleicher *et al.*, Z. Phys. A **359**, 201 (1997).
16. V. Frolov *et al.*, Phys. Rev. Lett. **82**, 45 (1999).
17. K. Joo *et al.*, Phys. Rev. Lett. **88**, 122001 (2002).
18. N. Sparveris, University of Athens, Ph.D. Thesis, in preparation.
19. D. Drechsel, L. Tiator, J. Phys. G: Nucl. Part. Phys. **18**, 449 (1992); A.S. Raskin, T.W. Donnelly, Ann. Phys. **191**, 78.
20. C.E. Carlson, J.L. Poor Phys. Rev. D **38**, 2758 (1988).
21. R.M. Davidson *et al.*, Phys. Rev. Lett. **56**,804 (1986); Phys. Rev. D **43**, 71 (1991); Phys. Lett. B **353**, 131 (1995).
22. D. Drechsel *et al.*, Nucl. Phys. A **645**, 145 (1999) and `http://www.kph.uni-mainz.de/MAID/maid2000/`.
23. S.S. Kamalov *et al.*, Phys.Rev. C **64**, 032201 (2001).
24. B. Pasquini *et al.*, Eur. Phys. J. A **11**, 185 (2001).
25. M. Vanderhaeghen, Nucl. Phys. A **595**, 219 (1995).
26. G.C. Gellas *et al.*, Phys. Rev. D **60**, 054022 (1999).
27. S. Dolfini *et al.*, Nucl. Instrum. Methods A **344**, 571 (1994).
28. J. Mandeville *et al.*, Nucl. Instrum. Methods A **344**, 583 (1994).
29. C. Vellidis, University of Athens, Ph.D. Thesis, (2001): ISBN:960-8313-05-8.
30. Christian Kunz, MIT PhD Thesis, 1999, unpublished.
31. A.J. Buchmann *et al.*, Phys. Rev. C **55**, 448 (1997); Phys. Rev. C **63**, 015202 (2000).

Eur. Phys. J. A **18**, 147–153 (2003)
DOI 10.1140/epja/i2002-10290-6

THE EUROPEAN PHYSICAL JOURNAL A

CP violation in B-meson decays

K.R. Schubert[a]

Technische Universität Dresden, D-01062 Dresden, Germany

Received: 30 September 2002 /
Published online: 22 October 2003 – © Società Italiana di Fisica / Springer-Verlag 2003

Abstract. 37 years after the discovery of *CP* violation in $\pi^+\pi^-$ decays of neutral K-mesons, the experiments BABAR and BELLE have found a second system which violates *CP* symmetry. $J/\psi K^0_S$ decays of neutral B-mesons show very large symmetry breaking. The effect has now, with the most recent data, a significance of ten standard deviations. The presentation describes the B-meson factories, the experiments, and their analyses. The results are in agreement with the Standard Model explanation of *CP* violation, *i.e.* with different couplings of the Higgs boson to quarks and antiquarks.

PACS. 14.40.Nd Bottom mesons – 12.15.Hh Determination of Kobayashi-Maskawa matrix elements – 11.30.Er Charge conjugation, parity, time reversal, and other discretesymmetries

1 Discovery of CP Violation

In today's language, *CP* symmetry of the charged weak interaction means equal couplings of left-handed fermions ν_L, e^-_L, u^-_L, d^-_L ... , and right-handed antifermions, $CP\,\nu_L = \overline{\nu}_R$, $CP\,e^-_L = e^+_R$ ... , to $W^\pm$-bosons. This symmetry was assumed to be perfect between 1957, when *P* violation was discovered, and 1964. In that year, Christenson *et al.* [1] discovered *CP* symmetry breaking in $\pi^+\pi^-$ decays of neutral K-mesons. These very strange particles have a non-exponential decay law because of transitions $K^0 \leftrightarrow \overline{K}^0$. There are two and only two linear superpositions which decay exponentially [2],

$$K^0_S = pK^0 + q\overline{K}^0\,, \qquad K^0_L = pK^0 - q\overline{K}^0\,. \tag{1}$$

CP symmetry requires $|p| = |q|$, but the 1964 discovery showed $|p| > |q|$. The simplest manifestation of this *CP* violation today has been observed by CPLEAR [3]. Figure 1 shows their rate asymmetry as a function of t, the time between K production and K decay,

$$A(t) = \frac{N(\overline{K}^0 \to \pi^+\pi^-) - N(K^0 \to \pi^+\pi^-)}{N(\overline{K}^0 \to \pi^+\pi^-) + N(K^0 \to \pi^+\pi^-)}\,.. \tag{2}$$

It can be expressed by standard K-meson parameters [2],

$$A(t) = \frac{-2|\eta_{+-}|e^{-t/2\tau}\cos(\Delta m_K \cdot t - \phi_{+-})}{e^{-t/\tau_S} + |\eta_{+-}|^2 e^{-t/\tau_L}}\,, \tag{3}$$

where τ_S and τ_L are the mean lives of the two states in eq. (1) and $1/\tau = 1/\tau_S + 1/\tau_L$, Δm_K is the mass difference

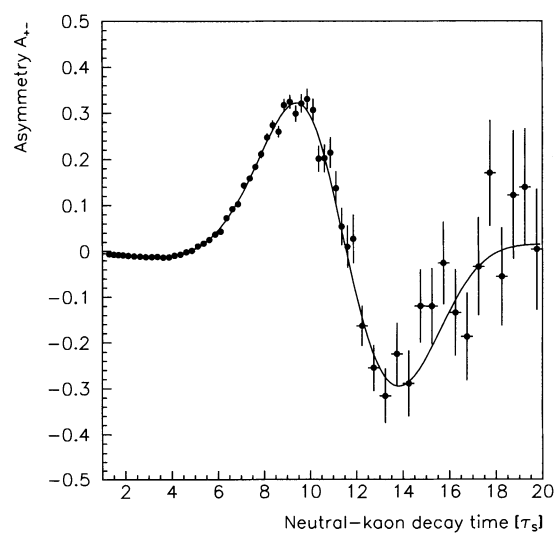

Fig. 1. The CPLEAR result [3] on the decay asymmetry of K^0 and $\overline{K}^0$ in the $\pi^+\pi^-$ mode. The abscissa is t/τ_S.

of the two states, $\Delta m_K = m(K^0_L) - m(K^0_S)$, and

$$\eta_{+-} = \frac{\langle\pi^+\pi^-|T|K^0_L\rangle}{\langle\pi^+\pi^-|T|K^0_S\rangle} = |\eta_{+-}| \cdot e^{i\phi_{+-}}\,. \tag{4}$$

The results in fig. 1 and in earlier experiments lead to a world average [4] of

$$\eta_{+-} = (2.27 \pm 0.02) \cdot 10^{-3} \cdot e^{i(43.3\pm0.5)^\circ}\,. \tag{5}$$

CP asymmetries have also been observed in decays of neutral kaons into the final state $\pi^0\pi^0$ and in the difference

[a] e-mail: K.R.Schubert@physik.tu-dresden.de

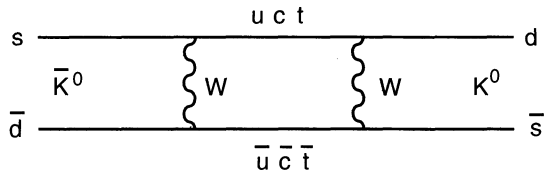

Fig. 2. Feynman diagram for transitions $K^0 \leftrightarrow \overline{K}^0$. *CP* symmetry is violated since the transition rates from left to right are larger than those from right to left.

between $\pi^+\pi^-$ and $\pi^0\pi^0$ decays. The parameters for these asymmetries are

$$\eta_{00} = \frac{\langle 2\pi^0|T|K_L^0\rangle}{\langle 2\pi^0|T|K_S^0\rangle},\ \epsilon_K = \frac{2\eta_{+-} + \eta_{00}}{3},\ \epsilon' = \frac{\eta_{+-} - \eta_{00}}{3} \tag{6}$$

and experimentally we have

$$\epsilon_K \approx \eta_{00} \approx \eta_{+-}\,, \qquad \epsilon' \approx 2 \cdot 10^{-3} \cdot \epsilon_K\,. \tag{7}$$

2 Expectations in the Standard Model

The Standard Model describes transitions $K^0 \leftrightarrow \overline{K}^0$ with the help of second-order weak interactions as shown in fig. 2. There are four weak vertices in this graph, each one contributes with the coupling constant $g_w \cdot V_{ik}$ to the transition amplitude, where g_w is the universal weak coupling and V_{ik} is the CKM matrix element [5,6] with $i = u, c, t$ and $k = d, s$. With three families of quarks, V is allowed to be a complex matrix, and the presence of six different complex V_{ik} values in the transition amplitude leads to an interference with the result

$$\Gamma(K^0 \to \overline{K}^0) < \Gamma(\overline{K}^0 \to K^0)\,. \tag{8}$$

More about the Standard Model interpretation of *CP* violation in sect. 7.

For 37 years, the K^0 was the only system in particle physics with observed *CP* symmetry breaking. In summer 2001, decays of B^0-mesons showed the second evidence. The search for this effect could be very well planned because of a clear Standard Model expectation,

$$\begin{aligned} A &= \frac{N(\overline{B}^0 \to J/\psi K_S^0) - N(B^0 \to J/\psi K_S^0)}{N(\overline{B}^0 \to J/\psi K_S^0) + N(B^0 \to J/\psi K_S^0)} \\ &= A(t) = \sin 2\beta \cdot \sin(\Delta m_B \cdot t)\,, \end{aligned} \tag{9}$$

where $\beta = \arg(V_{td}V_{tb}^*V_{cb}V_{cd}^*)$ is a Standard Model parameter and $\Delta m_B = m(B_H^0) - m(B_L^0)$. The states B_H^0 and B_L^0 are the exponentially decaying superpositions of B^0 and $\overline{B}^0$ as in eq. (1). Early experiments with B-mesons which had discovered $B^0 \leftrightarrow \overline{B}^0$ transitions [7,8] determined Δm_B to be 0.5/ps. The result for $|\eta_{+-}|$ in eq. (5) together with later measurements of $|V_{ub}|$ [9,10] and $\Delta m(B_s)$ [11] lead to the prediction $\sin 2\beta = 0.5$ to 0.8 if *CP* violation in the K system has only Standard Model origin. A conclusive measurement of the asymmetry in eq. (9), however, needs about $3 \cdot 10^7$ B-mesons, which required the construction of special "B-meson factories". The most promising method was electron-positron annihilation at $E_{CM} = 10.58$ GeV with formation of $\Upsilon(4S)$-mesons which decay predominantly into B^+B^- and $B^0\overline{B}^0$ pairs without any extra particles.

Two such high-luminosity e^+e^- storage rings have been built in the mid-90s. With present technologies for storage ring beam sizes and present space resolutions of silicon vertex detectors, measurements in the $\Upsilon(4S)$ rest frame would give unmeasurably small *CP* asymmetries, even for large values of $\sin 2\beta$ in eq. (9). Experiments must be done with moving $\Upsilon(4S)$-mesons, but modest boosts of $\beta\gamma(\Upsilon 4S) \approx 0.5$ are sufficient for seeing the effect. Both B-meson factories have, therefore, been built with unequal beam energies for electrons and positrons.

3 The B-meson factories PEP-II and KEK-B

The double storage ring PEP-II [12] at SLAC (Stanford, California) was designed around 1988, was approved in 1993, and started operation in 1998. The ring with a circumference of 2.2 km is located in the old tunnel of PEP. Electrons and positrons are injected with their nominal energy of 9.1 and 3.0 GeV, respectively, from the 3 km long SLAC linear accelerator. The E asymmetry leads to an $\Upsilon(4S)$ motion with $\beta\gamma = 0.55$. The luminosity in the only intersection region has now reached $\dot{\mathcal{L}} = 4.5 \cdot 10^{33}/\mathrm{cm}^2/\mathrm{s}$, corresponding to 5.0 produced $\Upsilon(4S)$-mesons per second. To obtain this luminosity, the circulating electron current is 0.98 A, for the positrons it is 1.68 A. Both beams are colliding head-on, *i.e.* with zero crossing angle. Two good days in BABAR give the same amount of data as ARGUS [8,9] at DESY collected in its whole lifetime from 1982 to 1992.

KEK-B [13] at KEK (Tsukuba, Japan) was designed, approved, and built on the same time scale as PEP-II. The beam energies are 8.0 and 3.5 GeV for e^- and e^+, respectively, corresponding to $\beta\gamma = 0.43$. The luminosity has now reached a value of $\dot{\mathcal{L}} = 7.2 \cdot 10^{33}/\mathrm{cm}^2/\mathrm{s}$, *i.e.* 8.0 produced $\Upsilon(4S)$-mesons per second. One reason for the higher luminosity compared to PEP-II is the beam crossing angle of 22 mrad in the interaction region. In spite of KEK-B's luminosity record, PEP-II has still the higher integrated luminosity $\mathcal{L} = \int \mathcal{L} dt$. Until 13 June 2002, the day before this presentation, it produced $\mathcal{L} = 91$ events/femptobarn recorded in the PEP-II detector BABAR, whereas the KEK-B detector BELLE recorded 85 events/fb until the same day.

4 The detectors BABAR and BELLE

The BABAR detector is described in detail in ref. [14]. It consits of a five-layer silicon vertex tracker, a 40-layer drift chamber, a detector of internally reflected Čerenkov light for charged-particle identification, and an electromagnetic calorimeter with 6580 CsI(Tl) crystals, all embedded in a solenoidal magnetic field of 1.5 T, and surrounded by

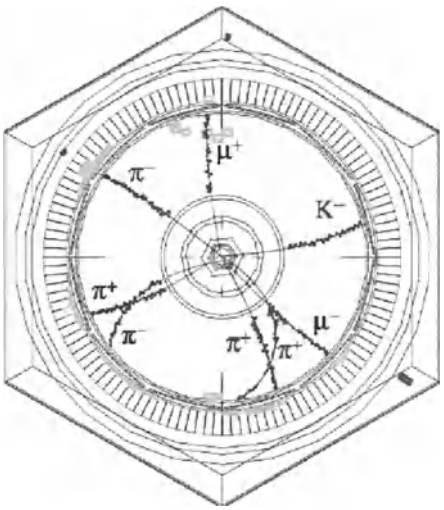

Fig. 3. A fully reconstructed event $e^+e^- \to \Upsilon(4S) \to B^0\overline{B}^0 \to [\psi(2S)K^0_S][D^{*+}\pi^-]$ in BABAR.

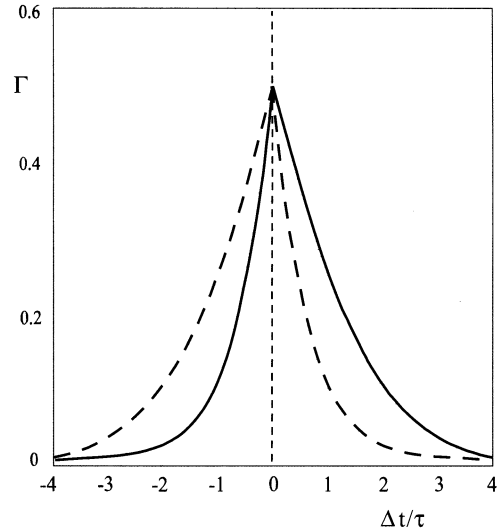

Fig. 4. The expected time dependence of B decays into $J/\psi K^0_S$ from the $\Upsilon(4S)$-resonance. The solid curve shows the decays tagged by a B^0, the dashed curve those with $\overline{B}^0$ tags.

an instrumented flux return for muon identification and K^0_L detection. The BABAR Collaboration has now 516 physicists from 73 institutions in USA, Italy, France, UK, Germany, Canada, Russia, Norway, and China.

The BELLE detector [15] is quite similar to BABAR. The main difference is in the charged-particle identification. Instead of a ring-image Čerenkov detector, it has a system of aerogel threshold Čerenkov detectors and scintillators for time-of-flight measurement. The BELLE Collaboration consists of about 300 physicists from 49 institutes in Australia, Austria, China, Germany, India, Korea, Japan, Philippines, Poland, Russia, Slovenia, Switzerland, Taiwan, and USA.

5 Principles of the measurement

A fully reconstructed event $e^+e^- \to \Upsilon(4S) \to B^0\overline{B}^0$ is shown in fig. 3, where one of the neutral B-mesons decays into a flavour eigenstate, $\overline{B}^0 \to D^{*+}\pi^-$, and the other one into the CP eigenstate $\psi(2S)K^0_S$ with the eigenvalue $CP = -1$. The CP eigenstate can be reached from either a B^0 or a $\overline{B}^0$. In fact it is reached from a linear superpostition of both, with coefficients which depend on the time difference between the two B-meson decays. This time-dependent coherent superposition is an important property for CP asymmetry measurements on the $\Upsilon(4S)$-resonance.

The $\Upsilon(4S)$ has the quantum numbers $C = P = -1$. It decays by strong interaction, so P and C are conserved. The final state with two neutral B-mesons at polar angles θ and $\pi - \theta$ has to be

$$\psi = [B^0(\theta)\overline{B}^0(\pi-\theta) - \overline{B}^0(\theta)B^0(\pi-\theta)]/\sqrt{2}\,. \qquad (10)$$

This state remains unchanged until the first of the two Beons decays. If it decays at time t_1 into a flavour-specific mode indicating that it was a B^0, the other Beon is a $\overline{B}^0$ at the same time. This $\overline{B}^0$ develops as single-particle state with $B^0\overline{B}^0$ oscillations until it decays at time t_2. The probabilities to decay as a B^0 or as a $\overline{B}^0$ are well-defined functions [2] of $\Delta t = t_2 - t_1$. These are used to derive the CP asymmetry in eq. (9), where for $\Upsilon(4S)$ measurements $t = t_2 - t_1 = \Delta t$, and $B^0 \to J/\psi K^0_S$ means a decay at t_2 with a flavour-specific decay, a so-called "tag", of a $\overline{B}^0$ at time t_1. The expression in eq. (9) is the same for $\Delta t < 0$. The expected Δt distributions for decays into $J/\psi K^0_S$ are shown in fig. 4 for $\Delta m_B = 0.47/\text{ps}$ and $\sin 2\beta = 0.7$.

The observed asymmetry will not be $A(\Delta t)$ because of resolution effects $r(\Delta\tilde{t} - \Delta t)$ and because of non-perfect flavour tagging resulting in a "dilution" D. The observed asymmetry $\tilde{A}$ as a function of the measured time difference $\Delta\tilde{t}$ will be

$$\tilde{A}(\Delta\tilde{t}) = D \cdot \sin 2\beta \cdot \int \sin(\Delta m_B \Delta t) \cdot r(\Delta\tilde{t} - \Delta t)\mathrm{d}t\,, \quad (11)$$

where D and r have to be determined experimentally with the help of control samples. The parameter $\sin 2\beta$ can then be obtained from a fit to the observed asymmetry $\tilde{A}(\Delta\tilde{t})$. In practice, it is obtained from a simultanuous fit to the two distributions $N(\overline{B}^0 \to J/\psi K^0_S)$ and $N(B^0 \to J/\psi K^0_S)$ as functions of $\Delta\tilde{t}$ and to the control samples. Before this fit, each candidate event needs to be reconstructed in several steps: reconstructing the K^0_S, the J/ψ, the B, the flavour of the tag, and the value of $\Delta\tilde{t}$.

6 Results

Examples from the BABAR analysis with 62 million $\Upsilon(4S)$ events [16], as obtained in March 2002, are shown in fig. 5. Selection of fully reconstructed B-mesons is performed with the help of the two quantities

$$\Delta E = E(J/\psi) + E(K^0) - m(\Upsilon 4S)/2\,,$$
$$m^2_{ES} = [m(\Upsilon 4S)/2]^2 - [\boldsymbol{p}(J/\psi) + \boldsymbol{p}(K^0)]^2\,, \qquad (12)$$

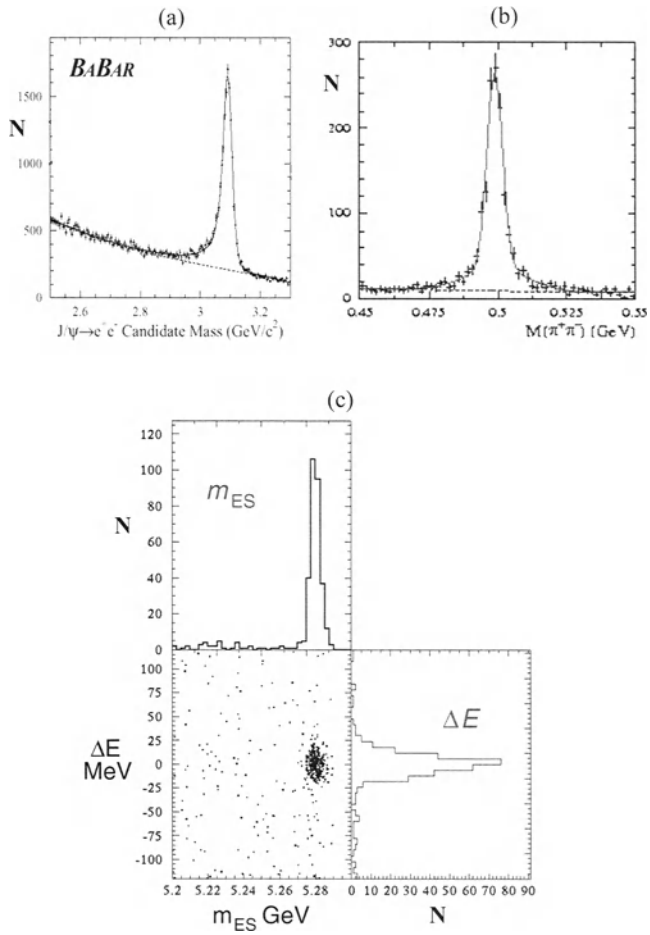

Fig. 5. Event reconstruction in BABAR. (a) $J/\psi \to e^+e^-$, (b) $K^0_S \to \pi^+\pi^-$, (c) $B \to J/\psi K^0_S$.

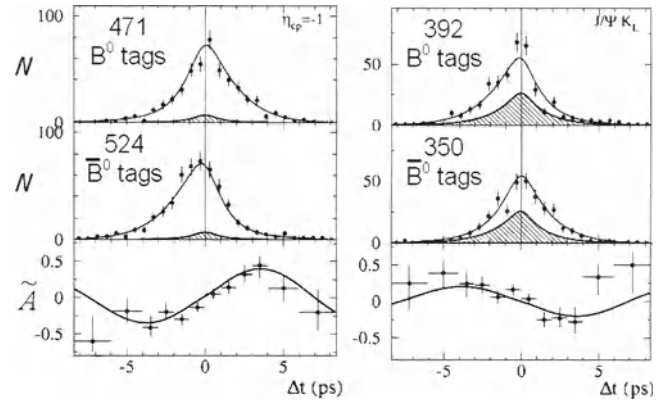

Fig. 6. BABAR results from 62M $B\overline{B}$ events. The left-hand side shows the time-dependent decay rates into $J/\psi K^0_S$ and other $c\bar{c}K$ modes with $CP = -1$, the right-hand side into $J/\psi K^0_L$ with $CP = +1$. The two top graphs show decays with B^0 tags, the middle ones with $\overline{B}^0$ tags, and the lower ones the raw asymmetries $\tilde{A}$ as defined in eqs. (9) and (11).

Table 1. All published results for the CP asymmetry $\sin 2\beta$ in B-meson decays. The first errors are statistical, the second ones systematic.

Experiment	Reference	Result
OPAL	[20]	$3.2\,^{+1.8}_{-2.0} \pm 0.5$
ALEPH	[21]	$0.84\,^{+0.82}_{-1.04} \pm 0.16$
CDF	[22]	$0.79\,^{+0.41}_{-0.44}$
BABAR	[16]	$0.75 \pm 0.09 \pm 0.04$
BELLE	[19]	$0.82 \pm 0.12 \pm 0.05$
Average		0.78 ± 0.08

where E and $\boldsymbol{p}$ are energies and momenta of the B decay daughters in the $\Upsilon(4S)$ frame. The "energy-substituted" mass m_{ES} is used because it has a smaller experimental error than the invariant mass with $E(J/\psi) + E(K^0)$ instead of $m(\Upsilon 4S)/2$. After requiring flavour tags in addition to B reconstruction, there remain 995 B candidates decaying into CP eigenstates with eigenvalue $CP = -1$ ($J/\psi K^0_S$, $\chi_{c1}K^0_S$, and $\psi(2S)K^0_S$) and 742 with $CP = +1$ ($J/\psi K^0_L$). 113 candidates are found in the mode J/ψ K^{*0} which contains events with $CP = -1$ and with $CP = +1$. Their relative contribution is determined experimentally from a Dalitz-plot analysis [17] resulting in $CP_{\text{eff}} = +0.65 \pm 0.07$.

Tagging is obtained by decays of the other B-meson into electrons, muons, charged kaons, or from a combination of all event information in a neural net. $(67.5 \pm 0.5)\%$ of all reconstructed CP eigenstates are tagged. The value of this tagging efficiency is not important; essential is only the "quality factor"

$$Q = \sum_i \epsilon_i (1 - 2w_i)^2 \ ,$$

where the sum runs over the four tagging categories, ϵ_i is the tagging efficiency and w_i the mistag fraction of each category. The value of Q determines the obtainable precision on $\sin 2\beta$,

$$\sin 2\beta \approx \frac{1.9}{\sqrt{N_{\text{sig}} \cdot Q}} \cdot \sqrt{1 + \frac{N_{\text{bg}}}{N_{\text{sig}}}} \ , \qquad (13)$$

where N_{sig} and N_{bg} are the numbers of signal and background events before tagging. In the presented analysis, BABAR has reached $Q = (25.1 \pm 0.8)\%$. The mistag fractions w_i for each tagging category are determined experimentally by tagging events of the "flavour sample", *i.e.* fully reconstructed events with known flavour like $B \to D^*\pi$, and by counting how often the tag is wrong.

The value of $\Delta\tilde{t}$ for each tagged event is determined from the distance $\Delta\tilde{z}$ between the reconstructed vertex of the CP eigenstate decay and that of the tagging decay, and

$$\Delta\tilde{t} = \Delta\tilde{z}/\beta\gamma c \ .$$

The Δt resolution function is determined from the $\Delta\tilde{t}$ distribution of events in which one neutral B decays into a fully reconstructed flavour state and the other one into one of the tagging categories. Because of $B^0\overline{B}^0$ oscillations, the $B^0\overline{B}^0$ events follow the distribution $e^{-|\Delta t|/\tau}(1 + \cos \Delta m_B \Delta t)$ and those with B^0B^0 and

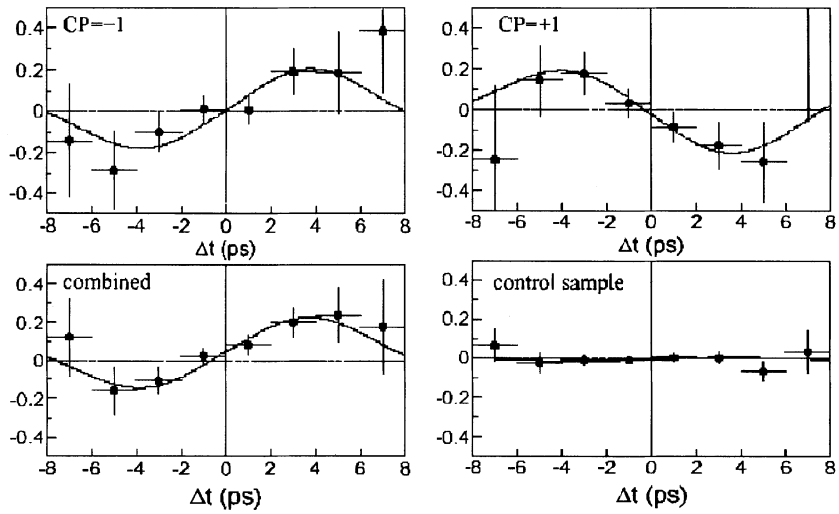

Fig. 7. BELLE results from 46M $B\overline{B}$ events. Shown are the raw asymmetries $\tilde{A}$ as defined in eqs. (9) and (11) for decays into $c\bar{c}K$ modes with $CP = -1$, with $CP = +1$, for both of them, and —as a control— for decays into flavour eigenstates where $\tilde{A} = 0$ is expected.

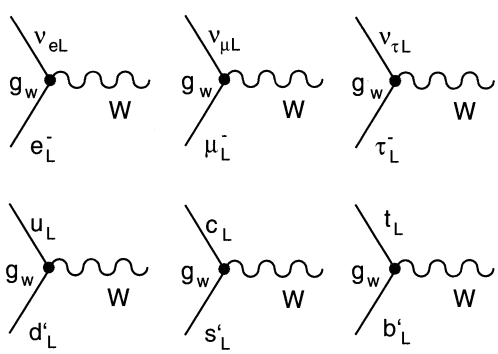

Fig. 8. Feynman diagrams for couplings of the charged weak interaction in the Standard Model.

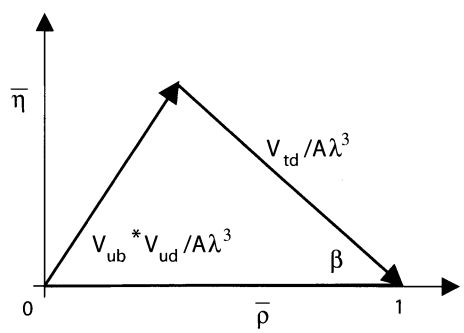

Fig. 9. The unitarity triangle of the CKM matrix, as defined by eq. (25). The angle β in this triangle determines the CP asymmetry $\sin 2\beta$ in $B \to c\bar{c}K$ decays.

$\overline{B}^0\overline{B}^0$ follow $e^{-|\Delta t/|\tau}$ $(1 - \cos \Delta m_B \Delta t)$. The two observed distributions of these events as a function of $\Delta\tilde{t}$ determine very well the time resolution function. They can also be used for a determination of the mass difference Δm_B, the BABAR result from this data sample is [18]

$$\Delta m_B = (0.516 \pm 0.016 \pm 0.010)\,\mathrm{ps}^{-1} \ . \qquad (14)$$

The last step in the determination of $\sin 2\beta$ is the final fit to the two $\Delta\tilde{t}$ distributions of CP eigenstate events, those with B^0 and those with $\overline{B}^0$ tags. The distributions are shown in fig. 6 for $CP = -1$ and $CP = +1$ events. CP violation is clearly seen, the time dependence of events with B^0 tags is very different from that of events tagged by $\overline{B}^0$. The lower part of the figure shows the raw asymmetries $\tilde{A}$ as introduced in eq. (11). The $CP = -1$ events give $\sin 2\beta = 0.76 \pm 0.10$, and those with $CP = +1$ give $\sin 2\beta = 0.73 \pm 0.19$. Together with the J/ψ K^{*0} sample of mixed CP eigenvalue composition, the final BABAR result from 62M $B\overline{B}$ events is

$$\sin 2\beta = 0.75 \pm 0.09 \pm 0.04 \ . \qquad (15)$$

Also in March 2002, the BELLE experiment has presented a $\sin 2\beta$ result obtained with 46M $B\overline{B}$ meson pairs [19]. The analysis is very similar to that of BABAR. Their raw asymmetries $\tilde{A}(\Delta\tilde{t})$, again as defined in eq. (11), are shown in fig. 7. Their combined result from fits to the $CP = -1$, $CP = +1$, and J/ψ K^{*0} events, is

$$\sin 2\phi_1 = 0.82 \pm 0.12 \pm 0.05 \ , \qquad (16)$$

where ϕ_1 is the Japanese name for β. Table 1 summarizes all $\sin 2\beta$ results obtained so far. Their mean value is

$$\sin 2\beta = 0.78 \pm 0.08 \ , \qquad (17)$$

i.e. CP asymmetry in B-meson decays is now established with a significance of about ten standard deviations.

7 Standard model explanation of CP violation in K and B decays

The measured values of $\sin 2\beta$ and ϵ_K are compatible with each other and with the assumption that they are completely determined by the charged weak interaction of the

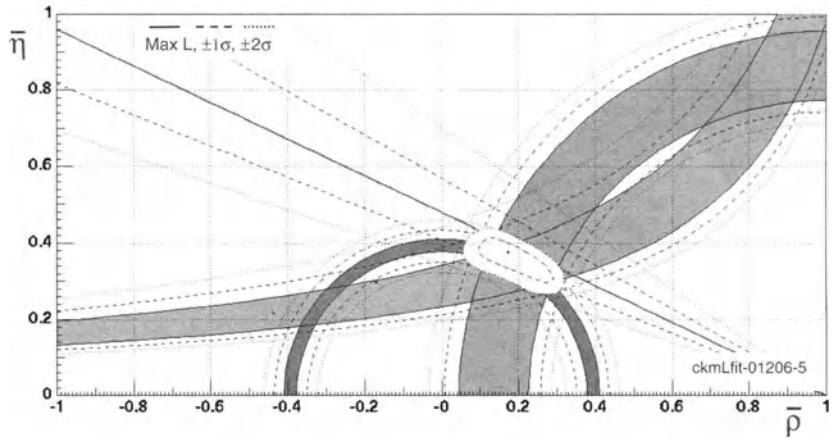

Fig. 10. Information on the CKM matrix parameters ρ and η. The circular band around $(0,0)$ is the result of exclusive and inclusive $b \to u\ell\nu$ decays; the circular band around $(1,0)$ results from measurements of $B^0\overline{B}^0$ and $B_s\overline{B}_s$ oscillations; the hyperbolic band results from the measurement of ϵ_K; and the linear band is given by $\sin 2\beta$. Solid lines correspond to maximum likelihood, dashed lines to $\pm 1\sigma$, and dotted lines to $\pm 2\sigma$. The region around $(0.20, 0.35)$ is the maximum-likelihood fit to all information [26].

Standard Model. In perturbation theory, processes of this interaction are calculated with the Feynman diagrams in fig. 8, where all six diagrams have the same universal weak coupling strength g_w.

The index L indicates that only the left-handed fractions $f_L = (1-\gamma_5)f/2$ of all fermions f participate in these couplings to the W field. The quarks u, c, t are mass eigenstates; their Glashow partners (*i.e.* members in the same doublet of weak isospin) are not. These partners d′, s′, b′ are linear superpositions of mass eigenstates d, s, b:

$$\begin{aligned} d' &= V_{ud} \cdot d + V_{us} \cdot s + V_{ub} \cdot b \ , \\ s' &= V_{cd} \cdot d + V_{cs} \cdot s + V_{cb} \cdot b \ , \\ b' &= V_{td} \cdot d + V_{ts} \cdot s + V_{tb} \cdot b \ , \end{aligned} \tag{18}$$

with the unitarity CKM matrix V as already introduced in sect. 2. In the Standard Model, the matrix elements are given by the coupling of the Higgs field to quarks. CPT symmetry requires how the Higgs couples to antiquarks, leading to the following relations between the Glashow partners of $\bar{u}$, $\bar{c}$, $\bar{t}$ and the mass eigentates $\bar{d}$, $\bar{s}$, $\bar{b}$:

$$\begin{aligned} \bar{d}' &= V_{ud}{}^* \cdot \bar{d} + V_{us}{}^* \cdot \bar{s} + V_{ub}{}^* \cdot \bar{b} \ , \\ \bar{s}' &= V_{cd}{}^* \cdot \bar{d} + V_{cs}{}^* \cdot \bar{s} + V_{cb}{}^* \cdot \bar{b} \ , \\ \bar{b}' &= V_{td}{}^* \cdot \bar{d} + V_{ts}{}^* \cdot \bar{s} + V_{tb}{}^* \cdot \bar{b} \ . \end{aligned} \tag{19}$$

If the CKM matrix is not real, the Higgs couplings mix antiquarks in a different way than quarks; this is the origin of *CP* violation in the Standard Model. However, not every complexity leads to observable *CP* asymmetries. The necessary and sufficient condition for *CP* violation is given by quartets of CKM matrix elements [23],

$$J = \mathrm{Im}(V_{ik} V_{il}^* V_{jl} V_{jk}^*) \neq 0 \ , \tag{20}$$

with $i \neq j$ and $k \neq l$. The CKM matrix has four observable parameters and has to be unitary, $VV^+ = 1$. The most widely used parametrisation of V was introduced by Wolfenstein [24]; a sufficient approximation is

$$V \approx \begin{pmatrix} 1-\lambda^2/2 & \lambda & A\lambda^3(\rho - i\eta) \\ -\lambda & 1-\lambda^2/2 & A\lambda^2 \\ A\lambda^3(1-\overline{\rho}-i\overline{\eta}) & -A\lambda^2 & 1 \end{pmatrix} \ ,$$

$$\overline{\rho} = (1-\lambda^2/2)\rho \ , \ \overline{\eta} = (1-\lambda^2/2)\eta \ , \ J \approx A^2\lambda^6\overline{\eta} \ . \tag{21}$$

The parameters A, λ, ρ and η are four of the 18 free parameters of the Standard Model. They have to be determined experimentally. From the observed rates of K-meson β-decays we know

$$\lambda = 0.223 \pm 1\% \ , \tag{22}$$

and from B-meson β-decays

$$A = 0.82 \pm 4\% \ . \tag{23}$$

Six unitarity conditions of V can be drawn as triangles in the complex $\overline{\rho}$-$\overline{\eta}$ plane. One example,

$$V_{ud}V_{ub}{}^* + V_{cd}V_{cb}{}^* + V_{td}V_{tb}{}^* = 0 \ , \tag{24}$$

$$\frac{V_{ub}{}^*(1-\lambda^2/2)}{A\lambda^3} - 1 + \frac{V_{td}}{A\lambda^3} = 0 \ , \tag{25}$$

is shown in fig. 9. The area of this triangle is $\overline{\eta}/2$, that of the unscaled triangle in eq. (24) is $J/2$. The Standard Model *CP* asymmetry in $B \to c\bar{c}K$ decays is given by the angle β of the triangle; expressed by the Wolfenstein paremeters we have

$$\sin 2\beta = \frac{2\,(1-\overline{\rho})\,\overline{\eta}}{(1-\overline{\rho})^2 + \overline{\eta}^2} \ . \tag{26}$$

Figure 10 shows the experimental informations which constrain ρ and η. With the exception of $\sin 2\beta$, all these constraints depend not only on measured values but also

on QCD parameters which have to be calculated. Details can be found in recent reviews on the CKM matrix [25]. Here I only want to show the result of a maximum-likelihood fit [26] to the informations in fig. 10:

$$\rho = 0.20 \pm 0.10\,, \qquad \eta = 0.36 \pm 0.06\,, \tag{27}$$

where the errors are given as $\pm 1\sigma$. Including the errors on λ and A, we obtain

$$J = (2.9 \pm 0.6) \cdot 10^{-5}\,. \tag{28}$$

The fit has the remarkable property that all input informations are very well compatible with each other. The now 30-year-old Standard Model contains CP violation, created by the same mechanism which gives masses to quarks and leptons, and the present value of its CP-violating parameter η accounts quantitatively for all observed CP asymmetries in K- and B-meson decays.

References

1. J.H. Christensen *et al.*, Phys. Rev. Lett. **13**, 138 (1964).
2. G.C. Branco, L. Lavoura, J.P. Silva, *CP Violation* (Clarendon Press, Oxford, 1999).
3. CPLEAR (A. Apostolakis *et al.*), Phys. Lett. B **458**, 545 (1999).
4. Particle Data Group (K. Hagiwara *et al.*), Phys. Rev. D **66**, 010001 (2002).
5. N. Cabibbo, Phys. Rev. Lett. **10**, 531 (1963).
6. M. Kobayashi, T. Maskawa, Progr. Theor. Phys. **49**, 652 (1973).
7. UA1 (C. Albajar *et al.*), Phys. Lett. B **186**, 247 (1987).
8. ARGUS (H. Albrecht *et al.*), Phys. Lett. B **192**, 245 (1987).
9. ARGUS (H. Albrecht *et al.*), Phys. Lett. B **234**, 409 (1990).
10. CLEO (R. Fulton *et al.*), Phys. Rev. Lett. **64**, 16 (1990).
11. For a complete list of references, see the review of O. Schneider in ref. [4].
12. PEP-II Conceptual Design Report, SLAC-R-418 (1993).
13. KEK report 2001-157, edited by E. Kikutani (2001).
14. BABAR (B. Aubert *et al.*), Nucl. Instrum. Methods A **479**, 1 (2002).
15. BELLE (A. Abashian *et al.*), Nucl. Instrum. Methods A **479**, 117 (2002).
16. BABAR (B. Aubert *et al.*), *Proceedings of the XXXVII Rencontres de Moriond on Electroweak Interactions and Unified Theories, Les Arcs, France, 9-16 March 2002*, a newer result is in Phys. Rev. Lett. **89**, 201802 (2002).
17. BABAR (B. Aubert *et al.*), Phys. Rev. Lett. **87**, 241801 (2001).
18. BABAR (B. Aubert *et al.*), Phys. Rev. Lett. **88**, 221802 (2002).
19. BELLE (K. Abe *et al.*), *Proceedings of the XXXVII Rencontres de Moriond on Electroweak Interactions and Unified Theories, Les Arcs, France, 9-16 March 2002*, a newer result is in Phys. Rev. D **66**, 071102R (2002).
20. OPAL (K. Ackerstaff *et al.*), Eur. Phys. J. C **5**, 379 (1998).
21. ALEPH (R. Barate *et al.*), Phys. Lett. B **492**, 259 (2000).
22. CDF (T. Affolder *et al.*), Phys. Rev. D **61**, 072005 (2000).
23. C. Jarlskog, Phys. Rev. Lett. **55**, 1039 (1985).
24. L. Wolfenstein, Phys. Rev. Lett. **51**, 1945 (1983).
25. A. Hoecker *et al.*, Eur. Phys. J. C **21**, 225 (2001).
26. R. Nogowski, Diplomarbeit, TU Dresden (2002).

Eur. Phys. J. A **18**, 155–158 (2003)
DOI 10.1140/epja/i2002-10291-5

THE EUROPEAN PHYSICAL JOURNAL A

Relativistic study of nucleon electroweak properties in a constituent-quark model

R.F. Wagenbrunn[1,a], S. Boffi[2], L.Ya. Glozman[1], W. Klink[3], W. Plessas[1], and M. Radici[2]

[1] Institut für Theoretische Physik, Universität Graz, Universitätsplatz 5, A-8010 Graz, Austria
[2] Dipartimento di Fisica Nucleare e Teorica, Università di Pavia, and Istituto Nazionale di Fisica Nucleare, Sezione di Pavia, Via Bassi 6, I-27100 Pavia, Italy
[3] Department of Physics and Astronomy, University of Iowa, Iowa City, IA 52242, USA

Received: 30 September 2002 /
Published online: 22 October 2003 – © Società Italiana di Fisica / Springer-Verlag 2003

Abstract. We discuss the predictions of the Goldstone-boson-exchange constituent-quark model for the proton and neutron electric and magnetic form factors as well as the nucleon axial and induced pseudoscalar form factors. The results are calculated in a covariant framework using the point-form approach to relativistic quantum mechanics. The only input into the calculations is the nucleon wave function from the constituent-quark model. A remarkably consistent picture, with all aspects of the electroweak nucleon structure close to existing experimental data, is obtained.

PACS. 12.39.-x Phenomenological quark models – 13.66.-a Lepton-lepton interactions – 14.20.Dh Protons and neutrons

To treat a system of several particles relativistically, one must employ a quantum theory fulfilling all the symmetry requirements imposed by the Poincaré group. According to Dirac [1] there exist three possibilities for a relativistic quantum theory such that the generators of the Poincaré group are minimally affected by interactions: the instant form, the front form, and the point form.

In the point-form approach only the components of the four-momentum operator $\hat{P}^\mu$ contain interactions. Moreover, all Lorentz transformations (in particular the Lorentz boosts) remain purely kinematic so that the point form is manifestly covariant.

To construct the interacting four-momentum operators for a quantum theory with a fixed number of particles (as in a constituent-quark model) we use the Bakamjian-Thomas (BT) construction [2]. Starting from the free generators of the Poincaré group one introduces the auxiliary operators $\hat{M}_{\rm fr} = \sqrt{\hat{P}^\mu_{\rm fr}\hat{P}_{{\rm fr}\mu}}$ (free mass operator) and $\hat{V}^\mu_{\rm fr}$ (free four-velocity operator) defined by $\hat{M}_{\rm fr}\hat{V}^\mu_{\rm fr} = \hat{P}^\mu_{\rm fr}$, where $\hat{P}^\mu_{\rm fr}$ is the free four-momentum operator. Thereby all the dynamics is introduced into the mass operator (the four-velocity operator remaining unaffected by interactions), and the four-momentum operator can be written as

$$\hat{P}^\mu := \hat{P}^\mu_{\rm fr} + \hat{P}^\mu_{\rm int} = \hat{M}\hat{V}^\mu_{\rm fr} = (\hat{M}_{\rm fr} + \hat{M}_{\rm int})\hat{V}^\mu_{\rm fr}. \quad (1)$$

Poincaré covariance requires that $\hat{M}$ commutes with $\hat{V}^\mu_{\rm fr}$ and is a scalar under Lorentz transformations. Eigenstates of the four-momentum operator arise as simultaneous eigenstates of the mass and the velocity operators. The motion of the system as a whole and the internal motion are separated. The latter is described by a wave function of internal degrees of freedom which is obtained by solving the eigenvalue problem for the mass operator

$$\hat{M}\Psi = M\Psi. \quad (2)$$

For a constituent-quark model (CQM) of baryons the Hilbert space is spanned by product states of three spin-$\frac{1}{2}$ particles

$$|p_1, p_2, p_3; \sigma_1, \sigma_2, \sigma_3\rangle = |p_1, \sigma_1\rangle \otimes |p_2, \sigma_2\rangle \otimes |p_3, \sigma_3\rangle\,. \quad (3)$$

In the point form, however, a more useful basis is provided by the so-called velocity states [3]

$$|v; \boldsymbol{k}_1, \boldsymbol{k}_2, \boldsymbol{k}_3; \mu_1, \mu_2, \mu_3\rangle = U_{B(v)}\,|k_1, k_2, k_3; \mu_1, \mu_2, \mu_3\rangle = \prod_{i=1}^{3} D^{1/2}_{\sigma_i\mu_i}[R_{\rm W}(k_i, B(v))]\,|p_1, p_2, p_3; \sigma_1, \sigma_2, \sigma_3\rangle\,. \quad (4)$$

Here, $B(v)$ is a boost with four-velocity v and $U_{B(v)}$ its unitary representation, $p_i = B(v)k_i$, where the $k_i = (\omega_i, \boldsymbol{k}_i)$ are momenta that are restricted by $\sum \boldsymbol{k}_i = 0$, and $D^{1/2}$ are the spin-1/2 representation matrices of Wigner

[a] e-mail: robert.wagenbrunn@uni-graz.at

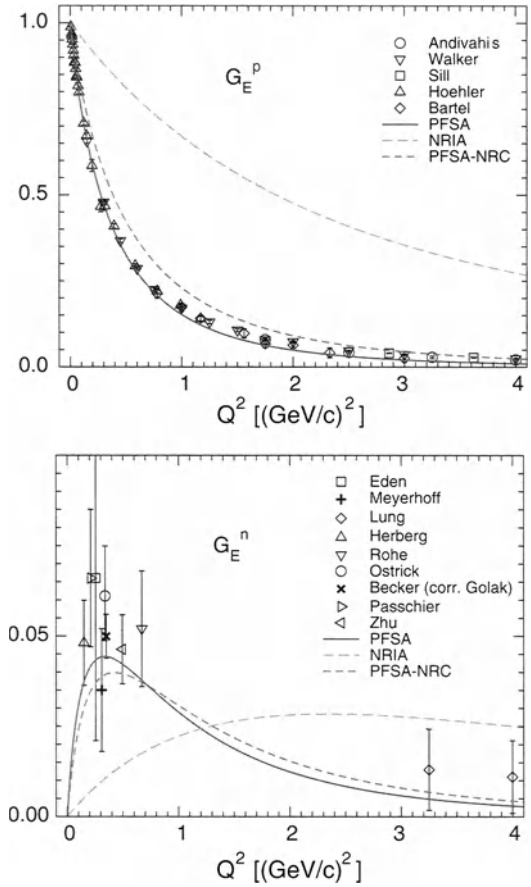

Fig. 1. Proton and neutron electric form factors.

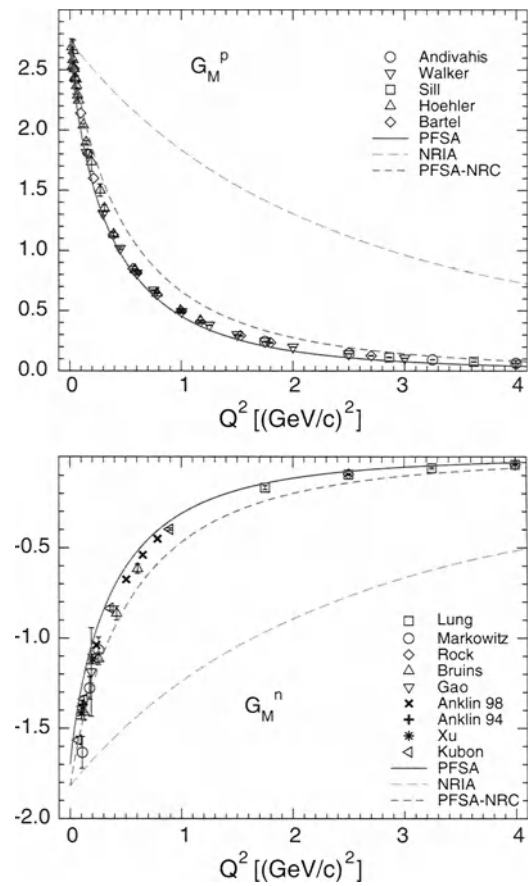

Fig. 2. Proton and neutron magnetic form factors.

rotations $R_{\rm W}(k_i, B(v))$. The velocity states are simultaneous eigenstates of the free mass and four-velocity operators. The baryon wave function is the velocity state representation of the mass operator eigenstate $|P, \Sigma\rangle$, where P and Σ are the eigenvalues of the total momentum and the z-component of the total angular momentum, respectively.

In a recent CQM [4] the interaction between two constituent quarks i, j was based on Goldstone-boson-exchange (GBE) dynamics in addition to a linear confinement. The corresponding mass operator is given by

$$\hat{M} = \sum_{i=1}^{3} \sqrt{\hat{m_i^2} + \hat{\boldsymbol{k}_i^2}} + \sum_{i<j} \left[\hat{V}_{\rm conf}(i,j) + \hat{V}_{\rm GBE}(i,j) \right] . \quad (5)$$

Even though $\hat{V}_{\rm conf}$ and $\hat{V}_{\rm GBE}$ are nonrelativistic potentials, we emphasize that this mass operator fulfills all the requirements of Poincaré covariance.

The electromagnetic and axial form factors of the nucleons are related to matrix elements of electromagnetic and axial current operators between states $|P, \Sigma\rangle$ and $|P', \Sigma'\rangle$ of the incoming and outgoing nucleon. For the current operator we apply the point-form spectator approximation (PFSA) [3]. It relies on the assumption that two constituent quarks are spectators in the sense that

$$\langle p_1', p_2', p_3'; \sigma_1', \sigma_2', \sigma_3' | \, \hat{J}^\mu(0) \, | p_1, p_2, p_3; \sigma_1, \sigma_2, \sigma_3 \rangle = 2E_2 \delta(\boldsymbol{p}_2' - \boldsymbol{p}_2) \delta_{\sigma_2' \sigma_2} 2E_3 \delta(\boldsymbol{p}_3' - \boldsymbol{p}_3) \delta_{\sigma_3' \sigma_3} \times \langle p_1', \sigma_1' | \, \hat{j}^\mu(0) \, | p_1, \sigma_1 \rangle \ , \quad (6)$$

and similarly for the axial current with $\hat{J}^\mu(0)$ replaced by $\hat{\boldsymbol{A}}^\mu(0)$ and $\hat{j}^\mu(0)$ by $\hat{\boldsymbol{a}}^\mu(0)$. Here, we indicate one-body currents of the constituent quarks by small letters. The axial current is a vector in isospin space. It is important to notice that the impulse delivered to the constituent quark, $\tilde{q} = p_1' - p_1$, is different from the impulse delivered to the nucleon, $q = P' - P$. The momentum transfer $\tilde{q}$ is uniquely determined by q and the two spectator conditions $\boldsymbol{p}_2' = \boldsymbol{p}_2$ and $\boldsymbol{p}_3' = \boldsymbol{p}_3$. For the remaining one-body current matrix element we employ the familiar expressions for the electromagnetic and axial currents of pointlike spin-$\frac{1}{2}$ particles

$$\langle p_1', \sigma_1' | \, \hat{j}^\mu(0) \, | p_1, \sigma_1 \rangle = \bar{u}(p_1', \sigma_1') \gamma^\mu e_1 u(p_1, \sigma_1), \quad (7)$$

$$\langle p_1', \sigma_1' | \, \hat{\boldsymbol{a}}^\mu(0) \, | p_1, \sigma_1 \rangle = \bar{u}(p_1', \sigma_1') \left[\gamma^\mu + \frac{2 f_\pi}{\tilde{Q}^2 + \mu_\pi^2} g_{\pi q} \tilde{q}^\mu \right] \gamma_5 \frac{\boldsymbol{\tau}_1}{2} u(p_1, \sigma_1). \quad (8)$$

In the electromagnetic current, e_1 is the charge of the constituent quark. In the first term of the axial current we

Table 1. Proton and neutron electric radii (in fm^2) and magnetic moments (in n.m.).

	Experiment	PFSA	NRIA	PFSA-NRC
r_p^2	0.757(14) [9]	0.82	0.10	0.57
r_n^2	−0.1161(22) [9]	−0.133	−0.009	−0.093
μ_p	2.792847337(29) [9]	2.70	2.74	2.74
μ_n	−1.91304270(5) [9]	−1.70	−1.82	−1.82

assume that the axial coupling of the constituent quark is equal to one as for a free bare fermion. The second term is due to the coupling of the pion to the constituent quark. It is proportional to the pion decay constant $f_\pi = 93.2$ MeV and the pion-quark coupling $g_{\pi q}$. For the latter we take $\frac{g_{\pi q}^2}{4\pi} = 0.67$; this is the same value as in the parametrization of the pion-exchange potential of ref. [4]; μ_π is the pion mass and $\tilde{Q}^2 = -\tilde{q}^\mu \tilde{q}_\mu$.

The predictions of the GBE CQM for the nucleon electromagnetic and axial form factors calculated in PFSA have been obtained in refs. [6–8]. Figures 1 and 2 show the electric and magnetic form factors of the proton and the neutron. The PFSA results (solid lines) fall rather close to the experimental data, while the predictions in nonrelativistic impulse approximation (NRIA) represented by the long-dashed lines deviate drastically. The short-dashed lines (labelled by PFSA-NRC) are the results of a calculation with a nonrelativistic current but with boosts included. One observes that the inclusion of boost effects brings the results already near to the PFSA predictions. Therefore, the main part of the difference between PFSA and NRIA is due to relativistic boosts, and effects from the relativistic current operator are of secondary importance.

The electric radii and magnetic moments of proton and neutron are given in table 1. The electric radii show the same characteristics as just outlined for the form factors. For the magnetic moments it appears at first instance that a nonrelativistic theory would be appropriate. A closer inspection, however, reveals that the PFSA results are governed by considerably large relativistic effects both from the relativistic current operator and from Lorentz boosts. In NRIA, *i.e.* using a nonrelativistic current operator, boosts have no influence, and incidentally a reasonable result is recovered, even though a covariant theory suggests large relativistic effects also for the magnetic moments.

In figs. 3 and 4 we show analogous results for the axial and induced pseudoscalar nucleon form factors. While the PFSA predictions are found in reasonable agreement with experimental data, the NRIA results appear again unacceptable. The dash-dotted curve in fig. 3 represents the result of a calculation with a relativistic current but without Lorentz boosts; it remains far away from a reasonable description. For the induced pseudoscalar form factor in fig. 4 the inclusion of the pion pole term for the axial current in eq. (8) is essential. The axial coupling constant (axial charge) $g_A = G_A(Q^2 = 0)$ is not affected by Lorentz boosts. The covariant result (*i.e.* using a relativistic current) is 1.15, thus slightly smaller than the experimental value 1.2670(30), while the nonrelativistic result of 1.65 is too large.

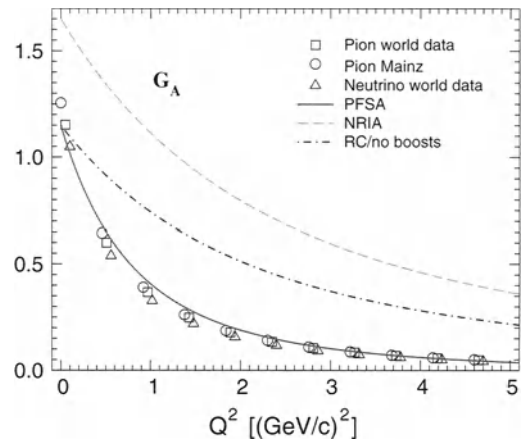

Fig. 3. Nucleon axial form factor.

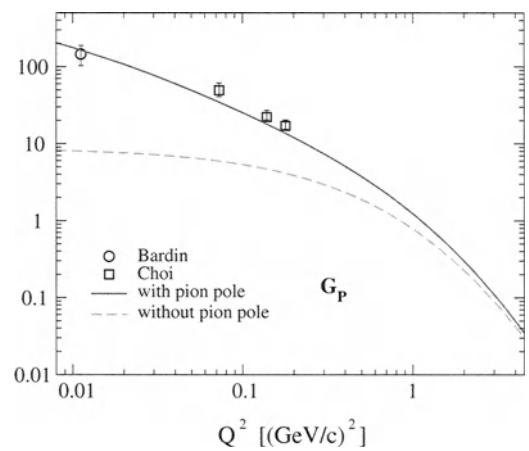

Fig. 4. Nucleon induced pseudoscalar form factor.

In summary the PFSA predictions for all electroweak nucleon form factors fall rather close to the experimental data. The nonrelativistic results deviate drastically. The inclusion of Lorentz boosts is most essential. Obviously, a reasonable description of the electroweak nucleon structure requires a covariant theory.

This work was supported by the Austrian Science Fund, Project No. P14806.

References

1. P.A.M. Dirac, Rev. Mod. Phys. **21**, 392 (1949).
2. B. Bakamjian, L.H. Thomas, Phys. Rev. **92**, 1300 (1953).
3. W.H. Klink, Phys. Rev. C **58**, 3587 (1998).
4. L. Ya. Glozman, W. Plessas, K. Varga, R.F. Wagenbrunn, Phys. Rev. D **58**, 094030 (1998).
5. L. Theußl, R.F. Wagenbrunn, B. Desplanques, W. Plessas, Eur. Phys. J. A **12**, 91 (2001).

6. R.F. Wagenbrunn, S. Boffi, W. Klink, W. Plessas, M. Radici, Phys. Lett. B **511**, 33 (2001).
7. L. Ya. Glozman, M. Radici, R.F. Wagenbrunn, S. Boffi, W. Klink, W. Plessas, Phys. Lett. B **516**, 183 (2001).
8. S. Boffi, L. Ya. Glozman, W. Klink, W. Plessas, M. Radici, R.F. Wagenbrunn, Eur. Phys. J. A **14**, 17 (2002).
9. K. Hagiwara *et al.*, Phys. Rev. D **66**, 010001 (2002).

Eur. Phys. J. A **18**, 159–161 (2003)
DOI 10.1140/epja/i2002-10292-4

THE EUROPEAN PHYSICAL JOURNAL A

Parity-violating electron scattering at MAMI

Strangeness in the nucleon

S. Baunack[a] and the A4 Collaboration

Institut für Kernphysik, Universität Mainz, Becherweg 45, D-55099 Mainz

Received: 30 September 2002 /
Published online: 22 October 2003 – © Società Italiana di Fisica / Springer-Verlag 2003

Abstract. A measurement of the parity-violating asymmetry in elastic scattering of polarized electrons on protons is currently running within the A4 Collaboration at the MAMI facility in Mainz. The aim is to reveal the contribution of strange quarks to the form factors of the nucleon at a $Q^2 = 0.23\,\mathrm{GeV}^2$. The expected asymmetry without strangeness is around 5.4×10^{-6}. After 600 hours of asymmetry data taking, an accuracy of 1×10^{-6} has been achieved.

PACS. 13.40.Gp Electromagnetic form factors – 11.30.Er Charge conjugation, parity, time reversal, and other discrete symmetries – 14.20.Dh Protons and neutrons – 13.60.-r Photon and charged-lepton interactions with hadrons

1 Introduction

Although there is no net strangeness in the nucleon, there is experimental evidence for the contribution of strange quark and antiquark pairs to the properties of the nucleon. From π-N scattering we know that strange quarks contribute to the mass of the nucleon [1], from deep inelastic scattering that there are contributions to spin and momentum of the nucleon. In this experiment, scattering of longitudinal polarized electrons on unpolarized protons is used for the determination of the contribution of the strange quarks to the vector form factors of the nucleon.

Weak interaction leads to a parity-violating (pv) asymmetry in the cross-section of elastic scattering of polarized electrons on unpolarized protons. At energies much smaller than m_Z the leading pv-term comes from the interference of photon and Z_0 exchange and is of the order Q^2/m_Z^2. The different coupling in weak and electromagnetic interaction allows a separation of the strange contribution to the vector form factors of the nucleon, provided the electric (G_E) and magnetic (G_M) form factors of the proton and neutron —or, alternatively, the Sachs form factors F_1 and F_2— are known [2].

The strange contribution can be written as an additive correction to the parity-violating asymmetry without strangeness, A_0:

$$A = A_0 \cdot (1 + a \cdot F_1^s + b \cdot F_2^s + c \cdot G_A^s)\,, \qquad (1)$$

where a, b and c are kinematical factors.

Given the Mainzer Microtron Facility (MAMI) maximum electron energy —at present 855 MeV— Figure of Merit (FOM) calculations led to the scattering angle of $\theta = (35 \pm 5)^\circ$, which corresponds to $Q^2 = 0.227\ \mathrm{GeV}^2/c^2$. The value for A_0 at 35° is 5.4×10^{-6}. For forward angles, as in our parity violation experiment, the asymmetry is most sensitive to F_1^s with small admixtures of F_2^s and G_A^s.

2 Experimental setup

2.1 Measurement principle

The experimental concept is very simple. It consists of counting the elastic scattered electrons N^+ and N^- for right- and left-handed polarized electrons and then getting the asymmetry in the cross-section by

$$A = \frac{N^+ - N^-}{N^+ + N^-}\,. \qquad (2)$$

For the desired statistical accuracy, about 2×10^{13} elastic electrons have to be counted. To achieve this within a measurement time of 1000 hours, a high luminosity of $L = 0.5 \times 10^{38}\ \mathrm{cm}^{-2}\mathrm{s}^{-1}$ is necessary. This luminosity leads to an elastic rate of about 10 MHz and a background rate of about 100 MHz in the detector.

Polarized electrons at a polarization between 75% and 80% are produced via photoeffect from strained layer GaAs-crystals. The electrons are then accelerated in the Mainz Microtron accelerator (MAMI) to an energy of 854.3 MeV. Helicity-correlated fluctuations of the beam are minimized by several stabilization systems. The small helicity-correlated fluctuations of the beam parameters are measured with high accuracy in our monitor system.

[a] e-mail: baunack@kph.uni-mainz.de

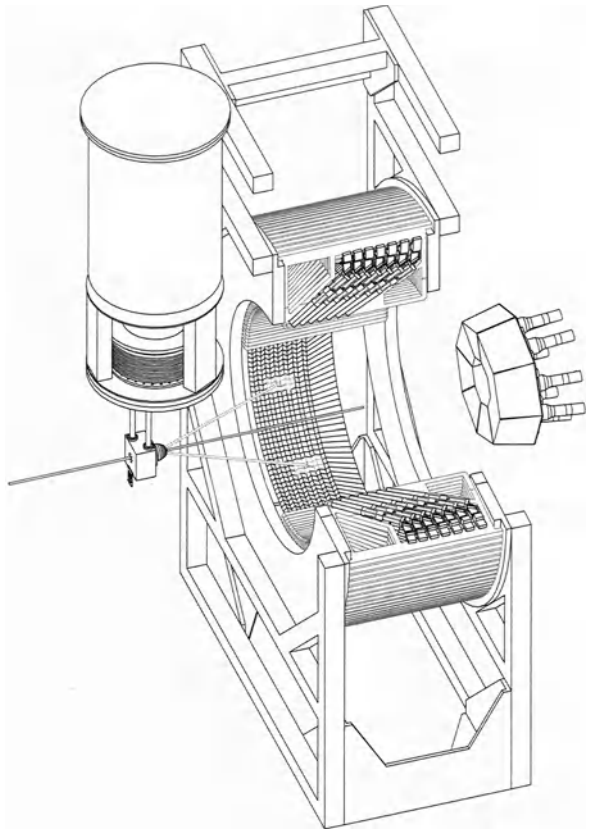

Fig. 1. Drawing of target, lead fluoride calorimeter and luminosity monitors.

In the measurements presented here the polarization of the electron beam has been measured with a Moeller polarimeter of the A1 Collaboration.

The electron beam hits the 10 cm long liquid-hydrogen target, which is designed to cool the 80 W of heating power from the 20 μA electron beam. The target does not show boiling, despite the fact that the beam is not rastered. The energy of the scattered particles is measured in our homogenous absorbing PbF_2 Čerenkov shower calorimeter. The luminosity is measured under small angles downstream of the target. The beam is dumped in a water-cooled beam dump.

2.2 PbF_2 calorimeter

The PbF_2 calorimeter is the central part of the MAMI parity experiment. It measures both position and energy of the scattered particles within a scattering angle between 30° to 40° within full azimuthal symmetry (total solid angle 0.7 sr). The energy and position signals are digitized and filled in histograms for positive and negative helicity states and stored on disk for later offline analysis. The calorimeter deals with high rates of about 100 MHz and provides an energy resolution of $3.5\%/\sqrt{E}$, which allows a separation of elastic scattered electrons from inelastic events. There are high demands on the calorimeter material as well as on the calorimeter electronics.

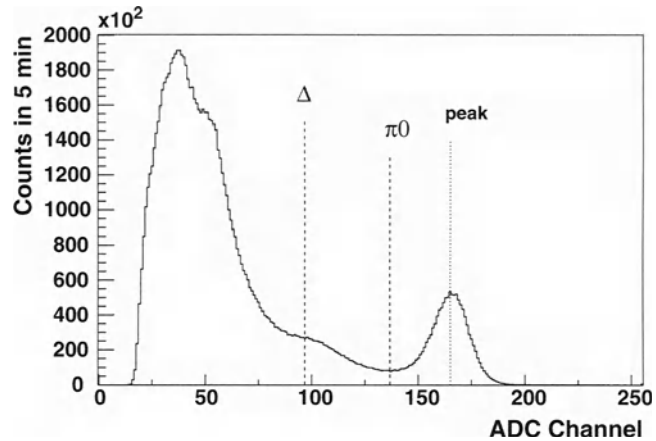

Fig. 2. Energy spectrum of the lead fluoride calorimeter. The spectrum is corrected for the differential non-linearities (DNL) of the ADC. x-axis = energy in ADC units. One can see the elastic peak at ADC channel 165, the π_0 production threshold at ADC channel 137 and the huge background. The cut-off at low ADC channels is due to thresholds in the electronics.

Lead fluoride (PbF_2) has been chosen as calorimeter material. PbF_2 has a high density and a short radiation length, as a pure Čerenkov radiator it is intrinsic fast and provides a good energy resolution. A schematic view of the PbF_2 calorimeter is shown in fig. 1. There are 1022 PbF_2 single crystals arranged in 146 columns and 7 rows.

For an almost complete coverage of the electromagnetic shower of an event, the signals of 3×3 crystals are summed up. This minimizes the energy loss, the energy resolution gets enhanced.

2.3 Electronics

The data acquisiton system has been developed at the Institute of Nuclear Physics, Mainz. Due to the high rates parallelisation of the electronics has been chosen. There are 1022 identical circuits, *i.e.* each crystal has such an electronics channel. The electronic circuit is divided into two parts, an analogue and a digital part. A dead time of 20 ns for the complete event is achieved. There is no individual channel information processed, each crystal is the center of a matrix of 9 channels and the analogue pulses of the matrix are summed by an analogue summing amplifier. The analogue summation signal is then digitized by a fast ADC. In addition, the center channel charge is integrated and also digitized. This gives information on the impact position on the individual crystal.

At the summation point of each channel, the analogue signals of the 8 direct neighbours need to be connected. Second hits within the integration time of 20 ns in the same crystal or in the a matrix of 25 crystals need to be recognised, so that on the veto level each crystals electronics circuit must be connected with the 24 neighbours. Due to this high connectivity, the topology of the electronics is the same as in the detector, a closed cylinder where neighbouring electronics channels correspond to neighbouring crystals in the detector.

Table 1. The table gives an overview over the small helicity-correlated fluctuations of the beam parameters and the resulting false asymmetries.

Parameter	Value	(False A)/A_0
I asym	$7.5 \cdot 10^{-8} \pm 2.3 \cdot 10^{-7}$	(0.9 ± 94.1) %
pos$X$ diff	(8.0 ± 1.0) nm	(0.3 ± 2.3) %
pos$Y$ diff	(82.2 ± 1.0) nm	(2.9 ± 6.0) %
angle$X$ diff	$(1.7 \cdot 10^{-7} \pm 1.8 \cdot 10^{-8})^\circ$	(0.1 ± 0.9) %
angle$Y$ diff	$(3.5 \cdot 10^{-7} \pm 2.2 \cdot 10^{-8})^\circ$	(0.3 ± 1.0) %
E diff	(5.2 ± 0.2) eV	(0.1 ± 0.3) %

2.4 Energy spectra

At the measurements presented here, one half of the PbF_2 calorimeter was equipped. Per run there are 1022 energy spectra as shown in fig. 2. With determination of the elastic line ("peak") the pion production threshold can be calculated. The knowledge of this threshold allows it to define an elastic cut and determine the counts of right- and left-handed elastic scattered electrons.

2.5 Beam parameters

Helicity-correlated beam fluctuations cause false asymmetries in the PbF_2 calorimeter. In order to control and minimize these beam fluctuations, beam monitor and stabilization systems for position, intensity and energy have been installed. Table 1 lists the achieved beam fluctuations and the resulting false asymmetries.

3 Analysis

In contrast to the simple approach in eq. (2), the elastic count rates are normalized to the target density $\rho = \frac{L}{I}$:

$$A_{\text{meas}} = \frac{\frac{N^+}{\rho^+} - \frac{N^-}{\rho^-}}{\frac{N^+}{\rho^+} + \frac{N^-}{\rho^-}} \tag{3}$$

The asymmetry is extracted by a linear regression in multiple dimensions. There is a $\lambda/2$-wave plate, which can be inserted in the laser system of the electron source. With this $\lambda/2$-wave plate in, the helicity of the electrons is reverted. This change is not known to the electronics and an important test of the whole apparatus. The sign of the observed asymmetries should correspond to the position of this plate. We have 17 data sets, 9 sets with $\lambda/2$-wave plate out and 8 sets with $\lambda/2$-wave plate in. The resulting physical asymmetries should change their sign corresponding to the position of the $\lambda/2$-wave plate. Figure 3 shows the preliminary results of the ongoing analysis. The change of sign for the individual data sets can be observed very well. The preliminary physical asymmetry at 35° that we get from all data sets together is

$$A_{\text{phys}} = (-7.3 \pm 0.9) \times 10^{-6}\,. \tag{4}$$

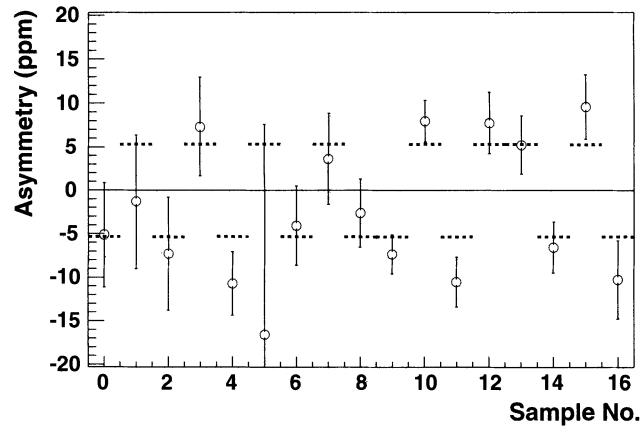

Fig. 3. Decorrelated physical asymmetries of the A4 experiment. The dashed lines indicate the expectation of the asymmetry without strangeness contribution.

The uncertainty in our result comes from three parts. One part arises from statistics, the correction for false asymmetries enters some error and the polarisation measurement contributes. The value of the asymmetrie has to be compared with A_0 without strangeness, 5.4×10^{-6}, which has some also some error due to the form factors that were put in to calculate A_0.

4 Outlook

The upgrade of the A4 experiment is currently on the way. The detector is fully equipped with all 1022 detectors and its electronics. The Compton backscattering polarimeter is being installed, which measures the absolute polarisation non-destructively during asymmetry data taking. Additionally, a Compton polarimeter is ready for installation downstream the calorimeter to provide fast measurements of relative changes in the beam polarisation. The future measurements will include

- measurements with increased statistics at 0.23 GeV under forward angles;
- 0.1 GeV under forward angles, which corresponds to the SAMPLE Q^2 under backward angles;
- 0.23 GeV under backward angles, which corresponds to our Q^2 under forward angles;
- 0.47 GeV under backward angles, which corresponds to the HAPPEX Q^2 under forward angles.

All these measurements together will allow for the first time a flavour separation of the form factors of the nucleon.

References

1. B. Borasoy, U.-G. Meissner, Ann. Phys. **254**, 192 (1997).
2. M.J. Musolf *et al.*, Phys. Rep. **239**, 1 (1994).

Eur. Phys. J. A **18**, 163–165 (2003)
DOI 10.1140/epja/i2002-10293-3

THE EUROPEAN PHYSICAL JOURNAL A

Baryon spectroscopy with the CB-ELSA detector at ELSA

V. Credé[a]

Helmholtz-Institut für Strahlen- und Kernphysik, Nußallee 14-16, 53115 Bonn, Germany

Received: 30 September 2002 /
Published online: 22 October 2003 – © Società Italiana di Fisica / Springer-Verlag 2003

Abstract. The investigation of the excitation spectrum of baryons provides important information on many open questions in baryon spectroscopy. The key to any progress is the identification of the effective degrees of freedom leading to a qualitative understanding of strong QCD. The problem of *missing resonances* predicted by quark models is discussed on the basis of recent experimental results of the CB-ELSA experiment at the e^- accelerator ELSA in Bonn. First hints for resonance production are given and cascades of the type $N^{**}(\Delta^{**}) \to N^*(\Delta^*) \to p\pi^0\pi^0(p\pi^0\eta)$ are observed. Indications for a Δ-resonance around 1900 MeV are seen. The latter is particularly interesting if it had negative parity because a confirmation of this state would be in contradiction with almost all constituent quark models, (S. Capstick, N. Isgur, Phys. Rev. D **34**, 2809 (1986); U. Löhring *et al.*, Eur. Phys. J. A **10**, 309 (2001)) for instance. Both, the quark models using one-gluon exchange and the quark model using instanton-induced forces as short-range residual quark-quark interaction predict the three states $\Delta_{5/2^-}(1930)$, $\Delta_{3/2^-}(1940)$ and $\Delta_{1/2^-}(1900)$ at masses in the 2200 MeV region.

PACS. 25.20.-x Photonuclear reactions

1 Introduction

All current models describing the spectrum of baryon resonances predict a series of hitherto unobserved states. This feature would clearly be a big problem for all models as they would have failed to describe physical reality. There are at least two possible explanations which account for this open question. One is that these *missing resonances* have to exist if the 3 valence quarks of the nucleon are not frozen into a quark-diquark substructure. In fact, this would reduce the number of effective degrees of freedom and, therefore, also the number of possible baryon states [1].

An alternative explanation is that those *missing resonances* are really missing and have simply not been observed up to now because almost all existing data result from πN elastic-scattering experiments. As a matter of fact, some models focussing on baryon strong decays predict baryon states missing in πN elastic-scattering analyses but showing strong evidence in electromagnetic production [2]. Those *missing resonances* should couple strongly to channels like $\Delta\pi$, for instance [3]. Thus, photoproduction experiments offer a large discovery potential.

2 Experimental configuration

Electrons extracted from the stretcher accelerator (ELSA) hit a primary radiation target and produce Bremsstrahlung. The corresponding energy of the photons ($E_\gamma = E_0 - E_{e^-}$) is determined in a tagging system by the deflection of the electrons in a magnetic field. This detector provides a tagged beam in the photon energy range from 25% up to 92% of the incoming electron energy. The calorimeter (Crystal Barrel) consisting of 1380 CsI(Tl) crystals covers about 98% of 4π solid angle for reactions *at rest* and is an ideal detector for photons. The photoproduction target in the center of the Crystal Barrel has a length of 5 cm and is filled with liquid hydrogen. It is surrounded by a scintillating fibre detector which was built to detect and trigger charged particles leaving the target.

3 Study of baryon decay cascades

The CB-ELSA detector is the ideal instrument to study various multi-photon final states over the full dynamical range. It allows to identify highly excited baryon states up to 2.6 GeV/c^2 by observing cascades of high-mass states to the ground state via the emission of single pions and η-mesons. The 4π acceptance of the detector system in combination with a good spatial and energy resolution guarantees a large efficiency and selectivity of many neutral final states in photoproduction off the proton. Data presented below were taken at an ELSA energy of $E_0 = 3.2$ GeV.

Figure 1(a) shows the total invariant mass for the $p\pi^0\eta$ final state. No structures are visible at first sight. Different mass regions are indicated and the corresponding $p\pi^0$ mass spectra given. Hints for baryon resonances

[a] e-mail: crede@iskp.uni-bonn.de

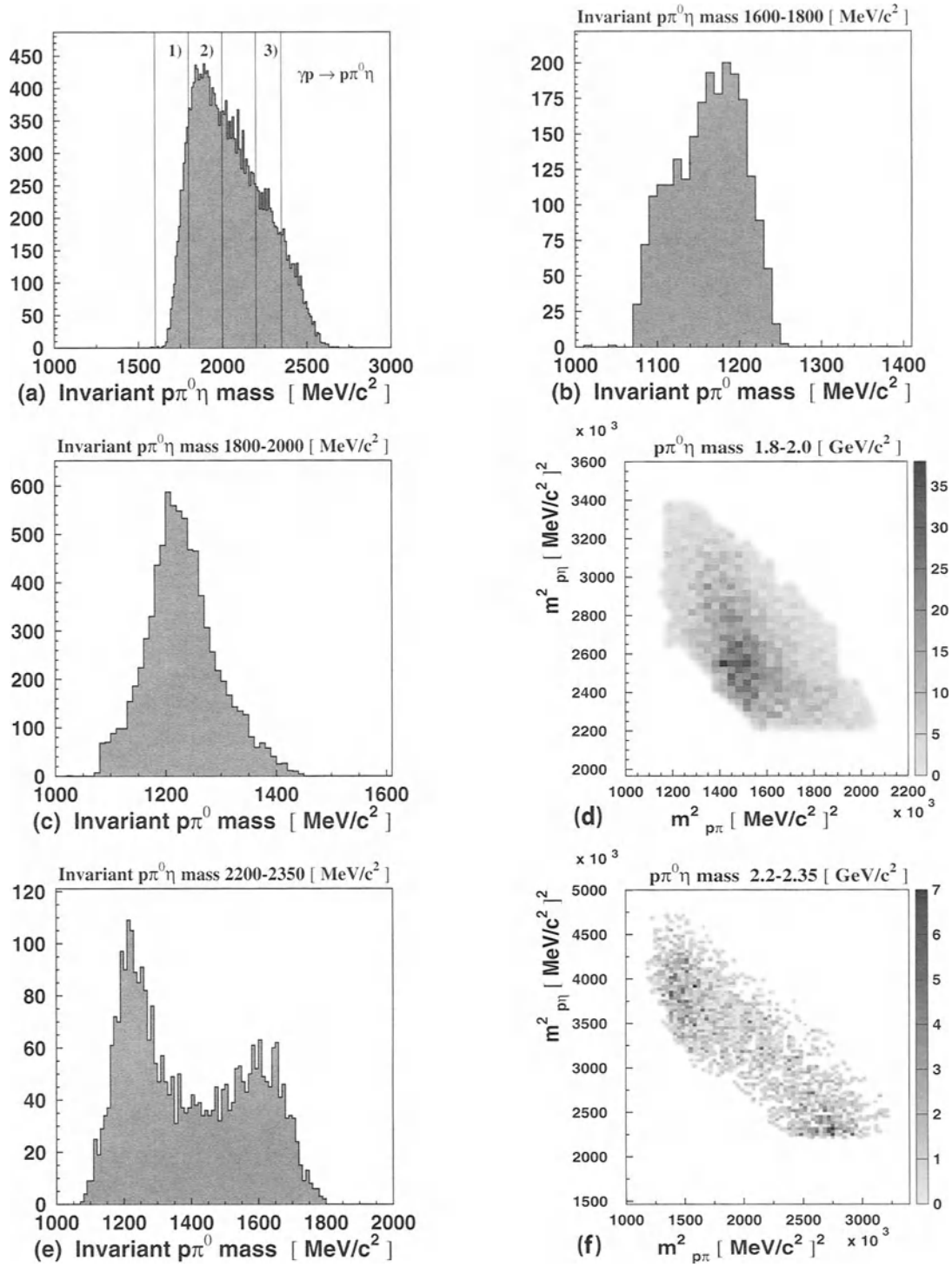

Fig. 1. Different plots on the reaction $\gamma\,\mathrm{p} \rightarrow \mathrm{p}\,\pi^0\,\eta$. (a) shows the total invariant $\mathrm{p}\pi^0\eta$ mass. In (b), (c), (e), the $\mathrm{p}\pi^0$ mass is plotted for the three different $\mathrm{p}\pi^0\eta$ mass regions indicated in (a). Clear evidence for the $\Delta(1232)$ can be observed and, thus, hints for resonances decaying via $\Delta\eta$ become obvious. (d) and (f) show the corresponding Dalitz plots for two different $\mathrm{p}\pi^0\eta$ mass regions. Resonance structures become even more transparent. All distributions are not efficiency corrected nor any photon flux normalisation has been carried out. However, the reconstruction efficiency is almost flat in $\cos(\theta)$ (of the proton in the center-of-mass system) and energy.

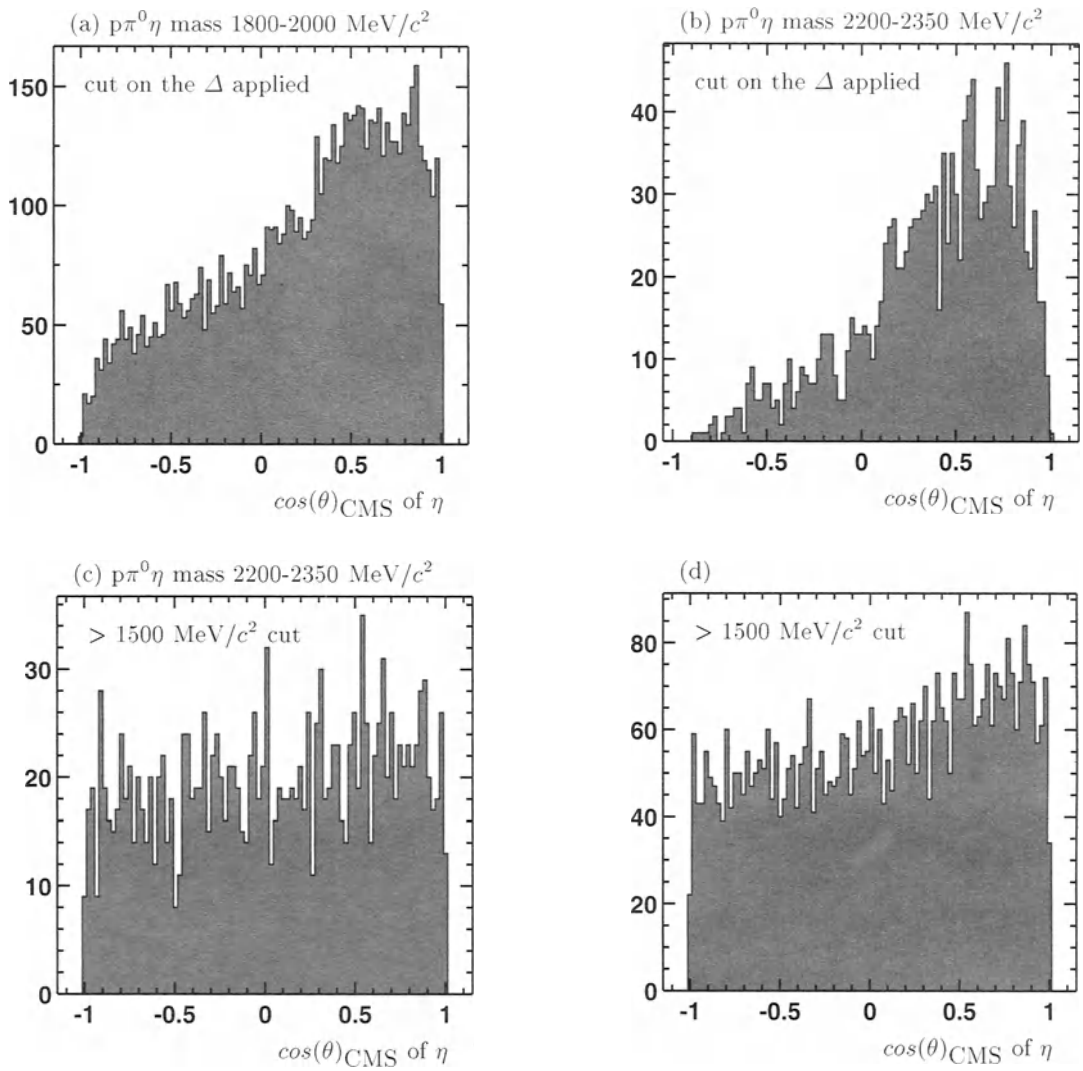

Fig. 2. $\cos(\theta)_{\mathrm{CMS}}$ of the η-meson in the reaction $\gamma\,\mathrm{p} \rightarrow \mathrm{p}\,\pi^0\,\eta$. A flat angular distribution can be interpreted as the decay of S-wave resonances. The $\Delta(1232)$ above 2.2 GeV likely does not stem from resonances but is created via more complicated processes.

decaying into $\Delta\eta$ now become visible. In the total mass region around 1700 MeV, no structure can be seen. However, a clear peak at the Δ mass can already be observed in the mass region around 1900 MeV. As a matter of fact, we expect a series of resonances in this mass region with positive as well as with negative parity. In principle, it would be very difficult to disentangle them. However, we expect a small angular momentum between the emitted meson (η-meson) and the known intermediate state ($\Delta(1332)$ in this case) due to the centrifugal barrier such that it should be possible to excite certain resonances selectively. In the case of the reaction $\gamma\,\mathrm{p} \rightarrow \mathrm{p}\,\pi^0\,\eta$, this idea will help to answer the question whether there are negative-parity Δ states in this region. For higher $\mathrm{p}\,\pi^0$ masses, further resonance intensity may be hidden in a structure around 1600 MeV. In fact, one has to be careful interpreting structures in the mass projections as those are often reflections of the corresponding Dalitz plots (fig. 1(d) and (f)).

More information is given by the CMS angular distributions of the η-meson for the same mass regions as indicated in fig. 1(a). These plots are given in fig. 2. A cut on the $\Delta(1232)$ in the $\mathrm{p}\,\pi^0$ system is applied as well as on higher masses ($m(\mathrm{p}\,\pi^0) > 1500$ MeV/c^2). The offset below the forward peak in fig. 2(a) and the flat angular distribution in 2(c) are likely to stem from resonant S-wave decays. On the other hand, the angular distribution in (b) is strongly shifted into the forward direction. This indicates the direct production of $\Delta(1232)$ which will be due to other mechanisms than resonance production.

References

1. D.B. Lichtenberg, Phys. Rev. **178**, 2197 (1969).
2. E.S. Ackleh *et al.*, Phys. Rev. D **54**, 6811 (1996).
3. S. Capstick, W. Roberts, Phys. Rev. D **49**, 4570 (1994).

Eur. Phys. J. A **18**, 167–169 (2003)
DOI 10.1140/epja/i2002-10294-2

THE EUROPEAN PHYSICAL JOURNAL A

A possible interpretation of the $\pi_1(1400)$ exotic meson

A.P. Szczepaniak[a]

Department of Physics, Indiana University, Bloomington, IN 47405, USA

Received: 30 September 2002 /
Published online: 22 October 2003 – © Società Italiana di Fisica / Springer-Verlag 2003

Abstract. I will discuss the current theoretical and experimental status of exotic mesons and a possible interpretation of the light, $\pi_1(1400)$ exotic meson as a final state interaction effect.

PACS. 12.39.Mk Glueball and nonstandard multi-quark/gluon states – 13.60.Le Meson production

1 Introduction

Gluonic excitations are expected to play a crucial role in light-quark spectroscopy by providing information on dynamical features of confinement. Strong interactions between colored gluons could result in a spectrum of gluon-dominated mesons —glueballs as well as hybrid states characterized by the presence of simultaneous gluonic and quark excitations. There is indeed strong evidence that the scalar-isoscalar π-π spectrum in the 1–2 GeV mass region has more states then expected from the valence quark model. The decay pattern of three scalar resonances observed in this mass region is consistent with the existence of a $J^{PC} = 0^{++}$ glueball with mass around 1.5 GeV. The possible mixing with ordinary mesons, however, makes the identification of glueballs and hybrids problematic with the exception of exotic states. These are mesons which have quantum numbers, J^{PC} that cannot originate from the valence quark and antiquark alone, *e.g.* $J^{PC} = 0^{--}, 0^{+-}, 1^{-+}, \ldots$. There is good evidence from lattice computations that the additional contribution to an exotic meson structure should come from exciting the gluonic field rather than from breakup channels, *e.g.* $(Q\bar{Q})^2$.

The spectrum of gluonic excitations and its connection to confinement has been extensively studied on the lattice. Numerical simulations of the energy of a static quark-antiquark system in the presence of dynamical gluons result in a linearly rising potential between the quarks —a characteristic feature of a confining interactions. There also exist lattice simulations of $Q\bar{Q}$ energies in the presence of excited gluon configurations. The first-excited state of the gluonic field turns out to have one unit of the total angular momentum along the axis connecting the static color sources, and has a negative product of parity and charge conjugation [1]. Combining the quantum numbers of the low-lying gluon excitation with those of the quark-antiquark pair leads to a spectrum of hybrid mesons including the exotic $J^{PC} = 1^{-+}$ state which arises from combining the orbitally excited gluon field with the $L = 0, S = 1$ quark-antiquark configuration. From lattice simulations of light-quark exotics it follows that the mass of the 1^{-+} state is slightly below 2 GeV [2–4]. Similarly, studies of the charmonium exotics indicate that the excitation of the gluonic degrees of freedom requires approximately 1 GeV. One should keep in mind, however, that the masses computed on the lattice are obtained with rather heavy u- and d-quark masses, > 50 MeV. Extrapolation to the chiral limit can shift downward the predicted hadron masses by 100–200 MeV [5]. An identification of exotic resonances can only be made if they are not too broad. This is indeed expected to be the case based on studies of exotic-mesons widths in the large-N_C limit [6]. Studies of the ground-state exotic-meson wave function on the lattice also show that it is well confined to a region where pair creation and string breaking are not expected to be significant [7].

To summarize, the current lattice and phenomenological studies indicate that the lightest exotic meson should have $J^{PC} = 1^{-+}$, mass between 1.8–2 GeV and a typical hadronic width of 100–200 MeV.

2 The $\eta\pi$ spectrum

Recently, a few exotic-mesons candidates have been reported, mainly by the E852 Collaboration. Some of the reported states, however, do not fit the theoretical profile discussed above. The E852 Collaboration reported a 1^{-+} exotic resonance in $\eta\pi^-$ and $\eta'\pi^-$ decay channels with widths of the order of 350 MeV and masses 1.4 and 1.6 GeV, respectively. The experiment used 18 GeV π^- beam on a hydrogen target and resonances were identified via the partial-wave analysis [8]. The Crystal Barrel experiment also found a signature of an exotic wave in

[a] *Present address*: Department of Physics, Indiana University, Bloomington, IN 47405, USA; e-mail: aszczepa@indiana.edu

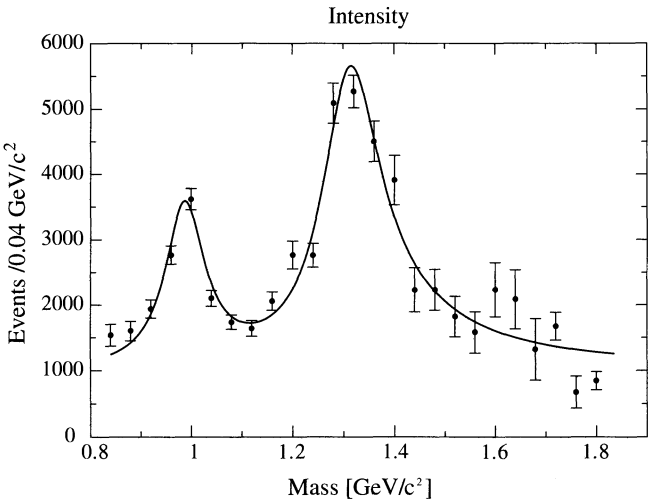

Fig. 1. Acceptance-corrected mass distribution of the $\eta\pi^0$ system for momentum transfer $t < 0.3$ GeV^2, from the reaction $\pi^-(18\text{ GeV})p \to \eta\pi^0 n$.

the $\eta\pi$ system consistent with the E852 result [9]. The $\eta\pi$ channel is particularly suited for exotic-meson identification, since the $\eta\pi$ P-wave has exotic quantum numbers. The resonance interpretation of the exotic wave in the $\eta\pi^-$ channel came from mass-dependent fits of the intensity and phase motion of the natural-parity P-waves. However, if the spin-1 exotic resonance is to be directly produced in the reaction

$$\pi^- p \to X^- p \to \eta\pi^- p\,, \tag{1}$$

it should be also found with the same mass and width in unnatural-parity exchange P-waves, P_- and P_0, even if the underlying production mechanisms are different.

More recently an analysis of the $\eta\pi^0$ spectrum has been performed [10]. The neutral channel has the added advantage of having well-defined charge conjugation. The final $\eta\pi^0$ data sample has approximately 35K events, and was comparable to the $\eta\pi^-$ sample discussed above. The $\eta\pi^0$ mass spectrum, shown in fig. 1 clearly indicates presence of the $a_0(980)$- and the $a_2(1320)$-resonances. The momentum transfer, $t-$ distribution of the D-waves representing the a_2 production were found consistent with the Regge exchange of ρ (natural) and b_1 mesons (unnatural). Limited statistics prevented t-dependent analysis for the a_0, however qualitatively it was also found consistent with the expected helicity-non-flip production. In the Gottfried-Jackson frame the η (or π^0) distribution can be written as

$$I(\Omega) = \sum_{\epsilon} \left| \sum_{L,M} a^{\epsilon}_{LM}(M_{\eta\pi^0}, t) Y^{\epsilon}_{LM}(\Omega) \right|^2, \tag{2}$$

where $0 < M \leq 1$ is the magnitude of the magnetic quantum number, $\epsilon = \pm$ labels the naturality (or reflectivity) of an amplitude, and Y^{ϵ} is the real or imaginary part of a spherical harmonic for $\epsilon = 1, -1$, respectively. In each mass, $M_{\eta\pi^0}$ and momentum transfer, t-bin there are seven complex amplitudes corresponding to $S = a_{00}$, $P_0 = a_{10}$, $P_+ = a^+_{11}$, $P_- = a^-_{11}$, and D_0, D_+ and D_-. Empirically the $D^{\epsilon}_2 = a^{\epsilon}_{22}$ waves were found to be negligible. Magnitudes and phases of these waves can be determined by fitting the angular distribution, $I(\Omega)$ or its moments. It is however well know that there are multiple sets of amplitudes which give identical intensity function, I. For this reason physical constraints have to be imposed on the amplitudes to eliminate the ambiguities. We have found that one can uniquely (modulo a few mass and t-bins) select the solution by imposing the requirement that all waves are continuous, the S dominates at threshold and is small at the a_2 region where the D-waves are large, and that the $D_0 - S$ phase motion corresponds to the interference of two resonances.

One can also study the mass dependence of the individual waves by fitting the mass distribution of moments, defined by

$$H_{LM} = \int \mathrm{d}\Omega I(\Omega) Y^*_{LM}(\Omega) \tag{3}$$

which, since given directly by the data, are unambiguous. The mass dependence of an individual wave was parameterized using a relativistic Breit-Wigner (BW) form consistent with the assumption that the spectrum can be described by an a_0, a_2 and an exotic P-wave resonance.

We have found that while the a_0- and a_2-resonance parameters are well reproduced, no consistent set of parameters of the P-wave resonance could be found for the P-waves. We should also point out that the natural-parity P_+-wave was found consistent with the one from the $\eta\pi^-$ analysis discussed earlier.

The difference in the interpretation of the observed P-wave is based on the type of analysis (fits) of the data. The resonance interpretation of ref. [8] was based on a fit to the P_+- and D_+-wave intensity, and the $P_+ - D_+$ phase differences in a single t-bin. No results were shown for different t-regions, other, unnatural P-wave amplitudes nor comparison of the fit to the amplitudes with the experimental moments. In contrast, our analysis takes all the above under consideration and then we find that resonance interpretation becomes problematic. This is illustrated, for example, in fig. 2 where the $H(10)$ moment, which is linear in the P-wave, is shown. The experimental data points prefer a "flatter" P-wave solution (solid line) as compared with the more varying one (dashed).

We also conclude that the data indeed indicate the presence of a P-wave but with a weak mass-dependence, while the "bump" structure seen in the P_+-wave in ref. [8] (in both $\eta\pi^0$ and $\eta\pi^-$) channels is most likely due to an imperfect acceptance and "leakage" from the dominant D_+-wave.

It has recently been shown that the observed light 2-meson spectra below 1–1.5 GeV can be well described by an effective, energy-independent interaction supplemented in some channels by direct coupling to a few underlying QCD states, *e.g.* the ρ in the $\pi\pi$, $I = S = 1$ channel [11–13]. These effective interactions in some cases, *e.g.* $\pi\pi$ $I = S = 0$, are well constrained by chiral symmetry while in others, *e.g.* $\pi\eta$ in the P-wave are more phenomenological [14]. The notion of a QCD resonance comes, in turn from the leading behavior of the meson spectrum in the

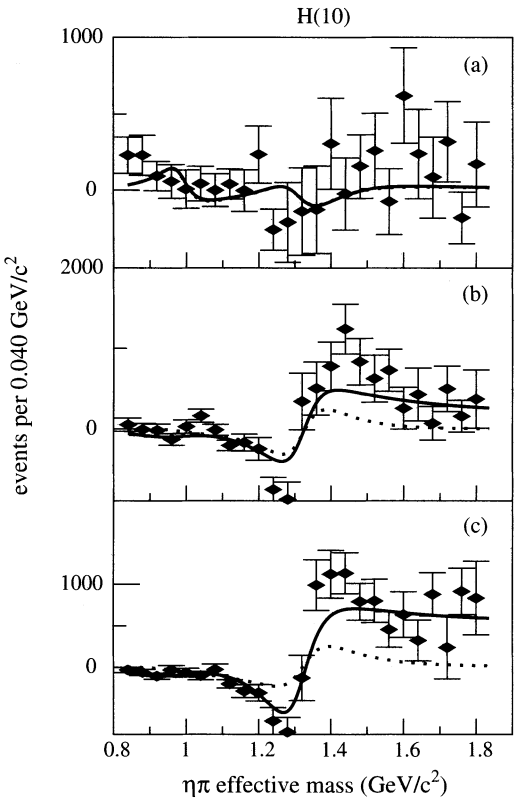

Fig. 2. Acceptance-corrected $H(10)$ moment, in three t-regions (a, b, c) of the $\eta\pi^0$ angular distribution as a function of the $\eta\pi^0$ invariant mass.

large-N_C limit where the meson loops are suppressed while quark bound states are expected to exist.

The E852 data in both $\eta\pi^0$ and $\eta\pi^-$ channels indicate that the P-wave phase is positive and slowly rising as a function of the $\eta\pi$ mass. Even though, as discussed above, this behavior cannot be unambiguously attributed to a simple BW pole on the complex energy plane near the real axis, the behavior can be due to a residual attractive interaction.

We thus assume that in the process,

$$\pi^- p \to \eta\pi^0 n \tag{4}$$

the $\eta\pi^0$ is directly produced with a slowly (or no) mass-dependent phase and then the observed P-wave phase comes from $\eta\pi^0 \to \eta\pi^0$ rescattering.

For illustration purposes consider a simple model for the $\eta\pi$ interaction given by a separable potential in the P channel of the form

$$\langle \eta\pi, q|V|\eta\pi, p\rangle = 4\pi\lambda \frac{qp}{f_\pi^2} g(p)g(q)\,. \tag{5}$$

The scale f_π is natural for low-energy meson-meson interactions and λ is a coupling constant of $O(1)$. Even though to lowest order in chiral expansion the P-wave $\eta\pi$ potential vanishes, one can expect the η_0-η_8 mixing effects to produce an effective interaction of the order $O(p^2/f_\pi^2)$ [14]. The form factors $g(p)$ are thus expected to cut off the interaction at a scale of the order of $4\pi f_\pi \sim 1$ GeV. The

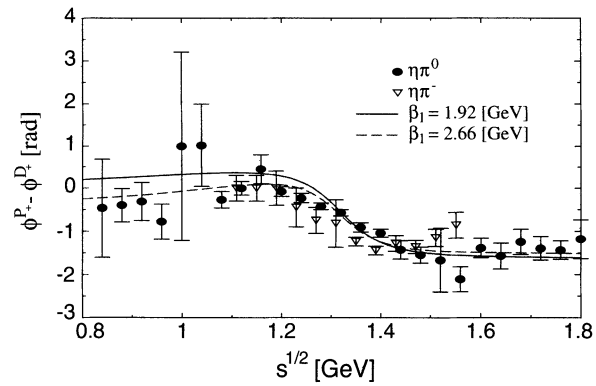

Fig. 3. Comparison of $P_+ - D_+$ wave phase differences with the $\eta\pi$ phase calculated using an effective interaction of eq. (5) with two different momentum cutoffs.

general features of the potential can also be inferred, for example by fitting the $S = I = 0$ $\pi\pi$ spectrum, where no QCD resonances are expected below 1.3 GeV. Comparison of the $\eta\pi$ elastic phase shift calculated using the above interaction with the $\eta\pi^0$ and $\eta\pi^-$ data is shown in fig. 3.

A more elaborate study of the rescattering effects, taking into account constraints from chiral symmetry and coupling to other channels are currently being investigated.

This work was done in collaboration with Alex Dzierba, Maciej Swat and Scott Teige, and was supported by the US Department of Energy.

References

1. K.J. Juge, J. Kuti, C.J. Morningstar, Nucl. Phys. Proc. Suppl. **63**, 326 (1998).
2. UKQCD Collaboration (P. Lacock *et al.*), Phys. Rev. D **54**, 6997 (1996); Phys. Lett. B **401**, 308 (1997).
3. TXL Collaboration (P. Lacock *et al.*), Nucl. Phys. Proc. Suppl. **73**, 261 (1999).
4. MILC Collaboration (C.W. Bernard *et al.*), Phys. Rev. D **56**, 7039 (1997).
5. A.W. Thomas, A.P. Szczepaniak, Phys. Lett. B **526**, 72 (2002).
6. T.D. Cohen, Phys. Lett. B **427**, 348 (1998).
7. K.J. Juge, J. Kuti, C.J. Morningstar, Phys. Rev. Lett. **82**, 4400 (1999).
8. E852 Collaboration (D.R. Thompson *et al.*), Phys. Rev. Lett. **79**, 1630 (1997); E852 Collaboration (S.U. Chung *et al.*), Phys. Rev. D **60**, 092001 (1999).
9. Crystal Barrel Collaboration (A. Abele *et al.*), Phys. Lett. B **423**, 175 (1998).
10. A.R. Dzierba *et al.*, *Study of the $\eta\pi^0$ spectrum and search for a $J^{PC} = 1^{-+}$ exotic meson*, Phys. Rev. D **67**, 094015 (2003).
11. J.A. Oller, E. Oset, Phys. Rev. D **60**, 074023 (1999).
12. J.A. Oller, E. Oset, J.R. Pelaez, Phys. Rev. D **59**, 074001 (1999); **60**, 099906 (1999) (E).
13. R. Kaminski, L. Lesniak, J.P. Maillet, Phys. Rev. D **50**, 3145 (1994).
14. S.D. Bass, E. Marco, Phys. Rev. D **65**, 057503 (2002).

Eur. Phys. J. A **18**, 171–176 (2003)
DOI 10.1140/epja/i2002-10305-4

THE EUROPEAN PHYSICAL JOURNAL A

Study of baryon and search for dibaryon resonances by the pp $\rightarrow$ pp$\pi^+\pi^-$ reaction

E. Doroshkevich[1], M. Bashkanov[1], W. Brodowski[1], R. Bilger[1], H. Calén[2], H. Clement[1,a], C. Ekström[2], K. Fransson[3], J. Greiff[4], S. Häggström[3], B. Höistad[3], J. Johanson[3], A. Johansson[3], T. Johansson[3], K. Kilian[5], S. Kullander[3], A. Kupść[2], P. Marciniewski[3], R. Meier[1], B. Morosov[6], W. Oelert[5], J. Pätzold[1], R.J.M.Y. Ruber[3], W. Scobel[4], J. Stepaniak[7], A. Sukhanov[6], A. Turowiecki[8], G.J. Wagner[1], Z. Wilhelmi[8], J. Zabierowski[9], and J. Zlomanczuk[3]

[1] Physikalisches Institut der Universität Tübingen, Morgenstelle 14, D-72076 Tübingen, Germany
[2] The Svedberg Laboratory, S-751 21 Uppsala, Sweden
[3] Department of Radiation Sciences, Uppsala University, S-751 21 Uppsala, Sweden
[4] I. Institut für Experimentalphysik der Universität Hamburg, D-22761 Hamburg, Germany
[5] IKP - Forschungszentrum Jülich GmbH, D-52425 Jülich, Germany
[6] Joint Institute for Nuclear Research Dubna, 101000 Moscow, Russia
[7] Soltan Institute for Nuclear Studies, PL-00681 Warsaw, Poland
[8] Institute of Experimental Physics, Warsaw University, PL-0061 Warsaw, Poland
[9] Soltan Institute for Nuclear Studies, PL-90137 Lódz, Poland

Received: 30 September 2002 /
Published online: 22 October 2003 – © Società Italiana di Fisica / Springer-Verlag 2003

Abstract. Exclusive measurements of the two-pion production channel $pp \rightarrow pp\pi^+\pi^-$ have been carried out near threshold at CELSIUS with the PROMICE/WASA detector. They reveal $pp \rightarrow pp^*(1440) \rightarrow pp\sigma \rightarrow pp(\pi^+\pi^-)_{I=\ell=0}$ as the dominant process at these energies, however, the data exhibit also significant contributions from $p^*(1440) \rightarrow \Delta\pi \rightarrow p(\pi^+\pi^-)_{I=\ell=0}$. From the observed interference of these Roper decay routes their relative branching ratio is derived. The status on the search for NN-decoupled $NN\pi$-resonances is reviewed with regard to recent experimental searches in the pionic double charge exchange in nuclei, the two-pion production in nucleon-nucleon collisions, the photo pion-production on the deuteron and the electro pion-production in nuclei.

PACS. 13.75.-n Hadron-induced low- and intermediate-energy reactions and scattering (energy ≤ 10 GeV) – 14.20.Gk Baryon resonances with $S = 0$ – 14.20.Pt Dibaryons – 25.40.Ve Nucleon-induced reactions: Other reactions above meson production thresholds (energies > 400 MeV)

1 Introduction

At the CELSIUS ring the availability of the PROMICE/WASA detector [1] has made it possible to reconstruct complete $pp \rightarrow pp\pi^+\pi^-$ events over a large part of phase space for the first time. We have performed exclusive measurements at $T_p = 725, 750$ and 775 MeV [2–4]. With four charged particles in the final state several subsystems may be investigated in great detail. In this contribution we focus on the $N\pi\pi$ and $NN\pi$ subsystems which are of interest for the decay properties of the Roper resonance in its low-energy tail and the search for the dibaryon state d', respectively.

1.1 The intriguing Roper resonance

In contrast to the $\Delta(1232)$ and other higher-lying resonances the second excited state of the nucleon, the Roper resonance $N^*(1440)$ is still poorly understood both theoretically and experimentally [5]. Being hardly observed in electromagnetic processes and having quantum numbers identical to those of the nucleon, the $N^*(1440)$ has been interpreted as the breathing-mode monopole excitation of the nucleon. Recent theoretical works [6,7] find the Roper excitation to rest solely on meson-nucleon dynamics, whereas another recent investigation [8] proposes it to be actually two resonances with one being the breathing mode and the other one a Δ excitation built on top of the $\Delta(1232)$. In all these aspects the decay modes of the Roper into the $N\pi\pi$ channels play a crucial role. There, the simplest decay is $N^* \rightarrow N(\pi\pi)_{I=l=0} := N\sigma$, *i.e.*, the

[a] e-mail: clement@pit.physik.uni-tuebingen.de

decay into the σ channel. A competitive and, according to present knowledge [5], actually much stronger decay channel is the Roper decay into the $\Delta(1232)$-resonance $N^* \to \Delta\pi$. However, this decay channel is not very well defined, since the Δ is not stable and decays nearly as fast as the Roper does. In fact, most of this decay will end up again in the $N\sigma$ channel and thus will interfere with the direct $N^* \to N\sigma$ decay.

Calculations of the Valencia group [9] predict the $pp \to pp\pi^+\pi^-$ reaction at energies not far above threshold to proceed dominantly via σ exchange in the initial NN collision with successive excitation of the Roper resonance in one of the nucleons. Our first exclusive measurements of this reaction at $T_p = 750\,\mathrm{MeV}$ [2] support very much this perception. This finding suggests $pp \to pp\pi\pi$ to be unique in the sense that it selectively provides the excitation mode "σ" $N \to N^*$ (where "σ" stands now for the σ exchange), which is not accessible in any other basic reaction process leading to the Roper excitation. We exploited this feature to study the decay properties of the Roper resonance in its low-energy tail.

1.2 The evasive dibaryon d′

In QCD-inspired models a large number of dibaryon states of basic $6q$ structure have been predicted [10]. However, despite a vast number of dedicated experiments in search of such states, not a single one could yet be identified unambiguously; for a review see, *e.g.*, [11]. In fact, dibaryons which by their quantum numbers can couple to the NN and/or $N\Delta$ channels cannot be expected to have narrow widths and hence should be hard to sense experimentally. But NN-decoupled dibaryon resonances may be rather narrow, if they are not far above the $NN\pi$ threshold. Indeed, such states at a mass as low as $m = 2.1\,\mathrm{GeV}/c^2$ with $I(J^P) = 0(0^-)$ and $0(2^-)$ have been predicted by Mulders *et al.* [10] though more recent theoretical work taking into account proper antisymmetrization [12] prefers the 0^--state to lie at a somewhat higher mass. Experimental studies for such dibaryon states were carried out in recent years in reactions of the pionic double charge exchange (DCX) in nuclei, in π^0 photoproduction on the deuteron and in direct measurements of 3-particle final-state invariant-mass distributions.

The measurements $A(\pi^+,\pi^-)B$ of the pionic DCX on nuclei exhibit at pion energies below the delta-resonance a peculiar resonance-like structure in the energy dependence of the forward-angle cross-section (fig. 1) [13–15]. This structure has peak cross-sections at incident energies $T_\pi \approx$ 40–60 MeV, *i.e.* far below the Δ excitation. Assuming a narrow $NN\pi$-resonance, the so-called d', with $I(J^P) =$ even (0^-), $m \approx 2.06\,\mathrm{GeV}/c^2$ and $\Gamma_{NN\pi} \approx 0.5\,\mathrm{MeV}$ the DCX data can be very well explained both in their energy and angular dependence.

However, since this reaction takes place in the nuclear medium, subtle medium effects cannot be excluded as origin of this structure. In fact, attempts have been made with some success to describe the observed resonance-like structures for specific nuclei by

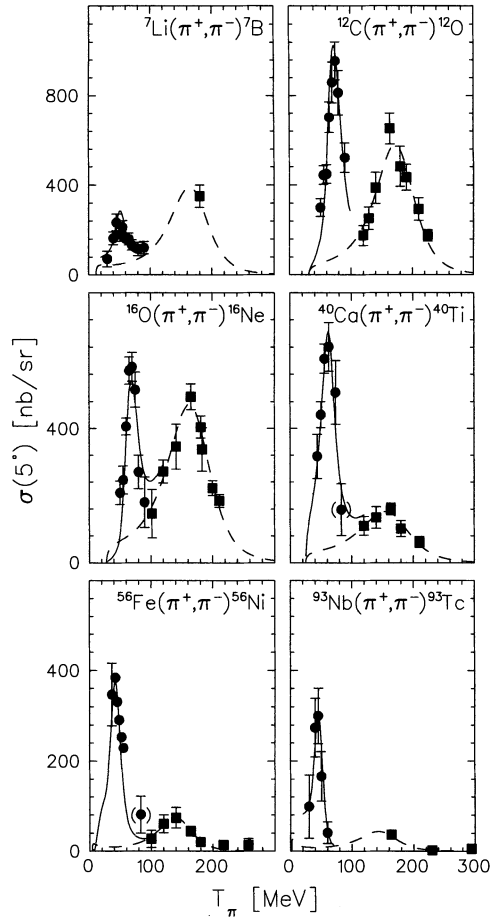

Fig. 1. Energy dependence of the forward-angle cross-section of the pionic DCX on nuclei. The solid lines show calculations assuming the formation of the hypothetical $NN\pi$-resonance d' interfering with the delta excitation (dashed lines) in this process (from ref. [13]).

conventional models [16–18]. In order to minimize the effects of the nuclear medium, the DCX reaction has also been carried out on ^{3}He and ^{4}He [19,20]. However, in these cases there is no longer a bound nuclear state in the exit channel, and the process leads to the nuclear continuum only. Unfortunately, this situation leads to a much less conclusive signature of d' production, in particular, if collision damping of the d'-resonance with the neighboring nucleons is included [19–21].

The search for narrow isoscalar or isovector resonances, which couple to the γd channel has been carried out [22] at MAMI. Deviations $\Delta\sigma$ of the data for the total π^0 production cross-section from a smoothed fit of data is shown in fig. 2. In the range $2020\,\mathrm{MeV}/c^2 < m < 2100\,\mathrm{MeV}/c^2$ no narrow structures have been found on the 3σ level with upper limits in the range of a few microbarn for the production of isoscalar or isovector dibaryons. Yet, this limit is still an order of magnitude above the prediction for d' production [23] and hence not conclusive for this particular dibaryon candidate either.

Therefore, in the search for the d', a hadronic process without medium effects such as the $pp \to pp\pi\pi$ reaction was highly interesting.

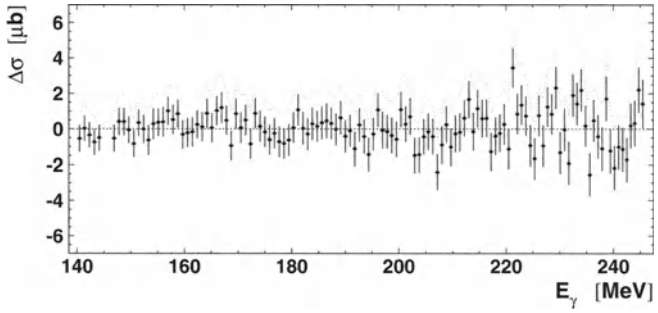

Fig. 2. Deviations $\Delta\sigma$ of the data for the total π^0 photoproduction cross-section on the deuteron. The deviations have been taken relative to a smoothed energy dependence fitted to the data. The dotted curve represents upper limits (90% C.L.) for underlying narrow structures averaged over the experimental energy resolution (from ref. [22]).

2 Experiment

We have carried out exclusive measurements of the $pp \to pp\pi^+\pi^-$ reaction at $T_p = 725, 750$ and 775 MeV using the PROMICE/WASA setup [1] with a hydrogen cluster jet target at the CELSIUS ring. The ejectiles were detected in the angular range $4° \leq \Theta_{\rm lab} \leq 21°$. Protons and pions were identified by the $\Delta E - E$ method, π^+-particles were in addition positively identified by the delayed pulse originating from μ^+ decay following the π^+ decay at rest. This way the two-pion production events could be clearly separated from the huge background of charged $\geq$ 3-prong events due to single-π^0 production with successive Dalitz decay or γ conversion into e^+e^--pairs. As a test of the energy resolution we constructed the missing-mass spectrum from identified $pp\pi^+$ tracks and obtained a clean single peak at the π^- mass with a width of $\Gamma \approx 8$ MeV FWHM (see fig. 1 in ref. [24]). Eventually the four-momenta of the full $pp\pi^+\pi^-$ events were reconstructed by kinematical fits with one over-constraint (1C) which requires that in the 3-particle missing mass $MM_{pp\pi^+}$ is equal to the pion mass m_{π^-}. About one thousand reconstructed events have been obtained at 725 MeV, whereas for 750 and 775 MeV this number was larger by nearly an order of magnitude.

3 Results and discussion

3.1 Decay routes for the Roper resonance

In fig. 3 we present a selection of the 750 and 775 MeV data [2,4]. To see whether the reaction indeed proceeds via N^* excitation, we inspect the measured distribution of the invariant mass $M_{p\pi^+\pi^-}$. At both energies the data are substantially enhanced towards the high-energy end compared to pure phase space (shaded areas in fig. 3) and compatible with the low-energetic tail of the N^* excitation as reproduced by the appropriate MC simulations. In these simulations the amplitude for the N^* decay is written as

$$\mathcal{A} \sim 1 + c\mathbf{k}_1 \cdot \mathbf{k}_2 \left(3D_{\Delta^{++}} + D_{\Delta^0}\right) \qquad (1)$$

which in the full reaction amplitudes complements the propagators for σ exchange and N^* excitation as well as the expression describing the final-state interaction between the outgoing protons in relative s-wave. $D_{\Delta^{++}}$ and D_{Δ^0} are the Δ propagators, the constant 1 stands for the process $N^* \to N\sigma$ and the second term for the decay route $N^* \to \Delta\pi \to N\sigma$, where $\mathbf{k}_1$ and $\mathbf{k}_2$ are the pion momenta. The mixing coefficient c of the two decay routes may be directly read off the data for $M_{\pi^+\pi^-}$ and $\sigma(\delta_{\pi^+\pi^-})$, where $\delta_{\pi^+\pi^-} = \sphericalangle(\mathbf{k}_1, \mathbf{k}_2)$ is the opening angle between the two pions. The latter distribution directly reflects the squared decay amplitude (1) averaged over all possible pion momenta at given $\delta_{\pi^+\pi^-}$, *i.e.*, $\sigma(\delta_{\pi^+\pi^-}) \sim (1 + a\cos\delta_{\pi^+\pi^-})^2$ with $a = c\langle k_1 k_2 (3D_{\Delta^{++}} + D_{\Delta^0})\rangle$, where the brackets denote the average over all possible combinations. For $a \ll 1$ the distribution $\sigma(\delta_{\pi^+\pi^-})$ is essentially linear in a, as exhibited by the data (fig. 3, right column).

In order to illustrate the sensitivity of the data to the mixing of both routes we show calculations for pure phase space, pure transitions $N^* \to N\sigma$ and $N^* \to \Delta\pi \to N\sigma$ as well as mixed scenarios corresponding to $a = -0.20, -0.25$ and -0.33. The negative sign reflects the destructive interference between both routes required by the data.

From a fit to the data the coefficient c can be determined and by this also the ratio $R(M_{N^*})$ of the partial decay widths for the routes $N^* \to \Delta\pi \to N\pi\pi$ and $N^* \to N\sigma$ in dependence of the N^* mass effectively excited in the reaction process. For $T_p = 750$ MeV we have the invariant $N\pi\pi$ mass $\langle M_{N_{\pi\pi}}\rangle = 1264$ MeV and for $T_p = 775$ MeV $\langle M_{N_{\pi\pi}}\rangle = 1272$ MeV with the average taken over the invariant-mass spectra. It is very gratifying for our model that the resulting values of c agree within their statistical errors of about 4%. This leads to branching ratios of $R(1264) = 0.040(4)$ and $R(1272) = 0.060(6)$, respectively. Note the dominance of the $N^* \to N\sigma$ decay route in the low-energy tail of the Roper resonance and the energy dependence of R which is exclusively due to the operators in eq. (1).

Assuming the validity of our model with a fixed value of c we tentatively extrapolate to the nominal Breit-Wigner resonance pole and obtain $R(1440) = 3.9(3)$ which agrees very favorably with the PDG values [5] of 4(2). The model dependence of our result is evident. However, we wanted to demonstrate that the $pp \to pp\pi^+\pi^-$ reaction has the potential to determine experimentally this ratio at the pole with good precision by measurements at appropriate higher energies. This reaction, moreover, provides a tool to map out the energy dependence of the $N^* \to N\pi\pi$ decay by successive increase of the incident proton energy —a program which is currently pursued at CELSIUS/WASA and COSY-TOF.

3.2 Status of the d′ search

The investigation of the $pp \to pp\pi^+\pi^-$ reaction should be a sensitive test of the d' hypothesis, since both invariant-mass spectra $M_{pp\pi^+}$ and $M_{pp\pi^-}$ can be observed simultaneously and the cross-section of the conventional process is small. Since the decay of the hypothetical d'-resonance

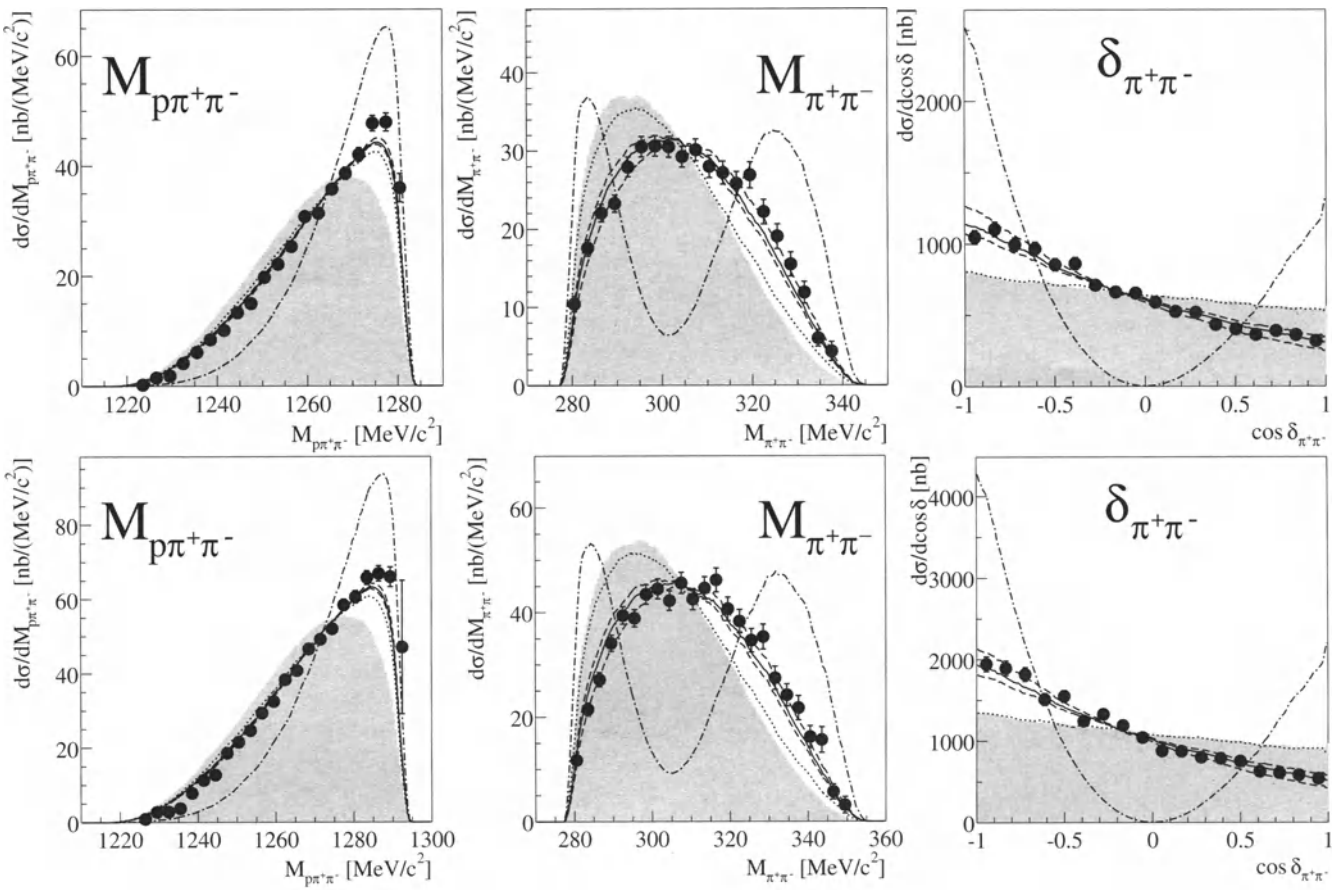

Fig. 3. Influence of the Roper resonance decay onto the differential cross-sections for the invariant masses $M_{p\pi^+\pi^-}$ and $M_{\pi^+\pi^-}$ as well as for the opening angle $\delta_{\pi^+\pi^-}$ between both pions in the reaction $pp \to pp\pi^+\pi^-$ at $T_p = 750\,\mathrm{MeV}$ (top) and $T_p = 775\,\mathrm{MeV}$ (bottom). Pure-phase-space calculations are shown by the shaded area, dotted lines show the case of a pure $N^* \to N\sigma$ decay, whereas the dash-dotted lines exhibit the scenario for a pure $N^* \to \Delta\pi \to N(\pi^+\pi^-)_{I=\ell=0}$ decay. Solid and dashed curves finally show calculations assuming interference from both decay routes with $a = -0.20, -0.25$ and -0.33 [4].

into $pp\pi^-$ is dominated by s-waves between outgoing particles, the two outgoing nucleons (*e.g.* two protons in the decay $d' \to pp\pi^-$) must be in the $^1S_0$-state. In this situation the pp invariant-mass spectrum is strongly affected by the well-known Migdal-Watson–type final-state interaction (FSI) [25,26] leading to a considerable enhancement of the decay rate at small M_{pp}. In order to enhance the sensitivity to d' in $M_{pp\pi^-}$, a cut on small M_{pp} masses, $M_{pp} < 1896\,\mathrm{MeV}/c^2$, has been imposed. In the resulting spectra shown in fig. 4 no narrow structures of statistical significance in $M_{pp\pi^-}$ are observed with the possible exception of an enhancement at $2087\,\mathrm{MeV}/c^2$. Since this data bin is right at the high-energy end of the experimental acceptance range, where instrumental corrections are already substantial and not easily under control, any interpretation of this enhancement would be premature. Its nature can only be solved by measurements at still higher energies. The upper limit (95% C.L.) for the production of narrow dibaryons is of the order $\sigma \lesssim 20\,\mathrm{nb}$ for $m < 2087\,\mathrm{MeV}/c^2$. With respect to d' this upper limit is more than an order of magnitude below the theoretical prediction of $\sigma_{d'} \approx 300$–$1000\,\mathrm{nb}$ [27,28].

We note in passing that in a preceding test run with much lower statistics a structure at $2.063\,\mathrm{GeV}/c^2$ in $M_{pp\pi^-}$ had been observed [24] with a statistical significance of 2 to 3σ depending on the treatment of background. At least part of this bump could meanwhile be associated with a previously unknown detector inefficiency [3,4,29]. We also note that in a measurement [30] of the same reaction at ITEP at $T_p = 920\,\mathrm{MeV}$ a bump has been observed, too, near 2.06 GeV in $M_{pp\pi^-}$, if a cut on small M_{pp} masses was imposed. To our knowledge, no follow-up studies are under way at ITEP to resolve the nature of that bump.

Finally there are the so-called beam gas data from ARGUS at DESY at $E_e = 5\,\mathrm{GeV}$, which contain the electro pion-production on $^{16}\mathrm{O}$ of the form $\gamma^{*16}\mathrm{O} \to pp\pi^\pm X$. From the measured four-momenta of protons and pions $M_{pp\pi^+}$ and $M_{pp\pi^-}$ spectra have been obtained [31] with and without a constraint on low M_{pp} masses. In both cases the $M_{pp\pi^+}$ data are in accordance with phase space, whereas in $M_{pp\pi^-}$ a bump near 2.06 GeV is observed with a significance of about 4σ under both conditions. From the analysis of the $M_{p\pi^-}$ spectrum an admixture of misiden-

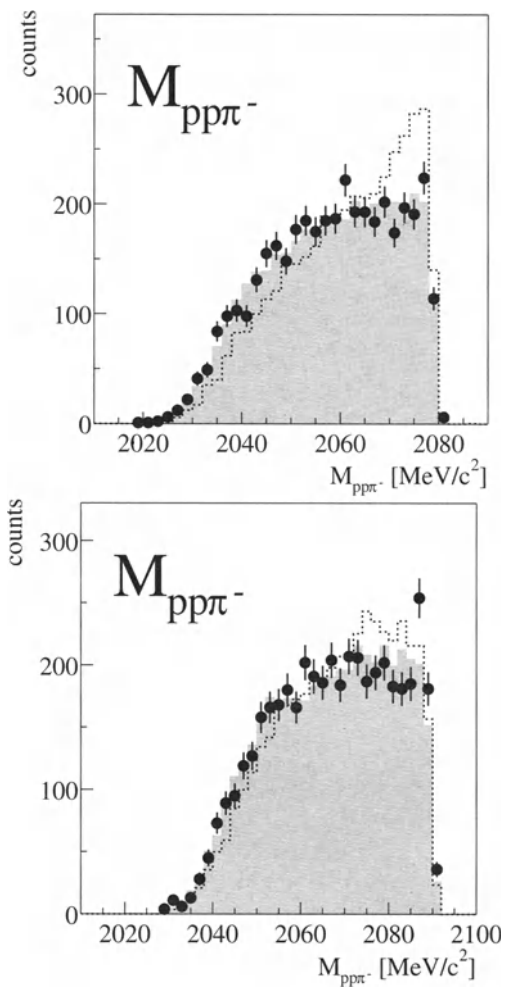

Fig. 4. Invariant-mass spectra $M_{pp\pi^-}$ obtained from the exclusive measurements of the $pp \to pp\pi^+\pi^-$ reaction at $T_p = 750\,\mathrm{MeV}$ (top) and $T_p = 775\,\mathrm{MeV}$ (bottom). The spectra contain only events meeting the condition $M_{pp} < 1896\,\mathrm{MeV}/c^2$ (see text). The dotted lines represent a MC simulation assuming pure phase space for the reaction process, the shaded areas represent a model calculation, which quantitatively describes all differential cross-sections of the reaction (from refs. [3,4, 29]).

tified Λ-particles as a possible reason for this bump can be excluded. For the $M_{pp\pi^-}$ region of the observed bump the corresponding M_{pp} spectrum exhibits an anomalously large pp FSI, in particular in connection with $M_{p\pi^-}$ values around the Λ mass. These findings would be in accordance with what is expected in case of d' production [31]. We note that the $M_{pp\pi^-}$ spectra constructed from $pp\pi^-\pi^\pm$ and $pp\pi^-\pi^+\pi^+$ event samples do not show any enhancements near 2.06 GeV —again as expected in case of d' electroproduction on a np-pair, since in this case there is only single-pion production. π^0-particles were not identified, hence their possible accompanying production cannot be excluded.

4 Conclusions

The kinematically complete, even overdetermined $pp \to pp\pi^+\pi^-$ data have enabled us to analyze several observables in great detail. This way we were able to demonstrate that the Roper resonance is excited by σ exchange in pp collisions. Furthermore we studied two interfering decay routes into the $N\pi\pi$ final channel. The ratio of the partial widths for decay via $\Delta\pi$ and $N\sigma$ was shown to be $R = 0.04$ and $R = 0.06$ at invariant masses of 1264 and 1272 MeV, respectively, within our model ansatz. Ongoing experiments at COSY-TOF and CELSIUS/WASA will test this ansatz at higher energies and see if our extrapolation to the Roper pole is justified.

In recent years high-statistics and high-resolution experiments have been carried out in search for a possible signature of d' in basic systems. In $\gamma d \to \pi^0 X$ and in $pp \to pp\pi^+\pi^-$ no narrow structures of statistical significance have been found. In the former reaction the deduced upper limits are still above the predicted d' production cross-sections; however, for the latter reaction they are below the predicted values by already one to two orders of magnitude. Together with the findings on nuclei (DCX, $\gamma^{*16}\mathrm{O} \to pp\pi^\pm X$) our results on the basic systems imply a number of consequences. Either d' does not exist at all, or its production cross-section in $pp \to pp\pi^+\pi^-$ is for some unknown reason much smaller than expected, or its mass outside the nuclear medium is above the mass range investigated so far, or it possibly exists only in the presence of the nuclear medium.

We acknowledge the support by BMBF (06 TU 987) and DFG (Europäisches Graduiertenkolleg 683).

References

1. H. Calen *et al.*, Nucl. Instrum. Methods A **379**, 57 (1996).
2. W. Brodowski *et al.*, Phys. Rev. Lett. **88**, 192301 (2002).
3. W. Brodowski, doctoral thesis, Universität Tübingen, 2001.
4. J. Pätzold, doctoral thesis, Universität Tübingen, 2002, `http://w210.ub.uni-tuebingen.de/dbt/volltexte/2002/550/` and submitted for publication.
5. Particle Data Group, Phys. Rev. D **66**, 1 (2002).
6. O. Krehl *et al.*, Phys. Rev. C **62**, 025207 (2000).
7. E. Hernández, E. Oset, M.J. Vicente Vacas, Phys. Rev. C **66**, 065201 (2002), nucl-th/0209009.
8. H.P. Morsch, P. Zupranski, Phys. Rev. C **61**, 024002 (1999).
9. L. Alvarez-Ruso, E. Oset, E. Hernández, Nucl. Phys. A **633**, 519 (1998) and private communication.
10. See, *e.g.*, P.J. Mulders, A.T. Aerts, J.J. de Swart, Phys. Rev. Lett. **40**, 1543 (1978); Phys. Rev. D **21**, 2653 (1980).
11. K.K. Seth, in *Proceedings of the International Workshop on Pions in Nuclei, Peniscola, Spain*, edited by E. Oset (World Scientific, Singapore, 1992) p. 205 and references therein.
12. A.J. Buchmann, G. Wagner, A. Faessler, Phys. Rev. C **57**, 3340 (1998).

13. J. Draeger *et al.*, Phys. Rev. C **62**, 064615 (2000).
14. J. Pätzold *et al.*, Phys. Lett. B **428**, 18 (1998); **443**, 77 (1998).
15. R. Bilger *et al.*, Phys. Rev. Lett. **71**, 42 (1993); **72**, 2972 (1994); **79**, 3849 (1997).
16. M. Nuseirat *et al.*, Phys. Rev. C **58**, 2292 (1998).
17. H.C. Wu, W.R. Gibbs, Phys. Rev. C **62**, 044614 (2000).
18. Y. Liu, A. Faessler, J. Schwieger, A. Bobyk, J. Phys. G **24**, 1135 (1998).
19. J. Gräter *et al.*, Phys. Lett. B **471**, 113 (1999); **420**, 37 (1998).
20. J.L. Clark *et al.*, Phys. Rev. C **66**, 054606 (2002).
21. A.V. Nefediev, M.G. Schepkin, H.A. Clement, Phys. Rev. C **67**, 015201 (2003).
22. U. Siodlaczek *et al.*, Eur. Phys. J. A **9**, 309 (2000).
23. R. Bilger *et al.*, Nucl. Phys. A **596**, 586 (1996).
24. W. Brodowski *et al.*, Z. Phys. A **355**, 5 (1996).
25. A.B. Migdal, JETP **28**, 3 (1955).
26. K.M. Watson, Phys. Rev. **88**, 1163 (1952).
27. M. Schepkin, O. Zaboronsky, H. Clement, Z. Phys. A **345**, 407 (1993).
28. H. Clement *et al.*, Prog. Part. Nucl. Phys. **36**, 369 (1996).
29. W. Brodowski *et al.*, Phys. Lett. B **550**, 147 (2002).
30. L. Vorobyev *et al.*, JETP Lett. **52**, 77 (1994).
31. E. Doroshkevich, status report, `www.pit.physik.uni-tuebingen.de/report.html`.

Eur. Phys. J. A **18**, 177–180 (2003)
DOI 10.1140/epja/i2002-10295-1

THE EUROPEAN PHYSICAL JOURNAL A

Antiproton physics at GSI: Studying the physics of hadronic matter

J. Ritman[a]

For the Antiproton Research Study Group[b]
II. Physikalisches Institut, Universität Gießen, Gießen, Germany

Received: 30 September 2002 /
Published online: 22 October 2003 – © Società Italiana di Fisica / Springer-Verlag 2003

Abstract. GSI/Darmstadt is planning a major upgrade of its accelerator and experimental facilities. One of the main components of the proposed GSI-upgrade is a storage ring, in which beams of antiprotons with unprecedented quality and intensity will be available with beam momenta up to 15 GeV/c. At this facility a wide physics program is planned to investigate the structure of hadrons in the charmonium mass range, with the goal to develop a better understanding of the transition from quarks and gluons to hadrons as effective degrees of freedom. An overview of the physics program and the detector system envisioned for this project are presented.

PACS. 13.75.-n Hadron-induced low- and intermediate-energy reactions and scattering (energy $\leq$ 10 GeV) – 25.43.+t Antiproton-induced reactions

1 Introduction

Quantum Chromodynamics (QCD) is generally accepted to be the correct theory to describe the interaction of particles via the strong force. In systems involving large momentum transfers, corresponding to small-distance scales, perturbative methods can be applied, thereby allowing high-precision tests of the theory. However, with decreasing momentum transfers, corresponding to increasing length scales, the magnitude of the strong-coupling constant increases to the point that the perturbative treatment is no longer valid. In this low-energy regime the structure of the hadrons is characterized by new unsettled phenomena:

- As a result of the rapid rise of the coupling constant, free quarks are not observed at length scales larger than the size of the nucleon, instead, quarks are bound to color neutral objects, called hadrons.
- The mass of hadrons is much larger than the sum of their valence quark masses. This is related to the interaction of the hadron with the complex structure of the QCD vacuum.
- The self-interaction of gluons should permit hadrons with valence quarks and gluons (so-called hybrids) and states of nearly pure glue (*i.e.* glueballs) to exist.

These properties are inherent in the specific nature of the strong force and are the objects of our attempts to understand the nature of multi-particle states bound by the strong force.

[a] e-mail: `james.ritman@exp2.physik.uni-giessen.de`

[b] *Antiproton Research Study Group*: J. Bacelar, KVI Groningen; R. Bertini, Torino University "A. Avogadro"; D. Bettoni, Ferrara, INFN; T. Bressani, Torino University I; K.-T. Brinkmann, Dresden University; R. Calabrese, Ferrara, INFN; M. Düren, Giessen University; C. Ekstrom, TSL Uppsala; W. Eyrich, Erlangen University; D. Frekers, Münster University; S. Ganzhur, Bochum University; P. Gianotti, Frascati; A. Gillitzer, FZ-Jülich IKP; O. Hartmann, GSI Darmstadt; V. Hejny, FZ-Jülich IKP; M. Holzscheiter, Los Alamos; B. Kamys, Kraków University; P. Kienle, Technical University Munich; J. Kisiel, University of Silesia; H. Koch, Bochum University; W. Kühn, Giessen University; U. Lynen, GSI Darmstadt; M. Macri, Genova University; A. Martin, Trieste University and INFN; J. Marton, Austrian Academy of Science (IMEP); R. Meier, Tuebingen University; V. Metag, Giessen University; P. Moskal, FZ-Jülich IKP; H. Orth, GSI Darmstadt; M. Pallavicini, Genova, INFN; S. Paul, Technical University Munich; K. Peters, Bochum University; J. Pochodzalla, Mainz University; G. Raciti, Catania University; J. Ritman, Giessen University; G. Rosner, Glasgow University; E.L. Rizzini, Brescia University and INFN II; A. Rotondi, Pavia University; M. Sapojnikov, JINR Dubna; L. Schmitt, Technical University Munich; C. Schwarz, GSI Darmstadt; K. Seth, Northwestern University; J. Smyrski, Kraków University; I. Tikhonov, BINP Novosibirsk; N. Vlassov, JINR Dubna; A. Vodopianov, JINR Dubna; U. Wiedner, Uppsala University; A. Zenoni, Brescia University and INFN I; B. Zwieglinski, SINS Warsaw.

2 Hadron physics with antiproton beams

Experimental studies of hadronic structure can be performed with various probes such as electrons or antiprotons. The interaction of electrons with hadrons provides the advantages of using a point-like probe that interacts via the well-known —but relatively weak— electromagnetic force. On the other hand, antiproton annihilation produces copious numbers of particle-antiparticle pairs in a gluon-rich environment, allowing spectroscopic studies with unprecedented statistics and precision. Antiprotons in the 1–15 GeV/c range are thus an ideal tool to study the questions mentioned above. Intense discussions within the international hadron physics community have been distilled into a physics program. This physics program, together with a facility to produce high-luminosity, cooled antiproton beams up to 15 GeV/c, has been included in the conceptual design report for the planned upgrade of the GSI-Darmstadt facility [1,2].

The physics program at the planned GSI facility includes the following main aspects:

- Charmonium spectroscopy: precision measurements of mass, width, decay branches of all charmonium states, especially to extract information on quark confinement.
- Firm establishment of the QCD-predicted gluonic excitations (charmed hybrids, glueballs) in the charmonium mass range (3–5 GeV/c^2).
- Search for modifications of meson properties in the nuclear medium, and their possible relationship to the partial restoration of chiral symmetry for light quarks. Particular emphasis is placed on mesons with open and hidden charm in order to learn more about the origin of hadron masses.
- Precision γ-ray spectroscopy of single and double hypernuclei for information on their structure and on the hyperon-nucleon and hyperon-hyperon interaction.

With increasing luminosity of the antiproton facility further possibilities will emerge. These include D-meson decay spectroscopy (rare leptonic and hadronic decays), the search for CP violation in the charm and strangeness sector (D-meson decays, Λ-$\bar{\Lambda}$ system), the extraction of generalized parton distributions from $\bar{p}$-p annihilation, and fundamental physics with stopped antiprotons.

The use of an antiproton beam allows several major advantages to study the physics program outlined above. For instance, antiproton beams can be cooled (stochastically and/or with electron cooling) to obtain momentum resolutions of the order of 10^{-5}. Furthermore, charmonium states of all quantum numbers can be directly formed, in contrast to e^+e^- reactions where only the vector states (*i.e.* $J^{PC} = 1^{--}$) could be directly formed. The possibility to measure charmonium states in formation reactions[1] allows the resolution of the mass and width to be limited only by the beam momentum (because of 4-momentum conservation). In contrast, the resolution of the mass and width in production reactions[2] is limited by the detector resolution which is on the order of 10^{-2}. Moreover, the possibility to measure both production and formation reactions is also a very important tool for the spin-exotic search, *i.e.* a particle that appears in production reactions but not in formation reactions is an interesting candidate. The large branching ratio to baryon-antibaryon pairs also is a useful tool, *e.g.* using the $\bar{\Xi}$ to tag a Ξ beam which is incident on a secondary target, as forseen in the double-hypernuclei program.

3 Proposed experimental facility

The antiproton beams needed to pursue the physics program outlined above will be produced by a primary proton beam from the planned fast-cycling, superconducting 100 Tm ring. The antiprotons will be collected with a rate of about 2×10^7/s and then stochastically cooled and stored. After 5×10^{10} antiprotons have been produced, they will be transferred to the High-Energy Storage Ring (HESR) where internal experiments in the momentum range 1.5–15 GeV/c can be performed.. Stochastic cooling in the HESR ring will allow a beam momentum resolution of $\delta p/p \sim 10^{-4}$ at luminosities up to $2 \times 10^{32}/\mathrm{cm}^2/\mathrm{s}$. For antiproton momenta below 8 GeV/c electron cooling will enable a higher momentum resolution ($\delta p/p \sim 10^{-5}$) at a reduced luminosity $10^{31}/\mathrm{cm}^2/\mathrm{s}$.

To serve the many experiments planned at this new facility, a general purpose detector is planned. This detector facility must be able to handle high rates (10^7 annihilations/s), with good particle identification and momentum resolution for γ, e, μ, π, K, and p. The experiments will use internal targets, *i.e.* either pellets of frozen H_2 or cluster jet targets for the reactions on proton targets, and wires for reactions on nuclear targets.

The proposed detector is comprised of a target spectrometer which has a 2 T solenoidal magnetic field, and a forward spectrometer that uses a 1 m gap dipole magnet with 2 Tm bending power. A schematic overview of the target spectrometer is given in fig. 1. The innermost detector is a microvertex detector (MVD) for precise measurements of particles produced at secondary vertices. The MVD will be a radiation hard silicon pixel detector, based on the design for LHC experiments [3,4]. A cylindrical array of straw tubes for tracking (STT) will surround the MVD. Particles at small polar angles will also be measured by a sequence of mini drift chambers (MDC) of the HADES type [5,6] located downstream of the target.

Kaon-pion discrimination will be performed with two types of ring imaging Čerenkov counters. For polar angles above 22°, the detection of internally reflected Čerenkov (DIRC) light [7] is used. The radiator will be constructed out of 1.7 cm thick quartz slabs. At smaller polar angles we plan to use proximity focusing Čerenkov counters similar to those in STAR/ALICE [8]. An important part of the detector is the electromagnetic calorimeter. In order to realize the desired compact structure and high-rate capability,

[1] Single-particle intermediate state, *e.g.* $\bar{p} + p \to \chi_{c1}$.

[2] Multi-particle intermediate state, *e.g.* $e^+ + e^- \to \gamma + \chi_{c1}$.

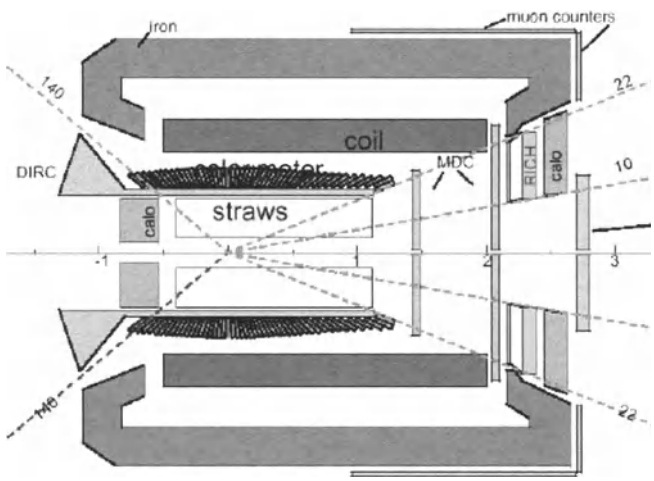

Fig. 1. Schematic overview of the detector concept for the planned HESR antiproton facility at GSI.

scintillators of the $PbWO_4$ type are very advantageous. Experiments using phototubes for readout show that they have good energy resolution for γ/e-detection [9]. Outside the iron yoke of the solenoid magnet the target spectrometer has two arrays of 72 scintillator strips for muon detection.

4 Simulations of the detector performance

The properties of the proposed detector system have been investigated extensively during the past year. All the main components of the target spectrometer are implemented in a simulation package based on the GEANT4 software [10]. The results of this simulation were analyzed with a software package based on ROOT [11], and the event generator is based on the package PLUTO++ [12].

To be able to examine reactions involving D-mesons a vertex resolution on the order of 100 μm is required. The simulations indicate a vertex resolution of about 50 μm in the transverse and 80 μm in the longitudinal direction.

The momentum resolution has been investigated at several polar angles as a function of transverse momentum. Typical transverse-momentum resolutions are 1-2%. Furthermore, the momentum resolution has been investigated by reconstructing events from the reaction $\overline{p}p \rightarrow J/\Psi + \phi$ at $\sqrt{s} = 4.4$ GeV/c^2. Gaussian fits to the $\mu^{\pm}$ and $K^{\pm}$ invariant-mass distributions, have widths of 36 and 3.6 MeV/c^2 for the J/Ψ and ϕ, respectively.

The DIRC provides information on the velocity of particles, thus by combining this with the momentum measurement from the tracking, the mass of the particle can be determined. Above about 0.6 GeV/c the efficiency to identify a kaon is over 95% and the probability to misidentify a pion as a kaon is about 1%.

The electromagnetic calorimeter is used to measure photon energies and to provide electron-hadron separation. The simulations indicate that the calorimeter has sufficient resolution to reconstruct the η-meson with about 20 MeV/c^2 resolution. Furthermore, the probability to misidentify a pion as an electron is on the order of 10^{-3}.

The muon counters are located outside of the solenoid magnet. The integrated efficiency of the muon counters is about 90% for muons above 1.3 GeV/c. In the most relevant momentum range the misidentification probability for pions to be registered as muons is between 1% and 2%.

The geometrical acceptance times the efficiency for detection and reconstruction of the target spectrometer has been investigated by simulating the reaction $\overline{p}p \rightarrow J/\Psi + \phi$ at $\sqrt{s} = 4.4$ GeV/c^2. The total acceptance times efficiency was determined for both dilepton decay branches of the J/Ψ as a function of the cosine of the J/Ψ center-of-mass polar angle. The acceptance is large ($\approx$ 50%) and quite uniform over the full allowed region, which is very important in order to perform accurate partial-wave analyses.

5 Summary

The annihilation of antiprotons on protons and nuclear target provides experimental access to a wide range of important questions in the non-perturbative range of QCD. The collisions of antiprotons with nuclei allow charm-nucleus interactions to be studied, which extend naturally the present program of GSI on the properties of hadrons in nuclear matter.

The simulations of the detector concept show its ability to measure electrons, muons, pions and kaons over a large phase space region. A momentum resolution of 1-2% is obtained and we have a high discriminating power for particle identification. Combining these features with the large solid-angle coverage (which is close to 4π) allows the application of strong kinematical constraints to the data which will serve for a high level of background suppression. One of the open question concerns the feasibility of a pellet target system. The forward spectrometer and the Ge array for the hypernuclei experiments still need to be included into the simulations.

The project described here has recently taken a big step forward in the approval process: The German Scientific Council has evaluated the proposals for a number of planned large research facilities in Germany and has recommended that the planned GSI upgrade should be funded when certain conditions are fulfilled [13]. Currently a collaboration is forming in order to develop a detailed technical proposal for the design and construction of the detector system presented here.

References

1. *Conceptual Design Report: An International Accelerator Facility for Beams of Ions and Antiprotons*, `http://www.gsi.de/GSI-Future/cdr`
2. P. Kienle, Nucl. Phys. A **655**, 381c (1999).
3. ATLAS TDR 11, CERN/LHCC 98-13.
4. CMS TDR 5, CERN/LHCC 98-6.
5. C. Müntz, Nucl. Phys. B **78**, 139 (1999).

6. C. Garabatos, Nucl. Instrum. Methods A **412**, 38 (1998).
7. R. Aleksan *et al.*, Nucl. Instrum. Methods A **397**, 261 (1997).
8. ALICE TDR 1, CERN/LHCC 98-19.
9. R. Novotny *et al.*, IEEE Trans. Nucl. Sci. **47**, 1499 (2000).
10. CERN `http://wwwinfo.cern.ch/asd/geant4`
11. CERN `http://root.cern.ch`
12. `http://www-hades.gsi.de/computing/pluto/html/PlutoIndex.html`
13. `http://www.wissenschaftsrat.de/liste_wr.htm#2002`

Eur. Phys. J. A **18**, 181–183 (2003)
DOI 10.1140/epja/i2002-10296-0

THE EUROPEAN PHYSICAL JOURNAL A

Measurement of the neutron electric form factor via recoil polarimetry

The Jefferson Laboratory E93-038 Collaboration

T. Reichelt[16,a], R. Madey[1,2], A.Yu. Semenov[1], S. Taylor[2], A. Aghalaryan[4], E. Crouse[5], G. MacLachlan[6], B. Plaster[3], S. Tajima[7], W. Tireman[1], Chenyu Yan[1], A. Ahmidouch[8], B.D. Anderson[1], R. Asaturyan[4], O. Baker[9], A.R. Baldwin[1], H. Breuer[10], R. Carlini[2], E. Christy[9], S. Churchwell[7], L. Cole[9], S. Danagoulian[2,8], D. Day[11], M. Elaasar[12], R. Ent[2], M. Farkondeh[3], H. Fenker[3], F.M. Finn[5], L. Gan[9], K. Garrow[2], P. Gueye[9], C. Howell[7], B. Hu[9], M.K. Jones[2], J.J. Kelly[10], C. Keppel[9], M. Khandaker[13], W.Y. Kim[14], S. Kowalski[3], A. Lung[3], D. Mack[2], D.M. Manley[1], P. Markowitz[15], J. Mitchell[2], H. Mkrtchyan[4], A.K. Opper[6], C. Perdrisat[5], V. Punjabi[13], B. Raue[15], J. Reinhold[15], J. Roche[5], Y. Sato[9], W. Seo[14], N. Simicevic[17], G. Smith[2], S. Stepanyan[4], V. Tadevosyan[4], L. Tang[9], P. Ulmer[18], W. Vulcan[2], J.W. Watson[1], S. Wells[17], F. Wesselmann[11], S. Wood[2], Chen Yan[2], L. Yuan[9], S. Yang[14], W.M. Zhang[1], H. Zhu[11], X. Zhu[9], and H. Arenhövel[19]

[1] Kent State University, Kent, OH 44242, USA
[2] Thomas Jefferson National Accelerator Facility, Newport News, VA 23606, USA
[3] Massachusetts Institute of Technology, Cambridge, MA 02139, USA
[4] Yerevan Physics Institute,Yerevan 375036, Armenia
[5] The College of William and Mary, Williamsburg, VA 23187, USA
[6] Ohio University Athens, OH 45701, USA
[7] Duke University, Durham, NC 27708, USA
[8] North Carolina A & T State University, Greensboro, NC 27411, USA
[9] Hampton University, Hampton, VA 23668, USA
[10] University of Maryland, College Park, MD 20742, USA
[11] University of Virginia, Charlottesville, VA 22904, USA
[12] Southern University of New Orleans, New Orleans, LA 70126, USA
[13] Norfolk State University, Norfolk, VA 23504, USA
[14] Kyungpook National University, Korea
[15] Florida International University, Miami, FL 33199, USA
[16] Rheinische Friedrich-Wilhelms-Universität Bonn, Germany
[17] Louisiana Tech University, Ruston, LA 71272, USA
[18] Old Dominion University, Norfolk, VA 23508, USA
[19] Johannes Guthenberg-Universität Mainz, Germany

Received: 30 September 2002 /
Published online: 22 October 2003 – © Società Italiana di Fisica / Springer-Verlag 2003

Abstract. The ratio G_e^n/G_m^n of the electric to the magnetic form factor of the neutron has been measured by analyzing the polarization of the recoiling neutron in quasi-elastic scattering of longitudinally polarized electrons from deuterium at the Q^2 values of 0.45, 1.15, and 1.47 $(\mathrm{GeV}/c)^2$. The experiment has been performed in Hall C of the Thomas Jefferson National Accelerator Facility. With G_m^n being known G_e^n can be deduced. The preliminary results show that the lowest Q^2 points follow the Galster parametrization and that the 1.47 $(\mathrm{GeV}/c)^2$ point rises above this parametrization.

PACS. 13.40.Gp Electromagnetic form factors – 14.20.Dh Protons and neutrons – 24.70.+s Polarization phenomena in reactions

1 Introduction

The electromagnetic form factors of the nucleon are fundamental quantities in hadron pysics. In the past the lack of data was unsatisfactorily severe for G_e^n, the electric form factor of the neutron. In the last years, however, substantial progress has been made by developing high-quality polarized electron beams and efficient neutron polarimeters allowing the measurement of the interference term in

[a] e-mail: reichelt@physik.uni-bonn.de

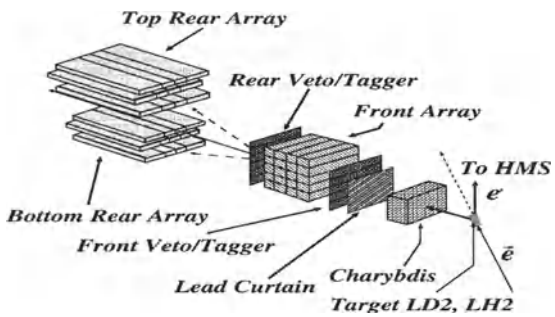

Fig. 1. Experimental set-up.

polarization experiments and extracting the electric form factor with small systematic and statistical errors.

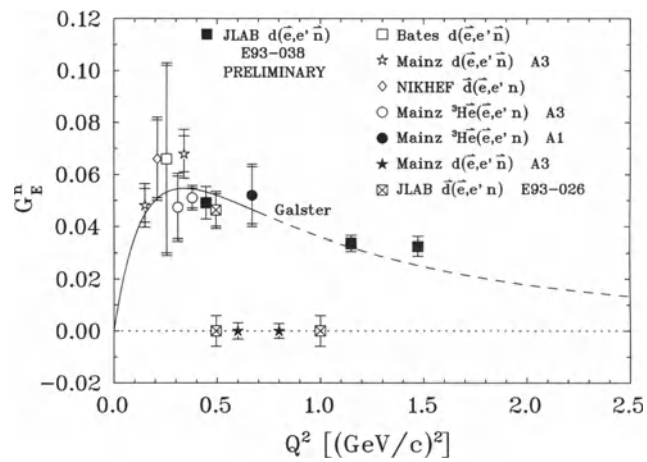

Fig. 2. World data on G_e^n *vs.* Q^2 as obtained from polarization experiments. The points on the abscissa are projections.

2 Experimental method

A sketch of the experimental set-up is shown in fig. 1. A beam of longitudinally polarized electrons scattered from a 15 cm liquid deuterium target. The scattered electrons were detected and momentum analyzed in the High-Momentum Spectrometer (HMS) of Hall C in coincidence with the recoiling neutrons, the polarization of which was measured in the polarimeter NPOL. NPOL consisted of an array of front detectors (20) and two arrays of rear detectors (12 each). It made use of the spin-dependent scattering of the neutrons in the front detectors resulting in an up/down asymmetry which is proportional to the transverse component of the polarization vector.

The 100 cm × 10 cm × 10 cm dimensions of each front detector were small enough to permit high luminosity. A double layer of thin tagging detectors directly ahead of and behind the front array identified charged particles. Each layer of the rear array consisted of two central scintillators, each 25.4 cm × 10.16 cm × 101.6 cm, with a 50.8 cm × 10.16 cm × 101.6 cm scintillator on each side. A 10 cm Pb curtain attenuated the flux of electromagnetic background from the target. The two sides of NPOL were shielded by ∼ 1.2 m concrete, the rear and front shielding consisted of steel blocks of ∼ 1.3 m thickness. A collimator in the front shielding prevented the rear detectors from direct sight to the target. The mean flight path for the neutrons was 7 m. Rejection of inelastic events was accomplished with two cuts: a missing-momentum cut of less than 100 MeV/c, and a relative momentum bite dP/P of −3% to +5%. The resulting solid angle for NPOL was 10 msr. Throughout the experiment NPOL remained positioned at 46 degrees relative to the beam. For the different Q^2 values the beam energy and the HMS angle and momentum were adjusted accordingly.

The polarization vector of the neutrons leaving the target lies in the scattering plane. The longitudinal component is given by kinematics when G_e^n is negligible. The transverse component is proportional to the ratio G_e^n/G_m^n. The dipole magnet Charybdis was positioned between the target and NPOL and the field was vertical. The interaction of the neutron's magnetic moment with the field resulted in a precession of the polarization vector by an angle χ.

When a pair of asymmetry measurements with two different precession angles is taken, the ratio $g = G_e^n/G_m^n$ can directly be expressed as a function of the precession angles χ and the ratio η of the corresponding asymmetries ξ. We chose the precession angles

$$\chi = 0°/90°, \qquad \eta = \xi_0/\xi_{90}, \qquad g = -K \cdot \eta \qquad \text{and}$$
$$\chi = -40°/+40°, \qquad \eta = \xi_-/\xi_+, \qquad g = -K \cdot \tan\chi \cdot \tfrac{\eta+1}{\eta-1},$$

where K is a known kinematical factor. A remarkable advantage of the ratio technique lies in the fact that in the ratio of the asymmetries the analyzing power and also the beam polarization cancel, provided the latter is stable.This has been verified by repeated measurements with the C beam-line Møller polarimeter.

3 Scattering asymmetries

An event is generated by a triple coincidence between an electron in the HMS, a neutral particle in the front array and either a neutral or charged particle in one of the rear arrays. TOF spectra were recorded for the time of flight between the HMS and a front detector (ctof) and between the front detector and a rear detector (dtof). These spectra allowed the subtraction of accidentals. The four dtof spectra (up, down, + helicity, − helicity) contain the information from which the asymmetry is extracted. From the yields in the dtof peaks, the ratio r is calculated, which is the ratio of the two geometric means $(N_U^+ N_D^-)^{1/2}$ and $(N_U^- N_D^+)^{1/2}$, where $N_U^\pm, N_D^\pm$ are the number of events for nucleons scattered up (down) when the beam helicity was positive (negative). The physical asymmetry is then given by $(r-1)/(r+1)$. By this method inherent asymmetries like different solid angles for the rear arrays or a beam charge asymmetry for the two helicity states cancel.

4 Preliminary results

In fig. 2 our preliminary results are plotted *vs.* Q^2 together with the current world data for G_e^n from polarization experiments [1–9]. The data from E 93-038 follow the Galster parametrization [10] up to 1.15 $(\mathrm{GeV}/c)^2$ and rises above at 1.47 $(\mathrm{GeV}/c)^2$. Schiavilla and Sick [11] extracted values for G_e^n from the nuclear physics data on the quadrupole form factor of the deuteron and obtained results up to $Q^2 \sim 1.65$ $(\mathrm{GeV}/c)^2$ consistent with the Galster parametrization. Our data together with those to be expected in the near future (Mainz, JLab) constitute a challenge for theoretical nucleon models [12–19], which must be able to reproduce all four electromagnetic form factors of the nucleon. They also allow a better determination of the interior charge distribution of the neutron [20].

The support of the Jefferson Lab scientific and engineering staff in Hall C and the accelerator staff is gratefully acknowleged. This work was supported in part by the National Science Foundation, the Department of Energy, and the Deutsche Forschungsgemeinschaft. The Southeastern Universities Research Association (SURA) operates the Thomas Jefferson National Accelerator Facility under the U.S. Department of Energy contract DE-AC05-84ER40150.

References

1. T. Eden *et al.*, Phys. Rev. C **50**, R 1749 (1994).
2. M. Meyerhoff *et al.*, Phys. Lett. B **327**, (1994), 201
3. J. Becker *et al.*, Eur. Phys. J A **6**, 329 (1999).
4. J. Golak *et al.*, Phys. Rev. C **63**, 034006-1 (2001).
5. M. Ostrick *et al.*, Phys. Rev. Lett. **83**, 276 (1999).
6. C. Herberg *et al.*, Eur. Phys. J. A **5**, 131 (1999).
7. I. Passchier *et al.*, Phys. Rev. Lett. **82**, 4988 (1999).
8. D. Rohe *et al.*, Phys. Rev. Lett. **83**, 4257 (1999).
9. H. Zhu *et al.*, Phys. Rev. Lett. **87**, 081801-1 (2001).
10. S. Galster *et al.*, Nucl. Phys. B **32**, 221 (1971).
11. R. Schiavilla, I. Sick, Phys. Rev. C **64**, 041002-1(R) (2001).
12. F. Cardarelli, A. Simula, Phys. Rev. C **62**, 065201-1 (2000).
13. M.F. Gari, W. Krümpelmann, Z. Phys. A **322**, 689 (1985).
14. M.F. Gari, W. Krümpelmann, Phys. Lett. B **274**, 159 (1992).
15. G. Holzwarth, Z. Phys. A **356**, 339 (1996).
16. S. Boffi *et al.*, Nucl. Phys. A **699**, 312c (2002).
17. R.F. Wagenbrunn, Phys. Lett. B **511**, 33 (2001).
18. P. Mergell *et al.*, Nucl. Phys. A **596**, 367 (1996).
19. D. Merten *et al.*, Eur. Phys. J. A **14**, 477 (2002), hep-ph/0204024.
20. J.J. Kelly, Phys. Rev. C **66**, 065203 (2002), hep-ph/0204239.

Eur. Phys. J. A **18**, 185–187 (2003)
DOI 10.1140/epja/i2002-10297-y

THE EUROPEAN PHYSICAL JOURNAL A

S = −1 meson-baryon scattering in coupled-channel unitarized Chiral Perturbation Theory*

C. García-Recio[1], J. Nieves[1], E. Ruiz Arriola[1,a], and M. Vicente Vacas[2]

[1] Departamento de Física Moderna, Universidad de Granada, E-18071 Granada, Spain
[2] Departamento de Física Teórica and IFIC, Centro Mixto Universidad de Valencia-CSIC, Ap. Correos 22085, E-46071 Valencia, Spain

Received: 30 September 2002 /
Published online: 22 October 2003 – © Società Italiana di Fisica / Springer-Verlag 2003

Abstract. The s-wave meson-baryon scattering amplitude is analyzed for the strangeness $S = -1$ and isospin $I = 0$ sector in a Bethe-Salpeter coupled-channel formalism incorporating Chiral Symmetry. Four two-body channels have been considered: $\bar{K}N$, $\pi\Sigma$, $\eta\Lambda$, $K\Xi$. The needed two-particle irreducible matrix amplitude is taken from lowest-order Chiral Perturbation Theory in a relativistic formalism. Off-shell behaviour is parameterized in terms of low-energy constants, which outnumber those assumed in previous works and provide a better fit to the data. The position of the complex poles in the second Riemann sheet of the scattering amplitude determines masses and widths of the $\Lambda(1405)$ and $\Lambda(1670)$ resonances which compare well with accepted numbers.

PACS. 11.10.St Bound and unstable states; Bethe-Salpeter equations – 11.30.Rd Chiral symmetries – 11.80.Et Partial-wave analysis – 13.75.Lb Meson-meson interactions

1 Introduction

The existence of baryon resonances is a non-perturbative feature of intermediate energy QCD. In addition to the standard relativistic invariance, Chiral Symmetry (CS) and unitarity prove extremely convenient tools to deal with this problem. In this energy range, hadronic degrees of freedom seem to be the relevant ones in terms of which the symmetries may be easily incorporated [1]. Heavy Baryon Chiral Perturbation Theory (HBChPT) [2, 3] incorporates CS at low energies in a systematic way, and has provided a satisfactory description of πN scattering in the region around threshold [4–6] but fails to reproduce the resonance region. The s-wave meson-baryon scattering for the strangeness $S = -1$ and isospin $I = 0$ sector incorporating CS and unitarization has been studied in previous works [7–13]. The need for unitarization in this reaction becomes obvious after the work of ref. [14], where it is shown that HBChPT to one loop fails completely in the $\bar{K}N$ channel already at threshold due to nearby subthreshold $\Lambda(1405)$-resonance.

We report here on results obtained for the s-wave $S = -1$, $I = 0$ meson-baryon reaction in a Bethe-Salpeter Equation (BSE) coupled-channel approach, extending the works of refs. [15–17]. We also improve on a previous approach [8] by reparameterizing off-shell effects as low-energy constants, in the spirit of an Effective Field Theory. We consider four coupled channels: $\pi\Sigma$, $\bar{K}N$, $\eta\Lambda$ and $K\Xi$ and take into account $SU(3)$-breaking symmetry effects but assume isospin symmetry. More details can be found in ref. [18].

2 Theoretical framework

The coupled-channel scattering amplitude for the baryon-meson process in the isospin channel $I = 0$ is given by

$$T_P = \bar{u}_B(P-k', s_B)t_P(k,k')u_A(P-k, s_A) \qquad (1)$$

Here, $u_A(P-k, s_A)$ and $u_B(P-k', s_B)$ are baryon Dirac spinors normalized as $\bar{u}u = 2M$, P is the conserved total CM four-momentum, $P^2 = s$, and $t_P(k,k')$ is a matrix in the Dirac and coupled-channel spaces. Further details on normalizations and definitions of the amplitudes can be seen in ref. [17]. To evaluate the amplitude t_P we solve the BSE

$$t_P(k,k') = v_P(k,k') + i\int \frac{\mathrm{d}^4 q}{(2\pi)^4} t_P(q,k')\Delta(q)S(P-q)v_P(k,q)\,, \qquad (2)$$

where $t_P(k,k')$ is the scattering amplitude defined in eq. (1), $v_P(k,k')$ the two-particle irreducible Green's function (or *potential*), and $S(P-q)$ and $\Delta(q)$ the baryon and

* Spokesperson: E. Ruiz Arriola.
[a] e-mail: earriola@ugr.es

meson exact propagators, respectively. The above equation turns out to be a matrix one, both in the coupled-channel and Dirac spaces. For any choice of the *potential* $v_P(k,k')$, the resulting scattering amplitude $t_P(k,k')$ fulfills the coupled-channel unitarity condition, discussed in eq. (21) of ref. [17]. The BSE requires some input potential and baryon and meson propagators to be solved. At lowest-order of the BSE-based chiral expansion [15], we approximate the iterated *potential* by the chiral expansion lowest order meson-baryon amplitudes in the desired strangeness and isospin channels, and the intermediate particle propagators by the free ones (which are diagonal in the coupled-channel space). From the meson-baryon chiral Lagrangian [1] (see sect. IIA of ref. [17]), one gets at lowest order for the *potential*:

$$v_P(k,k') = t_P^{(1)}(k,k') = \frac{D}{f^2}(\not{k} + \not{k}') \tag{3}$$

with D the coupled-channel matrix,

$$D = \frac{1}{4}\begin{array}{c} \begin{array}{cccc} \bar{K}N & \pi\Sigma & \eta\Lambda & K\Xi \end{array} \\ \begin{pmatrix} -3 & \sqrt{\frac{3}{2}} & -\frac{3}{\sqrt{2}} & 0 \\ \sqrt{\frac{3}{2}} & -4 & 0 & -\sqrt{\frac{3}{2}} \\ -\frac{3}{\sqrt{2}} & 0 & 0 & \frac{3}{\sqrt{2}} \\ 0 & -\sqrt{\frac{3}{2}} & +\frac{3}{\sqrt{2}} & -3 \end{pmatrix} \end{array} \begin{array}{c} \\ \bar{K}N \\ \pi\Sigma \\ \eta\Lambda \\ K\Xi \end{array} \tag{4}$$

The s-wave BSE can be solved and renormalized up to a numerical matrix inversion in the coupled-channel space [16].

3 Numerical results

We use the following numerical values for masses and weak decay constants of the pseudoscalar mesons (all in MeV), $m_K = m_{\bar{K}} = 493.68$, $m_\pi = 139.57$, $m_\eta = 547.3$, $M_p = 938.27$, $M_\Sigma = 1189.37$, $M_\Lambda = 1115.68$, $M_\Xi = 1318.0$ and $f_\pi = f_\eta = f_K = 1.15 \times 93.0$, where for the weak meson decay constants we take for all channels an averaged value.

3.1 Fitting procedure

We perform a χ^2-fit, with 12 free parameters, to the following set of experimental data and conditions:

1. $S_{01}(L_{2T2J})$ $\bar{K}N \to \bar{K}N$ and $\bar{K}N \to \pi\Sigma$ scattering amplitudes (real and imaginary parts) [19] in the CM energy range $1480\,\text{MeV} \leq \sqrt{s} \leq 1750\,\text{MeV}$. In this CM energy region, there are a total number of 56 data points (28 real and 28 imaginary parts) for each channel. The normalization used in ref. [19] is different from that used here and their amplitudes, T_{ij}^{Go77}, are related to ours by $T_{ij}^{\text{Go77}} = \text{sig}(i,j)|\boldsymbol{k}_i| \left[f_0^{\frac{1}{2}}(s)\right]_{j\leftarrow i}$, where $\text{sig}(i,j)$ is $+1$ for the elastic channel and -1 for the $\bar{K}N \to \pi\Sigma$ one. On the other hand, and because in ref. [19] errors are not provided, we have taken for those amplitudes errors given by $\delta T_{ij}^{\text{Go77}} = \sqrt{(0.12\, T_{ij}^{\text{Go77}})^2 + 0.05^2}$ in the spirit of those used in ref. [11].
2. $S_{01} - \pi\Sigma$ mass spectrum [20], $1330\,\text{MeV} \leq \sqrt{s} \leq 1440\,\text{MeV}$. In this CM energy region, there are a total of thirteen 10 MeV bins and the experimental data are given in arbitrary units. To compare with data, taking into account the experimental acceptance of 10 MeV, we compute

$$\Delta\sigma/\Delta[M_{\pi\Sigma}(i)] = C \int_{M^-}^{M^+} \left|\left[f_0^{\frac{1}{2}}(s = x^2)\right]_{2\leftarrow 2}\right|^2 \times |\boldsymbol{k}_2(s = x^2)|\, x^2\, \mathrm{d}x\,, \tag{5}$$

where C is an arbitrary global normalization factor[1], $M^\pm = M_{\pi\Sigma}(i) \pm 5\,\text{MeV}$ and i denotes the bin with central CM energy $M_{\pi\Sigma}(i)$. Hence, there are only 12 independent data points. Finally, we take the error of the number of counts, N_i, of the bin i to be $1.61\sqrt{N_i}$ as in ref. [21].
3. The $K^-p \to \eta\Lambda$ total cross-section of ref. [22], $1662\,\text{MeV} \leq \sqrt{s} \leq 1684\,\text{MeV}$. We use the Crystal Ball Collaboration precise new total cross-section measurements (a total of 17 data points compiled in table I of ref. [22]) for the near-threshold reaction $K^-p \to \eta\Lambda$, which is dominated by the $\Lambda(1670)$-resonance. We assume, as in ref. [22], that the p- and higher wave contributions do not contribute to the total cross-section.

Finally, we define the χ^2, which is minimized, as

$$\chi^2/N_{\text{tot}} = \frac{1}{N}\sum_{\alpha=1}^{N}\frac{1}{n_\alpha}\sum_{j=1}^{n_\alpha}\left(\frac{x_j^{(\alpha)\,\text{th}} - x_j^{(\alpha)}}{\sigma_j^{(\alpha)}}\right)^2, \tag{6}$$

where $N = 4$ stands for the four sets of data used and discussed above. Though we have considered four coupled channels, three-body channels, for instance the $\pi\pi\Sigma$ one, are not explicitly considered, as has been also assumed previously in refs. [12] and [22]. The fit is shown in fig. 1.

3.2 Poles and couplings

Resonances are defined as poles in the second Riemann sheet of the s-complex plane. Around them, the scattering matrix behaves as

$$[t(s)]_{ij} \to \frac{2M_R g_i g_j}{s - M_R^2 + \mathrm{i}M_R\Gamma_R}\,. \tag{7}$$

We find three poles in the second Riemann sheet whose positions are given in table 1. Errors have been transported

[1] We fix it by setting the area of our theoretical spectrum, $\sum_i \frac{\Delta\sigma}{\Delta[M_{\pi\Sigma}(i)]}$, to the total number of experimental counts $\sum_i N_i$.

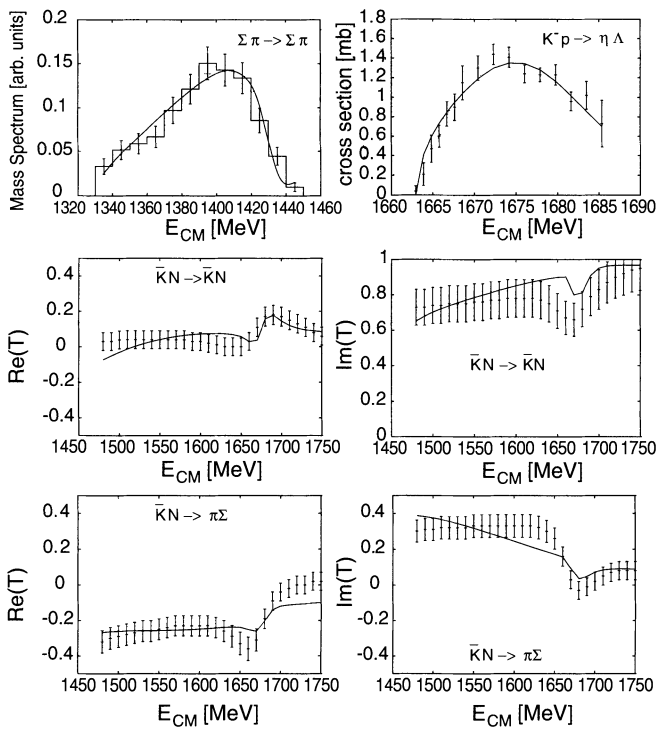

Fig. 1. Best-fit results for the Bethe-Salpeter Equation in the $S = -1$, $I = 0$ channel (solid lines). Upper panel: Experimental data for $\pi\Sigma \to \pi\Sigma$ and $K^-p \to \eta\Lambda$ are from refs. [20] and [22], respectively. Middle panel: The real (left panel) and imaginary (right panel) parts of the s-wave T-matrix, with normalization specified in the main text, for elastic $\bar{K}N \to \bar{K}N$ process in the $I = 0$ isospin channel as functions of the CM energy. Experimental data are taken from the analysis of ref. [19] with the errors stated in the main text. Lower panel: Same as middle panel for the inelastic channel $\bar{K}N \to \pi\Sigma$.

Table 1. Resonance masses and widths (in MeV).

	First	Second	Third
M_R	1368 ± 12	1443 ± 3	1677.5 ± 0.8
Γ_R	250 ± 20	50 ± 7	29.2 ± 1.4

from those in the best-fit parameters [18], taking into account the existing statistical correlations through a Monte Carlo simulation. As can be seen from fig. 2 besides the three poles appearing in the second Riemann sheet, unphysical poles show up in the physical sheet out of the real axis, but they do not influence the scattering. Our resonances are not of the Breit-Wigner form. For the $\Lambda(1670)$-resonance, branching ratios, as defined in ref. [18], are

$$B_{\bar{K}N} = 0.24, \qquad B_{\pi\Sigma} = 0.08, \qquad B_{\eta\Lambda} = 0.68\,. \tag{8}$$

These values reasonably agree with the values quoted in the PDG ($B_{\bar{K}N} = 0.20 \pm 0.05$, $B_{\pi\Sigma} = 0.40 \pm 0.20$, $B_{\eta\Lambda} = 0.25 \pm 0.10$) and in ref. [23] ($B_{\bar{K}N} = 0.37 \pm 0.07$, $B_{\pi\Sigma} = 0.16 \pm 0.06$, $B_{\eta\Lambda} = 0.39 \pm 0.08$, $B_{\pi\Sigma(1385)} = 0.08 \pm 0.06$).

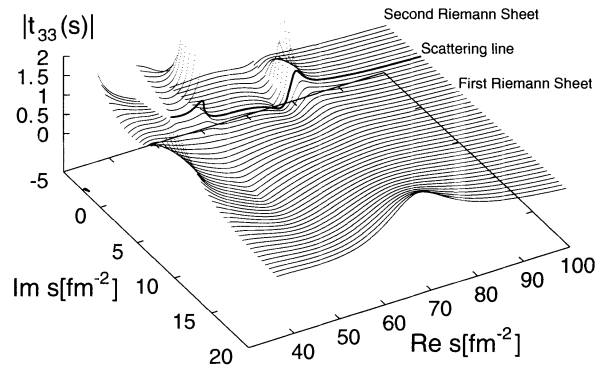

Fig. 2. Modulus of the $\eta\Lambda \to \eta\Lambda$ element of the scattering amplitude $t(s)$ (fm), analytically extended to the first and fourth quadrants of the s-complex plane. The solid line is the scattering line, $s + \mathrm{i}\ 0^+$, from the first threshold, $(m_\pi + M_\Sigma)^2$, on. The first (second) Riemann sheet is depicted in the first (fourth) quadrant of the s-complex plane.

This work has been supported by the DGES grants no. BFM200-1326 and PB98-1367 and the Junta de Andalucía.

References

1. A. Pich, Rep. Prog. Phys. **58**, 563 (1995).
2. E. Jenkins, A.V. Manohar, Phys. Lett. B **255**, 558 (1991).
3. V. Bernard, N. Kaiser, J. Kambor, Ulf G. Meissner, Nucl. Phys. B **388**, 315 (1992).
4. M. Mojzis, Eur. Phys. J. C **2**, 181 (1998).
5. N. Fettes, Ulf-G. Meissner, S. Steininger, Nucl. Phys. A **640**, 199 (1988).
6. N. Fettes, Ulf G. Meißner, Nucl. Phys. A **676**, 311 (2000).
7. N. Kaiser, P.B. Siegel, W. Weise, Nucl. Phys. A **594**, 325 (1995).
8. E. Oset, A. Ramos, Nucl. Phys. A **635**, 99 (1998).
9. B. Krippa, Phys. Rev. C **58**, 1333 (1998).
10. J.A. Oller, Ulf G. Meißner, Phys. Lett. **500**, 263 (2001).
11. M.Th. Keil, G. Penner, U. Mosel, Phys. Rev. C **63**, 045202 (2001).
12. E. Oset, A. Ramos, C. Bennhold, Phys. Lett. B **522**, 260 (2002).
13. M.F.M. Lutz, E.E. Kolomeitsev, Nucl. Phys. A **700**, 193 (2002).
14. N. Kaiser, Phys. Rev. **C 64** , 045204 (2001).
15. J. Nieves, E. Ruiz Arriola, Phys. Lett. B **455**, 30 (1999); Nucl. Phys. A **679**, 57 (2000).
16. J. Nieves, E. Ruiz Arriola, Phys. Rev. D **63**, 076001 (2001).
17. J. Nieves, E. Ruiz Arriola, Phys. Rev. D **64**, 481 (2001).
18. C. García Recio, J. Nieves, E. Ruiz Arriola, M. J. Vicente-Vacas, work in preparation.
19. G.P. Gopal *et al.*, Nucl. Phys. B **119**, 362 (1977).
20. R.J. Hemingway, Nucl. Phys. B **253**, 742 (1984).
21. R.H. Dalitz, A. Deloff, J. Phys. G **17**, 289 (1991).
22. A. Starostin *et al.*, Phys. Rev. C **64**, 055205 (2001).
23. D.M. Manley *et al.*, Phys. Rev. Lett. **88**, 012002-1 (2002).

Eur. Phys. J. A **18**, 189–192 (2003)
DOI 10.1140/epja/i2002-10298-x

THE EUROPEAN PHYSICAL JOURNAL A

The spectrum and strong decays of baryons in a relativistic quark model

B. Metsch[a], U. Löring, D. Merten, and H. Petry

Helmholtz-Institut für Strahlen- und Kernphysik, Universität Bonn, Nußallee 14-16, D-53115 Bonn, Germany

Received: 30 September 2002 /
Published online: 22 October 2003 – © Società Italiana di Fisica / Springer-Verlag 2003

Abstract. On the basis of the three-particle Bethe-Salpeter equation we formulated a relativistic quark model for baryons. With free constituent-quark propagators and instantaneous interaction kernels a good description of the overall baryonic mass spectrum up to the highest spin states is obtained. Preliminary results on strong two-body decays of baryon resonances are discussed.

PACS. 11.10.St Bound and unstable states; Bethe-Salpeter equations – 12.39.Ki Relativistic quark model – 12.40.Yx Hadron mass models and calculations – 13.30.Eg Hadronic decays

1 Introduction

The baryonic resonance spectrum exhibits some striking features: Linear Regge trajectories, which hint at a linear confinement potential; moderately large hyperfine splittings (*e.g.* the N-Δ splitting) hinting at a strong spin-spin interaction; parity doublets, such as *e.g.* $N^*_{\frac{5}{2}+}(1680)$-$N^*_{\frac{5}{2}-}(1675)$, which all are a challenge to explain theoretically. The most successful approaches to account for these have been constituent-quark models (in non-relativistic or "relativized" versions), see *e.g.* the excellent review by Capstick and Roberts [1] and references therein, which use one-gluon exchange or Goldstone-boson exchange as quark interaction in addition to a linear confinement potential. Although the results from such calculations are in general satisfactory, they do not reproduce the details of the N Regge trajectory nor explain the parity doublets found. Moreover, the role of the spin-orbit parts of the residual interactions remains obscure. On top of this, the conventional constituent-quark models have no real field-theoretical basis and lack relativistic covariance. As an extension of an earlier relativistic quark model description of mesons [2], we therefore developed a relativistic quark model for baryons on the basis of the three-particle Bethe-Salpeter equation.

2 A relativistic quark model

The details of our approach are extensively described in [3]; here we shall merely quote the basic assumptions and features. Starting point is the Bethe-Salpeter equation for bound states of three fermions, which is a homogeneous integral equation involving full quark propagators and irreducible interaction kernels in terms of the 8 relative momentum variables of the quarks. In order to solve this equation we made the following assumptions, which were inspired by the non-relativistic constituent-quark model being quite successful in describing the baryon spectrum. It is assumed that the self-energy in the quark propagators can be suitably approximated by introducing an effective, constituent-quark mass in the free Feynman propagator. Furthermore, we assume that interaction kernels do not depend on the relative energy variables of the quarks in the rest frame of the baryon. Although this also implies a technical simplification (Salpeter equation), the main reason is that we want to implement confinement by an instantaneous linearly rising three-body potential. These assumptions, after introducing an effective instantaneous kernel that approximates retardation effects in two-body interactions, allow for a formulation of the resulting Salpeter equation as an eigenvalue equation. The latter is solved by expanding the amplitudes in a suitable large, but finite, basis.

Confinement is implemented by a string-like three-body potential, which rises linearly with inter-quark distances and comprises a spin structure chosen such that spin-orbit splittings are suppressed, see [4] for details. In order to account for the hyperfine structure we adopted an effective two-body interaction based on instanton effects, which has the decisive property to solve the $U_A(1)$-problem in the pseudoscalar meson spectrum [2]. For two quarks it is a short-range two-body interaction acting on quark pairs with vanishing spin that are antisymmetric in flavour. Consequently, this force does not act on the flavour symmetric Δ-resonances. The Regge trajectory in

[a] e-mail: metsch@itkp.uni-bonn.de

Table 1. Comparison of experimental (PDG [5]) and calculated masses of resonances on positive-parity Regge trajectories [4].

State	Rating	J^π	PDG	Calc.
$\Delta(1232)$	****	$\frac{3}{2}^+$	1230–1234	1261
$\Delta(1950)$	****	$\frac{7}{2}^+$	1940–1960	1956
$\Delta(2420)$	****	$\frac{11}{2}^+$	2300–2500	2442
$\Delta(2950)$	**	$\frac{15}{2}^+$	2750–3090	2824
$N(939)$	****	$\frac{1}{2}^+$	939	939
$N(1680)$	****	$\frac{5}{2}^+$	1675–1690	1723
$N(2220)$	****	$\frac{9}{2}^+$	2180–2310	2221
$N(2700)$	**	$\frac{13}{2}^+$	2567–3100	2619
$\Lambda(1116)$	****	$\frac{1}{2}^+$	1116	1108
$\Lambda(1820)$	****	$\frac{5}{2}^+$	1815–1825	1834
$\Lambda(1350)$	****	$\frac{9}{2}^+$	2340–2370	2340
Λ		$\frac{13}{2}^+$		2754

this sector is then used to determine the (non-strange) constituent-quark mass and the constant and string tension parameters of the confinement potential. The results are given in table 1. The parameters of the instanton force are determined from the ground-state octet-decuplet splittings. The remaining spectrum is then a genuine prediction.

3 Mass spectra

The resulting mass spectra for non-strange and strange baryons can be found in [4] and [6], respectively. In general a very satisfactory description of the masses of states up to 2.5 GeV is found. The most prominent features are: Once the strengths of the instanton-induced interaction are fixed from the ground-state splittings, see fig. 1, the other prominent hyperfine splittings in the spectrum can be explained quite naturally. In contrast to an earlier calculation in the framework of the non-relativistic quark model with the same interactions [7], in the present relativistic setup the instanton-induced interaction is strong enough to account almost quantitatively for the low position of the Roper resonances and its analogues in the strange sectors. For a more extensive discussion of the interplay of the instanton-induced interaction, the parameterization of confinement and the relativistic treatment, we again refer to [4]. In addition, the N and Λ Regge trajectory can be very nicely reproduced, see also table 1, indicating that this force leads to a constant shift in M^2 for these states, in accordance with experimental data. Moreover this force also accounts for the occurrence of the parity doublets mentioned above: selectively those states from a particular shell (in the harmonic-oscillator classification), which

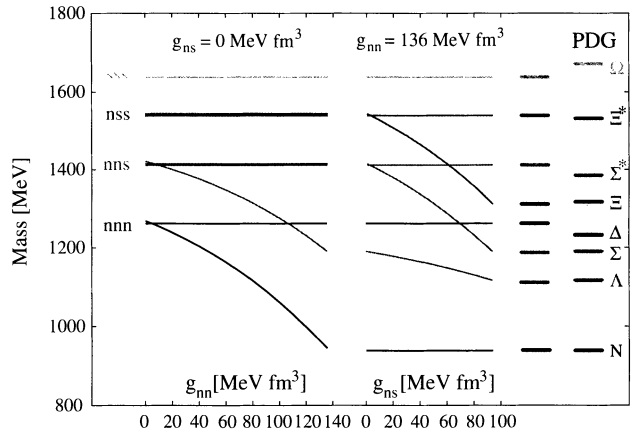

Fig. 1. Octet-decuplet splittings from the instanton-induced interaction. The strengths g_{nn} for non-strange and g_{ns} for non-strange–strange quark pairs increase from left to right, from [4]. Experimental data (PDG) from [5].

show scalar diquark configurations, are lowered enough to become degenerate with some states of the lower oscillator shell with opposite parity [4]. This is illustrated for some higher-spin states in the N-sector in fig. 2. Similar features have also been found for Λ-resonances [4], but not in the other strange sectors, where the instanton-induced force is in general too weak to produce parity doublets. An experimental verification of this would be very interesting.

4 Strong two-body decays

In the framework of the Mandelstam formalism, the amplitude for the strong mesonic decay of excited baryons can be obtained in lowest order by evaluating the simple quark-loop diagram of fig. 3, which involves the vertex functions (amputated Bethe-Salpeter amplitudes) of the participating meson, obtained from a previous calculation on mesons [2], and baryons. A similar procedure has been already used in a treatment of some selected two-meson decays of mainly scalar mesons [8]. Some preliminary results [9] on partial πN- and $\pi\Delta$-decay widths are listed in table 2. In view of the fact that these calculations do not involve any new parameters, we think that the results are quite remarkable. Although the calculated width of the $(\Delta \to N\pi)$-decay is only half the experimental value, we feel that this is quite realistic, since this value leaves room for final-state interaction effects (pion-loop effects), which in general are expected to increase the decay width. Apart from this factor of two we find in general a reasonable description of the partial decay widths of the lowest resonance of given spin-parity. The $N\pi$-decay width of the $N_{\frac{1}{2}}$-(1650), $N_{\frac{3}{2}}$-(1700) and $N_{\frac{5}{2}}$-(1675), which in our calculation are almost pure internal spin-$\frac{3}{2}$ resonances, is definitely too small. At this point we would like to stress that the reconstruction of the nucleon vertex function is approximate only, see [10,11], in contrast to the treatment of Δ-resonances, where no further approximations

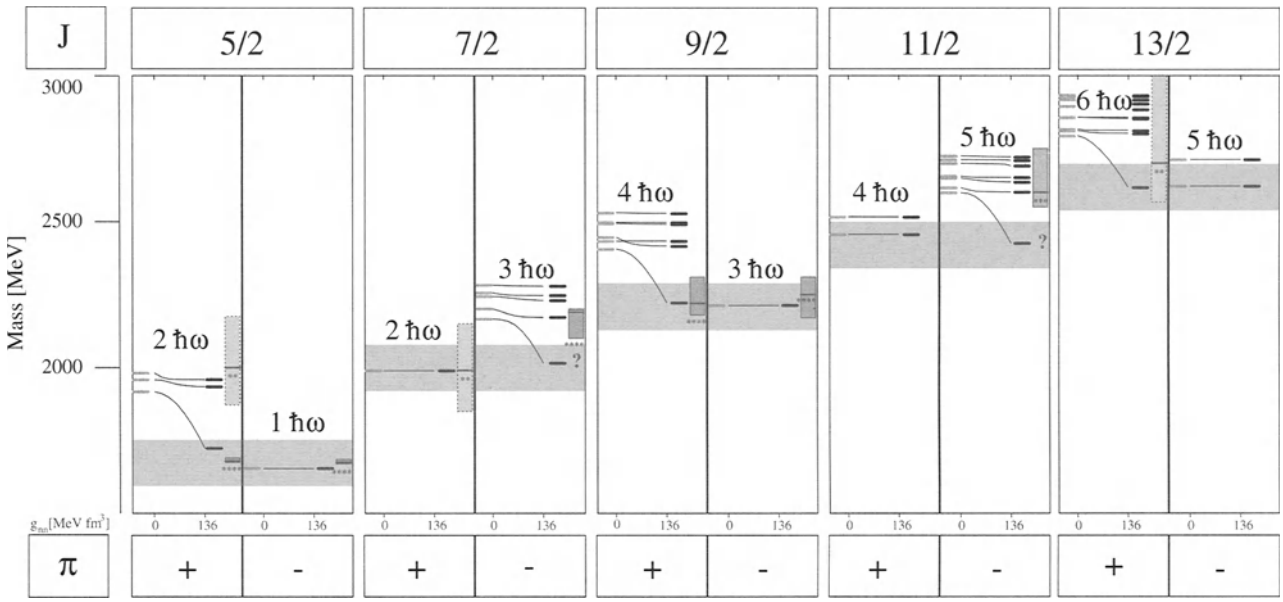

Fig. 2. Generation of parity doublets in the N spectrum through the instanton-induced quark force, from [4]. On the left of each column is the spectrum with the confinement potential alone; the strength of the instanton-induced interaction increases from left to right; experimental data from [5].

Table 2. Comparison of calculated partial decay widths (in MeV) of N- and Δ-resonances to the calculation ($^3P_0$) of Capstick and Roberts [12], and the experimental values (PDG) listed by the Particle Data Group [5].

Decay		Calc.	$^3P_0$	PDG
$P_{33}(1232)$	$\to N\pi$	63	108	$(119 \pm 0)^{+5}_{-5}$
$P_{11}(1440)$	$\to N\pi$	35	412	$(228 \pm 18)^{+65}_{-65}$
	$\to \Delta\pi$	35	11	$(88 \pm 18)^{+25}_{-25}$
$S_{11}(1535)$	$\to N\pi$	34	216	$(68 \pm 15)^{+45}_{-23}$
	$\to \Delta\pi$	1	2	< 2
$S_{11}(1650)$	$\to N\pi$	3	149	$(109 \pm 26)^{+29}_{-4}$
	$\to \Delta\pi$	6	13	$(6 \pm 5)^{+2}_{0}$
$D_{13}(1520)$	$\to N\pi$	39	74	$(66 \pm 6)^{+8}_{-5}$
	$\to \Delta\pi$	35	35	$(24 \pm 6)^{+3}_{-2}$
$D_{13}(1700)$	$\to N\pi$	0.1	34	$(10 \pm 5)^{+5}_{-5}$
	$\to \Delta\pi$	88	778	
$D_{15}(1675)$	$\to N\pi$	4	28	$(68 \pm 7)^{+14}_{-5}$
	$\to \Delta\pi$	35	32	$(83 \pm 7)^{+17}_{-6}$
$S_{31}(1620)$	$\to N\pi$	4	26	$(38 \pm 7)^{+8}_{-8}$
	$\to \Delta\pi$	71	18	$(68 \pm 23)^{+14}_{-14}$
$D_{33}(1700)$	$\to N\pi$	2	24	$(45 \pm 15)^{+15}_{-15}$
	$\to \Delta\pi$	52	262	$(135 \pm 45)^{+45}_{-45}$

are involved and where we get quite reasonable results. Also the issue whether the situation can be improved by taking into account mixings induced by coupling to, *e.g.*, the πN-channel, or that this constitutes a serious deficiency of our internal quark dynamics, will be the subject of future investigations. It can be noted here, that also the photon couplings to these states [10] are underpredicted. For the time being we consider these preliminary results, which, to our knowledge, are the first parameter-free calculations of strong-decay widths in a relativistically covariant framework, as encouraging.

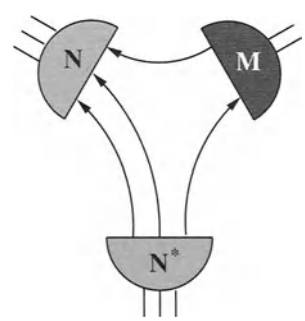

Fig. 3. Lowest-order quark-loop contribution to the strong ($N^* \to N + M$)-decay of excited baryons.

References

1. S. Capstick, W. Roberts, Prog. Part. Nucl. Phys., **45**, 241 (2000).
2. M. Koll, R. Ricken, D. Merten, B.Ch. Metsch, H. Petry, Eur. Phys. J. A **9**, 73 (2000).
3. U. Löring, K. Kretzschmar, B.Ch. Metsch, H.R. Petry, Eur. Phys. J. A **10**, 309 (2001).
4. U. Löring, B.Ch. Metsch, H.R. Petry, Eur. Phys. J. A **10**, 395 (2001).

5. Particle Data Group (D.E. Groom *et al.*), Eur. Phys. J. C **15**, 1 (2000).
6. U. Löring, B.Ch. Metsch, H.R. Petry, Eur. Phys. J. A **10**, 447 (2001).
7. W.H. Blask, U. Bohn, M.G. Huber, B.C. Metsch, H.R. Petry, Z. Phys. A **337**, 327 (1990).
8. Ch. Ritter, B.C. Metsch, C.R. Münz, H.R. Petry, Phys. Lett. B **380**, 431 (1996).
9. D. Merten, *Hadron Form Factors and Decays in a Covariant Quark Model*, PhD Thesis (Universität Bonn, Bonn, 2002).
10. D. Merten, U. Löring, B.C. Metsch, H. Petry, this issue, p. 705.
11. D. Merten, U. Löring, K. Kretzschmar, B. Metsch, H.R. Petry, Eur. Phys. J. A **14**, 477 (2002).
12. S. Capstick, W. Roberts, Phys. Rev D **49** 4570 (1994).

Eur. Phys. J. A **18**, 193–195 (2003)
DOI 10.1140/epja/i2002-10304-5

THE EUROPEAN PHYSICAL JOURNAL A

Electromagnetic properties of baryons in a relativistic quark model

D. Merten[a], U. Löring, B. Metsch, and H. Petry

Helmholtz-Institut für Strahlen- und Kernphysik, Universität Bonn, Nußallee 14-16, D-53115 Bonn, Germany

Received: 30 September 2002 /
Published online: 22 October 2003 – © Società Italiana di Fisica / Springer-Verlag 2003

Abstract. Results on electromagnetic form factors of the nucleon and photon transition form factors of non-strange baryon resonances calculated in a relativistically covariant quark model based on the Bethe-Salpeter equation are presented. The relevance of the instanton-induced quark interaction on these properties is discussed.

PACS. 11.10.St Bound and unstable states; Bethe-Salpeter equations – 12.39.Ki Relativistic quark model – 12.40.Yx Hadron mass models and calculations – 13.40.Gp Electromagnetic form factors

1 Introduction

From the very beginning electromagnetic properties of hadrons played a key role in tests of quark models of baryons. In particular the ratio of the magnetic moments of proton and neutron (experimental value 1.46) is often interpreted as "proving" the correctness of the non-relativistic quark model, which predicts the value 1.5 on the basis of spin-isospin matrix elements only. Also the electric and magnetic form factors of the nucleon have been intensely studied for a long time and constitute important tests for the charge and current distributions inside the nucleon. For a discussion of in particular the neutron form factor, see, *e.g.*, [1]. Most calculations of electromagnetic form factors in the framework of the constituent quark model essentially adopt the wave functions from a non-relativistic treatment of the quark dynamics[1] supplemented by a relativistic prescription for calculating the electromagnetic current matrix elements, see, *e.g.*, [3,4]. Indeed in this manner a remarkable good description of nucleonic form factors can be achieved [5].

In contrast to this in our relativistic quark model we have used the Bethe-Salpeter equation with instantaneous forces, which inherently respects relativistic covariance. On the basis of the amplitudes, obtained by solving the full Salpeter equation, see [6,7,3], the baryonic vertex function (amputated Bethe-Salpeter amplitude) can be reconstructed for any on-shell baryon momentum und thus form factors and various couplings can be calculated in impulse approximation without any additional parameters. The details of the calculation of electroweak form factors of non-strange baryons have been published recently [8]. Here, we shall merely quote the approximations made and briefly discuss also some additional results.

2 Baryonic currents

Insisting on an instantaneous treatment of the quark dynamics on the basis of the full Salpeter equation, even in the presence of two-body interactions, the retardation effects of these can be accounted for only perturbatively. In [9,7,10] it was shown that by the perturbative construction of an effective interaction potential, which parameterises the effects of two-body forces, in lowest order, nevertheless, a very satisfactory description of the baryonic mass spectra up to high masses and high spins can be achieved. The current operators, which enter the computation of form factors then should be calculated consistently with this effective treatment of retardation effects. Again in lowest order, for details see [11,8], the current matrix elements can then approximately be written as

$$\begin{aligned}
&\langle \bar{P}|j^\mu(0)|M\rangle = \\
&-3\int \frac{\mathrm{d}^4p_\xi}{(2\pi)^4}\frac{\mathrm{d}^4p_\eta}{(2\pi)^4}\bar{\Gamma}_P\left(p_\xi, p_\eta - \frac{2}{3}q\right) \\
&\times S_F^1\left(\frac{1}{3}M + p_\xi + \frac{1}{2}p_\eta\right)\otimes S_F^2\left(\frac{1}{3}M - p_\xi + \frac{1}{2}p_\eta\right) \\
&\otimes S_F^3\left(\frac{1}{3}M - p_\eta + q\right)\hat{e}\,\gamma^\mu S_F^3\left(\frac{1}{3}M - p_\eta\right)\Gamma_M\left(\boldsymbol{p}_\xi, \boldsymbol{p}_\eta\right),
\end{aligned}$$

where $\bar{\Gamma}_P, \Gamma_M$ stand for the vertex functions for baryons with on-shell 4-momentum P and $P' = M \equiv (M, \mathbf{0})$ in

[a] e-mail: merten@itkp.uni-bonn.de

[1] Although often a relativistic form for the single-quark kinetic energy is used and/or some relativistic effects are parameterised in the expressions for the interaction, see, *e.g.*, [2].

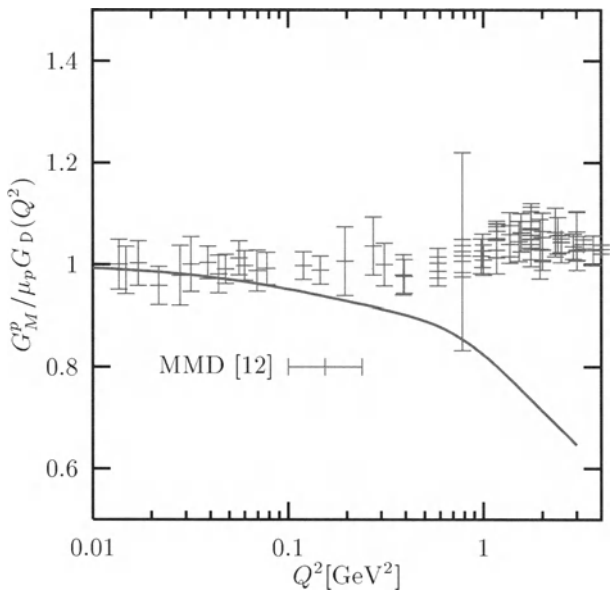

Fig. 1. Magnetic form factor of the proton; experimental data from the analysis of [12].

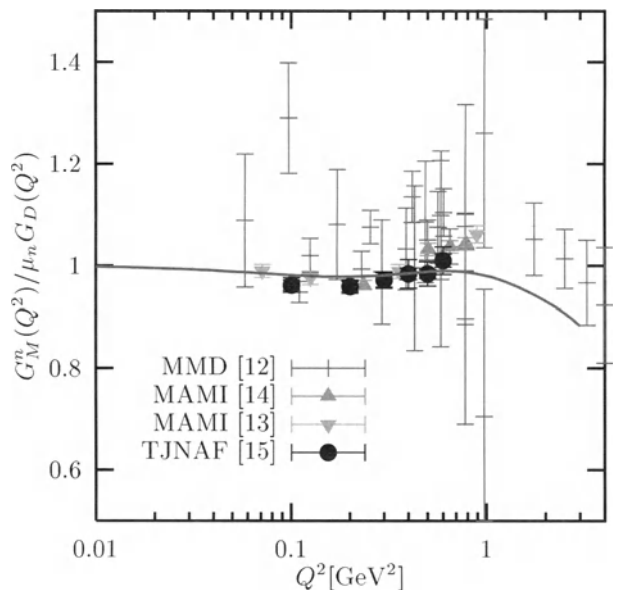

Fig. 2. Magnetic form factor of the neutron; experimental data from the analysis of [12].

the final and initial state, respectively, $q := P - P'$ is the momentum transfer, $\hat{e}$ the quark charge operator and the integration is over the relative 4-momenta of the quarks.

3 Results

Form factors and helicity amplitudes are then calculated by standard formulas [8]. Static properties of the nucleon, such as magnetic momenta, the axial coupling constant and radii are obtained from inspection of the $Q^2 = -q^2$ limit of the corresponding from factors and are in general in excellent agreement with experimental data, again see [8]. We found that the correct relativistic treatment of boosts of our amplitudes is imperative to achieve agreement with the experimental data: If, *e.g.*, we neglect this boost, the value for the magnetic moment of the proton drops by about one nuclear magneton. In this respect the apparent success of the non-relativistic quark model in explaining ratios of magnetic moments must be considered as accidental.

As an example for the quality of our calculations we compare the magnetic form factors of the nucleon relative to a dipole parameterisation in figs. 1 and 2 with experimental data mainly from the compilation of [12]. Although the calculated form factors drop too fast for large momentum transfer[2], the calculation of the neutron magnetic form factor nicely reproduces the shallow minimum around $Q^2 = 0.3$ GeV^2, recently measured at MAMI [13, 14] and Jefferson Lab [15].

As an illustration of the calculation of electro-excitation of baryon resonances of higher mass and spin

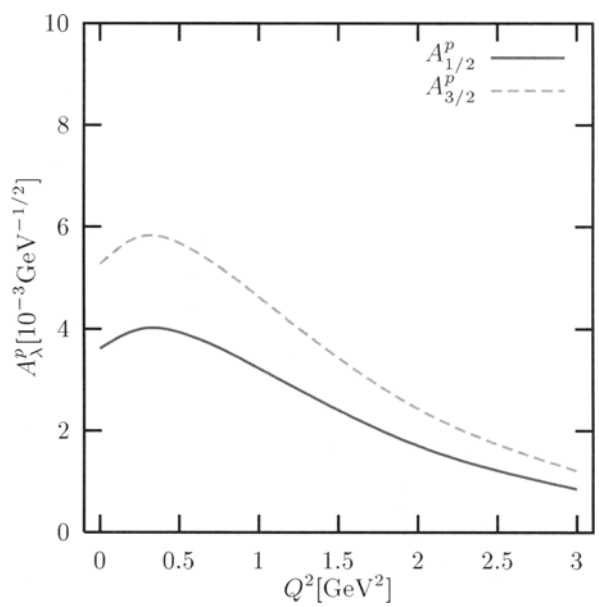

Fig. 3. $D_{15}(1675)$ proton electro-excitation helicity amplitudes.

we present the helicity amplitudes for electro-excitation on the proton for the mass degenerate "parity doublet" $D_{15}(1675)$-$F_{15}(1680)$ in figs. 3 and 4, respectively. We predict that the $D_{15}(1675)$ helicity amplitudes, which however is rather small, drops significantly faster with increasing momentum transfer than the corresponding $F_{15}(1680)$ amplitudes. In the present model this is due to the feature that the former state is (in the harmonic-oscillator nomenclature) dominantly a $L = 1$, $S = \frac{3}{2}$, $1\hbar\omega$-state, for which the instanton-induced interaction

[2] This also applies to the isovector electric form factor of the nucleon, see [8].

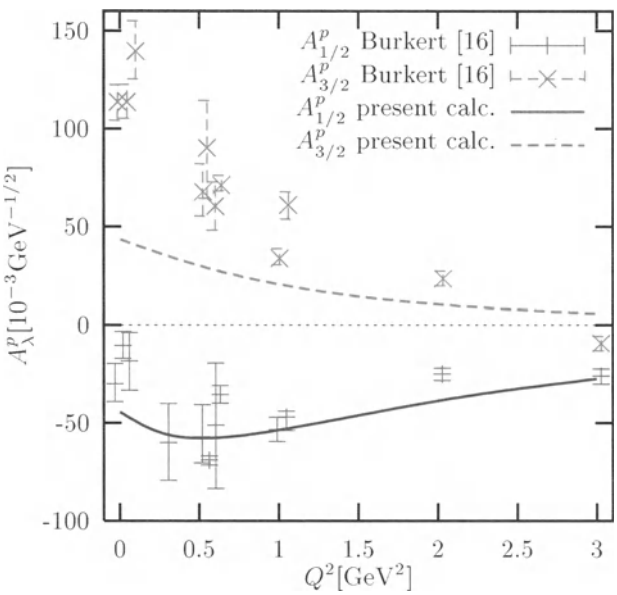

Fig.. 4. $F_{15}(1680)$ proton electro-excitation helicity amplitudes.

vanishes, whereas the latter state is mainly a $L = 2$, $S = \frac{1}{2}$, $2\hbar\omega$-state, with scalar diquark correlations from this interaction, which are sufficiently strong to lower this state to a mass almost degenerate with the other state. Furthermore at low Q^2 the experimental data indicate that for this resonance the $A_{\frac{3}{2}}$ amplitude dominates (which is unfortunately not quite reproduced by our calculation) and at large Q^2 the $A_{\frac{1}{2}}$ amplitude is larger, which is also found in the calculation, whereas for the $D_{15}(1675)$-resonance our calculation indicate that both amplitudes have the same magnitude. This different behaviour should be clearly visible in a measurement of an asymmetry $\propto |A_{\frac{1}{2}}|^2 - |A_{\frac{3}{2}}|^2$ in dependence on Q^2.

In conclusion we think that we have demonstrated, that a fully relativistic treatment of the quark dynamics and their electromagnetic couplings on the basis of the instantaneous Bethe-Salpeter equation with quark forces from a confinement potential and an instanton-induced interaction indeed leads to an encouraging description of the major features of baryonic excitations, which certainly still can and, in view of the approximate treatment of retardation effects from the two-body interaction, must be improved.

References

1. T. Reichelt, this issue, p. 181.
2. S. Capstick, W. Roberts, Phys. Rev. D **49**, 4570 (1994).
3. S. Capstick, B.D. Keister, Phys. Rev. D **51**, 3598 (1995).
4. R.F. Wagenbrunn, S. Boffi, W. Klink, W. Plessas, M. Radici, Phys. Lett. B **511**, 33 (2001); L.Ya. Glozmann, M. Radici, R.F. Wagenbrunn, S. Boffi, W. Klink, W. Plessas, Phys. Lett. B **516**, 183 (2001).
5. S. Boffi, M. Radici, L. Glozman, W. Plessas, R.F. Wagenbrunn, W. Klink, in *Proceedings of 9th International Conference on the Structure of Baryons (BARYONS 2002), Newport News, Virginia, 2002*, edited by C.E. Carlson, B.A. Mecking (World Scientific, Singapore, 2003), arXive:hep-ph/0205021.
6. B. Metsch, U. Löring, D. Merten, H. Petry, this issue, p. 189.
7. U. Löring, B.Ch. Metsch, H.R. Petry, Eur. Phys. J. A **10**, 395 (2001).
8. D. Merten, U. Löring, K. Kretzschmar, B. Metsch, H.R. Petry, Eur. Phys. J. A **14**, 477 (2002).
9. U. Löring, K. Kretzschmar, B.Ch. Metsch, H.R. Petry, Eur. Phys. J. A **10**, 309 (2001).
10. U. Löring, B.Ch. Metsch, H.R. Petry, Eur. Phys. J. A **10**, 447 (2001).
11. D. Merten, *Hadron Form Factors and Decays in a Covariant Quark Model*, PhD Thesis (Universität Bonn, Bonn, 2002).
12. P. Mergell, U.-G. Meißner, D. Drechsel, Nucl. Phys. A **596**, 367 (1996).
13. G. Kubon *et al.*, Phys. Lett. B **524**, 26 (2002).
14. H. Anklin *et al.*, Phys. Lett. B **428**, 248 (1998).
15. W. Xu *et al.*, Phys. Rev. C **67**, 012201 (2003), arXiv:nucl-ex/0208007; W. Xu. *et al.*, Phys. Rev. Lett. **85**, 2900 (2000).
16. V. Burkert, *Research Program at CEBAF II*, edited by V. Burkert (1986) p. 161; Phys. Lett. B **428**, 248 (1998).

Eur. Phys. J. A **18**, 197–199 (2003)
DOI 10.1140/epja/i2002-10306-3

THE EUROPEAN PHYSICAL JOURNAL A

t-dependence of pion production in $\pi^- p \to \pi^0\pi^0 n$

F.P. Sassen[a], S. Krewald, and J. Speth

IKP Theorie Forschungszentrum Jülich, Jülich, Germany

Received: 30 September 2002 /
Published online: 22 October 2003 – © Società Italiana di Fisica / Springer-Verlag 2003

Abstract. As the E852 and the GAMS Collaboration published their data for the dependence of the reaction $\pi^- p \to \pi^0\pi^0 n$ on the momentum transfered to the nucleon, questions rose, whether the $K\bar{K}$-molecule picture might be ruled out by their experiments. Here we report on our analysis of these data and our investigations into concerns raised in discussions, like the role of the $NN\pi\pi\pi$ contact term. We find the molecule picture capable to explain the experimental data.

PACS. 11.55.Fv Dispersion relations – 11.80.Gw Multichannel scattering – 13.75.Gx Pion-baryon interactions – 13.75.Lb Meson-meson interactions

1 Introduction

Both the GAMS Collaboration [1] and the BNL E852 experiment [2] observed a peculiar behaviour of the $f_0(980)$-resonance when measuring the t-dependence of the reaction $\pi^- p \to \pi^0\pi^0 n$. While for low momentum transfer t to the nucleon, *e.g.* $-t < 0.1\,\mathrm{GeV}^2$, the resonance shows as a distinct dip, a sharp peak is seen at the same position for large t, *e.g.* $-t > 0.2\,\mathrm{GeV}^2$. Based on this observation claims were made that there must be a hard $q\bar{q}$-component in the $f_0(980)$-resonance [3]. Looking at this phenomenon within the framework of the Jülich meson exchange model for $\pi\pi$ scattering [4] we also investigate claims that the $K\bar{K}$-molecule, generating the $f_0(980)$-resonance within this model, only forms because the independent empirical t-channel form factors can be used to generate the needed attraction in the $K\bar{K}$-channel. Instead of using those arbitrary form factors we develop a self-consistent procedure to calculate the meson form factors microscopically in the s-channel and use a dispersion relation to generate the t-channel form factors. In sect. 2 we describe the self-consistent procedure used to calculate these form factors. Section 3 gives a short description of how pion production is handled in our model. As we do not consider pion production by the $NN\pi\pi\pi$ contact term we give a short discussion on the influence of this term in sect. 4. Our results for the t-dependence observed in pion production are presented in sect. 5.

2 Self-consistent form factors

Since within the Jülich meson exchange model s- and t-channel form factors were treated independently, the possibility existed that the $K\bar{K}$-molecule was an artefact of too point-like t-channel form factors, which overestimate the generated attraction. In the old model the bare s-channel vertex f^0 gets dressed by the non-pole part of the T-matrix (T^{NP}) and the s-channel resonances aquire a self-energy contribution by means of the Bethe-Salpeter equation, which both do not happen in the t-channel. To account for those mechanisms also in the t-channel we calculate the s-channel form factor ($\Gamma(s)$) as an empirical form factor F plus dressing by meson exchanges (1), (2) and use dispersion relation (3) to continue the form factor to the t-channel. Here, F is chosen to be a formal interpolation of the old s- and t-channel form factors:

$$\Gamma(s)f^0(s) = f(s) = (1 + T^{\mathrm{NP}}G)\tilde{f}^0\,, \tag{1}$$

$$\tilde{f}^0 = Ff^0 = \frac{4\Lambda^4 + M^4}{4\Lambda^4 + 4\omega^4(k)} f^0\,, \tag{2}$$

$$\Gamma(t) = \frac{1}{\pi}\int_{4m_\pi^2}^{\infty} \mathrm{d}t' \frac{\Im(\Gamma(t'))}{t'-t} + \text{pole contributions}\,. \tag{3}$$

The same idea is applied to the self-energy. Care has to be taken in both cases since the empirical form factor introduces poles, which have to be accounted for in the dispersion relations. As the formulas for both form factors and self-energy depend on the latter two to be known, we start from the empirical values of the old model and use them to calculate a first estimate, which then is the starting point to calculate a second estimate and so forth until we obtain a self-consistent solution. During this iteration we make sure that $\pi\pi$ phase shifts and inelasticities keep their good agreement with experiment. The differences between the old and new form factors are not too large so that this calculation justifies the empirical form factors used in the model before.

[a] e-mail: F.P.Sassen@fz-juelich.de

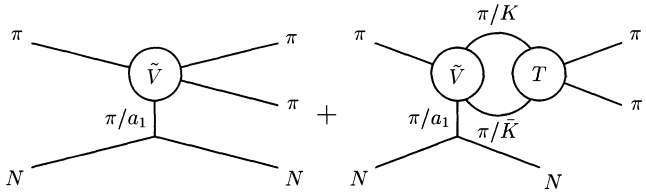

Fig. 1. Pion production as Born amplitude plus final-state interaction. For the potential $\tilde{V}$ only the π/a_1 emitted by the nucleon is allowed to be off its mass shell.

One aspect regarding the change in the s-channel form factors is worth mentioning. The poles introduced by the empirical form factor get closer to the physical region as we switch to our interpolated form factor. This is necessary since we want to use a dispersion relation in one variable, which means, that the poles of the old form factor lie in the region we want to continue to. This is why the poles of the new form factor had to contain a non-vanishing imaginary part. These poles, even though their contribution decreases during iteration, stay part of the self-consistent form factors. As those poles originate from an empirical form factor, which is as its predecessors acausal, we might shortly discuss their influence on our calculation even though we have not yet introduced our model for pion production. There are two main aspects in which the poles show up: Firstly they cause a pronounced decay into $K\bar{K}$. Secondly they cause a great part of the excess strength in the pion production at low invariant two pion masses in the region of high momentum transfer t to the nucleon (fig. 3b) below).

3 Pion production

In order to compare to the data provided by E852 and GAMS, we apply the model depicted in fig. 1. That is, we use a Born amplitude together with subsequent final-state interaction. We take the Jülich meson exchange description together with the self-consistent form factors described in sect. 2 to model the final-state interaction, *i.e.* the final-state interaction is calculated in a three-dimensional reduction of the Bethe-Salpeter equation with a kernel as described in [4] plus the four-pion contact terms added in [5]. As the production vertex $\tilde{V}$ is concerned, we only allowed the leg connected to the nucleon to be off-shell. $\tilde{V}$ contains t-channel exchanges for ρ and K^*, as well as s-channel resonances and the four-pion contact terms. The π and the a_1 emitted at the nucleon vertex have usually high momentum. So the question rises whether the Blankenbeclar-Sugar propagator we are using is a good enough approximation. To check this, we replace them by Regge propagators with the parameters taken from [6]. This replacement had only slight influence on the result. So we are justified in showing the results for the Blankenbeclar-Sugar propagators only. To be consistent with the experimental analysis we further adopted the use of exponential form factors at the nucleon vertex fitting their parameters to the t-dependence of the total cross-section.

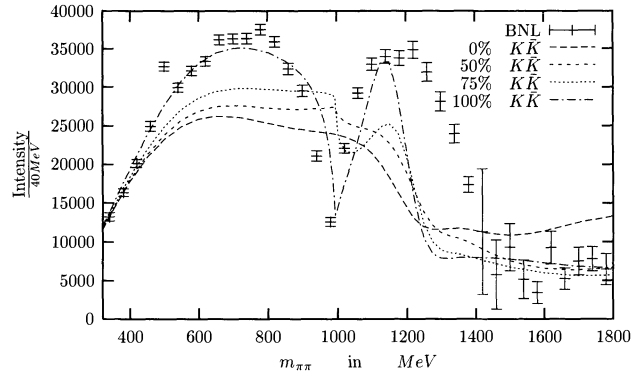

Fig. 2. Development of $f_0(980)$ while the coupling to the $K\bar{K}$-channel is increased. The data shown is taken from the BNL E852 experiment [2].

4 NN$\pi\pi\pi$ contact term in the production

At low momentum transfer to the nucleon and low invariant pion masses a sizeable contribution to the production comes from diagrams starting with the emission of a pion from the nucleon followed by a four-pion contact interaction, which at those masses is not yet cut off by its form factor. So there is the chance that this class of diagrams gets cancelled by diagrams starting with a $NN\pi\pi\pi$ point vertex. In the case of pion deuteron scattering this effect has for example been discussed by [7]. Two points should be noted in this respect:

1. When the ρ was introduced as a gauge particle our Lagrangian acquired a slightly different form compared to [7] plus an additional $\pi\pi\pi\pi$ contact term.
2. The cancellation occurs only at threshold in the chiral limit of vanishing pion mass. This can be seen when looking at the production amplitudes shown in the appendix of [8] (diagrams A) and B)).

Looking at the production in the discussed momentum transfer region one sees only partial cancellation of the amplitudes corresponding to the ungauged Lagrangian. Since these give only minor contribution to the overall production, an effect on the final result can hardly be noticed. This should be even more the case, if the $NN\pi\pi\pi$ contact term gets its own appropriate form factor instead of sharing the form factor for the $\pi\pi\pi\pi$ vertex as we chose to ensure maximum cancellation.

5 Results

We find that the formation of a $K\bar{K}$-molecule is by no means an artefact of the unconstrained t-channel form factors. This is demonstrated in fig. 2, where the low momentum transfer pion production is shown as calculated for self-consistent form factors. To demonstrate that the origin of the $f_0(980)$ seen here as a sharp dip really lies within the $K\bar{K}$-channel we start from the case of an uncoupled $\pi\pi$-channel (long dashes), which shows no distinct features. As we increase the coupling to the $K\bar{K}$-channel

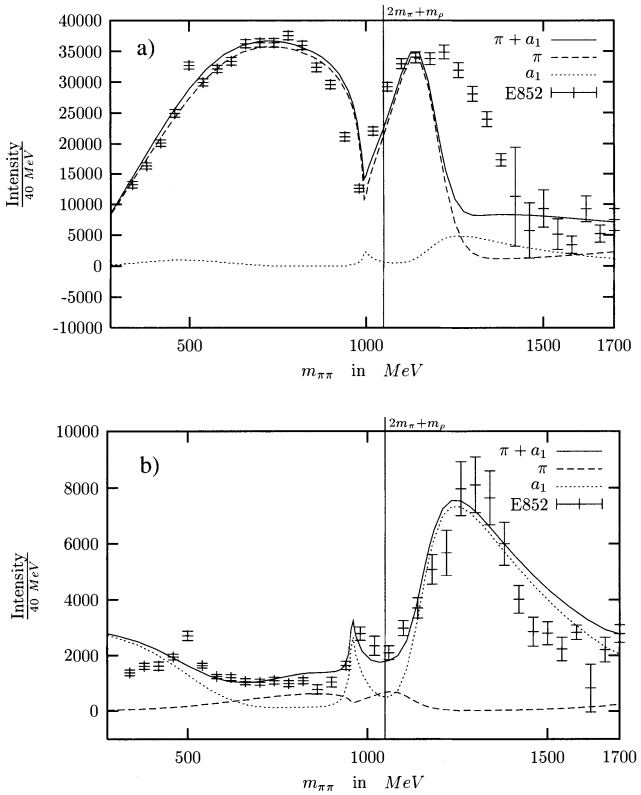

Fig. 3. t-dependence of pion production in the S-wave. a) shows low momentum transfer, *i.e.* $-t = 0.03\,\mathrm{GeV}^2$ calculations with data from [2] averaged for $0.01 < -t < 0.1\,\mathrm{GeV}^2$ and b) shows high momentum transfer, *i.e.* $-t = 0.8\,\mathrm{GeV}^2$ calculations with data from [2] averaged for $0.4 < -t < 1.5\,\mathrm{GeV}^2$.

as well as the interaction in this channel, a cusp structure (dashes) shows, which evolves into the sharp dip in the fully coupled case (dash-dotted line). This shows how the $f_0(980)$ is formed as a $K\bar{K}$-molecule. When looking at the full model (dash-dotted line in fig. 2) one clearly sees that we miss a lot of strength above 1.2 GeV. We will investigate this missing strength together with the t-dependence of the data. When looking at fig. 3 we see, apart from the afore-mentioned one, two further features that we miss. One is the strength at low invariant pion masses, which we already traced back to the close poles of our empirical s-channel form factors. The other is the distinct peak at 500 MeV, which we should not reproduce, since it stems from kaon decays and has nothing to do with the reaction under investigation.

But now let us discuss the t-dependence before analysing the missing strength. Looking at fig. 3 one sees the experimental t-dependence nicely reproduced. This is due to a change in the production mechanism. While in the low-t case depicted in 3a) the production via pion emission is dominant (dashed line), the production in the high-t case is mainly due to the a_1. This is demonstrated by the dotted line in 3b). The peak emerging in 3b) instead of the dip in 3a) is generated by destructive interference of the first diagram in fig. 1 and the parts of the second diagram having gone through the $K\bar{K}$ channel. When looking at the missing strength at high invariant two pion masses it should be stressed, that there are further channels to be considered and that there might be some problems with the S-wave data around 1.2–1.4 GeV as strong G-waves appear, which could be a misinterpretation of the S-wave strength [9]. Nevertheless, we tried to fill up the second bump of 3a) just by resonances. Using just a broader version of the $f_0(1370)$ fails to reproduce the high momentum transfer structure in 3b), whereas there is no problem to fill the missing strength by an additional resonance. This shows, that the t-dependence gives valuable information on the resonance structure. We also introduced a genuine, *i.e.* $q\bar{q}$, $f_0(980)$ in our model, which by itself was not able to reproduce the measured inelasticities, but cannot be excluded to contribute as an admixture to the $f_0(980)$-resonance if the coupling is small.

6 Summary

Good agreement with experiment has been achieved using our model for self-consistent form factors even though we had to move the unphysical singularities closer to the physical region, which has caused some artefacts like an increase of production close to threshold. The good agreement with experiment covers scattering phases and inelasticities as well as the t-dependence of the S-wave amplitudes. Further we had no problem to generate the attraction in the $K\bar{K}$-channel needed to form a molecule even though our form factors are now heavily constrained. Comparing our new form factors with the old empirical ones, we found good agreement and would consider the use of empirical form factors in the Jülich meson exchange model to be justified. To investigate the energy region up to 2 GeV, the $\rho\rho$, $\eta\eta$, $\pi\eta$ channels have to be considered [10].

References

1. D. Alde *et al.*, Z. Phys. C **66**, 375 (1995).
2. J. Gunter *et al.*, Phys. Rev. D **64**, 072003 (2001).
3. V.V. Anisovich *et al.*, Phys. Lett. B **355**, 363 (1995).
4. D. Lohse *et al.*, Nucl. Phys. A **516**, 513 (1990).
5. G. Janßen *et al.*, Phys. Rev. D **52**, 2690 (1995).
6. A.V. Anisovich *et al.*, Phys. Rev. D **62**, 051502 (2000).
7. M.R. Robilotta, C. Wilkin, J. Phys. G **4**, L115 (1978).
8. V. Bernard *et al.*, Nucl. Phys. A **359**, 83 (1997).
9. R. Kaminski *et al.*, Eur. Phys. J. Direct C **4**, 4 (2002), arXiv:hep-ph/0109268.
10. E. Klempt, arXiv:hep-ex/0101031.

Eur. Phys. J. A **18**, 201–205 (2003)
DOI 10.1140/epja/i2002-10299-9

THE EUROPEAN PHYSICAL JOURNAL A

Nuclear forces and currents in large-N_C QCD

D.O. Riska[a]

Helsinki Institute of Physics and Department of Physical Sciences, 00014 University of Helsinki, Finland

Received: 30 September 2002 /
Published online: 22 October 2003 – © Società Italiana di Fisica / Springer-Verlag 2003

Abstract. Expression of the nucleon-nucleon interaction to leading order in $1/N_C$ in terms of Fermi invariants allows a dynamical interpretation of the interaction and a consistent construction of the associated interaction currents. The numerically significant components of 4 different modern realistic phenomenological interaction models admit very similar meson exchange interpretations in the large-N_C limit. The ratio of the volume integrals of the leading, next-to-leading and next-to-next leading-order terms in these interaction models is roughly 300 : 5–10 : 0.1, which corresponds fairly well to the ratios of $1/N_C^2$ between the terms that would be suggested by the $1/N_C$ expansion if $N_C = 3$.

PACS. 13.75.Cs Nucleon-nucleon interactions (including antinucleons, deuterons, etc.) – 21.30.Cb Nuclear forces in vacuum

1 Introduction

The large color number limit of QCD allows a series expansion in $1/N_C$ for hadronic observables, where the first few terms capture the key phenomenological features of the structure of the baryons [1]. The leading terms in the $1/N_C$ series expansion of the components of the nucleon-nucleon interaction have been shown to correspond well with the strongly coupled exchange terms in a phenomenological meson exchange model for the interaction [2].

All the most commonly employed modern realistic phenomenological interaction models allow an interpretation in terms of phenomenological meson exchange and their numerically significant components correspond well to the leading terms in the $1/N_C$ expansion of the interaction components. The ratio of the volume integrals of the leading, next-to-leading and next-to-next leading-order terms in these interaction models is roughly $300 : 5 - 10 : 0.1$, which matches the ratios of $1/N_C^2$ between the terms that is suggested by the $1/N_C$ expansion for $N_C = 3$.

A dynamical interpretation of a phenomenological interaction model is possible if it is expressed in terms of the 5 Fermi invariants. That separates the interaction into linear combinations of scalar, vector, axial vector and pseudoscalar exchange mechanisms. These invariants define consistent interaction current operators [3,4], for which $1/N_C$ expansions follow from those of the corresponding potentials [5].

The nucleon-nucleon interaction models that are considered here are the V18 [6], the CD-Bonn [7], the Nijmegen(93) [8] and the Paris [9] potentials. All of these have long-range pion exchange tails, and phenomenological short-range terms. Their components in the Fermi invariant representation are remarkably similar in strength, and when parametrized in terms of single-meson exchange give rise to similar "effective" meson-nucleon couplings.

[a] e-mail: riska@pcu.helsinki.fi

2 The nucleon-nucleon interaction in the large-N_C limit

2.1 Phenomenological interactions

The nucleon-nucleon interaction is commonly expressed in terms of the following set of Galilean invariant spin and isospin operators:

$$V_{NN} = \sum_i^5 [\tilde{v}_j^+ + \tilde{v}_j^- \boldsymbol{\tau}^1 \cdot \boldsymbol{\tau}^2]\, \tilde{\Omega}_j, \tag{1}$$

where the coefficients $\tilde{v}_j^\pm$ are scalar functions and the spin operators $\tilde{\Omega}_j$ are defined as

$$\tilde{\Omega}_C = 1, \quad \tilde{\Omega}_{LS} = \boldsymbol{L} \cdot \boldsymbol{S}, \quad \tilde{\Omega}_T = S_{12},$$
$$\tilde{\Omega}_{SS} = \boldsymbol{\sigma}^1 \cdot \boldsymbol{\sigma}^2, \quad \tilde{\Omega}_{LS2} = \frac{1}{2}\{\boldsymbol{\sigma}^1 \cdot \boldsymbol{L}, \boldsymbol{\sigma}^2 \cdot \boldsymbol{L}\}_+ \quad . \tag{2}$$

The powers of the leading terms in the $1/N_C$ expansion for these potential components are the following [2]:

$$\tilde{v}_C^+ \tilde{\Omega}_C, \quad \tilde{v}_T^- \tilde{\Omega}_T, \quad \tilde{v}_{SS}^- \tilde{\Omega}_{SS} \quad \sim \quad \mathcal{O}(N_C),$$
$$\tilde{v}_C^- \tilde{\Omega}_C, \quad \tilde{v}_2^\pm \tilde{\Omega}_{LS}, \quad \tilde{v}_T^+ \tilde{\Omega}_T, \quad \tilde{v}_{SS}^+ \tilde{\Omega}_{SS}, \quad \tilde{v}_{LS2}^- \tilde{\Omega}_{LS2} \quad \sim \quad \mathcal{O}(1/N_C),$$
$$\tilde{v}_{LS2}^+ \tilde{\Omega}_{LS2} \quad \sim \quad \mathcal{O}(1/N_C^3). \tag{3}$$

A simple derivation of these scaling relations is given below.

For a dynamical interpretation re-expression of the interaction in terms of the 5 Fermi invariants S, V, T, A, P is required. These are defined as [10]

$$S = 1, \quad V = \gamma^1_\mu \gamma^2_\mu, \quad T = \frac{1}{2}\sigma^1_{\mu\nu}\sigma^2_{\mu\nu},$$
$$A = i\gamma^1_5\gamma^1_\mu \, i\gamma^2_5\gamma^2_\mu, \quad P = \gamma^1_5\gamma^2_5. \tag{4}$$

In terms of the Fermi invariants the interaction takes the form

$$V_{NN} = \bar{u}(p'_1)\bar{u}(p'_2)[v^+_j + v^-_j \, \boldsymbol{\tau}^1 \cdot \boldsymbol{\tau}^2] \, F_j \, u(p_1)u(p_2), \tag{5}$$

where the F_j, $j = 1...5$ represent the Fermi invariants in the order S, V, T, A, P.

The linear relation between the spin operators $\tilde{\Omega}_j$ and the Fermi invariants F_j is given (to order $1/m_N^2$) in ref. [4]. Since the nucleon mass $m_N \sim \mathcal{O}(N_C)$, only the leading terms in $1/m_N^2$ are needed for the present large-N_C limit considerations.

The N_C dependence of the components of the potential (1) may be inferred directly by quark model considerations. Consider the single quark operators $1, \sigma_j, \tau_k, \sigma_j\tau_k$. Matrix elements of the sum over N_C such quark operators in nucleon states then depend on N_C as follows [11]:

$$\langle N| \sum_{q=1}^{N_C} 1^q |N\rangle \sim N_C\,, \quad \langle N| \sum_{q=1}^{N_C} \sigma^q_j |N\rangle \sim N_C^0\,,$$
$$\langle N| \sum_{q=1}^{N_C} \tau^q_k |N\rangle \sim N_C^0\,, \quad \langle N| \sum_{q=1}^{N_C} \sigma^q_j\tau^q_k |N\rangle \sim N_C\,. \tag{6}$$

In the large-N_C limit the baryon-baryon interaction may be interpreted as meson exchange, since the gluon lines may be replaced by $q\bar{q}$ lines in all surviving (planar gluon) diagrams. The meson-baryon couplings are proportional to the quark operator matrix elements above and inversely proportional to the meson decay constants f_M, which scale like $\sqrt{N_C}$ [1]. Application of the scaling relations (6) and multiplication by $1/f_M^2$ to the two-nucleon system directly implies that

$$\tilde{v}^+_C\tilde{\Omega}_C, \quad \tilde{v}^-_T\tilde{\Omega}_T, \quad \tilde{v}^-_{SS}\tilde{\Omega}_{SS} \quad \sim \quad \mathcal{O}(N_C),$$
$$\tilde{v}^-_C\tilde{\Omega}_C, \quad \tilde{v}^+_T\Omega_T, \quad \tilde{v}^+_{SS}\tilde{\Omega}_{SS} \quad \sim \quad \mathcal{O}(1/N_C). \tag{7}$$

The order in N_C of the spin-orbit interaction may be found by noting that the momentum operator $\boldsymbol{P}$ in the spin-orbit interaction operator always appears in the combination $\boldsymbol{P}/m_N$, where $m_N \sim N_C$. The isospin-independent term $\tilde{v}^+_{LS}\tilde{\Omega}_{LS}$ contains the spin operator of one nucleon in combination with $\boldsymbol{P}/m_N$, and therefore the vertex scales as $1/N_C$. If the quark coupling at the other nucleon line is $\sim 1^q$, it follows that $\tilde{v}^+_{LS}\tilde{\Omega}_{LS} \sim \mathcal{O}(1/N_C)$ once the overall factor $1/f_M^2$ is taken into account. For the isospin-dependent spin-orbit interaction the scaling factor or the vertex with a spin operator multiplying $\boldsymbol{P}/m_N$ and an isospin operator is N_C^0. In this case the vertex at the other nucleon line also contains an isospin factor, so it also scales as N_C^0. Thus, it follows that $\tilde{v}^-_{LS}\tilde{\Omega}_{LS} \sim \mathcal{O}(1/N_C)$. The N_C scaling of the isospin independent quadratic spin-orbit interaction may be obtained by a direct extension of these arguments.

Table 1. Order of the leading term in the $1/N_C$ expansion of the Fermi invariant potential components.

Isospin	S	V	T	A	P
1	N_C	N_C	$1/N_C$	$1/N_C$	N_C
$\boldsymbol{\tau}^1 \cdot \boldsymbol{\tau}^2$	N_C	N_C	N_C	N_C	N_C^3

When the interaction is re-expressed in terms of Fermi invariant potential components $v^\pm_j$ as in ref. [4], with retention of only the leading terms in $1/m_N^2$ (*i.e.* in $1/N_C^2$) the order in $1/N_C$ of the terms is given in table 1 [5].

2.2 Dynamical interpretation of the potential components

The only isospin-independent potential components that are of order N_C are the scalar and vector components v^+_S and v^+_V as well as the pseudoscalar component v^+_P. The first one of these corresponds to the largest component in the two-pion exchange interaction between nucleons [12,13], which commonly is modeled in terms of a scalar ("σ") meson exchange mechanism [14,15]. The second corresponds to the short-range repulsion between nucleons, and is commonly modeled in terms of a ω meson exchange interaction, with an overstrength effective ω nucleon coupling constant [15]. The last (pseudoscalar) term, which may be interpreted as η meson exchange is large in the earlier potential models, but very small in the most recent models.

Among the isospin-dependent Fermi invariant potential components in table 1 the pseudoscalar component is of order N_C^3 and are thus the largest of all terms in the $1/N_C$ counting scheme. This strong pseudoscalar exchange component v^-_P is immediately interpretable in terms of the long-range pion exchange interaction between nucleons, which is expectedly "strong", because of its long range.

That the other isospin-dependent Fermi invariant potential components are of order N_C also corresponds to established nucleon-nucleon phenomenology. To see this, it is worth noting that an isospin 1 vector meson (ρ) exchange interaction may be expressed in terms of Fermi invariants as follows [16]:

$$\left(\gamma^1_\mu - \frac{\kappa}{2m_N}\sigma^1_{\mu\nu}\,k_\nu\right)\left(\gamma^2_\mu + \frac{\kappa}{2m_N}\sigma^2_{\mu\alpha}\,k_\alpha\right) = \frac{\kappa}{m_N^2}P^1_\mu P^2_\mu S$$
$$+(1+\kappa)V - \frac{\kappa(1+\kappa)k^2}{4m_N^2}T + \frac{\kappa(1+\kappa)}{m_N^2}P^1_\mu P^2_\mu P. \tag{8}$$

Phenomenological boson exchange interaction models typically contain a ρ-meson exchange interaction, where the "effective" tensor coupling of the ρ-meson to nuclei is

large $\kappa \sim 7$ [15]. Because of the large tensor coupling, such an isospin-dependent vector meson exchange interaction contributes strongly to all the Fermi invariant potential components, except the axial vector invariant. The order N_C of the potential components v_S^-, v_V^-, v_T^- thus may be interpreted in terms of a strong ρ-meson exchange interaction.

While the isospin-dependent pseudoscalar potential $v_P^- P$ is of order N_C^3, the corresponding isospin-independent potential $v_P^+ P$ is only of order N_C. This corresponds to the phenomenological finding in boson exchange models for the nucleon-nucleon interaction that the η-meson exchange term is much weaker than the π-meson exchange interaction component.

3 Large-N_C components of phenomenological interaction models

The simplest numerical estimates of the potential components are their volume integrals. These are given in table 2 for the 4 considered interaction models. In the case of the V18 potential, the operator form of which contains a quadratic spin-orbit interaction of the form $(\boldsymbol{L}\cdot\boldsymbol{S})^2$, we employ the relation

$$(\boldsymbol{L}\cdot\boldsymbol{S})^2 = 2\boldsymbol{L}^2 + 2\tilde{\Omega}_{LS2} - 2\tilde{\Omega}_{LS} \tag{9}$$

to reduce the interaction to the standard form (1) in combination with terms of the form $\boldsymbol{L}^2$.

In the case of the isospin-independent scalar interaction these volume integrals are all of the order 10 fm^2, ranging from $-6.3\,\mathrm{fm}^2$ for the Paris potential to -13.5 for the CD-Bonn potential.

If the isospin-independent scalar potential component is interpreted as due to a single scalar meson exchange interaction, the volume integral would equal $-g_S^2/m_S^2$, where g_S is the scalar meson-nucleon coupling constant, and m_S the scalar meson mass. If m_S is taken to be 600 MeV the value of the effective scalar meson coupling constant for these interactions range between 7.6 and 11.2 (table 3). It is striking how closely similar values obtain for the "effective" scalar meson coupling constants with the 4 different interaction models, two of which do not contain any scalar-meson–like term in their parametrized forms.

In a meson exchange interpretation the isospin-dependent scalar interaction arises from exchange of the $a_0(980)$ meson. The volume integrals of these interactions should equal $-g_{a_0}^2/m_{a_0}^2$, where g_{a_0} is the $a_0(980)$-nucleon coupling constant and m_{a_0} is the mass of the $a_0(980)$. If the value of the "effective" $a_0(980)$-nucleon coupling constant is extracted from these volume integrals, the values range from $g_{a_0} = 9.0$ to $g_{a_0} = 10.4$ (table 3).

The isospin-independent vector interaction admits an interpretation in terms of a repulsive ω-meson exchange interaction. The shape of this interaction component is very similar for all the interactions considered, and the volume integrals are also remarkably similar, ranging from 8.7 to 11.6 fm^2. If the "effective" ω-nucleon coupling constant is extracted from the volume integrals, by setting them equal to g_ω^2/m_ω^2 the values range between 11.7 and 13.5.

Table 2. Volume integrals (in fm^2) of the leading terms in the $1/N_C$ expansion of the Fermi invariant potential components phenomenological interaction models.

Component	V18	CD-Bonn	Nijmegen (93)	Paris
v_S^+	−8.7	−13.5	−10.3	−6.3
v_S^-	−3.2	−3.3	−3.3	−4.4
v_V^+	9.4	11.6	8.7	10.2
v_V^-	3.2	3.2	2.9	4.4
v_T^+	−0.1	0.0	0.0001	0.03
v_T^-	0.6	0.1	0.001	0.46
v_A^+	−0.1	0	0	0.03
v_A^-	0.6	0	0	0.46
v_P^+	9.8	0.0	0.35	18.0
v_P^-	360	338	323	352

Table 3. Effective meson-nucleon coupling values that correspond to phenomenological interaction models.

Component	V18	CD-Bonn	Nijmegen (93)	Paris
g_σ	9.0	11.2	9.8	7.6
g_{a_0}	9.0	9.0	9.0	10.4
g_ω	12.2	13.5	11.7	12.7
κ_ρ	7.0	7.0	6.3	10.1
g_η	8.7	0.0	1.8	11.7
g_π	13.4	13.0	12.7	13.2

The isospin-dependent vector interaction, by eq. (8), admits an interpretation in terms of ρ-meson exchange. This interaction component is roughly 3 times weaker than the corresponding isospin-independent interaction. The volume integrals of the isospin-dependent vector interaction range from 2.9 to 4.4 fm^2 for the 4 phenomenological interactions considered here. In a simple ρ-meson exchange model these volume integrals equal $(1+\kappa)g_\rho^2/m_\rho^2$, where g_ρ and κ are the vector and tensor ρ-nucleon coupling constants. The canonical value for the ρ-nucleon vector coupling constant is $g_\rho^2/4\pi \sim 0.5$. If this value for g_ρ is used in the expression for the volume integral, an "effective" value for κ_ρ can be determined. The volume integrals in table 2 for the 4 interaction models then give values for κ_ρ in the range 6.3–10.1, in agreement with the early finding that $\kappa_\rho \sim 6.6$ [17].

In a meson exchange model the tensor potential arises from vector meson exchange when the vector mesons couple to the nucleon with a Pauli (tensor) coupling. As in the CD-Bonn interaction model the isospin-independent ω-meson exchange interaction has no Pauli coupling term, v_T^+ vanishes in this interaction model.

By the N_C counting rules in table 1 the isospin-independent tensor interaction should be smaller by $1/N_C^2$ than the isospin-dependent tensor interaction.

Comparison of the corresponding set of volume integrals in table 2 shows that the phenomenological interaction models considered here satisfy this rule well.

The order N_C of the isospin-dependent tensor interaction alone does not explain why this interaction is one order of magnitude smaller than the corresponding vector interactions for all the phenomenological potential models. For boson exchange models the reason is readily seen in eq. (8), which shows that the tensor coupled vector meson exchange interaction is suppressed by an overall factor $1/m_N^2$, which is only partially counteracted by the large tensor coupling κ_ρ. For the phenomenological interaction models the reason for the weakness of the isospin-dependent tensor interaction is to be found in the fact that pion exchange gives rise to the bulk of the isospin-dependent spin-spin and vector interactions, and this pion (or pseudoscalar) exchange contribution is exactly cancelled in the combination of v_{SS}^- and v_T^-. This latter argument may also be extended to the isospin-independent tensor interaction, where the pseudoscalar —in this case the η-meson— exchange contribution cancels in the combination of v_{SS}^+ and v_T^+.

In single-meson exchange models only axial vector meson exchange gives rise to an axial vector interaction. Since the CD-Bonn and the Nijmegen (93) boson exchange interaction models do not contain any a_1-meson exchange terms, these interaction models have no axial vector exchange components. The phenomenological V18 and Paris potential models give rise to small A interaction components. These satisfy the N_C counting rules in table 1, by which the isospin-dependent axial vector interaction should be larger by N_C^2 than the isospin-independent one as seen in table 2.

In a single-meson exchange interpretation the longest-range mechanism that contributes to the isospin-independent pseudoscalar interaction, is η-meson exchange. This interaction component is not well constrained by nucleon-nucleon scattering data. As a consequence the phenomenological interaction models considered here give widely different results for this interaction component.

The η-nucleon coupling constant is not well known. An estimate for this coupling constant may be obtained from the volume integrals of the phenomenological interaction models if these are set to equal g_η^2/m_η^2. From the volume integral values listed in table 2 one then obtains values for g_η, which range from 1.8 (Nijmegen (93)) to 11.7 (Paris) (table 3). Analyses of observables, other than nucleon-nucleon scattering as, *e.g.*, η-meson photoproduction suggest that the coupling constant value should not exceed 2.2 [18].

The isospin-dependent pseudoscalar exchange interaction is strong and has long range. Its main component is the long-range pion exchange interaction, which is built into all the phenomenological interaction models considered here. Because of this all the interaction models converge for nucleon separations larger than 1 fm. This interaction component is also the strongest component by N_C counting, as it scales as N_C^3 (table 1). The volume integrals of this interaction component are listed in table 2 for the 4 interaction models considered, and range from 323 fm^2 to 360 fm^2. The corresponding values for the pseudoscalar pion-nucleon coupling constant g_π range from 12.7 to 13.4, when extracted by equating the numerically determined volume integrals with g_π^2/m_π^2 (table 3).

4 Exchange currents in the large-N_C limit

The scaling rules (6) may be applied to give the large-N_C scaling behavior of both the single-nucleon current operators as well as of the exchange currents that are associated with the interaction (1) [5]. As an example the axial current and charge operators of a single nucleon,

$$\boldsymbol{A}_\pm = -g_A \boldsymbol{\sigma}\tau_\pm, \quad A_\pm^0 = -g_A \frac{\boldsymbol{\sigma}\cdot\boldsymbol{p}}{m_N}\tau_\pm, \tag{10}$$

are of order N_C^1 and N_C^0, respectively.

There is no axial exchange charge operator that would be directly proportional to the pseudoscalar invariant potential component. There is, however, an axial exchange charge operator, which is of order N_C^0, and which arises from the long-range pion exchange interaction, which gives rise to the bulk of the pseudoscalar interaction component. This axial charge operator was derived in ref. [19], and has the form

$$A_\pm^0(\pi) = \frac{g_A}{4\pi}\left(\frac{m_\pi}{2f_\pi}\right)^2 \boldsymbol{\Sigma}_{12}\cdot\boldsymbol{r}_{12}(\boldsymbol{\tau}^1\times\boldsymbol{\tau}^2)_\pm \times\left(1+\frac{1}{m_\pi r_{12}}\right)\frac{e^{-m_\pi r_{12}}}{m_\pi r_{12}}, \tag{11}$$

where $\boldsymbol{\Sigma}_{12} = \boldsymbol{\sigma}^1 + \boldsymbol{\sigma}^2$. Because the pion decay constant $f_\pi \sim \sqrt{N_C}$ in the large-N_C limit, it is readily seen by the relations (6) that this operator is of order N_C^0.

The contributions of the two-nucleon exchange current terms to the axial charge operator are conventionally expressed in the form of an effective single-nucleon axial charge operator. The exchange current contributions then represent nuclear enhancement factors of the single-nucleon axial charge operator (10). Experimental studies of first-forbidden nuclear β-transitions reveal that this enhancement factor runs from about 1.7 in light nuclei [20] to about a factor 2 in heavy nuclei [21]. About one half of this enhancement may be attributed to the pion exchange operator (11), which is natural as its order in the $1/N_C$ expansion is the same as that of the single-nucleon operator (10). The bulk of the remainder arises from the exchange current, which is associated with the isospin-independent scalar interaction [3]. While the order of this term is $1/N_C$, it gives rise to a direct term matrix element, which enhances its value relative to that of the matrix element of the pion exchange term (11), which is an "exchange term".

A complete list of the N_C dependence of the axial and electromagnetic exchange current operators that are associated with the interaction components in the Fermi representation is given in [5], along with explicit expressions for the corresponding potential components.

5 Discussion

This analysis of 4 commonly employed phenomenological nucleon-nucleon interaction models reveals that the structure of their components is completely consistent with their corresponding dependence on N_C (or $1/N_C$). For all the interaction models the isospin-dependent pseudoscalar components, which contain the long-range pion exchange interaction, have volume integrals that are larger than those of any other interaction component by more than an order of magnitude. This interaction component also scales with the largest power of N_C (N_C^3) (table 2).

The interaction components that follow the isospin-dependent pseudoscalar interaction in strength are the isospin-independent scalar and vector interactions, which scale as N_C. These interaction components are those responsible for nuclear binding (v_S^+) and short-range repulsion between nucleons (v_V^-). For distances shorter than 0.4 fm the variation in form of these interaction components between the 4 considered phenomenological interaction models is substantial [5].

Next in strength are the isospin-dependent scalar and vector interactions, which also scale as N_C. The volume integrals of these interaction components are about half as large as those of the corresponding isospin-independent interactions.

The tensor and axial vector interaction components are very weak for all the considered phenomenological interaction models. For the isospin-independent tensor and axial vector components this is completely consistent with their N_C dependence, which is $1/N_C$. The smallness of the isospin-dependent tensor and axial vector exchange interaction components cannot be explained by their N_C dependence alone, as they scale as N_C. In meson exchange models the smallness of v_T^- is however natural, as it arises from tensor coupled vector mesons, and contains an overall factor $1/m_N^2$ (8).

The least well-understood interaction component is the isospin-independent pseudoscalar interaction. This component, which scales as N_C^1, is vanishingly small in two of the considered phenomenological interactions and even stronger than v_V^+ in the other two. The longest-range part of this interaction component arises from η-meson exchange. The large variation between the phenomenological interaction models for this interaction component reflects the continuing uncertainty concerning the strength of the η-nucleon coupling.

Research supported in part by the Academy of Finland by grant 54038.

References

1. E. Jenkins, Ann. Rev. Nucl. Sci. **48**, 41 (1999).
2. D.B. Kaplan, A.V. Manohar, Phys. Rev. C **56**, 76 (1997).
3. M. Kirchbach, D.O. Riska, K. Tsushima, Nucl. Phys. A **542**, 616 (1992).
4. K. Tsushima, D.O. Riska, P.G. Blunden, Nucl. Phys. A **559**, 543 (1993).
5. D.O. Riska, eprint nucl-th/0204016
6. R.B. Wiringa, V.G.J. Stoks, R. Schiavilla, Phys. Rev. C **51**, 38 (1995).
7. R. Machleidt, Phys. Rev. C **63**, 024001 (2001).
8. V.G.J. Stoks *et al.*, Phys. Rev. C **49**, 2950 (1994).
9. M. Lacombe *et al.*, Phys. Rev. C **21**, 861 (1980).
10. M.L. Goldberger *et al.*, Phys. Rev. **120**, 2250 (1960).
11. A. Wirzba, M. Kirchbach, D.O. Riska, J. Phys. G **20**, 1583 (1994).
12. M.H. Partovi, E.L. Lomon, Phys. Rev. Lett. **22**, 438 (1969).
13. M. Chemtob, J.W. Durso, D.O. Riska, Nucl. Phys. B **38**, 141 (1972).
14. D.O. Riska, G.E. Brown, Nucl. Phys. A **53**, 8 (1970).
15. R. Machleidt, K. Holinde, Ch. Elster, Phys. Rep. **149**, 1 (1987).
16. P.G. Blunden, D.O. Riska, Nucl. Phys. A **536**, 697 (1992).
17. G. Höhler *et al.*, Nucl. Phys. B **144**, 505 (1976).
18. L. Tiator, C. Bennhold, S.S. Kamalov, Nucl. Phys. A **580**, 455 (1994).
19. K. Kubodera, J. Delorme, M. Rho, Phys. Rev. Lett. **40**, 755 (1978).
20. T. Minamisono *et al.*, Phys. Rev. C **65**, 015209 (2002).
21. E.K. Warburton, Phys. Rev. Lett. **66**, 1823 (1991).

Eur. Phys. J. A **18**, 207–209 (2003)
DOI 10.1140/epja/i2002-10308-1

THE EUROPEAN PHYSICAL JOURNAL A

Polarization observables in high-energy deuteron photodisintegration within the Quark-Gluon Strings Model

V.Yu. Grishina[1,a], L.A. Kondratyuk[2,3], W. Cassing[4], E. De Sanctis[5], M. Mirazita[5], F. Ronchetti[5], and P. Rossi[5]

[1] Institute for Nuclear Research, 60th October Anniversary Prospect 7A, 117312 Moscow, Russia
[2] Institute for Theoretical and Experimental Physics, B. Cheremushkinskaya 25, 117259 Moscow, Russia
[3] IKP, Forschungszentrum Jülich, D-52425 Jülich, Germany
[4] Institute for Theoretical Physics, University of Giessen, Heinrich-Buff-Ring 16, D-35392 Giessen, Germany
[5] Frascati National Laboratories, INFN, CP 13, via E. Fermi, 40; I-00044, Frascati, Italy

Received: 30 September 2002 /
Published online: 22 October 2003 – © Società Italiana di Fisica / Springer-Verlag 2003

Abstract. Deuteron two-body photodisintegration is analysed within the framework of the Quark-Gluon Strings Model. The model describes fairly well the recent experimental data from TJNAF in the few GeV region. Angular distributions at different γ-energies are presented and the effect of a forward-backward asymmetry is discussed. New results from the QGSM for polarization observables from 1.5–6 GeV are presented and compared with the available data.

PACS. 13.40.-f Electromagnetic processes and properties – 25.20.-x Photonuclear reactions

In a recent paper [1] we have investigated high-energy deuteron photodisintegration within the framework of the Quark-Gluon Strings Model (QGSM). The QGSM —proposed by Kaidalov [2]— is based on two ingredients: i) a topological expansion in QCD and ii) a space-time picture of the interactions between hadrons that takes into account the confinement of quarks. In a more general sense the QGSM can be considered as a microscopic (nonperturbative) model of Regge phenomenology for the analysis of exclusive and inclusive hadron-hadron and photo-hadron reactions on the quark level. Within the QGSM the deuteron photodisintegration amplitude $T(\gamma d \to pn)$ can be described in first approximation by the planar graph with three-valence-quark exchange in t (or u) channels, which corresponds to a nucleon Regge trajectory. The intermediate s channel will consist of a $6q$ string (or color tube) with $1q$ and $5q$ states at the ends. Assuming that all the intermediate quark clusters have minimal spins and the s channel helicities in the quark-hadron and hadron-quark transition amplitudes are conserved, we can reconstruct the spin structure of the amplitude $T(\gamma d \to pn)$ as [1]

$$\langle p_3, \lambda_p; p_4, \lambda_n | \hat{T}(s,t) | p_2, \lambda_d; p_1, \lambda_\gamma \rangle = \bar{u}_{\lambda_p}(p_3) \hat{\epsilon}_{\lambda_\gamma} \left(A(s,t)\hat{p}_3 + B(s,t)m \right) \hat{\epsilon}_{\lambda_d} v_{\lambda_n}(p_4) \,. \quad (1)$$

The ratio $R = B(s,t)/A(s,t)$ is fixed by the model to the interval $R = 1$–2; calculations will be presented for the limiting values $R = 1$ and $R = 2$ (see below).

In ref. [1] we have analyzed deuteron photodisintegration within the framework of the QGSM employing nonlinear Regge trajectories. Parameters have been fixed by a previous analysis of pp data (*i.e.* the reaction $pp \to d\pi^+$) and the TJNAF data at $\Theta_{\text{c.m.}} = 36°$. We have found that the QGSM provides a reasonable description of all new TJNAF data [3–6] on deuteron photodisintegration at large momentum transfer t and that the energy dependence of $\mathrm{d}\sigma/\mathrm{d}t$ at $\Theta_{\text{c.m.}} = 36$–$90°$ gives new evidence for a nonlinearity of the Regge trajectory $\alpha_N(t)$. The best agreement with the data can be achieved using the —QCD motivated— logarithmic form of the Regge trajectory [1],

$$\alpha_N(t) = \alpha_N(0) - (\gamma\nu)\ln(1 - t/T_B). \quad (2)$$

Evidently the QGSM predicts that $\mathrm{d}\sigma/\mathrm{d}t$ at fixed c.m. angles will decrease faster than any finite power of s and at sufficiently large energies the perturbative regime will become dominant. Therefore, it is very important to have new data at larger energies to further check the energy behaviour of $\mathrm{d}\sigma/\mathrm{d}t$ as obtained from the QGSM.

We have also investigated the angular dependence of the cross-section at different energies. In fig. 1 we present the angular dependence of $\mathrm{d}\sigma/\mathrm{d}t \cdot s^{11}$ at two energies ($E_\gamma = 1.6$ and 3.98 GeV) for the logarithmic Regge trajectory (2). The two dashed curves have been calculated assuming isovector photon dominance [1]. In this case we

[a] e-mail: Grishina@heron.itep.ru

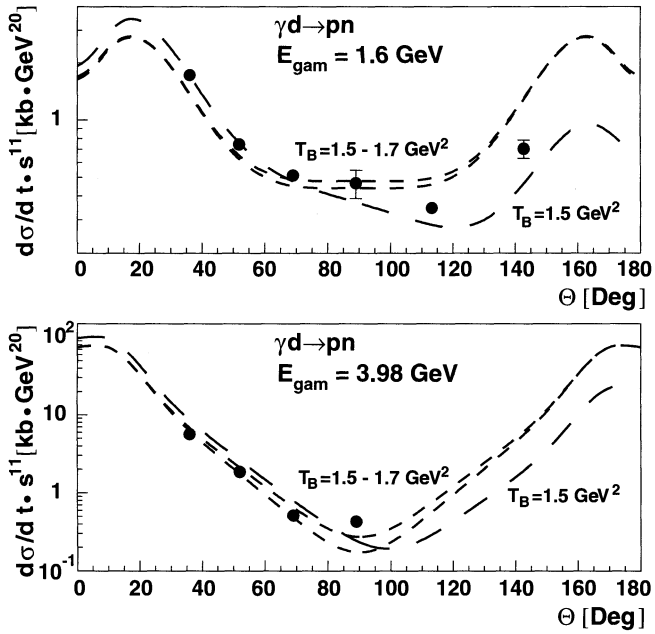

Fig. 1. Differential cross-section for the reaction $\gamma d \to pn$ (multiplied by s^{11}) as a function of the c.m. angle for E_γ = 1.6 GeV and 3.98 GeV [1]. The experimental data are from ref. [6]. The dashed curves are calculated within the QGSM with logarithmic Regge trajectories (2) using $T_B = 1.5$ and 1.7 GeV^2 (cf. [1]). The long-dashed curve presents the result of calculations which take into account the interference of the isoscalar and isovector parts of the $\gamma d \to pn$ amplitude (see text).

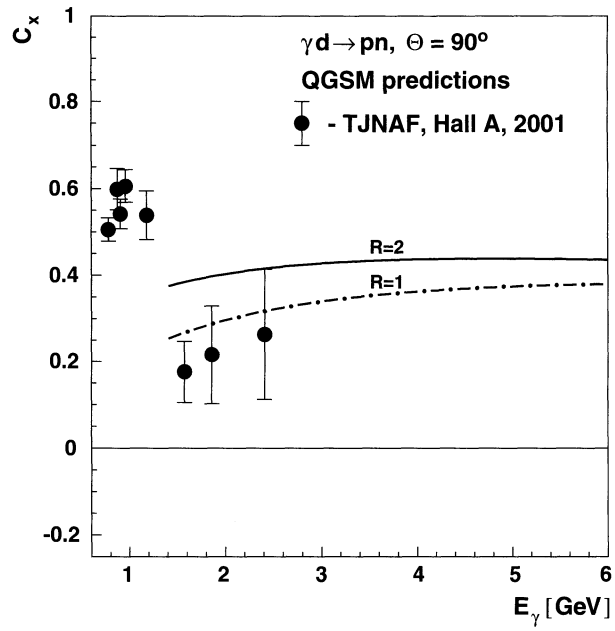

Fig. 2. Polarization transfer C_x for circularly polarized photons. The solid and dash-dotted curves correspond to $R = 2$ and 1, respectively. The experimental data are from [7] and have been corrected for spin rotation due to the lab.-c.m. transformation.

get a forward-backward symmetry of the differential cross-section. At 1.6 GeV the calculated angular distribution has a dip for $\Theta_{\rm c.m.} = 0°$ and 180° which is related to the choice of the ratio $R = 2$. This dip is absent for $R = 1$. The long-dashed curves in fig. 1 take into account the forward-backward asymmetry as discussed below.

We recall, that a forward-backward asymmetry arises from the interference of two amplitudes which describe the contribution of isovector (ρ like) and isoscalar (ω like) photons. In this case, the differential cross-section can be written as

$$\frac{{\rm d}\sigma^{\rho+\omega}_{\gamma d\to pn}}{{\rm d}t} = \frac{1}{64\,\pi s}\,\frac{1}{(p^{\rm c.m.}_\gamma)^2}\,\left|\langle\lambda_p;\lambda_n\left|\hat{T}^\rho(s,t)+\hat{T}^\omega(s,t)\right|\lambda_d;\lambda_\gamma\rangle - \langle\lambda_p;\lambda_n\left|\hat{T}^\rho(s,t)-\hat{T}^\omega(s,t)\right|\lambda_d;\lambda_\gamma\rangle\right|^2. \quad (3)$$

Using the Vector Dominance Model (VDM) we adopt

$$\hat{T}^\omega(s,t) = \hat{T}^\rho(s,t)/\sqrt{8}, \quad \hat{T}^\omega(s,u) = \hat{T}^\rho(s,u)/\sqrt{8}. \quad (4)$$

The data in fig. 1 at 1.6 GeV provide evidence for a forward-backward asymmetry because the differential cross-section at backward angles is smaller than for the corresponding angles in the forward region. The predictions of the QGSM model with ρ-ω interference are in qualitative agreement with the published data [6] (long-dashed lines). They are also in good agreement with the new preliminary data from the CLASS Collaboration at TJNAF [4,5].

Complementary information to the differential cross-sections is provided by polarization observables that should give important tests of nonperturbative calculations in the intermediate-energy regime. Data for recoil polarizations have been published recently [7]. Existing Meson-Baryon Models (MBM) fail to describe the data for the induced polarizations, which are surprisingly small for energies above about 1 GeV. Moreover, the polarization transfer data are inconsistent with hadron helicity conservation (HHC), which is generally expected for PQCD.

We present here the polarization observables as calculated within the QGSM. For the definitions of these observables in terms of helicity amplitudes we refer the reader to ref. [8]. We find that

i) the induced polarization P_y vanishes at $\Theta_{\rm c.m.} = 90°$, but is different from 0 for $\Theta_{\rm c.m.} \neq 90°$;
ii) the polarization transfers C_x and C_z for circularly polarized photons do not vanish at $\Theta_{\rm c.m.} = 90°$: $C_x \simeq$ 0.25–0.35 (fig. 2) and $C_z \simeq -0.1 \div -0.2$ at 1.5–2.5 GeV (fig. 3) ;
iii) the polarized photon asymmetry Σ is about 0.7 at $\Theta_{\rm c.m.} = 90°$ and $E_\gamma = 1.5$ GeV (fig. 4) and drops smoothly with E_γ.

We observe that for $E_\gamma \geq 1.5$ GeV the calculated values of C_x and C_z are in agreement with the new TJNAF data. We note that the term $\sim B(s,t)$ in (1) violates chirality; consequently our results for C_x and C_z are different from HHC prediction ($C_x = C_z = 0$), which is an essential property of PQCD. According to Brodsky and Hiller [9]

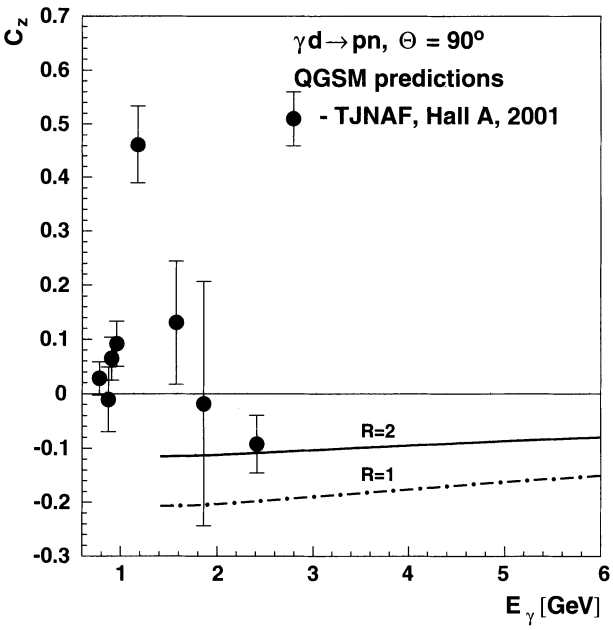

Fig. 3. Polarization transfer C_z for circularly polarized photons. The solid and dash-dotted curves correspond to $R = 2$ and 1, respectively. The experimental data are taken from [7] and have been corrected for spin rotation due to the lab.-c.m. transformation.

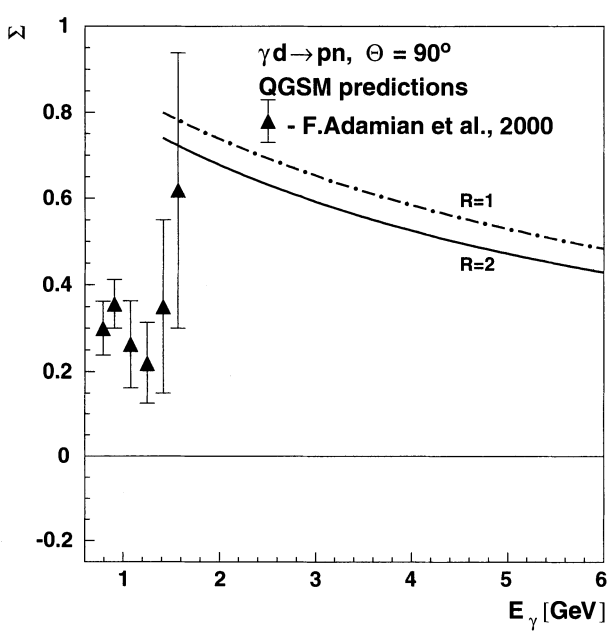

Fig. 4. The asymmetry $\Sigma(90°)$ for linearly polarized photons as a function of the photon energy. The solid and dash-dotted curves correspond to $R = 2$ and 1, respectively. The experimental data are from [10].

we should have $\lambda_d = \lambda_p + \lambda_n$ within PQCD independently of λ_γ. Assuming that —in the scaling limit— the transversedeuteron helicities are suppressed, as compared to the longitudinal ones, the asymmetry for linearly polarized photons

$$\Sigma(\theta) = (\mathrm{d}\sigma_{||} - \mathrm{d}\sigma_T)/(\mathrm{d}\sigma_{||} + \mathrm{d}\sigma_T) \tag{5}$$

should at 90° approach the value [11]:

$$\Sigma \simeq -2\mathrm{Re}(T^{10}_{+-}T^{10*}_{-+})/(|T^{10}_{+-}|^2 + |(T^{10}_{-+}|^2). \tag{6}$$

Nagornyi *et al.* [11] predicted —using the axial symmetry $T^{10}_{+-}(90°) = T^{10}_{-+}(90°)$— that $\Sigma(90°)$ should approach –1. We note, however, that the condition $T^{10}_{+-}(90°) = T^{10}_{-+}(90°)$ is valid only for "isoscalar" photons, where the isospin function is antisymmetric. But, in case of "isovector" photons, the isospin function is symmetric and, due to the Pauli principle, we have $T^{10}_{+-}(90°) = -T^{10}_{-+}(90°)$. Furthermore, according to the VDM, the isovector photon couples to hadrons more strongly that the isoscalar photon. Thus, one expects that in case of HHC the polarization $\Sigma(90°)$ should not be very different from +1.

As seen from fig. 4 the QGSM predicts a slow decrease of $\Sigma(90°)$ with photon energy from 0.7–0.8 at 1.5 GeV to 0.4–0.5 at 5–6 GeV. For photon energies below 1.5 GeV the polarizations C_x and C_z show quasi-resonance structures at $\sqrt{s} = 2.7$ GeV and $\sqrt{s} = 2.9$ GeV, respectively. Such resonance structures are conceptually out of the range of the QGSM. It is interesting to note that there are similar structures at exactly the same $\sqrt{s}$ in $\Delta\sigma_L$ for elastic *pp* scattering [12]. We speculate that these quasi-resonance structures might be related to the thresholds ρNN and $\rho N\Delta$.

In summarizing this contribution we have presented angular distributions at different γ-energies (1.68 GeV and 3.98 GeV) for deuteron photodisintegration within the QGSM and discussed the effect of a forward-backward asymmetry. In addition to ref. [1] new results from the QGSM for polarization observables from 1.5–6 GeV (cf. figs. 2–4) have been calculated and compared to the available data.

We are grateful to Ronald Gilman for sending us the experimental data on the polarizations C_x and C_z corrected for spin rotation due to the lab.-c.m. transformation. This work is supported by DFG, RFFI and Forschungszentrum Jülich.

References

1. V.Yu. Grishina *et al.*, Eur. Phys. J. A **10**, 355 (2001).
2. A.B. Kaidalov, Z. Phys. C **12**, 63 (2001).
3. E.C. Schulte *et al.*, Phys. Rev. Lett. **87**, 102302-1 (2002).
4. M. Mirazita, *Proceedings of the XL International Winter Meeting on Nuclear Physics, Bormio, January 21-26, 2002*; hep-ph/0206213.
5. F. Ronchetti, this issue, p. 409.
6. C. Bochna *et al.*, Phys. Rev. Lett. **81**, 4576 (1998).
7. K. Wijesooriya *et al.*, Phys. Rev. Lett. **86**, 2975 (2001).
8. V.P. Barannik *et al.*, Nucl. Phys. A **451**, 751 (1986).
9. S.J. Brodsky, J.R. Hiller, Phys. Rev. C **28**, 475 (1983).
10. F. Adamian *et al.*, Eur. Phys. J. A **8**, 423 (2000).
11. S.I. Nagornyi, Yu. A. Kasatkin, I.K. Kirichenko, Sov. J. Nucl. Phys. **55**, 189 (1992).
12. I.P. Auer *et al.*, Phys. Rev. Lett. **62**, 2649 (1989).

Eur. Phys. J. A **18**, 211–214 (2003)
DOI 10.1140/epja/i2002-10300-9

THE EUROPEAN PHYSICAL JOURNAL A

Phase diagram of the three-dimensional NJL model

C.G. Strouthos[a]

Department of Physics, University of Wales Swansea, Singleton Park, Swansea SA2 8PP, UK

Received: 30 September 2002 /
Published online: 22 October 2003 – © Società Italiana di Fisica / Springer-Verlag 2003

Abstract. With the exception of confinement the three-dimensional Nambu–Jona-Lasinio (NJL_3) model incorporates many of the essential properties of QCD. We discuss the critical properties of the model at non-zero temperature T and/or non-zero chemical potential μ. We show that the universality class of the thermal transition is that of the $d = 2$ classical spin model with the same symmetry. We provide evidence for the existence of a tricritical point in the (μ, T)-plane. We also discuss numerical results by Hands *et al.* which showed that the system is critical for $\mu > \mu_c$ and the diquark condensate is zero.

PACS. 71.10.Fd Lattice fermion models (Hubbard model, etc.) – 05.70.Fh Phase transitions: general studies

1 Introduction

Phase transitions in QCD at non-zero temperature and/or non-zero baryon density have been studied intensively over the last decade both analytically and numerically. However, since the problem of chiral symmetry breaking and its restoration is intrinsically non-perturbative, the number of available techniques is limited and most of our knowledge about the phenomenon comes from lattice simulations. Because of the complexity of QCD with dynamical fermions, studies so far have been done on lattices with modest size and in various cases the results are distorted by finite size and discretization effects.

The NJL model has been proved to be an interesting and tractable laboratory to study chiral phase transitions both numerically by means of lattice simulations and analytically in the form of large-N_f expansions [1–9]. The Lagrangian density of the $U(1)$-symmetric model is

$$\mathcal{L} = \bar{\psi}_i(\partial\!\!\!/ + m + \sigma + i\gamma_5\pi)\psi_i + \frac{N_f}{2g^2}(\sigma^2 + \pi^2), \quad (1)$$

where the index i runs over N_f fermion flavors. There are several features which make this model interesting for the modelling of strong interactions: i) The spectrum of excitations contains both "baryons" and "mesons", namely the elementary fermions f and the composite $f\bar{f}$ states [10]. ii) For sufficiently strong coupling $g^2 > g_c^2$ it exhibits spontaneous chiral symmetry breaking implying dynamical generation of a fermion mass m_f, the pion field π being the associated Goldstone boson. iii) For $2 < d < 4$ there is an interacting continuum limit at a critical value of the coupling, which for $d = 3$ has a numerical value $g_c^2/a \approx 1.0$ in the large-N_f limit if a lattice regularisation is employed [2]. There is a renormalisation group UV fixed point at $g^2 = g_c^2$, signalled by the renormalisability of the $1/N_f$ expansion [1], entirely analogous to the Wilson-Fisher fixed point in scalar field theory. iv) Numerical simulations with baryon chemical potential $\mu \neq 0$ show qualitatively correct behavior, in that the onset of matter occurs for μ of the same order as the constituent-quark scale m_f [3], rather than for $\mu \approx m_\pi/2$, which happens in gauge theory simulations with a real measure $\det(M^\dagger M)$ because of the presence of a baryonic pion in the spectrum. This makes NJL_3 an ideal arena in which to test strongly interacting thermodynamics.

In sect. 2 we discuss the universality of the $T \neq 0$ transition [4,5]. In sect. 3 we present results from a study of the phase diagram in the (μ, T)-plane [8] which support the existence of a tricritical point on the line that separates the chirally broken from the chirally symmetric phases. We also discuss numerical results which support the non-existence of a diquark condensate for $\mu > \mu_c$ [9].

2 Universality at non-zero temperature

Although there is little disagreement that the chiral phase transition in QCD with two massless fermions is second order, no quantitative work or simulations have been done that decisively determine its universality class. Universality arguments are very appealing due to their beauty and simplicity. In essence they can be phrased as follows: At finite T phase transitions, the correlation length diverges in the transition region and the long-range behavior is that

[a] e-mail: C.G.Strouthos@swansea.ac.uk

Table 1. Summary of FSS results and comparison with $2d$ Ising and mean-field scaling behavior.

Exponents	FSS	$Z(2)$	MF
ν	1.00(3)	1	0.5
β_m/ν	0.12(6)	0.125	1
γ/ν	1.66(9)	1.75	2

of the $(d-1)$ classical spin model with the same symmetry, because the IR region of the system is dominated by the zero mode of the bosonic field and the contribution of non-zero modes does not affect the critical singularities but can be absorbed into non-critical, non-universal aspects of the transition. Consequently, fermions, which satisfy anti-periodic boundary conditions, and do not have zero modes, are expected to decouple from the scalar sector. In another language, the classical thermal fluctuations whose energy is $O(K_B T)$ dominate over quantum fluctuations with energy $O(\hbar\omega)$ for soft modes of the field and the effective $(d-1)$-dimensional theory for the bosonic fields near T_c is a classical statistical theory. A possible loophole to this standard scenario is that the mesons are composite $f\bar{f}$ states and their size and density increase as $T \to T_c$. Therefore, if the transition region can be described as a system of highly overlapping composites, the violation of the bosonic character of the mesons may be maximal and the fermions become essential degrees of freedom irrespective of how heavy they are. At leading order in $1/N_f$ the model has a second-order phase transition at $T_c = \frac{m_f}{2\ln 2}$ [4] with Landau-Ginzburg mean-field scaling. We studied the critical behavior of the Z_2-symmetric model with finite N_f by performing lattice simulations in the vicinity of the critical point. The temporal lattice size was $L_t = 6$ and the spatial size varied from $L_s = 18$ to 50. The expectation value of the auxiliary sigma field ($\Sigma \equiv \langle\sigma\rangle$) serves as a convenient order parameter for the theory's critical point. We simulated the model exactly for $N_f = 12$ with the Hybrid Monte Carlo method. The staggered fermion lattice action and further details concerning the algorithm can be found in [2]. By using the finite-size scaling (FSS) method we extracted the critical exponents. The results which are summarized in table 1 support the dimensional reduction scenario, because the values of the exponents are in good agreement with those of the $2d$ Ising model rather than the mean-field theory ones.

Next we tried to understand how the large-N_f mean-field theory prediction reconciles with the dimensional reduction and universality arguments. The answer is that the large-N_f description has its applicability region. As we discuss in detail for a Yukawa theory in [5] the phenomenon which leads to an apparent contradiction is the suppression of the width of the non–mean-field critical region by a power of $1/N_f$. The $2d$ Ising critical behavior sets in when $T \gg m_\sigma(T)$ ($m_\sigma(T)$ is the thermal mass of the σ meson). If the cutoff $\Lambda \gg T$, the renormalized self-interaction coupling $\lambda(T)$ in the large-N_f limit is close to the IR fixed point of the Yukawa theory and is given by $\lambda(T) \sim T^{4-d}/N_f$ for $2 < d < 4$. The mean-field approximation breaks down because of self-inconsistency when the value of the coupling of the $(d-1)$-dimensional scalar theory $\lambda_{d-1} = T\lambda(T)$ on the scale $m_\sigma^{5-d}(T)$ (the power $d-5$ comes from dimensional analysis) is not small anymore. Therefore, for $d = 3$ the Ginzburg criterion for the applicability of the mean-field scaling is given by $m_\sigma(T) \gg T/\sqrt{N_f}$. This scenario was verified numerically in [5].

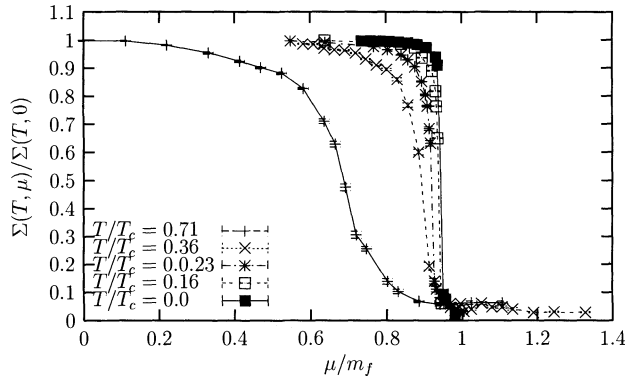

Fig. 1. $\Sigma(T,\mu)/\Sigma(T,0)$ *vs.* μ/m_f at different values of T.

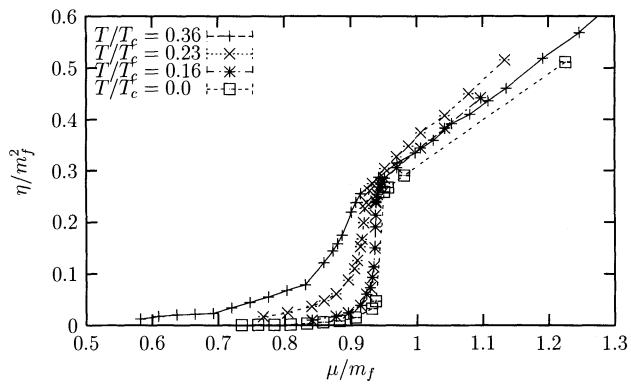

Fig. 2. $\eta(\mu)/m_f$ *vs.* μ/m_f at different values of T.

Additional evidence in favor of the dimensional reduction scenario was produced in studies of the $U(1)$-symmetric NJL$_3$ model [6]. Both analytical and numerical results showed that its phase structure at $T \neq 0$ is the same as the $2d$ XY model. It has two different chirally symmetric phases, one critical and one with finite correlation length, separated by a Berezinskii-Kosterlitz-Thouless transition.

3 Results at non-zero chemical potential

The action of the NJL model remains real even after the introduction of non-zero chemical potential μ, which means we can study the physics of the high-density regime using standard Monte Carlo techniques. In the presence of a Fermi surface with Fermi momentum p_F, the creation of $f\bar{f}$ pairs with zero net momentum is suppressed, because one can only create particles with $p > p_F$. So as the fermion number density $\eta(\mu)$ grows, the chiral symmetry breaking is suppressed. The large-N_f description of the $\mu \neq 0$ chiral phase transition predicts a first-order

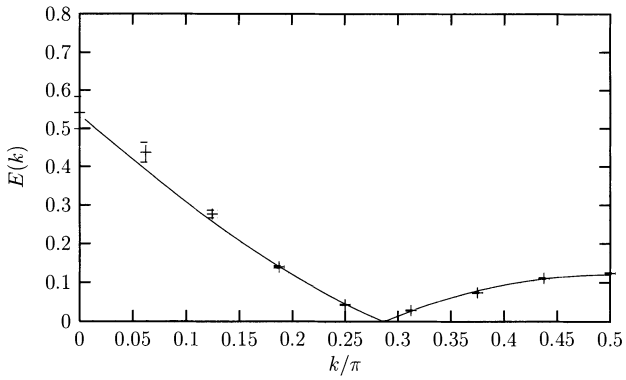

Fig. 3. Fermion dispersion relation at $\mu = 0.8$.

transition for $T = 0$ and a continuous transition for $T > 0$ [4]. Furthermore, the critical value of the chemical potential μ_c is equal to the value of the fermion mass at $\mu = 0$, which indicates that materialization of the fermion itself drives the symmetry restoration transition. Interactions as expected decrease μ_c below the mean-field result [3]. Work by Stephanov [7] suggests that any non-zero density simulation which incorporates a real path integral measure proportional to $\det(MM^\dagger)$ is doomed to failure due to the formation of a light baryonic pion from a quark q and a conjugate quark q^c. The NJL model, however, does not exhibit such a pathology, because the realization of the Goldstone mechanism in this model is fundamentally different from that in QCD. In the NJL model the Goldstone mechanism is realized by a pseudoscalar channel pole formed from disconnected diagrams and the connected diagrams yield a bound state of mass $\approx 2m_f$. This implies the absence of a light qq^c state.

As expected, our simulations of the Z_2-symmetric NJL$_3$ with $N_f = 4$ [8] did not provide any evidence for the existence of a nuclear liquid-gas transition at $\mu < \mu_c$. It was shown in [11] that in the NJL model there is no saturation density for stable matter. In order to get the saturation features the authors of [11] introduced a chirally invariant scalar-vector interaction term which cures the binding problem. Furthermore, our results showed that the second-order nature of the $T \neq 0$, $\mu = 0$ transition remains stable down to low T and large μ. In fig. 1 we plot the normalized order parameter $\Sigma(T,\mu)/\Sigma(T,0)$ as a function of μ/m_f at different values of T. It is clear from the shapes of these curves that the transition becomes sharper as we decrease the temperature. In fig. 2 we plot the normalized fermion number density as a function of the chemical potential at different values of T. In the limit $T \to 0$ we see that the fermion density is strongly suppressed before the transition and then jumps discontinuously. By performing detailed finite-size scaling analysis which allowed us to distinguish between second-order and weak first-order transitions we showed that the tricritical point lies on the section of the phase boundary defined by $T/T_c \leq 0.23$, $\mu/\mu_c \geq 0.97$ [8]. This result shows that higher-order corrections in the $1/N_f$ expansion for the nature and the location of the transition points in the phase diagram are small in this model.

It is well known that at high density the diquark condensate is non-zero in models of strongly interacting matter which either assume that the interaction between quarks is due to one-gluon exchange [12], or by using effective four-fermion vertices resulting from the presence of instantons in the QCD vacuum [13]. Unfortunately, theoretical studies of color superconductivity are limited to perturbative and self-consistent methods, because of the notorious "sign problem" in QCD. Hands *et al.* studied numerically the $(SU(2) \otimes SU(2))$-symmetric NJL$_3$ and found no evidence for a condensate $\langle qq \rangle \neq 0$ in the model's high-density phase. Their results with a non-zero diquark source are consistent with a critical behavior $\langle qq(j) \rangle \propto j^{\frac{1}{\delta}}$ throughout the dense phase with δ falling in the range 3–5 for the μ values studied. This suggests that the model is a two-dimensional superfluid as first described by Kosterlitz and Thouless for thin films of ^{4}He but with the universality class determined by the presence of massless relativistic fermions. Results for the dispersion relation $E(k)$ in the spin-$\frac{1}{2}$ sector are shown in fig. 3. For $k < k_F$ the lowest excitations vacate states in the Fermi sea, and hence are "hole-like", whereas for $k > k_F$, excitations add quarks to the system and are "particle-like". There is no sign for any discontinuity on the Fermi surface characteristic of a BCS gap $\Delta \neq 0$ in NJL$_3$. However, recent numerical results provided evidence that $\langle qq \rangle \neq 0$ in NJL$_4$ [14].

4 Summary

We discussed the basic features of the phase diagram of NJL$_3$. The universality class of the $T \neq 0$ transition is that of the $d = 2$ classical spin model with the same symmetry. The non-trivial critical region of the Z_2-symmetric model is suppressed by a factor $1/\sqrt{N_f}$. The non-zero density phase transition is strongly first order and the lattice simulations provided evidence for the existence of a tricritical point on the critical line at small T and large μ. The simulations showed no evidence for the existence of non-zero diquark condensate at $T = 0$ and $\mu > \mu_c$. The results are consistent with a critical behavior throughout the dense phase, suggesting that the model is a two-dimensional relativistic superfluid.

Support by the Leverhulme Trust is kindly acknowledged.

References

1. B. Rosenstein, B.J. Warr, S.H. Park, Phys. Rep. **205**, 59 (1991).
2. S.J. Hands, A. Kocić, J.B. Kogut, Ann. Phys. (N.Y.) **224**, 29 (1993).
3. S.J. Hands, S. Kim, J.B. Kogut, Nucl. Phys. B **442**, 364 (1995); I.M. Barbour, S.J. Hands, J.B. Kogut, M.-P. Lombardo, S.E. Morrison, Nucl. Phys. B **557**, 327 (1999).
4. K.G. Klimenko, Z. Phys. C **37**, 457 (1988); B. Rosenstein, B.J. Warr, S.H. Park, Phys. Rev. D **39**, 3088 (1989); S.J. Hands, A. Kocić, J.B. Kogut, Nucl. Phys. B **390**, 355 (1993); A. Kocić, J.B. Kogut, Nucl. Phys. B **455**, 229 (1995).

5. J.B. Kogut, M.A. Stephanov, C.G. Strouthos, Phys. Rev. D **58**, 096001 (1998).
6. E. Babaev, Phys. Lett. B **497**, 323 (2001); S.J. Hands, J.B. Kogut, C.G. Strouthos, Phys. Lett. B **515**, 407 (2001).
7. Misha A. Stephanov Phys. Rev. Lett. **76**, 4472 (1996).
8. J.B. Kogut, C.G. Strouthos, Phys. Rev. D **63**, 054502 (2001).
9. S.J. Hands, B. Lucini, S.E. Morrison, Phys. Rev. D **65**, 036004 (2002).
10. S.J. Hands, J.B. Kogut, C.G. Strouthos, Phys. Rev. D **65**, 114507 (2002); Nucl. Phys. B **645**, 321 (2002), hep-lat/0208030.
11. V. Koch, T.S. Biro, J. Kunz, U. Mosel, Phys. Lett. B **185**, 1 (1987). M. Buballa, Nucl. Phys. A **609**, 519 (1996).
12. B.C. Barrois, Nucl. Phys. B **129**, 390 (1977); D. Bailin, A. Love, Phys. Rep. **107**, 390 (1984).
13. R. Rapp, T. Schäfer, E.V. Shuryak, M. Velkovsky, Phys. Rev. Lett. **81**, 53 (1998); M. Alford, K. Rajagopal, F. Wilczek, Phys. Lett B **422**, 247 (1998).
14. S.J. Hands, D.N. Walters, Phys. Lett. B **548**, 196 (2002), hep-lat/0209140.

Eur. Phys. J. A **18**, 215–217 (2003)
DOI 10.1140/epja/i2002-10301-8

THE EUROPEAN PHYSICAL JOURNAL A

Nonperturbative contribution to the quark form factor within the instanton model

A.E. Dorokhov[1,a] and I.O. Cherednikov[1,2,b]

[1] Bogolyubov Laboratory of Theoretical Physics, Joint Institute for Nuclear Research, 141980 Dubna, Russia
[2] Institute for Theoretical Problems of Microphysics, Moscow State University, 119899 Moscow, Russia

Received: 30 September 2002 /
Published online: 22 October 2003 – © Società Italiana di Fisica / Springer-Verlag 2003

Abstract. The nonperturbative effects in the quark form factor are considered in the Wilson loop formalism, within the framework of the instanton liquid model. For the integration path corresponding to this form factor, the explicit expression for the vacuum expectation value of the Wilson operator is found to the leading order. It is shown that the instantons produce the power-like corrections to the perturbative result, which are comparable in magnitude with the perturbative part at the scale of order of the inverse average instanton size. It is demonstrated that the instanton contributions to the quark form factor are exponentiated to high orders in the small instanton density parameter.

PACS. 12.38.-t Quantum chromodynamics – 11.15.Tk Other nonperturbative techniques

In the present report, we start the investigation of the instanton-induced effects in the high-energy QCD processes by means of the Wilson integral formalism [1,2]. The basic object of study in such an approach is the gauge invariant vacuum average of the Wilson loop operator

$$W(C) = \frac{1}{N_c}\mathrm{Tr}\left\langle 0 \left| \mathcal{P}\exp\left(ig\int_C \mathrm{d}x_\mu \hat{A}_\mu(x)\right)\right| 0\right\rangle \ , \quad (1)$$

where the integration goes along the closed contour C and the gauge field $\hat{A}_\mu(x) = T^a A^a_\mu(x)$, $T^a = \frac{\lambda^a}{2}$, belongs to the Lie algebra of the gauge group $SU(N_c)$, while the Wilson loop operator $\mathcal{P}\mathrm{e}^{ig\int \mathrm{d}x A(x)}$ lies in its fundamental representation. We propose an approach which allows one to evaluate the instanton contributions to the Wilson integrals made of several (in)finite lines containing specific cusp, and/or cross singularities. For this purpose, we start with one of the simplest configurations, *i.e.*, the angle with infinite sides that corresponds to the integration path for the Wilson operator describing the soft part of the quark Sudakov form factor [3].

For brevity, we omit here the detailed discussion on the renormalization of cusp singularities, just say that it can be proven that there exists the consistent renormalization procedure for such quantities [4]. For details, see [5].

The leading nontrivial cusp-dependent term in the expansion of $W(C)$ (1) in powers of g^2 for the angle with two infinite straight-line rays contains the contributions from both perturbative and nonperturbative fields, which can be expressed in the following form:

$$W^{\mathrm{LO}}(\gamma) = -\frac{g^2 C_F}{2}\int_{C_\gamma}\mathrm{d}x_\mu \int_{C_\gamma}\mathrm{d}y_\nu\ D_{\mu\nu}(x-y)\ , \quad (2)$$

where $C_F = \frac{N_c^2-1}{2N_c}$. It is convenient to present the gauge field propagator $D_{\mu\nu}(z)$ as

$$D_{\mu\nu}(z) = \delta_{\mu\nu}\partial_z^2 d_1(z^2) - \partial_\mu\partial_\nu d_2(z^2)\ . \quad (3)$$

Here and in what follows, we use the dimensional regularization with $n = 4-2\varepsilon$, $\varepsilon < 0$ in order to control the IR-divergent terms in the integrals. The remaining UV singularity will be regularized by the corresponding UV cutoff.

The trajectories of the incoming and outgoing quarks may be parameterized as $x = v_1 s$ $(0 < s < \infty)$, $y = v_2\tau$ $(-\infty < \tau < 0)$. The angle between the vectors v_1 and v_2 is given in the Minkowski space by

$$\cosh\chi = (v_1 v_2) = \frac{(p_1 p_2)}{m^2} = 1 + \frac{Q^2}{2m^2}\ ,$$
$$-Q^2 = (p_2 - p_1)^2\ , \qquad v_{1,2}^2 = 1, \quad (4)$$

where the quark momenta are supposed to be on-shell: $p_1^2 = p_2^2 = m^2$. The continuation to the Euclidean space is defined as: $\chi \to i\gamma$ (see [6,7]). Hence we have within the one-loop accuracy

$$W(\gamma) = 1 - 4\pi\alpha_s C_F(n-2)h(\gamma)d_1(0)\ , \quad (5)$$

[a] e-mail: dorokhov@thsun1.jinr.ru
[b] e-mail: igorch@thsun1.jinr.ru

where

$$h(\gamma) = \gamma \cot\gamma - 1 \tag{6}$$

is the universal cusp factor. We should emphasize here that the expression (5) holds for the perturbative as well as for the nonperturbative part depending on the value $d_1(0)$.

Let us consider first the perturbative part $W_P^{\rm LO}(\gamma)$. The function $d_1(0)$ diverges at both upper and lower limit and then must be UV and IR regularized [5]. To this end, we may introduce the UV cutoff μ^2 and IR cutoff λ^2, and finally get the perturbative part with one-loop accuracy:

$$W_P(\gamma,\mu) = 1 - \frac{\alpha_s}{2\pi} C_F h(\gamma) \ln\frac{\mu^2}{\lambda^2} \ . \tag{7}$$

The nonperturbative contribution to $W(C)$ in the instanton model can be estimated as follows. The instanton field is given by

$$\hat{A}_\mu(x;\rho) = \frac{1}{g}\mathbf{R}^{ab}\sigma^a \eta^{\pm b}_{\ \mu\nu}(x-z_0)_\nu \varphi(x-z_0;\rho), \tag{8}$$

where $\mathbf{R}^{ab}$ is the color orientation matrix ($a,b=1,2,3$), σ^a's are the Pauli matrices, and ($\pm$) corresponds to the instanton, or anti-instanton. The averaging of the Wilson operator over the nonperturbative vacuum is reduced to the integration over the coordinate of the instanton center z_0, the color orientation and the instanton size ρ. The measure for the averaging over the instanton ensemble reads $\mathrm{d}I = \mathrm{d}\mathbf{R}\ \mathrm{d}^4 z_0\ \mathrm{d}n_\rho$, where $\mathrm{d}\mathbf{R}$ refers to the averaging over color orientation, and $\mathrm{d}n_\rho$ depends on the choice of the instanton size distribution. Taking into account (8), we write the Wilson integral (1) in *the single-instanton approximation* in the form

$$w_I(C) = \frac{1}{N_c}\langle 0|\mathrm{Tr}\exp\left(i\sigma^a\phi^a\right)|0\rangle \ , \tag{9}$$

where the phase is

$$\phi^a = \mathbf{R}^{ab}\eta^{\pm b}_{\ \mu\nu}\int_{C_\gamma}\mathrm{d}x_\mu\ (x-z_0)_\nu \varphi(x-z_0;\rho) \ . \tag{10}$$

For the sake of simplicity, in what follows we restrict ourselves to the investigation of the weak-field limit. In this limit, the leading instanton-induced term reads

$$w_I^{\rm LO}(\gamma) = -\frac{g^2\lambda^{n-4}}{2}\int \mathrm{d}n_\rho \int_{C_\gamma}\mathrm{d}x_\mu \int_{C_\gamma}\mathrm{d}y_\nu \times \int \frac{\mathrm{d}^n k}{(2\pi)^n}\ \tilde{A}^a_\mu(k;\rho)\tilde{A}^a_\nu(-k;\rho)\mathrm{e}^{-ik(x-y)} \ . \tag{11}$$

By using the Fourier transform of the instanton field $\tilde{A}^a_\mu(k;\rho)$ eq. (11) can be written in the form of eq. (3) with the instantonic analogue of the function $d_1(z^2)$: $d_1(z^2) \to d_1^I(z^2)$, where

$$d_1^I(z^2) = -\frac{1}{g^2 C_F}\int \mathrm{d}n_\rho D_I(z^2;\rho,\lambda) = -\frac{\lambda^{4-n}}{g^2 C_F}\int \mathrm{d}n_\rho \frac{\mathrm{d}^n k}{(2\pi)^n}\mathrm{e}^{-ikz}\left(2\tilde{\varphi}'(k^2;\rho)\right)^2 \ . \tag{12}$$

Above, $\tilde{\varphi}(k^2;\rho)$ is the Fourier transform of the instanton profile function $\varphi(z^2;\rho)$ and $\tilde{\varphi}'(k^2;\rho)$ is its derivative with respect to k^2. Now using the result (5) of the previous section, we get the instanton contribution in the form

$$w_I(\gamma;\varepsilon,\lambda) = (n-2)h(\gamma)\int \mathrm{d}n_\rho\ D_I(0;\varepsilon,\lambda,\rho) \ . \tag{13}$$

Consider now the renormalization of the nonperturbative part for the instanton field in the singular gauge, where the profile function is

$$\varphi(u;\rho) = \frac{\rho^2}{z^2(z^2+\rho^2)} \ . \tag{14}$$

For the complete expression for $D_I(0;\varepsilon,\lambda,\rho)$, see [5]. Applying the renormalization procedure as described in the previous section, we find in the leading order the instanton contribution to the Wilson loop:

$$w_I^{\rm LO}(\gamma,\lambda) - 1 = \pi^2 h(\gamma)\int \mathrm{d}n_\rho\ \rho^4 \ln(\rho\lambda) \ . \tag{15}$$

In order to estimate the magnitude of the instanton-induced effect we consider the distribution function which has been suggested in [8] (and discussed in [9] in the framework of the constrained instanton model) in order to describe the lattice data [10]:

$$\mathrm{d}n_\rho = \frac{\mathrm{d}\rho}{\rho^5}\ C_{N_c}\left(\frac{2\pi}{\alpha_s(\rho)}\right)^{2N_c}\mathrm{e}^{-\frac{2\pi}{\alpha_s(\rho)}}\mathrm{e}^{-2\pi\sigma\rho^2} \ , \tag{16}$$

where the numerical constant C_{N_c} is determined by the number of colours $C_{N_c} \approx 0.0015$ and the string tension is accepted to be $\sigma \approx (0.44\,\mathrm{GeV})^2$ [11,8]. Then, using the one-loop expression for the running coupling constant we find the instanton contribution (15) in the form (in the distribution (16), the slow-varying logarithmic factor due to the power of the coupling α_s is assumed to be constant, and taken at the point of the mean instanton size $\bar{\rho}$):

$$w_I^{\rm LO}(\gamma,\lambda) - 1 = \pi^2 h(\gamma)\frac{C_{N_c}\Gamma(\beta_0/2)}{4} \times \left(\frac{2\pi}{\alpha_s(\bar{\rho})}\right)^{2N_c}\left(\frac{\Lambda_{\rm QCD}}{\sqrt{2\pi\sigma}}\right)^{\beta_0}\ln\frac{\lambda^2}{2\pi\sigma} \ , \tag{17}$$

where β_0 is the first coefficient of the perturbative β-function. The expression (17) shows explicitly that the instantons yield the power-like corrections to the perturbative result, which is expected from general consideration, *e.g.*, from the renormalon analysis (see, *e.g.*, [12]).

It is instructive to express the result (17) in terms of the mean instanton size $\bar{\rho}$ and the instanton density $\bar{n}$ calculated directly from the distribution (16). To compare the instanton-induced and perturbative parts, we assume that the factorization scale μ (which divides the soft and hard regions of momenta in the factorized quark form factor) is of order of the inverse instanton size $\mu \approx \bar{\rho}^{-1} \approx 0.6\,\mathrm{GeV}$. Then we write the total leading-order

contribution to the Wilson loop expectation value in the form

$$W(\gamma,\bar{\rho},\lambda) = 1 + \frac{\alpha_s(\bar{\rho})}{2\pi} C_F h(\gamma) \ln(\bar{\rho}^2\lambda^2) \times \left(1 + K\,\frac{S_0\pi^2\bar{n}\bar{\rho}^4}{C_F}\right), \tag{18}$$

where $S_0 = \frac{8\pi^2}{g^2(\bar{\rho}^{-1})} \approx 10$ is the "classical enhancement" factor with the renormalized coupling constant $g(\mu)$ at the energy scale $\mu \approx \bar{\rho}^{-1}$, and $K \approx 0.74$. The ratio of the instanton correction to the perturbative leading term is about 0.5, what is estimated using the conventional value for the packing fraction [13] $\pi^2\bar{n}\bar{\rho}^4 \approx 0.1$. One can see using the main formula (17) that the strong power suppression of the instanton part is partially compensated by the large factor $S_0^{2N_c+1}$. This means that at the energy scale of order of $\bar{\rho}^{-1}$ the magnitude of the instanton-induced effects is comparable to the leading perturbative part, and must be taken into account as well. It is useful also to note that the two-loop–order perturbative contribution appears numerically to be of the same order as the instanton part [5]. Thus, the complete consideration of the quark form factor at the low-momentum scale must include both the two-loop perturbative part and the leading-order instanton one.

Expression (18) defines the first terms of the Wilson loop expansion in gauge fields. On the basis of the exponentiation theorem [14] for the non-Abelian path-ordered exponentials it is well known that perturbative corrections to the Sudakov form factor are exponentiated to high orders in the QCD coupling constant. Let us show briefly how the single-instanton contribution is exponentiated in the small instanton density parameter, treating the instanton vacuum as a dilute medium [15]. For details, see [5]. The gauge field is taken to be the sum of individual instanton fields in the singular gauge, (8),(14), with their centers at the points z_j's. Since the parameterization of the loop integral along rays of the angle plays the role of the proper time, a time-ordered series of instantons arises and has an effect on the Wilson loop. Then, the expression is simplified when averaging over the gauge orientations of instantons: the entire loop integral collapses to a product of traces,

$$W_I^{(n)}(\gamma) \to \lim_{n\to\infty} \prod_{j=1}^{n} w_I^{(j)}(\gamma). \tag{19}$$

Since the individual instantons are considered to be decoupled in the dilute medium, the total multiple instanton contribution to the vacuum average of the Wilson operator simply exponentiates the all-order single-instanton term $w_I(\gamma)$, and one has

$$W_I(\gamma) = \lim_{n\to\infty}\left\{1 + \frac{1}{n} w_I(\gamma)\right\}^n = \exp[w_I(\gamma)]. \tag{20}$$

To summarize, we have calculated, within the instanton vacuum model, the nonperturbative contribution to the soft part of the quark form factor, described in terms of the vacuum expectation value of the Wilson loop for the contour of a special form. We have proved that in the dilute regime, the full instanton contribution to the quark form factor is given by the exponentiated all-order single-instanton result, see (20). In the weak-field limit, the instanton contribution to the soft part of the color singlet quark form factor is found explicitly in terms of the instanton profile function in the singular gauge. It is shown that the instanton-induced effects are of a power type (17), but nevertheless they are comparable in magnitude to the perturbative ones at the scale of order of the inverse average size of the instanton in the instanton vacuum, see (18).

The authors are grateful for the fruitful discussions to D. Antonov, N.I. Kochelev, S.V. Mikhailov and S. Tafat. This work is partially supported by RFBR (nos. 02-02-16194, 01-02-16431) and INTAS (no. 00-00-366). The work of I.Ch. is supported also by the RFBR grant no. 00-15-96577.

References

1. Yu.M. Makeenko, A.A. Migdal, Phys. Lett. B **88**, 135 (1979); Nucl. Phys. B **188**, 269 (1981); A. Polyakov, *Gauge Fields and Strings* (Harwood, 1987).
2. A. Bassetto, M. Ciafaloni, G. Marchesini, Phys. Rep. **100**, 201 (1983); O. Nachtmann, Ann. Phys. (N.Y.) **209**, 436 (1991); G. Korchemsky, Phys. Lett. B **220**, 629 (1989); G. Korchemsky, G. Sterman, Nucl. Phys. B **437**, 415 (1995); G. Korchemsky, A. Radyushkin, Phys. Lett. B **279**, 359 (1992).
3. G. Korchemsky, Phys. Lett. B **217**, 330 (1989).
4. V. Dotsenko, S. Vergeles, Nucl. Phys. B **169**, 527 (1980); A. Polyakov, Nucl. Phys. B **164**, 171 (1980); R.A. Brandt, F. Neri, M.-A. Sato, Phys. Rev. D **24**, 879 (1981).
5. A.E. Dorokhov, I.O. Cherednikov, Phys. Rev. D **66**, 074009 (2002), hep-ph/0204172.
6. G. Korchemsky, A. Radyushkin, Nucl. Phys. B **283**, 342 (1987).
7. E. Meggiolaro, Phys. Rev. D **53**, 3835 (1996).
8. E. Shuryak, hep-ph/9909458.
9. A.E. Dorokhov, S.V. Esaibegyan, S.V. Mikhailov, Phys. Rev. D **56**, 4062 (1997); A.E. Dorokhov, S.V. Esaibegyan, A.E. Maximov, S.V. Mikhailov, Eur. Phys. J. C **13**, 331 (2000), hep-ph/9903450.
10. D.A. Smith, M.J. Teper, Phys. Rev. D **58**, 014505 (1998); J.W. Negele, Nucl. Phys. B (Proc. Suppl.) **73**, 92 (1999).
11. E. Shuryak, I. Zahed, Phys. Rev. D **62**, 085014 (2000); M. Nowak, E. Shuryak, I. Zahed, Phys. Rev. D **64**, 034008 (2001).
12. M. Beneke, Phys. Rep. **317**, 1 (1999).
13. E. Shuryak, Nucl. Phys. B **203**, 93; 116; 140 (1982).
14. J.G.M. Gatheral, Phys. Lett. B **133**, 90 (1983); J. Frenkel, J.C. Taylor, Nucl. Phys. B **246**, 231 (1984).
15. C.G. Callan, R. Dashen, D.J. Gross, Phys. Rev. D **17**, 2717 (1978).

Eur. Phys. J. A **18**, 219–221 (2003)
DOI 10.1140/epja/i2002-10302-7

THE EUROPEAN PHYSICAL JOURNAL A

Determination of vector meson properties by matching resonance saturation to a constituent quark model

S. Leupold[a]

Institut für Theoretische Physik, Universität Giessen, Giessen, Germany

Received: 30 September 2002 /
Published online: 22 October 2003 – © Società Italiana di Fisica / Springer-Verlag 2003

Abstract. The properties of mesonic resonances can be calculated in terms of the low-energy coefficients of chiral perturbation theory (χPT) by extending unitarized χPT to higher energies. On the other hand, these low-energy coefficients can be calculated in two different models, namely i) by assuming resonance saturation and ii) within a constituent quark model. By matching the expressions of the two models combined with the results of unitarized χPT and the Weinberg sum rules, the properties of vector and axial-vector mesons can be calculated in the combined large-N_c and chiral limit.

PACS. 12.39.Fe Phenomenological quark models: Chiral Lagrangians – 14.40.Cs Properties of specific particles: Other mesons with $S = C = 0$, mass < 2.5 GeV

1 Introduction

What determines the properties of hadrons made from light quarks, chiral symmetry breaking (χSB) and/or confinement? It is nowadays common wisdom that the mechanism of χSB causes large constituent quark masses of the order of 300–400 MeV. Hence even without confinement the creation of a quark-antiquark pair is rather expensive. Therefore, the role of confinement for the description of light hadrons is at least diminished by the appearance of χSB [1]. This suggests that the properties of light hadrons are *quantitatively* determined by the effect of χSB. In such a scenario confinement enters only *qualitatively* by excluding non-white states and quark-antiquark thresholds. It is well known that such a picture works very well for pions (*e.g.*, [2] and references therein). It is the purpose of the present work to apply that picture to ρ- and a_1-mesons. One reason why one does not need confinement to describe the properties of pions can be found in the fact that the mass of these quasi-Goldstone bosons is much below the (constituent!) quark-antiquark threshold. This is of course different for other types of mesons. At first glance it seems that this messes up the line of reasoning given above. The point however is that *e.g.* ρ-mesons leave a trace also in the low-energy region much below their pole mass by mediating, *e.g.*, pion-pion interactions [3]. Hence the key idea is that on the one hand (χSB aspect) one can describe the low-energy region reliably by a (chiral!) quark model (without confinement) —as this region is far away from the quark-antiquark production threshold. On the other hand (confinement aspect) the mesonic resonances are supposed to mediate the interactions in this low-energy regime. By matching corresponding expressions it should be possible to determine masses and coupling constants of mesonic resonances in terms of quark model expressions. This procedure is depicted schematically in fig. 1. For simplicity I work in the following in the combined large-N_c and chiral limit.[1]

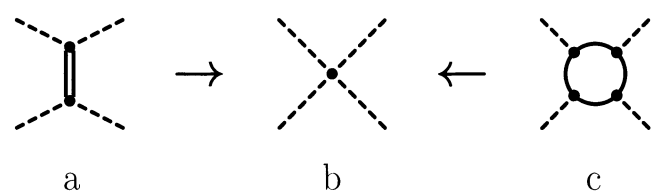

Fig. 1. Schematic view of the resonance saturation model (a) and the constituent quark model (c) and their respective low-energy reduction to χPT (b). The dashed lines denote Goldstone bosons, the double line mesonic resonances and the full lines quarks.

2 Chiral perturbation theory and unitarization

At low energies QCD reduces to an effective theory where only the lightest mesons —the pseudoscalar Goldstone bosons— appear which interact with each other and with external sources. χSB demands that the meson interaction

[a] e-mail: stefan.leupold@theo.physik.uni-giessen.de

[1] To be specific I take the large-N_c limit first, *i.e.* neglect the chiral log's which are suppressed by $1/N_c$.

vanishes with vanishing energy. Therefore a systematic expansion in terms of the derivatives of the meson fields is possible. These considerations lead to the effective Lagrangian of chiral perturbation theory (χPT) [4]:

$$\mathcal{L}_{\chi\mathrm{PT}} = \mathcal{L}_1 + \mathcal{L}_2 + \text{higher order derivatives} \tag{1}$$

with

$$\mathcal{L}_1 = \frac{1}{4} F_\pi^2 \,\mathrm{tr}(\nabla_\mu U^\dagger \nabla^\mu U) + \dots\,, \tag{2}$$

$$\begin{aligned}\mathcal{L}_2 = {} & L_1 \langle \nabla_\mu U^\dagger \nabla^\mu U\rangle^2 + L_2 \langle \nabla_\mu U^\dagger \nabla_\nu U\rangle \langle \nabla^\mu U^\dagger \nabla^\nu U\rangle \\ & + L_3 \langle \nabla_\mu U^\dagger \nabla^\mu U \nabla_\nu U^\dagger \nabla^\nu U\rangle \\ & - i L_9 \langle F^{\mathrm{R}}_{\mu\nu} \nabla^\mu U \nabla^\nu U^\dagger + F^{\mathrm{L}}_{\mu\nu} \nabla^\mu U^\dagger \nabla^\nu U\rangle + \dots\,,\end{aligned} \tag{3}$$

where I have only displayed the terms which are relevant for later use. In U the pseudoscalar meson fields are encoded. $F^{\mathrm{R,L}}_{\mu\nu}$ denotes the field strength which corresponds to (chirally covariant combinations of) external vector fields v_μ and axial-vector fields a_μ. F_π denotes the pion decay constant (in the chiral limit). I refer to [4] for further details. The four-point meson interaction induced by (3) is depicted schematically in fig. 1b.

As it stands the effective theory (1)-(3) is valid at low energies only. Especially unitarity is not fulfilled. In [5] the inverse amplitude method (IAM) is used to unitarize the effective theory and extend its applicability to the mesonic-resonance region. The IAM is very well suited to recover a resonance from its trace left at low energies [6] and therefore fits perfectly to the philosophy discussed above. In [5] it is demonstrated that the IAM is able to reproduce the scattering data of pions, kaons and etas up to 1.2 GeV including several mesonic resonances. Here I am interested in the large-N_c and chiral limit of the results presented in [5]. It is easy to show that in this limit the mass of the ρ-meson becomes [7]

$$M_V^2 = -\frac{F_\pi^2}{4L_3}\,. \tag{4}$$

3 Chiral constituent quark model

As already pointed out it should be reasonable to calculate the coefficients of the effective theory (1)-(3) from a chiral constituent quark model, as the low-energy region is (much) below the quark-antiquark production threshold. In the following I use the quark–Goldstone-boson Lagrangian (in Euclidean space)

$$\mathcal{L}_{\mathrm{quark}} = \bar{q}\,(\gamma_\mu \partial_\mu - M U^{\gamma_5} + \gamma_\mu v_\mu + \gamma_\mu \gamma_5 a_\mu + \dots)\, q\,. \tag{5}$$

This Lagrangian can be motivated in several ways (*e.g.* [8, 9]). I would like to stress that it is also the simplest model which one can write down which couples quarks to the Goldstone bosons of χSB. The latter are encoded in

$$U^{\gamma_5} = \frac{1-\gamma_5}{2}\, U + \frac{1+\gamma_5}{2}\, U^\dagger\,. \tag{6}$$

M denotes the mass of the constituent quark. The dots in (5) denote further couplings to external sources besides the displayed ones for vector and axial-vector fields. By integrating out the quarks, expanding the obtained effective action in terms of meson field derivatives and finally transforming the result to Minkowski space one arrives at the χPT Lagrangian (1) with predictions for the low-energy constants. This procedure is shown in fig. 1 as the transition from fig. 1c to fig. 1b. For the constants of interest one obtains [9]

$$\begin{aligned} L_1^{\mathrm{quark}} &= \frac{N_c}{384\pi^2}\,, & L_2^{\mathrm{quark}} &= 2L_1^{\mathrm{quark}}\,, \\ L_3^{\mathrm{quark}} &= -4L_1^{\mathrm{quark}}\,, & L_9^{\mathrm{quark}} &= 8L_1^{\mathrm{quark}}\,. \end{aligned} \tag{7}$$

Note that the results are pure numbers, *i.e.* do not depend on any model-dependent quantities like, *e.g.*, the UV cutoff which regulates UV singular integrals coming from the non-renormalizable Lagrangian (5). The reason is that the loop depicted in fig. 1c is actually UV finite.

4 Resonance saturation model

Assuming that (only) resonances mediate the low-energy interactions of (3) one can write down a Lagrangian which couples resonances to Goldstone bosons [10]. Here I concentrate on the ρ-meson and its interaction Lagrangian

$$\mathcal{L}_{\mathrm{int}} = \frac{F_V}{2\sqrt{2}}\,\mathrm{tr}(V_{\mu\nu} f_+^{\mu\nu}) + \frac{iG_V}{\sqrt{2}}\,\mathrm{tr}(V_{\mu\nu} u^\mu u^\nu)\,, \tag{8}$$

where basically u_μ is obtained from U, *i.e.* contains the pseudoscalar fields, while $f_+^{\mu\nu}$ contains the external vector fields (see [10] for details). $V_{\mu\nu}$ denotes the vector meson resonance in the tensor representation. Note that one does *not* assume here that the vector meson couples with the same strength to the external vector field (photon) as it couples to the pseudoscalars (*e.g.* pions). To phrase it differently, universality of the ρ-meson coupling is *not an input* of the resonance saturation model. As I will show below, however, one gains the universality as an *output* of my approach. Integrating out the resonance fields one obtains (3) with predictions for the low-energy coefficients (schematically shown in fig. 1 by the transition from a to b). For the ones governed solely by vector meson exchange one gets [10]

$$L_2^{\mathrm{res}} = \frac{G_V^2}{4M_V^2}\,, \quad L_9^{\mathrm{res}} = \frac{F_V G_V}{2M_V^2}\,. \tag{9}$$

Note that all the other low-energy constants are additionally influenced by the exchange of mesons with different quantum numbers.

5 Results from matching

In the last sections I have basically collected results from the literature. The new aspect is now that the results from the approaches with hadronic degrees of freedom (sects. 2, 4) are matched to the quark model calculations of sect. 3.

As already pointed out in the introduction, the idea behind that matching is that, on the one hand, the chiral quark model is supposed to give reliable results in the low-energy regime. On the other hand, confinement enforces the formation of resonances (instead of the production of free quarks and antiquarks). These resonances, however, are also visible at low energies, *i.e.* determine the low-energy structure of the strong interaction. From the matching procedure one obtains information about the resonances in terms of quark degrees of freedom.

Even without the results of sect. 4 one obtains from (4) and (7) for the ρ-meson mass:

$$M_V^2 = \frac{24\pi^2 F_\pi^2}{N_c}\,. \tag{10}$$

Using the physical value for the pion decay constant $F_\pi \approx 93\,\mathrm{MeV}$ the ρ-meson mass turns out to be $M_V \approx 826\,\mathrm{MeV}$, already close to the physical ρ-meson mass of 770 MeV. Note that this result was obtained in the chiral and large-N_c limit. Hence pion loops are absent in this framework, *i.e.* I have determined the mass of a bare ρ-meson without its pion cloud. Typically the ρ-pion interaction reduces the bare ρ mass by approximately 5–10% [11,12].

Using in addition (9) yields the coupling constants

$$F_V^2 = 2F_\pi^2\,, \qquad G_V^2 = \frac{F_\pi^2}{2}\,. \tag{11}$$

In particular, the relation $F_V = 2G_V$ states the universality of the vector meson coupling as can be most easily seen by inspecting (8). This automatically implies that the KSFR relation is fulfilled [13].

The connection of G_V to the usual $\rho\pi\pi$ coupling is provided by

$$g = \frac{G_V M_V}{F_\pi^2} \tag{12}$$

with g defined via the Lagrangian [12]

$$\mathcal{L}_{\mathrm{int}} = \frac{ig}{4}\,\mathrm{tr}(V^\mu\,[\partial_\mu \Phi, \Phi]) - \frac{g^2}{16}\,\mathrm{tr}([V^\mu, \Phi]^2)\,, \tag{13}$$

where V^μ is the vector meson resonance in the vector representation and Φ is connected to U via $U = \exp(i\Phi/F_\pi)$. Relation (12) can be obtained by calculating the decay width $\Gamma(\rho \to \pi\pi)$ in both approaches (8) and (13). From (10), (11) one gets

$$g = \sqrt{\frac{3}{N_c}}\,2\pi \tag{14}$$

as compared to the experimental value of 6.05 extracted from the decay width $\Gamma(\rho \to \pi\pi)$ [12].

Finally, properties of the axial-vector meson a_1 can be deduced from the Weinberg sum rules [13,10]:

$$F_V^2 = F_A^2 + F_\pi^2\,, \qquad M_V^2 F_V^2 = M_A^2 F_A^2\,. \tag{15}$$

In combination with the previous results this yields the a_1 mass

$$M_A = \sqrt{\frac{3}{N_c}}\,4\pi F_\pi \approx 1169\,\mathrm{MeV} \tag{16}$$

and the coupling of the a_1 to an external axial-vector current

$$F_A = F_\pi \approx 93\,\mathrm{MeV} \tag{17}$$

to be compared to the experimental values $M_{a_1} = 1230 \pm 40\,\mathrm{MeV}$ and $F_{a_1} = 124 \pm 27\,\mathrm{MeV}$ [10].

6 Summary and outlook

I have presented a somewhat indirect way to determine the properties of vector and axial-vector mesons in terms of quark degrees of freedom. The success of the presented approach suggests that it is indeed the phenomenon of χSB which quantitatively determines the properties of the studied mesonic resonances. Confinement enters the framework only qualitatively by demanding that color-white resonances are formed instead of quark-antiquark pairs.

There are things which still have to be clarified: First, I have utilized two different versions of resonance saturation. In the first one (sect. 2) resonances are created from a combination of the two Lagrangians (2) and (3) (cf. [5] for details), while in the second version (sect. 4) the resonances only influence the fourth-order Lagrangian (3). The connection of these two versions has to be studied in more detail. Second, there is a low-energy constant, namely L_{10}, which can be calculated both from the quark model and from the resonance saturation model using vector and axial-vector mesons. It turns out that one needs more than one meson per channel to achieve an agreement between the two calculations [14].

I expect that the presented framework can be extended from the vacuum case studied here to the case of a medium with finite temperature and/or quark density. This should provide interesting insight in the in-medium changes *e.g.* of the ρ-meson mass, its coupling to pions and photons and possible differences between longitudinal and transverse ρ-mesons.

References

1. D. Diakonov, Prog. Part. Nucl. Phys. **36**, 1 (1996).
2. S.P. Klevansky, Rev. Mod. Phys. **64**, 649 (1992).
3. J.F. Donoghue, C. Ramirez, G. Valencia, Phys. Rev. D **39**, 1947 (1989).
4. J. Gasser, H. Leutwyler, Ann. Phys. (N.Y.) **158**, 142 (1984); Nucl. Phys. B **250**, 465 (1985).
5. A. Gomez Nicola, J.R. Pelaez, Phys. Rev. D **65**, 054009 (2002).
6. J.A. Oller, E. Oset, J.R. Pelaez, Phys. Rev. D **59**, 074001 (1999); **60**, 099906 (1999) (E).
7. L. Jahnke, S. Leupold, in preparation.
8. D. Diakonov, V.Y. Petrov, Nucl. Phys. B **272**, 457 (1986).
9. D. Espriu, E. de Rafael, J. Taron, Nucl. Phys. B **345**, 22 (1990); **355**, 278 (1991) (E).
10. G. Ecker, J. Gasser, A. Pich, E. de Rafael, Nucl. Phys. B **321**, 311 (1989).
11. M. Herrmann, B.L. Friman, W. Nörenberg, Nucl. Phys. A **560**, 411 (1993).
12. F. Klingl, N. Kaiser, W. Weise, Z. Phys. A **356**, 193 (1996).
13. S. Weinberg, Phys. Rev. Lett. **18**, 507 (1967).
14. S. Leupold, in preparation.

Eur. Phys. J. A **18**, 223–226 (2003)
DOI 10.1140/epja/i2002-10303-6

THE EUROPEAN PHYSICAL JOURNAL A

Chromofields of strings and baryons

G. Martens[a], C. Greiner, S. Leupold, and U. Mosel

Institut für Theoretische Physik, Universität Giessen, Heinrich-Buff-Ring 16, 35392 Giessen, Germany

Received: 30 September 2002 /
Published online: 22 October 2003 – © Società Italiana di Fisica / Springer-Verlag 2003

Abstract. We calculate color electric fields of quark/antiquark ($\bar{q}q$) and 3-quark (qqq) systems within the Chromodielectric Model (CDM). We explicitly evaluate the string tension of flux tubes in the $\bar{q}q$-system and analyze their profile. To reproduce results of lattice calculations we use a bag pressure $B = (320\,\mathrm{MeV})^4$ from which an effective strong-coupling constant $\alpha_s \approx 0.3$ follows. With these parameters we get a Y-shaped configuration for large qqq-systems.

PACS. 11.10.Lm Field theory: Nonlinear or nonlocal theories and models – 11.15.Kc Gauge field theories: Classical and semiclassical techniques – 12.39.Ba Phenomenological quark models: Bag model

1 Introduction

Quantum Chromodynamics (QCD) is the widely accepted theory for the dynamics of quarks and gluons. Despite its success in the regime of high momemtum transfer it remains an outstanding task to explain the low-energy behavior of hadrons within QCD. Only in the last 10 years lattice QCD (lQCD) has found detailed evidence for the confinement of quarks in hadrons [1] but it still fails to give a dynamical description of this phenomenon. It is therefore necessary to rely on models, capable to describe confinement dynamically on the one hand and to reproduce static results of lQCD on the other hand.

In this paper we present static calculations within the Chromodielectric Model [2–4], namely the detailed analysis of quark-antiquark strings and three-quark configurations.

2 Phenomenology of the model

In the Chromodielectric Model (CDM) it is assumed, that the vacuum of QCD behaves in the long-range limit as a perfect color dielectric medium with vanishing dielectric constant $\kappa = 0$. The medium is generated through the non-Abelian part of the gluonic sector of QCD which is represented in the CDM as a scalar color singlet field σ. The remaining two Abelian gluon fields are able to propagate through this medium. The scalar field σ is driven by a scalar potential $U(\sigma)$ (see fig. 1) which exhibits two (quasi) stable points, separating the non-perturbative, perfect dielectric phase where $\sigma = \sigma_{\mathrm{vac}}$, from the perturbative phase with $\kappa = 1$, where the color fields can propagate freely and $\sigma = 0$.

[a] e-mail: Gunnar.Martens@theo.physik.uni-giessen.de

In our description quarks are treated classically and the gluons are coupled to the quark current $j^{\mu,a}$. This results in the following Lagrangian:

$$\mathcal{L} = \mathcal{L}_q + \mathcal{L}_g + \mathcal{L}_\sigma\,, \tag{1}$$

$$\mathcal{L}_q = -\sum_k m_k \sqrt{1-\dot{\boldsymbol{x}}_k^2}\; w\left(\boldsymbol{x}-\boldsymbol{x}_k(t)\right) - g_s\, j^a_\mu\, A^{\mu,a}\,, \tag{2}$$

$$\mathcal{L}_g = -\frac{1}{4}\kappa(\sigma) F^a_{\mu\nu} F^{\mu\nu,a}\,, \tag{3}$$

$$\mathcal{L}_\sigma = \frac{1}{2}\partial_\mu\sigma\partial^\mu\sigma - U(\sigma)\,, \tag{4}$$

$$F^{\mu\nu,a} = \partial^\mu A^{\nu,a} - \partial^\nu A^{\mu,a}, \quad a \in \{3,8\}\,, \tag{5}$$

$$j^{\mu,a} = \sum_k q^a_k\, u^\mu_k\, w\left(\boldsymbol{x}-\boldsymbol{x}_k(t)\right) = (\rho^a, \boldsymbol{\jmath}^{\,a}) \tag{6}$$

with u^μ_k being the 4-velocity of particle k with classical charge q^a_k (see fig. 1) and extension $w\left(\boldsymbol{x}-\boldsymbol{x}_k(t)\right)$. The scalar potential $U(\sigma)$ is chosen to be of a quartic form and is shown in fig. 1. In this work $U(\sigma)$ has no relative maximum between $\sigma = \sigma_{\mathrm{vac}}$ and $\sigma = 0$ and U is determined through the bag pressure $B = U(0)$ and σ_{vac} alone. The dielectric function is of the form $\kappa(\sigma) = \exp\left(-\frac{\sigma^3}{\sigma_0^3}\right)$ for $\sigma \geq 0$ and $\kappa(\sigma) = 1$ else and has $\kappa(\sigma_{\mathrm{vac}}) \equiv \kappa_{\mathrm{vac}} \ll 1$.

In the static case, the equations of motion for the electric potentials Φ^a and for the confinement field σ following from eq. (1) are

$$\boldsymbol{\nabla}\cdot\left(\kappa(\sigma)\,\boldsymbol{\nabla}\Phi^a\right) = -g_s\,\rho^a \tag{7}$$

and

$$\nabla^2\sigma = U'(\sigma) - \frac{1}{2}\frac{\kappa'(\sigma)}{\kappa(\sigma)^2}\left(\boldsymbol{D}^3\cdot\boldsymbol{D}^3 + \boldsymbol{D}^8\cdot\boldsymbol{D}^8\right), \tag{8}$$

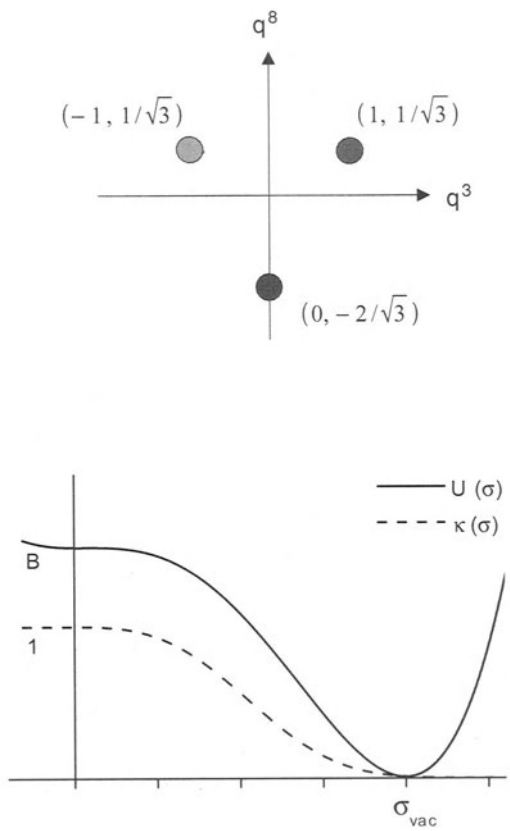

Fig. 1. Top: the color charges of the green (left), red (right) and blue (lower) quark. Bottom: The dielectric function $\kappa(\sigma)$ (dashed line) and the scalar potential $U(\sigma)$ (solid line).

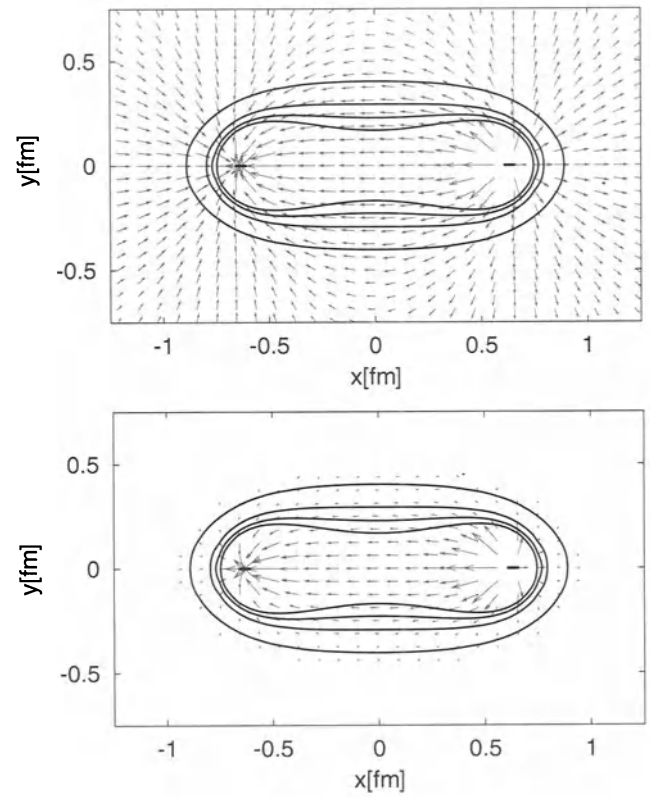

Fig. 2. The color fields $\boldsymbol{E}^3$ (upper panel) and $\boldsymbol{D}^3$ (lower panel). The contour lines give the electric energy density (11) $\varepsilon_g = 1, 3, 5, 7\ \mathrm{fm}^{-4}$ from the outside. Only the electric displacement $\boldsymbol{D}^a$ is confined to the flux tube.

where $\boldsymbol{D}^a = \kappa(\sigma)\boldsymbol{\nabla}\Phi^a$ denotes the color electric displacement. The energy (neglecting quark masses) is given by

$$E = E_\sigma + E_g \tag{9}$$

$$E_\sigma = \int \left(\frac{1}{2}(\nabla\sigma)^2 + U(\sigma)\right) \mathrm{d}^3r\,, \tag{10}$$

$$E_g = \frac{1}{2}\int \left(\boldsymbol{E}^3\cdot\boldsymbol{D}^3 + \boldsymbol{E}^8\cdot\boldsymbol{D}^8\right)\mathrm{d}^3r \equiv \int \varepsilon_g\,\mathrm{d}^3r. \tag{11}$$

Confinement of color fields in our model is achieved by means of Gauss's law in eq. (7) and the characteristic form of the dielectric function $\kappa(\sigma)$: A single colored quark would generate a spherical electric field. In the vicinity of the quark the field is strong enough to push the confinement field from $\sigma = \sigma_{\mathrm{vac}}$ towards smaller values and forms a cavity in the surrounding vacuum. As $\kappa(\sigma)$ drops to zero at the boundary of the cavity, the electric field $\boldsymbol{E}^a = \frac{\boldsymbol{D}^a}{\kappa(\sigma)}$ diverges and so does the electric-field energy (11). Note that in this version of CDM there is no direct coupling between the quarks and the confinement field as proposed in [2,5].

3 $\bar{q}q$ strings

In contrast to configurations with net color, all white configurations have finite energy and color fields are confined into well-defined spatial regions. Again, eq. (7) enforces an electric color field, but field lines now end on the anticolor and are parallel to the boundary of the cavity. In this case the color electric displacement is suppressed with the dielectric constant in the non-perturbative vacuum. Both the electric-field energy and the confinement field energy are negligible in the outside.

In this section we study the field configurations of color flux tubes stretching from a quark q to an antiquark $\bar{q}$. We start by showing the electric fields $\boldsymbol{E}^3$ and $\boldsymbol{D}^3$ in fig. 2. It is seen that the electric displacement vanishes outside the cavity. The flux tube can be characterized by the profile function, *i.e.* the component of $\boldsymbol{D}$ parallel to the string axis along the center line perpendicular to the string axis. This profile has been studied within lQCD in [6][1]. The profile depends mainly on the choice of $U(\sigma)$, *i.e.* on the bag constant B and the vacuum value σ_{vac} as shown in fig. 3. The bag constant acts as a pressure against the electric field and therefore an increasing B leads to decreasing width of the profile. In order to fulfill Gauss's law (7) the electric $\boldsymbol{D}$ field on the string axis must increase with increasing B.

The value of σ_{vac} controls the surface of the bag. Decreasing its value leads to a sharper surface. In our

[1] Note that in CDM the $\boldsymbol{D}$ field is confined and we compare it to the $\boldsymbol{E}$ field of reference [6].

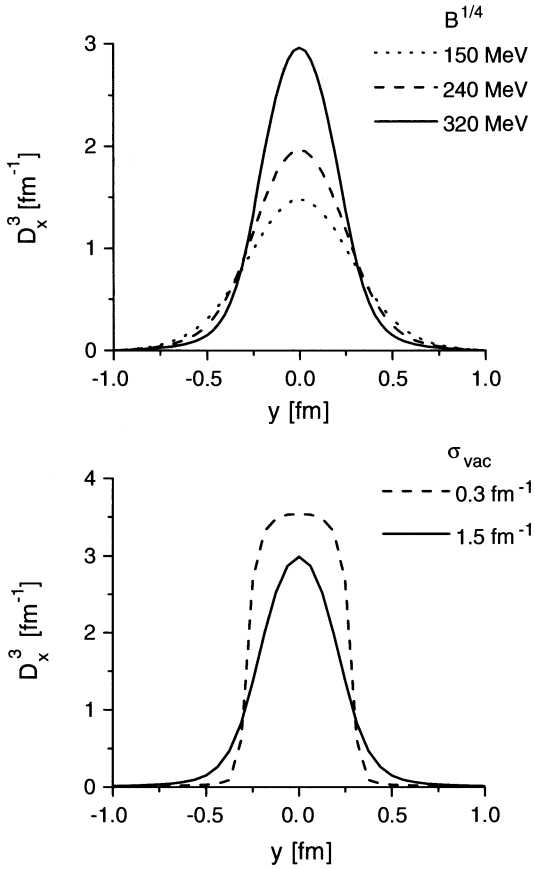

Fig. 3. The string profile of a 1.2 fm string. Increasing the bag pressure B decreases the width and simultanously increases the maximal value of the $\boldsymbol{D}$ field (top) and increasing σ_{vac} smoothes the surface (bottom). All constant parameters are taken from table 1.

Table 1. Model parameters used in this work.

$B^{\frac{1}{4}}$	σ_{vac}	κ_{vac}	g_s
320 MeV	1.5 fm^{-1}	0.01	1.0

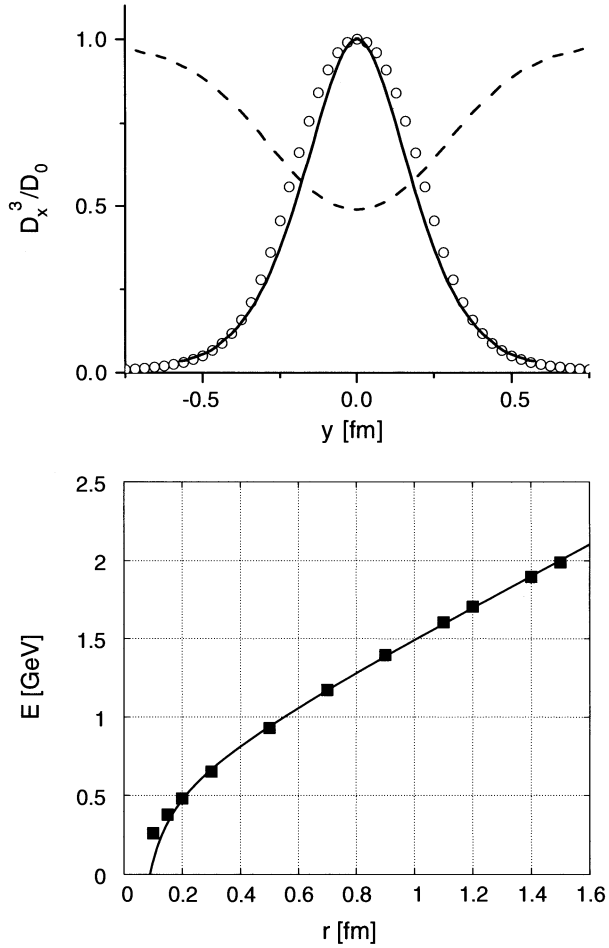

Fig. 4. Top: the string profile within the CDM (circles) compared to lQCD results (solid line) [1]. The confinement field (dashed line) drops to $\sigma \approx 0.5\sigma_{\text{vac}}$ inside the string. Bottom: the string potential within the CDM (squares) and a fit to the Cornell potential (12). The first two data points are not included in the fit as the Coulomb potential does not hold for too small distances due to finite extension of the charges with r.m.s. radius $\sqrt{\langle \boldsymbol{r}^2 \rangle} \approx 0.1$ fm.

simulations the detailed form of the dielectric function (see fig. 1) has little effect on the profile.

With the parameters given in table 1 we reproduce the results of lQCD [1,6] as can be seen in fig. 4.

Using the same parameters we can calculate the string tension of the flux tube. We vary the q-$\bar{q}$ distance r and plot the total energy of eq. (9) as a function of r in fig. 4. For $r > 0.5$ fm the energy rises linearly. We fit our results to a Cornell potential

$$E_c(r) = E_0 + \tau r - \frac{\alpha_{\text{eff}}}{r}, \tag{12}$$

where the linear term reflects the confinement behavior for large $\bar{q}q$ separations and the Coulomb term describes the one-gluon exchange dominant at small r. The constant term $E_0 = 560$ MeV is due to electric self-energies included in eq. (11). We find a string tension $\tau = 988$ MeV/fm and a value $\alpha_{\text{eff}} = 0.291$ which is to be compared to lQCD results where $\alpha_{\text{eff}} = 0.295$ [1]. It should be noted that, due to the high bag pressure B, the electric fields are not strong enough to expel totally the non-perturbative vacuum out of the string. The confinement field only drops to $\sigma \approx 0.5\sigma_{\text{vac}}$, *i.e.* the dielectric function rises to $\kappa \approx 0.5$. However, confinement is still achieved as the energy of the color fields does not leak into the outside.

4 Baryons

In this section we study color fields of baryon like qqq–configurations. Given that the energy scales linearly with the $\bar{q}q$ separation, one can argue that configurations with 3 quarks sitting on the corner of an equilateral triangle will form strings with minimal total string length. This would be a configuration with a central *Steiner* point, called a

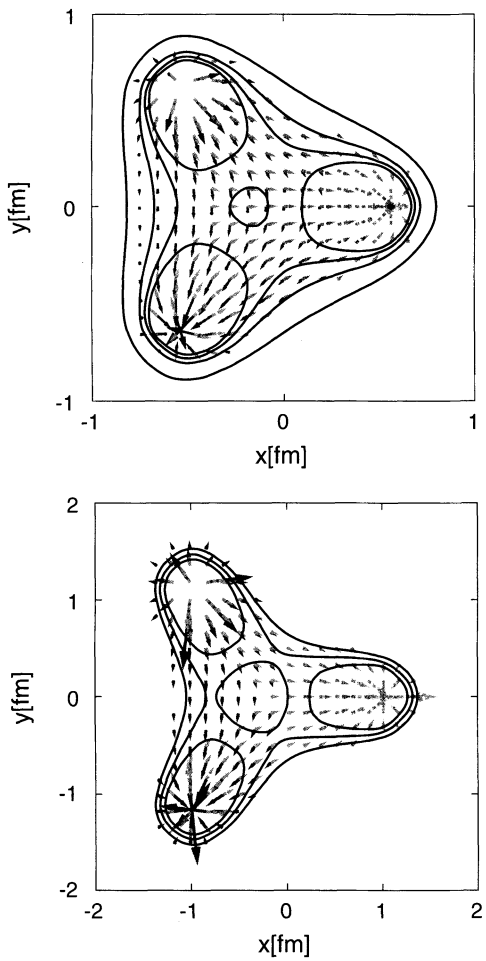

Fig. 5. The color fields of a qqq configuration with $\ell = 0.7(1.3)$ fm top (bottom). The contour lines correspond to $\varepsilon_g = 1, 3, 5, 7$ fm^{-4} (top) and $\varepsilon_g = 1, 1.4, 1.8$ fm^{-4} (bottom).

Y configuration. However, if only two-quark interactions are dominant, one might expect strings stretching pairwise from one quark to another, which would be the Δ configuration. In lQCD the qqq potential has been studied and there are indications for both the Δ-baryon [1,7] and the Y-baryon [8]. However, in the Gaussian Stochastic Vacuum model [9] clear evidence for the Y ansatz is found.

In fig. 5 we plot the electric field distribution for the baryon with the parameters given in table 1. The quarks are separated a distance $\ell = 0.7(1.3)$ fm from the Steiner point, *i.e.* the qq distance is $L = \sqrt{3}\ell \approx 1.2(1.7)$ fm.

The field is clearly different from a simple superposition of 3 flux tubes between the quarks (see fig. 2). The electric energy is pushed towards the center of the baryon, and a Y-shaped configuration (at least for large quark separations) is seen.

5 Summary

We have analyzed the $\bar{q}q$ string within the CDM and have reproduced the geometric profile function as well as the potential. With a bag constant $B = (320\,\text{MeV})^4$ and $\sigma_{\text{vac}} = 1.5$ fm^{-1} we get a string tension $\tau = 988$ MeV/fm and an effective strong-coupling $\alpha_{\text{eff}} = 0.29$. qqq configurations with large qq separations tend to show a Y-shaped geometry.

This work was supported by BMBF.

References

1. G.S. Bali, Phys. Rep. **343**, 1 (2001).
2. R. Friedberg, T.D. Lee, Phys. Rev. D **15**, 1694 (1977).
3. R. Friedberg, T.D. Lee, Phys. Rev. D **16**, 1096 (1977).
4. C.T. Traxler, U. Mosel, T.S. Biro, Phys. Rev. C **59**, 1620 (1999).
5. A. Schuh, H.J. Pirner, L. Wilets, Phys. Lett. B **174**, 10 (1986).
6. G.S. Bali, K. Schilling, C. Schlichter, Phys. Rev. D **51**, 5165 (1995).
7. C. Alexandrou, P. De Forcrand, A. Tsapalis, Phys. Rev. D **65**, 054503 (2002).
8. T.T. Takahashi, H. Suganuma, Y. Nemoto, H. Matsufuru, Phys. Rev. D **65**, 114509 (2002).
9. D.S. Kuzmenko, Y.A. Simonov, Phys. At. Nucl. **64**, 107 (2001).

Eur. Phys. J. A **18**, 227–230 (2003)
DOI 10.1140/epja/i2002-10205-7

THE EUROPEAN PHYSICAL JOURNAL A

Effective effective interactions

B.R. Holstein[a]

Department of Physics, University of Massachusetts, Amherst, MA 01003, USA

Received: 30 September 2002 /
Published online: 22 October 2003 – © Società Italiana di Fisica / Springer-Verlag 2003

Abstract. The use of effective field theory techniques allows the basic physics to be extracted from otherwise complex systems. We cite examples from quantum mechanics, condensed-matter physics, QCD, and quantum gravity.

PACS. 04.60.-m Quantum gravity – 12.20.-m Quantum electrodynamics

1 Introduction

There exist many situations in physics wherein two quite separate scales —one heavy and one light— are involved. In such cases, provided that one is working at an energy momentum small compared to the heavy scale, then one can write the interaction in terms of an "effective" Hamiltonian which is written only in terms of the light degrees of freedom but which fully incorporates all (virtual) effects associated with the heavy scale [1]. Such an effective interaction is often able to isolate and more clearly represent the underlying physics of a given process than is a rigorous treatment involving the entire system. A simple example from classical mechanics involves the use of the effective gravitational potential

$$V = mg(r - R_{\mathrm{E}})$$

in the vicinity of the earth's surface rather than the full Newtonian form

$$V = -\frac{GmM_{\mathrm{E}}}{r}$$

which is valid everywhere [2]. We give additional simple examples below from the realms of quantum mechanics, condensed-matter physics, QCD, and quantum gravity.

2 Examples

2.1 Quantum mechanics

A nice example of effective field theory (EFT) methods is found in quantum mechanics, from the classic problem of understanding why the sky is blue [3]. The answer, of course, comes from Compton scattering of visible light from the atoms which make up the earth's atmosphere. First, however, we outline the full analysis. Using the simple Hamiltonian [4]

$$H = \frac{(\boldsymbol{p} - e\boldsymbol{A})^2}{2m} + e\phi \tag{1}$$

and lowest-order perturbation theory, one finds the Kramers-Heisenberg amplitude

$$\begin{aligned}\mathrm{Amp} = -\frac{e^2}{m\sqrt{2\omega_i\omega_f}}\Bigg[&\hat{\epsilon}_i\cdot\hat{\epsilon}_f \\ &+\frac{1}{m}\sum_n\Bigg(\frac{\hat{\epsilon}_f\cdot\langle 0|\boldsymbol{p}e^{-i\boldsymbol{q}_f\cdot\boldsymbol{r}}|n\rangle\langle n|\boldsymbol{p}e^{i\boldsymbol{q}_i\cdot\boldsymbol{r}}|0\rangle\cdot\hat{\epsilon}_i}{\omega_i + E_0 - E_n} \\ &+\frac{\hat{\epsilon}_i\cdot\langle 0|\boldsymbol{p}e^{i\boldsymbol{q}_i\cdot\boldsymbol{r}}|n\rangle\langle n|\boldsymbol{p}e^{-i\boldsymbol{q}_f\cdot\boldsymbol{r}}|0\rangle\cdot\hat{\epsilon}_f}{E_0 - \omega_f - E_n}\Bigg)\Bigg].\end{aligned} \tag{2}$$

When the energy of the photons is small compared to a typical excitation energy, the use of simple quantum-mechanical identities allows one to simplify eq. (2) to the form

$$\mathrm{Amp} \propto \omega^2\,,$$

where the constant of proportionality involves the electric polarizability of the atom. The corresponding cross-section is proportional to ω^4 and explains why the sky is blue.

A corresponding EFT discussion is much simpler. An effective interaction which describes Compton scattering from an atomic system must satisfy certain basic strictures. It must be quadratic in the vector potential $\boldsymbol{A}$, must be a rotational scalar, be gauge invariant, and be symmetric under spatial inversion and time reversal. After a little thought it becomes clear that the lowest order effective Hamiltonian must have the form

$$H_{\mathrm{eff}} = \frac{1}{2}4\pi\alpha_{\mathrm{E}}\boldsymbol{E}^2 + \frac{1}{2}4\pi\beta_M\boldsymbol{H}^2\,. \tag{3}$$

[a] e-mail: holstein@physics.umass.edu

Since $\boldsymbol{E}, \boldsymbol{H} \sim \omega\hat{\epsilon}$ we easily find the desired form

$$\frac{\mathrm{d}\sigma}{\mathrm{d}\Omega} \propto |\langle f|H_{\mathrm{eff}}|i\rangle|^2 \propto \omega^4 . \tag{4}$$

Obviously then EFT has isolated the basic physics with a minimum of formalism.

2.2 Superconductivity

A second example, this time from condensed-matter physics, is that of superconductivity. In this case electron-lattice interactions lead, in a complex fashion, to the effective BCS Hamiltonian, which involves an effective attractive interaction between electron pairs which are anticorrelated in spin and momentum [5],

$$H_{\mathrm{BCS}} = \sum_{\boldsymbol{k},s} \psi^\dagger_{\boldsymbol{k},s} \left(i\frac{\partial}{\partial t} - \frac{\boldsymbol{k}^2}{2m} - \mu \right) \psi_{\boldsymbol{k},s} - g \sum_{\boldsymbol{k}} \psi^\dagger_{\boldsymbol{k},\uparrow} \psi^\dagger_{-\boldsymbol{k},\downarrow} \psi_{-\boldsymbol{k},\downarrow} \psi_{\boldsymbol{k},\uparrow} . \tag{5}$$

However, while the physics of superconductivity can be found by a detailed many-body solution of eq. (5) [6], it is certainly not apparent from the form of the Hamiltonian. Nevertheless, one can spotlight the essential physics by rewriting the BCS Hamiltonian in terms of the "right" degrees of freedom —the anticorrelated electron pairs. Defining

$$\phi = \psi_{q\uparrow}\psi_{-q\downarrow}$$

and rewriting eq. (5) in terms of ϕ at fixed temperature T, via imaginary-time methods, yields the familiar Landau-Ginzburg Hamiltonian [7]

$$H_{\mathrm{eff}} = c(T)\phi^\dagger \frac{(-i\boldsymbol{\nabla} - e^*\boldsymbol{A})^2}{2m^*} + a(T)\phi^\dagger\phi + b(T)(\phi^\dagger\phi)^2 + \dots , \tag{6}$$

where $e^* = 2e$, $m^* = 2m$. Here $b(T), c(T)$ are positive monotonic functions of temperature, but [8]

$$a(T) \propto \ln \frac{T}{T_{\mathrm{c}}}$$

and changes sign at a critical temperature T_{c}. Then when $T > T_{\mathrm{c}}$, the effective potential has a single-well shape with the minimum at $\phi^\dagger\phi = 0$. However, when $T < T_{\mathrm{c}}$ the effective potential has a double well, with a minimum at $\phi^\dagger\phi \neq 0$, corresponding to the superconducting phase. Here too then the use of EFT methods has allowed the extraction of the basic physics of the system.

2.3 QCD

A particularly nice example of the use of EFT in particle/nuclear physics is the utilization of chiral perturbation theory in order to understand low-energy QCD [9]. Since such methods will be extensively covered in parallel session, I will not give a detailed discussion here. However, it is worth pointing out that there exist in this case interesting parallels with the superconducting discussion given above. As in superconductivity, we begin with an interaction:

$$\mathcal{L}_{\mathrm{QCD}} = \bar{q}(i\not{D} - m)q - \frac{1}{4}G_{\mu\nu}G^{\mu\nu} , \tag{7}$$

which is difficult (impossible!) to solve. However, at low energies we can make contact between theory and experiment by rewriting eq. (7) in terms of new variables

$$\phi = \psi_{q\uparrow}\bar{\psi}_{-q\downarrow}$$

and the nonlinear quantity

$$U = \exp\left(\frac{i}{F_\pi} \sum_i \lambda_i \phi_i \right)$$

which are the pseudoscalar mesons. What results is a lowest-order effective interaction:

$$\mathcal{L}_{\mathrm{eff}} = \frac{F_\pi^2}{4}\mathrm{Tr}(\partial_\mu U \partial^\mu U^\dagger) + \frac{F_\pi^2}{4}\mathrm{Tr}(B_0 m(U + U^\dagger) \tag{8}$$

in terms of the physical degrees of freedom —π, K, η— rather than in terms of the quarks and gluons in terms of which eq. (7) is written. This effective chiral Lagrangian encodes the underlying symmetries of QCD and has had enormous phenomenological success [10].

2.4 Quantum gravity

I will close with a brief discussion of a subject that folklore says is impossible —quantum gravity. I agree that we do not know how to represent such a theory at all scales, but I want to show you that provided that we treat things as an EFT and only try to represent the long-range aspects, then quantum gravity can be made fully consistent [11]. In order to demonstrate this, we have recently calculated the radiation (photon loop) corrections to the energy-momentum tensor, which describes the coupling of a charged point mass to the gravitational field. In the case of a spin-(1/2) system, the most general form of such a matrix element is [12]

$$\langle p'|T_{\mu\nu}|p\rangle = \bar{u}(p')\Big[F_1(q^2)P_\mu P_\nu - F_2(q^2)\frac{i}{4M}\left(\sigma_{\mu\lambda}q^\lambda P_\nu + \sigma_{\nu\lambda}q^\lambda P_\mu\right) + F_3(q^2)\frac{1}{4M^2}(q_\mu q_\nu - q^2\eta_{\mu\nu})\Big] , \tag{9}$$

where $P_\mu = \frac{1}{2}(\boldsymbol{p}' + p)_\mu$, $q_\mu = (p - p')_\mu$ and we have calculated each of these form factors. The general form of each is found to be [12,13]

$$F_i(q^2) = 1 + \frac{\alpha}{\pi}\left(a\frac{q^2}{M^2}\sqrt{\frac{M^2}{-q^2}} + b\frac{q^2}{M^2}\ln - \frac{q^2}{M^2} + c\frac{q^2}{M^2} + \dots \right) . \tag{10}$$

The surprising thing about these forms is the appearance of the nonanalytic terms $\propto \sqrt{-q^2}, q^2 \ln -q^2$, for which the usual structure measure

$$\langle r^2 \rangle = \frac{6}{F(q^2)} \frac{\mathrm{d}F(q^2)}{\mathrm{d}q^2}\bigg|_{q^2=0} = \infty .$$

The meaning of these forms can be found ty taking the Fourier transform in order to go to coordinate space [14]

$$T_{\mu\nu}(\boldsymbol{r}) = \int \frac{\mathrm{d}^3 q}{(2\pi)^3} e^{-i\boldsymbol{q}\cdot\boldsymbol{r}} T_{\mu\nu}(q) = \frac{GM}{r^2} + a\frac{G\alpha}{r^4} + b\frac{G\alpha\hbar}{Mr^5} + \dots . \tag{11}$$

The meaning of such terms is clear. The classical correction $\propto \frac{G\alpha}{r^4}$ arises from the energy momentum of the electric/magnetic fields which extend outside the charged mass [15]. Indeed, the energy-momentum tensor for the electromagnetic field is given by

$$T^{EM}_{\mu\nu} = -F_{\mu\lambda}F_{\nu}{}^{\lambda} + \frac{1}{4}F_{\lambda\delta}F^{\lambda\delta} . \tag{12}$$

Using the Dirac value —two— for the gyromagnetic ratio, this yields forms

$$\begin{aligned} T^{EM}_{00}(\boldsymbol{r}) &= \frac{1}{2}\boldsymbol{E}^2 = \frac{\alpha}{8\pi r^4} , \\ T^{EM}_{0i}(\boldsymbol{r}) &= -(\boldsymbol{E}\times\boldsymbol{B})_i = -\frac{\alpha}{4\pi m r^6}(\boldsymbol{S}\times\boldsymbol{r})_i , \\ T^{EM}_{ij}(\boldsymbol{r}) &= -E_iE_j + \frac{1}{2}\delta_{ij}\boldsymbol{E}^2 = \\ &\quad -\frac{\alpha}{4\pi r^4}\left(\frac{r_ir_j}{r^2} - \frac{1}{2}\delta_{ij}\right) , \end{aligned} \tag{13}$$

which agree precisely with the classical piece of eq. (11), while the quantum corrections $\propto \frac{G\alpha\hbar}{Mr^5}$ can be understood in terms of the feature that a classical distance must be modified in going to quantum mechanics by an uncertainty of order the Compton wavelength. Then

$$r \to r + \frac{\hbar}{m}$$

and

$$\frac{1}{r^4} \to \frac{1}{r^4} - \frac{\hbar}{mr^5} + \dots ,$$

so that the quantum pieces of eq. (11) are seen to be zitterbewegung modifications to the distance scale r [16].

Alternatively, one can use the Einstein equation

$$\Box h_{\mu\nu} = -16\pi G(T_{\mu\nu} - \frac{1}{2}\eta_{\mu\nu}T) \tag{14}$$

to convert these modifications of $T_{\mu\nu}$ to changes in the metric, leading to forms

$$h_{\mu\nu} \sim \frac{GM}{r} + a\frac{G\alpha}{r^2} + b\frac{G\alpha\hbar}{Mr^3} + \dots . \tag{15}$$

Here the classical corrections

$$\begin{aligned} h^{cl}_{00}(\boldsymbol{r}) &= \frac{G\alpha}{r^2} , \\ h^{cl}_{0i}(\boldsymbol{r}) &= -\frac{G\alpha}{mr^4}(\boldsymbol{S}\times\boldsymbol{r})_i , \\ h^{cl}_{ij}(\boldsymbol{r}) &= \frac{G\alpha}{r^4} r_ir_j \end{aligned} \tag{16}$$

are again well known and agree precisely with the Kerr-Newman metric, which describes a rotating massive charge [17]. However, we also find unique quantum corrections which of necessity go along with this classical form.

We see then that when treated as an effective field theory, quantum gravity is well defined and leads to specific long-distance corrections to the lowest-order forms. Such modifications are required and follow simply from the feature that electromagnetism and gravity must be described in terms of both classical and quantum mechanics.

In closing, I want to mention that we are currently in the process and calculating the corresponding *gravitational* loop corrections to the gravitational couplings [18]. In this case, the metric corrections from classical loop contributions are higher order in G and can be shown to be identical to the $\mathcal{O}(G^2)$ corrections to the classical Kerr-Newman metric, and there are corresponding and unique quantum-mechanical corrections of $\mathcal{O}(G^2\hbar/m)$. Again, however, when interpreted in terms of effective field theory, quantum gravity contains completely consistent and understandable forms in the long distance regime.

3 Conclusions

We have shown above, in a variety of circumstances,

i) Quantum Mechanics,
ii) Superconductivity,
iii) Quantum Chromodynamics,
iv) Quantum Gravity,

how the use of EFT methods allows extraction of the relevant physics in a fully consistent and efficient fashion. Such methods truly are effective!

This work was supported in part by the National Science Foundation under award PHY-98-01875.

References

1. See, *e.g.*, A. Manohar, hep-ph/9606222; D. Kaplan, nucl-th/9506035; H. Georgi, Ann. Rev. Nucl. Sci. **43**, 209 (1995).
2. D. Phillips, nucl-th/0203040.
3. B.R. Holstein, Am. J. Phys. **67**, 422 (1999).
4. See, *e.g.*, J.J. Sakurai *Advanced Quantum Mechanics* (Addison-Wesley, Reading, Mass., 1967).
5. J. Bardeen, L.N. Cooper, J.R. Schrieffer, Phys. Rev. **108**, 1175 (1957).

6. S. Weinberg *Quantum Field Theory*, Vol. **II** (Cambridge University Press, Cambridge 1996)
7. V.L. Ginzburg, L.D. Landau, Sov. Phys. JETP **20**, 1064 (1950).
8. L.P. Gorkov, Sov. Phys. JETP **7**, 505 (1959).
9. J. Gasser, H. Leutwyler, Ann. Phys. (N.Y.) **158**, 142 (1984); Nucl. Phys. B **250**, 465 (1985).
10. See, *e.g.*, B.R. Holstein, Int. J. Mod. Phys. A **7**, 7873 (1992).
11. J.F. Donoghue, Phys. Rev. D **50**, 3974 (1994).
12. F. Berends, R. Gastmans, Phys. Lett. B **55**, 311 (1975) and Ann. Phys. (N.Y.) **98**, 225 (1976).
13. K. Milton, Phys. Rev. D **15**, 538 (1977).
14. J.F. Donoghue, B.R. Holstein, B. Garbrecht, T. Konstandin, Phys. Lett. B **529**, 132 (2002).
15. See, *e.g.* J.D. Jackson, *Classical Electrodynamics* (Wiley, New York 1975).
16. See, *e.g.*, B.R. Holstein, *Topics in Advanced Quantum Mechanics* (Addison-Wesley, Reading, Mass., 1992).
17. R. Kerr, Phys. Rev. Lett. **11**, 237 (1963); E.T. Newman, E. Couch, K. Chinnapared, A. Exton, A. Prakash, R. Torrence, J. Math. Phys. **6**, 918 (1965).
18. N.E.J. Bjerrum-Bohr, J.F. Donoghue, B.R. Holstein, in preparation.

Eur. Phys. J. A **18**, 231–235 (2003)
DOI 10.1140/epja/i2002-10206-6

THE EUROPEAN PHYSICAL JOURNAL A

Facets of confinement and dynamical chiral symmetry breaking

P. Maris[1], A. Raya[2], C.D. Roberts[3,4,a], and S.M. Schmidt[5]

[1] Department of Physics, North Carolina State University, Raleigh NC 27695-8202, USA
[2] Instituto de Física y Matemáticas, Universidad Michoacana de San Nicolás de Hidalgo, Apartado Postal 2-82, Morelia, Michoacán, México
[3] Physics Division, Argonne National Laboratory, Argonne IL 60439-4843, USA
[4] Fachbereich Physik, Universität Rostock, D-18051 Rostock, Germany
[5] Helmholtz-Gemeinschaft, Ahrstrasse 45, D-53175 Bonn, Germany

Received: 30 September 2002 /
Published online: 22 October 2003 – © Società Italiana di Fisica / Springer-Verlag 2003

Abstract. The gap equation is a cornerstone in understanding dynamical chiral symmetry breaking and may also provide clues to confinement. A symmetry-preserving truncation of its kernel enables proofs of important results and the development of an efficacious phenomenology. We describe a model of the kernel that yields: a momentum-dependent dressed-quark propagator in fair agreement with quenched lattice-QCD results; and chiral limit values, $f_\pi^0 = 68\,\mathrm{MeV}$ and $\langle\bar{q}q\rangle = -(190\,\mathrm{MeV})^3$. It is compared with models inferred from studies of the gauge sector.

PACS. 12.38.Aw General properties of QCD (dynamics, confinement, etc.) – 11.30.Rd Chiral symmetries

1 Introduction

We will address these topics from the perspective of QCD's Dyson-Schwinger equations (DSEs) [1]. The DSEs are a keystone in proving renormalisability and provide a generating tool for perturbation theory. The latter point is very important in applications to low-energy phenomena because it means that the model-dependence which necessarily appears in continuum studies of nonperturbative QCD is restricted to the infrared; *i.e.*, to momentum scales $\lesssim 1\,\mathrm{GeV}^2$. This feature has successfully been exploited in applications to the spectra [2,3], and strong [4] and electroweak [5] interactions of mesons. It also mitigates, to a useful extent, some of the problems with the approach; *e.g.*, it helps in developing reliable truncations for the coupled system of DSEs.

Recent successes are founded on an accurate understanding of dynamical chiral symmetry breaking (DCSB), and its role in resolving the dichotomy of the pion [6] (as both a Goldstone mode and a massless bound state of massive constituents) and its relation to the long-range behaviour of the effective coupling between quarks [7].

[a] e-mail: cdroberts@anl.gov

2 Dynamical chiral symmetry breaking

This is a purely nonperturbative phenomenon that can be studied via QCD's gap equation:

$$S(p)^{-1} = (i\gamma\cdot p + m) + \int \frac{\mathrm{d}^4 q}{(2\pi)^4}\, g^2 D_{\mu\nu}(p-q)\frac{\lambda^a}{2}\gamma_\mu S(q)\Gamma^a_\nu(q,p)\,, \qquad (1)$$

wherein m is the current-quark bare mass, g is the coupling constant, $D_{\mu\nu}(p-q)$ is the dressed-gluon propagator, $\Gamma^a_\nu(q,p)$ is the dressed-quark-gluon vertex; and the solution is the dressed-quark propagator

$$S(p) = \frac{1}{i\gamma\cdot p\,A(p^2) + B(p^2)} = \frac{Z(p^2)}{i\gamma\cdot p + M(p^2)}\,. \qquad (2)$$

(Equation (1) is the unrenormalised equation: renormalisation will only be mentioned as necessary.)

As noted in the introduction, one can use the gap equation to evaluate the fermion self-energy perturbatively and thereby obtain

$$B(p^2) = m\left(1 - \frac{\alpha}{\pi}\ln\left[\frac{p^2}{m^2}\right] + \ldots\right)\,, \qquad (3)$$

wherein the ellipsis denotes two- and higher-loop contributions. It is apparent that each term is proportional to

the current-quark mass and vanishes as $m \to 0$. Hence, in perturbation theory, if there is no quark mass to begin with, interactions do not generate one; *i.e.*, DCSB is impossible in perturbation theory.

In the chiral limit, namely, $m = 0$, eq. (1) always admits the trivial solution $B(p^2) \equiv 0$; *i.e.*, the solution accessible perturbatively. However, as is characteristic of gap equations, when the integrated strength of the kernel exceeds some critical value, a $B(p^2) \neq 0$ solution is generated. This nonperturbative, dynamical generation of a quark mass *from nothing* is DCSB. The integrated strength of the kernel can be characterised by an interaction tension, σ^{Δ}, for which the critical value is [8] $\sigma_c^{\Delta} \sim 2.5\,\mathrm{GeV/fm}$: this strength provides for DCSB *but only just*. An acceptable description of hadrons requires [2] $\sigma^{\Delta} \sim 25\,\mathrm{GeV/fm}$, which is an order of magnitude larger.

2.1 Symmetry-preserving truncation

It is apparent that the gap equation's kernel is formed from a product of the dressed-gluon propagator and dressed-quark-gluon vertex. It may be calculated in perturbation theory but that is inadequate for the study of intrinsically nonperturbative phenomena. Consequently, to make sensible statements about DCSB, one must employ an alternative systematic and chiral symmetry-preserving truncation scheme.

One must also focus on more than just the gap equation's kernel. Chiral symmetry is expressed via the axial-vector Ward-Takahashi identity:

$$P_\mu \Gamma_{5\mu}(k;P) = S^{-1}(k_+)\, i\gamma_5 + i\gamma_5\, S^{-1}(k_-)\,, \tag{4}$$

$k_\pm = k \pm P/2$, wherein $\Gamma_{5\mu}(k;P)$ is the dressed axial-vector vertex. This three-point function satisfies an inhomogeneous Bethe-Salpeter equation:

$$[\Gamma_{5\mu}(k;P)]_{tu} = [\gamma_5\gamma_\mu]_{tu} + \int \frac{\mathrm{d}^4 q}{(2\pi)^4} [S(q_+)\Gamma_{5\mu}(q;P)S(q_-)]_{sr} K^{rs}_{tu}(q,k;P)\,, \tag{5}$$

in which $K(q,k;P)$ is the fully amputated quark-antiquark scattering kernel. The Ward-Takahashi identity, eq. (4), means that the kernel in the gap equation and that in the Bethe-Salpeter equation are intimately related. Therefore, a qualitatively reliable understanding of chiral symmetry and its dynamical breaking can only be obtained using a truncation scheme that preserves this relation, and hence guarantees eq. (4) without a *fine-tuning* of model-dependent parameters.

One such scheme exists [9]. Its leading-order term is the renormalisation-group-improved rainbow-ladder truncation and the general procedure provides a means to identify, *a priori*, those channels in which that truncation is likely to be accurate. This scheme underlies the successful application of a rainbow-ladder model to flavour-nonsinglet pseudoscalar mesons and vector mesons [2–5]. The systematic nature of the scheme has also made possible a proof of Goldstone's theorem in QCD [6] and the derivation of a mass formula that unifies the light- and heavy-quark sectors [10].

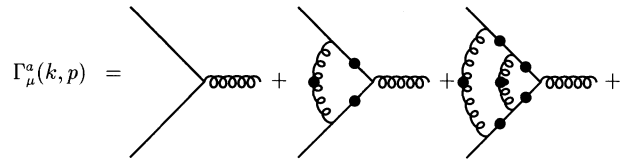

Fig. 1. Planar dressed-quark-gluon vertex obtained by neglecting contributions associated with explicit gluon self-interactions. The solid circles indicate fully dressed propagators. The quark-gluon vertices are not dressed.

Table 1. π- and ρ-meson masses obtained with $\mathcal{G} = 0.48\,\mathrm{GeV}$. (Dimensioned quantities in GeV.) n is the number of dressed-gluon rungs retained in the planar vertex, see fig. 1, and hence the order of the vertex-consistent Bethe-Salpeter kernel.

	$M_H^{n=0}$	$M_H^{n=1}$	$M_H^{n=2}$	$M_H^{n=\infty}$
π, $m = 0$	0	0	0	0
π, $m = 0.011$	0.152	0.152	0.152	0.152
ρ, $m = 0$	0.678	0.745	0.754	0.754
ρ, $m = 0.011$	0.695	0.762	0.770	0.770

In this scheme, as in perturbation theory, it is impossible, in general, to obtain complete closed-form expressions for the kernels of the gap and Bethe-Salpeter equations. However, for the planar dressed-quark-gluon vertex depicted in fig. 1, closed forms can be obtained and a number of significant features illustrated [11] when one uses the following model for the dressed-gluon line [12]:

$$g^2\, D_{\mu\nu}(k) = \left[\delta_{\mu\nu} - \frac{k_\mu k_\nu}{k^2}\right] (2\pi)^4\, \mathcal{G}^2\, \delta^4(k)\,, \tag{6}$$

where $\mathcal{G}$, measured in GeV, sets the model's mass-scale. This form is a precursor to the class of renormalisation-group-improved models. It has many positive features in common with that class and, furthermore, its particular momentum-dependence works to advantage in reducing integral equations to character-preserving algebraic equations. Naturally, there is a drawback: the simple momentum dependence also leads to some model-dependent artefacts, but they are easily identified and hence not cause for concern.

It is a general result [11] that with any vertex whose diagrammatic content is known explicitly; *e.g.*, fig. 1, it is always possible to construct a unique Bethe-Salpeter kernel which ensures the Ward-Takahashi identities are automatically fulfilled: that kernel is necessarily non-planar. This becomes transparent with the model in eq. (6), using which the gap equation obtained with the vertex depicted in fig. 1 reduces to an algebraic equation, irrespective of the number of dressed-gluon rungs that are retained, and the same is true of the Bethe-Salpeter equations in every channel: pseudoscalar, vector, etc.

Results for the π and ρ are illustrated in table 1. It is evident that, irrespective of the order of the truncation; *i.e.*, the value of n, the number of dressed gluon

rungs in the quark-gluon vertex, the pion is massless in the chiral limit. (N.B. This pion is composed of heavy dressed quarks, as is evident in the calculated scale of the dynamically generated dressed-quark mass function: $M(0) \approx 0.5\,\mathrm{GeV}$.) The masslessness of the π is a model-independent consequence of the consistency between the Bethe-Salpeter kernel and the kernel in the gap equation. Furthermore, the bulk of the ρ-π mass splitting is present in the chiral limit and with the simplest ($n = 0$; *i.e.*, rainbow-ladder) kernel, which makes plain that this mass difference is driven by the DCSB mechanism: it is not the result of a finely adjusted hyperfine interaction. Finally, the quantitative effect of improving on the rainbow-ladder truncation; *i.e.*, including more dressed-gluon rungs in the gap equation's kernel and consistently improving the kernel in the Bethe-Salpeter kernel, is a 10% correction to the vector meson mass. Simply including the first correction ($n = 1$, *i.e.*, retaining the first two diagrams in fig. 1) yields a vector meson mass that differs from the fully resummed result by $\lesssim 1\%$. The rainbow-ladder truncation is clearly accurate in these channels.

2.2 Rainbow-ladder truncation

The renormalisation-group-improved rainbow-ladder truncation is based on the fact that in QCD, on the domain for which $Q^2 := (k-q)^2 \sim k^2 \sim q^2$ is large and spacelike,

$$\begin{aligned} M(q,k;P) &:= g^2(\mu^2)\, D_{\mu\nu}(k-q) \\ &\quad \times \left[\Gamma^a_\mu(k_+,q_+) S(q_+)\right] \otimes \left[S(q_-)\,\Gamma^a_\nu(q_-,k_-)\right] \\ &= 4\pi\,\alpha(Q^2)\, D^{\mathrm{free}}_{\mu\nu}(k-q) \\ &\quad \times \left[\frac{\lambda^a}{2}\gamma_\mu\, S^{\mathrm{free}}(q_+)\right] \otimes \left[S^{\mathrm{free}}(q_-)\,\frac{\lambda^a}{2}\gamma_\nu\right], \end{aligned} \tag{7}$$

where $\alpha(Q^2)$ is the strong running coupling and, *e.g.*, S^{free} is the free quark propagator. The dressed-ladder truncation supposes that eq. (7) is valid for all momenta and is thus an assumption about the long-range ($Q^2 \lesssim 1\,\mathrm{GeV}^2$) behaviour of the interaction. Requiring that Ward-Takahashi identities be automatically fulfilled by any truncation entails [9,11] that the kernel in the renormalised gap equation is expressed through

$$\mathcal{G}(Q^2)\, D^{\mathrm{free}}_{\mu\nu}(Q)\frac{\lambda^a}{2}\gamma_\mu S(q)\frac{\lambda^a}{2}\gamma_\nu\,, \tag{8}$$

where we have introduced $\mathcal{G}(Q^2)$, an effective interaction, to emphasise that, while $\mathcal{G}(Q^2) = 4\pi\alpha(Q^2)$ is well determined for $Q^2 \gtrsim 1\,\mathrm{GeV}^2$, the behaviour at $Q^2 < 1\,\mathrm{GeV}^2$, *i.e.*, at infrared length-scales ($\gtrsim 0.2\,\mathrm{fm}$), of the kernels in the gap and Bethe-Salpeter equations is unknown.

Contemporary DSE studies employ a model for the infrared behaviour. The most extensively applied is [3]

$$\begin{aligned} \frac{\mathcal{G}(Q^2)}{Q^2} &= \frac{4\pi^2}{\omega^6} D\, Q^2 \mathrm{e}^{-Q^2/\omega^2} \\ &\quad + 8\pi \frac{\pi\,\gamma_m}{\ln\left[\tau + \left(1 + Q^2/\Lambda^2_{\mathrm{QCD}}\right)^2\right]}\,\mathcal{F}(Q^2)\,, \end{aligned} \tag{9}$$

Table 2. Calculated pion decay constant and vacuum quark condensate. Experimentally, $f_\pi = 0.092$, and a best phenomenological value of the condensate is $-\langle\bar{q}q\rangle^0_{1\,\mathrm{GeV}} = (0.236 \pm 0.008)^3$ [13]. (All quantities are listed in GeV.)

Model	f_π	$(-\langle\bar{q}q\rangle^0_{1\,\mathrm{GeV}})^{1/3}$
eqs. (9), (10)	0.092	0.24
eqs. (14), (15)	0.053	0.15
eqs. (14), (16)	0.099	0.25

where $\mathcal{F}(Q^2) = [1 - \exp(-k^2/[4m_t^2])]/k^2$, $m_t = 0.5\,\mathrm{GeV}$, $\tau = \mathrm{e}^2 - 1$, $\gamma_m = 12/(33 - 2N_f)$, $N_f = 4$, and $\Lambda_{\mathrm{QCD}} = \Lambda^{(4)}_{\overline{\mathrm{MS}}} = 0.234\,\mathrm{GeV}$ [14] (N.B. eq. (9) gives $\alpha(m_Z^2) = 0.126$. Comparison with a modern value [15], $0.113^{+0.009}_{-0.013}$, means that a smaller Λ_{QCD} is acceptable in the model, if one wants to avoid overestimating the coupling in the ultraviolet, but not a larger value.) The true parameters in eq. (9) are D and ω, which together determine the interaction tension in the model. However, they are not independent: in fitting, a change in one is compensated by altering the other; *e.g.*, on the domain $\omega \in [0.3, 0.5]\,\mathrm{GeV}$, the fitted observables are approximately constant along the trajectory $\omega D = (0.72\,\mathrm{GeV})^3$. This correlation, a reduction in D compensating for an increase in ω, acts to keep a fixed value of the interaction tension; *i.e.*, the interaction's integrated strength on the infrared domain. With

$$D = (0.96\,\mathrm{GeV})^2\,,\ \omega = 0.4\,\mathrm{GeV} \tag{10}$$

and current-quark masses

$$m_u^{1\,\mathrm{GeV}} = 5.5\,\mathrm{MeV}\,,\ m_s^{1\,\mathrm{GeV}} = 125\,\mathrm{MeV}\,, \tag{11}$$

one obtains the excellent description of meson observables described in the introduction, which can be illustrated via the calculated values of the leptonic decay constant and vacuum quark condensate in table 2.

2.3 Comparison with lattice-QCD simulations

The scalar functions characterising the renormalised dressed-quark propagator, *i.e.* the wave function renormalisation, $Z(p^2)$, and the mass function, $M(p^2)$, obtained by solving the renormalised gap equation using eq. (9), are depicted in figs. 2, 3. The infrared suppression of $Z(p^2)$ and enhancement of $M(p^2)$ are long-standing predictions of DSE studies, as ref. [16] makes plain and could be anticipated from ref. [17]. This prediction has recently been confirmed in numerical simulations of quenched lattice-QCD, as is evident in the figures.

It is not yet possible to reliably determine the chiral limit behaviour of lattice Schwinger functions. Hence one does not have a lattice estimate for the quantities in table 2. To obtain such an estimate, we used the DSE model described previously, varying (D, ω) in order to reproduce the lattice data. Our current best result, obtained with

$$D = (0.74\,\mathrm{GeV})^2\,,\ \omega = 0.3\,\mathrm{GeV}\,, \tag{12}$$

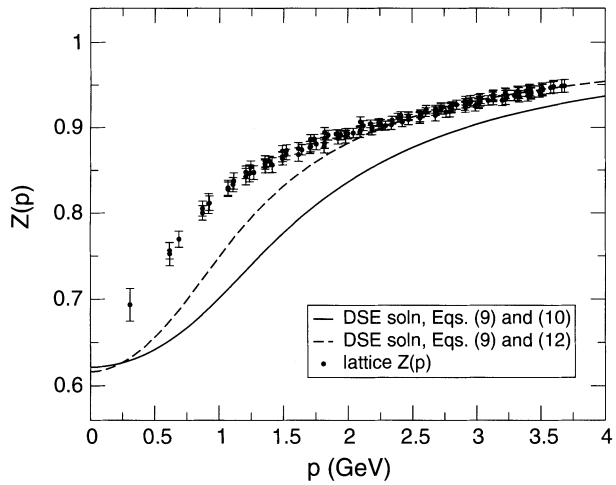

Fig. 2. Wave function renormalisation. Solid line: solution of the renormalised gap equation using eqs. (9), (10); data: lattice simulations [18], $m = 0.036/a \sim 60\,\mathrm{MeV}$; dashed line: gap equation solution using eqs. (9), (12). (In the DSE studies, the renormalisation point $\zeta = 19\,\mathrm{GeV}$ and the current-quark mass is $0.6\,m_s^{1\,\mathrm{GeV}}$ (eq. (11)).)

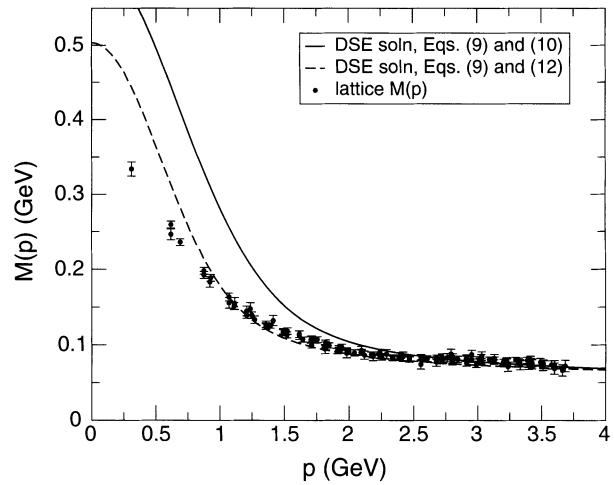

Fig. 3. Mass function. Solid line: solution of the renormalised gap equation using using eqs. (9), (10); data: lattice simulations [18], $m = 0.036/a \sim 60\,\mathrm{MeV}$; dashed line: gap equation solution using eqs. (9), (12). (In the DSE studies, the renormalisation point $\zeta = 19\,\mathrm{GeV}$ and the current-quark mass is $0.6\,m_s^{1\,\mathrm{GeV}}$ (eq. (11)).)

at a current-quark mass of $0.6\,m_s^{1\,\mathrm{GeV}}$, eq. (11), is also depicted in figs. 2, 3, and yields $f_\pi = 0.094\,\mathrm{GeV}$, $m_\pi = 0.48\,\mathrm{GeV}$. (N.B. These are values for a pion-like bound state constructed from constituents whose current-quark mass is $m \approx 14\,m_u$. Our DSE-calculated meson mass *versus* current-quark mass trajectory is consistent with results of recent quenched lattice-QCD simulations obtained on $m \in [1,2]\,m_s$ [10].) The parameters in eq. (12) give chiral limit results:

$$f_\pi^0 = 0.068\,\mathrm{GeV}\,,\ -\langle\bar{q}q\rangle^0_{1\,\mathrm{GeV}} = (0.19\,\mathrm{GeV})^3\,. \tag{13}$$

2.4 Gap equation and QCD's gauge sector

Contemporary Landau gauge DSE studies of QCD's gauge sector have been used to infer a form of the effective interaction [19], which is well represented by ($x = Q^2/\Lambda^2_{\mathrm{QCD}}$)

$$\frac{1}{4\pi}\mathcal{G}(x) := \alpha(x) = \frac{a_0 + a_1 x}{1 + a_2 x + a_3 x^2 + a_4 x^3} + \frac{\pi\,\gamma_m}{\ln(e + x)}\,, \tag{14}$$

a_0	a_1	a_2	a_3	a_4
1.47	0.881	0.314	0.00986	0.00168

(15)

Aspects of these DSE studies are in qualitative agreement with quenched lattice-QCD results [20]; *e.g.*, the feature that the dressed-gluon propagator is finite at $Q^2 = 0$. This effective interaction yields the results in the second row of table 2: apparently, f_π is too small by a factor of ~ 2 and the scale of DCSB too small by a factor of $\sim 4 = 1.6^3$ [21]. This outcome could have been anticipated from ref. [7].

Equations (7), (8) are correct on the ultraviolet domain in which perturbation theory is applicable. However, modelling is involved in extrapolating onto the infrared domain. One may require that multiplicative renormalisability of the dressed fermion propagator be preserved in this modelling [22]. The *Ansatz* of ref. [23] incorporates this constraint; however, it implicitly specifies a kernel in the gap equation that violates a more important constraint, namely, Lorentz covariance [24]. A minimal *Ansatz* that satisfies both constraints and eq. (7) finds expression in the kernel of the renormalised gap equation as

$$4\pi\alpha(Q^2)\frac{1}{Z^2(Q^2)}\,D^{\mathrm{free}}_{\mu\nu}(Q)\frac{\lambda^a}{2}\gamma_\mu S(q)\frac{\lambda^a}{2}\gamma_\nu\,. \tag{16}$$

The gap equation's solution now gives the results in the third row of table 2. (We simplified the numerical study by using a well-tried angle approximation: $\alpha((k-q)^2)/Z^2((k-q)^2) \approx \alpha((k-q)^2)/Z^2(\max(k^2,q^2))$.) This procedure is evidently a candidate for providing a bridge between DSE studies of the gauge sector and what is known, from the calculation of observables, to be the infrared strength required in the effective interaction. The increased interaction tension arises because the enhancement of $1/Z(p^2)$, evident in fig. 2, persists with this kernel and amplifies the effective coupling: the interaction tension calculated with eq. (14) alone is $\sigma^\Delta = 12\,\mathrm{GeV/fm}$, but using eq. (16) we estimate that the $1/Z^2(Q^2)$ factor raises this to $\sigma^\Delta \sim 25\,\mathrm{GeV/fm}$.

3 Confinement

This is a statement about the properties of coloured Schwinger functions; *i.e.*, gauge-dependent quantities. Hence it is plausible that the expression of confinement will depend on the gauge-fixing procedure one employs. Linear covariant gauges are most widely employed in DSE studies. While the problem of Gribov copies is unresolved, it affects only the far infrared behaviour of coloured Schwinger functions and hence is hoped to have little impact on physical observables. This conjecture is supported

by the close correspondence between Landau and Laplacian gauge two-point quark and gluon Schwinger functions obtained in quenched lattice-QCD simulations [25]. (Laplacian gauge fixing is a nonlocal prescription that is identical to Landau gauge at ultraviolet momenta. It is free of Gribov copies.)

It has long been known [26] that for confinement it is sufficient that no coloured Schwinger function possess a spectral representation. This is equivalent to the statement that all coloured Schwinger functions violate reflection positivity. That property can manifest itself *almost* as simply as, say, dressed-gluons being described by a propagator with a large width. The connection between confinement and the violation of reflection positivity has cleanly been illustrated in QED3 [27], and it is a result of DSE studies that a sufficiently large interaction tension will always produce a dressed-quark propagator that violates reflection positivity. (N.B. Gap equation solutions that violate reflection positivity also exhibit DCSB. The converse is not necessarily true.) Thus, it is a widespread conjecture that confinement in QCD is realised this way.

A Schwinger function that violates reflection positivity is easily identified: it is sufficient that the function exhibit a maximum or inflection at some spacelike four-momentum-squared. In lattice-QCD simulations, this feature is evident in the two-point gluon Schwinger function [20] and incipient in the scalar functions characterising the dressed-quark two-point function [18]. It is plain in our results for the dressed-quark propagator, figs. 2, 3, and apparent in the DSE result for the gluon two-point function [28]. The DSE solution for the ghost two-point function also violates reflection positivity but in this case it is manifest in the strength of its singularity at $k^2 = 0$.

A consistent picture may be emerging It is complemented by the fact that the colour-singlet S-matrix elements which describe physical processes do not exhibit unphysical quark and gluon production thresholds when calculated using coloured Schwinger functions that violate reflection positivity. The ideas we have described also ensure that coloured composites such as diquarks do not appear in the spectrum [9,11].

4 Epilogue

The momentum-dependent dressing of quark and gluon propagators is a fact. It is certainly the keystone of DCSB and quite likely plays a central role in confinement. Its incorporation into models of low-energy phenomena facilitates the development of a qualitatively reliable understanding and makes possible an excellent description of experiment. That has provided guidance for modelling the long-range behaviour of the interaction between light-quarks. A remaining challenge is to calculate it and progress is being made.

We thank P.O. Bowman for the lattice data and P.C. Tandy for a careful reading of the manuscript. PM and AR are grateful for the hospitality and support of the Physics Division at ANL during visits in which part of this work was conducted. This work was supported by the Deutsche Forschungsgemeinschaft, contract no. Ro 1146/3-1; the US Department of Energy (DOE), Nuclear Physics Division, contract no. W-31-109-ENG-38; DOE grant nos. DE-FG02-96-ER-40947, DE-FG02-97-ER-41048; and benefited from the resources of the US National Energy Research Scientific Computing Center.

References

1. C.D. Roberts, S.M. Schmidt, Prog. Part. Nucl. Phys. **45**, S1 (2000); R. Alkofer, L. v. Smekal, Phys. Rep. **353**, 281 (2001).
2. P. Maris, C.D. Roberts, Phys. Rev. C **56**, 3369 (1997).
3. P. Maris, P.C. Tandy, Phys. Rev. C **60**, 055214 (1999).
4. P. Bicudo, *et al.*, Phys. Rev. D **65**, 076008 (2002); D. Jarecke, P. Maris, P.C. Tandy, *Strong decays of light vector mesons*, nucl-th/0208019.
5. P. Maris, P.C. Tandy, Phys. Rev. C **62**, 055204 (2000); C.R. Ji, P. Maris, Phys. Rev. D **64**, 014032 (2001); P. Maris, P.C. Tandy, Phys. Rev. C **65**, 045211 (2002).
6. P. Maris, C.D. Roberts, P.C. Tandy, Phys. Lett. B **420**, 267 (1998).
7. F.T. Hawes, P. Maris, C.D. Roberts, Phys. Lett. B **440**, 353 (1998).
8. C.D. Roberts, *Continuum strong QCD: Confinement and dynamical chiral symmetry breaking*, nucl-th/0007054.
9. A Bender, C.D. Roberts, L. v. Smekal, Phys. Lett. B **380**, 7 (1996).
10. C.D. Roberts, Nucl. Phys. Proc. Suppl. **108**, 227 (2002).
11. A. Bender, W. Detmold, A.W. Thomas, C.D. Roberts, Phys. Rev. C **65**, 065203 (2002).
12. H.J. Munczek, A.M. Nemirovsky, Phys. Rev. D **28**, 181 (1983).
13. D.B. Leinweber, Ann. Phys. (N.Y.) **254**, 328 (1997).
14. Particle Data Group Collaboration (L. Montanet *et al.*), Phys. Rev. D **50**, 1173 (1994).
15. Particle Data Group Collaboration (D.E. Groom *et al.*), Eur. Phys. J. C **15**, 1 (2000).
16. C.D. Roberts, A.G. Williams, Prog. Part. Nucl. Phys. **33**, 477 (1994).
17. K. Johnson, M. Baker, R. Willey, Phys. Rev. **136**, B1111 (1964).
18. P.O. Bowman, U.M. Heller, A.G. Williams, Phys. Rev. D **66**, 014505 (2002).
19. R. Alkofer, C.S. Fischer, L. v. Smekal, Acta Phys. Slov. **52**, 191 (2002) and references therein.
20. F.D. Bonnet, *et al.*, Phys. Rev. D **64**, 034501 (2001).
21. These results are in agreement with M. Bhagwat, M.A. Pichowsky, P.C. Tandy, private communication.
22. D.C. Curtis, M.R. Pennington, Phys. Rev. D **42**, 4165 (1990).
23. J.C.R. Bloch, *Multiplicative renormalizability and quark propagator*, hep-ph/0202073.
24. C.J. Burden, C.D. Roberts, Phys. Rev. D **47**, 5581 (1993).
25. P.O. Bowman, U.M. Heller, A.G. Williams, Nucl. Phys. Proc. Suppl. **109**, 163 (2002); P.O. Bowman, U.M. Heller, D.B. Leinweber, A.G. Williams, *Gluon propagator on coarse lattices in Laplacian gauges*, hep-lat/0206010.
26. G. Krein, C.D. Roberts, A.G. Williams, Int. J. Mod. Phys. A **7**, 5607 (1992).
27. P. Maris, Phys. Rev. D **52**, 6087 (1995).
28. R. Alkofer, L. v. Smekal, Nucl. Phys. A **680**, 133 (2000).

Eur. Phys. J. A **18**, 237–240 (2003)
DOI 10.1140/epja/i2002-10207-5

THE EUROPEAN PHYSICAL JOURNAL A

Experimental tests of Chiral Perturbation Theory

H. Merkel[a]

For the MAMI A1 Collaboration
Institut für Kernphysik, Johannes Gutenberg-Universität Mainz, 55099 Mainz, Germany

Received: 12 August 2002 /
Published online: 22 October 2003 – © Società Italiana di Fisica / Springer-Verlag 2003

Abstract. In this paper the current status of the threshold photo- and electroproduction of neutral pions as test of Chiral Perturbation Theory is summarized. The combination of differential cross-section data with polarized photon asymmetries allows to determine a complete set of s- and p-wave amplitudes at threshold for the photoproduction case. These extracted amplitudes are in good agreement with predictions and fits of Heavy Baryon Chiral Perturbation Theory. On the other hand, new data on pion electroproduction shows a significant deviation from the predicted cross-sections at a four-momentum transfer of $Q^2 = 0.05\,\mathrm{GeV}^2/c^2$. For the coherent pion production from the deuteron the photoproduction data agree with Chiral Perturbation Theory. The former reported severe disagreement between the electroproduction s-wave amplitude at a four-momentum transfer of $Q^2 = 0.1\,\mathrm{GeV}^2/c^2$ and first calculations seems to be resolved now.

PACS. 25.30.Rw Electroproduction reactions – 13.60.Le Meson production – 12.39.Fe Chiral Lagrangians

1 Neutral pion photoproduction

Chiral Perturbation Theory is a consistent scheme to utilize the symmetries of QCD to predict observables at the confinement scale. A short introduction on the basic principles of ChPT was given in this conference [1]. A more complete overview of the status of this field can be found, *e.g.*, in ref. [2].

In this paper, the current status of the neutral pion photo- and electroproduction experiments near threshold is discussed. Since the pion is the Goldstone Boson of the chiral symmetry breaking, these experiments are well suited to test calculations in the framework of Heavy Baryon Chiral Perturbation Theory (HBChPT) [3].

First experiments [4] on threshold pion photoproduction were aimed at testing the predictions of Low Energy Theorems [5] for the threshold value of the s-wave multipole amplitude E_{0+}. The severe disagreement between these theorems and the experiments was resolved in the following years by refined calculations in HBChPT [6], which also gave predictions for the p-wave multipole combinations:

$$\begin{aligned} P_1 &= 3E_{1+} + M_{1+} - M_{1-}\,, \\ P_2 &= 3E_{1+} - M_{1+} + M_{1-}\,, \\ P_3 &= 2M_{1+} + M_{1-}\,. \end{aligned}$$

The calculations showed that the s-wave amplitude is only slow converging in the chiral expansion, while the p-wave combinations P_1 and P_2 are strong predictions in this framework. P_3 is given by a low-energy constant of HBChPT and has to be determined by the experiment.

The first experimental access to the multipoles is the measurement of the differential cross-section. With the assumption that only s- and p-waves contribute at threshold, the angular structure of the cross-section is given by

$$\sigma(\theta) = \frac{q}{k}\left(A + B\,\cos\theta + C\,\cos^2\theta\right)$$

with the phase space factor $\frac{q}{k}$ and three angular coefficients,

$$\begin{aligned} A &= E_{0+}^2 + \frac{1}{2}\left({P_2}^2 + {P_3}^2\right)\,, \\ B &= 2\,Re\left(E_{0+}{P_1}^*\right)\,, \\ C &= {P_1}^2 - \frac{1}{2}\left({P_2}^2 + {P_3}^2\right)\,. \end{aligned}$$

Experiments at SAL [7] and MAMI [8,9] are in good agreement and allow for an extraction of the full angular structure of the differential cross-section. But from unpolarized cross-section experiments, only the modulus of the s-wave multipole $|E_{0+}|$ and the p-wave combinations P_1 and $P_{23} := \frac{1}{2}({P_2}^2 + {P_3}^2)$ can be extracted. To further decompose all multipoles, a further observable has to be measured. A convenient choice is the polarized photon asymmetry Σ with the multipole decomposition

$$\Sigma(\theta)\,\sigma(\theta) \sim \sin(\theta)\frac{1}{2}\left(P_3^2 - P_2^2\right).$$

[a] e-mail: merkel@kph.uni-mainz.de

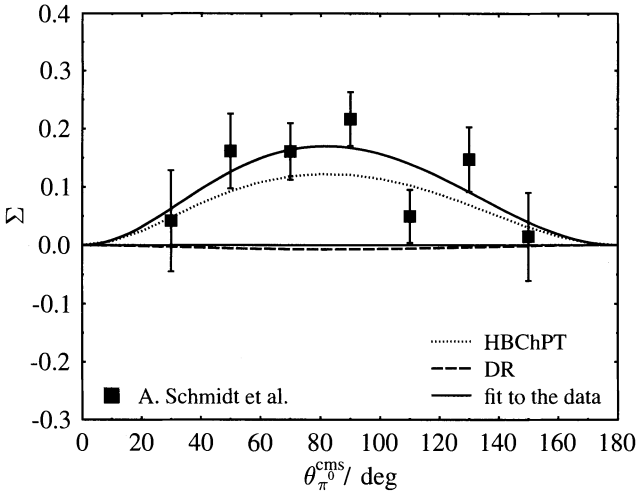

Fig. 1. Polarized photon asymmetry measured at MAMI [9] in comparison with calculations in ChPT [6] and in Dispersion Relations formalism [10].

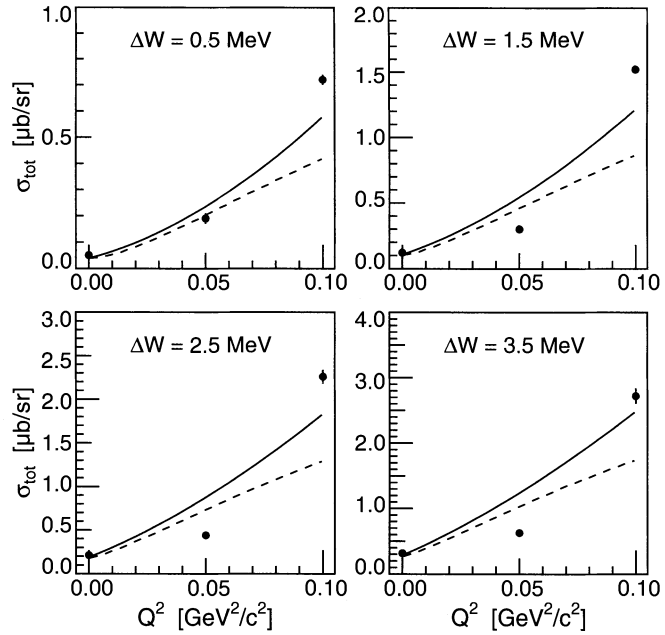

Fig. 2. The total cross-section $\sigma_{\rm tot}$ *versus* Q^2, at a value of $\epsilon = 0.8$. The solid (dashed) line is the prediction of ChPT [13] (MAID [15]), data points at $Q^2 = 0$ and $0.1\,\mathrm{GeV}^2/\mathrm{c}^2$ from [9,12].

Such an experiment was performed at MAMI [9] at the tagged-photon beam of the A2 Collaboration with the TAPS detector for the detection of the π^0 decay photons. The polarized photon beam was produced by coherent Bremsstrahlung from a diamond crystal. Figure 1 shows the asymmetry Σ, averaged over the energy range of the experiment.

With this experiment, for the first time a complete separation of the p-waves is possible. The results are given in table 1, in comparison with the predictions of Chiral Perturbation Theory (ChPT) [6] and Dispersion Relations(DR) [10]. Within the error bars, the two existing high-resolution experiments and the quoted calculations agree. The deviation for P_3 of ChPT can be removed by re-fitting the low-energy constants to the new data set.

2 Electroproduction at low Q^2

Additional information on the pion production mechanism can be extracted from electroproduction experiments.

While, *e.g.*, the multipole combination P_3 is basically a fit parameter in the description of the photoproduction data, the extention of this quantity to virtual photons is given in ChPT without further degrees of freedom. In addition, the longitudinal s-wave amplitude L_{0+} and two further longitudinal p-wave combinations can be extracted.

First experiments at a photon virtuality of $Q^2 = 0.1\,(\mathrm{GeV}/c)^2$ aimed at extracting the s-wave amplitudes at threshold [11,12]. These experiments were in reasonable agreement with calculations [13], but the value of $Q^2 = 0.1\,(\mathrm{GeV}/c)^2$ is somewhat to high for the convergence radius of ChPT.

Therefore, a further experiment at the intermediate value of the photon virtuality $Q^2 = 0.05\,(\mathrm{GeV}/c)^2$, halfway between photoproduction and the existing data was performed at MAMI [14].

This experiment showed a surprising discrepancy to the calculations. Figure 2 shows the total cross-section as a function of Q^2. In this observable, the statistical error of all data points is very small and only systematic errors contribute. Thus, the clear discrepancy between data and calculations, but also the increasing discrepancy between ChPT and MAID [15] is visible.

In ref. [14] also an extraction of multipoles in a model-independent manner was attempted. While the resolution of the experiments is not yet good enough to perform a reliable separation of the multipoles, it seems that the deviation is burried in the multipole combination P_{23}, which is already fixed by photoproduction and cannot be adjusted in the calculations to describe the new data set.

Since the discrepancy is large and surprising, this subject urgently needs further investigation. An experiment at MAMI is planned to cover a continuous range in Q^2, while an independent experiment is planned at JLab [16] with extended kinematical coverage using a large acceptance spectrometer.

3 Electroproduction from the deuteron

The low-energy constants of ChPT were adjusted, as shown above, to describe the existing pion photo- and electroproduction data from the proton. By this, one looses some of the predictive power of ChPT, since in threshold experiments the complete amplitude is already given by only few parameters. On the other hand, from the description of the proton amplitudes one can extract predictions for the pion production from the neutron without introducing further degrees of freedom.

Despite this theoretical advantage, the experimental access to the free neutron amplitude is quite difficult. The

Table 1. Experimental multipole amplitudes for photoproduction from MAMI [9] and SAL [7] in comparison with Chiral Perturbation Theory (ChPT)) [6] and Dispersion Relations (DR).

	E_{0+} $(10^{-3}/m_\pi)$	P_1 $(qk \cdot 10^{-3}/m_\pi^3)$	P_2 $(qk \cdot 10^{-3}/m_\pi^3)$	P_3 $(qk \cdot 10^{-3}/m_\pi^3)$
MAMI	-1.31 ± 0.08	10.02 ± 0.2	-10.5 ± 0.2	13.1 ± 0.1
SAL	-1.32 ± 0.05	10.26 ± 0.1		
ChPT	-1.16	10.33 ± 0.6	-11.0 ± 0.6	11.7 ± 0.6
DR	-1.22	10.54	-11.4	10.2

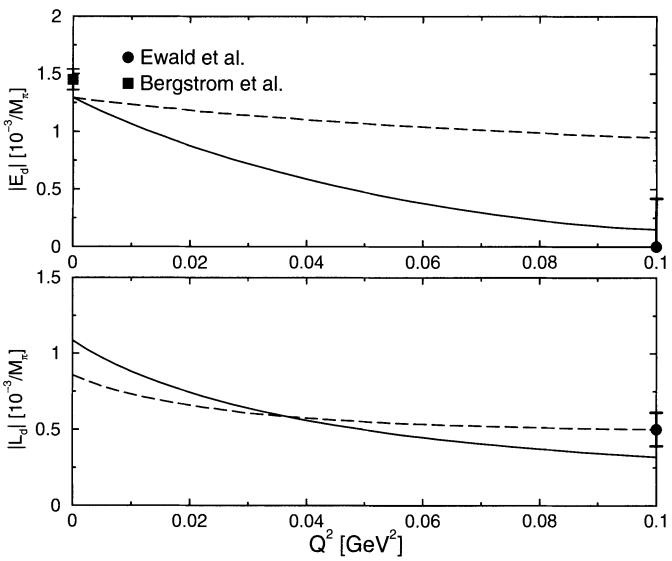

Fig. 3. The extracted s-wave multipoles from MAMI [19] (circles) in comparison with the prediction of ChPT [21]. The solid line shows the fit to the data, while the dashed line was fitted with additional constrains from resonance saturation.

most promising method seems to be the coherent pion production from a deuteron target. In impulse approximation, the production amplitude is basically given by the coherent iso-scalar sum of the free proton and free neutron amplitude, corrected by form factors as parameterization of the deuteron structure.

A first measurement of the photoproduction amplitude was performed at SAL [17]. The IGLOO detector was used to detect the decay photons of the π^0 decay in coincidence. By this technique, the missing mass resolution is not sufficient to separate the coherent channel from the deuteron breakup. By calculating this contribution in a simple model, the authors were able to extract the threshold value of the s-wave amplitude to $E_d = (-1.45 \pm 0.09) \times 10^{-3}/m_\pi$.

This value falls about 20% below the prediction of ChPT [18] of $E_d = (-1.8 \pm 0.6) \times 10^{-3}/m_\pi$ but the agreement seems reasonable within the error bars.

The extension of this experiments to finite Q^2 introduced further experimental difficulties. Due to the background conditions for electroproduction the detection of the pion decay photons had to be replaced by the detection of the recoil deuteron, which suffers at the low energies at threshold from energy loss and multiple scattering. On the other hand, by this technique the coherent channel is clearly separated from the deuteron break-up reaction and can be extracted without model assumptions.

A first threshold measurement of $d(e, e'd)\pi^0$ was performed at MAMI [19]. The detection of the deuteron limited this experiment to a four-momentum transfer of $Q^2 = 0.1\,(\mathrm{GeV}/c)^2$. As for the similar experiments from the proton, the full center-of-mass angle was covered up to 4 MeV above threshold and a Rosenbluth separation was performed.

The first prediction in ChPT for electroproduction [20] could not explain the extracted s-wave amplitudes $|E_d| \approx 0 \cdot 10^{-3}/m_\pi$ and $|L_d| = 0.5 \cdot 10^{-3}/m_\pi$ and missed the experiment by nearly an order of magnitude. The improved calculation [21] showed that it is necessary to calculate elementary nucleon amplitudes and multi-body currents in consistent schemes. Figure 3 shows the result of this calculation in comparison with the data. Within the large systematic error of the data, finally consistency could be achieved. Of course, a measurement at lower Q^2 would be necessary to further test these concepts.

References

1. B. Holstein, this issue, p. 227.
2. A.M. Bernstein, J.L. Goity, Ulf.-G. Meißner (Editors), *Chiral Dynamics* (World Scientific, Singapore, 2001).
3. V. Bernard *et al.*, Nucl. Phys. B **383**, 442 (1992).
4. E. Mazzucato *et al.*, Phys. Rev. Lett. **57**, 3144 (1986); R. Beck *et al.*, Phys. Rev. Lett. **65**, 1841 (1990).
5. P. de Baenst, Nucl. Phys. B **24**, 633 (1970); I.A. Vainshtein, V.I. Zakharov, Nucl. Phys. B **36**, 589 (1972).
6. V. Bernard, N. Kaiser, J. Gasser, Ulf-G. Meißner, Phys. Lett. B **268**, 291 (1991); V. Bernard, N. Kaiser, Ulf-G. Meißner, Z. Phys. C **70**, 483 (1996).
7. J. C. Bergstrom *et al.*, Phys. Rev. C **53**, R1052 (1996).
8. M. Fuchs *et al.*, Phys. Lett. B **368**, 20 (1996); A.M. Bernstein *et al.*, Phys. Rev. C **55**, 1509 (1997).
9. A. Schmidt *et al.*, Phys. Rev. Lett. **87**, 232501 (2001).
10. O. Hanstein *et al.*, Phys. Lett. B **399**, 13 (1997).
11. H.B. van den Brink *et al.*, Phys. Rev. Lett. **74**, 3561 (1995); T.P. Welch *et al.*, Phys. Rev. Lett. **69**, 2761 (1992).
12. M.O. Distler *et al.*, Phys. Rev. Lett. **80**, 2294 (1998).
13. V. Bernard, N. Kaiser, Ulf-G. Meißner, Nucl. Phys. A **607**, 379 (1996); **633**, 695(E) (1998).
14. H. Merkel *et al.*, Phys. Rev. Lett. **88**, 012301 (2002).
15. D. Drechsel *et al.*, Nucl. Phys. A **645**, 145 (1999); S.S. Kamalov *et al.*, Phys. Lett. B **522**, 27 (2001).

16. R. Lindgren *et al.*, Experiment E01-014, JLab, 2001.
17. J.C. Bergstrom *et al.*, Phys. Rev. C **57**, 3203 (1998).
18. S.R. Beane *et al.*, Nucl. Phys. A **618**, 381 (1997).
19. I. Ewald *et al.*, Phys. Lett. B **499**, 238 (2001).
20. V. Bernard, H. Krebs, Ulf-G. Meißner, Phys. Rev. C **61**, 58201 (2000).
21. Ulf-G. Meißner, this issue, p. 487; H. Krebs, V. Bernard, Ulf-G. Meißner, nucl-th/0207072.

Eur. Phys. J. A **18**, 241–245 (2003)
DOI 10.1140/epja/i2002-10208-4

THE EUROPEAN PHYSICAL JOURNAL A

Recent developments in quark nuclear physics

A.W. Thomas[a], D.B. Leinweber, and R.D. Young

Special Research Centre for the Subatomic Structure of Matter and Department of Physics and Mathematical Physics, University of Adelaide, Adelaide 5005, Australia

Received: 30 September 2002 /
Published online: 22 October 2003 – © Società Italiana di Fisica / Springer-Verlag 2003

Abstract. We provide an overview of recent work exploring the quark-mass dependence of hadronic observables and the associated role of chiral non-analytic behavior due to the meson-cloud of hadrons. In particular, we address an issue of great current interest, namely the degree of model independence of results obtained through a controlled extrapolation of lattice QCD simulation results. Physical insights gained from this research are highlighted. We emphasize how chiral effective field theory formulated with a finite-range regulator provides a reliable and *model-independent* extrapolation to the physical world.

PACS. 12.38.Gc Lattice QCD calculations – 11.30.Rd Chiral symmetries – 24.85.+p Quarks, gluons, and QCD in nuclei and nuclear processes

1 Introduction

Quark nuclear physics describes our attempts to understand the structure of hadronic systems, including nuclei and dense matter, in terms of quarks and gluons —the fundamental degrees of freedom in QCD. It is impossible in just a few pages to provide even a vague outline of the many exciting physics issues currently being addressed in this field —from the possible phase transition to one or more quark-gluon phases at high temperature or density [1], to suggestions of changes of hadron properties in-medium [2,3]. Instead, we shall concentrate on just one development which offers considerable insight into hadron structure from QCD itself, an approach which has led to surprisingly accurate comparisons between lattice QCD data and experiment as well as remarkable insights into how one might improve hadron models.

As the time for calculations within lattice QCD [4] with dynamical fermions (including q-$\bar{q}$ creation and annihilation in the vacuum) scales as $m_q^{-3.6}$ [5], current calculations have been limited to light quark masses 6–10 times larger than the physical ones. With the next generation of supercomputers, around 10 Teraflops, it should be possible to get as low as 2–3 times the physical quark mass, but to actually reach that goal on an acceptable volume will require at least 500 Teraflops. This is probably 10–20 years away.

Since a major motivation for lattice QCD must be to unambiguously compare the calculations of hadron properties with experiment, this is somewhat disappointing. The only remedy for the next decade at least is to find a way to extrapolate masses, form-factors, and so on, calculated at a range of masses considerably larger than the physical ones, to the chiral limit. In an effort to avoid theoretical bias this has usually been done through low-order polynomial fits as a function of quark mass. Unfortunately, as we discuss in sect. 2, this is incorrect and can yield quite misleading results because of the Goldstone nature of the pion.

The essential problem in performing calculations at realistic quark masses (of order 5 MeV) is the approximate chiral symmetry of QCD. Goldstone's theorem tells us that chiral symmetry is dynamically broken and that the non-perturbative vacuum is highly non-trivial [6], with massless Goldstone bosons in the limit $m_q \to 0$. For finite quark mass these bosons are the three charge states of the pion with a mass $m_\pi^2 \propto m_q$. Although this result strictly holds only for m_π^2 near zero (the Gell-Mann–Oakes–Renner relation), lattice simulations show it is a good approximation for m_π^2 up to 1 GeV^2 or so, and we shall use m_π^2 here as a measure of the deviation from the chiral limit.

On these very general grounds, one is therefore compelled to incorporate the non-analyticity into any extrapolation procedure. The classical approach to this problem is chiral perturbation theory (χpt), an effective field theory built upon the symmetries of QCD [7]. There is considerable evidence that the scale naturally associated with chiral symmetry breaking in QCD, $\Lambda_{\chi\mathrm{SB}}$, is of order $4\pi f_\pi$, or about 1 GeV. χpt then leads to an expansion in powers of $m_\pi/\Lambda_{\chi\mathrm{SB}}$ and $p/\Lambda_{\chi\mathrm{SB}}$, with p a typical momentum scale for the process under consideration. At $\mathcal{O}(p^4)$, the corresponding effective Lagrangian has only a small

[a] e-mail: athomas@physics.adelaide.edu.au

number of unknown coefficients which can be determined from experiment. On the other hand, at $\mathcal{O}(p^6)$ there are more than 100 unknown parameters [8], far too many to determine phenomenologically.

While this situation seems formidable, the resolution is already in hand. We must first realize that the lattice data obtained so far represents a wealth of information on the properties of hadrons within QCD itself over a range of quark masses. Just as the study of QCD as a function of N_c has taught us a great deal, so the behaviour as a function of m_q can yield considerable insight into hadronic physics.

The first thing that stands out, once one views the data as a whole, is just how smoothly every hadron property behaves in the region of large quark mass. In fact, baryon masses behave like $a + b\,m_q$, magnetic moments like $(c + d\,m_q)^{-1}$, charge radii squared like $(e + f\,m_q)^{-1}$ and so on. Thus, if one defined a light "constituent quark mass" as $M \equiv M_0 + \tilde{c}\,m_q$ (with $\tilde{c} \sim 1$), one would find baryon masses proportional to M (times the number of u and d quarks), magnetic moments proportional to M^{-1} and so on —just as in the constituent quark picture. There is little or no evidence for the rapid non-linearity associated with the branch cuts created by Goldstone boson loops.

Over the past few years we have come to a deep understanding of why QCD exhibits these features. It will be helpful to summarise those conclusions here:

- In the region of quark masses $m_q > 60$ MeV or so (m_π greater than typically 400–500 MeV) hadron properties are smooth, slowly varying functions of something like a constituent quark mass, $M \sim M_0 + c\,m_q$ (with $c \sim 1$).
- Indeed, $M_N \sim 3\,M, M_{\rho,\omega} \sim 2\,M$ and magnetic moments behave like $1/M$.
- As m_q decreases below 60 MeV or so, chiral symmetry leads to rapid, non-analytic variation, with $\delta M_N \sim {m_q}^{3/2}, \delta\mu_H \sim {m_q}^{1/2}$ and $\delta\langle r^2\rangle_{\rm ch} \sim \ln m_q$.
- Chiral quark models like the cloudy bag [9–11] provide a natural explanation of this transition. The scale is basically set by the inverse size of the composite source, above which chiral loops are strongly suppressed. Below this scale, the pion Compton wavelength is larger than the source and one begins to see rapid, non-analytic chiral corrections.

These are remarkable results that will have profound consequences for our further exploration of hadron structure within QCD as well as the analysis of the vast amount of data now being taken concerning unstable resonances. In terms of immediate results for the structure of the nucleon, we note that the careful incorporation of the correct chiral behaviour of QCD into the extrapolation of its properties calculated on the lattice has produced:

i) The most accurate values of the proton and neutron magnetic moments from lattice QCD [12].
ii) The most accurate value of the sigma commutator from lattice QCD [13].
iii) The most accurate values for the charge radii of the baryon octet from lattice QCD [14].
iv) The most accurate values for the magnetic moments of the hyperons from lattice QCD [15,16].
v) Good agreement between the extrapolated moments of the non-singlet distribution, $u-d$, calculated in lattice QCD and the experimentally measured moments [17, 18].
vi) The most accurate estimates of the low moments of the spin-dependent parton distribution functions at the physical quark mass from lattice QCD [19].
vii) An understanding of the failures of the assumption of universality of quark electromagnetic properties [20] and an improved lattice estimate of the strangeness magnetic moment of the proton G_M^s [21].

Furthermore, this approach, together with the observed constituent-quark–like behaviour seen in the lattice data for $m_q > 50$ MeV (as noted earlier), has suggested a novel way of modelling hadron structure [22,23].

Apart from the original publications, these developments have been fairly widely reported at various conferences —*e.g.* see refs. [24,25]. Here we focus particularly on the question of the extrapolation of hadron masses in order to clarify an issue of great current interest, namely the degree of model independence of the results obtained after a controlled chiral extrapolation.

2 Effective field theory

Chiral perturbation theory is a low-energy effective field theory for QCD. Low-energy properties of QCD can be expanded about the limit of vanishing momenta and quark mass. In relation to the extrapolation of lattice data, χpt provides a functional form applicable in the limit $m_\pi \to 0$.

Goldstone boson loops give rise to specific corrections to baryon properties —most importantly, they give rise to non-analytic behaviour as a function of quark mass. The low-order, non-analytic contributions arise from the pole in the Goldstone boson propagator and hence are *model-independent* [26]. Analytic variation of hadron properties is not constrained via the symmetry and hence expansions contain free parameters which must be determined by comparison with data.

Effective field theory then tells us that the general expansion of the nucleon mass about the $SU(2)$ chiral limit is

$$m_N = \alpha_0 + \alpha_2\,m_\pi^2 + \alpha_4\,m_\pi^4 + \sigma_{N\pi}(m_\pi, \Lambda) + \sigma_{\Delta\pi}(m_\pi, \Lambda) + \dots, \quad (1)$$

where $\sigma_{B\pi}$ is the self-energy arising from a $B\pi$ loop ($B = N$ or Δ). The expansion has been written explicitly in this form to highlight that the theory is equivalently defined for an arbitrary regulator —see ref. [27] for a complete discussion.

The traditional approach within the literature is to use dimensional regularisation to evaluate the self-energy integrals. Under such a scheme, the $NN\pi$ contribution simply becomes $\sigma_{N\pi}(m_\pi, \Lambda) \to c_{\rm LNA}\,m_\pi^3$ and the analytic terms, $\alpha_n\,m_\pi^n$, undergo an infinite renormalisation. The Δ contribution behaves similarly, producing a logarithm and

one obtains a series expansion of the nucleon mass about $m_\pi = 0$:

$$m_N = c_0 + c_2\, m_\pi^2 + c_4\, m_\pi^4 + c_{\rm LNA}\, m_\pi^3 + c_{\rm NLNA}\, m_\pi^4 \ln m_\pi + \dots\,, \qquad (2)$$

where the α_i have been replaced by the renormalised (and finite) parameters c_i.

It is not clear, *a priori*, that any such truncated expansion will be capable of reliably fitting lattice data. The first empirical indication of serious problems in this approach came with the realization that lattice data could not recover the *model-independent* coefficient, $c_{\rm LNA}$. Truncating the power series at the m_π^3 term and allowing $c_{\rm LNA}$ to vary as a free fit parameter, together with c_0 and c_2, produced a value $c_{\rm LNA} \sim -0.76$ GeV^{-2} [28]. This should be compared with the physical value of -5.6 GeV^{-2} —a factor of 8 larger! This tells us immediately that *either* there are serious convergence problems with the third-order expansion *or* lattice QCD is in error. Clearly, most readers would opt for the first possibility and so do we.

Even by retaining all terms as described in eq. (2), it is not clear that reliable extrapolation can be guaranteed by fitting lattice data over a range of (heavy) quark masses. One point of issue is that it is derived in the limit $m_\pi \ll \Delta(\equiv m_\Delta - m_N)$, whereas the lowest lattice data with dynamical fermions that one can expect in the next decade is perhaps 200–250 MeV —cf. $\Delta = 292$ MeV. It should be clear to those familiar with lattice simulations that even at this lightest pion mass the branch cut will not be observed due to the restricted phase space on a finite-volume lattice. Consequently, all lattice data will still lie above Δ. Mathematically, the region $m_\pi \approx \Delta$ is dominated by a square-root branch cut which starts at $m_\pi = \Delta$. Using dimensional regularisation this takes the form[29]

$$\frac{6g_A^2}{25\pi^2 f_\pi^2}\left[(\Delta^2 - m_\pi^2)^{\frac{3}{2}} \ln(\Delta + m_\pi - \sqrt{\Delta^2 - m_\pi^2}) - \frac{\Delta}{2}(2\Delta^2 - 3m_\pi^2)\ln m_\pi\right], \qquad (3)$$

for $m_\pi < \Delta$, while for $m_\pi > \Delta$ the first logarithm becomes an arctangent. No serious attempt has been made to extend the formal expansion in eq. (2) to incorporate this cut in an analysis of lattice data and, given the number of parameters to be determined if one works to order m_π^6, it is not likely that it will be done in the next decade.

Even ignoring the $\Delta\pi$ cut for a short time, studies of the formal expansion of the $N \to N\pi \to N$ self-energy integral, $\sigma_{N\pi}$, suggest that it has abysmal convergence properties. Using a sharp, ultra-violet cut-off, Wright showed [30] that the series diverged for $m_\pi > 0.4$ GeV. If one instead uses a dipole cut-off, which in view of the phenomenological shape of the nucleon's axial form-factor is much more realistic, it is worse —with the radius of convergence being around 0.25 GeV. We return to this in sect. 3.

The main issue of the convergence of this truncated series, eq. (2), has its origin fixed in the formalism that it is derived from the general form of eq. (1). The dimensionally regulated approach requires that the pion mass remain much lighter than every other mass scale involved in the problem. This requires that $m_\pi/\Lambda_{\chi\rm SB} \ll 1$ and $m_\pi/\Delta \ll 1$. A further scale, as addressed in the introduction, is set by the physical extent of the source of the pion field. This scale, $\Lambda \sim R^{-1}_{\rm SOURCE}$, corresponds to the transition between rapid, non-linear variation and smooth, *constituent-like* quark mass behaviour. An alternative procedure would be to regulate eq. (1) with a finite Λ which physically corresponds to the source of the meson cloud having an extended structure.

In summary, the low-energy effective field theory can be very useful in describing the quark mass behaviour of hadron properties. These powers have unfortunately been lost in the literature, where only a single type of regulator (*i.e.* dimensional) has been studied in detail.

3 Accurate, model-independent method of chiral extrapolation

We now turn to the direct application of eq. (1), written in a regulator independent form, to the extrapolation of lattice data. By studying a range of different regulators, both finite-ranged, and the dimensional approach, we can study the sensitivity to the form chosen.

The additional analytic term, $\alpha_4\, m_\pi^4$, differs from previous studies using a finite-ranged regulator [28]. Since one is working to non-analytic order $m_\pi^4 \log m_\pi$, one is certainly permitted freedom in α_4 [27]. In practice, whether or not this can be reliably determined, together with Λ, will depend on the data available.

The self-energies, $\sigma_{B\pi}$, are evaluated with a variety of regulators. Included here are both that of the truncated power series resulting from dimensional regularisation and also those of finite range, including sharp cut-off, monopole, dipole and Gaussian. The coefficients of non-analytic terms are constrained to their phenomenological values, while the parameters α_i and Λ are then determined by fitting *lattice data*.

It is again worth noting that, independent of regulator, precisely the same expansion of eq. (2) will be obtained in the limit $m_\pi \ll \Lambda$. Although the parameters α_i *will* depend upon the choice of regulator, one can expand the self-energy terms to order m_π^2 (or higher) to obtain the chiral coefficients at the appropriate order and compare with the truncated expansion of eq. (2) —see ref. [27] for a full discussion of this issue.

The results of our fits to lattice data studied with a range of regulators are shown in fig. 1. The short-dashed curve shows the fit obtained using the dimensionally regulated form of eq. (2) extended to a further term in the expansion, $\alpha_6\, m_\pi^6$. This additional term is necessary for a more reasonable fit due to the large NLNA contribution. The long-dashed curve is the result of using a sharp cut-off regulator, while the following three fits (solid curves), *indistinguishable in this plot* correspond to the monopole, dipole and Gaussian regulated forms.

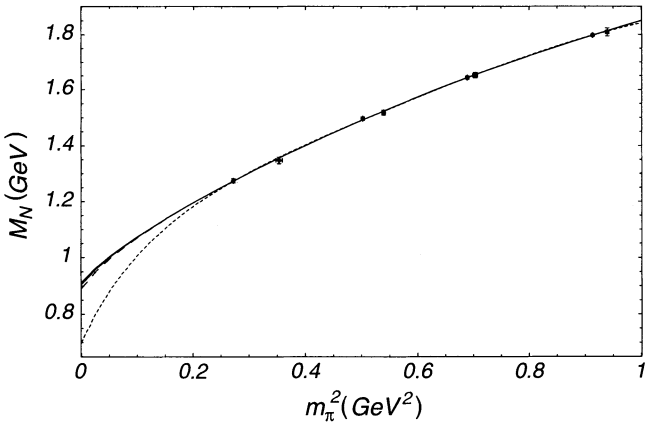

Fig. 1. Fits to lattice data [31] for five different ultra-violet regulators.

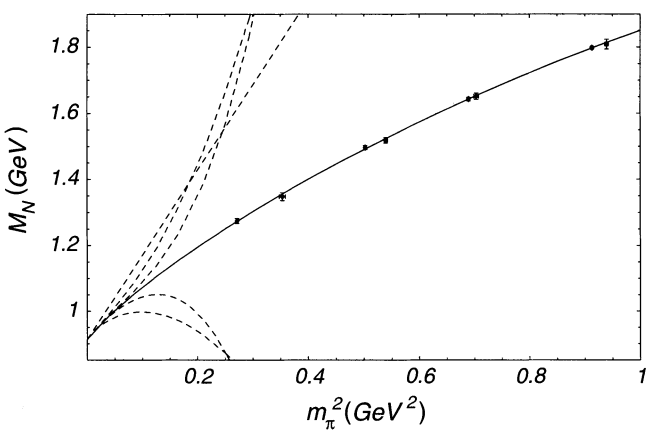

Fig. 2. The fit to the lattice data using the dipole regulator. The dashed curves show power series expansions of this fit to successive orders in m_π for $m_\pi^2 \to m_\pi^6$.

The extrapolation of lattice data is clearly independent of the choice of finite, ultra-violet regulator. Knowing this, we can examine the range of convergence of a truncated power series. Selecting the dipole form and neglecting the $\Delta\pi$ contribution to the nucleon self-energy, one can obtain a closed analytic expression. An expansion in powers of the pion mass is shown in fig. 2. Here we see that convergence of the expansion to order m_π^6 breaks down above $m_\pi \sim$ 250 MeV.

For the reasons outlined, it is essential that the self-energies are evaluated using some ultra-violet regulator —a sharp cut-off or a dipole form, for example. Whatever is chosen does not effect the non-analytic structure which is guaranteed correct. The branch points at m_π equal zero and Δ are incorporated naturally. The use of a finite regulator then automatically produces the transition scale associated with the physical extent of the meson source.

The essential point is that studies of the nucleon (cf. ref. [30] and fig. 1), the Δ (cf. fig. 4 of Leinweber *et al.* [28]) and the ρ meson [32] suggest that *this procedure will result in little or no model dependence in the extrapolation to the physical pion mass once there is accurate lattice data for* $m_\pi \sim 0.3$ GeV *or less.* Physically, this is possible because

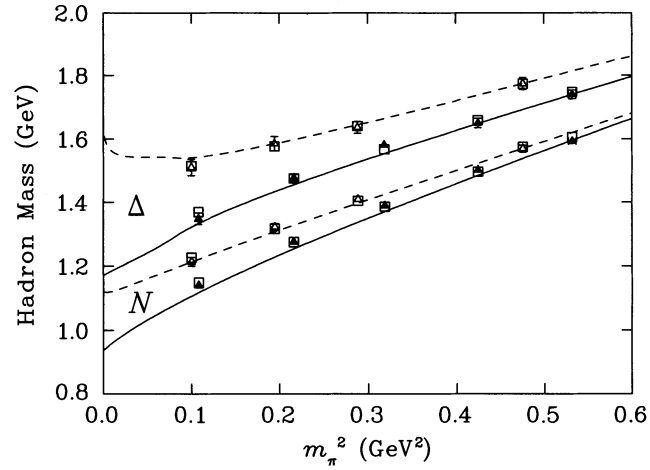

Fig. 3. Fits to both quenched (open triangles) and dynamical (closed triangles) lattice data [33] using a dipole regulator [34].

the self-energy loops are rapidly suppressed in the region $m_\pi > 0.4$ GeV. Thus, an extrapolation based on eq. (1) formulated with the selection of a long-distance regulator allows one to respect *all the chiral constraints*, keep the number of fitting parameters low and yield essentially model-independent results at the physical pion mass. No other approach can do this.

4 Possible connection to QQCD

Although quenched QCD (QQCD) is an unphysical theory, it provides an alternative avenue for enhancing our understanding of chiral extrapolation. Multi-mass techniques allow a dense set of quark masses to be simulated with relative computational ease. Together with recent advances in numerical techniques, which allow simulations to be performed at light quarks masses [35], one will be able to very accurately determine the quark mass dependence of quenched simulations within the light-quark-mass regime.

The study of baryon spectroscopy in quenched lattice QCD has recently made great progress. We have already noted that the lattice data behaves like a constituent quark model for quark masses above 50–60 MeV because Goldstone boson loops are strongly suppressed in this region. This not only provides a very natural explanation of the similarity of quenched and full data in this region but it also suggests a much more ambitious approach to hadron spectra. It suggests that one might remove the small effects of Goldstone boson loops in QQCD (including the η') and then estimate the hadron masses in full QCD by introducing the Goldstone loops which yield the LNA and NLNA behaviour in full QCD.

As a first test of this idea, Young *et al.* [34] recently analysed the MILC data [33] for the N and Δ, using eq. (1) (with $\alpha_4 = 0$) for full QCD and the appropriate generalization for QQCD —*i.e.* using quenched pion couplings as well as the single- and double-"hairpin" η' loops [36,37]. The results illustrated in fig. 3 are remarkable. The values

of α_0 and α_2 for the N (or the Δ) obtained in QQCD agree within statistical errors with those obtained in full QCD. Certainly this result (unlike the result for the extrapolation of individual hadron masses as noted above) is somewhat dependent on the shape of the ultra-violet cut-off chosen —although the extent of that is yet to be studied in detail. Nevertheless, given that the study involved the phenomenologically favoured dipole form, it is a remarkable result and merits further investigation.

5 Conclusion

At the present time we have a wonderful conjunction of opportunities. Modern accelerator facilities are providing data of unprecedented precision over a tremendous kinematic range at the same time as numerical simulations of lattice QCD are delivering results of impressive accuracy. It is therefore timely to ask how to use these advances to develop a new and deeper understanding of hadron structure and dynamics.

We have demonstrated that the use of chiral effective field theory can provide accurate extrapolation formulae. In particular, we have shown that the extrapolation of the nucleon mass exhibits minimal model dependence in the choice of finite-ranged, ultra-violet regulator.

In combination with the very successful techniques for chiral extrapolation, lattice QCD will finally yield accurate data on the consequences of non-perturbative QCD. Furthermore, the physical insights obtained from the study of hadron properties as a function of quark mass will guide the development of new quark models and hence a much more realistic picture of hadron structure.

We would like to thank those colleagues who have contributed to our understanding of the problems discussed here, notably Jonathon Ashley, Ian Cloet, Will Detmold, Wally Melnitchouk, Stewart Wright and James Zanotti. This work was supported by the Australian Research Council and the University of Adelaide.

References

1. L. McLerran, arXiv:hep-ph/0202025.
2. S. Dieterich *et al.*, Phys. Lett. B **500**, 47 (2001), arXiv:nucl-ex/0011008.
3. D.H. Lu, K. Tsushima, A.W. Thomas, A.G. Williams, K. Saito, Phys. Rev. C **60**, 068201 (1999), arXiv:nucl-th/9807074.
4. H.J. Rothe, World Sci. Lect. Notes Phys. **59** (1997) 1.
5. T. Lippert, S. Gusken, K. Schilling, Nucl. Phys. Proc. Suppl. **83**, 182 (2000).
6. A.W. Thomas, W. Weise, *The Structure of the Nucleon*, (Wiley-VCH, Berlin, 2001).
7. J. Gasser, H. Leutwyler, Ann. Phys. (N.Y.) **158**, 142 (1984).
8. H.W. Fearing, S. Scherer, Phys. Rev. D **53**, 315 (1996), arXiv:hep-ph/9408346.
9. A.W. Thomas, Adv. Nucl. Phys. **13**, 1 (1984).
10. G.A. Miller, A.W. Thomas, S. Theberge, Phys. Lett. B **91**, 192 (1980).
11. S. Theberge, G.A. Miller, A.W. Thomas, Can. J. Phys. **60**, 59 (1982).
12. D.B. Leinweber *et al.*, Phys. Rev. D **60**, 034014 (1999).
13. D.B. Leinweber, A.W. Thomas, S.V. Wright, Phys. Lett. B **482**, 109 (2000), arXiv:hep-lat/0001007.
14. E.J. Hackett-Jones *et al.*, Phys. Lett. B **494**, 89 (2000), hep-lat/0008018.
15. E.J. Hackett-Jones, D.B. Leinweber, A.W. Thomas, Phys. Lett. B **489**, 143 (2000), arXiv:hep-lat/0004006.
16. T.R. Hemmert, W. Weise, arXiv:hep-lat/0204005.
17. W. Detmold, W. Melnitchouk, J.W. Negele, D.B. Renner, A.W. Thomas, Phys. Rev. Lett. **87**, 172001 (2001), arXiv:hep-lat/0103006.
18. W. Detmold *et al.*, Eur. Phys. J. directC **13**, 1 (2001), arXiv:hep-lat/0108002.
19. W. Detmold, W. Melnitchouk, A.W. Thomas, arXiv:hep-lat/0206001.
20. D.B. Leinweber *et al.*, Phys. Rev. Lett. **86**, 5011 (2001), arXiv:hep-ph/0101211.
21. D.B. Leinweber, A.W. Thomas, Phys. Rev. D **62**, 074505 (2000), arXiv:hep-lat/9912052.
22. I.C. Cloet *et al.*, Phys. Rev. C **65**, 062201 (2002), arXiv:hep-ph/0203023.
23. I.C. Cloet *et al.*, in *Proceedings of the Joint Workshop on Physics at Japanese Hadron Facility* (World Scientific, 2002), pp. 125-35.
24. W. Detmold *et al.*, Pramana **57**, 251 (2001), arXiv:nucl-th/0104043.
25. A.W. Thomas, in *Boundary of nuclear physics and QCD*, edited by E. Norman, L. Schroeder, G. Wozniak, AIP Conf. Proc. vol. **610**, 262-280 (2002), arXiv:nucl-th/0111001.
26. L.F. Li, H. Pagels, Phys. Rev. Lett. **26**, 1204 (1971).
27. J.F. Donoghue, B.R. Holstein, B. Borasoy, Phys. Rev. D **59**, 036002 (1999).
28. D.B. Leinweber, A.W. Thomas, K. Tsushima, S.V. Wright, Phys. Rev. D **61**, 074502 (2000), arXiv:hep-lat/9906027.
29. M.K. Banerjee, J. Milana, Phys. Rev. D **54**, 5804 (1996).
30. S.V. Wright, PhD Thesis, The University of Adelaide (2002).
31. CP-PACS Collaboration (A. Ali Khan *et al.*), Phys. Rev. D **65**, 054505 (2002), arXiv:hep-lat/0105015.
32. D.B. Leinweber *et al.*, Phys. Rev. D **64**, 094502 (2001), arXiv:hep-lat/0104013.
33. C.W. Bernard *et al.*, Phys. Rev. D **64**, 054506 (2001), arXiv:hep-lat/0104002.
34. R.D. Young *et al.*, Phys. Rev. D **66**, 094507 (2002), arXiv:hep-lat/0205017.
35. CSSM Lattice Collaboration (J.M. Zanotti *et al.*), Phys. Rev. D **65**, 074507 (2002), arXiv:hep-lat/0110216.
36. J.N. Labrenz, S.R. Sharpe, Phys. Rev. D **54**, 4595 (1996), arXiv:hep-lat/9605034.
37. R.D. Young *et al.*, Nucl. Phys. Proc. Suppl. A **109**, 55 (2002).

Eur. Phys. J. A **18**, 247–252 (2003)
DOI 10.1140/epja/i2002-10209-3

THE EUROPEAN PHYSICAL JOURNAL A

FLIC fermions and hadron phenomenology

D.B. Leinweber[1,a], J.N. Hedditch[1], W. Melnitchouk[1,2], A.W. Thomas[1], A.G. Williams[1], R.D. Young[1], J.M. Zanotti[1], and J.B. Zhang[1]

[1] Centre for the Subatomic Structure of Matter and Department of Physics and Mathematical Physics, University of Adelaide, Adelaide, SA 5005, Australia
[2] Jefferson Lab, 12000 Jefferson Avenue, Newport News, VA 23606, USA

Received: 30 September 2002 /
Published online: 22 October 2003 – © Società Italiana di Fisica / Springer-Verlag 2003

Abstract. A pedagogical overview of the formulation of the Fat-Link-Irrelevant-Clover (FLIC) fermion action and its associated phenomenology is described. The scaling analysis indicates FLIC fermions provide a new form of nonperturbative $\mathcal{O}(a)$ improvement where near-continuum results are obtained at finite lattice spacing. Spin-(1/2) and spin-(3/2), even- and odd-parity baryon resonances are investigated in quenched QCD, where the nature of the Roper resonance and $\Lambda^*(1405)$ are of particular interest. FLIC fermions allow efficient access to the light-quark-mass regime, where evidence of chiral nonanalytic behavior in the Δ mass is observed.

PACS. 12.38.Gc Lattice QCD calculations – 12.38.Aw General properties of QCD (dynamics, confinement, etc.)

1 FLIC Fermions

The CSSM lattice Collaboration has been examining the merits of a new lattice fermion action [1] in which the (irrelevant) operators introduced to remove fermion doublers and lattice spacing artifacts are constructed with smoothed links. These links are created via APE smearing [2]; a process that averages a link with its nearest transverse neighbors in a gauge-invariant manner. Iteration of the averaging process generates a "fat" link. The use of links in which short-distance fluctuations have been removed simplifies the determination of the coefficients of the improvement terms [3]. Perturbative renormalizations are small for smeared links and tree-level estimates, or the mean-field improved estimates used here, are sufficient to remove $\mathcal{O}(a)$ errors in the lattice spacing a, to all orders in the strong-coupling g. The key is that both the energy dimension-five Wilson term and the Clover term [4] are constructed with smooth links, while the relevant operators, surviving in the continuum limit, are constructed with the original untouched links generated via standard Monte Carlo techniques. We call this action the Fat-Link-Irrelevant-Clover (FLIC) fermion action.

The established approach to nonperturbative (NP) improvement [5] tunes the coefficient of the clover operator to all powers in g^2. Unfortunately, this formulation of the clover action is susceptible to the problem of exceptional configurations as the quark mass becomes small. Chiral symmetry breaking in the clover fermion action introduces an additive mass renormalization into the Dirac operator that can give rise to singularities in quark propagators at small quark masses. In practice, this prevents the simulation of small quark masses and the use of coarse lattices ($\beta < 5.7 \sim a > 0.18$ fm) [3,6].

The clover term of the fermion action requires a lattice determination of the QCD field strength tensor $F_{\mu\nu}$. The so-called clover version of $F_{\mu\nu}(x)$ involves the product of links around the four plaquettes centered at x in the μ-ν plane. This simple formulation is commonly used in clover actions, but it is now known to have large $\mathcal{O}(a^2)$ errors. These errors lead to 10% errors in the topological charge even on very smooth configurations [7].

A key feature of FLIC fermions is that the construction of irrelevant operators using smoothed links facilitates the use of highly improved definitions of the QCD field strength tensor $F_{\mu\nu}$. In particular, we employ an $\mathcal{O}(a^4)$ improved definition of $F_{\mu\nu}$ [8] in which the standard clover-sum of four 1×1 Wilson loops is combined with 1×2, 1×3, 2×2 and 3×3 Wilson-loop clovers.

The scaling analysis of FLIC fermions is performed at three different lattice spacings and two different volumes. The tree-level $\mathcal{O}(a^2)$–Symanzik-improved [9] gauge action is used on $12^3 \times 24$ and $16^3 \times 32$ lattices with lattice spacings of 0.093, 0.122 and 0.165 fm determined from a string tension analysis incorporating the lattice Coulomb term [10]. Where necessary, we take $\sqrt{\sigma} = 440$ MeV. A

[a] Plenary talk presented by Derek Leinweber; e-mail: dleinweber@physics.adelaide.edu.au

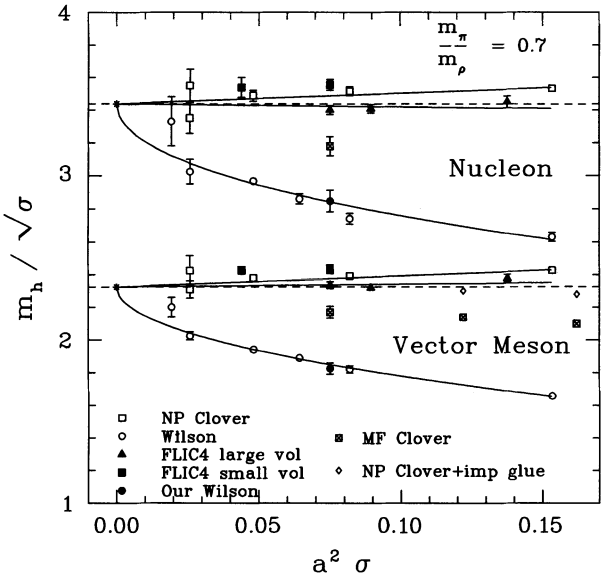

Fig. 1. Nucleon and vector meson masses for the Wilson, mean-field (MF) improved, NP-improved clover and FLIC actions obtained by interpolating simulation results to $m_\pi/m_\rho = 0.7$. For the FLIC action ("FLIC4"), fat links are constructed with $n = 4$ APE-smearing sweeps with smearing fraction $\alpha = 0.7$. Results from the CSSM lattice Collaboration are indicated by the solid symbols; those from earlier simulations by open or hatched symbols. The solid-lines illustrate fits, constrained to have a common continuum limit, to FLIC, NP-improved clover and Wilson fermion action results obtained on physically large lattice volumes.

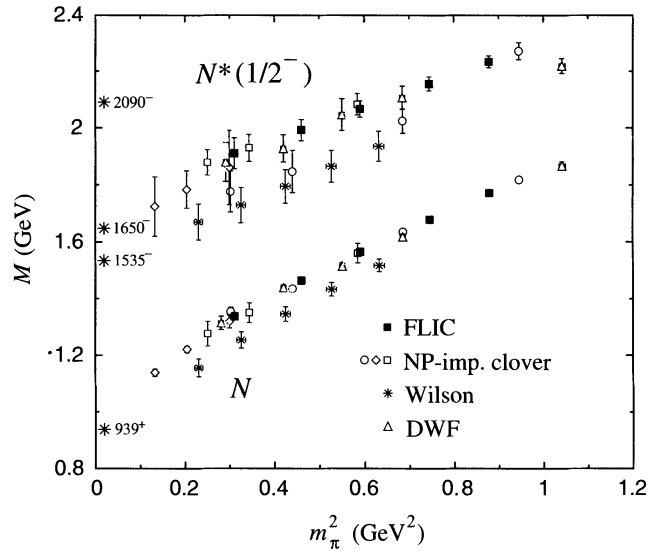

Fig. 2. Masses of the nucleon (N) and the lowest $J^P = 1/2^-$ excitation ("N^*"), obtained from the standard nucleon interpolating field. The FLIC and Wilson results are from the present analysis.

total of 200 configurations are used in the scaling analysis at each lattice spacing and volume. In addition, for the light quark simulations, 94 configurations are used on a $20^3 \times 40$ lattice with $a = 0.134$ fm. The error analysis is performed by a third-order, single-elimination jackknife, with the χ^2 per degree of freedom obtained via covariance matrix fits. A fixed boundary condition and smeared sources [11] are used for the fermions.

Figure 1 displays our most comprehensive scaling analysis to date. The present results for the Wilson action agree with those of ref. [12]. The FLIC action performs systematically better than the mean-field–improved clover action and competes well with those obtained with the NP-improved clover fermion action [12].

Our two different volumes used at $a^2\sigma \sim 0.075$ indicate a finite-volume effect, which increases the mass for the smaller volumes at $a^2\sigma \sim 0.075$ and ~ 0.045. Examination of points from the small and large volumes separately indicates continued scaling toward the continuum limit. While the finite-volume effect will produce a different continuum limit value, the slope of the points from the smaller and larger volumes agree.

Focusing on simulation results from physical volumes with extents ~ 2 fm and larger, we perform a simultaneous fit of the FLIC, NP-improved clover and Wilson fermion action results. The fits are constrained to have a common continuum limit and assume errors are $\mathcal{O}(a^2)$ for FLIC and NP-improved clover actions and $\mathcal{O}(a)$ for the Wilson action. An acceptable χ^2 per degree of freedom is obtained for both the nucleon and ρ-meson fits. These results indicate that FLIC fermions provide a new form of nonperturbative $\mathcal{O}(a)$ improvement. The FLIC fermion results display nearly perfect scaling indicating $\mathcal{O}(a^2)$ errors are small for this action.

2 Baryon resonances

Lattice studies of baryon excitations [13–17] provide valuable insight into the forces of confinement and the nature of QCD in the nonperturbative regime. They complement the high-precision measurements of the N^* spectrum under way at Jefferson Lab. The simulations presented here are performed on 392 $\mathcal{O}(a^2)$–Symanzik-improved [9] configurations of size $16^3 \times 32$ at $\beta = 4.60$ providing a lattice spacing of $a = 0.122(2)$ fm. FLIC fermions are implemented with 4 sweeps of APE smearing at $\alpha = 0.7$.

2.1 Spin-(1/2) baryon resonances

There are two nucleon interpolating fields commonly considered in exciting the nucleon from the vacuum. The standard interpolating field couples a u-d quark pair to a scalar diquark and is $\mathcal{O}(1)$ in a nonrelativistic reduction. The alternate interpolator is $\mathcal{O}(p^2/E^2)$ in a nonrelativistic reduction placing two quarks in relative P waves. Odd-parity states may be projected from correlation functions of these interpolators. The standard interpolator is expected to have stronger overlap with the lowest-lying odd-parity state due to the scalar-diquark construction of the interpolator.

In fig. 2 we show the N and $N^*(1/2^-)$ masses from FLIC fermions as a function of m_π^2. For comparison, we

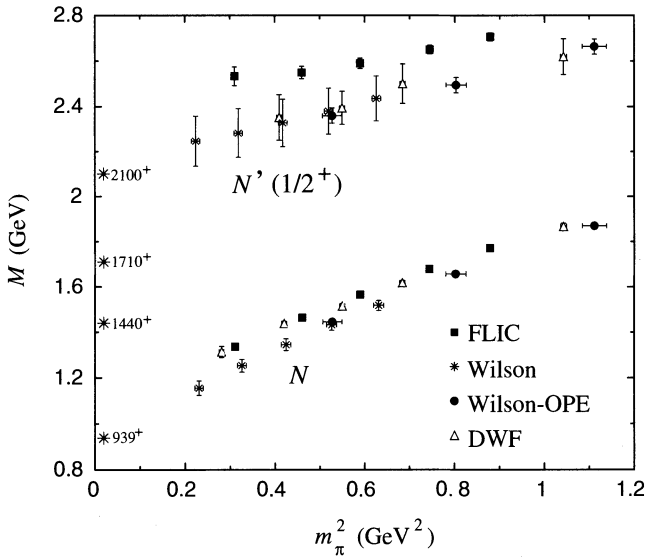

Fig. 3. Masses of the nucleon, and the lowest $J^P = 1/2^+$ excitation ("N'") obtained from the alternate interpolating field. The FLIC and Wilson results are from this analysis.

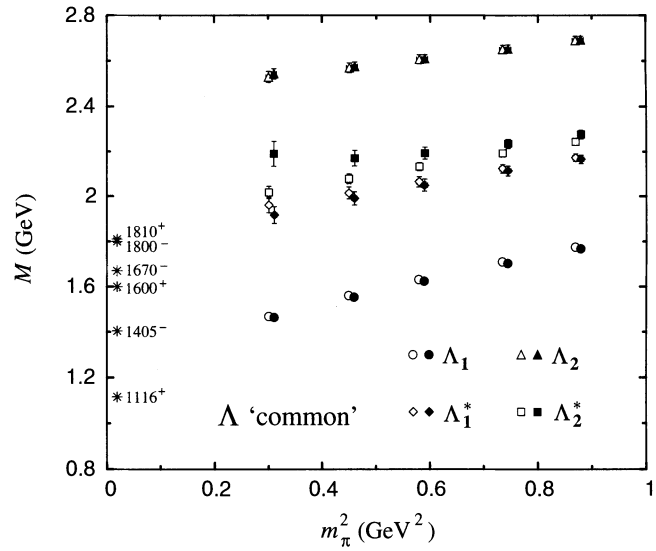

Fig. 4. Masses of the $\Lambda(1/2^\pm)$ states, obtained from the standard (Λ_1) and alternate (Λ_2) interpolating fields. The symbols are described in the text.

also show results from simulations with Wilson [17] and domain wall fermions (DWF) [16], and the NP-improved clover action [15] with different source smearing and volumes. There is excellent agreement between the different improved actions for the nucleon mass. The Wilson results lie systematically low in comparison to these due to large $\mathcal{O}(a)$ errors in this action [1].

A similar pattern is seen for the lowest-lying $N^*(1/2^-)$ masses. A mass splitting of approximately 400 MeV is clearly visible between the N and N^* for all actions, including the Wilson. The trend of the $N^*(1/2^-)$ data with decreasing m_π is also consistent with the mass of the lowest physical negative-parity N^* state.

The mass of the $J^P = 1/2^+$ state obtained from the alternate nucleon interpolating field [13], which vanishes in a nonrelativistic reduction, is shown in fig. 3. In addition to the FLIC and Wilson results from the present analysis, also shown are the DWF results [16], and results from an earlier analysis with Wilson fermions analyzed via the operator product expansion [13]. The most striking feature of the data is the relatively large excitation energy of the N', some 1 GeV above the nucleon. It has been speculated that the alternate interpolator may have overlap with the lowest $1/2^+$ excited state [16]. However, there is little evidence that this state is the $N^*(1440)$. It is likely that the alternate nucleon interpolator simply does not have good overlap with either the nucleon or the Roper, but rather a (combination of) excited $1/2^+$ state(s).

The spectrum of positive- and negative-parity Λ states is shown in fig. 4. Here we consider an interpolating field which contains terms common to the $SU(3)$-flavor singlet and octet interpolating fields. It is the $SU(2)$-isospin analogue of the Σ^0 interpolating field and does not bias the flavor symmetry of the Λ-resonances. The positive (negative) parity states labeled Λ_1 (Λ_1^*) and Λ_2 (Λ_2^*) are constructed from the traditional and alternate Λ interpolators analogous to those of the nucleon. The pattern of mass splittings is similar to that observed for the N^*'s in figs. 2 and 3. The importance of the correlation matrix analysis projecting the eigenstates of the Hamiltonian (filled symbols) is evident from a comparison with the naive fits to single correlation functions (open symbols). There is little evidence that the Λ_2 has any significant overlap with the first positive-parity excited state, $\Lambda^*(1600)$ (cf. the Roper resonance, $N^*(1440)$, in fig. 3).

While it seems plausible that nonanalyticities in a chiral extrapolation [18] of N_1 and N_1^* results could eventually lead to agreement with experiment, the situation for the $\Lambda^*(1405)$ is not as compelling. Whereas a 150 MeV pion-induced self-energy is required for the N_1, N_1^* and Λ_1 states, 400 MeV is required to approach the empirical mass of the $\Lambda^*(1405)$. This large discrepancy suggests that relevant physics may be absent from simulations in the quenched approximation or perhaps more exotic interpolating fields are required to obtain significant overlap with the $\Lambda^*(1405)$. Investigations at lighter quark masses involving quenched chiral perturbation theory will assist in resolving these issues.

2.2 Spin-(3/2) baryon resonances

We consider the following isospin-(1/2), spin-(3/2) interpolator [19]: $\chi_\mu^{N^+}(x) = \epsilon^{abc}(u^{Ta}(x)\ C\gamma_5\gamma_\mu\ d^b(x))\gamma_5 u^c(x)$, which transforms as a pseudo-vector under parity, in accord with a positive-parity Rarita-Schwinger spinor. For the Δ^{++}-resonance we use the standard interpolator as in ref. [20]. Since the spin-(3/2) Rarita-Schwinger spinor-vector is a tensor product of a spin-1 vector and a spinor, the spin-(3/2) interpolating field contains spin-(1/2) contributions. To project a spin-(3/2) state one needs to use a

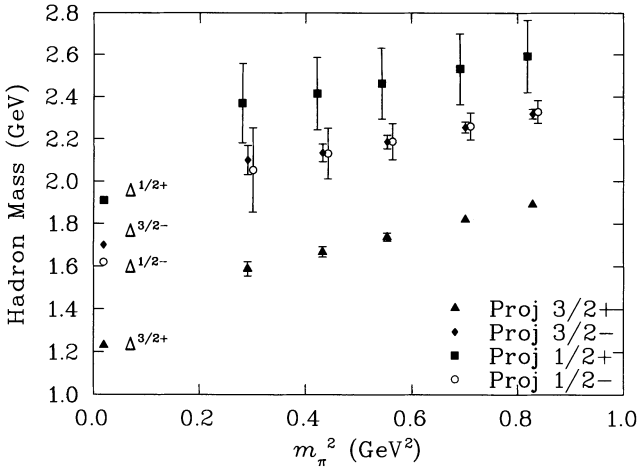

Fig. 5. Masses of the spin-parity–projected $\Delta(3/2^{\pm})$ and $\Delta(1/2^{\pm})$ states. The empirical masses are indicated along the ordinate.

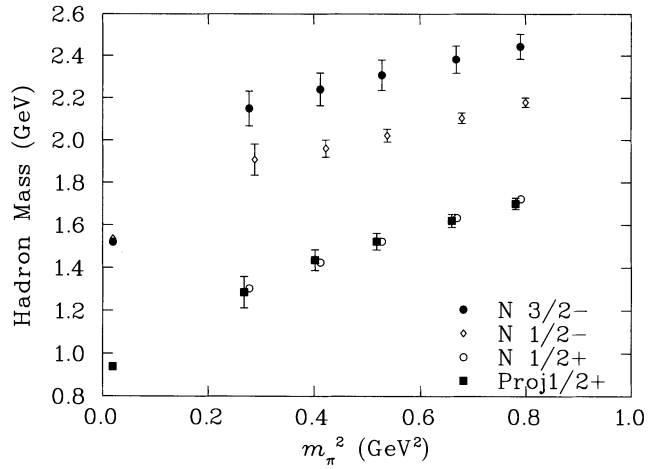

Fig. 6. Masses of the spin-projected $N(3/2^-)$ and $N(1/2^+)$ states, compared with the nucleon and $N(1/2^-)$ masses from sect. 2.1.

spin-(3/2) projection operator [21]. Following spin projection, the correlation function for a given spin still contains positive- and negative-parity states. In an analogous procedure to that used for spin-(1/2) resonances with a fixed boundary condition in the time direction, positive- and negative-parity states are obtained by taking the trace of the correlation function with the parity-projection operators $\Gamma_{\pm} = (1 \pm \gamma_4)/2$.

In fig. 5 the spin-parity-projected $\Delta(3/2^+)$ (triangles) and $\Delta(3/2^-)$ (diamonds) masses are shown. We find a clear signal for the P-wave $\Delta(3/2^-)$ parity partner of the Δ ground state. The mass of the $\Delta(3/2^-)$ lies some 500 MeV above that of its parity partner. A discernible signal is detected for the $\Delta(1/2^{\pm})$ states. The level ordering of the Δ states is consistent with that observed in the empirical mass spectrum.

In the isospin-(1/2) sector, large statistical fluctuations make it difficult to obtain a clear signal, even with 392 configurations. Parity projecting to extract the $N(3/2^+)$ state, we find that the correlation function changes sign and has a large negative contribution for time slices in the range $t = 7$–11 following the source at $t = 3$. This behavior is an artifact associated with the quenched decay of the excited state into $N+\eta'$ and is further explored in ref. [19].

The $N(1/2^+)$ channel also displays the interplay of a quenched decay channel and the ground state contribution. A strong P-wave coupling of the $N^*(1/2^+)$ to $N\eta'$ forces the correlation function to be negative at small times, which then turns positive at larger times when the ground-state nucleon begins to dominate the correlation function. This suggests that the first-excited state of the nucleon has a strong coupling to the quenched η' which remains degenerate with the pion in the quenched approximation. These results imply a gluon-rich structure for the Roper resonance and further indicate that it may be impossible to directly observe the Roper resonance at light quark masses in the quenched approximation. While there are claims to have observed the Roper in quenched QCD [22], these results follow from a Bayesian analysis, and the credibility of the Bayesian-prior information used in the analysis requires further examination [23,24].

The extracted masses of the $N(3/2^-)$ and $N(1/2^+)$ states are displayed in fig. 6. Earlier results from sect. 2.1 using the standard spin-(1/2) interpolating field are also shown in fig. 6 for reference. There is excellent agreement between the spin-projected $1/2^+$ state obtained from the spin-(3/2) interpolating field and the earlier $1/2^+$ results.

3 Chiral nonanalytic behavior

The FLIC fermion action has extremely impressive convergence rates for matrix inversion [1,25], and this provides great promise for performing cost-effective simulations at quark masses closer to the physical values. Problems with exceptional configurations have prevented such simulations with Wilson-type fermion actions in the past.

In the absence of exceptional configurations, the standard deviation of an observable will be independent of the number of configurations considered in the average. Exceptional configurations reveal themselves by introducing a significant jump in the standard deviation as the configuration is introduced into the average. In severe cases, exceptional configurations can lead to divergences in correlation functions or prevent the matrix inversion process from converging.

The ease with which one can invert the fermion matrix using FLIC fermions leads us to attempt simulations down to small quark masses corresponding to $m_\pi/m_\rho = 0.35$. The simulations are on a $20^3 \times 40$ lattice with a physical length of 2.7 fm. We have used an initial set of 100 configurations, using $n = 6$ sweeps of APE-smearing and a five-loop improved lattice field-strength tensor. Preliminary results indicate exceptional configurations at the few percent level [19]. For the current results, these configurations have been identified and removed from the ensemble.

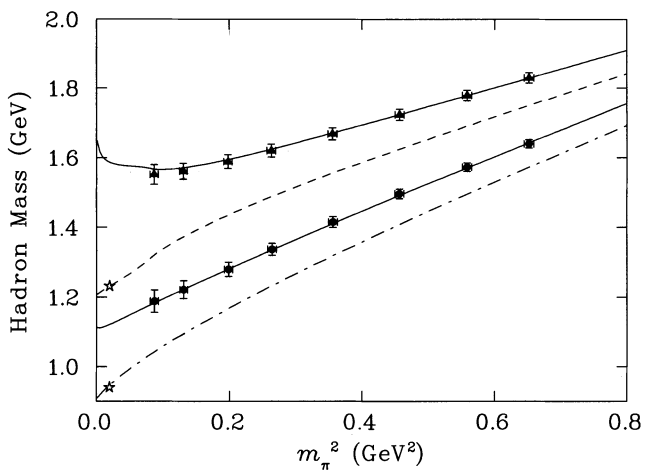

Fig. 7. Nucleon and Δ masses for the FLIC-fermion action on a $20^3 \times 40$ lattice with $a = 0.134$ fm. The solid curves illustrate fits of finite-range regulated quenched chiral perturbation theory to the lattice QCD results. The dot-dashed and dashed curves estimate the correction that will arise in unquenching the lattice QCD simulations for the N and Δ, respectively. Stars at the physical pion mass denote experimental values.

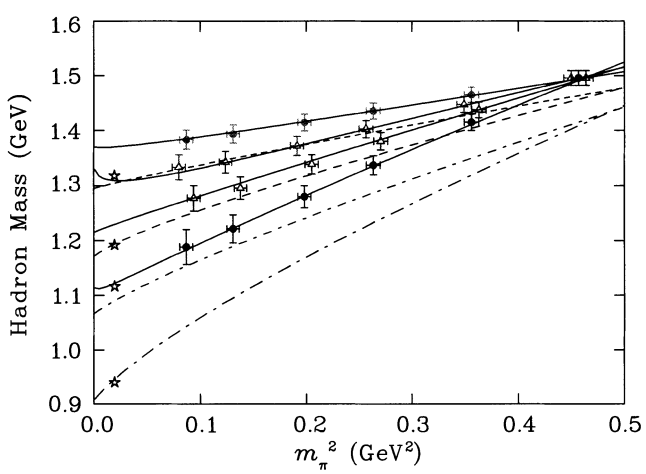

Fig. 8. Octet baryon masses for the FLIC-fermion action. Points are offset for clarity. Symbols are as described for fig. 7.

Figure 7 shows the N and Δ masses as a function of m_π^2 for eight quark masses. An upward curvature in the Δ mass for decreasing quark mass is observed in the FLIC fermion results. This behavior, increasing the quenched $N - \Delta$ mass spitting, was predicted by Young *et al.* [26] using quenched chiral perturbation theory (QχPT) formulated with a finite-range regulator. This QχPT fit to the FLIC-fermion results is illustrated by the solid curves. The dashed curves estimate the correction that will arise in unquenching the lattice QCD simulations. A similar preliminary analysis incorporating the light-meson cloud of the baryon octet is illustrated in fig. 8. Inclusion of the kaon-cloud is in progress.

4 Conclusions

In constructing the irrelevant operators of clover fermion actions with APE-smeared links, FLIC fermions provide a new form of nonperturbative $\mathcal{O}(a)$ improvement. The technique allows the use of highly improved operators, provides optimal scaling and reduces the exceptional configuration problem. Quenched simulations at quark masses down to $m_\pi/m_\rho = 0.35$ have been successfully performed on a $20^3 \times 40$ lattice with a lattice spacing of 0.134 fm. Simulations at such light quark masses have already revealed the non-analytic behavior of quenched chiral perturbation theory in the Δ-baryon mass. We expect to see more evidence of chiral nonanalytic behavior in forthcoming simulations of the electromagnetic form factors of hadrons.

We thank the Australian National Computing Facility for Lattice Gauge Theory, and the Australian Partnership for Advanced Computing (APAC) for supercomputer time. This work was supported by the Australian Research Council. W.M. was supported by the US Department of Energy contract DE-AC05-84ER40150, under which the Southeastern Universities Research Association (SURA) operates the Thomas Jefferson National Accelerator Facility (Jefferson Lab).

References

1. J.M. Zanotti *et al.*, Phys. Rev. D **60**, 074507 (2002); Nucl. Phys. Proc. Suppl. **109**, 101 (2002).
2. M. Falcioni *et al.*, Nucl. Phys. B **251**, 624 (1985).
3. MILC Collaboration (T. DeGrand), Phys. Rev. D **60**, 094501 (1999).
4. B. Sheikholeslami, R. Wohlert, Nucl. Phys. B **259** 572, (1985).
5. M. Luscher *et al.*, Nucl. Phys. B **478**, 365 (1996). M. Luscher *et al.*, Nucl. Phys. B **491**, 323, 344 (1997).
6. W. Bardeen *et al.*, Phys. Rev. D **57**, 1633 (1998); W. Bardeen *et al.*, Phys. Rev. D **57**, 3890 (1998).
7. F.D. Bonnet *et al.*, Phys. Rev. D **62**, 094509 (2000).
8. S. Bilson-Thompson *et al.*, Nucl. Phys. Proc. Suppl. **109**, 116 (2002); hep-lat/0203008.
9. K. Symanzik, Nucl. Phys. B **226**, 187 (1983).
10. R. G. Edwards *et al.*, Nucl. Phys. B **517**, 377 (1998) [hep-lat/9711003].
11. S. Gusken, Nucl. Phys. Proc. Suppl. **17**, 361 (1990).
12. R.G. Edwards, U.M. Heller, T.R. Klassen, Phys. Rev. Lett. **80**, 3448 (1998); see also R.D. Kenway, Nucl. Phys. Proc. Suppl. **73**, 16 (1999), for a review.
13. D. B. Leinweber, Phys. Rev. D **51**, 6383 (1995).
14. F. X. Lee, D. B. Leinweber, Nucl. Phys. Proc. Suppl. **73**, 258 (1999).
15. C. R. Allton *et al.*, Phys. Rev. D **47**, 5128 (1993); D. G. Richards *et al.*, Nucl. Phys. Proc. Suppl. **109**, 89 (2002); M. Göckeler *et al.*, Phys. Lett. B **532**, 63 (2002).
16. S. Sasaki, T. Blum, S. Ohta, Phys. Rev. D **65**, 074503 (2002).
17. W. Melnitchouk *et al.*, hep-lat/0202022; Nucl. Phys. Proc. Suppl. **109**, 96 (2002).
18. D. B. Leinweber *et al.*, Phys. Rev. D **61**, 074502 (2000).
19. J. M. Zanotti *et al.*, in preparation.

20. Y. Chung *et al.*, Nucl. Phys. B **197**, 55 (1982).
21. M. Benmerrouche *et al.*, Phys. Rev. C **39**, 2339 (1989).
22. F. X. Lee, *et al.*, Lattice '02, hep-lat/0208070; S. J. Dong, *et al.*, Lattice '02, hep-lat/0208055.
23. D. B. Leinweber, Phys. Rev. D **51** (1995) 6369.
24. C. Allton *et al.*, in preparation.
25. W. Kamleh *et al.*, Phys. Rev. D **66**, 014501 (2002).
26. R.D. Young *et al.*, hep-lat/0205017.

Eur. Phys. J. A **18**, 253–256 (2003)
DOI 10.1140/epja/i2002-10210-x

THE EUROPEAN PHYSICAL JOURNAL A

Lattice calculations

K. Jansen[a]

NIC/DESY Zeuthen, Platanenallee 6, D-15738 Zeuthen, Germany

Received: 30 September 2002 /
Published online: 22 October 2003 – © Società Italiana di Fisica / Springer-Verlag 2003

Abstract. In this contribution we describe how an exact chiral symmetry can be realized on the lattice. A practical realization of a lattice Dirac operator that leads to a chiral invariant lattice action is discussed and a simulation with this operator is presented that aims at testing the phenomenon of spontaneous chiral symmetry breaking in QCD.

PACS. 11.15.Ha Lattice gauge theory – 12.38.Gc Lattice QCD calculations

1 Introduction

Since its formulation in 1974 [1], lattice QCD has matured to a well-established part of theoretical high-energy physics and it nowadays provides many non-perturbatively obtained, *ab initio* computations and results in a variety of fields. These include, besides QCD, the electroweak standard model, spin systems, tests of semi-classical pictures (instantons etc.) and even quantum gravity (see, *e.g.*, [2]). One of the reasons why the impact of lattice calculations is becoming stronger and stronger is the fact that (parallel) computers, the workhorses for lattice physicists, have become more and more powerful. However, a certainly equal important reason is that over the years a number of conceptual developments have been established that help in making simulations faster and much better controlled:

- *Accelerating the continuum limit*
  Lattice QCD actions that are used in the past give rise to lattice discretization errors that are linear in the lattice spacing a. Considering pure gauge theories, these effects are only quadratically in the lattice spacing [3, 4] and hence simulations including fermions slow down the approach to the continuum limit substantially. Following the concept of *Symanzik improvement* [5,6], this drawback can be overcome: it can be shown that at $O(a)$ only one additional term can be added to the standard Wilson fermion action. This term, called the *Sheikoleslami-Wohlert* term [7], is multiplied by a free, tunable parameter $c_{\rm sw}$. It is possible to compute this coefficient non-perturbatively in such a way that it exactly cancels the linear lattice discretization effects coming from the standard Wilson fermion action and hence the discretization errors are reduced from $O(a)$ to $O(a^2)$ [8,9]. Of course, the continuum limit itself still has to be performed, but it is reached with a much faster rate by using these so-called *non-perturbative O(a)-improved Wilson fermions.*
  Finite-size effects
  Lattice simulations have necessarily to be done in a finite, 4-dimensional box of physical size L^4. In order to fit physical quantities like a proton into this box, it is necessary that the physical size is large enough. The linear physical extent L is given by $L = Na$, where N is the number of lattice points. If the lattice spacing a is kept small enough to avoid large discretization effects, the number of points to be simulated becomes easily very large. Therefore, trying to avoid finite-size effects results in very costly and demanding simulations.
  However, in many circumstances it is possible to turn this drawback around and promote it to an advantage. It is possible to use the finite volume as a probe of the system and extract from the finite-volume effects of physical quantities infinite-volume properties of the system under consideration. One prominent application is to use the finite size of the box as the scale used in non-perturbative renormalization (see the reviews [10,11]). Another strategy is to develop finite-size formulae that actually describe the finite-size effects analytically and allow for a well-controlled determination of infinite-volume quantities. An example of this strategy is given below.
- *Dynamical fermions*
  QCD, as a quantum field theory allows for the creation and annihilation of virtual quark-antiquark pairs that lead to renormalization effects like the running of the strong-coupling constant, *i.e.* the value of the strong-coupling constant depends on the energy where it is measured. In order to take these effects into account, the full theory including the fermionic degrees of

[a] e-mail: kjansen@ifh.de

freedom has to be simulated. The algorithms that are known today for these simulations lead to very costly simulations [12]. Although, by a continuous development of the algorithms it was possible to gain a factor about 20 in the, say, last 10 years, physical results with well-controlled errors would need computers that can deliver 10–100 teraflops performance, something that cannot be reached today.

Therefore, many simulations performed so far neglect the dynamical quark effects and work in the so-called *quenched approximation.* It is surprising —and not really understood— that this approximation (or better truncation) of the theory still gives results that often differ from experimental data by only 20% to 30%. Of course, eventually the quenched approximation has to be given up and the lattice community worldwide is in a transition period to switch to real dynamical-fermion simulations.

– *Chiral symmetry*

The lattice and chiral symmetry, *i.e.* the invariance of the action under exchange of left-handed and right-handed massless quarks, were two concepts that did not seem to fit together for a very long time. Only recently a solution to this longstanding problem could be found and in the remaining part of this contribution we explain this new development.

2 Spontaneous chiral symmetry breaking

In our theory of strong interactions, quantum chromodynamics, chiral symmetry is assumed to be spontaneously broken. This symmetry allows for an interchange of left-handed and right-handed quarks while leaving physics invariant —at least when these quarks are massless. In this case a scalar quark-antiquark $q\bar{q}$ condensate is assumed to be developed and the Goldstone particles are identified with the light pions that are observed in nature.

As stated above, the occurrence of spontaneous symmetry breaking *is an assumption.* The phenomenon is inherently non-perturbative and cannot be addressed with approximative methods like perturbation theory. However, even with numerical simulations it is difficult to test spontaneous chiral symmetry breaking (SχSB). The reason for this becomes clear when the way to detect SχSB is considered. Let us choose a system that has a finite physical volume V, as would be required for numerical simulations. Further, we introduce a quark mass m. SχSB is tested in a double limit, where first the volume of the system is sent to infinity and then the quark mass is sent to zero. If a non-vanishing scalar quark condensate remains, SχSB is identified. Obviously, such a procedure is infeasible within the approach of numerical simulations.

The way out is the use of chiral perturbation theory [13]. In this approach chiral symmetry breaking is also taken as an assumption with the consequences of the appearance of non-vanishing field expectation values and Goldstone particles. A special situation arises when the size of the box becomes comparable to or even smaller than the Compton wavelength of the Goldstone particle. Then, the corresponding field can be considered as being uniform and it is possible to set up a systematic expansion that starts in the lowest order with an effective Lagrangian of this constant mode and then taking systematically higher-order fluctuations into account [14].

3 Chiral symmetry on the lattice

Chiral perturbation theory as well as the lattice method was developed for quantum chromodynamics in order to deepen our understanding of the strong interactions. Still, until relatively recently, both approaches could not really come together, at least in the region of very small quark masses where chiral symmetry starts to get restored. The reason was that the lattice seemed to be lacking the concept of chiral symmetry and for many years the infamous Nielson-Ninomiya theorem [15] has been telling us that it would even be impossible to implement chiral symmetry in a consistent way on a lattice.

The situation only changed a few years ago, when an old work by Ginsparg and Wilson [16] was rediscovered [17]. The Ginsparg-Wilson paper contained actually a clue for answering the problem of chiral fermions on the lattice. The interaction of the fermions is described by some particular operator, the Dirac operator, the details of which should not be discussed here. In the continuum theory this Dirac operator anti-commutes, of course, with γ_5. On a lattice with non-vanishing lattice spacing a, such an anti-commutation property cannot be demanded. If the anti-commutation property is insisted on, the fermion spectrum of the lattice theory does not correspond to the one of the target continuum theory.

The suggestion of Ginsparg and Wilson was to replace the anti-commutation condition by a relation (now known as the Ginsparg-Wilson (GW) relation) for a lattice Dirac operator D:

$$\gamma_5 D + D\gamma_5 = aD\gamma_5 D \; . \tag{1}$$

Clearly, in the limit that the lattice spacing vanishes, the usual anti-commutation relation of the continuum theory is recovered.

The fact that renders the relation eq. (1) conceptually extremely fruitful is that it implies an exact chiral symmetry on the lattice even if the value of the lattice spacing does not vanish [18]. The notion of a chiral symmetry on the lattice is a conceptual breakthrough and renders the lattice theory in many respects to behave like its continuum counterpart with far-reaching consequences.

However, as nice as the theoretical progress that followed the rediscovery of the Ginsparg-Wilson relation was, as much of a challenge are realizations of operators D that satisfy the Ginsparg-Wilson relation (see [19–21] for reviews). Let us give a particular example for such a solution as found by H. Neuberger [22] from the overlap formalism [23], based on the pioneering work of D. Kaplan [24]. To this end, we first consider the standard Wilson Dirac operator on the lattice:

$$D_{\mathrm{w}} = \frac{1}{2}\left\{\gamma_\mu(\nabla_\mu^* + \nabla_\mu) - a\nabla_\mu^*\nabla_\mu\right\} \tag{2}$$

with ∇_μ, ∇^*_μ the lattice forward, backward derivatives, *i.e.* nearest-neighbour differences, acting on a field $\Phi(x)$:

$$\nabla_\mu \Phi(x) = \Phi(x+\mu) - \Phi(x)\,,$$
$$\nabla^*_\mu \Phi(x) = \Phi(x) - \Phi(x+\mu)\,.$$

We then define

$$A = 1 + s - D_{\rm w} \tag{3}$$

with $0 < s < 1$ a tunable parameter. Then Neuberger's operator $D_{\rm N}$ with mass m is given by

$$D_{\rm N} = \left\{ 1 - \frac{m}{2(1+s)} D_{\rm N}^{(0)} + m \right\}\,, \tag{4}$$

where

$$D_{\rm N}^{(0)} = (1+s)\left[1 - A(A^\dagger A)^{-1/2}\right]\,. \tag{5}$$

What is important here in the definition of Neuberger's operator is the appearance of the square root of the operator $A^\dagger A$. This means that $D_{\rm N}$ connects all points of the lattice with each other. Note, however, that despite this the operator is a local operator in the field-theoretical sense [25]. In practice, the operator $A^\dagger A$ is represented by a matrix that is, unfortunately, very large. Having a physical volume of size L^4, the number of sites is $N^4 = (L/a)^4$. As the internal number of degrees of freedom per lattice point is 12, we end up with A being a $(12N^4) \otimes (12N^4)$ complex matrix with N typically in the range $10 < N < 30$ for present days simulations. Hence we have to construct the square root of a very large matrix. What is worse, to compute relevant physical observables, we don't need the operator $D_{\rm N}$ itself but its inverse. Such an inverse is constructed by iterative methods like the conjugate gradient algorithm and its relatives [26].

The square root can be constructed by a polynomial expansion, normally based on a Chebyshev approximation, or by rational approximations. Both methods give comparable performances in practice. The convergence of the approximation to the square root is determined by the condition number of the (positive definite) matrix $A^\dagger A$. When the matrix $A^\dagger A$ is normalized such that the largest eigenvalue is 1, the condition number is given by the inverse of the lowest eigenvalue.

It was shown that very low-lying eigenvalues of the operator $A^\dagger A$ can appear in numerical simulations resulting in large condition numbers [27]. In such situations the convergence of the approximations chosen can be rather slow and special tricks have to be implemented to accelerate the convergence. The most fruitful improvement is to treat a part of the low-lying end of the spectrum exactly by projecting this part out of the matrix $A^\dagger A$ [28, 27]. Further improvements can be implemented, examples of which are discussed in ref. [27].

Despite all these technical improvements it is found that a typical value for the degree of a polynomial is $O(100)$ and a typical value for the number of iterations to compute the inverse of $D_{\rm N}$ is again $O(100)$. Since in each iteration to compute $D_{\rm N}^{-1}$ the Chebyshev polynomial has to be evaluated, this means that for a value of a physical observable on a single configuration ten thousand applications of a huge matrix on a vector has to be performed. To compute the expectation value of some observable, this observable has to be averaged over many gluonic configurations. Clearly, this results in a very demanding computational effort.

4 The scalar condensate

The existence of an exact lattice chiral symmetry allows the use of finite-size effects to test for SχSB in QCD. Using a chiral invariant formulation of lattice QCD, it is possible to reach the region of very small quark masses where it is to be expected that chiral symmetry starts to get restored.

The order parameter of chiral symmetry breaking in quantum chromodynamics is the condensate of a quark-antiquark state $\Sigma = \langle \psi\bar{\psi}\rangle$. A (standard) caveat here is the fact that all computations are done in the quenched approximation. In QCD there is a peculiarity: the field configurations can have topological properties, characterized by the so-called topological charge which can be measured —unambiguously— through the number of zero modes of the operator $D_{\rm N}$. In fact, the formulae from quenched chiral perturbation theory are parameterized by the topological charge and it is hence very important to be able to identify the topological charge of the gauge field configurations. Without the special properties of lattice Dirac operators that satisfy the Ginsparg-Wilson relation such an identification would be very difficult.

The complete theoretical formula from quenched chiral perturbation theory in lowest order is

$$\Sigma_\nu(m,V) = \Sigma\, z\, [I_\nu(z)K_\nu(z) + I_{\nu+1}(z)K_{\nu-1}(z)] + C\cdot m/a^2\,. \tag{6}$$

The only important thing to notice here is that this relatively involved combination of Bessel functions only depend on one scaling variable,

$$z = \Sigma m V\,, \tag{7}$$

that contains the quantity of interest, namely the infinite volume, chiral limit scalar condensate Σ. The additional term $C\cdot m/a^2$ is a power divergence that comes from the renormalization properties of the theory. We will not discuss this field-theoretical aspect here but just notice that this term has to be included in the fit.

In fig. 1, we show the result of our numerical computation of the scalar condensate [29] in a fixed topological charge sector $|\nu| = 1$ as a function of the quark mass at several volumes. The solid line is a fit to the prediction of chiral perturbation theory, eq. (6). We find that the simulation data are described by this prediction very well. This means that we find evidence for the basic assumption on which the theoretical prediction relies: the appearance of spontaneous chiral symmetry breaking in (quenched) QCD.

We want to remark that this work was the first of this kind. After this work, a number of other groups repeated

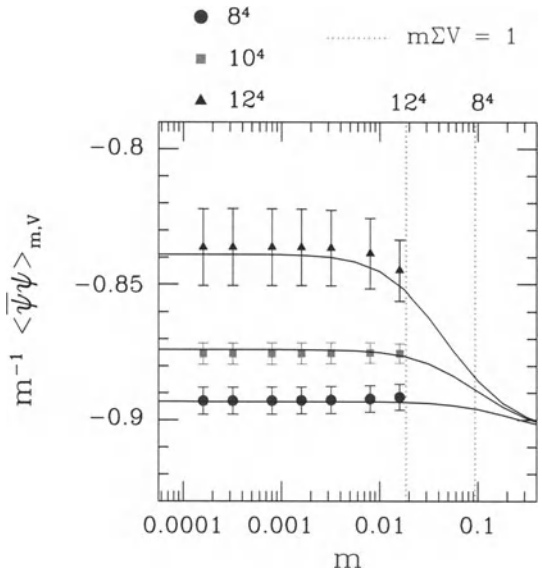

Fig. 1. The scalar condensate computed on lattices of various size as a function of the quark mass. The solid lines are 2-parameter (Σ and the constant C of eq. (6)) fits, according to the prediction of chiral perturbation theory.

such an analysis [30–32] and it was reassuring to observe that very consistent results were found. In a sub-sequel work [33,34] we developed also a quite general method for renormalizing the value of the bare scalar condensate as extracted from the finite-size scaling analysis performed here.

5 Conclusion

In this contribution we have demonstrated that by a combination of theoretical ideas, improved numerical methods and the use of powerful supercomputer platforms it is possible to test basic properties of field theories. Of particular interest was the question of whether the phenomenon of spontaneous symmetry breaking (SSB) does occur in certain field theories important in elementary-particle physics. The phenomenon of SSB leads to far-reaching consequences in theories like QCD or the scalar sector of the electroweak interactions. In the work performed here, we found strong evidence for the appearance of spontaneous chiral symmetry breaking in quenched lattice QCD.

The results presented here have been obtain in a most enjoyable collaboration with my colleagues and friends P. Hernández, L. Lellouch and H. Wittig.

References

1. K.G. Wilson, Phys. Rev. D **10**, 2445 (1974).
2. M. Müller-Preussker, W. Bietenholz, K. Jansen, F. Jegerlehner, I. Montvay, G. Schierholz, R. Sommer, U. Wolff, Nucl. Phys. Proc. Suppl. **106** (2002), hep-lat/0203004.
3. M. Lüscher, P. Weisz, Phys. Lett. B **158**, 250 (1985).
4. M. Lüscher, P. Weisz, Commun. Math. Phys. **97**, 59 (1985).
5. K. Symanzik, Nucl. Phys. B **226**, 187 (1983).
6. K. Symanzik, Nucl. Phys. B **226**, 205 (1983).
7. B. Sheikholeslami, R. Wohlert, Nucl. Phys. B **259**, 572 (1985).
8. M. Lüscher *et al.*, Nucl. Phys. B **491**, 323 (1997), hep-lat/9609035.
9. K. Jansen, R. Sommer, Nucl. Phys. B **530**, 185 (1998).
10. R. Sommer, *Lectures at Scladming 1997*, hep-lat/9711243.
11. M. Lüscher, *Lectures given at the Les Houches Summer School "Probing the Standard Model of Particle Interactions", July 28 - September 5, 1997*, hep-lat/9802029.
12. C. Bernard *et al.*, Nucl. Phys. Proc. Suppl. **106**, 199 (2002).
13. S. Weinberg, Physica A **96**, 327 (1979); J. Gasser, H. Leutwyler, Ann. Phys. (N.Y.) **158**, 142 (1984).
14. J. Gasser, H. Leutwyler, Phys. Lett. B **188**, 477 (1987); H. Neuberger, Phys. Rev. Lett. **60**, 889 (1988); Nucl. Phys. B **300**, 180 (1988);
F.C. Hansen, Nucl. Phys. B **345**, 685 (1990); F.C. Hansen, H. Leutwyler, Nucl. Phys. B **350**, 201 (1991);
P. Hasenfratz, H. Leutwyler, Nucl. Phys. B **343**, 241 (1990).
15. H.B. Nielsen, M. Ninomiya, Phys. Lett. B **105**, 219 (1981).
16. P.H. Ginsparg, K.G. Wilson, Phys. Rev. D **25**, 2649 (1982).
17. P. Hasenfratz, Nucl. Phys. B Proc. Suppl. **63**A-C, 53 (1998); P. Hasenfratz, V. Laliena, F. Niedermayer, Phys. Lett. B **427**, 125 (1998), hep-lat/9801021.
18. M. Lüscher, Phys. Lett. B **428**, 342 (1998), hep-lat/9802011.
19. F. Niedermayer, Nucl. Phys. Proc. Suppl. **73**, 105 (1999), hep-lat/9810026.
20. T. Blum Nucl. Phys. Proc. Suppl. **73**, 167 (1999), hep-lat/9810017.
21. P. Hernández, Nucl. Phys. Proc. Suppl. **106**, 80 (2002), hep-lat/0110218.
22. H. Neuberger, Phys. Lett. B **417**, 141 (1998), hep-lat/9707022.
23. R. Narayanan, H. Neuberger, Nucl. Phys. B **412**, 574 (1994), hep-lat/9307006.
24. D.B. Kaplan, Phys. Lett. B **288**, 342 (1992).
25. P. Hernández, K. Jansen, M. Lüscher, Nucl. Phys. B **552**, 363 (1999), hep-lat/9908010.
26. W.H. Press, S.A. Teukolsky, W.T. Vetterling, B.P. Flannery, *Numerical Recipes*, second edition (Cambridge University Press, Cambridge, 1992).
27. P. Hernández, K. Jansen, L. Lellouch, hep-lat/0001008.
28. R.G. Edwards, U.M. Heller, R. Narayanan, Phys. Rev. D **59**, 094510 (1999), hep-lat/9811030.
29. P. Hernández, K. Jansen, L. Lellouch, Phys. Lett. B **469**, 198 (1999), hep-lat/9907022.
30. T. DeGrand, Phys. Rev. D **63**, 034503 (2001), hep-lat/0007046.
31. L. Giusti, C. Hoelbling, C. Rebbi, hep-lat/0108007.
32. P. Hasenfratz, S. Hauswirth, K. Holland, T. Jorg, F. Niedermayer, Nucl. Phys. Proc. Suppl. **106**, 751 (2002), hep-lat/0109007.
33. P. Hernández, K. Jansen, L. Lellouch, H. Wittig, JHEP **07**, 18 (2001).
34. P. Hernández, K. Jansen, L. Lellouch, H. Wittig, (2000), in preparation.

Eur. Phys. J. A **18**, 257–260 (2003)
DOI 10.1140/epja/i2002-10211-9

THE EUROPEAN PHYSICAL JOURNAL A

Beyond the quark model of hadrons from lattice QCD

C. Michael[a]

Theoretical Physics Division, Mathematical Sciences Department, University of Liverpool, Liverpool L69 3BX, UK

Received: 30 September 2002 /
Published online: 22 October 2003 – © Società Italiana di Fisica / Springer-Verlag 2003

Abstract. Lattice QCD can give direct information on OZI-violating contributions to mesons. Here we explore the contributions that split flavour singlet and non-singlet meson masses. I discuss in detail the spectrum and decays for scalar mesons (*i.e.* including glueball effects). I also review the status of hybrid mesons and their decays.

PACS. 12.38.Gc Lattice QCD calculations – 12.39.Mk Glueball and nonstandard multi-quark/gluon states

1 Introduction

Lattice QCD is a first-principles approach to solving QCD non-perturbatively. It enables theorists to explore the consequences of QCD for quarks of different mass and so complements experimental studies. It is especially valuable for validitating phenomenological models. Direct comparison with experiment is hampered by two obstructions: i) the continuum limit (lattice spacing $a \to 0$) should be taken but this is not computationally feasible in many cases and ii) the u- and d-quark masses are too light to be successfully explored on a lattice so that one has to rely on chiral perturbation theory and extrapolate from heavier quark masses. Nevertheless, lattice QCD enables exploration of the hadron spectrum and matrix elements and can be used to quantify the success (and failure) of quark models. One area where the quark model is deficient is in flavour singlet mesons. Here the gluonic degrees of freedom are likely to make a significant contribution.

2 Flavour singlet mesons

In lattice QCD, one studies mesons by creating a quark-antiquark pair at time 0 with the quantum numbers of that meson and then annihilating the quark-antiquark pair at time t. The quark sources and sinks are then combined using the fully non-perturbative quark propagators determined on the lattice. For flavour singlet mesons, there will be two contributions: disconnected $D(t)$ and connected $C(t)$ as illustrated in fig. 1.

At large t where ground-state contributions dominate, these measured correlations satisfy $C(t) = ce^{-m_1 t}$ and

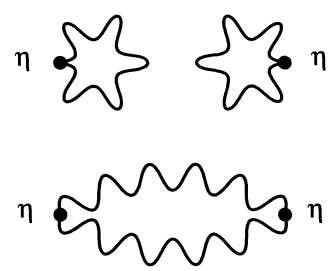

Fig. 1. The disconnected (above) and connected (below) correlators for flavour singlet mesons at time separation t. Here the wiggly lines represent full quark propagators. The illustration is for a pseudoscalar meson (η) but the same diagrams apply to all mesonic quantum numbers.

$C(t)+D(t) = de^{-m_0 t}$, where m_0 is the flavour singlet mass and m_1 the flavour non-singlet mass. Then, by a study of D/C which is given by $(d/c)\exp((m_1 - m_0)t) - 1$, one can explore the mass splitting between flavour singlet and non-singlet which is a measure of the OZI-violating gluonic contribution arising from the disconnected diagram.

From a lattice study of this for all mesonic quantum numbers [1] the only significant disconnected contributions were found for scalar and for pseudoscalar mesons. This is not unexpected: both from the phenomenology of the observed meson masses and from the expectation that the lightest glueball has scalar quantum numbers and that topological charge fluctuations have pseudoscalar quantum numbers.

For a review of the situation concerning pseudoscalar mesons see ref. [2]. We now discuss the glueballs and their impact on the meson spectrum.

[a] e-mail: smi@liv.ac.uk

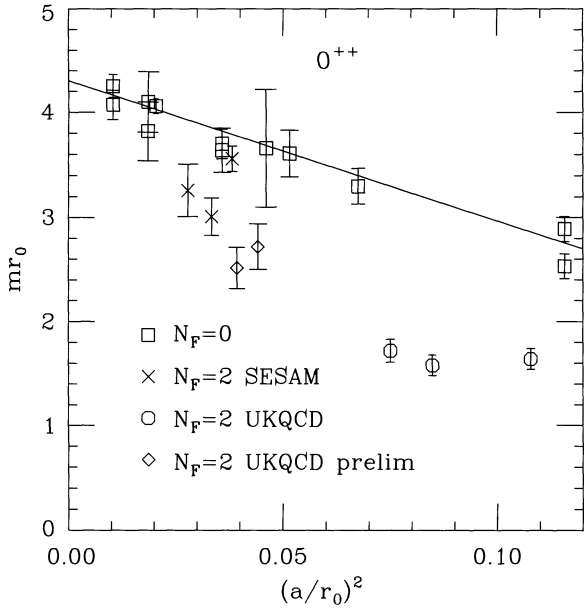

Fig. 2. The value of mass of the lightest $J^{PC} = 0^{++}$ meson (glueball) from quenched data ($N_f = 0$)[3–6] in units of r_0, where $r_0 \approx 0.5$ fm. The straight line shows a fit describing the approach to the continuum limit as $a \to 0$. Results [7–9] for the lightest scalar meson with $N_f = 2$ flavours of sea-quarks are also shown.

3 Glueballs and scalar mesons

Glueballs are defined to be hadronic states made primarily from gluons. The full non-perturbative gluonic interaction is included in quenched QCD. In the quenched approximation, there is no mixing between such glueballs and quark-antiquark mesons. A study of the glueball spectrum in quenched QCD is thus of great theoretical value.

This has been studied extensively [5,10] and the consensus is that the lightest glueball has scalar quantum numbers with the tensor ($J^{PC} = 2^{++}$) and pseudoscalar glueballs ($J^{PC} = 0^{-+}$) next in mass. The quenched results have been explored to very small lattice spacings and there is convincing evidence that the continuum limit values have been extracted —see fig. 2. Since the quenched approximation does *not* reproduce experiment, different ways to set the scale will differ —by ±10%. Using a conventional scale assignment ($r_0 = 0.5$ fm) gives masses of around 1.6 GeV for the scalar glueball and 2.2 GeV for the tensor.

One signal of great interest would be a glueball with J^{PC} not allowed for $q\bar{q}$ —a spin-exotic glueball or *oddball*— since it would not mix with $q\bar{q}$ states. These states are found [4,5,10] to be high lying: considerably above $2m(0^{++})$. Thus, they are likely to be in a region very difficult to access unambiguously by experiment.

Within the quenched approximation, the glueball states are unmixed with $q\bar{q}$, $q\bar{q}q\bar{q}$, etc. Furthermore, the $q\bar{q}$ states have degenerate flavour singlet and non-singlet states in the quenched approximation. This gives rise to anomalies in the quenched approximation: for example the scalar meson propagation can have the wrong sign [11] because the $\eta\pi$ intermediate state is mistreated. Once quark loops are allowed in the vacuum, then these anomalies are removed. Indeed, for the flavour singlet states of any given J^{PC}, there will be mixing between the $s\bar{s}$ state, the $u\bar{u}+d\bar{d}$ state and the glueball. Since the scalar glueball is lightest, we expect the largest effects here and one can explore this by measuring directly the scalar mass eigenstates in a study with $N_f = 2$ flavours of sea-quark.

Most studies have shown no significant change of the glueball spectrum as dynamical quarks are included [7]. However, the larger lattice spacing result [8] shows a significant reduction in the lightest scalar mass. Before concluding that this implies a lower scalar mass in the continuum limit, one needs to check whether an enhanced order a^2 correction might be present. Studies using the same approach at a finer lattice spacing [12,9] do suggest that this large order a^2 effect is significant, but studies even nearer to the continuum or with improved actions are needed to resolve this fully.

Let us now discuss the mixing of the scalar glueball and scalar mesons. In quenched QCD there is the problem described above concerning scalar mesons. For heavy enough quarks this is unimportant and one can measure the mixing strength on a quenched lattice even though no mixing actually occurs. On a rather coarse lattice ($a^{-1} \approx 1.2$ GeV), two groups have attempted this [13,8]. Their results expressed as the mixing for two degenerate quarks of mass around the strange-quark mass are similar, namely $E \approx 0.36$ GeV [13] and 0.44 GeV [8]. Opinions differ [13,8] as to whether this large mixing which would shift the glueball mass down by 20% will persist to the continuum limit.

From dynamical fermion studies with $N_f = 2$, one can determine the flavour singlet and non-singlet mass spectrum. No glueball, as such, can be defined. What we find [8,9] is that the lightest flavour singlet scalar meson is lighter than the lightest flavour non-singlet. This is in qualitative agreement with the mixing scenario described above.

As well as this mixing of the glueball with $q\bar{q}$ states, there will be mixing with $q\bar{q}q\bar{q}$ states which will be responsible for the hadronic decays. A first attempt to study this [14] in quenched QCD yields an estimated width for decay to two pseudoscalar mesons from the scalar glueball of order 100 MeV. A more realistic study would involve taking account of mixing using gluonic, $q\bar{q}$ and $q\bar{q}q\bar{q}$ operators in full QCD.

4 Hybrid mesons

A hybrid meson has the gluonic degrees of freedom which are excited non-trivially. The most significant consequence of this, experimentally, will be mesons with J^{PC} values not allowed in the quark model for a $q\bar{q}$ system (such as 1^{-+}).

On the lattice one can easily deal with relatively light quarks (down to the strange-quark mass) or extremely heavy quarks (treated as static or using NRQCD). I first discuss hybrid mesons with static heavy quarks where the description can be thought of as an excited colour string.

The lattice results [15–17] can then be presented as potential energy *versus* quark-antiquark separation R. The ground state will correspond to the usual interquark potential, whereas excited states will have non-trivial representations of the symmetries, *e.g.* the lightest excited state (Π_u) has colour flux which is a difference of paths from quark to antiquark of the form $\sqcap - \sqcup$.

From the potential corresponding to these excited gluonic states, one can determine the spectrum of hybrid quarkonia using the Schrödinger equation in the Born-Oppenheimer approximation. The Π_u symmetry state will produce a degenerate set of eight hybrid mesons of which those with $J^{PC} = 1^{-+}$, 0^{+-} and 2^{+-} are spin-exotic and hence will not mix with $Q\bar{Q}$ states. They thus form a very attractive goal for experimental searches for hybrid mesons.

Within the quenched approximation, the lattice evidence for $b\bar{b}$-quarks points to a lightest hybrid spin-exotic meson H with $J^{PC} = 1^{-+}$ at an energy given by [18] $(m_H - m_{2S})r_0 = 1.9 \pm 0.1$. This has been checked with $N_f = 2$ studies [19,20] which find similar mass ratios $(m_H - m_{1S})/(m_{1P} - m_{1S})$ but a larger splitting in terms of r_0, namely [19] $(m_H - m_{2S})r_0 = 2.4 \pm 0.2$. Using the experimental mass of the $\Upsilon(2S)$, these results imply that the lightest spin-exotic hybrid is in the mass range 10.7 to 10.9 GeV. Above this energy there will be many more hybrid states, many of which will be spin-exotic.

Within this static quark framework, one can explore the decay mechanisms. One special feature is that the symmetries of the quark and colour fields about the static quarks must be preserved exactly in decay. This has the consequence that the decay from a Π_u hybrid state to the open b-mesons ($B\bar{B}$, $B^*\bar{B}$, $B\bar{B}^*$, $B^*\bar{B}^*$) will be forbidden [20] if the light quarks in the B- and B^*-mesons are in an S-wave relative to the heavy quark. The decay to B^{**}-mesons with light quarks in a P-wave is allowed by symmetry but not energetically. The only allowed decays are to $\chi_b + M$, where M is a light quark-antiquark meson in a flavour singlet. Lattice estimates [20] of these transitions have been made and the dominant mode (with a width of around 100 MeV) is found to be with M as a scalar meson. This decay analysis does not take into account heavy-quark motion or spin-flip and these effects will be significantly more important for charm quarks than for b-quarks.

Several lattice groups [21–24] have studied hybrid spectra for light quarks and find the lightest spin-exotic hybrid to have $J^{PC} = 1^{-+}$ and mass (for s-quarks) of around 2 GeV. The corresponding light-quark (u, d) state would be around 120 MeV lighter. The light-quark results have also been [22] extrapolated to charm quarks and masses near 4.4 GeV are found for the corresponding state. A recent study has confirmed this value but with a very long extrapolation [24]. These mass estimates can be compared to naive estimates [16] of the spin-exotic charm state mass of 4.0 GeV from the static quark approach which will have an uncontrolled systematic error.

It is not easy to reconcile these lattice results with experimental indications [25] for resonances at 1.4 GeV and 1.6 GeV, especially the lower mass value. Mixing with $q\bar{q}q\bar{q}$ states such as $\eta\pi$ is not included for realistic quark masses in the lattice calculations. This can be interpreted, dependent on one's viewpoint, as either that the lattice calculations are incomplete or as an indication that the experimental states may have an important meson-meson component in them.

An attractive prospect to study hybrid mesons is from $p\bar{p}$ annihilation. Spin-exotic hybrids, which provide the best signal, will only be produced in association with other hadrons. The decay channel to $\chi_c + \pi + \pi$ with the two π-mesons in an S-wave is a promising detection channel. Lattice studies give first estimates of the masses and decay widths but more work needs to be done to constrain the systematic errors on these estimates.

References

1. UKQCD Collaboration (C. McNeile, C. Michael, K.J. Sharkey), Phys. Rev. D **65**, 014508 (2002).
2. UKQCD Collaboration (C. McNeile, C. Michael), Phys. Lett. B **491**, 123 (2000).
3. P. De Forcrand *et al.*, Phys. Lett. B **152**, 107 (1985).
4. C. Michael, M. Teper, Nucl. Phys. B **314**, 347 (1989).
5. UKQCD Collaboration (G. Bali *et al.*), Phys. Lett. B **309**, 378 (1993).
6. H. Chen *et al.*, Nucl. Phys. B (Proc. Suppl.) **34**, 357 (1994); A. Vaccarino, D. Weingarten, Phys. Rev. D **60**, 114501 (1999).
7. SESAM and TχL Collaboration (G. Bali *et al.*), Nucl. Phys. B (Proc. Suppl.) **63**, 209 (1998); Phys. Rev. D **62**, 054503 (2000).
8. C. McNeile, C. Michael, Phys. Rev. D **63**, 114503 (2001)
9. UKQCD Collaboration (A. Hart, C. McNeile, C. Michael), in preparation.
10. C. Morningstar, M. Peardon, Phys. Rev. D **56**, 4043 (1997); **60**, 034509 (1999).
11. W. Bardeen *et al.*, Phys. Rev. D **65**, 014509 (2002).
12. UKQCD Collaboration (A. Hart, M. Teper), Phys. Rev. D **65**, 034502 (2002).
13. W. Lee, D. Weingarten, Nucl. Phys. B (Proc. Suppl.) **63**, 194 (1998); hep-lat/9805029; Phys. Rev. D **61**, 014015 (2000).
14. J. Sexton, A. Vaccarino, D. Weingarten, Nucl. Phys. B (Proc. Suppl.) **42**, 279 (1995); Phys. Rev. Lett. **75**, 4563 (1995)
15. L.A. Griffiths, C. Michael, P.E.L. Rakow, Phys. Lett. B **129**, 351 (1983).
16. S. Perantonis, C. Michael, Nucl. Phys. B **347**, 854 (1990).
17. K. Juge , J. Kuti, C. Morningstar, Phys. Rev. Lett. **82**, 1999 (4400); Nucl. Phys. B (Proc. Suppl.) **83**, 304 (2000).
18. C. Michael, *Proceedings of the 8th International Symposium on Heavy Flavour Physics, Southampton, 25-29 July 1999*, edited by P. Dauncey, C. Sachrajda, JHEP, PRHEP-hf8/001, 1-10 (2000); hep-ph/9911219.
19. CP-PACS Collaboration (T. Manke *et al.*), Phys. Rev. Lett. **82**, 4396 (1999); Phys. Rev. D **64**, 097505 (2001).
20. UKQCD Collaboration (C. McNeile, C. Michael, P. Pennanen), Phys. Rev. D **65**, 094505 (2002).
21. UKQCD Collaboration (P. Lacock, C. Michael, P. Boyle, P. Rowland), Phys. Rev. D **54**, 6997 (1996); Phys. Lett. B **401**, 308 (1997).

22. C. Bernard *et al.*, Phys. Rev. D **56**, 7039 (1997); Nucl. Phys. B (Proc. Suppl.) **73**, 264 (1999).
23. P. Lacock, K. Schilling, Nucl. Phys. B (Proc. Suppl.) **73**, 261 (1999).
24. Z.H. Mei, X.Q. Luo, hep-lat/0206012.
25. D. Thompson *et al.*, Phys. Rev. Lett. **79**, 1630 (1997); S.U. Chung *et al.*, Phys. Rev. D **60**, 092001 (1999); D. Adams *et al.*, Phys. Rev. Lett. **81**, 5760 (1998); E.I.Ivanov *et al.*, Phys. Rev. Lett. **86**, 3977 (2001).

Eur. Phys. J. A **18**, 261–264 (2003)
DOI 10.1140/epja/i2002-10212-8

THE EUROPEAN PHYSICAL JOURNAL A

Infrared exponents and the running coupling of Landau gauge QCD and their relation to confinement

R. Alkofer[1,a], C.S. Fischer[1], and L. von Smekal[2]

[1] Institute for Theoretical Physics, University of Tübingen, Auf der Morgenstelle 14, D-72076 Tübingen, Germany
[2] Institute for Theoretical Physics III, University of Erlangen-Nürnberg, Staudtstr. 7, D-91058 Erlangen, Germany

Received: 30 September 2002 /
Published online: 22 October 2003 – © Società Italiana di Fisica / Springer-Verlag 2003

Abstract. The infrared behaviour of the gluon and ghost propagators in Landau gauge QCD is reviewed. The Kugo-Ojima confinement criterion and the Gribov-Zwanziger horizon condition result from quite general properties of the ghost Dyson-Schwinger equation. The numerical solutions for the gluon and ghost propagators obtained from a truncated set of Dyson-Schwinger equations provide an explicit example for the anticipated infrared behaviour. The results are in good agreement with corresponding lattice data obtained recently. The resulting running-coupling approaches a fix point in the infrared, $\alpha(0) = 8.92/N_c$. Two different fits for the scale dependence of the running coupling are given and discussed.

PACS. 12.38.Aw General properties of QCD (dynamics, confinement, etc.) – 14.70.Dj Gluons – 12.38.Lg Other nonperturbative calculations – 11.15.Tk Other nonperturbative techniques – 02.30.Rz Integral equations

1 Aspects of confinement

Quarks and gluons, the elementary fields of QCD, are not directly detected in experiments. Instead, a plethora of hadrons, interpreted as colourless bound states, are observed. This phenomenon, called *confinement*, is still not properly understood, a clear and undisputable mechanism responsible for this effect has not been found yet. Moreover it seems not even clear, at present, whether the phenomenon of confinement is at all compatible with a description of quark and gluon correlations in terms of local fields in the usual sense of quantum field theory.

It is interesting to note that the two-point correlations functions of QCD, the quark, gluon and ghost propagators, might show some signals of the underlying structures of the theory which are responsible for confinement. It has been argued that the infrared behaviour of the ghost and the gluon propagator of ordinary Faddeev-Popov gauge is related to both, the Kugo-Ojima confinement criterium [1] and the Gribov-Zwanziger horizon condition [2,3].

In the Kugo-Ojima scenario a physical state space that contains colourless states only is generated if two conditions are fulfilled: *First*, one should not have massless particle poles in transverse gluon correlations and *second*, one needs a well-defined, *i.e.* unbroken, global colour charge. The second condition can be related to the behaviour of the ghost propagator in Landau gauge. For it to be satisfied, the propagator must be more singular than a massless particle pole in the infrared [4].

The Gribov-Zwanziger horizon condition is connected to the gauge fixing ambiguities in the linear covariant gauge. Ideally one would eliminate Gribov copies along gauge orbits by a restriction of the functional integral of the QCD partition function to the so-called fundamental modular region. This part of configuration space lies inside the first Gribov region, a convex region in gauge field space which contains the trivial configuration $A \equiv 0$. At the boundary of the first Gribov region, the lowest eigenvalue of the Faddeev-Popov operator approaches zero. Entropy arguments have been employed to reason that the infrared modes of the gauge field are close to this Gribov horizon [3]. As the ghost propagator is the inverse of the Fadeev-Popov operator we therefore encounter the presence of the Gribov horizon in the infrared behaviour of the ghost: The ghost propagator is required to be more singular than a simple pole if the restriction to the Gribov region is correctly implemented. Furthermore, by the same entropy arguments, the gluon propagator has to vanish in the infrared [3].

Our framework to investigate the behaviour of the propagators of QCD are the Dyson-Schwinger equations (DSEs) [5]. Being complementary to lattice Monte Carlo simulations which have to deal with finite-volume effects, DSEs allow for analytical investigations of the infrared behaviour of correlation functions. In Landau gauge we have the particularly simple situation that the ghost-gluon

[a] e-mail: Reinhard.Alkofer@uni-tuebingen.de

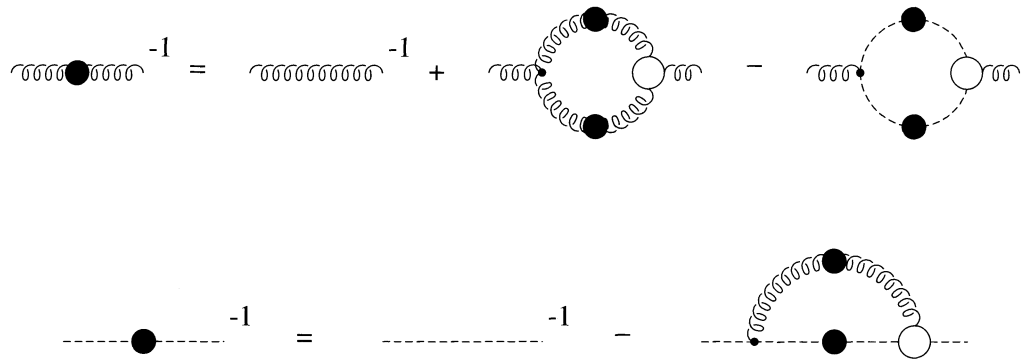

Fig. 1. Diagrammatic representation of the truncated gluon and ghost Dyson-Schwinger equations (DSE) studied here. Terms with four-gluon vertices have been dismissed.

vertex does not suffer from ultraviolet infinities. Based on this observation one can use the general structure of the ghost DSE, the properties of multiplicative renormalizability and the assumption that all involved Green's functions can be expanded in a power series to show that the Kugo-Ojima criterion as well as the Gribov-Zwanziger horizon condition are satisfied [6,7]. Furthermore, it has been shown that the infrared behaviour of the ghost and the gluon propagators are uniquely related: Both fulfill power laws such that the corresponding powers in the running coupling (as extracted from the ghost-gluon vertex) exactly cancel and one obtains an infrared fix point for the coupling.

2 Infrared exponents and running coupling

More detailed information on the propagators of Landau gauge QCD can be obtained from the DSEs once the system is truncated and *ansaetze* for the vertices have been made. The resulting closed system of equations can be solved both analytically in the infrared and numerically for non-vanishing momenta. The considerations presented in the previous section suggest that for small momenta the ghost loop dominates in the gluon DSE. Assuming this dominance, effects from a wide class of possible dressings for the ghost-gluon vertex have been investigated in ref. [7] and found to be of negligible influence to the qualitative findings.

Thus, for the purpose of this paper we concentrate on the simplest of these truncation schemes which has been developed in detail in refs. [8,9]. This scheme employs bare three-point functions and neglects four-gluon vertices, see fig. 1[1]. It provides the correct one-loop anomalous dimensions of the ghost and gluon dressing functions, $G(k^2)$ and $Z(k^2)$, respectively[2], and thus correctly describes the leading logarithmic behaviour of the propagators in the ultraviolet. Furthermore, this scheme reproduces the infrared exponents found in refs. [7,11]: $Z(k^2) \sim (k^2)^{2\kappa}$ and $G(k^2) \sim (k^2)^{-\kappa}$ with $\kappa \approx 0.595$. These exponents are close to the ones extracted from lattice calculations [12–14]. Interestingly enough they are also close to the ones obtained in a comparable truncation scheme in stochastically quantized Landau gauge Yang-Mills theory [15].

The numerical solutions are compared to recent lattice calculations [14] in fig. 2. Differences mainly occur for the gluon propagator in the region around the bending point, *i.e.* somewhat below one GeV. These can be attributed to the omission of the two-loop diagrams in the DSE truncation. Given the limitations of both methods the qualitative and partly even quantitative agreement is remarkable.

The DSE-based result for the running coupling can be seen in fig. 3. The analytically obtained value for the fix point of the running coupling in the infrared is $\alpha(0) \approx 2.97$ for the gauge group $SU(3)$ in this truncation scheme. Corrections from possible dressings for the ghost-gluon vertex have been found to be such that $2.5 < \alpha(0) \leq 2.97$ [7]. The maximum at non-vanishing momenta seen in our result for the running-coupling results in a multi-valued beta-function. On the other hand, it appears in a region where the above comparison to lattice data suggests that our results are least reliable. (The physical scale has been fixed by requiring the experimental value $\alpha(M_Z^2 = (91.2\,\mathrm{GeV})^2) = 0.118$.) We therefore summarize our result for the running coupling in the monotonic fit functions[3]:

$$\text{Fit A:} \quad \alpha(x) = \frac{\alpha(0)}{\ln(e + a_1(x/\Lambda^2)^{a_2} + b_1(x/\Lambda^2)^{b_2})}, \quad (1)$$

$$\text{Fit B:} \quad \alpha(x) = \frac{1}{a + (x/\Lambda^2)^b}\left(a\,\alpha(0) + \left(\frac{1}{\ln(x/\Lambda^2)} - \frac{1}{x/\Lambda^2 - 1}\right)(x/\Lambda^2)^b\right). \quad (2)$$

The value $\alpha(0) = 2.972 = 8.915/N_c$ is known from the infrared analysis. In both fits the ultraviolet behaviour

[1] A coupled system of gluon and ghost DSEs has been studied for the first time in ref. [10].

[2] These quantities are defined via the gluon and the ghost propagators via the relations $D_{\mu\nu}^{\mathrm{Gluon}}(k^2) = \left(\delta_{\mu\nu} - \frac{k_\mu k_\nu}{k^2}\right) Z(k^2)/k^2$ and $D^{\mathrm{Ghost}}(k^2) = -G(k^2)/k^2$.

[3] The β-function corresponding to fit A can be found in ref. [16].

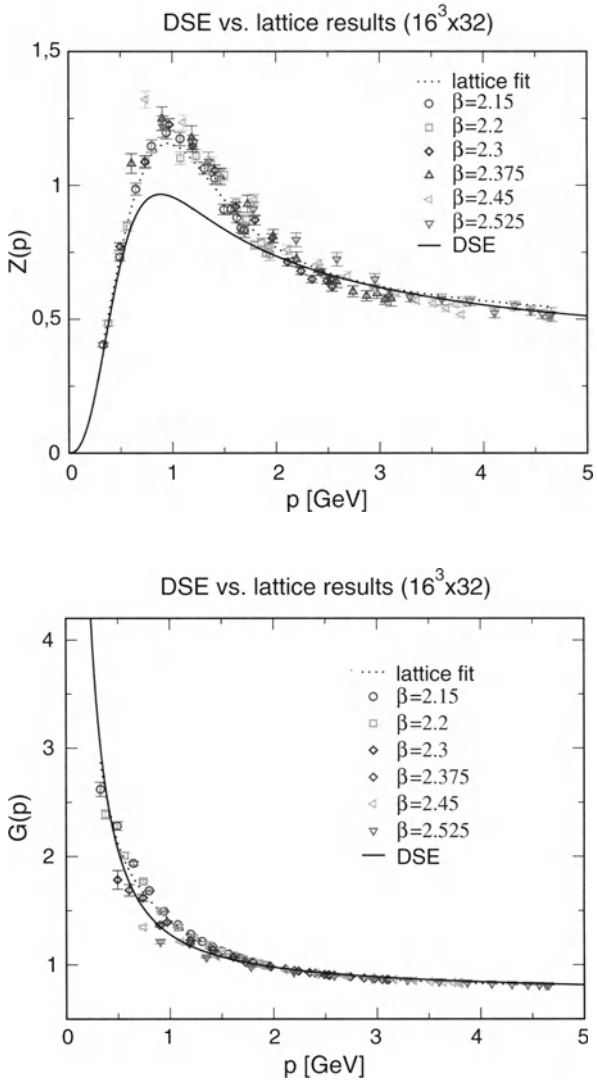

Fig. 2. Solutions of the Dyson-Schwinger equations compared to recent lattice results for two colours [14].

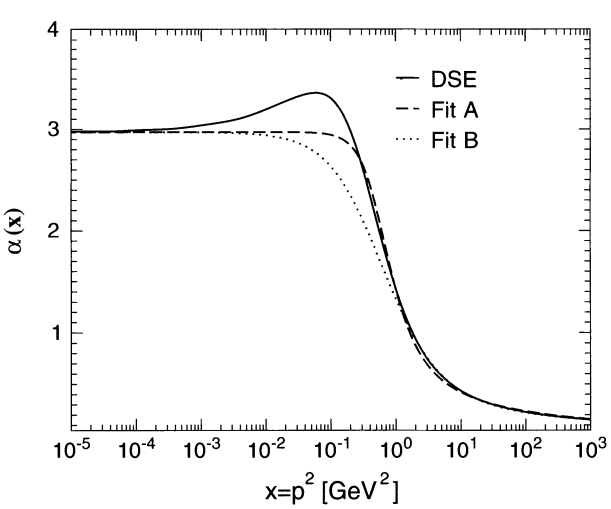

Fig. 3. The strong running coupling from the DSEs and the fits A and B, cf. eqs. (1), (2).

of the solution fixes the scale, $\Lambda = 0.714\,\mathrm{GeV}$. Note that we have employed a MOM scheme, and thus Λ has to be interpreted as $\Lambda_{\mathrm{MOM}}^{N_f=0}$, *i.e.* this scale has the expected magnitude. Fit A employs the four additional parameters: $a_1 = 1.106$, $a_2 = 2.324$, $b_1 = 0.004$, $b_2 = 3.169$. Fit B (which provides a better description in the ultraviolet at the expense of some deviations at smaller momenta) has only two free parameters: $a = 1.020$, $b = 1.052$.

In summary, we have employed analytical as well numerical studies of the gluon and ghost Dyson-Schwinger equations in Landau gauge Yang-Mills theories to verify the Kugo-Ojima confinement criterion. We have shown that the resulting infrared behaviour of gluon and ghost propagators, namely a highly infrared singular ghost and an infrared suppressed gluon propagator, is related to the Gribov-Zwanziger horizon condition. The solution for these propagators has then be used to calculate the running coupling for all spacelike momentum scales.

R.A. thanks the organizers of *Quark Nuclear Physics 2002* for the possibility to participate in this conference. We are grateful to K. Langfeld, H. Reinhardt, D. Shirkov, P. Watson and D. Zwanziger for helpful discussions. This work has been supported by the DFG under contract Al 279/3-4 and by the European graduate school Tübingen-Basel (DFG contract GRK 683).

References

1. T. Kugo, I. Ojima, Prog. Theor. Phys. Suppl. **66**, 1 (1979).
2. V.N. Gribov, Nucl. Phys. B **139**, 1 (1978).
3. D. Zwanziger, Nucl. Phys. B **364**, 127 (1991); **399**, 477 (1993); **412**, 657 (1994).
4. T. Kugo, in *Proceedings of the International Symposium on the BRS symmetry, Kyoto, Sep. 18-22, 1995*, edited by M. Abe, N. Nakanishi, I. Ojima (Universal Academic Press, Tokyo, 1996), arXiv:hep-th/9511033.
5. R. Alkofer, L. von Smekal, Phys. Rep. **353**, 281 (2001), arXiv:hep-ph/0007355.
6. P. Watson, R. Alkofer, Phys. Rev. Lett. **86**, 5239 (2001), arXiv:hep-ph/0102332; R. Alkofer, L. von Smekal, P. Watson, *Proceedings of the ECT* Collaboration Meeting on Dynamical Aspects of the QCD Phase Transition, Trento, Italy, March 12-15, 2001*, arXiv:hep-ph/0105142.
7. C. Lerche, L. von Smekal, Phys. Rev. D **65**, 125006 (2002), arXiv:hep-ph/0202194.
8. C.S. Fischer, R. Alkofer, H. Reinhardt, Phys. Rev. D **65**, 094008 (2002), arXiv:hep-ph/0202195.
9. C.S. Fischer, R. Alkofer, Phys. Lett. B **536**, 177 (2002), arXiv:hep-ph/0202202.
10. L. von Smekal, R. Alkofer, A. Hauck, Phys. Rev. Lett. **79**, 3591 (1997), arXiv:hep-ph/9705242; Ann. Phys. (N.Y.) **267**, 1 (1998), arXiv:hep-ph/9707327.
11. D. Zwanziger, Phys. Rev. D **65**, 094039 (2002), arXiv:hep-th/0109224.
12. F.D. Bonnet, P.O. Bowman, D.B. Leinweber, A.G. Williams, Phys. Rev. D **62**, 051501 (2000), arXiv:hep-lat/0002020.
13. F.D. Bonnet, P.O. Bowman, D.B. Leinweber, A.G. Williams, J.M. Zanotti, Phys. Rev. D **64**, 034501 (2001), arXiv:hep-lat/0101013.

14. K. Langfeld, H. Reinhardt, J. Gattnar, Nucl. Phys. B **621**, 131 (2002), arXiv:hep-ph/0107141; see also K. Langfeld *et al.*, arXiv:hep-th/0209173.
15. D. Zwanziger, Phys. Rev. D **67**, 105001 (2003), arXiv:hep-th/0206053.
16. R. Alkofer, C.S. Fischer, L. von Smekal, Acta Phys. Slovaca **52**, 191 (2002), arXiv:hep-ph/0205125.

Eur. Phys. J. A **18**, 265–268 (2003)
DOI 10.1140/epja/i2002-10213-7

THE EUROPEAN PHYSICAL JOURNAL A

Spectral functions of quarks in quark matter

F. Frömel[a], S. Leupold, and U. Mosel

Institut für Theoretische Physik, Universität Giessen, D-35392 Giessen, Germany

Received: 30 September 2002 /
Published online: 22 October 2003 – © Società Italiana di Fisica / Springer-Verlag 2003

Abstract. We present a simple albeit self-consistent approach to the spectral function of light quarks in infinite quark matter. Relations between correlation functions and collision rates are used to calculate the spectral function in an iterative procedure. The quark interactions are described by the $SU(2)$ Nambu–Jona-Lasinio model. Calculations were performed in the chirally restored phase at zero temperature.

PACS. 24.85.+p Quarks, gluons, and QCD in nuclei and nuclear processes – 12.39.Fe Chiral Lagrangians – 12.39.Ki Relativistic quark model

1 Introduction

It is well known that short-range correlations have influence on the properties of nuclear matter and finite nuclei; a substantial amount of high-momentum processes is contained in the nucleon spectral function. There have been many theoretical approaches trying to understand the short-range correlations. Of particular interest are the self-consistent calculations for the spectral function of nucleons in nuclear matter from Lehr *et al.* [1]. The results of their simple model are in good agreement with sophisticated calculations from many-body theory. It is striking that their model is very successful in describing the influence of short-range correlations on the properties of nuclear matter using a simple pointlike nucleon interaction with a constant scattering amplitude.

Motivated by the success of this model we have taken up the concept to investigate the properties of light quarks in infinite quark matter [2]. It is our basic assumption that the properties of the spectral function are dominated by phase space effects and the overall strength of the interaction just like in the case of the nucleons. The detailed structure of the interaction should be relatively unimportant as long as the relative symmetries are respected. We use relations between the spectral function and the collisional self-energies to construct a simple albeit self-consistent model. The spectral function can then be calculated in an iterative process beyond the quasiparticle approximation. The quark interactions are described by the Nambu–Jona-Lasinio (NJL) model [3]. It has the same symmetries as QCD and describes an effective pointlike interaction.

As a first step the model has been applied to the simplest system, namely the chirally restored phase at zero temperature. Mean-field effects were neglected, diquark condensates that arise in the color superconducting phase were not included. For the collisional self-energies only the lowest-order contributions, the Born diagrams, were considered. In the numerical calculations the influence of the coupling strength and the chemical potential on the properties of the spectral function was investigated.

2 The model

In this section we will briefly review our model. For more details we refer to [2]. The underlying Green's function formalism is discussed in much detail in [4,5]. Note that current quark masses are neglected throughout this work and only systems in thermal equilibrium are considered. We use the Nambu–Jona-Lasinio model to describe the quark interactions in our approach. It is an effective interaction model that was designed to resemble the symmetries of QCD. The $SU(2)$ Lagrangian is given by

$$\mathcal{L}_{\mathrm{NJL}} = \bar{\psi} i \partial\!\!\!/ \psi + G[(\bar{\psi}\psi)^2 + (\bar{\psi} i \gamma_5 \boldsymbol{\tau} \psi)^2], \qquad (1)$$

where G is the coupling strength, independent of energy and momentum, and the τ_i are isospin Pauli matrices. Due to the pointlike interaction this model is nonrenormalizable and a three-momentum cutoff Λ is introduced. Currently we do not consider any extensions to the Lagrangian that lead to color superconductivity, cf. [2].

The correlation functions

$$ig^{>}(1,1') = \langle \psi(1)\bar{\psi}(1')\rangle,$$
$$-ig^{<}(1,1') = \langle \bar{\psi}(1')\psi(1)\rangle$$

are the fundamental elements of our model. In thermal equilibrium they are related to the spectral function $\mathcal{A}$

[a] e-mail: Frank.Froemel@theo.physik.uni-giessen.de

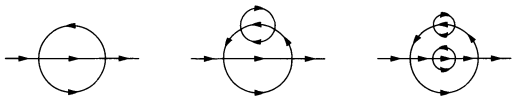

Fig. 1. Examples for diagrams that are resummed in our calculation. The lines correspond to free propagators.

via the thermal Fermi distribution $n_{\mathrm{F}}(p_0)$:

$$-ig^{<}(p) = \mathcal{A}(p)n_{\mathrm{F}}(p_0), \quad (2)$$

$$ig^{>}(p) = \mathcal{A}(p)[1 - n_{\mathrm{F}}(p_0)]. \quad (3)$$

Note that the Green's functions and the spectral function are matrices in spinor space. The single-particle self-energy can be decomposed into a mean-field part Σ^{mf} and the collisional self-energies $\Sigma^{\gtrless}$. Thus, the retarded self-energy Σ^{ret} is given by

$$\Sigma^{\mathrm{ret}}(1,1') = \Sigma^{\mathrm{mf}}(1,1') + \Theta(t_1 - t_{1'})\left[\Sigma^{>}(1,1') - \Sigma^{<}(1,1')\right]. \quad (4)$$

The time local mean-field self-energy corresponds to the motion of particles in a potential. It is responsible for the dynamical generation of the constituent-quark masses. The collisional self-energies contain the effects of particle decays and collisions in the medium. In lowest order they are given by the Born diagrams (cf. left diagram in fig. 1). One finds

$$\pm i\Sigma^{\gtrless}(p) \sim \iiint \cdots G^2 g^{\lessgtr}(p_2) g^{\gtrless}(p_3) g^{\gtrless}(p_4), \quad (5)$$

where $g^{>}$ and $g^{<}$ are full propagators and the integrals run over p_2, p_2, and p_4. Equations (5) look like total collision rates and can be used to determine the width of the spectral function:

$$\Gamma(p) = -2\mathrm{Im}\Sigma^{\mathrm{ret}}(p) = i[\Sigma^{>}(p) - \Sigma^{<}(p)]. \quad (6)$$

The real part of Σ^{ret} is related to Γ by a dispersion relation. If the width is known over the full energy range $\mathrm{Re}\Sigma^{\mathrm{ret}}$ can be calculated dispersively. Using Γ and $\mathrm{Re}\Sigma^{\mathrm{ret}}$ the spectral function can be explicitly written as

$$\mathcal{A}(p) = -2\mathrm{Im}g^{\mathrm{ret}}(p) = -2\mathrm{Im}\frac{1}{\not{p} - \mathrm{Re}\Sigma^{\mathrm{ret}} + i\Gamma/2} \quad (7)$$

Equations (2),(3), and (5)-(7) form a set of equations describing a self-consistency problem. A direct solution is not easily possible. It is possible, however, to solve the problem iteratively by starting from an initial guess for one of the quantities. In this way we can find a solution for the spectral function. The effect of self-consistency can be nicely illustrated in the language of Feynman diagrams. Using full propagators $g^{\gtrless}$ that depend themselves on $\Sigma^{\gtrless}$ in eqs. (5) means that we sum nonperturbatively over a whole class of diagrams. Some examples are shown in fig. 1.

Finally, we have to discuss the matrix structure of the spectral function in spinor space. To find the most general form $\mathcal{A}$ can be decomposed in terms of the 16 independent products of the γ matrices. Demanding invariance under parity and time reversal symmetry we find for the rest frame of the medium (in thermal equilibrium) [6]:

$$\mathcal{A}(p) = \rho_{\mathrm{s}}(p_0, \boldsymbol{p}^2) + \rho_0(p_0, \boldsymbol{p}^2)\gamma^0 + \rho_{\mathrm{v}}(p_0, \boldsymbol{p}^2)\hat{\boldsymbol{p}} \cdot \boldsymbol{\gamma}, \quad (8)$$

where $\hat{\boldsymbol{p}}$ is a unit vector in the momentum direction. Note that the density of states is given by ρ_0 alone and that ρ_{s} has to be zero in the chirally restored phase. It follows from eqs. (2)-(7) that Γ and $\Sigma^{\gtrless}$ must have the same structure as ρ.

Currently we apply two simplifications to the model. First, we restore chiral symmetry "manually" by setting Σ^{mf} to zero. This can be done for any density and temperature since $m = 0$ is always a solution of the equation for the constituent-quark mass [3]. However, one has to be aware that this might not be the thermodynamically favored phase when also a finite solution for m exists. Second, we neglect the real part of Σ^{ret} due to technical reasons [2]. For nuclear matter this was a reasonable approximation [1]. To make sure that the effects of this violation of analyticity are not significant we have checked that $\mathrm{Re}\Sigma^{\mathrm{ret}}$ is small compared to $\not{p}$, cf. eq.(7).

3 Results

All our calculations were performed at zero temperature and in the chirally restored phase. The calculations were initialized with a constant width, $\Gamma_0 = 1\,\mathrm{MeV}$ and $\Gamma_{\mathrm{v}} = 0$. Self-consistency was achieved after two iterations. First, we chose the quark matter density such that it is comparable to regular nuclear matter, $\rho_{\mathrm{qm}} = 3 \cdot \rho_{\mathrm{nm}} = 3 \cdot 0.17\,\mathrm{fm}^{-3}$. This yields a Fermi energy of $\omega_{\mathrm{F}} = 0.268\,\mathrm{GeV}$. The cutoff Λ and the coupling constant G of the NJL model were chosen so that the model reproduces the known values [3] for the quark condensate and the pion coupling constant f_π in vacuum. To investigate the influence of the coupling on the spectral function we did also calculations with two times and four times larger coupling strengths. In reality quark matter with a chemical potential of $\omega_{\mathrm{F}} = 0.268\,\mathrm{GeV}$ would not be in the chirally restored phase. Therefore we made additional calculations with a higher density of $\rho_{\mathrm{qm}} = 1.53\,\mathrm{fm}^{-3}$, corresponding to $\omega_{\mathrm{F}} = 0.387\,\mathrm{GeV}$. This chemical potential is well beyond the chiral phase transition in the NJL model [3].

Figure 2 shows our results for the spectral function and its width at several momenta and coupling strengths using $\omega_{\mathrm{F}} = 0.268\,\mathrm{GeV}$. Due to the pointlike interaction the width seems to increase explosively for large $|p_0|$. At even higher $|p_0|$, however, the opening of phase space is suppressed by the NJL cutoff and the width decreases again. Physically the most interesting area lies in the energy range $0 < p_0 < \omega_{\mathrm{F}}$ since that is the region of the populated quark states. All states above the Fermi energy as well as the anti-quark states at negative p_0 are unoccupied (no holes in the Dirac sea). The structure of the spectral function is dominated by the on-shell peaks of the quarks and anti-quarks at $p_0 = |\boldsymbol{p}|$ and $p_0 = -|\boldsymbol{p}|$. The peaks get broader when the coupling is increased. Strength is distributed away from the peaks to the off-shell regions, the

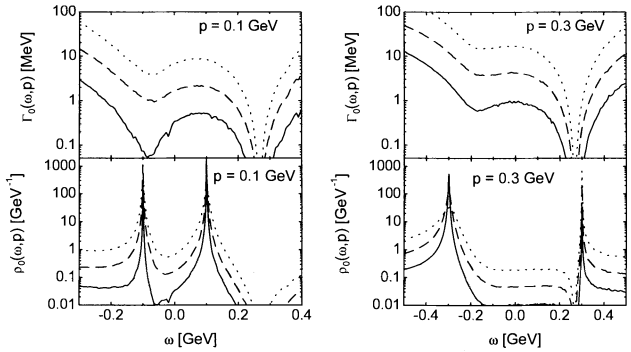

Fig. 2. The width Γ_0 and the spectral function ρ_0 of quarks at different momenta. Solid lines correspond to the usual NJL coupling strength, dashed lines to a coupling twice as large. Dotted lines have been obtained with a coupling four times larger than the usual value.

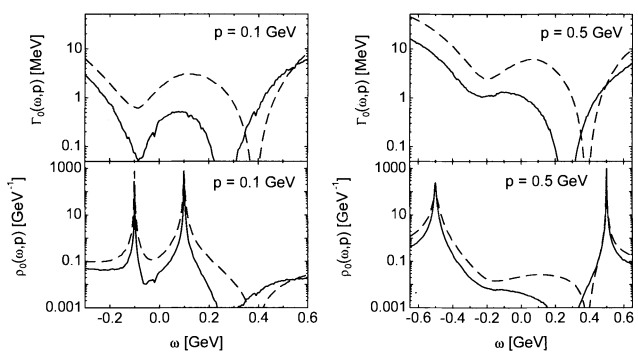

Fig. 3. The width Γ_0 and the spectral function ρ_0 of quarks at different momenta. Solid lines correspond to $\omega_F = 0.268\,\mathrm{GeV}$, dashed lines to $\omega_F = 0.387\,\mathrm{GeV}$.

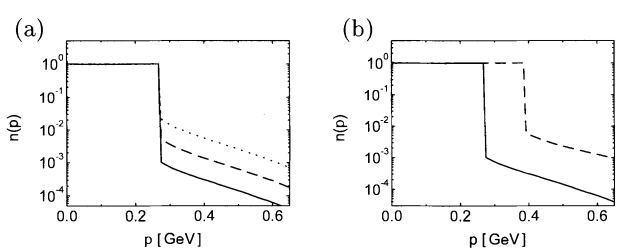

Fig. 4. (a) Quark momentum distribution in quark matter for $\omega_F = 0.268\,\mathrm{GeV}$ and three different couplings (see fig. 2 for details). (b) Momentum distribution for two different chemical potentials (see fig. 3 for details).

width of the peaks increases from 0.1–1 MeV to 10 MeV. The width seems to scale with the coupling strength (respectively G^2, cf. eqs. (5)) while the general shape remains unchanged.

Figure 3 shows the width and the spectral function for the two chemical potentials $\omega_F = 0.268\,\mathrm{GeV}$ and $\omega_F = 0.387\,\mathrm{GeV}$ using the regular coupling strength. The effect of the higher density is comparable to increasing the coupling. The width approximately scales with the chemical potential while the shape remains unchanged. This leads again to a broadening of the peaks of the spectral function.

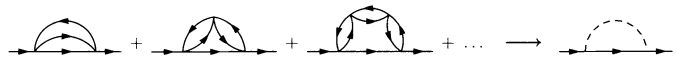

Fig. 5. Series of diagrams corresponding to dynamically generated mesons.

In the momentum distribution of nucleons in nuclear matter a depletion of the occupation probabilites by about 10% is seen [1]. The resulting high-energy tail is taken as a universal sign of short-range correlations. We show the momentum distribution of the quarks for the different coupling strengths in fig. 4(a). At the lowest coupling a depletion of only 0.1% is found. For the coupling twice as large the short-range correlations increase but still the depletion effect is below 1%. Only for the largest couplings we find a high momentum tail of a few percent, comparable to the case of nucleons. In fig. 4(b) it can be seen again that the effect of the larger chemical potential is similar to an increased coupling. The depletion for $\omega_F = 0.387\,\mathrm{GeV}$ grows by almost one order of magnitude compared to $\omega_F = 0.268\,\mathrm{GeV}$.

4 Summary and outlook

Based on a successful model for nuclear matter we have presented a simple but fully self-consistent approach to the spectral function of quarks in quark matter. It uses a pointlike interaction and goes beyond the quasiparticle approximation. The numerical results indicate that the influence of short-range correlations is rather small compared to nuclear matter. This finding might be an artifact of the present model, the NJL model with vacuum parameters in the Born approximation. Furthermore we have not considered broken symmetries. However, the calculations have shown that the model is technically feasible and suitable for further development.

At present, the model is extended in two ways. First, a more realistic phase with broken symmetries —the chirally broken phase— is considered. In this phase large constituent-quark masses must be taken into account and the analytic structure of the spectral function (8) is more complicated. Second, a new class of diagrams is incorporated into the collisional self-energies (5). This series of diagrams is shown in fig. 5. The lowest-order contribution is again the Born diagram. The full series can be interpreted as a dynamically generated meson that couples to the quarks [3,7]. First estimates show that this extension will increase the effective quark coupling and should lead to significantly higher widths of the spectral function. In addition, it will be possible to investigate the properties of the self-consistently calculated pions and sigmas.

This work was supported by DFG.

References

1. J. Lehr, M. Effenberger, H. Lenske, S. Leupold, U. Mosel, Phys. Lett. B **483**, 324 (2000); J. Lehr, H. Lenske, S. Leupold, U. Mosel, Nucl. Phys. A **703**, 393 (2002).

2. F. Frömel, S. Leupold, U. Mosel, Phys. Rev. C **67**, 015206 (2003), nucl-th/0111004.
3. S.P. Klevansky, Rev. Mod. Phys. **64**, 649 (1992).
4. L.P. Kadanoff, G. Baym, *Quantum Statistical Mechanics* (Benjamin, New York, 1962).
5. P. Danielewicz, Ann. Phys. (N.Y.) **152**, 305 (1984).
6. J.D. Bjorken, S.D. Drell, *Relativistic Quantum Fields* (McGraw-Hill, New York, 1965).
7. P. Rehberg, Phys. Rev. C **57**, 3299 (1998).

Eur. Phys. J. A **18**, 269–272 (2003)
DOI 10.1140/epja/i2002-10214-6

THE EUROPEAN PHYSICAL JOURNAL A

Moments of isovector quark distributions in lattice QCD

W. Detmold[1,2,a], W. Melnitchouk[3], and A.W. Thomas[2]

[1] Department of Physics, University of Washington, Box 351560, Seattle, WA 98195, USA
[2] Special Research Centre for the Subatomic Structure of Matter, University of Adelaide, Adelaide, SA 5005, Australia
[3] Jefferson Lab, 12000 Jefferson Avenue, Newport News, VA 23606, USA

Received: 30 September 2002 /
Published online: 22 October 2003 – © Società Italiana di Fisica / Springer-Verlag 2003

Abstract. We investigate the connection of lattice calculations of moments of isovector parton distributions to the physical regime through extrapolations in the quark mass. We consider the one-pion loop renormalisation of the nucleon matrix elements of the corresponding operators and thereby develop formulae with which to extrapolate the moments of the unpolarised, helicity and transversity distributions. These formulae are consistent with chiral perturbation theory in chiral limit and incorporate the correct heavy-quark limits. In the polarised cases, the inclusion of intermediate states involving the Δ-isobar is found to be very important. The results of our extrapolations are in general agreement with the phenomenological values of these moments where they are known, and for the first time we make reliable predictions for the low moments of the isovector transversity distribution.

PACS. 12.38.Gc Lattice QCD calculations – 11.30.Rd Chiral symmetries

1 Introduction

Until recently, state of the art studies [1] of the moments of parton distributions within lattice QCD have led to large discrepancies with experimental data [2]. Lattice calculations are performed at quark masses much greater than those of the physical light quarks. Consequently, an extrapolation to the physical mass regime must be made in order to compare with experiment. A naive linear extrapolation results in values for the first three non-trivial moments of the unpolarised $u-d$ distribution that are 50% above the phenomenological values [2]. For the polarised distributions the results are no better; g_A (the 0th moment of $\Delta u - \Delta d$) is significantly underestimated by a linear extrapolation, while the lack of accuracy in the data (both experimental and lattice) on higher moments precludes definitive statements. Such a large disagreement in such basic hadronic observables casts doubt on the current reliability of the lattice approach to hadronic physics.

We present an improved extrapolation scheme [3–6] that for the first time resolves much of this discrepancy. Using constraints from chiral symmetry and the heavy-quark limit, we develop a formalism for the extrapolation of the moments of the isovector, unpolarised, helicity and transveristy distributions. These are related to the forward nucleon matrix elements of various twist-2 operators which are calculated on the lattice through the operator product expansion. In particular, we find that contributions from intermediate states involving the Δ-isobar are large, and their effects cannot be ignored in any quantitative analysis. With their inclusion, we are able to make reliable, almost model-independent[1] extrapolations of the moments of parton distributions and make predictions for the low-spin transversity moments which can be tested by future measurements.

2 Pion-loop renormalisation of moments of parton distribution functions

General constraints from the approximate chiral symmetry of QCD lead to the appearance of non-analytic terms in the quark mass expansion of many hadronic quantities. In particular, the moments of quark distributions behave as [8,9]

$$\langle x^n \rangle_{q,\Delta q,\delta q} \sim m_\pi^2 \log m_\pi^2, \tag{1}$$

where the Gell-Mann–Oakes–Renner relation, $m_q \sim m_\pi^2$, has been used to express the quark mass in terms of the pion mass. This behaviour arises from the infrared properties of the one-pion loop renormalisation of the matrix elements of the corresponding twist-2 operators $\mathcal{O}_{q,\Delta q,\delta q}$ (see

[a] e-mail: wdetmold@physics.adelaide.edu.au

[1] Results are independent of the shape of the pion-nucleon form factor to 1-2% [7].

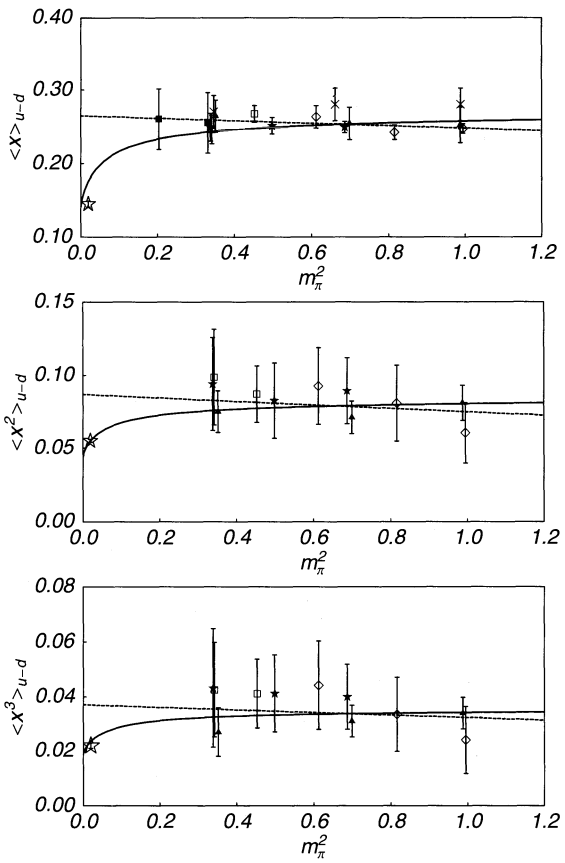

Fig. 1. Lowest three non-trivial moments of the unpolarised isovector parton distribution. Data are taken from various lattice simulations (see ref. [5] for details). The linear extrapolation (dashed-line) significantly overestimates the experimental results (stars), whilst the extrapolation using eq. (3) is in reasonable agreement.

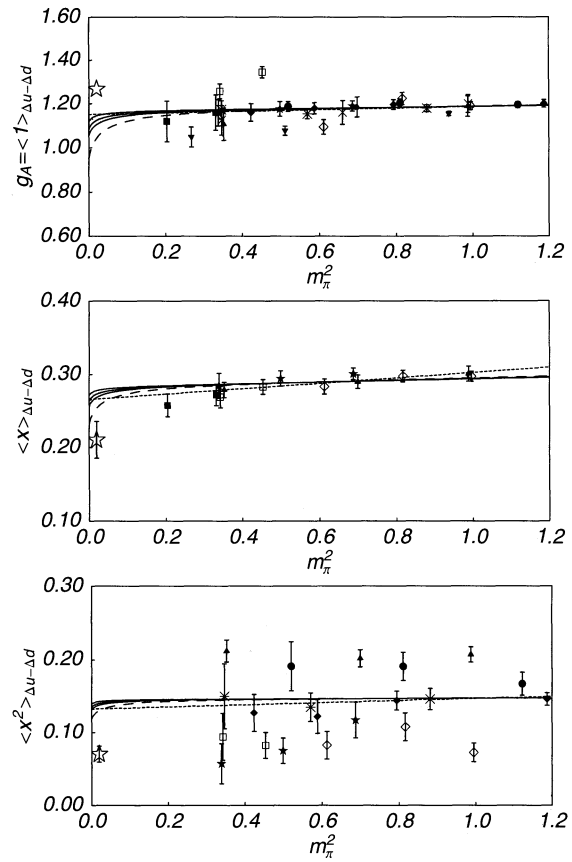

Fig. 2. Lowest three non-trivial moments of the helicity isovector parton distribution. Curves shown are (dotted line) linear extrapolation, (dashed-line) extrapolation using the polarised analog of eq. (3) but ignoring Δ contributions, and (solid lines) extrapolations for varying values of the $\pi N\Delta$ coupling. (Data as for fig. 1.)

ref. [5] for their definitions and further details). That is,

$$\langle N|\mathcal{O}_i^{\mu_1\cdots\mu_n}|N\rangle_{\text{dressed}} = \frac{Z_2}{Z_i}\langle N|\mathcal{O}_i^{\mu_1\cdots\mu_n}|N\rangle_{\text{bare}}\,, \qquad (2)$$

where Z_2 is the nucleon wave function renormalisation and Z_i, $i = q, \Delta q, \delta q$, are the operator renormalisations arising from πN, $\pi\Delta$, and $\pi(N\Delta$ transition) intermediate states.

In the case of the unpolarised moments, simple one-loop calculations of the renormalisation using a variety of form factors (cutoff, monopole, dipole) for the pion-nucleon coupling all lead to a simple extrapolation formula

$$\langle x^n\rangle_{u-d} = a_n\left(1 + c_{\text{LNA}} m_\pi^2 \log\frac{m_\pi^2}{m_\pi^2+\mu^2}\right) + b_n m_\pi^2\,, \qquad (3)$$

with three free parameters, a_n, b_n, μ (c_{LNA} is fixed by chiral perturbation theory). Similar expressions are found for the helicity and transversity moments in ref. [5]. The parameter μ describes the physical scale of the pion source [10] and ideally would be constrained by lattice data. However, until sufficiently accurate lattice data at low quark masses are available, alternative methods (such as the one used here) must be used to fix μ.

As shown by the solid curves in fig. 1 this formula provides an excellent description of the lattice data, the experimental values of the moments and (with suitable modification —see ref. [4]) the values known in the heavy-quark limit. However, when a similar formula is applied to the moments of the helicity distributions, the extrapolation is considerably worse than a naive linear extrapolation, as shown by the dashed lines in fig. 2.

When we turn to the moments of polarised parton distributions, there is considerable evidence from phenomenological models that suggests the Δ-resonance will play an important role. Although the Δ contributions formally enter at higher order in m_π, the coefficients of these next-to-leading non-analytic terms are large, and they cannot be ignored in any quantitative analysis. This is clearly demonstrated by fig. 3 where the pion mass dependence of the one-loop renormalisation of helicity matrix elements is shown calculated with a dipole form factor with varying values of the $\pi N\Delta$ coupling, $g_{\pi N\Delta}$. Full details are given in ref. [5]. For these helicity (and transversity) operator matrix elements the difference between $g_{\pi N\Delta}/g_{\pi NN} = 0$ (no Δ) and $g_{\pi N\Delta}/g_{\pi NN} = 2$

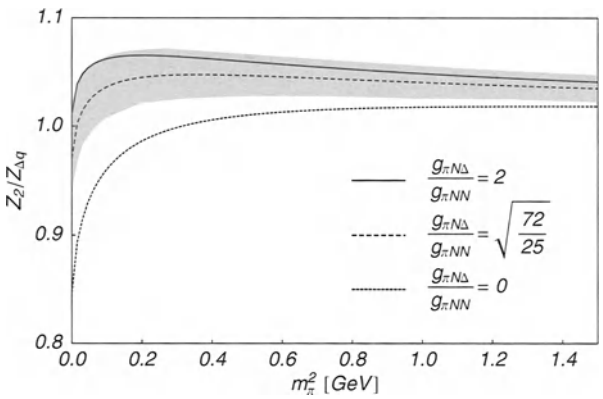

Fig. 3. One-loop renormalisation of the nucleon matrix elements of the polarised, isovector, twist-2 operators using a dipole form factor ($\Lambda = 0.8$ GeV) and varying values of the coupling ratio $g_{\pi N\Delta}/g_{\pi NN}$. The shaded region corresponds to variation of the Weinberg-Tomozawa coupling —see ref. [5].

Table 1. Values of the unpolarized, helicity and transversity moments, extrapolated to the physical pion mass using eq. (3). For comparison, experimental values of the moments, where known [2], are also listed.

Moment	Experimental	Extrapolated
$\langle x\rangle_{u-d}$	0.145(4)	0.17(3)
$\langle x^2\rangle_{u-d}$	0.054(1)	0.05(2)
$\langle x^3\rangle_{u-d}$	0.022(1)	0.02(1)
$\langle 1\rangle_{\Delta u-\Delta d}$	1.267(4)	1.12(8)
$\langle x\rangle_{\Delta u-\Delta d}$	0.210(25)	0.27(3)
$\langle x^2\rangle_{\Delta u-\Delta d}$	0.070(11)	0.14(4)
$\langle 1\rangle_{\delta u-\delta d}$	?	1.22(8)
$\langle x\rangle_{\delta u-\delta d}$	?	0.5(1)

(phenomenological value) is up to 15% —much greater than in the unpolarised case where the overall effect is less than 2% over the entire mass range studied here.

In order to incorporate these effects into the extrapolations of lattice data, we calculate the required renormalisations for the phenomenologically preferred dipole parameter, $\Lambda = 0.8$ GeV, and for varying values of the coupling ratio $g_{\pi N\Delta}/g_{\pi NN}$. We then determine μ by fitting to the calculated renormalisations using eq. (3) (with $c_{\rm LNA}$ calculated in the $\Delta M = M_\Delta - M_N \to 0$ limit). With μ thus fixed, we then use the lattice data to determine the fit parameters a_n and b_n. The resulting curves are then shown in each panel of fig. 2 for $g_{\pi N\Delta}/g_{\pi NN} = 0$ (no Δ), $\sqrt{72/25}$, 1.85 and 2 [2].

Table 1 shows the resulting extrapolated values along with uncertainties resulting from the $\pi N\Delta$ and Weinberg-Tomozawa couplings, statistical and (estimated) systematic errors. Also listed are the experimental moments where known [2]. It is evident that the agreement between the experimental and extrapolated results is very good for the unpolarised moments, but significantly worse in the helicity sector. The extrapolated value of g_A is 10% below its experimental value, with 8% errors. However, there is some evidence that lattice simulations of this quantity are particularly susceptible to finite-volume effects [11]. For the higher helicity moments, statistical errors on the lattice data are not yet sufficiently small to make definitive statements. Since the renormalisation of the transversity matrix elements is almost identical to that of the helicity matrix elements, we are also able to make an estimate of the values of these moments which can be compared with future experimental determinations.

[2] Reasonable variation of the strength of the Weinberg-Tomozawa contact term is also included —see ref. [5] for details.

3 Conclusion

We have investigated the extrapolation of lattice data on the low moments of the isovector, unpolarised, helicity and transversity parton distribution functions. In the case of the polarised moments, the Δ-isobar, even though not leading non-analytic, was found to play a significant role and its inclusion in the operator renormalisation and extrapolation procedure is vital. With this accounted for, we have the surprising result that the effect of the non-analytic behaviour is strongly suppressed for the polarised moments, and a naive linear extrapolation of the moments provides quite a good approximation to the more accurate form.

Talk given by W.D. who is grateful to R. Alkofer and the Institut für Theoretische Physik, Universität Tübingen for their hospitality and to DFG grant Al279/3-3 for support. W.M. is supported by the U.S. Department of Energy contract DE-AC05-84ER40150, under which the South-eastern Universities Research Association (SURA) operates the Thomas Jefferson National Accelerator Facility (Jefferson Lab).

References

1. M. Fukugita *et al.*, Phys. Rev. Lett. **75**, 2092 (1995); S. Aoki *et al.*, Phys. Rev. D **56**, 433 (1997); S. Güsken *et al.*, Phys. Rev. D **59**, 114502 (1999); M. Göckeler *et al.*, Phys. Rev. D **53**, 2317 (1996); M. Göckeler *et al.*, Nucl. Phys. Proc. Suppl. **53**, 81 (1997); C. Best *et al.*, arXiv:hep-ph/9706502; M. Gockeler *et al.*, arXiv:hep-ph/9909253; D. Dolgov *et al.*, Nucl. Phys. Proc. Suppl. **94**, 303 (2001); LHPC Collaboration (D. Dolgov *et al.*), Phys. Rev. D **66**, 034506 (2002).
2. H.L. Lai *et al.*, Eur. Phys. J. C **12**, 375 (2000); A.D. Martin, R.G. Roberts, W.J. Stirling, R.S. Thorne, Eur. Phys. J. C **14**, 133 (2000); M. Glück, E. Reya, A. Vogt, Eur. Phys. J. C **5**, 461 (1998); J. Blümlein, H. Böttcher, Nucl. Phys. B **636**, 225 (2002), arXiv:hep-ph/0203155.
3. W. Detmold, W. Melnitchouk, J.W. Negele, D.B. Renner, A.W. Thomas, Phys. Rev. Lett. **87**, 172001 (2001).
4. W. Detmold, W. Melnitchouk, A.W. Thomas, Eur. Phys. J. direct C **13**, 1 (2001).
5. W. Detmold, W. Melnitchouk, A.W. Thomas, Phys. Rev. D **66**, 054501 (2002).

6. W. Detmold, *Nonperturbative approaches to Quantum Chromodynamics*, PhD Thesis, University of Adelaide, 2002.
7. R.D. Young, A.W. Thomas, D. Leinweber, in preparation.
8. A.W. Thomas, W. Melnitchouk, F.M. Steffens, Phys. Rev. Lett. **85**, 2892 (2000).
9. D. Arndt, M.J. Savage, Nucl. Phys. A **697**, 429 (2002); J.W. Chen, X. Ji, Phys. Lett. B **523**, 107 (2001).
10. W. Detmold, D.B. Leinweber, W. Melnitchouk, A.W. Thomas, S.V. Wright, Pramana **57**, 251 (2001).
11. S. Sasaki, T. Blum, S. Ohta, K. Orginos, Nucl. Phys. Proc. Suppl. **106**, 302 (2002), arXiv:hep-lat/0110053.

Eur. Phys. J. A **18**, 273–276 (2003)
DOI 10.1140/epja/i2002-10215-5

THE EUROPEAN PHYSICAL JOURNAL A

Mapping gluonic excitations and confinement

The GlueX/Hall D project at Jefferson Lab

A.R. Dzierba[a]

Department of Physics, Indiana University, Bloomington, IN 47405, USA

Received: 30 September 2002 /
Published online: 22 October 2003 – © Società Italiana di Fisica / Springer-Verlag 2003

Abstract. One of the outstanding and fundamental questions in physics is the quantitative understanding of the confinement of quarks and gluons in quantum chromodynamics (QCD). Confinement is a unique feature of QCD. Exotic hybrid mesons manifest gluonic degrees of freedom and their spectroscopy will provide the crucial data needed to test assumptions in lattice QCD and phenomenology leading to confinement. Photoproduction is expected to be particularly effective in producing exotic hybrids but data using photon probes are sparse. At Jefferson Lab, plans are underway to use the coherent bremsstrahlung technique to produce a linearly polarized photon beam. A solenoid-based hermetic detector will be used to collect data on meson production and decays with statistics that will exceed the current photoproduction data in hand by several orders of magnitude after the first year of running. In order to reach the ideal photon energy of 9 GeV/c for this mapping of the exotic spectra, the energy of the Jefferson Lab electron accelerator, CEBAF, will be doubled from its current maximum of 6 GeV to 12 GeV. The physics and project are described.

PACS. 12.39.Mk Glueball and nonstandard multi-quark/gluon states – 13.60.Le Meson production

1 Science of confinement

The observation nearly four decades ago that mesons are grouped in nonets, each characterized by unique values of J^{PC} —spin (J), parity (P) and charge conjugation (C) quantum numbers— led to the development of the quark model. Within this picture, mesons are bound states of a quark (q) and antiquark ($\bar{q}$). The three light-quark flavors (*up*, *down* and *strange*) suffice to explain the spectroscopy of most —but not all— of the lighter-mass mesons (*i.e.* below 3 GeV/c^2) that do not explicitly carry heavy flavors (charm or beauty). Early observations yielded only those J^{PC} quantum numbers consistent with a fermion-antifermion bound state. The J^{PC} quantum numbers of a $q\bar{q}$ system with total quark spin, $\boldsymbol{S}$, and relative angular momentum , $\boldsymbol{L}$, are determined as follows: $\boldsymbol{J} = \boldsymbol{L} + \boldsymbol{S}$, $P = (-1)^{L+1}$ and $C = (-1)^{L+S}$. Thus, J^{PC} quantum numbers such as 0^{--}, 0^{+-}, 1^{-+} and 2^{+-} are not allowed and are called *exotic* in this context.

Our understanding of how quarks form mesons has evolved within quantum chromodynamics (QCD) and we now expect a richer spectrum of mesons that takes into account not only the quark degrees of freedom but also the gluonic degrees of freedom. Gluonic mesons with no quarks (*glueballs*) are expected. These are bound states of gluons and since the quantum numbers of low-lying glueballs are not necessarily exotic, they should manifest themselves as extraneous states that cannot be accommodated within $\bar{q}q$ nonets. But their identification is complicated since they do mix with $\bar{q}q$. Excitations of the gluonic field binding the quarks can also give rise to so-called *hybrid* mesons that can be viewed as bound states of a quark, antiquark and valence gluon ($q\bar{q}g$). An alternative picture of hybrid mesons, one supported by lattice QCD [1], is one in which a gluonic flux tube forms between the quark and antiquark and the excitations of this flux tube lead to so-called *hybrid* mesons. Actually the idea of flux tubes, or strings connecting the quarks, originated in the early 1970s [2] to explain the observed linear dependence of the mass-squared of hadrons on spin (Regge trajectories). Conventional $\bar{q}q$-mesons arise when the flux tube is in its ground state. Hybrid mesons arise when the flux tube is excited and some hybrid mesons can have a unique signature, exotic J^{PC}, and therefore the spectroscopy of exotic hybrid mesons is not complicated by possible mixing with conventional $\bar{q}q$ states.

The level splitting between the ground-state flux tube and the first-excited transverse modes is π/r, where r is the separation between the quarks, so the hybrid spectrum should lie about 1 GeV/c^2 above the ground-state spectrum. According to the flux tube model [3] and lattice

[a] *Present address*: Department of Physics, Indiana University, Bloomington, IN 47405 USA; e-mail: `dzierba@indiana.edu`

gauge calculations [4], one expects the lightest $J^{PC} = 1^{-+}$ exotic hybrid to have a mass of about 1.9 GeV/c^2.

In this discussion the motion of the quarks was ignored, but we know from general principles [3] that the an approximation that ignores the impact of the flux tube excitation and quark motion on each other seems to work quite well.

In the coming years there will be significant computational resources [5], using lattice techniques, dedicated to understanding non-perturbative QCD including confinement. The prediction of the hybrid spectrum, including decays, will be part of this program but experimental data will be needed to validate assumptions. The spectroscopy of exotic mesons provides a clean and attractive starting point for the study of gluonic excitations.

2 Experimental situation

After about two decades of experimental searches there have been reports of observations of states with $J^{PC} = 1^{-+}$ by the Brookhaven E852 Collaboration. One of these was reported in the reaction $\pi^- p \to \pi^+\pi^-\pi^- p$ using an 18 GeV/c π^- beam. The state has a mass of (1593 ± 8) MeV/c^2 and width of (168 ± 20) MeV/c^2 and decays into $\rho^0\pi^-$ [6]. A partial-wave analysis (PWA) of the 3π system uncovered the exotic signal as a P-wave between the ρ^0 and π^- with a line shape in the P-wave amplitude and interference with the nearby $\pi_2(1670)$ ($J^{PC} = 2^{-+}$) characteristic of a Breit-Wigner resonance. The exotic state's contribution to the 3π spectrum is much smaller than the dominant $a_1(1260)$, $a_2(1320)$ and $\pi_2(1670)$ so uncovering the signal is a challenge.

The E852 Collaboration also reported observation of another $J^{PC} = 1^{-+}$ state with mass (1370 ± 16) MeV/c^2 and a width of (385 ± 40) MeV/c^2 decaying into $\eta\pi^-$ [7] and soon after confirmed by the Crystal Barrel group [8] but this result is not without controversy. If an $\eta\pi$ system exists in a P-wave it has exotic J^{PC} but the identification of a Breit-Wigner resonance is particularly challenging since the $a_2(1320)$ dominates the $\eta\pi$ spectrum. Critical to the identification of an exotic state is not only showing the presence of a P-wave, but also that the resulting line shape is consistent with a Breit-Wigner and that the phase motion of the P-wave, as determined by its interference with the dominant D-wave, cannot be due solely to the $a_2(1320)$-resonance. A recent analysis of E852 data from the reaction $\pi^- p \to \eta\pi^0 n$ indicates that a P-wave is present but is not consistent with a Breit-Wigner resonance [9] and is likely due to final-state re-scattering. This reaction has some advantages. Both the $a_0(980)$ and $a_2(1320)$ are produced and this aids in the PWA and for $\eta\pi^0$ —in contrast to $\eta\pi^-$— C, charge conjugation, is well defined.

3 Using photons as probes

The data to date are tantalizing and suggest that exotic hybrid mesons may exist but the extensive data collected to date with π probes have not uncovered the hybrid meson spectrum. Lattice QCD and phenomenology, however, indicate the photon is a probe that should be particularly effective in producing exotic hybrids but data on photoproduction of light mesons are sparse indeed.

The first-excited transverse modes of the flux tube are degenerate and correspond to clockwise or counterclockwise rotations of the flux tube about the axis joining the quark and antiquark fixed in space with $J = 1$ [3]. Linear combinations of these two modes are eigenstates of parity and lead to $J^{PC} = 1^{+-}$ and $J^{PC} = 1^{-+}$ for the excited flux tube. When these quantum numbers are combined with those of the $q\bar{q}$ with $\boldsymbol{L} = 0$ and $\boldsymbol{S} = 1$ (quark spins aligned), three of the six possible J^{PC} have exotic combinations: 0^{+-}, 1^{-+} and 2^{+-}. A photon probe is a virtual $q\bar{q}$ with quark spins aligned. In contrast, when the $q\bar{q}$ have $\boldsymbol{L} = 0$ and $\boldsymbol{S} = 0$ (spins antialigned), the resulting quantum numbers of the hybrid meson are not exotic. Pion probes are $q\bar{q}$ with quark spins antialigned. If we view one outcome of the scattering process as exciting the flux tube binding the quarks in the probe, the suppression of exotic hybrids in π-induced reactions is not surprising —a spin-flip of one of the quarks is required followed by the excitation of the flux tube. In contrast, the spins of the virtual quarks in the photon probe are properly aligned to lead to exotic hybrids. Phenomenological studies quantitatively support this picture predicting that the photoproduction cross-sections for exotic mesons are comparable to those for copiously produced mesons such the $a_2(1320)$ [10,11].

4 The GlueX/Hall D project

Based on this guidance from theory and experiment, the GlueX/Hall D Collaboration was formed to design a photon beam and detector to map the exotic hybrid spectrum [12,13]. The goal of the experiment is to reach meson masses up to about 3 GeV/c^2 and collect sufficient statistics on the production of mesons with a sensitivity to a wide variety of decay modes. In order to identify the quantum numbers, the PWA technique will be used. This requires a detector that has excellent resolution, is hermetic and has good rate capability. It is essential to kinematically identical exclusive reactions in order to apply PWA.

4.1 Photon beam

The optimal photon energy for this study is around 9 GeV. The photon energy must be large enough to produce the higher mass states with sufficient boost in the laboratory so that their decay products will be detected and measured with sufficient resolution. It is also important that the energy be high enough to avoid line shape distortions that arise due to relatively large values of $|t_{\min}|$ occurring near threshold —$|t_{\min}|$ is the minimum momentum transfer squared from the incident photon beam to the produced meson.

As will be described below, a solenoid-based detector design will be used. This represents the optimal design

for fixed-target photoproduction experiment as the intense photon beam produces large electromagnetic backgrounds (e^+e^- pairs) that can be trapped within a tight region along the beam by the axial field of the solenoid. However, with this geometry, the momentum resolution of two-body decays of lighter mesons degrades if the photon beam energy exceeds 9 GeV/c^2.

The photon beam must also be linearly polarized due to the PWA requirements. This is related to the fact that states of linear polarization, in contrast to states of circular polarization, are eigenstates of parity. The linear polarization of the photon beam will also be used as an exotics filter [14].

Coherent bremsstrahlung will be used to produce linearly polarized photons. Instead of using an amorphous radiator, a diamond crystal is used. At special settings for the orientation of the crystal with respect to the electron beam, the atoms of the crystal can be made to recoil together from the radiating electron leading to an enhanced emission at particular photon energies and yielding linearly polarized photons. The resulting spectrum of photons is a sum of incoherent bremsstrahlung, whose spectrum falls like $1/E_\gamma$, and the coherent spectrum. The correlation of emitted photon energy and angle also allows one to substantially collimate out the incoherent portion of the photon spectrum before the photons reach the detector. A collimator with a 3.4 mm diameter hole placed 80 m from the radiator will be used to greatly reduce the backgrounds from unwanted lower-energy photons in the detector target. The collimation is also needed to increase the degree of linear polarization to 40% in the current design. The employment of coherent bremsstrahlung and collimation is made possible by the superb characteristics of the electron beam at Jefferson Lab including the continuous wave feature leading to a duty factor close to unity, the small spot size and the emittance characteristics. In addition, recent advances in growing and thinning diamond wafers down to 20 μm result in negligible multiple scattering allowing collimation to be effective.

The diamond crystal in the electron beam will be immediately followed by a focal-plane spectrometer (photon tagger) that will be used to measure the electron energy after the radiator thus allowing an energy determination of each photon into the detector with a resolution of 0.1%.

4.2 Accelerator upgrade

In order to produce 9 GeV photons with sufficient degree of linear polarization an electron energy of 12 GeV will suffice. For example, increasing the electron energy to 20 GeV will only double the degree of polarization of 9 GeV photons from 40% to 80% while requiring a major modification of the accelerating section and arcs. However, dropping from 12 GeV to 10 GeV electrons would reduce the degree of linear polarization of 9 GeV photons by nearly an order of magnitude.

Figure 1 shows the configuration of the proposed 12 GeV CEBAF upgrade at Jefferson Lab. The present

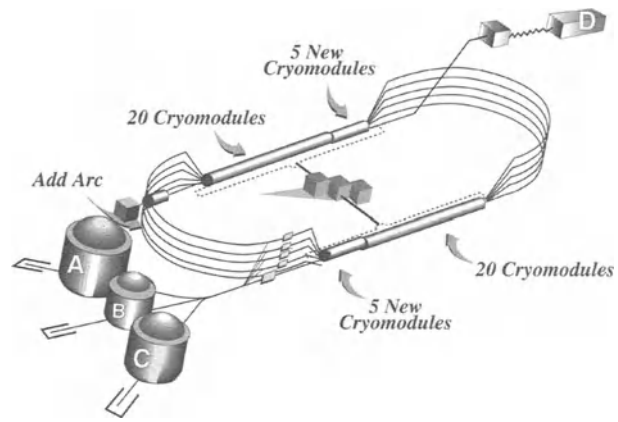

Fig. 1. The proposed configuration for the 12 GeV upgrade of CEBAF at Jefferson Lab showing the additional new Hall D for the GlueX experiment. Details are given in the text.

CEBAF accelerator consists of two linear accelerating sections, each about 250 m long. Re-circulating arcs of magnets allow multiple-passes of the electrons through the accelerating regions. Currently, beam is delivered to three existing experimental halls labelled A, B and C. The proposal calls for the construction of a fourth hall (D) preceded by the photon tagger to which 12 GeV electrons will be delivered. To accomplish the energy upgrade 5 new accelerating superconducting cryomodules will be added to the 20 existing cryomodules in each of the two accelerating sections. The space for the additional modules already is available. In addition, 3 of the existing 20 cryomodules in each of the two straight sections will be replaced. A tenth added arc will allow for 11 full passes of the electrons before delivery to Hall D. More details of the accelerator upgrades along with the proposed GlueX/Hall D project and the planned upgrades for the existing halls for the upgrade project are described in ref. [15].

4.3 Detector

Figure 2 shows a schematic of the proposed detector for Hall D. Central to the detector is a superconducting solenoid with a clear bore diameter of 73 in and a length of 183 in. The central field is 2.5 T. The magnet was originally constructed for the LASS experiment at SLAC and then moved to LANL where it was used for the MEGA experiment. It will be moved, refurbished and shipped to Jefferson Lab for use in the GlueX/Hall D experiment. The inside bore of the solenoid will be lined with an electromagnetic calorimeter surrounding the target and the central and forward particle tracker. That will be followed by an atmospheric Čerenkov counter, a time-of-flight wall and then a 2500-element lead glass calorimeter. The latter was originally built and used in the E852 experiment and has since been moved to Jefferson Lab for the GlueX/Hall D experiment.

Initially the detector will run with an incident photon flux of 10^7 photons per second. With this flux and after the first year of data-taking, the collected sample will

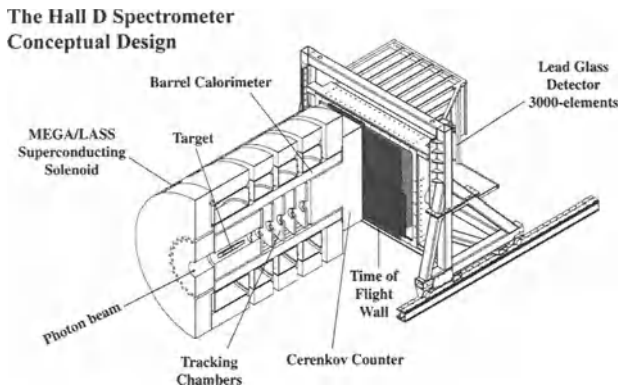

Fig. 2. The conceptual design for the proposed GlueX/Hall D project. Details are given in the text.

exceed current photoproduction data by several orders of magnitude and current π-induced data by an order of magnitude. Later the beam flux will be increased by a factor of 10. Data will be recorded at the rate of 100 MB/s leading to roughly 1 PetaByte of stored data per year. This is comparable to the size of the data sets planned for the LHC experiments.

4.4 Plan for analysis

Extensive Monte Carlo studies have been carried out to evaluate the proposed detector design. The acceptance of the proposed detector over relevant kinematic variables including decay angles is high and uniform. Double-blind Monte Carlo studies have included exotic signals at low levels mixed with conventional mesons. Generated events have been smeared according to the expected resolution and passed through acceptance simulations. The surviving sample has then been acceptance corrected, reconstructed and passed through PWA-fitting programs. Signals at the few percent level have been successfully recovered.

In addition to Monte Carlo studies, the fundamental assumptions behind the PWA are also under study including any model assumptions (*e.g.*, the *isobar* assumption), mathematical ambiguities, and issues of analyticity. It is essential to minimize possible biases and uncertainties from the dynamical unknowns.

5 Conclusions

The question of the quantitative understanding of the confinement mechanism in QCD is still an open, important and fundamental issue in physics. There has been recent impressive theoretical progress on this issue and ambitious plans are underway to significantly increase the computational resources for lattice QCD leading to further progress. Data on the spectrum of gluonic excitations is essential in this effort —experiment is the ultimate arbiter. Although some tantalizing data suggest that gluonic excitations have been uncovered, their detailed mapping awaits new data from photoproduction which is expected to be a rich source. The energy upgraded CEBAF at Jefferson Lab, along with the construction of a new photon beam and detector dedicated to spectroscopy will provide the unique opportunity to carry out the definitive experiment. This has been recognized in the recent long-range plan for nuclear science in the next decade in the US [16].

The author expresses his gratitude to the late Nathan Isgur for his deep insights and guidance. He also benefitted from discussions with Geoffrey Fox, George Lolos, Curtis Meyer, Elton Smith, Adam Szczepaniak and Scott Teige and other members of the GlueX/Hall D Collaboration. The author also thanks Lawrence Cardman for his valuable input. This work was supported by a grant from the US Department of Energy.

References

1. SESAM/TCL Collaboration (G.S. Bali *et al.*), Phys. Rev. D **62**, 054503 (2000).
2. Y. Nambu, University of Chicago report No. 70-70 (1970), unpublished.
3. N. Isgur, J. Paton, Phys. Rev. D **31**, 2910 (1985).
4. MILC Collaboration (C. Bernard *et al.*), Phys. Rev. D **56**, 7039 (1997).
5. `http://www.lqcd.org/`, National Computational Infrastructure for Lattice Gauge Theory.
6. G.S. Adams *et al.*, Phys. Rev. Lett. **81**, 5760 (1998).
7. D.R. Thompson *et al.*, Phys. Rev. Lett. **79**, 175 (1997).
8. A. Abele *et al.*, Phys. Lett. B **423**, 175 (1998); A. Abele *et al.*, Phys. Lett. B **446**, 349 (1999).
9. See A.P. Szczepaniak, this issue, p. 167.
10. A. Afanasev, P.R. Page, Phys. Rev. D **57**, 6771 (1998).
11. A.P. Szczepaniak, M. Swat, Phys. Lett. B **516**, 72 (2001).
12. The Hall D Project Design Report (2000); `http://www.gluex.org`.
13. A.R. Dzierba, N. Isgur, CERN Courier, **40**, No. 7, 23 (2000).
14. A.P. Szczepaniak, A.V. Afanasev, Phys. Rev. D **61**, 114008 (2002), hep-ph/9910268 (1999).
15. *The Science Driving the 12 GeV Upgrade of CEBAF*, Jefferson Lab (2001).
16. *Opportunities in Nuclear Science - A Long Range Plan for the Next Decade*, DOE/NSF Nuclear Science Advisory Committee (2002).

Eur. Phys. J. A **18**, 277–281 (2003)
DOI 10.1140/epja/i2002-10216-4

THE EUROPEAN PHYSICAL JOURNAL A

Meson production at CELSIUS

T. Johansson[a]

Representing the CELSIUS/WASA Collaboration[b]
Department of Radiation Sciences, Uppsala University, Uppsala, Sweden

Received: 30 September 2002 /
Published online: 22 October 2003 – © Società Italiana di Fisica / Springer-Verlag 2003

Abstract. The experimental programme of the CELSIUS/WASA Collaboration at the CELSIUS cooler/storage ring of the The Svedberg Laboratory, Uppsala, focuses on meson production and decay studies using light-ion collisions near threshold. The production of η-mesons has been studied in pp and pd collisions and 2π reactions have been studied in pp collisions, using the PROMICE/WASA detector. Both total and differential cross-sections have been investigated and some of the reaction channels have been measured for the first time in any detail. The data on η production reveal effects which can be attributed to a strong and attractive η-N interaction. Both the η and two-pion production data contain new information on the importance of different nucleon resonances in these reactions. The PROMICE/WASA detector is now an integrated part of the recently commissioned WASA detector at CELSIUS, which has a nearly 4π acceptance for both charged particles and photons. This will provide significantly improved conditions for a new generation of experiments on meson production and decays.

PACS. 13.75.-n Hadron-induced low- and intermediate-energy reactions and scattering (energy $\leq$ 10 GeV) – 14.20.Gk Baryon resonances with $S = 0$ – 25.40.Ve Other reactions above meson production thresholds (energies > 400 MeV)

1 Introduction

Cooler/storage rings, with their high-quality beams and thin windowless internal targets, offer an ideal environment for measurements of meson production in the threshold region. Such studies have therefore been a major topic of research at the CELSIUS, COSY and IUCF machines.

This paper reviews results from CELSIUS taken by the CELSIUS/WASA Collaboration on η-meson production in proton-proton and proton-deuteron collisions and 2π production in proton-proton collisions. The motivation for the study is twofold; to learn about a) the reaction mechanism, and b) the interaction between the final-state particles. The fact that only a few partial waves are important near threshold will facilitate any interpretation of the data. Furthermore, the relatively high and well-defined momentum transfers involved makes these processes good candidates to probe short-range physics. Kinematical considerations ensure that, close to threshold, the final-state particles are all emitted with low relative velocities, allowing the possibility of studying interactions between these particles.

The CELSIUS ring at the The Svedberg Laboratory, Uppsala, currently provides protons up to a maximum kinetic energy of 1.35 GeV. This makes η-mesons energetically accessible for experimental studies in free proton-proton collisions up to a centre-of-mass (CM) excess energy, $Q_{\rm cm}$ ($= \sqrt{s} - \sum m_{\rm final}$), of 37 MeV above the reaction threshold. This limitation has been circumvented by taking advantage of the Fermi motion of the struck nucleon in quasi-free reactions using deuterium as a target. A $Q_{\rm cm}$ of more than 100 MeV can be reached through this technique.

A complication when using internal targets at storage rings is that the beam pipe limits the access in the very forward direction. This drawback can be turned into an advantage by using a magnetic system that bends the produced charged particles out of the beam trajectory for subsequent detection. Alternatively, for short-lived mesons, one may detect the decay products. Both techniques have been employed at CELSIUS. The experiments with the PROMICE/WASA (PW) set-up used an internal cluster jet target, giving a typical target density of 10^{14} atoms/cm^2. With a circulating beam of a few times 10^{10} protons, this provides luminosities of the order of 5×10^{30} cm^2 s^{-1}. More details of the PW set-up can be found in ref. [1].

[a] e-mail: tord.johansson@tsl.uu.se
[b] www.tsl.uu.se/wasa

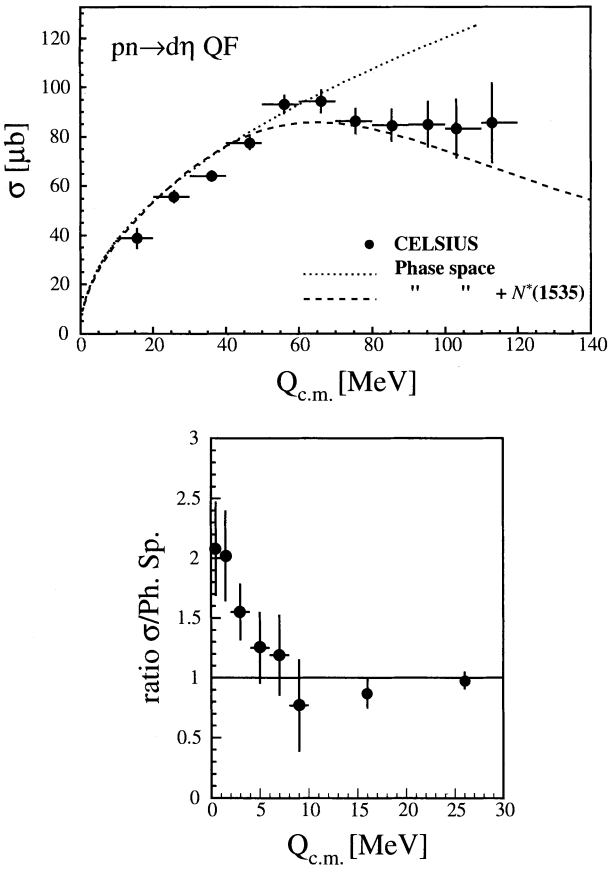

Fig. 1. Energy dependence for the quasifree $pn \to d\eta$ reaction. The upper figure shows data in the region $16 \leq Q_{\rm cm} \leq 113$ MeV [5]. Also shown is a two-body phase-space curve (dotted line) and a Breit-Wigner shape (dashed line) representing the $N^*(1535)$. The lower curve shows the ratio between the measured cross-section and the phase-space in the vicinity of the threshold [6].

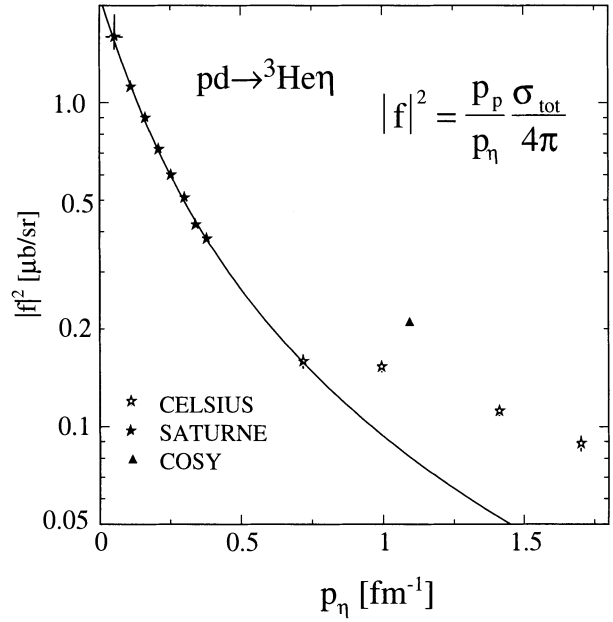

Fig. 2. Amplitude squared of the $pd \to {}^3\mathrm{He}\,\eta$ reaction, averaged over spin and angle, as a function of the CM η momentum. Full and empty stars represent the result from SACLAY [10] and CELSIUS [12], respectively. The COSY point is denoted by a closed triangle. The solid line represents an s-wave optical model fit to Saclay ${}^3\mathrm{He}\,\eta$ and ${}^4\mathrm{He}\,\eta$ data [10,11] data.

2 Meson production experiments

2.1 η production in pN collisions

Low-energy η production is believed to be dominated by an isospin-$\frac{1}{2}$ s-wave resonance, the $N^*(1535)S_{11}$. This resonance has a large decay branching ratio (30%–55%) into the $N\eta$ channel and its width of ≈ 150 MeV overlaps the $N\eta$ threshold. The presence of this resonance should influence the observables near threshold, where s-waves dominate, and also give rise to a strong and attractive $N\eta$ final-state interaction (FSI). It has even been suggested that this interaction might be strong enough for quasi-bound states to be formed already in the two-nucleon sector [2–4].

Effects relating to the $N^*(1535)$ have been observed in the $pn \to d\eta$ reaction. The two-body phase space gives a good description of the energy dependence of the cross-section up to a $Q_{\rm cm}$ of about 60 MeV, from where it starts to overpredict. This can be cured by including a Breit-Wigner function that describes the shape of the $N^*(1535)$-resonance [5], as shown in the upper part of fig. 1. This constitutes the first direct evidence for the importance of this resonance in nucleon-induced η production. A relative enhancement of the cross-section with respect to phase space is observed very close to threshold [6]. This is shown in the lower part of fig. 1 and is an effect that would follow from an attractive d-η FSI. Effects of a similar nature have also been observed for the $pp \to pp\eta$ reaction [7,8].

2.2 η production in pd collisions

The renewed interest in η production over the last 10 years started with measurements of the $pd \to {}^3\mathrm{He}\,\eta$ reaction at SATURNE [9,10]. These data are remarkable for both their magnitude and energy variation close to threshold. The amplitude squared falls over a factor of three in the first few MeV above threshold, as shown in fig. 2. This energy variation is certainly associated with an interaction between the η and the ^{3}He in the final state [11]. More recent data taken by the PW experiment at higher energies ($Q_{\rm cm} > 50$ MeV) [12] are also shown in fig. 2 together with a datum point from COSY [13].

The first CELSIUS point lies on a line which corresponds to an s-wave optical model fit of the earlier SATURNE data from ref. [10,11]. Data at higher energies lie above the curve. This is not surprising as higher partial waves become increasingly more important as the energy increases. This is also illustrated in fig. 3, which shows an increasing anisotropy of the angular distributions with energy.

The same data sample also contains information on the $pd \to pd\eta$ reaction. The first, very preliminary, results

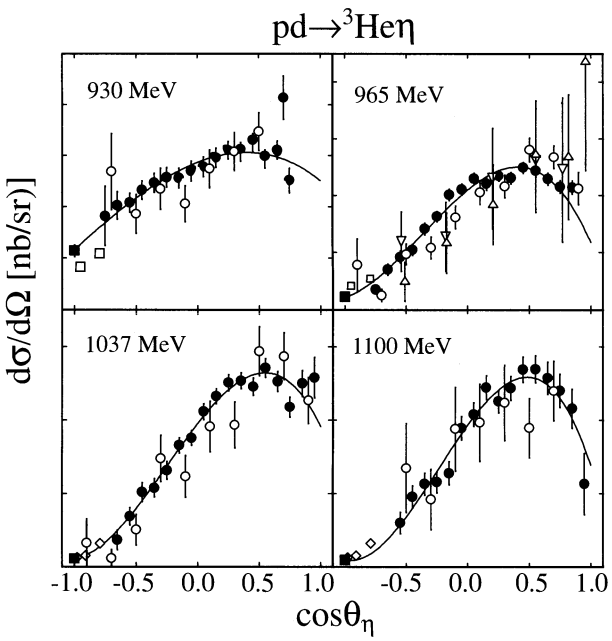

Fig. 3. Angular distributions for the $pd \rightarrow {}^3\mathrm{He}\,\eta$ reaction at four energies. The full and empty circles represent PW data [12] taken with only the ^{3}He detected and with the ^{3}He and two photons detected in coincidence, respectively. The full squares come from an interpolation in energy from SATURNE data [15]. The open squares and diamonds were taken from the same reference at 950 MeV and 1050 MeV, respectively. The triangles are COSY data [13] scaled by an empirical factor of 0.71 to agree with the trend of our data shown in fig. 2. The solid lines represent third-order polynomial fits to the data.

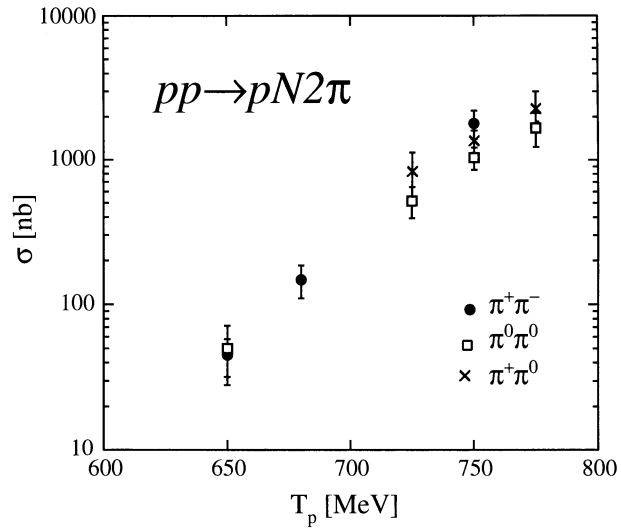

Fig. 4. Total cross-sections for the $pp \rightarrow pp\pi^+\pi^-$ (filled circles), $pp\pi^0\pi^0$ (open squares) and $pn\pi^0\pi^+$ (crosses) reactions between 650 and 775 MeV.

indicate much more isotropic angular distributions than for the $^3\mathrm{He}\,\eta$ final state [14]. The invariant mass spectra show a threshold $\eta\,d$ enhancement that is very similar to the one observed in the pN interactions discussed in the previous section.

2.3 2π production

Two-pion production in proton-proton collisions contains information about the nucleon-nucleon, pion-nucleon and pion-pion interactions. The production mechanism for these reactions is likely to be dominated by resonance production with the $N^*(1440)P_{11}$ and $\Delta(1232)P_{33}$ resonances being prime candidates. We have obtained data for the two-pion production from the $pp \rightarrow pp\pi^+\pi^-$, $pp\pi^0\pi^0$, $pn\pi^0\pi^+$ reactions at energies ranging from 650 to 775 MeV. This corresponds to excess energies from approximately 20 to 85 MeV, *i.e.* a region very close to threshold where no previous data are available. The PW results on the total cross-sections are shown in fig. 4.

We note that the magnitude for all three reactions is approximately the same. This information can be used within an isospin analysis to get a clue on the underlying reaction dynamics. The total $NN \rightarrow NN\pi\pi$ cross-section can be expressed in terms of isospin matrix elements $M_{T_\mathrm{i}T_{2\pi}T_\mathrm{f}}$, where T_i denotes the isospin of the initial nucleon pair, T_f is the isospin of the nucleons in the final state and $T_{2\pi}$ the isospin of the produced pion pair. Assuming that $\ell_{2\pi} = 0$, being close to threshold, it can be shown that the amplitude squared $|M_{121}|^2$ is about twice as large as $|M_{101}|^2$ [16]. Furthermore, the channel $N^*(1440) \rightarrow p + (2\pi)^{T=0}_{\ell=0}$ can only be involved in $|M_{101}|^2$, while $\Delta\Delta$ excitation is allowed in both $|M_{101}|^2$ and $|M_{121}|^2$. This could mean that the double-Δ excitation is the dominant reaction amplitude. However, the $N^*(1440)$ Roper resonance could still dominate the $pp \rightarrow pp\pi^+\pi^-$ cross-section due to the large isospin coupling factor for this matrix element [16]. The latter is confirmed from a study of the differential distributions from this reaction for the 750 MeV data [17]. Here it is shown that the differential distributions can be fully described by the $N^*(1440)$-resonance with decay branching ratios of $\approx 80\%$ for $N^* \rightarrow p + 2\pi$ decay and 20% for $N^* \rightarrow \Delta\pi$ decay. The contribution from the $\Delta\Delta$ channel turns out to be negligible at this energy. This is in agreement with the findings of Alvarez-Ruso *et al.* [18]. It should be noted, however, that they underpredict the magnitude of the $pp \rightarrow pn\pi^+\pi^0$ for which the $N^*(1440) \rightarrow N(\pi\pi)^{T=0}_{\ell=0}$ is forbidden by isospin conservation.

These findings show that the $pp \rightarrow pp\pi^+\pi^-$ reaction in the threshold region has the potential to give new information on the decay properties of the poorly known $N^*(1440)P_{11}$ Roper resonance. More details on this issue can be found in the contribution from H. Clement in these proceedings (see p. 171).

3 First results from the WASA detector

To investigate the different aspects of meson production in more detail, one needs high-quality data on the differential distributions from these reactions. The restricted

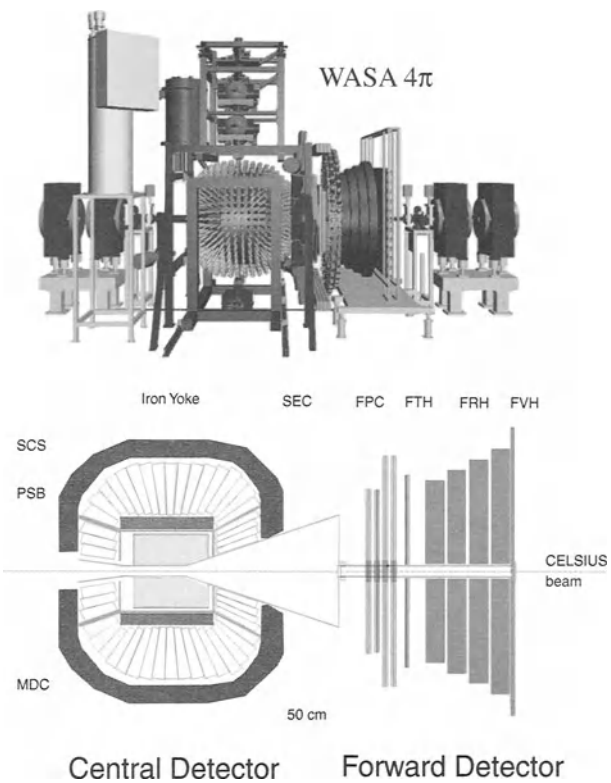

Fig. 5. The WASA 4π experimental set-up [19]. The upper figure shows a CAD view of the facility. The lower figure shows a cross-section of the detector. The forward detector is identical to the one used in the PW experiment [1].

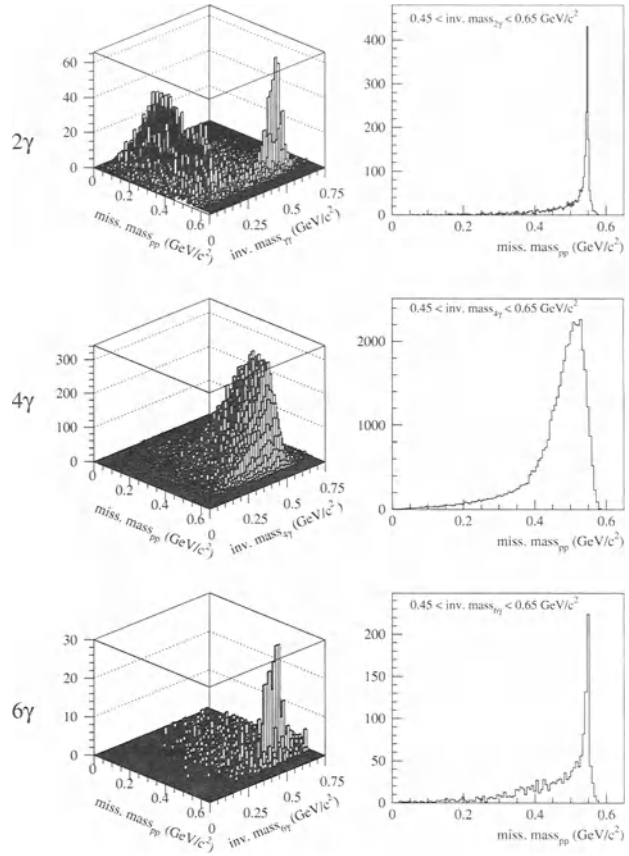

Fig. 6. Experimental data from the WASA detector at a proton kinetic energy of 1350 MeV with two protons identified in the forward detector and two, four and six γ's measured in the central detector. The left column shows the invariant mass of the γ's *versus* the two-proton missing mass. The right column shows the two-proton missing mass taken from a band around the η mass in the invariant multiple γ distributions.

acceptance of the PW experiment was a drawback in this respect. This limitation is overcome by the recently commissioned WASA 4π detector at CELSIUS [19], of which the PW set-up is a subset. The detector is designed for the measurements of rare η and π^0 decays, where it should be capable of handling luminosities of about 10^{32} $s^{-1}cm^{-2}$ using frozen droplets (pellets) of hydrogen or deuterium as targets. It measures charged particles and photons over a solid angle close to 4π ($\approx 96\%$) with high accuracy both in energy and track coordinates. This is accomplished with a central detector (CD) whose outer part (SEC) is made from a large array of CsI(Na) crystals. The inner part is surrounded by a very thin-walled ($0.16X_0$) superconducting solenoid (SCS) and comprises a vertex detector (MDC) made from 16 layers of straw chambers organized in stereo-layers and a plastic scintillator barrel (PSB). The forward detector is the same as was used in the PW experiments. A CAD view of the WASA detector is shown in the upper part of fig. 5 and a cross-section of the detector is shown in the lower part.

An example of the present performance of the WASA detector is shown in fig. 6. The data were taken at a proton energy of 1350 MeV using a hydrogen pellet target. Two protons were identified in the forward detector with 2, 4 and 6 γ's measured in the central detector. Prominent η peaks can be seen in the 2γ and 6γ samples coming from the $\eta \to 2\gamma$ and the $\eta \to 3\pi^0$ decays. No η signal is seen in the 4γ sample, as expected, since this decay is forbidden by CP invariance. The continuum in the projection of the two-proton missing-mass plot comes mainly from the direct $pp \to \pi^0\pi^0\pi^0$ process and will lead to the first measurement of this cross-section in this energy region.

The power of the WASA detector to resolve the $pp \to pp\pi^0\pi^0$ reaction from the same data sample can be seen in fig. 7. Here the combinations of 2γ invariant masses that are closest to the π^0 masses are plotted. A clean $2\pi^0$ peak is then seen. No corrections have yet been made for acceptance and efficiencies.

4 Conclusions

η production has been investigated in pN and pd interactions and 2π production has been studied in pp interactions at the CELSIUS cooler/storage ring at the The Svedberg Laboratory. The results point to the importance of nucleon isobars in the production of these mesons. The 2π reaction is especially interesting in this respect and may

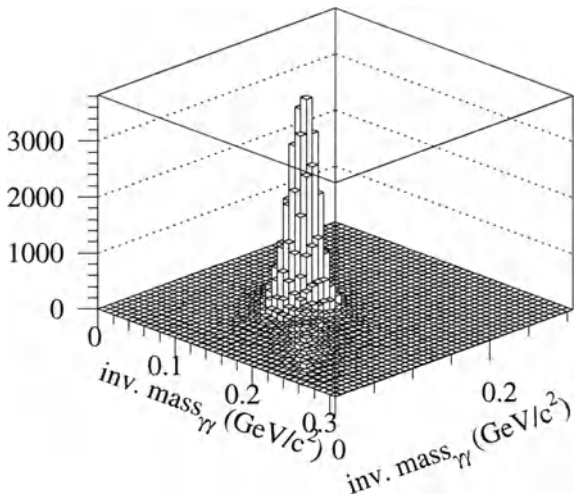

Fig. 7. Experimental data from the WASA detector at a proton kinetic energy of 1350 MeV with two protons identified in the forward detector and four γ's measured in the central detector. The invariant-mass combination of the two $\gamma\gamma$ which best fit the π^0 assumption are plotted against each other.

prove to be an important tool to study the decay properties of the $N^*(1440)P_{11}$ Roper resonance. The newly commissioned WASA detector will be a powerful tool for continued studies of these reactions as well as for studies of other rare processes and meson decay properties.

References

1. H. Calén *et al.*, Nucl. Instrum. Methods A **379**, 57 (1996).
2. T. Ueda, Phys. Rev. Lett. **66**, 297 (1991).
3. S.A. Rakityansky *et al.*, Phys. Rev. C **53**, R2043 (1996).
4. A.M. Green, J.A. Niskanen, S. Wycech, Phys. Rev. C **54**, 1970 (1996).
5. H. Calén *et al.*, Phys. Rev. Lett. **79**, 2642 (1997).
6. H. Calén *et al.*, Phys. Rev. Lett. **80**, 2069 (1998).
7. H. Calén *et al.*, Phys. Lett. B **366**, 39 (1996).
8. P. Moskal *et al.*, Phys. Lett. B **482**, 356 (2000).
9. J. Berger *et al.*, Phys. Lett. **61**, 919 (1988).
10. B. Mayer *et al.*, Phys. Rev. C **53**, 2068 (1996).
11. N. Willis *et al.*, Phys. Lett. B **406**, 143 (1997).
12. R. Bilger *et al.*, Phys. Rev. C **47**, 044608 (2002).
13. M. Betigeri *et al.*, Phys. Lett. B **472**, 267 (2000).
14. J. Złomańczuk, private communication.
15. P. Berthet *et al.*, Nucl. Phys. A **443**, 589 (1985).
16. J. Johanson *et al.*, Nucl. Phys. A **712**, 75 (2002).
17. W. Brodowsky *et al.*, Phys. Rev. Lett. **88**, 192301 (2002).
18. L. Alvarez-Ruso, E. Oset, E. Hernandez, Nucl. Phys. A **633**, 519 (1998).
19. J. Zabierowski *et al.*, Phys. Scr. T **99**, 159 (2002).

Eur. Phys. J. A **18**, 283–287 (2003)
DOI 10.1140/epja/i2002-10217-3

THE EUROPEAN PHYSICAL JOURNAL A

Progress in hypernuclear physics

T. Nagae[a]

High Energy Accelerator Research Organization (KEK), 1-1 Oho, Tsukuba, Ibaraki 305-0801, Japan

Received: 30 September 2002 /
Published online: 22 October 2003 – © Società Italiana di Fisica / Springer-Verlag 2003

Abstract. The recent progress in hypernuclear physics is discussed in this paper. The topics include recent results on hypernuclear gamma-ray spectroscopy, non-mesonic weak decay, and double-Λ hypernuclei. Future prospects at the 50 GeV PS are also discussed.

PACS. 21.80.+a Hypernuclei – 25.80.-e Meson- and hyperon-induced reactions

1 Introduction

Since the 1980s, the Alternating-Gradient Synchrotron (AGS) in Brookhaven National Laboratory (BNL) and the 12 GeV proton synchrotron (PS) in KEK have played a very important role in Hypernuclear Physics by providing high-intensity K^- and $\pi^\pm$ beams. The (π^+, K^+) and (K^-, π^-) reactions were used for the production of Λ hypernuclei, and the (K^-, K^+) reaction for the investigation on the strangeness $S = -2$ systems, such as double-Λ hypernuclei, Ξ^- hypernuclei, and the hypothetical H dibaryon. These experiments at BNL-AGS and KEK-PS have extended the scope of hypernuclear physics to the physics of hadron many-body systems with strangeness degrees of freedom, *i.e.* Strangeness Nuclear Physics.

Recently, Jefferson Laboratory (JLab) started hypernuclear spectroscopy with a different reaction of $(e, e'K^+)$. In 2007, the new 50 GeV proton synchrotron, now in construction in Japan, will be in operation. Then, it will be the opening of a new era in Strangeness Nuclear Physics.

2 Recent topics

2.1 Spectroscopy of Λ hypernuclei

The spectroscopy of Λ hypernuclei has been successfully carried out in KEK by using the SKS spectrometer [1]. An overview of the measurements with the (π^+, K^+) reactions was given in ref. [2]. The SKS spectrometer improved the energy resolution in Λ hypernuclear spectroscopy from 3–4 $\mathrm{MeV_{FWHM}}$ to $\sim$ 2 MeV, and further improved it to 1.45 MeV in the recent measurement [3]. The energy resolution resolved the major shell structure of Λ-orbits up to ${}^{208}_{\Lambda}$Pb [4] owing to the selectivity of the (π^+, K^+) reaction due to the high-momentum transfer ($\sim$ 350 MeV/c) of the reaction. It also revealed, for the first time, several core-excited states of ${}^{12}_{\Lambda}$C [4,3]. Some of them were not simply explained in naive weak-coupling structure, and it was suggested that the parity-mixing intershell couplings mediated by a Λ-particle should be taken into account [5].

The great progress in Λ hypernuclear spectroscopy has taken place with a success of a hypernuclear γ-ray measurement by using a germanium (Ge) detector system, called Hyperball, in KEK [6]. The detector consisted of fourteen N-type coaxial Ge detectors of 60% relative efficiency. It covered 15% of the 4π sr. The energy resolution of 3–4 $\mathrm{keV_{FWHM}}$ was achieved at 1.33 MeV. It is a great improvement. So far, a few hypernuclear γ-rays were well-identified with NaI counters in worse energy resolutions.

The measurement observed the spin-flip $M1(\frac{3}{2}^+ \to \frac{1}{2}^+)$ γ-ray at 691.7±0.6(stat)±1.0(syst) keV in ${}^{7}_{\Lambda}$Li, for the first time. The energy splitting provided a stringent constraint to the strength of the ΛN spin-spin interaction.

It also observed the $E2(\frac{5}{2}^+ \to \frac{1}{2}^+)$ γ-ray transition at $2050.1 \pm 0.4(\mathrm{stat}) \pm 0.7(\mathrm{syst})$ keV. Because of the good energy resolution of the Hyperball, we could measure the lifetime of the $\frac{5}{2}^+$ state from the peak shape analysis, the so-called Doppler-shift attenuation method [7]. The large momentum transfer of the (π^+, K^+) reaction ($\sim$ 350 MeV/c) makes the stopping time of the recoiling ${}^{7}_{\Lambda}$Li ($\sim$ 13 ps) comparable to the expected lifetime (3–10 ps) of the $\frac{5}{2}^+$ state. The observed γ-ray peak at 2050 keV had two components; a sharp peak and a Doppler-broadened tail part. The sharp peak corresponds to the γ-rays emitted after the stopping of the recoiling ${}^{7}_{\Lambda}$Li. From the two-component fitting by changing the lifetime of the $\frac{5}{2}^+$ state, the lifetime was obtained to be $5.8^{+0.9}_{-0.7} \pm 0.7$ ps, from which the reduced transition probability, $B(E2)$, was estimated to be $3.6 \pm 0.5^{+0.5}_{-0.4} e^2\,\mathrm{fm}^4$. This value is about one-third of the $B(E2)$ of the corresponding $E2(3^+ \to 1^+)$ transition in ^{6}Li. The $B(E2)$ is very sensitive to size contraction; in

[a] e-mail: tomofumi.nagae@kek.jp

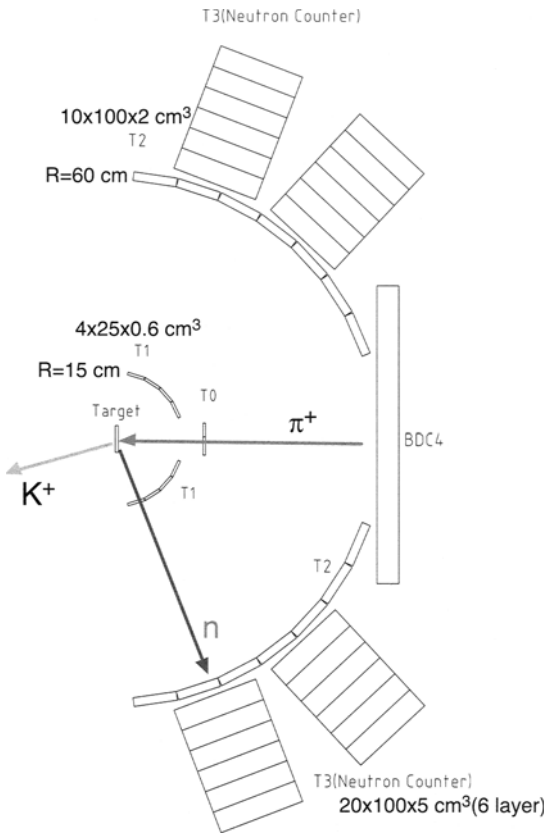

Fig. 1. Detector setup for the coincidence measurement of neutrons and protons emitted from non-mesonic weak decays in KEK-PS E369.

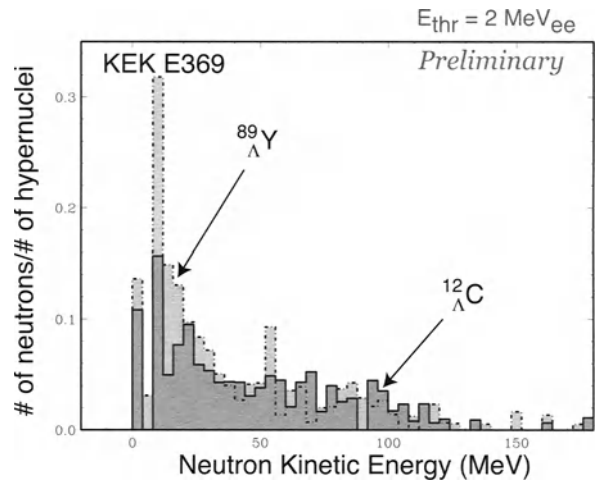

Fig. 2. The neutron energy spectra with a 2 MeV_{ee} threshold for ${}^{12}_{\Lambda}$C and ${}^{89}_{\Lambda}$Y. The vertical scale is normalized to the number of hypernuclei in the bound region.

this case, the shrinkage of the ^{6}Li core in the ${}^{7}_{\Lambda}$Li hypernucleus.

The further γ-ray measurements in p-shell Λ hypernuclei are in progress at BNL-AGS with the (K^-, π^-) reactions by using the Hyperball.

2.2 Weak decay of Λ hypernuclei

The weak decay properties of a Λ-hyperon in hypernuclei is another interesting subject. It is well known that the mesonic free Λ decay($\Lambda \to \pi N$) is strongly suppressed because of the Pauli blocking and the dominant decay mode is the non-mesonic decay($\Lambda N \to NN, \Lambda NN \to NNN$). However, the present experimental data have too large ambiguities on the total decay rate and the neutron emission probability to pin down the reaction mechanism.

In the study of non-mesonic weak decays of Λ hypernuclei, a large ratio of $\Gamma_n(\Lambda n \to nn)/\Gamma_p(\Lambda p \to np) \sim 1$ has been a puzzle not to be simply explained. The importance of two-nucleon–induced weak decay ($\Lambda NN \to NNN$) was suggested in ref. [8] related to this puzzle. However, available data were not enough to distinguish the one-nucleon–induced decay and two-nucleon–induced one. For example, the energy spectra of emitted nucleons should have different shapes in two decay processes [9]. An enhancement of the low-energy component is expected in the two-nucleon–induced process. The proton measurements so far done, however, usually had high energy thresholds of 40–50 MeV, which lost sensitivity to detect the low-energy component from the two-nucleon–induced process, if it existed. Therefore, we carried out the neutron measurement, in which the detection energy threshold could be reduced to $\leq$10 MeV. The quality of the neutron measurements so far has been very bad in statistics and signal-to-noise ratio.

The experimental setup for coincidence measurements of neutrons and protons emitted from non-mesonic weak decays of ${}^{89}_{\Lambda}$Y is shown in fig. 1. Since the mesonic weak-decay rate is expected to be negligibly small, all kinds of weak-decay products were measured in this setup.

The emitted timing of protons was measured with the T1 counter located 15 cm apart from the target. The flight time difference of protons was corrected with the velocity measured from the time of flight between the T1 and T2 counters. The overall timing resolution for protons was found to be $\sim$ 150 ps (rms).

Neutral particles, such as γ's and neutrons, were measured in the T3 counter with T1 and T2 as veto counters. The T3 counter consisted of six layers of a plastic scintillator (BC420) of 20[W]$\times$100[L]$\times$5[T] cm^3. The velocity of a neutral particle was obtained with a time-of-flight measurement between T0 and T3 counters. The relative timing of all 24 neutron counters was adjusted with the prompt γ's from the (π^+, pX) reaction. The typical resolution for the prompt γ's was $\sim$ 200 ps (rms).

The time-of-flight spectra of neutral particles in coincidence with bound states of ${}^{12}_{\Lambda}$C and ${}^{89}_{\Lambda}$Y showed that the n/γ separation was very clean and we had a very good signal-to-noise ratio for neutrons. Gated to the neutron component, the energy spectra of neutrons from ${}^{12}_{\Lambda}$C and ${}^{89}_{\Lambda}$Y are obtained as shown in fig. 2.

Here, we notice that there exists no prominent bump structure around $\sim$ 75 MeV expected from the one-nucleon–induced decay process ($\Lambda N \to NN$) even for ${}^{12}_{\Lambda}$C,

while the total shape seems to be very similar to that for the two-nucleon–induced process [9]. The recent measurement of the neutron spectrum from ${}^{5}_{\Lambda}$He [10] also shows a very similar shape with that for ${}^{12}_{\Lambda}$C. This suggests that rescattering effects after the one-nucleon–induced decay were unexpectedly large and/or the two-nucleon–induced decay plays a dominant role in the non-mesonic weak decay.

2.3 Double-Λ hypernuclei

There has been three emulsion events which showed the existence of double-Λ hypernuclei [11–13]. However, these events had some ambiguities on interpretation etc., and the ground-state binding energy was not determined definitely.

In 2001, two new observations were reported from BNL-AGS and KEK-PS.

The KEK-PS E373 experiment [14] reported a double-hyperfragment event in a hybrid-emulsion measurement. The event is uniquely identified as the sequential decay of ${}^{6}_{\Lambda\Lambda}$He emitted from a Ξ^- hyperon nuclear capture at rest,

$$
\begin{aligned}
{}^{12}\mathrm{C} + \Xi^- &\rightarrow {}^{6}_{\Lambda\Lambda}\mathrm{He} + {}^{4}\,\mathrm{He} + t\,,\\
{}^{6}_{\Lambda\Lambda}\mathrm{He} &\rightarrow {}^{5}_{\Lambda}\mathrm{He} + p + \pi^-.
\end{aligned}
$$

The binding energy of ${}^{6}_{\Lambda\Lambda}$He has been measured to be $7.25\pm0.19^{+0.18}_{-0.11}$ MeV, for the first time. It corresponds to the $\Delta B_{\Lambda\Lambda} = 1.01\pm0.20^{+0.18}_{-0.11}$ MeV, where $\Delta B_{\Lambda\Lambda}$ is defined by $\Delta B_{\Lambda\Lambda}({}^{A}_{\Lambda\Lambda}Z) = B_{\Lambda\Lambda}({}^{A}_{\Lambda\Lambda}Z) - 2B_{\Lambda}({}^{A-1}_{\Lambda}Z)$. It means the Λ-Λ interaction is weakly attractive. Two of the past measurements gave a value of $\Delta B_{\Lambda\Lambda}$ to be about 4.5 MeV. Thus, the new value is smaller than these.

The other experiment at BNL-AGS [15] demonstrated the production of double-Λ hypernuclei in the (K^-, K^+) reaction on ^{9}Be. It used a quite new technique to identify double-Λ hypernuclei by using a Cylindrical Drift chamber System (CDS). In the CDS, two π^-'s emitted through sequential weak decays of hypernuclei were detected in a good momentum resolution. The result indicated the production of a significant number of the double-Λ hypernucleus ${}^{4}_{\Lambda\Lambda}$H and the twin hypernuclei ${}^{4}_{\Lambda}$H and ${}^{3}_{\Lambda}$H.

3 Future prospects at the 50 GeV PS

The 50 GeV proton synchrotron (PS) is now under construction in the Joint Project between KEK and Japan Atomic Energy Research Institute (JAERI). The average beam current is 15.7 μA, which will produce the world's highest-intensity K^- beams. The construction will be completed early in 2007.

In the experimental area for the slow-extracted beam, two secondary beam lines, K1.8 and K1.1, are proposed for the studies of strangeness nuclear physics; the former for the $S = -2$ systems, and the latter for the $S = -1$ systems.

A letter of intent for experiments on strangeness nuclear physics [16] well summarizes the initial experimental programs in this field. Among the various topics discussed in the letter of intent, I introduce two interesting programs: the investigation of new hadronic many-body systems with strangeness $S = -2$ and high-resolution γ-ray spectroscopy.

3.1 Spectroscopic study of S = −2 systems

The high-intensity K^- beam at $\sim$ 1.8 GeV/c available at the 50 GeV PS is quite unique to open a new frontier of Strangeness Nuclear Physics in the spectroscopic studies of strangeness $S = -2$ systems. This is not only a step forward from the $S = -1$ systems as a natural extension, but also a significant step to explore the multi-strangeness hadronic systems; in the course of the limit, strange hadronic matter ($S = -\infty$) in the core of a neutron star is our concern. Also, it is important to extract some information on ΞN and Λ-Λ interactions from the spectroscopic data.

The (K^-, K^+) reaction is one of the best tools to implant the $S = -2$ through an elementary process $K^-+p \rightarrow K^++\Xi^-$, the cross-section of which in the forward direction has a broad maximum around this energy.

At present, the experimental information on the $S = -2$ systems mainly comes from several emulsion data in limited statistics. As for the Ξ hypernuclei, there exist some hints of emulsion events for their existence. However, it is still not conclusive. Some upper limits on the Ξ-nucleus potential have been obtained from the production rate in the bound region of a Ξ hypernucleus via the (K^-, K^+) reaction.

The energy difference between the (Ξ^-p) system and the ($\Lambda\Lambda$) system is only 28.3 MeV in free space. Therefore, a relatively large configuration mixing between Ξ^-+A and $\Lambda\Lambda+(A-1)$ states is suggested. It is very interesting to investigate whether the single-particle picture of Ξ^- is valid or not in such a system.

It is expected that the spectroscopy of the Ξ hypernuclei is promising. Here we use the (K^-, K^+) reaction in which we can use the same method for the (π^+, K^+) reaction in the Λ-hypernuclear spectroscopy. In fact, two reactions have very similar characteristics of large recoil momentum of a produced hyperon: $p_{\Xi^-} \sim 500$ MeV/c and $p_{\Lambda} \sim 350$ MeV/c. Therefore, even for heavy targets well-separated peak structures are expected in spite of many possible excitations, because the spin-stretched configurations with $\ell_p + \ell_{\Xi} + J =$ even are strongly populated as in the case of the (π^+, K^+) reaction, or more strongly.

For the spectroscopy of the (K^-, K^+) reaction, we need two spectrometers as in the (π^+, K^+) reaction: a beam line spectrometer for the incident K^- and a K^+ spectrometer.

A 2 GeV/c kaon beam line for the JHF was designed by J. Doornbos [17]. A beam line spectrometer is installed in the last part of the beam line. It consists of a QDQDQ system. It is estimated that the momentum resolution of 2×10^{-4} could be achievable.

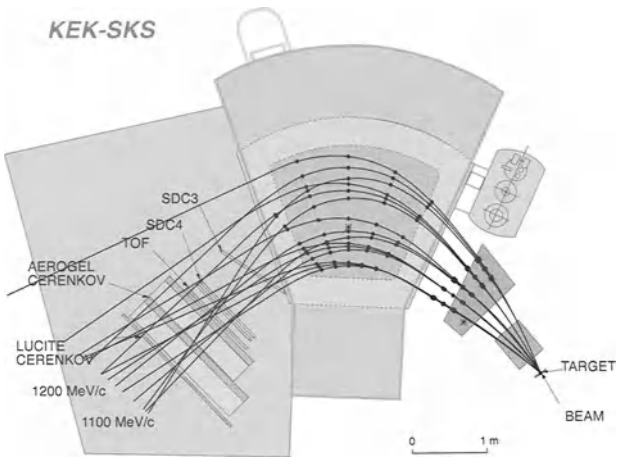

Fig. 3. Schematic layout of the SKS spectrometer for the (K^-, K^+) reaction at 1.65 GeV/c.

For the K^+ spectrometer, we will use the existing SKS spectrometer with some modifications. In fig. 3, the setup of the SKS spectrometer for the (K^-, K^+) reaction is shown schematically.

Since the radius for the central momentum is larger than that for the (π^+, K^+) reaction, the target point is moved away from the magnet. So that, the acceptance of the spectrometer is reduced to be $\sim$ 50 msr. The overall energy resolution is estimated to be 2 MeV(FWHM) for a 2 g/cm^2 target thickness.

The production cross-section of the Ξ hypernuclei in the (K^-, K^+) reaction is calculated to be $\sim$ 0.1 μb/sr/MeV around the middle of the bound region for various types of potentials. Thus, the yield for the ^{208}Pb target with 2 g/cm^2 thickness is estimated to be $\simeq$ 6 events/MeV/day. So, even for the heaviest case, we could get enough statistics within $\sim$ 20 days to obtain spectroscopic information. For lighter targets such as ^{28}Si and ^{58}Ni, the yields are several times higher with the normalized target thickness of 2 g/cm^2.

3.2 High-resolution hypernuclear γ-ray spectroscopy

High-resolution hypernuclear γ-ray spectroscopy will be extended further and exciting new physics fields will be opened up at the 50 GeV PS.

The (K^-, π^-) reaction at 1.1 GeV/c is used in order to produce Λ hypernuclei. This reaction has a large spin-flip amplitude and allows population of various hypernuclear states including spin-flip states with unnatural parities.

We require a secondary beam line whose intensity is optimized to 1.1 GeV/c. It should have a double-stage mass separator to obtain pure K^- beams in order to minimize the counting rates of Ge detectors and tracking devices in the spectrometer. The beam intensity of 1.1 GeV/c K^- is expected to be 1.9×10^7 K^- per spill (2×10^{14} protons) in 3.4 s cycle.

The momentum of the K^- beam is measured event-by-event with a beamline spectrometer having $<$ 0.2% FWHM resolution. The outgoing π^- is measured with a spectrometer similar to SKS, which is required to have an acceptance of more than 50 msr and momentum resolution of $<$ 0.2% FWHM. An overall mass resolution better than 3 MeV is necessary.

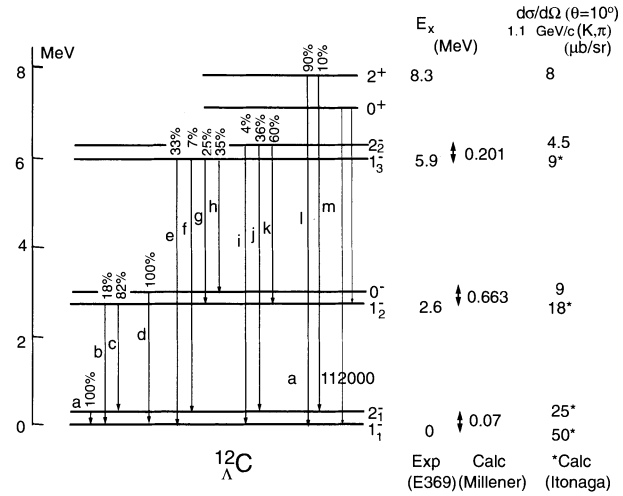

Expected Yield (5 days)

single				$\gamma\gamma$ coincidnece with a		with c		with d	
a	112000	h	1700	c	1900	a	1900	h	55
b	2600	i	64	f	50	g	39		
c	12000	j	580	g	150	k	50		
d	7500	k	1400	j	94				
e	1100	l	2000	k	170				
f	240	m	230	m	31				
g	1300								

Fig. 4. Top: Expected level energies and γ transitions of $^{12}_{\Lambda}$C. Bottom: Expected yields of γ transitions of $^{12}_{\Lambda}$C for 5 days' run. Yields of γ-γ coincidence events are also shown.

Around the target, we install a new Ge detector system, which is similar to the present Hyperball but has a much larger efficiency. In the present design, we expect to use 14 sets of "Segmented Super Clover Ge detectors", which has recently become commercially available. One detector set consists of four Ge crystals of 7 cm$\varnothing \times$ 14 cm, and the electrode of each crystal is segmented into 4 readout channels. Such a fine segmentation is necessary for Doppler-shift correction. The Ge crystals cover about 40% of the total solid angle. The Ge detector system has a photo-peak efficiency of 12% at 1 MeV in total. Each of the Ge detectors is surrounded by a set of BGO or GSO counters, which are used to veto Compton scattering and high-energy γ-rays from π^0.

An example of the γ-ray measurement in the case of $^{12}_{\Lambda}$C for 5-day data taking is shown in fig. 4. The production cross-sections of the $^{12}_{\Lambda}$C states (except for the first 2^+ state) were calculated by Itonaga *et al.* for the 1.1 GeV/c (K^-, π^-) reaction [18]. The energy levels are taken from the experimental values from KEK-E369 [3], but the doublet spacing energies are taken from the new parameter set of the spin-dependent interactions by Millener [19].

We will have quite enough yields for almost all the γ transitions. We can expect good statistics even for γ-γ

coincidence spectra, which enable us to completely reconstruct the level scheme.

4 Summary

There has been a lot of progress in Hypernuclear Physics in the last decade. The recent success of hypernuclear γ-ray spectroscopy with the Hyperball detector opened a new stage of hypernuclear spectroscopy in precision. As for non-mesonic weak decays, new neutron spectra from several Λ-hypernuclei gave a new information to investigate the reaction mechanism. There was also important progress in double-Λ hypernuclei.

We hope these efforts will be in full bloom at the 50 GeV PS with high-intensity K^- beams.

References

1. T. Fukuda *et al.*, Nucl. Instrum. Methods A **361**, 485 (1995).
2. T. Nagae, Nucl. Phys. A **691**, 76c (2001).
3. H. Hotchi *et al.*, Phys. Rev. C **64**, 044302 (2001).
4. T. Hasegawa *et al.*, Phys. Rev. C **53**, 1210 (1996).
5. T. Motoba, Nucl. Phys. A **639**, 135c (1998).
6. H. Tamura *et al.*, Phys. Rev. Lett. **84**, 5963 (2000).
7. K. Tanida *et al.*, Phys. Rev. Lett. **86**, 1982 (2001).
8. W.M. Alberico, A. De Pace, M. Ericson, A. Molinari, Phys. Lett. B **256**, 134 (1991).
9. A. Ramos, M.J. Vincente-Vacas, E. Oset, Phys. Rev. C **55**, 735 (1997).
10. H. Outa *et al.*, KEK E462 experiment, private communication.
11. D.J. Prowse, Phys. Rev. Lett. **17**, 782 (1966).
12. M. Danysz *et al.*, Nucl. Phys. **49**, 121 (1963).
13. S. Aoki *et al.*, Prog. Theor. Phys. **85**, 1287 (1991).
14. H. Takahashi *et al.*, Phys. Rev. Lett. **87**, 212502 (2001).
15. J.K. Ahn *et al.*, Phys. Rev. Lett. **87**, 132504 (2001).
16. JHF Strangeness Nuclear Physics Group, *Letter of Intent for Experiments on Strangeness Nuclear Physics at the 50-GeV Proton Synchrotron*, July 2000, unpublished, `http://www-jhf.kek.jp/JHF_WWW/LOI/50GeVNP-LOI-v1.0.pdf`).
17. J. Doornbos, KEK Report 97-5 (1997).
18. K. Itonaga *et al.*, Prog. Theor. Phys. Suppl. **117**, 17 (1994).
19. D.J. Millener, *Proceedings of the International Workshop on Hypernuclear Physics with Electromagnetic Probes (HYPJLAB99), Hampton, Virginia, 2-4 December, 1999.*

Eur. Phys. J. A **18**, 289–291 (2003)
DOI 10.1140/epja/i2002-10218-2

THE EUROPEAN PHYSICAL JOURNAL A

Parity non-conservation in proton-proton elastic scattering

V.R. Brown[1,a], B.F. Gibson[2], J.A. Carlson[2], and R. Schiavilla[3]

[1] Massachusetts Institute of Technology, Cambridge, MA 02139, and University of Maryland, College Park, MD 20742-4111, USA
[2] Los Alamos National Lab, Los Alamos, NM 87545, USA
[3] Old Dominion University, Norfolk, VA 20742, USA

Received: 30 September 2002 /
Published online: 22 October 2003 – © Società Italiana di Fisica / Springer-Verlag 2003

Abstract. The parity–non-conserving longitudinal asymmetry in proton-proton (*pp*) elastic scattering is calculated in the lab energy range 0–350 MeV using contemporary, realistic strong-interaction potentials combined with a weak-interaction potential comprised of ρ- and ω-meson exchanges as exemplified by the DDH model. Values for the ρ- and ω-meson coupling constants, h_ρ^{pp} and h_ω^{pp}, are determined from comparison with the measured asymmetries at 13.6 MeV, 45 MeV, and 221 MeV.

PACS. 21.30.-x Nuclear forces – 24.80.+y Nuclear tests of fundamental interactions and symmetries – 25.40.Cm Elastic proton scattering

1 Introduction

The parity-violating longitudinal asymmetry in proton-proton *pp* elastic scattering is calculated in the lab energy range 0–350 MeV. Contemporary, realistic strong-interaction potentials such as the Argonne V_{18} [1], the Bonn 2000 [2], and the Nijmegen I [3] models are combined with a weak-interaction potential comprised of ρ- and ω-meson exchanges as exemplified by the well-known DDH model [4]. The full scattering problem in the presence of the strong parity-conserving, the Coulomb, and the weak parity-non-conserving forces is solved.

The meson exchange terms in the weak interaction are assumed to have the same cut-off as in the Bonn 2000 strong interaction. Values for the ρ- and ω-meson coupling constants, h_ρ^{pp} and h_ω^{pp}, are determined from comparison with the measured asymmetries at 13.6 MeV [5], 45 MeV [6], and 221 MeV [7].

2 Parity–non-conserving potentials

The DDH parity–non-conserving interaction can be defined as

$$\begin{aligned} V_{NN}^{\rm PV}(ij) = {} & i\frac{g_\pi f_\pi}{2\sqrt{2}}\,\frac{1}{m}\,\tau_i\times\tau_j\cdot\hat{z}\,(\sigma_i+\sigma_j)\cdot[\mathbf{p}_{ij},Y_\pi(r_{ij})] \\ & -g_\rho\Bigg(h_\rho^0\tau_i\cdot\tau_j+\frac{1}{2}h_\rho^1(\tau_i+\tau_j)\cdot\hat{z} \\ & +\frac{h_\rho^2}{(2\sqrt{6})}(3\tau_i\cdot\hat{z}\tau_j\cdot\hat{z}-\tau_i\cdot\tau_j)\Bigg) \\ & \times\Bigg(\frac{1}{m}(\sigma_i-\sigma_j)\cdot\{\mathbf{p}_{ij},Y_\rho(r_{ij})\} \\ & +i\frac{1+\kappa_\rho}{m}(\sigma_i\times\sigma_j)\cdot[\mathbf{p}_{ij},Y_\rho(r_{ij})]\Bigg) \\ & -g_\omega[h_\omega^0+\frac{1}{2}h_\omega^1(\tau_i+\tau_j)\cdot\hat{z}] \\ & \times\Bigg(\frac{1}{m}(\sigma_i-\sigma_j)\cdot\{\mathbf{p}_{ij},Y_\omega(r_{ij})\} \\ & +i\frac{1+\kappa_\omega}{m}(\sigma_i\times\sigma_j)\cdot[\mathbf{p}_{ij},Y_\omega(r_{ij})]\Bigg) \\ & -\frac{1}{2m}(g_\omega h_\omega^1-g_\rho h_\rho^1)(\tau_i-\tau_j)\cdot\hat{z} \\ & \times(\sigma_i+\sigma_j)\cdot\{\mathbf{p}_{ij},Y_\rho(r_{ij})\} \\ & -\frac{1}{2m}g_\rho h_\rho^{1\prime}i(\tau_i\times\tau_j)\cdot\hat{z} \\ & \times(\sigma_i+\sigma_j)\cdot[\mathbf{p}_{ij},Y_\rho(r_{ij})]\,. \end{aligned}$$

DDH emphasizes the major difficulties in attempting to provide reliable estimates for these weak parity-violating couplings:

- the large S-P factorization term due to the dependence upon the absolute size of the current u, d quark masses;
- enhancement factors associated with the renormalization group treatment of the effective weak Hamiltonian;
- use of a relativistic *vs.* a non-relativistic quark model;
- the size of the sum rule contribution to pion emission due to $SU(3)$ breaking;

[a] e-mail: vrbrown@lns.mit.edu

Table 1. Original DDH weak-coupling constants.

Coupling	DDH range	DDH "best" value
f_π	[0, 30]	12
h_ρ^0	[30, −81]	−30
h_ρ^1	[−1, 0]	−0.5
h_ρ^2	[−20, −29]	−25
h_ω^0	[15, −27]	−5
h_ω^1	[−2, −5]	−3

- the size of the vector meson *vs.* pion emission amplitudes due to $SU(6)$ breaking effects;
- etc.

The DDH weak-coupling constants quoted in units of the "sum rule" value of 3.8×10^{-8} are given in table 1.

The DDH approach has been generally successful in describing a wide variety of data involving the weak-interaction effects in nucleon and nuclear systems. However, the determination of weak meson exchange couplings from measurements in nuclei [8] is difficult because the observables depend on the nuclear wave functions.

The most fundamental appearance of the weak interaction in the purely hadronic sector is parity violation in the two-nucleon system, where the strong interaction is well represented. For $\boldsymbol{pp}$ scattering, the parity non-conserving weak interaction becomes

$$\begin{aligned} v^{\mathrm{PV}} = &- \frac{g_\rho\, h_\rho^{pp}}{4\pi}\frac{m_\rho}{m}\Big\{(\sigma_1-\sigma_2)\cdot\{\mathbf{p}\,,\,Y(m_\rho r)\} \\ &+ i(1+\kappa_\rho)(\sigma_1\times\sigma_2)\cdot[\mathbf{p}\,,\,Y(m_\rho r)]\Big\} \\ &- \frac{g_\omega\, h_\omega^{pp}}{4\pi}\frac{m_\omega}{m}\Big\{(\sigma_1-\sigma_2)\cdot\{\mathbf{p}\,,\,Y(m_\omega r)\} \\ &+ i(1+\kappa_\omega)(\sigma_1\times\sigma_2)\cdot[\mathbf{p}\,,\,Y(m_\omega r)]\Big\}\ , \end{aligned}$$

where $\kappa_\omega \approx 0$ in the Bonn model is used to define the strong-interaction parameters in the analysis. The coupling constants h_ρ^{pp} and h_ω^{pp} result from evaluating the isospin operators for the pp system in the first DDH parity non-conserving interaction above.

Since the $\boldsymbol{pp}$ longitudinal asymmetry depends only on h_ρ^{pp} and h_ω^{pp}, the energy dependence of this process alone can determine the two parameters. However, the energy dependence of the partial waves [9] enhances the sensitivity of this determination. Below 50 MeV the ${}^1S_0$-${}^3P_0$ partial wave dominates and the two spin terms add coherently, such that the asymmetry is approximately proportional to

$$h_\rho^{pp} g_\rho(2+\kappa_\rho) + 2h_\omega^{pp} g_\omega\,.$$

At energies close to 225 MeV the ${}^3P_2$-${}^1D_2$ partial wave dominates (because the ${}^1S_0$-${}^3P_0$ partial wave is near zero) and the two spin terms subtract, such that the asymmetry is approximately proportional to

$$h_\rho^{pp} g_\rho \kappa_\rho\,.$$

Consequently, the data near 225 MeV are more sensitive to h_ρ^{pp} alone, and the data at 13.6 MeV and 45 MeV can determine the linear combination of h_ρ^{pp} and h_ω^{pp}.

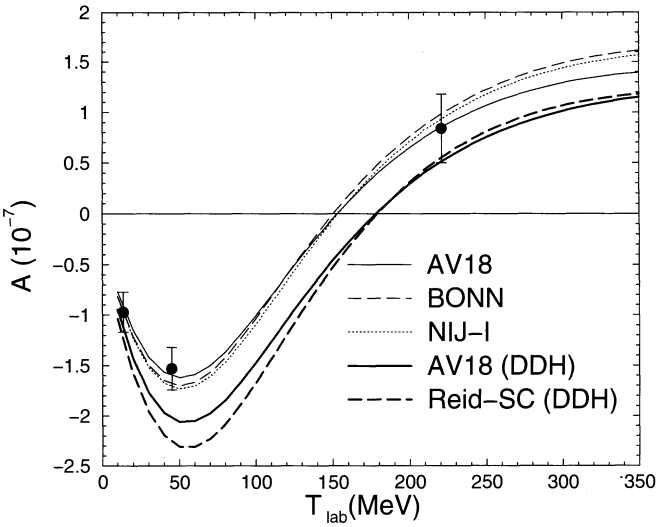

Fig. 1. Asymmetry in $\boldsymbol{pp}$ scattering as a function of energy.

3 Results

The energy dependence of the $\boldsymbol{pp}$ asymmetry can help dial in the relative contribution of the ρ and ω, and thus provide enough constraints to determine the h_ρ^{pp} and h_ω^{pp} weak-coupling constants. With the the recent publication [7] of the Triumf results at 221 MeV, there now exist enough data from 13.5 MeV to 221 MeV with the accuracy to make this determination.

A comparison of our theoretical calculations [10] with the available total asymmetry (A) data is shown in fig. 1. The calculated nuclear asymmetries are obtained by retaining in the partial-wave expansion all channels with J up to $J_{\max} = 8$. The curves labeled AV18, BONN, and NIJ-I all use the DDH potential with the coupling constants h_ρ^{pp} and h_ω^{pp} determined by a rough fit to data (the AV18 is used in the fitting procedure). There is very little sensitivity to the input strong-interaction potential, as seen by comparing the top three curves labeled AV18, BONN, and NIJ-I. The results are generally similar to those of earlier calculations [11,12].

Also presented in fig. 1 are AV18 (DDH) and Reid-SC (DDH), where the label (DDH) corresponds to using the "best"estimates for the h_ρ^{pp} and h_ω^{pp} coupling constants [4]. Notice that these two curves differ significantly from those using the DDH-adj parameters obtained by fitting to the $\boldsymbol{pp}$ asymmetry data.

A summary of parameter values used for the ρ and ω components of the strong- and weak-interactions in this study [10] along with the weak-coupling constants of the original DDH model [4] is provided in table 2.

In the fit to data h_ρ^{pp} is essentially determined by the 221 MeV measurement, and to reproduce the data at 13.6 MeV and 45 MeV h_ω^{pp} must be opposite in sign to h_ρ^{pp}. Nonetheless, the values extracted for h_ρ^{pp} and h_ω^{pp} are still compatible with the "reasonable" ranges quoted by DDH.

Table 2. Parameter values used for coupling of the ρ- and ω-meson to the nucleon in the strong- and weak-interaction models.

	$g_\alpha^2/4\pi$	κ_α	$10^7 h_\alpha^{pp}$ (DDH-adj)	$10^7 h_\alpha^{pp}$ (DDH-orig)	Λ_α (GeV/c)
ρ	0.84	6.1	−22.3	−15.5	1.31
ω	20.	0.	+5.17	−3.04	1.50

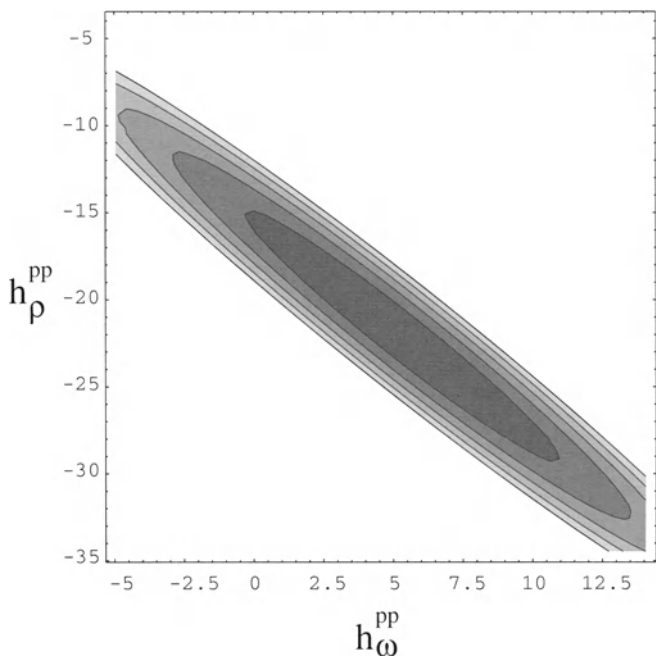

Fig. 2. Curves of constant total χ^2 obtained by analyzing the experimental pp data with the AV18 model, and ρ- and ω-meson strong-interaction couplings in the DDH potential from the Bonn 2000 model. The curves indicate surfaces of total $\chi^2 = 1$, 2, 3, 4, and 5 for various values of h_ρ^{pp} and h_ω^{pp}.

The DDH-adjusted values for coupling constants h_ρ^{pp} and h_ω^{pp} are somewhat insensitive to the ingredients of our calculational procedure as illustrated in fig. 1. Although the angular distribution of the longitudinal asymmetry does depend sensitively on the Coulomb interaction at small angles, the total asymmetry (integrated over angles) does not. In any case, our calculation [10] includes the effects of the Coulomb potential. The sensitivity to the cut-off in the weak-interaction potential [10] is more significant and could affect the determination of these coupling constants. The use of a cut-off in the weak-interaction corresponding to the one used in the strong interaction was introduced earlier [12].

Curves of constant total χ^2 obtained by analyzing the experimental pp data with the AV18 model, and ρ- and ω-meson strong-interaction couplings in the DDH potential from the Bonn 2000 model are plotted in fig. 2. The curves indicate surfaces of total $\chi^2 = 1$, 2, 3, 4, and 5 for various values of h_ρ^{pp} and h_ω^{pp}. The low-energy data put a tight constraint on linear combinations of h_ρ^{pp} and h_ω^{pp}. The Triumf data point at 221 MeV then fixes h_ρ^{pp}.

4 Conclusions

The DDH-adjusted values for coupling constants h_ρ^{pp} and h_ω^{pp} reported here [10] are fairly reliable and somewhat insensitive to the ingredients of our calculation. For a more precise determination of these weak-coupling constants, the use of the cut-off prescription for the short-range weak interaction should be examined further. The use of a cut-off is appropriate for the strong force, but it is not so well motivated for the short-range weak interaction. A measurement of the pp longitudinal asymmetry at an energy between 50 and 221 MeV would also be useful.

Future few-nucleon weak-interaction experiments involving both neutrons and protons can help tie down the weak-coupling constants, including that for the weak π-meson exchange, which introduces the parity-violating isospin-changing triplet-triplet transition. The empirical determination of the meson weak-coupling parameters from the few-nucleon sector, where strong-interaction effects are reasonably under control, can lead to a better understanding of weak-interaction effects in nuclei, where strong-interaction effects are problematic.

References

1. R.B. Wiringa, V.G.J. Stoks, R. Schiavilla, Phys. Rev. C **51**, 38 (1995).
2. R. Machleidt, Phys. Rev. C **63**, 024001 (2001).
3. V.G.J. Stoks, R.A.M. Klomp, C.P.F. Terheggen, J.J. de Swart, Phys. Rev. C **49**, 2950 (1994).
4. B. Desplanques, J.F. Donoghue, B.R. Holstein, Ann. Phys. (N.Y.) **124**, 449 (1980).
5. P.D. Eversheim *et al.*, Phys. Lett. B **256**, 11 (1991).
6. S. Kistryn *et al.*, Phys. Rev. Lett. **58**, 1616 (1987).
7. A.R. Berdoz *et al.*, Phys. Rev. Lett. **87**, 272301 (2001).
8. W. Haxton, C. Wieman, Annu. Rev. Nucl. Part. Sci. **51**, 261 (2001).
9. M. Simonius, Phys. Lett. B **41**, 415 (1972).
10. J. Carlson, R. Schiavilla, V.R. Brown, B.F. Gibson, Phys. Rev. C **65**, 035502 (2002).
11. V.R. Brown, E.M. Henley, F.R. Krejs, Phys. Rev. C **9**, 935 (1973); Phys. Rev. Lett. **30**, 770 (1973).
12. D.E. Driscoll, G.A. Miller, Phys. Rev. C **39**, 1951 (1989); **40**, 2159 (1989).

Eur. Phys. J. A **18**, 293–296 (2003)
DOI 10.1140/epja/i2002-10219-1

THE EUROPEAN PHYSICAL JOURNAL A

pd scattering at 250 MeV and three-nucleon forces

K. Hatanaka[1,a], J. Kamiya[1], Y. Maeda[2], T. Noro[3], K. Sagara[3], H. Sakai[2], Y. Sakemi[1], K. Sekiguchi[2], Y. Shimizu[1], A. Tamii[2], T. Wakasa[1], K. Yako[2], H.P. Yoshida[1], and V.P. Ladygin[4]

[1] Research Center for Nuclear Physics, Osaka University, Ibaraki, Osaka 567-0047, Japan
[2] Department of Physics, University of Tokyo, Bunkyo, Tokyo 113-0033, Japan
[3] Department of Physics, Kyushu University, Hakozaki, Fukuoka 812-8581, Japan
[4] Joint Institute for Nuclear Researches, 141980 Dubna, Russia

Received: 30 September 2002 /
Published online: 22 October 2003 – © Società Italiana di Fisica / Springer-Verlag 2003

Abstract. We have measured angular distributions of the differential cross-section, the analyzing power and all of the spin transfer coefficients $K_y^{y'}$, $K_x^{x'}$, $K_z^{x'}$, $K_x^{z'}$, and $K_z^{z'}$ for the pd elastic scattering at 250 MeV. These are the first measurements of a complete set of proton polarization observables for pd elastic scattering at intermediate energies. The present data are compared with theoretical predictions based on exact solutions of the three-nucleon Faddeev equations and modern realistic nucleon-nucleon potentials combined with three-nucleon forces (3NF), namely the Tucson-Melbourne (TM) 2π-exchange model, a modification thereof (TM′) closer to chiral symmetry, and the Urbana IX model.

PACS. 21.45.+v Few-body systems – 21.30.-x Nuclear forces – 24.70.+s Polarization phenomena in reactions

1 Introduction

Studies of few-nucleon systems offer a good opportunity to investigate the nature of nuclear forces. Owing to intensive theoretical and experimental efforts, a so-called new generation of realistic nucleon-nucleon (NN) potentials has been obtained using meson-exchange or other more phenomenological approaches, namely AV18 [1], CD Bonn [2], Nijm I, II and 93 [3]. They describe the rich set of experimental NN data up to 350 MeV which is well above the pion threshold of 290 MeV. These realistic two-nucleon forces (2NF), however, fail to reproduce experimental binding energies for light nuclei where rigorous solutions of the Schrödinger equation are available, clearly showing underbinding. For instance, the underbinding amounts to 0.5–1 MeV in the case of ^{3}H and ^{3}He and to 2–4 MeV in the case of ^{4}He. One can achieve correct three-nucleon (3N) and four-nucleon (4N) binding energies by including the Tucson-Melbourne (TM) [4] or Urbana IX [5] three-nucleon forces (3NF) which are refined versions of the Fujita-Miyazawa force [6], a 2π-exchange between three nucleons with an intermediate Δ excitation. In recent years, it became possible to perform rigorous numerical Faddeev-type calculations for the 3N scattering processes by the advances in computational capabilities.

In addition to the first signal on 3NF effects resulting from discrete states, strong 3NF effects were observed in a study of the minima of the Nd elastic scattering cross-section at incoming nucleon energies higher than about 60 MeV [7]. On the other hand, a recent study at RIKEN [8] shows that the inclusion of the 3NF does not always improve the description of precise data taken at intermediate deuteron energies. Proton vector analyzing power data at 70–200 MeV have revealed the deficiency of 3NF [9,10], which produces large but wrong effects. These results may be caused by a wrong spin structure of present-day 3NF. Clearly, the present situation is only the very beginning of the investigation of the spin structure of the 3NF. In addition, one can expect relativistic effects with increasing energy. However, the existing higher-energy database for the proton analyzing power is rather poor. There are no measurements of two-spin observables except for the spin correlation coefficient C_{yy} at 197 MeV at IUCF [11]. Precise data at intermediate energies including higher-rank spin observables are needed to provide constraints on theoretical 3NF models.

In the present study, we have measured angular distributions of the differential cross-section, the analyzing power A_y and all proton spin transfer coefficients $K_x^{x'}$, $K_x^{z'}$, $K_z^{x'}$, $K_z^{z'}$, and $K_y^{y'}$ for pd elastic scattering at 250 MeV. This energy is slightly above the pion threshold at 215 MeV. Realistic NN potentials have been obtained by analyzing the existing NN database up to 350 MeV. The corresponding proton energy in the pd system is 259 MeV to give the same center-of-mass (c.m.) energy.

[a] e-mail: hatanaka@rcnp.osaka-u.ac.jp

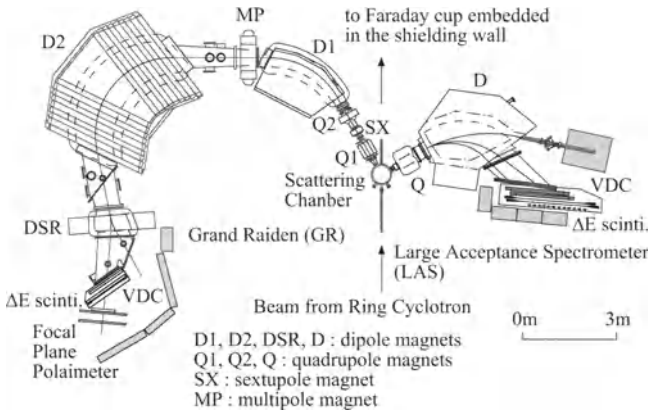

Fig. 1. Schematic layout of the RCNP dual spectrometer consisting of Grand Raiden and LAS.

Most of the effects caused by the pion production are expected to be taken into account in the realistic NN potentials. The cross-section of elastic pd scattering shows a smooth energy dependence in the 200–300 MeV range indicating a small effect of the pion production and a possibly larger relativistic effect in this energy region [12].

2 Experimental results and discussions

The experiment was performed at the Research Center for Nuclear Physics (RCNP), Osaka University. Polarized protons were produced in an atomic beam polarized ion source [13], injected into and accelerated by the $K = 120$ MeV AVF (azimuthally varying field) cyclotron up to 46.7 MeV. Subsequently the beam was injected into the $K = 400$ MeV ring cyclotron and accelerated to the final energy of 250 MeV. The polarization axis was vertical after the AVF cyclotron. Two superconducting solenoids located in the beam transfer line between the AVF cyclotron and the ring cyclotron were used to precess the proton spin polarization into the horizontal plane so as to have either of the two spin states sideways or longitudinal on the target. The proton polarization was continuously measured with two beamline polarimeters separated by a total bending angle of 115°, precessing the spin of 250 MeV protons by about 260° between the two polarimeters. Both the horizontal and vertical components of the polarization vector were determined. During the measurements, typical values for polarization and beam current were 70% and 200 nA, respectively. Analyzing power of the beamline polarimeter was precisely determined to be 0.362 ± 0.003 at the laboratory angle of 17° [14].

Measurements were performed using self-supporting 99% isotopically enriched deuterated polyethylene foils (CD_2) with total thicknesses of 21 and 44 mg/cm^2. A 15 mg/cm^2 thick, natural carbon target was used to subtract contributions due to scattering on carbon. It is essential to get precise absolute cross-sections for comparison with Faddeev calculations. Therefore, in a later measurement, a gaseous D_2 target was used to normalize cross-sections taken with the solid CD_2 target. The uncertainty

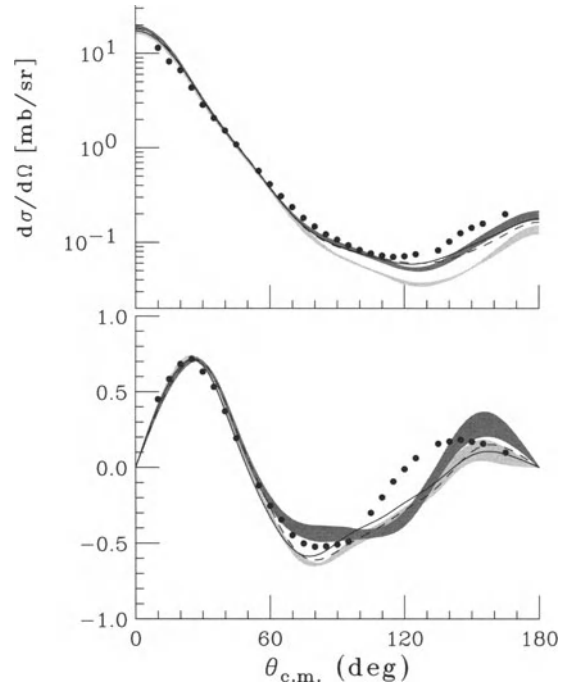

Fig. 2. The differential cross-section $d\sigma/d\Omega$ (top) and proton analyzing powers (bottom) of elastic pd scattering at $E_p = 250$ MeV. The light-shaded bands contain NN force predictions (AV18, CD-Bonn, Nijm I, II, and 93); the dark-shaded bands contain the NN + TM 3NF predictions. The solid and dashed lines are the AV18 + Urbana IX and CD-Bonn + TM′ predictions, respectively.

in the overall normalization was estimated to be 3% by comparing pp scattering data with calculations by the phase-shift analysis program code SAID.

Scattered protons or recoil deuterons in the pd scattering were momentum analyzed by the Grand Raiden spectrometer [15]. The layout of the system is shown in fig. 1. The LAS spectrometer was used to monitor the luminosity. The polarization transfer (PT) coefficients ($K_i^{j'}$) are defined by the following relation:

$$\begin{pmatrix} p'_{x'} \\ p'_{y'} \\ p'_{z'} \end{pmatrix} = \frac{1}{1 + p_y A_y} \times \left[\begin{pmatrix} 0 \\ P_{y'} \\ 0 \end{pmatrix} + \begin{pmatrix} K_x^{x'} & 0 & K_z^{x'} \\ 0 & K_y^{y'} & 0 \\ K_x^{z'} & 0 & K_z^{z'} \end{pmatrix} \cdot \begin{pmatrix} p_x \\ p_y \\ p_z \end{pmatrix} \right], \quad (1)$$

where p_i and $p'_{j'}$ (i or $j = x, y, z$) denote the polarization of the incident and scattered protons, respectively. The polarization of elastically scattered protons from CD_2 targets was measured by the FPP after momentum analysis in the Grand Raiden spectrometer (fig. 1). Detailed descriptions are found in ref. [16] about the procedures to measure the PT coefficients.

The experimental results for the differential cross-section ($d\sigma/d\Omega$), the vector analyzing power (A_y) and the PT coefficients ($K_x^{x'}$, $K_x^{z'}$, $K_z^{x'}$, $K_z^{z'}$, and $K_y^{y'}$) are shown in figs. 2 and 3. The quoted errors are statistical

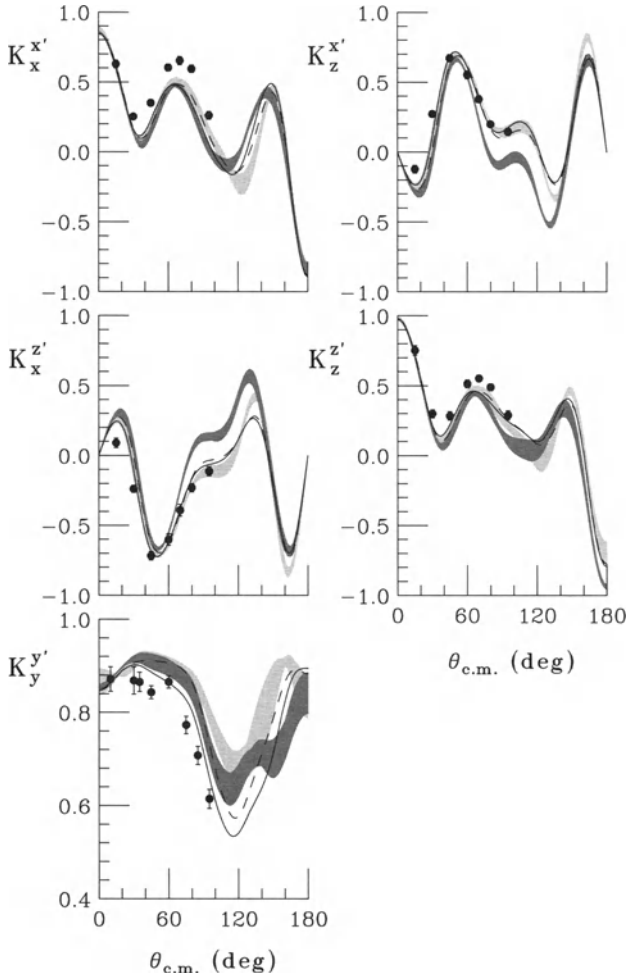

Fig. 3. Polarization transfer coefficients ($K_x^{x'}$, $K_x^{z'}$, $K_z^{x'}$, $K_z^{z'}$, and $K_y^{y'}$) of elastic pd scattering at $E_p = 250$ MeV. For the description of bands and lines see legend of fig. 2.

ones only. The overall uncertainty in the absolute normalization of the cross-section is estimated to be 3% from the calibration by the gaseous target measurements as previously described. There is also the relative uncertainty of 2.5% attributed to the inhomogeneity of CD_2 foils. The analyzing power has an uncertainty of 1% in the absolute normalization owing to the precise calibration of the beamline polarimeter in this experiment. The PT coefficients have an uncertainty of 2.5% in the normalization due to the uncertainty of the effective analyzing power of the FPP. For the PT coefficients, axes $\hat{i}$ and $\hat{j}'$ are defined in the laboratory scattering frame and $K_i^{j'}$ are plotted as function of the c.m. angles.

In the top panel of fig. 2, the measured differential cross-section is compared with rigorous Faddeev solutions by H. Kamada [17]. The various 2NF predictions are very similar and are depicted by a narrow band (light shaded), which reflects the small dependence on the particular NN interaction used. The inclusion of the TM 3NF (dark-shaded band) leads to a much better description at angles larger than 70°. This supports the claim of the clear evidence [7,8] of the 3NF from the systematic analysis of the energy dependence of the cross-section data. The inclusion of the TM′ (dashed curve) and the Urbana IX (solid curve) 3NF also leads to a good agreement to the data. However, discrepancies remain at angles larger than 120°. From the analysis of the dp data at the equivalent proton energy of 135 MeV [8], it has been shown that the TM 3NF and the Urbana IX 3NF provided a good description of the cross-section even at very backward angles.

In the bottom panel of fig. 2, we compare the experimental analyzing power A_y with different nuclear-force predictions. The differences (narrow light-shaded band) between the 2NF predictions are rather small at forward angles and become larger at backward angles. These predictions are in good agreement with the experimental data at forward angles, but deviate dramatically at backward angles larger than 60°. The experimental analyzing power A_y changes the sign at about 120°, while the calculations predict this change only around 140°. In the angular range 60°–120°, 2NF predictions are clearly larger in absolute value than experimental data. By including the TM 3NF (dark-shaded band) the agreement with the data becomes better in the minimum around $\theta_{c.m.} = 60°–100°$ but the discrepancies at more backward angles remain. This is again in contrast to the results for the deuteron vector analyzing power as shown in ref. [8], where predictions with the TM 3NF describe the data very well not only in the minimum but also at backward angles.

Our PT data are shown in fig. 3 together with theoretical predictions. The PT coefficients in the horizontal plane ($K_x^{x'}, K_x^{z'}, K_z^{x'}$, and $K_z^{z'}$) are reasonably well described by calculations with 2NF only (light-shaded bands). The inclusion of the TM 3NF (dark-shaded bands) rather deteriorates the agreement with the experimental data. The TM′ (dashed curves) and the Urbana IX (solid curves) 3NF do not have a large effect on these PT coefficients and give a reasonably good agreement with the data. In the case of the PT coefficient in the vertical plane ($K_y^{y'}$), the inclusion of the TM 3NF (dark-shaded band) and especially the Urbana IX 3NF (solid curve) give results in better agreement with the measurements. This is similar to the case of the analyzing power which is also a polarization observable in the vertical plane. Present measurements were limited to relatively forward angles $\theta_{c.m.} \leq 95°$. In fig. 3, large differences are observed between theoretical predictions with and without 3NFs at more backward angles for some PT coefficients. At angles larger than 100°, the energies of scattered protons are less than 120 MeV, where the present FPP at the Grand Raiden has a poor efficiency [16]. A low-energy FPP is now under development at the RCNP to enable measurements of proton polarization below 120 MeV.

At intermediate energies, our data are the first complete set of PT coefficients for pd elastic scattering covering a wide angular range and serve as a good testing ground of the investigation of the spin structure of 3NF and the effects of relativity. In order to offer further valuable sources of information, a rich spectrum of spin observables will be measured not only for elastic scattering

but also for the Nd breakup process. For both of them, large 3NF effects have been predicted at higher energies.

References

1. R.B. Wiringa *et al.*, Phys. Rev. C **51**, 38 (1995).
2. R. Machleidt *et al.*, Phys. Rev. C **53**, R1483 (1996).
3. V.G.J. Stoks *et al.*, Phys. Rev. C **49**, 2950 (1994).
4. S.A. Coon, M.T. Peña, Phys. Rev. C **48**, 2559 (1993).
5. B.S. Pudliner *et al.*, Phys. Rev. C **56**, 1720 (1997).
6. J. Fujita, H. Miyazawa, Prog. Theor. Phys. **17**, 360 (1957).
7. H. Witała *et al.*, Phys. Rev. Lett. **81**, 1183 (1998).
8. K. Sekiguchi *et al.*, Phys. Rev. C **65**, 034003 (2002).
9. E.J. Stephenson *et al.*, Phys. Rev. C **60**, 061001(R) (1999).
10. K. Ermisch *et al.*, Phys. Rev. Lett. **86**, 5862 (2001).
11. R.V. Cadman *et al.*, Phys. Rev. Lett. **86**, 967 (2001).
12. H. Rohdjeß *et al.*, Phys. Rev. C **57**, 2111 (1998).
13. K. Hatanaka *et al.*, Nucl. Instrum. Methods Phys. Res. A **384**, 575 (1997).
14. K. Hatanaka *et al.*, to be published in *IX Workshop on High Energy Spin Physiscs, Spin-01, Dubna, August 2-7, 2001* (The Bogoliubov Laboratory of Theoretical Physics, JINR).
15. M. Fujiwara *et al.*, Nucl. Instrum. Methods Phys. Res. A **422**, 484 (1999).
16. T. Kawabata *et al.*, Phys. Rev. C **65**, 064316 (2002).
17. H. Kamada, private communication.

Eur. Phys. J. A **18**, 297–299 (2003)
DOI 10.1140/epja/i2002-10220-8

THE EUROPEAN PHYSICAL JOURNAL A

Experiments on the search for the NN-decoupled NNπ-resonance d′

E. Doroshkevich[a], W. Brodowski, J. Pätzold, H. Clement, R. Meier, and G.J. Wagner

Physikalisches Institut, Universität Tübingen, Auf der Morgenstelle 14, 72076 Tübingen, Germany

Received: 30 September 2002 /
Published online: 22 October 2003 – © Società Italiana di Fisica / Springer-Verlag 2003

Abstract. The status on the search for NN-decoupled $NN\pi$-resonances is reviewed with regard to recent experimental searches in the pionic double-charge exchange in nuclei, the two-pion production in nucleon-nucleon collisions, the photo pion-production on the deuteron and the electro pion-production in nuclei.

PACS. 14.20.Gk Baryon resonances with $S = 0$ – 13.75.-n Hadron-induced low- and intermediate-energy reactions and scattering (energy $\leq$ 10 GeV) – 25.40.Ve Other reactions above meson production thresholds (energies 400 MeV)

1 Introduction

In QCD-inspired models a large number of dibaryon states of basic $6q$ structure have been predicted [1]. However, despite a vast number of dedicated experiments in search of such states not a single one could yet be identified unambiguously; for a review see, *e.g.*, [2]. In fact, dibaryons which by their quantum numbers can couple to the NN and/or $N\Delta$ channels cannot be expected to have narrow widths and hence should be hard to sense experimentally. But NN-decoupled dibaryon resonances may be rather narrow, if they are not far above the $NN\pi$ threshold. Indeed, such states at a mass as low as $m = 2.1$ GeV/c^2 with $I(J^P) = 0(0^-)$ and $0(2^-)$ have been predicted by Mulders *et al.* [1], though more recent theoretical work taking into account proper antisymmetrization [3] prefers the 0^- state to lie at a somewhat higher mass. Experimental studies for such dibaryon states were carried out in recent years in reactions of the pionic double-charge exchange (DCX) in nuclei, in π^0 photoproduction on the deuteron and in direct measurements of 3-particle final-state invariant-mass distributions.

2 Experiments

The measurements of the pionic DCX on nuclei $A(\pi^+, \pi^-)B$ exhibit at pion energies below the delta-resonance a peculiar resonance-like structure in the energy dependence of the forward-angle cross-section (fig. 1) [4–6]. This structure has peak cross-sections at incident energies of $T_\pi \approx$ 40–60 MeV, *i.e.* far below the Δ excitation. Assuming a narrow $NN\pi$-resonance, the so-called d', with $I(J^P)$ = even (0^-), $m \approx 2.06$ GeV/c^2 and $\Gamma_{NN\pi} \approx 0.5$, MeV the DCX data can be very well explained both in their energy and angular dependence.

However, since this reaction takes place in the nuclear medium, subtle medium effects cannot be excluded as origin of this structure. In fact, attempts have been made with some success to describe the observed resonance-like structures for specific nuclei by conventional models [7–9]. In order to minimize the effects of the nuclear medium, the DCX reaction has also been carried out on ^{3}He and ^{4}He [10]. However, in these cases there is no longer a bound nuclear state in the exit channel, and the process leads to the nuclear continuum only. Unfortunately, this situation leads to a much less conclusive signature of d' production, in particular, if collision damping of the d'-resonance with the neighboring nucleons is included [10].

The search for narrow isoscalar or isovector resonances, which couple to the γd channel has been carried out [11] at MAMI. Deviations $\Delta\sigma$ of the data for the total π^0 production cross-section from a smoothed fit of data is shown in fig. 2. In the range 2020 MeV/$c^2 < m <$ 2100 MeV/c^2, no narrow structures have been found on the 3σ level with upper limits in the range of a few microbarns for the production of isoscalar or isovector dibaryons. Yet, this limit is still an order of magnitude above the prediction for d' production [12] and hence not conclusive for this particular dibaryon candidate either.

The investigation of the $pp \to pp\pi^+\pi^-$ reaction should be a more sensitive test of the d' hypothesis, since both invariant-mass spectra $M_{pp\pi^+}$ and $M_{pp\pi^-}$ can be observed simultaneously and the cross-section of the conventional process is small. Exclusive measurements of the two-pion production in pp collisions have been carried out at CELSIUS at T_p = 725, 750 and 775 MeV using the

[a] e-mail: evd@pit.physik.uni-tuebingen.de

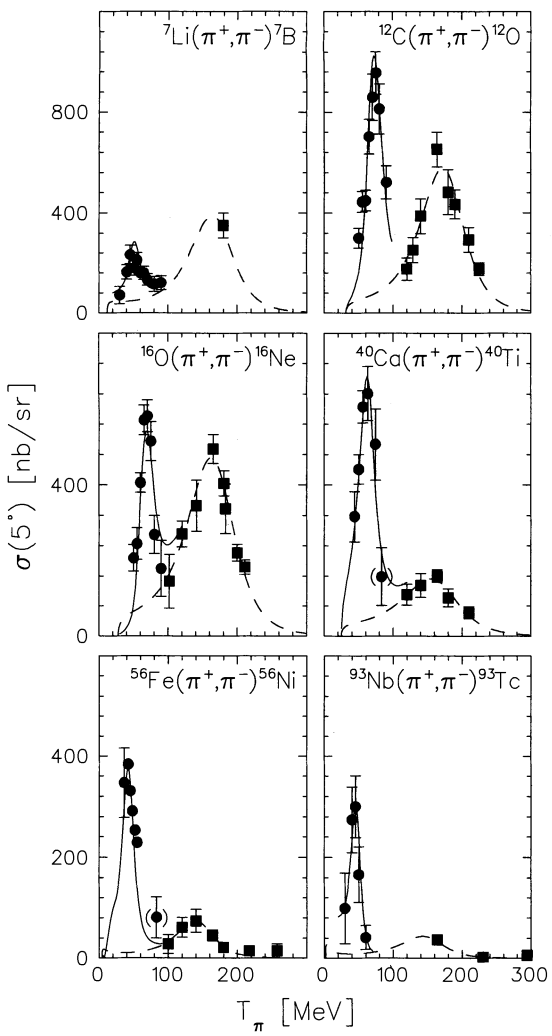

Fig. 1. Energy dependence of the forward-angle cross-section of the pionic DCX on nuclei. The solid lines show calculations assuming the formation of the hypothetical $NN\pi$-resonance d' interfering with the delta excitation (dashed lines) in this process. (from ref. [4]).

PROMICE/ WASA setup with a hydrogen cluster jet target [13]. For details of these measurements see refs. [14–18]. Since the decay of the hypothetical d'-resonance into $pp\pi^-$ is dominated by s-waves between outgoing particles, the two outgoing nucleons (*e.g.* two protons in the decay $d' \to pp\pi^-$) must be in the $^1S_0$-state. In this situation, the pp invariant-mass spectrum is strongly affected by the well-known Migdal-Watson–type final-state interaction (FSI) [19] leading to a considerable enhancement of the decay rate at small M_{pp}. In order to enhance the sensitivity to d' in $M_{pp\pi^-}$, a cut on small M_{pp} masses, $M_{pp} < 1896$ MeV/c^2, has been imposed. In the resulting spectra shown in fig. 3 no narrow structures of statistical significance in $M_{pp\pi^-}$ are observed with the possible exception of an enhancement at 2087 MeV/c^2 . Since this data bin is right at the high-energy end of the experimental acceptance range, where instrumental corrections are already substantial and not easily under control, any interpretation of this enhancement would be premature.

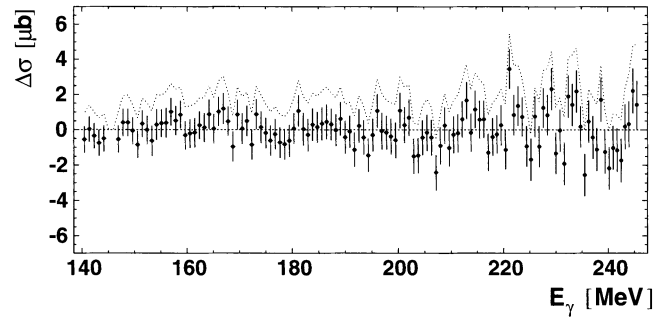

Fig. 2. Deviations $\Delta\sigma$ of the data for the total π^0 photoproduction cross-section on the deuteron. The deviations have been taken relative to a smoothed energy dependence fitted to the data. The dotted curve represents upper limits (90% C.L.) for underlying narrow structures averaged over the experimental energy resolution (from ref. [11]).

Its nature can only be solved by measurements at still higher energies. The upper limit (95% C.L.) for the production of narrow dibaryons is of the order $\sigma \lesssim 20$ nb for $m < 2087$ MeV/c^2. With respect to d', this upper limit is more than one order of magnitude below the theoretical prediction of $\sigma_{d'} \approx 300$–1000 nb [19,20].

We note in passing that in a preceding test run with much lower statistics a structure at 2.063 GeV/c^2 in $M_{pp\pi^-}$ had been observed [21] with a statistical significance of 2 to 3σ, depending on the treatment of background. At least part of this bump could meanwhile be associated to a previously unknown detector inefficiency [14–17]. We also note that in a measurement [22] of the same reaction at ITEP at $T_p = 920$ MeV a bump has been observed, too, near 2.06 GeV in $M_{pp\pi^-}$, if a cut on small M_{pp} masses was imposed. To our knowledge, no follow-up studies are under way at ITEP to resolve the nature of that bump.

Finally, there are so-called beamgas data from ARGUS at DESY at $E_e = 5$ GeV, which contain the electro pion-production on ^{16}O of the form $\gamma^*\ ^{16}\mathrm{O} \to pp\pi^\pm X$. From the measured four-momenta of protons and pions $M_{pp\pi^+}$ and $M_{pp\pi^-}$ spectra have been obtained [23] with and without a constraint on low M_{pp} masses. In both cases, the $M_{pp\pi^+}$ data are in accordance with phase space, whereas in $M_{pp\pi^-}$ a bump near 2.06 GeV is observed with a significance of about 4σ under both conditions. From analysis of the $M_{p\pi^-}$ spectrum an admixture of misidentified Λ particles as a possible reason for this bump can be excluded [23]. For the $M_{pp\pi^-}$ region of the observed bump the corresponding M_{pp} spectrum exhibits an anomalously large pp FSI, in particular in connection with $M_{p\pi^-}$ values around the Λ mass. These findings would be in accordance with what is expected in case of d' production [23]. We note that the $M_{pp\pi^-}$ spectra constructed from $pp\pi^-\pi^\pm$ and $pp\pi^-\pi^+\pi^+$ event samples do not show any enhancements near 2.06 GeV —again as expected in case of d' electro-production on a np pair, since in this case there is only single-pion production. π^0 particles were not identified, hence their possible accompanying production cannot be excluded.

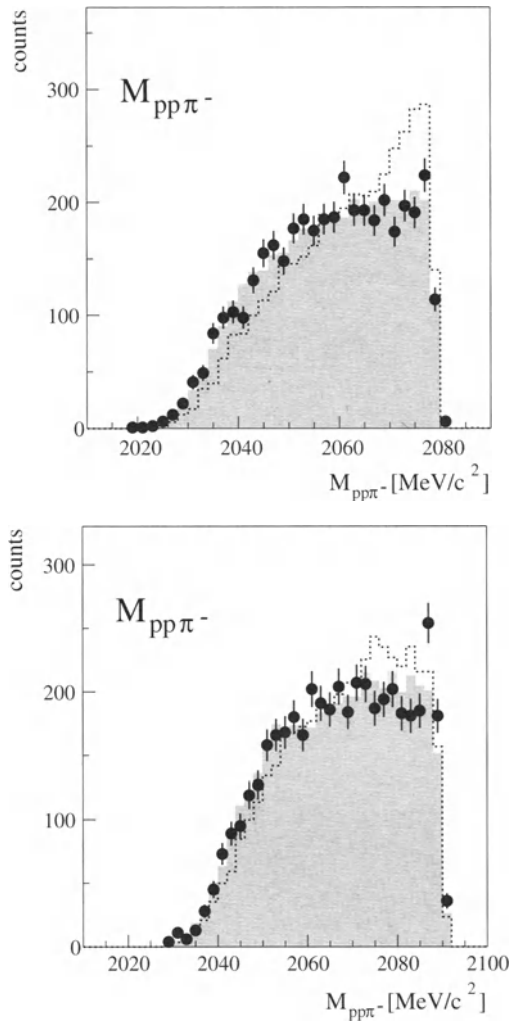

Fig. 3. Invariant mass spectra $M_{pp\pi^-}$ obtained from the exclusive measurements of the $pp \to pp\pi^+\pi^-$ reaction at $T_p = 750$ MeV (top) and $T_p = 775$ MeV (bottom). The spectra contain only events meeting the condition $M_{pp} < 1896$ MeV/c^2 (see text). The dotted lines represent a MC simulation assuming pure phase space for the reaction process, the shaded areas represent a model calculation, which quantitatively describes all differential cross-sections of the reaction (from ref. [14,15, 17]).

3 Conclusions

In recent years, high-statistics and high-resolution experiments have been carried out in search for a possible signature of d' in basic systems. In $\gamma d \to \pi^0 X$ and in $pp \to pp\pi^+\pi^-$ no narrow structures of statistical significance have been found. In the former reaction the deduced upper limits are still above the predicted d' production cross-sections; however, for the latter reaction they are below the predicted values by already one to two orders of magnitude.

Together with the findings on nuclei (DCX, $\gamma^*\ {}^{16}\mathrm{O} \to pp\pi^{\pm}X$) our results on the basic systems imply a number of consequences. Either d' does not exist at all, or its production cross-section in $pp \to pp\pi^+\pi^-$ is for some unknown reason much smaller than expected, or its mass outside the nuclear medium is above the mass range investigated so far, or it possibly exists only in the presence of the nuclear medium.

We acknowledge the support by BMBF (06 TU 987) and DFG (Europäisches Graduiertenkolleg 683).

References

1. See, *e.g.*, P.J. Mulders, A.T. Aerts, J.J. de Swart, Phys. Rev. Lett **40**, 1543 (1978); Phys. Rev. D **21**, 2653 (1980).
2. K.K. Seth, in *Proceedings of the International Workshop on Pions in Nuclei, Peniscola, Spain*, edited by E. Oset (World Scientific, 1992) p. 205 and references therein.
3. A.J. Buchmann, G. Wagner, A. Faessler, Phys. Rev. C **57**, 3340 (1998).
4. J. Draeger *et al.*, Phys. Rev. C **62**, 064615 (2000).
5. J. Pätzold *et al.*, Phys. Lett. B **428**, 18 (1998); **443**, 77 (1998).
6. R. Bilger *et al.*, Phys. Rev. Lett. **71**, 42 (1993); **72**, 2972 (1994); **79**, 3849 (1997).
7. M. Nuseirat *et al.*, Phys. Rev. C **58**, 2292 (1998).
8. H.C. Wu, W.R. Gibbs, Phys. Rev. C **62**, 044614 (2000).
9. Y. Liu, A. Faessler, J. Schwieger, A. Bobyk, J. Phys. G **24**, 1135 (1998).
10. J. Gräter *et al.*, Phys. Lett. B **471**, 113 (1999); **420**, 37 (1998); Phys. Rev. D **66**, 054606 (2002).
11. U. Siodlaczek *et al.*, Eur. Phys. J. A **9**, 309 (2000).
12. R. Bilger *et al.*, Nucl. Phys. A **596**, 586 (1996).
13. H. Calen *et al.*, Nucl. Instrum. Methods A **379**, 57 (1996).
14. W. Brodowski *et al.*, Phys. Lett. B **550**, 147 (2002), nucl-ex/0206020.
15. W. Brodowski *et al.*, Phys. Rev. Lett. **88**, 192301 (2002).
16. W. Brodowski, doctoral thesis, Universität Tübingen (2001).
17. J. Pätzold, doctoral thesis, Universität Tübingen (2002).
18. R. Bilger *et al.*, Prog. Part. Nucl. Phys. **36**, 379 (1996).
19. A.B. Migdal, Sov. Phys. JETP **28**, 3 (1955); K.M. Watson Phys. Rev. **88**, 1163 (1952); M. Schepkin, O. Zaboronsky, H. Clement, Z. Phys. A **345**, 407 (1993).
20. H. Clement *et al.*, Prog. Part. Nucl. Phys. **36**, 369 (1996).
21. W. Brodowski *et al.*, Z. Phys. A **355**, 5 (1996).
22. L. Vorobyev *et al.*, JETP Lett. **52**, 77 (1994).
23. E. Doroshkevich, status report, `www.pit.physik.uni-tuebingen.de/report.html`.

Eur. Phys. J. A **18**, 301–304 (2003)
DOI 10.1140/epja/i2002-10221-7

THE EUROPEAN PHYSICAL JOURNAL A

The Bethe-Salpeter equation and the Low Energy Theorems for πN scattering

I.R. Afnan[1,a] and A.D. Lahiff[2]

[1] School of Chemistry, Physics & Earth Sciences, Flinders University, GPO Box 2100, Adelaide 5001, Australia
[2] TRIUMF, 4004 Wesbrook Mall, Vancouver, BC, Canada V6T 2A3

Received: 30 September 2002 /
Published online: 22 October 2003 – © Società Italiana di Fisica / Springer-Verlag 2003

Abstract. The Bethe-Salpeter (BS) amplitude for πN scattering is evaluated at the off-mass-shell points corresponding to the Low Energy Theorems (LET) based on PCAC and current algebra. The results suggest a way of maintaining constructing between BS equation and LET.

PACS. 25.80.Dj Pion elastic scattering – 11.30.Rd Chiral symmetries – 24.80.+y Nuclear tests of fundamental interactions and symmetries

1 Introduction

The formulations of πN scattering can be divided into two approaches. On the one hand, we have the Effective Field Theory (EFT) approach where the emphasis is on preserving the symmetries of QCD. This is achieved by the expansion for the amplitude in powers of the pion mass or external momenta divided by a typical QCD cut-off of ≈ 1 GeV. For the πN system, the commonly used EFT is Chiral Perturbation Theory (ChPT) [1] which results in an off-mass-shell amplitude that is consistent with the Low Energy Theorems (LET). These LET are based on current algebra and PCAC. On the other hand, we have the more traditional approach of using the two-body scattering equation (*e.g.*, the Bethe-Salpeter equation) in which the potential is based on s-, t-, and u-channel pole diagrams derived from a chirally invariant Lagrangian. In this case, unitarity is the main uniting feature which allows the examination of πN scattering at higher energies.

2 The Bethe-Salpeter amplitude

With the advent of solutions to the Bethe-Salpeter (BS) equation for the off-mass-shell πN amplitude [2], it is now possible to compare the results of the traditional approach based on two-body scattering, with the LET. Here we will present solutions to the BS equation based on a potential derived from the chirally invariant Lagrangian [2]:

$$\begin{aligned}\mathcal{L}_{\rm int} = & \frac{g_{\pi NN}}{2m_N}\bar{\psi}_N\gamma_5\gamma^\mu\boldsymbol{\tau}\cdot\partial_\mu\boldsymbol{\pi}\psi_N \\ & +\frac{f_{\pi N\Delta}}{m_\pi}\bar{\psi}^\mu_\Delta(g_{\mu\nu}+x_\Delta\gamma_\mu\gamma_\nu)\boldsymbol{T}\psi_N\cdot\partial^\nu\boldsymbol{\pi}+\text{h.c.} \\ & +g_{\rho NN}\bar{\psi}_N\frac{1}{2}\boldsymbol{\tau}\cdot\left(\gamma^\mu\boldsymbol{\rho}_\mu+\frac{\kappa_\rho}{2m_N}\sigma^{\mu\nu}\partial_\mu\boldsymbol{\rho}_\nu\right)\psi_N \\ & +g_{\rho\pi\pi}\boldsymbol{\rho}_\mu\cdot(\partial^\mu\boldsymbol{\pi}\times\boldsymbol{\pi}) \\ & +g_{\sigma NN}\bar{\psi}_N\psi_N\sigma \\ & +\frac{g_{\sigma\pi\pi}}{2m_\pi}\sigma\partial_\mu\boldsymbol{\pi}\cdot\partial^\mu\boldsymbol{\pi}\,. \end{aligned} \tag{1}$$

The tree level diagrams that contribute to the potential include the s- and u-channel diagrams with nucleon and Δ poles, and t-channel diagrams with ρ and σ poles. To solve the four-dimensional BS equation, we have introduced form factors for each of the vertices in the Lagrangian. Here we considered two classes of form factors

$$f_{\alpha\beta\gamma}(p_\alpha^2,p_\beta^2,p_\gamma^2)=f_\alpha(p_\alpha^2)\,f_\beta(p_\beta^2)\,f_\gamma(p_\gamma^2)\quad\text{(type I)} \tag{2}$$

and

$$f_{\alpha\beta\gamma}(p_\alpha^2,p_\beta^2,p_\gamma^2)=f_\pi(p_\pi^2)\qquad\text{(type II)}\,, \tag{3}$$

where

$$f_\alpha(p_\alpha^2)=\left(\frac{\Lambda_\alpha^2-m_\alpha^2}{\Lambda_\alpha^2-p_\alpha^2}\right)^{n_\alpha}\,. \tag{4}$$

In the above, m_α and Λ_α are the mass and cut-off associated with the hadron α. The parameters in the Lagrangian are adjusted to fit the s- and p-wave scattering data up to pion laboratory energy of 300 MeV. In fig. 1 we present a

[a] e-mail: Iraj.Afnan@Flinders.edu.au

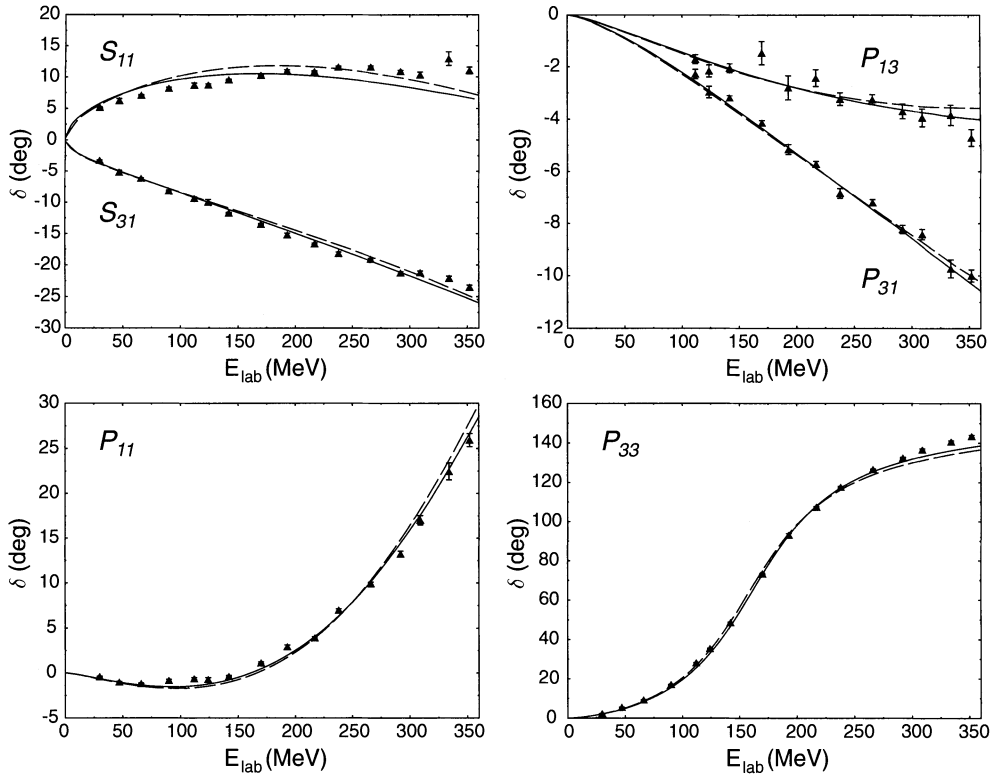

Fig. 1. The S and P wave phase shifts for the form factors type I (solid line) and II (dashed line), the data is SM95 [3].

fit to the data for the form factors type I and II ($n = 4$). Similar fits are achieved for the form factors II ($n = 2$) and II ($n = 10$). Here, the form factors determine the off-mass-shell behaviour of the BS amplitudes. In this way we can vary the off-mass-shell amplitudes when comparing the results of the BS equations with those based on current algebra and PCAC.

3 The Low Energy Theorems

The LET for πN scattering are based on current algebra and PCAC. The latter is implemented by defining the pion field, π^a, in terms of the derivative of the axial vector current, *i.e.* $\partial^\mu A^a_\mu = f_\pi m_\pi^2 \pi^a$. This allows us to write the πN amplitude in terms of the commutation relation of the currents. In this way we can use current algebra to determine the πN amplitude in the soft pion limit.

The πN amplitude with off-shell pion can be written as

$$T^{ab}_{\pi N} = \bar{u}(p') \left\{ T^{(+)}\delta_{ab} + \tfrac{1}{2}\left[\tau_a, \tau_b\right] T^{(-)} \right\} u(p) \ , \qquad (5)$$

where p (p') is the initial (final) on-shell nucleon momentum, and

$$T^{(\pm)} = D^{(\pm)} + \frac{i}{2m}\sigma^{\mu\nu} q_\mu q'_\nu B^{(\pm)} \ . \qquad (6)$$

Here the (+), (−) refer to isospin even and odd components of the amplitude, and q (q') are the off-mass-shell pion initial (final) momentum. The amplitudes D and B with the pion off mass shell are a function of ν, ν_B, q^2 and q'^2, *i.e.* $D^{(\pm)} = D^{(\pm)}(\nu, \nu_B, q^2, q'^2)$ with $\nu = \frac{1}{4m}(s-u)$ and ν_B being the value of ν at the s-channel nucleon pole, and s and u being the standard Mandelstam variables. Current algebra and PCAC can impose constraints on these off-mass-shell amplitudes. In particular, we can write the isospin even amplitude with the nucleon pole subtracted, *i.e.* $\tilde{D}^+(\nu, \nu_B, q^2, q'^2)$ at three off-shell points. The amplitude at Weinberg (W) [4], Adler (A) [5] and the Cheng-Dashen (CD) [6] points are

$$\tilde{D}^+(0,0,0,0) = -\frac{\sigma_{\pi N}(0)}{f_\pi^2} \ , \qquad (7)$$

$$\tilde{D}^+(0,0,m_\pi^2,0) = 0 = \tilde{D}^+(0,0,0,m_\pi^2) \ , \qquad (8)$$

$$\tilde{D}^+(0,0,m_\pi^2,m_\pi^2) = \frac{\sigma_{\pi N}(0)}{f_\pi^2} + \mathcal{O}(m_\pi^4) + \cdots \ , \qquad (9)$$

respectively. Here we observe that the amplitude at the Weinberg and Cheng-Dashen points are opposite in sign, while that at the Adler point is zero. Since the sigma-term $\sigma_{\pi N}(0)$ is a measure of chiral-symmetry breaking, *i.e.*

$$\sigma_{\pi N}(0) = \frac{1}{2}\sum_{a=1}^{3} \langle N(p)| \left[Q_a^5, [Q_a^5, H]\right] |N(p)\rangle \ , \qquad (10)$$

in the absence of any mechanism for chiral-symmetry breaking, the πN amplitude is zero at all three points.

Table 1. The coupling constants and masses for the optimum fit to the data for different choices for the form factors. All coupling constants are $g^2/4\pi$.

	I ($n=1$)	II ($n=2$)	II ($n=4$)	II ($n=10$)
$g^{(0)2}_{\pi NN}$	1.80	4.23	4.68	5.98
$f^{(0)2}_{\pi n\Delta}$	0.37	0.17	0.20	0.196
x_Δ	−0.11	−0.13	−0.24	−0.18
$g_{\rho NN}g_{\rho\pi\pi}$	2.88	2.67	2.63	2.80
κ_ρ	2.66	2.18	2.03	2.15
$g_{\sigma\pi\pi}g_{\sigma NN}$	−0.41	0.86	0.39	0.48
$m^{(0)}_N$	1.34	1.18	1.14	1.11
$m^{(0)}_\Delta$	2.305	1.495	1.492	1.435
m_σ	0.65	0.88	0.62	0.64
Λ^{R}_π	1.22	0.874	0.868	0.822
Δ_π	1.3%	2.47%	2.51%	2.79%

Table 2. The BS amplitude at the Adler [5], Weinberg [4] and Cheng-Dashen [6] points in units of m_π^{-1} for different form factors. Also included are the σ-term $\sigma_{\pi N}(0)$ and the isospin-even S-wave scattering length.

Model	A	W	CD	$\sigma_{\pi N}(0)$	a^+
I	0.366	0.355	0.379	23.8	−0.025
II ($n=2$)	0.0949	0.102	0.106	6.64	−0.05
II ($n=4$)	0.0411	0.0462	0.0494	3.10	−0.048
II ($n=10$)	0.0180	0.0218	0.0259	1.62	−0.049

4 Results

To examine the variation in the off-mass-shell BS amplitude when comparing with the results from the LET, we have considered four possible form factors for our potential. In table 1 we have the parameters that give the optimum fit to the data up to pion energy of 300 MeV for the form factor types I ($n=1$), II ($n=2$), and II ($n=4$) and II ($n=10$). Also included in the table are the equivalent cut off mass for a monopole Λ^{R}_π, and the difference in the form factor at the pion pole and at $q^2=0$, *i.e.* $\Delta_\pi = 1 - f^{\mathrm{R}}_\pi(0)$. Here, R refers to the fact that these quantities are calculated for the renormalised form factor. From the table we observe that the dressing of the nucleon and Δ is substantially more for type-I form factors than is the case for type-II form factors. At the same time the type-I form factors give a value for Δ_π that is closer to the commonly accepted value of 3% from the Goldberger-Treiman relation.

In table 2 we present the off-shell amplitude resulting from the solution of the BS equations at the Adler (A), Weinberg (W), and the Cheng-Dashen(CD) points for different choices for our form factor. Also included are the values for the πN σ-term $\sigma_{\pi N}(0)$ and the isospin even scattering length a^+. Here we observe that:

1. The off-mass-shell amplitude is sensitive to the choice of cut off form factor, and in particular, model I gives a larger σ-term than model II.
2. The amplitudes at the three off-mass-shell points are approximately the same. This is in contrast to the fact that the amplitudes at the Weinberg and Cheng-Dashen points are equal and opposite in sign.
3. Finally, the amplitude at the Adler point is not zero.

To understand the difference between the amplitude resulting from the solution of the BS equation and the LET, we first examined the Born amplitude for the πN potentials considered. Here we found that the Born amplitude at all three points is zero, consistent with the requirement of chiral-symmetry conservation. (The σ-term is a measure of chiral-symmetry breaking). This suggests that the higher terms in the multiple-scattering series give all the contribution to the amplitude at the three off-mass-shell points. To examine the source of this chiral-symmetry–breaking contribution, we have examined the contribution of each term in the potential to the amplitude at the Adler, Weinberg and Cheng-Dashen points. This exercise revealed that the source of chiral-symmetry breaking is the higher-order multiple-scattering t-channel ρ exchange. In particular, it is the $\rho\pi\pi$-term in the Lagrangian that gives rise to the symmetry breaking. Since this $\rho\pi\pi$ Lagrangian is of the form $g_{\rho\pi\pi}\,\boldsymbol{\rho}_\mu\cdot(\partial^\mu\boldsymbol{\pi}\times\boldsymbol{\pi})$, then the only time this term in the Lagrangian contributes to chiral-symmetry breaking is when the external pion is represented by $\boldsymbol{\pi}$ rather than $\partial^\mu\boldsymbol{\pi}$. It is possible to restore chiral symmetry to the amplitude by introducing a symmetric form for the coupling of the ρ to the π, *e.g.* $(\partial_\mu\rho_\nu-\partial_\nu\rho_\mu)\cdot(\partial^\mu\boldsymbol{\pi}\times\partial^\nu\boldsymbol{\pi})$ [7], which is equivalent on the mass shell to the form employed in the present calculation. The resultant amplitude would then satisfy chiral symmetry. Chiral-symmetry breaking could then be introduced in a controlled form via a non-derivative $\sigma\pi\pi$ coupling.

5 Conclusion

In the above analysis we have established that the Bethe-Salpeter amplitude for a Lagrangian that satisfies chiral symmetry is inconsistent with the Low Energy Theorems of current algebra. The source of the disagreement is the mode of chiral-symmetry breaking via the higher-order multiple scattering of t-channel ρ exchange. This could be overcome with the introduction of a symmetric $\rho\pi\pi$ Lagrangian, and a mode of chiral-symmetry breaking that is consistent with the LET.

The authors would like to thank the Australian Research Council for their financial support during the course of this work. The work of ADL was supported in part by a grant from the National Science and Engineering Research Council of Canada.

References

1. J. Gasser, H. Leutwyler, Ann. Phys. (N.Y.) **158**, 142 (1984); Nucl. Phys. B **250**, 465 (1985).
2. A.D. Lahiff, I.R. Afnan, Phys. Rev. C **60**, 024608 (1999).

3. R.A. Arndt, I.I. Strakovsky, R.L. Workman, M.M. Pavan, Phys. Rev. C **52**, 2120 (1995).
4. S. Weinberg, Phys. Rev. Lett. **17**, 616 (1966).
5. S. L. Adler, Phys. Rev. B **139**, 1638 (1965).
6. T.P. Cheng, R.F. Dashen, Phys. Rev. Lett. **26**, 594 (1971).
7. J. Wess, B. Zumino, Phys. Rev. **163**, 1727 (1967).

Eur. Phys. J. A **18**, 305–307 (2003)
DOI 10.1140/epja/i2002-10222-6

THE EUROPEAN PHYSICAL JOURNAL A

Exclusive and semi-inclusive strangeness and charm production in πN and NN reactions

A.M. Gasparyan[1,2,a], V.Yu. Grishina[3], L.A. Kondratyuk[1,2], and W. Cassing[4]

[1] IKP, Forschungszentrum Jülich, D-52425 Jülich, Germany
[2] Institute for Theoretical and Experimental Physics, B. Cheremushkinskaya 25, 117259 Moscow, Russia
[3] Institute for Nuclear Research, 60th October Anniversary Prospect 7A, 117312 Moscow, Russia
[4] Institute for Theoretical Physics, University of Giessen, Heinrich-Buff-Ring 16, D-35392 Giessen, Germany

Received: 30 September 2002 /
Published online: 22 October 2003 – © Società Italiana di Fisica / Springer-Verlag 2003

Abstract. Using the Quark-Gluon Strings Model (QGSM) combined with Regge phenomenology we consider the reactions $\pi^- p \to K^0 \Lambda$ and $\pi^- p \to D^- \Lambda_c^+$ which are dominated by the contributions of the K^* and D^* Regge trajectories, respectively. The spin structure of the amplitudes is described by introducing Reggeized Born terms. It is found that the existing data for the reaction $\pi^- p \to K^0 \Lambda$ are in reasonable agreement with the model predictions. To describe the absolute values of the cross-sections it is necessary to introduce also suppression factors which can be related to absorption corrections. Furthermore, assuming the $SU(4)$ symmetry to hold for Regge residues and the universality of absorption corrections we calculate the cross-section of the reaction $\pi^- p \to D^- \Lambda_c^+$. Employing the latter results from $\pi^- p$ reactions we then estimate the contributions of the pion exchange mechanism to the cross-sections of the reactions $NN \to NK\Lambda$ and $NN \to N\bar{D}\Lambda_c$ and compare them with the contributions of the K and D exchanges. We find that the NN reactions are dominated not by pion exchange but by K and D exchanges, respectively. Moreover, assuming the $SU(4)$ symmetry to hold approximately for the coupling constants $g_{ND\Lambda_c} = g_{NK\Lambda}$ we analyze also the production of leading Λ_c-hyperons in the reaction $NN \to \Lambda_c X$. It is shown that the non-perturbative mechanism should give an essential contribution to the Λ_c yield for $x \geq 0.5$.

PACS. 13.85.Fb Inelastic scattering: two-particle final states – 13.85.Hd Inelastic scattering: many-particle final states – 14.20.Lq Charmed baryons – 14.40.Lb Charmed mesons

Recently it has been argued [1] that the open-charm enhancement observed in nucleus-nucleus collisions [2] at the SPS might be due to secondary reaction mechanisms such as $\pi N \to \bar{D}\Lambda_c$ or $NN \to N\bar{D}\Lambda_c$. In this work we present estimates of these elementary cross-sections using the anology with strangeness production in πN and NN collisions. We consider also semi-inclusive Λ and Λ_c production in the reactions $NN \to NX\Lambda$ and $NN \to NX\Lambda_c$.

It is well known that the methods of perturbative QCD cannot be applied for a calculation of the cross-sections mentioned above especially at invariant energies closer to threshold. For the analysis of binary reactions we instead use the non-perturbative Quark-Gluon String Model [3] and for reactions with three particles in the final state we employ the meson exchange model taking into account the exchanges of the lowest meson states —pseudoscalar and vector.

The amplitudes for the reactions $\pi N \to K\Lambda$ and $\pi N \to D\Lambda_c$ are calculated using the Reggeized–Born-term approach (see, *e.g.*, refs. [4,5]) with contributions of K^* and D^* Regge trajectories, respectively. The parameters of the trajectories are taken from ref. [6], whereas for the coupling constants we assume $SU(4)$ symmetry, as suggested recently by Lin and Ko [7]. With these parameters the energy dependence of the total $\pi^- p \to K^+\Lambda$ cross-section (solid line in fig. 1) as well as the t-dependence of the differential $\pi^- p \to K^+\Lambda$ cross-section are described rather well, except for the region close to threshold where the dominant contribution stems from the well-established s- and p-wave resonances [8]. We note that to obtain the absolute value of the cross-section one has to introduce a suppression factor of ~ 0.4, which can be interpreted as an absorption correction. Assuming its universality we will introduce the same suppression factor for charm production, too. The resulting total cross-section of the reaction $\pi^- p \to D^- \Lambda_c^+$ is shown by the dashed line in fig. 1.

Our next step is to study NN reactions where we first apply our model to strangeness production. Using the method of Yao [9] one can express the π exchange cross-section for the reaction $pp \to pK^+\Lambda$ in terms of the $g_{NN\pi}$

[a] e-mail: g.achot@fz-juelich.de

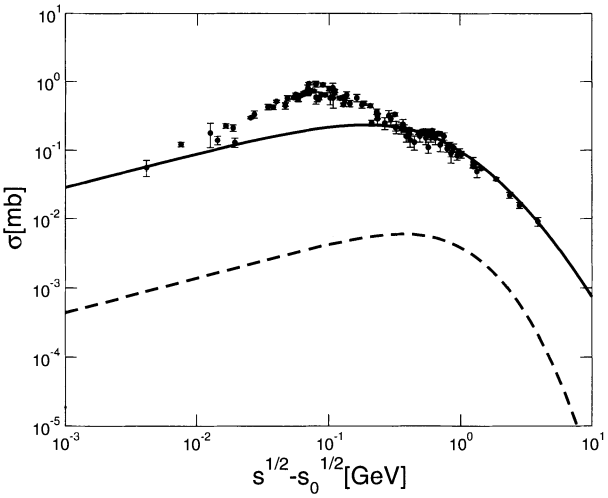

Fig. 1. Total cross-section for the reaction $\pi^- p \to K^+\Lambda$ (solid line) and $\pi^- p \to D^- \Lambda_c^+$ (dashed line) as a function of the invariant energy above thresholds in comparison to the data from ref. [10].

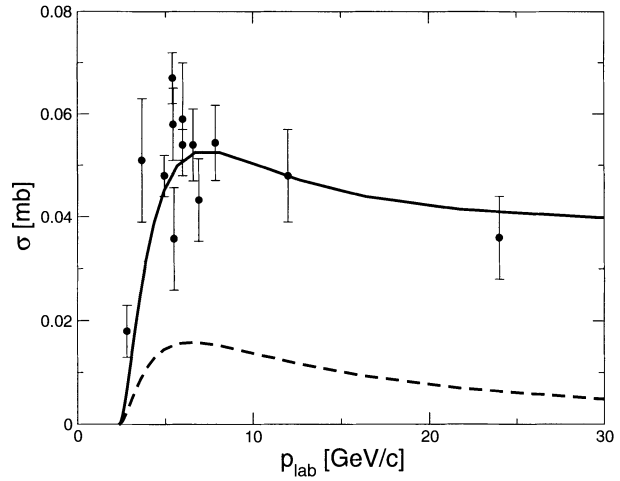

Fig. 2. The total cross-section for the reaction $pp \to K^+\Lambda p$ as a function of proton laboratory momentum $p_{\rm lab}$. The dashed line denotes the π exchange contribution, while the solid line corresponds to the K exchange with the cutoff $\Lambda_K = 1.0$ GeV.

coupling constant and the $\pi^0 p \to K^+\Lambda$ cross-section as

$$\sigma = \frac{g_{NN\pi}^2}{8\pi^2 p_i^2 s} \int_{W_{\min}}^{W_{\max}} k\, W^2\, \sigma(\pi^0 p \to K^+\Lambda, W)\, \mathrm{d}W \times \int_{t_{\min}(W)}^{t^{\max}(W)} F_\pi^4(t) \frac{1}{(t-m_\pi^2)^2}\, t\, \mathrm{d}t, \quad (1)$$

where W is the c.m. energy in the $K^+\Lambda$ subsystem and t is the 4-momentum transfer squared between the initial and final baryons. The form factor was chosen to be of the standard monopole type: $F_\pi(t) = (\Lambda_\pi^2 - m_\pi^2)/(\Lambda_\pi^2 - t)$ with $\Lambda_\pi = 1.3$ GeV. A similar expression —but with $\sigma(K^+p)$— can be written for the K exchange. For the K^+p elastic cross-section employed in this case we use the parametrization of Cugnon *et al.* [11].

The total cross-section of the reaction $pp \to K^+\Lambda p$ as a function of the laboratory momentum $p_{\rm lab}$ is shown in Fig. 2. The dashed and solid lines describe the π- and K exchange contributions, respectively, with the cutoff $\Lambda_K = 1.0$ GeV. An interesting observation is that the pion exchange contribution is substantially smaller than the K exchange and can be neglected especially at higher energies. The reason for that is a difference in the energy dependence of the elementary cross-sections: $\sigma(\pi^- p \to K\Lambda)$ falls off with energy, whereas $\sigma(K^+p)$ is almost constant since it is dominated by pomeron exchange. Moreover, the K exchange alone is able to reproduce the experimental data when choosing the cutoff $\Lambda_K = 1.0$ GeV.

We see that using the approach of Yao [9] we can express the cross-section for the reaction $pp \to K^+p\Lambda$ through the coupling constant $g_{K^+p\Lambda}$ and the elastic K^+p scattering cross-section $\sigma_{\rm el}(K^+p)$. Similarly, the cross-section for the leading-Λ production in the reaction $pp \to X\Lambda$ can be expressed through the same coupling constant and the total K^+p scattering cross-section $\sigma_{\rm tot}(K^+p)$.

As follows from fig. 2 the cross-section of the reaction $pp \to K^+p\Lambda$ is about 40–50 μb for $p_{\rm lab} \geq 5$ GeV/c. The ratio of the cross-sections $\sigma_{\rm tot}(K^+p)/\sigma_{\rm el}(K^+p) \simeq 7$–8. Thus we expect that the cross-section for semi-inclusive leading-Λ production in the reaction $pp \to X\Lambda$ via K exchange should be about $\sigma_{K\text{-exch}}(pp \to X\Lambda) \simeq 300$–400 μb. Furthermore, the ratio of the coupling constants $g_{K^*+p\Lambda}/g_{K+p\Lambda} \simeq 2$ [5], which implies that the contribution of the K^* exchange to the cross-section of the leading-Λ production might be ~ 4 times larger. Thus, we expect the cross-section for the semi-inclusive leading-Λ production to be about

$$\sigma_{K\text{-exch}}(pp \to X\Lambda) + \sigma_{K*\text{-exch}}(pp \to X\Lambda) \simeq 1.5\text{–}2\,\text{mb}.$$

We note that Erhan *et al.* [12] quote total cross-sections for the reaction $pp \to \Lambda + X$ of 4.4 ± 0.2 and 4.7 ± 0.2 mb at $\sqrt{s} = 53$ and 62 GeV, respectively. This comparison shows that the mechanism considered above gives a dominant contribution to the semi-inclusive leading-Λ production in the reaction $pp \to X\Lambda$.

Using the analogy of strangeness and charm production we can expect that the main contributions to the cross-sections of the reactions $NN \to \bar{D}_c(\bar{D}_c^*)\Lambda_c N$ come from the D_c and D_c^* exchanges, respectively. The coupling constants —involving a charm quark— can be related to the strange ones using $SU(4)$ symmetry, *i.e.* $g_{KN\Lambda} = g_{D_c N\Lambda_c}$ and $g_{K^*+N\Lambda} = g_{D_c^* N\Lambda_c}$. Within the approach of Yao [9] we then can express the cross-section of the reaction $pp \to \bar{D}_c^0 p\Lambda_c^+$ through the coupling constant $g_{\bar{D}_c^0 p\Lambda_c^+}$ and the elastic $\bar{D}_c^0 p$ scattering cross-section $\sigma_{\rm el}(\bar{D}_c^0 p)$. Similarly, the cross-section for the leading-Λ_c production in the reaction $pp \to X\Lambda_c$ can be expressed through the same coupling constant and the total $\bar{D}_c^0 p$ scattering cross-section $\sigma_{\rm tot}(\bar{D}_c^0 p)$.

In our calculations we assume $\sigma_{\rm el}(\bar{D}_c^0 p) = \sigma_{\rm el}(K^+p)$ and $\sigma_{\rm tot}(\bar{D}_c^0 p) = \sigma_{\rm tot}(K^+p)$, while the form factor is taken as

$$F_D(t) = \Lambda_D^2/(\Lambda_D^2 - t). \quad (2)$$

In fig. 3 we present the total cross-section for the reaction $pp \to \bar{D}_c^0 \Lambda_c^+ p$ as a function of the invariant energy

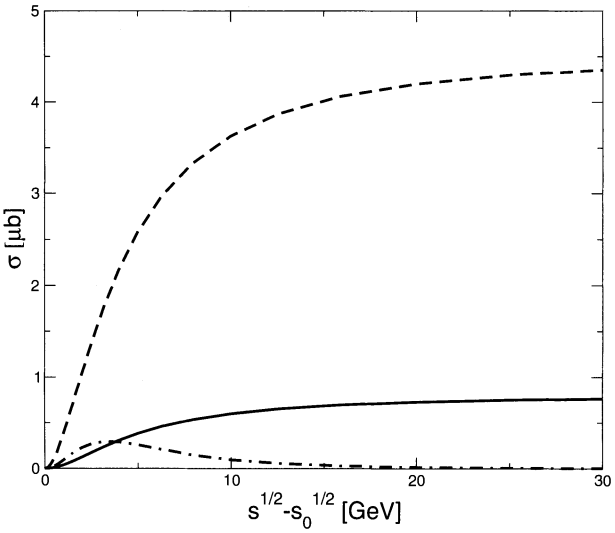

Fig. 3. The predicted total cross-section for the reaction $pp \to \bar{D}^0 \Lambda_c^+ p$ as a function of the invariant energy above threshold. The dash-dotted line denotes the contribution from the π exchange, while the solid line and the dashed line correspond to the D_c exchange with the cutoff $\Lambda_D = 1.0$ GeV and 1.5 GeV, respectively.

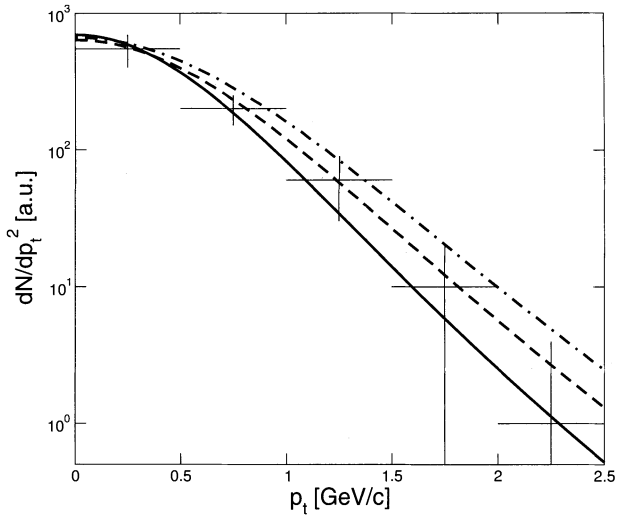

Fig. 4. The p_t dependence of the differential cross-section for the reaction $pp \to X\Lambda_c$ at $\sqrt{s} = 62$ GeV. The theoretical curves correspond to the differential cross-section $\mathrm{d}^2\sigma/\mathrm{d}p_t^2\mathrm{d}x$ calculated at $x = 0.9$ (where it peaks) for the cutoffs $\Lambda_D = 1.0$ GeV (solid line), $\Lambda_D = 1.3$ GeV (dashed line), $\Lambda_D = 1.5$ GeV (dash-dotted line). The results are normalized to the data from [14] at small transverse momentum p_t.

above threshold for $\Lambda_{D_c} = 1.5$ GeV (dashed line) and $\Lambda_{D_c} = 1.0$ GeV (solid line). The dash-dotted line denotes the contribution from the π exchange alone. Note that for the elementary reaction $\pi^0 p \to \bar{D}^0 \Lambda_c^+$ we use the amplitude calculated in the approach discussed above, while for the $\bar{D}^0 p$ cross-section we adopt a value corresponding to the asymptotic $K^+ p$ cross-section, *i.e.* ~ 3 mb, which is consistent with the values used in the literature (see, *e.g.*, [13]).

We find that the main contribution to the cross-section for the reaction $NN \to \bar{D}\Lambda_c N$ (a few GeV above threshold) comes from the D_c exchange which is much larger than the pion exchange for cutoff parameters $\Lambda_D \geq 1$ GeV.

To find restrictions on the cutoff parameter Λ_D in (2) we use the data from ref. [14] on semi-inclusive Λ_c production in the reaction $pp \to X\Lambda_c$. We assume now that the same D exchange mechanism also gives a large contribution to the semi-inclusive Λ_c production at x close to 1. (In fact, in our calculation the cross-section is peaked at $x \sim 0.9$.) Of course, in this case one has to insert the total $\bar{D}^0 p$ cross-section in the corresponding analog of eq. (1). As shown in fig. 4 the p_t dependence of the differential cross-section constrains Λ_D to 1–1.5 GeV.

To make a rough estimate of the absolute value of the D exchange contribution to the leading-Λ_c production in the reaction $pp \to X\Lambda_c$ we assume that the total $\bar{D}^0 p$ cross-section is the same as in case of $K^+ p$ scattering, *i.e.* ~ 20 mb. Then at c.m. energies larger than 10 GeV we obtain a cross-section of $\sim$ 10–40 μb depending on the choice of the cutoff. As in the case of strangeness production the contribution from D^* exchange might be approximately 4 times larger. Therefore, according to our estimates the cross-section of the semi-inclusive leading-Λ_c production at high energy should be as large as $\sim$ 50–200 μb. This estimate agrees with the experimental value of 40–200 μb at $\sqrt{s} = 62$ GeV quoted in ref. [14] which implies that the non-perturbative mechanism considered here gives an essential contribution to the leading-Λ_c production.

We finally note, that the same mechanism with D and D^* exchanges should provide a similar contribution to the open-charm production in $p\bar{p}$ collisions.

This work was supported by DFG, RFFI and Forschugszentrum Jülich.

References

1. W. Cassing, L.A. Kondratyuk, G.I. Lykasov, M.V. Rzjanin, Phys. Lett. B **513**, 1 (2001).
2. NA50 Collaboration (M.C. Abreu *et al.*), Eur. Phys. J. C **14**, 443 (2000).
3. A.B. Kaidalov, Z. Phys. C **12**, 63 (1982).
4. A.C. Irving, R.P. Worden, Phys. Rep. **34**, 117 (1977).
5. M. Guidal, J.-M. Laget, M. Vanderhaeghen, Nucl. Phys. A **627**, 645 (1997).
6. K.G. Boreskov, A.B. Kaidalov, Yad. Fiz. **37**, 174 (1983).
7. Z.W. Lin, C.M. Ko, J. Phys. G **27**, 617 (2001).
8. T. Feuster, U. Mosel, Phys. Rev. C **58**, 457 (1998).
9. T. Yao, Phys. Rev. **125**, 1048 (1961).
10. A. Baldini, V. Flaminio, W.G. Moorhead, D.R. Morrison and H. Schopper, *Total Cross-Sections for Reactions of High-Energy Particles, Landolt-Böernstein New Series*, Vol. **1/12** (Springer-Verlag, Berlin, Heidelberg, 1988) pp. 409.
11. J. Cugnon, P. Deneye, J. Vandermeulen, Phys. Rev. C **41**, 1701 (1990).
12. S. Erhan *et al.*, Phys. Lett. B **85**, 447 (1979).
13. W. Cassing, Y.S. Golubeva, L.A. Kondratyuk, Eur. Phys. J. A **7**, 279 (2000).
14. G. Bari *et al.*, Nuovo Cimento A **104**, 571 (1991).

Eur. Phys. J. A **18**, 309–312 (2003)
DOI 10.1140/epja/i2002-10223-5

THE EUROPEAN PHYSICAL JOURNAL A

Coupled-channel analysis of isoscalar f_0-mesons in $\bar{N}N$ annihilation and $\pi\pi$ scattering

T.S. Belozerova and V.K. Henner[a]

Perm State University, Perm, 614600, Russia

Received: 30 September 2002 /
Published online: 22 October 2003 – © Società Italiana di Fisica / Springer-Verlag 2003

Abstract. The properties of $f_0(980)$, $f_0(1370)$ and $f_0(1500)$ mesons are studied by means of a generalization of the Breit-Wigner approach preserving unitarity in case of several overlapping resonances.

PACS. 11.80.-m Relativistic scattering theory – 13.25.Jx Decays of other mesons – 13.75.Lb Meson-meson interactions – 14.40.Cs Other mesons with $S = C = 0$, mass < 2.5 GeV

1 Introduction

A goal of this work is to find the parameters of f_0-mesons using a method appropriate for broad overlapping resonances. The obvious advantage of the Breit-Wigner (BW) approach is that its parameters have a direct physical meaning. Simple BW parameterization is applicable only in case of well-separated resonances, far away from the channels' thresholds. In this generalization, the multichannel scattering amplitudes are sums of BW terms with relative phases that are not free parameters but determined by the unitarity relations. The partial and total widths may be energy dependent; they are approximately constant only if the resonances are far away from all thresholds.

We also show how to apply this BW method for production processes and use it to describe the f_0 states in $\bar{N}N$ annihilation.

2 Unitary BW S-matrix for overlapping resonances

In a previous work [1], we developed a generalization of the BW method applied to the problem of several resonances which could be strongly overlapping. This work also includes a comparison of different methods suitable for application to overlapping resonances. An approach has been to write down the S-matrix as a sum of resonance terms, and then to try to solve the constraints imposed by unitarity on the resonance parameters. The K-matrix method in which unitarity is satisfied is a common way used to describe experimental data. However, the "physical" states and the poles in the K-matrix formalism are not equivalent, the "physical" particles are more closely related to BW description. Thus, writing down the S-matrix as a sum of resonance terms with no redundant parameters could give a more direct way to extract the resonances parameters from data. Our purpose is to give an algebraic derivation of the unitarity constraints and their solutions for the BW approach. Having done this, the formalism can be applied to production reactions in which the overlapping resonances appear in the final states, together with another particle, or particles (in a similar manner to the K-matrix method [2]). Some features of our method are close to the approach of work [3].

For scalar mesons the threshold energy dependence is very important. In the development of work [1] the scattering matrix contains phase space factors, $\rho_k(E)$:

$$S(E) = I - i\sqrt{\rho(E)}\, T(E)\, \sqrt{\rho(E)}. \qquad (1)$$

Lets write $T(E)$ in a resonance form

$$T = \sum_{r=1}^{N} \frac{\boldsymbol{g}_r \boldsymbol{g}_r}{E - \varepsilon_r(E)}, \qquad T_{ij} = \sum_{r=1}^{N} \mathrm{e}^{i\varphi_{ij}^{(r)}} \frac{|g_{ir}|\ \ |g_{rj}|}{E - \varepsilon_r(E)},$$

where $\boldsymbol{g}_r \equiv \boldsymbol{g}_r^x + i\boldsymbol{g}_r^y$ are complex, energy-independent N-components vectors (N is the number of coupled channels), g_{ri} are coupling constants, $\varepsilon_r(E) \equiv \varepsilon_r^x(E) + i\varepsilon_r^y(E)$. The interference of the resonances with the same decay channels is the key aspect of any analysis and interpretation. In the BW approach this interference is often taken into account by relative phases in BW terms which are treated as free parameters, the most often just 0 or π. The results of analysis critically depend on the choice of this phase set. Whether or not these phases are included, such a sum of BW terms is depleted of unitarity which is the basic point in the BW description. In our approach, real energy-independent phases φ_{ri} are not free parameters but

[a] e-mail: henner@psu.ru

should be determined in such a way which preserves unitarity. The scattering matrix T is free of threshold singularities which are included in the diagonal $M \times M$ matrix $\rho(E)$ with the elements $\rho_k(E)$. Function $\rho_k(E)$ is imaginary below the k-th threshold, and real when $E \geq E_k$. (We use energy E rather than $s = E^2$ only in order to simplify some formulae.) A general way to include background is described in work [1] and in the case when it is elastic, formula (1) for S_{ij} should be multiplied by $e^{i(\delta_i^B + \delta_j^B)}$ (background phases can depend on energy).

To find the relations that should be imposed on the vectors $\boldsymbol{g}_r$ to keep the matrix S unitary and symmetric, we compose their imaginary parts through the real ones:

$$\boldsymbol{g}_r^y = u_{r1}\boldsymbol{g}_1^x + u_{r2}\boldsymbol{g}_2^x + ... + u_{rN}\boldsymbol{g}_N^x, \quad (r = 1, ..., N),$$

where $U = \{u_{rk}\}_{r,k=1}^N$ is a real antisymmetric matrix. Vectors $\boldsymbol{g}_r$ satisfy the relations

$$\sum_{k=1}^M \rho_k(E)\theta_k(E)\,|g_{rk}|^2 = -\frac{2}{S}[S + 2Q_r]\varepsilon_r^y,$$
$$\sum_{k=1}^M \rho_k\theta_k \mathrm{Re}(g_{qk}^* g_{rk}) = -\frac{2}{S}[F_{qr}(\varepsilon_q^x - \varepsilon_r^x) + G_{qr}(\varepsilon_q^y + \varepsilon_r^y)],$$
$$\sum_{k=1}^M \rho_k\theta_k \mathrm{Im}(g_{qk}^* g_{rk}) = -\frac{2}{S}[G_{qr}(\varepsilon_q^x - \varepsilon_r^x) - F_{qr}(\varepsilon_q^y + \varepsilon_r^y)].$$

Here $r = 1, ..., N$, $q = r + 1, ..., N$ and $\theta_k(E)$ is the step function: $\theta_k(E) = 0$, if $E < E_k$; $\theta_k(E) = 1$, if $E \geq E_k$. The (constant) coefficients S, Q_r, F_{qr} G_{qr} are determined via the elements of the coupling matrix U (see [1]).

Matrix U gives a measure of resonances overlap. If $|m_r - m_{r'}| \gg \Gamma_r + \Gamma_{r'}$, the matrix elements $u_{rk} \to 0$ and vectors $\boldsymbol{g}_r$ are getting real and orthogonal: $g_r = g_r^x$, $(\boldsymbol{g}_r\boldsymbol{g}_q) = 0$, thus we obtain an expression similar to Flatte's one-resonance formula [4]:

$$T_{ij} = \sum_{r=1}^N \frac{g_{ir}g_{rj}}{E - m_r + \frac{i}{2}\sum\limits_{k=1}^M \rho_k(g_{rk})^2}. \tag{2}$$

In the general case unitarity provides the expressions for energy-dependent masses and widths:

$$\Gamma_r(E) = -2\varepsilon_r^y(E) = \frac{S}{S + 2Q_r}\sum_{k=1}^M \rho_k(E)\theta_k(E)\,|g_{rk}|^2,$$
$$\varepsilon_r^x(E) = \varepsilon_1^x(E) + \frac{S}{2(F_{1r}^2 + G_{1r}^2)}\sum_{k=1}^M \rho_k(E)\theta_k(E)$$
$$\times\,[F_{1r}\mathrm{Re}(g_{1k}^* g_{rk}) + G_{1r}\mathrm{Im}(g_{1k}^* g_{rk})],$$
$$\varepsilon_1^x(E) = m_1 - i\,\frac{S}{2(S + 2Q_1)}\sum_{k=1}^M \rho_k(E)(1 - \theta_k(E))|g_{1k}|^2.$$

m_1 is the "bare" mass in the first BW term. For three resonances the coefficients in these formulae are:

$$S = 1 - \alpha^2 - \beta^2 - \gamma^2,$$
$$Q_1 = \alpha^2 + \beta^2, \qquad Q_2 = \alpha^2 + \gamma^2, \qquad Q_3 = \beta^2 + \gamma^2,$$
$$F_{12} = -\alpha, \qquad F_{13} = -\beta, \qquad F_{23} = -\gamma,$$
$$G_{12} = \beta\gamma, \qquad G_{13} = -\alpha\gamma, \qquad G_{23} = \alpha\beta.$$

Real parameters α, β, γ are the elements of the matrix

$$U = \begin{pmatrix} 0 & -\alpha & -\beta \\ \alpha & 0 & -\gamma \\ \beta & \gamma & 0 \end{pmatrix},$$

and are restricted by the relation $\alpha^2 + \beta^2 + \gamma^2 < 1$. The rest of the constraints on $\boldsymbol{g}_r$ are quadratic equations for each $k = 1, ..., M$.

It is simple to consider the slightly more general case in which g_{ir} is replaced by f_{pr}, where p (the production channel, $\bar{N}N$ in our case) does not occur in the sums in $\Gamma_r(E)$ and $\varepsilon_r(E)$. We would then have for the transition from the production state p to final state k

$$F_{pk} = \sum_{r=1}^N \frac{f_{pr}g_{rk}}{E - \varepsilon_r^x(E) + \frac{i}{2}\Gamma_r(E)} \tag{3}$$

Vectors $\boldsymbol{f}_r$ like vectors $\boldsymbol{g}_r$ are complex. The amplitudes F have the same poles as the amplitudes T.

The "running mass" $\varepsilon_r^x(E)$ is approximately constant only in case when all the resonances are far away from thresholds. The equation $E - \varepsilon_r^x(E) = 0$ gives the mass of the r-th resonance, m_r (generally it can have several roots, but for f_0 states we obtain one root for each r).

Branching ratios of the decay of the r-th resonance into the k-th channel are given by

$$B_{rk} = \frac{\Gamma_{rk}}{\Gamma_r} = \frac{\rho_k(m_r)\theta_k(m_r)\,|g_{rk}|^2}{\sum\limits_{k=1}^M \rho_k(m_r)\theta_k(m_r)\,|g_{rk}|^2}. \tag{4}$$

3 Analysis of $f_0(980)$, $f_0(1370)$, $f_0(1500)$ states

Similar to a number of other analyses, our model includes four channels: $\pi\pi$, $\bar{K}K$, $\eta\eta$, 4π. We do not include the $\eta\eta'$-channel due to lack of data. Phase state factors are:

$$\rho_k(s) = \sqrt{(s - s_k)/s},$$
$$s_1 = 4m_\pi^2, \qquad s_2 = 4m_K^2, \qquad s_3 = 4m_\eta^2,$$
$$\rho_4(s) = \sqrt{(s - s_4)/s}\,/\,(1 + \exp[\Lambda \cdot (s_0 - s)]),$$
$$s_4 = 16m_\pi^2, \qquad s_0 = 2.8\,(\mathrm{GeV}^{-2}), \qquad \Lambda = 3.5\,(\mathrm{GeV}^{-2}).$$

For ρ_4 we use the strongly energy-dependent 4π phase factor [5] that approximates either the $\rho\rho$ or $\sigma\sigma$ phase space. With a small change in the parameter s_0 one can assume that the 4π simulates all inelastic channels not included in our scheme directly.

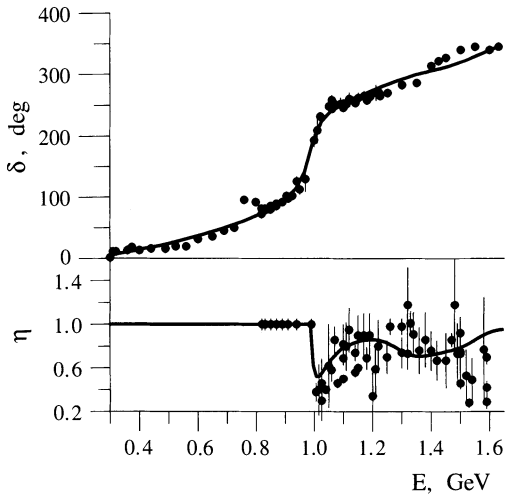

Fig. 1. Phase δ and inelasticity η for $I = J = 0$ $\pi\pi$ scattering. Experimental points are from [6].

Table 1. Branching ratios (in %) and relative to $f_{0.98}$ phases (in degrees).

State	$B_{f_{0.98}}$	$B_{f_{1.37}}$	$\varphi_{f_{1.37}}$	$B_{f_{1.50}}$	$\varphi_{f_{1.50}}$
$\pi\pi$	77.3	8.2	−28.9	4.0	28.4
$\bar{K}K$	20.8	5.8	−38.0	3.4	19.2
$\eta\eta$	1.9	52.7	68.2	57.8	16.6
4π	0.01	33.3	88.7	34.8	26.5

Figure 1 shows the $\pi\pi$ S-wave within the model including three f_0 states. Ignoring complications connected with identical pions in the final states, the formula which was used in a number of paper (see [7]) for the resonant mass spectra in the reactions $\bar{N}N \to (k)\pi^0$ can be written as

$$\frac{\mathrm{d}N_k}{\mathrm{d}m} = C_k\sqrt{\left[1-\frac{(m-m_\pi)^2}{4m_N^2}\right]\left[1-\frac{(m+m_\pi)^2}{4m_N^2}\right]}\frac{2m}{\pi} \times|\rho_k(m)F_{pk}(m)|^2,$$

where F_{pk} are the production amplitudes (3). The fit of some Crystal Barrel data is shown in figs. 2 and 3.

Masses and widths of f_0 states (in GeV) are

$$m_1 = 0.987, \quad m_2 = 1.356, \quad m_3 = 1.549,$$
$$\Gamma_1 = 0.117, \quad \Gamma_2 = 0.269, \quad \Gamma_3 = 0.151.$$

These numbers are compatible with previous findings [8]. Table 1 contains other parameters having physical meaning. The number of free parameters in the unitarized BW method is MN comparing to $N(M+1)$ in a naive BW (if we take a sum of terms (2)) and K-matrix methods. Here we use the "bare" mass m_1, coefficients α, β, γ, and 8 out of 12 real parts of vectors g_{ir} as free parameters. The fit of $\bar{N}N$ annihilation processes also requires N complex numbers f_{pr}. The $\pi\pi$ background phase shift is a linear function of energy and is about 90° near $\bar{K}K$ threshold.

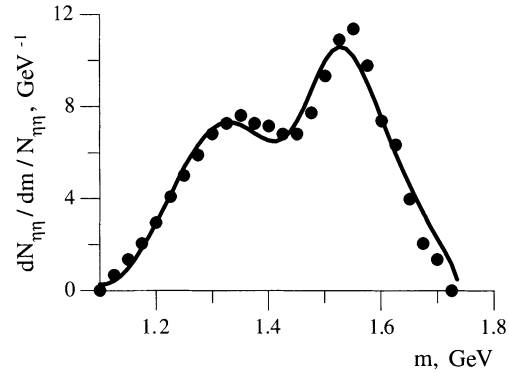

Fig. 2. Normalized $\eta\eta$ mass spectra in $\bar{p}p \to (\eta\eta)\pi^0$ at rest. The data are from [9].

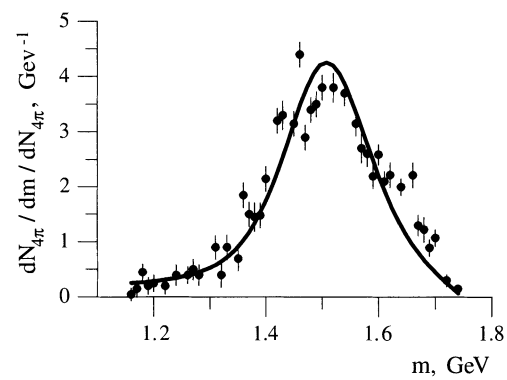

Fig. 3. Normalized $4\pi^0$ mass spectra in $\bar{N}N \to (4\pi^0)\pi^0$ at rest. The data are from [10].

4 Conclusion

We present a scheme of unitarization of a sum of BW terms which can be useful to the study of several overlapping resonances within the same partial wave. The resulting formula (1) resembles a traditional sum of BW terms with the relative phases that are not free parameters but are determined from the unitarity constraints.

We apply this approach to the analysis of the scalar f_0-mesons in the $\pi\pi$ scattering and $\bar{N}N$ annihilation at rest. The results show that $f_0(1370)$ and $f_0(1500)$ states strongly interfere. This stresses the necessity to use unitary description. Masses and widths of these states are compatible with previous findings. In a model with four coupled channels, the main decay modes for $f_0(1370)$ and $f_0(1500)$ are $\eta\eta$ and 4π, while the $\pi\pi$ and $\bar{K}K$ decays are suppressed.

References

1. T.S. Belozerova, V.K. Henner, Phys. Part. Nucl. **29**, 63 (1998); Yad. Fiz. **60**, 1998 (1997); **61**, 127 (1998).
2. I.J.R. Aitchison, Nucl. Phys. A **189**, 417 (1972).
3. N.A. Tornqvist, Z. Phys. C **68**, 647 (1995).
4. S.M. Flatte, Phys. Lett. B **63**, 228 (1976).

5. D.V. Bugg, A.V. Sarantsev, B.S. Zou, Nucl. Phys. B **471**, 59 (1996).
6. B. Hyams, *et al.*, Nucl. Phys. B **100**, 205 (1975).
7. N.N. Achasov, G.N. Shestakov, Phys. Rev. D **53**, 3539 (1996), and references therein.
8. D.E. Groom, *et al.*, Eur. Phys. J. C **15**, 1 (2000).
9. V.V. Anisovich, *et al.*, Phys. Lett. B **323**, 233 (1994).
10. A. Abele, *et al.*, Eur. Phys. J. C **19**, 667 (2001); A. Lanaro, Nucl. Phys. A **558**, 13c (1993); A. Adamo *et al.*, Phys. Lett. B **287**, 368 (1992).

Eur. Phys. J. A **18**, 313–315 (2003)
DOI 10.1140/epja/i2002-10224-4

THE EUROPEAN PHYSICAL JOURNAL A

Probing the deuteron structure at small N-N distances by cumulative pion production

A.Yu. Illarionov[a], A.G. Litvinenko, and G.I. Lykasov

Joint Institute for Nuclear Research, 141980 Dubna, Moscow Region, Russia

Received: 30 September 2002 /
Published online: 22 October 2003 – © Società Italiana di Fisica / Springer-Verlag 2003

Abstract. The fragmentation of deuterons into pions emitted forward in the kinematic region forbidden for free nucleon-nucleon collisions is analyzed. It is shown that the inclusion of the non-nucleonic degrees of freedom in a deuteron results in a satisfactory description of the data for the inclusive pion spectrum and improves the description of the data about T_{20}. According to the data, T_{20} has very small positive values, less than 0.2, which contradicts the theoretical calculations ignoring these degrees of freedom.

PACS. 24.70.+s Polarization phenomena in reactions – 25.10.+s Nuclear reactions involving few-nucleon systems

The investigation of polarization phenomena by deuteron fragmentation at intermediate and high energies in the kinematic region forbidden for hadron emission by free N-N scattering has recently become very topical. These are the so-called cumulative processes.

Cumulative proton production in the collision of polarized deuterons with the target results in information about the deuteron spin structure at small inter-nuclear distances. This can be seen from the experimental and theoretical study of deuteron fragmentation into protons at a zero angle (see [1] and references therein). The theoretical analysis of this reaction has shown that the tensor analyzing power T_{20} and the polarization transfer coefficient κ are more sensitive to the deuteron wave function (DWF), particularly to the reaction mechanism, than the inclusive spectrum. At present, not a single DWF relativistic form can describe T_{20} measured by $Dp \to pX$ stripping at light-cone variable $x \geq 1.7$. On the other hand, the inclusion of the reaction mechanism, namely the impulse approximation and the secondary interaction of the produced hadrons, can describe both the inclusive spectrum and T_{20} at $x \leq 1.7$ using only the nucleonic degrees of freedom [1]. Among other things this phenomenon can be due to the fact that the deuteron structure at a high ($>$ 0.20 GeV/c) internal momentum (short inter-nuclear distances $<$ 1 fm) is determined by non-nucleonic degrees of freedom. The inclusion of non-nucleonic degrees of freedom, (it can be a six-quark state, $\Delta\Delta$, $NN^\star$, $NN\pi$ and other states in the deuteron) allowed one to describe the data on the inclusive proton spectrum at $x \geq 1.7$ [1].

If we try to study the manifestation of non-nucleonic degrees of freedom, it is natural to investigate the cumulative production of different hadrons having different quark contents. Interesting experimental data on T_{20} in the reaction $Dp \to \pi X$, where the pion is emitted forward, have been published recently [2]. These data are presented as a function of the so-called cumulative scaling variable x_C ("cumulative number") [3]. (The value of x_C corresponds to the minimum mass, in nucleon mass units, of the part of the projectile nucleus (deuteron) involved in the reaction. Values of $x_C \sim x$ larger than 1 correspond to cumulative pions.) It was found a very small, approximately constant, value of the tensor analyzing power T_{20} for the deuteron fragmentation into pions $Dp \to \pi X$ at $x_C \geq 1$.

In recent papers [4,5] we have investigated the reaction of deuteron fragmentation into pions within the framework of the relativistic impulse approximation. The mechanism of this reaction is mainly an impulse approximation as the secondary interaction or the final-state interaction is very small and can be neglected [6]. The main goal was to describe this reaction in a consistent relativistic approach using a nucleon model of the deuteron. A fully covariant expression for all quantities was obtained within the Bethe-Salpeter formalism. In this way we have obtained general conclusions about the amplitude of the process, which cannot be drawn in the non-relativistic approach. The main investigation results can be summarized as follows: I) It was evident from the behavior of the inclusive pion spectrum and particularly the tensor analyzing power T_{20} at large x_C, that the relativistic effects are sizeable. However, the state of theory is such that the unique procedure to include relativistic effects in the deuteron has not been found yet. An extreme sensitivity to different

[a] e-mail: Alexei.Illarionov@jinr.ru

methods of the relativistic deuteron wave function was found for T_{20} at $x_C \geq 1$. It was shown that the inclusion of the $\mathcal{P}$-wave contribution to the DWF within the Bethe-Salpeter approaches [7,8] results in a better (but not satisfactory) description of the data over the cumulative region. II) It was demonstrated a large sensitivity of the inclusive spectrum of pions to the vertex of the $NN \to \pi X$ subprocess. In contrast to this, a small sensitivity of T_{20} to this vertex was found. This polarization observable is very sensitive to the DWF form, that can be used for systematic investigation of the DWF. III) For the deuteron fragmentation into protons emitted forward, the tensor analyzing power T_{20} is not described by standard nuclear physics using the nucleonic degrees of freedom at $x_C \geq 1.7$ [1]. On the contrary, T_{20} for the fragmentation $Dp \to \pi X$ cannot be described within the same assumptions over the whole region $x_C \geq 1$ [4].

In this paper we try to include the non-nucleonic degrees of freedom within the approach suggested in [1,9], the use of which has reproduced the data for the proton spectrum in the deuteron stripping rather well.

We consider the inclusive reaction of deuteron fragmentation into a pion, $\vec{D} + p \to \pi(0^\circ) + X$, for the polarized deuteron and pion emitted forward at initial energies of order few GeV. If the initial deuteron is only tensor aligned due to their p_D^{ZZ} component, the inclusive spectrum of this reaction can be written in the form

$$\rho_{pD}^{\pi}\left(p_D^{ZZ}\right) = \rho_{pD}^{\pi}\left[1 + A_{ZZ}\, p_D^{ZZ}\right], \qquad (1)$$

where $\rho_{pD}^{\pi} \equiv \varepsilon_\pi \;\; \mathrm{d}\sigma_{pD}^{\pi}/\mathrm{d}^3 p_\pi$ is the inclusive spectrum for the case of unpolarized deuterons and $A_{ZZ} \equiv \sqrt{2}T_{20}$ $(-\sqrt{2} \leq T_{20} \leq 1/\sqrt{2})$ is the tensor analyzing power. In the relativistic impulse approximation they can be written in a fully covariant manner within the Bethe-Salpeter formalism [4]:

$$\rho_{pD}^{\pi} = \frac{1}{(2\pi)^3} \int \frac{\sqrt{\lambda(p,n)}}{\sqrt{\lambda(p,D)}} \left[\rho_{pN}^{\pi} \cdot \Phi^{(u)}(|\boldsymbol{q}|)\right] \frac{m^2 \mathrm{d}^3 q}{E_{\boldsymbol{q}}}, \qquad (2)$$

$$\rho_{pD}^{\pi}\, \mathrm{A}_{ZZ} = -\frac{1}{(2\pi)^3} \int \frac{\sqrt{\lambda(p,n)}}{\sqrt{\lambda(p,D)}} \times \left[\rho_{pN}^{\pi} \cdot \Phi^{(t)}(|\boldsymbol{q}|)\right] \left(\frac{3\cos^2\vartheta_{\boldsymbol{q}} - 1}{2}\right) \frac{m^2 \mathrm{d}^3 q}{E_{\boldsymbol{q}}}, \qquad (3)$$

where $\lambda(p_1, p_2) \equiv (p_1 p_2)^2 - m_1^2 m_2^2 = \lambda(s_{12}, m_1^2, m_2^2)/4$ is the flux factor; p, n are the four-momenta of the proton-target and intra-deuteron nucleon, respectively; ρ_{pN}^{π} is the relativistic invariant inclusive spectrum of pions arising from the interaction of the intra-deuteron nucleon with the target proton. The functions $\Phi^{(u)}(|\boldsymbol{q}|)$ and $\Phi^{(t)}(|\boldsymbol{q}|)$ depend on the relative momentum $q = n - D/2$ and contain full information about the structure of deuteron with one on-shell nucleon [4].

According to [10], large momenta of nucleons are due to few-nucleon correlations in the nucleus. Then the deuteron structure can be described by assuming quark degrees of freedom [11,12]. On the other hand, the shape of the high momentum tail of the nucleon distribution in

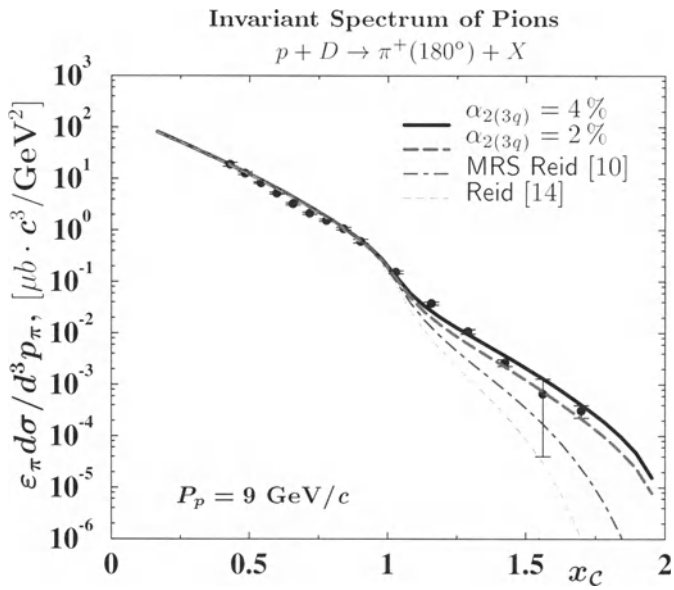

Fig. 1. The invariant pion spectrum calculated within the relativistic impulse approximation where non-nucleonic components in the DWF [1,9] have been included; its probability $\alpha_{2(3q)}$ is 0.02–0.04 (long-dashed and solid curves, respectively). One can have a good description of the data [13] for all x_C.

the deuteron can be constructed on the basis of its true Regge asymptotic at $x \to 2$ [9], and the corresponding parameters can be found from the good description of the inclusive proton spectrum in the deuteron fragmentation $Dp \to pX$ [9]. According to [1,9], one can write the following form for $\widetilde{\Phi}^{(u)}(|\boldsymbol{q}|)$:

$$\Phi^{(u)}(|\boldsymbol{q}|) = \frac{E_{\boldsymbol{k}}/E_{\boldsymbol{q}}}{2(1-x)} \widetilde{\Phi}^{(u)}(|\boldsymbol{k}|), \qquad (4)$$

where

$$\widetilde{\Phi}^{(u)}(|\boldsymbol{k}|) = N_D^{-1} \frac{M_D^2}{m^2} \Big[(1 - \alpha_{2(3q)}) \left(U^2(|\boldsymbol{k}|) + W^2(|\boldsymbol{k}|)\right) + \alpha_{2(3q)} \frac{8\pi x(1-x)}{E_{\boldsymbol{k}}} G_{2(3q)}(x, \boldsymbol{k}_\perp)\Big], \qquad (5)$$

where $(x, \boldsymbol{k}_\perp)$ are the light-cone variables [10] and $\boldsymbol{k}^2 = (m^2 + \boldsymbol{k}_\perp^2)/(4x(1-x)) - m^2$. The normalization factor $N_D^{-1} = \pi\sqrt{2/M_D}$ is chosen according to the non-relativistic normalization DWF [4]. The parameter $\alpha_{2(3q)}$ is the probability for a non-nucleonic component in the deuteron which is a state of two colorless $(3q)$ systems:

$$G_{2(3q)}(x, \boldsymbol{k}_\perp) = \frac{b^2}{2\pi} \frac{\Gamma(A+B+2)}{\Gamma(A+1)\Gamma(B+1)} x^A (1-x)^B \mathrm{e}^{-b|\boldsymbol{k}_\perp|} \qquad (6)$$

Figure 1 presents the invariant pion spectrum calculated within the relativistic impulse approximation including the non-nucleonic component in the DWF [1,9]; its probability $\alpha_{2(3q)}$ is 0.02–0.04 (long-dashed and solid curves, respectively). One can see that the inclusion of the non-nucleonic degrees of freedom within the approach suggested in [1,9], the use of which has reproduced the data for the proton spectrum in the deuteron stripping, allows

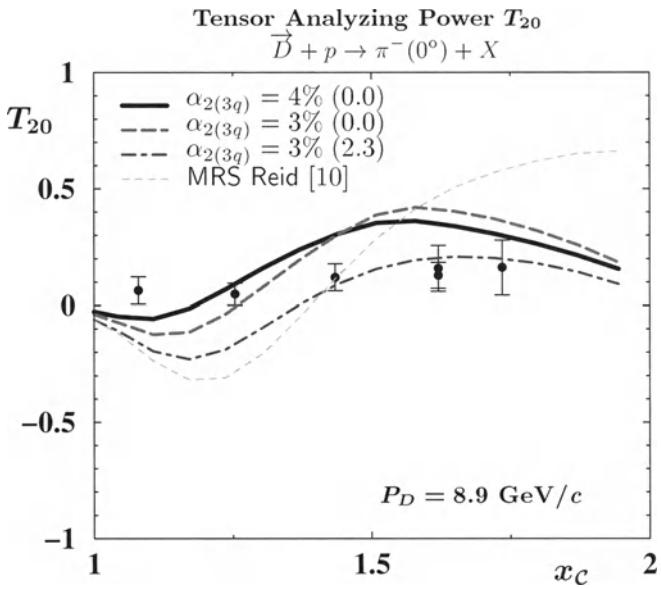

Fig. 2. The tensor analyzing power T_{20} calculated within the relativistic impulse approximation allowing for non-nucleonic components in the DWF. The solid and long-dashed lines represent the calculations with the mixing parameter $a = 0.0$ and the probability $\alpha_{2(3q)} = 4\,\%, 3\,\%$, respectively. The dot-dashed line corresponds to the calculation with the mixing parameter $a = 2.3$, which gives the curve closest to the data at $x_C \geq 1.5$. The thin dashed curve corresponds to the Reid DWF [14] obtained by the minimal relativistic scheme (MRS) [10].

us also to describe the inclusive pion spectrum at all values of x_C rather well (fig. 1). However, the information contained in both observables is redundant, since it is the same deuteron properties that are the main ingredient in the analysis of both $Dp \to pX$ and $Dp \to \pi X$ reactions in the impulse approximation. Therefore, the calculation of the tensor analyzing power including the non-nucleonic degrees of freedom in the fragmentation of the deuteron into pions can give us new independent information about the deuteron structure at small N-N distances and its comparison with the data can be considered as a test of the modified DWF model used. Actually, in [9] only a form of $\widetilde{\Phi}^{(u)}(|\boldsymbol{k}|)$ has been constructed. However, to calculate T_{20} it is not enough, the corresponding orbital waves have to be known. Let us assume that non-nucleonic degrees of freedom result in the main contribution to the $\mathcal{S}$ and $\mathcal{D}$ waves of the deuteron wave function. Constructing new forms of these waves by including the non-nucleonic degrees of freedom we have to require that the square of the new DWF be equal to the one determined by eq. (5). Introducing a mixing parameter $\alpha = \pi a/4$ one can find the following forms of new $\mathcal{S}$ and $\mathcal{D}$ waves

$$\widetilde{U}(|\boldsymbol{k}|) = \sqrt{1-\alpha_{2(3q)}}U(|\boldsymbol{k}|) + \cos(\alpha)\Delta(|\boldsymbol{k}|)\,, \quad (7)$$

$$\widetilde{W}(|\boldsymbol{k}|) = \sqrt{1-\alpha_{2(3q)}}W(|\boldsymbol{k}|) + \sin(\alpha)\Delta(|\boldsymbol{k}|)\,, \quad (8)$$

where the function $\Delta(|\boldsymbol{k}|)$ has been obtained from the equation

$$\widetilde{\Phi}^{(u)}(|\boldsymbol{k}|) \;=\; N_D^{-1}\frac{M_D^2}{m^2}\Big[\widetilde{U}^2(|\boldsymbol{k}|) + \widetilde{W}^2(|\boldsymbol{k}|)\Big]\,. \quad (9)$$

Figure 2 presents the analyzing power T_{20} calculated by using the functions $\widetilde{U}, \widetilde{W}$ including the non-nucleonic components in the DWF, according to [1,9]. It is evident from fig. 2 that the inclusion of non-nucleonic components in the DWF improves the description of the data for T_{20} at $x_C > 1$. The best description of the observable is obtained for the value $a = 2.3$ of the parameter a entering into eqs. (7), (8).

The main results can be summarized as follows. Very interesting experimental data on T_{20} [2] showing approximately zero values at $x_C \geq 1$ are not reproduced by a theoretical calculus using even different kinds of the relativistic DWF [4]. This may indicate the possible existence of non-nucleonic degrees of freedom or a basically new mechanism of pion production in the kinematic region forbidden for free N-N scattering.

The inclusion of the non-nucleonic degrees of freedom within the approach suggested in [1,9] allows us to describe experimental data about the inclusive pion spectrum at all the values of x_C rather well, fig. 1, and improve the description of data [2] concerning the analyzing power T_{20} in the fragmentation of the deuteron into pions, fig. 2. Of course, the inclusion of the non-nucleonic degrees of freedom in the analysis of T_{20} is approximate, but can be considered as the indication of an important role of these degrees of freedom in studying polarization phenomena in the type of reactions considered.

A.Yu.I. is grateful to the Organizers of the International Conference on Quark Nuclear Physics 2002 for the kind invitation and financial support towards the participation.

References

1. G.I. Lykasov, Phys. Part. Nucl. **24**, 59 (1993).
2. S. Afanasev *et al.*, Phys. Lett. B **445**, 14 (1998), JINR-E2-98-319.
3. V.S. Stavinsky, Fiz. Elem. Chastits. At. Yadra **10**, 949 (1979).
4. A. Yu. Illarionov, A.G. Litvinenko, G.I. Lykasov, Eur. Phys. J. A **14**, 247 (2002), hep-ph/0007358.
5. A. Yu. Illarionov, A.G. Litvinenko, G.I. Lykasov, Czech. J. Phys., Suppl. A **51**, A307 (2001), hep-ph/0012290.
6. N.S. Amelin, G.I. Lykasov, Sov. J. Nucl. Phys. **33**, 100 (1981).
7. R. Gilman, F. Gross, J. Phys. G **28**, R37 (Apr. 2002), nucl-th/0111015.
8. A.Y. Umnikov, Z. Phys. A **357**, 333 (1997), hep-ph/9605292.
9. A.V. Efremov, A.B. Kaidalov, V.T. Kim, G.I. Lykasov, N.V. Slavin, Sov. J. Nucl. Phys. **47**, 868 (1988).
10. L.L. Frankfurt, M.I. Strikman, Phys. Rep. **76**, 215 (1981).
11. V.K. Lukyanov, A.I. Titov, Fiz. Elem. Chastits. At. Yadra **10**, 815 (1979).
12. V.V. Burov, V.K. Lukyanov, A.I. Titov, Fiz. Elem. Chastits. At. Yadra **15**, 1249 (1984).
13. A.M. Baldin, Nucl. Phys. A **434**, 695 (1985).
14. R.V. Reid, jr., Ann. Phys. (N.Y.) **50**, 411 (1968).

Eur. Phys. J. A **18**, 317–319 (2003)
DOI 10.1140/epja/i2002-10225-3

THE EUROPEAN PHYSICAL JOURNAL A

Short-range NN properties in the processes pd → dp and pd → (pp)n

Yu.N. Uzikov[1,2,a], V.I. Komarov[2], F. Rathmann[3], and H. Seyfarth[3]

[1] Kazakh National University, 480078 Almaty, Kazakhstan
[2] Laboratory of Nuclear Problems, Joint Institute for Nuclear Research, Dubna, 141980 Russia
[3] Institut für Kernphysik, Forschungszentrum Jülich, 52425 Jülich, Germany

Received: 30 September 2002 /
Published online: 22 October 2003 – © Società Italiana di Fisica / Springer-Verlag 2003

Abstract. The data from the first measurement, performed at ANKE/COSY, of the unpolarized cross-section of the reaction $pd \to (pp)n$ in the kinematics of backward elastic $pd \to dp$ scattering at proton beam energies between 0.6 and 1.9 GeV are analyzed in a phenomenological approach. The $pd \to (pp)n$ data and the triplet cross-section of the reaction $pd \to (pn)p$, calculated from the $pd \to dp$ data on the basis of the Fäldt-Wilkin extrapolation, are used here to derive the ratio ζ of the singlet production matrix element squared to the triplet one. This ratio, defined in our earlier analysis of $pd \to (pn)p$ data in a largely model-independent way, depends on the dynamics of the pd interaction. We find here $\zeta \approx 0.02$ and show that the smallness of this value may point toward softness of the deuteron at short NN distances.

PACS. 13.75.Cs Nucleon-nucleon interactions (including antinucleons, deuterons, etc.) – 25.10.+s Nuclear reactions involving few-nucleon systems

1 Introduction

The structure of the lightest nuclei at short distances in the nucleon overlap region $r_{NN} < 0.5$ fm, *i.e.* at high relative momenta $q_{NN} \sim 1/r_{NN} > 0.4$ GeV/c between the nucleons, is a fundamental problem of nuclear physics. The structure can be tested by electromagnetic probes at high transferred momenta. However, a self-consistent picture of electro- and photo-nuclear processes is not yet developed due to the unknown strength of the meson exchange currents. Hadron-nucleus collisions can give important independent information. The theoretical analysis of hadron processes is complicated by initial- and final-state interactions and the excitation/de-excitation of nucleons in intermediate states. For instance, a large contribution of the double pN scattering with excitation of the $\Delta(1232)$-resonance was found in proton-deuteron backward elastic scattering $pd \to dp$ at ~ 0.5 GeV [1–5]. At higher beam energies the role of heavier baryon resonances is expected to increase. Unfortunately, these contributions are not well controlled in theory due to the rather poor information about the $pN \rightleftharpoons NN^*$and $pN \rightleftharpoons N\Delta$ amplitudes. To some extent these effects are taken into account in the one-pion exchange (OPE) model [1] with a virtual subprocess $pp \to d\pi^+$, but another important contribution, *i.e.* the one-nucleon exchange (ONE) amplitude, cannot be included in this model.

To minimize these complicating effects, it was proposed [6] to study the deuteron breakup reaction $pd \to (pp)n$ in the kinematics of backward elastic pd scattering. For low excitation energies $E_{pp} \leq 3$ MeV, the final pp pair can be assumed to be in the $^1S_0$ spin singlet (isotriplet) state. This feature, in contrast to the $pd \to dp$ process, results in a considerable suppression of the Δ- (and N^*-) excitation amplitudes by the isospin factor 1/3 in comparison with the one-nucleon exchange (ONE). Recently it was shown [7] that the same suppression factor acts for a broad class of diagrams with isovector meson-nucleon rescattering in the intermediate state including the excitation of any baryon resonance. Furthermore, the node in the half-off-shell $pp(^1S_0)$ scattering amplitude at the off-shell momentum $q \sim 0.4$ GeV/c results in remarkable irregularities in the spin observables and leads to a dip in the unpolarized cross-section for the ONE mechanism [6, 8]. In the $pd \to dp$ and $pd \to pX$ processes, the node in the deuteron S-wave is hidden by the large contribution of the D-wave. The irregularities of the observables allow new studies of i) the commonly used potentials of the NN interaction at short distances and ii) possible contributions from N^*-exchanges [9] and exotic three-baryon states [2].

The first data on the reaction $pd \to (pp)n$ at high beam energies $T_p = 0.6$–1.9 GeV with forward emission of a fast

[a] e-mail: uzikov@nusun.jinr.ru

proton pair of low excitation energy E_{pp} were obtained at ANKE/COSY [10]. Using a largely model-independent approach based on the Migdal-Watson and the Fäldt-Wilkin FSI theory, we discuss the relative strength of the measured singlet in comparison to the triplet channel. We present also the results of a calculation of the deuteron breakup cross-section performed within the main mechanisms of the $pd \to dp$ process [5].

2 The FSI theory

At excitation energies around 1 MeV, the $pd \to (pn)p$ cross-section is strongly influenced by the np FSI. The resulting peak is well described by the Migdal-Watson formulae [11,12] which take into account the nearby poles in the FSI triplet (t) and singlet (s) pn-scattering amplitudes:

$$\mathrm{d}\sigma_{s,t} = \mathrm{FSI}_{s,t}(k^2)\, K\, |A_{s,t}|^2. \tag{1}$$

Here $A_{s,t}$ is the production matrix element for the singlet and triplet state, K is the kinematical factor, and $\mathrm{FSI}_{s,t}$ is the Goldberger-Watson factor [12]:

$$\mathrm{FSI}_{s,t}(k^2) = \frac{k^2 + \beta_{s,t}^2}{k^2 + \alpha_{s,t}^2}. \tag{2}$$

Here k is the relative momentum in the pn system at the excitation energy $E_{np} = k^2/m$, where m is the nucleon mass. The parameters α and β are determined by the known properties of the on-shell NN scattering amplitudes at low energies: $\alpha_t = 0.232\,\mathrm{fm}^{-1}$, $\alpha_s = -0.04\,\mathrm{fm}^{-1}$, $\beta_t = 0.91\,\mathrm{fm}^{-1}$, $\beta_s = 0.79\,\mathrm{fm}^{-1}$ [13]. Information on the $pd \to pnp$ mechanism and the off-shell properties of the NN system is contained in the matrix elements $A_{s,t}$ and their ratio [14]:

$$\zeta = \frac{|A_s|^2}{|A_t|^2}. \tag{3}$$

The $pd \to (pp)n$ data, obtained at ANKE/COSY [10], are presented as cms cross-sections

$$\overline{\frac{\mathrm{d}\sigma}{\mathrm{d}\Omega_n}} = \frac{1}{\Delta\Omega_n}\int_0^{E_{\max}} \mathrm{d}E_{pp} \int\int m \frac{\mathrm{d}^3\sigma}{\mathrm{d}k^2\mathrm{d}\Omega_n}\mathrm{d}\Omega_n, \tag{4}$$

integrated over E_{pp} from 0 to 3 MeV and averaged over the neutron cms angle $\theta_n^* = 172° - 180°$, where

$$\frac{\mathrm{d}^3\sigma}{\mathrm{d}k^2\mathrm{d}\Omega_n} = \frac{1}{(4\pi)^5}\frac{p_n}{p_i}\frac{k}{s\sqrt{m^2+k^2}}\frac{1}{2}\int\int \mathrm{d}\Omega_{\mathbf{k}}\overline{|M_{fi}|^2} \tag{5}$$

and $\Delta\Omega_n$ is the neutron solid angle. In eq. (5) p_i and p_n are the cms momenta of the incident proton and the final neutron, respectively; M_{fi} is the full matrix element of the reaction. Due to the isospin invariance the following relation holds in the singlet cannel

$$\frac{\mathrm{d}\sigma}{\mathrm{d}\Omega^*}(pd \to (np)_s p) = \frac{1}{2}\frac{\mathrm{d}\sigma}{\mathrm{d}\Omega^*}(pd \to (pp)_s n). \tag{6}$$

Using the Fäldt-Wilkin extrapolation [15] for the bound and the scattering S-wave functions in the triplet state at short pn distances $r < 1$ fm, and taking into account the short-range character of the interaction mechanism, the triplet cross-section $pd \to (pn)_t n$ is obtained as

$$\frac{\mathrm{d}\sigma_t}{\mathrm{d}\Omega^*} = \frac{p_f}{p_i} f^2(k^2)\frac{\mathrm{d}\sigma}{\mathrm{d}\Omega^*}(pd \to dp), \tag{7}$$

where

$$f^2(k^2) = \frac{2\pi\, m}{\alpha_t(k^2 + \alpha_t^2)} \tag{8}$$

and $\mathrm{d}\sigma/\mathrm{d}\Omega^*$ is the $pd \to pd$ cms cross-section. After integration over E_{pp} the triplet cross-section (7) takes the form

$$\overline{\frac{\mathrm{d}\sigma_t}{\mathrm{d}\Omega^*}} = \frac{p_f}{p_i} Z \frac{\mathrm{d}\sigma}{\mathrm{d}\Omega^*}(pd \to dp), \tag{9}$$

where

$$Z = \frac{1}{2\pi}\frac{2}{\alpha_t}\left\{k_{\max} - \alpha_t \arctan\left(\frac{k_{\max}}{\alpha_t}\right)\right\}. \tag{10}$$

On the other side, the triplet (t) and singlet (s) cross-sections can be obtained by integration of eq. (1) over E_{pp}. K, $|A_s|^2$, and $|A_t|^2$, being very smooth functions of E_{pp}, can be assumed as constant. A ratio of the integrals $R = y_s/y_t$ can be defined, where

$$y_{s,t} = \int_0^{k_{\max}^2} \mathrm{FSI}_{s,t}(k)\, k\, \mathrm{d}k^2. \tag{11}$$

With this ratio one finally gets the singlet-to-triplet ratio ζ defined by eq. (3) as

$$\zeta = \frac{1}{2\,R\,Z}\frac{\frac{\mathrm{d}\sigma}{\mathrm{d}\Omega^*}(pd \to (pp)_s n)}{\frac{\mathrm{d}\sigma}{\mathrm{d}\Omega^*}(pd \to dp)}. \tag{12}$$

It is obvious that ζ is not a direct ratio of the $pd \to (pp)n$ and $pd \to dp$ cross-sections, but contains also the additional factor $1/(2\,R\,Z)$.

3 Results and discussion

For the numerical calculations of ζ, defined by eq. (12), we use the experimental data on the $pd \to dp$ cross-section [16] and the new ANKE/COSY data for the $pd \to (pp)n$ reaction [10]. From eqs. (2) and (11) and with the values for α_i and β_i, given above, we get $Z = 0.101$ and $R = 2.29$ for $E_{pp}^{\max} = 3$ MeV. With these numbers and assuming systematic uncertainties of 10% for both the $pd \to dp$ cross-section and the Fäldt-Wilkin ratio (7), we obtain $\zeta = (2.3 \pm 0.5)\%$ for 0.6, $\zeta = (1.6 \pm 0.3)\%$ for 0.7, and $\zeta = (2.1 \pm 1.2)\%$ for 1.9 GeV beam energy. We find the surprising fact that ζ is constant within the errors over the whole investigated beam energy range from 0.6 to 1.9 GeV.

The present, model-independent small result for ζ can be compared with $\zeta < 5\%$, obtained recently [14] for the $pd \to (pn)p$ reaction data, measured exclusively at 585 MeV and cms angle $\theta^* = 92°$ [17]. A similar, small value for the singlet admixture of a few percent was found

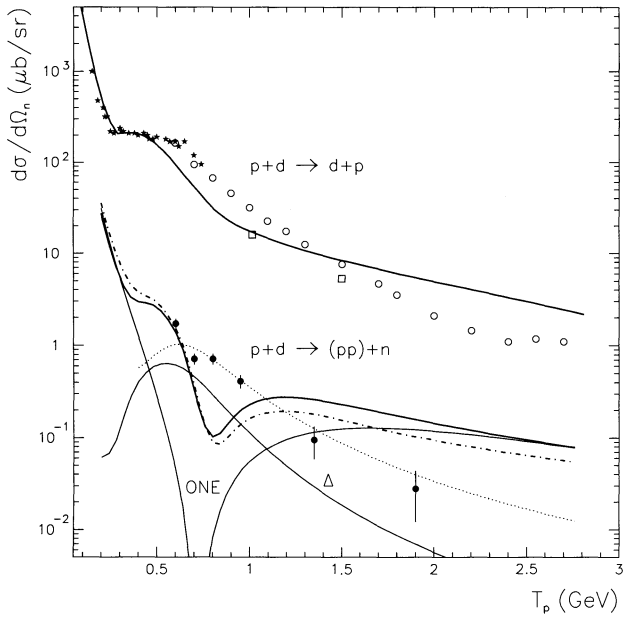

Fig. 1. Experimental cross-section of the reactions $pd \to dp$ [16] and $pd \to (pp)n$ [10] as a function of the beam energy in comparison with ONE + SS + Δ model calculations (thick full lines) using the RSC potential with cutoff momentum $\Lambda_\pi = 0.53$ GeV/c in the πNN and $\pi N\Delta$ vertices [4]. Inclusion of rescattering in the initial and final states, taken into account within the ONE(DWBA) + SS + Δ model [8], yields the dash-dotted line. The dotted line results from a calculation using only the Δ mechanism with cutoff momentum $\Lambda_\pi = 0.7$ GeV/c.

for the reaction $pp \to pn\pi^+$ in the FSI region at beam energies of 492 MeV [18] and 800 MeV [19], too. The smallness of the singlet contribution in the Δ-region of the reaction $pd \to (pn)p$ can be explained by dominance of the OPE mechanism with the subprocess $pp \to (pn)_s\pi^+$ [14].

The singlet-to-triplet ratio can be estimated as $\zeta_{th} = R_S \times R_I \times R_X$. Here $R_S = 1/3$ is the spin statistical factor. The isospin ratio R_I is 1 for the ONE and 1/9 for both the Δ mechanism and the vector meson-nucleon exchanges [7]. R_X is the ratio of the spatial singlet and triplet amplitudes. For the Δ mechanism, it reflects the difference of the $^1S_0$ and $^3S_1$ wave functions at $r < 1$ fm. Since ζ, according to eqs. (1) and (2), does not contain the FSI factor, R_X is ≈ 1 for the Δ amplitude. For the ONE it is ≈ 0.5 due to the contribution of the D-wave in the triplet and its absence in the singlet state. The calculation using eqs. (5) and (4) with the Reid-Soft-Core (RSC) NN potential [20] gives $\zeta_{\rm ONE} = 5$–8% for $T_p = 1.4$–1.9 GeV for the ONE which is 3 to 4 times the experimental value. For the Δ mechanism this ratio $\zeta_\Delta = R_S \times R_I = 1/27$ is in better agreement with the experimental value.

Calculations [4,8] with use of the RSC NN potential and the ONE + SS + Δ model [2,5], including single pN scattering (SS), describe the $pd \to (pp)n$ cross-section data for the beam energies 0.6 and 0.7 GeV, as is seen in fig. 1. In this region the Δ mechanism dominates due to the nearby minimum of the ONE cross-section. At higher energies the strong disagreement with the data is obvious. The data show no indication of the dip around 0.8 GeV, and for $T_p > 1.3$ GeV they are by a factor 2 to 4 below the prediction. A very similar discrepancy is observed for $pd \to dp$ backward elastic scattering, as can be seen from the upper part of fig. 1. Both the earlier $pd \to dp$ and the recent $pd \to (pp)n$ data show that in the until now used model the contribution by the ONE, dominating for $T_p > 1.3$ GeV, is too strong. On the other side, a calculation, using only the Δ mechanism with a cutoff momentum $\Lambda_\pi = 0.7$ GeV/c allows one to describe the $pd \to (pp)n$ data for $T_p > 0.7$ GeV. This mechanism does not involve such high-momentum components of the NN wave function as the ONE. A possible conclusion would be that the deuteron and the $pp(^1S_0)$ system at short NN distances are softer than modeled by the RSC NN potential. As one should note, the assumption about softness of the deuteron at short NN distances is supported by i) a rather successful description of the $pd \to dp$ cross-section within the OPE model only [21,5], and ii) the strong disagreement between the ONE calculations and the T_{20} data [22]. Detailed analyses of this conjecture are in progress.

This work was supported by the BMBF project grant KAZ 99/001 and the Heisenberg-Landau program.

References

1. N.S. Craigie, C. Wilkin, Nucl. Phys. B **14**, 477 (1969).
2. L.A. Kondratyuk, F.M. Lev, L.V. Schevchenko, Yad. Fiz. **33**, 1208 (1981).
3. A. Boudard, M. Dillig. Phys. Rev. C **31**, 302 (1985).
4. O. Imambekov, Yu.N. Uzikov, Yad. Fiz. **47**, 1089 (1988); O. Imambekov, Yu.N. Uzikov, L.V. Schevchenko, Z. Phys. A **332**, 349 (1989).
5. Yu.N. Uzikov, Phys. Part. Nucl. **29**, 583 (1998).
6. O. Imambekov, Yu.N. Uzikov, Sov. J. Nucl. Phys. **52**, 862 (1990).
7. Yu.N. Uzikov, Pis'ma Zh. Eksp. Teor. Fiz. **75**, 7 (2002).
8. Yu.N. Uzikov, J. Phys. G **28**, B13 (2002).
9. A.K. Kerman, L.S. Kisslinger, Phys. Rev. **180**, 1483 (1969).
10. V.I. Komarov *et al.*, Phys. Lett. B **553**, 179 (2003), arXiv:nucl-ex/0210017 v2.
11. K.M. Watson, Phys. Rev. **88**, 1163 (1952); A.B. Migdal, Sov. Phys. JETP **28**, 3 (1955).
12. M.L. Goldberger, K.M. Watson, *Collision Theory* (John Wiley, New York, 1964).
13. R. Machleidt, Phys. Rev. C **63**, 024001 (2001).
14. Yu.N. Uzikov, V.I. Komarov, F. Rathmann, H. Seyfarth, Phys. Lett. B **524**, 303 (2002).
15. G. Fäldt, C. Wilkin, Phys. Scr. **56**, 566 (1997).
16. P. Berthet *et al.*, J. Phys. G **8**, L111 (1982).
17. T. Witten *et al.*, Nucl. Phys. A **254**, 269 (1975).
18. V.V. Abaev *et al.*, Phys. Lett. B **521**, 158 (2001).
19. Yu.N. Uzikov, C. Wilkin, Phys. Lett. B **511**, 191 (2001).
20. J.R.V. Reid, Ann. Phys. (N.Y.) **50**, 411 (1968).
21. V.M. Kolybasov, N.Ya. Smorodinskaya, Yad. Fiz. **17**, 1211 (1973).
22. L.S. Azhgirey *et al.*, Phys. Lett. B **391**, 22 (1997).

Eur. Phys. J. A **18**, 321–322 (2003)
DOI 10.1140/epja/i2002-10226-2

THE EUROPEAN PHYSICAL JOURNAL A

Charge "asymmetry" from the isospin symmetry in pp $\rightarrow$ pp$\pi^+\pi^-$

I. Seluzhenkov[1,a], M. Schepkin[1], and H. Clement[2]

[1] Institute of Theoretical and Experimental Physics, B. Cheremushkinskaja 25, Moscow, 117259, Russia
[2] Physikalisches Institut der Universität Tübingen, Morgenstelle 14, D-72076 Tübingen, Germany

Received: 30 September 2002 /
Published online: 22 October 2003 – © Società Italiana di Fisica / Springer-Verlag 2003

Abstract. Charge "asymmetry" meant as $\sigma_{+-} = \mathrm{d}\sigma/\mathrm{d}M_{p\pi^+} - \mathrm{d}\sigma/\mathrm{d}M_{p\pi^-}$ is easy to reproduce by the simple-minded reaction mechanism, which stems on the interference of Δ^{++} and Δ^0 excited in one of the colliding protons. High-quality experimental data for the $pp \rightarrow pp\pi^+\pi^-$ reaction taken at CELSIUS storage ring with the PROMICE/WASA detector can be described by the Lorentz-invariant phenomenological approach. The same approach is applied for the description of the asymmetry between $M_{pp\pi^+}$ and $M_{pp\pi^-}$ invariant-mass spectra.

PACS. 13.75.-n Hadron-induced low- and intermediate-energy reactions and scattering (energy $\leq$ 10 GeV) – 25.40.Ve Other reactions above meson production thresholds (energies > 400 MeV)

1 Introduction

Recent measurements of the two-pion production, $pp \rightarrow pp\pi^+\pi^-$ at the CELSIUS storage ring [1] reveal a pronounced asymmetry between $p\pi^+$ and $p\pi^-$, as well as between $pp\pi^+$ and $pp\pi^-$ invariant-mass spectra.

In this paper a possibility of the description of the observed anisotropy via $\Delta(1232)$ excitation in the intermediate state off one of the participating protons is examined. As follows from the isospin symmetry, contributions of Δ^{++} and Δ^0 are different, their relative contributions to the amplitude being independent of the isospin of the exchanged mesons. Besides, it looks probable that charge "asymmetry" is not sensitive to the particular dynamics of the $\Delta(1232)$ excitation. Schematically such a mechanism is depicted in figs. 1(a)-(b). Figure 1(c) stands for the contributions not concerned with $\Delta(1232)$ excitation (non-Δ terms). One of the possible scenarios of this kind has been considered in ref. [2]. The authors of this paper claim that the leading contribution is due to the excitation of the Roper resonance $N^*(1440)$ decaying as $N^* \rightarrow \Delta\pi$ or directly $N^* \rightarrow N\pi\pi$. However, the phenomenological approach [1] based on the results of the work [2] is not capable of describing the charge "asymmetry" observed in the reaction $pp \rightarrow pp\pi^+\pi^-$.

A simple phenomenological approach, discussed in this paper, allows to successfully describe the observed "asymmetry" within the framework of minimal assumptions.

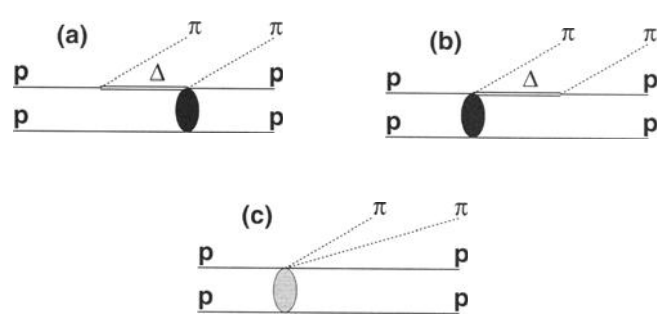

Fig. 1. Diagrams for the two-pion production reaction $pp \rightarrow pp\pi^+\pi^-$: (a) and (b): $\Delta(1232)$ excitation; (c): non-Δ terms.

The approach is Lorentz invariant, and is therefore applicable at higher energies.

2 Amplitude of the reaction pp $\rightarrow$ pp$\pi^+\pi^-$

The Lorentz-invariant reaction amplitude, corresponding to the diagrams in figs. 1(a)-(c) can be written as

$$\mathcal{A} \sim A + B\, k_1^\mu k_2^\nu \left[\mathcal{D}_{\mu\nu}(P_{\Delta^0}) + 3\mathcal{D}_{\mu\nu}(P_{\Delta^{++}})\right] , \qquad (1)$$

where $k_{1,2}$ are pions 4-momenta, P_{Δ^0} and $P_{\Delta^{++}}$ are 4-momenta of the Δ^0 and Δ^{++}, respectively. A and B are considered as smooth functions of k_1 and k_2. $\mathcal{D}_{\mu\nu}(P)$

[a] e-mail: seluzhen@heron.itep.ru

stands for the symmetric part of the Δ-propagator:

$$\mathcal{D}_{\mu\nu}(P) = \frac{g_{\mu\nu}P^2 - P_\mu P_\nu}{P^2 - M^2 + iM\Gamma} \,. \tag{2}$$

M and Γ are the mass and width of the $\Delta(1232)$-resonance. Δ^0 and Δ^{++} contribute to the amplitude with different weights (see also [2]). It is this consequence of the isospin symmetry which gives rise to the asymmetry σ_{+-} between $p\pi^+$ and $p\pi^-$ invariant-mass spectra. The same holds true for the asymmetry between $pp\pi^+$ and $pp\pi^-$ spectra.

The complete expression for the Δ-propagator used in the numerical calculations looks as (see, *e.g.*, the review [3])

$$\frac{\hat{P} + M}{P^2 - M^2 + iM\Gamma} \times \left(-g_{\mu\nu} + \frac{\gamma_\mu\gamma_\nu}{3} + \frac{\gamma_\mu P_\nu - \gamma_\nu P_\mu}{3M} + \frac{2}{3}\frac{P_\mu P_\nu}{M^2} - \frac{2}{3}\frac{P^2 - M^2}{M^2}\left[\gamma_\mu P_\nu - \gamma_\nu P_\mu + (\hat{P} + M)\gamma_\mu\gamma_\nu\right]\right) \,. \tag{3}$$

This particular form of the Δ-propagator is dictated by the following physical requirements: low-energy πN scattering via Δ should follow a typical p-wave behaviour. By neglecting small antisymmetric terms in the propagator we arrive at the simple form (1) for the amplitude.

3 Results

Shown in figs. 2(a)-(b) are the numerical results of our calculations in comparison with the experimental data. We stress once again that the charge "asymmetry" is only slightly dependent on the particular parameterization of the functions A and B entering eq. (1). It points to an independence of the asymmetry from the details of the dynamics of the intermediate Δ production thus leaving room for a fit of the other invariant-mass spectra.

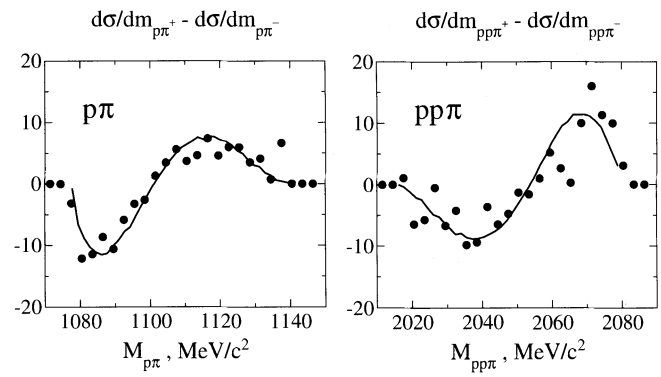

Fig. 2. The asymmetry σ_{+-} (nb $\cdot$ c^2/MeV) as a function of $p\pi$-invariant mass (left) and $pp\pi$-invariant mass (right). Solid lines: results of the calculations with the amplitude (1); dots: experimental data taken at CELSIUS [1].

This work has been supported by DFG (Europ. Graduiertenkolleg 683) and RFBR grant 00-15-96562.

References

1. W. Brodowski *et al.*, Phys. Rev. Lett. **88**, 192301 (2002).
2. L. Alvarez-Ruso, E. Oset, E. Hernández, Nucl. Phys. A **633**, 519 (1998).
3. A.I. Vaishtein, V.I. Zakharov, Usp. Fiz. Nauk **100**, 225 (1970).

Eur. Phys. J. A **18**, 323–326 (2003)
DOI 10.1140/epja/i2002-10227-1

THE EUROPEAN PHYSICAL JOURNAL A

Hadronic threshold reactions

W. Oelert[a]

IKP-I, Forschungszentrum Jülich, D-52425 Jülich, Germany

Received: 30 September 2002 /
Published online: 22 October 2003 – © Società Italiana di Fisica / Springer-Verlag 2003

Abstract. First investigations on meson production at threshold in the strong interaction began in the fifties when sufficient energies of accelerated protons were available. Early experiments performed with bubble chambers revealed already typical ingredients of threshold studies, which were superseded by more complete meson production investigations at the nucleon beam facilities TRIUMF, LAMPF, PSI, LEAR and SATURNE. Currently, at the cooler rings IUCF, CELSIUS and COSY the field is entering a new domain of precision and further progress. The analysis of this new data in the short-range limit permits a more fundamental consideration and a quantitative comparison of the production processes for different mesons in the few-body final states. The interpretation of the data takes advantage of the fact that production reactions close to threshold are characterized by only a few degrees of freedom between a well-defined combination of initial and exit channels. Deviations from predictions of phase-space–controlled one-meson exchange models are indications of new physics. Precision data on differential cross-sections, isospin and spin observables —partly but by no means adequately available— are presently turning up.

PACS. 13.60.Le Meson production – 13.75.Cs Nucleon-nucleon interactions – 13.85.Lg Total cross-sections – 14.40.-n Mesons

1 Introduction

The physics program at the medium energy hadron accelerators was and is focusing on studies of the production and the decay of light-mesons and baryon resonances and the conservation or violation of symmetries.

Production of mesons and meson pairs at threshold will be discussed with the features depicted by the interaction view of fig. 1, [1] where in the nucleon-nucleon (NN) scattering a meson X is created in a one-boson exchange model. For the particular case the questions have to be answered: how is the distortion of the incident NN waves (ISI) included, which mesons contribute to the exchange process, is there an intermediate baryon resonance, how significant are rescattering contributions of the exchange mesons and what is a reasonable treatment of the NN and NX final state interactions (FSI)? Especially for the NN interaction the FSI is crucial because of the nearby poles in the S-wave amplitudes corresponding to the deuteron bound state in the $^3S_1$ channel or the $^1S_0$ virtual state [1]. These poles and the phase space factors tend to determine much of the energy dependence of the total cross-section for meson production. Furthermore, in any region where these poles dominate, it is possible to link quantitatively meson production in cases where the two nucleons emerge separately or as a bound deuteron

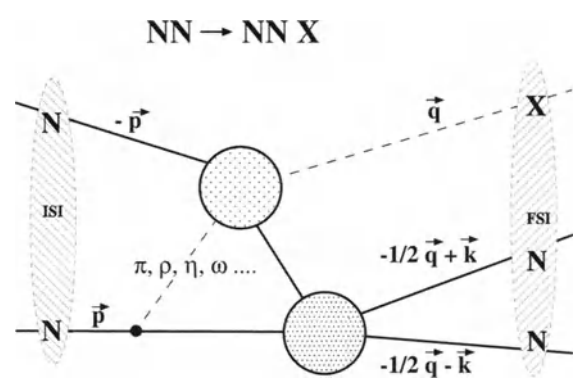

Fig. 1. Diagrammatic view of the one-boson exchange meson production process. Produced meson = X, nucleon momentum = $\boldsymbol{p}$, meson momentum = $\boldsymbol{q}$, relative NN momentum = $2\,\boldsymbol{k}$ [1].

state. Even at threshold the reaction mechanism of the basic process for the interrelation between real pions and virtual exchange meson currents as, for instance, in the pion production ($NN \to NN\pi$) is still not fully understood. Though first data suggested that s-wave pions were produced in a heavy-meson exchange process, later measurements resulted in an interpretation of an interference among transition amplitudes as Ss, Ps, Pp, Sd and Ds, where the capital letter indicates the NN final-state wave and the small letter the angular momentum between the two nucleons and the meson produced. In addition, it has

[a] e-mail: w.oelert@fz-juelich.de

been concluded that for higher partial waves π exchange rather than a heavier-meson exchange is more significant.

Especially the pion-nucleon interaction went through several stages of increasing sensitivity for tests of nuclear theory. More than a decade after the initial work [2,3] only in the sixties explicit calculations on cross-sections of the $pp \to pp\pi^0$, $pn\pi^+$ transitions were possible [4, 5] which, however, failed the total cross-section [6–8] by a factor of five. After further theoretical developments, see, *e.g.*, ref. [9], only recently detailed calculations were provided within the Jülich meson exchange model [10–12] including transitions in the threshold region beyond $l_\pi = 0$ and predicting analyzing powers and spin correlation coefficients making use of i) the basic diagrams, ii) final-state interactions, iii) off-shell effects, iv) the exchange of heavier mesons and v) influences of intermediate excitation of the Δ-resonance. On the other hand, the Jülich model does not account for quark degrees of freedom, *i.e.* calculations within the framework of the χPT which, in fact, predict cross-sections too small [13] compared to experiments. The heavier the meson produced in nucleon-nucleon scattering the larger the momentum transfers and thus in such processes the short-range parts of the production operators are tested.

Double-meson production processes with both mesons being either identical (*e.g.* $\pi^0\pi^0$ or $K^0\overline{K^0}$) or different (*e.g.* $\pi\eta$) are in principle similar to the single ones; however, the possibly associated baryon resonances as intermediate states differ significantly. For instance, the two-pion production very likely is dominated by either the P_{11} $N^*(1440)$-resonance —via an effective σ exchange giving information of a scalar meson excitation of the P_{11} $N^*(1440)$-resonance— or the simultaneously excited P_{33} $\Delta(1232)$-resonances. Due to selection rules here the choice of definite quantum numbers in the initial and final state might help to sort out the reaction mechanism.

Much knowledge about the π-π interaction has been obtained by the $\pi N \to \pi\pi N$ reaction, whereas data employing proton beams just start to come.

As long as only S-wave processes are involved, which is the privilege of threshold production studies, scattering length and effective range approaches are used to describe the interaction sign and strength. In case of strong attractive interactions a distinction between the final-state scattering and the formation of a baryonic resonance leading to bound or quasi-bound states cannot be made uniquely.

Isospin violation or charge symmetry breaking processes are a topical and interesting field of threshold production physics. The essential contribution to isospin breaking is the possible π^0-η mixing. Therefore experiments around the η threshold as, *e.g.*, $dd \to \alpha\,\pi^0(\eta)$ or $pd \to {}^3\mathrm{He}\,\pi^0({}^3\mathrm{H}\,\pi^+)$ should identify the π^0-η mixing angle which, in turn, might give hints to the mass difference of the up and down quarks.

There is an exciting field of physics studying the threshold production of mesons in the fundamental processes of $NN \to NNX$. There is work for the years to come and thus it is a very positive sign that the Research Centre Jülich is presently upgrading COSY by projecting a new linear injector for higher intensities and especially for polarized beams of high quality.

2 Aspects of threshold production

Threshold production experiments are characterized by excess energies which are small compared to the produced masses. Consequently, in fixed-target experiments the momenta of the final-state particles transverse with respect to the direction of the incoming beam are small compared to the longitudinal components. Thus, ejectiles are confined to a narrow forward cone in the laboratory system around the centre-of-mass movement and —close to threshold— an experimental acceptance covering the full solid angle is feasible with comparatively small dedicated detector arrangements.

Small relative momenta in the final state effectively limit the number of partial waves contributing, simplifying the theoretical interpretation of experimental results. It should be noted, that already three-body final states require —in principle— a three-body Faddeev-like approach, which has not been accomplished so far [14, 15]. However, as first described by Watson [16], with two strongly interacting particles in the final state, the energy dependence of the total cross-section close to threshold is essentially determined by the (three-body) phase space and the energy dependence of the on-shell final-state interaction (FSI). Due to small relative velocities FSI effects are inherent to the experimental observables. Thus, the interpretation of data in terms of reaction dynamics requires a correct treatment of both initial- (ISI) and final-state interactions [17] (for a review see [18]). On the other hand, FSI effects might provide access to low-energy scattering parameters, which are difficult to obtain otherwise in case of unstable particles.

Meson production at threshold implies high momentum transfers Δp, given by

$$\Delta p = \frac{1}{2}\sqrt{(m_N + m_B + m_X)^2 - 4\,m_N^2}$$

for the reaction type $NN \to NBX$ with N, B and X denoting a nucleon, baryon or meson in the initial and final state and m_N, m_B and m_X as the respective masses. With momentum transfers in the range of $0.37\,\mathrm{GeV}/c$ to $1.10\,\mathrm{GeV}/c$ for π^0- and ϕ-meson production, threshold production probes with corresponding distances between 0.53 fm and 0.18 fm the short-range part of the nucleon-nucleon interaction. Consequently, the energy dependence of the primary production amplitude is expected to be weak, motivating Watson's approach [16].

Theoretical studies have been carried out mainly within the framework of hadronic meson exchange models, *i.e.* with baryons and mesons as effective degrees of freedom (for a recent review see [19]). Chiral perturbation theory has been applied for the description of data on π production close to threshold [20]. However, in view of the characteristic distances mentioned above, QCD-inspired models [21,22] with constituent quarks and gluons or instantons as relevant degrees of freedom, might turn out to

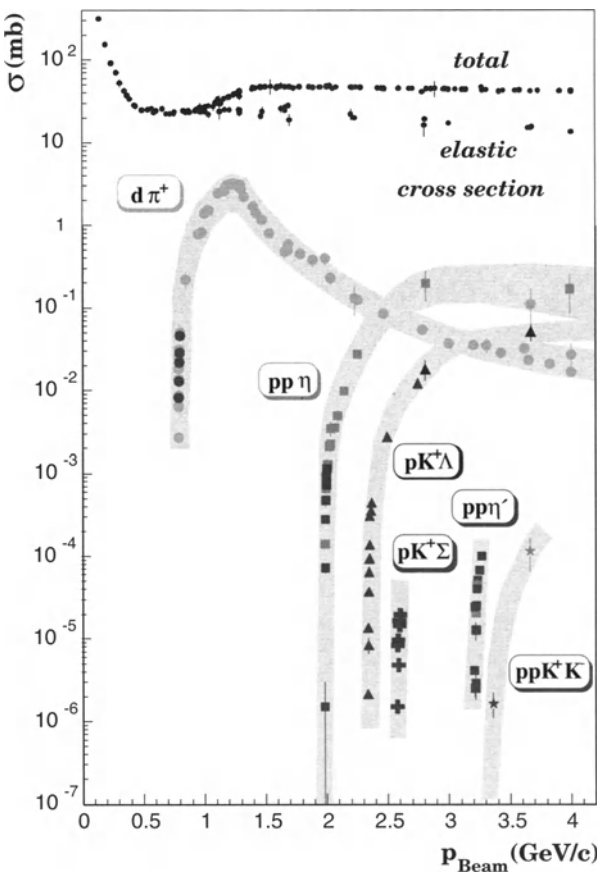

Fig. 2. Proton-proton cross-sections for different reactions of the light-meson production in the threshold region. For comparison also the total and elastic cross-sections of proton-proton scattering are shown. Relevant references to the data are given throughout the present article at the appropriate sections.

be appropriate. High-quality exclusive data on close-to-threshold meson production in the energy range of non-perturbative strong-interaction physics will be crucial for exploring the boundary between effective meson exchange models and (so far phenomenological) approaches based on quark-gluon degrees of freedom.

3 Features of hadronic probes

It seems that the χPT is of limited value once strangeness is involved in the hadronic systems and non-perturbative coupled-channel considerations beyond χPT are on the market [23,24]. High-quality data on the meson ($\pi, \eta, \eta', \omega, K^+, K^-$) production at threshold have been and are being produced at the hadronic beam cooler rings using the baryon number $B = 2$ systems (essentially pp and pn). At least equally important are studies with hadronic interactions in the $B = 1$ sector. However, most measurements with π- or K-beams used bubble chamber techniques which naturally suffer from very poor statistics.

Accurate investigations of differential cross-sections for meson production from the initial π plus proton or K plus proton systems are needed at several momenta to study the s- and p-wave dynamics and their interplay. There are indications that both the S_{11}-resonance and the $K\Sigma$ quasi-bound state —followed by a final-state interaction leading to nucleon and meson— are essential and could be investigated best via the $B = 1$ sector.

Until now, most of the data for threshold meson production were observed with proton beams. The use of antiprotons has contributed considerably to the knowledge of the meson spectroscopy up to serious candidates for glueballs and exotic hybrids but is still suffering from the lack of unique interpretations.

A comparison of the meson production in the fundamental process to productions on heavier nucleons would give constraints to eliminate uncertainties in the basic interactions. As outlined in ref. [25], precise measurements of such processes set the necessary constraints for the effective Lagrangian of low-energy QCD with strange quarks. Its knowledge has impacts on several other important issues, such as the strange-quark content of the nucleon.

Cross-sections are very small in the threshold region down to eight orders of magnitude compared to the total yield. Due to the rapid growth of the phase space volume the total cross-section of the meson production reactions increases by orders of magnitudes in a few MeV range of excess energy. Such studies have been made possible only due to the low-emittance and small-momentum spread proton beams available at the storage ring facilities. Figure 2 demonstrates threshold production measurements of light mesons in the proton-proton interaction.

References

1. C. Wilkin, nucl-th/9810047 and *Proceedings of the 8th International Conference On The Structure Of Baryons (Baryons 98), September 22–26, 1998, Bonn, Germany*, edited by D.W. Menze, B. Metsch (World Scientific, Singapore, 1999) p. 505.
2. M. Gell-Mann, K.M. Watson, Annu. Rev. Nucl. Sci. **4**, 219 (1954).
3. A.H. Rosenfeld, Phys. Rev. **96**, 130 (1954).
4. D. Koltun, A. Reitan, Phys. Rev. **141**, 1413 (1966).
5. M.E. Schillaci *et al.*, Phys. Rev. **179**, 1539 (1969).
6. H.O. Meyer *et al.*, Nucl. Phys. A **539**, 633 (1992).
7. H.O. Meyer *et al.*, Phys. Rev. Lett. **65**, 2846 (1990).
8. W.W. Daehnick *et al.*, Phys. Rev. Lett. **74**, 2913 (1995).
9. T.S.H. Lee, D.O. Riska, Phys. Rev. Lett. **70**, 2237 (1993).
10. C. Hanhart *et al.*, Phys. Lett. B **358**, 21 (1995).
11. C. Hanhart *et al.*, Phys. Lett. B **444**, 25 (1998).
12. C. Hanhart *et al.*, Phys. Rev. C **61**, 064008 (2000).
13. B. Blankleider, A.N. Kvinikhidze, Few-Body Syst. Suppl. **12**, 223 (2000).
14. S. Wycech, A.M. Green, Nucl. Phys. A **663**, 529 (2000).
15. A. Fix, H. Arenhovel, Nucl. Phys. A **697**, 277 (2002).
16. K.M. Watson, Phys. Rev. **88**, 1163 (1952).
17. C. Hanhart, K. Nakayama, Phys. Lett. B **454**, 176 (1999).
18. F. Kleefeld, nucl-th/0108064 and *Proceedings of the Symposium on Threshold Meson Production in pp and pd Interactions, June 20–24, 2001, Cracow, Poland, Schriften des FZ-Jülich, Matter and Materials*, edited by P. Moskal, M. Wolke, Vol. **11**, (Forschungszentrum Jülich, 2002) p. 51.

19. K. Nakayama, nucl-th/0108032 and *Proceedings of the Symposium on Threshold Meson Production in pp and pd Interactions, June 20–24, 2001, Cracow, Poland, Schriften des FZ-Jülich, Matter and Materials*, edited by P. Moskal, M. Wolke, Vol. **11**, (Forschungszentrum Jülich, 2002).
20. C. Hanhart, U. van Kolck, G.A. Miller, Phys. Rev. Lett **85**, 2905 (2000).
21. N.I. Kochelev, V. Vento, A.V. Vinnikov, Phys. Lett. B **472**, 247 (2000).
22. M. Dillig, hep-ph/0202067.
23. N. Kaiser, P.B. Siegel, W.Weise, Nucl. Phys. A **594**, 325 (1995).
24. N. Kaiser, T. Waas, W. Weise, Nucl. Phys. A **612**, 297 (1997).
25. W. Weise, U.-G. Meißner, GSI – HESR-Project, Contributions to the Scientific Case (1999) p. 103.

Eur. Phys. J. A **18**, 327–329 (2003)
DOI 10.1140/epja/i2002-10228-0

THE EUROPEAN PHYSICAL JOURNAL A

Manifestations of anomalous glue: Light-mass exotic mesons and $g_{\eta' NN}$

S.D. Bass[a]

Institute for Theoretical Physics, University of Innsbruck, Technikerstrasse 25, A-6020 Innsbruck, Austria

Received: 30 September 2002 /
Published online: 22 October 2003 – © Società Italiana di Fisica / Springer-Verlag 2003

Abstract. The light-mass exotics with $J^{PC} = 1^{-+}$ observed at BNL and CERN may have a simple explanation as dynamically generated resonances in $\eta'\pi$ rescattering in the final-state interaction. This dynamics is mediated by the same anomalous glue which also generates the large mass of the η'. OZI-violating processes are also potentially important to η' production in proton-proton collisions close to threshold.

PACS. 12.39.Mk Glueball and nonstandard multi-quark/gluon states – 13.75.Lb Meson-meson interactions – 13.75.Cs Nucleon-nucleon interactions (including antinucleons, deuterons, etc.)

1 Introduction

Searching for evidence of gluonic degrees of freedom in low-energy QCD is one of the main themes driving present experimental and theoretical studies of the strong interaction. Key probes include glueball and $J^{PC} = 1^{-+}$ exotic-meson searches plus OZI violation in η' physics [1] which is sensitive to gluonic degrees of freedom through the $U(1)$ axial anomaly [2]. Exotic mesons are particularly interesting because the quantum numbers $J^{PC} = 1^{-+}$ are inconsistent with a simple quark-antiquark bound state [3]. Two such exotics, with masses 1400 and 1600 MeV, have been observed in experiments at BNL [4] and CERN [5] in decays to $\eta'\pi$ and $\eta\pi$. These exotics have been a puzzle to theorists and experimentalists alike because the lightest-mass $q\bar{q}g$ state with exotic quantum numbers predicted by lattice calculations [6,7] and QCD-inspired models [8] has mass about 1800–1900 MeV. As we explain here, the presently observed light-mass exotics seen at BNL and CERN may have a simple explanation [9] as dynamically generated resonances in $\eta'\pi$ rescattering (in the final-state interaction). The anomalous glue which generates the large η' mass plays an essential role in this dynamics.

The physics of anomalous glue also yields interesting phenomenology in the η'-nucleon system. The flavor-singlet Goldberger-Treiman relation [10] relates the flavor-singlet axial-charge $g_A^{(0)}$ extracted from polarized deep inelastic scattering [11] to the η'-nucleon coupling constant. The small value of $g_A^{(0)}$ (about 50% of the OZI value 0.6) measured in polarized DIS and the large mass of the η' point to large violations of OZI in the flavor-singlet $J^{PC} = 1^{++}$ channel. OZI-violating processes may also play an important role [12] in η' production in proton-nucleon collisions close to threshold [13]. This process is presently under investigation at COSY [14].

We first review the puzzle of light-mass exotics. We then explain how the presently observed states may be understood as dynamically generated resonances in $\eta'\pi$ rescattering. Here we briefly review the $U_A(1)$-extended effective Lagrangian for low-energy QCD [15,16]. This Lagrangian is constructed so that it successfully includes the effects of the strong $U(1)$ axial anomaly and the large η' mass. Finally, we discuss η' production in proton-nucleon collisions close to threshold where new effects [12] of OZI violation are suggested by coupling this Lagrangian to the nucleon.

2 Light-mass exotics

The $J^{PC} = 1^{-+}$ light-mass exotics discovered at BNL [4] and CERN [5] were observed in decays to $\eta\pi$ and $\eta'\pi$. Two such exotics, denoted π_1, have been observed through $\pi^- p \to \pi_1 p$ at BNL [4]: with masses 1400 MeV (in decays to $\eta\pi$) and 1600 MeV (in decays to $\eta'\pi$ and $\rho\pi$). The $\pi_1(1400)$ state has also been observed in $\bar{p}N$ processes by the Crystal Barrel Collaboration at CERN [5]. While the exotic quantum numbers $J^{PC} = 1^{-+}$ are inconsistent with a quark-antiquark bound state, they can be generated through a "valence" gluonic component —for example through coupling to the operator $[\bar{q}\gamma_\mu q G^{\mu\nu}]$. However, the observed exotics are considerably lighter than

[a] e-mail: Steven.Bass@cern.ch

the predictions (about 1800–1900 MeV) of quenched lattice QCD [6,7] and QCD-inspired models [8] for the lowest mass $q\bar{q}g$ state with $J^{PC} = 1^{-+}$ These results suggest that, perhaps, the "exotic" states observed by the experimentalists might involve significant meson-meson bound-state contributions. Furthermore, the decays of the light-mass exotics to η- or η'-mesons plus a pion suggest a possible connection to axial $U(1)$ dynamics.

This idea has recently been investigated [9] in a model of final-state interaction in $\eta\pi$ and $\eta'\pi$ rescattering using the $U_A(1)$-extended chiral Lagrangian [15,16], coupled channels and the Bethe-Salpeter equation, following the approach of the Valencia group [17].

The $U_A(1)$-extended low-energy effective Lagrangian used in these calculations is

$$\begin{aligned}\mathcal{L}_{\rm m} = & \frac{F_\pi^2}{4}\mathrm{Tr}(\partial^\mu U \partial_\mu U^\dagger) + \frac{F_\pi^2}{4}\mathrm{Tr}\left[\chi_0\ (U + U^\dagger)\right] \\ & + \frac{1}{2} i Q \mathrm{Tr}\left[\log U - \log U^\dagger\right] + \frac{3}{\tilde{m}_{\eta_0}^2 F_0^2} Q^2 \\ & + \lambda\ Q^2\ \mathrm{Tr}\ \partial_\mu U \partial^\mu U^\dagger\,. \end{aligned} \tag{1}$$

Here $U = \exp\left(i\frac{\phi}{F_\pi} + i\sqrt{\frac{2}{3}}\frac{\eta_0}{F_0}\right)$ is the unitary meson matrix where $\phi = \sum_k \phi_k \lambda_k$ with ϕ_k denoting the octet of would-be Goldstone bosons (π, K, η_8) associated with spontaneous chiral $SU(3)_L \otimes SU(3)_R$ breaking, and η_0 is the singlet boson; Q denotes the topological charge density $\left(Q = \frac{\alpha_s}{4\pi} G\tilde{G}\right)$. Also, $\chi_0 = \mathrm{diag}[m_\pi^2, m_\pi^2, (2m_K^2 - m_\pi^2)]$ is the quark-mass–induced meson mass matrix, $\tilde{m}_{\eta_0}$ is the gluonic-induced mass term for the singlet boson and λ is an OZI-violating coupling —see below. The pion decay constant $F_\pi = 92.4$MeV and F_0 renormalizes the flavor-singlet decay constant $F_{\rm singlet} = F_\pi^2/F_0 \sim 100$MeV.

The gluonic potential involving Q is constructed so that the effective theory reproduces the QCD axial anomaly [2] in the divergence of the gauge invariantly renormalized axial-vector current. This potential also generates the gluonic contribution to the η and η' masses: Q is treated as a background field with no kinetic term; it may be eliminated through its equation of motion to yield

$$\frac{1}{2} i Q \mathrm{Tr}\left[\log U - \log U^\dagger\right] + \frac{3}{\tilde{m}_{\eta_0}^2 F_0^2} Q^2 \ \mapsto\ -\frac{1}{2}\tilde{m}_{\eta_0}^2 \eta_0^2\,. \tag{2}$$

The η-η' mass matrix resulting from eq. (1) gives η and η' masses:

$$\begin{aligned} m_{\eta',\eta}^2 = & (m_{\rm K}^2 + \tilde{m}_{\eta_0}^2/2) \\ & \pm \frac{1}{2}\sqrt{(2m_{\rm K}^2 - 2m_\pi^2 - \frac{1}{3}\tilde{m}_{\eta_0}^2)^2 + \frac{8}{9}\tilde{m}_{\eta_0}^4}\,. \end{aligned} \tag{3}$$

If the gluonic term $\tilde{m}_{\eta_0}^2$ were zero in this expression, one would have $m_{\eta'} = \sqrt{2m_{\rm K}^2 - m_\pi^2}$ and $m_\eta = m_\pi$. Without any extra input from glue, in the OZI limit, the η would be approximately an isosinglet light-quark state $(\frac{1}{\sqrt{2}}|\bar{u}u + \bar{d}d\rangle)$ degenerate with the pion and the η' would be a strange-quark state $|\bar{s}s\rangle$ —mirroring the isoscalar vector ω- and ϕ-mesons. Indeed, in an early paper [18] Weinberg argued that the mass of the η would be less than $\sqrt{3}m_\pi$ without any extra $U(1)$ dynamics to further break the axial $U(1)$ symmetry. The gluonic contribution to the η and η' masses is about 300–400 MeV [1].

In the model calculations [9] of FSI the meson-meson (re-)scattering potentials in the Bethe-Salpeter equation were derived from the Lagrangian (1). The OZI-violating interaction $\lambda\ Q^2\ \mathrm{Tr}\ \partial_\mu U \partial^\mu U^\dagger$ [16] was found to play a key role in the $J^{PC} = 1^{-+}$ channel. A simple estimate for the coupling λ can be deduced from the decay $\eta' \to \eta\pi\pi$ yielding two possible solutions with different signs. Especially interesting is the negative-sign solution. When substituted into the Bethe-Salpeter equation this solution was found to yield a dynamically generated p-wave resonance with exotic quantum numbers $J^{PC} = 1^{-+}$. Furthermore, this resonance was found to have mass $\sim$ 1400 MeV and width $\sim$ 300 MeV —close to the observed exotics. (The width of the $\pi_1(1400)$ state measured in decays to $\eta\pi$ is 385 ± 40 MeV; the width of the $\pi_1(1600)$ measured in decays to $\eta'\pi$ is 340 ± 64 MeV.) The topological charge density mediates the coupling of the dynamically generated light-mass exotic to the $\eta\pi$ and $\eta'\pi$ channels in these calculations. For detailed discussion and the amplitudes for the individual channels which contribute to this dynamics, see [9].

3 OZI violation in the η'-nucleon system

Going beyond the meson sector, it is interesting to look for evidence of OZI violation in the η'-nucleon system. Some guidance is provided by coupling the $U_A(1)$-extended chiral Lagrangian to the nucleon [12]. Here we find a gluon-induced contact interaction in the $pp \to pp\eta'$ reaction close to threshold:

$$\mathcal{L}_{\rm contact} = -\frac{i}{F_0^2}\ g_{QNN}\ \tilde{m}_{\eta_0}^2\ \mathcal{C}\ \eta_0\ \left(\bar{p}\gamma_5 p\right)\ \left(\bar{p}p\right). \tag{4}$$

Here g_{QNN} is an OZI-violating coupling which measures the one-particle irreducible coupling of the topological charge density Q to the nucleon and $\mathcal{C}$ is a second OZI-violating coupling which also features in $\eta' N$ scattering. The physical interpretation of the contact term (4) is a "short distance" ($\sim$ 0.2 fm) interaction where glue is excited in the interaction region of the proton-proton collision and then evolves to become an η' in the final state. This gluonic contribution to the cross-section for $pp \to pp\eta'$ is extra to the contributions associated with meson exchange models [19,20]. There is no reason, *a priori*, to expect it to be small.

What is the phenomenology of this OZI-violating interaction?

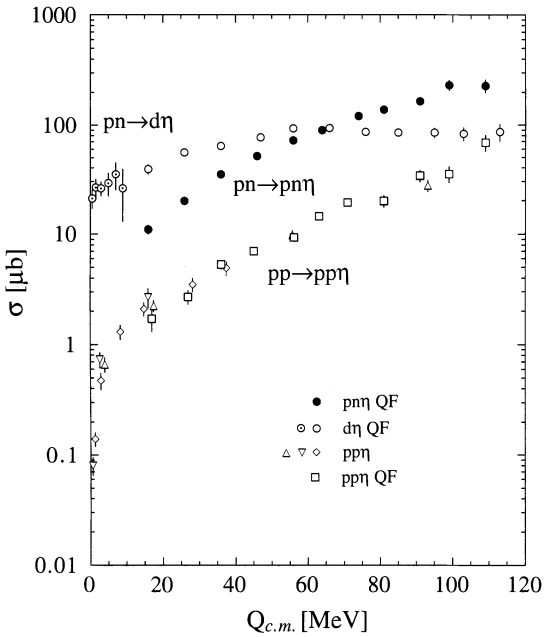

Fig. 1. CELSIUS data on η production.

Since glue is flavor-blind, the contact interaction (4) has the same size in both the $pp \to pp\eta'$ and $pn \to pn\eta'$ reactions. CELSIUS [21] have measured the ratio $R_\eta = \sigma(pn \to pn\eta)/\sigma(pp \to pp\eta)$ for quasifree η production from a deuteron target up to 100 MeV above threshold. They observed that R_η is approximately energy independent $\simeq 6.5$ over the whole energy range —see fig. 1. The value of this ratio signifies a strong isovector exchange contribution to the η production mechanism [21]. This experiment can be repeated for η' production. The cross-section for $pp \to pp\eta'$ close to threshold has been measured at COSY [14]. A new experiment [22] has been initiated to carry out the $pn \to pn\eta'$ measurement. In the formal limit that the $pp \to pp\eta'$ reaction were dominated by gluonic-induced production, the ratio

$$R_{\eta'} = \sigma(pn \to pn\eta')/\sigma(pp \to pp\eta') \qquad (5)$$

would approach unity close to threshold after we correct for the final-state interaction [23] between the two outgoing nucleons. It will be interesting to compare future measurements of $R_{\eta'}$ with the CELSIUS measurement [21] of R_η. Given that η' phenomenology is characterised by large OZI violations, it is natural to expect large OZI effects in the $pp \to pp\eta'$ process.

SDB is supported by a Lise-Meitner Fellowship, M683, of the Austrian FWF. I thank W. Oelert and the COSY-11 Collaboration for hospitality in Juelich, P. Moskal for helpful discussions and E. Marco for collaboration on light-mass exotics.

References

1. S.D. Bass, Phys. Scr. T **99**, 96 (2002), hep-ph/0111180.
2. G.M. Shore, Lecture at 1998 Zuoz Summer School, hep-ph/9812354.
3. A.R. Dzierba, hep-ex/0106010 and this issue, p. 273.
4. The E852 Collaboration (D.R. Thompson *et al.*), Phys. Rev. Lett. **79**, 1630 (1997); (S.U. Chung *et al.*), Phys. Rev. D **60**, 092001 (1999); (G.S. Adams *et al.*), Phys. Rev. Lett. **81**, 5760 (1998); (E.I. Ivanov *et al.*), Phys. Rev. Lett. **86**, 3977 (2001).
5. The Crystal Barrel Collaboration (A. Abele *et al.*), Phys. Lett. B **423**, 246 (1998).
6. P. Lacock *et al.* (UKQCD), Phys. Rev. D **54**, 6997 (1996); Phys. Lett. B **401**, 308 (1997); C. Bernard *et al.* (MILC), Phys. Rev. D **56**, 7039 (1997); Nucl. Phys. B Proc. Suppl. **53**, 228 (1997).
7. A.W. Thomas, A.P. Szczepaniak, Phys. Lett. B **526**, 72 (2002).
8. N. Isgur, R. Kokoski, J. Paton, Phys. Rev. Lett. **54**, 869 (1985); F.E. Close, P.R. Page, Nucl. Phys. B **443**, 233 (1995); T. Barnes, F.E. Close, E.S. Swanson, Phys. Rev. D **52**, 5242 (1995).
9. S.D. Bass, E. Marco, Phys. Rev. D **65**, 057503 (2002), hep-ph/0108189.
10. G. Veneziano, Mod. Phys. Lett. A **4**, 1605 (1989); G.M. Shore, G. Veneziano, Nucl. Phys. B **381**, 23 (1992); T. Hatsuda, Nucl. Phys. B **329**, 376 (1990).
11. S.D. Bass, Eur. Phys. J A **5**, 17 (1999), hep-ph/9902280; E. Reya, B. Lampe, Phys. Rept. **332**, 1 (2000); B.W. Filippone, X. Ji, hep-ph/0101224.
12. S.D. Bass, Phys. Lett B **463**, 286 (1999), hep-ph/9907373.
13. G. Fäldt, T. Johannson, C. Wilkin, Phys. Scr. T **99**, 146 (2002).
14. The COSY-11 Collaboration (P. Moskal *et al.*), Phys. Rev. Lett. **80**, 3202 (1998); Phys. Lett. B **474**, 416 (2000); **482**, 356 (2000).
15. P. Di Vecchia, G. Veneziano, Nucl. Phys. B **171**, 253 (1980).
16. P. Di Vecchia, F. Nicodemi, R. Pettorino, G. Veneziano, Nucl. Phys. B **181**, 318 (1981).
17. J.A. Oller, E. Oset, Nucl. Phys. A **620**, 438 (1997); A **652**, 407(E) (1997).
18. S. Weinberg, Phys. Rev. D **11**, 3583 (1975).
19. R. Machleidt, K. Holinde, Ch. Elster, Phys. Rept. **149**, 1 (1987).
20. J.-F. Germond, C. Wilkin, Nucl. Phys. A **518**, 308 (1990); G. Fäldt, C. Wilkin, Z. Phys. A **357**, 241 (1997); K. Nakayama, H.F. Arellano, J.W. Durso, J. Speth, Phys. Rev. C **61**, 024001 (1999).
21. The CELSIUS Collaboration (H. Calen *et al.*), Phys. Rev. Lett. **80**, 2069 (1998); Phys. Rev. C **58**, 2667 (1998).
22. The COSY-11, Uppsala University Collaboration (P. Moskal, T. Johansson *et al.*), COSY Proposal No.100; P. Moskal, in *Proceedings of the Symposium on Threshold Meson Production in pp and pd Interactions, June 20-24, 2001, Crakow, Poland, Schriften des FZ-Jülich, Matter and Materials*, edited by P. Moskal, M. Wolke, Vol. **11** (Forschungszentrum, Jülich, 2002), nucl-ex/0110001.
23. G. Fäldt, C. Wilkin, Phys. Scr. **56**, 566 (1997); Am. J. Phys. **66**, 876 (1998).

Eur. Phys. J. A **18**, 331–334 (2003)
DOI 10.1140/epja/i2002-10229-y

THE EUROPEAN PHYSICAL JOURNAL A

Exclusive η production in pp reactions

I. Fröhlich[1,a], F. Balestra[2], Y. Bedfer[3,b], R. Bertini[2,3], L.C. Bland[4], A. Brenschede[1,c], F. Brochard[3,d], M.P. Bussa[2], Seonho Choi[4,e], M.L. Colantoni[2], R. Dressler[6,f], M. Dzemidzic[4,d], J.-Cl. Faivre[3,b], A. Ferrero[2], L. Ferrero[2], J. Foryciarz[9,5,g], V. Frolov[7], R. Garfagnini[2], A. Grasso[2], S. Heinz[2,3], W.W. Jacobs[4], W. Kühn[1], A. Maggiora[2], M. Maggiora[2], A. Manara[2,3], D. Panzieri[8], H.-W. Pfaff[1,h], G. Piragino[2], A. Popov[7], J. Ritman[1], P. Salabura[5], V. Tchalyshev[7], F. Tosello[2], S.E. Vigdor[4], and G. Zosi[2]

[1] II. Physikalisches Institut, University of Gießen, Gießen, Germany
[2] Dipartimento di Fisica "A. Avogadro" and INFN, Torino, Italy
[3] Laboratoire National Saturne, CEA Saclay, France
[4] Indiana University Cyclotron Facility, Bloomington, Indiana, USA
[5] M. Smoluchowski Institute of Physics, Jagellonian University, Kraków, Poland
[6] Forschungszentrum Rossendorf, Germany
[7] JINR, Dubna, Russia
[8] Università del Piemonte Orientale and INFN, Torino, Italy
[9] H. Niewodniczanski Institute of Nuclear Physics, Kraków, Poland

Received: 30 September 2002 /
Published online: 22 October 2003 – © Società Italiana di Fisica / Springer-Verlag 2003

Abstract. Angular distributions for the exclusive reaction $pp \to pp\eta$ observed via the $\pi^+\pi^-\pi^0$ decay channel have been measured at $T_{\rm beam} = 2.15$ GeV, 2.50 GeV and 2.85 GeV (excess energies $Q = 324$ MeV, 412 MeV and 554 MeV). The polar angle of the η shows an anisotropy with respect to the beam direction for the lowest energy, which vanishes for the higher energies. The anisotropy of the pp polar angle increases slightly with the beam energy.

PACS. 13.75.Cs Nucleon-nucleon interactions (including antinucleons, deuterons, etc.) – 14.40.Aq π, K, and η mesons – 25.40.Ve Other reactions above meson production thresholds (energies > 400 MeV)

1 Introduction

The production of η-mesons in nucleon-nucleon collisions plays a role in elementary hadron physics to test various production models based on one-boson exchange [1–5]. In contrast to pion production, η production is dominated by the near-threshold resonance $S_{11}(1535)N^*$, which has a large coupling to the η-decay. Moreover, differential and total cross-section distributions measured in elementary η production are important for heavy-ion physics, where they are folded into model calculations. In nucleon-nucleon collisions, η production has been measured in early bubble chamber experiments with sufficient statistic for total cross-sections and in near-threshold experiments with differential cross-section distributions up to a beam energies of 1.5 GeV [6–12], where the small phase space covers only a fraction of the $S_{11}(1535)N^*$ signal.

In ref. [12], angular distributions of the η-meson in the Center-of-Mass system (CM) as well as for the pp system have been presented at near-threshold energies (excess energies 16 and 37 MeV). It has been shown that the distribution of the η CM polar angle ($\cos\theta_\eta^{\rm CM}$) is not isotropic and has a maximum flow of η-mesons perpendicular to the beam direction. The sign of this anisotropy is the same as observed in photoproduction [13], but opposite to the η production with pion beams [14]. Using the idea of the vector dominance model, where the photon is coupling to the proton-η vertex by an intermediate vector meson, this is a hint for a dominant vector meson exchange in this energy region. A more detailed interpretation of these data shows a dominant exchange of ρ vector mesons [5] with a destructive ρ/π interference. The sign of the anisotropy should be opposite if π exchange were dominant.

[a] e-mail: Ingo.Froelich@exp2.physik.uni-giessen.de
[b] *Present address*: DAPNIA/SPhN, CEA Saclay, France.
[c] *Present address*: Syngenio AG, Stuttgart
[d] *Present address*: LPHNHE, Ecole Polytechnique 91128 Palaiseau, France.
[e] *Present address*: Temple University, Philadelphia, PA, USA.
[f] *Present address*: Paul Scherrer Institut, Villigen, CH-5232.
[g] *Present address*: Motorola Polska Software Center, Kraków, Poland.
[h] *Present address*: d-fine GmbH, Eschborn.

In this report, angular distributions of the exclusive reaction $pp \to pp\eta$ are presented, which have been measured with the DISTO-Spectrometer at higher energies. First, an overview of the apparatus and the data analysis techniques are given. In the second part, the measured angular distributions of the η as well as the of recoiling pp system are shown.

2 Experimental setup and analysis steps

The DISTO magnetic spectometer [15] was located at the SATURNE II accelerator. Proton beams with kinetic energies of 2.15 GeV, 2.50 GeV and 2.85 GeV were directed to a liquid hydrogen target. The relevant components of the detector for the results presented here were a large dipole magnet which covered the target, two sets of multiwire proportional chambers (MWPC) mounted outside the magnetic field and an array of water Čerenkov detectors, which allowed a separation of protons and pions over a large momentum range. The large solid angle of the detector allowed final states with four charged particles to be measured. Various kinematically complete reactions have been investigated simultanously under the same conditions of four charged particles in the final state, *e.g.*, ppK^+K^-, $pp\pi^+\pi^-(\pi^0)$ and pKY, $Y = \Sigma, \Lambda$ [16–18].

The exclusive η production has been observed via the reaction $pp \to pp\eta \to pp\pi^+\pi^-\pi^0$ ($\eta \to \pi^+\pi^-\pi^0$ branching ratio: 23% [19]). The momentum of each track has been calculated using the hit pattern information of the MWPC. The four-momentum vectors were determined by assigning a mass hypothesis (p or π^+) to the positively charged tracks. A χ^2-test was applied to the measured three-momenta and Čerenkov light outputs to find the best assignment of the positive tracks to the $pp\pi^+$ hypothesis. Futhermore, a requirement of $\chi^2_{\text{best}} < 3$ has been used to suppress events from other reactions (*e.g.*, $pp \to pK\Lambda \to ppK\pi$).

After the identification of all four charged particles in the final state, energy and momentum conservation can be used to reconstruct the invariant mass M_X^{inv} and missing mass M_X^{miss} of specific particle combinations X. To select the reaction $pp\pi^+\pi^-\pi^0$ *versus* other reaction channels with $pp\pi^+\pi^-$ in the final state a missing π^0 has been required with the conditions $0.002\,\text{GeV}^2/c^4 < (M^{\text{miss}}_{pp\pi^+\pi^-})^2 < 0.037\,\text{GeV}^2/c^4$ and $(M^{\text{inv}}_{\pi^+\pi^-})^2 < (M^{\text{miss}}_{pp})^2$. A further suppression of background and gain in momentum resolution have been archieved by refitting the four tracks with the additional constraint that $M^{\text{miss}}_{pp\pi^+\pi^-} = M_{\pi^0}$ [17].

To evaluate the acceptance of the detector, Monte Carlo simulations have been used, which were processed through the same analysis chain as the measured data. The simulations indicate a very low acceptance of the apparatus for the η produced in the backward hemisphere in the CM frame. However, since the initial system consists of two identical particles, a reflection symmetry about $\theta^{\text{CM}} = 90°$ exists, thus the backward data are redundant for the cross-section determination. In the forward hemisphere the detector acceptance was found to be non-zero in every bin over the full kinematically allowed region, thus eliminating the need for any model-dependent extrapolations of the cross-section into unmeasured regions of phase space.

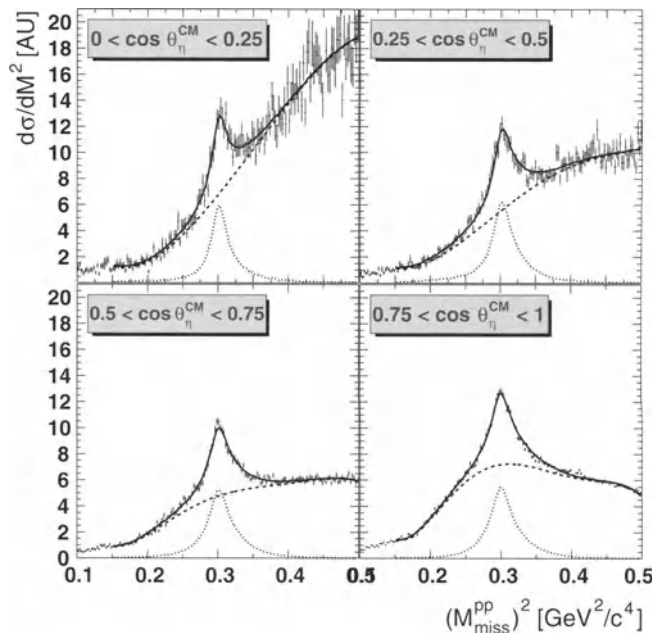

Fig. 1. Proton-proton missing-mass squared for 4 different $\cos\theta_\eta^{\text{CM}}$-bins (2.85 GeV data) before absolute normalization. Dotted line: η line shape from Monte Carlo simulation. Dashed line: background (polynomial of 6th order). Solid line: signal plus background. Both data and simulation have been corrected for acceptance in the η invariant mass region.

The kinematically allowed phase space of the three-body $pp\eta$ final state has been divided into 4-dimensional kinematic bins. We have chosen the invariant masses $M^{\text{inv}}_{p_1\eta}$, $M^{\text{inv}}_{p_2\eta}$ and three Euler angles θ_η^{CM}, ϕ_η^{CM}, ψ_{pp}^{CM} as the degrees of freedom, where symmetry reasons ensure that the ϕ_η^{CM} distribution must be isotropic. The efficiency correction factor was determined for each bin separately by dividing the number of generated $pp\eta$ events by the number of reconstructed events in the corresponding acceptance bin. The data presented below have been corrected on an event-by-event basis via this weighting factor. For a detailed discussion see [18].

The data which has been selected by all conditions still contain background, mostly from non-resonant $\pi^+\pi^-\pi^0$ production. A χ^2 minimization routine has been applied to a parametrization of the background and signal. The background has been parameterized by a 6th-order polynomial. The line shape of the η signal was derived from Monte Carlo simulation for each individual bin of the angular distributions. Figure 1 shows the pp missing-mass distribution (2.85 GeV data) for four ranges of $\cos\theta_\eta^{\text{CM}}$, which is the polar angle of the η-meson with respect to the beam direction in the $pp\eta$ CM system.

Due to the large systematic uncertainty of the beam current normalization, we did not measure the total cross-section of the $pp \to pp\eta$ reaction. However, the total

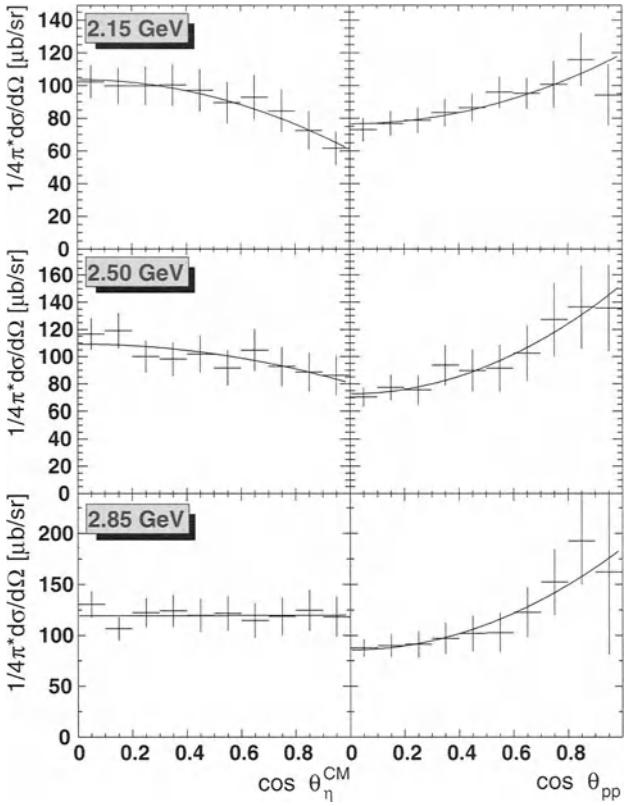

Fig. 2. Angular distributions of the η with respect to the beam direction (left column) and of the pp system in the pp rest frame (right column). The data have been fitted with the first two even Legendre polynomials. The error bars include both statistical and systematical uncertainties. The histograms on the right side have been scaled by a factor of $\frac{1}{2}$ since $\cos\theta_{pp}$ is only defined between 0 and 1.

cross-section of $pp \to pp\eta$ is known from many other experiments, allowing us to obtain the absolute normalization of the angular distributions, as shown in [18]. Following the same procedure, we used $90 \pm 20\,\mu$b, $100 \pm 30\,\mu$b and $120 \pm 40\,\mu$b for the $T_{\text{beam}} = 2.15$ GeV, 2.50 GeV and 2.85 GeV data, respectively. Since the absolute normalization enters only as a global scale, the related error bars have not been included in the errors of the individual bins in the presented angular distributions.

However, each bin of the angular distributions has an individual error due to systematic effects, which are dominated by the acceptance correction and background substraction. To evaluate those bin-by-bin errors, both the statistical error from the minimization routine and the bin-by-bin systematical error have been taken into account. The systematic error has been obtained by comparing background fits with similar χ^2 values but different conditions on both the polynomials and the signal shape and included in the angular differential cross-sections presented in this work.

3 Results

The differential cross-section has been evaluated as a function of $\cos\theta_\eta^{\text{CM}}$ and $\cos\theta_{pp}$, as shown in fig. 2. Here, θ_{pp} is the polar alignment of the pp system in the pp rest frame with respect to the beam axis. The observables have been divided into 10 bins, for each bin the yield has been extracted by fitting and subtracting the background. Both angular distributions have been fitted with the sum of the first two even Legendre polynomials $\frac{\mathrm{d}\sigma}{\mathrm{d}\Omega} \propto L_{0,2}(\cos\theta) = c_0[1 + c_2 L_2(\cos\theta)]$ to evaluate the contributions of c_0 and c_2. The c_2 parameters at the different beam energies are compared in table 1. These results indicate an anisotropy of the produced η-meson perpendicular to the beam direction at 2.15 GeV, which is smaller for the 2.50 GeV data and vanishes for the highest energy. The c_2 contribution of the protons increases with the beam energy. The inclusion of Legendre polynomials of higher order were not neccessary to describe the data points.

Table 1. Contribution c_2 of the 2nd Legendre polynomial.

Beam energy	Excess energy	$c_2(\eta)$	$c_2(pp)$
2.15 GeV	324 MeV	-0.33 ± 0.20	0.31 ± 0.06
2.50 GeV	412 MeV	-0.19 ± 0.15	0.38 ± 0.07
2.85 GeV	554 MeV	-0.01 ± 0.10	0.50 ± 0.06

In conclusion, we have measured the angular distribution in the reaction $pp \to pp\eta$ with the DISTO spectrometer at beam energies of 2.15 GeV, 2.50 GeV and 2.85 GeV. The anisotropy of the η-meson polar angle at 2.15 GeV gradually vanishes at larger beam energies. This behaviour should be considered in upcoming theoretical approaches together with the new near-theshold data from COSY [20] with higher statistics in one framework.

We acknowledge the work provided by the SATURNE II accelerator staff and technical support groups in delivering an excellent proton beam and assisting this experimental program. This work has been supported by CNRS-IN2P3, CEA-DSM, NSF, INFN, KBN (5P03B14020) and GSI.

References

1. J.-F. Germond, C. Wilkin, Nucl. Phys. A **518**, 308 (1990).
2. T. Vetter, A. Engel, T. Biró, U. Mosel, Phys. Lett. **263**, 153 (1991).
3. J.M. Laget, F. Wellers, J.F. Lecolley, Phys. Lett. B **257**, 254 (1991).
4. A. Sibirtsev, W. Cassing, Few-Body Systems Suppl. **99**, 1 (1999).
5. G. Fäldt, C. Wilkin, Phys. Scr. **64**, 427 (2001).
6. E. Chiavassa *et al.*, Phys. Lett. B **322**, 270 (1994); E. Chiavassa *et al.*, Phys. Lett. B **337**, 192 (1994).
7. A.M. Bergdolt *et al.*, Phys. Rev. D **48**, R2969 (1993); F. Hibou *et al.*, Phys. Lett. B **438**, 41 (1998).
8. A. Khoukaz *et al.*, Nucl. Phys. A **663** & **664**, 565c (2000); J. Smyrski *et al.*, Phys. Lett B **474**, 182 (2000).
9. Roderburg *et al.*, Acta Phys. Pol. B **31**, 2299 (2000).
10. H. Calén *et al.*, Phys. Lett. B **366**, 39 (1996).
11. H. Calén *et al.*, Phys. Rev. C **58**, 2667 (1998).
12. H. Calén *et al.*, Phys. Lett. B **458**, 190 (1999).
13. B. Krusche *et al.*, Phys. Rev. Lett. **74**, 3736 (1995).

14. W. Deinet *et al.*, Nucl. Phys. B **11**, 495 (1969).
15. F. Balestra *et al.*, Nucl. Instrum. Methods **426**, 385 (1999).
16. F. Balestra *et al.*, Phys. Rev. Lett. **81**, 4572 (1999).
17. F. Balestra *et al.*, Phys. Lett. B **491**, 29 (2000).
18. F. Balestra *et al.*, Phys. Rev C **63**, 024004 (2000).
19. D.E. Groom *et al.*, Eur. Phys. Jour. C **15**, 1 (2000).
20. P. Moskal *et al.*, PiN Newslett. **16**, 367 (2002), nucl-ex/0110018; The COSY-TOF Collaboration (M. Abdel-Bary *et al.*), Eur. Phys. J. A **16**, 127 (2003), nucl-ex/0205016.

Eur. Phys. J. A **18**, 335–338 (2003)
DOI 10.1140/epja/i2002-10231-5

THE EUROPEAN PHYSICAL JOURNAL A

Eta physics at threshold

P. Moskal[1,2,a], H.-H. Adam[3], A. Budzanowski[4], R. Czyżykiewicz[2], D. Grzonka[1], M. Janusz[2], L. Jarczyk[2], B. Kamys[2], A. Khoukaz[3], K. Kilian[1], P. Kowina[1,6], T. Lister[3], W. Oelert[1], T. Rożek[1,6], R. Santo[3], G. Schepers[1], T. Sefzick[1], M. Siemaszko[6], J. Smyrski[2], S. Steltenkamp[3], A. Strzałkowski[2], P. Winter[1], M. Wolke[1], P. Wüstner[5], and W. Zipper[6]

[1] IKP, Forschungszentrum Jülich, D-52425 Jülich, Germany
[2] M. Smoluchowski Institute of Physics, Jagellonian University, PL-30-059 Kraków, Poland
[3] IKP, Westfälische Wilhelms-Universität, D-48149 Münster, Germany
[4] Institute of Nuclear Physics, PL-31-342 Kraków, Poland
[5] ZEL, Forschungszentrum Jülich, D-52425 Jülich, Germany
[6] Institute of Physics, University of Silesia, PL-40-007 Katowice, Poland

Received: 30 September 2002 /
Published online: 22 October 2003 – © Società Italiana di Fisica / Springer-Verlag 2003

Abstract. The production of η- and η'-mesons in elementary nucleon-nucleon collisions has been investigated at the synchrotrons CELSIUS, COSY and SATURNE. The high-quality proton beam with low emittance and small momentum spread permits to study the creation of these mesons very close to the kinematical threshold, where —due to the rapid growth of the phase space volume— the total cross-section increases by orders of magnitude over a few MeV range of the excess energy. The magnitude and energy dependence of the total cross-section as well as the occupation distribution of the phase space serve as observables for investigating the mechanisms underlying the production processes and the interaction of mesons with nucleons. The precise data on the η and η' creation via the $pp \to pp\eta(\eta')$ reactions allowed to settle the general features of the η- and η'-meson production and revealed the sensitivity of the mentioned observables to the nucleon-nucleon-meson final-state interaction. The particular production properties, like for example, the determination of the dominating exchange processes which lead to the excitation of the S_{11} nucleon isobar in the case of η creation, must be established by confrontation with other observables. The present status of this investigation with an emphasis on the results of the COSY-11 Collaboration is briefly presented. The available data are interpreted in view of the production mechanism and the meson-nucleon interaction.

PACS. 13.60.Le Meson production – 13.75.-n Hadron-induced low- and intermediate-energy reactions and scattering (energy $\leq$ 10 GeV) – 13.85.Lg Total cross sections – 25.40.-h Nucleon-induced reactions

1 Manifestation of the η-nucleon-nucleon interaction

In the last decade, large experimental as well as theoretical efforts were concentrated on the study of the creation of η- and η'-mesons via the hadronic interactions. Measurements of the production of these mesons in the elementary nucleon-nucleon collision have been performed in the vicinity of the kinematical threshold where only one partial wave in both initial and final state is expected to contribute to the production process. For example, in case of the proton-proton collision the dominance of the $^3P_0 \to Ss$ transition is expected up to an excess energy of about 40 MeV and 100 MeV for η- and η'-meson, respectively [1]. This simplifies significantly the interpretation of the data, yet still appears to be challenging due to the three-particle final-state system with a complex hadronic potential. The determined energy dependences of the total cross-section for η' [2,3] and η [3,4] mesons in proton-proton collisions are presented in figs. 1 and 2. Comparing the data to the arbitrarily normalized phase-space integral (dashed lines) reveals that the proton-proton FSI enhanced the total cross-section by more than one order of magnitude for low excess energies. One recognizes also that in the case of the η'-meson the calculation —assuming that the on-shell proton-proton amplitude exclusively determines the phase-space population— describes the data very well (solid line). This indicates that the proton-η' interaction is too small to be observed within the present accuracy [5]. In the case of the η-meson the increase of the total cross-section for very low and very high energies is much larger than expected from the final-state interaction between protons. The excess at higher energies can

[a] e-mail: p.moskal@fz-juelich.de

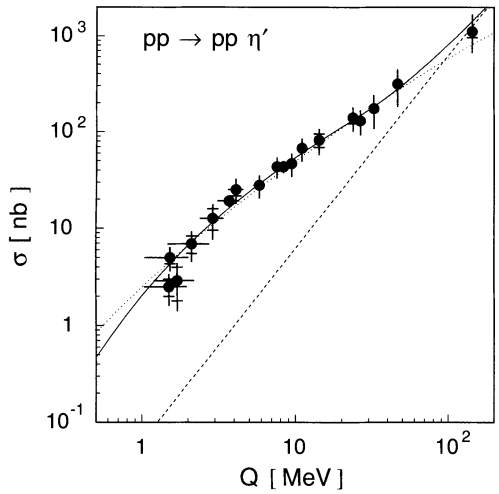

Fig. 1. Total cross-section for the $pp \to pp\eta'$ reaction as a function of the centre-of-mass excess energy Q. Data are from refs. [2,3]. The solid line shows the phase-space distribution with inclusion of proton-proton strong and Coulomb interactions. The dotted line indicates the parametrization of reference [6] with $\epsilon = 0.3$ and the dashed line indicates a phase-space integral normalized arbitrarily. Figure and title are adapted from ref. [1].

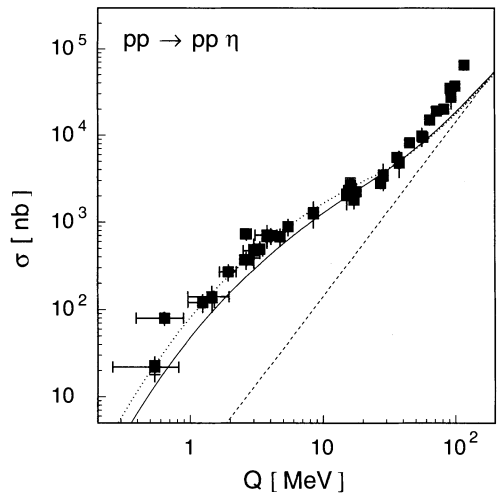

Fig. 2. Total cross-section for the $pp \to pp\eta$ reaction as a function of the centre-of-mass excess energy Q. Data are from refs. [3,4]. The dashed line indicates a phase-space integral normalized arbitrarily. The phase-space distribution with inclusion of proton-proton strong and Coulomb interactions fitted to the data in the excess energy range between 15 and 40 MeV is shown as the solid line. Additional inclusion of the proton-η interaction is indicated by the dotted line. The scattering length $a_{p\eta} = 0.7\,\text{fm} + i\,0.4\,\text{fm}$ and the effective range parameter $b_{p\eta} = -1.50\,\text{fm} - i\,0.24\,\text{fm}$ [7] have been arbitrarily chosen. The figure and caption are adapted from ref. [1].

be assigned to the onset of higher partial waves, and the enhancement at threshold can be plausibly explained by the influence of the attractive interaction between the η-meson and the proton.

Though the simple phenomenological treatment —based on factorization of the transition amplitude into the constant primary production and the on-shell incoherent pairwise interaction among particles— works well for the energy dependence of the total cross-section, it fails completely as far as the description of the differential cross-section is concerned (see the thin solid line in fig. 3).

This discrepancy is rather too large to be utterly caused by the underestimation of the S-wave proton-η interaction. An explanation could be a contribution from P-wave proton-proton interaction [8] or a significant influence of the off-shell effects of the interaction between outgoing particles. Indeed, a much better description of the differantial cross-section shown in fig. 3 is achieved when the enhancement due to the proton-proton FSI is modeled by the inverse of the squared Jost function instead of the on-shell amplitude of the elastic proton-proton scattering (see thick solid line in fig. 3). The Jost function accounts for the off-shell effects of the interacting particles, however it gives wrong energy dependence of the total cross-section, and unfortunately it depends rather strongly on the potential model [9,1] and applied formalism [10]. Therefore, in the framework of this phenomenology it is not possible —with a satisfactory accuracy— to separate the contribution of the proton-η interaction from other effects in a model-independent way. Thus, more sophisticated theoretical calculations are required. An estimation of the nucleon-η scattering parameters has successfully been performed by comparing the close-to-threshold data of the η-meson photoproduction on a deuteron [11] to the calculations performed to the first-order rescattering in the two-body subsystems [12]. The recent investigation of Fix and Arenhövel [13] shows, however, that the three-body dynamics contribute substantially to the total and differential cross-sections of the η photoproduction on the deuteron, and thus it cannot be neglected in the quantitative analysis.

Data of the η-NN system created via the hadronic interaction of nucleons still awaits a strict theoretical explanation. The hitherto performed analysis of the energy dependence of the total cross-section reveals the sensitivity of the data to the η-nucleon interaction. Clearly, further comparative studies of the η-nucleon-nucleon system created in photo- and hadro-production should lead to a better determination of the η-nucleon potential and specifically should be helpful in distinguishing between effects due to the production dynamics and the final-state interaction among the produced particles.

2 Production dynamics

It is rather well established that close to threshold the energy dependence of the total cross-section is due to the interaction among the outgoing particles and that the entire production dynamics manifests itself only in a single constant which determines the magnitude of the total cross-section [1]. Therefore, in spite of the precise measurements of the total cross-section for the creation of η- and η'-mesons in proton-proton as well as of η-meson in

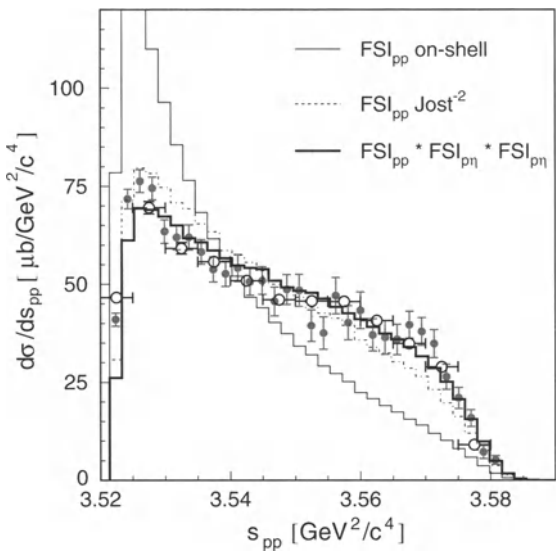

Fig. 3. Experimental distribution of the square of the proton-proton invariant mass (s_{pp}) determined experimentally for the $pp \to pp\eta$ reaction at the excess energy of $Q = 15.5$ MeV by the Collaborations COSY-11 [14] (closed circles) and TOF [15] (open circles). The TOF data have been normalized to give the same total cross-section as those of the COSY-11. The integral of the phase space weighted by the proton-proton on-shell scattering amplitude and by the inverse of the proton-proton squared Jost function [16] is represented by the thin solid and dashed line, respectively. The thick solid line shows the result of the calculations where the occupation density of the phase space was weighted by the inverse of the Jost function multiplied by the square of the proton-η scattering amplitude. The latter was calculated taking arbitrarily the scattering length $a_{p\eta} = 0.7\,\mathrm{fm} + i\,0.4\,\mathrm{fm}$. The lines have been normalized in amplitude to the data.

proton-neutron collisions there are still a lot of ambiguities in the description of the mechanism underlying the production process. It is generally anticipated [17–19] that the η-meson is produced predominantly via the excitation of the S_{11} baryonic resonance $N^*(1535)$, whose creation is induced through the exchange of the virtual π, η, ρ, σ and ω mesons; however, at present it is still not established what are the relative contributions originating from a particular meson. Measurements of the total cross-section in different isospin channels put some more limitations to the models, yet still the η-meson production in the $pp \to pp\eta$ and $pn \to pn\eta$ can be equally well described by, *e.g.*, assuming the ρ-meson exchange dominance [18] or by taking contributions from the pseudoscalar and vector meson exchanges [19]. Therefore, for a full understanding of the production dynamics the determination of polarisation observables is mandatory. Already the precise measurement of the beam analyzing power could exclude one of the above-mentioned possibilities. The first measurement of that quantity has been recently performed [20], but for a conclusive inference a better accuracy of the data is required.

Until now it was also not possible to determine unambiguously the mechanism of the production of the η'-meson [1]. Model uncertainties and in practice only one number —namely the magnitude of the total cross-section of the $pp \to pp\eta'$ reaction— serving as input for theory are by far not sufficient to distinguish between the mesonic, nucleonic or resonant production currents [21]. The understanding of that mechanism on the hadron and quark-gluon level will shed a light on the structure of the η'-meson. A possibly large glue content of the η' wave function and the dominant flavour-singlet combination of its quarks component may cause that the dynamics of its production process in nucleon-nucleon collisions is significantly different from that responsible for the production of other mesons. A creation of that meson via a fusion of gluons excited in the interaction region should lead to the same production yield in proton-proton and proton-neutron collisions, because gluons do not distinguish between flavours [22]. Therefore, it is interesting to determine experimentally the ratio $R_{\eta'} = \sigma(pn \to pn\eta')/\sigma(pp \to pp\eta')$ and to compare it to the already known value of $R_\eta \approx 6.5$ [23]. In the extreme case when the η'-meson is created only from glue excited in the interaction region the ratio $R_{\eta'}$ should be close to unity after the correction for the final- and initial-state interactions between the interacting nucleons [22]. On the contrary, a production mechanism dominated by the isovector meson exchange would yield a significantly larger ratio as already observed in the case of the η-meson. The appropriate experiments are in preparation at the COSY-11 facility [24] and the first feasibility study has already been accomplished sucessfully.

The work has been partly supported by the European Community - Access to Research Infrastructure action of the Improving Human Potential Programme.

References

1. P. Moskal, M. Wolke, A. Khoukaz, W. Oelert, Prog. Part. Nucl. Phys. **49**, 1 (2002), hep-ph/0208002.
2. F. Balestra *et al.*, Phys. Lett. B **491**, 29 (2000); P. Moskal *et al.*, Phys. Lett. B **474**, 416 (2000); P. Moskal *et al.*, Phys. Rev. Lett. **80**, 3202 (1998); A. Khoukaz *et al.*, Ann. Rep. 2001, IKP Universität Münster.
3. F. Hibou *et al.*, Phys. Lett. B **438**, 41 (1998).
4. H. Calén *et al.*, Phys. Lett. B **366**, 39 (1996); J. Smyrski *et al.*, Phys. Lett. B **474**, 182 (2000); E. Chiavassa *et al.*, Phys. Lett. B **322**, 270 (1994); A.M. Bergdolt *et al.*, Phys. Rev. D **48**, R2969 (1993); H. Calén *et al.*, Phys. Rev. Lett. **79**, 2642 (1997); P. Moskal *et al.*, e-Print Archive: nucl-ex/0110018.
5. P. Moskal *et al.*, Phys. Lett. B **482**, 356 (2000).
6. G. Fäldt, C. Wilkin, Phys. Lett. B **382**, 209 (1996).
7. A.M. Green, S. Wycech, Phys. Rev. C **55**, R2167 (1997).
8. Ch. Hanhart, private communication (2002).
9. V. Baru *et al.*, Phys. Atom. Nucl. **64**, 579 (2001).
10. F. Kleefeld, e-Print Archive: nucl-th/0108064
11. V. Hejny *et al.*, Eur. Phys. J. A **13**, 493 (2002);
12. Ch. Elster *et al.*, e-Print Archive: nucl-th/0207052.
13. A. Fix, H. Arenhövel, e-Print Archive: nucl-th/0209085.
14. P. Moskal *et al.*, e-Print Archive: nucl-ex/0208004.

15. M. Abdel-Bary *et al.*, e-Print Archive: nucl-ex/0205016.
16. J.A. Niskanen, Phys. Lett. B **456**, 107 (1999)
17. M. Batinić *et al.*, Phys. Scr. **56**, 321 (1997); A. Moalem *et al.*, Nucl. Phys. A **600**, 445 (1996); J.F. Germond, C. Wilkin, Nucl. Phys. A **518**, 308 (1990); J.M. Laget *et al.*, Phys. Lett. B **257**, 254 (1991); T. Vetter *et al.*, Phys. Lett. B **263**, 153 (1991); B.L. Alvaredo, E. Oset, Phys. Lett. B **324**, 125 (1994); M. Dillig, e-Print Archive: hep-ph/0202067.
18. G. Fäldt, C. Wilkin, Phys. Scr. **64**, 427 (2001).
19. K. Nakayama *et al.*, Phys. Rev. C **65**, 045210 (2002).
20. P. Winter *et al.*, Phys. Lett. B **544**, 251 (2002).
21. K. Nakayama *et al.*, Phys. Rev. C **61**, 024001 (2000).
22. S.D. Bass, e-Print Archive: hep-ph/0006348; S.D. Bass, Phys. Lett. B **463**, 286 (1999); S.D. Bass *et al.*, Nucl. Phys. A **686**, 429 (2001).
23. H. Calén *et al.*, Phys. Rev. C **58**, 2667 (1998).
24. P. Moskal, e-Print Archive nucl-ex/0110001.

Eur. Phys. J. A **18**, 339–341 (2003)
DOI 10.1140/epja/i2002-10230-6

THE EUROPEAN PHYSICAL JOURNAL A

Investigation of the $a_0^+(980)$-resonance with ANKE

P. Fedorets[1,a] and V. Kleber[2]
For the ANKE Collaboration[b]

[1] Institute for Theoretical and Experimental Physics, 117218 Moscow, Russia
[2] Institut für Kernphysik, Forschungszentrum Jülich, 52425 Jülich, Germany

Received: 30 September 2002 /
Published online: 22 October 2003 – © Società Italiana di Fisica / Springer-Verlag 2003

Abstract. Two experiments on the production of the $a_0^+(980)$-resonance in the reaction $pp \to da_0^+$ were performed with the ANKE spectrometer at COSY-Jülich. The decay channels $a_0^+ \to K^+\overline{K^0}$ and $a_0^+ \to \pi^+\eta$ were measured simultaneously at energies $T = 2.65$ GeV and $T = 2.83$ GeV. For the reaction $pp \to dK^+\overline{K^0}$ a total production cross-section of ~ 50 nb has been deduced for $T = 2.65$ GeV. Further goals of the data analysis are to determine differential cross-sections like angular distributions and the branching ratio $a_0^+ \to K^+\overline{K^0}/\pi^+\eta$.

PACS. 13.75.Cs Nucleon-nucleon interactions (including antinucleons, deuterons, etc.) – 25.40.Ve Other reactions above meson production thresholds (energies > 400 MeV)

1 Introduction

The $a_0(980)$- and $f_0(980)$-resonances are the focus of experimental and theoretical studies because their structure is not yet understood. According to different theoretical works [1–5] they could be $q\overline{q}$ states, four-quark states, $K\overline{K}$ molecules, or be of dynamical origin, *i.e.* generated via strong final-state interaction effects. Due to a possible mixing between the neutral $a_0^0(980)$- and the $f_0(980)$-resonances via the coupling to $K\overline{K}$ intermediate states [6], the unmixed, pure isospin-1 state $a_0^+(980)$ was studied in a first series of experiments with ANKE [7,8]. Simultaneous detection of the two main decay channels $a_0^+ \to K^+\overline{K^0}$ and $a_0^+ \to \pi^+\eta$ has been achieved. The most important benefits of such measurements are

- The a_0^+ was measured at energies $T = 2.65$ GeV and $T = 2.83$ GeV. This is close to the $K^+\overline{K^0}$ threshold and allows to study the a_0^+-resonance in direct production, and not via the decay from higher-lying resonances.
- The simultaneous measurement of both decay channels reduces systematic errors, *e.g.* for the determination of their branching ratio.
- The deuteron in the final state is a spin-isospin filter that might simplify the interpretation of the data.
- Meson-meson and meson-deuteron FSI can be studied.
- ANKE allows to measure absolute production cross-sections.

2 Event identification with ANKE

The first measurement of $a_0^+(980)$ production was performed in Jan./Feb. 2001 at a beam energy of $T = 2.65$ GeV. All spectra shown in this article have been obtained from these data. The ANKE spectrometer [9,10] is located at an internal target position of the proton synchrotron COSY-Jülich. The experimental setup of ANKE is shown in fig. 1. A hydrogen cluster-jet target built at the University of Münster was used for our measurements.

For the detection of K^+- and π^+-mesons the positive detector system was exploited, which consists of 23 TOF-start counters, 2 MWPCs, 6 side-wall counters and 15 range telescopes located in the focal plane of the ANKE dipole. Kaons (pions) were selected from the background by using their time-of-flight (TOF) between the start counters and the telescopes (side-wall counters) as well as their energy losses. The information from the MWPCs was used to reject particles scattered at the pole shoes of D2. Figure 2(a) shows the TOF spectra for particles in the positive-particle detectors. After the cuts mentioned above, a clear peak from K^+-mesons is visible (inset in fig. 2(a)). The remaining background under the kaon peak is suppressed subsequently by requiring the coincidence with a deuteron.

Deuterons were detected in the forward detection system (3 MWPCs and a 2-layer scintillator hodoscope).

[a] e-mail: p.fedorets@fz-juelich.de
[b] Complete collaboration list available via: http://www.fz-juelich.de/ikp/anke

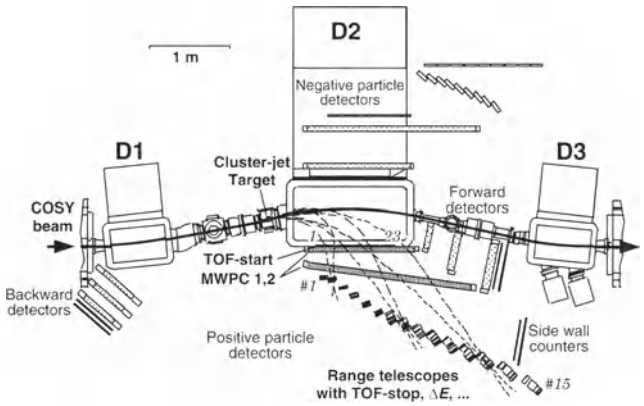

Fig. 1. The ANKE facility comprises the spectrometer dipole D2 and four detection systems: backward detectors, forward detectors, negative- and positive-particle detectors. For the investigation of the $a_0^+(980)$-resonance the forward detectors (2 layer scintillator hodoscopes, 3 MWPCs) and the positive-particle detectors (23 TOF-start counters, 2 MWPCs, 6 side-wall counters, 15 range telescopes) were used.

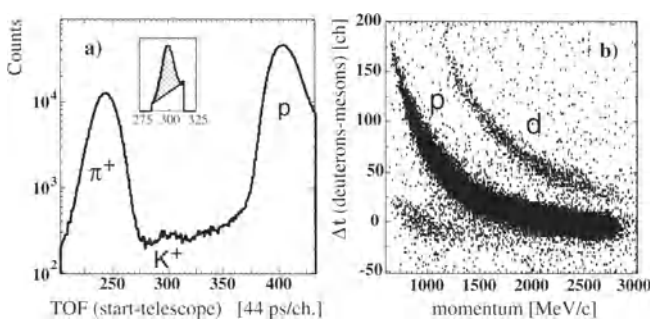

Fig. 2. Particle identification: a) TOF of K^+/π^+ in the positive-particle detectors. After TOF, energy loss and MWPCs cuts a clear peak of K^+-mesons becomes visible (small inset). b) Selection of deuterons in the forward detectors via 2d spectrum, Δt (between mesons and d) *versus* momentum. Bands corresponding to protons and deuterons are seen. The cut along deuteron band allows to separate them from protons.

They were separated from the more abundant protons by a cut in a 2d spectrum of Δt (between K^+/π^+ and d) *versus* momentum (fig. 2(b)).

3 Missing-mass spectra

Figure 3 presents the missing-mass distributions for the selected deuteron-meson pairs. The upper row shows the results for the dK^+-events, the lower for $d\pi^+$. All spectra are not yet efficiency and acceptance corrected. Corresponding simulations are in progress. The (pp, dK^+) missing-mass distribution is shown in fig. 3(a). It exhibits a narrow peak around the $\overline{K^0}$ mass, which confirms the clean selection of the reaction channel $pp \to dK^+\overline{K^0}$. The missing mass of the (pp, d) system is shown in fig. 3(b). This distribution is limited at the left side by the $K^+\overline{K^0}$ threshold and at the right side by the maximum accessible

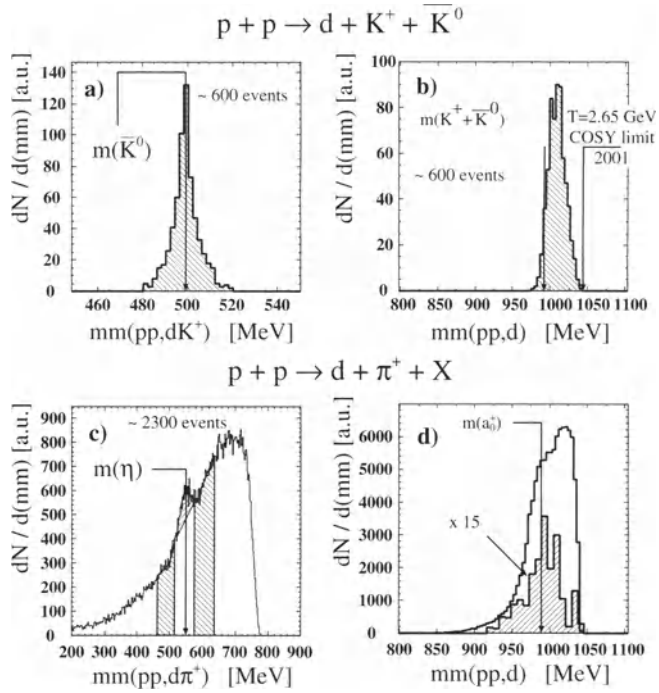

Fig. 3. Missing-mass spectra for the selected dK^+ (upper row) and $d\pi^+$ (lower row) pairs at $T = 2.65$ GeV. The spectra are not efficiency and acceptance corrected. The hatched distribution in picture (d) presents the remaining events after background subtraction.

mass for $T = 2.65$ GeV. For such a narrow missing-mass range it is difficult to separate resonant (via the a_0^+) and non-resonant components of the $K^+\overline{K^0}$ channel, because the shapes of both distributions are very similar [11]. According to model calculations [12–15], the resonant part should dominate ($\approx 85\%$) at $T = 2.65$ GeV. The predicted cross-section for the reaction $pp \to da_0^+ \to dK^+\overline{K^0}$ [15] is in good agreement with our preliminary value of ~ 50 nb for the reaction $pp \to dK^+\overline{K^0}$, which is based on the determination of the luminosity described in sect. 4 and on simulation calculations of the ANKE acceptance. After acceptance correction of the missing-mass (pp, K^+) spectrum (not shown) it should be possible to obtain information about the $d\overline{K^0}$ final-state interaction, which is expected to be strong close to the $K\overline{K^0}$ threshold [5].

The $(pp, d\pi^+)$ missing-mass spectrum (fig. 3(c)) exhibits a peak around the η mass containing ~ 2300 events on top of background from multi-pion production $pp \to d\pi^+(n\pi)$ $(n \geq 2)$. The corresponding deuteron missing-mass distribution mm(pp, d) from fig. 3(d) has a shoulder around 980 MeV/c^2. Assuming a smooth behavior of the background in mm$(pp, d\pi^+)$, the events in the shaded areas of the lower left figure are used for background subtraction. The remaining events show a clear peak structure around 980 MeV/c^2 with a width of ~ 40 MeV. This corroborates the interpretation that the peak in mm$(pp, d\pi^+)$ at ~ 550 MeV/c^2 is connected with the $pp \to da_0^+ \to d\eta\pi^+$ reaction. For the extraction of the cross-section value

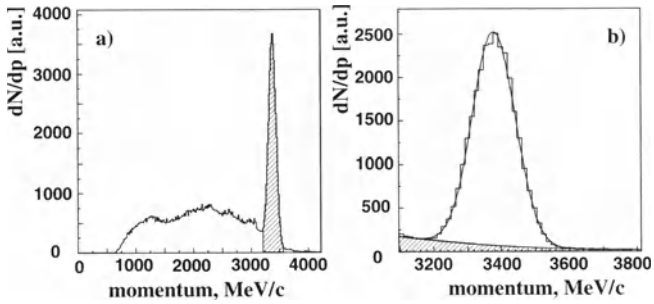

Fig. 4. Luminosity determination via the pp elastic scattering reaction. (a) Raw momentum spectrum of particles detected in the forward counters. (b) Peak of elastically scattered protons with emission angles $\vartheta = (5.5\text{–}9)^\circ$ after correction for the MWPC efficiencies. A Gaussian fit of the peak and a polynomial fit for the background are shown.

a careful investigation of the shape of the multi-pion background below the η peak is in progress.

4 Luminosity determination

The luminosity during the a_0^+ beam times was determined with the help of pp elastic scattering events taken simultaneously with the a_0^+ data [16]. A peak from this reaction is seen in the momentum distribution of protons detected inclusively with the forward detectors (fig. 4(a)). For the luminosity determination protons scattered into the angular range $\vartheta = (5.5\text{–}9)^\circ$ were selected, since GEANT simulations show that the ANKE acceptance changes smoothly for these angles and the elastic peak in the momentum distribution is easily distinguished from the background. The elastic peak region was fitted by a Gaussian distribution, and events were selected within 2σ from the fitted average value. The background was fitted by a polynomial and subtracted. For the detector-efficiency correction of these data two-dimensional efficiency maps for each MWPC plane were created. Figure 4(b) shows the peak from elastically scattered protons in the $\vartheta = (5.5\text{–}9)^\circ$ angular range after this correction. Finally, an average luminosity $L \sim 2.7 \times 10^{31}$ s^{-1}cm^{-2} for the a_0^+ measurement at $T = 2.65$ GeV was obtained. This corresponds to an areal target density of $\sim 5 \cdot 10^{14}$ cm^{-2} [17].

5 Summary

The ANKE spectrometer has been exploited for a simultaneous measurement of the $K^+\overline{K^0}$ and $\pi^+\eta$ decay channels of the $a_0^+(980)$-resonance.

At $T = 2.65$ GeV the measured cross-section for the reaction $pp \to dK^+\overline{K^0}$ is ~ 50 nb. The separation between resonant (via the a_0^+) and non-resonant $K^+\overline{K^0}$ production is difficult due to the narrow available $K^+\overline{K^0}$ mass interval. According to model calculations [12–15], the resonant contribution into the kaon channel is expected to be dominant.

For the $\pi^+\eta$ channel a peak from η-mesons on a broad background from multi-pion production is seen in the missing-mass distribution mm$(pp, d\pi^+)$. After background subtraction a peak structure in mm(pp, d) at 980 MeV/c^2 with a width of about 40 MeV/c^2 is obtained. A detailed analysis of this channel, in particular simulations of the multi-pion background, is in progress.

In Febr./March 2002 a second measurement on a_0^+-resonance production was performed at $T = 2.83$ GeV, which currently is the upper energy limit of the COSY accelerator. Due to the higher energy, the range of accessible missing masses becomes significantly wider. This should allow a model-independent separation of resonant and non-resonant contributions also in the kaon decay. The data analysis is in progress.

In the future we intend to investigate neutral a_0/f_0 resonances at ANKE, using a neutron (*i.e.* deuteron) target and detecting three decay channels, $\pi^0\eta, K^+K^-$ and $\pi^+\pi^-$ [18]. A photon detector for the study of the $\pi^0\eta$ channel is under development [19]. The detection system for negatively charged particles was installed at ANKE and successfully tested in spring 2002.

This work has been supported by grants RFBR99-02-04034, RFBR02-02-16349, RFBR02-02-06518, WTZ-RUS-684-99, ISTC-1966, DFG-436RUS-113/561.

References

1. F.E. Close *et al.*, Phys. Lett. B **319**, 291 (1993).
2. M. Genovese *et al.*, Nuovo Cimento A **107**, 1249 (1994).
3. G. Janssen *et al.*, Phys. Rev. D **52**, 2690 (1995).
4. V.V. Anisovich *et al.*, Phys. Lett. B **355**, 363 (1995).
5. E. Oset *et al.*, Eur. Phys. J. A **12**, 435 (2001).
6. O. Krehl *et al.*, Phys. Lett. B **390**, 23 (1997).
7. V. Chernyshev *et al.*, COSY proposal #55 *Study of a_0^+-mesons at ANKE (1997)*; available via `http://www.fz-juelich.de/ikp/anke`.
8. M. Büscher *et al.*, Beam-time request for COSY experiment #55; available via `http://www.fz-juelich.de/ikp/anke`.
9. S. Barsov *et al.*, Nucl. Instrum. Methods Phys. Res. A **462**, 364 (2001).
10. M. Büscher *et al.*, Nucl. Instrum. Methods Phys. Res. A **481**, 378 (2002).
11. V. Chernyshev *et al.*, nucl-th/0110069.
12. V.Yu. Grishina *et al.*, Eur. Phys. J. A **9**, 277 (2000).
13. V.Yu. Grishina *et al.*, Phys. Lett. B **521**, 217 (2001).
14. E. Bratkovskaya *et al.*, J. Phys. G **28**, 2423 (2002), nucl-th/ 0107071.
15. V.Yu. Grishina *et al.*, *Proceedings of the International Workshop MESON 2002, May 24-28, 2002, Cracow, Poland* (World Scientific Publishing) in press.
16. P. Fedorets *et al.*, Annual Report 2001 of the IKP, FZ Jülich; available via www: `http://www.fz-juelich.de/ikp/publications/AR2001`.
17. H.J. Stein *et al.*, Annual Report 2001 of the IKP, FZ Jülich; available via www: `http://www.fz-juelich.de/ikp/publications/AR2001`.
18. M. Büscher *et al.*, COSY proposal #97; available via `http://www.fz-juelich.de/ikp/anke`.
19. V. Hejny *et al.*, Nucl. Instrum. Methods Phys. Res. A **486**, 126 (2002).

Eur. Phys. J. A **18**, 343–346 (2003)
DOI 10.1140/epja/i2002-10232-4

THE EUROPEAN PHYSICAL JOURNAL A

Chiral dynamics in the pp $\to$ dK$^+\bar{K}^0$ and pp $\to$ d$\pi^+\eta$ reactions

E. Oset[1,a], J.A. Oller[2], and U.-G. Meißner[3]

[1] Departamento de Física Teórica and IFIC, Centro Mixto Universidad de Valencia-CSIC, Institutos de Investigación de Paterna, Aptad. 22085, 46071, Valencia, Spain
[2] Departamento de Fisica, Universidad de Murcia, Spain
[3] Forschungszentrum Jülich, Institut für Kernphysik (Theorie), D-52425 Jülich, Germany and Karl-Franzens-Universität Graz, Institut für Theoretische Physik, A-8010 Graz, Austria

Received: 30 September 2002 /
Published online: 22 October 2003 – © Società Italiana di Fisica / Springer-Verlag 2003

Abstract. We perform a study of the final-state interactions of the $K^+\bar{K}^0$ and the $\bar{K}^0 d$ systems in the reactions $pp \to dK^+\bar{K}^0$ and $pp \to d\pi^+\eta$. The interactions of the mesons are accounted for by using chiral unitary techniques, which generate dynamically the $a_0(980)$-resonance, and the $\bar{K}^0 d$ interaction is also taken into account. The amount of $\pi^+\eta$ *versus* $K^+\bar{K}^0$ production is shown to depend critically on the primary mixture of the two mechanisms, with large interference effects due to final-state interactions

PACS. 12.39.Fe Chiral Lagrangians – 13.75.Lb Meson-meson interactions – 13.75.Cs Nucleon-nucleon interactions (including antinucleons, deuterons, etc.) – 13.75.Gx Pion-baryon interactions

1 Introduction

The reaction $pp \to dK^+\bar{K}^0$ is presently the subject of experimental study by the ANKE Collaboration at the Cooler Synchrotron COSY at Jülich with the aim (among others) of learning about the nature and properties of the $a_0(980)$-resonance [1]. The problem has attracted also the interest of theoretical groups [2,3] (see furthermore the contributed papers in [4]). The prospect of gaining novel information about the $a_0(980)$-resonance, which might help to shed further light from the experimental side on the disputed nature of this resonance, is one of the attractive features of this reaction. This controversy originates from the observation that there are several different models to deal with the isospin $I = 0$, 1 scalar sector, all of them reproducing the scattering data to some extent, but with different conclusions with respect to the origin of the underlying dynamics. In particular, in refs. [5–9] these resonances are considered as pre-existing ones (genuine quark model states), while in ref. [10] they appear as meson-meson resonances generated by a potential.

2 Basic reaction mechanisms

The reaction measured in [1] is

$$pp \to dK^+\bar{K}^0 \ . \tag{1}$$

We study it theoretically in connection with the accompanying process

$$pp \to d\pi^+\eta \ , \tag{2}$$

since the dynamics of coupled channels, which we use here, deals with both channels simultaneously. On the other hand, the energy of the ANKE experiment is fixed to $\sqrt{s} = 2912.88$ MeV just about 45 MeV above the $dK^+\bar{K}^0$ threshold.

Reaction (1) forces the $K^+\bar{K}^0$ system to be in an $I = 1$ state which, given the proximity of the $a_0(980)$-resonance, would have its rate of production and invariant-mass distributions very much influenced by the tail of that resonance. Reaction (2), which is also planned to be measured by the ANKE Collaboration, could see the actual shape of the $a_0(980)$-resonance through the mass distribution of the $\pi^+\eta$ system.

Due to total angular momentum and parity conservation as well as to the antisymmetry of the initial state, the two mesons cannot be simultaneously in intrinsic S-wave and in S-wave relative to the deuteron. At low energies they can only be in $\ell = 0$, $L = 1$ or $\ell = 1$, $L = 0$, where $\ell = 0$ is the orbital angular momentum of the CM motion of the two pseudoscalars PQ and the deuteron, and L the orbital angular momentum of the pseudoscalar mesons in their own CM frame, that we also call intrinsic angular momentum of the two mesons. These two possibilities lead

[a] e-mail: oset@condor1.ific.uv.es

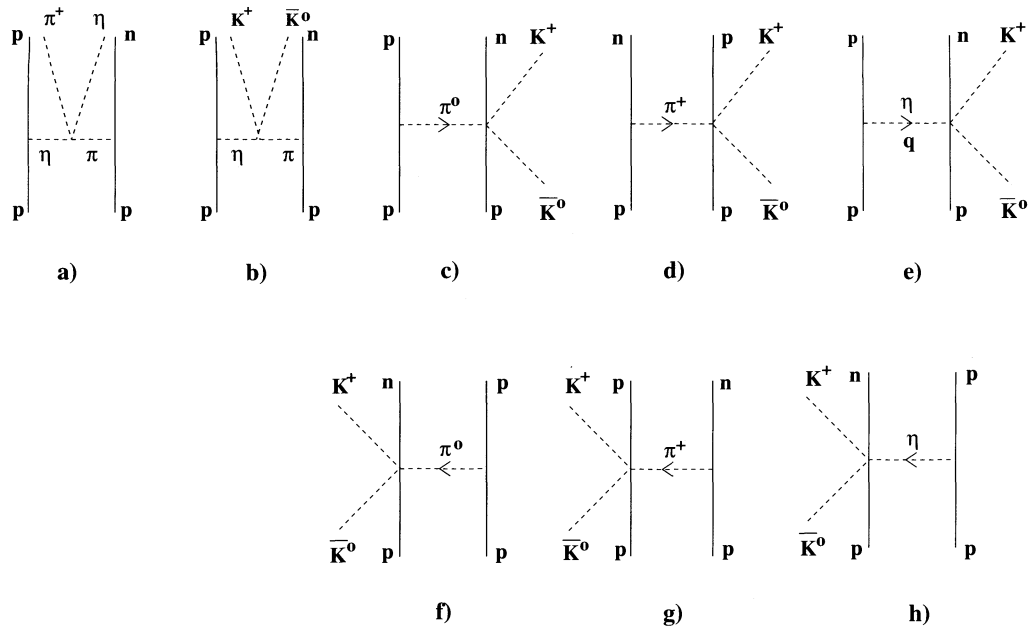

Fig. 1. Chiral model for the primary production used to extract the structures given in eq. (3).

to the following amplitudes for $K\bar{K}$ production:

$$\begin{aligned} &\text{I)}\ \boldsymbol{\sigma}^{(1)}\boldsymbol{p}_1\,\boldsymbol{\sigma}^{(2)}(\boldsymbol{p}_{K^+}-\boldsymbol{p}_{\bar{K}^0})+\boldsymbol{\sigma}^{(1)}(\boldsymbol{p}_{K^+}-\boldsymbol{p}_{\bar{K}^0})\,\boldsymbol{\sigma}^{(2)}\boldsymbol{p}_1\ , \\ &\text{II)}\ -\boldsymbol{\sigma}^{(1)}\boldsymbol{p}_1\,\boldsymbol{\sigma}^{(2)}\boldsymbol{p}_d-\boldsymbol{\sigma}^{(1)}\boldsymbol{p}_d\,\boldsymbol{\sigma}^{(2)}\boldsymbol{p}_1\ . \end{aligned} \tag{3}$$

Should the $K\bar{K}$ system be in an intrinsic S-wave, $L=0$, we would have eq. (3II) and the cross-section contains the factor $\boldsymbol{p}_d^2$, as correctly stated in ref. [11], which largely affects the shape of the $K\bar{K}$ invariant-mass distribution.

3 Final-state interactions

The $K^+\bar{K}^0$ system in $I=1$ will interact strongly and couple to the $\pi^+\eta$ system. In [12] the input of the lowest-order chiral Lagrangian was used as the kernel (potential) of the Bethe-Salpeter equation which produced exact unitarization in coupled channels. Diagrammatically it means that starting from the tree-level diagrams of fig. 1 we will have final production of $K^+\bar{K}^0$ and $\pi^+\eta$ from diagrams of fig. 1 which originally give rise to $\pi^+\eta$ and $K^+\bar{K}^0$, respectively. By calling G the loop function of the mesons, the sums in fig. 2 will dress the structure eq. (3II) containing the $\boldsymbol{p}_d$ vector corresponding to the case when the two mesons are in S-wave in their CM reference system, $L=0$. So we will have

$$\begin{aligned} \pi^+\eta:\ & f^S_{\pi\eta}|\boldsymbol{p}_1||\boldsymbol{p}_d|\mathrm{Y}_{1m}(\hat{p}_d)\to|\boldsymbol{p}_1||\boldsymbol{p}_d|\mathrm{Y}_{1m}(\hat{p}_d)\,\big(f^S_{\pi\eta} \\ & +f^S_{\pi\eta}G_{\pi\eta}t_{\pi\eta\to\pi\eta}+f^S_{K\bar{K}}G_{K\bar{K}}t_{K\bar{K}\to\pi\eta}\big)\ , \\ K^+\bar{K}^0:\ & f^S_{K\bar{K}}|\boldsymbol{p}_1||\boldsymbol{p}_d|\mathrm{Y}_{1m}(\hat{p}_d)\to|\boldsymbol{p}_1||\boldsymbol{p}_d|\mathrm{Y}_{1m}(\hat{p}_d)\,\big(f^S_{K\bar{K}} \\ & +f^S_{K\bar{K}}G_{K\bar{K}}t_{K\bar{K}\to K\bar{K}}+f^S_{\pi\eta}G_{\pi\eta}t_{\pi\eta\to K\bar{K}}\big)\ . \end{aligned} \tag{4}$$

Now we consider the FSI from the $\bar{K}d$ system. The interaction of the K^+ with the protons and neutrons is

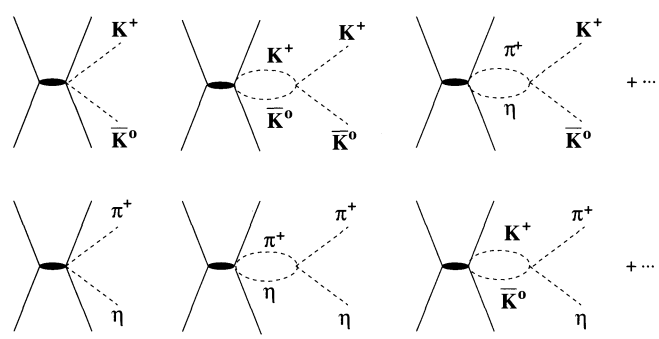

Fig. 2. Diagrams relevant to take into account the meson-meson FSI. The $a_0(980)$-resonance is dynamically generated through the iteration of the meson-meson bubbles. This iteration is indicated in the figure by the ellipses.

rather weak and we neglect it. However, this is not the case for the $\bar{K}^0n$ interaction which is very strong close to threshold due to the $\Lambda(1405)$-resonance below the $\bar{K}^0n$ threshold [13–16]. On the other hand what we need here is the $\bar{K}^0$ interaction with the deuteron that is quite strong close to the threshold due to extra reinforcement of the multiple scattering of the $\bar{K}$ in the deuteron as proved in multiple evaluations of this quantity using Faddeev equations [17–21]. A reanalysis of this quantity in the light of the new $\bar{K}N$ amplitudes generated in the chiral dynamical approach of [15] was done in [22] within the fixed scatterer approximation for the deuteron, which proves rather accurate comparing the results with those of the non-static calculation of [21]. A sizeable $\bar{K}d$ scattering length of about $(-1.6+i1.9)$ fm is obtained in [22]. In order to take into account this extra interaction we first extrapolate the results of the $\bar{K}d$ scattering amplitude at threshold of [22] to the small finite $\bar{K}$ energies of the ANKE experiment [1].

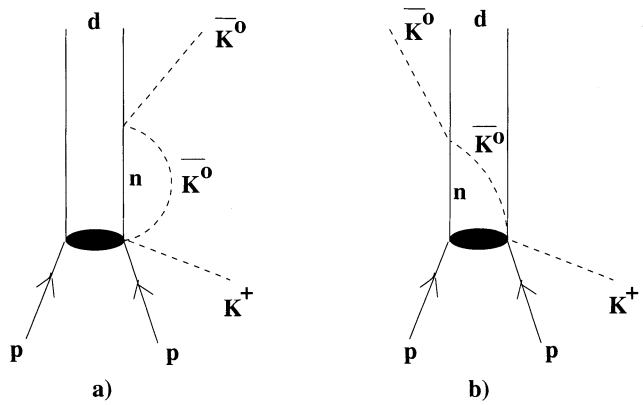

Fig. 3. Diagrams to take into account the $\bar{K}^0 d$ FSI.

The $\bar{K}d$ FSI are diagrammatically represented in fig. 3, and the corresponding terms are renormalized by changing them by

$$1 + G_d\, t_{\bar{K}d}\,, \tag{5}$$

where G_d is the meson-deuteron loop function for the $\bar{K}N$ interaction. Further details can be seen in ref. [23].

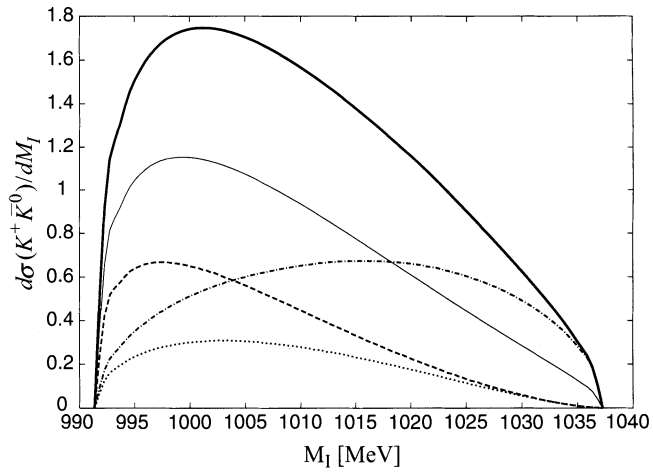

Fig. 4. $d\sigma(K^+\bar{K}^0)/dM_I$ for the whole range of available M_I in the reaction $pp \to dK^+\bar{K}^0$ with $\sqrt{s} = 2912.88$ MeV. The thick (thin) solid line is the full result with $a_{\bar{K}N} = -1.84\,(-1.34)$. The dashed line corresponds to including only meson-meson FSI, the dash-dotted one includes only $\bar{K}^0 d$ FSI and the dotted line includes no FSI with a $\boldsymbol{p}_d^2$ factor for the modulus squared of the amplitude.

4 Results and discussion

Apart from the absolute normalization of the amplitudes, our chiral model for the primary production depends on two free parameters, θ and ϕ, such that

$$f^S_{K\bar{K}} = \cos\theta\,, \quad f^S_{\pi\eta} = \sin\theta\cos\phi\,, \quad f^P_{K\bar{K}} = \sin\theta\sin\phi\,, \tag{6}$$

where $f^p_{K\bar{K}}$ provides the strength for the amplitude of eq. (3I).

First, in order to show the relevance of the FSI, we take $\theta = \phi = 0$, implying $f^S_{\pi\eta} = 0$ and $f^P_{K\bar{K}} = 0$. In fig. 4 we display several curves corresponding to $d\sigma_{K^+\bar{K}^0}/dM_I$ neglecting either the two considered FSI and including either one or two of them. The distribution in the absence of any FSI (dotted line) peaks around $M_I = 1003$ MeV. If the $K^+\bar{K}^0$ interaction is switched on (dashed line) the strength is shifted considerably towards low invariant mass and the peak moves to about $M_I = 997$ MeV. This is an obvious consequence of the presence of the $a_0(980)$-resonance around 980 MeV and the $K^+\bar{K}^0$ distribution feels the tail of that resonance which increases the strength the closer one is to the resonance position, and hence to smaller values of the $K^+\bar{K}^0$ invariant mass. If one switches on only the $\bar{K}^0 d$ FSI (dash-dotted line) the distribution is rather broad and there is an accumulation of strength to higher values of the M_I. Finally, when all the interactions are considered (thick solid line) the peak of the distribution moves back to lower masses around 1 GeV, where the pure phase space peaks as well. The strength is furthermore increased by about a factor five due to the combined effects of both FSI.

We can see that the distributions are rather dependent on the values of the θ and ϕ and so are the angular distributions. This fact could be used to extract the optimal parameters from the data on $K^+\bar{K}^0$ mass distributions and angular distributions, assuming that a good fit is possible. Should this be the case, the theory would then predict absolute rates and mass distribution for the $\pi^+\eta$ production or other experimental yields, which would be a real prediction of the approach in spite of having started from two unknown parameters. The final results of the ANKE experiment are thus awaited to test the theoretical ideas exposed here.

This paper is partially supported by the DGICYT contract number BFM 2000-1326, the EU TMR network Eurodaphne, contract no. ERBFMRX-CT98-0169 and the Deutsche Forschungsgemeinschaft.

References

1. S. Barsov *et al.*, Nucl. Instrum. Methods A **462**, 364 (2001).
2. V.Yu. Grishina, L.A. Kondratyuk, E.L. Bratkovskaya, M. Büscher, W. Cassing, Eur. Phys. J. A **9**, 277 (2000).
3. E.L. Bratkovskaya, V.Yu. Grishina, L.A. Kondratyuk, M. Büscher, W. Cassing, J. Phys. G **28**, 2423 (2000).
4. *Proceedings of the Workshop on* $a_0(980)$ *Physics with ANKE, Moscow, July 13/14, 2000*, edited by M. Büscher, V. Kleber, Berichte des Forschungszentrum Jülich, 2000.
5. N.A. Tornqvist, Phys. Rev. Lett. **49**, 624 (1982); N.A. Tornqvist, M. Roos, Phys. Rev. Lett. **76**, 1575 (1996).
6. R. Jaffe, Phys. Rev. D **15**, 267; 281 (1977).
7. N.N. Achasov, Nucl. Phys. A **675**, 279c (2000); N.N. Achasov, S.A. Devyanin, G.N. Shestakov, Sov. J. Nucl. Phys. **32**, 566 (1980), (Yad. Fiz. **32**, 1098 (1980)).

8. E. van Beveren, T.A. Rijken, K. Metzger, C. Dullemond, G. Rupp, J.E. Ribeiro, Z. Phys. C **30**, 615 (1986). E. van Beveren, G. Rupp, Eur. Phys. J. C **22**, 493 (2001), hep-ex/0106077.
9. D. Black, A.H. Fariborz, S. Moussa, S. Nasri, J. Schechter, Phys. Rev. D **64**, 014031 (2001). D. Black, A.H. Fariborz, J. Schechter, hep-ph/0008246.
10. J. Weinstein, N. Isgur, Phys. Rev. Lett. **48**, 659 (1982); J. Weinstein, N. Isgur, Phys. Rev. D **27**, 588 (1983); **41**, 2236 (1990).
11. V. Chernyshev, P.V. Fedorets, A.E. Kudryavtsev, V.E. Tarasov, ANKE preprint.
12. J.A. Oller, E. Oset, Nucl. Phys. A **620**, 438 (1997); Nucl. Phys. A **652**, 407 (1999)(E).
13. R.H. Dalitz, T.C. Wong, G. Rajasekaran, Phys. Rev. **153**, 1617 (1967).
14. N. Kaiser, P.B. Siegel, W. Weise, Nucl. Phys. A **594**, 325 (1995). N. Kaiser, T. Waas, W. Weise, Nucl. Phys. A **612**, 297 (1997).
15. E. Oset, A. Ramos, Nucl. Phys. A **635**, 99 (1998).
16. J.A. Oller, U.-G. Meißner, Phys. Lett. B **500**, 263 (2001).
17. G. Toker, A. Gal, J.M. Eisenberg, Nucl. Phys. A **362**, 405 (1982).
18. M. Torres, R.H. Dalitz, A. Deloff, Phys. Lett. B **174**, 213 (1986).
19. A. Bahaoui, C. Fayard, G.H. Lamot, T. Mizutani, Nucl. Phys. A **508**, 335 (1990).
20. R.C. Barrett, A. Deloff, Phys. Rev. C **60**, 025201 (1999).
21. A. Deloff, Phys. Rev. C **61**, 024004 (2000).
22. S.S. Kamalov, E. Oset, A. Ramos, Nucl. Phys. A **690**, 494 (2001).
23. E. Oset, J.A. Oller, U.-G. Meißner, Eur. Phys. J. A **12**, 435 (2001).

Eur. Phys. J. A **18**, 347–349 (2003)
DOI 10.1140/epja/i2002-10233-3

THE EUROPEAN PHYSICAL JOURNAL A

Hyperon production in proton-proton collisions at the time-of-flight spectrometer COSY-TOF

W. Schroeder[a]

For the COSY-TOF Collaboration
Physikalisches Institut, Universität Erlangen-Nürnberg, Erwin-Rommel-Str. 1, 91058 Erlangen, Germany

Received: 30 September 2002 /
Published online: 22 October 2003 – © Società Italiana di Fisica / Springer-Verlag 2003

Abstract. The associated strangeness production in elementary proton-induced reactions is studied exclusively at the external COSY beam using the time-of-flight spectrometer TOF. The complete measurement of all charged-particle tracks allows the extraction of total and differential cross-sections and Dalitz plots as well. Especially the analysis of the Dalitz plots of the reaction $pp \longrightarrow K^+\Lambda p$ shows a strong influence of N^*-resonances.

PACS. 13.75.Cs Nucleon-nucleon interactions (including antinucleons, deuterons, etc.) – 14.20.Jn Hyperons

1 Introduction

The main interest in the investigation of the associated strangeness production in the reaction $pp \longrightarrow K^+\Lambda p$ close to the reaction threshold is the insight in the dynamics of the $s\bar{s}$ production. The reaction mechanism can be described within meson exchange models. In these models the contribution of strange and non-strange exchange particles can be investigated as well as the influence of N^*-resonances. Moreover, measurements near threshold can give information about the role of the hyperon nucleon final-state interaction (FSI) [1].

2 Experiment

The external experiment COSY-TOF is a large angle, non magnetic spectrometer, with various start and stop detector components to measure the time of flight. The detector combines high efficieny and acceptance with a moderate energy and momentum resolution. The whole detector together with a tiny liquid-hydrogen target is installed inside a vacuum vessel (see fig. 1). This ensures a rather precise definition of the interaction point and a strongly reduced contamination from background reactions in air.

The outer detector, which gives the stop timing, consists of a huge cylindrical segmented scintillator barrel with about three meters length and diameter each and a circular endcap in the forward direction. The endcap is made of two seperate hodoscopes, a central one ("Quirl") with a diameter of one meter and a ring-like one with an outer diameter of three meters. Both consist of three segmented scintillator layers, one of wedge-like parts and two of left- and right-hand spirally formed elements.

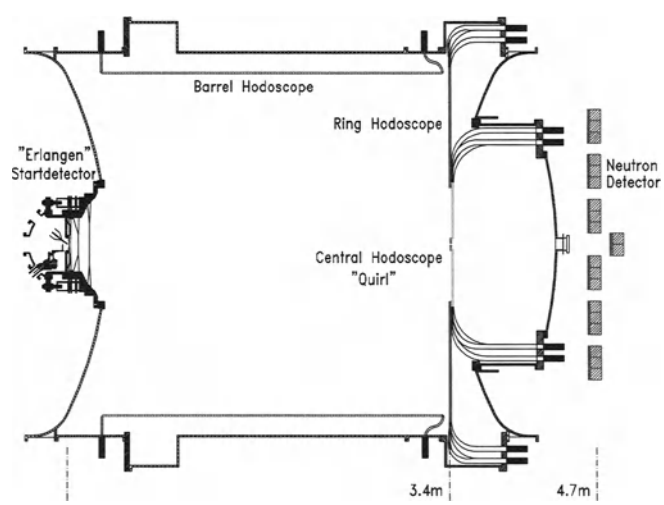

Fig. 1. Scheme of the TOF detector.

The inner detector, shown in fig. 2 together with a typical $K^+\Lambda p$ event, is optimized for track and vertex reconstruction. It consists of the "Starttorte", made of two layers of thin scintillators providing the start timing, a highly granulated double-sided silicon microstrip detector and two scintillating fibre hodoscopes. This system covers the whole angular range of the reaction products for the investigated hyperon production from threshold up to the

[a] e-mail: schroeder@physik.uni-erlangen.de

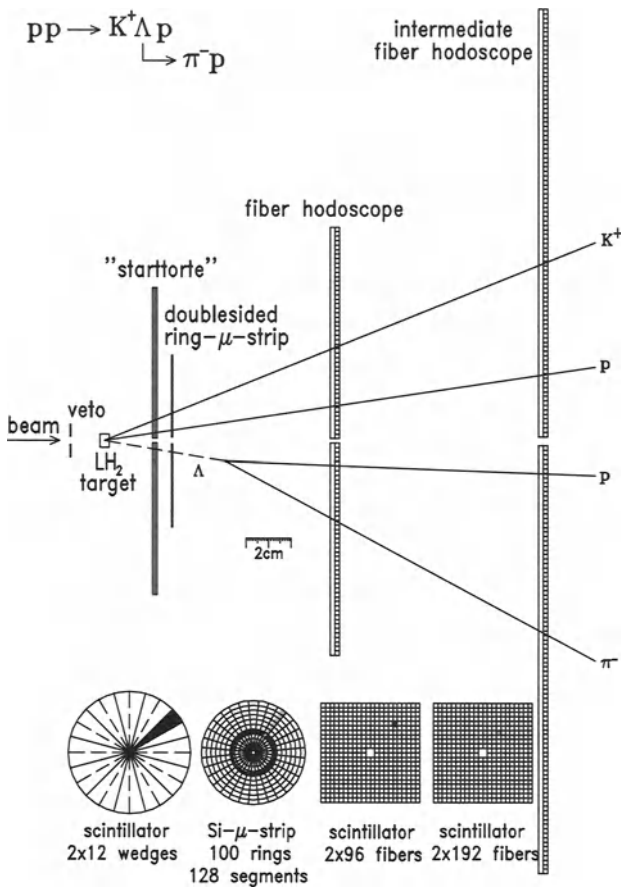

Fig. 2. Scheme of the Erlangen startdetector.

COSY limit at 3.4 GeV/c. It allows the complete reconstruction of the $pp \longrightarrow K^+\Lambda p$ events including the precise measurement of the delayed decay of the Λ-hyperon in two charged particles.

3 Results and discussion

The reaction $pp \longrightarrow K^+\Lambda p$ has been investigated in detail between 2.5 GeV/c and 3.2 GeV/c beam momentum. For all measurements clean event samples on a very low background have been extracted. To demonstrate this, the missing-mass spectra of the reconstructed Λ-hyperons are shown in figs. 3 for the beam momenta of 2.95 and 3.2 GeV/c, respectively.

One big advantage of the TOF experiment is the coverage of the full phase space which allows to extract various exclusive observables model indepentently. A powerful tool to investigate the influence of N^*-resonances and the FSI is the analysis of Dalitz plots. In figs. 4 and 6 the squared masses of the subsystems $K\Lambda$ *versus* $p\Lambda$ are shown for the data at 2.95 and 3.20 GeV/c. A strong deviation from pure phase space is observed.

To investigate this in more detail, we use a meson exchange model of Sibirtsev *et al.* [2] where various contributions can be added in a coherent way. Besides a non-resonant meson exchange which leads to a uniform distribution of the Dalitz plots, the code allows to include the

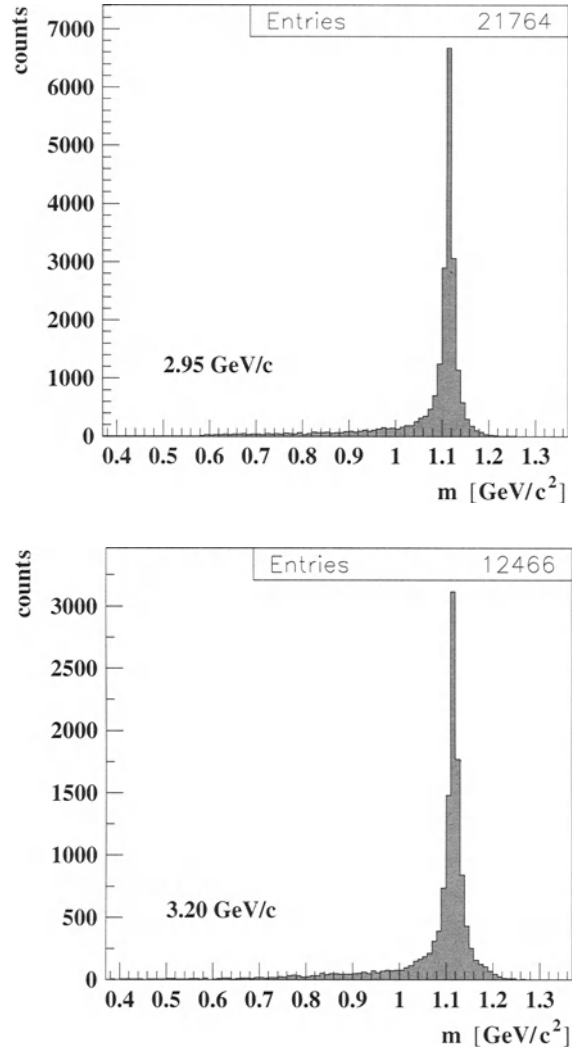

Fig. 3. Λ missing-mass distributions at 2.95 GeV/c (top) and 3.20 GeV/c (bottom).

resonant exchange via the N^*-resonances at 1650, 1710 and 1720 MeV/c^2. The resonances are known to have a significant decay branch into the $K\Lambda$ system. Moreover, $p\Lambda$ FSI can be included.

The contribution of the N^*-resonances without FSI leads to horizontal bands in the investigated Dalitz plots corresponding to their masses and widths. The FSI together with a non-resonant contribution without resonances shows up in an enhancement at low $p\Lambda$ masses. As shown in figs. 5 and 7, the experimental result can only be explained by a coherent addition of both FSI and N^*-resonances. Together with the data at 2.85 GeV/c which are not presented here, the analysis shows a clear and unique result concerning the influence of the N^*-resonances discussed. There is a strong energy dependence; whereas at 2.85 GeV/c only the $N^*(1650)$ is relevant, at 2.95 GeV/c in addition there is already a significant contribution of the $N^*(1710)$. At 3.20 GeV/c the amplitudes of both resonances are equal within the precision of the analysis. This behavior is in good agreement with the prediction of Shyam [3].

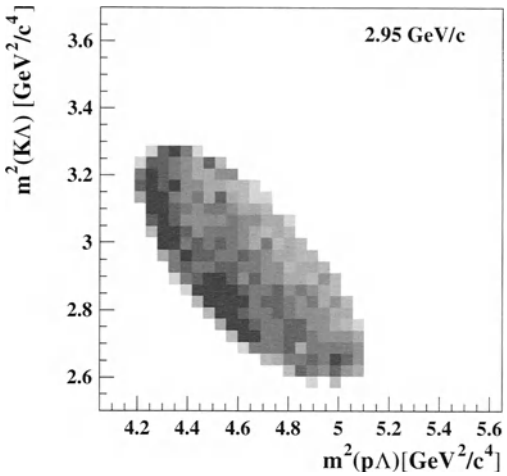

Fig. 4. Dalitz plot at 2.95 GeV/c.

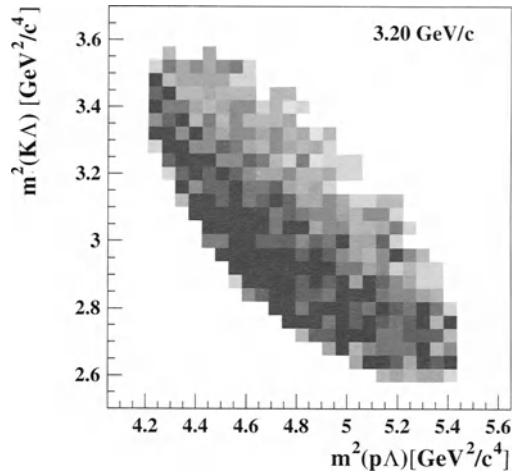

Fig. 6. Dalitz plot at 3.20 GeV/c.

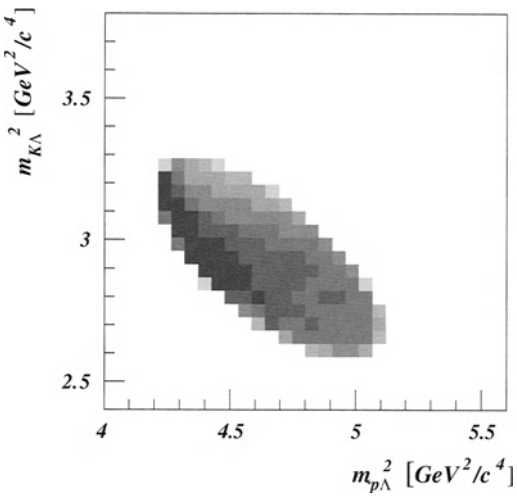

Fig. 5. Result of model calculations at 2.95 GeV/c.

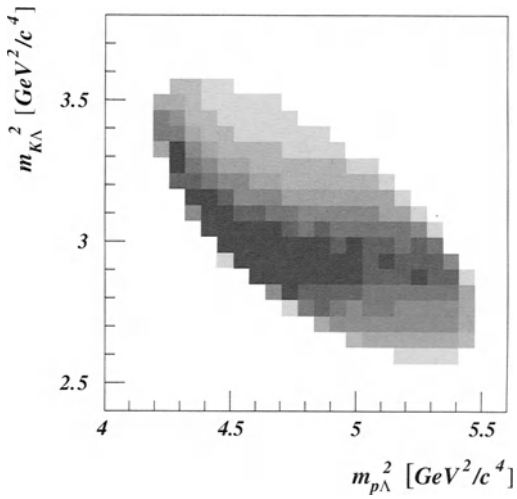

Fig. 7. Result of model calculations at 3.20 GeV/c.

4 Conclusion

The analysis of the Dalitz plots of the COSY-TOF data show for the first time in a clear way the strong influence of N^*-resonances in the Λ production in proton-proton collision close to threshold.

In a further step this method will be extended to the Σ production especially in the channel $pp \longrightarrow K^0\Sigma^+p$ for which first data could already be extracted in the COSY-TOF experiment.

Moreover, the use of a polarized beam will provide additional information for a more detailed analysis including exclusive spin observables.

This work was supported by German BMBF and FZ Jülich.

References

1. A. Bilger *et al.*, Phys. Lett. B **420**, 217 (1998).
2. A. Sibirtsev, private communication (2002).
3. R. Shyam, Phys. Rev. C **60**, 055213 (1999),

Eur. Phys. J. A **18**, 351–354 (2003)
DOI 10.1140/epja/i2002-10234-2

THE EUROPEAN PHYSICAL JOURNAL A

Associated strangeness production at threshold

P. Kowina[1,2,a], M. Wolke[1], H.-H. Adam[3], A. Budzanowski[5], R. Czyżykiewicz[4], D. Grzonka[1], M. Janusz[4], L. Jarczyk[4], B. Kamys[4], A. Khoukaz[3], K. Kilian[1], T. Lister[3], P. Moskal[1,4], W. Oelert[1], T. Rożek[1,2], R. Santo[3], G. Schepers[1], T. Sefzick[1], M. Siemaszko[2], J. Smyrski[4], S. Steltenkamp[3], A. Strzałkowski[4], P. Winter[1], P. Wüstner[6], and W. Zipper[2]

[1] IKP, Forschungszentrum Jülich, D-52425 Jülich, Germany
[2] Institute of Physics, University of Silesia, PL-40-007 Katowice, Poland
[3] IKP, Westfälische Wilhelms-Universität, D-48149 Münster, Germany
[4] Institute of Physics, Jagellonian University, PL-30-059 Kraków, Poland
[5] Institute of Nuclear Physics, PL-31-342 Kraków, Poland
[6] ZEL, Forschungszentrum Jülich, D-52425 Jülich, Germany

Received: 30 September 2002 /
Published online: 22 October 2003 – © Società Italiana di Fisica / Springer-Verlag 2003

Abstract. The associated strangeness dissociation at threshold has been studied at the COSY-11 facility measuring the hyperon and the K^+K^- meson pair production. Measurements of the near-threshold Λ and Σ^0 production via the $pp \to pK^+\Lambda/\Sigma^0$ reaction (S. Sewerin *et al.*, Phys. Rev. Lett. **83**, 682 (1999)) at COSY-11 have shown that the Λ/Σ^0 cross-section ratio exceeds the value at high excess energies ($Q \geq$ 300 MeV (A. Baldini *et al.*, *Total Cross-Sections for Reactions of High-Energy Particles, Landolt-Börnstein, New Series*, Vol. **I/12** (Springer, Berlin, 1988))) by an order of magnitude. For a better understanding additional data have been taken between 13 MeV and 60 MeV excess energy. The near-threshold production of the charged kaon-antikaon pair is related to the discussion about the nature of the scalar states in the 1 GeV/c^2 mass range, *i.e.* the $f_0(980)$ and $a_0(980)$ (O. Krehl, R. Rapp, J. Speth, Phys. Lett. B **390**, 23 (1997)). The interpretation as a $K\overline{K}$ molecule is strongly dependent on the K-$\overline{K}$ interaction which can be studied via the production channel. A first total cross-section value on the reaction $pp \to ppK^+K^-$ at an excess energy of 17 MeV (C. Quentmeier *et al.*, Phys. Lett. B **515**, 276 (2001)), *i.e.* below the ϕ production threshold, was measured.

PACS. 13.75.-n Hadron-induced low- and intermediate-energy reactions and scattering (energy $\leq$ 10 GeV) – 14.20.Jn Hyperons – 14.40.Aq π, K, and η mesons – 25.40.Ep Inelastic proton scattering

1 The Λ/Σ^0 production ratio close to threshold

One of the main investigations of the COSY-11 Collaboration is the associated strangeness production of the neutral Λ and Σ^0 hyperons in the reactions $pp \to pK^+\Lambda/\Sigma^0$. Since the quark structures of these hyperons are analogous to each other, one can expect similar production mechanisms. In such a case the cross-section ratio $\mathcal{R}_{\Lambda/\Sigma^0} \equiv \frac{\sigma(pp\to pK^+\Lambda)}{\sigma(pp\to pK^+\Sigma^0)}$ should be mainly determined by the isospin relation which leads to $\mathcal{R}_{\Lambda/\Sigma^0} = 3$. That is consistent with the ratio of about 2.5 observed at high excess energies ($Q \geq 300$ MeV) [1]. Very close to threshold, in the range of excess energies $Q \leq 13$ MeV, the total cross-sections for the Λ- and Σ^0-hyperon production were measured exclusively at the COSY-11 facility [2,3] at COSY Jülich [4]. The most remarkable feature of the data [5,6] was that at the same excess energy the total cross-section for the Σ^0 production appeared to be about a factor of 28^{+6}_{-9} smaller than for the Λ-particle.

Enhancements in the missing mass distribution at the Λp and ΣN thresholds observed in inclusive K^+ production data, taken at SPES 4 [7] in proton-proton scattering at $Q = 252$ MeV, both having about the same magnitude, suggest a strong $\Sigma N \to \Lambda p$ final-state conversion. This conversion might be responsible for the decrease of the Σ^0 production yield close to threshold as seen in the COSY-11 data. Strong $\Sigma N \to \Lambda p$ conversion effects are also suggested when interpreting the results of K^- scattering on deuterons [8]. Here a sharp peak is clearly seen at an effective mass of the Λ-proton system $m_{\Lambda p} = 2131$ MeV/c^2 corresponding exactly to the $\Sigma^0 p$ threshold.

However, in calculations within the Jülich meson exchange model [9], the final-state conversion is rather excluded as a dominant origin of the observed Σ^0 suppression. In these calculations both the π and the K exchange

[a] e-mail: P.Kowina@fz-juelich.de

are taken into account with inclusion of final-state interaction (FSI) effects. Λ production is found to be dominated by kaon exchange, which is consistent with the experimental results obtained by the DISTO Collaboration [10] at higher excess energies ($Q = 430\,\mathrm{MeV}$). Here the importance of the K exchange is confirmed by a measurement of the polarisation transfer coefficient. On the other hand, in the case of Σ^0 production both the π and the K exchanges are found to contribute with about the same strength. A destructive interference of the π and K exchanges, suggested by Gasparian *et al.* [9], is able to describe the suppression of the Σ^0 production observed in the close-to-threshold data.

Studies of the production ratio in [11] consider two different models: either a π plus K exchange approach or the excitation of intermediate N^*-resonances via an exchange of π- and heavier non-strange mesons, where the N^*'s couple to the K^+Y channel [12], but any interference of the amplitudes is neglected.

The latter mechanism is also taken into account in an effective Lagrangian approach [13] where the strangeness production mechanism is modeled by the exchange of π, ρ, ω and σ mesons, which excite the nucleon resonances $N^*(1650)$, $N^*(1710)$, and $N^*(1720)$. In both calculations experimental data are reproduced within a factor of two.

The one-boson exchange calculation performed by Laget [14] takes into account interference effects of pion and kaon exchange by selecting the relative sign for these two mechanism to maximise the cross-section and reproduce not only the data of the Λ/Σ^0 ratio within a factor of two, but also the polarisation transfer results of the DISTO experiment [10].

Recent COSY-11 measurements [15] extend the Λ/Σ^0 production ratio in proton-proton collisions up to an excess energy $Q = 60\,\mathrm{MeV}$. This allows the study of the behaviour of the cross-section ratio in the transition region between the low-energy range $Q \leq 13\,\mathrm{MeV}$ and data at high excess energies $Q \gg 60\,\mathrm{MeV}$. Together with the new [15] and earlier [5] experimental data, calculations obtained within the approach of Gasparian *et al.* [9] are presented in fig. 1. Here a destructive interference of π and K exchange is assumed, with different choices of the hyperon-nucleon interaction model for low-energy scattering in the final state. The results of the calculations are very sensitive to the off-shell properties of the microscopic hyperon-nucleon interaction.

Both the rather good description of the experimental data very close to threshold by the Jülich model A [16] and the fair agreement for the Nijmegen model (dashed line in fig. 1) with the right tendency of the cross-section ratio should not be regarded as being very conclusive. In the case of the Nijmegen model an explicit isospin symmetry breaking had to be introduced [17]. As a consequence, the relation between amplitudes of the $\Sigma^{\pm}p$ and $\Sigma^0 p$ channels is not uniquely defined [18].

As already emphasised in [19], constant elementary amplitudes and S-waves alone in the final state may not be justified for excess energies above 20 MeV and thus the calculation based on the new Jülich model [20] (solid line in fig. 1) does not reproduce the excitation function of the experimental cross-section ratios.

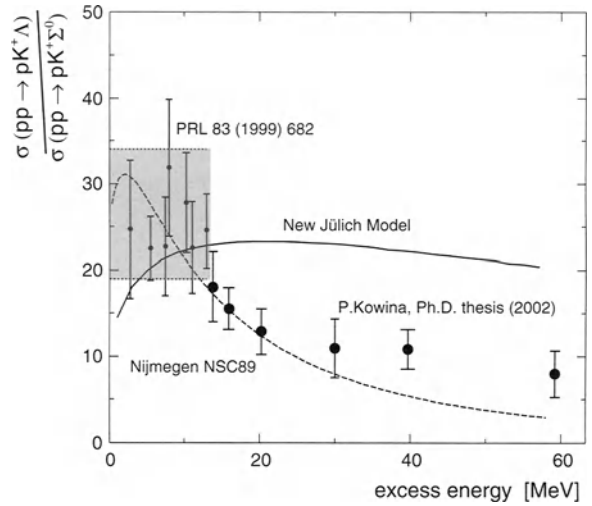

Fig. 1. Energy dependence of the cross-section ratio for Λ/Σ^0 production in proton-proton collisions. Experimental data within the range up to 13 MeV are from [5], data at higher excess energies from [15]. Calculations are performed within the Jülich meson exchange model, assuming a destructive interference of K and π exchange [19] and employing the microscopic YN interaction models Nijmegen NSC89 (dashed line [17]) and the new Jülich model (solid line [20]), respectively.

The data for the Λ production in the excess energy range up to 60 MeV are described fairly well by calculations of the phase space behaviour, which is modified by the p-Λ FSI [15] consistent with the scattering parameters from [21]. In contrast, in the case of Σ^0 there is almost no deviation from the phase space behaviour in the energy dependence of the cross-section for Σ^0 production, which might indicate a very weak p-Σ^0 FSI [15]. However, it should be noted that the apparently weak influence of the p-Σ^0 FSI could be feigned by either higher partial-wave contributions or an energy dependence of the elementary amplitude [19]. Therefore further measurements at an excess energy of $Q \approx 60\,\mathrm{MeV}$ are highly desirable to study the angular distribution of the produced Λ and Σ^0 hyperons.

2 Exclusive kaon-antikaon production at COSY-11

Different interpretations of the structure of the scalar resonances $f_0(980)$ and $a_0(980)$ are known [22,23]. Some motivations for measurements of the K^+K^- production were calculations within the Jülich meson exchange model for the $\pi\pi$ and $\pi\eta$ scattering. The results of these calculation are very sensitive on a strength of the $K\overline{K}$ interaction [24]. Therefore, measurements of the energy dependence of the cross-section can help to confirm or exclude the hypothesis, that the production of K^+K^- occurs via the excitation of the intermediate resonance. Unfortunately those calculations are done only for $\pi\pi$ scattering. However,

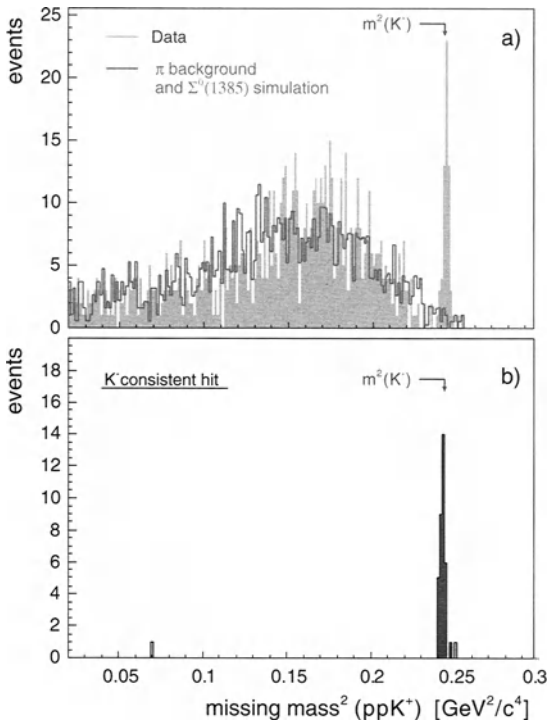

Fig. 2. Missing-mass distribution with respect to an identified (ppK^+) subsystem at an excess energy of 17 MeV above the $pp \to ppK^+K^-$ production threshold without (a) and with (b) K^- detection [25].

similar effects are expected in the case of the pp interaction [26].

From the reconstruction of the full four-momentum vectors for all positively charged ejectiles one obtains the missing-mass spectrum of the (ppK^+) system shown in the upper part of fig. 2, where a clear peak with a resolution (FWHM) of $\approx 2\,\mathrm{MeV}/c^2$ is seen at the mass of the charged kaon. The physical background shown is mainly due to the excitation of the hyperon resonances $\Lambda(1405)$ and $\Sigma(1385)$, where the proton originating from the hyperon resonance decay is detected.

Requiring an additional K^- hit in the dedicated negative particle detector installed at the COSY-11 facility [2] one obtains an almost background-free spectrum of the missing mass of the ppK^+ system shown in the lower part of fig. 2. The number of entries in the K^- peak is slightly reduced compared to the upper figure due to the influence of the kaon decay and acceptance. The analysis resulted in a first total cross-section for the elementary K^+K^- production below the Φ threshold at $Q = 17\,\mathrm{MeV}$, measured in proton-proton scattering. Its value is $\sigma = 1.80 \pm 0.27^{+0.28}_{-0.35}$ nb with statistical and systematical errors, respectively [25]. The cross-section for the $pp \to pK^+\Lambda$ [5,6,15] reaction, which is the elementary K^+ production is two orders of magnitude larger compared to the cross-section for the elementary K^- production in the $pp \to ppK^+K^-$ reaction at corresponding excess energies.

At the present stage it is not possible to judge whether K^+K^- proceeds via a resonant production with the excitation of the $f_0(980)$ and $a_0(980)$ scalar resonances.

The energy dependence of the total cross-section for K^+K^- below [25] and above [27] the Φ threshold might be compared to data for η' [1,28] production, where for an excess energy range $100 \leq Q \leq 1000\,\mathrm{MeV}$ the excitation function is well described by a three-body phase space ($\sigma \propto Q^2$). To describe the data below 100 MeV at least the FSI between the final-state protons and possibly even the FSI between the final-state proton and meson have to be considered.

This is not the case for the K^+K^- production, where calculations based on a one-boson exchange [29] neglecting FSI effects give significantly different results than simply assuming a four-body phase space behaviour. Contrary to the $\pi N \to \eta' N$ amplitudes, the K^+p and especially the K^-p amplitudes are strongly energy dependent [30]. The reason might be a compensation of the interaction of the two strongly interacting subsystems pp and K^-p in the final state or an additional degree of freedom given by the four-body exit channel. In such a case the influence of the FSI effects should be more pronounced at the K^+K^- production threshold [30].

Additional data were taken at the COSY-11 facility at excess energies 10 MeV and 28 MeV, *i.e.* close to the K^+K^- production threshold and slightly below threshold for the Φ production. The data analysis is presently in progress.

References

1. A. Baldini *et al.*, *Total Cross-Sections for Reactions of High Energy Particles, Landolt-Börnstein, New Series*, Vol. **I/12** (Springer, Berlin, 1988).
2. S. Brauksiepe *et al.*, Nucl. Instrum. Methods A **376**, 397 (1996).
3. M. Wolke, Nucl. Phys. News **9**, 27 (1999).
4. R. Maier, Nucl. Instrum. Methods A **390**, 1 (1997).
5. S. Sewerin *et al.*, Phys. Rev. Lett. **83**, 682 (1999).
6. J.T. Balewski *et al.*, Phys. Lett. B **420**, 211 (1998).
7. R. Siebert *et al.*, Nucl. Phys. A **567**, 819 (1994).
8. T.H. Tan, Phys. Rev. Lett. **23**, 395 (1969).
9. A. Gasparian *et al.*, Phys. Lett. B **480**, 273 (2000).
10. F. Balestra *et al.*, Phys. Rev. Lett. **83**, 1534 (1999).
11. A. Sibirtsev *et al.*, e-Print nucl-th/0004022 (2000).
12. K. Tsushima *et al.*, Phys. Rev. C **59**, 369 (1999).
13. R. Shyam *et al.*, Phys. Rev. C **63**, 022202 (2001).
14. J.-M. Laget, Phys. Lett. B **259**, 24 (1991); Nucl. Phys. A **691**, 11c (2001).
15. P. Kowina, PhD Thesis, Silesian University Katowice (2002).
16. B. Holzenkamp *et al.*, Nucl. Phys. A **500**, 485 (1989).
17. P.M.M. Maessen *et al.*, Phys. Rev. C **40**, 2226 (1989).
18. J. Haidenbauer, private communications.
19. A. Gasparyan, *Proceedings of the Symposium on threshold meson production in pp and pd interactions*, edited by P. Moskal, M. Wolke, *Schriften des FZ-Jülich, Matter and Materials*, Vol. **11** (Forschungszentrum Jülich, 2002) p. 205.

20. J. Haidenbauer *et al.*, AIP Conf. Proc. **603**, 421 (2001).
21. J.T. Balewski *et al.*, Eur. Phys. J. A **2**, 99 (1998).
22. U. Thoma, this issue p. 135.
23. D. Morgan, M.R. Pennington, Phys. Rev. D **48**, 1185 (1993); F. Kleefeld *et al.*, Phys. Rev. D **66**, 034007 (2002); R.L. Jaffe, Phys. Rev. D **15**, 267 (1977); F.E. Close, Rep. Prog. Phys. **51**, 833 (1988); F.E. Close *et al.*, Phys. Lett. B **319**, 291 (1993); J. Weinstein, N. Isgur, Phys. Rev. D **41**, 2236 (1990); D. Lohse *et al.*, Nucl. Phys. A **516**, 513 (1990); Z.S. Wang *et al.*, Nucl. Phys. A **684**, 429c (2000).
24. O. Krehl, R. Rapp, J. Speth, Phys. Lett. B **390**, 23 (1997).
25. C. Quentmeier *et al.*, Phys. Lett. B **515**, 276 (2001).
26. J. Haidenbauer, *Proceedings of the Symposium on threshold meson production in pp and pd interactions*, edited by P. Moskal, M. Wolke, *Schriften des FZ-Jülich, Matter and Materials*, Vol. **11** (Forschungszentrum Jülich, 2002) p. 225.
27. F. Balestra *et al.*, Phys. Rev. C **63**, 024004 (2001).
28. F. Hibou *et al.*, Phys. Lett. B **438**, 41 (1998); P. Moskal *et al.*, Phys. Rev. Lett. **80**, 3202 (1998); P. Moskal *et al.*, Phys. Lett. B **474**, 416 (2000); F. Balestra *et al.*, Phys. Lett. B **491**, 29 (2000).
29. A. Sibirtsev *et al.*, Z. Phys. A **358**, 101 (1997).
30. A. Sibirtsev, *Proceedings of the Symposium on threshold meson production in pp and pd interactions*, edited by P. Moskal, M. Wolke, *Schriften des FZ-Jülich, Matter and Materials*, Vol. **11** (Forschungszentrum Jülich, 2002) p. 239.

Eur. Phys. J. A **18**, 355–357 (2003)
DOI 10.1140/epja/i2002-10237-y

THE EUROPEAN PHYSICAL JOURNAL A

First close-to-threshold measurement of the analysing power A_y in the reaction $\vec{p}p \to pp\eta$

P. Winter[1,a], H.-H. Adam[2], A. Budzanowski[3], R. Czyżykiewicz[4], D. Grzonka[1], M. Janusz[4], L. Jarczyk[4], B. Kamys[4], A. Khoukaz[2], K. Kilian[1], P. Kowina[1,6], T. Lister[2], P. Moskal[1,4], W. Oelert[1], C. Piskor-Ignatowicz[4], T. Rożek[1,6], R. Santo[2], G. Schepers[1], T. Sefzick[1], M. Siemaszko[6], J. Smyrski[4], S. Steltenkamp[2], A. Strzałkowski[4], A. Täschner[2], M. Wolke[1], P. Wüstner[5], and W. Zipper[6]

[1] IKP, Forschungszentrum Jülich, D-52425 Jülich, Germany
[2] IKP, Westfälische Wilhelms-Universität, D-48149 Münster, Germany
[3] Institute of Nuclear Physics, PL-31-342 Kraków, Poland
[4] M. Smoluchowski Institute of Physics, Jagellonian University, PL-30-059 Kraków, Poland
[5] ZEL, Forschungszentrum Jülich, D-52425 Jülich, Germany
[6] Institute of Physics, University of Silesia, PL-40-007 Katowice, Poland

Received: 30 September 2002 /
Published online: 22 October 2003 – © Società Italiana di Fisica / Springer-Verlag 2003

Abstract. At the internal facility COSY-11 a first measurement of the reaction $\vec{p}p \to pp\eta$ near the production threshold has been performed. Results for the analysing power will be presented and a comparison with one-meson exchange models will be discussed.

PACS. 12.40.Vv Vector-meson dominance – 13.60.Le Meson production – 13.88.+e Polarization in interactions and scattering – 24.70.+s Polarization phenomena in reactions

1 Introduction

Triggered by an extensive database on η-meson production in NN collisions through measurements of total [1–6] as well as differential cross-sections [7–11] lots of theoretical investigations have been performed in this field of physics over the last years. Several one-meson exchange models —differing mainly in the assumptions for the production mechanism— reproduce the existing data quite well so that additional measurements are needed. Polarisation observables —analysing powers or spin correlation coefficients— present a powerful tool because they are sensitive to the influence of higher partial waves.

2 Experiment

The measurement was performed at the internal facility COSY-11 [12,13] at the COoler SYnchrotron COSY [14] in Jülich with a beam momentum of $p_{\text{beam}} = 2.096\,\text{GeV}/c$ corresponding to an excess energy $Q = 40\,\text{MeV}$. The reaction takes place in a cluster target [15] mounted in front of a COSY dipole magnet. A set of drift chambers and a time-of-flight measurement with scintillation detectors allows for a four-momentum determination of positively charged ejectiles. An identification of the unregistered meson succeeds with the missing-mass method (see fig. 1).

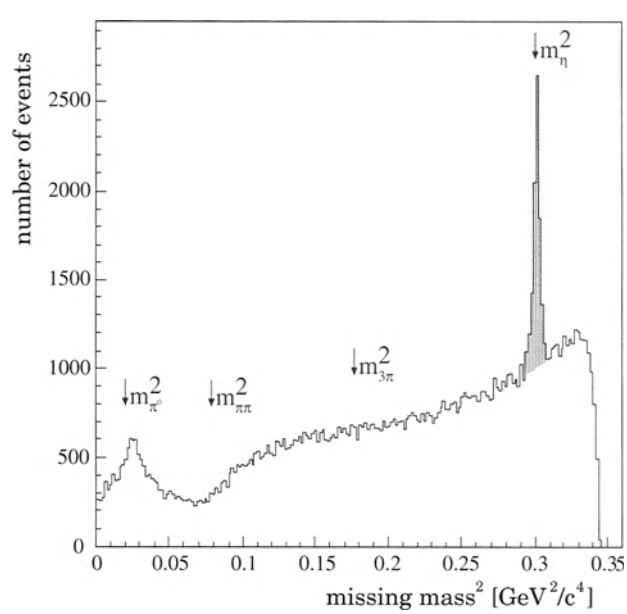

Fig. 1. Missing-mass spectrum of events with two identified protons in the exit channel.

[a] e-mail: p.winter@fz-juelich.de

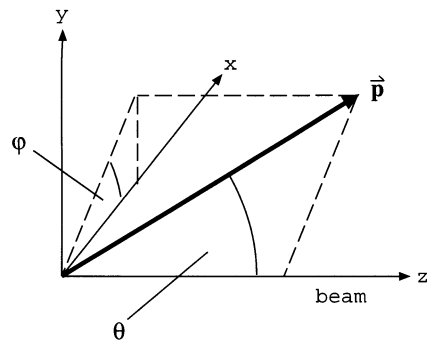

Fig. 2. Definition of the angles. θ is defined as the angle between momentum vector and the z-axis, φ between the x-axis and the projection of $\vec{p}$ onto the x-y plane.

Table 1. Averaged beam polarisation obtained with the simultaneous measurement at the EDDA experiment.

	Time block 1	Time block 2
$P_\uparrow$	0.381 ± 0.007	0.497 ± 0.006
$P_\downarrow$	-0.498 ± 0.007	-0.572 ± 0.007

Besides a clear signal from the η-meson there is a broad background due to multi-pion reactions. The rising shape of this background results from the acceptance behaviour of the detection system. A subtraction of the background with a polynomial fit allows the determination of the number of η-events. An efficiency correction for the polar and azimuthal angle of the relative proton-proton momentum in the pp rest system was applied. This is necessary for an extraction of interference terms from contributing partial waves. The detailed analysing procedure is described in [16,17].

3 Results

For later purposes, fig. 2 depicts the definition of the used polar (θ) and azimuthal (φ) angle. The indices p and q refer to the pp rest system and the η-meson in the CMS, respectively. The angle θ_p is chosen such that $0 \leq \theta_p \leq \pi/2$. This choice guarantees that all observables are invariant under the transformation $\vec{p} \to -\vec{p}$, as required by the identity of the two protons in the final state.

The determination of the analysing power needs the knowledge of the averaged beam polarisation $P_{\uparrow,\downarrow}$ for the cycles with spin up and down, respectively, the relative time-integrated luminosity $\mathcal{L}_{\rm rel} := \int \mathcal{L}_\downarrow \, {\rm d}t_\downarrow \, / \int \mathcal{L}_\uparrow \, {\rm d}t_\uparrow$ and the number of events $N_{\uparrow,\downarrow}$.

Via a simultaneous measurement of the $\vec{p}p$ elastic scattering at the internal experiment EDDA [18,19] the beam polarisation was determined for two time blocks (see table 1). The slight increase between the two blocks was caused by improved tuning of the beam with respect to polarisation.

The relative luminosity was extracted from the comparison of the measured angular distribution of the elastically scattered protons with the distribution known from the literature [18,19] (see table 2).

Table 2. Time-integrated relative luminosity $\mathcal{L}_{\rm rel}$.

	Time block 1	Time block 2
$\mathcal{L}_{\rm rel}$	$1.004 \pm 0.004\,^{+0.002}_{-0.002}$	$0.949 \pm 0.004\,^{+0.001}_{-0.001}$

Table 3. Analysing power as a function of the emission angle θ_q^* of the η-meson in the CMS.

$\cos\theta_q^*$	$\bar{A}_y(\cos\theta_q^*)$
-0.75 ± 0.25	0.19 ± 0.21
-0.25 ± 0.25	-0.02 ± 0.09
0.25 ± 0.25	0.05 ± 0.06
0.75 ± 0.25	-0.05 ± 0.06

In order to account for the detection efficiency the data has been corrected on an event-by-event basis by the weighting factors determined via Monte Carlo simulations [16,17]. Using a GEANT-3 code, 10^7 events were generated and for each event a detection system response was calculated. The simulated data sample was analysed with the same programme which is used for the analysis of the experimental data.

The determined averaged values $\bar{A}_y(\cos\theta_q^*)$ of the analysing power for the $\vec{p}p \to pp\eta$ reaction are presented in table 3 as a function of the center-of-mass polar angle $\cos\theta_q^*$ of the η-meson. Explicitely, $\bar{A}_y(\cos\theta_q^*)$ is defined via

$$\bar{A}_y(\cos\theta_q^*) := \tag{1}$$

$$\iiint \frac{{\rm d}^2\sigma}{{\rm d}\Omega_p {\rm d}\Omega_q}(\xi)\, A_y(\xi)\, {\rm d}\cos\theta_p {\rm d}\varphi_p {\rm d}\varphi_q^* \,/\, \frac{{\rm d}\sigma}{{\rm d}\cos\theta_q^*}\,, \tag{2}$$

where ξ denotes the set of the five variables which kinematically completely describe the exit channel, namely (θ_p, φ_p, θ_q^*, φ_q^*, E_{pp}). The kinetic energy E_{pp} of the two final protons in their CM system is given by $E_{pp} = \sqrt{s_{12}} - 2m_p$ with $\sqrt{s_{12}} = 2\sqrt{\vec{p}^2 + m_p^2}$ as the energy in the pp subsystem. θ_q^* and φ_q^* denote the angles of the η-meson in the CMS.

For the derivation of these values for the analysing power $\bar{A}_y(\cos\theta_q^*)$, we used an ansatz for the spin-dependent cross-section as already applied in case of the $\vec{p}\vec{p} \to pp\pi^0$ reaction [20]. With the inclusion of the efficiency correction, an integration gives (details can be reviewed in [16])

$$\iint \frac{{\rm d}^2\sigma}{{\rm d}\Omega_p {\rm d}\Omega_q}(\xi)\, A_y(\xi)\, {\rm d}\cos\theta_p\, {\rm d}\varphi_p =$$

$$2\pi \left(G_1^{y0} \sin\theta_q^* + (H_1^{y0} + I^{y0}) \sin 2\theta_q^* \right) \cos\varphi_q^*, \tag{3}$$

where G_1^{y0}, H_1^{y0} and I^{y0} described in [20] correspond to the explicit interference terms $(PsPp)$, $(Pp)^2$ and $(SsSd)$ of the partial-wave amplitudes. Here, the relative angular momentum of the two outgoing protons in their rest system is denoted by capital letters $l_p = S, P, D \ldots$, the one of the η-meson in the CMS by small letters $l_q = s, p, d \ldots$.

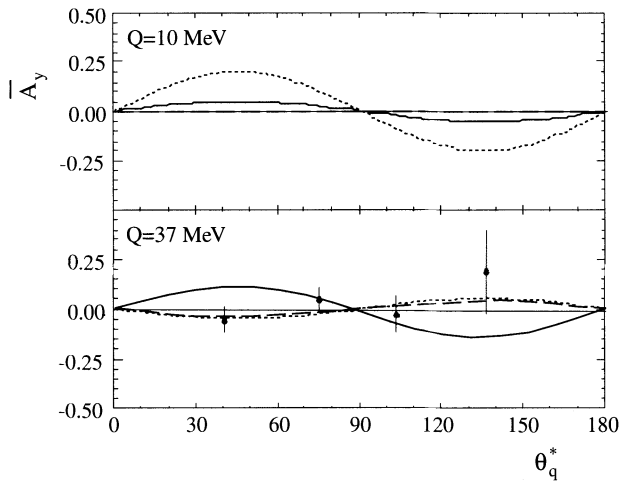

Fig. 3. Analysing power for the reaction $\vec{p}p \to pp\eta$ in dependence on θ_q^* for the two excess energies $Q = 10\,\mathrm{MeV}$ and $37\,\mathrm{MeV}$.

With eqs. (2) and (3), it can be shown that an extraction of the interference terms G_1^{y0} and $H_1^{y0} + I^{y0}$ is possible from the experimental data via

$$G_1^{y0} = \frac{1}{\pi^2} \sum_{\cos\theta_q^*} \frac{\mathrm{d}\sigma}{\mathrm{d}\cos\theta_q^*} \bar{A}_y \cdot \Delta\cos\theta_q^* ,$$

$$H_1^{y0} + I^{y0} = \frac{2}{\pi^2} \sum_{\cos\theta_q^*} \frac{\mathrm{d}\sigma}{\mathrm{d}\cos\theta_q^*} \bar{A}_y \cos\theta_q^* \cdot \Delta\cos\theta_q^* ,$$

and results in

$$G_1^{y0} = (0.003 \pm 0.004)\,\mu\mathrm{b}$$

and

$$H_1^{y0} + I^{y0} = (-0.005 \pm 0.005)\,\mu\mathrm{b}\,.$$

4 Comparison with theory

Figure 3 shows a comparison of the data (triangles) with two model predictions taken from [21] (dotted line) and [22] (solid and dashed lines) for $Q = 10\,\mathrm{MeV}$ and $37\,\mathrm{MeV}$.

While Fäldt and Wilkin [21] conclude a dominant ρ-meson exchange for the underlying production mechanism, the authors of ref. [22] find a dominance of π and η exchange (solid line). The dashed curve represents a reduction of their full model to a vector dominance model with an exclusion of π and η exchange. It seems that the data favours slightly the vector dominance exchange models.

The observable structure of the experimental values show a slight deviation from the $\sin\theta_q^* \cos\theta_q^*$-dependence of both models. This deviation indicates a non-vanishing value of G_1^{y0}. As this corresponds to the $(PpPs)$-term, an influence of the P-wave must be suspected but right now the experimental result for G_1^{y0} is compatible with zero. A non-zero G_1^{y0} would imply that H_1^{y0} —describing the $(Pp)^2$ interference— should have a non-negligible contribution, too. For further detailed studies the data are not yet precise enough to disentangle the sum of H_1^{y0} and I^{y0}. Therefore, new data at $Q = 37\,\mathrm{MeV}$ has been taken in September 2002 in order to reduce the error bars by more than a factor of 2. The data analysis is currently in progress but it is already obvious that the much higher statistics and polarisation of $P \approx 80\%$ will enable to achieve a significant increase in precision.

Furthermore, additional measurements are scheduled in the first half of 2003 at $Q = 2$, 10 and 25 MeV for tests on the predictions of the different models for the energy dependence of $A_y(\theta_q^*)$.

This work was partly supported by the European Community – Access to Research Infrastructure action of the Improving Human Potential Programme.

References

1. A.M. Bergdolt *et al.*, Phys. Rev. D **48**, 2969 (1993).
2. E. Chiavassa *et al.*, Phys. Lett. B **322**, 270 (1994).
3. Calén, H. *et al.*, Phys. Lett. B **366**, 39 (1996).
4. Calén, H. *et al.*, Phys. Rev. Lett. **79**, 2642 (1997).
5. F. Hibou *et al.*, Phys. Lett. B **438**, 41 (1998).
6. J. Smyrski *et al.*, Phys. Lett. B **474**, 182 (2000).
7. Calén, H. *et al.*, Phys. Lett. B **458**, 190 (1999).
8. B. Tatischeff *et al.*, Phys. Rev. C **62**, 054001 (2000).
9. P. Moskal *et al.*, πN Newslett. **16**, 367 (2001).
10. The COSY-TOF Collaboration (M. Abdel-Bary *et al.*), Eur. Phys. J. A **16**, 127 (2003) nucl-ex/0205016.
11. P. Moskal *et al.*, Nucl. Phys. A **721**, 657 (2003), nucl-ex/0212003
12. S. Brauksiepe *et al.*, Nucl. Instrum. Methods A **376**, 397 (1996).
13. P. Moskal *et al.*, Nucl. Instrum. Methods A **466**, 444 (2001).
14. R. Maier, Nucl. Instrum. Methods A **390**, 1 (1997).
15. H. Dombrowski *et al.*, Nucl. Instrum. Methods A **386**, 228 (1997).
16. P. Winter *et al.*, Phys. Lett. B **544**, 251 (2002).
17. P. Winter, Diploma thesis, Rheinische Friedrich-Wilhelms-Universität Bonn, 2002, IKP Jül-3943.
18. D. Albers *et al.*, Phys. Rev. Lett. **78**, 1652 (1997).
19. M. Altmeier *et al.*, prl, **85**, 1819 (2000).
20. H.O. Meyer *et al.*, Phys. Rev. C **63**, 064002 (2001).
21. G. Fäldt, C. Wilkin, Phys. Scr. **64**, 427 (2001).
22. K. Nakayama, J. Speth, T.S.H. Lee, Phys. Rev. C **65**, 045210 (2002).

Eur. Phys. J. A **18**, 359–361 (2003)
DOI 10.1140/epja/i2002-10235-1

THE EUROPEAN PHYSICAL JOURNAL A

Aspects of a_0^0-f_0 mixing in the reaction pn $\rightarrow$ dX

C. Hanhart[a]

Institut für Kernphysik, Forschungszentrum Jülich, D-52425 Jülich

Received: 30 September 2002 /
Published online: 22 October 2003 – © Società Italiana di Fisica / Springer-Verlag 2003

Abstract. Possibilities to study the a_0^0-f_0 mixing amplitude in meson production reactions in nucleon-nucleon collisions are discussed. It is argued that, even without knowing the production operator, it is possible to gain valuable insights from these reactions.

PACS. 13.60.Le Meson production – 13.75.-n Hadron-induced low- and intermediate-energy reactions and scattering (energy ≤ 10 GeV) – 14.40.Cs Other mesons with $S = C = 0$, mass < 2.5 GeV

The structure as well as the properties of the lightest scalar mesons is not yet understood. It is believed that the a_0^0-f_0 mixing amplitude will give some hint on the nature of these resonances. In this paper the experimental signal from the reaction $pn \rightarrow d(\pi\eta)_{(s\text{-wave})}$ induced by a_0^0-f_0 mixing is discussed in a model-independent way. It was observed recently that this reaction is an ideal system to study the mixing, for the deuteron in the final state acts as an isospin filter that kinematically enhances the signal of the mixing [1]. We will come back to this point later.

Naturally there are two ingredients that contribute to any observable of the reaction $pn \rightarrow d(\pi\eta)_{(s\text{-wave})}$, namely the primary production of the two-meson system and its propagation. It is the latter that we are interested in, however, we first need to understand the former to draw definite conclusions. In the close-to-threshold regime it should be sufficient to include the lowest partial waves possible only. However, even this simplification is still insufficient to allow us to construct the production operator directly. But it limits the number of partial waves allowed sufficiently that it is still possible to make definite statements. The energy dependence of the initial-state interaction as well as the one of the production operator should scale with the initial momentum. The interactions in the outgoing system, however, should scale with the typical momentum in the final-state $k \simeq \sqrt{2M_N Q}$, where $Q = \sqrt{s} - \sqrt{s_{\text{thr}}} = \sqrt{s} - \sqrt{2M_N + m}$. Note, since we study the production of an unstable meson or more exactly a two-meson system, one has to generalize the definition of the excess energy: the mass m in the above equation denotes the invariant mass of this system. Following the same philosophy as that of effective field theories, we simply construct the most general structure of the amplitude consistent with the symmetries of the underlying theory. The coefficients appearing can be assumed constant (up to corrections of the order $(|\boldsymbol{k}|/|\boldsymbol{p}|)^2$). Thus, based on rather general arguments it should be possible to study the final state even without knowing anything about the actual mechanism of production.

The goal of the present investigation is to study the a_0^0-f_0 mixing that demands the presence of charge symmetry breaking. However, the resonance parameters of f_0 and a_0 are very close to each other. Therefore, as long as we stay close to the resonance mass, the mixing in the propagating meson system should be far more important than any possible mechanism of charge symmetry breaking in the primary production amplitude. This is the central assumption of this investigation.

As was stated in the beginning, in this presentation we consider the mesons to be in a relative s-wave. This largely simplifies the construction of the transition operator, for under this assumption only $\boldsymbol{k}$ (the center-of-mass momentum of the deuteron), $\boldsymbol{S}$ (the spin of the initial NN system), $\boldsymbol{p}$ (the beam momentum) and ϵ (the deuteron polarization) can appear explicitly in the transition operator. In addition, conservation of angular momentum, isospin and parity demands that an isospin-one scalar state is to be produced in a p-wave with respect to the deuteron. Therefore, only the following four transitions are possible: ${}^3P_J \rightarrow ({}^3S_1 - {}^3D_1)p$ and ${}^3F_2 \rightarrow ({}^3S_1 - {}^3D_1)p$, where $J = 0, 1, 2$. Having said this it is a straightforward task to express all observables for the isospin-one system in terms of the partial-waves amplitudes. However, there is a more transparent way to come to the same result, that at the same time allows for a more straightforward interpretation of the observables in terms of the spin structure of the production operator. For that one just has to construct

[a] e-mail: c.hanhart@fz-juelich.de

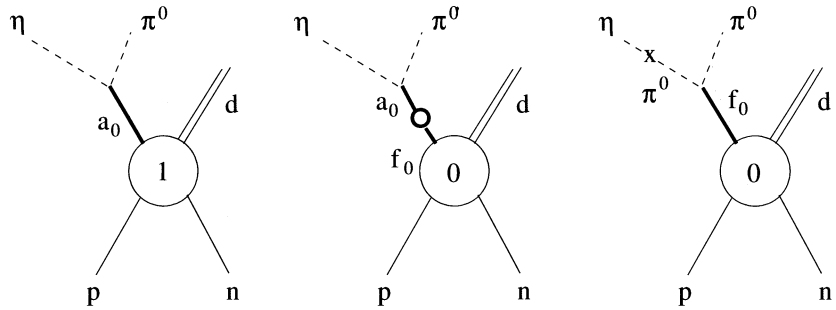

Fig. 1. Diagrammatic representation of the approach for the π-η final state. The large circles denote the primary production amplitudes, whereas the little circle indicates the a_0^0-f_0 transition amplitude. The thick solid lines denote the propagation of the resonances.

all possible scalars from the vectors available. We get

$$M_1 = a\,(\boldsymbol{p}\cdot\boldsymbol{S})\,(\boldsymbol{k}\cdot\boldsymbol{\epsilon}^*) + b\,(\boldsymbol{p}\cdot\boldsymbol{k})\,(\boldsymbol{S}\cdot\boldsymbol{\epsilon}^*) + c\,(\boldsymbol{k}\cdot\boldsymbol{S})\,(\boldsymbol{p}\cdot\boldsymbol{\epsilon}^*) + d\,(\boldsymbol{p}\cdot\boldsymbol{S})\,(\boldsymbol{p}\cdot\boldsymbol{\epsilon}^*)\,(\boldsymbol{k}\cdot\boldsymbol{p})\,. \quad (1)$$

This procedure was advocated in ref. [2] and applied more rigorously in ref. [3].

The isoscalar f_0, on the other hand, can be produced in an s-wave and we find

$$M_0 = f\,(\boldsymbol{S}\cdot\boldsymbol{\epsilon}^*) + g\,(\boldsymbol{p}\cdot\boldsymbol{S})\,(\boldsymbol{p}\cdot\boldsymbol{\epsilon}^*)\,. \quad (2)$$

It is obvious from eqs. (1) and (2) that $\mathcal{M}_1 \propto k$ and $\mathcal{M}_0 \propto$ const near the threshold. For the isospin-conserving case we therefore get

$$\frac{\mathrm{d}\sigma}{\mathrm{d}m^2}(pn \to da_0) \propto Q^{3/2} \text{ and } \frac{\mathrm{d}\sigma}{\mathrm{d}m^2}(pn \to df_0) \propto Q^{1/2}\,.$$

Thus, if we study a channel where the two-meson system is produced in an isovector state, namely $\pi^0\eta$, only the occurrence of charge symmetry breaking allows the contribution of s-wave production. This is the kinematical enhancement mentioned in the beginning. In addition, that the symmetry conserving piece starts with a p-wave has a large influence on any differential observable as we will discuss below.

Since the main focus of the paper is the $\pi\eta$ channel it is convenient to introduce a mixing parameter ξ by

$$\xi(m) = \Sigma_{01}(m)\,\tilde{G}_{f_0}(m^2), \quad (3)$$

where Σ_{01} was defined in ref. [3] and is related to the a_0^0-f_0 transition amplitude. Let $\boldsymbol{p}\cdot\boldsymbol{k} = pk\cos\theta$ and $\boldsymbol{\zeta}\cdot[\boldsymbol{k}\times\boldsymbol{p}] = \zeta\,pk\sin\theta\,\sin\varphi$ ($\zeta = |\boldsymbol{\zeta}|$). Using those expressions we get

$$\overline{|\mathcal{M}(\theta,\varphi)|^2} = C_0 + C_1\cos\theta + C_2\cos^2\theta + \zeta\,\sin\theta\,\sin\varphi\,(D_0 + D_1\cos\theta)\,, \quad (4)$$

where

$$C_0 = \frac{1}{2}\left(|a|^2 + |c|^2\right)p^2k^2 + \left(|f|^2 + \frac{1}{2}|f + p^2g|^2\right)|\xi|^2\,,$$

$$C_1 = pk\,\mathrm{Re}\left(\left[(a + b + c + p^2d)^*(f + p^2g) + 2b^*f\right]\xi\right)\,,$$

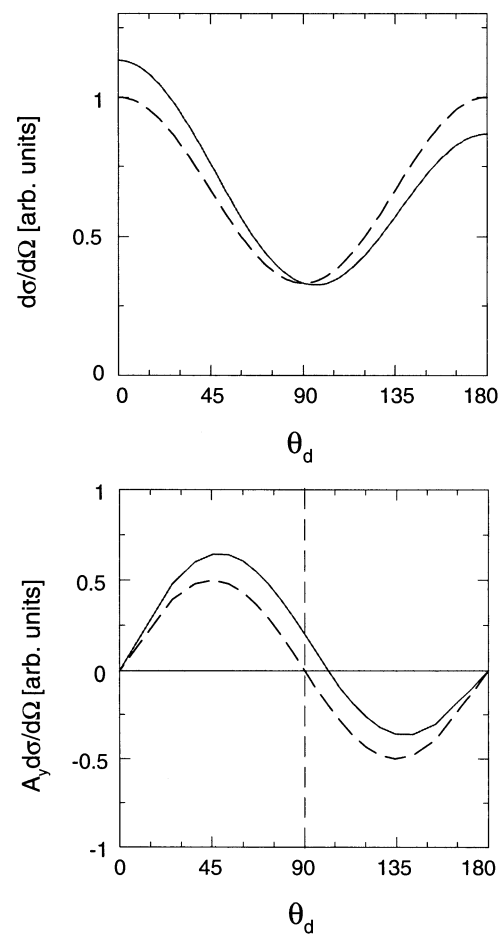

Fig. 2. Sketch of the possible signal for both the differential cross-section as well as the analyzing power in the reaction $pn \to \pi\eta d$. The dashed line corresponds to the observables without isospin breaking, whereas the solid line shows the expected signal in the presence of isospin violation.

$$C_2 = p^2k^2\left[|b|^2 + \frac{1}{2}|b + p^2d|^2 + \mathrm{Re}\left(a^*c + (a + c)^*(b + p^2d)\right)\right],$$

$$D_0 = pk\,\mathrm{Im}\left(\left[a^*f - c^*(f + p^2g)\right]\xi\right)\,,$$

$$D_1 = p^2k^2\,\mathrm{Im}(a^*b + a^*c + b^*c + p^2d^*c)\,.$$

Here, also the role of the deuteron as isospin filter becomes clear: since it is an isoscalar, the isospin of the two-meson system determines the isospin of the initial two-nucleon system, as long as isospin is conserved. Therefore, in the absence of isospin breaking the differential cross-section is necessarily forward-backward symmetric. Therefore any forward-backward asymmetry is a direct measure of isospin violation. This is indicated in the upper panel of fig. 2. Please note that the curves are not based on a calculation but are meant as a sketch for illustration.

Another interesting observable is the analyzing power. As one can read directly of eq. (4), in the absence of isospin violation the analyzing power vanishes at 90°. Thus, any deviation from zero at 90° directly measures the isospin violation. This is true not only if only the lowest partial waves are included, but also in the presence of higher partial waves, as long as we restrict ourselves to a relative s-wave in the two-meson system. However, it should be stressed that a relative p-wave in the two-meson system can also lead to a shift of the zero in the analyzing power, even in the absence of any isospin breaking. This effect can be studied in the reaction $pp \to d\pi^+\eta$, since a charged two-meson state does not mix with an isospin-zero state.

In ref. [4] it was argued recently that especially in the $K\bar{K}$ channel not only the resonances in the two-meson system, but also a meson-baryon resonance, namely the $\Lambda(1405)$, should play a significant role in the reaction under consideration. The authors predicted a significant change in the invariant-mass distributions of the final particles. Since this resonance favors an s-wave of the $\bar{K}$ and the deuteron, it is this additional final-state interaction that should strongly enhance the p-waves in the meson-meson system. Again, also this point can already be studied in the reaction $pp \to d\pi^+\eta$. It should be stressed, that preliminary data from the ANKE Collaboration at COSY indicate, that there is indeed a sizable amount of p-wave strength in the $K\bar{K}$ system.

To summarize, in this paper recent studies were presented, that demonstrate, that the production of scalar mesons in nucleon-nucleon collisions might be the ideal reaction to investigate the properties of scalar mesons, especially their mixing. It is the latter attribute that is believed to be the key to an understanding of the nature of scalar mesons.

References

1. A.E. Kudryavtsev, V.E. Tarasov, JETP Lett. **72**, 401 (2000), nucl-th/0102053.
2. V.Yu. Grishina, L.A. Kondratyuk, M. Büscher, W. Cassing, H. Ströher, Phys. Lett. B **521**, 217 (2001).
3. A.E. Kudryavtsev, V.E. Tarasov, J. Haidenbauer, C. Hanhart, J. Speth, Phys. Rev. C **66**, 015207 (2002).
4. E. Oset, J.A. Oller, Ulf-G. Meißner, Eur. Phys. J. A **12**, 435 (2001).

Eur. Phys. J. A **18**, 363–365 (2003)
DOI 10.1140/epja/i2002-10238-x

THE EUROPEAN PHYSICAL JOURNAL A

Surface pion condensation in finite nuclei

H. Toki[1,2,a], K. Ikeda[2], and S. Sugimoto[2]

[1] Research Center for Nuclear Physics (RCNP), Osaka University, Ibaraki, Osaka, 567-0047, Japan
[2] RIKEN, 2-1 Hirosawa, Wako, Saitama 351-0105, Japan

Received: 30 September 2002 /
Published online: 22 October 2003 – © Società Italiana di Fisica / Springer-Verlag 2003

Abstract. We discuss here the possible occurrence of surface pion condensation in finite nuclei. We show the argument for this possibility by the recent findings in few-body calculations and the spin-flip experiments. We show the calculated results on various $N = Z$ nuclei using the relativistic mean-field theory with a pion.

PACS. 21.60.-n Nuclear-structure models and methods

1 Introduction

The pion was conjectured by Yukawa as the mediator of the nucleon-nucleon interaction [1]. It has the properties $J^\pi = 0^-$ spin parity and $T = 1$ isospin, which result in rich phenomena in hadron and nuclear physics. The pion plays a central role in hadron physics, particularly for low-energy phenomena. The chiral perturbation approach, with the pion acting as the essential degree of freedom, is a powerful tool in the study of hadron properties and their interactions.

Since the proposal of the shell model, nuclear structure has been studied in terms of the single-particle basis [2]. In that treatment, single-particle orbits are obtained with the parity-conserved mean field given by the central and spin-orbit potential. However, when a virtual pion is emitted and absorbed by a nucleon in a good-parity orbit, the nucleon makes a jump from one single-particle state to another with opposite parity, accompanied by a spin flip due to the pion-nucleon coupling. Therefore, to incorporate the effect of the correlation caused by the pion exchange interaction in the parity-conserved single-particle space, we must treat higher configurations, like 2p-2h (2 particle-2 hole) states, crossing over major shells. To avoid such complications, we renormalize the central and the spin-orbit interactions in nuclei to take into account the strong correlations caused by the pion in the restricted model space. This means that we assume a model space in which the parity of a single-particle state is conserved and then define an effective interaction acting between nucleons in the model space. Hence, the pion is not treated explicitly in conventional nuclear physics. One of the main motivations of the present study is to expand the model space so that the important role of the pion is explicitly accounted for in order to see the effect of the correlation induced by the pion on nuclear structure [3].

With regard to the importance of the pion, we recall findings concerning few-body systems, which can be treated rigorously without the restriction of model space, explicitly using a realistic nucleon-nucleon interaction that has a short-range repulsive core and a tensor force [4,5]. The calculations are performed in a non-relativistic framework, and hence the pion appears mainly as a tensor force, which is much stronger than the central force in the one-pion exchange interaction. There are many existing extensive calculations that employ variational principles and sophisticated numerical techniques, and the calculated results compare with experiments very well [4,5]. The calculated results demonstrate the dominant role of the tensor force in few-body systems. Recent variational calculations carried out by the Argonne group up to $A = 8$ also demonstrate the dominant role of the pion, which amounts to 70–80% of the strength of the two-body interaction part in $3 \leq A \leq 8$ systems.

There are several sets of experimental data that make apparent the important role of the pion in medium and heavy nuclei. The (p, n) reactions with medium and heavy nuclei demonstrate that slightly more than one half of the Gamow-Teller $(\sigma\tau)$ strength is carried by 1p-1h excitations, while most of the rest is interpreted as being carried by 2p-2h excitations, due to the coupling with the 1p-1h states by the strong tensor force, which distributes the strength up to at least 50 MeV in excitation energy [6]. A further dramatic result is that the ratio of the longitudinal and transverse spin responses is found to be close to 1, while the strong pionic correlations should provide a large enhancement in the longitudinal channel [7]. This experimental result seems to imply the need for a special

[a] e-mail: toki@rcnp.osaka-u.ac.jp

improvement of the treatment of the pion in nuclear spin response.

The above considerations seem to indicate the importance of the correlation induced by the pion in the description of nuclear many-body systems. For this reason, we would like to construct a framework in which the pionic effect is treated explicitly under a mean-field approximation for medium and heavy nuclei. To this end, we break the parity, spin, and isospin symmetries of single-particle states to treat the pion in the mean-field approximation. This treatment may oppose the common sense belief that pion condensation does not occur in nuclear matter at the saturation density. This fact does not mean, however, that the pion mean field vanishes in a finite nuclear system. The pion is a pseudoscalar meson; it couples with a nucleon through the $\boldsymbol{\sigma}\cdot\boldsymbol{\nabla}$ coupling, and therefore the source term of the pion field needs parity mixing and spin-density modulation. In infinite matter in a high-density region, we have to provide this spin-density modulation (ALS structure) for the pion to act, which requires a large amount of energy [8]. In a finite nuclear system, we have the nuclear surface, and automatically there arises the spin-density modulation necessary for the pion to act. Details are published in ref. [3].

2 Relativistic mean-field theory with a pion

We take the standard expression for the relativistic mean-field Lagrangian together with the pion field. We give here only the equations of motion for the nucleon and the pion explicitly. They are

$$[i\gamma^\mu\partial_\mu - M - g_\pi\boldsymbol{\nabla}\pi\gamma_5\boldsymbol{\gamma}\tau_0]\psi = 0 \tag{1}$$

for the nucleon and

$$(\boldsymbol{\nabla}^2 - m_\pi^2)\pi = -g_\pi\boldsymbol{\nabla}\langle\bar{\psi}\gamma_5\boldsymbol{\gamma}\tau_0\psi\rangle \tag{2}$$

for the pion. Here, the brackets $\langle\cdots\rangle$ denote the ground-state expectation value. The other mesons obey equations of motion similar to those above. Their explicit forms are given in ref. [9].

Equations (1) and (2) describe the structure of the pion mean field. These equations reveal why we have not included the pion mean field until now. If single-particle states in a mean field have good parity, the source term of the pion field becomes zero. Hence, we must break parity in the construction of the single-particle states. The violation of parity is caused by the pion term in the above Dirac equation for nucleons. The pion field is finite when the source term breaks parity symmetry. The pion field is enhanced by the spatial dependence of the source term due to the derivative of the coupling of the pion and the nucleon. When the pion field is finite in (1), the nucleon single-particle state breaks the parity symmetry, which makes the pion source term finite. The self-consistency condition is used to obtain a convergent solution to the above equations. If the pion mean field becomes finite, the parity symmetry is broken, and this is interpreted as the occurrence of pion condensation in the finite nuclei.

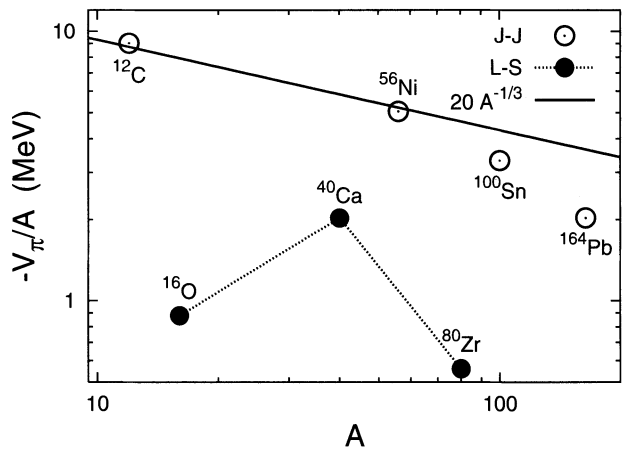

Fig. 1. The pion energy per nucleon as a function of the mass number in the log-log plot. There are two groups; one is for the jj-closed-shell nuclei denoted by open circles and the other is for the LS-closed-shell nuclei denoted by closed circles. The pion energy per nucleon for the jj-closed-shell nuclei decreases monotonically and follows more steeply than $A^{-1/3}$, which is shown by the solid line.

Hence, the single-particle state is expressed as

$$\psi_{njm} = \sum_\kappa \begin{pmatrix} iG_{n\kappa}\mathcal{Y}_{\kappa m} \\ F_{n\kappa}\mathcal{Y}_{\bar{\kappa}m} \end{pmatrix} = \begin{pmatrix} iG_{n\kappa}\mathcal{Y}_{\kappa m} + iG_{n\bar{\kappa}}\mathcal{Y}_{\bar{\kappa}m} \\ F_{n\kappa}\mathcal{Y}_{\bar{\kappa}m} + F_{n\bar{\kappa}}\mathcal{Y}_{\kappa m} \end{pmatrix}. \tag{3}$$

Here, $\mathcal{Y}_{\kappa m}$ is the eigenfunction of the total angular momentum $j = l + s$ and $\mathcal{Y}_{\bar{\kappa}m} = \boldsymbol{\sigma}\cdot\hat{r}\mathcal{Y}_{\kappa m}$. We assume spherical symmetry (jm is a good quantum number) for the intrinsic state. G and F are the radial parts of the single-particle wave function. The summation over κ represents the parity mixing, where κ is $\kappa = -(l_\downarrow + 1)$ for $l_\downarrow = j - 1/2$ and $\kappa = l_\uparrow$ for $l_\uparrow = j + 1/2$.

3 Numerical results with a finite pion field

We present here our numerical results. We use the TM1 parameter set of ref. [9] for all the parameters except for the pion-nucleon coupling. For this we use the value of the Bonn-A potential, which corresponds to setting $g_\pi = f_\pi/m_\pi$, with $f_\pi \sim 1$. Since we are especially interested in the appearance of a finite pion mean field and wish to see its effect under the simplest conditions, we ignore the Coulomb term. We carried out calculations for the $N = Z$ closed-shell nuclei ^{12}C, ^{16}O, ^{40}Ca, ^{56}Ni, ^{80}Zr, ^{100}Sn and ^{164}Pb.

We plot the mass number dependence of the pion energy per nucleon in fig. 1. We mention here that the kinetic energy and the sigma and omega energies per particle are almost independent of the mass number. We see, on the other hand, peculiar behavior in the pion energy. The magnitudes of the pion energy are clearly separated into two groups. One group is large, and their common feature is the jj-closed-shell nuclei, the magic number nuclei due to a larger spin-orbit partner (j-upper) being filled. The other

group is small, and they are LS-closed-shell nuclei. The pion energy per nucleon for jj-closed-shell nuclei decreases monotonically with the mass number. The rate of this decrease is more rapid than $A^{-1/3}$. This means that the pion mean-field energy behaves proportionally with the nuclear surface or even stronger than that. For this reason, we use the expression of "surface pion condensation". That separation into two groups for the pion energy: LS-closed and jj-closed-shell cases, is related with the spin-orbit splitting. The spin-orbit partner having larger total spin near the Fermi-surface does not contribute to the total energy for the case of surface pion condensation in the LS-closed-shell nuclei [3].

We discuss here the examples of the qualitative consequence of finite pion mean field. First, we discuss the Gamow-Teller (GT) transitions. Without pion condensation, there exist no transitions for LS-closed-shell nuclei as ^{16}O, ^{40}Ca and only two transitions, for example, for ^{90}Zr. However, the mixing of parity in the intrinsic state allows transitions of 2p-2h states. This makes the spectrum of the GT transitions with some GT strengths above the two dominant peaks in ^{90}Zr [6]. Hence, naturally we have strengths in the region of the higher excitation energy in the mean-field theory with the pion as the experiment demands. Second, the longitudinal spin response functions, which are caused by the pionic correlations, should be largely modified due to pion condensation. Since the large pionic strength is used up to construct the nuclear ground state, the pionic fluctuation ought to be reduced largely. This should make the spin response in the pion channel weak. This remains to be demonstrated in the future work.

Until now phenomena involving high-momentum components have been assigned as nuclear correlations induced by the repulsive core and the tensor force. Surface pion condensation provides us with the possibility to describe the part of the correlation effect induced by the tensor force. This fact implies that we are now able to separate the short-range correlation phenomena into that due to the pion and that due to the repulsive core. In fact, as seen above in the investigation of the parity projection, the surface pion condensation provides a large amount of the 2p-2h excitations in the nuclear ground state automatically. There should be many other consequences of surface pion condensation in nuclear phenomena. The pairing correlations and the spin-orbit couplings are all surface phenomena and surface pion condensation should couple with these correlations and provide rich phenomena.

4 Conclusion

We have studied the possible existence of a finite pion mean field in finite nuclei by introducing a pion field into the relativistic mean-field (RMF) theory. We have extended the RMF theory by introducing the parity-mixed single-particle basis to accommodate the finite pion mean field. We have employed the TM1 parameter set in the RMF theory and introduced the pion field in the pseudovector coupling with the nucleon. With the use of the pion-nucleon coupling constant in free space, we have carried out calculations for $N = Z$ closed-shell nuclei and demonstrated the actual appearance of a finite pion mean field. We have shown that the potential energy associated with the pion behaves roughly proportional to the nuclear surface. For this reason, we refer to the onset of the finite pion mean field as "surface pion condensation". We have given qualitative discussion on the consequences of surface pion condensation on the Gamow-Teller strengths, the spin response functions, and the short-range correlations.

We would like to stress here that we are in the initial stage of our investigation of the role of the pion in finite nuclei. We must carry out various studies in order to establish the mean-field theory with the inclusion of the pion, pursued in this paper for medium and heavy nuclei. We must introduce the rho-meson tensor coupling term, which acts to oppose the appearance of a pion finite mean-field. We should also include the delta-isobar pion coupling terms, which favor a finite pion mean field. In addition, we must study carefully the effect of the short-range repulsions, the so called g' term in the non-relativistic framework. We would like also to work out the exchange terms, *i.e.* the Fock terms in the relativistic many-body theory. We then have to conduct a parameter search for the coupling constants in the Lagrangian. We shall end up with the reduction of the sigma and omega coupling constants, which enhances the effect of the pion mean field. We should further perform a study of the parity projection in the framework of the variation after projection (VAP). There are many studies to be carried out in order to establish the existence of surface pion condensation. We are at the gate of exploring both theoretically and experimentally the phenomena caused by the most important boson, the pion, in nuclear physics.

This is a talk presented by H. Toki at the International Workshop on Quark Nuclear Physics held through June 9-14, 2002 in Juelich. We acknowledge fruitful discussions with Prof. H. Horiuchi and Prof. Y. Akaishi and Prof. I. Tanihata on the role of the pion in light nuclei and the experimental consequence of surface pion condensation.

References

1. H. Yukawa, Proc. Phys.-Math. Soc. Jpn. **17**, 48 (1935).
2. M.G. Mayer, Phys. Rev. **75**, 1969 (1949). O. Haxel, J.H.D. Jensen, H.E. Suess, Phys. Rev. **75**, 1766 (1949).
3. H. Toki, S. Sugimoto, K. Ikeda, Prog. Theor. Phys. **108**, 903 (2002).
4. J. Carlson, R. Schiavilla, Rev. Mod. Phys. **70**, 743 (1998).
5. R.B. Wiringa, S.C. Pieper, J. Carlson, V.R. Pandharipande, Phys. Rev. C **62**, 014001 (2000).
6. T. Wakasa *et al.*, Phys. Rev. C **55**, 2909 (1997).
7. T. Wakasa *et al.*, Phys. Rev. C **59**, 3177 (1999).
8. T. Takatsuka, R. Tamagaki, Prog. Theor. Phys. **55**, 624 (1976).
9. Y. Sugahara, H. Toki, Nucl. Phys. A **579**, 557 (1994).

Eur. Phys. J. A **18**, 367–370 (2003)
DOI 10.1140/epja/i2002-10286-2

THE EUROPEAN PHYSICAL JOURNAL A

Study of $p + d \rightarrow {}^3A + \pi$ reactions in the Δ-resonance region

S. Abdel-Samad[1], J. Bojowald[1], A. Budzanowski[3], A. Chatterjee[9], J. Ernst[7], D. Frekers[8], P. Hawranek[1,3], J. Ilieva[1,5], L. Jarczyk[3], K. Kilian[1], S. Kliczewski[4], W. Klimala[1,3], D. Kolev[6], M. Kravčíková[12], T. Kutsarova[5], J. Lieb[10], H. Machner[1], A. Magiera[1,3], G. Martinská[12], H. Nann[11], L. Pentchev[5], D. Protić[1], P. von Rossen[1], B.J. Roy[9], R. Siudak[4], A. Strzałkowski[3], R. Tsenov[6], M. Uličný[1,12], J. Urbán[7,12,a], and K. Zwoll[2]

[1] Institut für Kernphysik, Forschungszentrum Jülich, Jülich, Germany
[2] Zentrallabor für Elektronik, Forschungszentrum Jülich, Jülich, Germany
[3] Institute of Physics, Jagellonian University, Kraków, Poland
[4] Institute of Nuclear Physics, Kraków, Poland
[5] Institute of Nuclear Physics and Nuclear Energy, Sofia, Bulgaria
[6] Physics Faculty, University of Sofia, Sofia, Bulgaria
[7] Institut für Strahlen- und Kernphysik der Universität Bonn, Bonn, Germany
[8] Institut für Kernphysik, Universität Münster, Münster, Germany
[9] Nuclear Physics Division, BARC, Bombay, India
[10] Physics Department, George Mason University, Fairfax, VA, USA
[11] IUCF, Indiana University, Bloomington, IN, USA
[12] P.J. Safarik University, Košice, Slovakia
[13] Technical University, Košice, Košice, Slovakia

Received: 30 September 2002 /
Published online: 22 October 2003 – © Società Italiana di Fisica / Springer-Verlag 2003

Abstract. A stack of annular detectors made of high-purity germanium was used to measure $p + d \rightarrow {}^3\mathrm{He} + \pi^0$ and $p + d \rightarrow {}^3\mathrm{H} + \pi^+$ differential and total cross-sections at beam momenta from 900 MeV/c to 1050 MeV/c. The total cross-sections are consistent with Δ-excitation. The differential data consist of two components. One corresponds to large momentum transfer from the projectile to the pion, the other to small momentum transfer. The former shows an independence of the slope as a function of the momentum transfer t (scaling). The scale parameter is different for π^+ and π^0 emission which violates isospin symmetry. The second component which is almost isotropic is in agreement with isospin symmetry. It is approximately a quarter of the total yield in the Δ-resonance region.

PACS. 25.10.+s Nuclear reactions involving few-nucleon systems – 25.40.Qa (p, π) reactions – 25.70.Ef Resonances

1 Introduction

The study of pion production in $p+d$ collisions is expected to provide information about the underlying reaction dynamics. Various reaction mechanisms involving different number of nucleons as well as the response of the bound residual nuclei to high momentum transfers should be considered. The deuteron is a loosely bound system making it an ideal case for the use of impulse approximation. Also the knowledge of wave functions for $A = 2$ and $A = 3$ nuclei allows a more accurate treatment. At the experimental side, data for $pd \rightarrow {}^3\mathrm{He} + \pi^0$ reaction exist near threshold ($\eta < 0.5$) where only the S-wave pion production is important and near the resonance region ($\eta \simeq 1.5$) where the Δ-resonance is the dominant one. The data in the intermediate region, where S-D interference is expected to be large, are missing. The present experiments are performed to bridge the gap between these two intervals. The simultaneous detection of $pd \rightarrow {}^3\mathrm{H} + \pi^+$ is also performed to investigate one of the most interesting aspects of strong interaction —the isospin invariance.

2 GEM detectors and target system

The experimental technique and methods are unique and differ from the ones used to study the above-mentioned reactions. This new experimental design enabled a large-angular-acceptance (full-solid-angle) measurement with a very good energy resolution [1]. The measurements were performed with the Germanium Wall of the GEM detector system. It is a stack of annular diodes made of high-purity

[a] e-mail: urban@kosice.upjs.sk

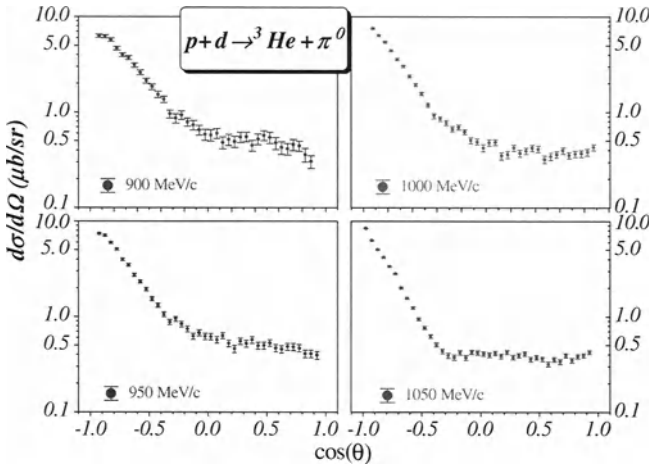

Fig. 1. Differential cross-sections for the $p + d \rightarrow {}^3\mathrm{He} + \pi^0$ reaction as a function of the cosines of the angle of the recoiling ^{3}He. The beam momenta are indicated in the figure. All quantities are in the cm system.

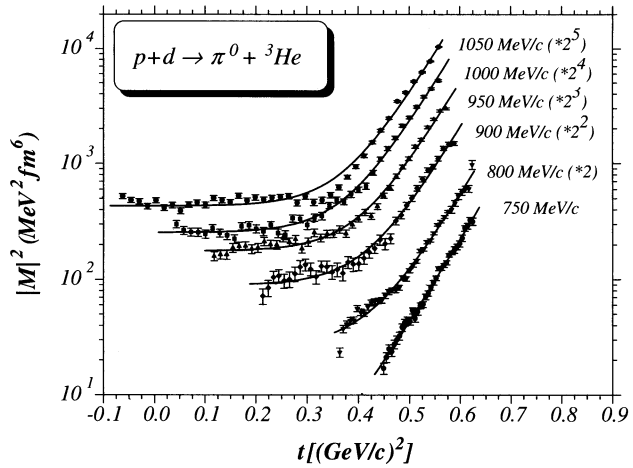

Fig. 2. Matrix elements squared fitted by eq. (1). The data are shown by dots and the fitted functions by solid curves. The laboratory beam momenta and scale factors are given next to the appropriate data.

Ge. The first detector (ΔE, quirl) is position sensitive segmented with 200 Archimedes spirals of opposite orientation on the front and rear sides. Each spiral from the front side crosses one spiral on the rear side defining thus 40000 pixels of sizes between 0.01–0.1 mm^2. The quirl detector is 1.3 mm thick with a 5.8 mm diameter hole in the centre. It was followed by two E detectors (pizzas) segmented into 32 wedges. Each of these pizzas was 15 mm thick. The detector system accepts particles emitted between 50 and 290 mrad. In the present experiment a thinner 2.2 mm liquid-deuterium target was used compared to the 6.4 mm applied in previous one [2].

3 Results on $\mathbf{p + d \rightarrow {}^3He + \pi^0}$ and $\mathbf{p + d \rightarrow {}^3H + \pi^+}$ reactions

The counts were lumped for each CMS angular bin as a function of CMS momenta or missing mass. Gaussian and smooth polynomial were fitted to the resulting spectra in order to separate the background. Finally the integrated counts in the Gaussians were converted to differential cross-sections. For ^{3}He the results are illustrated in fig. 1.

The proper theoretical description of data taken in full-solid-angle arrangement may lead to a revision of the deuteron model, *e.g.* to match the angular distribution the isovector component should be included into the deuteron [3].

The CMS angular distributions of ^3A at lower energies are backward peaked —with an almost exponential slope. With increasing collision energy an isotropic component appears. This happens at large momentum transfers from the projectile to the ion. In order to study these two components the matrix element squared $|M(t)|^2 \propto \mathrm{d}\sigma/\mathrm{d}t$, t being the four-momentum transfer squared from proton to pion, was fitted with a function

$$|M(t)|^2 = a \exp(bt) + c. \qquad (1)$$

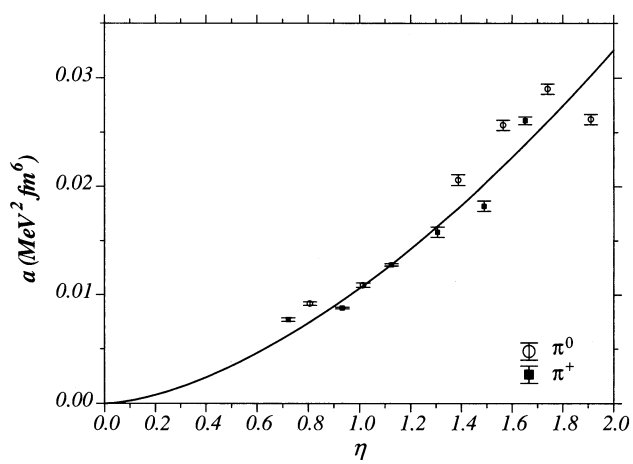

Fig. 3. The fit parameter a as a function of the pion centre of mass momentum $\eta = p^*_\pi/m_\pi$ with fixed value for b. The solid curve is to guide the eye.

The fit results in rather parallel slopes (see fig. 2):

$$b = 16.87 \pm 0.17\ (\mathrm{GeV}/c)^{-2} \quad (\chi^2/\mathrm{ndf} = 0.5) \quad \text{for } \pi^0,$$
$$b = 18.71 \pm 0.34\ (\mathrm{GeV}/c)^{-2} \quad (\chi^2/\mathrm{ndf} = 3.2) \quad \text{for } \pi^+.$$

The errors of the slope values b are 1% for π^0 and 2% for π^+ although the dimensionless variable $\eta = p^*_\pi/m_\pi$ changes more than 1 unit for π^0.

In the fitting procedure further on parameter b was fixed and a and c varied freely. The results are shown as functions of the dimensionless variable η. The values of a, as can be seen in fig. 3, increase with increasing pion CMS momenta and at a given beam energy they are slightly smaller for π^+ than for π^0.

The fitted values for c seem to fulfill the isospin symmetry. The fit results for $^3\mathrm{He} + \pi^0$ final states in fig. 4 are multiplied by isospin factor 2. Obviously, the results obey this symmetry within the error bars. A smooth curve is fitted to the data to guide the eyes. The maximum at $\eta \approx 1.3$ is below the Δ-resonance.

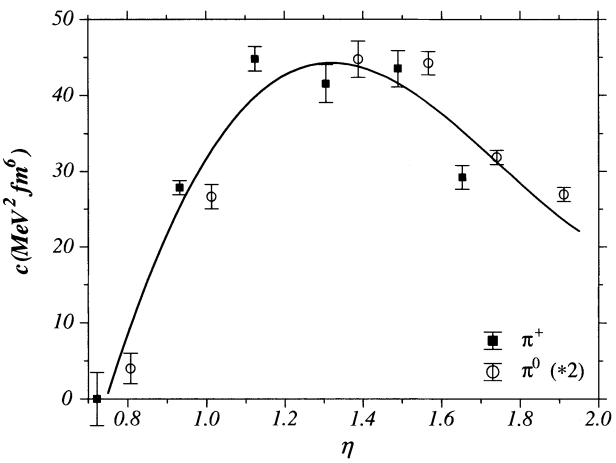

Fig. 4. Same as fig. 3, but for the parameter c.

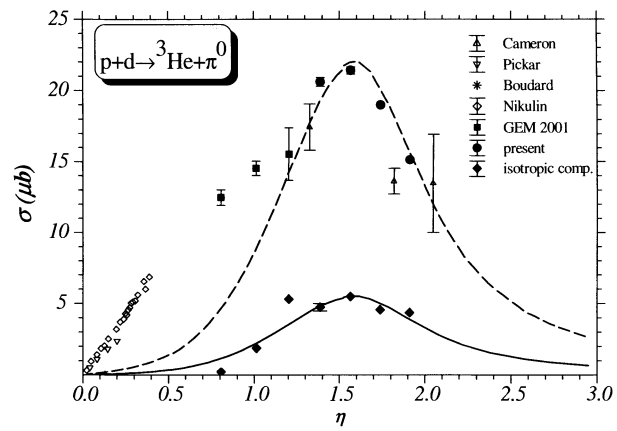

Fig. 5. Excitation function for the $p + d \to {}^3\mathrm{He} + \pi^0$ reaction.

In the Glauber approach applied to meson production on nuclei [4] the steep raising component is due to coherent, while the almost isotropic component is connected with incoherent meson production. The slope parameter is in a simple relation with the strong absorption radius (R) of the optical model $R = 2\sqrt{b}\ \hbar c$. For π^0 channels one gets $R = 1.622 \pm 0.008$ fm and for π^+ the radius is $R = 1.708 \pm 0.016$ fm. It is interesting to note that a similar analysis of the elastic $p + d$ scattering at 1 GeV/c [5] yields $b = 15.4 \pm 1.3$ (GeV/c)$^{-2}$ and an absorption radius of 1.55 ± 0.07 fm.

Most models applied to the present reactions are variations of the so-called spectator model [6]. The t-dependence is due to a form factor containing the deuteron and ${}^3A$ wave functions and the more elementary $NN \to d\pi$ cross-section. One would naively expect R to scale with the ^{3}He and ^{3}H wave functions. However, the present finding is in contrast to the results for the charge radii from electron scattering [7] $r_{\mathrm{ch}}({}^3\mathrm{He}) = 1.959 \pm 0.030$ fm $> r_{\mathrm{ch}}({}^3\mathrm{H}) = 1.755 \pm 0.086$ fm. Since the Coulomb energy between π^+ and ^{3}H is rather small, the present effect is more likely due to the Coulomb force between the two protons in the ^{3}He wave function. In the entrance channel we are dealing with the same system. Therefore, another possibility for the different radii may be different forces between the pions and the ${}^3A$ systems for the present partial waves involved.

Reaction cross-sections were extracted fitting Legendre polynomials to the angular distributions. The found cross-sections and the world data are shown in fig. 5 as functions of η for the case of the $p + d \to {}^3\mathrm{He} + \pi^0$ reaction, where existing data are primarily in the threshold region. The present data are shown as full dots, those from refs. [8–11, 2] by the indicated symbols. The dashed and full curves are the $p + p \to d + \pi^+$ cross-sections scaled down by factors of 145.4 and 581.6, respectively. The points near the full curve represent the isotropic component of the cross-section. For the reaction $p + d \to {}^3\mathrm{H} + \pi^+$ there were more data mainly from pion absorption. The excitation function in fig. 5 for the $p + p \to d + \pi^+$ reaction exhibits a wide peak around $\eta \simeq 1.6$ caused by Δ-excitation. The ${}^3A$ cross-sections follow in the peak region the same dependence.

The data points around the full curve correspond to the extracted contributions of the isotropic part and are approximately 25% of the reaction cross-section. The momentum dependence again follows the Δ-resonance excitation. The underlying reaction mechanism is presently unclear. It must be of a more complicated origin than the exponential part, since it is almost independent of the momentum transfer. Its onset at a certain collision energy and its coupling to the Δ may shed light on this reaction mechanism.

4 Summary

Diffferential and total cross-sections for the reactions $p + d \to {}^3\mathrm{He} + \pi^0$ and $p + d \to {}^3\mathrm{H} + \pi^+$ were measured in the Δ-excitation region. The CMS angular distributions show two components: one strongly increasing with momentum transfer to the pion and a smaller one almost independent of momentum transfer. Parametrization of

$$\mathrm{d}\sigma/\mathrm{d}t = \tilde{a} \exp(bt) + \tilde{c}$$

yields constant values of slopes, but different for the two reactions. The slope parameters seem to carry more isospin information than a_1. The reaction mechanism behind the $a_1 \simeq$ const must be of more complicated nature than the exponential part, since it is independent of momentum transfer. Its onset at $\eta \approx 0.9$ corresponds to the threshold for the free $NN \to d\pi$ and needs further studies.

We are grateful to the COSY operation crew for their efforts making a good beam. Support by BMBF Germany (06 MS 568 I TP4), Internationales Büro des BMBF (X081.24 and 211.6), SCSR Poland (2P302 025 and 2P03B 88 08), GAS Slovakia (1/8041/01), and COSY Jülich is gratefully acknowledged.

References

1. M. Betigeri *et al.*, Nucl. Instrum. Methods Phys. Res. A **421**, 447 (1999).
2. M. Betigeri *et al.*, Nucl. Phys. A **690**, 473 (2001).

3. L. Cantom, private communication.
4. B. Margolis, K.S. Kölbig, Nucl. Phys. B **6**, 85 (1968).
5. N.E. Booth *et al.*, Phys. Rev. D **4**, 1261 (1971).
6. M. Ruderman: Phys. Rev. **87**, 383 (1952).
7. A. Amroun *et al.*, Nucl. Phys. A **579**, 596 (1994).
8. A. Boudard *et al.*, Phys. Lett. B **214**, 6 (1988).
9. J.M. Cameron *et al.*, Nucl. Phys. A **472**, 718 (1987).
10. M.A. Pickar *et al.*, Phys. Rev. C **46**, 397 (1992).
11. V. Nikulin *et al.*, Phys. Rev. C **54**, 1732 (1996).

Eur. Phys. J. A **18**, 371–375 (2003)
DOI 10.1140/epja/i2002-10239-9

THE EUROPEAN PHYSICAL JOURNAL A

Strangeness production and other recent results from Hall B at Jefferson Lab

R.A. Schumacher[a]

For the CLAS Collaboration
Department of Physics, Carnegie Mellon University, Pittsburgh, PA 15213, USA

Received: 30 September 2002 /
Published online: 22 October 2003 – © Società Italiana di Fisica / Springer-Verlag 2003

Abstract. Recent results using the CLAS detector at Jefferson Lab are discussed. We emphasize strangeness photo- and electro-production in the baryon resonance region between $W = 1.6$ and 2.3 GeV, where indications of s-channel structure are suggestive of high-mass baryon resonances coupling to kaons and hyperons in the final state. Other CLAS results, for the E_{1+}/M_{1+} transition form factor at the first Δ-resonance, two-pion electroproduction, and η photoproduction are also briefly mentioned.

PACS. 13.30.-a Decays of baryons – 13.30.Eg Hadronic decays – 13.40.-f Electromagnetic processes and properties – 13.60.-r Photon and charged-lepton interactions with hadrons

1 Introduction

The CLAS detector at Jefferson Lab [1–5] serves as a large-acceptance, moderate-momentum resolution facility for probing nucleon excitations, meson production, and correlations in light nuclear systems. This presentation features highlights from a series of measurements dedicated to the study of open strangeness systems in the baryon resonance region. New results for both photo- and electro-production of strangeness-containing final states will be discussed. Complementary work in resonance excitation in the non-strange final states will be mentioned and the reader will be referred to the recent literature.

Baryon resonances are a basic problem of interest in non-perturbative QCD. The masses, quantum numbers, and decay branches of the higher-mass baryon resonances have remained difficult to establish, both experimentally and theoretically. Experimentally, most of what we know comes from the use of hadron beams, most commonly pions, interacting with nucleon targets, followed by detection of one or more pions plus the nucleons in the final state. At higher energies, both the energy overlap problem, and, above the two-pion threshold, ρ-meson production, make it more difficult to separate the resonance contributions. The large number of poorly established higher-mass resonances listed by the Particle Data Group [6] attests to the challenge of doing accurate work above the strangeness threshold near 1600 MeV. Theoretically, there is the well-known over-supply of baryons predicted in quark models, the so-called "missing baryons" problem [7], and various suggested ways that dynamical effects such as di-quarks could prune the spectrum to something close to what has been observed [8].

Electromagnetic production of resonances that decay into strange particles offers two advantages. First, two-body KY final states are experimentally easier to analyze than the three-body $\pi\pi N$ final states that dominate decays at higher masses. So, while the cross-sections for strangeness production tend to be small (on the order of 1 or 2 μb in electromagnetic production) there can be a pay-off in terms of ease of interpretation of energy and angular distributions. Second, couplings of resonances to strangeness-containing final states are expected to be different than coupling to pionic final states [7]. Therefore, the strangeness sector casts a different light on the resonance excitation spectrum, and thus offers an opportunity for seeing resonances not revealed clearly using pions.

It must be added, however, that to date the PDG compilation lists only five well-established resonances with poorly known coupling to the $K\Lambda$ final state, and none with couplings to the $K\Sigma^0$ final state. The most widely available theoretical calculation of the electromagnetic $K\Lambda$ production, the Kaon-MAID code [9], includes a mere three well-known resonances: the $S_{11}(1650)$, the $P_{11}(1710)$, and the $P_{13}(1720)$. Thus it is timely and interesting to have additional good-quality photo- and electro-production data of these channels to see what additional resonance formation and decay information can be found.

[a] e-mail: schumacher@cmu.edu

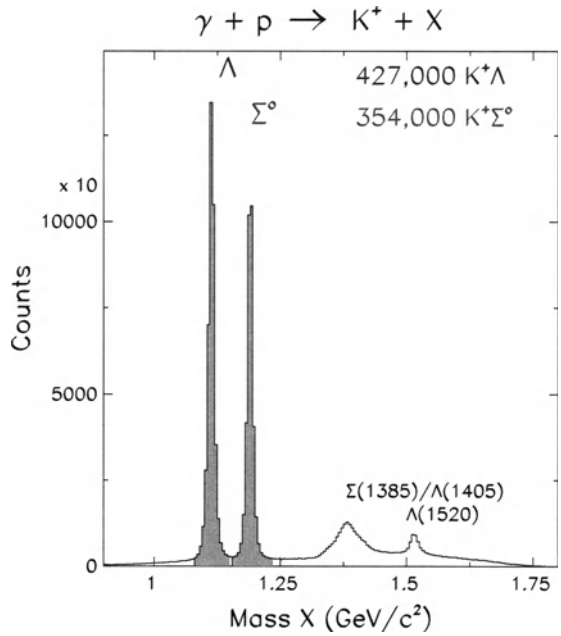

Fig. 1. Missing-mass plot for the CLAS photoproduction data set with 2.4 GeV endpoint energy, summed over all kaon detection angles.

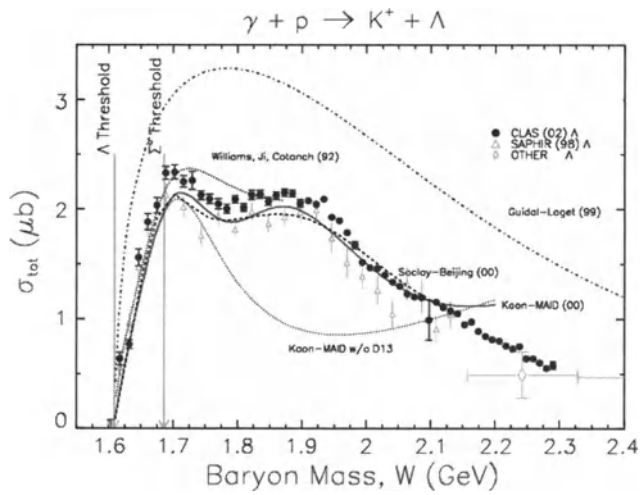

Fig. 2. Total cross-section for Λ-hyperon photoproduction measured at CLAS (solid circles). Data from SAPHIR/Bonn [11] (open triangles) are also shown. The curves are for effective Lagrangian calculations of Bennhold *et al.* as computed by Kaon-MAID [9] (solid), Williams, Ji, and Cotanch [12] (upper dotted), Saghai [13] (dashed), and a Regge-model calculation of Guidal *et al.* [14,15] (dot-dashed). The lower dotted curve illustrates the effect when the $D_{13}(1900)$ resonance in the Kaon-MAID calculation is switched off.

2 KY photoproduction

Figure 1 shows the missing-mass spectrum obtained with CLAS for the real photon reaction $\gamma + p \to K^+ + X$ after kaon selection cuts. The beam of tagged photons had an electron endpoint energy of 2.4 GeV, and spanned all photon energies from threshold at $E_\gamma = 0.911$ GeV up to 2.3 GeV. A mass resolution of $\sigma = 6.1$ MeV was obtained when averaging over all detection angles and photon energies. The Λ and Σ^0 events were separated from the background of mis-identified pions using lineshape fits to missing-mass spectra in each bin of photon energy and kaon angle.

Our results were binned in 25 MeV steps in W and in 20 bins in the center-of-mass angle of the kaons, $\cos(\theta_K^{\mathrm{c.m.}})$. CLAS has acceptance holes in the forward and backward directions for $\cos(\theta_K^{\mathrm{c.m.}}) > 0.9$. A Legendre polynomial moment analysis of the angular distributions was used to extrapolate into these regions, causing a source of systematic uncertainty into the total cross-section results shown here. The full analysis of the angular distributions will be discussed in a future publication.

Figure 2 shows the total cross-section for Λ-hyperon photoproduction. Overall there is fair agreement between CLAS and previous data from SAPHIR at Bonn [11]. The CLAS data are preliminary in that we are still working on 10%-level corrections to the normalization and acceptances. Most notable above the threshold region where the known S_{11}, P_{11}, and P_{13} resonances dominate, is the broad unexplained structure centered at 1.9 GeV. This structure, first seen in the Bonn data, was interpreted by Mart and Bennhold [10] and collaborators as evidence for a "missing" resonance at this mass. Based on theoretical considerations from a particular quark model [7], an assignment of $D_{13}(1900)$ seemed consistent with the angular distributions. However, other groups showed that the same data could be accommodated either with u-channel exchanges [13] or with an extra P-wave resonance [16]. We expect the CLAS data to resolve this question when the full angular distributions are released.

The Regge-model calculation [14,15] shown in fig. 2 is too high by a substantial factor for this channel. The calculation uses only K and K^* exchanges, with no resonances at all. The prediction was made using a model that fit high-energy kaon electroproduction data very well. However, extrapolated into the resonance region, the model fails. As seen below, it behaves much more as expected in the case of Σ^0 production.

In fig. 3 the total cross-section for the Σ^0-hyperon is shown. In this case, both isospin-(1/2) and isospin-(3/2) nucleon resonances can contribute. Here there is a peak in the total cross-section near 1.9 GeV, which has in the past been associated with the cluster of Δ-resonances in this mass range. As mentioned earlier, no such resonances have been reliably shown to have decay branches to strange final states. These data, as do the previous Bonn data, clearly show the imprint of resonant decays to $K\Sigma^0$.

With an unpolarized photon beam and an unpolarized target, hyperons can still be produced polarized along the axis perpendicular to the production plane. This is known as the "recoil" polarization. The large acceptance of CLAS made it straightforward to detect protons from the decay of hyperons in coincidence with the K-mesons. The well-known parity-violating weak decay asymmetry in hyperon decays permits us to determine this polarization by measuring the angular distribution of the decay protons.

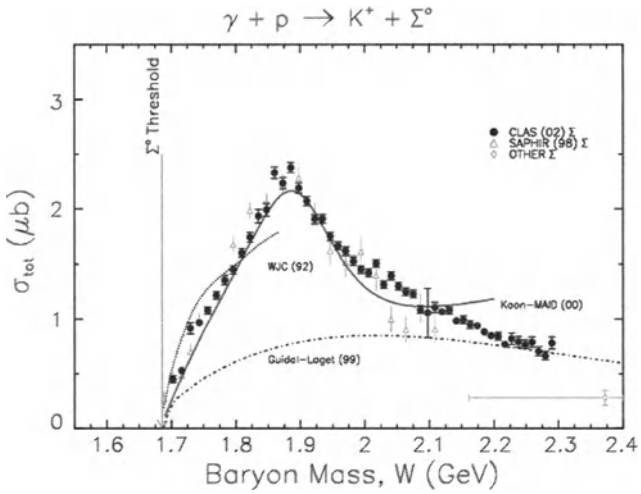

Fig. 3. Total cross-section for Σ^0-hyperon photoproduction measured at CLAS (solid circles). Data from SAPHIR/Bonn [11] (open triangles) are also shown. The curves are for effective Lagrangian calculations of Bennhold *et al.* [17] as computed by Kaon-MAID [9] (solid), Williams, Ji, and Cotanch [12] (dotted), and a Regge-model calculation of Guidal *et al.* [14,15] (dot-dashed).

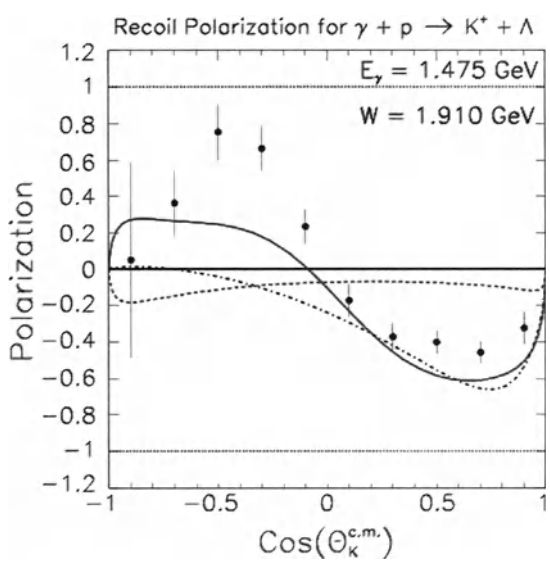

Fig. 4. Polarization of the Λ-hyperon as a function of kaon center-of-mass production angle for a total system mass, W, of 1.90 GeV. For comparison, the curves are for the hadrodynamic calculation of Bennhold *et al.* [17] as computed by Kaon-MAID [9] (full), and a Regge-model calculation of Guidal *et al.* [14,15] (dot-dashed). The dashed curve illustrates the effect when the $D_{13}(1900)$-resonance in the Kaon-MAID calculation is switched off.

Measurement of this observable is interesting since it is related to interferences of the imaginary parts of the resonant amplitudes with other amplitudes, including Born terms.

In fig. 4 we show an example of the data obtained at CLAS, for an energy bin at the peak of the broad $K\Lambda$ cross-section rise, $W = 1.9$ GeV, and for the full range of kaon angles in the c.m. frame. We see strong negative polarization of the Λ hyperons when the kaons are in the forward direction, and an equally strong positive polarization when the kaons go backward. Our results are consistent with a few older data points from Bonn [11], although they had no data at this particular energy. It is interesting to see that the MAID calculation is very sensitive to the presence of the $D_{13}(1900)$ (dashed curve), for indeed this is the only resonant amplitude included in this calculation in this mass range. This observation is in contradiction to the statement made in ref. [10] when discussing the MAID model in relation to the Bonn data. It is clear that the MAID model, while providing some back-angle recoil polarization via a D_{13} at 1900 MeV, still misses the measured polarization by a factor of 2 at some angles. The Regge model is not able to provide any back-angle polarization, since by construction it has only a t-channel dominated (forward-angle) production mechanism. CLAS has polarization data of the sort shown in fig. 4 for the full range of energies shown in fig. 2, but final systematic checks are still in progress.

3 KY electroproduction

Moving away from the 4-momentum transfer $Q^2 = 0$ limit of photoproduction, CLAS has measured exclusive $K^+\Lambda$ and $K^+\Sigma^0$ electroproduction on the proton for $0.5 < Q^2 < 1.1$ GeV/c^2 at a beam energy of 2.6 GeV. For unpolarized electrons and target, and after dividing out the flux of virtual photons in a given bin of W and Q^2, the cross-section for pseudo-scalar meson electroproduction reads:

$$\frac{d\sigma_\gamma}{d\Omega_K} = \sigma_T + \epsilon\sigma_L + \epsilon\sigma_{TT}\cos(2\phi) + \sqrt{2\epsilon_L(\epsilon+1)}\sigma_{LT}\cos(\phi)\,,$$

where ϵ is the polarization parameter of the virtual photon, and ϕ is the azimuthal angle between the electron-scattering (e, e') and the hadronic (KY) planes. Exploiting the ϕ-dependence of the process allows one to pick out the interference cross-sections at a given Q^2, W, $\cos(\theta_K^{\mathrm{c.m.}})$, and ϵ, or, using the Rosenbluth technique, separating the transverse (σ_T) and longitudinal (σ_L) cross-sections.

At CLAS we have determined the so-called unseparated transverse and longitudinal cross-sections $(\sigma_T + \epsilon\sigma_L)$ and, for the first time in the resonance region, the interference cross-sections σ_{LT} and σ_{TT}. The W range was the same as in photoproduction. At the amplitude level, the electron scattering interference responses σ_{LT} and σ_{TT} are related to real photon measurements of polarized beam asymmetries, and so they are sensitive to some of the same structure information [18].

In fig. 5 we show the missing-mass spectrum for hyperon electroproduction, again summed over all of CLAS,

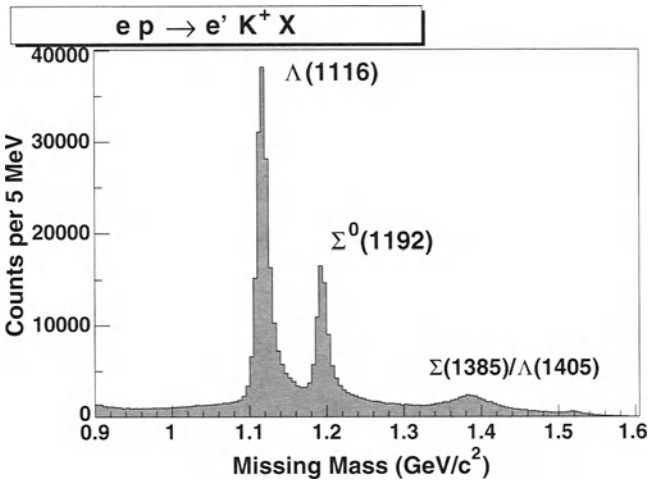

Fig. 5. Missing-mass plot for the CLAS data set with 2.6 GeV electron energy, summed over all kaon detection angles. The resolution is 7.5 MeV. The background, due to mis-identified pions, was removed via line-shape fitting that included radiative effects.

and for the full range of Q^2 that was measured. The resolution is similar to the real photoproduction case shown in fig. 1. The radiative tails can be seen on the high-mass sides of the hyperon peaks. After dividing into bins according to the kinematic variables in the problem (W, Q^2, $\cos(\theta_K)$, ϕ), the missing-mass spectra were fit to individually calculated lineshapes that included pion background.

In fig. 6 we show the ϕ-dependence of the cross-section for Λ and Σ^0 electroproduction in one specific bin, near $W = 1.9$ GeV, where in photoproduction there is a broad maximum in the cross-section. One sees that the interference behavior is very different: $\sigma_{\rm LT}$ for the two hyperons will have opposite signs, and $\sigma_{\rm TT}$ for the Λ is small while for the Σ^0 it is large. The kinematic dependence of the cross-section structure functions show that Λ's and Σ^0's are produced very differently. t-channel processes seem to dominate Λ production, with large contributions from the longitudinal part of the interaction. Production of the Σ^0-hyperon is more s-channel resonance dominated. The cross-section results are not quite final enough for inclusion here.

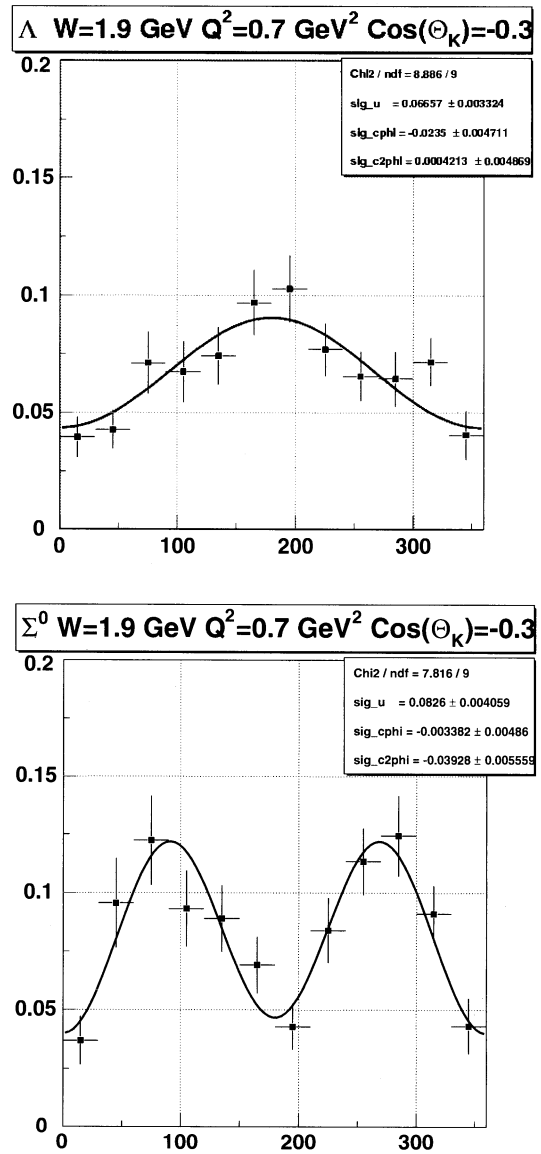

Fig. 6. Dependence of the hyperon electroproduction cross-sections on ϕ in a given kinematic bin: $W = 1.900 \pm 0.025$ GeV, $Q^2 = 0.7 \pm 0.2$ (GeV/c)^2, and $\cos(\theta_K^{\rm c.m.}) = -0.3 \pm 0.1$ The vertical scales are arbitrary. The fits are of the form $A + B\cos(\phi) + C\cos(2\phi)$.

4 Other CLAS results

Space does not permit an extensive review of the other CLAS results discussed in this presentation. In several cases the results are now available elsewhere. The CLAS results for E_{1+}/M_{1+} for the $N \to \Delta$ transition have been published [19] and will not be reproduced here.

Recent measurements of η photoproduction have been made that extend the differential and total cross-section measurements up to $W = 2.13$ GeV, well above the previous limits defined by experiments at Mainz and GRAAL. These results have been submitted for publication and are available [20].

CLAS data for electroproduction of two-pion and of ω-meson final states show some evidence [21] for new structure in the higher-mass baryon resonance excitation region. Collectively, the new results from CLAS indicate that we have entered a new era of experimental progress in the baryon resonance problem.

Work on finalizing the hyperon cross-sections and polarizations shown here should be completed by the end of 2002. The main qualitative conclusion is already clear: these data show significant unexplained baryon resonance structure at higher masses. New amplitude-level analyses are called for to more fully unravel the structure of hyperon photo- and electro-production.

References

1. W. Brooks *et al.*, Nucl. Phys. A **663**, 1077 (2000).
2. M.D. Mestayer *et al.*, Nucl. Instrum. Methods A **449**, 81 (2000).
3. E.S Smith *et al.*, Nucl. Instrum. Methods A **432**, 265 (1999).
4. G. Adams *et al.*, Nucl. Instrum. Methods A **465**, 414 (2001).
5. A. Amarian *et al.*, Nucl. Instrum. Methods A **460**, 239 (2001).
6. Particle Data Group, Phys. Rev. D **66**, 1 (2002).
7. Simon Capstick, W. Roberts, Phys. Rev. D **58**, 1 (1998), and references therein.
8. See for example: E. Klempt, nucl-ex/0203002.
9. T. Mart, C. Bennhold, H. Haberzettl, L. Tiator, *KaonMAID 2000* at `www.kph.uni-mainz.de/MAID/kaon/kaonmaid.html`.
10. T. Mart, C. Bennhold, Phys. Rev. C **61**, 012201 (2000).
11. M.Q. Tran *et al.*, Phys. Lett. B **445**, 20 (1998); C. Bennhold *et al.*, nucl-th/9901066; M. Bockhorst *et al.*, Z. Phys. C **63**, 37 (1994).
12. Robert A. Williams, Cheung-Ryong Ji, Stephen R. Cotanch, Phys. Rev. C **46**, 1617 (1992); see also Stephen Cotanch, Shian Hsiao, Nucl. Phys. A **450**, 419 (1986)c.
13. B. Saghai, private communication. See also: J.C. David, C. Fayard, G.H. Lamot, B. Saghai, Phys. Rev. C **53**, 2613 (1996).
14. M. Guidal, J.-M. Laget, M. Vanderhaegen, Nucl. Phys. A **627**, 645 (1997).
15. M. Vanderhaegen, M. Guidal, J.-M. Laget, Phys. Rev. C **57**, 1454 (1998).
16. S. Janssen, J. Ryckebusch, D. Debruyne, T. Van Cauteren, Phys. Rev C **65**, 015201 (2001); S. Janssen, J. Ryckebusch, W. Van Nespen, D. Debruyne, T. Van Cauteren, Eur. Phys. J. A **11**, 105 (2001).
17. C. Bennhold, H. Haberzettl, T. Mart, in *Proceedings of the 2nd ICTP International Conference on Perspectives in Hadron Physics, Trieste, Italy, 10-14 May 1999*, edited by S. Boffi, C. Ciofi degli Atti, M. Giannini (World Scientific, Singapore, 2000), nucl-th/9909022.
18. See for example: G. Knoechlein, D. Drechsel, L. Tiator, Zeit. Phys. A **352**, 327 (1995).
19. K. Joo *et al.*, Phys. Rev. Lett. **88**, 122001 (2002).
20. M. Dugger *et al.*, Phys. Rev. Lett. **89**, 222002 (2002), `www.public.asu.edu/ britchie/etaPRL.pdf`.
21. M. Ripani *et al.*, in preparation.

Eur. Phys. J. A **18**, 377–381 (2003)
DOI 10.1140/epja/i2002-10240-4

THE EUROPEAN PHYSICAL JOURNAL A

The (spin) structure of the nucleon

G. van der Steenhoven[a]

For the HERMES Collaboration
Nationaal Instituut voor Kernfysica en Hoge-Energiefysica (NIKHEF), P.O. Box 41882, 1009 DB Amsterdam, The Netherlands

Received: 30 September 2002 /
Published online: 22 October 2003 – © Società Italiana di Fisica / Springer-Verlag 2003

Abstract. A selection of new data obtained by the HERMES experiment at DESY is presented, which provides new insight into the QCD structure of the nucleon. Using polarized lepton beams and polarized targets, the spin-dependent structure function $g_1(x)$ has been determined for ^{1}H, ^{2}H and ^{3}He. By also observing one of the produced hadrons it has been possible to extract the polarization distribution of individual quark flavours in the nucleon as well. Further information on nucleon structure has been obtained by observing (almost) exclusive reactions, which can be interpreted in terms of the recently introduced generalized parton distributions (GPDs). As an example of such data measurements of both the beam-spin and beam-charge asymmetries resulting from deeply virtual Compton scattering (DVCS) are presented. By embedding the deep-inelastic scattering process in the nuclear environment additional information can be obtained on nucleon structure and some QCD effects. The potential of this technique is illustrated by showing new results on tagged structure functions and hadronization in nuclei.

PACS. 13.60.Hb Total and inclusive cross-sections (including deep-inelastic processes) – 13.88.+e Polarization in interactions and scattering – 14.20.Dh Protons and neutrons – 24.85.+p Quarks, gluons, and QCD in nuclei and nuclear processes

1 Introduction

Studies of the QCD structure of the nucleon are entering a new phase because of a wealth of new measurements that recently has come available, and because of some recent theoretical developments. Two examples are mentioned. Experimentally, new data on the longitudinal spin-structure of the nucleon enable a precise determination of the flavour-separated quark polarization distributions in the nucleon. Theoretically, the introduction of generalized parton distributions provides a new unified framework to access dynamic correlations between partons in the nucleon on the basis of various —quite different— reactions.

Moreover, progress is also reported from more familiar areas of research such as studies of the effect of the nuclear medium on deep-inelastic scattering. The renewed interest in this domain is exemplified by the claim that energy-loss measurements based on semi-inclusive deep-inelastic scattering data on nuclei can be linked to energy loss phenomena in relativistic heavy-ion collisions [1]. Furthermore, first data on recoil detection in deep-inelastic scattering have created considerable interest as well.

In this paper many of these developments are summarized with emphasis on those subjects where recent HERMES data are available. The paper is organized as follows. In the next section new results on the spin structure of the nucleon are presented. Subsequently, in sect. 3 the subject of Generalized Parton Distributions is discussed. The fourth section is devoted to nuclear effects, while the paper is concluded in the last section.

[a] e-mail: gerard@nikhef.nl

2 The spin structure of the nucleon

So far most of the experimental effort in the field of spin physics has been dedicated to precise measurements of the inclusive spin-dependent structure function $g_1(x)$. In subsect. 2.1 the presently available data on $g_1(x)$ are reviewed. In recent years, both SMC and HERMES have been able to decompose the quark spin distribution into several distinct distributions for each quark flavour [2,3] including a determination of the flavour dependence of the sea-quark spins. These data are presented in subsect. 2.2.

2.1 The spin structure function $g_1(x)$

The polarized structure function $g_1(x)$ contains information on the helicity-dependent quark contribution to the deep-inelastic scattering cross-section. The available data on $g_1(x)$ on the proton [4–7] are displayed in the top

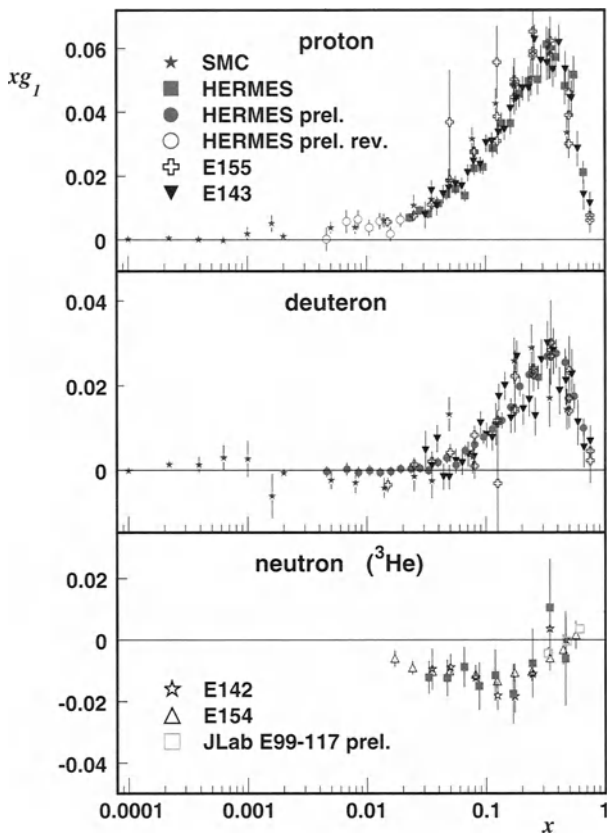

Fig. 1. The longitudinal spin-dependent structure function $g_1(x)$ (mutiplied by x) as measured on longitudinally polarized hydrogen (top panel), deuterium (middle panel) and ^{3}He (lower panel) targets. All data are shown at the *measured* Q^2 values.

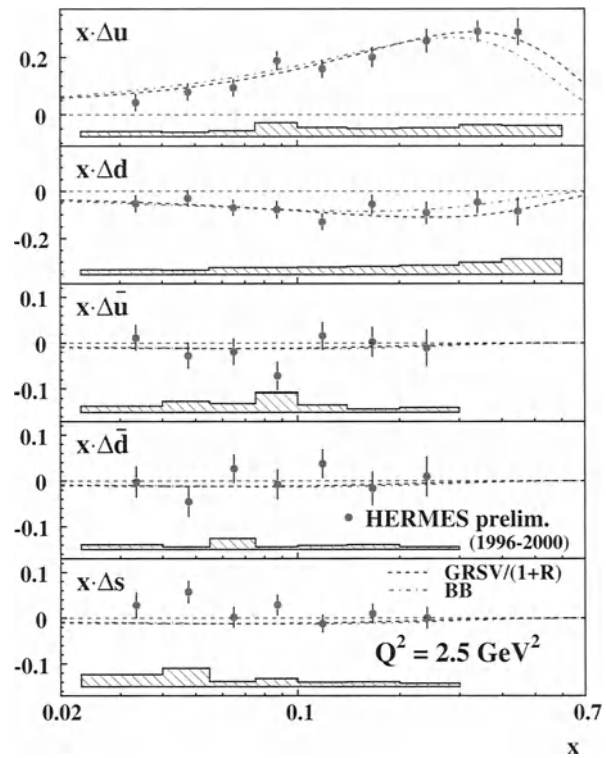

Fig. 2. The x-weighted longitudinal quark spin distribution for u-quarks, d-quarks, $\bar{u}$-quarks, $\bar{d}$-quarks and s-quarks (from top to bottom). The hatched areas represent the systematic uncertainties of the data.

panel of fig. 1. The most recent HERMES measurements focussed on the structure function $g_1^d(x)$. In the middle panel of fig. 1 the corresponding results are shown, which are based on data collected in the years 1998 through 2000 using a longitudinally polarized deuterium target. The results are seen to agree with those obtained at SLAC [4,7] and CERN [6], but have an improved precision.

The data shown in the bottom panel of fig. 1 have been obtained on a polarized ^{3}He target [8–10]. These data confirm the general conclusion that can be derived from fig. 1, *i.e.* that all presently available data are in good agreement which each other for each target. Improvements of the data are mainly needed at very low values of x (below 0.004) and very high values of x (above 0.6).

2.2 Flavour decomposition

Semi-inclusive deep-inelastic scattering experiments that make use of both polarized lepton beams and polarized targets in principle enable the determination of the polarized quark distributions $\Delta q_f(x)$ for each flavour f. From the experimental data the double spin-asymmetries $A_1^h(x)$ are extracted for different hadron types h. The asymmetries $A_1^h(x)$ are related to the quark distributions $\Delta q_f(x)$ through the so-called purity matrix p_f^h, which describes the probability that a hadron h originates from a quark of flavour f. The values of the matrix elements p_f^h are determined from Monte Carlo simulations based on the Lund string fragmentation model. Using this technique the HERMES Collaboration has obtained values for $x\Delta u$, $x\Delta d$, $x\Delta\bar{u}$, $x\Delta\bar{d}$, and $x\Delta s$, which are shown in fig. 2. In the analysis a s-$\bar{s}$ symmetric strange quark polarisation is assumed, and the data were evolved to a common Q^2 value of 2.5 GeV^2. As compared to previous data of this kind [2,3], the accuracy of the data on Δu and Δd has improved considerably, while it is the first time that separate spin distributions for the three sea-quark flavours have been obtained.

From the data shown in fig. 2 it is concluded that the u-quarks are strongly polarized in a direction parallel to that of the proton spin, while the d-quarks are weakly polarized in the opposite direction. The u and d sea quarks are seen to carry a small amount of spin, while there is a hint for a small positive s-quark polarization at low x (where the systematic uncertainty is largest).

The data are compared to two parameterisations of particle distribution functions, which are based on inclusive data only. The dashed line represents the GRSV parameterisation [11] using the so-called "standard scenario" in leading order. The dashed-dotted line represents the result of a leading order QCD parameterisation due to Bluemlein and Boettcher [12]. In all cases a reasonable to good description of the data is obtained.

3 Generalized parton distributions

Generalized parton distributions (GPDs) represent a new theoretical development, which encompasses both the well-known parton distribution functions (PDFs) and the nucleon form factors as limiting cases. While the PDFs describe the probability to find a parton with fractional momentum x in the nucleon (forward scattering), the GPDs describe the interference between quarks with momentum fractions $x+\xi$ and $x-\xi$ in the nucleon (off-forward scattering). Hence, the GPDs are sensitive to partonic correlations.

In 1997 Ji [13] has shown that the first moment of certain GPDs, which are accessible in deeply virtual Compton scattering (DVCS), are related to the total angular momentum of the quarks and the gluons in the nucleon. Experimentally one has to distinguish the DVCS process from the Bethe-Heitler (BH) process, which is usually largely dominant in an electron scattering environment. However, by exploiting the interference between the DVCS and BH processes, it is possible to obtain access to the DVCS amplitude [14]. As the interference term in the cross-section depends on the polarization and charge of the beam, and the azimuthal angle ϕ of the emitted photon (about the direction of the virtual photon), measurements of the ϕ-dependence of the beam-spin and beam-charge asymmetry are needed.

3.1 Beam-spin asymmetry in DVCS

The beam-spin asymmetry in hard electroproduction of photons has been measured both by the HERMES experiment at DESY [15] and the CLAS experiment at JLab [16]. In both cases an asymmetry with respect to the helicity state of the incoming lepton beam is observed if the missing energy is chosen to be close to the proton mass. The observed asymmetry has a clear $\sin\phi$ dependence, as expected from the DVCS-BH interference.

Since the first results were published, additional DVCS analyses have been carried out by the HERMES Collaboration. In fig. 3 the beam-spin asymmetry is shown as a function of ϕ for data collected in 2000. The previous observations (which were based on data collected in 1997) are confirmed with improved statistics. Moreover, the beam-spin analyzing power $A_{LU}^{\sin\phi} = \frac{2}{N}\sum_{i=1}^{N}\frac{\sin\phi_i}{(P_l)_i}$ with $(P_l)_i$ the beam polarization measured during the beam burst of the i-th event, has been evaluated. The quantity $A_{LU}^{\sin\phi}$ corresponds to the amplitude of the $\sin\phi$-fit of the single spin asymmetry. The data do not reveal any strong x, t or Q^2 dependence of $A_{LU}^{\sin\phi}$, but unfortunately the available statistics do not allow to make a 3-dimensional binning in these 3 variables. As there can be compensating kinematic dependences, considerably more data are needed before more definite conclusions can be drawn.

3.2 Beam-charge asymmetry in DVCS

While the beam-spin asymmetries give information on the imaginary part of the DVCS-BH interference amplitudes,

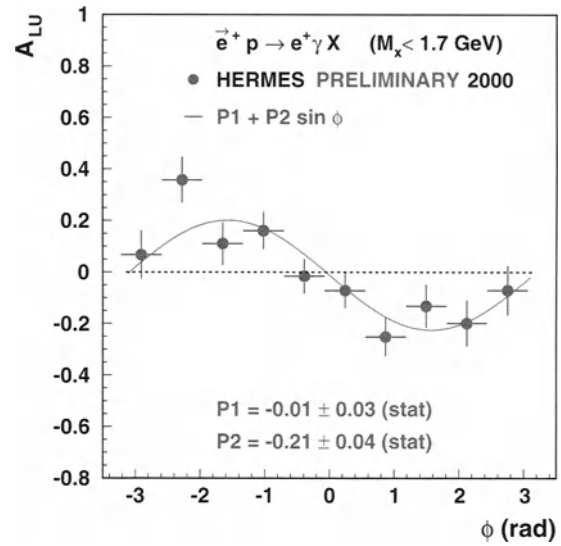

Fig. 3. Single beam-spin asymmetry for electroproduction of real photons on an unpolarized hydrogen target as a function of the azimuthal angle ϕ. The curve represents a $\sin\phi$-fit to the data, of which the amplitude ($P2$) and offset ($P1$) are shown.

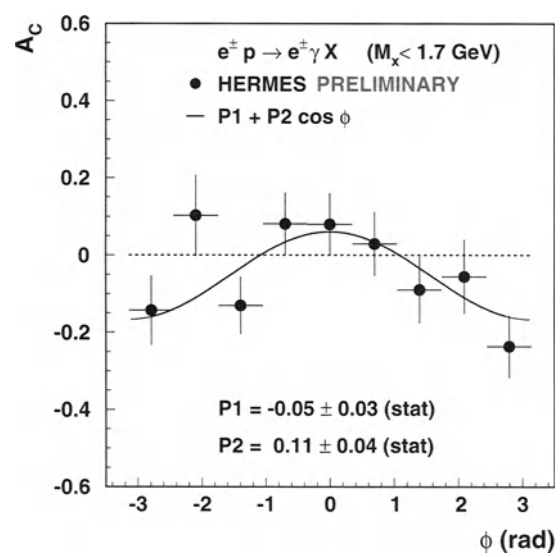

Fig. 4. Single beam-charge asymmetry for electroproduction of real photons on an unpolarized hydrogen target as a function of the azimuthal angle ϕ. The curve represents a $\cos\phi$-fit to the data, of which the amplitude ($P2$) and offset ($P1$) are shown.

the beam-charge asymmetry is sensitive to the real part of these amplitudes. A measurement of the beam-charge asymmetry requires the availability of both electron and positron beams at the same experimental set-up; both beams are available at HERA.

In fig. 4 the first measurements of the single beam-charge asymmetry for electroproduction of real photons on an unpolarized hydrogen target are shown. The data have low statistics, but show evidence of the expected $\cos\phi$ dependence [14]. If the $\cos\phi$-moment of the data is evaluated non-zero values are only seen in the "exclusive" region around $M_x \approx m_{\text{proton}}$.

The new DVCS data demonstrate the feasibility of studying Compton scattering at the partonic level. It is also clear that the statistics (and kinematic coverage) of such measurements has to be dramatically improved before DVCS data can be used to extract information on the total angular momentum carried by quarks.

4 Quark nuclear physics

The nuclear medium represents an additional degree of freedom in our efforts to study nucleon structure. In inclusive deep-inelastic lepton scattering, for instance, the A-dependence of the unpolarized structure function $F_2(x)$ may provide information on a possible density or nucleon momentum dependence of the quark distributions. In a similar vein it has been investigated whether the ratio of the longitudinal to transverse photon absorption cross-sections $R(x, Q^2)$ is A-dependent. A careful analysis of new ^{84}Kr data (and a reanalysis of existing ^{14}N data) has provided no conclusive evidence supporting such an A-dependence[1].

If additional hadrons are observed in deep-inelastic scattering on nuclear targets a possible momentum dependence of $F_2(x)$ can be studied (subsect. 4.1) and parton energy loss mechanisms can be investigated (subsect. 4.2).

4.1 Tagged structure functions

In order to study the feasability of observing (relatively slow) recoil protons in deep-inelastic lepton scattering a small Silicon Test Counter (STC) was built and installed just below the internal target of the HERMES experiment [19,20]. The STC was successfully operated for several months with unpolarized ^{1}H and ^{2}H targets. As the instrument was installed *inside* the vacuum of the HERA storage ring, and the HERMES internal target has a very thin cell wall ($\approx 75\,\mu$m), recoil protons with momenta down to 100 MeV/c could be observed.

While the primary physics purpose of recoil detection in deep-inelastic scattering is the identification of exclusive processes such as DVCS (see sect. 3), the low momentum threshold of the STC makes it also possible to study tagged structure functions. In fact, data collected at HERMES during the few months in which the STC was tested are sufficient for a first study of this subject.

When a slow recoil proton is observed in DIS on ^{2}H it can either be due to target fragmentation or it is a spectator proton that can be used as a tag of a DIS event on a neutron. The latter type of events can be isolated by subtracting recoil data collected on a ^{1}H target from the ^{2}H data properly weighted by the corresponding integrated luminosities. If the resulting recoil momentum spectrum is subsequently corrected for acceptance effects and kinematics, the nucleon momentum distribution $n(p)$ in ^{2}H can be derived from the data under the assumption that the integral (over x and Q^2) of the tagged and untagged structure functions are roughly the same. The derived values of $n(p)$ are displayed in fig. 5. Within the relatively large systematic uncertainties (of about 16%), the data are seen to be in surprisingly good agreement with both a relativistic plane-wave calculation of Tjon [21], and a parameterisation of existing data obtained in *quasi-elastic* kinematics [22].

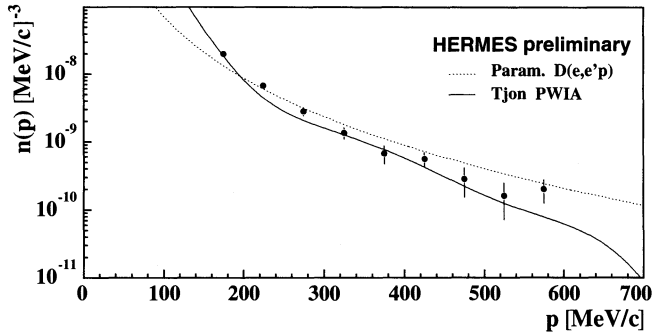

Fig. 5. Momentum distribution of spectator protons observed in deep-inelastic scattering off ^{2}H. Fragmentation products are subtracted using data collected on ^{1}H. The dotted curve corresponds to a parameterisation of ^{2}H$(e, e'p)$ data obtained in quasi-elastic kinematics [23], while the solid curve represents a calculation of the plane-wave momentum distribution of the nucleons in ^{2}H [21].

It is concluded that the spectator mechanism is at work in deep-inelastic scattering, and can thus be used to tag structure functions. Consequently, high-statistics data of this kind will enable a study of the nucleon momentum dependence of $F_2(x, Q^2)$. Such a momentum dependence of $F_2(x, Q^2)$ has been proposed as a possible explanation of the EMC effect [24]. Furthermore, the success of the spectator model implies that the nucleon momentum distribution in ^{2}H can —in principle— be measured as well in deep-inelastic scattering. Usually, the momentum distribution $n(p)$ is determined in quasi-elastic knock-out experiments. However, such measurements are known to be hampered by relatively large meson-exchange and $\Delta(1232)$ contributions [23] —in particular at high p, neither of which contribute in deep-inelastic scattering. On the other hand, a proper treatment of the final-state interaction between the fragmentation products and the spectator proton will require further theoretical study.

4.2 Quark propagation in nuclei

In a recent paper Wang [25] calculated the energy loss of propagating partons in hot or cold nuclear matter. The effect of parton rescattering and energy loss is cast in an effective modification of the fragmentation function, $D_{\text{eff}}(z) \approx \frac{1}{1-\Delta E/E} D(\frac{z}{1-\Delta E/E})$ with ΔE the average partonic energy loss. By comparing this type of calculation to results obtained from semi-inclusive deep-inelastic scattering data collected by the HERMES Collaboration on ^{14}N and ^{84}Kr, a value for ΔE in cold nuclear matter is obtained. The resulting calculation of D_{eff}/D is compared to the data in fig. 6. In this figure the ratio of

[1] The previously reported [17] A-dependence of R turned out to be due to an artefact of the analysis [18].

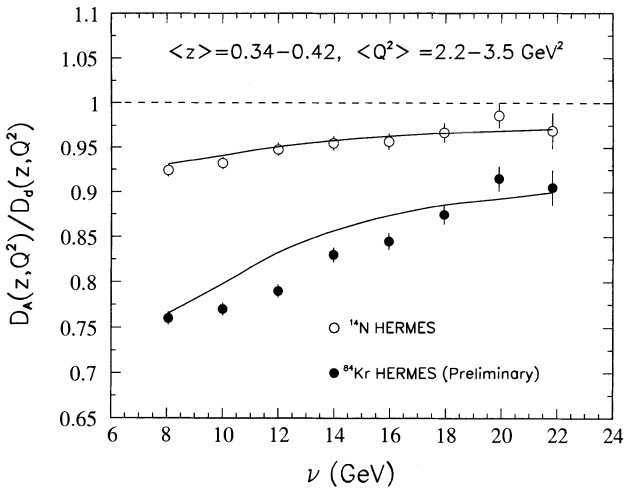

Fig. 6. Multiplicity ratio of hadrons produced on ^{14}N (open circles) and ^{84}Kr (solid circles) normalized to the multiplicity ratio as obtained on ^{2}H. (This superratio is expressed as a ratio of fragmentation functions [1].) The curves are from ref. [1] in which the parton energy-loss was adjusted to 0.3 GeV/fm.

the hadron yields per DIS event on ^{14}N (and ^{84}Kr) to the same yield as obtained on deuterium is plotted *versus* the energy transfer ν. The data show a significant (energy-dependent) attenuation, which is larger for ^{84}Kr than for ^{14}N. This hadron attenuation is well described by the aforementioned calculations of Wang if an energy loss per unit of distance of about 0.3 GeV/fm is taken.

This value for the partonic energy loss in cold nuclear matter can be compared to the energy loss derived from recent PHENIX data [26] on π^0 production in Au + Au collisions at $\sqrt{s} = 130$ GeV, yielding 0.25 GeV/fm [25]. If the PHENIX number is converted to the corresponding energy loss in the initial hot stage of the Au + Au collision, a value of about 4.5 GeV/fm is found. Comparing this number to the value derived from the HERMES data for cold nuclear matter, it is concluded that the gluon density (which drives the energy loss) is a factor 15 higher in the initial phase of the Au + Au collision. This result reflects an interesting link between two fields that used to be essentially independent: relativistic heavy-ion collisions, and deep-inelastic scattering.

5 Outlook

Experiments studying the structure of the nucleon have expanded considerably beyond the well-known inclusive deep-inelastic lepton scattering experiments, which —by now— have yielded precise data on the unpolarized structure function $F_2(x)$ and the spin-dependent structure function $g_1(x)$. As an example of these developments the new data on the flavour decomposed quark spin distributions were presented, showing that the sea quarks carry only little spin angular momentum. Another example is offered by data on deeply virtual Compton scattering, which —if pursued at higher luminosity— may give information on the *total* angular momentum carried by the partons.

Several new results have also been obtained with unpolarized experiments on heavy nuclei, the true domain of *quark nuclear physics*. The first measurement of the momentum spectrum of recoil protons in deep-inelastic scattering on ^{2}H demonstrated the validity of the spectator model, which will enable the study of the p-dependence of $F_2(x)$ in the future. The attenuation of hadrons produced in semi-inclusive experiments provided a value for the parton energy loss in cold nuclear matter, which is of great relevance as a benchmark for the interpretation of relativistic heavy-ion collisions.

These developments, which in several cases represent only first low-statistics measurements demonstrating the feasability of a new technique, call for the construction of new high-luminosity deep-inelastic lepton scattering facilities. Both in Europe and the US such plans are being actively discussed [27].

I would like to thank all my collegues from the HERMES Collaboration for making it possible to perform an experiment that has produced so many high-quality data. Ed Kinney and Dirk Ryckbosch are kindly acknowledged for carefully reading the manuscript.

References

1. X. Guo, X.N. Wang, Phys. Rev. Lett. **85**, 3591 (2000).
2. B. Adeva *et al.*, Phys. Lett. B **420**, 180 (1998).
3. K. Ackerstaff *et al.*, Phys. Lett. B **464**, 123 (1999).
4. P.L. Anthony *et al.*, Phys. Lett. B **463**, 339 (1999); Phys. Lett. B **493**, 19 (1999).
5. A. Airapetian *et al.*, Phys. Lett. B **442**, 484 (1998).
6. B. Adeva *et al.*, Phys. Rev. D **58**, 112001 (1998); Phys. Rev. D **60**, 072004 (1999).
7. K. Abe *et al.*, Phys. Rev. Lett. **76**, 587 (1996); Phys. Rev. D **58**, 112003 (1998).
8. P.L. Anthony *et al.*, Phys. Rev. Lett. **71**, 959 (1993); Phys. Rev. D **54**, 6620 (1996).
9. K. Abe *et al.*, Phys. Rev. Lett. **79**, 26 (1997).
10. K. Ackerstaff *et al.*, Phys. Lett. B **404**, 383 (1997).
11. M. Glück, E. Reya, M. Stratmann, W. Vogelsang, Phys. Rev. D **63**, 094005 (2001).
12. J. Blumlein, H. Boettcher, hep-ph/0203155 (scen. 1).
13. X. Ji, Phys. Rev. D **55**, 7114 (1997).
14. M. Diehl *et al.*, Phys. Lett. B **411**, 193 (1997).
15. A. Airapetian *et al.*, Phys. Rev. Lett. **87**, 182001 (2001).
16. S. Stepanyan *et al.*, Phys. Rev. Lett. **87**, 182002 (2001).
17. K. Ackerstaff *et al.*, Phys. Lett. B **475**, 386 (2000).
18. A. Airapetian *et al.*, submitted to Phys. Lett. B (2002).
19. K.T. Fiedler, PhD Thesis, University of Nürnberg-Erlangen, 2001.
20. J. Visser, PhD Thesis, University of Groningen, 2002.
21. E. Hummel, J. Tjon, Phys. Rev. C **49**, 21 (1994), and private communication.
22. F. Krautschneider, PhD Thesis, University of Bonn, 1976.
23. W.-J. Kasdorp *et al.*, Few-Body Systems **25**, 115 (1998).
24. J. Ashman *et al.*, Phys. Lett. B **206**, 364 (1988).
25. X.N. Wang, hep-ph/0111404; E. Wang, X.N. Wang, hep-ph/0202105.
26. K. Adcox *et al.*, Phys. Rev. Lett. **88**, 022301 (2002).
27. G. van der Steenhoven, *Concluding remarks on QCD-N'02 Workshop in Ferrara*, Nucl. Phys. A **711**, 363c (2002).

Eur. Phys. J. A **18**, 383–388 (2003)
DOI 10.1140/epja/i2002-10241-3

THE EUROPEAN PHYSICAL JOURNAL A

HERA results on the structure of the proton

B. Foster[a]

H.H. Wills Physics Laboratory, University of Bristol, Bristol, UK and DESY, Notkestrasse 85, Hamburg, Germany

Received: 30 September 2002 /
Published online: 22 October 2003 – © Società Italiana di Fisica / Springer-Verlag 2003

Abstract. A selection of results from the H1 and ZEUS experiments at HERA are reviewed, particularly in the area of deep inelastic scattering and diffraction. Quantum chromodynamics gives a good explanation of these data down to surprisingly low values of the four-momentum transfer, Q^2. Data at smaller Q^2 can be described by Regge models as well as by dipole models including parton-saturation effects. The latter can also give a unified description of many features of diffractive data.

PACS. 13.66.-a Lepton-lepton interactions – 13.60.-r Photon and charged-lepton interactions with hadrons

1 Introduction

Results from HERA have revolutionised our view of the structure of the proton. The increased kinematic range has not only extended the range upwards in Q^2, the negative of the squared four-momentum transfer to the proton, but also downwards in x, the fractional momentum carried by the struck parton. ZEUS data reaches down to $x \sim 10^{-6}$. The rapid rise of the gluon density as x decreases, discovered at HERA, implies that the density is very high at these values of x, so that it is interesting to see if non-linear effects in gluon evolution, often referred to as saturation, become visible. Other deviations from the standard DGLAP evolution in quantum chromodynamics (QCD) may also become visible in specific kinematic regions, particularly at low x. Here, there is a transition from the QCD description that works exceedingly well at high Q^2 to a Regge description that is applicable at low Q^2. These features are illustrated with reference to next-to-leading-order QCD fits carried out both by H1 and ZEUS. The description of these phenomena by dipole models is discussed. These form a natural way to explore the relationship between inclusive deep inelastic scattering and diffractive interactions.

2 The F_2 structure function

The double-differential cross-section, $\mathrm{d}^2\sigma/\mathrm{d}Q^2\mathrm{d}x$, for the deep inelastic scattering (DIS) of an unpolarised positron from a proton can be described by

$$\frac{\mathrm{d}^2\sigma}{\mathrm{d}x\mathrm{d}Q^2} = \frac{2\pi\alpha^2}{xQ^4}\left[Y_+ \cdot F_2(x,Q^2) - y^2 F_L(x,Q^2) - Y_- \cdot xF_3(x,Q^2)\right] , \quad (1)$$

where $Y_\pm$ are kinematic factors given by

$$Y_\pm = 1 \pm (1-y)^2 ; \quad (2)$$

$y = Q^2/sx$, s is the total squared centre-of-mass energy and F_2, F_L and F_3 are structure functions. At low Q^2, the effects of xF_3 can be ignored and, since the effects of F_L are small except at high y, the double-differential cross-section is approximately proportional to F_2. The measurement of the differential cross-section therefore gives information on F_2, which in its turn can be decomposed (in the DIS normalisation scheme) into

$$F_2(x,Q^2) = \sum_{i=u,d,s,c,b} A_i(Q^2)\left[xq_i(x,Q^2) + x\overline{q}_i(x,Q^2)\right] . \quad (3)$$

The parton densities $q_i(x,Q^2)$ and $\overline{q}_i(x,Q^2)$ refer to quarks and antiquarks of type i. At low Q^2, the quantities $A_i(Q^2)$ are given by the square of the electric charge of quark or antiquark i. Figure 1 shows the F_2 structure function measured by the ZEUS and H1 Collaborations [1–3] at high x, together with data from the fixed-target experiments NMC [4], BCDMS [5,6] and E665 [7] as a function of Q^2 in bins of x. The region of scaling around $x = 0.2$ can be seen clearly, together with the strong scale breaking as x falls, caused by gluon radiation. The fit to the predictions of next-to-leading-order (NLO) QCD [2] can be seen to give an excellent fit to the data over the whole kinematic range. ZEUS has performed an NLO QCD fit which is also of excellent quality [8]. Both experiments

[a] e-mail: b.foster@bris.ac.uk

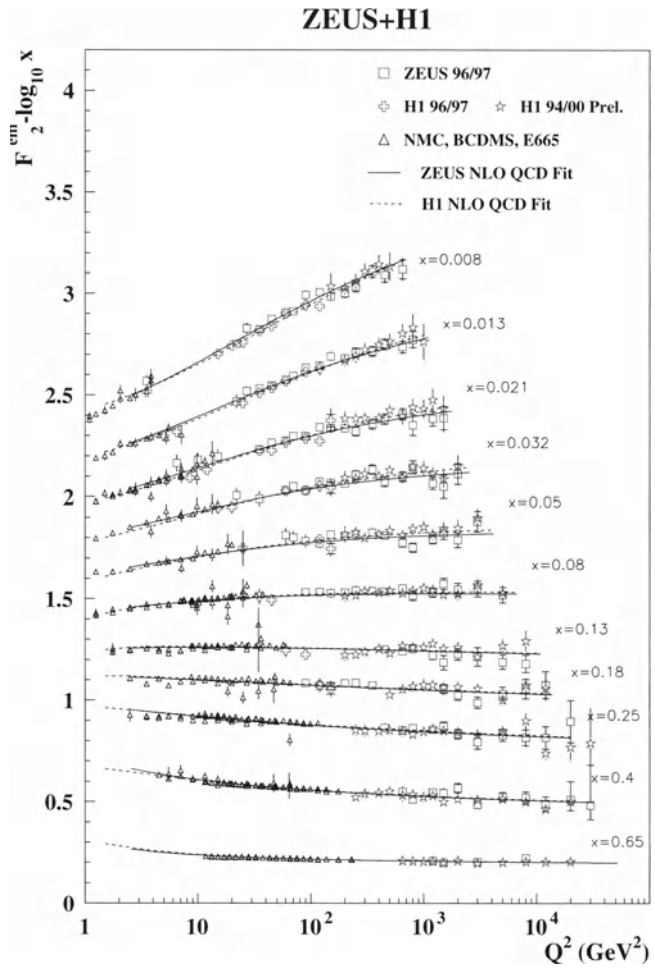

Fig. 1. The H1 and ZEUS data on F_2 at high x as a function of Q^2. Also shown are points from the fixed-target experiments NMC, BDCMS and E665. The solid curve shows the NLO QCD fit. Each bin in x is displaced by the factor $\log_{10} x$ as indicated for ease of visibility.

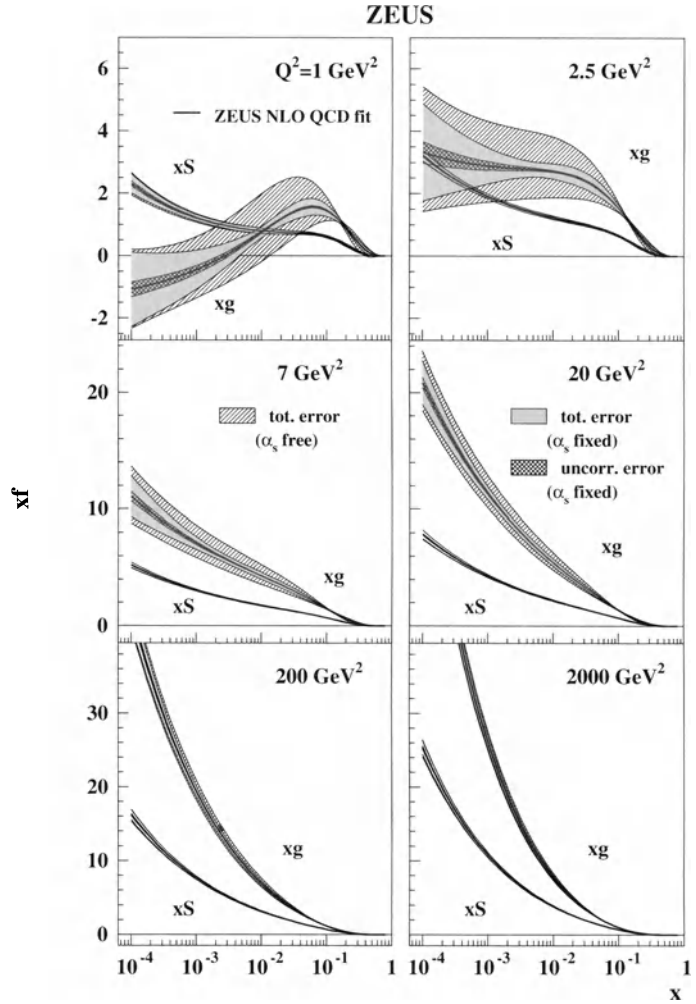

Fig. 2. The ZEUS determination of the gluon and singlet-quark densities in six bins of Q^2 as a function of $\ln x$. The shaded bands show the uncorrelated error on the parton density, the total error if the strong coupling is fixed, and the total error if α_s is allowed to vary.

have used the results of the fit to determine the parton density distributions through relations analogous to that given by eq. (3). Some of the results from ZEUS are shown in fig. 2.

Several conclusions can be drawn from these sorts of determinations. Firstly, the strong rise of the gluon density as x falls at medium and high Q^2 can clearly be seen. The singlet quark densities have a lower density than that of the gluon, as would be expected since the sea is considered to be generated by the emission of gluons from the valence quarks. However, at $Q^2 \sim 1$ GeV^2 and at low x, the gluon density drops considerably below that of the sea and, even more strikingly, seems to become negative. Although worrying and difficult to interpret, this behaviour is not necessarily pathological since parton densities are not observables; however, at around the same Q^2, F_L also seems to become negative. The conclusion is, therefore, that the NLO QCD formalism begins to break down at $Q^2 \sim 1$ GeV^2. In fact, the biggest surprise is probably that QCD and the concept of partons do indeed seem to work down to such low values of Q^2.

3 F_2 at low Q^2

For values of Q^2 less than 1 GeV^2, a good representation of the data can be achieved using Regge theory, particularly at low x, since this corresponds to high W, where W is the centre-of-mass energy of the photon-proton system, at which Regge theory is most applicable. This can be seen in fig. 3, which shows the high-precision ZEUS BPT F_2 data [9] at low Q^2, together with other H1 and ZEUS data, as a function of y *versus* $\log Q^2$. For $Q^2 > 1$ GeV^2, the data are approximately flat, consistent with the expectations from QCD. Below 1 GeV^2, the data fall rapidly, consistent with the Q^{-2}-dependence expected from conservation of the electromagnetic current. The form is well fitted by a parameterisation [9] based on Regge theory.

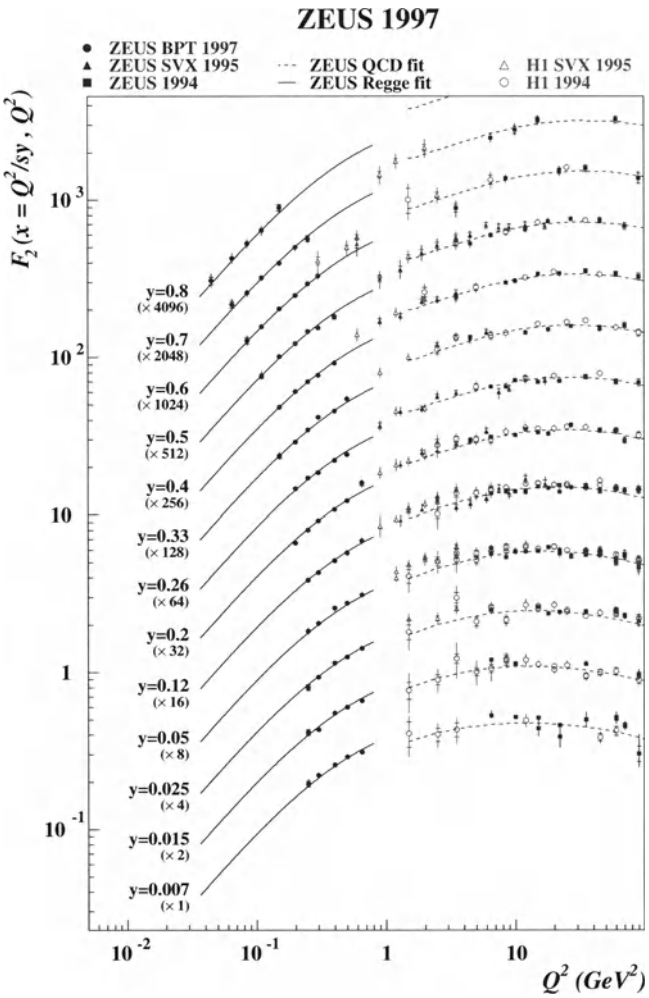

Fig. 3. H1 and ZEUS F_2 data as a function of $\log Q^2$. Each y bin is multiplied by the number in parentheses for clarity of presentation. For $Q^2 > 1$ GeV^2, the curves show an NLO QCD fit to the data. For the ZEUS data below 1 GeV^2, a fit to a Regge-based parameterisation is shown.

These features are confirmed by recent H1 data taken with the interaction vertex shifted to give access to smaller values of Q^2. These data [10] cover the Q^2 region between the ZEUS BPT data and that taken in the central detectors with $Q^2 > 2$–3 GeV^2.

3.1 Low-x phenomenology

We have seen that the QCD description of the DIS data begins to break down around $Q^2 \sim 1$ GeV^2, and that for values below this, a good description can be given by Regge theory. Neither theory can describe the entire HERA kinematic range. One possibility to achieve this is via dipole models, which consider the DIS process in the rest frame, rather than the more usual infinite-momentum frame, of the proton. In such a frame, the virtual photon can be considered to fluctuate into partonic subsystems, typically a quark-antiquark pair, or dipole, or a quark-antiquark-gluon state. By combining such a treatment with the concept of parton saturation, models such as that of Golec-Biernat and Wüsthoff [11,12] can give a good description of the data over all ranges of Q^2. Parton saturation effects would be expected to set in at low x when the parton density becomes so large that their probability of interacting with each other becomes non-negligible. Fits of the Golec-Biernat and Wüsthoff model to the HERA data, including one modified to take account of QCD-evolution effects [13], is shown in fig. 4 for the higher-Q^2 data. The fit is significantly improved by including QCD evolution. The model also gives a good fit to the ZEUS BPT data (not shown).

4 Diffraction

Dipole models not only successfully fit the DIS data over the full HERA kinematic range, but also give a natural connection to another important process, diffraction. In diffractive processes at HERA, a hard interaction occurs but nevertheless the proton leaves the interaction intact. This can be understood if the proton exchanges a colour-singlet object which transfers energy and momentum to the interaction with the virtual photon. This object is normally called the pomeron; it can be considered to have a partonic structure analogous to that of the proton, which can be investigated by examining the debris of the hard collision, as is done in the measurement of the proton structure functions. The connection between this process and standard inclusive DIS in dipole models is that the inclusive DIS processes can be considered to be the sum of single-gluon and two-gluon exchange between the proton and the dipole fluctuation of the virtual photon, whereas diffraction can be considered to originate from colour-singlet two-gluon exchange only. Such a picture implies a simple connection between two apparently rather different processes.

The success of the dipole picture can be seen in fig. 5, which shows the ratio of the diffractive cross-section to the total cross-section as a function of W in various Q^2 and M_X bins, where M_X is the mass of the diffractive system. The very flat behaviour of this ratio as a function of W is in contradiction to simple ideas from Regge theory and the optical theorem; the former would predict a W-dependence of diffraction like $W^{0.16}$ compared to that of the total cross-section of $W^{0.4}$. Similarly, if diffraction is related to the exchange of a colour-singlet two-gluon system, then it should have a $W \sim 1/x$-dependence like the gluon-density squared, compared to the single-gluon dependence of the inclusive cross-section, which ought to result in the ratio strongly rising as W increases. The flatness of this ratio is therefore a surprise, but, at least for the smallest values of M_X, it is rather well fitted by the Golec-Biernat and Wüsthoff model.

A similar picture emerges if one examines more exclusive processes, such as elastic vector-meson production [14]. Here the light mesons, ρ and ϕ, show a similarly flat cross-section ratio. In the case of the J/ψ, however, where the mass of the charmed quark is sufficiently large

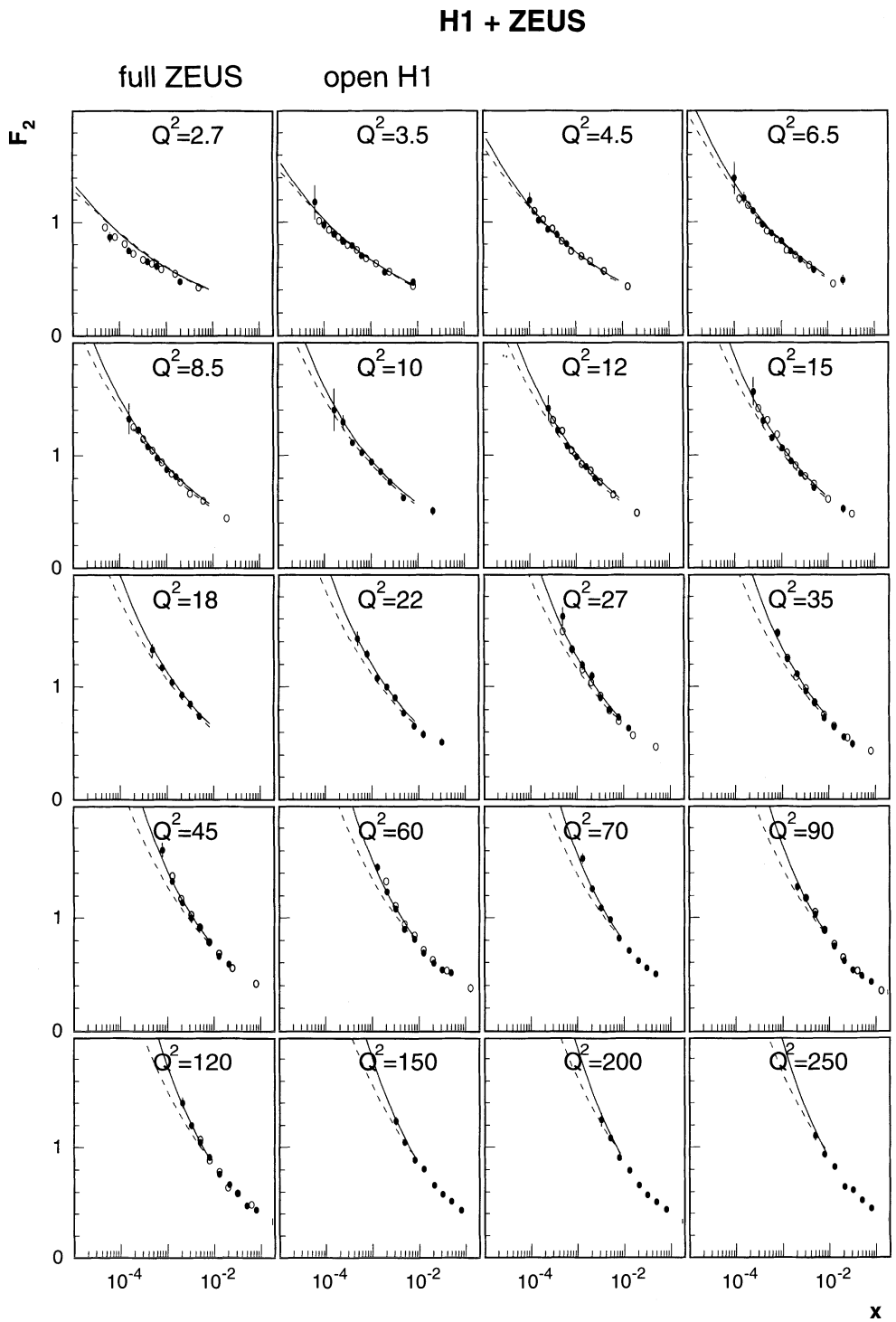

Fig. 4. The ZEUS (full points) and H1 (open circles) F_2 data as a function of x in bins of Q^2. Also shown are two fits to the Golec-Biernat and Wüsthoff model. The dotted line shows the fit to the original model without QCD evolution; the full curve shows the prediction taking such evolution into account.

to form a hard scale, the behaviour of the ratio in photoproduction is very different, with a steep dependence on W which flattens at higher Q^2. This is a clear indication of the interplay of hard scales in QCD and the study of such processes is likely to be very interesting.

The study of vector-meson production as a function of t, the momentum transfer at the proton vertex, is also interesting [15]. There is considerable evidence that t can also form a hard scale in QCD. Forshaw and Poludniowski [16] have looked at the production rate of ρ, ϕ and J/ψ mesons as a function of t and found that models based on conventional two-gluon exchange cannot fit the data. Their model, based on a BKFL-like [17] pomeron, can fit the data over the full t range for all mesons. This is one of

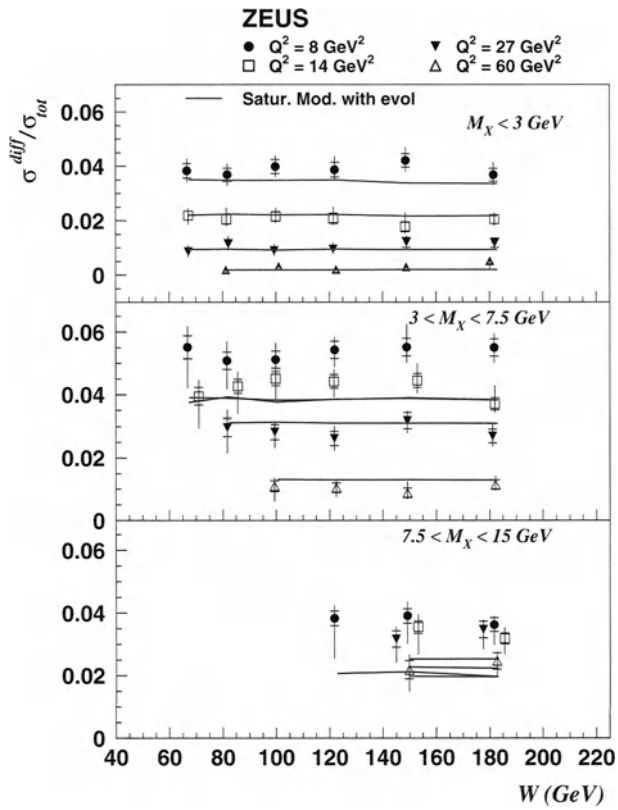

Fig. 5. The ratio of the diffractive cross-section to the total cross-section as a function of W in four bins of Q^2 and in three regions on M_X. The curve shows the predictions of the Golec-Biernat and Wüsthoff model.

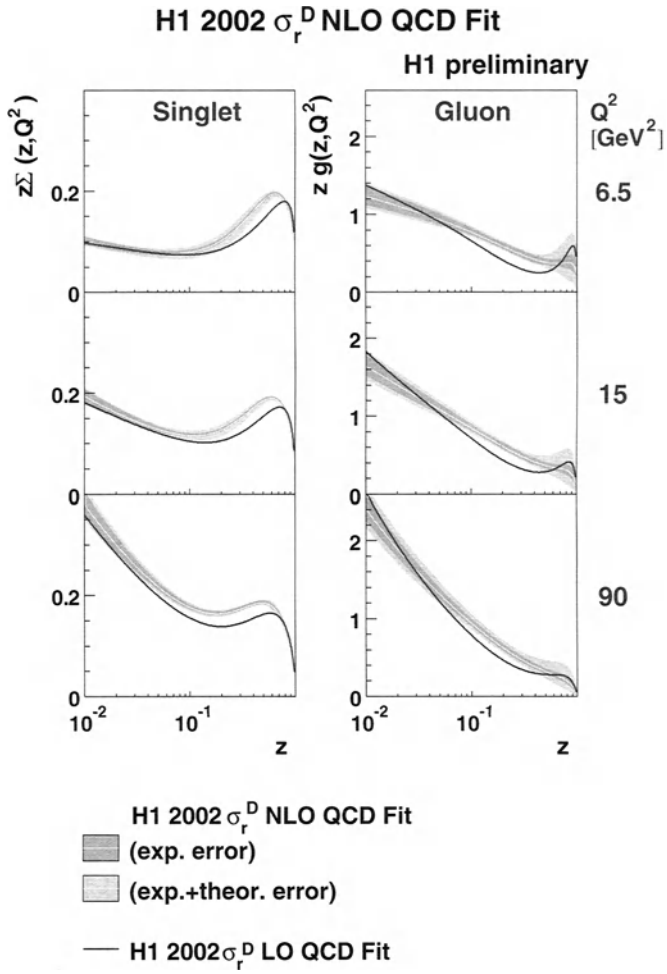

Fig. 6. The singlet and gluon parton distribution functions of the pomeron as obtained from the H1 reduced diffractive cross-sections as functions of z, the fractional momentum of the pomeron carried by the parton. The distributions are shown in three bins of Q^2. The line shows the LO QCD fit, while the shaded bands indicate the results of the NLOQCD fit with uncertainties as indicated in the legend.

the few concrete indications of the importance of BFKL evolution at HERA.

The H1 Collaboration has recently produced [18] a determination of the parton content of the pomeron from a NLOQCD fit to the reduced cross-sections obtained from the inclusive diffractive data, analogous to that discussed above for the F_2 data. The results of this fit for the singlet and gluon distributions in the pomeron are shown in fig. 6 as a function of z, the fractional momentum of the pomeron carried by the parton. The fits clearly show that the pomeron is dominated by gluons and that, similarly to the proton, the gluon distribution rises strongly as z falls, driving in turn a rise in the singlet distribution at higher Q^2. These data are in agreement with the idea that diffraction is mediated by an exchange of some form of two-gluon ladder.

Finally in this section, although not strictly diffractive, it is instructive to consider the data on the pion structure function. Virtual pions can be probed in ep DIS by tagging leading neutrons in a dedicated calorimeter at 0° far downstream of the interaction point in the proton direction. Such a process can be shown in particular kinematic regions to be dominated by exchange of another colourless object, the virtual pion. Thus, similarly to the H1 determination of the pomeron pdfs discussed above, ZEUS has used the cross-sections for inclusive leading neutron production to determine the pion structure function [19]. The data are generally compatible with the factorisation of the lepton and proton vertices, although a factorisation breaking with Q^2 of around 20% is observed, which may be caused by absorptive rescattering of the neutron. The overall normalisation of the pion structure function derived from these data is uncertain to around a factor of two, due to the lack of an unambiguous model for the virtual-pion flux. Nevertheless, the shape of the pion structure in the accessible kinematic region is remarkably similar to that of the proton.

5 Summary

Within the limited space of this write-up, it is not possible to cover a vast field of other HERA physics, in particular that at high Q^2 and the search for physics beyond the Standard Model of particle physics. This area will be the

focus of the HERA II programme, which will not only benefit from a substantial upgrade in the luminosity, but also from the availability of polarised lepton beams. Thus, the field of heavy-quark physics, electroweak studies and exotic physics will take centre stage at HERA II. The richness of the HERA I data, particularly in the areas of the low-Q^2 interface, diffraction and jet physics are far from exhausted, however, and the next few years should bring further illumination in this poorly understood and theoretically challenging area of physics.

I am grateful to many colleagues, particularly of ZEUS and H1, for helpful discussions. I am particularly grateful to M. Kuze for a critical reading of this manuscript.

References

1. H1 Collaboration (C. Adloff *et al.*), Eur. Phys. J. C **13**, 609 (2000).
2. H1 Collaboration (C. Adloff *et al.*), Eur. Phys. J. C **21**, 33 (2001).
3. ZEUS Collaboration (S. Chekanov *et al.*), Eur. Phys. J. C **21**, 443 (2001).
4. NMC Collaboration (M. Arneodo *et al.*), Nucl. Phys. B **483**, 3 (1997).
5. BCDMS Collaboration (A.C. Benvenuti *et al.*), Phys. Lett. B **223**, 485 (1989).
6. BCDMS Collaboration (A.C. Benvenuti *et al.*), Phys. Lett. B **237**, 592 (1990).
7. E665 Collaboration (M.R. Adams *et al.*), Phys. Rev. D **54**, 3006 (1996).
8. ZEUS Collaboration (S. Chekanov *et al.*), Phys. Rev. D **67**, 012007 (2002), hep-ex/0208023.
9. ZEUS Collaboration (J. Breitweg *et al.*), Phys. Lett. B **481**, 213 (2000).
10. H1 Collaboration, Paper 975, in *Proceedings of the XXXI International Conference on High Energy Physics, ICHEP02, Amsterdam, The Netherlands, 25-31 July 2002*, edited by S. Bentvelsen, P. de Jong, J. Koch, E. Koch, Nucl. Phys. B Proc. Suppl. **117** (2003).
11. K. Golec-Biernat, M. Wüsthoff, Phys. Rev. D **59**, 014017 (1999).
12. K. Golec-Biernat, M. Wüsthoff, Phys. Rev. D **60**, 114023 (1999).
13. J. Bartels, K. Golec-Biernat, H. Kowalski, Phys. Rev. D **66**, 014001 (2002).
14. ZEUS Collaboration, Paper 820, in *Proceedings of the XXXI International Conference on High Energy Physics, ICHEP02, Amsterdam, The Netherlands, 25-31 July 2002*, edited by S. Bentvelsen, P. de Jong, J. Koch, E. Koch, Nucl. Phys. B Proc. Suppl. **117** (2003).
15. ZEUS Collaboration (S. Chekanov *et al.*), Eur. Phys. J. C **26**, 389 (2003), hep-ex/0205081.
16. J. Forshaw, G. Poludniowski, Eur. Phys. J. C **26**, 411 (2003), hep-ph/0107068.
17. E.A. Kuraev, L.N. Lipatov, V.S. Fadin, Phys. Lett. B **60**, 50 (1975); Sov. Phys. JETP **44**, 433 (1976); **45**, 199 (1977); Ya.Ya. Balitsky, L.N. Lipatov, Sov. J. Nucl. Phys. **28**, 822 (1978).
18. H1 Collaboration, Paper 980, in *Proceedings of the XXXI International Conference on High Energy Physics, ICHEP02, Amsterdam, The Netherlands, 25-31 July 2002*, edited by S. Bentvelsen, P. de Jong, J. Koch, E. Koch, Nucl. Phys. B Proc. Suppl. **117** (2003).
19. ZEUS Collaboration (S. Chekanov *et al.*), Nucl. Phys. B **637**, 3 (2002).

Eur. Phys. J. A **18**, 389–394 (2003)
DOI 10.1140/epja/i2002-10242-2

THE EUROPEAN PHYSICAL JOURNAL A

An introduction to the Generalized Parton Distributions

M. Garçon[a]

DAPNIA/SPhN, CEA-Saclay, 91191 Gif-sur-Yvette, France

Received: 30 September 2002 /
Published online: 22 October 2003 – © Società Italiana di Fisica / Springer-Verlag 2003

Abstract. The recently introduced concepts of Generalized Parton Distributions (GPD) are reviewed in an introductory and phenomenological fashion. These distributions provide a rich and unifying picture of the nucleon structure. Their physical meaning is discussed. The GPD are in principle measurable through exclusive deeply virtual production of photons (DVCS) or of mesons (DVMP). Experiments are starting to test the validity of these concepts. First results are discussed and new experimental projects presented, with an emphasis on this program at Jefferson Lab.

PACS. 12.38.-t Quantum chromodynamics – 13.60.-r Photon and charged-lepton interactions with hadrons – 14.20.Dh Properties of protons and neutrons

In Memoriam : René Beurtey died a few days before this conference began. His work has had a determining influence on the technical and physical developments in our field. His ideas were innovative and he shared them generously, not being concerned with "publishing first". He developed the first adiabatic transitions in a polarized deuteron source, promoted original technics for the study of nucleon-nucleon scattering as a continuous function of energy (cluster jet inside a synchrotron ring and the "Beurtey-Saudinos" wheel), and triggered the "Tatischeff experiments" on narrow dibaryons search. In addition, he participated in the accelerator research that made SATURNE the first synchrotron to successfully cross proton depolarizing resonances. Beyond his professional talents, René had an expansive and enjoyable personality that made him a true pleasure to work with or around, or to consult. His lively wit and sense of humor were a stimulus for many of us.

1 Foreword

This presentation is intended to provide a pedagogical introduction to the subject of Generalized Parton Distributions and associated phenomenology. It cannot be exhaustive on the subject, and the reader should consult reviews or papers such as refs. [1–5], and references therein, for a more rigourous and complete account of the subject. At this conference, M. Vanderhaeghen gave another talk on the subject, with more emphasis on theory and its latest developments [6].

[a] e-mail: mgarcon@cea.fr

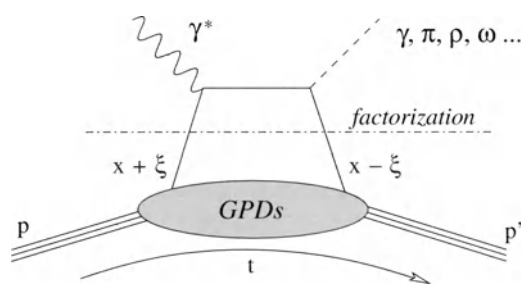

Fig. 1. Representation of the deeply virtual exclusive processes DVCS and DVMP, also referred to as the "handbag" diagram.

2 Basic concepts

In the last few years, significant theoretical advances were made that allow, using Quantum Chromodynamics (QCD) and within some conditions, to factorize the amplitude for exclusive electroproduction processes into a hard scattering at the parton level and non-perturbative *Generalized Parton Distributions* (GPD) —see fig. 1. From the theoretical point of view, as a particular case of factorization theorems, the introduction of these distributions builds a bridge between fundamental QCD, phenomenology and experimental observables. The processes under consideration are the deeply virtual Compton scattering (DVCS: $ep \to ep\gamma$) and the deeply virtual meson production (DVMP: $ep \to ep\ \rho, \omega, \pi \ldots$). We understand by "deeply virtual" a kinematical regime where the virtuality Q^2 of the exchanged photon γ^* is large and where the available energy in the $\gamma^* p$ system is above the resonance region, typically larger than 2 GeV.

The GPDs contain the hitherto most complete description of the internal quark-gluon structure of hadrons. For each of the quark flavours (we will not consider the gluon sector in this paper), there are four of these distributions, H, E, $\tilde{H}$ and $\tilde{E}$, which depend on three variables: the average longitudinal momentum fraction x of the struck parton in the initial and final states, a skewness parameter ξ which measures the difference between these two momentum fractions, and the momentum transfer t to the target nucleon. The above-mentioned factorization theorems are applicable for $|t|/Q^2 \ll 1$.

The physical content of the GPDs is quite rich: in simple terms, whereas ordinary parton distributions yield, for example, the probability $|\psi(x)|^2$ that a quark carries a fraction x of the momentum of a fast-moving nucleon, the GPDs measure the *coherence* $\psi^*(x-\xi)\cdot\psi(x+\xi)$ between two different (quark) momentum states of the nucleon and in this way quark momentum correlations in the nucleon. In quantum mechanics, one cannot reduce the knowledge of a system formed of a superposition of states (in our case, an infinite number of states described by the variable x) to the sole probabilities that the system be in a particular state. The interferences between these states, or *coherences*, or off-diagonal elements, are necessary for a full description of the system.

If one of the momentum fractions ($x+\xi$ or $x-\xi$) is negative, it is interpreted as representative of an antiquark. Meson-like $q\bar{q}$ configurations in the nucleon may then be investigated. As mentioned in sect. 3.2, the GPDs are expected to exhibit a rich structure at $|x|<\xi$ which is related in particular to the pion cloud around the nucleon.

Whereas x and ξ characterize solely the longitudinal momenta of the partons involved, the t-dependence of the GPDs is related to their transverse momenta. By Fourier transform, it is conceivable to access simultaneously the longitudinal momentum fraction of quarks and their position in the transverse plane [7]. This would open the way to a *femto-photography* of the nucleon [8].

The richness of information contained in the GPDs may be illustrated by several quite remarkable relations, among which

– *the forward limit:*

$$\lim_{t\to 0,\xi\to 0} H(x,\xi,t) = q(x), \text{ or } -\bar{q}(-x) \text{ if } x<0$$

and

$$\lim_{t\to 0,\xi\to 0} \tilde{H}(x,\xi,t) = \Delta q(x), \text{ or } \Delta\bar{q}(-x).$$

As expected from the above discussion, the ordinary parton distributions, both unpolarized $q(x)$ and polarized $\Delta q(x)$, are but a limiting case of the GPDs. Note that, though the GPDs are defined functions for $\xi=0$ or $t=0$, these variables take only finite, non-zero values in any experiment. Note also that the functions E and $\tilde{E}$ have no connection with the ordinary parton distributions. They are not constrained by deeply inelastic scattering, which corresponds to this forward limit.

– *the form factor limit:*

$$\forall\xi, \quad \int_{-1}^{+1} H(x,\xi,t)\cdot \mathrm{d}x = F(t)$$

(4 relations of this type for each quark flavor). After integration over x, the t-dependence of the GPDs is given by the nucleon elastic form factors ($H\to$ Dirac, $E\to$ Pauli, $\tilde{H}\to$ axial vector and $\tilde{E}\to$ pseudoscalar form factors).

– *Ji's sum rule:*

$$\forall\xi, \quad \lim_{t\to 0}\frac{1}{2}\int_{-1}^{+1} x\cdot(H+E)(x,\xi,t)\cdot \mathrm{d}x = J_q,$$

where J_q is the total angular momentum, *i.e.* the sum of intrinsic spin and of orbital angular momentum, carried by the quarks. This sum rule provides a way to understand the origin of the nucleon spin. Indeed, the contribution of the quark intrinsic spin ($\frac{1}{2}\Delta\Sigma$) was measured at CERN/SMC, SLAC and DESY/HERMES. The gluon contribution (ΔG) will be determined at CERN/COMPASS, RHIC/STAR and SLAC. The knowledge of GPDs allows one to isolate the contribution of the quark orbital angular momentum to the total spin of the nucleon: $\frac{1}{2} = J_q + J_g = (\frac{1}{2}\Delta\Sigma + L_q) + (\Delta G + L_g)$.

The first two relations demonstrate the new unifying frame given by the GPDs: observables as different as elastic form factors and parton distributions are related to each other through these new functions. However, the knowledge of limits, or projections, does not imply a complete knowledge of the GPDs themselves. Models are being developed for a complete representation.

3 GPD calculations

We give here a short summary of selected calculations of the GPDs. For a more complete account, see refs. [3,5,6].

3.1 Constrained parametrizations

The "double distributions" [9] are well suited for the description of the GPDs. They incorporate the GPDs mathematical properties (polynomiality of the Mellin moments) and have a definite physical content. They satisfy positivity bounds, a number of inequalities that GPDs have been shown to obey. Elastic form factors and parton distributions are included as limiting values.

An alternate, "dual" parametrization, based on a partial-wave expansion, has recently been proposed [10].

3.2 Model calculations

QCD-inspired models are very useful to understand how non-perturbative mechanisms generate various structures in GPDs.

Table 1. Comparative merits of DVCS and DVMP for the study of Generalized Parton Distributions.

DVCS	DVMP
Factorization established (virtual photon is transverse at leading order)	Factorization established for longitudinal photons (σ_L must be extracted experimentally)
Measures a combination of $H, E, \tilde{H}, \tilde{E}$	Vector mesons : combination of H and E (the GPD's entering Ji's sum rule) Pseudoscalar mesons : combination of $\tilde{H}$ et $\tilde{E}$ Various decompositions in quark flavours according to the nature of the meson
$\sigma_T(\gamma^* p \to \gamma p) \propto Q^{-4}$	$\sigma_L(\gamma^* p \to p \text{ meson}) \propto Q^{-6}$ (larger at least for π^+, ρ and ω at moderate Q^2)
Contribution of Bethe-Heitler process: - useful through interferences (polarization or charge asymmetries measurements) - decreases quickly with increasing energy	
	A manageable complication: the meson structure
Smaller higher-twist contributions	Larger higher-twist contributions, but cancel in ratios ρ/ω and polarization asymmetries

In the simple bag model, GPDs have but a weak dependence on ξ, and show no structure for $|x| < \xi$. A number of calculations in different constituent quark models are being developed.

In contradistinction, in the chiral quark-soliton model, where the quarks interact through a highly non-linear pion field, the GPDs exhibit a rich structure for $|x| < \xi$. The same model leads also to a t-dependence which can be approximated by $H(x,0,t) \sim x^{-at}q(x)$ and deviates significantly from the early factorized *ansatz* $H(x,0,t) \sim F(t)q(x)$.

In the region $x > \xi$, the use of light-cone wave functions for the nucleon allows to write GPDs as overlap integrals. In considering the nucleon as a superposition of Fock states, *e.g.* $|p\rangle = |uud\rangle + |uudq\bar{q}\rangle + |uudg\rangle + \cdots$, the GPDs are useful to understand the role of given states.

3.3 Lattice QCD

Moments of ordinary parton distributions are being evaluated using QCD calculations on a lattice [11]. Likewise, it is conceivable that GPD moments could be calculated, but this has not been attempted yet.

4 Observables

Both DVCS and DVMP processes are sensitive to GPDs of the nucleon, once it is established that the handbag diagram of fig. 1 dominates in the kinematical regions where measurements are performed. These processes have different merits and sensitivities summarized in table 1. The sensitivity of specific observables, including polarization observables, has been studied in detail in refs. [3,5].

While ξ and t are variables fixed by the kinematics of the process under study, x enters the amplitude as an integration variable. Therefore, in most cases, observables are expressed in terms of integrals over x of GPDs. The only exception is in observables sensitive only to the imaginary part of the handbag amplitude: because of the propagators $(x \pm \xi + i\varepsilon)^{-1}$ in the diagram of fig. 1, the GPDs enter then with an argument $x = \pm\xi$. This is the case for the DVCS beam spin asymmetries discussed in sect. 6.

In general, the extraction of GPDs from observables requires a deconvolution and, in principle, an infinite set of data. In practice, this problem has mathematical properties analogous to, *e.g.*, tomography [12] and may be solved (with associated uncertainties) with a finite set of data. This complete exercise remains to be done with either real or simulated data.

5 Finite Q^2

Most of the discussion so far was based on a high momentum transfer approximation (Bjorken limit). In practice, the measurements of the exclusive processes under study are or will be performed at rather moderate Q^2, 1 to 6 GeV^2. The relevant corrections are listed in this section.

As is the case for the ordinary parton distributions, the GPD evolution leads to logarithmic corrections ($\ln Q^2$): the dependence of the GPDs on a factorization scale μ results from the evolution equation

$$\mu \frac{\partial}{\partial \mu} H(x,\xi,t;\mu) = \int \mathcal{K}(x,y,\xi;\alpha_s(\mu)) \cdot H(y,\xi,t;\mu) \cdot \mathrm{d}y \,,$$

where α_s is the strong-coupling constant. The kernel $\mathcal{K}$ has been calculated at next-to-leading order (NLO).

At order $\mathcal{O}(1/Q)$ (twist-3), beyond a minimal gauge restoring term, the contribution of a longitudinal exchanged photon γ_L^* to DVCS can be expressed in terms of derivatives of (twist-2) GPDs. This is the so-called Wandzura-Wilczek approximation. The exchange of a gluon between the quark in the handbag loop and the nucleon core would give an additional contribution, thought to be very small, in analogy with a similar case in deeply inelastic scattering.

At the next order in Q, trivial kinematical corrections $\mathcal{O}(t/Q^2, M^2/Q^2)$, surprisingly enough, are not always considered. There are also dynamical target mass corrections $\mathcal{O}(M^2/Q^2)$. Finally the transverse momenta of quarks modify the quark propagators in the diagram of fig. 1: $(x \pm \xi + i\varepsilon)^{-1} \to (x \pm \xi + k_\perp^2/Q^2 + i\varepsilon)^{-1}$. Many other twist-4 contributions remain to be evaluated.

The aim of the first-generation experiments (see sect. 6) is then to establish that observables have the anticipated Q^2-dependence in order to validate the GPD approach at leading twist or to disentangle higher-twist contributions.

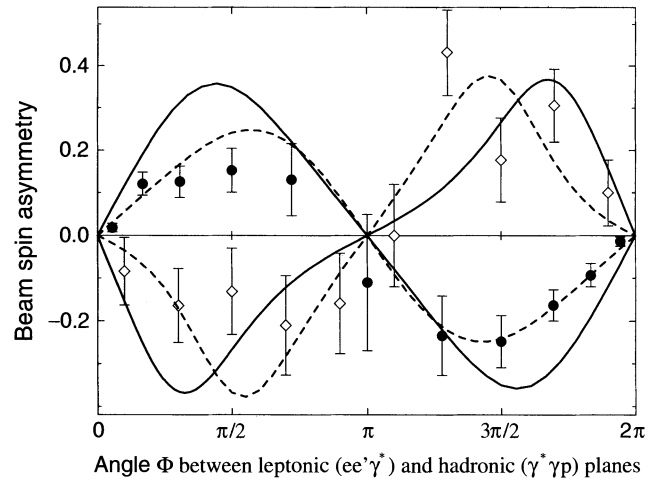

Fig. 2. Beam spin asymmetry in $ep \to ep\gamma$. The full circles are from JLab/CLAS [17], the diamonds from HERMES [16]. The kinematics are different for the two experiments. The corresponding calculations are from [5] (dashed lines) and [3] (solid lines). The asymmetry is of opposite sign between the two experiments because one uses an electron beam, while the other uses positrons. The approximate $\sin\Phi$ dependence is strongly suggestive of the validity of the GPD approach at leading order.

6 Experiments

The difficulty in the experimental study of GPDs is the measurement of exclusive processes, of rather low cross-sections, at the highest possible momentum transfer Q^2. This requires high beam energy and luminosity, as well as large-acceptance and high-resolution detectors. At present, these studies have been initiated at HERMES (sufficient energy, 27 GeV, but relatively low luminosity) and at Jefferson Lab (beam energy of 4 to 6 GeV, but high product luminosity × acceptance). In the next few years, significant progress could be achieved with a 12 GeV upgrade at JLab/CEBAF [13], and using the 200 GeV muon beam at COMPASS [14]. A new high-luminosity, high-duty-cycle machine, operating in the 25–50 GeV range, would be ideally suited for these studies [15].

DVCS should be the cleanest process for GPD studies. Through the optical theorem, it is linked to deeply inelastic scattering for which the evolution of the structure functions is well understood down to $Q^2 \sim 1$ GeV^2. In addition, the $\gamma\gamma^*\pi^0$ form factor, whose calculation proceeds through the same type of handbag diagram as in fig. 1, gives also a good indication that DVCS should scale early. Corrections may then be expected to be understood at rather low Q^2. As mentioned in table 1, DVCS is indistinguishable from the known Bethe-Heitler (BH) process where the final photon is emitted by the incident or scattered electron. DVCS dominates over BH only at very high energies (COMPASS, HERA). At beam energies accessible at JLab or HERMES, the large BH process may be turned into an advantage by measuring interferences in spin or charge asymmetries; DVCS could then be accessed at the amplitude level.

The first experimental indications of DVCS at the quark level were published last year [16,17]. DVCS was also observed at HERA [18], in a kinematical region that makes it more sensitive to gluons. The approximate $\sin\Phi$ dependence of the observed beam spin asymmetry (see fig. 2) is expected from any process which conserves helicity in the $\gamma^* p \to \gamma p$ scattering [19]. The process described by the (leading order) handbag diagram of fig. 1 has such a property. The comparison with first calculations using the GPD formalism is very encouraging. From the experimental point of view, it should be noted that at HERMES, the 800 MeV missing-mass resolution in the $ep \to e\gamma X$ reaction is not sufficient to select unambiguously the (dominating) $ep \to ep\gamma$ events, while at JLab/CLAS, the 110 MeV missing-mass resolution in the $ep \to epX$ reaction causes the $ep \to ep\gamma$ and $ep \to ep\pi^0$ to mix, but a separation was done using a shape analysis of the relevant spectra. First results of beam charge asymmetry measurement in DVCS were also reported from HERMES [20].

Both experiments will soon obtain more statistics. Furthermore, both detection systems will be improved in the next couple of years. In particular, at JLab/CLAS, a forward lead-tungstanate calorimeter, covering the photon angles between 3° and 12°, is being built, together with a specially designed two-coil solenoid acting as a trap for background Möller electrons [21]. A luminosity of 2×10^{34} cm^{-2}s^{-1} is anticipated with this large acceptance spectrometer. Another DVCS experiment will run in 2003 at JLab/Hall A [22], using one High-Resolution Spectrometer for detection of the scattered electrons, a new lead-fluoride calorimeter for the outgoing photons, and a ring of thick plastic scintillators for the recoil protons [22]. Preliminary tests indicate that a luminosity of 10^{37} cm^{-2}s^{-1} can be reached, in spite of the rather open geometry and forward disposition of the proton detector.

Because of the necessary additional gluon exchange to create a meson, the asymptotic regime should be reached at higher Q^2 in DVMP processes. However observables

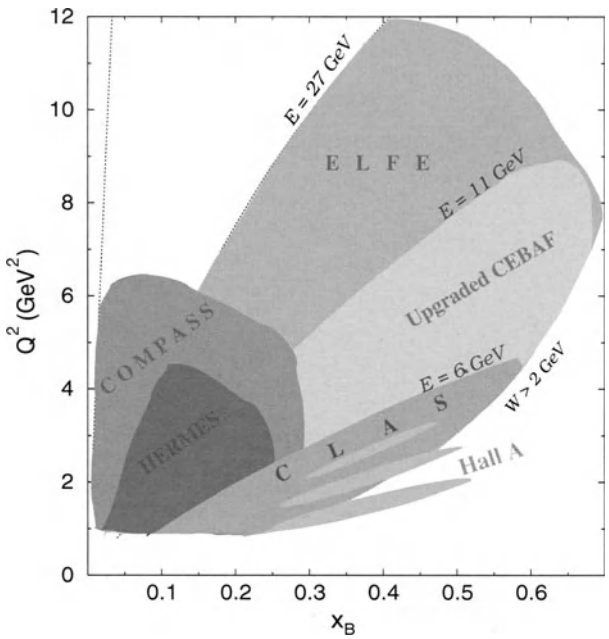

Fig. 3. Kinematical domain (Q^2 *vs.* x_B) accessible at various facilities (existing or in project) for the measurement of deeply virtual exclusive processes. x_B is the usual Bjorken variable, from which ξ is calculated. "ELFE" does not refer here to a specific project, but to a —yet to be defined— high-luminosity machine, in this case at 27 GeV. See text for additional comments.

such as asymmetries and ratios (*e.g.*, ρ/ω) are expected to scale earlier. As illustrated in table 1, DVMP, at leading order, is sensitive to different combinations of GPDs as DVCS. Also the different quark content of various mesons gives access to different flavour combinations of these distributions. Since factorization has been proven only for longitudinal photons [23], the corresponding contribution must be extracted from the experiment. For vector mesons, this is done via a measurement of the meson polarization through the angular distribution of its decay products ($\rho \to \pi^+\pi^-$, $\omega \to \pi^+\pi^-\pi^0$, $\phi \to K^+K^-$) and the verifiable application of s-channel helicity conservation to relate the virtual-photon helicity to the one of the emitted vector meson. For pseudoscalar mesons, one has to resort to a Rosenbluth separation to extract σ_L (this has not been attempted yet in the considered kinematical regime).

The first results of (almost) exclusive electroproduction of ρ-mesons (longitudinal cross-sections) [24] in a kinematical region where the handbag diagram is expected to dominate are also very suggestive of the validity of the GPD approach. Systematic studies and tests of the predicted Q^{-6} scaling of the longitudinal cross-sections are underway at JLab/CLAS: data taken at beam energies of 4.2 GeV [25] and 5.75 GeV [26], up to $Q^2 \sim 4$ GeV^2, are being analyzed.

The kinematical domain accessible with existing and projected facilities is illustrated in fig. 3. The high Q^2 approximate limit for the existing high-energy facilities results from count rate limitations due to a lower luminosity and decreasing cross-sections as Q^2 and x_B increase.

7 Conclusions and outlook

Generalized Parton Distributions have emerged in the past few years as a powerful, attractive and unifying concept for the hadron structure. Their Q^2 evolution has been worked out to next-to-leading order, and twist-3 (and some twist-4) contributions to deeply virtual and exclusive processes have been calculated. The interpretation and significance of GPDs are under intense study.

The deconvolution problem posed by the extraction of GPDs from experimental observables was barely touched upon, but mathematical methods exist, or are being developed, that address this particular issue.

On the experimental side, we are still at a very early stage. There are indications that the handbag diagram is at work. In the next two or three years, more dedicated and higher statistics experiments will attempt to establish on firm grounds the validity of this theoretical approach; this includes tests of Q^2-scaling laws and of factorization. Beyond that, systematic measurements of GPDs will be performed in a large kinematical domain at several facilities.

References

1. M. Vanderhaeghen, P.A.M. Guichon, M. Guidal, Phys. Rev. D **60**, 094017 (1999); P.A.M. Guichon, M. Vanderhaeghen, Prog. Part. Nucl. Phys. **41**, 125 (1998).
2. B.W. Filippone, Xiandong Ji, Adv. Nucl. Phys. **26**, 1 (2001).
3. K. Goeke, M.V. Polyakov, M. Vanderhaeghen, Prog. Part. Nucl. Phys. **47**, 401 (2001).
4. A.V. Radyushkin, hep-ph/0101225.
5. A.V. Belitsky, D. Müller, A. Kirchner, Nucl. Phys. B **629**, 323 (2002).
6. M. Vanderhaeghen, this issue, p. 429.
7. M. Burkardt, Phys. Rev. D **62**, 071503(R) (2000).
8. J.P. Ralston, B. Pire, hep-ph/0110075; M. Diehl, Eur. Phys. J. C **25**, 223 (2002); J.P. Ralston, P. Jain, hep-ph/0207129; M. Burkardt, hep-ph/0209179.
9. A.V. Radyushkin, Phys. Rev. D **59**, 014030 (1999).
10. M.V. Polyakov, A.G. Shuvaev, hep-ph/0207153.
11. A.W. Thomas *et al.*, this issue, p. 241.
12. O.V. Teryaev, Phys. Lett. B **510**, 125 (2001).
13. The Science Driving the 12 GeV Upgrade of CEBAF, Jefferson Lab report, February 2001.
14. N. d'Hose *et al.*, Letter of intent to the CSTS/SPhN-Saclay (2000), `http://www-dapnia.cea.fr/Sphn/Vcs/Deep/`.
15. *Declaration of Ferrara*, `http://www.fe.infn.it/qcd-n02/`.
16. HERMES Collaboration (A. Airapetian *et al.*), Phys. Rev. Lett. **87**, 182001 (2001).
17. CLAS Collaboration (S. Stepanyan *et al.*), Phys. Rev. Lett. **87**, 182002 (2001).
18. H1 Collaboration (C. Adloff *et al.*), Phys. Lett. B **517**, 47 (2001).
19. M. Diehl *et al.*, Phys. Lett. B **411**, 193 (1997).
20. G. van der Steenhoven, this issue, p. 377.
21. V. Burkert, L. Elouadrhiri, M. Garçon, S. Stepanyan *et al.*, CEBAF experiment 01-113.
22. P. Bertin, C. Hyde-Wright, R. Ransome, F. Sabatié *et al.*, CEBAF experiment 00-110.

23. J.C. Collins, L. Frankfurt, M. Strikman, Phys. Rev. D **56**, 2982 (1997).
24. HERMES Collaboration (A. Airapetian *et al.*), Eur. Phys. J. C **17**, 389 (2000).
25. C. Hadjidakis, private communication.
26. M. Guidal, M. Garçon, E. Smith *et al.*, CEBAF experiment 99-105.

Eur. Phys. J. A **18**, 395–399 (2003)
DOI 10.1140/epja/i2002-10243-1

THE EUROPEAN PHYSICAL JOURNAL A

Flavor structure of the nucleon sea

J.-C. Peng[a]

University of Illinois at Urbana-Champaign, Urbana 61801 IL, USA

Received: 30 September 2002 /
Published online: 22 October 2003 – © Società Italiana di Fisica / Springer-Verlag 2003

Abstract. The recent progress on our understanding of the flavor structure of unpolarized and polarized nucleon sea is reviewed. The large flavor asymmetry between the up and down sea quark distributions is now well established. This asymmetry strongly suggests the importance of the mesonic degrees of freedom in the description of the nucleon sea. The strong connection between the flavor structure and the spin structure of the nucleon sea is emphasized. Possible future measurements for testing various theoretical models are also discussed.

PACS. 14.20.Dh Properties of specific particles: Protons and neutrons – 24.85.+p Quarks, gluons, and QCD in nuclei and nuclear processes

1 Introduction

One of the most active areas of research in nuclear and particle physics during the last several decades is the study of quark and gluon distributions in the nucleons and nuclei. Several major surprises were discovered in Deep-Inelastic Scattering (DIS) experiments which profoundly changed our views of the partonic substructure of hadrons. In the early 1980s, the famous "EMC" effect found in muon DIS provided the first unambiguous evidence that the quark distributions in nuclei are significantly different from those in free nucleons. More recently, surprising results on the spin and flavor structures of the nucleons were discovered in DIS experiments. The so-called "spin crisis", revealed by the polarized DIS experiments, has led to extensive efforts to understand the partonic content of proton's spin. Subsequently, the observation [1] of the violation of the Gottfried Sum Rule [2] in DIS revealed a surprisingly large asymmetry between the up and down antiquark distributions in the nucleon, shedding new light on the origins of the nucleon sea.

In this article, we review the status of our current knowledge on the flavor dependence of the sea quark distributions in hadrons. In sect. 2, we summarize the experimental evidence for the flavor asymmetry of the nucleon sea. Implications of various theoretical models for explaining the $\bar{d}/\bar{u}$ asymmetry are also discussed. Section 3 is devoted to the subject of the flavor structure of polarized nucleon sea. Finally, we present future prospects and conclusion in sect. 4.

[a] e-mail: jcpeng@uiuc.edu

2 Flavor structure of unpolarized nucleon sea

The earliest parton models assumed that the proton sea was flavor symmetric, even though the valence quark distributions are clearly flavor asymmetric. Inherent in this assumption is that the content of the sea is independent of the valence quark's composition. The flavor symmetry assumption was not based on any known physics, and it remained to be tested by experiments. Neutrino-induced charm production experiments [3,4], which are sensitive to the $s \to c$ process, showed that the strange-quark content of the nucleon is only about half of the up or down sea quarks. Such flavor asymmetry is attributed to the much heavier strange-quark mass compared to the up and down quarks. The similar masses for the up and down quarks suggest that the nucleon sea should be nearly up-down symmetric.

The issue of the equality of $\bar{u}$ and $\bar{d}$ was first encountered in measurements of the Gottfried integral [2], defined as

$$I_{\mathrm{G}} = \int_0^1 \left[F_2^p(x,Q^2) - F_2^n(x,Q^2)\right]/x \,\mathrm{d}x, \qquad (1)$$

where F_2^p and F_2^n are the proton and neutron structure functions measured in DIS experiments. Under the assumption of a $\bar{u}$, $\bar{d}$ flavor-symmetric sea in the nucleon, the Gottfried Sum Rule (GSR) [2], $I_{\mathrm{G}} = 1/3$, is obtained. The most accurate test of the GSR was reported by the New Muon Collaboration (NMC) [1], which measured F_2^p and F_2^n over the region $0.004 \le x \le 0.8$. They determined the Gottfried integral to be 0.235 ± 0.026, significantly below 1/3. This surprising result has generated much interest. Although the violation of the GSR can be explained by assuming unusual behavior of the parton distributions at

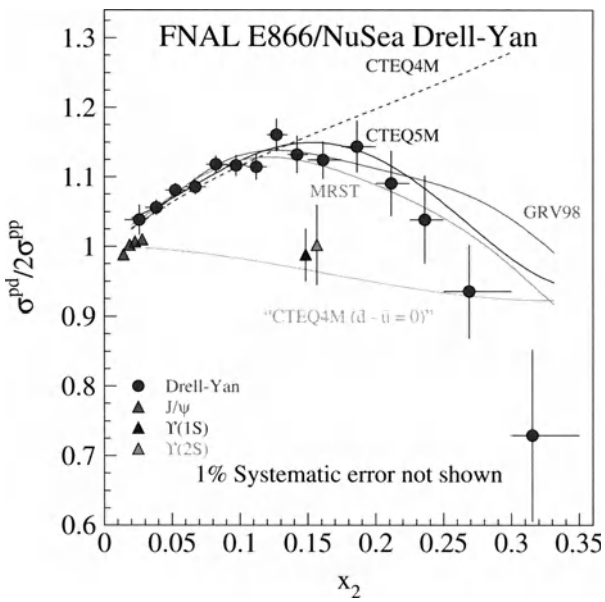

Fig. 1. Cross-section ratios of $p+d$ over $2(p+p)$ for Drell-Yan, J/Ψ, and Υ production from FNAL E866. The curves are the calculated next-to-leading-order cross-section ratios for the Drell-Yan using various parton distribution functions.

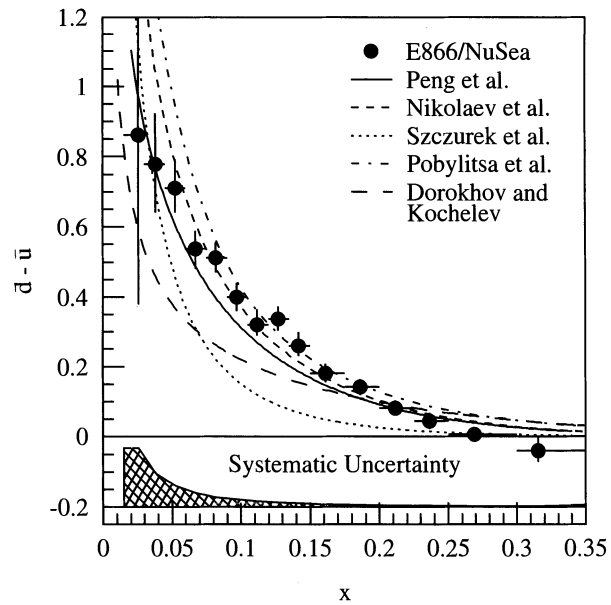

Fig. 2. Comparison of the measured $\bar{d}(x)-\bar{u}(x)$ at $Q^2 = 54\,\mathrm{GeV}^2/c^2$ to predictions of several models of the nucleon sea. The solid and short-dashed curves show pion cloud calculations [8,14]. The dotted curve is a chiral-quark model calculation [15], while the dot-dashed curve shows the chiral-quark soliton calculation [16]. The long-dashed curve shows the instanton model prediction [17].

very small x, a more natural explanation is to abandon the assumption $\bar{u}=\bar{d}$.

The proton-induced Drell-Yan (DY) process provides an independent means to probe the flavor asymmetry of the nucleon sea [5]. An important advantage of the DY process is that the x-dependence of $\bar{d}/\bar{u}$ can be determined. The NA51 Collaboration at CERN carried out the first dedicated dimuon production experiment to study the flavor structure of the nucleon sea [6]. Using a 450 GeV proton beam, NA51 obtained $\bar{u}/\bar{d} = 0.51 \pm 0.04(\mathrm{stat}) \pm 0.05(\mathrm{syst})$ at $x = 0.18$ and $\langle M_{\mu\mu}\rangle = 5.22\,\mathrm{GeV}$. This important result established the asymmetry of the quark sea at a single value of x. What remained to be done was to map out the x-dependence of this asymmetry.

At Fermilab, a DY experiment (E866/NuSea) aimed at a higher statistical accuracy with a much wider kinematic coverage than the NA51 experiment, has been completed [7–9]. The DY cross-section ratio per nucleon for $p+d$ to that for $p+p$ is shown in fig. 1. At positive x_{F} this ratio is given as

$$\sigma_{\mathrm{DY}}(p+d)/2\sigma_{\mathrm{DY}}(p+p) \simeq \left(1+\bar{d}(x_2)/\bar{u}(x_2)\right)/2. \quad (2)$$

Figure 1 shows that the DY cross-section per nucleon for $p+d$ clearly exceeds $p+p$, and it indicates an excess of $\bar{d}$ with respect to $\bar{u}$ over an appreciable range in x_2. In contrast, the $\sigma(p+d)/2\sigma(p+p)$ ratios for J/Ψ and Υ production, also shown in fig. 1, are very close to unity. This reflects the dominance of gluon-gluon fusion process for quarkonium production and the expectation that the gluon distributions in the proton and in the neutron are identical.

The Drell-Yan cross-section ratios from E866 were analysed to obtain $\bar{d}-\bar{u}$ over the region $0.02 < x < 0.345$ as shown in fig. 2. The HERMES Collaboration has reported a semi-inclusive DIS measurement of charged pions from hydrogen and deuterium targets [10]. Based on the differences between charged-pion yields from the two targets, $\bar{d}-\bar{u}$ is determined in the kinematic range, $0.02 < x < 0.3$ and $1\,\mathrm{GeV}^2/c^2 < Q^2 < 10\,\mathrm{GeV}^2/c^2$. The HERMES results are consistent with the E866 results obtained at significantly higher Q^2. In table 1 we list the values of the integral $\int_0^1[\bar{d}(x)-\bar{u}(x)]\mathrm{d}x$ determined from the NMC, HERMES, and FNAL E866 experiments. The agreement among these results, obtained using different techniques including DIS, semi-inclusive DIS, and Drell-Yan, is quite good.

Table 1. Values of the integral $\int_0^1[\bar{d}(x)-\bar{u}(x)]\mathrm{d}x$ determined from the DIS, semi-inclusive DIS, and Drell-Yan experiments.

Experiment	$\langle Q^2\rangle$ (GeV^2/c^2)	$\int_0^1[\bar{d}(x)-\bar{u}(x)]\mathrm{d}x$
NMC/DIS	4.0	0.147 ± 0.039
HERMES/SIDIS	2.3	0.16 ± 0.03
FNAL E866/DY	54.0	0.118 ± 0.012

Many theoretical models, including meson cloud model, chiral-quark model, Pauli-blocking model, instanton model, chiral-quark soliton model, and statistical model, have been proposed to explain the $\bar{d}/\bar{u}$ asymmetry. For details of these various models, we refer to several recent review articles [11–13]. As shown in fig. 2, these models can describe the $\bar{d}-\bar{u}$ data very well. However, they all have difficulties explaining the $\bar{d}/\bar{u}$ data at large x ($x > 0.2$) [18]. Thus, it would be very important to

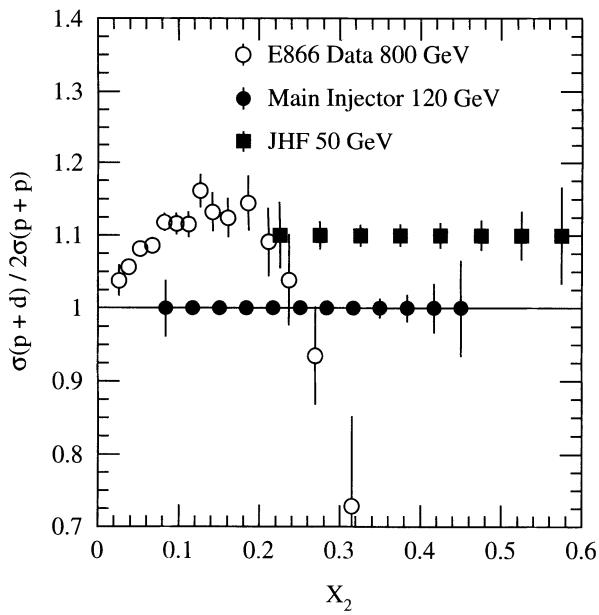

Fig. 3. Projected statistical accuracy for $\sigma(p+d)/2\sigma(p+p)$ in a 100-day run at JHF [20]. The E866 data and the projected sensitivity for a proposed measurement [21] at the 120 GeV Fermilab Main Injector are also shown.

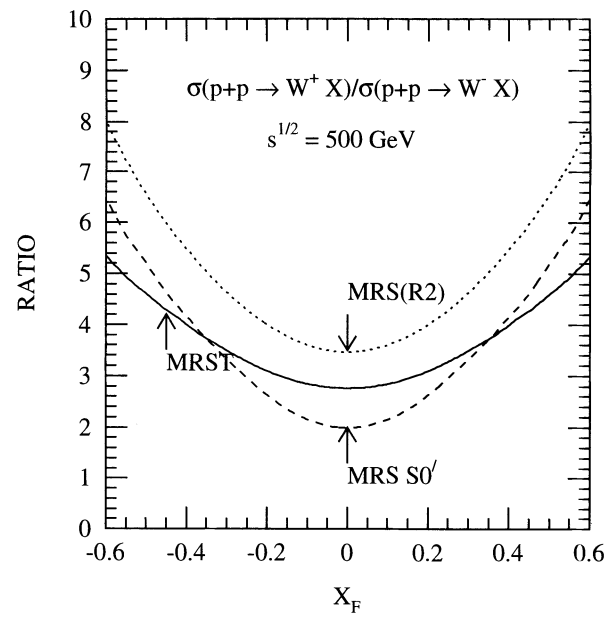

Fig. 4. Predictions of $\sigma(p+p \to W^+x)/\sigma(p+p \to W^-x)$ as a function of x_F at $\sqrt{s} = 500$ GeV. The dashed curve corresponds to the $\bar{d}/\bar{u}$ symmetric MRS S0′ structure functions, while the solid and dotted curves are for the $\bar{d}/\bar{u}$ asymmetric structure function MRST and MRS(R2), respectively.

extend the DY measurements to larger-x_2 regimes. The new 120 GeV Fermilab Main Injector (FMI) and the proposed 50 GeV Japanese Hadron Facility [19] (JHF) present opportunities for extending the $\bar{d}/\bar{u}$ measurement to larger x ($0.25 < x < 0.7$). Figure 3 shows the expected statistical accuracy for $\sigma(p+d)/2\sigma(p+p)$ at JHF [20] compared with the data from E866 and a proposed measurement [21] using the 120 GeV proton beam at the FMI. A definitive measurement of the $\bar{d}/\bar{u}$ over the region $0.25 < x < 0.7$ could indeed be obtained at FMI and JHF.

To disentangle the $\bar{d}/\bar{u}$ asymmetry from the possible charge-symmetry violation effect [22,23], one could consider W-boson production in $p+p$ collision at RHIC. An interesting quantity to be measured is the ratio of the $p+p \to W^+ + x$ and $p+p \to W^- + x$ cross-sections [24]. It can be shown that this ratio is very sensitive to $\bar{d}/\bar{u}$. An important feature of the W production asymmetry in $p+p$ collision is that it is completely free from the assumption of charge symmetry. Figure 4 shows the predictions for $p+p$ collision at $\sqrt{s} = 500$ GeV. The dashed curve corresponds to the $\bar{d}/\bar{u}$ symmetric MRS S0′ structure functions, while the solid and dotted curves are for the $\bar{d}/\bar{u}$ asymmetric structure function MRST and MRS(R2), respectively. Figure 4 clearly shows that W asymmetry measurements at RHIC could provide an independent determination of $\bar{d}/\bar{u}$.

Models in which virtual mesons are admitted as degrees of freedom have implications that extend beyond the $\bar{d}, \bar{u}$ flavor asymmetry addressed above. They create hidden strangeness in the nucleon via such virtual processes as $p \to \Lambda + K^+, \Sigma + K$, etc. Such processes are of considerable interest as they imply different s and $\bar{s}$ parton distributions in the nucleon, a feature not found in gluonic production of $s\bar{s}$ pairs. This subject has received a fair amount of attention in the literature [25–27] but experiments have yet to clearly identify such a difference. Thus, in contrast to the $\bar{d}, \bar{u}$ flavor asymmetry, to date there is no positive experimental evidence for $s\bar{s}$ contributions to the nucleon from virtual meson-baryon states [28–30].

A difference between the s and $\bar{s}$ distribution can be made manifest by direct measurement of the s and $\bar{s}$ parton distribution functions in DIS neutrino scattering, or in the measurement of the q^2-dependence of the strange-quark contribution ($F^p_{1s}(q^2)$) to the proton charge form factor. Measurement of these form factors allows extraction of the strangeness contribution to the nucleon's charge and magnetic moment and axial form factors. The portion of the charge form factor $F^p_{1s}(q^2)$ due to strangeness clearly is zero at $q^2 = 0$, but if the s and $\bar{s}$ distributions are different the form factor becomes nonzero at finite q^2. These "strange" form factors can be measured in neutrino elastic scattering [31] from the nucleon, or by selecting the parity-violating component of electron-nucleon elastic scattering, as is now being done at the Bates [32] and Jefferson Laboratories [33].

3 Flavor structure of polarized nucleon sea

The flavor structure and the spin structure of the nucleon sea are closely connected. Many theoretical models originally proposed to explain the $\bar{d}/\bar{u}$ flavor asymmetry also have specific implications for the spin structure of the nucleon sea. In the meson cloud model, for example, a quark would undergo a spin flip upon an emission of a pseudoscalar meson ($u^\uparrow \to \pi^\circ(u\bar{u}, d\bar{d}) + u^\downarrow$, $u^\uparrow \to \pi^+(u\bar{d}) + d^\downarrow$,

$u^\uparrow \to K^+ + s^\downarrow$, etc.). The antiquarks $(\bar{u}, \bar{d}, \bar{s})$ are unpolarized ($\Delta\bar{u} = \Delta\bar{d} = \Delta\bar{s} = 0$) since they reside in spin-0 mesons. The strange quarks (s), on the other hand, would have a negative polarization since the up valence quarks in the proton are positively polarized and the $u^\uparrow \to K^+ + s^\downarrow$ process would lead to an excess of $s^\downarrow$. By considering a vector meson (ρ) cloud, non-zero $\bar{u}, \bar{d}$ sea quark polarizations with $\Delta\bar{d} - \Delta\bar{u} > 0$ were predicted [34–37].

The Pauli-blocking model [38] predicts that an excess of $q^\uparrow(q^\downarrow)$ valence quarks would inhibit the creation of a pair of $q^\uparrow\bar{q}^\downarrow$ ($q^\downarrow\bar{q}^\uparrow$) sea quarks. Since the polarization of the $u(d)$ valence quarks is positive (negative), this model predicts a positive (negative) polarization for the $\bar{u}(\bar{d})$ sea ($\Delta\bar{u} > 0 > \Delta\bar{d}$).

In the instanton model [17], the quark sea can result from a scattering of a valence quark off a non-perturbative vacuum fluctuation of the gluon field, instanton. The interaction induced by an instanton is given by the 't Hooft effective Lagrangian which allows processes such as $u^\uparrow \to u^\downarrow d^\uparrow \bar{d}^\downarrow$, $d^\downarrow \to d^\uparrow u^\downarrow \bar{u}^\uparrow$, etc. Since the flavor of the quark-antiquark produced in this process is different from the flavor of the initial valence quark, this model readily explains $\bar{d} > \bar{u}$. Furthermore, the correlation between the sea quark helicity and the valence quark helicity in the 't Hooft effective Lagrangian (*i.e.* $u^\uparrow$ leads to a $\bar{d}^\downarrow$) naturally predicts a positively (negatively) polarized $\bar{u}(\bar{d})$ sea. In particular, this model predicts [39] a large $\Delta\bar{u}, \Delta\bar{d}$ flavor asymmetry with $\Delta\bar{u} > \Delta\bar{d}$, namely, $\int_0^1 [\Delta\bar{u}(x) - \Delta\bar{d}(x)]\mathrm{d}x = \frac{5}{3}\int_0^1 [\bar{d}(x) - \bar{u}(x)]\mathrm{d}x$.

In the chiral-quark soliton model [40,41], the large N_c limit of QCD becomes an effective theory of mesons with the baryons appearing as solitons. Quarks are described by single-particle wave functions which are solutions of the Dirac equation in the field of the background pions. In this model, the polarized isovector distributions $\Delta\bar{u}(x) - \Delta\bar{d}(x)$ appear in leading-order (N_c^2) in a $1/N_c$ expansion, while the unpolarized isovector distributions $\bar{u}(x) - \bar{d}(x)$ appear in next-to-leading order (N_c). Therefore, this model predicts a large flavor asymmetry for the polarized sea $[\Delta\bar{u}(x) - \Delta\bar{d}(x)] > [\bar{d}(x) - \bar{u}(x)]$.

In the statistical approach, the nucleon is treated as a collection of massless quarks, antiquarks, and gluons in thermal equilibrium within a finite-size volume. The momentum distributions for quarks and antiquarks follow a Fermi-Dirac distributions function characterized by a common temperature and a chemical potential μ which depends on the flavor and helicity of the quarks. It can be shown that

$$\mu_{\bar{q}\uparrow} = -\mu_{q\downarrow}; \qquad \mu_{\bar{q}\downarrow} = -\mu_{q\uparrow}. \tag{3}$$

Equation (3), together with the constraints of the valence quark sum rules and inputs from polarized DIS experiments, can readily lead to the prediction that $\bar{d} > \bar{u}$ and $\Delta\bar{u} > 0 > \Delta\bar{d}$.

Predictions of various model calculations for I_Δ, the first moment of $\Delta\bar{u}(x) - \Delta\bar{d}(x)$, are listed in table 2. While the meson cloud model gives small negative values for I_Δ, all other models predict a positive I_Δ with a magnitude comparable or greater than the corresponding integral for unpolarized sea (recall that $\int_0^1 [\bar{d}(x) - \bar{u}(x)]\mathrm{d}x \simeq 0.12$). Several meson cloud calculations for the direct contribution of ρ-meson cloud are in good agreement. However, the large $\pi - \rho$ interference effect reported in [35] was not confirmed in a more recent study [36]. It is worth noting that a recent work [44] on $\pi - \sigma$ interference predicts a large effect on $\Delta\bar{d} - \Delta\bar{u}$, and with a sign opposite to other meson cloud model calculations.

Table 2. Prediction of various theoretical models on the integral $I_\Delta = \int_0^1 [\Delta\bar{u}(x) - \Delta\bar{d}(x)]\mathrm{d}x$.

Model	I_Δ prediction	Reference
Meson cloud (π-meson)	0	[42,43]
Meson cloud (ρ-meson)	$\simeq -0.0007$ to -0.027	[34]
Meson cloud ($\pi - \rho$ interf.)	$= -6\int_0^1 g^p(x)\mathrm{d}x$ $\simeq -0.7$	[35]
Meson cloud (ρ and $\pi - \rho$ interf.)	$\simeq -0.004$ to -0.033	[36]
Meson cloud (ρ-meson)	< 0	[37]
Meson cloud ($\pi - \sigma$ interf.)	$\simeq 0.12$	[44]
Pauli-blocking (bag-model)	$\simeq 0.09$	[36]
Pauli-blocking (ansatz)	$\simeq 0.3$	[45]
Pauli-blocking	$= \frac{5}{3}\int_0^1 [\bar{d}(x) - \bar{u}(x)]\mathrm{d}x$ $\simeq 0.2$	[46]
Chiral-quark soliton	0.31	[47]
Chiral-quark soliton	$\simeq \int_0^1 2x^{0.12}[\bar{d}(x) - \bar{u}(x)]\mathrm{d}x$	[48]
Instanton	$= \frac{5}{3}\int_0^1 [\bar{d}(x) - \bar{u}(x)]\mathrm{d}x$ $\simeq 0.2$	[39]
Statistical	$\simeq \int_0^1 [\bar{d}(x) - \bar{u}(x)]\mathrm{d}x$ $\simeq 0.12$	[49]
Statistical	$> \int_0^1 [\bar{d}(x) - \bar{u}(x)]\mathrm{d}x$ > 0.12	[50]

If the flavor asymmetry of the polarized sea is indeed as large as the predictions of many models shown in table 2, it would imply that a significant fraction of the Bjorken sum, $\int_0^1 [g_1^p(x) - g_1^n(x)]\mathrm{d}x$, comes from the flavor asymmetry of polarized nucleon sea.

Measurements of $\Delta\bar{u}(x)$ and $\Delta\bar{d}(x)$ are clearly of great current interest. The HERMES Collaboration has reported their preliminary results on the extraction of $\Delta\bar{u}(x)$ and $\Delta\bar{d}(x)$ using polarized semi-inclusive DIS data [51]. A global analysis of inclusive spin asymmetries for π^+, π^-, K^+, and K^- has been carried out for longitudinally polarized hydrogen and deuterium targets. As a result, $\Delta u(x)$, $\Delta d(x)$, $\Delta\bar{u}(x)$, $\Delta\bar{d}(x)$, $\Delta s(x)(= \Delta\bar{s}(x))$ polarized quark densities were extracted for $0.03 < x$ at $Q^2 = 2.5\,\mathrm{GeV}^2$. These very interesting preliminary results showed that Δs has a trend of being positive, in disagreement with

the predictions of theoretical models which attributed the violation of Ellis-Jaffe sum rule to a large negative polarization of the strange sea. Furthermore, the preliminary HERMES result does not support the prediction of a large positive $\Delta\bar{u} - \Delta\bar{d}$. Although the statistics are still limited, the HERMES preliminary result shows that $\Delta\bar{u}, \Delta\bar{d}, \Delta\bar{u} - \Delta\bar{d}$ are all consistent with being zero.

Another promising technique for measuring sea quark polarization is W-boson production [52] at RHIC. The longitudinal single-spin asymmetry for W production in polarized $p+p \to W^{\pm}+x$ can be written in leading order as

$$A_{\mathrm{L}}^{W^+} \approx -\frac{\Delta\bar{d}(x)}{\bar{d}(x)}, \qquad A_{\mathrm{L}}^{W^-} \approx -\frac{\Delta\bar{u}(x)}{\bar{u}(x)} \tag{4}$$

at suitable kinematic regions. Therefore, A_{L} gives a direct measure of sea quark polarization. The RHIC W production and the HERMES SIDIS measurements are clearly complementary tools for determining polarized sea quark distributions.

4 Conclusion

The flavor asymmetry of the nucleon sea has been clearly established by recent DIS and Drell-Yan experiments. The x-dependence of $\bar{d}/\bar{u}$ indicates that a $\bar{d}, \bar{u}$ symmetric sea dominates at small ($x < 0.05$) and large x ($x > 0.3$). But for $0.1 < x < 0.2$ a large and significant flavor non-symmetric contribution determines the sea distributions. The surprisingly large asymmetry between $\bar{u}$ and $\bar{d}$ is unexplained by perturbative QCD, and it strongly suggests the presence of virtual isovector mesons, mostly pions, in the nucleon sea. Additional clues on the origins of the flavor asymmetry will come from future studies including:

- Measurements of $\bar{d}/\bar{u}$ for $x > 0.25$.
- Measurements of $\Delta\bar{u}$ and $\Delta\bar{d}$ using semi-inclusive DIS, and W production in polarized p-p collision.
- Direct measurement of the meson cloud in DIS experiments tagging on forward-going nucleons. Interesting first measurements were performed recently at HERA [53].
- More precise measurements on the s *versus* $\bar{s}$ distributions in the nucleon.

References

1. P. Amaudruz *et al.*, Phys. Rev. Lett. **66**, 2712 (1991); M. Arneodo *et al.*, Phys. Rev. D **55**, R1 (1994).
2. K. Gottfried, Phys. Rev. Lett. **18**, 1174 (1967).
3. H. Abromowicz *et al.*, Z. Phys. C **15**, 19 (1982).
4. J.M. Conrad, M.H. Shaevitz, T. Bolton, Rev. Mod. Phys. **70**, 1341 (1998).
5. S.D. Ellis, W.J. Stirling, Phys. Lett. B **256**, 258 (1991).
6. A. Baldit *et al.*, Phys. Lett. B **332**, 244 (1994).
7. E.H. Hawker *et al.*, Phys. Rev. Lett. **80**, 3715 (1998).
8. J.C. Peng *et al.*, Phys. Rev. D **58**, 092004 (1998).
9. R.S. Towell *et al.*, Phys. Rev. D **64**, 052002 (2001).
10. K. Ackerstaff *et al.*, Phys. Rev. Lett. **81**, 5519 (1998).
11. S. Kumano, Phys. Rep. **303**, 183 (1998).
12. J. Speth, A.W. Thomas, Adv. Nucl. Phys. **24**, 83 (1998).
13. G.T. Garvey, J.C. Peng, Prog. Part. Nucl. Phys. **47**, 203 (2001).
14. N.N. Nikolaev, W. Schäfer, A. Szczurek, J. Speth, Phys. Rev. D **60**, 014004 (1999).
15. A. Szczurek, A. Buchmans, A. Faessler, J. Phys. G **22**, 1741 (1996).
16. P.V. Pobylitsa *et al.*, Phys. Rev. D **59**, 034024 (1999).
17. A.E. Dorokhov, N.I. Kochelev, Phys. Lett. B **259**, 335 (1991); **304**, 167 (1993).
18. W. Melnitchouk, J. Speth, A.W. Thomas, Phys. Rev. D **59**, 014033 (1999).
19. JHF Project Office. Proposal for Japan Hadron Facility, KEK Rep. 97-3 (1997).
20. J.C. Peng, S. Sawada *et al.*, hep-ph/0007341.
21. E906 Collaboration (D.F. Geesaman *et al.*), Fermi National Accelerator Laboratory Proposal E906, 1999.
22. B.Q. Ma, Phys. Lett. B **274**, 111 (1992).
23. C. Boros, J.T. Londergan, A.W. Thomas, Phys. Rev. Lett. **81**, 4075 (1998).
24. J.C. Peng, D.M. Jansen, Phys. Lett. B **354**, 460 (1995).
25. A.I. Signal, A.W. Thomas, Phys. Lett. B **191**, 205 (1987).
26. X.D. Ji, J. Tang, Phys. Lett. B **362**, 182 (1995).
27. S. Brodsky, B.-Q. Ma, Phys. Lett. B **381**, 317 (1996).
28. A.O. Bazarko *et al.*, Z. Phys. C **65**, 189 (1995).
29. V. Barone, C. Pascaud, F. Zomer, Eur. Phys. J. C **12**, 243 (2000).
30. M. Goncharov *et al.*, Phys. Rev. D **64**, 112006 (2001).
31. G. Garvey, W. Louis, H. White, Phys. Rev. C **48**, 761 (1993).
32. B. Mueller *et al.*, Phys. Rev. Lett. **78**, 3824 (1997).
33. K. Aniol *et al.*, Phys. Rev. Lett. **82**, 1096 (1999).
34. R.J. Fries, A. Schäfer, Phys. Lett. B **443**, 40 (1998).
35. K.G. Boreskov, A.B. Kaidalov, Eur. Phys. J. C **10**, 143 (1999).
36. F.G. Cao, A.I. Signal, Eur. Phys. J. C **21**, 105 (2001).
37. S. Kumano, M. Miyama, Phys. Rev. D **65**, 034012 (2002).
38. F.M. Steffens, A.W. Thomas, Phys. Rev. C **55**, 900 (1997).
39. A. Dorokhov, hep-ph/0112332.
40. D.I. Diakonov *et al.*, Nucl. Phys. B **480**, 341 (1996).
41. M. Wakamatsu, T. Kubota, Phys. Rev. D **57**, 5755 (1998).
42. E. Eichten, I. Hinchliffe, C. Quigg, Phys. Rev. D **45**, 2269 (1992).
43. A.W. Thomas, Phys. Lett. B **126**, 97 (1983).
44. R.J. Fries, A. Schäfer, C. Weiss, hep-ph/0204060.
45. M. Glück *et al.*, Phys. Rev. D **63**, 094005 (2001).
46. F.M. Steffens, Phys. Lett. B **541**, 346 (2002).
47. B. Dressler *et al.*, hep-ph/9809487.
48. M. Wakamatsu, T. Watabe, Phys. Rev. D **62**, 017506 (2000).
49. C. Bourrely, J. Soffer, F. Buccella, Eur. Phys. J. C **23**, 487 (2002).
50. R.S. Bhalerao, Phys. Rev. C **63**, 025208 (2001).
51. H.E. Jackson, Int. J. Mod. Phys. A **17**, 3551 (2002).
52. G. Bunce, N. Saito, J. Soffer, W. Vogelsang, Annu. Rev. Nucl. Part. Sci. **50**, 525 (2000).
53. C. Adloff *et al.*, Eur. Phys. J. C **6**, 587 (1999).

Eur. Phys. J. A **18**, 401–404 (2003)
DOI 10.1140/epja/i2002-10244-0

THE EUROPEAN PHYSICAL JOURNAL A

Helicity dependence of the γN interaction and the GDH sum rule

P. Pedroni[a]

For the GDH and A2 Collaborations
INFN-Sezione di Pavia, via Bassi 6, Pavia, Italy

Received: 30 September 2002 /
Published online: 22 October 2003 – © Società Italiana di Fisica / Springer-Verlag 2003

Abstract. First measurements of pion photoproduction using circularly polarized photons on longitudinally polarized protons were carried out at MAMI (Mainz) in the energy range $E_\gamma = 200$–800 MeV. Results of the helicity dependence of the total inclusive photoabsorption cross-section and of the pion photoproduction channels will be presented. These data provide new input for multipole analyses and determine the main contribution to the Gerasimov-Drell-Hearn integral and the forward spin polarizability γ_0.

PACS. 13.60.Le Meson production – 14.20.Gk Baryon resonances with $S = 0$

1 Introduction

The helicity-dependent total cross-sections for the absorption of real photons on nucleons, $\sigma_{3/2}$ and $\sigma_{1/2}$, corresponding to the two parallel or antiparallel relative spin configurations, respectively, are related to the anomalous magnetic moment κ of the nucleon via the Gerasimov-Drell-Hearn (GDH) sum rule [1]:

$$\int_0^\infty \left(\sigma_{3/2} - \sigma_{1/2}\right)\frac{\mathrm{d}\nu}{\nu} = \frac{2\pi\alpha}{m^2}\kappa^2. \qquad (1)$$

In a similar way, the forward spin polarizability γ_0, a structure constant of the nucleon still unmeasured, can be obtained as

$$\gamma_0 = -\frac{1}{4\pi^2}\int_0^\infty \left(\sigma_{3/2} - \sigma_{1/2}\right)\frac{\mathrm{d}\nu}{\nu^3}. \qquad (2)$$

Both equations connect the ground-state properties of the nucleon (m, e, κ, γ_0) with the dynamics of the excitation spectrum.

The GDH sum rule is based on very general physics principles (low-energy theorems, optical theorem, unsubtracted dispersion relation) applied to the Compton forward amplitude and gives important constraints for the models of the nucleon. Due to its fundamental character this prediction, formulated in the 1960s, deserves a verification which has been awaiting technical developments that only recently have taken place.

Apart from the GDH sum rule, another important motivation to study the helicity structure of single- and double-pion photoproduction lies in the fact that it provides completely new and up to now inaccessible information on partial-wave amplitudes. The inclusion of this new observable into multipole analyses will allow to access small resonance amplitudes and help to separate them from the dominating ones and from the non-resonant background.

The aim of the GDH Collaboration[1] is to provide an extensive data set of helicity-dependent cross-sections for all the partial and total reactions channels both on the proton and on the neutron with a combined use of the MAMI (Mainz) ($m_\pi \leq E_\gamma \leq 800$ MeV) and ELSA (Bonn) ($E_\gamma \leq 3$ GeV) accelerators. In the following, the first results from the Mainz experimental part will be presented.

2 Experimental set-up

The experiment was carried out at the tagged-photon facility of the MAMI accelerator in Mainz.

Circularly polarized electrons were produced by bremsstrahlung of longitudinally polarized electrons. The electron source, based on the photoeffect on strained GaAs crystals, delivered routinely electrons with a degree of polarization of $\sim$ 75% [2]. The degree of polarization was continuously measured throughout the experiment by Möller scattering in a magnetized iron foil.

[a] e-mail: pedroni@pv.infn.it

[1] This collaboration is formed by researchers from the Universities of Mainz, Bonn, Bochum, Erlangen, Göttingen, Lund, Nagoya, Pavia, Tübingen and from INFN-Sezione di Pavia, RUG Gent, CEA Saclay, INR Moscow.

Polarized nucleons were available in the frozen-spin target [3] that consisted of a horizontal dilution refrigerator and a superconducting polarization magnet, which was used in the polarization phase together with a microwave system for dynamical nuclear polarization (DNP). The polarization was maintained during the measurement in the "frozen-spin" mode at temperatures of about 50 mK by an internal superconducting coil ($B \simeq 0.4$ T) which is integrated into the dilution refrigerator.

The target material was butanol (C_4H_9OH). At 2.5 T maximum polarization values close to 90% were obtained for the protons with a typical relaxation time of about 200 hours.

The photon-induced reaction products were registered by means of the detector DAPHNE [4], made by CEA Saclay and INFN-Sezione di Pavia, which is complemented by forward detectors to increase the solid-angle acceptance. DAPHNE is essentially a charged-particle tracking detector having a cylindrical symmetry. It consists of 3 coaxial layers of multi-wire proportional chambers, surrounded by a segmented ΔE-E-ΔE plastic scintillator telescope and by a double scintillator-absorber sandwich which allows the detection of neutral pions with a useful efficiency.

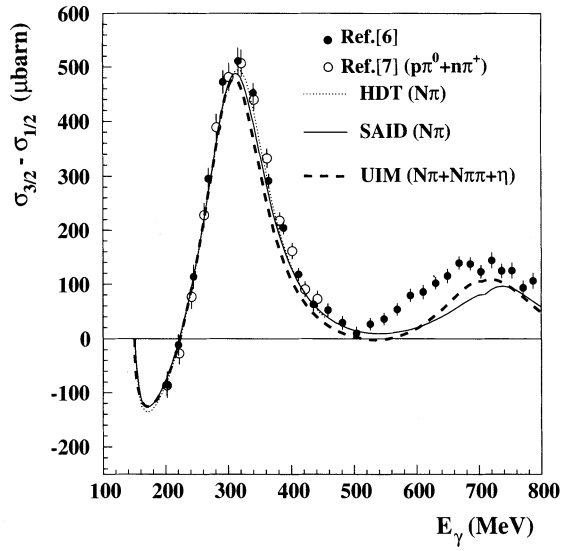

Fig. 1. The helicity-dependent total cross-section $\sigma_{3/2} - \sigma_{1/2}$ on ^{1}H [6] (filled points) is compared to the sum of the $N\pi$ channels [7] (empty points) and to the predictions of the HDT [8], SAID [9] and UIM [10] analyses. Only statistical errors are shown.

3 Results and comments

3.1 Inclusive total cross-section

An inclusive method of data analysis has been developed to determine the total absorption cross-section. Its characteristics are fully described in [5,6].

The helicity-dependent total photoabsorption cross-section $\Delta\sigma = (\sigma_{3/2} - \sigma_{1/2})$ on the proton [6] (full circles) is shown in fig. 1. Only statistical errors are shown. The estimated total systematic error is about 6% on the measured $\Delta\sigma$ [6].

These data are compared with the sum of our previously published helicity dependence for the $n\pi^+$ and $p\pi^0$ channels in the Δ region [7]. The good agreement found between the different analyses gives us confidence in their reliability.

In the same figure the predictions of the HDT [8], SAID [9], and UIM [10] analyses are also shown. In the Δ-resonance region, there is a good agreement between experiment and theories. In the second resonance region, a significant contribution from double-pion photoproduction is clearly visible. This feature is not completely reproduced by the UIM model. The measured value of the GDH integral between 200 and 800 MeV amounts to 226 ± 5 (stat) $\pm$ 12 (sys) μb. Due to the ν^{-3} weighting, the γ_0 integral is almost saturated by $E_\gamma = 800$ MeV. The value of the γ_0 integral between 200 and 800 MeV amounts to $(-187 \pm 8$ (stat) ± 10 (sys)$) \cdot 10^{-6}\,\mathrm{fm}^4$.

Although the measured photon energy interval is too narrow to draw any definitive conclusion, a reasonable estimate of the GDH sum rule value can be deduced if we use the existing models for the evaluation of the missing contributions. The UIM model [10] gives a contribution of $-30\,\mu$b for $E_\gamma < 200$ MeV and $+40\,\mu$b for $800 < E_\gamma < 1650$ MeV. For $E_\gamma > 1650$ MeV, ref. [11] gives a contribution of $-26\,\mu$b. The combination of our experimental result with these predictions yields an estimate ($210\,\mu$b) which within the experimental errors is consistent with the GDH sum rule value (1). It should be kept in mind that, especially above $E_\gamma = 800$ MeV, none of the models has yet been validated experimentally and only a measurement in this energy region can lead to a definitive conclusion about the high-energy contribution to the GDH integral. Our collaboration is performing such a measurement at ELSA (Bonn) up to $E_\gamma \simeq 3$ GeV.

In case of the γ_0 integral (2) the contribution from $E_\gamma < 200$ MeV is important, the UIM prediction being $+104 \cdot 10^{-6}\,\mathrm{fm}^4$. The missing high-energy contribution, according to UIM and ref. [11], is $-3 \cdot 10^{-6}\,\mathrm{fm}^4$ only. The combination with our experimental result gives an estimate of $-86 \cdot 10^{-6}\,\mathrm{fm}^4$ for γ_0. This value is within the range of values predicted by dispersion theories [12,13].

3.2 Exclusive measurements

The identification and the energy determination of the charged particles is performed, with high efficiency ($\geq 80\%$) by the maximum likelihood method described in [14], while neutrons and π^0's can only be identified (without any energy determination) with an efficiency of 10–30%. These combined features allow the separation of all the single and double photoproduction channels up to 800 MeV.

As an example, in fig. 2 the helicity-dependent cross-section $(\mathrm{d}\sigma/\mathrm{d}\Omega)_{3/2} - (\mathrm{d}\sigma/\mathrm{d}\Omega)_{1/2}$ for the $\gamma p \to p\pi^0$ channel as a function of pion scattering angle in the CM system

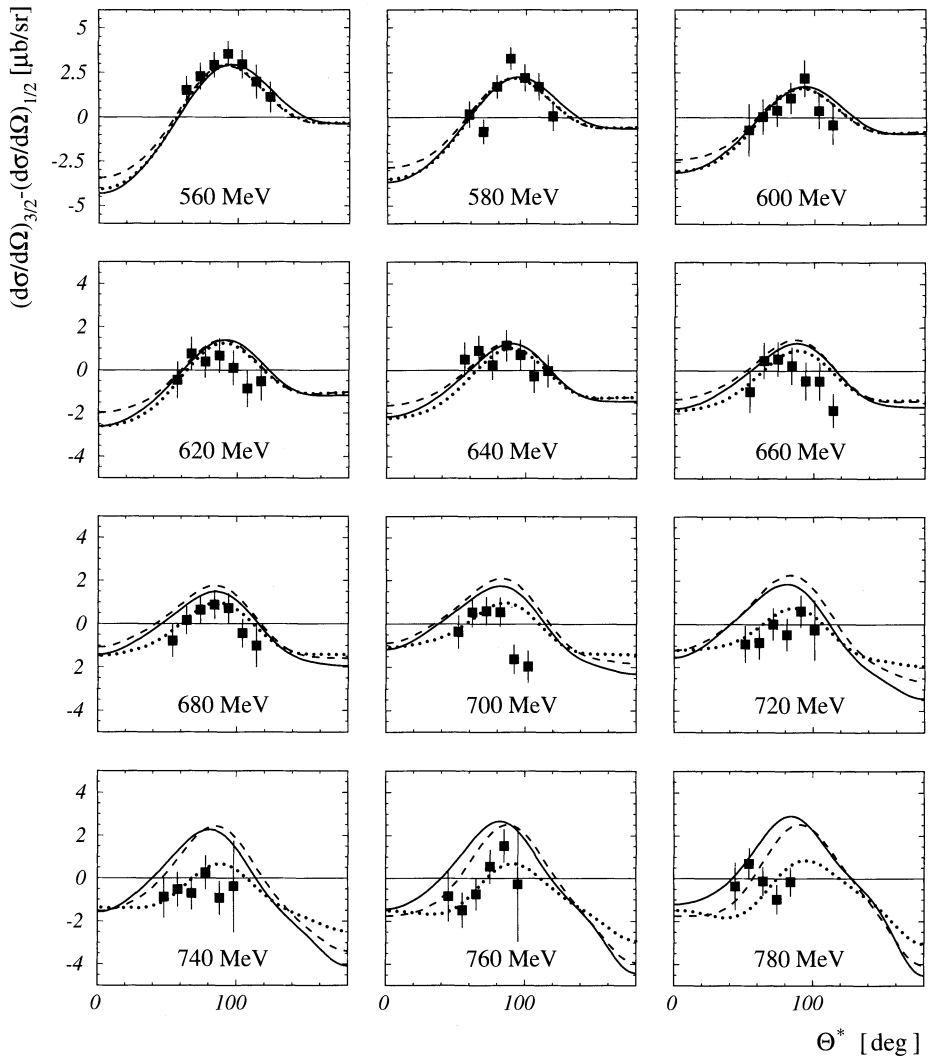

Fig. 2. The measured helicity-dependent differential cross-section for $\gamma p \to p\pi^0$ (solid squares) is compared to the SAID [9] (solid line) and UIM [10] (dashed line) analyses. The dotted curve presents the modified solution of UIM (see text). The errors shown are statistical only.

θ^* is shown in the photon energy region from 550 MeV up to 790 MeV [15].

At the lower photon energies, the data are in a good agreement with SAID and UIM models, while a clear, systematic discrepancy is present when the energy region of the $D_{13}(1520)$-resonance is approached. The dotted line represents a modified UIM solution which was fitted to our data. With respect to the standard UIM solution, the most relevant changes were found for the $M_{2-}^{1/2}$ (11% increase) and $E_{2-}^{1/2}$ (19% decrease) multipoles. This produces a sizeable change in the helicity amplitudes $A_{1/2}$ and $A_{3/2}$, as shown in table 1.

Finally, in fig. 3 [16] the preliminary results for the helicity-dependent total cross-section of all double-pion photoproduction channels on the proton are shown.

According to the existing models [17], the large positive $(\sigma_{3/2}-\sigma_{1/2})$ values for the $p\pi^+\pi^-$ channel, are mainly due to an intermediate excitation of a $\Delta\pi$ state, with the D_{13}-resonance playing a minor role. On the contrary, the intermediate excitation of the D_{13} should give the dominant contribution to the $n\pi^+\pi^0$ channel, through the $D_{13} \to n\rho$ decay mode. The intermediate D_{13} excitation is expected to play a major role also for the $p\pi^0\pi^0$ channel (through the $D_{13} \to \Delta\pi$ decay mode) but the small quantity of data analysed up to now for this reaction (about 1/4 of the total statistics) prevents to draw any clear experimental conclusion.

Table 1. The D_{13} helicity amplitudes $A_{1/2}$, $A_{3/2}$ for the proton (in units of $\mathrm{GeV}^{-1/2}$) estimated from the modified UIM analysis, are compared to the standard UIM solution, and to the PDG latest estimate [18].

Solution	$A_{1/2}$	$A_{3/2}$
Standard UIM	-0.017	0.164
PDG estimate	-0.024 ± 0.009	0.166 ± 0.005
Modified UIM	-0.038 ± 0.003	0.147 ± 0.010

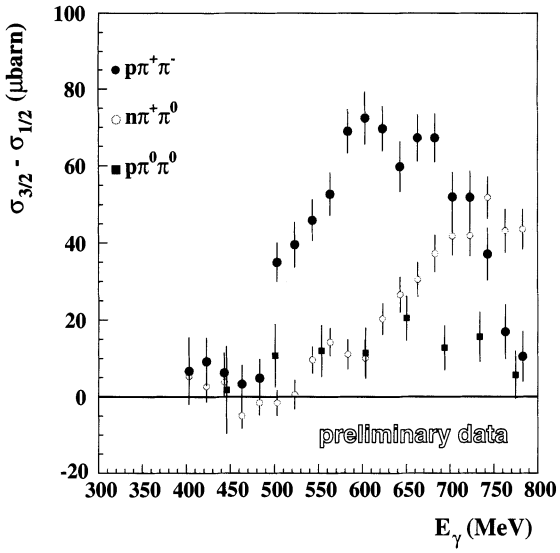

Fig. 3. Preliminary helicity-dependent total cross-section ($\sigma_{3/2} - \sigma_{1/2}$) for all $\pi\pi$ photoproduction channels on ^{1}H.

4 Summary and outlook

First data on the helicity dependence of the photon-nucleon reactions in the energy range from 200 to 800 MeV have been obtained at MAMI.

The helicity dependence of the total cross-section gives valuable information on the nucleon spin structure and allows a test of the GDH sum rule together with a measurement of the forward spin polarizability γ_0. In addition, new input for multipole analyses is also available from the data on the single- and double-pion production channels.

References

1. S.B. Gerasimov, Sov. J. Nucl. Phys. **2**, 430 (1966); S.D. Drell, A.C. Hearn, Phys. Rev. Lett. **16**, 430 (1966).
2. K. Aulenbacher *et al.*, Nucl. Instrum. Methods A **391**, 498 (1997).
3. C. Bradtke *et al.*, Nucl. Instrum. Methods A **436**, 430 (1999).
4. G. Audit *et al.*, Nucl. Instrum. Methods. A **301**, 473 (1991).
5. M. Mac Cormick *et al.*, Phys. Rev. C **53**, 41 (1996).
6. J. Ahrens *et al.*, Phys. Rev. Lett. **87**; 02203 (2001).
7. J. Ahrens *et al.*, Phys. Rev. Lett. **84**, 26 (2000).
8. O. Hanstein, Nucl. Phys. A **632**, 561 (1998).
9. R.A. Arndt *et al.*, Phys. Rev. C **53**, 430 (1996), solution SP01.
10. D. Drechsel *et al.*, Nucl. Phys. A **645**, 145 (1999).
11. N. Bianchi, T. Thomas, Phys. Lett. B **450**, 439 (1999).
12. D. Babusci *et al.*, Phys. Rev. C **58**, 1013 (1998).
13. D. Drechsel *et al.*, Phys. Rev. C **61**, 015204 (2000).
14. A. Braghieri *et al.*, Nucl. Instrum. Methods A **343**, 623 (1994).
15. J. Ahrens *et al.*, Phys. Rev. Lett. **88**, 232002 (2002).
16. H. Holvoet, PhD Thesis, University of Gent, 2001; M. Lang, PhD thesis, University of Mainz, in preparation; F. Zapadtka, PhD Thesis, University of Göettingen, in preparation.
17. J.C. Nacher, E. Oset, Nucl. Phys. A **697**, 372 (2002), e-print nucl-th/0106005.
18. D.E. Groom *et al.*, Eur. Phys. J. C **15**, 1 (2000).

Eur. Phys. J. A **18**, 405–408 (2003)
DOI 10.1140/epja/i2002-10245-y

THE EUROPEAN PHYSICAL JOURNAL A

Photon-induced reactions

S. Schadmand[a]

II. Physikalisches Institut, JLU Gießen, Gießen, Germany

Received: 30 September 2002 /
Published online: 22 October 2003 – © Società Italiana di Fisica / Springer-Verlag 2003

Abstract. An overview over the experimental research programs with photon beams is given with the focus on the electromagnetic excitation of the nucleon and the subsequent decay via mesons. Photoproduction of mesons on the free proton and on nucleons embedded in nuclei up to 1 GeV incident-photon energy are discussed.

PACS. 13.60.Le Meson production – 13.60.Rj Baryon production – 14.20.Gk Baryon resonances with $S = 0$ – 25.20.Lj Photoproduction reactions

1 Introduction

The advent of continuous-wave electron accelerators providing intense electron beams and tagged photon beams has enabled high-quality measurements. The experimental programs discussed here concentrate on the structure of the nucleon and observe resonance decays via their decay into mesons. In sect. 2, the experimental status of meson photoproduction in the non-strange regime is summarized. A further aspect is the modification of hadron properties in the nuclear medium. The underlying questions are the origin of hadron masses in the context of spontaneous chiral symmetry breaking and their modification in a hadronic environment due to chiral dynamics and partial restoration of chiral symmetry [1,2]. Section 3 discusses recent advances in photon-induced reactions on nuclei.

2 Meson photoproduction on the proton

The complex structure of the nucleon is reflected in its excitation spectrum which is observed in photoabsorption experiments. Here, the photohadronic method is applied where a shower detector at small forward angles rejects electromagnetic events and a large solid-angle hadronic detector registers events at larger angles. Figure 1 shows a compilation of photoabsorption cross-sections as measured on the proton. Several resonance regions can be discerned containing the contributions of broad and overlapping nucleon resonances. The lowest resonance is called $\Delta(1232)$ which is a P_{33} state in the common notation $(L_{(2I)(2J)})$ with a pole mass of 1232 MeV. It is prominently excited by incident photons of 0.2–0.5 GeV. The following group of resonances is called second resonance region ($E_\gamma = 0.5$–0.9 GeV). The contributing states together

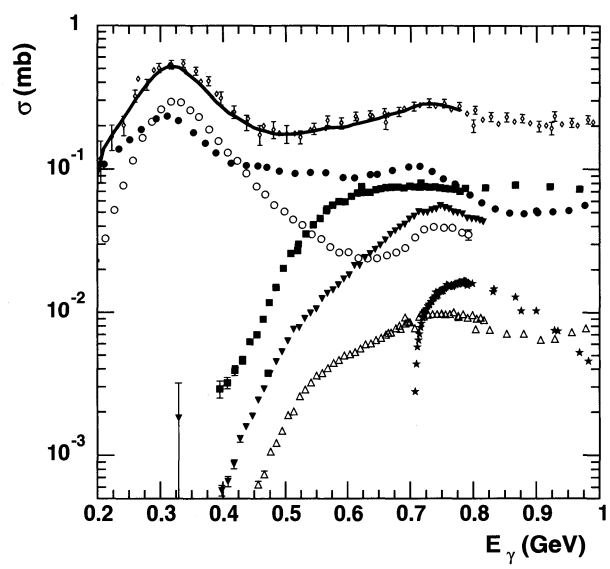

Fig. 1. The photoabsorption cross-section on the proton and its decomposition into the meson production channels. Diamonds are the photoabsorption data compilation from [3]. The experimental meson production cross-sections are: single π^+ (solid circles) from [4,5], single π° (open circles) from [6], $\pi^+\pi^-$ (solid squares) from [7,8], $\pi^+\pi^\circ$ (downward solid triangles) from [9], $\pi^\circ\pi^\circ$ (upward open triangles) from [10,11], and η (stars) from [12,13]. The solid line is the sum of the meson channels up to 800 MeV.

with their width and the incident-photon energies needed to produce their pole mass are listed in the following table:

State (Mass)	Width	E_γ
$P_{11}(1440)$	≈ 350 MeV	0.636 GeV
$D_{13}(1520)$	≈ 120 MeV	0.763 GeV
$S_{11}(1535)$	≈ 150 MeV	0.787 GeV

[a] e-mail: s.schadmand@physik.uni-giessen.de

Figure 1 also provides the status of meson photoproduction cross-sections. The shapes of the meson cross-sections reflect the resonance structure observed in photoabsorption showing that they are mostly decay products of the respective resonances. In the region of the Δ-resonance single-pion production is dominant. The π° (open circles) and π^+ (full circles) cross-sections are shown. The three resonances in the second resonance region decay roughly to 50% via single-pion emission which is used for partial wave analyses. Above $E_\gamma \approx 0.4\,\mathrm{GeV}$, the production of two pions is kinematically possible and single-π production looses its dominance. It can also be noted that the meson production channels involving charged pions are dominant as expected in electromagnetic excitation processes.

The η production threshold is located at $E_\gamma \approx 700\,\mathrm{MeV}$. The steeply rising η cross-section in fig. 1 is characteristic for an S-wave resonance. The angular distributions of the η emission are consistent with this observation and the cross-section peaks around the mass pole of the $S_{11}(1535)$-resonance. This resonance is the only one with a strong decay branch of 30–55% into η-mesons and 35–55% into single pions. Thus, η production is considered characteristic for the $S_{11}(1535)$-resonance. Above the η threshold the cross-section basically displays the resonance line shape enabling detailed studies of that state. At the production threshold, studies of ηN final-state interactions are currently investigated and discussed in the contribution by S. Schneider (this issue, p. 421).

In the second resonance region, pion production can stem from the three resonances, $P_{11}(1440)$, $D_{13}(1520)$, and $S_{11}(1535)$. The dominant contribution comes from the $D_{13}(1520)$-resonance which has the strongest coupling to the incident photon. The single- as well as the double-pion production channels display structure at the corresponding resonance mass, *i.e.* around $E_\gamma \approx 760\,\mathrm{MeV}$. On the proton, three isospin combinations of pion pairs can be produced. $\pi^\circ\pi^\circ$ and $\pi^+\pi^-$ production revealed that the resonance decays sequentially via an intermediate Δ state. In $\pi^+\pi^\circ$ the same behavior was found and a decay branch of 20% $N^\star \to N\rho$ is deduced. On account of its dominance, the $D_{13}(1520)$-resonance is said to be tagged by double-pion production. In calculations by Gomez Tejedor and Oset [14], the N^* contribution to double-pion photoproduction by itself is not large but rather stems from an interference with other terms. At ca. 0.52 GeV, the threshold for $\pi\pi\pi$ production opens up, part of which stems from the $\eta \to 3\pi$ decay. Finally, the solid line in fig. 1 represents the sum of all meson cross-sections up to 0.8 GeV and demonstrates that the photoabsorption cross-section on the proton can be explained by its decomposition into meson production.

3 Meson photoproduction on nuclei

Experiments on nuclear photoabsorption and photofission have provided intriguing results. Figure 2(a) shows the nuclear photoabsorption data on carbon and averaged over a series of nuclei. For comparison, the photoabsorption cross-section on the proton is also shown. The $\Delta(1232)$-resonance appears broadened and slightly shifted in position. In contrast, the nuclear cross-section does not show any sign of resonance structure above 0.6 GeV. It has been shown in systematic studies that nuclear cross-sections from nuclei heavier than ^{6}Li show this behavior. Overall, the cross-sections scale with the atomic mass number due to the fact that the photon probe illuminates the entire nucleus. The comparative study of the nuclear and the elementary photoabsorption cross-section yields several observations:

- The cross-sections follow a universal behavior $\sigma \sim 1/A$.
- The Δ-resonance is broadened and slightly shifted.
- The higher resonance regions appear to have "disappeared".
- The absolute value of the cross-section for incident-photon energies above 0.6 GeV is reduced.

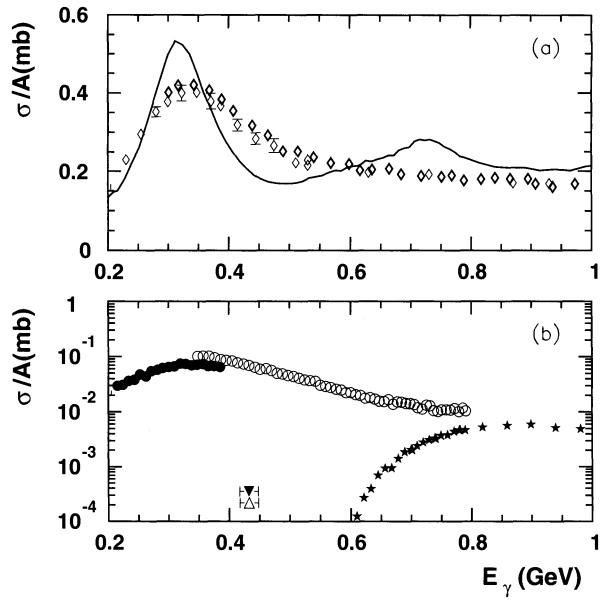

Fig. 2. The photoabsorption cross-section per nucleon on carbon (a) and its decomposition into the meson production channels (b). Diamonds are nuclear photoabsorption data from [15], the solid line shows the $\gamma + p$ cross-section. The experimental meson production cross-sections are: single π^+ (solid circles) from [16], single π° (open circles) from [17], $(\pi^\circ\pi^+ + \pi^\circ\pi^-)$ (solid triangles) and $\pi^\circ\pi^\circ$ (open triangles) from [18], and η (stars) from [19,20]. The solid line represents a fit to photoabsorption from the proton [15].

"Trivial" medium effects on baryon resonance parameters cannot explain the disappearance of resonance structure. These effects are summarized in the following table:

Mechanism	Modification
Fermi motion	Resonance broadening
Collisions $N^\star N \to N^\star N$	Resonance broadening
Quenching $N^\star N \to NN$	Reduction of meson yield
Meson decay $N^\star \to N + \mathrm{meson}$	Pauli blocking

The depletion of nuclear cross-sections in the second resonance region has been taken as evidence for modifications of hadron properties in the nuclear medium which have to date not been explained in a model-independent way. The phenomenon is commonly referred to as the disappearance of the D_{13}-resonance because of its dominant excitation in the $\gamma + p$ reaction.

It has been argued by Mosel *et al.* [21] that an in-medium broadening of the $D_{13}(1520)$-resonance is a likely cause of the suppressed photoabsorption cross-section. The broadening could arise from a coupling of the resonance to the $N\rho$ final state since the ρ-meson itself is expected to be appreciably broadened in the nuclear medium [22]. In the approach of Hirata *et al.* [23], the main point is a modification of double-pion production. The model predicts the disappearance of the peak around the position of the D_{13}-resonance via a cooperative effect of the interference in double-pion production processes, Fermi motion, collision broadening of the Δ- and N^*-resonances, and pion distortion in the nuclear medium.

A deeper understanding of the situation is anticipated from a detailed experimental study of meson photoproduction from nuclei. The investigations aim at various aspects, the meson-meson and meson-nucleus interaction and medium modifications of the excited states of the nucleon. Three different reaction mechanisms can contribute to meson production from nuclei. In coherent production the reaction amplitudes from all nucleons add coherently and the nucleus remains in its ground state while in incoherent production the nucleus is excited in the final state. In breakup reactions at least one nucleon is knocked out of the nucleus. At sufficiently high energies, it can be assumed that a quasifree reaction has taken place, in accordance with the coherence wavelength of the incident photon. Thus, in-medium properties of the nucleon resonances in the second resonance region have been investigated via quasifree pion or eta photoproduction. The meson resonances themselves are influenced by absorption as well as rescattering processes (final-state interactions). Any modification of meson properties can feed back on the baryon resonance parameters. The modification of the pion-pion interaction in the nuclear medium is of current interest and is discussed in the contributions of J. Messchendorp (this issue, p. 417) and M.J. Vicente Vacas (this issue, p. 479).

Compared to the elementary case, experimental information on meson photoproduction off nuclei is scarce. Figure 2(b) provides an overview over the experimental π, $\pi\pi$, and η total cross-sections that are currently available for carbon (^{12}C). Single-charged-pion cross-sections have only been measured below the double-pion production threshold ($E_\gamma \approx 0.4\,\mathrm{GeV}$). The cross-section $\sigma_{\pi^+}(E_\gamma)$ is displayed, which is roughly the same as $\sigma_{\pi^-}(E_\gamma)$. The single-pion cross-sections exhibit a broad maximum between 0.2 and 0.4 GeV and explain the shape of the photoabsorption data indicating that the $\Delta(1232)$-resonance is a dominant producer of single pions.

Single-π° photoproduction has also been studied in the second resonance region. The systematic study over a series of nuclei has not provided any hint for a depletion of the resonance yield. The observed reduction and change of shape can be explained by trivial effects like absorption, Fermi smearing and Pauli blocking, and collision broadening. A similar result is obtained in systematic studies of η photoproduction cross-section from nuclei. The data shown in fig. 2(b) clearly show the line shape of the $S_{11}(1535)$-resonance. This means that the two resonances of the second resonance region, $D_{13}(1520)$ and $S_{11}(1535)$, which are dominantly excited by photons, seem to maintain their structure in the nuclear medium and do not contribute to an explanation for the disappearance of the second resonance region. However, judging from the elementary case as seen in fig. 1, the neutral final meson states do not contribute dominantly to the total reaction cross-section. Total cross-sections for charged- and double-pion production channels are needed in order to complete the picture. Figure 2 shows first total cross-sections for double-pion photoproduction from carbon which need to be determined for higher energies.

4 Summary and outlook

As an introduction to photon-induced reactions, meson production on the free proton and on nucleons embedded in nuclei have been discussed. In this contribution, an overview of the available total meson production cross-sections in the non-strange regime has been given. These studies are successfully employed to study the structure of the nucleon by tagging on the broad and overlapping nucleon resonances via their characteristic meson decay. The experimental results from photoabsorption on nuclei show clear signs of in-medium modifications of hadron properties by the fact that the resonances above the $\Delta(1232)$ seem to have disappeared. This phenomenon is not yet understood in a model-independent way. A deeper understanding can come from detailed studies of meson photoproduction from nuclei where the meson-meson and meson-nucleus interaction and medium modifications of the excited states of the nucleon could be traced.

References

1. T. Hatsuda, S.H. Lee, Phys. Rev. C **46**, 34 (1992).
2. G.E. Brown, M. Rho, Phys. Rev. Lett. **66**, 2720 (1991).
3. Particle Data Group, `http://pdg.lbl.gov/~sbl/gammap_total.dat`.
4. K. Buechler *et al.*, Nucl. Phys. A **570**, 580 (1994).
5. M. MacCormick *et al.*, Phys. Rev. C **53**, 41 (1996).
6. F. Härter, PhD Thesis, University of Mainz (1996) KPH15/96.
7. A. Braghieri *et al.*, Phys. Lett. B **363**, 46 (1995).
8. J. Wißkirchen, PhD Thesis, University of Bonn (1999) BONN-IR-99-21.
9. W. Langgärtner *et al.*, Phys. Rev. Lett. **87**, 052001 (2001).
10. M. Kotulla, PhD Thesis, University of Giessen (2001).
11. E. Hourany, *INCP 2001*, AIP Conf. Proc. **610**, 362 (2001).
12. B. Krusche *et al.*, Phys. Rev. Lett. **74**, 3736 (1995).
13. F. Renard *et al.*, Phys. Lett. B **528**, 215 (2002).

14. J.A. Gomez Tejedor *et al.*, Nucl. Phys. A **600**, 413 (1996).
15. V. Muccifora *et al.*, Phys. Rev. C **60**, 064616 (1999).
16. J. Arends *et al.*, Z. Phys. A **305**, 205 (1982).
17. B. Krusche *et al.*, Phys. Rev. Lett. **86**, 4764 (2001).
18. J.G. Messchendorp *et al.*, Phys. Rev. Lett. **89**, 222302 (2002).
19. M. Roebig-Landau *et al.*, Phys. Lett. B **373**, 45 (1996).
20. H. Yamazaki *et al.*, Nucl. Phys. A **670**, 202 (2000).
21. U. Mosel *et al.*, Prog. Part. Nucl. Phys. **42**, 163 (1999).
22. F. Klingl *et al.*, Nucl. Phys. A **624**, 527 (1997).
23. M. Hirata *et al.*, Phys. Rev. C **66**, 014612 (2002).

Eur. Phys. J. A **18**, 409–411 (2003)
DOI 10.1140/epja/i2002-10246-x

THE EUROPEAN PHYSICAL JOURNAL A

Deuteron photodisintegration at high energy

F. Ronchetti[a]

INFN, Laboratori Nazionali di Frascati, Via E. Fermi 40, 00044 Frascati, Roma, and Università di Roma Tre, Dipartimento di Fisica, Via della Vasca Navale 84, 00146 Roma, Italy

Received: 30 September 2002 /
Published online: 22 October 2003 – © Società Italiana di Fisica / Springer-Verlag 2003

Abstract. The high-energy two-body deuteron break-up is a very well-suited process to identify quark effects in nuclei. In particular, its study in the few GeV region can clarify the transition from the nucleonic to the QCD picture of hadrons. The CEBAF Large Angle Spectrometer (CLAS) at JLab allowed for the first time the complete measurement of the angular distributions of the two-body deuteron photodisintegration differential cross-section at photon energies from 0.5 to 2.95 GeV. First results from the analysis of 30% of the total collected data show persistent forward-backward asymmetry and are well described by a calculation derived in the non-perturbative framework of the Quark Gluon String Model (QGSM).

PACS. 21.45.+v Few-body systems – 25.20.-x Photonuclear reactions

1 Introduction

A fundamental issue in nuclear physics concerns the study of the interplay between hadronic and partonic degrees of freedom in nuclei.

To this purpose, the deuteron photodisintegration is well suited for studying nuclear reactions in the intermediate-energy regime where neither the traditional meson exchange models nor perturbative QCD (pQCD) describe the data well. It is an exclusive reaction in which a large momentum is imparted to the constituents [1].

At high incident-photon energy and intermediate angles, conventionally 90°, where both the t-dominance and u-dominance are suppressed, the $\gamma d \to pn$ differential cross-section is well described by the Constituents Counting Rule (CCR) [2]:

$$\frac{\mathrm{d}\sigma}{\mathrm{d}t} = \frac{1}{s^{N-2}} f(\theta_{\mathrm{CM}}),$$

where N is the minimum number of microscopic fields involved in the reaction, s is the square of the total energy, and θ_{CM} is the proton scattering angle. In this case, with $N = 13$, the CCR predicts $\mathrm{d}\sigma/\mathrm{d}t \propto s^{-11}$.

Before the present experiment, the deuteron photodisintegration differential cross-section for $E_\gamma > 1\,\mathrm{GeV}$ was measured only at few proton angles ([3–5]) as can be seen in fig. 1. These data show s^{-11} scaling only at large angles: $\theta_{\mathrm{CM}} = 69°$ and 89°.

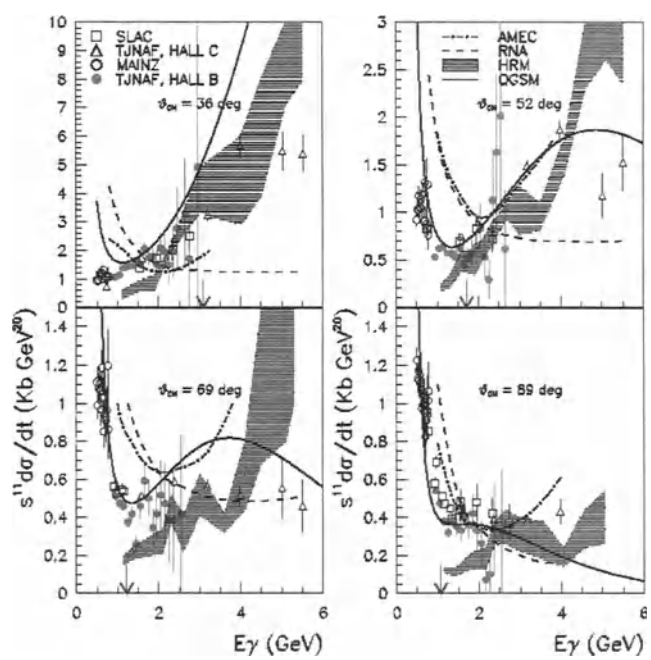

Fig. 1. Deuteron photodisintegration cross-section multiplied by s^{11}. Experimental data are from Mainz [3], JLab Hall C [4], SLAC [5] and CLAS. Points are multiplied by s^{11}, and arrows indicate the expected threshold for the onset of the scaling, where $t > 1\,\mathrm{GeV}$ [2]. For the theoretical curves, see [6–9].

For intermediate energies, the cross-section data indicate a deviation from the predictions of the simple CCR and more sophisticated models have been developed.

In the Reduced Nuclear Amplitude (RNA) model [10, 6] the binding of the quarks inside the nucleons and the

[a] *Present address*: Laboratori Nazionali di Frascati, CP 13, Via E. Fermi 40, 00044 Frascati, Roma, Italy; e-mail: `ronchetti@lnf.infn.it`

deuteron is taken into account with empirical form factors and the elementary cross-section is computed assuming CCR scaling. This approach is able to describe the $\gamma d \to pn$ cross-section with an appropriate normalization factor for $\theta_{\rm CM} = 89°$ and $69°$ with $E_\gamma > 2\,{\rm GeV}$.

In the Hard quark Rescattering Model (HRM) [7], the elementary interaction consists of a quark exchange between the two nucleons. The incoming photon is absorbed by a quark of one nucleon which then gives up its momentum via a hard gluon exchange with a quark of the other nucleon. The model assumes that this rescattering mechanism is analogous, with some approximation, to the wide-angle p-n scattering which is also dominated by quark exchange. The limits for the applicability of the model are $E_\gamma > 2.5\,{\rm GeV}$ and momentum transfer $t > 2\,{\rm GeV}^2$, but, under particular assumptions for the short-distance p-n interaction, they can be extended. However, the agreement with the data is poor, especially at higher energies where the uncertainty is large, due to the limited knowledge of the pn cross-section for the actual kinematic conditions.

A non-pQCD calculation has been done in the framework of the Quark Gluon String Model (QGSM) [8]. It assumes that the scattering amplitude at high energy is dominated by the exchange of three quarks in the t-channel, and the duality property allows its extension at lower energies. The intermediate three-quarks state can be identified with the nucleon Regge trajectory.

A short overview of the QGSM and the comparison with data are given in sect. 3.

Traditional models based on the N-π picture fail to reproduce data at $E_\gamma > 1\,{\rm GeV}$. However, this approach was extended in the few GeV region in the Asymptotic Meson Exchange Current (AMEC) model [9], using form factors to describe the d-NN interaction vertex and an overall normalization factor fixed by fitting the experimental data at 1 GeV. The results reproduce the energy dependence of the cross-section only for $\theta_{\rm CM} = 89°$. It is worth noticing that also this non–QCD-based model provides a scaling law for the cross-section, with an exponent depending on the scattering angle.

Complementary information to the differential cross-section is provided by polarization observables. At high energies, a signature of pQCD effects is the Hadron Helicity Conservation (HHC) [11–14].

The proton polarization was measured in the $\gamma d \to pn$ reaction only for proton angle $\theta_{\rm CM} = 90°$ [15]. Above 1 GeV, data show that the induced polarization is small, consistent with HHC. However, the transverse and longitudinal, in-plane, polarizations are non-zero, and indicate that helicity is not conserved at least up to 2 GeV. Thus, it can be concluded that experimental data at $\theta_{\rm CM} = 90°$ on cross-section and polarization give results that cannot be consistently interpreted in a perturbative picture.

2 The JLab experiment E93-017

A new dataset for the $\gamma d \to pn$ cross-section was obtained using the CLAS detector [16]. A *bremsstrahlung* photon beam is produced from a continuous electron beam by hitting a thin radiator, and then tagged [17] using a spectrometer operating in the range between 0.20 and 0.95 of the electron energy with a resolution about 0.1%. Scattered hadrons are detected with the CLAS [18], a nearly 4π spectrometer based on a toroidal magnetic field generated by 6 superconducting coils which define 6 independent modules. Each module is implemented with 3 regions of drift chambers [19] to track charged particles, and time-of-flight (TOF) scintillators [20] for charged-hadron identification.

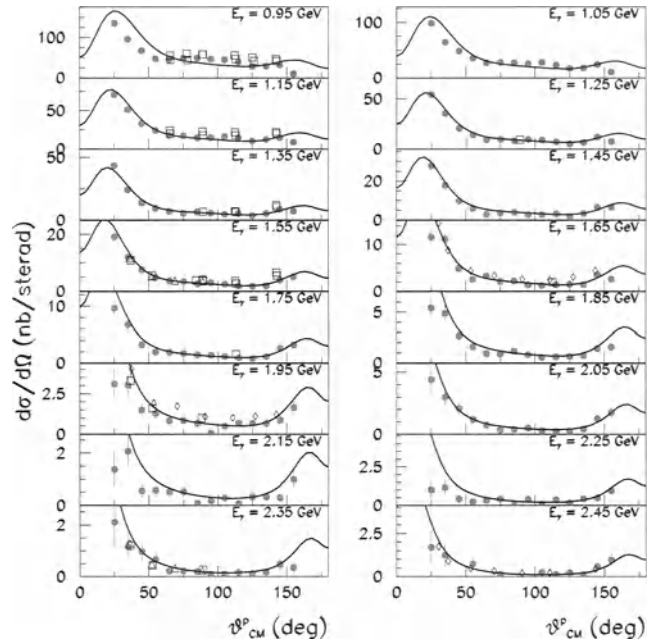

Fig. 2. First results of the deuteron photodisintegration differential cross-section measured with the CLAS (full dots), compared with the published data from JLab Hall C of [4] (open triangles) and SLAC [5] (open squares). The curve is the QGSM calculation [8].

The resolution of the proton momentum is of the order of a few percent, while the proton efficiency is better than 90% in the fiducial region of the detector.

Data were taken with photon energy ranging from 0.5 to 2.95 GeV with a trigger given by the coincidence between the tagger and the CLAS detector (TOF) signals. The total number of recorded triggers is about $2.5 \cdot 10^9$.

Photodisintegration events are selected requiring the identification of a photon in the tagger and a charged hadron in the CLAS, and then applying a missing-mass cut to the reaction $\gamma d \to pX$. The detector acceptance and proton efficiency have been evaluated by Monte Carlo simulations of the photodisintegration reaction, and the background contribution has been computed fitting the experimental missing-mass distributions.

In fig. 2 the differential cross-section $d\sigma/d\Omega$ is reported as a function of the proton angle in the CM frame, for fixed photon energy above 0.9 GeV. The present preliminary results are obtained from the analysis of about 30% of the accumulated statistic. Moreover, an additional cut $\theta_{\rm CM} > 20°$ has been applied, that will be removed in the

final analysis. The agreement with the other available data from SLAC [5] and JLab Hall C [4] is good at all energies and angles. Notice that, in spite of the limited data set, the statistical error is lower than 5% for $E_\gamma < 1.5\,\mathrm{GeV}$. The statistical error will be improved by a factor 3 or more for photon energies up to 2.5 GeV when the whole CLAS dataset will be analyzed.

3 The Quark Gluon String Model

The QGSM is a non-pQCD approach [21,22], used in the description of hadronic reactions at high energies [23]. Due to the duality property of amplitudes, it can be applied at intermediate energies for reactions without explicit resonances in the direct channel [24]. This approach has also been used for the description of heavy-ion collisions at high energy [25].

In particular, the reaction $\gamma d \to pn$ is described by the exchange of three valence quarks in the t-channel plus any number of gluons: this corresponds to the formation and break-up of a quark-gluon string in the intermediate state, leading to the factorization of the amplitudes. Such a string can also be identified with the nucleon Regge trajectory since the QGSM can be considered as a microscopic model for the Regge phenomenology, and can be used for the calculation of different quantities that have been considered before only at a phenomenological level [23].

In ref. [8], the QGSM has been applied for the description of the deuteron photodisintegration reaction, using QCD-motivated non-linear nucleon Regge trajectories [26] and including the photon spin variables with the assumptions of the dominance of the amplitudes that conserve s-channel helicity. The interference between the isoscalar and isovectorial components of the photon has been taken into account, leading to forward-backward asymmetry in the cross-section.

The result of this model is shown in fig. 2 as full line. The agreement between data and QGSM calculations is very good and the angular dependence of the cross-section at fixed photon energy is reproduced together with the forward-backward asymmetry showed by the data.

From fig. 2 it is clear the importance of the CLAS datum at very forward angles, in order to check the QGSM prediction of a decreasing cross-section at 10°–20°.

The QGSM model accounts for the decrease of $\mathrm{d}\sigma/\mathrm{d}t$ at fixed angle as a function of the photon energy, as shown in fig. 1 for four CM proton angles.

4 Conclusions

For its simplicity, the deuteron is very suitable to study the quark structure of nuclear matter and the $\gamma d \to pn$ is an ideal reaction, since γ-quark interactions are well known and momentum transfers are large. The experimental data for the cross-section at 90° are consistent with the CCR scaling, while the proton polarizations show that HHC is not conserved at least up 2 GeV giving the indication that a plain pQCD interpretation of the process may not be correct.

New measurements of the cross-section have been performed using the CLAS, with tagged-photon energy between 0.5 and 2.95 GeV, covering for the first time almost all proton angles in the CM frame. The preliminary results of about 30% of the total CLAS statistics are in good agreement with the already published data.

The CLAS data have been interpreted in the framework of the QGSM, a non-perturbative approach used for the description of binary hadronic reactions. This model works well for all proton angles and photon energy above 1 GeV.

References

1. R.J. Holt, Nucl. Phys. A **684**, 148c (2001).
2. S.L. Brodsky, G.L. Farrar, Phys. Rev. Lett. **31**, 1153 (1973); V. Matveev *et al.*, Lett. Nuovo Cimento **7**, 719 (1973).
3. R. Crawford *et al.*, Nucl. Phys. A **603**, 303 (1996).
4. C. Bochna *et al.*, Phys. Rev. C **41**, 4576 (1998); E.C. Shulte *et al.*, Phys. Rev. Lett. **87**, 102302-1 (2001).
5. S.J. Freedman *et al.*, Phys. Rev. C **48**, 1864 (1993); J.E. Beltz *et al.*, Phys. Rev. Lett. **74**, 646 (1995).
6. S.J. Brodsky, B.T. Chertok, Phys. Rev. D **14**, 3003 (1976); Phys. Rev. Lett. **37**, 269 (1976); S.J. Brodsky, C.-R. Ji, G.P. Lepage, Phys. Rev. Lett. **51** 83 (1983); L.C. Alexa *et al.*, Phys. Rev. Lett. **82**, 1374 (1999); D. Abbott *et al.*, Phys. Rev. Lett. **82**, 1879 (1999).
7. L.L. Frankfurt *et al.*, Phys. Rev. Lett. **84**, 3045 (2000); Nucl. Phys. A **663** & **664**, 349 (2000).
8. V.Yu. Grishina *et al.*, Eur. Phys. J. A **10**, 355 (2001).
9. A.E.L. Dieperink, S.I. Nagorny, Phys. Lett. B **456**, 9 (1999).
10. S.L. Brodsky, J.R. Hiller, Phys. Rev. C **28**, 475 (1983).
11. G.P. Lepage, S.J. Brodsky, Phys. Rev. D **22**, 2157 (1980); S.J. Brodsky, G.P. Lepage, Phys. Rev. D **24**, 2848 (1981).
12. D.G. Grabb *et al.*, Phys. Rev. Lett. **65**, 3241 (1990).
13. T. Gousset *et al.*, Phys. Rev. D **53**, 1202 (1996); C. Carlson, M. Chachkhunashvili, Phys. Rev. D **45**, 2555 (1992).
14. A. Afanasev *et al.*, Phys. Rev. D **61**, 034014 (2000).
15. K. Wijesooriya *et al.*, Phys. Rev. Lett. **86**, 2975 (2001), and references therein.
16. N. Bianchi *et al.*, CEBAF proposal E-93-017.
17. D.I. Sober *et al.*, Nucl. Instrum. Methods A **440**, 263 (2000).
18. W. Brooks, Nucl. Phys. A **663** & **664**, 1077c (2000).
19. D. Carman *et al.*, Nucl. Instrum. Methods A **449**, 81 (2000).
20. E.S. Smith *et al.*, Nucl. Instrum. Methods A **432**, 265 (2000).
21. G. 't Hooft, Nucl. Phys. B **72**, 461 (1974).
22. G. Veneziano, Phys. Lett. B **52**, 220 (1974); Nucl. Phys. Lett. B **117**, 519 (1976).
23. A.B. Kaidalov, Z. Phys. C **12**, 63 (1982); Surv. High Energy Phys. **13**, 265 (1999).
24. A.B. Kaidalov, Sov. J. Nucl. Phys. **53**, 872 (1991); C. Guaraldo *et al.*, Yad. Fiz. **59**, 1896 (2000); Phys. At. Nucl. **63**, 1395 (2000).
25. E.E. Zabrodin *et al.*, Phys. Lett. B **508**, 184 (2001).
26. M.M. Brisudova *et al.*, Phys. Rev. D **61**, 054013 (2000).

Eur. Phys. J. A **18**, 413–416 (2003)
DOI 10.1140/epja/i2002-10248-8

THE EUROPEAN PHYSICAL JOURNAL A

Measurement of π^- and π^+ photoproduction in deuterium at large momentum transfer for E = 1.7–5.6 GeV

H. Xiang[a]

For the Jefferson Lab Hall A and E94-104 Collaborations
MIT Laboratory for Nuclear Science, Cambridge, MA, 02139-4307, USA

Received: 30 September 2002 /
Published online: 22 October 2003 – © Società Italiana di Fisica / Springer-Verlag 2003

Abstract. Single-π^- and -π^+ photoproduction from deuterium has been measured at energies $E = 1.7$–5.6 GeV and momentum transfers $|t| = 0.4$–$5.6\,(\mathrm{GeV}/c)^2$. The ratio π^-/π^+ for data taken at $E = 3.4$ GeV is presented. Also the ratio of the π^+ from hydrogen to the π^+ from deuterium is extracted to examine the nucleon spectator assumption used in the cross-section ratio analysis. Results are discussed in conjunction with the existing measurements with frameworks ranging from a hadronic description to parton constituent models which successfully characterize the scaling behaviors observed in the exclusive measurements.

PACS. 13.60.Le Meson production – 24.85.+p Quarks, gluons, and QCD in nuclei and nuclear processes – 25.10.+s Nuclear reactions involving few-nucleon systems – 25.20.Lj Photoproduction reactions

1 Introduction

High-energy photoreactions, especially when measured at high momentum transfer, have been used to probe the quark-gluon structure of the hadronic particles involved in the reactions. It is of primary interest to develop insight into the transition between the hadronic and quark-gluon descriptions of the fundamental photoproduction processes, particularly in the energy regions accessible with CEBAF at Jefferson Lab.

Current understanding presents two complementary scenarios of the photoreaction process. In the low-energy and low-momentum-transfer region, models built with nucleon-meson degrees of freedom through effective hadronic Lagrangian have proved to be valid in describing the existing data [1,2]. At high energy and large momentum transfer, constituent counting rules (CCR), a description based on the quark and gluon degrees of freedom within the domain of perturbative QCD, have been successful in characterizing the photoreaction cross-section data [3,4]. Also, successful agreements between data and perturbative QCD calculations have been reported for high-energy pion photoproduction at large transverse momentum for the inclusive process of $\gamma + N \to \pi^0 + X$ [5, 6]. However, in the same momentum transfer region where the CCR are valid, another pQCD-based prediction, hadronic helicity conservation (HHC), has not been successful in explaining the newly emerged polarization data from experiments at Jefferson Lab [7,8].

Among the proposed physics observables, the ratio of the differential cross-section $\frac{d\sigma}{dt}(\gamma n \to \pi^- p)/\frac{d\sigma}{dt}(\gamma p \to \pi^+ n)$ is shown to be explicitly sensitive to the mechanisms of the scattering processes at high energy and high momentum transfer where pQCD-based models presumably apply [9–15]. However, previous data on this observable have been available only in the momentum transfer region of $|t|$ below $2.8\,(\mathrm{GeV}/c)^2$ [16–18] where they are compared to different hadronic-model–based calculations [1,2].

This paper reports a recent measurement of the charged-pion cross-section ratio from experiment E94-104 at Jefferson Lab [19] where single pions from the following processes are measured: $\gamma d \to \pi^- X$, $\gamma d \to \pi^+ X$ and $\gamma p \to \pi^+ X$. After a description of the measurement and data analysis, results of this experiment will be discussed in connection to the existing measurements and models based on both hadronic and quark-gluon degrees of freedom.

2 Experiment and analysis

This experiment was performed in Hall A of the Continuous Electron Beam Accelerator Facility (CEBAF) at Jefferson Lab in the spring of 2001. The photon beam was generated via bremsstrahlung of the electron beam in a thin 6% Cu radiator located upstream of the target. The typical electron beam current was $\sim 30\,\mu$A and data were taken at beam energies $E = 1.723, 2.561, 3.400, 4.236$ and

[a] *Present address*: Schlumberger-Doll Research, Old Quarry Road, Ridgefield, CT 06877-4108, USA; e-mail: hxiang@mit.edu

5.614 GeV. The liquid-hydrogen target was operated at a temperature of 19 K and a pressure of $\sim$ 0.17 MPa, giving a density of 0.072 g/cm^3. The liquid-deuterium target was operated at a temperature of 22 K and a pressure of $\sim$ 0.15 MPa, giving a density of 0.167 g/cm^3. The target cells for both the hydrogen and deuterium loops consisted of aluminum cylinders with their axes oriented along the beam direction. Special runs with radiator removed were taken for subtraction of the backgrounds from the electroproduction processes. In addition, dummy target cells were used to measure empty target backgrounds.

Independent measurements of the oppositely charged pions were performed with both of the High Resolution Spectrometers (HRS) in Hall A. The beam-left HRS arm was used to measure positively charged particles and the beam-right arm to measure negatively charged particles. The position and angle of the emitted particles were tracked with two vertical drift chambers in each of the two HRS arms. Particle identification for positive tracks was obtained with a combination of scintillators and two aerogel Čerenkov counters. For negative tracks, particle separation was obtained by using a gas Čerenkov counter and two layers of lead glass shower counters in the right arm.

Charged-pion cross-section ratios are obtained from the analysis of bremsstrahlung yield curves. The incident-photon energy is reconstructed on the basis of single-pion production kinematics under the assumption that the nucleon spectator model is valid. It is believed that the following is a good approximation

$$\frac{\pi^-}{\pi^+} \equiv \frac{\mathrm{d}\sigma/\mathrm{d}t(\gamma n \longrightarrow \pi^- p)}{\mathrm{d}\sigma/\mathrm{d}t(\gamma p \longrightarrow \pi^+ n)} \simeq \frac{\mathrm{d}\sigma/\mathrm{d}t(\gamma d \longrightarrow \pi^- pp)}{\mathrm{d}\sigma/\mathrm{d}t(\gamma d \longrightarrow \pi^+ nn)}, \quad (1)$$

where the known effects that cause differences in cross-sections between free nucleons in hydrogen and in deuterium partially cancelled out when the above ratio is formed [18], including 1) the Pauli exclusion principle, and 2) the Glauber corrections for interactions of the pion with the spectator nucleon and the final-state interactions of the two nucleons.

In extracting the π^-/π^+ ratios, it was required that the photon energy, calculated from the momentum and angle of the detected pion, fall within a range $E - 125\,\mathrm{MeV} < E_\gamma < E - 25\,\mathrm{MeV}$ for both π^+ and π^-. This procedure effectively eliminated multipion processes because of their higher threshold. By varying both the width and the location of this E_γ cut, the contribution of multipion processes to the π^-/π^+ ratio was examined and found to be less than $\sim$ 3%. Contaminations of electrons and protons to the measured π^- and π^+ yields are found to be at a level below $\sim$ 1%. Variations of both the acceptance cuts and the PID cuts reveal a maximum uncertainty in the π^-/π^+ ratio at a level below $\sim$ 3%. Other systematic errors should essentially cancel out when taking the ratio of π^- and π^+ yields.

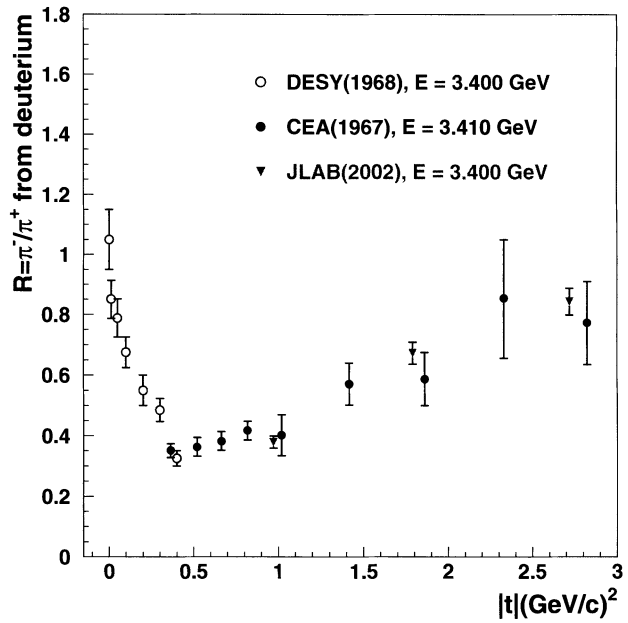

Fig. 1. $\frac{\pi^-}{\pi^+}$ ratio from deuterium measured at $E = 3.400$ GeV, comparing to the CEA and DESY data taken at same energy.

3 Results and discussion

3.1 Ratio π^-/π^+ at E = 3.400 GeV

The $|t|$-dependence of the π^-/π^+ ratio from deuterium for data taken at $E = 3.400$ GeV is shown in fig. 1, together with previous data obtained at the same beam energy from the Cambridge Electron Accelerator (CEA) [16] and DESY [17]. Using the same analysis approach as used in the previous measurements, results from this experiment suggest a very good agreement with the CEA results in their overlap region of momentum transfer. The π^-/π^+ ratio is close to unity in the forward direction, then falls sharply as $|t|$ increases, reaching a $\sim 1/3$ minimum at $|t| \simeq 0.4\,(\mathrm{GeV}/c)^2$. Further, the π^-/π^+ ratio rises smoothly as $|t|$ continue to increase between $|t| \simeq 0.4$–$2.8\,(\mathrm{GeV}/c)^2$.

3.2 Ratio of π^+ in hydrogen over π^+ in deuterium

As an examination of the validity of the assumption in eq. (1), the ratio of the π^+ produced in hydrogen to the π^+ produced in deuterium was also extracted over the same momentum transfer region of $|t| = 0.4$–$2.8\,(\mathrm{GeV}/c)^2$,

$$\frac{\pi^+(H)}{\pi^+(D)} = \frac{\mathrm{d}\sigma/\mathrm{d}t(\gamma p \longrightarrow \pi^+ n)}{\mathrm{d}\sigma/\mathrm{d}t(\gamma d \longrightarrow \pi^+ nn)}, \quad (2)$$

where the neutron in the deuterium target is viewed as a spectator when the π^+ is produced from the interaction between the photon and the struck proton. This ratio is plotted as a function of $|t|$ in fig. 2. Explicitly, the result reveals a prominent departure from unity as the measurement proceeded to increasingly higher momentum transfer. In the lower region of $|t|$ below $\sim 1.5\,(\mathrm{GeV}/c)^2$, this ratio is found to be in the vicinity of unity which is in good

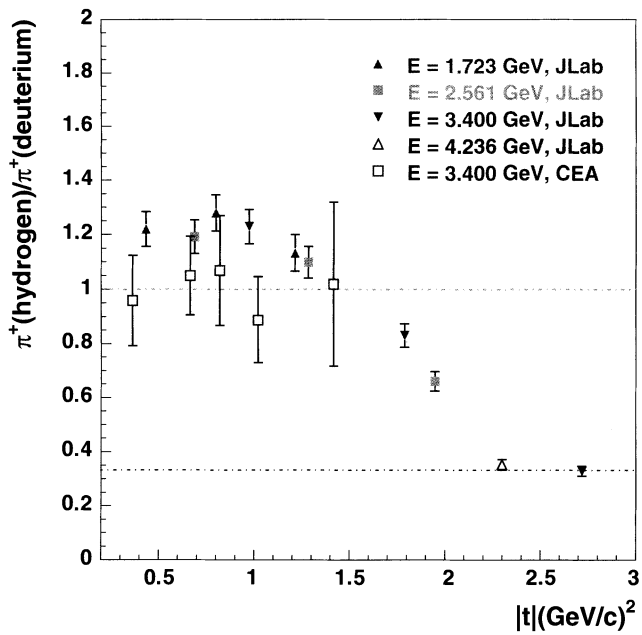

Fig. 2. Ratio of π^+ from hydrogen target over the π^+ from deuterium target. An earlier result from CEA [16] is also shown as open squares.

agreement with the same check done in the CEA data [16]. Furthermore, in a window of $|t| = 1.5$–$2.0\,(\mathrm{GeV}/c)^2$, this ratio dropped abruptly from ~ 1 down to a value of $\sim 1/3$.

It is interesting to examine this apparent breakdown of the simple nucleon spectator picture within the context of a series of exclusive cross-section measurements, including the previous measurements at SLAC on the $\gamma p \to \pi^+ n$ process [18,20] and the latest measurements on both the $\gamma p \to \pi^+ n$ and $\gamma n \to \pi^- p$ processes from this experiment [21].

First, as shown in fig. 2, both of the two data points down to the 1/3 ratio region are from measurements at center-of-mass energy $\sqrt{s}$ larger than 2.7 GeV, corresponding to a photon energy of 3.4 GeV, and at center-of-mass angle θ_{cm} larger than 70°. It has been observed that for $\sqrt{s}$ larger than 2.7 GeV, the differential cross-section for both $\gamma n \to \pi^- p$ and $\gamma p \to \pi^+ n$ at $\theta_{\mathrm{cm}} = 90°$ can be represented approximately by $\mathrm{d}\sigma/\mathrm{d}t \sim s^{-7} f(\theta_{\mathrm{cm}})$ [18,20, 21], which are in good agreement with the prediction of the parton constituent models [22–24].

Secondly, the breakdown point in the vicinity of $|t| \sim 2.0\,(\mathrm{GeV}/c)^2$ from fig. 2 is coincident with the earlier observations made in the measurements at SLAC [20] where the cross-section of $\mathrm{d}\sigma/\mathrm{d}t(\gamma p \to \pi^+ n)$ was measured as a function of momentum transfer $|t|$ for $E = 4.0$–7.5 GeV. It revealed that after an exponential ($\sim e^{3|t|}$) fall-off for $|t|$ values up to about $2.0\,(\mathrm{GeV}/c)^2$, the cross-section $\mathrm{d}\sigma/\mathrm{d}t$ entered a central region of momentum transfer where $\mathrm{d}\sigma/\mathrm{d}t$ is independent of $|t|$ and the cross-section has a steep energy dependence of s^{-7}. In addition, by extracting the effective value of the Regge trajectory parameter $\alpha(|t|)$, as defined in $\mathrm{d}\sigma/\mathrm{d}t \sim s^{2[\alpha(|t|)-1]}$ [25,26], it was found that this parameter underwent a transition at $|t| \simeq 2.0\,(\mathrm{GeV}/c)^2$ from its nominal zero value at lower momentum transfer to a definitive departure from zero into the higher-$|t|$ region where the cross-section scales with center-of-mass energy s^{2-n} with $n \simeq 7.3 \pm 0.4$.

With the convergent observations made in this measurement and other available data on the exclusive cross-sections [20,21], it appears that in the region of energy and momentum transfer accessed by this experiment, *i.e.* $E = 1.7$–5.6 GeV and $|t| = 0.4$–$2.8\,(\mathrm{GeV}/c)^2$, an apparent transition might have happened where scaling in cross-section is observed to set in as the process proceeds over a joint threshold in the center-of-mass energy $\sqrt{s}$ at ~ 2.7 GeV and momentum transfer $|t|$ at $\sim 2.0\,(\mathrm{GeV}/c)^2$. Nevertheless, the significance of other potential mechanisms such as multistep pion production processes in driving the high-t behavior of the ratio in eq. (2) remains to be investigated before a definitive conclusion may be drawn.

4 Summary

Data of single π^- and π^+ have been taken for the beam energies $E = 1.7$–5.6 GeV and momentum transfer $|t| = 0.4$–$5.6\,(\mathrm{GeV}/c)^2$. The ratio π^-/π^+ from deuterium for data taken at $E = 3.400$ GeV is in good agreement with the CEA data taken over a region of overlapped kinematics. In addition, the ratio of the π^+ from hydrogen to the π^+ from deuterium is extracted with an intention to examine the validity of the nucleon spectator model. A prominent breakdown from the naive expectation is observed at $|t| \simeq 2.0\,(\mathrm{GeV}/c)^2$. This finding, though revealed with a different observable, is concurrent to the observations made by earlier measurements from SLAC on the exclusive cross-sections. Due to this apparent breakdown, π^-/π^+ ratios at higher momentum transfer are to be investigated with additional input from the exclusive measurements.

We acknowledge the support of JLab Hall A technical staff and the Accelerator Division during this experiment. This work is supported in part by the US Department of Energy under the contracts DE-AC05-84ER40150, DE-FC02-94ER40818 and by the National Science Foundation. The Southeastern Universities Research Association operates the Thomas Jefferson National Accelerator Facility under the Department of Energy contract DE-AC05-84ER40150.

References

1. M. Guidal *et al.*, Phys. Lett. B **400**, 6 (1997).
2. M. Rahnama, J.K. Storrow, J. Phys. G, **17**, 243 (1991).
3. E.C. Schulte *et al.*, Phys. Rev. Lett. **87**, 102302 (2001).
4. C. Bochna *et al.*, Phys. Rev. Lett. **81**, 4576 (1998).
5. E. Auge *et al.*, Phys. Lett. B **168**, 163 (1986).
6. P. Aurenche *et al.*, Phys. Lett. B **135**, 164 (1984).
7. K. Wijesooriya *et al.*, Phys. Rev. Lett. **14**, 2975 (2001).
8. K. Wijesooriya *et al.*, Phys. Rev. Lett. **66**, 034614 (2002).
9. S.J. Brodsky *et al.*, Phys. Lett. B **449**, 306 (1997).
10. X. Ji, Phys. Rev. D **55**, 7114 (1997).

11. X. Ji, J. Osborne, Phys. Rev. D **58**, 094018 (1998).
12. A.V. Radyushkin, Phys. Rev. D **56**, 5524 (1997).
13. J.C. Collins *et al.*, Phys. Rev. D **56**, 2982 (1997).
14. C.E. Carlson, A.B. Wakely, Phys. Rev. D **48**, 2000 (1993).
15. A. Afanasev, C.E. Carlson, C. Wahlquist, Phys. Rev. D **58**, 054007 (1998).
16. Z. Bar-Yam *et al.*, Phys. Rev. Lett. **19**, 40 (1967).
17. P. Heide *et al.*, Phys. Rev. Lett. **21**, 248 (1968).
18. A.M. Boyarski *et al.*, Phys. Rev. Lett. **21**, 1767 (1968).
19. H. Gao, R. Holt *et al.*, JLab experiment E94-104.
20. R.L. Anderson *et al.*, Phys. Rev. D **14**, 679 (1976).
21. L.Y. Zhu *et al.*, in preparation.
22. S.J. Brodsky, G.R. Farrar, Phys. Rev. Lett. **31**, 1153 (1973).
23. S.J. Brodsky, G.R. Farrar, Phys. Rev. D **11**, 1309 (1975).
24. V.A. Matveev *et al.*, Lett. Nuovo Cimento **7**, 719 (1973).
25. G. Zweig, Nuovo Cimento **32**, 689 (1964).
26. P. Stichel, Z. Phys. **178**, 519 (1964).

Eur. Phys. J. A **18**, 417–419 (2003)
DOI 10.1140/epja/i2002-10249-7

THE EUROPEAN PHYSICAL JOURNAL A

$\pi\pi$ correlations in $\gamma + A$ reactions

J.G. Messchendorp[a]

For the TAPS and A2 Collaborations
II. Physikalisches Institut, University of Gießen, Germany

Received: 30 September 2002 /
Published online: 22 October 2003 – © Società Italiana di Fisica / Springer-Verlag 2003

Abstract. Preliminary differential cross-sections of the reactions $A(\gamma, \pi^0\pi^0)$ and $A(\gamma, \pi^0\pi^+ + \pi^0\pi^-)$ with $A = {}^1$H, ^{12}C, and ${}^{\rm nat}$Pb are presented. A significant nuclear-mass dependence of the $\pi\pi$ invariant-mass distribution is found in the $\pi^0\pi^0$ channel. The dependence is not observed in the $\pi^0\pi^\pm$ channel. The in-medium observation in the $\pi^0\pi^0$ channel is consistent with an in-medium modification of the $\pi\pi$ interaction in the $I = J = 0$ channel, changing width and pole position of a $\pi\pi$ resonant state.

PACS. 13.60.Le Meson production – 21.65.+f Nuclear matter

1 Introduction

One of the challenges in nuclear physics is to study the properties of hadrons embedded in a nuclear many-body system. This contribution reports on the photoproduction of correlated pion pairs on nuclei in the scalar-isoscalar $J = I = 0$ channel, also known as the σ-meson. In ref. [1] the σ-meson is identified as the $f_0(400\text{–}1200)$. The large natural width in free space of $\Gamma = 400\text{–}500$ MeV [2] makes it doubtful that this particle is a mesonic $q\bar{q}$ state. Alternatively, the σ-meson is considered to be a resonant state of two pions [3,4]. In vacuum, the $\pi\pi$ system is mildly attractive. However, in the nuclear medium the $\pi\pi$ interaction strength could increase thereby changing width and pole position of the resonant state. Experimental data on correlated $\pi\pi$ pairs in dense nuclear matter can clarify the nature of the σ-meson.

The first measurement of the in-medium $\pi\pi$ mass was obtained by a pion-induced experiment by the CHAOS Collaboration [5]. A rising accumulation of strength at low $\pi^+\pi^-$ mass was observed with increasing nuclear mass whereas such an enhancement was not seen in the $\pi^+\pi^+$-mass distributions. This effect was interpreted as a signature for an in-medium modification of the $\pi\pi$ interaction in the $I = J = 0$ channel. A similar effect was found by a pion-induced experiment of the Crystal Ball Collaboration [6] where a nuclear-mass dependence of the $\pi^0\pi^0$-mass distribution was observed.

For the interpretation of the pion-induced measurements the strong interaction of the initial-state pion with the medium has to be taken into account. As a result, only the surface of the nucleus is probed, leading to a small effective nuclear density. It was proposed to produce in-medium $\pi\pi$ pairs with electromagnetic probes which illuminate the complete nucleus and lead to a larger effective density.

In this contribution, measurements of $A(\gamma, \pi^0\pi^0)$ and $A(\gamma, \pi^0\pi^\pm)$ for $A = {}^1$H, ^{12}C, and ${}^{\rm nat}$Pb are presented. The measurements allow to study the different $\pi\pi$-isospin states at average effective densities of 35% (^{12}C) to 65% (^{208}Pb) [7] of the interior nuclear density of $0.17\,\text{fm}^{-3}$. Data are presented for an incident-photon energy of $E_\gamma = 400\text{–}460$ MeV. The energy was chosen to be small to minimize the effect of final-state interactions of the two pions with the medium and to prevent background from the $\eta \to 3\pi^0$ channel.

2 Experiment and analysis

The experiment was performed at the photon-beam facility at MAMI-B. Tagged photons [8] were produced with energies between 200 and 820 MeV. The beam intensity in the energy range of interest, $E_\gamma = 400\text{–}460$ MeV, was $10^7\,\text{s}^{-1}$ with a photon-energy resolution of about 2 MeV. A series of measurements were carried out using liquid-hydrogen, carbon, and lead targets.

The angles and energies of the pions were measured using the TAPS photon spectrometer [9] consisting of 510 hexagonal BaF_2 scintillators. The detector is depicted in fig. 1. The complete setup covered $\approx$ 40% of the total solid angle. Photons and charged pions were identified by exploiting the time-of-flight information of each detector. A 5 mm thick plastic scintillator was placed in front of each crystal to differentiate between neutral and charged particles.

Neutral pions were identified by an invariant-mass analysis of the two decay photons. For the identification of

[a] e-mail: messchendorp@kvi.nl

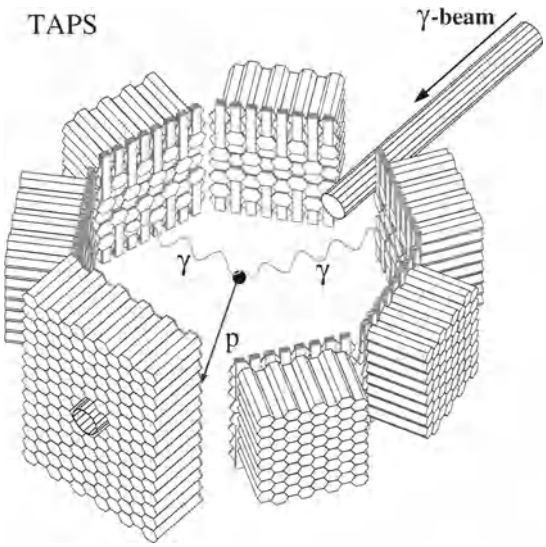

Fig. 1. The photon spectrometer TAPS consisting of 510 hexagonal BaF_2 scintillators and the 5 mm thick plastic scintillators. An event originating from π^0 production on a quasi-free proton is illustrated.

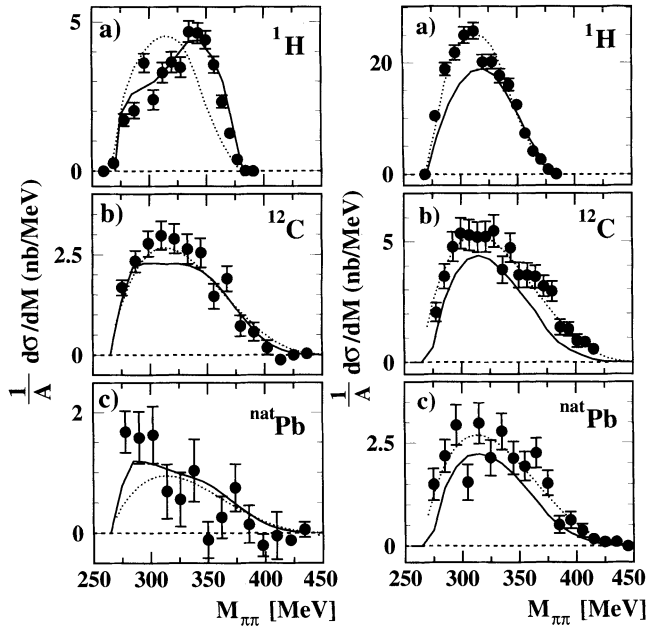

Fig. 2. Preliminary differential cross-sections of the reaction $A(\gamma, \pi^0\pi^0)$ (left panel) and $A(\gamma, \pi^0\pi^\pm)$ (right panel) for incident photons in the energy range of 400–460 MeV (solid circles). Error bars denote statistical uncertainties and the curves are explained in the text.

the $A(\gamma, \pi^0\pi^0)$ reaction, all four final-state photons were registered in the detector. Charged pions from $A(\gamma, \pi^0\pi^\pm)$ were selected by exploiting the information on the time-of-flight of the charged pion relative to the one of the photons of the π^0 decay and its deposited energy in the BaF_2 crystals [10]. Since the TAPS detector does not include a magnetic field, positively charged particles cannot be discriminated from negatively charged particles.

The dominant reaction mechanism in $A(\gamma, \pi^0\pi^0)$ and $A(\gamma, \pi^0\pi^\pm)$ channels is the quasi-free production on the constituent nucleons. Under this assumption, the undetected recoil nucleon was deduced from the incident photon energy and the momenta of the final-state pions. Its reconstructed mass distribution was found to be consistent with Monte Carlo simulations using a quasi-free event generator. The background of the $\eta \to 3\pi^0$ production channel does not contribute, since the incident-photon energy of $E_\gamma = 400$–460 is below the η production threshold.

3 Results and discussion

The measured $M_{\pi^0\pi^0}$-mass distributions for incident-photon energies of $E_\gamma = 400$–460 MeV are shown in the left panel of fig. 2. A strong increase in strength towards small $M_{\pi^0\pi^0}$ with increasing A is observed. The dotted curves in fig. 2 indicate phase space distributions. The experimentally observed peak position for $A = {}^1$H (a) lies higher than the phase space prediction, whereas for $A = {}^{12}$C (b) the measured mass distribution is compatible with phase space. For $A = {}^{nat}$Pb (c), most of the observed strength lies below the peak of the phase space distribution. The experimentally determined angular distributions in the $A(\gamma, \pi^0\pi^0)$ reaction of the $\pi^0\pi^0$ center-of-mass system are found to be isotropic [10] and are compatible with $J = 0$, supporting the conclusion that a significant A-dependence is found in the $\pi\pi$ $I = J = 0$ channel in photon-induced reactions.

The right panel of fig. 2 depicts preliminary results of the reactions $A(\gamma, \pi^0\pi^\pm)$. The data do not show an A-dependence in shape as was observed in the corresponding $M_{\pi^0\pi^0}$ distributions. For all targets, the data follow the phase space distributions depicted as dotted curves, indicating that significant in-medium effects in the isospin $I = 1$ channel are not observed. Furthermore, this observation indicates that the in-medium modification in the $\pi^0\pi^0$ channel cannot be explained by final-state interactions of the individual pions with the medium, as a similar behaviour for both exit channels would otherwise be expected.

The solid curves in fig. 2 are predictions by Roca *et al.* [4,7]. Here, the meson-meson interaction in the scalar-isoscalar channel is studied in the framework of a chiral-unitary approach at finite baryonic density. The model dynamically generates the σ-resonance, reproducing the meson-meson phase shifts in vacuum and accounts for the absorption of the pions in the nucleus. It qualitatively predicts a mass shift as observed in the $\pi^0\pi^0$ data. The basic ingredient driving this shift is the p-wave interaction of the pion with the baryons in the medium, resulting in an in-medium modification of the $\pi\pi$ interaction. A similar calculation [11] is not able to describe the observed A-dependence effect in the $A(\pi^-, \pi^0\pi^0)$ data [6], which might be due to the interaction of the initial-state pion. Since the σ-resonance does not couple to $\pi^0\pi^\pm$, the model does not show significant change in the shape of the mass distributions between $A = $ H, $A = {}^{12}$C, and $A = {}^{nat}$Pb,

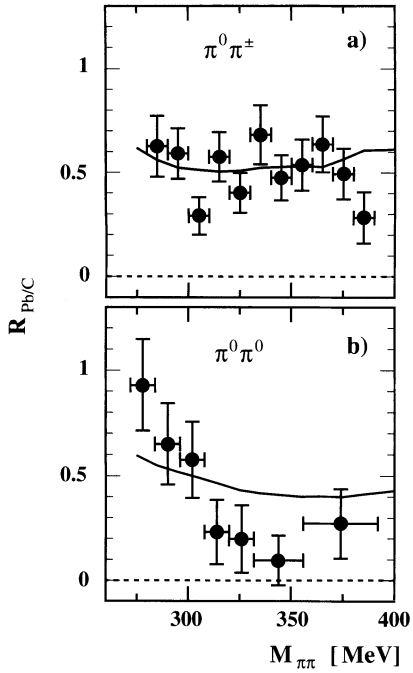

Fig. 3. Preliminary ratios between the differential cross-sections for $A = {}^{\text{nat}}\text{Pb}$ and $A = {}^{12}\text{C}$ for $A(\gamma, \pi^0\pi^\pm)$ (a) and $A(\gamma, \pi^0\pi^0)$ (b). The solid curves represent predictions by Roca *et al.* [4,7].

which agrees with the experimental observation as shown in the right panel of fig. 2.

Figure 3 shows the ratio $R_{\text{Pb/C}}$ between the differential cross-sections per nucleon for $A = {}^{\text{nat}}\text{Pb}$ and $A = {}^{12}\text{C}$ of the reactions $A(\gamma, \pi^0\pi^\pm)$ (a) and $A(\gamma, \pi^0\pi^0)$ (b) up to $M_{\pi\pi}$ masses of 400 MeV. The ratio $R_{\text{Pb/C}}$ indicates that about half of the final-state pions is absorped in the nucleus. The final-state effects of the pions become larger with increasing mass number A. The experimentally determined ratio $R_{\text{Pb/C}}$ for the $\pi^0\pi^\pm$ reaction is found to be flat, indicating that final-state interactions, absorption, and rescattering of the individual pions with the medium do not modify the shape in the mass distribution significantly. The model of Roca *et al.* [7] supports this conclusion as can be observed from the solid curve. Furthermore, the predictions for $R_{\text{Pb/C}}$ agree in magnitude with the experimental data, which indicates that the final-state effects of pions are properly taken into account by the calculations. In contrast to the $\pi^0\pi^\pm$ data, a significant in-medium shape effect is observed in the ratio $R_{\text{Pb/C}}$ for the $\pi^0\pi^0$ channel as depicted in fig. 3(b). Since final-state interactions of neutral and charged pions are expected to be similar, such large effect cannot be explained by an A-dependence in the final-state interactions of the individual pions with the medium. Hence, the observed in-medium effect points to an A-dependence in the $I = J = 0$ $\pi\pi$ interaction. The prediction by Roca *et al.* [4] with a theoretical uncertainty of 10% [7] is depicted as the solid curve in fig. 3(b).

4 Conclusion

An effect consistent with a significant in-medium modification in the $A(\gamma, \pi^0\pi^0)$ ($I = J = 0$) channel has been observed. With increasing A, the strength in these distributions is shifting towards smaller invariant masses. Earlier measurements using pion beams found a similar, but less pronounced effect. Photon-induced experiments have the advantage that initial-state interactions are absent and larger effective densities can be reached which enhance in-medium effects. The distortion of the $\pi\pi$-mass distribution due to final-state interactions of the individual pions with the constituents of the nucleus has been studied by measuring the $\pi^0\pi^\pm$ mass distribution concurrently. A significant in-medium effect was not observed. According to Roca *et al.* [4], a dominant part of the modification observed in the $\pi^0\pi^0$-mass distributions can be attributed to a change of the $\pi\pi$ interaction. The comparison with the experimental data hints at the nature of the σ-meson as a $\pi\pi$-resonance.

The author gratefully acknowledges the outstanding support of the accelerator group of the Mainz Microtron MAMI, as well as the other technicians and scientists of the Institut für Kernphysik at the Universität Mainz. We thank E. Oset, M.J. Vicente Vacas, and L. Roca for making their calculations available to us prior to publication. We also acknowledge many fruitful discussions with W. Cassing, R. Meier, B. Nefkens, and E. Oset. The data are part of the dissertations of S. Janssen and M.J. Kotulla. This work was supported by the Deutsche Forschungsgemeinschaft (SFB 201), the U.K. Engineering and Physical Sciences Research Council, and the Schweizerischer Nationalfond.

References

1. D.E. Groom *et al.*, Eur. Phys. J. C **15**, 1 (2000).
2. J.A. Oller *et al.*, Phys. Rev. Lett. **80**, 3452 (1998).
3. E. Oset *et al.*, nucl-th/0112033, 2001.
4. L. Roca *et al.*, Phys. Lett. B **541**, 77 (2002).
5. F. Bonutti *et al.*, Phys. Rev. Lett. **77**, 603 (1996).
6. A. Starostin *et al.*, Phys. Rev. Lett. **85**, 5539 (2000).
7. L. Roca, E. Oset, M.J. Vicente Vacas, private communications.
8. I. Anthony *et al.*, Nucl. Instrum. Methods A **301**, 230 (1991).
9. A.R. Gabler *et al.*, Nucl. Instrum. Methods A **346**, 168 (1994).
10. S. Janssen, dissertation, University of Gießen (2002).
11. M.J. Vicente Vacas, E. Oset, Phys. Rev. C **60**, 064621 (1999).

Eur. Phys. J. A **18**, 421–424 (2003)
DOI 10.1140/epja/i2002-10250-2

THE EUROPEAN PHYSICAL JOURNAL A

ηN final-state interaction in incoherent photoproduction of η-mesons from the deuteron

S. Schneider[1,a], A. Sibirtsev[1], Ch. Elster[1,2], J. Haidenbauer[1], S. Krewald[1], and J. Speth[1]

[1] Institut für Kernphysik, Forschungszentrum Jülich, D-52425 Jülich, Germany
[2] Institute of Nuclear and Particle Physics, Ohio University, Athens, OH 45701, USA

Received: 30 September 2002 /
Published online: 22 October 2003 – © Società Italiana di Fisica / Springer-Verlag 2003

Abstract. An analysis of incoherent photoproduction of η-mesons from the deuteron is presented. We concentrate here on the threshold region. The dominant contribution, the γN-ηN amplitude is described within an isobar model. Effects of the final-state interaction in the NN as well as the ηN systems are included by employing models derived within a meson-exchange approach.

PACS. 13.60.Le Meson production – 13.75.Cs Nucleon-nucleon interactions (including antinucleons, deuterons, etc.) – 14.40.Aq Π, K, and η mesons

1 Introduction

The incoherent photoproduction of η-mesons from the deuteron near threshold offers an opportunity to gain insight into the final-state interactions between the outgoing nucleons and the η-meson. Measurements by the TAPS Collaboration [1,2] at MAMI on photoproduction of η-mesons from ^{2}H and ^{4}He show an enhancement in the total cross-sections close to the reaction threshold. Such a threshold enhancement was also observed in π, η, η' and ω production in NN collisions at IUCF, COSY and CELSIUS [3–7]. With the exception of η production, this threshold enhancement could be well described by theoretical calculations including the NN final-state interaction [6,7]. For the η production, also the ηN final-state interaction could play a role [4].

Our knowledge of the ηN interaction is rather poor. Values of the scattering length have been extracted from reactions like $\pi N \to \eta N$ and $\gamma N \to \eta N$. Their real parts range from 0.25 fm to 1.05 fm, as indicated in fig. 1. It is important to study a wider class of η production reactions in order to see to what extent predicted values are compatible with each other.

We now investigate the effect of the ηN interaction in the reaction $\gamma d \to np\eta$. We take into account the lowest-order contributions of the scattering series: the impulse approximation and the NN and ηN final-state interactions.

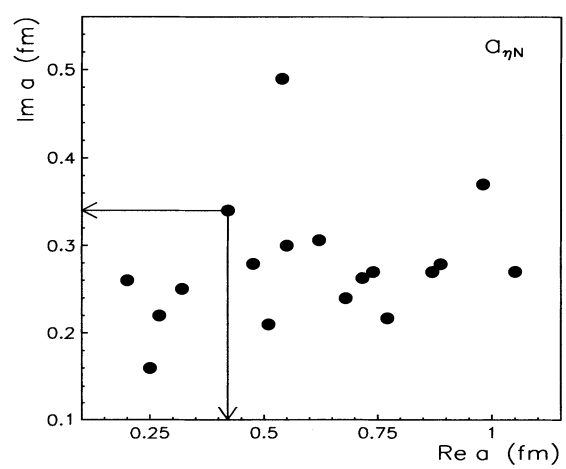

Fig. 1. The real and imaginary parts of the ηN scattering length as reviewed in [8]. The arrows indicate the value employed in our work.

2 The reaction γd $\to$ npη

The photoproduction amplitude for η-mesons on a single nucleon is described within an isobar model. We only consider the dominant contribution via excitation of the $S_{11}(1535)$-resonance, since other contributions as from t-channel vector meson exchange and the nucleon pole graph were found to be negligible [9,10]. Details of the production mechanism can be found in ref. [11].

For the reaction $\gamma d \to np\eta$ the amplitude $\mathcal{M}_{\rm IA}$ of the impulse approximation can be written as

$$\mathcal{M}_{\rm IA} = A^T(s_1)\Phi(p_2) - (-1)^{S+T}A^T(s_2)\Phi(p_1). \quad (1)$$

[a] e-mail: s.schneider@fz-juelich.de

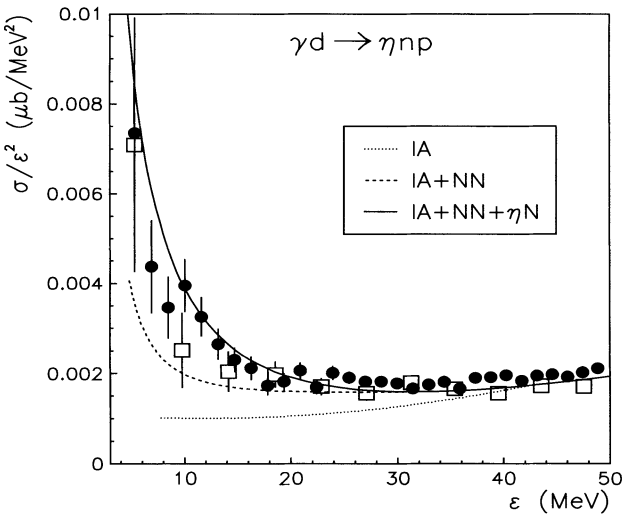

Fig. 2. The total cross-sections divided by ϵ^2 for incoherent η photoproduction off the deuteron as a function of the excess energy ϵ. The dotted line shows the impulse approximation, the dashed line results from inclusion of the NN final-state interaction, and the solid line shows the full calculation, including in addition the ηN final-state interaction. The data are from refs. [1] (squares) and [2] (circles).

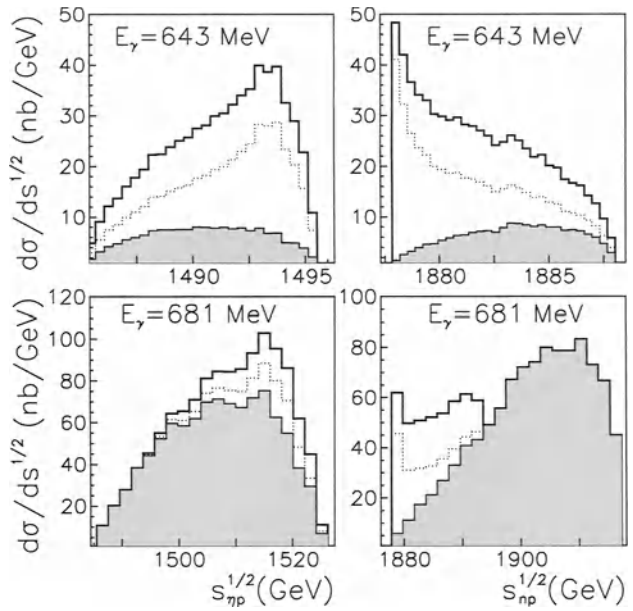

Fig. 3. The invariant-mass spectra of the ηp and the np systems in the reaction $\gamma d \to np\eta$. The shaded areas show the results for the impulse approximation, the dashed line was calculated by including also the np final-state interaction, while the solid line represents the full calculation including np and ηN FSI.

Here, S and T denote the spin and isospin of the outgoing two-nucleon system, $\Phi(p_i)$ stands for the deuteron wave function, p_1 and p_2 are the momenta of the proton or neutron in the deuteron rest frame, and $A^T(s_i)$ gives the η-meson photoproduction amplitude at the invariant collision energy of the corresponding γ-nucleon system.

In the next order of the scattering series, the final-state interaction between the two nucleons and between the η and a nucleon have to be accounted for. The np scattering matrix in the $^1S_0$ and $^3S_1$ partial waves was taken from the CD-Bonn potential [12]. However, it should be pointed out that the use of other realistic NN potentials did not have any observable effect on the results. This is not too surprising, for the deuteron wave function falls off rapidly with increasing momentum. Thus it cuts off contributions from higher off-shell momenta in the intermediate NN state, for which the differences in the various NN models are most pronounced.

Finally, to obtain the ηN scattering amplitude in the S_{11} partial wave, we employ the Jülich coupled-channel meson-exchange model developed for πN scattering [13].

The results for the total cross-sections of the reaction $\gamma d \to np\eta$ are shown in fig. 2. Here we divide our calculations and the data by the square of the excess energy, $\epsilon = \sqrt{s} - m_n - m_p - m_\eta$, since the phase space is proportional to ϵ^2. This representation is more illustrative when considering deviations from the energy dependence of the phase space. While the agreement of the calculation within the impulse approximation (dotted line) with the data is quite good for excess energies $\epsilon > 40\,\mathrm{MeV}$, in the threshold region we observe a sizeable underestimation.

The inclusion of the np and ηN FSI in the s-waves leads to an enhancement in the threshold region while it has no effect for $\epsilon > 40\,\mathrm{MeV}$. The results of the full calculation (solid line) are in good agreement with the data.

It may be instructive to study the interplay between the impulse approximation and the final-state interactions more closely. In fig. 3 we present the calculated mass spectra in the ηp and np system, respectively. The shaded areas stand for the invariant-mass distributions resulting from the impulse approximation alone, the dashed lines show the results including the np final-state interaction, and the solid lines show the results of the full calculation.

The full calculation differs from the impulse approximation not only in size, but also in shape. For the lower photon energy, $E_\gamma = 643\,\mathrm{MeV}$, the inclusion of np FSI enhances the cross-section substantially, especially for small np invariant masses. This forces the cross-section also to peak at higher ηp invariant masses. The inclusion of the ηN FSI in addition does not change the shape of both distributions but leads to an overall enhancement. At $E_\gamma = 681\,\mathrm{MeV}$, the shape of the ηp mass distribution is similar to that at $E_\gamma = 643\,\mathrm{MeV}$. The np system shows a double-peak structure with a pronounced peak at high invariant masses coming from the impulse approximation and a structure at low invariant masses which is due to the NN and ηN final-state interactions. The observation of such a double-peak structure could serve as direct evidence of the presence of FSI effects. It should be mentioned that the analysis of the reaction $pp \to pp\eta$ measured at COSY [14] shows quite a similar structure in the pp invariant-mass spectra.

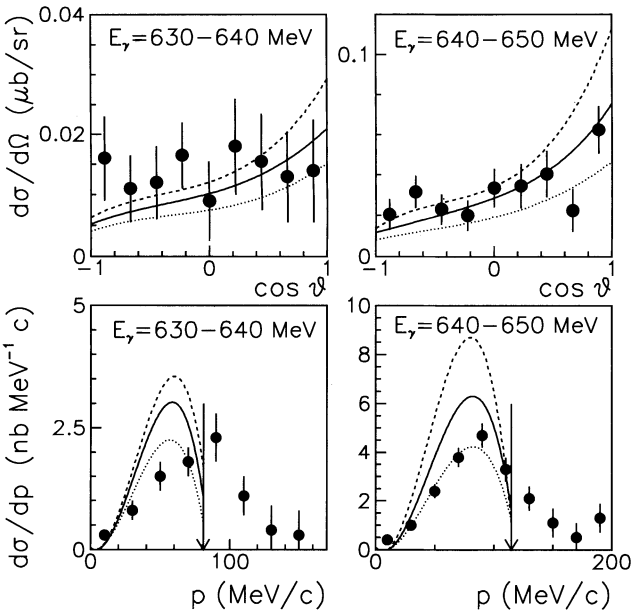

Fig. 4. The angular (upper part) and momentum (lower part) distributions of the η-meson in the γd center-of-mass system. The lines show our calculations with different scattering lengths: $a_{\eta N} = 0.42 + i0.32$ (solid), $0.74 + i0.27$ (dashed) and $0.25 + i0.16$ fm (dotted). The data are from ref. [2]. The arrows show the kinematical limit for η-meson momenta.

It is interesting to investigate to what extent our results depend on the properties of the ηN interaction employed. In [8] we found that the amplitude calculated with the ηN t-matrix from the full model is numerically identical to the amplitude obtained from an effective range expansion of the same t-matrix,

$$\left[iq - \frac{1}{a_{\eta N}}\right]^{-1} = \pi \frac{\sqrt{q^2+m_N{}^2}\sqrt{q^2+m_\eta{}^2}}{\sqrt{q^2+m_N{}^2}+\sqrt{q^2+m_\eta{}^2}} t_{\eta N}(q,q), \quad (2)$$

where q is the on-shell momentum of the η-meson in the ηN center-of-mass system. This can be explained through the good description of the (on-shell) ηN scattering matrix by the effective range expansion up to $q \approx 350$ MeV, as well as through the weak dependence of the half-shell ηN t-matrix on the off-shell momentum. The scattering length $a_{\eta N}$ calculated from the Jülich πN model is

$$a_{\eta N} = 0.42 + i0.34\,\text{fm}\,. \quad (3)$$

This lies roughly in the mid-range of the values for $a_{\eta N}$ given in the literature spreading from $0.25 + i0.16$ fm to $1.05 + i0.27$ fm.

Since we found the effective range expansion to give the same results for the ηN amplitude as the full calculation with the Jülich model, we can now investigate the influence of the strength of the low-energy ηN interaction on the observables of the reaction $\gamma d \to np\eta$. Figure 4 shows the angular and momentum distributions of the η-meson in the threshold region, together with our calculations for $a_{\eta N} = 0.42 + i0.34$ fm (solid line), $a_{\eta N} = 0.25 + i0.16$ fm [15] (dotted line) and $a_{\eta N} = 0.74 + i0.27$ fm [16] (dashed line). In order to make the theoretical predictions comparable to experiment, the result of the calculation was averaged over the energy bins. For the momentum distributions, the arrows indicate the maximum of the kinematically allowed momenta of the η-meson for the maximal photon energy in the energy bin. In the shown momentum spectra, a substantial fraction of the data lies above this limit, indicating perhaps a larger experimental uncertainty in the determination of the η momentum. Unfortunately, we can thus not make a clean comparison between our results and the data. However, we can observe that the data show a preference for smaller values of the ηN scattering length.

3 Conclusion

We calculated total and differential cross-sections for the reaction $\gamma d \to np\eta$ taking into account the dominant contribution from the $S_{11}(1535)$-resonance in the production amplitude as well as the final-state interactions in the NN and ηN systems. FSI effects enhance the cross-sections close to the reaction threshold, at higher energies they have no influence. The Dalitz plots show an enhancement at low invariant masses of the np subsystem due to the inclusion of final-state interaction. At $E_\gamma = 681$ MeV this enhancement leads to a double-peak structure. The experimental observation of such a structure could serve as direct evidence for the presence of FSI effects.

We found that the uncertainty of our calculation is dominated by the uncertainty in the value of the ηN scattering length $a_{\eta N}$. For our calculation we employed the Jülich meson-baryon model and found our results to be compatible with the data. The data taken in the threshold region show a sensitivity to the size of $a_{\eta N}$ and favour smaller values for the real part of the scattering length.

References

1. B. Krusche *et al.*, Phys. Lett. B **358**, 40 (1995).
2. V. Hejny *et al.*, Eur. Phys. J. A **13**, 493 (2002).
3. H.O. Meyer *et al.*, Phys. Rev. Lett. **65**, 2846 (1990); H.O. Meyer *et al.*, Nucl. Phys. A **539**, 633 (1992).
4. H. Calén *et al.*, Phys. Lett. B **366**, 39 (1996); H. Calén *et al.*, Phys. Rev. Lett. **80**, 2069 (1998).
5. P. Moskal *et al.*, Phys. Rev. Lett. **80**, 3202 (1998); P. Moskal *et al.*, Phys. Lett. B **474**, 416 (2000).
6. P. Moskal *et al.*, Phys. Lett. B **482**, 356 (2000).
7. For an overview and further references see, *e.g.*, H. Machner, J. Haidenbauer, J. Phys. G **25**, R231 (1999).
8. A. Sibirtsev, S. Schneider, Ch. Elster, J. Haidenbauer, S. Krewald, J. Speth, Phys. Rev. C **65**, 044007 (2002).
9. G. Knöchlein, D. Drechsel, L. Tiator, Z. Phys. A **352**, 327 (1995).
10. M. Benmerrouche, N.C. Mukhopadhyay, Phys. Rev. D **51**, 3237 (1995).

11. A. Sibirtsev, Ch. Elster, J. Haidenbauer, J. Speth, Phys. Rev. C **64**, 024006 (2001).
12. R. Machleidt, Phys. Rev. C **63**, 024001 (2001).
13. O. Krehl, C. Hanhart, S. Krewald, J. Speth, Phys. Rev. C **62**, 025207 (2000).
14. E. Roderburg and the TOF Collaboration, IKP/COSY Annual Report 2001.
15. C. Bennhold, H. Tanabe, Nucl. Phys. A **530**, 625 (1991).
16. A.M. Green, S. Wycech, Phys. Rev. C **55**, R2167 (1997).

Eur. Phys. J. A **18**, 425–427 (2003)
DOI 10.1140/epja/i2002-10251-1

THE EUROPEAN PHYSICAL JOURNAL A

Prospects for measurements of parity-violating photoproduction of $\pi^{\pm}$

J.W. Martin[a]

W.K. Kellogg Radiation Laboratory 106-38, California Institute of Technology, Pasadena, CA 91125, USA

Received: 30 September 2002 /
Published online: 22 October 2003 – © Società Italiana di Fisica / Springer-Verlag 2003

Abstract. I address the experimental feasibility of two measurements related to the photoproduction of pions, in the context of the G^0 experiment. The first involves an extraction of the parity-violating pion-nucleon coupling constant $h^{(1)}_{\pi NN}$ via a measurement of parity-violating threshold pion photoproduction. The second involves an extraction of d_Δ, which parameterizes parity-violating photoproduction of pions on the Δ-resonance. The second process might have an anomalously large asymmetry, from a model based on hyperon decays.

PACS. 11.30.Er Charge conjugation, parity, time reversal, and other discrete symmetries – 13.60.Le Meson production – 14.20.Gk Baryon resonances with $S = 0$

1 Physics and motivation

1.1 Threshold pion photoproduction: a possibility to extract $h^{(1)}_{\pi NN}$

The constant $h^{(1)}_{\pi NN}$ (sometimes called h_π, H^1_π, f_π, etc.) is the parity-violating isovector pion-nucleon coupling. This coupling constant is believed to be particularly sensitive to weak neutral currents inside the nucleon. It is also poorly constrained both theoretically and experimentally.

Theoretical estimates give $h^{(1)}_{\pi NN} = 0\text{–}11 \times 10^{-7}$, and a commonly referred to theoretical benchmark is the Desplanques, Donohue, and Holstein (DDH) "best value" [1] $h^{(1)}_{\pi NN}(\text{DDH}) = 4.6 \times 10^{-7}$. The current experimental results span the full theoretical range and tend to disagree with one another. The most sensitive measurements have been performed using various nuclei. This situation motivates new precise measurements with light nuclei.

Parity-violating threshold photoproduction of pions has recently been theoretically related to $h^{(1)}_{\pi NN}$ in the framework of chiral perturbation theory [2]. Calculations of the cross-section in this framework are good to roughly 10%.

The asymmetry in the parity-violating process is directly proportional to $h^{(1)}_{\pi NN}$. For the DDH value of $h^{(1)}_{\pi NN}$, the resultant asymmetry is $A_\gamma(\text{DDH}) = 2.5 \times 10^{-7}$.

1.2 Photoproduction of pions on the Δ-resonance: a measurement of d_Δ

As part of the G^0 backward angle measurements [3] of parity-violating elastic and quasi-elastic electron scattering, inelastic electron scattering will also be detected. A separate proposal exists for the inelastic measurements that will be carried out [4].

Recently, the electroweak radiative corrections to this process were calculated [5]. They depend on two new parameters that are theoretically difficult to estimate: a_Δ and d_Δ. The contribution of d_Δ is expected to be larger. However, d_Δ can be extracted from charged-pion photoproduction on the Δ-resonance [6].

The size of d_Δ has been estimated from a model of hyperon non-leptonic and weak-radiative decays, referred to as the resonance saturation model [7]. This model is known to solve two problems in hyperon decay:

- it fits simultaneously the S-wave and P-wave strength in hyperon non-leptonic decay,
- it generates the large asymmetries observed in hyperon weak-radiative decays that are forbidden by $SU(3)$ symmetry.

The model accomplishes this by allowing for mixing with intermediate negative-parity states that are higher resonances. Incorporating all the resonances allows enough freedom to adequately describe the hyperon decay data.

In the case of the $N \to \Delta$ transition, this gives extra freedom in the ranges that d_Δ can have. Constraining the mixing amplitudes based on the resonance saturation model gives a value for d_Δ in the range 10–25 g_π,

[a] For the G^0 Collaboration; e-mail: jmartin@krl.caltech.edu

where $g_\pi \equiv G_F F_\pi^2/2\sqrt{2} = 5 \times 10^{-8}$ is the scale of weak charged-current hadronic processes. This is many times the result obtained from naive dimensional analysis, which would give $d_\Delta \sim g_\pi$. The asymmetry could be further enhanced by V_{ud}/V_{us} as well as neutral-current contributions, increasing the value of d_Δ by up to a factor of four. The authors of ref. [6] therefore quote a "reasonable range" of $d_\Delta = 1 - 100 g_\pi$, with a best value $d_\Delta(\text{ZHMRM}) = 25 g_\pi$. The charged-pion photoproduction asymmetry is directly proportional to d_Δ, and for the best value of d_Δ, the parity-violation asymmetry has a value $A_\gamma(\text{ZHMRM}) = 1.3 \times 10^{-6}$.

2 Experimental possibilities for G^0

The G^0 experiment will measure quasi-elastic electron scattering from an LD_2 target at backward angles. A large background from the photoproduction of π^-, will exist for these backward angles. Čerenkov detectors will be constructed to reject this pion background [3]. Instead we may try to use these photoproduced pions for physics.

2.1 $h^{(1)}_{\pi NN}$

The G^0 backward angle measurements are conducted at too high an energy and with too low a luminosity for them to be useful for a measurement of $h^{(1)}_{\pi NN}$. The beam energy would have to be reduced to 335 MeV, and the beam current increased to about 400 μA. Such a low-energy, high-current beam has never been produced at Jefferson Lab and significant development would have to be done.

Nonetheless, given the chance of such a beam, we can study the experimental feasibility of such a measurement.

Such a high current would cause significant boiling in any known liquid target. One way to get around this problem would be to run the beam through a radiator, then divert the scattered electrons to a beam dump, keeping only the polarized photons to interact with the liquid target. Another possibility would be to use a solid nuclear target (such as a 20% radiation length of carbon) that will not boil. However, this solution is less attractive, as it requires a nucleus, and would possibly introduce nuclear uncertainties into the extraction of $h^{(1)}_{\pi NN}$.

Two studies were carried out for G^0:

- using a liquid-hydrogen target and diverting the electron beam after a 10% radiator to achieve a polarized photon beam,
- using a thick (20% r.l.) solid carbon target which itself provides a Bremsstrahlung flux of real photons.

The G^0 spectrometer magnet current and beam energy were chosen to maximize pion rates in the threshold region (defined in ref. [2]). The experimental parameters for the two possibilities, and the resultant G^0 coincidence rates and statistical uncertainties for 800 hours of running are shown in table 1. From these studies, it can be seen that a several hundred MHz rate must be accepted in order to achieve a reasonable statistical accuracy. Because this would result in unacceptably high accidental coincidence rates, it would likely be necessary to convert the G^0 CED/FPD setup to an integrating mode. This would make the apparatus more susceptible to backgrounds, and would require further study.

Table 1. Experimental parameters for two possible versions of an $h^{(1)}_{\pi NN}$ measurement using the G^0 apparatus.

Beam energy	335 MeV	
Beam current	400 μA	
Beam polarization	80%	
Target	40 cm LH_2	20% r.l. carbon
Radiator thickness	10% r.l.	half of target
CED/FPD coincidence rate	396 MHz	500 MHz
A_γ(DDH)	2.4×10^{-7}	
δA_γ(DDH)	18%	16%

In order to perform this experiment using the G^0 apparatus, significant changes to the setup would have to be made.

2.2 d_Δ

By contrast, an extraction of d_Δ appears to be within the reach of the backward-angle phase of the G^0 experiment, with a few relatively minor modifications. In fact the π^- that would be accepted by the experiment in a future run at 424 MeV beam energy on an LD_2 target would have kinematics such that they are on or very close to the Δ-resonance! The experiment could be conducted with either positive pions and a liquid-hydrogen target, or negative pions and a liquid-deuterium target.

Two cases were explored for the possibility of measuring d_Δ:

- Normal G^0 running at 424 MeV on LD_2 target with nominal 40 μA beam currrent and nominal G^0 spectrometer magnet settings.
- Additional running with the spectrometer tuned to maximally accept pions on the Δ-resonance.

Note that the first case would require additional electronics to be purchased for the experiment. The second case would require additional running, and therefore the addition of a radiator to boost the photoproduction rate was also considered.

The asymmetry calculated in ref. [6] assumes no background. However, physics backgrounds due to non-resonant pion production and multi-pion production can occur. For non-resonant background, it can be argued that the asymmetry is likely small, due to the fact that the asymmetry must be proportional to $h^{(1)}_{\pi NN}$. Therefore, this background can be treated as a dilution. A preliminary estimate of the non-resonant background finds that this background accounts for roughly 40% of the total rate. Multi-pion production was found to be nearly kinematically forbidden, and the background due to this process is therefore negligible.

Table 2. Experimental parameters for two possible versions of a d_Δ measurement using the G^0 apparatus.

	Standard G^0	Δ Tune
Beam energy	424 MeV	
Beam current	40 μA	
Beam polarization	80%	
Radiator thickness	half target + virtual photons	
Pion rate	6.8 MHz	22 MHz
A_γ(ZHMRM)	1.3×10^{-6}	
δA_γ(ZHMRM)	47%	27%
δd_Δ	$12 g_\pi$	$7 g_\pi$

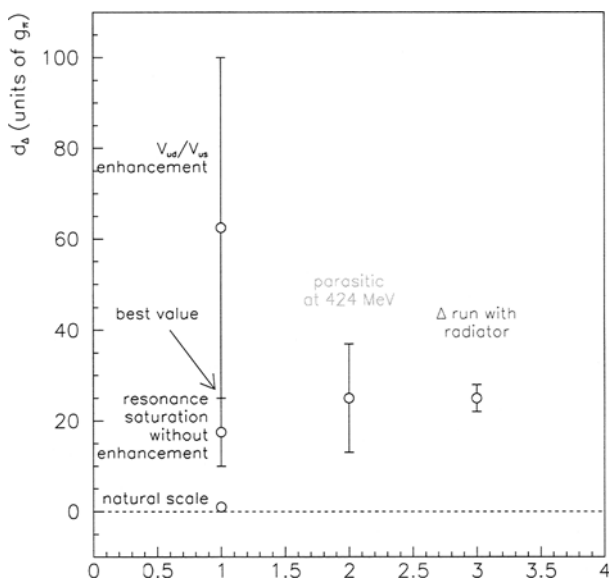

Fig. 1. Summary of theoretical predictions and the two cases studied for the G^0 experiment to contribute to the knowledge of d_Δ.

Table 2 shows the experimental settings and resultant rates for the two cases considered. The results again assume 800 hours of running time.

If we were to propose a dedicated Δ run, it would be wise to boost the photoproduction rate by placing a radiator upstream of the G^0 liquid target. For instance, a 10% radiation length radiator would boost the pion rate to 103 MHz. This would yield a 12% or $\delta d_\Delta = 3g_\pi$ extraction. We see no immediate problem with placing a radiator upstream of the target. For a 10% radiator, multiple scattering will increase the electron beam angular divergence by about 0.5°. This level of divergence would not cause the primary beam to hit the small entrance window to the target. The beam spot radius at the beam dump would be roughly 0.5 ft, which is smaller than the dump size and therefore should not strongly affect background rates in the detector.

Figure 1 summarizes the theoretical predictions for d_Δ and the two possibilities for G^0 to contribute.

The author would like to thank S.-L. Zhu, C. Maekawa, and M.J. Ramsey-Musolf for useful discussions, and R.D. McKeown for help in developing these ideas. This work was supported by NSF grant PHY-0071856.

References

1. B. Desplanques, J.F. Donohue, B.R. Holstein, Ann. Phys. **124**, 449 (1980).
2. J.-W. Chen, X. Ji, Phys. Rev. Lett. **86**, 4239 (2001).
3. JLab E-01-116, D.H. Beck, spokesperson, the G^0 Collaboration.
4. JLab E-01-115, S. Wells, N. Simicevic, spokespersons, the G^0 Collaboration.
5. S.-L. Zhu *et al.*, Phys. Rev. D **65**, 033001 (2002).
6. S.-L. Zhu *et al.*, Phys. Rev. Lett. **87**, 201802 (2001).
7. B. Borasoy, B.R. Holstein, Phys. Rev. D **59**, 054019 (1999).

Eur. Phys. J. A **18**, 429–432 (2003)
DOI 10.1140/epja/i2002-10252-0

THE EUROPEAN PHYSICAL JOURNAL A

Generalized parton distributions

M. Vanderhaeghen[a]

Institut für Kernphysik, Johannes Gutenberg-Universität, D-55099 Mainz, Germany

Received: 30 September 2002 /
Published online: 22 October 2003 – © Società Italiana di Fisica / Springer-Verlag 2003

Abstract. We discuss how generalized parton distributions (GPDs) enter in a variety of hard exclusive processes such as deeply virtual Compton scattering (DVCS) and hard meson electroproduction reactions on the nucleon. We show some key observables which are sensitive to the various hadron structure aspects of the GPDs, and discuss their experimental status.

PACS. 13.60.Fz Elastic and Compton scattering – 13.60.Le Meson production – 12.38.Bx Perturbative calculations

1 Introduction

Generalized parton distributions (GPDs), are universal non-perturbative objects entering the description of hard exclusive electroproduction processes (see refs. [1–3] for reviews and references). In leading twist there are four GPDs for the nucleon, *i.e.* H, E, $\tilde{H}$ and $\tilde{E}$, which are defined for each quark flavor (u, d, s). These GPDs depend upon the different longitudinal momentum fractions $x+\xi$ $(x-\xi)$ of the initial (final) quark and upon the overall momentum transfer $t = \Delta^2$ to the nucleon (see fig. 1). As the momentum fractions of initial and final quarks are different, one accesses quark momentum correlations in the nucleon. Furthermore, if one of the quark momentum fractions is negative, it represents an antiquark and, consequently, one may investigate $q\bar{q}$ configurations in the nucleon. Therefore, these functions contain a wealth of new nucleon structure information, generalizing the information obtained in inclusive deep inelastic scattering.

In particular, the GPDs allow to access the fraction of the nucleon spin carried by the quark total angular momentum (J^u, J^d, etc.), $\bar{q}q$ components of the nucleon wave function (in particular the D-term [4]), the strength of the skewedness effects in the GPDs (encoded in their ξ-dependence), the quark structure of $N \to N^*$, Δ transitions, flavor $SU(3)$ breaking effects, and others. Furthermore, it has been shown that by a Fourier transform of the t-dependence of GPDs, it is conceivable to access the distributions of parton in the transverse plane [5,6].

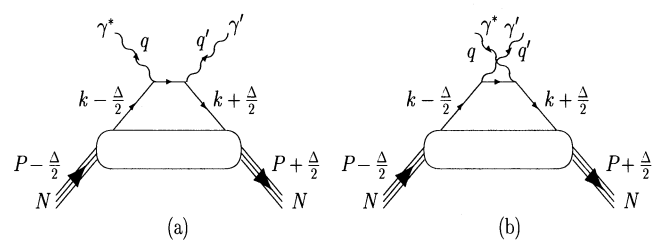

Fig. 1. "Handbag" diagrams for the DVCS process, containing the GPDs.

2 DVCS beam-helicity asymmetry

We first turn to the DVCS observables and their dependence on the GPDs. At intermediate lepton beam energies, one can extract the imaginary part of the DVCS amplitude through the $ep \to ep\gamma$ reaction with a polarized lepton beam, by measuring the out-of-plane angular dependence (in the angle ϕ) of the produced photon [7]. It was found in refs. [8,9] that the resulting electron single spin asymmetry (SSA)

$$\mathcal{A}^{\rm SSA} = \frac{\sigma_{e,h=+1/2} - \sigma_{e,h=-1/2}}{\sigma_{e,h=+1/2} + \sigma_{e,h=-1/2}}\,, \qquad (1)$$

with $\sigma_{e,h}$ the cross-section for an electron of helicity h, can be sizeable for HERMES ($E_e = 27\,\mathrm{GeV}$) and JLab ($E_e =$ 4–11 GeV) beam energies. The SSA for the $ep \to ep\gamma$ reaction has recently been measured in pioneering experiments at HERMES [10] and JLab/CLAS [11], as shown in fig. 2. They display already at the accessible values of $Q^2 \simeq 1$–$2.5\,\mathrm{GeV}^2$ predominantly a $\sin\phi$-dependence, indicating a dominance of the twist-2 DVCS amplitude. Furthermore, the observed magnitude is in good agreement with the

[a] e-mail: marcvdh@kph.uni-mainz.de

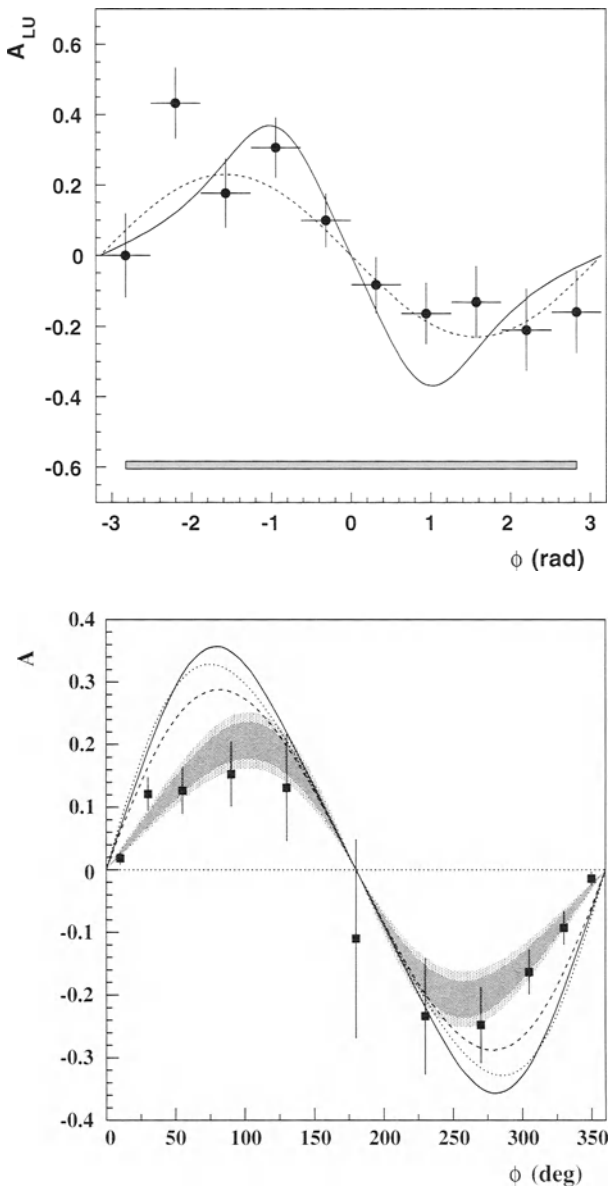

Fig. 2. The DVCS beam helicity asymmetry as measured at HERMES [10] (upper panel) and JLab/CLAS [11] (lower panel). Full curves: twist-2 + twist-3 predictions of ref. [12].

theoretical calculations [12,13] in terms of GPDs. Once the leading-order mechanism is confirmed by experiment, the measured helicity difference is directly proportional to the GPDs along the line $x = \xi$.

Dedicated experiments to measure the SSA with improved accuracy in a large kinematic range are already planned and underway both at JLab and HERMES.

Recently, the double deeply virtual Compton scattering (DDVCS) process has been studied [14] through the scattering of a spacelike virtual photon with large virtuality resulting in the production of a timelike virtual photon, decaying into an e^+e^- pair. For DDVCS, by varying the virtualities of both incoming and outgoing virtual photons, one can vary independently the variables ξ and ξ', where $-2\xi'$ is the longitudinal momentum fraction of the

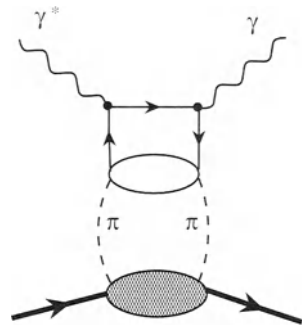

Fig. 3. Model contribution to the D-term entering the GPDs H and E.

incoming virtual photon. In contrast, in DVCS, only one variable can be varied as $\xi \approx \xi'$. It was then shown in ref. [14] that the imaginary part of the DDVCS amplitude (which can be directly measured through the beam helicity asymmetry as discussed for the DVCS process above) will access, in a concise notation, the GPD$(2\xi' - \xi, \xi, t)$, and allows to map out the GPDs as a function of its three arguments independently. In particular, in this way one can access the domain $x < \xi$ of the GPD(x, ξ, t), where one is sensitive to $q\bar{q}$ correlations in the nucleon. Although the cross-sections for the DDVCS process are small, their measurement seems feasible with a dedicated experiment at JLab and at a future high-energy, high-luminosity lepton facility.

3 DVCS beam-charge asymmetry

Besides the beam-helicity asymmetry for the $ep \to ep\gamma$ reaction, which accesses the imaginary part of the DVCS amplitude, one gets access to the real part of the DVCS amplitude by measuring both $e^+p \to e^+p\gamma$ and $e^-p \to e^-p\gamma$ processes. In those reactions, besides the mechanism where the photon originates from a quark (handbag diagrams of fig. 1), the photon can also be emitted by the lepton lines, in the so-called Bethe-Heitler (BH) process. However, in the difference $\sigma_{e^+} - \sigma_{e^-}$, the BH drops out, and one measures the real part of the BH-DVCS interference [15],

$$\sigma_{e^+} - \sigma_{e^-} \sim \Re\Big[T^{\mathrm{BH}} T^{\mathrm{DVCS}*}\Big], \tag{2}$$

which is sensitive to (a convolution integral of) GPDs away from the line $x = \xi$.

It has been shown in [12] that this beam-charge asymmetry (BCA) gets a sizeable contribution from the D-term. The latter encodes $q\bar{q}$ scalar-isoscalar correlations in the nucleon as shown in fig. 3, and has been estimated in the chiral quark soliton model [16].

The DVCS BCA has been accessed experimentally at HERMES [17], and the preliminary data are shown in fig. 4, together with the theoretical predictions. The measured asymmetry shows a $\cos\phi$-dependence with magnitude $\sim$ 0.10–0.15, and favors the calculations which include the D-term. This opens up the perspective to study

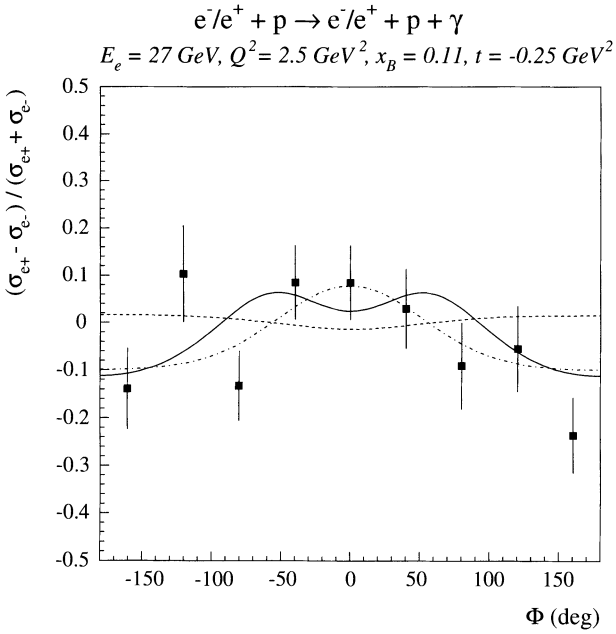

Fig. 4. The DVCS beam-charge asymmetry with preliminary HERMES data [17]. Theoretical predictions from [12]. Dashed-dotted (dashed) curves: twist-2 DVCS with (without) D-term. Full curve: twist-3 effects in addition to the D-term.

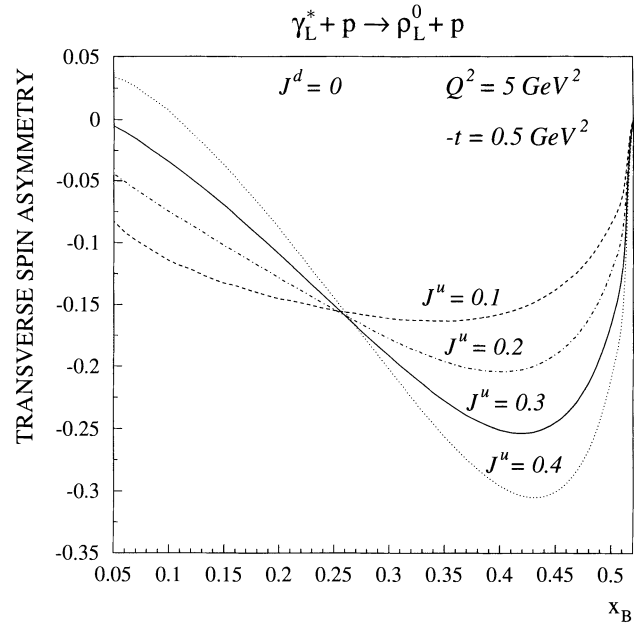

Fig. 5. x_B-dependence of the transverse target spin asymmetry for the $\gamma_L^* p \to \rho_L^0 p$ reaction. The estimates are given using the model of ref. [3] for the GPDs E^u and E^d. The sensitivity is shown to different values of J^u (for a value $J^d = 0$).

systematically (mesonic) $q\bar{q}$ components in the nucleon. Further measurements, with improved statistics, of the DVCS BCA are planned at HERMES.

4 Hard meson electroproduction

The GPDs reflect the structure of the nucleon independently of the reaction which probes the nucleon. In this sense, they are universal quantities and can also be accessed, in different flavor combinations, through the hard exclusive electroproduction of mesons, for which a QCD factorization proof was given [18]. This factorization theorem applies when the virtual photon is longitudinally polarized, which corresponds to a small-size configuration compared to a transversely polarized photon.

For the longitudinal vector meson (V_L) electroproduction processes $\gamma_L^* + N \to V_L + N$ at large Q^2, the GPDs enter in different isospin combinations for $V_L = \rho_L^0, \rho_L^+, \omega_L$, allowing for a flavor decomposition of GDPs.

An $\gamma_L^* + N \to V_L + N$ observable of particular interest is the transverse spin asymmetry (TSA) for a nucleon polarized perpendicular to the reaction plane [3]. The TSA is proportional to the imaginary part of the *interference* of the amplitudes which contain the GPDs H and E, respectively. Therefore, the TSA provides a unique observable to extract the GPD E. Besides, one may expect that the theoretical uncertainties for the meson electroproduction cross-sections largely disappear for the TSA, as it involves a ratio of cross-sections, suggesting that the leading-order expression is already accurate at accessible values of Q^2 (of a few GeV^2). Due to its linear dependence on the GPD E, the TSA for longitudinally polarized vector mesons opens up the perspective to get information on the total angular momentum contributions J^u and J^d of the u- and d-quarks to the proton spin. Due to the different u- and d-quark content of the vector mesons, the asymmetries for the ρ_L^0, ω_L and ρ_L^+ channels are sensitive to different combinations of J^u and J^d, with ρ_L^0 production sensitive to $2J^u + J^d$, ω_L to $2J^u - J^d$, and ρ_L^+ to $J^u - J^d$.

In fig. 5, the TSA for ρ_L^0 production is shown. One observes that it displays a pronounced sensitivity to J^u. It will therefore be very interesting to provide a first measurement of this asymmetry in the near future, for a transversely polarized target, such as is currently available at HERMES.

5 Outlook

We have seen some very promising first glimpses of GPDs entering hard exclusive reactions at existing facilities. A dedicated program aiming at the extraction of the full physics potential contained in the GPDs will require a dedicated facility combining high luminosity and a good resolution.

References

1. X. Ji, J. Phys. G **24**, 1181 (1998).
2. A.V. Radyushkin, in *the Boris Ioffe Festschrift "At the Frontier of Particle Physics / Handbook of QCD"*, edited by M. Shifman (World Scientific, Singapore, 2001).
3. K. Goeke, M.V. Polyakov, M. Vanderhaeghen, Prog. Part. Nucl. Phys. **47**, 401 (2001).

4. M.V. Polyakov, C. Weiss, Phys. Rev. D **60**, 114017 (1999).
5. M. Burkardt, Phys. Rev. D **62**, 071503 (R) (2000); hep-ph/0207047.
6. M. Diehl, Eur. Phys. J. C **25**, 223 (2002).
7. P. Kroll, M. Schürmann, P.A.M. Guichon, Nucl. Phys. A **598**, 435 (1996).
8. M. Vanderhaeghen, P.A.M. Guichon, M. Guidal, Phys. Rev. Lett. **80**, 5064 (1998); Phys. Rev. D **60**, 094017 (1999).
9. P.A.M. Guichon, M. Vanderhaeghen, Prog. Part. Nucl. Phys. **41**, 125 (1998).
10. A. Airapetian *et al.* (HERMES Collaboration), Phys. Rev. Lett. **87**, 182001 (2001).
11. S. Stepanyan *et al.* (CLAS Collaboration), Phys. Rev. Lett. **87**, 182002 (2001).
12. N. Kivel, M.V. Polyakov, M. Vanderhaeghen, Phys. Rev. D **63**, 114014 (2001).
13. A.V. Belitsky, D. Müller, A. Kirchner, Nucl. Phys. B **629**, 323 (2002).
14. M. Guidal, M. Vanderhaeghen, Phys. Rev. Lett. **90**, 012001 (2003), hep-ph/0208275.
15. S.J. Brodsky, F.E. Close, J.F. Gunion, Phys. Rev. D **6**, 177 (1972).
16. V. Petrov *et al.*, Phys. Rev. D **57**, 4325 (1998).
17. F. Ellinghaus (on behalf of the HERMES Collaboration), hep-ex/0207029.
18. J.C. Collins, L.L. Frankfurt, M. Strikman, Phys. Rev. D **56**, 2982 (1997).

Eur. Phys. J. A **18**, 433–435 (2003)
DOI 10.1140/epja/i2002-10253-y

THE EUROPEAN PHYSICAL JOURNAL A

Deep inelastic scattering of leptons on nuclei: Hadron formation, cumulative particles production

S.M. Eliseev[a]

Bogoliubov Laboratory of Theoretical Physics, Joint Institute for Nuclear Research, 141980, Dubna

Received: 30 September 2002 /
Published online: 22 October 2003 – © Società Italiana di Fisica / Springer-Verlag 2003

Abstract. We introduce a space-time model for propagation of quark and gluon jets in nuclear matter, taking into account the formation zone phenomena (Landau-Pomeranchuk-Migdal, LPM, effect) and cascading of soft particles in a nucleus. The measured final-state hadrons, including cumulative nucleons produced in neutrino interactions with nuclei are investigated and the formation length of hadrons is obtained.

PACS. 13.60.Le Meson production – 13.15.+g Neutrino interactions – 25.30.Pt Neutrino scattering

1 Introduction

Recently, there has been considerable interest in the study of highly relativistic ion collisions. Such an interest stems from the possibility of creating hadron matter of high-energy density. The creation of a domain of high-energy density may allow one to study matter under unusual state, *i.e.*, quark-gluon plasma. In order to investigate the possible emergence of quark-gluon plasma, it is necessary to understand the properties of ordinary multiparticle productions mechanisms in more simple conditions than in the relativistic collisions of heavy ions (see, *e.g.*, [1,2]).

In addition, the question of fundamental importance in QCD is the hadronization-mechanism which converts quark and gluon quanta into integrally charged final-state hadrons. Landau, Pomeranchuk and Migdal [3,4] investigated the classical radiation process in the random field inside the medium. They showed that after the first scattering the electron "shakes off" its field and until this field is re-established the scattering takes placed without emission of a photon leading to suppression of the radiation. The role of long distances in physics of strong interactions was noted by Feinberg [5].

Lepton-nucleus scattering provides a nontrivial possibility to study space-time evolution of jets inside a nuclear matter. In contrast with hadron production, intranuclear cascading can be studied without complicate effects of projectile rescattering or interactions of projectile constituent [6,7]. The physics of such reactions [6,7] is very interesting. However, at the present time it is not possible to calculate accurately all peculiarities of such reactions according to "the first principles" of QCD. Instead of this we apply a simple phenomenological concept of the formation zone (see, *e.g.*, ref. [6]). The last few years have witnessed a great revival of interest in inclusive DIS (HERMES, NOMAD and other collaborations) [8–10].

The aim of this work is to examine a multiproduction process of charged-current deep inelastic ν_μ-emulsion scattering and to estimate quantitatively the value of a formation length. We also concentrate on the production of cumulative protons (CP), *i.e.* the final-state protons from backward angles.

2 The model

For the time being, the explicit theoretical description of hadronization is difficult, as it is impossible to treat the soft fragmentation processes in the framework of QCD. Consequently, one has to a address this process with model calculation. We developed a cascade model of multiproduction from neutrino-nuclei interaction. (More detailed description of the model can be found in ref. [11]).

We assume that the interaction between an incident lepton and a target nucleus takes place via a lepton-nucleon interaction. The nucleus is excited by a series of collisions between secondaries, produced in the first lepton-nucleon interaction. At high energies the secondaries traverse the nucleus in such a short time that the nucleons cannot rearrange themselves until the probe has left. In short, the target nucleons are just static spectators, so that the scattering problem is in first approximation a sequence of two-body scattering processes. This process continues until all secondaries escape the target nucleus. A part of the energy is spread through the nucleus to produce a nucleus in equilibrium, which then decays statistically [11]. The process of particle generation is simulated by a Monte Carlo method.

[a] e-mail: selis@thsun1.jinr.ru

The characteristics of the interactions of the neutrino and of the produced particles with nucleons in nucleus are taken from experiments with free nucleons [11–13]. Since the interaction cross-section of neutrino with a nucleon is small, we assume that the neutrino can interact with any nucleon of the nucleus with equal probability. Following experiments and the quark parton model, we take into account that the interaction cross-section of neutrino with a neutron is twice that with a proton, $\sigma(\nu + n)/\sigma(\nu + p) \approx 2$. Nuclear effects such as the Fermi motion and Pauli blocking are also taken into consideration [11]. The space-time characteristics of lepton-nucleon interactions inside the target nucleus are taken into consideration. After a time τ from the intranuclear collision the cross-section for the next collision of a secondary particle with a nucleon inside the nucleus is given by

$$\sigma_{hN} = \sigma_{hN}^{\exp}\left(1 - e^{-\tau/\tau_0}\right), \tag{1}$$

where $\sigma_{hN}^{\exp}$ is the experimentally determined total interaction cross-section of a hadron with a free nucleon at the corresponding energy of the secondary particle produced. Thus, only after a relatively long time τ the cross-section of intranuclear interaction reaches the value $\sigma_{hN}^{\exp}$. In our equation, the parameter τ_0 is characteristic for the formation time of the secondary generated hadron. The equation for σ_{hN} can be rewritten in a formation parameter L. It should be noted that for $L \to 0$ ($\tau_0 \to 0$), our model will reduce to the old fashioned cascade model in which secondary hadrons are produced instantly. In the present model, at a finite value of L, secondary particles (*e.g.*, pions) are formed after a certain time.

The Fermi gas model of the nucleus is utilized. The nuclear density is taken from a Woods-Saxon expression

$$\rho(r) \sim 1/\left(1 + e^{(r-c)/\alpha}\right), \tag{2}$$

with the parameters $\alpha = 0.57\,\mathrm{fm}$ and $c = 1.19A^{1/3} - 1.61A^{-1/3}\,\mathrm{fm}$. Moreover, our calculations use three-dimensional geometry.

According to the matter composition, a nucleus (of mass number A) with which the neutrino would interact is chosen randomly. Then, knowing the nuclear density, we can place A nucleons inside the nucleus. For each simulation of A nucleons, we fix the coordinates of the center of intranuclear nucleons throughout the process of developing the cascade. The characteristics of charged-particle production in the first νN interaction inside the nucleus are taken from experimental data [11–13], which were obtained from reactions induced by the same neutrino beam used in the present work. The multiplicities of neutral particles (pions) are also taken from the experiment (see [11–13]). These multiplicities for νn and νp are

$$n_{\pi^0} = 0.72 + 0.22 n_{\pi^-} \tag{3}$$

and

$$n_{\pi^0} = 0.14 + 0.73 n_{\pi^-}, \tag{4}$$

where n_{π^-} is the multiplicity of negatively charged particles. The angular and momentum distributions of neutral particles are assumed to be the same as those of positively and negatively charged particles.

Table 1. The average multiplicities of s- and g-particles, produced in charged-current ν_μ-emulsion interaction.

Experimental data	Calculations of the model		
	$L = 0.2\,\mathrm{fm}$	$L = 0.5\,\mathrm{fm}$	$L = 1\,\mathrm{fm}$
N_s 5.28 ± 0.26	5.60 ± 0.04	5.12 ± 0.03	4.08 ± 0.02
N_g 1.33 ± 0.15	1.71 ± 0.02	1.35 ± 0.02	0.82 ± 0.01

Table 2. The average multiplicity of N_g and N_b particles associated with a different number $k = 0, 1$ and $k \geq 2$ of final-state cumulative protons. The experimental data are given in parentheses.

k	N_g ($\vartheta \leq \pi$)	N_g ($\pi/2 \leq \vartheta \leq \pi$)	N_b
0	1.1 (1.4 ± 0.1)	1.1 (1.4 ± 0.1)	3.9 (4.4 ± 0.2)
1	2.8 (3.0 ± 0.3)	1.8 (2.0 ± 0.3)	5.2 (5.4 ± 0.6)
≥ 2	5.6 (5.6 ± 0.5)	3.0 (3.1 ± 0.6)	9.0 ($10. \pm 1.0$)

3 Results and discussion

In this section we present the theoretical results for neutrino-emulsion interaction and compare with experimental data [11–13]. (The full list of the references of experimental data can be found in ref. [11].) The neutrino energy spectrum peaks at about 15 GeV, and extends to about 200 GeV.

Secondary particles in high-energy experiments with emulsion are divided into three classes [11]. The first includes relativistic, hot *shower* particles (s-particles) of velocity $\beta > 0.7$. These particles are almost all charged pions of kinetic energy ≥ 60 MeV and fast protons of kinetic energy ≥ 400 MeV. The second class consists of *grey*-track particles (g-particles) with $0.23 \leq \beta \leq 0.7$. Those are mainly protons in the energy range 27–400 MeV. The third class consists of *black*-track particles (b-particles). They are low-energy particles emitted mainly due to evaporation.

The average multiplicities of s- and g-particles, produced in charged-current ν_μ-emulsion interactions are compared with the corresponding quantities calculated in our model at different values of L and are presented in table 1. One can see from table 1 that the experimental and calculated data at $L = 0.5\,\mathrm{fm}$ are in good agreement.

It is important to note that in our approach the evolution of quark-gluon jets in nuclei is accompanied by a nucleon emission at backward angles and with momentum ≥ 300 MeV/c. In our model the underlying mechanism responsible for energetic particle production is as quasi-deuteron intranuclear absorption process. Such cumulative protons were observed in deep inelastic charged-current neutrino-emulsion interactions. The experimental multiplicity of CP 0.33 ± 0.07 is in good agreement with the calculated one and equal to 0.29 [11–13].

In table 2 we compare our calculated multiplicities of g- and b-particles accompanied by a different number k of cumulative protons with data.

Figure 1 shows the multiplicity distribution of particles for charged-current ν_μ-emulsion interactions. The dotted

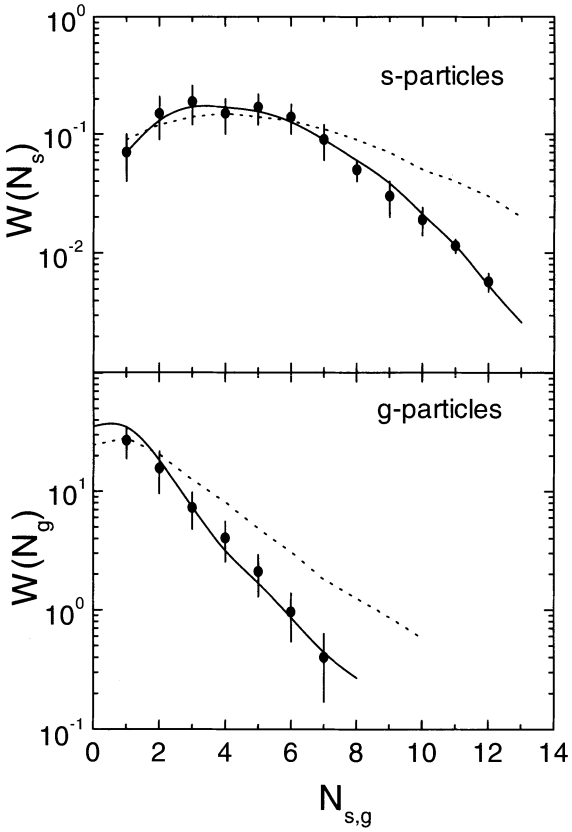

Fig. 1. Multiplicity distribution of s- and g-particles. See main text for details.

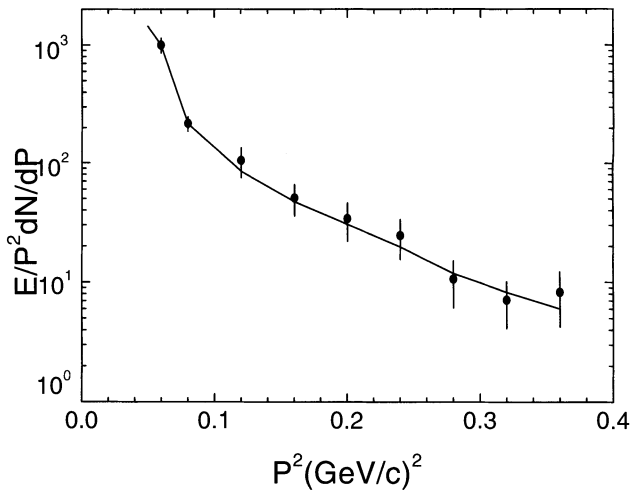

Fig. 2. Invariant momentum distributions for backward-going protons. See main text for details.

curve corresponds to calculation according to our model with a formation zone parameter $L = 0$. The solid line is the prediction with $L = 0.5$ fm. The experimental data are taken from refs. [11–13].

Figure 2 displays invariant momentum distributions for backward going protons. The solid line is the prediction with $L = 0.5$ fm. The nucleon emission process at backward angles can be divided into two parts with a different slope parameter of the spectra. In our approach the evaporation mechanism is responsible for production of protons with momentum ≤ 300 MeV/c. However, highly energetic nucleons are emitted in a direct process of neutrino-nucleus collision (the absorption of pions in nucleus by a correlated pair of nucleons along with rescattering).

In this way, we can include some exotic states (for example intranuclear multiquarks bags) to produce more energetic cumulative protons. Any discussion of this possibility and a more detailed investigation of the formation zone effect are, however, beyond the scope of the present analysis.

In summary, the cascade-evaporation model for the description of produced particles from deep inelastic collisions of neutrino with nuclei was developed. The model can be used for the extraction of the information of space-time property of the process of the formation of the secondary particles. Note that the formation time of particles plays a leading role in the various present-day investigations of the different nuclear reactions [14–17]. Moreover, the effect of the formation time is essential for the search of a powerful signature for quark-gluon plasma formation (see, *e.g.*, ref. [14]). We have shown that our model can be very useful not only to reveal the main physical effects of deep inelastic scattering, but also to perform accurate quantitative analyses and large systematics.

References

1. A. Capella, A.B. Kaidalov *et al.*, Phys. Rev. C **65**, 054908 (2002).
2. Bin Zhang *et al.*, Phys. Rev. C **65**, 054909 (2002).
3. L.D. Landau, I.J. Pomeranchuk, Dokl. Akad. Nauk. SSSR **92**, 535 (1953); **92**, 735 (1953).
4. A.B. Migdal, Phys. Rev. **103**, 1811 (1956).
5. E.L. Feinberg, in *Problems of Theoretical Physics* (Nauka, Moscow, 1972) pp. 248.
6. N.N. Nikolaev, Sov. Phys. Usp. **24**, 531 (1981).
7. B.B. Levchenko, N.N. Nikolaev, Yad. Fiz. **36**, 453 (1982).
8. NOMAD, P. Astier *et al.*, Nucl. Phys. B **609**, 255 (2001).
9. HERMES (A. Airapetian *et al.*), Eur. Phys. J. C **20**, 479 (2001).
10. HERMES (M. Düren), in *Proceedings of the International Workshop XXIX on Gross Properties on Nuclei and Nuclear Excitations, Hirschegg, Austria, January 14–20, 2001*, edited by H. Feldmeier, J. Knoll, W. Nörnberg, J. Wambach (GSI, Darmstadt, 2001) p. 130.
11. El-Naghy, S.M. Eliseev, J. Phys. G: Nucl. Part. Phys. **16**, 39 (1990), and references therein.
12. R.G. Ammar *et al.*, JETP Lett. **49**, 189 (1989).
13. R.G. Ammar *et al.*, JETP Lett. **49**, 480 (1998).
14. Sa Ben-Hao *et al.*, Phys. Rev. C **59**, 2728 (1999).
15. T. Falter, U. Mosel, nucl-th/0202011.
16. T. Falter, U. Mosel, Phys. Rev. C **66**, 024608 (2002).
17. W. Cassing, E.L. Bratkovskaya, O. Hansen, nucl-th/0203026.

Eur. Phys. J. A **18**, 437–440 (2003)
DOI 10.1140/epja/i2002-10254-x

THE EUROPEAN PHYSICAL JOURNAL A

High-density QCD and saturation of nuclear partons

I.P. Ivanov[1,2], N.N. Nikolaev[1,3,a], W. Schäfer[4], B.G. Zakharov[3], and V.R. Zoller[5]

[1] Institut f. Kernphysik, Forschungszentrum Jülich, D-52425 Jülich, Germany
[2] Institute of Mathematics, Novosibirsk, Russia
[3] L.D. Landau Institute for Theoretical Physics, Chernogolovka, Russia
[4] NORDITA, Blegdamsvej 17, DK-2100 Copenhagen Ø, Denmark
[5] Institute for Theoretical and Experimental Physics, Moscow, Russia

Received: 30 September 2002 /
Published online: 22 October 2003 – © Società Italiana di Fisica / Springer-Verlag 2003

Abstract. We review the recent finding of the two-plateau momentum distribution of sea quarks in deep inelastic scattering off nuclei in the saturation regime. The diffractive plateau which dominates for small $\mathbf{p}$ measures precisely the momentum distribution of quarks in the beam photon, the rôle of the nucleus is simply to provide an opacity. The plateau for truly inelastic DIS exhibits a substantial nuclear broadening of the momentum distribution. Despite this nuclear broadening, the observed final-state and initial-state sea quark densities do coincide exactly. We emphasize how the saturated sea is generated from the nuclear-diluted Weizsäcker-Williams because of the anti-collinear splitting of gluons into sea quarks.

PACS. 11.80.La Multiple scattering – 13.87.-a Jets in large-Q^2 scattering – 24.85.+p Quarks, gluons, and QCD in nuclei and nuclear processe

1 Introduction

The saturation of nuclear partons is one of the hot issues in high-energy physics. The interpretation of nuclear opacity in terms of a fusion and saturation of nuclear partons has been introduced in 1975 [1] way before the QCD parton model: the Lorentz contraction of relativistic nuclei entails a spatial overlap of partons with $x \lesssim x_A \approx 1/R_A m_N$ from different nucleons and the fusion of overlapping partons results in the saturation of parton densities per unit area in the impact parameter space. The pQCD link between nuclear opacity and saturation has been considered by Mueller [2] and the pQCD discussion of fusion of nuclear gluons has been revived by McLerran *et al.* [3].

In this paper we review the recent consistent derivation of nuclear parton densities in the opacity/saturation regime [4]. We demonstrate that despite the strong nuclear distortions the common wisdom that in deep inelastic scattering (DIS) the observed final-state (FS) momentum distribution of struck partons coincides with the initial-state (IS) density of partons in the probed target holds for nuclei too. The key to this derivation is the Weizsäcker-Williams (WW) glue of the relativistic nucleus as defined according to [5]. We pay a special attention to an important point that diffractive DIS in which the target nucleus does not break and is retained in the ground state, makes precisely 50 per cent of the total DIS events [6]. We point out that the saturated diffractive plateau measures precisely the momentum distribution of (anti-)quarks in the $q\bar{q}$ Fock state of the photon. We show how the anti-collinear splitting of WW gluons into sea quarks gives rise to nuclear saturation of the sea, despite the substantial nuclear dilution of the WW glue.

2 Nuclear distortions of the parton spectra

We illustrate our ideas on an example of DIS at $x \sim x_A \ll 1$ which is dominated by interactions of $q\bar{q}$ Fock states of the photon [6–10]. The total cross-section for interaction of the color dipole $\mathbf{r}$ with the target nucleon equals

$$\sigma(r) = \alpha_S(r)\sigma_0 \int \mathrm{d}^2\boldsymbol{\kappa} f(\boldsymbol{\kappa})\big[1 - \exp(i\boldsymbol{\kappa}\mathbf{r})\big], \tag{1}$$

where the unintegrated glue of the target nucleon is

$$f(\boldsymbol{\kappa}) = \frac{4\pi}{N_c\sigma_0} \cdot \frac{1}{\kappa^4} \cdot \frac{\partial G}{\partial \log \kappa^2}, \quad \int \mathrm{d}^2\boldsymbol{\kappa} f(\boldsymbol{\kappa}) = 1. \tag{2}$$

For DIS off a free nucleon target, see figs. 1a-d, the spectrum of the FS quark prior to the hadronization,

$$\frac{\mathrm{d}\sigma_N}{\mathrm{d}^2\mathbf{p}\,\mathrm{d}z} = \frac{\sigma_0\alpha_S(\mathbf{p}^2)}{2(2\pi)^2} \int \mathrm{d}^2\boldsymbol{\kappa} f(\boldsymbol{\kappa}) \times \big|\langle\gamma^* \mid \mathbf{p}\rangle - \langle\gamma^* \mid \mathbf{p} - \boldsymbol{\kappa}\rangle\big|^2, \tag{3}$$

[a] e-mail: N.Nikolaev@fz-juelich.de

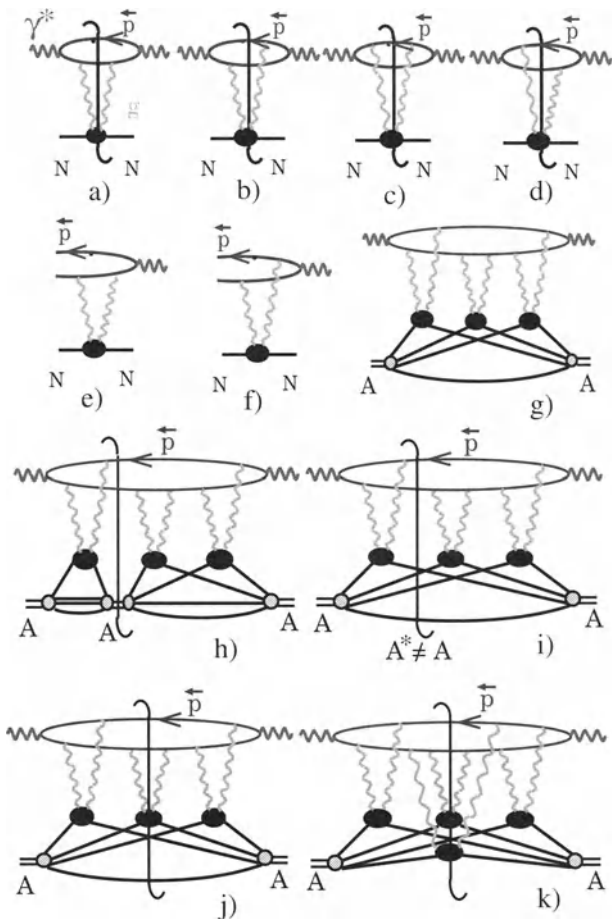

Fig. 1. The pQCD diagrams for inclusive (a-d) and diffractive (e, f) DIS off protons and nuclei (g-k). Diagrams (a-d) show the unitarity cuts with color excitation of the target nucleon, (g) a generic multiple-scattering diagram for Compton scattering off nucleus, (h) the unitarity cut for a coherent diffractive DIS, (i) the unitarity cut for quasielastic diffractive DIS with excitation of the nucleus A^*, (j, k) the unitarity cuts for truly inelastic DIS with single and multiple color excitation of nucleons of the nucleus.

where $\mathbf{p}$ is the transverse momentum, and z the Feynman variable, coincides, upon the z integration, with the conventional IS unintegrated $\mathbf{p}$ distribution of partons in the target. Notice that the target nucleon is color-excited and there is no rapidity gap in the FS.

In DIS off nuclei one must distinguish the three principal processes with distinct unitarity cuts of the forward Compton amplitude (fig. 1g): the coherent diffraction dissociation (D) of the photon (fig. 1h), quasielastic diffraction dissociation (qel) followed by excitation and breakup of the target nucleus (fig. 1i) —in both of them there is no color flow between the photon debris and the nucleus—, and the truly inelastic (in) DIS with color excitation of nucleons of the target nucleus (fig. 1j, k).

The technical trick with separation of the color dipole-nucleon S-matrix into the color-octet and color-singlet components, and the derivation of the full two-parton momentum spectrum are found in [4], here we only cite the single-parton spectrum

$$\frac{\mathrm{d}\sigma_{\mathrm{in}}}{\mathrm{d}^2\mathbf{p}\,\mathrm{d}z} = \frac{1}{(2\pi)^2}\int \mathrm{d}^2\mathbf{b}\int \mathrm{d}^2\mathbf{r}'\,\mathrm{d}^2\mathbf{r}\exp\left[i\mathbf{p}(\mathbf{r}'-\mathbf{r})\right] \times\Psi^*(\mathbf{r}')\Psi(\mathbf{r})\times\left\{\exp\left[-\frac{1}{2}\sigma(\mathbf{r}-\mathbf{r}')T(\mathbf{b})\right] - \exp\left[-\frac{1}{2}\left[\sigma(\mathbf{r})+\sigma(\mathbf{r}')\right]T(\mathbf{b})\right]\right\} \tag{4}$$

Evidently, the dependence of nuclear attenuation factors on $\mathbf{r}, \mathbf{r}'$ shall distort strongly the observed momentum distribution of quarks.

3 WW glue of nuclei

In the further parton model interpretation of this spectrum we resort to the NSS representation [5]

$$\Gamma_A(\mathbf{b},\mathbf{r}) = 1-\exp\left[-\frac{1}{2}\sigma(r)T(\mathbf{b})\right] = \int \mathrm{d}^2\boldsymbol{\kappa}\phi_{\mathrm{WW}}(\boldsymbol{\kappa})\left[1-\exp(i\boldsymbol{\kappa}\mathbf{r})\right], \tag{5}$$

where, driven by a close analogy to (1), (2) in terms of $f(\boldsymbol{\kappa})$, we interpret

$$\phi_{\mathrm{WW}}(\boldsymbol{\kappa}) = \sum_{j=1}^{\infty}\nu_A^j(\mathbf{b})\cdot\frac{1}{j!}f^{(j)}(\boldsymbol{\kappa})\exp\left[-\nu_A(\mathbf{b})\right] \tag{6}$$

as the WW unintegrated glue of a nucleus per unit area in the impact parameter plane. Here

$$\nu_A(\mathbf{b}) = \frac{1}{2}\alpha_S(r)\sigma_0 T(\mathbf{b})$$

defines the nuclear opacity and the j-fold convolutions

$$f^{(j)}(\boldsymbol{\kappa}) = \int\prod_{i=1}^{j}\mathrm{d}^2\boldsymbol{\kappa}_i f(\boldsymbol{\kappa}_i)\delta\left(\boldsymbol{\kappa}-\sum_{i=1}^{j}\boldsymbol{\kappa}_i\right) \tag{7}$$

describe the contribution to the diffractive amplitudes from j split pomerons [5].

A discussion of the nuclear antishadowing property of the hard WW glue is found in [5]. A somewhat involved analysis of the properties of the convolutions (7) in the soft region shows that they develop a plateau-like behaviour with the width of the plateau which expands $\propto j$. The gross features of the WW nuclear glue in the soft region are well reproduced by

$$\phi_{\mathrm{WW}}(\boldsymbol{\kappa}) \approx \frac{1}{\pi}\frac{Q_A^2}{\left(\boldsymbol{\kappa}^2+Q_A^2\right)^2}, \tag{8}$$

where the saturation scale $Q_A^2 = \nu_A(\mathbf{b})Q_0^2 \propto A^{1/3}$. Notice the nuclear dilution of soft WW glue, $\phi_{\mathrm{WW}}(\boldsymbol{\kappa}) \propto 1/Q_A^2 \propto A^{-1/3}$. The soft parameters Q_0^2 and σ_0 are related to the integrated glue of the proton in the soft region:

$$Q_0^2\sigma_0 \sim \frac{2\pi^2}{N_c}G_{\mathrm{soft}}, \quad G_{\mathrm{soft}} \sim 1.$$

4 An exact equality of the IS and FS parton densities

Making use of the NSS representation, the total nuclear photoabsorption cross-section can be cast in the form

$$\sigma_A = \int \mathrm{d}^2\mathbf{b} \int \mathrm{d}z \int \frac{\mathrm{d}^2\mathbf{p}}{(2\pi)^2} \times \int \mathrm{d}^2\boldsymbol{\kappa}\phi_{\mathrm{WW}}(\boldsymbol{\kappa})\big|\langle\gamma^* \mid \mathbf{p}\rangle - \langle\gamma^* \mid \mathbf{p}-\boldsymbol{\kappa}\rangle\big|^2, \quad (9)$$

which has a profound semblance to (3) and one is tempted to take the differential form of (9) as a definition of the IS sea quark density in a nucleus:

$$\frac{\mathrm{d}\bar{q}_{\mathrm{IS}}}{\mathrm{d}^2\mathbf{b}\,\mathrm{d}^2\mathbf{p}} = \frac{1}{2}\frac{Q^2}{4\pi^2\alpha_{\mathrm{em}}}\frac{\mathrm{d}\sigma_A}{\mathrm{d}^2\mathbf{b}\,\mathrm{d}^2\mathbf{p}}. \quad (10)$$

Remarkably, in terms of the NSS-defined WW nuclear glue, all intranuclear multiple-scattering diagrams of fig. 1g sum up to precisely the same four diagrams fig. 1a-d as in DIS off free nucleons. Although $\mathbf{p}$ emerges here just as a formal Fourier parameter, we shall demonstrate that it can be identified with the momentum of the observed final state antiquark.

Indeed, making use of the NSS representation, after some algebra one finds

$$\frac{\mathrm{d}\sigma_{\mathrm{in}}}{\mathrm{d}^2\mathbf{b}\,\mathrm{d}^2\mathbf{p}\,\mathrm{d}z} = \frac{1}{(2\pi)^2} \times\left\{\int \mathrm{d}^2\boldsymbol{\kappa}\phi_{\mathrm{WW}}(\boldsymbol{\kappa})\big|\langle\gamma^* \mid \mathbf{p}\rangle - \langle\gamma^* \mid \mathbf{p}-\boldsymbol{\kappa}\rangle\big|^2 - \left|\int \mathrm{d}^2\boldsymbol{\kappa}\phi_{\mathrm{WW}}(\boldsymbol{\kappa})\big(\langle\gamma^* \mid \mathbf{p}\rangle - \langle\gamma^* \mid \mathbf{p}-\boldsymbol{\kappa}\rangle\big)\right|^2\right\}, \quad (11)$$

$$\frac{\mathrm{d}\sigma_{\mathrm{D}}}{\mathrm{d}^2\mathbf{b}\,\mathrm{d}^2\mathbf{p}\,\mathrm{d}z} = \frac{1}{(2\pi)^2} \times\left|\int \mathrm{d}^2\boldsymbol{\kappa}\phi_{\mathrm{WW}}(\boldsymbol{\kappa})\big(\langle\gamma^* \mid \mathbf{p}\rangle - \langle\gamma^* \mid \mathbf{p}-\boldsymbol{\kappa}\rangle\big)\right|^2. \quad (12)$$

As far as diffraction is concerned, the analogy between (12) and its counterpart for free nucleons [5,8,11], and nuclear WW glue $\phi_{\mathrm{WW}}(\boldsymbol{\kappa})$ and $f(\boldsymbol{\kappa})$ thereof, is complete. Putting the inelastic and diffractive components of the FS quark spectrum together, we evidently find the FS parton density which exactly coincides with the IS parton density (10) such that $\mathbf{p}$ is indeed the transverse momentum of the FS sea quark. The interpretation of this finding is not trivial, though.

5 The two-plateau spectrum of sea quarks

Consider first the domain of $\mathbf{p}^2 \lesssim Q^2 \lesssim Q_A^2$ such that the nucleus is opaque for all color dipoles in the photon. Hereafter we assume that the saturation scale Q_A^2 is so large that $\mathbf{p}^2, Q^2$ are in the pQCD domain and neglect the quark masses. In this regime the nuclear counterparts of the crossing diagrams of figs. 1b, d, f can be neglected. Then, in the classification of [5], diffraction will be dominated by the contribution from the Landau-Pomeranchuk diagram of fig. 1e with the result

$$\left.\frac{\mathrm{d}\bar{q}_{\mathrm{FS}}}{\mathrm{d}^2\mathbf{b}\,\mathrm{d}^2\mathbf{p}}\right|_{\mathrm{D}} \approx \frac{1}{2}\frac{Q^2}{4\pi^2\alpha_{\mathrm{em}}}\int \mathrm{d}z \times\left|\int \mathrm{d}^2\boldsymbol{\kappa}\phi_{\mathrm{WW}}(\boldsymbol{\kappa})\right|^2 \big|\langle\gamma^* \mid \mathbf{p}\rangle\big|^2 \approx \frac{N_c}{4\pi^4}. \quad (13)$$

Remarkably, diffractive DIS measures the momentum distribution of quarks and antiquarks in the $q\bar{q}$ Fock state of the photon. This result, typical of the Landau-Pomeranchuk mechanism, is a completely generic one and would hold for any beam particle such that its coupling to colored partons is weak. In contrast to diffraction off free nucleons [8,11,12], diffraction off opaque nuclei is dominated by the anti-collinear splitting of hard gluons into soft sea quarks, $\boldsymbol{\kappa}^2 \gg \mathbf{p}^2$. Precisely for this reason one finds the saturated FS quark density, because the nuclear dilution of the WW glue is compensated for by the expanding plateau. The result (13) has no counterpart in DIS off free nucleons because diffractive DIS off free nucleons is negligibly small even at HERA, $\eta_{\mathrm{D}} \lesssim 6$–$10\%$.

The related analysis of the FS quark density for truly inelastic DIS in the same domain of $\mathbf{p}^2 \lesssim Q^2 \lesssim Q_A^2$ gives

$$\begin{aligned}\left.\frac{\mathrm{d}\bar{q}_{\mathrm{FS}}}{\mathrm{d}^2\mathbf{b}\,\mathrm{d}^2\mathbf{p}}\right|_{\mathrm{in}} &= \frac{1}{2}\frac{Q^2}{4\pi^2\alpha_{\mathrm{em}}}\int \mathrm{d}z \times\int \mathrm{d}^2\boldsymbol{\kappa}\phi_{\mathrm{WW}}(\boldsymbol{\kappa})\big|\langle\gamma^* \mid \mathbf{p}-\boldsymbol{\kappa}\rangle\big|^2 \\ &= \frac{Q^2}{8\pi^2\alpha_{\mathrm{em}}}\phi_{\mathrm{WW}}(0)\int^{Q^2} \mathrm{d}^2\boldsymbol{\kappa}\int \mathrm{d}z\big|\langle\gamma^* \mid \boldsymbol{\kappa}\rangle\big|^2 \\ &\approx \frac{N_c}{4\pi^4}\frac{Q^2}{Q_A^2}\theta\big(Q_A^2 - \mathbf{p}^2\big). \end{aligned} \quad (14)$$

It describes final states with color excitation of a nucleus, but as a function of the photon wave function and nuclear WW gluon distribution it is completely different from (3) for free nucleons. The θ-function simply indicates that the plateau for inelastic DIS extends up to $\mathbf{p}^2 \lesssim Q_A^2$. For $Q^2 \ll Q_A^2$ the inelastic plateau contributes little to the transverse-momentum distribution of soft quarks, $\mathbf{p}^2 \lesssim Q^2$, but the inelastic plateau extends way beyond Q^2 and its integral contribution to the spectrum of FS quarks is exactly equal to that from diffractive DIS. Such a two-plateau structure of the FS quark spectrum is a new finding and has not been considered before.

Now notice, that in the opacity regime the diffractive FS parton density coincides with the contribution $\propto |\langle\gamma^* \mid \mathbf{p}\rangle|^2$ to the IS sea parton density from the spectator diagram 1a, whereas the FS parton density for truly inelastic DIS coincides with the contribution to IS sea partons from the diagram of fig. 1c. The contribution from the crossing diagrams 1b, d is negigibly small.

Our results (13) and (14), especially nuclear broadening and unusually strong Q^2-dependence of the FS/IS parton density from truly inelastic DIS, demonstrate clearly

a distinction between diffractive and inelastic DIS. Our considerations can readily be extended to the spectrum of soft quarks, $\mathbf{p}^2 \lesssim Q_A^2$, in hard photons, $Q^2 \gtrsim Q_A^2$. In this case the result (13) for diffractive DIS is retained, whereas in the numerator of the result (14) for truly inelastic DIS one must substitute $Q^2 \to Q_A^2$, so that in this case $\mathrm{d}q_{\,\mathrm{FS}}|_{\mathrm{D}} \approx \mathrm{d}q_{\,\mathrm{FS}}|_{\mathrm{in}}$ and $\mathrm{d}q_{\,\mathrm{IS}} \approx 2\mathrm{d}q_{\,\mathrm{FS}}|_{\mathrm{D}}$. The evolution of soft nuclear sea, $\mathbf{p}^2 \lesssim Q_A^2$, is entirely driven by an anti-collinear splitting of the NSS-defined WW nuclear glue into the sea partons.

The early discussion of the FS quark density in the saturation regime is due to Mueller [13]. Mueller focused on $Q^2 \gg Q_A^2$ and discussed neither a distinction between diffractive and truly inelastic DIS nor a Q^2-dependence and broadening (8) for truly inelastic DIS at $Q^2 \lesssim Q_A^2$.

6 More signals of saturation in diffractive DIS

The flat $\mathbf{p}^2$ distribution of forward $q, \bar{q}$ jets in truly inelastic DIS in the saturation regime must be contrasted to the $\propto G(\mathbf{p}^2)/\mathbf{p}^2$ spectrum for the free nucleon target. In the diffractive DIS the saturation gain is much more dramatic: flat $\mathbf{p}^2$ distribution of forward $q, \bar{q}$ jets in diffractive DIS in the saturation regime must be contrasted to the $\propto 1/(\mathbf{p}^2)^2$ spectrum for the free nucleon target [8, 11]. In the exclusive diffractive DIS, *i.e.*, the vector meson production, the relevant hard scale for the proton target equals $\bar{Q}^2 \approx \frac{1}{4}(Q^2 + m_V^2)$ and the transverse cross-section has been predicted to behave as [14]

$$\sigma_{\mathrm{T}} \propto G^2\big(x, \bar{Q}^2\big)\big(\bar{Q}^2\big)^{-4}. \tag{15}$$

At $\bar{Q}^2 > Q_A^2$ the same would hold for nuclei too, but in the opposite case of $\bar{Q}^2 < Q_A^2$ the $\bar{Q}^2$-dependence is predicted to change to

$$\sigma_{\mathrm{T}} \propto G^2\big(x, \bar{Q}^2\big)\big(Q_A^2\big)^{-2}\big(\bar{Q}^2\big)^{-2}. \tag{16}$$

7 Conclusions

We reported a derivation of the FS parton spectrum. Our result (4) summarizes in an elegant way intranuclear distortions due to multiple diffractive rescatterings and color excitations of the target nucleus. In conjunction with the NSS definition of the WW glue of the nucleus, eqs. (5), (6), it gives an explicit form of the FS parton densities. The two-plateau FS quark density with the strong Q^2-dependence of the plateau for truly inelastic DIS has not been discussed before. A comparison with the IS nuclear parton densities which evolve from the NSS-defined WW nuclear glue shows an exact equality of the FS and IS parton densities. The plateau-like saturated nuclear quark density is suggestive of the Fermi statistics, but our principal point that for any projectile which interacts weakly with colored partons the saturated density measures the momentum distribution in the $q\bar{q}, gg, \ldots$ Fock state of the projectile disproves the Fermi-statistics interpretation. The spin and color multiplet of colored partons the photon couples to is completely irrelevant, what only counts is an opacity of heavy nuclei. The anti-collinear splitting of WW nuclear glue into soft sea partons is a noteworthy feature of the both diffractive DIS and IS sea parton distributions. The emergence of a saturated density of IS sea partons from the nuclear-diluted WW glue is due to the nuclear broadening of the plateau (8). Because the predominance of diffraction is a very special feature of DIS [6], one must be careful with applying the IS parton densities to, for instance, nuclear collisions, in which diffraction would not be of any significance.

One can go one step further and consider interactions with the opaque nucleus of the $q\bar{q}g$ Fock states of the photon. Then the above analysis can be extended to $x \ll x_A$ and the issue of the x-dependence of the saturation scale Q_A^2 can be addressed following the discussion in [9]. We only mention here that as far as diffraction and IS parton densities are concerned, the NSS-defined WW glue remains a useful concept and the close correspondence between $\phi_{\mathrm{WW}}(\boldsymbol{\kappa})$ for the nucleus and $f(\boldsymbol{\kappa})$ for the nucleon is retained.

This work has been partly supported by DAAD and Nordita, the INTAS grants 97-30494 & 00-00366 and DFG grant 436RUS17/119/01.

References

1. N.N. Nikolaev, V.I. Zakharov, Sov. J. Nucl. Phys. **21**, 227 (1975); (Yad. Fiz. **21**, 434 (1975)); Phys. Lett. B **55**, 397 (1975).
2. A.H. Mueller, Nucl. Phys. B **335**, 115 (1990).
3. L. McLerran, R. Venugopalan, Phys. Rev. D **49**, 2233 (1994); **55**, 5414 (1997); E. Iancu, A. Leonidov, L. McLerran, *Lectures at the Cargèse Summer School, August 6-18, 2001*, arXiv:hep-ph/0202270.
4. I.P. Ivanov, N.N. Nikolaev, W. Schafer, B.G. Zakharov, V.R. Zoller, arXiv: hep-ph/0207045; N.N. Nikolaev, W. Schafer, B.G. Zakharov, V.R. Zoller, arXiv: hep-ph/0207210.
5. N.N. Nikolaev, W. Schäfer, G. Schwiete, JETP Lett. **72** 583 (2000); (Pisma Zh. Eksp. Teor. Fiz. **72**, 583 (2000)); Phys. Rev. D **63**, 014020 (2001).
6. N.N. Nikolaev, B.G. Zakharov, V.R. Zoller, Z. Phys. A **351**, 435 (1995).
7. N.N. Nikolaev, B.G. Zakharov, Z. Phys. C **49**, 607 (1991).
8. N.N. Nikolaev, B.G. Zakharov, Z. Phys. C **53**, 331 (1992).
9. N.N. Nikolaev, B.G. Zakharov, J. Exp. Theor. Phys. **78**, 806 (1994); (Zh. Eksp. Teor. Fiz. **105**, 1498 (1994)); Z. Phys. C **64**, 631 (1994).
10. N.N. Nikolaev, B.G. Zakharov, V.R. Zoller, JETP Lett. **59**, 6 (1994).
11. N.N. Nikolaev, B.G. Zakharov, Phys. Lett. B **332**, 177 (1994).
12. M. Genovese, N.N. Nikolaev, B.G. Zakharov, Phys. Lett. B **378**, 347 (1996).
13. A.H. Mueller, Nucl. Phys. B **558**, 285 (1999); *Lectures at the Cargèse Summer School, August 6-18, 2001*, arXiv:hep-ph/0111244.
14. J. Nemchik, N.N. Nikolaev, B.G. Zakharov, Phys. Lett. B **341**, 228 (1994).

Eur. Phys. J. A **18**, 441–444 (2003)
DOI 10.1140/epja/i2002-10255-9

THE EUROPEAN PHYSICAL JOURNAL A

Measurement of the polarized parton distribution functions at HERMES

J. Stewart[a]

For the HERMES Collaboration
DESY Zeuthen, 15738 Zeuthen, Germany

Received: 30 September 2002 /
Published online: 22 October 2003 – © Società Italiana di Fisica / Springer-Verlag 2003

Abstract. The HERMES experiment at DESY has measured the inclusive and semi-inclusive double-spin asymmetries of polarized positrons scattering from polarized hydrogen and deuterium targets in the kinematic range of Bjørken-x $0.023 < x < 0.06$ and $1\,\mathrm{GeV}^2 < Q^2 < 10\,\mathrm{GeV}^2$. A RICH detector was installed for the deuterium running period and by providing the identification of charged pions and kaons has enabled the first measurement of charged kaon asymmetries. Based on the measured proton and deuterium asymmetries the polarized quark distributions have been extracted in leading-order pQCD.

PACS. 13.60.Hb Total and inclusive cross-sections (including deep-inelastic processes) – 13.88.+e Polarization in interactions and scattering

1 Introduction

The study of the nucleon spin structure has attracted great interest since the EMC experiment [1] reported that only a small fraction of the proton's spin is carried by the quarks' spins. Several experiments have been carried out since which have confirmed this result [2]. The HERMES experiment [3] was designed to perform precise measurements of the polarized parton distribution functions (PDFs). It utilizes the 27.6 GeV polarized electron or positron beam of the HERA accelerator in combination with a polarized internal gaseous target. With its large forward acceptance, the spectrometer is well suited to measure inclusive reactions where only the scattered positron is detected as well as semi-inclusive processes where a hadron is detected in coincidence. The study of semi-inclusive channels is particularly important as the identity of fast hadrons from the fragmentation process is correlated with the flavor of the struck quark. This "flavor-tagging" correlation can be used to determine the polarized PDFs for each quark flavor.

2 Formalism of the analysis

Assuming factorization of the hard-scattering process and the fragmentation process, the photo-absorption spin asymmetry A_1^h for the production of a hadron of type h can be written in LO QCD as

$$A_1^h(x,z,Q^2) = C_R \cdot \frac{\sum_f e_f^2 \Delta q_f(x,Q^2) D_f^h(z,Q^2)}{\sum_{f'} e_{f'}^2 q_{f'}(x,Q^2) D_{f'}^h(z,Q^2)} . \quad (1)$$

Here, $C_R = (1 + R(x,Q^2))/(1+\gamma^2)$, where $\gamma^2 = Q^2/\nu^2$ and $R = \sigma_\mathrm{L}/\sigma_\mathrm{T}$ is the ratio of the longitudinal (σ_L) and transverse (σ_T) virtual-photon absorption cross-sections. The symbol e_f denotes the charge of the quark with flavor f. The fragmentation functions $D_f^h(z,Q^2)$ give the probability that a struck quark of flavor f will fragment into a hadron h; $z = E_h/\nu$ is the fraction of the virtual photon's energy carried by the hadron. The data are analyzed for $0.2 < z < 0.8$ and $x_\mathrm{F} > 0.1$, therefore the fragmentation functions are evaluated over this range as well. These selection criteria were chosen to enhance the contribution of hadrons from the current fragmentation region. The upper cut $z < 0.8$ eliminates exclusive events from the sample. In eq. (1), $q_f(x,Q^2)$ and $\Delta q_f(x,Q^2)$ are the unpolarized and polarized parton distribution functions where $\Delta q_f(x,Q^2) \equiv q^+(x,Q^2) - q^-(x,Q^2)$ and $q^{+(-)}$ is the number density of quarks with spin parallel (antiparallel) to the nucleon's spin.

As seen in eq. (1), a measured semi-inclusive asymmetry is related to a linear combination of all polarized PDFs. The set of all inclusive and semi-inclusive asymmetries measured on both polarized proton and deuterium targets form a set of linear equations which can be solved for the quark polarizations. After integrating over the Q^2 and z ranges for each x-bin, the set of asymmetries can

[a] e-mail: James.Stewart@desy.de

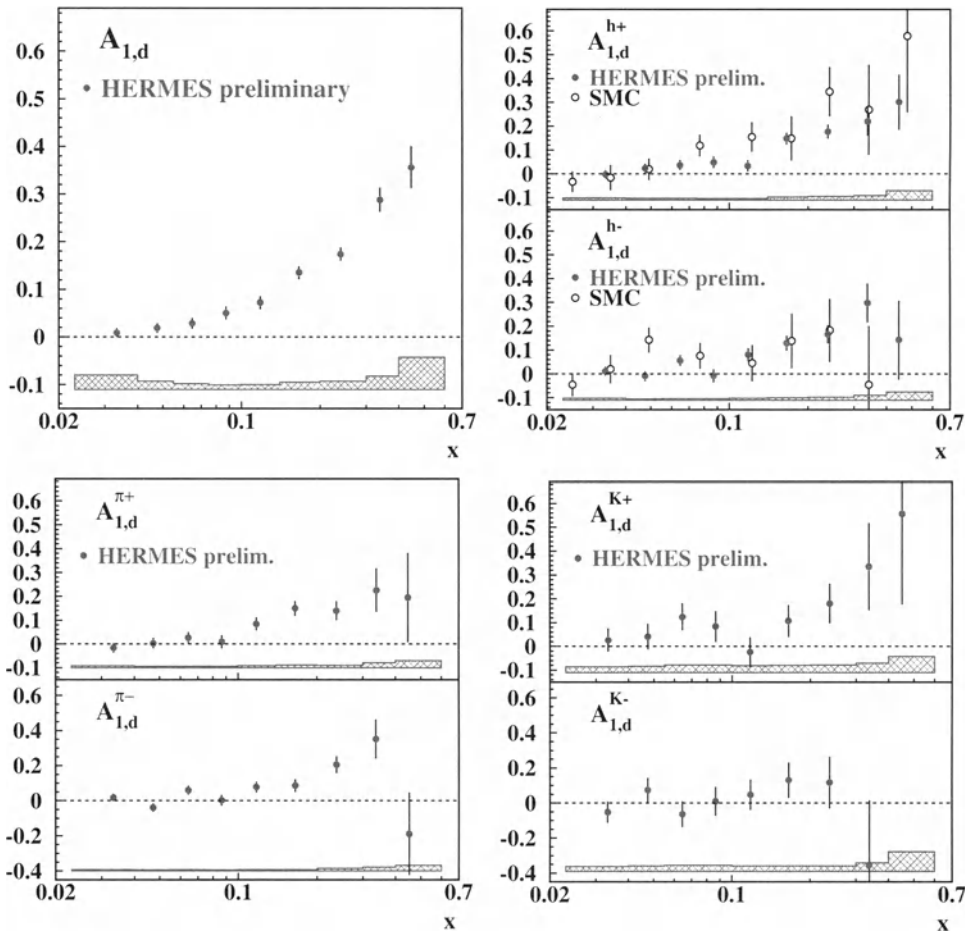

Fig. 1. Preliminary HERMES results on inclusive and semi-inclusive DIS asymmetries $A_{1,d}(x)$ as defined in eq. (1), here d denotes the polarized deuterium target. The shaded bands are the systematic uncertainties for the HERMES data.

be rewritten in matrix form as

$$\boldsymbol{A}(x) = C_R \cdot \boldsymbol{\mathcal{P}}\boldsymbol{Q}(x). \tag{2}$$

The vectors $\boldsymbol{A}(x)$ and $\boldsymbol{Q}(x)$ contain the measured asymmetries and the polarizations $\Delta q/q$ of the different quark flavors to be extracted.

The elements of the purity matrix $\boldsymbol{\mathcal{P}}$ depend solely on unpolarized quantities and can be written as follows:

$$P_f^h(x) \equiv \frac{e_f^2 q_f(x) \int_{0.2}^{0.8} \mathrm{d}z D_f^h(z)}{\sum_{f'} e_{f'}^2 q_{f'}(x) \int_{0.2}^{0.8} \mathrm{d}z D_f^h(z)}. \tag{3}$$

The purity $P_f^h(x)$ describes the probability that a hadron h originates from an event where a quark of flavor f was struck. It depends on the fragmentation functions and the unpolarized PDFs. It also contains the influence from the limited acceptance of the spectrometer. The fragmentation was modeled in the LUND string model implemented in the JETSET 7.4 [4] package. In order to obtain a reliable model of the fragmentation at HERMES energies, the string breaking parameters have been tuned to reproduce the measured hadron multiplicities at HERMES. The systematic uncertainties associated with the fragmentation were estimated by repeating the analysis with an alternative fit to the measured multiplicities and with the default LUND parameter setting valid for the PETRA e^+e^- collider. The resulting variations in the quark polarizations were added in quadrature to the other sources of the systematic error. The CTEQ5LO parameterizations from ref. [5] were used for the unpolarized PDFs in this analysis.

3 Experimental results

The preliminary data presented here are based on 6.5 (1.8) million DIS events taken on a deuterium (hydrogen) target in the kinematic range $Q^2 > 1\,\mathrm{GeV}^2$ and $W^2 > 10\,\mathrm{GeV}^2$. The average Q^2 of the data sample was $2.5\,\mathrm{GeV}^2$. The HERMES dual radiator RICH was installed in 1998 at the start of the deuterium data taking period. It made possible the identification of pions, kaons, and protons over the momentum range $2 < p < 15\,\mathrm{GeV}$. A Monte Carlo simulation was used to correct the asymmetries for kinematic smearing in the variable x due to instrumental resolution and QED radiative effects. Figure 1 shows the new HERMES measurements of the inclusive and of the semi-inclusive $\pi^{+/-}$ and $\mathrm{K}^{+/-}$ asymmetries. This first measurement of

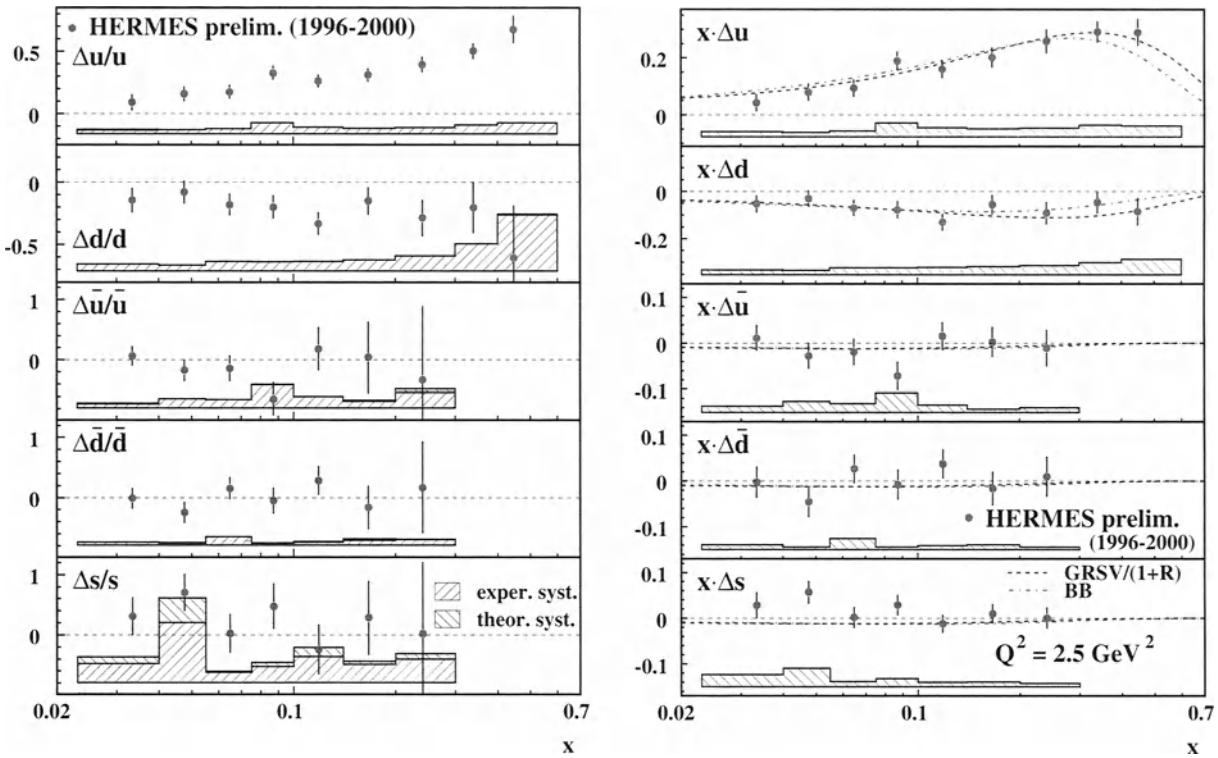

Fig. 2. HERMES preliminary results on the polarizations of the u, $\bar{u}$, d, $\bar{d}$, and $s+\bar{s}$ quark flavors *versus* x (left panel). The right panel shows the results on the corresponding polarized quark distributions at a common scale of $Q^2 = 2.5\,\mathrm{GeV}^2$. The dashed and dot-dashed lines are parameterizations from refs. [6,7]. The errors are statistical, while the shaded bands indicate the systematic uncertainties of the results. The contribution labeled "theor. syst." in the left panel gives the uncertainty due to the use of two different unpolarized parton densities [5,8].

the semi-inclusive kaon asymmetries is based on a sample of 86 (35) thousand identified $K^{+(-)}$. Also shown in fig. 1 are the semi-inclusive hadron asymmetries for comparison with the previous results from SMC [9].

A new refined analysis is also available for the earlier inclusive and semi-inclusive asymmetries for charged hadrons and pions produced from a hydrogen target (1996-1997 data taking) [10]. Pion identification was accomplished for particles in the momentum range $4.5 < p < 13.5\,\mathrm{GeV}$ using a gas threshold Čerenkov counter. No kaon identification was possible. For this analysis the effects due to smearing, resolution, and QCD effects were treated in the same way as for the deuterium data. Compared to the previous HERMES publication of these results [11], a new analysis of the target data has been performed yielding updated values for the target polarization: $P_z = 0.75 \pm 0.06$ for 1996 and $P_z = 0.85 \pm 0.05$ for 1997.

Using the asymmetries in fig. 1 and the re-analyzed proton asymmetries, eq. (2) has been solved using a least-squares minimization technique for the vector of quark polarizations $\boldsymbol{Q}(x)$. In this analysis the light quark sea is fit independently and the only remaining assumption is that the strange sea is symmetric; therefore $\boldsymbol{Q}(x) = (\frac{\Delta u}{u}, \frac{\Delta d}{d}, \frac{\Delta \bar{u}}{\bar{u}}, \frac{\Delta \bar{d}}{\bar{d}}, \frac{\Delta s}{s} = \frac{\Delta \bar{s}}{\bar{s}})$. In the fit procedure the polarization of all sea quark flavors was set to zero for $x > 0.3$ to avoid large uncertainties from correlations between the elements of $\boldsymbol{Q}(x)$. Figure 2 shows the obtained quark polarizations as well as the polarized quark momentum distributions. The polarized quark distributions Δu and Δd are consistent with earlier inclusive analyses [7,8]. Within their total uncertainties, all extracted sea quark polarizations are zero; no asymmetry between the $\Delta\bar{u}$ and $\Delta\bar{d}$ flavors is observed, and the polarized strange quark distributions favor slightly positive values in contrast to fits to inclusive data [7,8].

4 Conclusions

HERMES has measured with high precision a large set of double-spin asymmetries in the inclusive and semi-inclusive cross-sections. For the first time the semi-inclusive charged kaon asymmetries have been measured on a deuterium target. Based on a LO QCD analysis, Δu, $\Delta\bar{u}$, Δd, $\Delta\bar{d}$, and $\Delta s + \Delta\bar{s}$ have been extracted as a function of x in the range $0.023 < x < 0.6$. Within the accuracy of this first measurement, the flavor symmetry of the light quark see is compatible with the $SU(2)_f$ assumption and the strange sea polarization is consistent with zero.

References

1. J. Ashman *et al.*, Phys. Lett. B **206**, 364 (1988); Nucl Phys. B **328**, 1 (1989).

2. B.W. Filippone, X. Ji, hep-ph/0101224, and references therein.
3. The HERMES Collaboration, Nucl. Instrum. Methods A **417**, 230 (1988).
4. T. Sjöstrand, Comp. Phys. Commun. **82**, 74 (1994).
5. H.L. Lai *et al.*, Eur. Phys. J. C **12**, 375 (2000).
6. M. Glück *et al.*, Phys. Rev. D **63**, 094005 (2001).
7. J. Blümlein, H. Böttcher, Nucl. Phys. B **636**, 225 (2002), hep-ph/0203155.
8. M. Glück *et al.*, Eur. Phys. J. C **5**, 461 (1998).
9. B. Adeva *et al.*, Phys. Lett. B **420**, 180 (1998).
10. C.M. Simani, *Proceedings of the X International Workshop on Deep Inelastic Scattering (DIS2002)*, Acta Phys. Pol. B, in press.
11. The HERMES Collaboration, Phys. Lett. B **464**, 123 (1999).

Eur. Phys. J. A **18**, 445–447 (2003)
DOI 10.1140/epja/i2002-10256-8

THE EUROPEAN PHYSICAL JOURNAL A

Perturbative versus nonperturbative effects at medium energies in the $\gamma\gamma \to \pi^+\pi^-$ reaction

A. Szczurek[1,2,a] and J. Speth[3]

[1] Institute of Nuclear Physics, PL-31-342 Kraków, Poland
[2] University of Rzeszów, PL-35-959 Rzeszów, Poland
[3] Institut für Kernphysik, Forschungszentrum Jülich, D-52425 Jülich, Germany

Received: 30 September 2002 /
Published online: 22 October 2003 – © Società Italiana di Fisica / Springer-Verlag 2003

Abstract. The interplay of pQCD, pion exchange and FSI effects is studied for the $\gamma\gamma \to \pi^+\pi^-$ reaction in the region of $2\,\mathrm{GeV} < W_{\gamma\gamma} < 6\,\mathrm{GeV}$. We find strong interference effects between pQCD and soft-pion-exchange amplitudes up to $W_{\gamma\gamma} \sim 4\,\mathrm{GeV}$. We discuss to which extend the conventional hadronic FSI effects cloud the pQCD effects. We study multipole soft- and hard-scattering effects as well as the coupling between final-state hadronic channels.

PACS. 12.38.Bx Perturbative calculations – 11.80.La Multiple scattering

1 Introduction

It was predicted long ago [1] that at large t and large u the angular distribution of pions from the reaction $\gamma\gamma \to \pi^+\pi^-$ should be described by means of perturbative QCD due to the exchange of t-channel (u-channel) quarks. This reaction is commonly considered as a gold-plated reaction for pQCD effects to be observed. There is no common consensus how large t (or u) should be so that the pQCD behaviour of the angular distributions could be observed.

In the leading-twist perturbative treatment, the transition amplitude factorizes into a hard-scattering amplitude and a pion distribution amplitude. The pion distribution amplitude was found to be strongly constrained by the photon-pion transition form factor [2]. For the "realistic" distribution amplitude the pQCD contribution to the reaction $\gamma\gamma \to \pi^+\pi^-$ [3] is well below the experimental data above the resonance region ($2\,\mathrm{GeV} < W < 3.5\,\mathrm{GeV}$) [4, 5]. Recent analyses of the DELPHI and ALEPH Collaborations at LEP2 [6,7] extend the energy range.

Recently we have shown [8] that in the pion-pion elastic scattering at $W > 2\,\mathrm{GeV}$ the multipole soft rescatterings play an important role up to very large momenta transferred. Inspired by the result of [8], we have discussed the role of the final-state interaction (FSI) effects in $\gamma\gamma \to \pi^+\pi^-$ [9].

[a] e-mail: szczurek@alf.ifj.edu.pl

2 A sketch of calculation details and main results

According to the rules proposed in [10], at large energies and large center-of-mass angles the amplitude for the reaction $\gamma\gamma \to \pi^+\pi^-$ can be factorized into a perturbatively calculable hard-scattering amplitude and a nonperturbative distribution amplitude of finding a valence quark in each pion:

$$M_{\lambda_1\lambda_2}(W,\theta) = \int_0^1 \mathrm{d}x_1 \int_0^1 \mathrm{d}x_2 \times \Phi^*_\pi(x_1,\tilde{Q}_1) T^H_{\lambda_1\lambda_2}(x_1,x_2,W,\theta) \Phi^*_\pi(x_2,\tilde{Q}_2). \quad (1)$$

The indices λ_1 and λ_2 are photon helicities. In general, the distribution amplitudes Φ_π undergo a slow logarithmic QCD evolution, depending on scales $\tilde{Q}_1$ and $\tilde{Q}_2$. Because in the present analysis we concentrate mainly on pion exchange and FSI effects, we shall limit the approximation for T^H to the leading order (LO) in α_s only. The distribution amplitudes cannot be calculated from first principles. Based on phenomenology of a few reactions, it seems at present that the distribution amplitude is rather close to the asymptotic one:

$$\Phi_\pi(x) = \sqrt{3} f_\pi x(1-x), \quad (2)$$

where f_π is the pion decay constant.

In our calculation we followed [11] rather than [1] and used running coupling constant with simple analytic models for freezing [9].

The pQCD amplitude (1) contains singularities at $\theta = 0$ and $\theta = \pi$ (see [1]) which are artifacts of the collinear approximation. Furthermore the small-angle scattering is probably of soft nonperturbative character due to meson or reggeon exchanges which are explicitly included in the present approach. Therefore, in order to avoid double counting and make the use of the pQCD amplitudes in the multiple-scattering series possible, we smoothly cut off the small t and small u regions in the perturbative amplitude [9].

The QED pion-exchange Born amplitude for the reaction $\gamma\gamma \to \pi^+\pi^-$ with point-like particles has been known for long time [12]. An interesting problem is how to generalize the QED amplitude for real finite-size pions. We follow the idea of Poppe [13] and correct the QED amplitude by an overall t and u dependent form factor

$$A_{fs}(t,u,s) = \Omega(t,u,s) \cdot A_{\mathrm{QED}}(t,u,s). \tag{3}$$

This form by construction guarantees crossing symmetry. At sufficiently high energies the following simple Ansatz fulfils this requirement

$$\Omega(t,u,s) = \frac{F^2(t) + F^2(u)}{1 + F^2(-s)}, \tag{4}$$

where F is a standard vertex function such that $F(0) \approx 1$ and $F(t) \to 0$ when $t \to \infty$. In the limit of large s the Ansatz (4) generates standard vertex form factors [9]. The finite-size pion exchange leads to a cross-section which decreases with energy faster than the pQCD cross-section. An interesting question is: at what energy the pion exchange can be neglected.

The size of the interference effects can be estimated by comparing the incoherent sum of the pQCD process and the soft pion exchange $\sigma_{\mathrm{inc}} \propto |A_{\mathrm{pQCD}}| + |A_\pi|^2$ and the coherent sum $\sigma_{\mathrm{coh}} \propto |A_{\mathrm{pQCD}} + A_\pi|^2$. It was found [9] that the interference effects are generally large and positive. The coherent sum $|\mathrm{pQCD} + \pi|^2$ depends only weakly on the functional form of the form factor used. The interference of the pQCD and pion exchange amplitudes improves considerably the agreement with the recent DELPHI [6] and ALEPH [7] data. The constructive interference can be observed over the whole angular range [9].

The f_2-resonance is known to be strongly populated in the $\gamma\gamma$ collisions (see for instance [14,15]). It is rather broad with $\Gamma \sim 0.2\,\mathrm{GeV}$. The leading-twist pQCD contribution drops strongly with energy. Therefore one should look at the interplay of the high energy flank of f_2 with the strongly decreasing continuum. Then all kinds of energy dependence of kinematical and dynamical origin must be included. In the relativistic approach, the total cross-section for the resonance contribution reads

$$\sigma_{\gamma\gamma\to\pi\pi}(W) = 8\pi(2J+1)\left(\frac{M_R}{W}\right)^2 \times \frac{\Gamma_{\gamma\gamma}\Gamma_{\mathrm{tot}}(W) Br\left(f_2 \longrightarrow \pi^+\pi^-\right)}{\left(W^2 - M_R^2\right)^2 + M_R^2\Gamma_{\mathrm{tot}}^2}. \tag{5}$$

Table 1. Brief summary of double-scattering processes considered in this paper for $\gamma\gamma \to \pi^+\pi^-$.

Number	First step	Intermediate channel	Second step
1	soft π exch.	$\pi^+\pi^-$	$IP + f_2 + \rho$ exch.
2	pQCD	$\pi^+\pi^-$	$IP + f_2 + \rho$ exch.
3	soft VDM	$\rho^0\rho^0$	π exch.
4	pQCD	$\rho^+(0)\rho^-(0)$	π exch.

One usually parametrizes Γ_{tot} as

$$\Gamma_{\mathrm{tot}}(W) = \Gamma_{\mathrm{tot}}^0 \left(\frac{p}{p_0}\right)^{2l+1} \mathcal{F}_{\mathrm{dyn}}(p), \tag{6}$$

where $\mathcal{F}_{\mathrm{dyn}}(p)$ is a function of dynamical origin usually obtained in a simple nuclear-physics–inspired model of resonances.

It was recently demonstrated that for elastic pion-pion scattering, soft FSI effects lead to a damping of the cross-section at small angles and a considerable enhancement in the region of intermediate angles where they compete with the two-gluon exchange amplitude. In the following we shall discuss only some selected FSI effects for the reaction under consideration. In table 1 we list double-scattering terms considered in the present analysis.

In the language of multiple scattering at high energies [16] the amplitude for the reaction $\gamma\gamma \to \pi^+\pi^-$ can be written as an infinite series of the type

$$\begin{aligned} A_{\gamma\gamma\to\pi^+\pi^-}(s,t,u) &= \sum_\alpha A^{(\alpha)}_{\gamma\gamma\to\pi^+\pi^-}(s,t,u) \\ &+ \sum_{ij}\sum_{\alpha,\beta} \frac{i}{32\pi^2 s} \int \mathrm{d}^2\boldsymbol{k}_1 \mathrm{d}^2\boldsymbol{k}_2 \delta^2(\boldsymbol{k} - \boldsymbol{k}_1 - \boldsymbol{k}_2) \\ &+ A^{(\alpha)}_{\gamma\gamma\to ij}(s,\boldsymbol{k}_1) A^{(\beta)}_{ij\to\pi^+\pi^-}(s,\boldsymbol{k}_2) \\ &+ (\cdots). \end{aligned} \tag{7}$$

Here Greek indices label type of exchange, while Latin indices ij, etc. label two-body intermediate states.

The first component in (7) corresponds to single-scattering terms. In the following we shall include only $\alpha = \pi$ (pion exchange) or $\alpha = 2q$ (pQCD quark exchange) single-exchange amplitudes. We include only $ij = \pi^+\pi^-$ and $ij = \rho\rho$ intermediate states. The parameters of pion-pion interaction are taken from ref. [8].

In fig. 1 we present the result corresponding to the coherent sum of all processes discussed. For comparison we show the pQCD result. For $W > 2\,\mathrm{GeV}$ the final result is practically independent of the phase of the resonance contribution with respect to the other contributions. As can be seen by comparison of the solid and dashed line the inclusion of the processes considered in the present paper leads to a considerable improvement with respect to the pQCD calculation. The final result describes the ALEPH [7] and DELPHI [6] data surprisingly well.

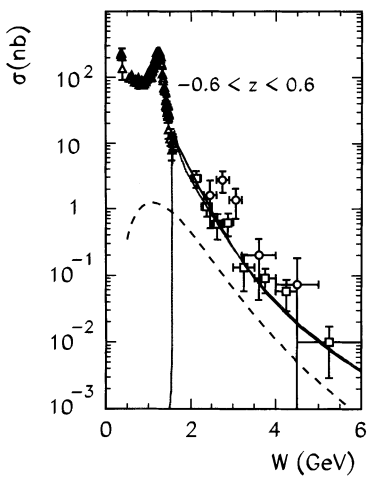

Fig. 1. The result corresponding to the coherent sum of all processes (solid line) *versus* pQCD result (dashed line). The vertical solid line shows the expected lower limit of the range of applicability of the present multipole-scattering approach.

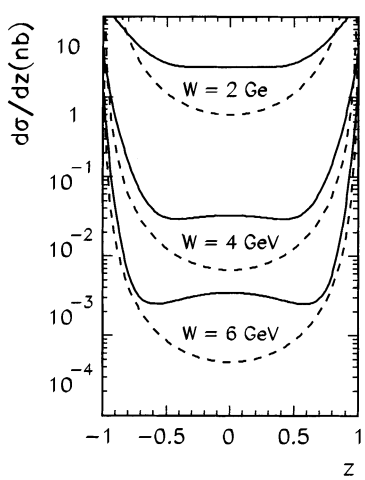

Fig. 2. The result corresponding to the coherent sum of all processes (solid line) *versus* pQCD result (dashed line).

To complete our results we present in fig. 2 the corresponding angular distributions. A large enhancement with respect to pQCD at intermediate angles ($z \sim 0$) is clearly visible. We predict an almost flat $d\sigma/dz$ in the experimentally measured region of $-0.6 < z < 0.6$. This is due to the competition of pion-exchange, pQCD, the tail of the f_2-resonance and multiple scattering effects.

3 Conclusions

Recent LEP2 results for the reaction $\gamma\gamma \to \pi^+\pi^-$, when combined with the present understanding of the pion distribution amplitudes, clearly demonstrate a failure of the leading-twist pQCD in explaining the data.

It was found that the soft-pion exchange, which is known to be the dominant mechanism below the f_2-resonance, remains important also above the resonance. Because the pQCD contribution strongly decreases with the photon-photon energy the high-energy flank of the broad f_2-resonance gives a contribution of comparable size to the pQCD continuum in a rather broad energy range above the resonance.

Using phenomenological, yet realistic, pion-pion interaction found in a recent analysis, we have estimated the contribution of the FSI processes. We have found that pion-pion FSI as well as the coupling with the $\rho\rho$ channel modify the total amplitude at the level of 20%.

In the light of our analysis, we conclude that the reaction $\gamma\gamma \to \pi^+\pi^-$ is not the best choice to identify the pQCD predictions.

References

1. S.J. Brodsky, G.P. Lepage, Phys. Rev. D **24**, 1808 (1981).
2. P. Kroll, M. Raulfs, Phys. Lett. B **387**, 848 (1996).
3. C. Vogt, hep-ph/9911253, hep-ph/0010040.
4. TPC/Two-Gamma Collaboration (H. Aihara *et al.*), Phys. Rev. Lett. **57**, 404 (1986).
5. CLEO Collaboration (J. Dominick *et al.*), Phys. Rev. D **50**, 3027 (1994).
6. DELPHI Collaboration (K. Grzelak), a talk at the *International Conference PHOTON2001, Ascona, Switzerland, September 2-7, 2001.*
7. ALEPH Collaboration (A. Finch), a private information.
8. A. Szczurek, N.N. Nikolaev, J. Speth, Phys. Rev. C **66**, 055206 (2002).
9. A. Szczurek, J. Speth, hep-ph/0207265.
10. G.P. Lepage, S.J. Brodsky, Phys. Rev. Lett. **43**, 545 (1979); Phys. Rev. D **22**, 2157 (1980).
11. Ch.-R. Ji, F. Amiri, Phys. Rev. D **42**, 3764 (1990).
12. S.J. Brodsky, T. Kinoshita, H. Terazawa, Phys. Rev. D **4**, 1532 (1971).
13. M. Poppe, Int. J. Mod. Phys. A **1**, 545 (1986).
14. Mark II Collaboration (J. Boyer *et al.*), Phys. Rev. D **42**, 1350 (1990).
15. Crystal Ball Collaboration (H. Marsiske *et al.*), Phys. Rev. D **41**, 3324 (1990).
16. K.A. Ter-Martirosyan, Sov. J. Nucl. Phys. **10**, 600 (1970).

Eur. Phys. J. A **18**, 449–451 (2003)
DOI 10.1140/epja/i2002-10257-7

THE EUROPEAN PHYSICAL JOURNAL A

Parton symmetries and the NuTeV anomaly

A.I. Signal[a] and F.G. Cao

Institute of Fundamental Sciences, Massey University, Palmerston North, New Zealand

Received: 30 September 2002 /
Published online: 22 October 2003 – © Società Italiana di Fisica / Springer-Verlag 2003

Abstract. Recently the NuTeV Collaboration (Phys. Rev. Lett. **88**, 091802 (2002)) announced a new measurement of $\sin^2\theta_W$ which was approximately three standard deviations above the currently accepted standard model value. The NuTeV analysis depends on the assumption that various quark-parton model symmetries are not broken. In particular the analysis takes $\bar{s}(x) = s(x)$ and $d_V^n(x) = u_V^p(x)$. However models which break these symmetries are known. We examine the predictions of these models and their effect on the NuTeV result. In most instances the effect is to decrease the discrepancy between the NuTeV result and the accepted value.

PACS. 13.15.+g Neutrino interactions – 11.30.Hv Flavor symmetries

1 Introduction

The NuTeV Collaboration has measured NC to CC ratios in deep-inelastic $\nu(\bar{\nu})$-nucleon scattering. This enables them to determine the effective couplings to left- and right-handed quarks (g_L and g_R) and, via the Paschos-Wolfenstein (PW) ratio

$$R_{PW} = \frac{\sigma_{NC}^{\nu} - \sigma_{NC}^{\bar{\nu}}}{\sigma_{CC}^{\nu} - \sigma_{CC}^{\bar{\nu}}} = g_L^2 - g_R^2 = \frac{1}{2} - \sin^2\theta_W, \qquad (1)$$

the value of the weak mixing angle

$$\sin^2\theta_W = 0.2277 \pm 0.0013(\text{stat}) \pm 0.0009(\text{syst}). \qquad (2)$$

Compared with the accepted value [1] of 0.2227 ± 0.0037 there is a 3σ discrepancy.

While this discrepancy may point to new physics, there are possible explanations in the standard model. As discussed by Davidson and collaborators [2], the PW ratio receives both electro-weak corrections and higher-order QCD corrections. However these appear to be too small to explain the discrepancy. Another possibility [3] is corrections arising from nuclear shadowing, which would be a higher twist effect. The possibility we will explore here is that the breaking of symmetries by the parton distributions can cause the observed discrepancy.

2 Parton symmetry breaking

There are two possible symmetry-breaking contributions to the PW ratio at leading order: quark-anti-quark asymmetries in the sea distributions and charge symmetry breaking in the valence distributions. Including both these effects the PW ratio becomes (to leading order in α_S)

$$R_{PW} = \frac{1}{2} - \sin^2\theta_W + \frac{3b_1 + b_2}{\langle x(u_V + d_V)\rangle/2}\Big[\langle x(c-\bar{c})\rangle - \langle x(s-\bar{s})\rangle + \frac{1}{2}\big(\langle x\delta u_V\rangle - \langle x\delta d_V\rangle\big)\Big], \qquad (3)$$

where

$$\delta u_V = u_V^p - d_V^n; \qquad \delta d_V = d_V^p - u_V^n \qquad (4)$$

are the charge symmetry-breaking valence distributions and

$$b_1 = \Delta_u^2 = g_{L_u}^2 - g_{R_u}^2; \qquad b_2 = \Delta_d^2 = g_{L_d}^2 - g_{R_d}^2 \qquad (5)$$

At the NuTeV scale ($Q^2 = 16\,\text{GeV}^2$) the coefficient in front of the square brackets of eq. (3) is about 1.3, so a symmetry-breaking term inside the square brackets of -0.0038 would explain the discrepancy between the NuTeV value and the accepted value of $\sin^2\theta_W$.

As the charm component of the sea is generated perturbatively, we expect $c(x) = \bar{c}(x)$, however processes such as $N \to \Lambda K$ can generate a non-perturbative component to the strange sea [4] and different shapes for $s(x)$ and $\bar{s}(x)$. The meson cloud model (MCM) [5] is a useful model for calculating the contributions to the strange sea from processes involving the meson cloud. We have used two approaches for the parton distributions of the baryons (Λ, Σ) and the kaon:

1. Take the baryon distributions to be $SU(3)$ symmetric *i.e.* $s^{\Lambda}(x) = s^{\Sigma}(x) = u^p(x)/2$, and for the kaon distribution use the Dortmund group parametrization [6].

[a] e-mail: a.i.signal@massey.ac.nz

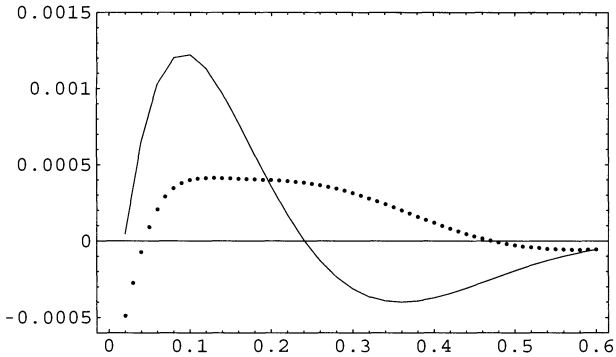

Fig. 1. The strange sea asymmetry calculated in the meson cloud model with $SU(3)$ symmetric baryon distributions (solid line) and the bag model baryon and kaon distributions (dotted line).

2. Calculate the distributions using the bag model [7], which breaks $SU(3)$.

While these two methods give different shapes for $x(s-\bar{s})$ (see fig. 1) they give similar results for the sign and magnitude of the integral of this distribution. For the MCM cut-off parameter $\Lambda = 1.08\,\mathrm{GeV}$ we find

$$\langle x(s-\bar{s})\rangle \approx 0.0001, \tag{6}$$

and varying the value of Λ does not significantly change the order of magnitude of this result. Thus it appears that any strange sea asymmetry is probably an order of magnitude too small to affect the NuTeV result.

It is interesting to note that one PDF fit [8] does allow $s(x) \neq \bar{s}(x)$, finding $\langle x(s-\bar{s})\rangle = 0.002 \pm 0.0028$ at $Q^2 = 20\,\mathrm{GeV}^2$, however the difference is mostly at large x rather than small x as in the MCM. NuTeV have also looked for a strange asymmetry [9], and find a small negative value for $\langle x(s-\bar{s})\rangle$, with a large (100%) uncertainty. Also the fit they used did not satisfy $\langle s-\bar{s}\rangle = 0$.

Charge symmetry is usually a good symmetry in quark phenomenology. The scale of any violation of CS is set by $(M_n - M_p)/M_p \approx 0.1\%$, however this may be enough to affect the significance of the NuTeV result. In the MCM charge symmetry breaking (CSB) can arise from mass differences in isospin multiplets. Cao and Signal [10] found a small effect in valence distributions: $\langle x\delta u_{\mathrm{V}}\rangle = -0.00018$ and $\langle x\delta d_{\mathrm{V}}\rangle = -0.00015$ with the MCM cut-off parameter $\Lambda = 1.08\,\mathrm{GeV}$. However CSB can also occur in the "bare" valence distributions, and this is much harder to estimate. There can be contributions from the mass difference between the proton and neutron, from the shift in mass of the intermediate state (Bickerstaff and Thomas [11] estimate $(m_{dd} - m_{uu}) = 4\,\mathrm{MeV}$), and from any change in the quark wave function due to changes in quark mass and changes in the boundary conditions. Using the bag model Sather [12] found $\langle x\delta u_{\mathrm{V}}\rangle - \langle x\delta d_{\mathrm{V}}\rangle = -0.0047$. A more extensive calculation by Rodionov, Thomas and Londergan [13] found that the valence distributions could be changed by as much as 5%, especially in the large x region. They concluded that shifts in the intermediate state mass give the most important CSB effect. The changes in the nucleon mass and the quark wavefunction both give 1% effects.

We have investigated the effect of varying the intermediate state mass M_n and the initial mass M using the formalism of the Adelaide group [14]. The parton distribution can be written

$$q(x) = M \sum_n \int_{p_m}^{\infty} p_n \,\mathrm{d}p_n G(pn),$$
$$p_m = \left|\frac{M^2(1-x)^2 - M_n^2}{2M(1-x)}\right|, \tag{7}$$

and we restrict our discussion to diquark intermediate states. A change in M or M_n then causes a change in the parton distribution

$$\mathrm{d}q(x) = \frac{\partial q(x)}{\partial M_n}\mathrm{d}M_n + \left(\frac{\partial q(x)}{\partial M} + \frac{\partial q(x)}{\partial x}\frac{\mathrm{d}x}{\mathrm{d}M}\right)\mathrm{d}M, \tag{8}$$

where the second term is a total derivative as x and M are not independent. We then obtain

$$\mathrm{d}q(x) = \frac{\partial q(x)}{\partial x} g(x)\mathrm{d}M_n + \frac{1}{M}\frac{\partial}{\partial x}(xq(x))\mathrm{d}M, \tag{9}$$

where

$$g(x) = \frac{2M_n(1-x)}{M^2(1-x)^2 + M_n^2}. \tag{10}$$

Comparing this expression with that of Sather, we see that the second term agrees, and the first term is the same if p_m is kept constant. Taking moments then gives

$$\langle x^j\,\mathrm{d}q(x)\rangle = -\left[j\langle x^{j-1}q(x)g(x)\rangle + \left\langle x^j q(x)\frac{\partial g(x)}{\partial x}\right\rangle\right]\mathrm{d}M_n - \frac{j}{M}\langle x^j q(x)\rangle \mathrm{d}M. \tag{11}$$

The second term can be evaluated using the full parton distribution $q(x)$, but the first should be evaluated using just the diquark intermediate states. We can do this using the bag model calculation of Boros and Thomas [7] and evolving at NLO up to $16\,\mathrm{GeV}^2$. We obtain the CSB in the valence distributions (giving the contribution of each term in eq. (11)):

$$\langle x\delta d_{\mathrm{V}}(x)\rangle = 0.0011 + 0.00017, \tag{12}$$
$$\langle x\delta u_{\mathrm{V}}(x)\rangle = 0 + 0.00033. \tag{13}$$

As the u_{V} distribution always arises from (ud) diquark intermediate states, these is no effect on this distribution from the 4 MeV splitting between dd and ud intermediate states. We also see that the shift in the intermediate state mass gives the dominant CSB contribution to the d_{V} distribution, in agreement with the results of ref. [13]. We find a total CSB contribution to the PW ratio of

$$\frac{1}{2}\langle x\delta u_{\mathrm{V}}(x)\rangle - \frac{1}{2}\langle x\delta d_{\mathrm{V}}(x)\rangle \approx -0.0006, \tag{14}$$

which is not large enough in magnitude to bring the NuTeV result into agreement with the accepted value of $\sin^2\theta_{\mathrm{W}}$, but does decrease the discrepancy a little.

3 Summary

We have investigated the possible role of symmetry breaking among parton distributions as an explanation of the anomalous NuTeV result for $\sin^2\theta_W$. The most important symmetry-breaking contributions are an asymmetry in the strange sea and charge symmetry breaking in the valence distributions. However detailed calculation shows that both these contributions are too small in magnitude to explain the anomaly, but the tendency is for them to reduce the size of the difference between the NuTeV value and the accepted value, so that the discrepancy is now at the 2σ level. We note that there is very little experimental information on these symmetry-breaking contributions.

This work is supported by the Marsden Fund of the Royal Society of New Zealand, and by the Science and Technology Postdoctoral Fellowship of the Foundation for Research Science and Technology.

References

1. LEPEWWG, Report CERN-EP/2001-098, hep-ex/0112021.
2. S. Davidson *et al.*, JHEP **02**, 037 (2002).
3. G.A. Miller, A.W. Thomas, hep-ex/0204007.
4. A.I. Signal, A.W. Thomas, Phys. Lett. B **191**, 205 (1987).
5. H. Holtmann, A. Szczurek, J. Speth, Nucl. Phys. A **596**, 631 (1996); J. Speth, A.W. Thomas, Adv. Nucl. Phys. **24**, 83 (1997).
6. M. Glück, E. Reya, M. Stratmann, Eur. Phys. J. C **2**, 159 (1998).
7. C. Boros, A.W. Thomas, Phys. Rev. D **60**, 074017 (1999).
8. V. Barone, C. Pascaud, F. Zomer, Eur. Phys. J. C **12**, 2 (2000).
9. NuTeV Collaboration (M. Goncharov *et al.*), Phys. Rev. D **64**, 112006 (2001).
10. F.G. Cao, A.I. Signal, Phys. Rev. C **62**, 015203 (2000).
11. R.P. Bickerstaff, A.W. Thomas, Phys. Rev. D **35**, 108 (1987).
12. E. Sather, Phys. Lett. B **191**, 205 (1992).
13. E.N. Rodionov, A.W. Thomas, J.T. Londergan, Mod. Phys. Lett. A **9**, 1799 (1994).
14. A.I. Signal, A.W. Thomas, Phys. Rev. D **40**, 2832 (1989); A.W. Schreiber, A.I. Signal, A.W. Thomas, Phys. Rev. D **44**, 2653 (1991).

Eur. Phys. J. A **18**, 453–458 (2003)
DOI 10.1140/epja/i2002-10258-6

THE EUROPEAN PHYSICAL JOURNAL A

Hadrons in dense and hot matter

J. Wambach[a]

Institut für Kernphysik, Technische Universität Darmstadt, Schloßgartenstr. 9, D-64289 Darmstadt, Germany

Received: 30 September 2002 /
Published online: 22 October 2003 – © Società Italiana di Fisica / Springer-Verlag 2003

Abstract. Theoretical issues and perspectives of hadronic matter at high baryon density are discussed with focus on the restoration of chiral symmetry and observable consequences.

PACS. 25.75.-q Relativistic heavy-ion collisions – 21.65.+f Nuclear matter

1 Introduction

The properties of strongly interacting matter under extreme conditions in temperature and density are the central focus of the relativistic heavy-ion program. One of the aims is to explore the phase diagram in the (T, μ)-plane which becomes experimentally accessible provided thermal equilibrium is reached during the early stages of the collision. The hadrochemical analysis of freeze-out abundances indicates that this may indeed be the case over a wide range of collision energies [1]. Our understanding of the phase structure and possible phase transitions remains sketchy. Stringent results from *ab initio* lattice simulations are only available along the T-axis [2] due to numerical difficulties at finite μ. The $\mu = 0$ lattice results indicate that, for physical values of the bare strange quark mass m_s° there is a smooth crossover at a transition temperature of $\sim 170\,\mathrm{MeV}$ at which chiral symmetry is restored, accompanied by a rapid change in the bulk thermodynamic variables. The latter signals the opening up of new degrees of freedom and is interpreted as a signature of deconfinement. It remains to be understood why chiral symmetry restoration and deconfinement seem to occur at the same value of the temperature. Several model studies [3] indicate that at values of $\mu \sim 1\,\mathrm{GeV}$ and small temperatures a chiral phase transition of first order should occur. This implies the existence of a critical point at which the critical line ends. The exact location of this point sensitively depends on the value of m_s° and its experimental determination would be an important milestone in the study of the phase diagram. Possible signatures have been suggested [4] and relate to the long-wavelength fluctuations of the in-medium chiral condensate.

In this paper I will focus on aspects of the restoration of spontaneously broken chiral symmetry which, in my opinion, are better understood than the issues related to deconfinement. Spontaneous chiral-symmetry breaking in the QCD vacuum and its restoration at finite μ and T is intimately related to the question of mass generation for light hadrons and the medium modification of their spectral properties.

2 The restoration of chiral symmetry

The starting point for the equilibrium description of strongly interacting matter is the QCD partition function in the grand canonical ensemble

$$\mathcal{Z}_{\mathrm{QCD}}(V, T, \mu_q) = \mathrm{Tr}\, e^{-(H_{\mathrm{QCD}} - \mu_q N_q)/T}, \qquad (1)$$

where N_q is the quark number operator and $\mu_q = \mu/3$ the quark chemical potential. From the free energy $\Omega(T, \mu) = -T \lim_{V\to\infty} 1/V \ln \mathcal{Z}_{\mathrm{QCD}}(V, T, \mu_q)$ all thermodynamic quantities such as pressure, internal energy, entropy, etc. can be derived in a standard way. In addition, an expression for the chiral condensate is obtained as

$$\langle\langle \bar{q}q \rangle\rangle = \frac{\partial \Omega(T, \mu)}{\partial m_q^\circ}, \qquad (2)$$

where m_q° denotes the current quark mass. Finally, through the corresponding susceptibilities, the free energy also determines the fluctuation properties of matter and hence the criticality near a phase transition. Besides the specific heat, the compressibility etc., the scalar (chiral) susceptibility

$$\chi_S = \frac{T}{V} \frac{\partial^2 \Omega(T, \mu)}{\partial m_q^{\circ 2}} = \langle\langle (\bar{q}q)^2 \rangle\rangle - \langle\langle \bar{q}q \rangle\rangle^2 \qquad (3)$$

which relates to the fluctuations of the chiral condensate, plays an important role.

[a] e-mail: wambach@physik.tu-darmstadt.de

2.1 Evolution of the chiral condensate

The chiral condensate is one of the order parameters for chiral-symmetry breaking and its evolution with temperature and number density, $n(\mu)$, reflects the restoration of the symmetry. Starting from low T or μ close to the chemical potential of nuclear matter at saturation, μ_0, it is more economical to work with confined hadrons rather than quark-gluon degrees of freedom. The connection can be made rigorous. Using eq. (2) in conjunction with the Gell-Mann Oakes Renner relation (GOR) which is well obeyed in vacuum [5] one can express the ratio of the in-medium condensate to that in the vacuum as a sum over all hadronic states present in matter as

$$\frac{\langle\langle\bar{q}q\rangle\rangle}{\langle\bar{q}q\rangle} \equiv R_\chi = 1 - \sum_h \frac{\Sigma_h \varrho_h^s(T,\mu)}{f_\pi^2 m_\pi^2} \tag{4}$$

with

$$\Sigma_h = m_q^\circ \frac{\partial m_h}{\partial m_q^\circ} = \frac{1}{m_q^\circ}\langle h|\bar{q}q|h\rangle; \quad \varrho_h^s(T,\mu_q) = \frac{\partial\tilde{\Omega}(T,\mu)}{\partial m_h} \tag{5}$$

($\tilde{\Omega}(T,\mu) = \Omega(T,\mu) - \Omega(0)$). There are two ingredients that enter eq. (4). One relates to the chiral properties of the hadron in question and is determined by the corresponding "sigma commutator", Σ_h. Physically, Σ_h represents the amount of energy required to displace the vacuum condensate in the vicinity of the hadron. The second involves the scalar density $\varrho_h^s(T,\mu)$ of hadrons in the interacting matter which is determined by $\partial\Omega(T,\mu)/\partial m_h$, where m_h denotes the vacuum mass of the hadron. Here the full complications of the many-body problem enter.

There are only two regions in the phase diagram where we have complete knowledge for the condensate evolution. One is for small T and μ, *i.e.* close to vacuum, and the other near cold nuclear matter at saturation characterized by $T = 0$, $\mu = \mu_0$. For small T and μ, hadronic matter can be viewed as a weakly interacting gas of thermally excited pions. Similarly, nuclear matter in the vicinity of μ_0 and small temperatures approximately behaves as a dilute gas of nucleons interacting with pions. In both cases chiral perturbation theory as a rigorous effective field theory can be applied, to obtain a model-independent leading-order expansion for eq. (4):

$$\frac{\langle\langle\bar{q}q\rangle\rangle}{\langle\bar{q}q\rangle} = 1 - \frac{T^2}{8f_\pi^2} - 0.3\frac{n(\mu)}{n(\mu_0)} + \cdots, \tag{6}$$

which corresponds to the free gas approximation. Thus, the mere presence of an ideal gas of hadrons diminishes the chiral condensate without changing the vacuum properties of the hadrons! Obviously, medium modifications and the corresponding non-trivial changes of the chiral condensate have to involve hadronic interactions. They become increasingly important as the matter grows hotter and denser, *i.e.* one moves deeper into the (T,μ)-plane and approaches the phase boundary. According to eq. (4), more and more hadronic states will enter, which severely limits the description near the phase transition. Chiral perturbation theory ceases to be applicable and one has to resort to chiral effective Lagrangians that treat higher-mass hadrons as explicit degrees of freedom. In the vicinity of the phase boundary, non-perturbative many-body methods are called for, in addition.

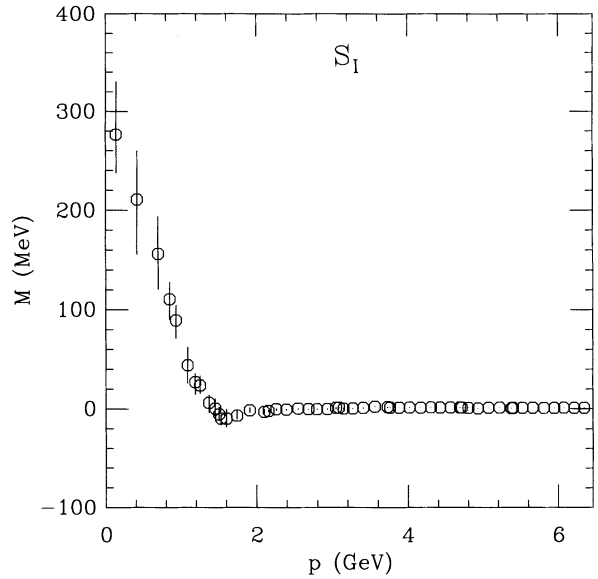

Fig. 1. The lattice quark mass function in Landau gauge [8].

2.2 Hadrons and chiral symmetry

Spontaneous chiral-symmetry breaking plays a decisive role in the mass generation of light hadrons [6,7]. On the other hand, chiral-symmetry breaking is an infrared phenomenon. This is clearly seen in lattice calculations of the Euclidean quark mass function in the Landau gauge [8] (fig. 1) and also follows from Dyson-Schwinger approaches [9]. As a consequence, high-mass mesons and baryons should decouple from the chiral condensate leading to parity doublets. This implies that their respective sigma commutators vanish (or at least become very small). Hence, according to eq. (4), they do not contribute to the condensate evolution. There is some evidence for parity doubling in the meson and baryon spectrum. The recent τ-decay measurements [10] of the vector- and axial-vector spectral distribution suggest that both spectral functions become identical between 1.5 GeV and 2 GeV and coincide with the PQCD limit [11]. This energy scale would be consistent with the lattice results in fig. 1. For the nucleon there are also tantalizing hints for parity doubling in the same range of excitation energy as suggested in ref. [12]. To put this conjecture on firmer grounds, detailed baryon spectroscopy of overlapping resonances is required. This difficult task is being discussed at electron accelerators such as ELSA in Bonn [13].

The fact that high-mass mesons and baryons do not contribute to the evolution of the chiral condensate opens the possibility to construct chiral Lagrangians with a limited number of degrees of freedom, including only hadrons with masses less than $\sim$ 2 GeV. To what extent such

hadrons are elementary quark states or dynamically generated resonances remains an open question and is of great importance to evaluate their sigma commutators. For the nucleon, significant progress in this direction is being made by calculating the bare quark mass dependence of the mass, supplemented by chiral extrapolations to realistic values of $m^{\circ}_{u,d}$. Such studies allow for an *ab initio* evaluation of Σ_N. A similar lattice analysis for excited states would be highly desirable.

3 Medium modification of hadrons

What are the signatures of chiral-symmetry restoration in hadronic matter? Being renormalization scale dependent, the chiral condensate is not an observable. Changes in $\Omega(T,\mu)$ and possible phase transitions are, however, reflected in the measurable excitation spectrum. The strategy is therefore to study the in-medium hadronic spectral functions as the elementary excitations the matter in equilibrium. In condensed matter this approach is known as "soft-mode spectroscopy". Quite generally, the restoration of broken chiral symmetry will lead to identical spectral functions for channels of opposite parity.

In QCD, the spectral properties of hadrons are encoded in the two-point correlation functions involving currents with the appropriate quantum numbers,

$$D_i(q_0,\boldsymbol{q}) = i\int \frac{\mathrm{d}^4x}{(VT)} e^{iqx}\theta(x_0)\langle\langle[J_i(x),J_i(0)]\rangle\rangle, \qquad (7)$$

where J_i are local operators composed of elementary quark fields. Notice the separate dependence on energy q_0 and three-momentum $\boldsymbol{q}$ due to loss of covariance in the medium. The spectral function

$$\rho_i(q_0,\boldsymbol{q}) = -\frac{1}{\pi}\,\mathrm{Im}\,D_i(q_0,\boldsymbol{q}) \qquad (8)$$

represents the excitation spectrum in a given channel of spin and parity. By means of the dispersion relation

$$D_i(q_0,\boldsymbol{q}) = \int_0^\infty \mathrm{d}q_0'^2 \frac{\rho_i(q_0',\boldsymbol{q})}{q_0'^2 - q_0^2 + i\eta}, \qquad (9)$$

ρ_i determines the entire correlation function. Rather than as derivatives of the free energy (eq. (3)), the susceptibilities can also be obtained directly from the spectral functions $\rho_i(q_0,\boldsymbol{q})$ as

$$\chi_i = \langle\langle J_i^2\rangle\rangle - \langle\langle J_i\rangle\rangle^2 = \lim_{(q_0,\boldsymbol{q})\to 0} D_i(q_0,\boldsymbol{q})$$
$$= \int_0^\infty \mathrm{d}q_0'^2 \frac{\rho_i(q_0',0)}{q_0'^2 + i\eta} \qquad (10)$$

which shows that enhanced fluctuations are related to the low-energy and low-momentum behavior of the spectral function.

First-principles lattice calculations of in-medium hadronic spectral functions in Minkowski space have been carried out for finite T and vanishing μ. Using maximum-entropy methods results are reported in refs. [14,15]. Due to the limited number of temporal data points they are still quite crude. At present, more detailed insight into the temperature dependence and the behavior at finite μ is obtained from hadronic models. Formally, the pertinent currents $J_i(x)$ are identified with elementary fields $\phi(x)$ such as the nucleon, Δ-isobar, pion, ρ-meson etc., that constitute the relevant hadronic degrees of freedom. For these, effective field theories, consistent with chiral symmetry, are utilized to calculated the in-medium spectral properties as reliably as possible.

In connection with chiral-symmetry restoration, there are several suggestions for exploring hadrons in the medium. In the following, I will discuss two examples in more detail. One deals with the behavior of the scalar-isoscalar f_0-meson and relates directly to the fluctuations of the chiral condensate. The second concerns the ρ-meson which plays a prominent role for low-mass dilepton production in heavy-ion collisions and has been discussed extensively [16] in connection with the CERES data from the CERN-SpS.

3.1 Scalar modes

As mentioned in sect. 2, the fluctuations of the chiral condensate are indicators for the restoration of chiral symmetry. In a rapid crossover or a weak first-order transition the scalar susceptibility χ_s is strongly enhanced (it diverges in a second-order transition with critical exponents determined by universal behavior). Since χ_s can be obtained directly from the free energy $\Omega(T,\mu)$ (eq. (3)) it can be reliably evaluated on the lattice for vanishing μ. A strong enhancement in the vicinity of the crossover is found [2]. According to eq. (10), this implies that the scalar spectral function must be shifted to lower energy. Within various models there have been several studies of this behavior [17–20] which all come to similar conclusions. As a representative example, I discuss recent results within the linear sigma model in the $1/N$-expansion [21]. Here the scalar quark current $J_s(x) = \bar{q}q(x)$ is identified with the sigma field $\sigma(x)$ [22] and the scalar correlator becomes the in-medium σ-propagator:

$$D_s(q_0,\boldsymbol{q}) \equiv D_\sigma(q_0,\boldsymbol{q})$$
$$= i\int \frac{\mathrm{d}^4x}{(VT)} e^{iqx}\theta(x_0)\langle\langle[\sigma(x),\sigma(0)]\rangle\rangle. \qquad (11)$$

The results displayed in fig. 2 show a strong softening as a function of number density $n(\mu)$. A similar reshaping is also found as a function of temperature. It has been shown explicitly that this effect is also found in non-linear realizations of chiral symmetry [23] and is therefore generic.

What are the experimental signatures? Since the σ- or f_0-meson strongly couples to two-pion states, a softening of the in-medium scalar spectral function leads to the emission of soft pions which should be observable in the p_T spectra or HBT correlations in heavy-ion collisions. There is a precursor to this phenomenon which may have

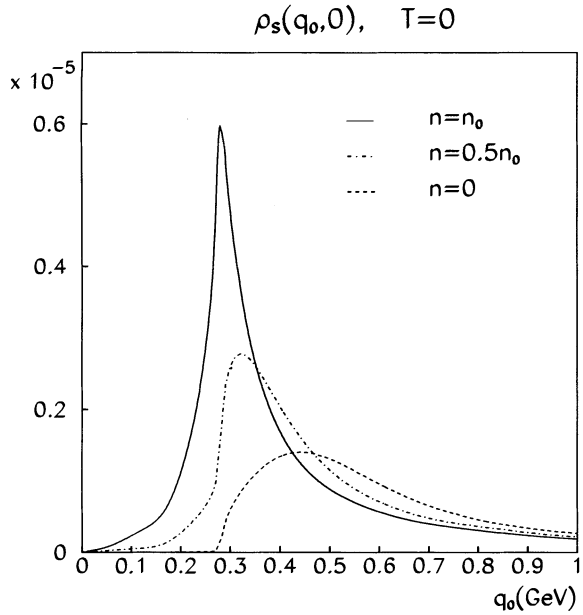

Fig. 2. The in-medium spectral function of the σ-meson for various values of density.

been observed already. According to eq. (6), the chiral condensate in the interior of cold nuclei is reduced by about 30%. Therefore, its fluctuations are enhanced — in fact quite substantially— as can be seen from fig. 2. This prediction can be tested in experiments where two pions with small cms momentum and the quantum numbers $J = I = 0$ of the f_0 are produced near threshold in nuclei. Such experiments have been conducted by the CHAOS Collaboration at TRIUMF using an incident π^+ beam on various nuclear targets [24] identifying charged pions in the final state. A second experiment was performed by the Crystal Ball (CB) Collaboration at BNL with an incident π^- beam [25] detecting a π^0 pair in the final state through coincident 4γ decay. Quite recently, the π_0-pair spectrum has also been measured in photon-induced reactions at MAMI-B using the TAPS spectrometer [26]. The photon has the advantage of weak initial-state interaction. In all cases, a shift to lower invariant masses for heavier nuclei has been reported. A quantitative understanding of the details of the distributions still awaits final clarification. Uniquely establishing the results of the measurements as a consequence of the in-medium s-wave $\pi\pi$ interaction would be an important milestone in the study of the chiral-symmetry restoration.

3.2 Vector- and axial-vector spectral functions

The ρ-meson appears as a prominent resonance in the e^+e^--annihilation cross-section as well as in $\tau \to 2n\pi\nu_\tau$ decay. It therefore plays a central role for dilepton production in heavy-ion collisions at invariant masses below 1 GeV. Medium-modifications of the ρ-meson have been suggested as another signal of chiral-symmetry restoration. The conjecture that the (pole) mass is proportional to some power of the condensate ratio R_χ [27]

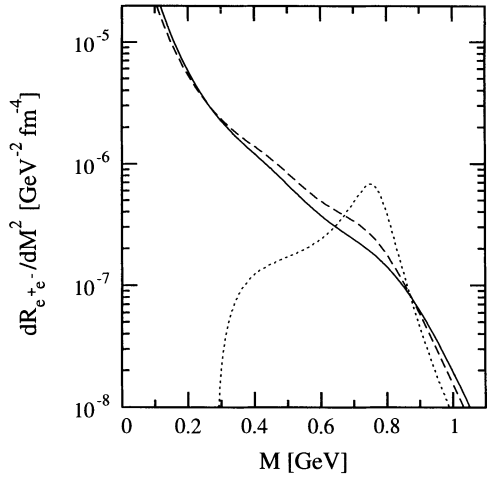

Fig. 3. The theoretical dilepton rate at $T = 150$ MeV and $\mu_B = 3\mu_q = 452$ MeV [28].

("Brown-Rho" (BR) scaling) implies a dropping of the ρ mass as R_χ decreases.

In general, the dilepton-production rate is given by the in-medium electromagnetic spectral function as

$$\frac{\mathrm{d}N_{l^+l^-}}{\mathrm{d}^4x\,\mathrm{d}^4q} = L^{\mu\nu}\left(-\frac{i}{\pi}\right)\int \mathrm{d}^4x e^{iqx}\theta(x_0) \times \langle\langle [J_\mu^{\mathrm{elm}}(x), J_\nu^{\mathrm{elm}}(0)]\rangle\rangle, \tag{12}$$

where $L^{\mu\nu}$ denotes the lepton tensor. In the vector dominance model (VDM) [29] which describes the vacuum properties of the ρ very well, the electromagnetic current correlator directly relates to its in-medium properties. In the calculations [16], two important medium effects can be identified. The first is the modification of the intermediate two-pion states to which the ρ-meson strongly couples. Here proper care has to be taken to ensure gauge invariance. The second is a direct coupling to baryonic resonances, most prominently the $N^*(1520)$-resonance. The inclusion of both effects leads to a large broadening of the spectral function at high density and temperature and results in a dramatic reshaping of the dilepton rate, as indicated in fig. 3. Since theses rates are very close to those obtained in hard-thermal-loop resumed perturbation theory for the quark-gluon plasma [30], one would conclude that the signal for chiral-symmetry restoration in the vector sector is a smooth evolution for the hadronic spectral function into that of the plasma. Once the local rate is space-time evolved through a realistic fireball expansion until thermal freeze-out and detector acceptances and background rates from Dalitz decays are properly accounted for, the resulting rates compare favorably with the measurements of the CERES Collaboration. Also the transverse spectra are well reproduced.

The relevance of such results for the restoration of chiral symmetry is not apparent, though. To make a stringent connection requires a simultaneous evaluation of both the vector- and the axial-vector correlator. In the vacuum and

in the chiral limit both are related by two "Weinberg sum rules" [31]:

$$\int_0^\infty \frac{\mathrm{d}s}{s}\left(\rho_V^\circ(s) - \rho_A^\circ(s)\right) = f_\pi^2;$$

$$\int_0^\infty \mathrm{d}s\left(\rho_V^\circ(s) - \rho_A^\circ(s)\right) = 0, \qquad (13)$$

where the first directly links the vacuum spectral functions to the pion decay constant, f_π. Similar sum rules also hold in the hadronic medium [32] and they serve as an important constraint of effective field theories that intend to properly implement chiral symmetry in the correlators. This is quite difficult especially when dealing with high baryon density. Here baryonic resonances of both parities enter as chiral partners and an understanding of their chiral structure is a necessity. As mentioned earlier, possible parity doubling for high masses is an important issue in this connection.

In the purely mesonic sector, relevant for RHIC energies, there have been several recent attempts to calculate the vector- and axial-vector correlator simultaneously, maintaining gauge invariance and chiral symmetry. One such approach [33,34] starts from the linear sigma model which is globally gauged with elementary ρ and a_1 fields as chiral partners. At high temperatures, a significant reshaping of distributions is observed, especially in the low-energy region. Nevertheless, the ρ and a_1 peaks remain present, even in the vicinity of the phase boundary. The parameters of the model Lagrangian can be adjusted such that, at the tree level, the ρ-meson mass is proportional to the in-medium chiral condensate $\langle\langle\sigma\rangle\rangle$. This is the BR-scaling scenario. To one-loop order, however, it can be proven analytically that the pole mass of the ρ-meson remains unchanged to order T^2 and only receives contributions of order T^4 and higher, hence putting BR-scaling into question. In a series of recent papers [35–37] the original BR scaling conjecture has been revisited in the context of the "vector manifestation" of broken chiral symmetry [38]. At the chiral phase transition this alternative way of breaking chiral symmetry requires the presence of a massless vector meson which is identified with the (longitudinal) ρ-meson. From the dilepton measurements a the BR scenario cannot be rule out, *a priori*, and it will presumably have to be decided in lattice simulations of the pertinent in-medium spectral functions whether the VM is a viable alternative to describe chiral-symmetry restoration.

4 Outlook

Progress has been made in our understanding of the in-medium properties of hadrons and their relation to the restoration of broken chiral symmetry. Several questions and issues remain open, though. They include: 1) the chiral structure of low-mass hadrons, 2) the role of high-mass mesons and baryons and the possible occurrence of parity doubling, 3) further developments of chirally consistent non-perturbative many-body methods that uniquely link the equilibrium properties of matter to those of the spectral functions, 4) comparison of hadronic models for in-medium properties with lattice data, 5) the confinement mechanism for light hadrons, and 6) the role and signatures of deconfinement in the (T, μ) phase diagram.

This work was supported in part by GSI and BMBF.

References

1. P. Braun-Munzinger, J. Stachel, J. Phys. G **28**, 1971 (2002).
2. F. Karsch, Lect. Notes Phys. **583**, 209 (2002).
3. S.P. Klevansky, Rev. Mod. Phys. **64**, 649 (1992); A. Barducci *et al.*, Phys. Rev. D **49**, 426 (1994); M.A. Stephanov, Phys. Rev. Lett. **76**, 4472 (1996); M.A. Halasz *et al.*, Phys. Rev. D **58**, 096007 (1998).
4. M. Stephanov, Nucl. Phys. A **661**, 403 (1999).
5. G. Colangelo, J. Gasser, H. Leutwyler, Nucl. Phys. B **603**, 125 (2001).
6. J.W. Negele, Nucl. Phys. Proc. Suppl. **73**, 92 (1999).
7. T. Schäfer, E.V. Shuryak, Rev. Mod. Phys. **70**, 323 (1998).
8. J. Skullerud, D.B. Leinweber, A.G. Williams, Phy. Rev. D **64**, 074508 (2001).
9. P. Maris *et al.*, arXiv:nucl-th/0208071.
10. R. Barate *et al.* (ALEPH), Eur. Phys. J. C **4**, 409 (1998).
11. R. Rapp, arXiv:nucl-th/0204003.
12. T.D. Cohen, L.Ya. Glozman, Int. J. Mod. Phys. A **17**, 1327 (2002); L.Ya. Glozman, Phys. Lett. B **539**, 257 (2002).
13. B. Schoch, private communication.
14. Y. Nakahara, M. Asakawa, T. Hatsuda, Phys. Rev. D **60**, 091503 (1999).
15. I. Wetzorke *et al.*, Nucl. Phys. Proc. Suppl. **106**, 510 (2002).
16. R. Rapp, J. Wambach, Adv. Nucl. Phys. **25**, 1 (2000).
17. Z. Aouissat, P. Schuck, J. Wambach, Nucl. Phys. A **618**, 402 (1997).
18. M.J. Vicente-Vacas, E. Oset, Phys. Rev. C **60**, 64621 (1999).
19. R. Rapp *et al.*, Phys. Rev. C **59**, R1237 (1999).
20. T. Hatsuda, T. Kunihiro, H. Shimizu, Phys. Rev. Lett. **82**, 2840 (1999).
21. Z. Aouissat, G. Chanfray, P. Schuck, J. Wambach, Phys. Rev. C **61**, 12202 (2000).
22. G. Chanfray, M. Ericson, arXiv:nucl-th/0106069.
23. D. Jido, T. Hatsuda, T. Kunihiro, Phys. Rev. D **63**, 011091 (2001).
24. F. Bonutti *et al.*, Nucl. Phys. A **677**, 213 (2000).
25. A.B. Starostin *et al.*, Phys. Rev. Lett. **85**, 5539 (2000).
26. J.G. Messchendorp *et al.*, arXiv:nucl-ex/0205009.
27. G.E. Brown, M. Rho, Phys. Rev. Lett. **66**, 2720 (1991).
28. M. Urban, M. Buballa, J. Wambach, Nucl. Phys. A **673**, 357 (2000).
29. J.J. Sakurai, Ann. Phys. **11**, 1 (1960).
30. E. Braaten, R.D. Pisarski, T.C. Yuan, Phys. Rev. Lett. **64**, 2242 (1990).
31. S. Weinberg, Phys. Rev. Lett. **18**, 507 (1967).
32. J. Kapusta, E.V. Shuryak, Phys. Rev. D **49**, 4694 (1994).

33. M. Urban, M. Buballa, J. Wambach, Nucl. Phys. A **697**, 338 (2002).
34. M. Urban, M. Buballa, J. Wambach, Phys. Rev. Lett. **88**, 042002 (2002).
35. M. Harada, S. Sasaki, Phys. Lett. B **537**, 280 (2002).
36. M. Harada, Y. Kim, M. Rho, Phys. Rev. D **66**, 016003 (2002).
37. G.E. Brown, M. Rho, Phys. Rep. **363**, 85 (2002).
38. M. Harada, K. Yamawaki, Phys. Rev. Lett. **86**, 757 (2001).

Eur. Phys. J. A **18**, 459–462 (2003)
DOI 10.1140/epja/i2002-10259-5

THE EUROPEAN PHYSICAL JOURNAL A

Hadrons in hot and dense matter

R. Rapp[a]

Department of Physics and Astronomy, SUNY Stony Brook, NY 11794-3800, USA

Received: 30 September 2002 /
Published online: 22 October 2003 – © Società Italiana di Fisica / Springer-Verlag 2003

Abstract. The description of excitations in hot and dense (hadronic) matter is discussed with emphasis on the use of correlation functions as a common framework for comparing different model (and QCD lattice) calculations with each other. Typical regimes of applicability of hadronic approaches are assessed, together with possibilities to confront them with experiment. We also elaborate on recent developments to relate baryonic in-medium effects to chiral-symmetry restoration.

PACS. 25.75.-q Relativistic heavy-ion collisions – 21.65.+f Nuclear matter

1 Introduction

The study of the phase structure of strong interactions (*i.e.*, QCD phase diagram) not only consists of determining the correct ground state, but also of identifying the relevant excitations, which are, after all, the probes amenable to experiment. At low-to-intermediate matter densities, this corresponds to the widely investigated topic of in-medium modifications of the hadronic spectrum as we know it from the vacuum. When passing through a phase transition (or cross-over region) an important question then is how changes in the ground-state symmetries (or order parameters) reflect themselves in the spectrum, schematically sketched in fig. 1. A general approach to the problem obviously requires a common framework which allows to compare results of individual models.

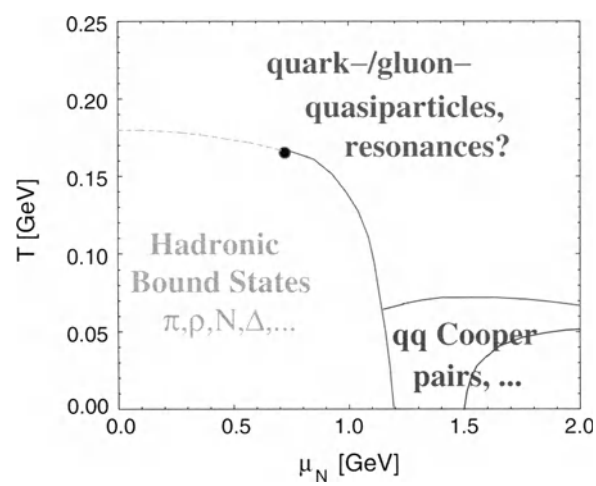

Fig. 1. Schematic phase structure and pertinent excitations of the QCD phase diagram.

2 Correlation and spectral functions

2.1 Definition

The general description of an excitation in a given quantum-number channel α can be formulated by correlation functions of the pertinent current operators [1], averaged over the thermodynamic partition function at temperature T and (baryon-) chemical potential $\mu_{\rm B}$. In coordinate space one has

$$\Pi_\alpha(x) = \mathrm{tr}\left(\left[j_\alpha(x) j_\alpha^\dagger(0)\right] \mathrm{e}^{-(\hat{H}-\mu_{\rm B}\hat{N})/T}\right)/\mathcal{Z} = \int \frac{\mathrm{d}^4 q}{(2\pi)^4} \Pi_\alpha(q) \mathrm{e}^{-iqx}. \quad (1)$$

Its interpretation becomes more transparent in momentum space: in the timelike region, $M^2 = q_0^2 - \boldsymbol{q}^2 > 0$, the "spectral function" $\mathrm{Im}\,\Pi_\alpha$ contains the information on the physical excitation spectrum, whereas the spacelike region, $M^2 < 0$, encodes screening phenomena as well as fluctuation and susceptibility properties (see refs. [2,3] for recent examples in scalar and vector channel).

In lattice QCD one typically evaluates $\Pi_\alpha(x)$ in (Euclidean) coordinate space; at finite temperatures, the transformation into Minkowski space is complicated by the shrinking of the "Matsubara box" $\tau\epsilon\{0, 1/T\}$ (due to periodic boundary conditions). However, model calculations in Minkowski space can, in principle, be straightforwardly transformed into Euclidean space for direct comparison with lattice data, see subsect. 3.2 below.

[a] *Present address*: NORDITA, Blegdamsvej 17, DK-2100 Copenhagen; e-mail: `ralf.rapp@stonybrook.edu`

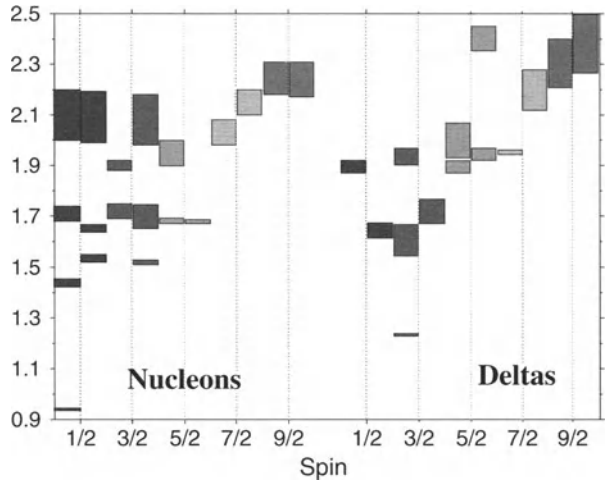

Fig. 2. Baryon spectrum according to PDG [6]. For given spin, left and right column correspond to positive and negative parity, respectively. Note the mass gaps of $\Delta E \simeq 0.5\,\mathrm{GeV}$ for low-lying spin-1/2 and -3/2 states, and the approximate degeneracy at higher masses, especially for $J \geq 5/2$.

2.2 Vacuum: chiral breaking vs. confinement

Correlation functions in free space are determined by the propagation and interaction of anti-/quarks in the non-perturbative QCD vacuum, which is characterized by two main phenomena, confinement and spontaneous breaking of chiral symmetry (SBCS). Whereas an understanding of the former is still elusive, the latter is widely believed to be due to instantons, which successfully reproduce QCD vacuum properties as well as low-lying meson and baryon correlation functions, see, *e.g.*, ref. [4]. However, attempts to obtain confinement from instantons have failed so far. On the other hand, the well-known Regge-behavior of hadronic masses, $J \propto M^2$, is suggestive for string-like excitations associated with a confining force. Furthermore, at masses $M \geq 2\,\mathrm{GeV}$, hadronic chiral partners seem to develop a degeneracy pattern suggestive for an "effective" restoration of chiral symmetry [5]. Most of these features are indeed supported by the appearance of the baryonic spectrum as extracted from the particle data group [6], cf. fig. 2.

2.3 In medium: hadronic approaches

Various methods to address medium effects on hadronic properties (and the equation of state) are available, cf. table 1.

At low densities and/or temperatures, systematic expansions using chiral perturbation theory [7] or a reduction formalism [8] can be performed.

At intermediate hadronic densities, as, *e.g.*, encountered in the later stages of heavy-ion collisions, many-body effects necessitating (partial) resummations, become important. *E.g.*, in the vector ($J^P = 1^-$) channel, the "melting" of the ρ-meson [9] enables to describe the dilepton excess observed at CERN-SPS energies [10] (cf. ref. [11] for an alternate view, and ref. [12] for a review). Likewise, in the scalar (0^+) channel, nuclear many-body effects contribute significantly to the threshold enhancement found in two-pion production experiments on nuclei [13].

Table 1. Applicability domains of approaches to hot+dense matter (ex = extrapolation, $n_0 = 0.16\ \mathrm{fm}^{-3}$).

T [MeV]	≤ 120	120–150	150–T_c	$\geq T_c$
ε [GeV/fm^3]	≤ 0.05	0.05–0.3	0.3–0.8	≥ 1
n_{had} [n_0]	≤ 0.5	0.5–2	2–5	N/A
Method	χPT	many-body	had-ex	pQCD-ex

In the expected phase transition region, both hadronic (below T_c) and partonic (above T_c) approaches have to rely on extrapolations. An important realization is, however, that medium modifications of light hadrons already encode precursor phenomena of chiral symmetry restoration. This connection can be made explicit by addressing the modifications of the respective chiral partners on an equal footing (*e.g.*, π-σ, ρ-a_1, N-$N^*(1535)$).

3 Recent applications: axial-/vector channel

3.1 Dileptons and a_1 spectral function

There is general consensus that the large excess in low-mass ($M \leq 1\,\mathrm{GeV}$) dilepton production observed in central Pb(158 AGeV)+Pb collisions by CERES/NA45 [10] is due to in-medium radiation from strongly modified ρ-mesons. The importance of baryon-induced effects [9] is supported by an even larger (relative) enhancement at lower SPS energies (40 AGeV), cf. fig. 3. The final interpretation on the nature of chiral restoration is still under debate. As argued above, this requires the evaluation of the in-medium axial-vector spectral function. Such an

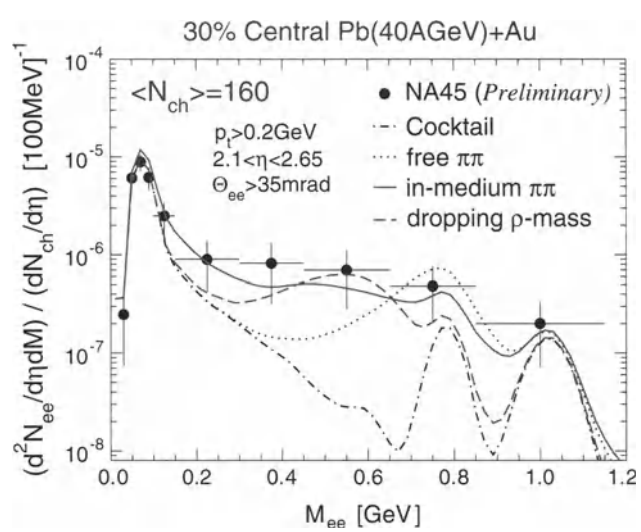

Fig. 3. Theoretical predictions using in-medium ρ-mesons [9] compared to recent NA45 data [10].

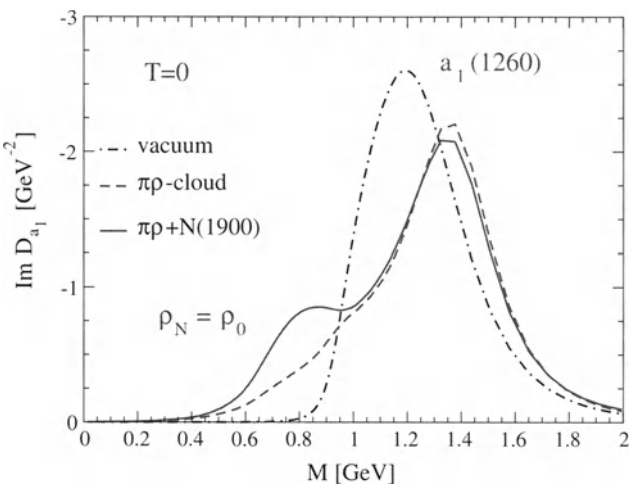

Fig. 4. a_1 spectral function in vacuum (dash-dotted line) and at normal nuclear matter density.

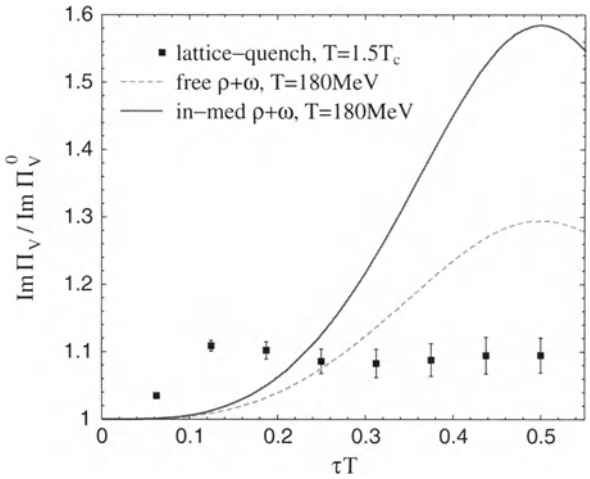

Fig. 5. Temporal vector correlator at $T = 180$ MeV (normalized to the $\mathcal{O}(\alpha_s^0)$ pQCD result) obtained from a hadronic model for ρ and ω spectral functions [15] in vacuum (dotted line) and with medium effects at $\mu_B \simeq 25$ MeV (solid line). Quenched lattice results (squares) at $T = 1.5T_c$ are from ref. [16].

analysis has been performed, *e.g.*, in ref. [14] for a thermal $\pi\sigma\rho a_1$ gas. However, even in a *net* baryon-free environment, the presence of baryon-antibaryon pairs at temperatures close to T_c has appreciable impact on the ρ spectral function [15]. Preliminary results for the $a_1(1260)$ within a many-body framework at finite density are shown in fig. 4. In addition to an in-medium modified $\pi\rho$-cloud, significant contributions arise from $a_1 \to N^*(1900)N^{-1}$ excitations, the putative $SU(2)$ chiral partner of the $\rho \to N(1520)N^{-1}$ bubble. Experimental information on the decay modes of baryon resonances, here $N(1900) \to Na_1$ (possibly measurable with the HADES detector using π-beams at GSI), would be of great help to constrain such calculations.

3.2 Vector correlator in Euclidean space

We finally return to the question of model comparisons with lattice-QCD results. In a "mixed" representation, the temporal Euclidean correlator is related to the spectral function in Minkowski space via

$$\Pi_\alpha(\tau, q) = \int_0^\infty \frac{\mathrm{d}q_0}{\pi} \,\mathrm{Im}\,\Pi_\alpha(q_0, q) \frac{\cosh\left(q_0[\tau - \frac{1}{2T}]\right)}{\sinh(q_0/2T)}. \quad (2)$$

A quenched lattice analysis of the vector correlator at zero 3-momentum, $\Pi_V(\tau, q = 0)$, above T_c has recently been presented in ref. [16]. For illustration, we show in fig. 5 results for the same quantity using the sum of (free and in-medium) ρ and ω spectral functions, supplemented with a perturbative continuum above $q_0 \simeq 1.3$ GeV. We stress that the enhancement at large $\tau T \simeq 0.5$ is at the origin of the dilepton excess at low-mass (cf. solid line in fig. 3).

4 (Some) open issues

The investigation of hadronic excitations and their medium modifications provides important insights into nonperturbative properties of the QCD phase diagram. In vacuum, confinement and chiral-symmetry breaking establish themselves in different (mass-) regimes of the spectrum, whereas associated phase transitions seem to occur at the same critical temperature (whether this holds true at high baryon densities is an open question). In particular, the role of (baryonic) resonances requires further understanding: on the one hand, they importantly figure into medium effects on, *e.g.*, light (axial-) vector mesons (as inferred from dilepton spectra) and thus into (the approach towards) chiral restoration; on the other hand, their copious population close to T_c significantly reduces the "jump" in the number of degrees of freedom in the transition to an (almost) ideal Quark-Gluon Plasma. Hadronic model calculations can thus be expected to remain an important tool to interpret both experimental and lattice data.

This work has been supported in part by US DOE grant no. DE-FG02-88ER40388.

References

1. E.V. Shuryak, Rev. Mod. Phys. **65**, 1 (1993).
2. G. Chanfray, M. Ericson, nucl-th/0106069.
3. M. Prakash *et al.*, Phys. Rev. C **65**, 034906 (2002).
4. T. Schäfer, E. Shuryak, Phys. Rev. D **54**, 1099 (1996).
5. T. Cohen, L. Glozman, Phys. Rev. D **65**, 016006 (2001).
6. Particle Data Group, Eur. Phys. J. C **15**, 1 (2000).
7. N. Kaiser, S. Fritsch, W. Weise, Nucl. Phys. A **697**, 255 (2002).
8. J. Steele, H. Yamagishi, I. Zahed, Phys. Rev. D **56**, 5605 (1997).
9. R. Rapp, J. Wambach, Eur. Phys. J. A **6**, 415 (1999).
10. CERES Collaboration (D. Adamova *et al.*), Nucl. Phys. A **698**, 253 (2002); J.P. Wessels, this issue, p. 521.
11. G.E. Brown, M. Rho, nucl-th/0206021.

12. R. Rapp, J. Wambach, Adv. Nucl. Phys. **25**, 1 (2000).
13. M.J. Vicente Vacas, E. Oset, nucl-th/0204055; M.J. Vicente Vacas, this issue, p. 479.
14. M. Urban, M. Buballa, J. Wambach, Phys. Rev. Lett. **88**, 042002 (2002).
15. R. Rapp, Phys. Rev. C **63**, 054907 (2001).
16. F. Karsch *et al.*, Phys. Lett. B **530**, 147 (2002).

Eur. Phys. J. A **18**, 463–466 (2003)
DOI 10.1140/epja/i2002-10260-0

THE EUROPEAN PHYSICAL JOURNAL A

Scalar and pseudoscalar QCD susceptibilities in nuclei

M. Ericson[1,2,a] and G. Chanfray[1]

[1] IPN Lyon, IN2P3-CNRS et UCB Lyon I, F-69622 Villeurbanne Cedex, France
[2] Theory division, CERN, CH-12111 Geneva, Switzerland

Received: 30 September 2002 /
Published online: 22 October 2003 – © Società Italiana di Fisica / Springer-Verlag 2003

Abstract. We study the staticscalar and pseudoscalar susceptibilities of QCD in the nuclear medium. We show that they become much closer than in the vacuum at normal nuclear matter density, a strong signal of the partial restoration of chiral symmetry.

PACS. 24.85.+p Quarks, gluons, and QCD in nuclei and nuclear processes – 11.30.Rd Chiral symmetries – 12.40.Yx Hadron mass models and calculations – 13.75.Cs Nucleon-nucleon interactions (including antinucleons, deuterons, etc.)

We focus in this paper on an aspect of chiral symmetry which has received little attention: the effect of the partial restoration on the susceptibilities of QCD, related to the fluctuations of the quark densities. In the phase of broken symmetry, there exist two susceptibilities. One along the spontaneous magnetization axis, and the second one along the perpendicular direction.

In QCD, the scalar susceptibility represents the modification of the order parameter, *i.e.*, of the quark condensate, to a small perturbation of the parameter responsible for the explicit breaking of the symmetry, which is the quark mass:

$$\chi_{\mathrm{S}} = \frac{\partial\langle\bar{q}q\rangle}{\partial m_q} = 2\int \mathrm{d}t'\,\mathrm{d}\mathbf{r}' G_{\mathrm{R}}(\mathbf{r}=0, t=0, \mathbf{r}', t'), \quad (1)$$

where G_{R} is the retarded quark scalar correlator:

$$G_{\mathrm{R}}(\mathbf{r}, t, \mathbf{r}', t') = \Theta(t-t')\big\langle -i\big[\bar{q}q(\mathbf{r}, t), \bar{q}q(\mathbf{r}', t')\big]\big\rangle. \quad (2)$$

The susceptibility represents space- and time-integrated correlators.

In the linear σ model the symmetry-breaking part of the Lagrangian is proportional to the σ field:

$$\mathcal{L}_{\chi\mathrm{SB}} = c\sigma \quad (3)$$

with $c = f_\pi m_\pi^2$. This quantity plays the role of the symmetry-breaking Lagrangian of QCD:

$$\mathcal{L}_{\chi\mathrm{SB}}^{\mathrm{QCD}} = -2m_q\bar{q}q, \quad (4)$$

which entails the following correspondence between the QCD and effective theory correlators:

$$\frac{\langle\bar{q}q(x)\bar{q}q(0)\rangle}{\langle\bar{q}q\rangle_{\mathrm{vac}}^2} = \frac{\langle\sigma(x)\sigma(0)\rangle}{f_\pi^2}, \quad (5)$$

where $\langle qq\rangle_{\mathrm{vac}}$ is the vacuum value of the condensate. The fluctuations of the quark density are thus carried by the σ field, the chiral partner of the pion. The in-medium propagation of the σ in the energy domain near the two-pion threshold, has been the object of several investigations (see, *e.g.*, [1–3]). Here we will focus on the low-energy region, below the particle-hole excitation energies.

The scalar susceptibility is given by

$$\begin{aligned}\chi_{\mathrm{S}} &= 2\frac{\langle\bar{q}q\rangle_{\mathrm{vac}}^2}{f_\pi^2}\int_0^\infty \mathrm{d}\omega\left(\frac{2}{\pi\omega}\right)\mathrm{Im}\,D_{\mathrm{SS}}(\mathbf{q}=0,\omega)\\ &= 2\frac{\langle\bar{q}q\rangle_{\mathrm{vac}}^2}{f_\pi^2}\,\mathrm{Re}\,D_{\mathrm{SS}}(\mathbf{q}=0,\omega=0),\end{aligned} \quad (6)$$

where $D_{\mathrm{SS}}(\mathbf{q},\omega)$ is the Fourier transform of the scalar correlator:

$$\begin{aligned}D_{\mathrm{SS}}(\mathbf{q},\omega) &= \int \mathrm{d}t\,\mathrm{d}\mathbf{r} e^{i\omega t} e^{-i\mathbf{q}\cdot\mathbf{r}}\\ &\times\big\langle -iT\big(\sigma(\mathbf{r},t)-\langle\sigma\rangle, \sigma(0)-\langle\sigma\rangle\big)\big\rangle.\end{aligned} \quad (7)$$

In a simple picture where the sharp σ mass is reduced in the nuclear medium, *i.e.* m_σ replaced by some dropped value, m_σ^* [2], the static correlator is $\exp(-m_\sigma^* r)/r$. As m_σ^* goes to zero at full chiral symmetry restoration, the fluctuations acquire an infinite range as for fluids near the critical temperature. In the work of Hatsuda *et al.* [2] the σ mass modification arises from the tadpole term. Here, we

[a] e-mail: Magda.Ericson@cern.ch

include the polarization of the nuclear medium by the σ field. The lowest excitations are the nuclear ones, where a nucleon-hole state is excited. At higher energy the σ transforms into two pions. When at least one pion is a nuclear one this process also produces an in-medium modification of the σ propagator. At present we have only included the nuclear states. The coupling of the σ to the nucleon-hole excitations modifies the scalar field propagator as follows:

$$D_{\rm SS} = D_{\rm S}^0\big(1 + D_{\rm S}^0 g_{\rm S}^2 \Pi_{\rm SS}\big). \tag{8}$$

Here $D_{\rm S}^0 = 1/(q^2 - m_\sigma^2)$ is the bare σ propagator, $\Pi_{\rm SS}$ is the full scalar NN^{-1} polarization propagator and the quantity $g_{\rm S}$ is the σNN coupling constant. In the linear σ model, as well as in quantum hadrodynamics, this quantity has a value close to 10. Using this value, for a first estimate, and the free Fermi gas expression for the nucleon-hole propagator: $\mathrm{Re}\,\Pi^0(\mathbf{q} = \mathbf{0}, \omega = 0) \simeq -2M_N k_{\rm F}/\pi^2$ we get

$$\chi_{\rm S} \simeq \chi_{\rm S,vac}\left(1 + \frac{2g_{\rm S}^2 M_N k_{\rm F}}{\pi^2 m_\sigma^2}\right). \tag{9}$$

Notice that the scalar susceptibility is, as the quark condensate, negative. This first-order correction leads to a large modification of the σ propagator at normal density: $D_{\rm S} \sim 12 D_{\rm S}^0$ at $\rho = \rho_0$ indicating a sizable in-medium increase of the scalar susceptibility. This effect can be seen as arising from an in-medium decrease of the σ mass. This mass is a screening mass and not the energy of the pole of the σ propagator at zero momentum.

Now, quantitatively, we have to know the full $\Pi_{\rm SS}(\mathbf{q} = 0, \omega = 0)$, which is a pure nuclear physics problem, on which experimental information can be obtained. Indeed, at low densities where non-relativistic effects are unimportant the scalar polarization propagator $\Pi_{\rm SS}$ is identical to the one for the ordinary density. It is then linked to the incompressibility factor K of nuclear matter, the magnitude of which is known experimentally

$$\frac{\Pi_{\rm SS}(\mathbf{q} = 0, \omega = 0)}{g_{\rm S}^2} = -\frac{9\rho_{\rm S}}{K}, \tag{10}$$

where $\rho_{\rm S}$ is the nucleon scalar density. With the currently suggested value, $K = 230\,\mathrm{MeV}$, which is practically the free Fermi gas one: $K = 3k_{\rm F}^2/M_N$, the quantity $\Pi_{\rm SS}(\mathbf{q} = 0, \omega = 0)$ also has the free Fermi gas value, which should validate the previous estimate.

However we have to discuss also in more detail the value of the σNN coupling constant entering the renormalization factor in eq. (8), which may depend on the density. This is the case in the quark-meson coupling model (QMC) of Guichon [4] which has a relevance for this problem. It is an extension of the quantum hadrodynamics model (QHD), but formulated at the quark level. In QMC the scalar and vector mesons couple directly to the quarks inside the nucleons, described by a bag model. The crucial ingredient of the model is the internal structure of the nucleon which adjusts to the presence of the scalar field. Under the influence of this attractive field the quark mass is lowered according to: $m_q^* = m_q - g_\sigma^q \langle\sigma\rangle$, where g_σ^q is the σ-quark coupling constant. Accordingly, the valence quark scalar number, which depends on the quark mass, also decreases, the quarks becoming more relativistic. This effect is directly related to the QCD scalar susceptibility of the bag, $\chi_{\rm S}^{\rm bag}$. Introducing the scalar charge, $Q_{\rm S}$, defined as the valence quark scalar number:

$$\begin{aligned} Q_{\rm S}(\langle\sigma\rangle) &= \int_{\rm bag} \mathrm{d}\mathbf{r}\big(\langle\bar{q}q(\mathbf{r})\rangle - \langle\bar{q}q\rangle_{\rm vac}\big) \\ &= Q_{\rm S}(m_q) + \chi_{\rm S}^{\rm bag}\big(m_q^* - m_q\big) \\ &= Q_{\rm S}(\langle\sigma\rangle = 0) - g_\sigma^q \chi_{\rm S}^{\rm bag}\langle\sigma\rangle. \end{aligned} \tag{11}$$

Now, the scalar charge acting as the source of the scalar field, a decrease of the scalar charge amounts to a lowering of the σNN coupling constant when the mean scalar field, *i.e.*, the density, increases:

$$g_{\rm S}(\rho) = g_\sigma^q Q_{\rm S}(\langle\sigma\rangle). \tag{12}$$

In QMC this mechanism is responsible for the saturation of nuclear matter. The introduction of $\chi_{\rm S}^{\rm bag}$, which is positive, amounts to an increase of the σ mass:

$$m_\sigma^{*2}(\rho) = m_\sigma^2 + (g_\sigma^q)^2 \chi_{\rm S}^{\rm bag}\rho_{\rm S}, \tag{13}$$

which partly counteracts the decrease due to the mixing with NN^{-1} states. Note that the direct contribution of the bag susceptibility to the nuclear one is by itself small and effects mostly the mean scalar field. We use the values of Guichon *et al.* [5] for the density-dependent scalar coupling constant and also, for consistency, their value of the incompressibility: $K = 280\,\mathrm{MeV}$ (also compatible with the experimental allowed range). The enhancement factor of the scalar susceptibility is $\chi_{\rm S}(\rho_0)/\chi_{\rm S,vac} = 6.2$, still quite a large medium effect.

We now turn to the transverse susceptibility, linked to the fluctuations of the pseudoscalar quark density. We define it in such a way that it coincides with the scalar susceptibility in the restored phase:

$$\begin{aligned} \chi_{\rm PS} = 2 &\int \mathrm{d}t'\,\mathrm{d}\mathbf{r}'\Theta(t - t')x \\ &\times\left\langle -i\left[\bar{q}i\gamma_5\frac{\tau_\alpha}{2}q(0), \bar{q}i\gamma_5\frac{\tau_\alpha}{2}q(\mathbf{r}'t')\right]\right\rangle. \end{aligned} \tag{14}$$

This pseudoscalar susceptibility is related to the correlator of the divergence of the axial current since

$$\partial^\mu \mathcal{A}_\mu^\alpha(x) = 2m_q\bar{q}i\gamma_5\frac{\tau_\alpha}{2}q(x). \tag{15}$$

In the representations where PCAC holds the interpolating pion field is proportional to the divergence of the axial current according to

$$\partial^\mu \mathcal{A}_\mu^\alpha(x) = f_\pi m_\pi^2 \Phi^\alpha(x). \tag{16}$$

The pseudoscalar susceptibility $\chi_{\rm PS}$ is then linked to the pion propagator, taken at zero momentum and energy:

$$\begin{aligned} \chi_{\rm PS} &= \frac{f_\pi^2 m_\pi^4}{2m_q^2}\int \mathrm{d}t'\,\mathrm{d}\mathbf{r}'\Theta(t - t')\big\langle -i\big[\Phi^\alpha(0), \Phi^\alpha(\mathbf{r}'t')\big]\big\rangle \\ &= \frac{f_\pi^2 m_\pi^4}{2m_q^2}\,\mathrm{Re}\,D_\pi(\mathbf{q} = 0, \omega = 0). \end{aligned} \tag{17}$$

Since the factor multiplying the pion propagator can be written as $2\langle\bar{q}q\rangle^2_{\rm vac}/f_\pi^2$, this equation is the analog of the one for the scalar susceptibility, with the pion replacing the σ. Thus in the linear σ model, where PCAC holds, the propagators of the two chiral partners, σ and π, govern the evolutions of the two susceptibilities. In the medium we denote $S(\mathbf{q},\omega)$ the pion self-energy so that

$$D_\pi(\mathbf{q}=0,\omega) = \left[\omega^2 - m_\pi^2 - S(\mathbf{q}=0,\omega)\right]^{-1}. \tag{18}$$

The expression of the self-energy depends on the representation. The one that should enter here is the one which applies to the PCAC representation. Its expression is not simple [6]. This complexity is, however, irrelevant for establishing a link with the condensate evolution. At zero four-momentum

$$\mathrm{Re}\, D_\pi(\mathbf{q}=0,\omega=0) = -\frac{1}{m_\pi^2 + S(0,0)}\,. \tag{19}$$

On the other hand, the evolution with density of the condensate is governed by the nuclear Σ commutator: Σ_A/A per nucleon, according to the exact expression:

$$\frac{\langle\bar{q}q(\rho)\rangle}{\langle\bar{q}q\rangle_{\rm vac}} = 1 - \frac{(\Sigma_A/A)\rho}{f_\pi^2 m_\pi^2}\,, \tag{20}$$

which follows from the very definition of the nuclear Σ commutator as the expectation value over the nuclear ground state of the commutator between the axial charge and its time derivative. In the PCAC representation, the nuclear Σ commutator also represents the scattering amplitude for soft pions on the nuclear medium, $T(0,0)$ (per unit volume), with

$$\frac{(\Sigma_A/A)\rho}{f_\pi^2} = T(0,0). \tag{21}$$

This quantity is related to the pion self-energy, $S(q,\rho)$, which depends on the density, through

$$T(0,0) = \frac{S(0,0)}{1 + S(0,0)/m_\pi^2}\,. \tag{22}$$

In this expression the denominator represents the coherent rescattering of the soft pion [7], which is needed in order to make the nuclear Σ commutator independent of the representation, ref. [6]. The link between the pseudoscalar susceptibility and the in-medium condensate is established by writing the condensate from its expression (eq. (20)) as

$$\frac{\langle\bar{q}q(\rho)\rangle}{\langle\bar{q}q\rangle_{\rm vac}} = 1 - \frac{T(0,0)}{m_\pi^2} = \frac{1}{1 + S(0,0)/m_\pi^2}\,. \tag{23}$$

From the expression of the pseudoscalar susceptibility (eq. (17)) and using the GOR relation, one finally obtains the result

$$\chi_{\rm PS} = \frac{\langle\bar{q}q\rangle_{\rm vac}}{m_q}\frac{1}{1 + S(0,0)/m_\pi^2} = \frac{\langle\bar{q}q(\rho)\rangle}{m_q}\,. \tag{24}$$

The pseudoscalar susceptibility follows the condensate evolution, *i.e.*, its magnitude decreases with density, with a linear dependence in the dilute limit where the relation $(\Sigma_A/A) = \Sigma_N$ holds. At normal density the susceptibility has thus decreased by 35%.

Our previous relation (24) between the transverse (pseudoscalar) susceptibility and the order parameter (the condensate) can be understood from the magnetic analogy. The rotational symmetry is intrinsically broken by a magnetic field $\mathbf{H}_0$ which aligns the spontaneous magnetization along its direction. The application of a small transverse field $\mathbf{H}_\perp$ rotates the magnetization $\mathbf{M}$ by an angle θ, such that it is now aligned in the direction of the resulting field $\mathbf{H}_0 + \mathbf{H}_\perp$. The transverse magnetization is $M_\perp = M\theta = M(H_\perp/H_0)$ and the transverse susceptibility is $\chi_\perp = M_\perp/H_\perp = M/H_0$, which is the analog of our formula (24).

Our results lead to the conclusion that at normal density the scalar and pseudoscalar susceptibilities become much closer than in the vacuum. As in the phase of restored symmetry they should become degenerate, the question is if this convergence is a signal of the partial symmetry restoration. The decrease in magnitude of the pseudoscalar one is clearly linked to the restoration since it follows the condensate. As for the scalar one which is the derivative of the order parameter with respect to the quark mass its evolution is also linked to the restoration process, which can be shown explicitly.

We have also explored how the convergence effect evolves at higher densities. However this extrapolation does not rely as previously on the experimental data of the incompressibility. For the scalar susceptibility we have taken the scalar coupling constant from ref. [5] and we have assumed that the polarization propagator keeps the free Fermi-gas expression with the effective nucleon mass of ref. [5]. The increase of the scalar susceptibility stabilizes or even decreases somewhat due to the fact that the nucleon reaction to the σ field manifests itself more with increasing density. However the influence of the two-pion continuum should also be included, which will be our next step, before a definite conclusion can be drawn. In summary we have studied the in-medium modifications of the two QCD susceptibilities, linked to the fluctuations of the scalar-isoscalar and the pseudoscalar-isovector quark densities. The first one is linked, through the linear σ model, to the propagator of the σ-meson, which in the nucleus mixes with the low-lying scalar-isoscalar nuclear excitations. At normal nuclear density this mixing produces an increase of the scalar susceptibility by a factor of about 6. This effect does not appear to increase further with increasing density. As for the pseudoscalar susceptibility, which is linked to the pion propagator, it follows the evolution of the condensate, *i.e.*, it decreases with density. The two combined effects make the scalar and pseudoscalar susceptibilities appreciably closer, at ρ_0, than in the vacuum. Their convergence is a clear, and amplified, signal of chiral symmetry restoration.

References

1. Z. Aouissat *et al.*, Nucl. Phys. A **581**, 471 (1995).
2. T. Hatsuda, T. Kunihiro, H. Shimizu, Phys. Rev. **82**, 2840 (1999).
3. J. Wambach, Z. Aouissat, P. Schuck, Nucl. Phys. A **690**, 127c (2001).
4. P.A.M. Guichon, Phys. Lett. B **200**, 235 (1988).
5. P.A.M. Guichon, K. Saito, E. Rodionov, A.W. Thomas, Nucl. Phys. A **601**, 349 (1996).
6. J. Delorme, G. Chanfray, M. Ericson, Nucl. Phys. A **603**, 239 (1996).
7. M. Ericson, Phys. Lett. B **101**, 11 (1993).

Eur. Phys. J. A **18**, 467–470 (2003)
DOI 10.1140/epja/i2002-10261-y

THE EUROPEAN PHYSICAL JOURNAL A

Transport analysis of in-medium hadron effects in pA and AA collisions

W. Cassing[a]

Institut für Theoretische Physik, Justus Liebig Universität Giessen, D-35392 Giessen, Germany

Received: 30 September 2002 /
Published online: 22 October 2003 – © Società Italiana di Fisica / Springer-Verlag 2003

Abstract. The production and decay of vector mesons (ρ, ω) in pA and AA reactions is studied with particular emphasis on their in-medium spectral functions. It is explored within transport calculations if hadronic in-medium decays like $\pi^+\pi^-$ or $\pi^0\gamma$ might provide complementary information to their dilepton (e^+e^-) decays. Whereas the $\pi^+\pi^-$ signal from the ρ-meson is found to be strongly distorted by pion rescattering, the ω-meson Dalitz decay to $\pi^0\gamma$ appears promising even for more heavy nuclei in γA and pA reactions. Furthermore, the influence of nucleon and kaon/antikaon potentials on the $K^\pm$ yields and spectra in pA collisions is calculated and compared to the recent data from the ANKE Collaboration.

PACS. 13.60.Le Meson production – 13.75.Jz Kaon-baryon interactions – 14.40.Aq π, K, and η mesons – 25.40.-h Nucleon-induced reactions

1 Introduction

The modification of the meson properties [1,2] in nuclear matter has become a challenging subject in hadron physics from γA, pA and AA collisions. Here the dilepton (e^+e^-) radiation from ρ's and ω's propagating in finite-density nuclear matter is directly proportional to their spectral function which becomes distorted in the medium due to the interactions with nucleons. Apart from the vacuum width Γ_V^0 $(V = \rho, \omega)$ these modifications are described by the real and imaginary part of the retarded self-energies Σ_V, where the real part $\Re\Sigma_V$ yields a shift of the meson mass pole and the additional imaginary part $\Im\Sigma_V$ (half) the collisional broadening of the vector meson in the medium. We recall that the meson self-energy in the t-ρ approximation is proportional to the complex forward VN scattering amplitude $f_{VN}(P, 0)$ and the nuclear density $\rho(X)$, *i.e.* $\Sigma_V(P, X) = -4\pi\rho(X) f_{VN}(P, 0)$. The scattering amplitude itself, furthermore, obeys dispersion relations between the real and imaginary parts [3], while the imaginary part can be determined from the total VN cross-section according to the optical theorem. Thus the vector meson spectral function,

$$A_V(X,P) \sim \frac{\Im\Sigma_V(X,P)}{\left(P^2 - M_V^2 - \Re\Sigma_V(X,P)\right)^2 + \Im\Sigma_V(X,P)^2}, \quad (1)$$

can be constructed once the VN elastic and inelastic cross-sections are known. Note that in (1) all quantities depend on space-time X and 4-momentum P.

2 Production and decay of vector mesons

Though strong modifications of the ρ-meson properties in relativistic $A + A$ reactions have been reported by the CERES Collaboration [4], the interpretation of the data is not unique since the latter may be explained by a dropping of the pole mass as well as by ordinary nuclear many-body effects [1,2]. In general, the medium effects on the ρ-meson are expected to increase when decreasing the bombarding energy from 160 A · GeV down to about 2 A · GeV for central Au + Au collisions [5]. At the lower range of bombarding energies we expect new data coming up from the HADES Collaboration in the near future [6]. Nevertheless, it is inevitable to study also γA and pA reactions where the time evolution of the baryon density is much better under control and the vector-meson spectral function is essentially tested at density ρ_0 in heavy nuclei [7,8].

The in-medium vector meson spectral functions can be measured directly by the leptonic decay $V \to e^+e^-$ (cf. refs. [7,8]), the strong decay $\rho^0 \to \pi^+\pi^-$ or the Dalitz decay $\omega \to \pi^0\gamma$, respectively. Thus it remains to be seen which of the decay modes is most effective for experimental studies.

The actual transport calculations have been performed for pA and γA collisions by introducing a real and

[a] In collaboration with E.L. Bratkovskaya, M. Büscher, Ye.S. Golubeva, V. Grishina, V. Hejny, V. Metag, J. Messchendorp, B. Kamys, L.A. Kondratyuk, P. Kulessa, Z. Rudy, S. Schadmand, A.A. Sibirtsev, H. Ströher; e-mail: Wolfgang.Cassing@theo.physik.uni-giessen.de

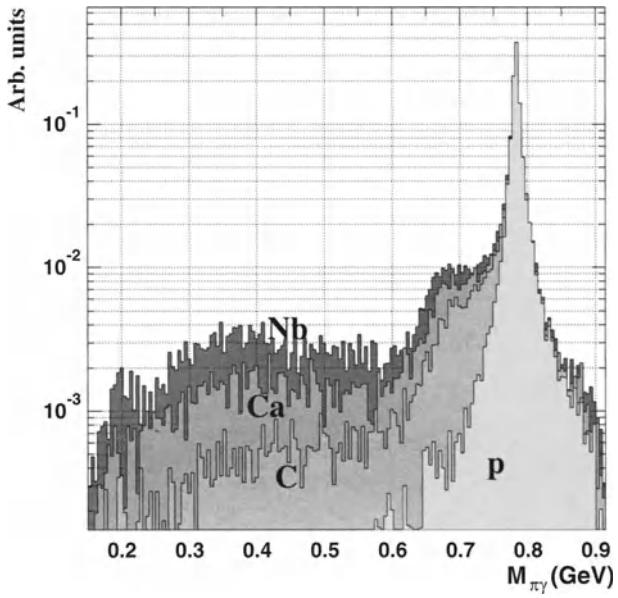

Fig. 1. The $\pi^0\gamma$ invariant-mass distribution from ω-meson decays in γA reactions including an attractive mass shift and collisional broadening at $E_\gamma = 1.2\,\mathrm{GeV}$ for a proton, ^{12}C, ^{40}Ca and Nb target according to ref. [12]. The spectra have been normalized to the vacuum decay peak at 0.783 GeV.

imaginary part of the vector meson self-energy and width as

$$U_V = \frac{\Re\Sigma_V}{2M_0} \simeq M_0\beta\frac{\rho(X)}{\rho_0}\,, \tag{2}$$

$$\Gamma^* = \frac{\Im\Sigma_V}{2M_0} \simeq \Gamma_V^0 + \Gamma_{\mathrm{coll}}\frac{\rho(X)}{\rho_0}\,, \tag{3}$$

in the t-ρ approximation. Here M_0 and Γ_V^0 denote the bare mass and width of the vector meson in vacuum, while $\rho(X)$ is the local baryon density ($\rho_0 = 0.16\,\mathrm{fm}^{-3}$). The parameter $\beta \simeq -0.16$ was adopted from the models discussed in refs. [1,2]. The predictions for the ω-meson collisional width Γ_{coll} at density ρ_0 range from 20 to 50 MeV [9] —depending on the number of ωN final channels taken into account— while the collisional width of the ρ-meson should be about 100–120 MeV at ρ_0 due to the strong coupling to baryon resonances (cf. fig. 6 of ref. [3]).

As a first remark we quote the result from ref. [10], where it has been found that the $\pi^+\pi^-$ decay mode of the ρ^0 in nuclei is not well suited to reconstruct the in-medium ρ^0 spectral function except for very light nuclei due to the strong $\pi^\pm$ final-state interactions. The situation changes for the in-medium ω-meson Dalitz decay since here only a single pion might rescatter whereas the photon escapes practically without reinteraction. In this case it is found [11,12] that though most of the ω-mesons — produced in photon induced reactions on nuclear targets— decay in the vacuum, there is a sizeable contribution of ω's decaying in the medium leading to $\pi^0\gamma$ pairs of invariant mass 0.6–0.9 GeV, however, also π^0 rescattering gives a substantial background essentially below 0.65 GeV.

As an example we show in fig. 1 the $\pi^0\gamma$ invariant-mass distribution from ω-meson decays including an attractive mass shift and collisional broadening at $E_\gamma = 1.2\,\mathrm{GeV}$ for a proton, ^{12}C, ^{40}Ca and Nb target according to ref. [12]. The background —in the invariant-mass range $0.6 \le M \le 0.9\,\mathrm{GeV}$ of interest— can be suppressed effectively by kinematical cuts on higher π^0 energies [12] or angular correlations between the photon and the pion [13] which provides good perspectives for the $\pi^0\gamma$ decay mode of the ω-meson.

3 K$^\pm$ production

The in-medium properties of kaons (and antikaons) show up in their suppressed (enhanced) yields in pA or AA collisions [14,15] as well as in their low-momentum spectra [1], which are most sensitive to the meson nuclear potentials. The experiments of the FOPI [16] and KaoS Collaboration [17] on nucleus-nucleus collisions at SIS energies have demonstrated that the abundancy and collective flow of kaons and antikaons indicate slightly repulsive potentials for K^+ and more strongly attractive potentials for K^-. However, as pointed out in ref. [15], the K^- yield is dominated by the strange flavor exchange reaction $\pi + Y \leftrightarrow \bar{K}N$ which by strangeness conservation strongly links the K^+ and K^- yields. The problem is that the cross-section for the latter reaction at high baryon density is not sufficiently known and that data from AA reactions do not allow for a unique conclusion. Thus $K^\pm$ production in pA reactions is a necessary and complementary study since in this type of reactions the $\pi + Y \to \bar{K}N$ channel plays a minor role and the $K^\pm$ potentials can be extracted with less ambiguities.

In pA reactions the $K^\pm$-mesons are dominantly produced with a finite momentum relative to the nucleus at rest and —once they do not rescatter elastically or inelastically— are accelerated or decelerated by the nuclear and Coulomb potential. For orientation the effective nuclear and Coulomb potentials are displayed in fig. 2 for a ^{12}C and ^{197}Au target as a function of the coordinate z. Here the $K^\pm$ nuclear potentials have been approximated by

$$V_{\mathrm{N}}^{\pm}(\mathbf{r}) = V_0^{\pm}\frac{\rho(\mathbf{r})}{\rho_0}\,, \tag{4}$$

with $V_0^+ = 20\,\mathrm{MeV}$ [18] and $V_0^- = -60\,\mathrm{MeV}$ [19]. As seen from fig. 2 the Coulomb potential V_{C} plays only a minor role for ^{12}C, however, is even larger than the K^+ potential in case of a ^{197}Au target. Thus the minimum kinetic energy of a K^+-meson —produced in the center of a Au target— (without rescattering) is about 45 MeV in the continuum and about 23 MeV in case of ^{12}C. Kaons produced at the nuclear surface will have a minimum kinetic energy that is determined by V_{C} at the point of production. Thus K^+ ratios from heavy-to-light targets have to show a strong suppression for low K^+ momenta. In fact, it has been demonstrated in ref. [20] that ratios of cross-sections for light and heavy targets in pA reactions provide a sensitive tool to measure the K^+ potentials in an almost model-independent way.

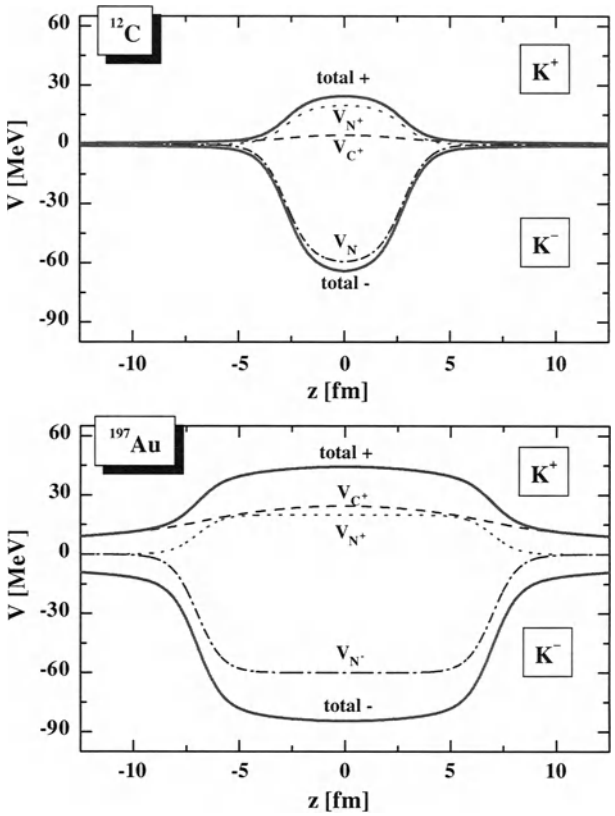

Fig. 2. The effective nuclear (4) (dotted lines) and Coulomb (dashed lines) potentials for K^+- and K^--mesons in case of a ^{12}C and ^{197}Au target (see text).

The situation is quite different for antikaons since K^- produced with low kinetic energy in the medium cannot escape to the continuum without elastic rescattering. Most of them are absorbed in the flavor exchange reaction $K^-N \to Y+\pi$ or, if their energy $E_K < 0$, they might form antikaonic atoms when escaping the nuclear medium.

We now turn to the kinematical conditions of the ANKE experiments at COSY-Jülich, that have taken K^+ spectra in forward direction for $\theta_{\rm lab} \leq 12°$. The calculated differential K^+ spectra for $p + {}^{12}$C at 1.0 GeV for $\theta_{\rm lab} \leq 12°$ are displayed in fig. 3 in comparison to the data from ref. [21]. The dotted line is obtained from transport calculations without baryon and kaon potentials, the dashed line shows the result with baryon potentials included while the solid line corresponds to a calculation with both, nucleon and kaon potentials. At this low bombarding energy the net attractive baryon potential in the final state enhances the K^+ yield by about a factor of 2 whereas the additional repulsive K^+ potential leads to a decrease by a factor ~ 3. The data from ref. [21] are rather well described by the calculations that include the baryon and K^+ potentials (solid line), whereas the other limits clearly fail. This might be considered as a first indication for the observation of a repulsive K^+ potential in pA reactions, however, a full systematics in target mass A and laboratory energy $T_{\rm lab}$ will be needed to pin down this effect unambiguously.

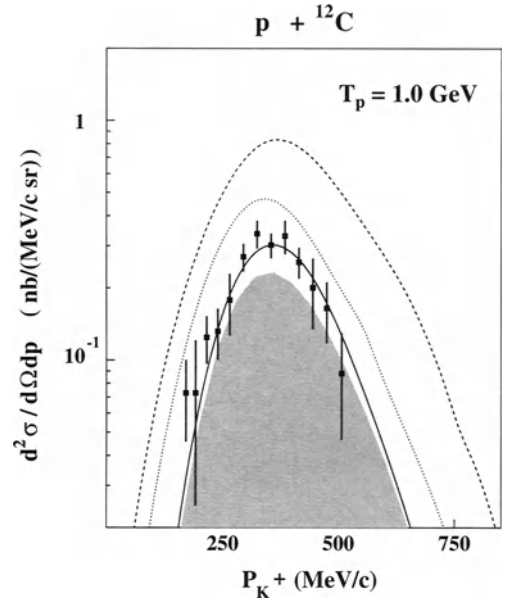

Fig. 3. The calculated differential K^+ spectra for $p + $ C at 1.0 GeV for $\theta_{\rm lab} \leq 12°$ within the acceptance of the ANKE spectrometer (from ref. [14]) in comparison to the data from [21]. The dotted (middle) line is obtained from transport calculations without baryon and kaon potentials, the dashed (top) line shows the results with baryon potentials included, while the solid line corresponds to calculations including both, nucleon and kaon potentials.

The shaded area in fig. 3 indicates the contributions from the two-step mechanisms $\Delta N \to K^+YN$ and $\pi N \to K^+Y$, respectively, for the case of nucleon and kaon potentials included (solid line). Thus secondary (Δ and π induced) reaction channels give the dominant fraction of the K^+ yield at 1 GeV even for the light target ^{12}C.

4 Summary

The production and decay of vector mesons (ρ, ω) especially in γA and pA reactions has been studied with particular emphasis on signals from their in-medium spectral functions. Whereas the $\pi^+\pi^-$ decay mode from the ρ-meson is found to be strongly distorted by pion rescattering with the surrounding nucleons, the ω-meson Dalitz decay to $\pi^0\gamma$ appears promising even for more heavy nuclei. Furthermore, the influence of nucleon and kaon/antikaon potentials on the $K^\pm$ yields and spectra has been evaluated within the transport approach. A comparison to the recent data from the ANKE Collaboration [21] yields a repulsive K^+ potential of ≈ 20 MeV at normal nuclear matter density [14,20] which is in line with the data from AA reactions at SIS energies [16,17].

References

1. W. Cassing, E.L. Bratkovskaya, Phys. Rep. **308**, 65 (1999).
2. R. Rapp, J. Wambach, Adv. Nucl. Phys. **25**, 1 (2000).

3. L.A. Kondratyuk *et al.*, Phys. Rev. C **58**, 1078 (1998).
4. B. Lenkeit *et al.*, Nucl. Phys. A **654**, 627c (1999).
5. W. Cassing *et al.*, Nucl. Phys. A **674**, 249 (2000).
6. R. Schicker *et al.*, Nucl. Instrum. Methods A **380**, 586 (1996).
7. Ye.S. Golubeva *et al.*, Nucl. Phys. A **625**, 832 (1997).
8. E.L. Bratkovskaya, Nucl. Phys. A **696**, 761 (2001).
9. G.I. Lykasov *et al.*, Eur. Phys. J. A **6**, 71 (1999).
10. A. Sibirtsev, W. Cassing, Nucl. Phys. A **629**, 717 (1998).
11. A. Sibirtsev *et al.*, Phys. Lett. B **483**, 405 (2000).
12. J. Messchendorp *et al.*, Eur. Phys. J. A **11**, 95 (2001).
13. Ye.S. Golubeva *et al.*, Eur. Phys. J. A **11**, 237 (2001).
14. Z. Rudy *et al.*, Eur. Phys. J. A **15**, 303 (2002), nucl-th/0201069.
15. W. Cassing *et al.*, Nucl. Phys. A **614**, 415 (1997).
16. P. Crochet *et al.*, Phys. Lett. B **486**, 6 (2000).
17. F. Laue *et al.*, Eur. Phys. J. A **9**, 397 (2000).
18. A. Sibirtsev *et al.*, Nucl. Phys. A **641**, 476 (1998).
19. L. Tolos *et al.*, Phys. Rev. C **65**, 054907 (2002), nucl-th/0202057.
20. M. Nekipelov *et al.*, Phys. Lett. B **540**, 207 (2002).
21. V. Koptev *et al.*, Phys. Rev. Lett. **87**, 022301 (2001).

Eur. Phys. J. A **18**, 471–473 (2003)
DOI 10.1140/epja/i2002-10262-x

THE EUROPEAN PHYSICAL JOURNAL A

Few-body correlations in the QCD phase diagram

M. Beyer[a]

Fachbereich Physik, Universität Rostock, 18051 Rostock, Germany

Received: 30 September 2002 /
Published online: 22 October 2003 – © Società Italiana di Fisica / Springer-Verlag 2003

Abstract. From the viewpoint of statistical physics, nuclear matter is a strongly correlated many-particle system. Several regimes of the QCD phase diagram should exhibit strong correlations. Here I focus on three- and four-body correlations that might be important in the phase diagram.

PACS. 21.65.+f Nuclear matter – 21.45.+v Few-body systems

1 Introduction

Lattice and effective model calculations provide a rich and exciting sketch of the phase diagram of Quantum Chromodynamics (QCD). Two regions may coarsely be distinguished: a hadronic phase and a plasma phase. Since quarks are considered part of the fundamental building blocks of matter, the existence of a hadronic phase is already an indication of strong correlations between quark-antiquark and three-quarks. Further on, in both phases correlations lead to more interesting phenomena, such as clustering of nucleons to form nuclei, or superfluidity (in nuclear matter) and color superconductivity (in quark matter). In particular in the later cases a weak residual interaction is enough to destabilize the ground state (just as is the case for the formation of Cooper pairing). These investigations are usually based on the study of two-particle correlations. There are reasons to go beyond two-particle correlations, *e.g.*:

- Particle production even in a dense environment such as deuteron formation in a heavy-ion reaction, need a third particle to conserve energy momentum [1].
- To study the properties of α-particles [2] or determine the critical temperature of a possible α-particle condensate [3–5] needs an in-medium four-body equation.
- Recent results in the Hubbard model indicate, that three-particle contributions may lead to a different (lower) critical temperature compared to the simple Thouless criterion [6]. Question of this type have not been addressed for nuclear matter.
- The chiral phase transition is often discussed along with a confinement-deconfinement transition based on investigating mesons (quark-antiquark states), see, *e.g.*, ref. [7]. Does this transition happen for nucleons (three-quark states) at the same density/temperature?

To investigate these issues a first step is to develop and solve proper effective in-medium three- and four-body equations that are valid at *finite temperatures and densities* analogous to the Feynman-Galitskii or Bethe-Goldstone equations [8]. This has been achieved in the past for the nonrelativistic problem [2,9–11]. These equations have been derived on the basis of statistical Green functions [8]. The Green functions have been decoupled utilizing a cluster expansion, see, *e.g.*, [12]. To tackle these questions in the (deconfined) quark-phase, in addition, such in-medium few-body equations must obey special relativity. As chiral symmetry breaking is presumably restored (up to small current masses) the quarks may become very light objects and therefore relativistic effects should play a larger role than for isolated systems. Here, relativity is realized using the light front form of relativistic dynamics [13]. First results are given in refs. [14,15] on the confinement-deconfinement (Mott) transition.

2 Theory

We use Dyson equations to tackle the many-particle problem, see, *e.g.*, ref. [12]. This enables us to decouple the hierarchy of Green functions. The Dyson equation approach used here is based on two ingredients: i) all particles of a cluster are taken at the same global time, ii) the ensemble averaging for a cluster is done for an uncorrelated medium. The resulting decoupled Green functions may be economically written as resolvents in the n-body space, where $n = 2, 3, 4, \ldots$ is the number of particles in the considered cluster.

The solution of the one-particle problem in the Hartree-Fock approximation leads to the following quasiparticle energy:

$$\varepsilon_1 = \frac{k_1^2}{2m_1} + \sum_2 V_2(12, \widetilde{12}) f_2 \simeq \frac{k_1^2}{2m_1^{\mathrm{eff}}} + \Sigma^{\mathrm{HF}}(0). \quad (1)$$

[a] e-mail: michael.beyer@physik.uni-rostock.de

The last equation introduces the effective mass that is a valid concept for the rather low densities considered here and $\mu^{\rm eff} \equiv \mu - \Sigma^{\rm HF}(0)$. The Fermi function $f_i \equiv f(\varepsilon_i)$ for the i-th particle is given by

$$f(\varepsilon_i) = \frac{1}{e^{\beta(\varepsilon_i - \mu)} + 1}. \quad (2)$$

The resolvent G_0 for n noninteracting quasiparticles is

$$G_0(z) = (z - H_0)^{-1} N \equiv R_0(z) N, \quad H_0 = \sum_{i=1}^{n} \varepsilon_i, \quad (3)$$

where G_0, H_0, and N are formally matrices in n-particle space. The Matsubara frequency z_λ has been analytically continued into the complex plane, $z_\lambda \to z$ [8]. The Pauli blocking for n-particles is

$$N = \bar{f}_1 \bar{f}_2 \ldots \bar{f}_n \pm f_1 f_2 \ldots f_n, \quad \bar{f} = 1 - f, \quad (4)$$

where the upper sign is for Fermi-type and the lower for Bose-type clusters. The full resolvent $G(z)$ is given by

$$G(z) = (z - H_0 - V)^{-1} N, \quad V \equiv \sum_{\text{pairs } \alpha} N_2^\alpha V_2^\alpha. \quad (5)$$

Note that $V^\dagger \neq V$. For the two-body case as well as for a two-body subsystem embedded in the n-body cluster the standard definition of the t-matrix leads to the Feynman-Galitskii equation for finite temperature and densities [8],

$$T_2^\alpha(z) = V_2^\alpha + V_2^\alpha N_2^\alpha R_0(z) T_2^\alpha(z). \quad (6)$$

Introducing the Alt-Grassberger-Sandhas (AGS) [16] transition operator $U_{\alpha\beta}(z)$ the effective inhomogeneous in-medium AGS equation reads

$$U_{\alpha\beta}(z) = (1 - \delta_{\alpha\beta}) R_0^{-1}(z) + \sum_{\gamma \neq \alpha} N_2^\gamma T_2^\gamma(z) R_0(z) U_{\gamma\beta}(z). \quad (7)$$

The homogeneous in-medium AGS equation uses the form factors defined by

$$|F_\beta\rangle \equiv \sum_\gamma \bar{\delta}_{\beta\gamma} N_2^\gamma V_2^\gamma |\psi_{B_3}\rangle \quad (8)$$

to calculate the bound state ψ_{B_3}

$$|F_\alpha\rangle = \sum_\beta \bar{\delta}_{\alpha\beta} N_2^\beta T_2^\beta(B_3) R_0(B_3) |F_\beta\rangle. \quad (9)$$

Finally, the four-body bound state is described by

$$|\mathcal{F}_\beta^\sigma\rangle = \sum_{\tau\gamma} \bar{\delta}_{\sigma\tau} U_{\beta\gamma}^\tau(B_4) R_0(B_4) \times N_2^\gamma T_2^\gamma(B_4) R_0(B_4) |\mathcal{F}_\gamma^\tau\rangle, \quad (10)$$

where $\alpha \subset \sigma$, $\gamma \subset \tau$ and σ, τ denote the four-body partitions. The two-body input is given in (6) and the three-body input by (7). Note that, although we have managed to rewrite the above equations in a way close to the ones for the isolated case, they contain all the relevant in-medium corrections in a systematic way, *i.e.* correct Pauli-blocking and self-energy corrections. The numerical solution requires some mild approximations that are however well understood in the context of the isolated few-body problem.

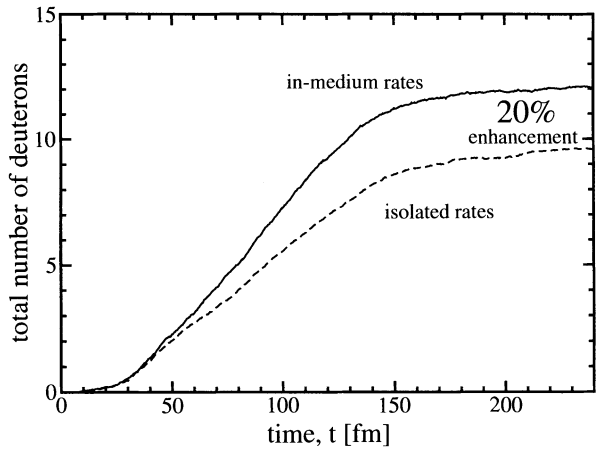

Fig. 1. BUU simulation of the deuteron formation during the central collision of ^{129}Xe + ^{119}Sn at 50 MeV/A.

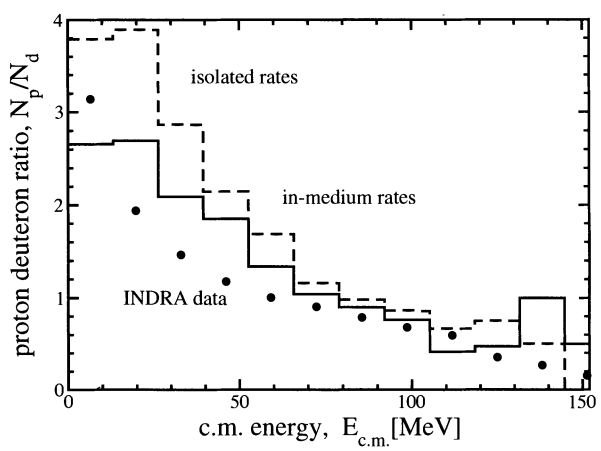

Fig. 2. Ratio of proton to deuteron numbers as a function of c.m. energy. The experimental data are from the INDRA Collaboration.

3 Results

An experiment to explore the equation of state of nuclear matter is heavy-ion collisions at various energies. Here we focus on intermediate to low scattering energies and compare results to a recent experiment ^{129}Xe + ^{119}Sn at 50 MeV/A by the INDRA Collaboration [17]. A microscopic approach to tackle the heavy-ion collision is given by the Boltzmann equation for different particle distributions and solved via a Boltzmann-Uehling-Uhlenbeck (BUU) simulation [18,19]. The reaction rates appearing in the collision integrals are *a priori* medium dependent. However, previously this medium dependence has been neglected. Within linear response theory for infinite nuclear matter the use of in-medium rates leads to faster time scales for the deuteron lifetime and the chemical relaxation time, as has been shown in detail in refs. [20,21]. This faster time scales should have consequences for the freeze-out of fragments.

We use the in-medium AGS equations (7) that reproduce the experimental data in the limit of an isolated three-body system. For details on the specific interaction

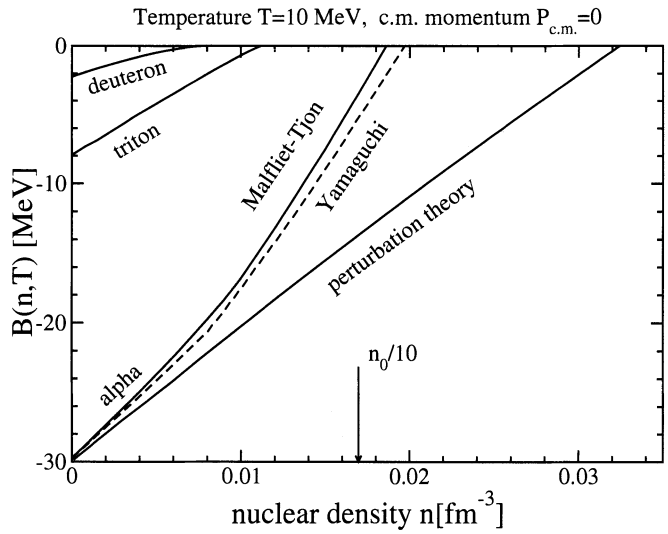

Fig. 3. Difference between the pole energy of the bound state and the continuum, $B(n,T) = E_{\text{pole}} - E_{\text{cont}}$.

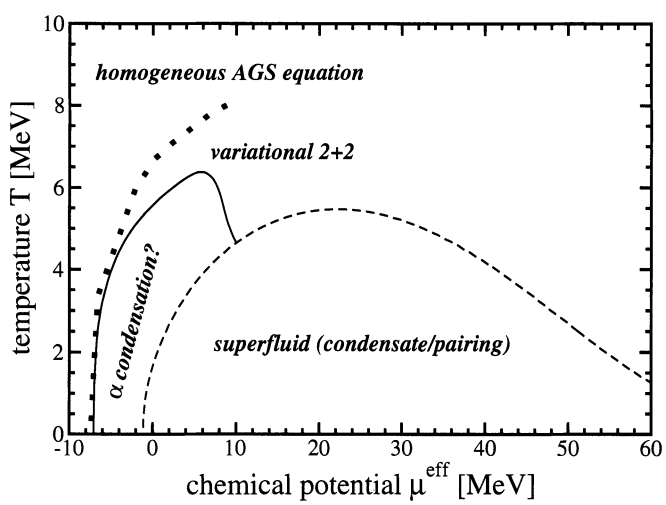

Fig. 4. Critical temperatures of condensation/pairing leading to superfluid nuclear matter. For an explanation see text.

model see ref. [9]. We investigate the influence of medium-dependent rates in the BUU simulation of the heavy-ion collision as compared to the use of isolated (*i.e.* experimental) rates. Figure 1 shows that the net effect (gain-minus-loss) of deuteron production becomes larger for the use of in-medium rates (solid line) compared to using the isolated rates (dashed line). The change is significant, however, a comparison with experimental data is difficult since deuterons may also be evaporating from larger clusters that have not been taken into account in the present calculation so far. The ratio of protons to deuterons may be better suited for a comparison to experiments that is shown in fig. 2. The use of in-medium rates (solid line) lead to a shape closer to the experimental data (dots) than the use of isolated rates (dashed line). In these calculation, besides the change of rates, also the Mott effect has been taken into account.

Figure 3 shows the dependence of the binding energy for different clusters at a given temperature $T = 10\,\text{MeV}$ and at rest in the medium.

In fig. 4 part of the phase diagram of nuclear matter is shown. The condition for the onset of superfluidity for α-particles is $B(T_c, \mu, P = 0) = 4\mu$. The critical temperature found by solving the homogeneous AGS equation for $\mu < 0$ confirms the onset of α condensation even at higher values (dotted line) than given earlier (solid line, from [3]) based on a variational calculation using the $2+2$ component of the α-particle. For $\mu > 0$ the condition $E = 4\mu$ for the phase transition can also be fulfilled. However, the significance for a possible quartetting needs further investigation. Due to the many-channel situation of more than two-particles equations, the Thouless criterion might be revisited.

Work supported by the Deutsche Forschungsgemeinschaft.

References

1. C. Kuhrts, M. Beyer, P. Danielewicz, G. Röpke, Phys. Rev. C **63**, 034605 (2001) and references therein.
2. M. Beyer, S.A. Sofianos, C. Kuhrts, G. Röpke, P. Schuck, Phys. Lett. B **488**, 247 (2000).
3. G. Röpke, A. Schnell, P. Schuck, P. Nozieres, Phys. Rev. Lett. **80**, 3177 (1998).
4. A. Tohsaki, H. Horiuchi, P. Schuck, G. Ropke, Phys. Rev. Lett. **87**, 192501 (2001).
5. Y. Suzuki, M. Takahashi, Phys. Rev. C **65**, 064318 (2002).
6. M. Himmerich, M. Letz, Phys. Rev. B **64**, 144519 (2001).
7. D. Blaschke, F. Karsch, C.D. Roberts (Editors), *Proceedings of the International Workshop on Understanding Deconfinement in QCD, Trento, 1-13 March, 1999* (World Scientific, Singapore, 1999) p. 354.
8. L.P. Kadanoff, G. Baym, *Quantum Statistical Mechanics* (Benjamin, New York, 1962); A.L. Fetter, J.D. Walecka, *Quantum Theory of Many-Particle Systems* (McGraw-Hill, New York, 1971).
9. M. Beyer, G. Röpke, A. Sedrakian, Phys. Lett. B **376**, 7 (1996).
10. M. Beyer, Few-Body Syst. Suppl. **10**, 179 (1999).
11. M. Beyer, W. Schadow, C. Kuhrts, G. Röpke, Phys. Rev. C **60**, 034004 (1999).
12. J. Dukelsky, G. Röpke, P. Schuck, Nucl. Phys. A **628**, 17 (1998).
13. P.A. Dirac, Rev. Mod. Phys. **21**, 392 (1949).
14. M. Beyer, S. Mattiello, T. Frederico, H.J. Weber, Phys. Lett. B **521**, 33 (2001).
15. S. Mattiello, M. Beyer, T. Frederico, H.J. Weber, Few-Body Syst. **31**, 159 (2002).
16. E.O. Alt, P. Grassberger, W. Sandhas, Nucl. Phys. B **2**, 167 (1967).
17. INDRA Collaboration (D. Gorio *et al.*), Eur. Phys. J. A **7**, 245 (2000) and references therein.
18. P. Danielewicz, G.F. Bertsch, Nucl. Phys. A **533**, 712 (1991).
19. P. Danielewicz, Q. Pan, Phys. Rev. C **46**, 2002 (1992).
20. M. Beyer, G. Röpke, Phys. Rev. C **56**, 2636 (1997).
21. C. Kuhrts, M. Beyer, G. Röpke, Nucl. Phys. A **668**, 137 (2000).

Eur. Phys. J. A **18**, 475–478 (2003)
DOI 10.1140/epja/i2002-10263-9

THE EUROPEAN PHYSICAL JOURNAL A

Hadrons with charmed quarks in matter

A. Sibirtsev[a]

Institut für Kernphysik, Forschungszentrum Jülich, D-52425 Jülich, Germany

Received: 30 September 2002 /
Published online: 22 October 2003 – © Società Italiana di Fisica / Springer-Verlag 2003

Abstract. We investigate the $D\bar{D}$ decay width of excited charmonium states at finite nuclear density with simultaneous modification of both D- and $\bar{D}$-mesons in nuclear matter. The strongest effect is found for the Ψ'-meson. The medium modification can be detected by dilepton spectroscopy as substantial Ψ' broadening and anomalous Ψ' absorption.

PACS. 13.25.Gv Decays of J/Ψ, Υ, and other quarkonia – 14.40.Lb Charmed mesons – 14.65.Dw Charmed quarks – 24.85.+p Quarks, gluons, and QCD in nuclei and nuclear processes

1 Introduction

In dense and hot nuclear matter the light-quark condensates $q\bar{q}$ might be substantially reduced. This affects the light-quark content of mesons and baryons and therefore results in-medium modification of hadron properties [1–3]. Even if the changes in quark condensates are small, the absolute difference between the in-medium and bare masses of hadrons is expected [3,4] to be larger for heavier hadrons.

The charmed mesons, which consist of light q, $\bar{q}$ and heavy c, $\bar{c}$ quarks, are considered suitable probes of in-medium modification of hadron properties. Similarly to $\bar{K}$ ($\bar{q}s$) and K ($q\bar{s}$) mesons, the D ($\bar{q}c$) and $\bar{D}$ ($q\bar{c}$) satisfy different dispersion relations in matter because of the different sign of q and $\bar{q}$ vector couplings [3]. While the D-meson mass is reduced in nuclear matter, the $\bar{D}$ mass is raised, as is illustrated by fig. 1a). Calculations with the Quark-Meson Coupling model (QMC) [5] show that already at normal nuclear density ρ_0 the mass splitting between D- and $\bar{D}$-mesons is about 160 MeV.

It was proposed [4] that the modification of the D-meson in nuclear matter can be identified by enhanced subthreshold production of open charm in $\bar{p}A$ annihilation. Because of charm conservation, D- and $\bar{D}$-mesons are produced pairwise. As is shown in fig. 1b) the sum of D and $\bar{D}$ masses depends substantially on nuclear density. The downward shift of the $D\bar{D}$ threshold at ρ_0 is $\simeq -100$ MeV. A QCD sum rule estimate [6] predicts about the same shift.

Furthermore, an attractive D-nucleus potential can be measured by investigating charmed mesic nuclei [3]. The reduction of D mass in matter might affect open-charm production [7] and J/Ψ suppression [8] in relativistic heavy-ion collisions.

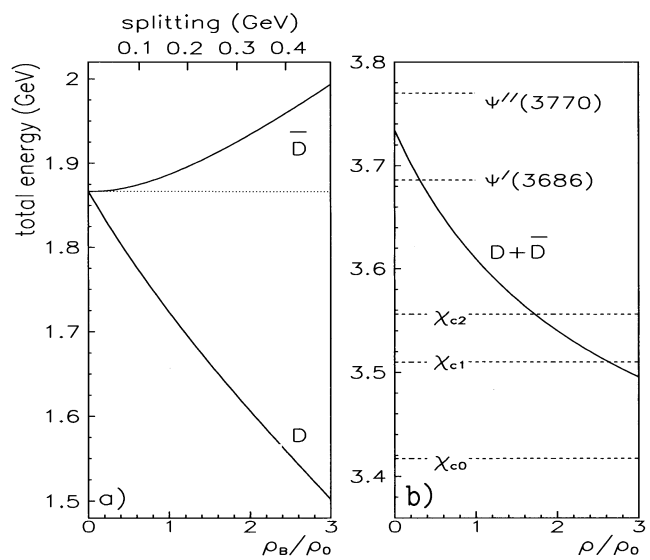

Fig. 1. a) The in-medium mass of D- and $\bar{D}$-mesons as a function of nuclear density ρ/ρ_0, with $\rho_0 = 0.16\,\mathrm{fm}^{-3}$ and the $D\bar{D}$ mass splitting (upper axis). b) The solid line shows the overall $D\bar{D}$ mass as a function of density. The dashed lines indicate the masses of excited charmonia.

In contrast to open charm, charmonium mesons consist of heavy $c\bar{c}$ quarks and can be affected only by gluonic condensates. It was expected that the modification of properties of heavy quarkonia in matter would be almost negligible [9]. In that case, the overall $D\bar{D}$ mass at some nuclear density might cross the masses of excited charmonium states, as is illustrated by fig. 1b).

[a] e-mail: a.sibirtsev@fz-juelich.de

The crossing of the charmonium states levels and the $D\bar{D}$ threshold in nuclear medium might result in the melting [10] of excited charmonium mesons.

Here, we investigate the modification of widths of charmonium states at finite nuclear density with D and $\bar{D}$ in-medium masses predicted by QMC [3]. We consider simultaneous modification of both D- and $\bar{D}$-mesons, as is illustrated in fig. 1 and study $\Psi''(3770)$, $\Psi'(3686)$ and χ_{c2} decay into $D\bar{D}$ in nuclear matter. The χ_{c0} modification is not discussed since the $D\bar{D}$ threshold does not cross its mass even at $\rho = 3\rho_0$, as is shown in fig. 1. The $\chi_{c1} \to D\bar{D}$ decay is suppressed by parity conservation.

2 $\Psi''(3770)$

The Ψ''-charmonium lies above the $D\bar{D}$ threshold in free space and its dominant decay width into $D\bar{D}$ channel is given by

$$\Gamma_{\Psi''\to D\bar{D}} = \frac{g^2_{\Psi'' D\bar{D}}}{3\pi}\frac{q^3}{m^2_\Psi}, \tag{1}$$

where m_Ψ is the $\Psi''(3770)$ mass and q is the D-meson momentum in the charmonium rest frame,

$$q = \frac{\left[\left(m^2_\psi - m^2_D - m^2_{\bar{D}}\right)^2 - 4m^2_D m^2_{\bar{D}}\right]^{1/2}}{2m_\Psi}, \tag{2}$$

with m_D and $m_{\bar{D}}$ the masses of D- and $\bar{D}$-mesons, respectively, while the coupling constant $g_{\Psi'' D\bar{D}} = 14.89$ is fixed by the vacuum decay width $\Gamma_{\Psi''\to D\bar{D}} = 23.6\,\mathrm{MeV}$.

If $\Psi'' D\bar{D}$ coupling does not change in matter the modification of the $\Psi(3770)$ width is entirely given by D and $\bar{D}$ in-medium masses and is determined by the phase space dependence of the charmonium decay width. In that case the in-medium $\Psi(3770)$ width depends substantially on nuclear-matter density, as is shown by the solid line in fig. 2a).

Within the $^3P_0$ model [11] the $\Psi'' D\bar{D}$ coupling itself depends on the D and $\bar{D}$ masses via

$$g^2_{\Psi'' D\bar{D}} = \frac{\pi^{3/2}2^{11}\gamma^2 m_\Psi}{5\beta^7 3^{10}}\left[\left(q^2+m^2_D\right)\left(q^2+m^2_{\bar{D}}\right)\right]^{1/2} \times\left(15\beta^2-2q^2\right)^2\exp\left(-q^2/6\beta^2\right), \tag{3}$$

where the oscillator length scale $\beta = 360\,\mathrm{MeV}$ is fixed by light-mesons decays [11], while the interaction strength $\gamma = 0.33$ is determined by $\Psi'' \to D\bar{D}$ decay.

Finally, the dashed line in fig. 2 shows the dependence of the $\Psi'' \to D\bar{D}$ decay width on nuclear-matter density resulting from the $^3P_0$ model. At normal nuclear density $\rho_0 = 0.16\,\mathrm{fm}^{-3}$ the $\Psi''(3770)$ in-medium width almost saturates $\Gamma_{\Psi''\to D\bar{D}} \simeq 90\,\mathrm{MeV}$, which is $\simeq 3.8$ times larger than in vacuum. Furthermore, the $^3P_0$ result substantially differs from the phase space estimate.

The Ψ'' modification in nuclear matter might be studied by dilepton spectroscopy from AA as well as $\bar{p}A$ interactions, since the effect is measurable already at normal nuclear densities. The $\Psi''(3770)$-charmonium does not decay into J/Ψ and thus its modification in matter cannot be considered as an additional source of J/Ψ suppression in heavy-ion collisions.

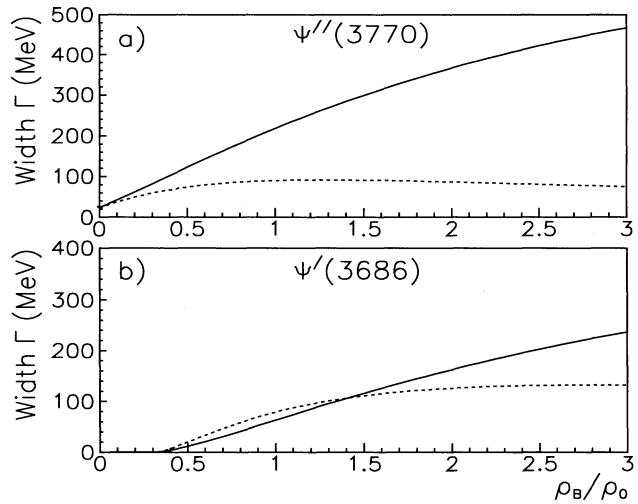

Fig. 2. Decay widths of $\Psi''(3770)$ (a) and $\Psi'(3686)$ (b) charmonium states into $D\bar{D}$ as a function of nuclear-matter density in units of ρ_0. The solid lines show the phase space dependence, while the dashed lines are the results from the $^3P_0$ model. In both calculations the D and $\bar{D}$ in-medium masses are given by the QMC model.

3 $\Psi'(3686)$

The Ψ'-charmonium lies below the $D\bar{D}$ threshold in free space, but the $D\bar{D}$ decay channel becomes open at nuclear density $\rho \simeq 0.05\,\mathrm{fm}^{-3}$, as illustrated by fig. 1. The Ψ' is narrow, its total width is 0.277 MeV and partial decay into J/Ψ accounts for $\simeq 54\%$ of the total width.

Although, the $\Psi(3686)$ coupling to $D\bar{D}$ is not directly accessible, it can be estimated within the framework of Vector Meson Dominance model as

$$g^2_{\Psi' D\bar{D}} = \frac{16\pi\alpha^2}{27}\frac{m_\Psi}{\Gamma_{\Psi'\to e^+e^-}}, \tag{4}$$

where α is the fine-structure constant, m_Ψ is the $\Psi'(3686)$ mass and $\Gamma_{\Psi'\to e^+e^-} = 2.35\,\mathrm{keV}$ is the radiative $\Psi' \to e^+e^-$ decay width. Finally, the $\Psi' D\bar{D}$ coupling constant is 12.84; the $\Psi'' D\bar{D}$ coupling from VMD is to 19.94, which is close to the result from direct $\Psi'' \to D\bar{D}$ decay given by eq. (1).

The phase space dependence of the Ψ' in-medium width from eq. (1) is shown by the solid line in fig. 2b). This result again can be compared with the prediction of the $^3P_0$ model given by [11]

$$\Gamma_{\Psi'\to D\bar{D}} = \frac{\pi^{1/2}2^9\gamma^2}{m_\Psi\beta^7 3^{11}}\left[\left(q^2+m^2_D\right)\left(q^2+m^2_{\bar{D}}\right)\right]^{1/2} \times q^3\left(15\beta^2-2q^2\right)^2\exp\left(-q^2/6\beta^2\right) \tag{5}$$

and shown by the dashed line in fig. 2b). Here the calculations were done with parameters β and γ evaluated

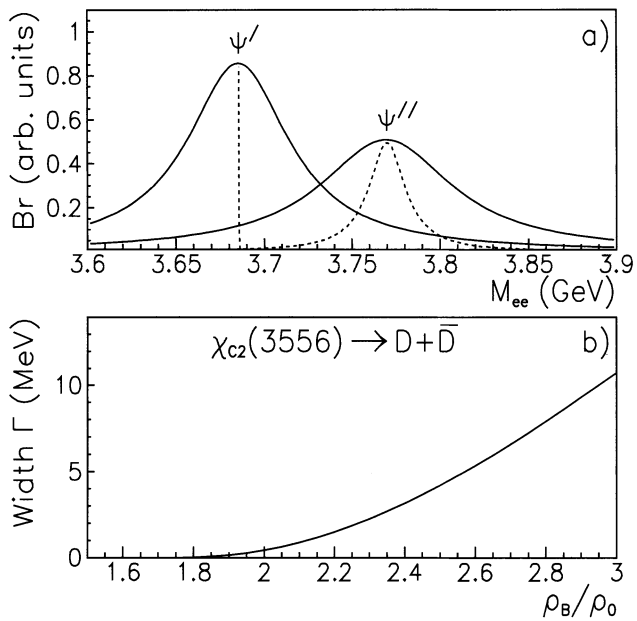

Fig. 3. a) Dilepton spectra from Ψ' and Ψ'' decays at normal nuclear density $\rho = \rho_0 = 0.16\,\mathrm{fm}^{-3}$ (solid lines) and in vacuum (dashed lines). b) Decay width of the $\chi_{c2}(3556)$-charmonium into $D\bar{D}$ as a function of nuclear-matter density in units of ρ_0 predicted by the $^3P_0$ model with D and $\bar{D}$ in-medium masses given by QMC.

above. Note that at nuclear densities $\rho \leq 1.5\rho_0$ both the $^3P_0$ model and VMD phase space estimates are in reasonable agreement. An exciting observation is that at normal nuclear density $\rho_0 = 0.16\,\mathrm{fm}^{-3}$ the Ψ' width is $\simeq 70\,\mathrm{MeV}$, which is $\simeq 250$ times larger than that in vacuum.

Again, the Ψ' modification in nuclear matter can be measured through dilepton spectroscopy. As we found, the dilepton spectrum from $\Psi'(3686)$ decay in matter might strongly overlap with $\Psi''(3770)$-charmonium decay. Figure 3a) shows dilepton spectra from Ψ' and Ψ'' decays unfolded from the production cross-section. The solid lines show the results for matter at normal nuclear density, while the dashed lines indicate the spectra in free space. The measurement of a broad peak around Ψ' pole might be considered as an direct indication of in-medium modification of charmonia.

On the other hand, a large $D\bar{D}$ component of Ψ'-charmonium should result in strong Ψ' absorption in nuclear matter, similar to that found [8] for J/Ψ dissociation. Moreover, Ψ' melting in nuclear matter will additionally suppress $\Psi' \to J/\Psi$ decay and partially eliminate J/Ψ yield in heavy-ion collisions.

4 $\chi_{c2}(3556)$

The χ_{c2}-charmonium level crosses the $D\bar{D}$ threshold at a nuclear density of about $0.28\,\mathrm{fm}^{-3}$. In vacuum the χ_{c2} width is 2 MeV and partial decay into the J/Ψ is $\simeq 13.5\%$. There is no reliable way to estimate $\chi_{c2}D\bar{D}$ coupling and to evaluate the phase space dependence of the χ_{c2} in-medium width.

In the $^3P_0$ model the $\chi_{c2} \to D\bar{D}$ width is given as [11]

$$\Gamma_{\chi_{c2}\to D\bar{D}} = \frac{\pi^{1/2}2^{12}\gamma^2}{5m_\chi\beta^5 3^8}\left[\left(q^2+m_D^2\right)\left(q^2+m_{\bar{D}}^2\right)\right]^{1/2} \times q^5 \exp\left(-q^2/6\beta^2\right), \tag{6}$$

where m_χ is the χ_{c2} mass and parameters β and γ are listed above. The in-medium χ_{c2} width is shown in fig. 3b) as a function of nuclear-matter density. The χ_{c2} modification becomes significant only at large densities.

5 Conclusion

Modification of the D- and $\bar{D}$-meson masses in nuclear matter leads to a substantial increase of the χ_{c2}, Ψ' and Ψ'' decay widths into the $D\bar{D}$ channel.

The calculations with the density-independent coupling constants between the Ψ'- and Ψ''-charmonium and the $D\bar{D}$-pair results in strong and monotonic density dependence of the Ψ' and Ψ'' in-medium widths due to the increase of the final-state phase space. Within the $^3P_0$ model these couplings are also considered as a function of the in-medium D and $\bar{D}$ masses and as a result the Ψ'- and Ψ''-charmonium widths do not increase monotonically with nuclear density, but saturate at $\rho_0 = 0.16\,\mathrm{fm}^{-3}$. It was found that the saturation limits are $\Gamma_{\Psi'\to D\bar{D}} \simeq 70\,\mathrm{MeV}$ and $\Gamma_{\Psi''\to D\bar{D}} \simeq 90\,\mathrm{MeV}$, which can be compared with vacuum widths of 0.277 MeV and 23.6 MeV, respectively.

The χ_{c2}-charmonium level crosses the $D\bar{D}$ threshold at $\rho \simeq 1.25\rho_0$ and its width increases with nuclear-matter density. At $\rho \simeq 3\rho_0$ the χ_{c2} decay width into $D\bar{D}$ is about 11 MeV, which may be compared with total $\Gamma_{\chi_{c2}} = 2\,\mathrm{MeV}$ width in vacuum.

We conclude that the modification of the D and $\bar{D}$ in matter most dramatically affects the Ψ'-charmonium. This can be detected by dilepton spectroscopy as the appearance of a broad peak near the Ψ' pole or as anomalous Ψ' suppression in nuclear matter.

Our results are in agreement with the most recent findings [12] that both the mass and width of $\Psi''(3770)$ depend significantly on the D-meson mass.

References

1. T. Hatsuda, T. Kunihiro, Phys. Rep. **247**, 221 (1994).
2. W. Weise, Nucl. Phys. A **610**, 35c (1996).
3. K. Tsushima *et al.*, Phys. Rev. C **59**, 2824 (1999); Nucl. Phys. A **680**, 279 (2000).
4. A. Sibirtsev, K. Tsushima, A.W. Thomas, Eur. Phys. J. A **6**, 351 (1999).
5. P.A.M. Guichon, Phys. Lett. B **200**, 235 (1988); K. Tsushima, K. Saito, J. Haidenbauer, A.W. Thomas, Nucl. Phys. A **630**, 691 (1998).

6. A. Hayashigaki, Phys. Lett. B **487**, 96 (2000).
7. Z. Lin, M. Gyulassy, Phys. Rev. C **51**, 2177 (1995); E.V. Shuryak, Phys. Rev. C **55**, 961 (1997); A. Sibirtsev, Nucl. Phys. A **680**, 274 (2000); W. Cassing, E.L. Bratkovskaya, A. Sibirtsev, Nucl., Phys. A **691**, 753 (2001).
8. A. Sibirtsev, K. Tsushima, K. Saito, A.W. Thomas, Phys. Lett. B **484**, 23 (2000); Phys. Rev. C **63**, 044906 (2001).
9. S.J. Brodsky, G.F. Teramond, Phys. Rev. Lett. **64**, 1011 (1990); F. Klingl *et al.*, Phys. Rev. Lett. **82**, 3396 (1999); A. Hayashigaki, Prog. Theor. Phys. **101**, 923 (1999).
10. S. Digal, P. Petreczky, H. Satz, Phys. Lett. B **514**, 57 (2001); C.Y. Wong, Phys. Rev. C **65**, 034902 (2002); C.Y. Wong, T. Barnes, E.S. Swanson, H.W. Crater, nucl-th/0112023.
11. G. Busetto, L. Oliver, Z. Phys. C **20**, 247 (1983); R. Kokoski, N. Isgur, Phys. Rev. D **35**, 907 (1987); E.S. Ackleh, Ted Barnes, E.S. Swanson, Phys. Rev. D **54**, 6811 (1996); T. Barnes, F.E. Close, P.R. Page, E.S. Swanson, Phys. Rev. D **55**, 4157 (1997).
12. B. Friman, S.H. Lee, T. Song, Phys. Lett. B **548**, 153 (2002), nucl-th/0207006; C.M. Ko, S.H. Lee, Phys. Rev. C **67**, 038202 (2003), nucl-th/0208003.

Eur. Phys. J. A **18**, 479–481 (2003)
DOI 10.1140/epja/i2002-10264-8

THE EUROPEAN PHYSICAL JOURNAL A

Experimental signals of σ-mesons in nuclei and chiral symmetry

M.J. Vicente Vacas[a]

Departamento de Física Teórica and IFIC, Universidad de Valencia-CSIC, Ap. Correos 22085, E-46071 Valencia, Spain

Received: 30 September 2002 /
Published online: 22 October 2003 – © Società Italiana di Fisica / Springer-Verlag 2003

Abstract. The $\pi\pi$ interaction in the scalar isoscalar channel is studied as a function of the baryonic density in the framework of a chiral unitary approach which successfully reproduces vacuum π-π phase shifts. We present some results on the σ-meson pole, which is generated dynamically in our model, in nuclear matter. Finally, we analyze the $(\gamma, \pi\pi)$ reaction on nucleons and nuclei in the kinematical region where the scalar isoscalar $\pi\pi$ scattering amplitude is influenced by the low mass of the σ in nuclei, and thus, presents a large enhancement close to the position of its pole. Indeed, we find, that the final-state interaction of the pions modified by the nuclear medium produces a large shift of strength of the two-pion invariant-mass distribution in the $(\gamma, \pi^0\pi^0)$ channel consistent with recent experimental data.

PACS. 14.40.-n Properties of specific particles: Mesons – 25.20.-x Photonuclear reactions – 21.65.+f Nuclear matter

1 Introduction

In the past years, much effort has been devoted to the study of the $\pi\pi$ scattering amplitude in nuclei and its possible experimental signals, like the enhancement of the $\pi\pi$ invariant-mass distributions close to the $\pi\pi$ threshold, seen in the experiments of pion-induced two-pion production in nuclei [1], and the large strength shift found in the $(\pi, \pi^0\pi^0)$ process [2].

The idea of strong threshold effects due to the $\pi\pi$ interaction in a dense nuclear medium was first suggested in ref. [3]. These effects would show up in the scalar-isoscalar —σ— channel and could be interpreted as due to a drop of the σ mass in nuclear matter. Later works, paying attention to the chiral constraints of the $\pi\pi$ amplitude and trying to use realistic potentials, found indeed an appreciable enhancement of the $\pi\pi$ scattering amplitude close to threshold [4–7].

These theoretical $\pi\pi$ scattering amplitudes in the nuclear medium have been used in the analysis of the $(\pi, \pi\pi)$ reactions in nuclei [8–10]. Although the modifications of the $\pi\pi$ invariant-mass distributions produced by the $\pi\pi$ scattering go in the right direction, the calculations have not been successful in fully reproducing the medium effects found in the experiment. A much better agreement has been obtained in the case of the $(\gamma, \pi\pi)$ reaction [11, 12], which has the obvious advantage of exploring higher nuclear densities. Additionally, the $N(\gamma, \pi\pi)N$ scattering amplitude is simpler and does not have the strong interference between different mechanisms that occurs in the elementary $\pi N \to (\pi\pi)_{I=0}N$ reaction.

[a] e-mail: Manuel.J.Vicente@uv.es

Fig. 1. Terms of the meson-meson scattering amplitude accounting for ph and Δh excitation.

In this paper, we will present briefly our results on the in-medium $\pi\pi$ interaction in the s-wave, $I = 0$ channel. We will consider the σ pole dependence on the nuclear density and finally, we will discuss the experimental signature of these medium effects in the $(\gamma, \pi\pi)$ reaction.

2 σ-meson in the medium

2.1 $\pi\pi$ interaction and the σ pole

The pion pion interaction in nuclear matter has been calculated in the framework of a chiral unitary approach which generates the f_0- and σ-resonances and reproduces well the meson-meson phase shifts in vacuum. The pions undergo multiple scattering which is accounted for by means of the Bethe-Salpeter equation,

$$T = V + VG_{\pi\pi}T, \tag{1}$$

where V is given by the lowest-order chiral amplitude for $\pi\pi \to \pi\pi$ in s-wave and $I = 0$, and $G_{\pi\pi}$ is the loop function of the two-pion propagators properly renormalized. The nuclear medium effects are basically driven by the attractive p-wave pion self-energy, represented by the particle-hole bubbles in fig. 1, and are incorporated by

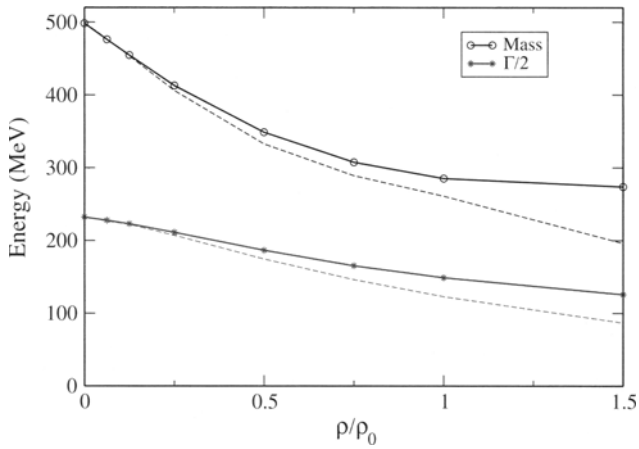

Fig. 2. σ mass and half-width as a function of the density. Dashed lines include also the $2ph$ pion self-energy pieces.

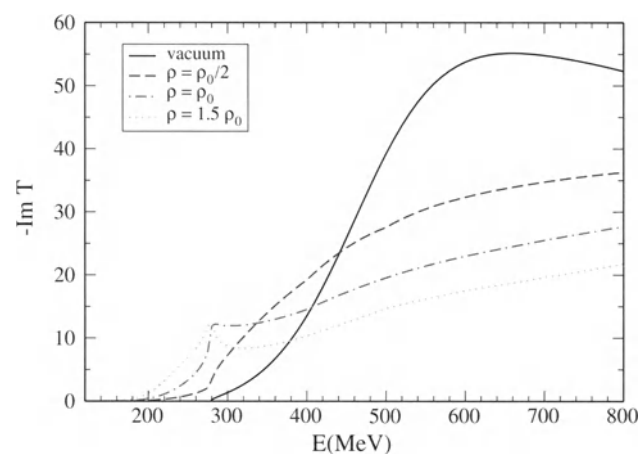

Fig. 3. Imaginary part of the $\pi\pi$ scattering amplitude at several densities.

modifying the pion propagators and including new pieces in the Bethe-Salpeter equation. Some of these pieces are shown in fig. 1. Full details of the calculation can be found in refs. [6] and [13].

In fig. 2, we present our results for the σ mass and its width as a function of the baryon density [13]. We find that both mass and width decrease as the density increases, reaching a mass around 250 MeV and a similar width at 1.5 times the nuclear density. Even at intermediate densities the σ pole is close to the 2π threshold. The influence of this pole is clear over the real energy axis and produces a peak in the $\pi\pi$ scattering amplitude at low energies as can be seen in fig. 3. The accumulation of strength depends quite strongly on the density, and therefore one should not expect any dramatic enhancement in peripheral reactions like $A(\pi,\pi\pi)X$.

2.2 The A($\gamma,\pi\pi$)X reaction

In contrast with the $(\pi,\pi\pi)$ reactions, the photon beam is not strongly distorted, and two-pion photoproduction probes deeper regions of the nuclei. For the elementary

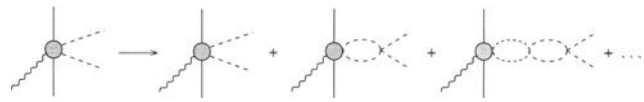

Fig. 4. Diagrammatic series for pion final-state interaction in $I = 0$.

$(\gamma,\pi\pi)$ reaction we follow the model of ref. [14] which couples the photons to mesons, nucleons and the resonances $\Delta(1232)$, $N^*(1440)$, $N^*(1520)$ and $\Delta(1700)$. This model reproduces all the charge channels at low energies well. Final-state interaction of the πN system is accounted for by means of the explicit use of resonances with their widths.

The two final pions undergo multiple scattering which can be accounted for by means of the Bethe-Salpeter equation as shown diagrammatically in fig. 4.

The two-pion final-state interaction is incorporated in the $I = 0$ part of the $(\gamma,\pi\pi)$ amplitude by factorizing the on-shell tree level $\gamma N \to \pi\pi N$ and $\pi\pi \to \pi\pi$ amplitudes in the loop functions:

$$T^{I_{\pi\pi}=0}_{(\gamma,\pi^0\pi^0)} \longrightarrow T^{I_{\pi\pi}=0}_{(\gamma,\pi^0\pi^0)}\left(1 + G_{\pi\pi} t^{I=0}_{\pi\pi}(M_I)\right), \qquad (2)$$

where $G_{\pi\pi}$ is the loop function of the two-pion propagators, which appears in the Bethe-Salpeter equation, and $T^{I=0}_{\pi\pi}$ is the $\pi\pi$ scattering matrix in isospin $I = 0$, taken from ref. [6].

In fig. 5, we can see the results for the invariant-mass distribution of the two pions for hydrogen, ^{12}C and ^{208}Pb. Apart from the in-medium $\pi\pi$ interaction, other nuclear effects like the nucleons Fermi motion and Pauli blocking and the final pion distortion (absorption + quasielastic scattering) have been included in the calculation. That these other effects are well under control can be seen in the right panels showing the reactions $(\gamma,\pi^+\pi^0)$ and $(\gamma,\pi^-\pi^0)$. In this case the two pions have isospin one or two and therefore interact weakly at these low energies. Our calculation incorporating the elementary $\gamma N \to \pi\pi N$ and the quoted trivial nuclear effects agrees well with the experiment.

On the other hand, as one can see in the figure, there is an appreciable shift of strength to the low invariant-mass region due to the in medium $\pi\pi$ interaction in the $\pi^0\pi^0$ channel. Whereas in hydrogen the distribution peaks around 340 MeV, in nuclei the peak moves towards the 2π threshold. This shift is also well reproduced by our calculation.

These results show a clear signature of the modified $\pi\pi$ interaction in the medium. The fact that the photons are not distorted has certainly an advantage over the pion-induced reactions and allows one to see inner parts of the nucleus. In this sense, it is worth noting that, from our calculations, we can determine the average nuclear density felt by the reaction which turns out to be 35% and 65% of the normal nuclear density for ^{12}C and ^{208}Pb, respectively.

Although we have been mostly discussing this reaction in terms of the $\pi\pi$ interaction in the nuclear medium, its relation to the modification of the σ-meson in the medium

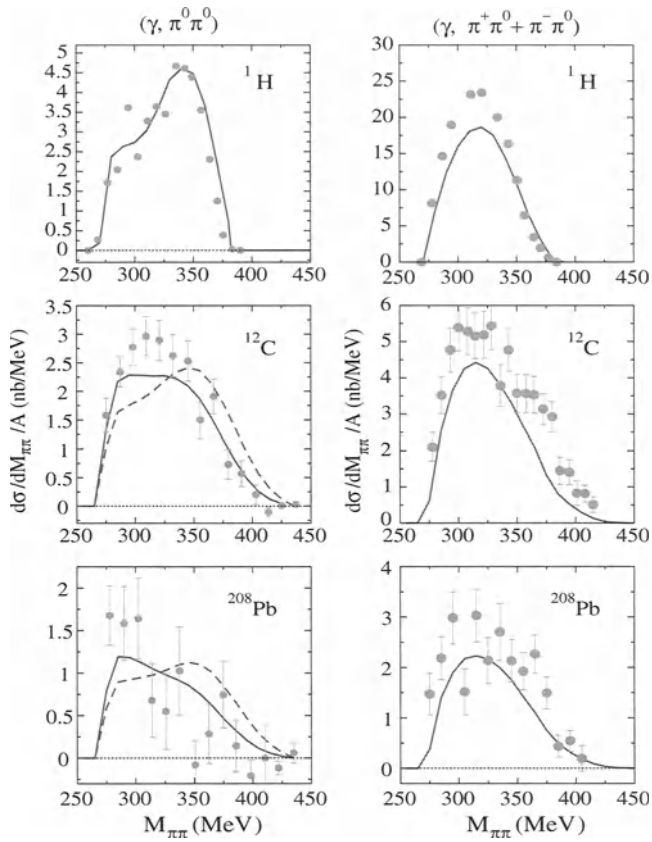

Fig. 5. 2π invariant-mass distribution for the $(\gamma, \pi\pi)$ reaction in hydrogen, ^{12}C and ^{208}Pb. Solid lines: full model including medium final $\pi\pi$ interaction. Dashed lines: idem using vacuum $\pi\pi$ interaction. Experimental data from [11].

is clear. We have mentioned that the reason for the shift of strength to lower invariant masses in the mass distribution is due to the accumulated strength in the scalar isoscalar $\pi\pi$ amplitude in the medium. Yet, this strength is mostly governed by the presence of the σ pole.

3 Conclusions

Present experimental data on both $(\pi, 2\pi)$ and $(\gamma, 2\pi)$ processes seem to confirm the importance of the 2π final state interaction in the scalar-isoscalar —"σ"— channel. In our approach, which is based on a conventional many-body expansion beginning with the standard chiral Lagrangians, the σ-meson both in the free space and in the nucleus is generated dynamically. Studying the evolution of the σ poles as a function of the nuclear density we find that the pole position of the σ moves to smaller energies as the density increases and produces as a consequence some accumulation of strength in the $\pi\pi$ interaction close to threshold.

Using this model, we are able to reproduce the experimental results of the $(\gamma, 2\pi)$ reaction from hydrogen to lead. Given that the $(\pi, 2\pi)$ reaction is more peripheral, and therefore sensitive to lower densities we expect the effects of the final-state interaction to be smaller in this case, what calls for some additional mechanism that could explain the large enhancements found experimentally.

References

1. CHAOS Collaboration (F. Bonutti *et al.*), Phys. Rev. Lett. **77**, 603 (1996); Nucl. Phys. A **638**, 729 (1998); P. Camerini, N. Grion, R. Rui, D. Vetterli, Nucl. Phys. A **552**, 451 (1993); **572**, 791 (1993)(E); F. Bonutti *et al.* (CHAOS Collaboration), Phys. Rev. C **60**, 018201 (1999).
2. Crystal Ball Collaboration (A. Starostin *et al.*), Phys. Rev. Lett. **85**, 5539 (2000).
3. P. Schuck, W. Norenberg, G. Chanfray, Z. Phys. A **330**, 119 (1988).
4. R. Rapp, J.W. Durso, J. Wambach, Nucl. Phys. A **596**, 436 (1996).
5. Z. Aouissat, R. Rapp, G. Chanfray, P. Schuck, J. Wambach, Nucl. Phys. A **581**, 471 (1995).
6. H.C. Chiang, E. Oset, M.J. Vicente Vacas, Nucl. Phys. A **644**, 77 (1998).
7. M.J. Vicente Vacas, E. Oset, H.C. Chiang, Acta Phys. Pol. B **29**, 3137 (1998).
8. R. Rapp *et al.*, Phys. Rev. C **59**, 1237 (1999).
9. M.J. Vicente Vacas, E. Oset, Phys. Rev. C **60**, 064621 (1999).
10. M.J. Vicente Vacas, E. Oset, arXiv:nucl-th/0002010.
11. J.G. Messchendorp *et al.*, Phys. Rev. Lett. **89**, 222302 (2002), arXiv:nucl-ex/0205009.
12. L. Roca, E. Oset, M.J. Vicente Vacas, Phys. Lett. B **541**, 77 (2002), arXiv:nucl-th/0201054.
13. M.J. Vicente Vacas, E. Oset, arXiv:nucl-th/0204055.
14. J.C. Nacher, E. Oset, M.J. Vicente Vacas, L. Roca, Nucl. Phys. A **695**, 295 (2001), arXiv:nucl-th/0012065.

Eur. Phys. J. A **18**, 483–485 (2003)
DOI 10.1140/epja/i2002-10265-7

THE EUROPEAN PHYSICAL JOURNAL A

Naturalness of nonlinear σ, ω self-couplings in relativistic mean-field models for neutron stars

E.F. Lütz[1], S.S. Rocha[1], A.R. Taurines[1], G.F. Marranghello[1], M. Dillig[2,a], and C.A.Z. Vasconcellos[1]

[1] Instituto de Física, Universidade Federal do Rio Grande do Sul, 15051 Porto Alegre, Brazil
[2] Institut für Theoretische Physik III, Universität Erlangen-Nürnberg, 91058 Erlangen, Germany

Received: 30 September 2002 /
Published online: 22 October 2003 – © Società Italiana di Fisica / Springer-Verlag 2003

Abstract. We investigate dense hadronic matter in a relativistic mean-field approach. For a generalized baryon-meson Lagrangian effective field theory, we confront expansions from naive dimensional analysis for the nonlinear self-couplings of the σ, ω fields with estimates from microscopic $q\bar{q}$ pair creation models from Quantum Chromodynamics. Upon adjusting the model parameters to ordinary nuclear matter, we discuss implications of the approach to dense hadronic matter and in particular to neutron stars.

PACS. 11.10.-z Field theory – 21.65.+f Nuclear matter – 26.60.+c Nuclear matter aspects of neutron stars

The investigation of hadronic matter is presently one of the leading topics in nuclear physics. One efficient approach to dense hadronic matter is based on Quantum Hadrodynamics (QHD) [1]: within the framework of effective meson and baryon degrees of freedom, the nuclear many-body problem is treated in a relativistic mean-field approach. This has turned out as a very economical parameterization: in the simplest approximation, keeping only the Hartree self-energy, classical σ and ω fields exhaust the overwhelming part of the effective NN interaction in the nuclear medium at ordinary nuclear matter density $\rho_0 \cong 0.15\,\mathrm{fm}^{-3}$.

Exploring hadronic matter at higher densities, the original Walecka Lagrangian [1] has to be extended significantly: besides the excitation of hyperons or the inclusion of leptons e^-, μ^- for charge neutrality, in particular nonlinear self couplings of the σ- and ω-mesons become increasingly important, as genuine many-body forces are expected to dominate with increasing matter density. A natural way to classify their contribution is to expand the Lagrangian density in terms of the characteristic scales of QCD. Here different expansion schemes are possible: fundamental scales are the renormalization invariant parameter $\Lambda_{\mathrm{QCD}} \sim 200\,\mathrm{MeV}$ or an expansion in the number of colours of quarks, N_c, reminiscent of the $SU(3)$ group structure of QCD. However, focusing on meson and baryons as effective low-energy degrees of freedom (equivalently realized in the large-N_c limit) as a result of chiral-symmetry breaking, the appropriate scales are the low-energy chiral parameters of QCD, *i.e.* the weak pion decay constant f_π and the chiral parameter Λ_χ: $f_\pi = 93\,\mathrm{MeV}$, $\Lambda_\chi \sim 1\,\mathrm{GeV}$, $\Lambda_\chi \leq 4\pi f_\pi$. The corresponding interaction Lagrangian is then given as [2]

$$L_{\mathrm{eff}} = \left(\frac{\bar{\psi}\Gamma\psi}{f_\pi^2 M}\right)^\ell \sum_{i,k=0}^{\infty} \frac{c_{i,k}}{i!k!}\left(\frac{\sigma}{f_\pi}\right)^i \left(\frac{\omega}{f_\pi}\right)^k f_\pi^2 \Lambda_\chi^2\,, \qquad (1)$$

with unknown expansion coefficients $c_{i,k}$. While there is evidence for ordinary nuclear matter that the expansion in the nonlinear mesonic couplings quickly converges —keeping only the cubic and quartic couplings of the σ-meson provides a semi-quantitative fit to nuclear matter data [3]— a controlled and useful extension to significantly higher densities ($\rho \geq 5\rho_0$) requires some assumption on a natural ordering of the expansion coefficients. Evidently, at least two schemes allow a compact summation of the full expansion series, *i.e.*

$$c_{i,k} = 1 \longrightarrow L_{\mathrm{eff}} = \left(\frac{\bar{\psi}\Gamma\psi}{f_\pi^2 M}\right)^\ell \exp\left(\frac{\sigma}{f_\pi}\frac{\omega}{f_\pi}\right), \qquad (2)$$

or, alternatively,

$$c_{i,k} = i!k! \longrightarrow L_{\mathrm{eff}} = \left(\frac{\bar{\psi}\Gamma\psi}{f_\pi^2 M}\right)^\ell \frac{1}{1+(\sigma/f_\pi)}\frac{1}{1+(\omega/f_\pi)}\,. \qquad (3)$$

A more phenomenological, but otherwise more flexible parameterization for nuclear matter, which combines the two limits derived above, taking into account σ-, ω- and

[a] e-mail: mdillig@theorie3.physik.uni-erlangen.de

ϱ-meson fields, is given as [4,5]

$$\begin{aligned}\mathcal{L} = &\sum_B \bar{\psi}_B\left[i\gamma_\mu\partial^\mu - (M_B - g^\star_{\sigma B}\sigma) - g^\star_{\omega B}\gamma_\mu\omega^\mu\right]\psi_B \\ &- \sum_B \psi_B\left[\frac{1}{2}g^\star_{\varrho B}\gamma_\mu\boldsymbol{\tau}\cdot\boldsymbol{\varrho}^\mu\right]\psi_B + \sum_\lambda \bar{\psi}_\lambda[i\gamma_\mu\partial^\mu - m_\lambda]\psi_\lambda \\ &+ \frac{1}{2}(\partial_\mu\sigma\partial^\mu\sigma - {m_\sigma}^2\sigma^2) - \frac{1}{4}\omega_{\mu\nu}\omega^{\mu\nu} + \frac{1}{2}{m_\omega}^2\omega_\mu\omega^\mu \\ &- \frac{1}{4}\boldsymbol{\varrho}_{\mu\nu}\cdot\boldsymbol{\varrho}^{\mu\nu} + \frac{1}{2}m_\varrho^2\boldsymbol{\varrho}_\mu\cdot\boldsymbol{\varrho}^\mu\,,\end{aligned}$$

where $g^\star_{\sigma B} \equiv m^\star_{\alpha B}g_\sigma$; $g^\star_{\omega B} \equiv m^\star_{\beta B}g_\omega$; $g^\star_{\varrho B} = m^\star_{\gamma B}g_\varrho$ and $m^\star_{nB} \equiv (1 + \frac{g_\sigma\sigma}{nM_B})^{-n}$; $n = \alpha, \beta, \gamma$. We assume, guided by phenomenology, α, β and γ as real and positive numbers (similar interaction terms may be associated to the vector and isovector sector of the Lagrangian density). Notice that we have assumed as a convenient starting point a universal coupling by setting $g_{(\sigma,\omega,\varrho)B} \to g_{(\sigma,\omega,\varrho)}$; the exponential and geometrical series above are recovered in the limit $n \to \infty$ and $n \to 1$, respectively. Evidently the parameterization above is identified with the ansatz in ref. [4] for the sigma-meson, upon rescaling the expansion parameters as

$$\frac{\sigma}{f_\pi} \cong \frac{g_\sigma\sigma}{\Lambda_\chi} \cong \frac{g_\sigma\sigma}{M}\,, \tag{4}$$

where M denotes the bare mass of the nucleon.

The crucial question for the relevance of the parameterizations formulated above is the naturalness of the coefficients: for example, for a rigorous summation in the exponential form, the coefficients have to be strictly equal to 1. In practice, such a constraint is never met; however, dimensional analysis and re-summation of infinite series might be still qualitatively an organizational scheme to control the expansion of —otherwise completely arbitrary— effective Lagrangians and to define their continuation to higher densities. With a full QCD calculation presently beyond any reach, one approach is to evolve the couplings of higher orders from a perturbative loop expansion based on effective intermediate mesonic degrees of freedom; alternative are (still rather phenomenological) constituent quark and effective non-perturbative $q\bar{q}$ pair creation models, which take into account the quark structure of the interacting mesons.

Focusing in this note briefly on the second route, among the various QCD-inspired models for $q\bar{q}$ production, we are currently pursuing the investigation of 3 different parameterizations: the effective one-gluon exchange ${}^3S_1$ model [6], the instanton-induced $q\bar{q}$ excitation [7] and the vacuum pair creation ${}^1P_0$ model [8]. In their structural form these models are very similar with their characteristic $q\bar{q}$ operator

$$L_{q\to q(q\bar{q})} \approx c(a,b)\lim_{\gamma\to\infty}\frac{\mathrm{d}}{\mathrm{d}\gamma}\delta(\boldsymbol{r}_i - \boldsymbol{r}_k + \boldsymbol{\sigma}_k\gamma); \tag{5}$$

where the main difference is contained in the operator $c_{a,b}$ involving the colours of the interacting quarks. In practice, the ansatz above is significantly simplified in the zero-range approximation for the radial form factor which is reduced to a δ-function in coordinate space For typical mass scales of $m_g \sim 0.3\,\mathrm{fm}^{-1}$ for non-perturbative gluon exchange or instanton models, the zero-range limit seems qualitatively well justified; finite-range corrections are readily estimated. For the mesonic structure a simple $q\bar{q}$ quark configuration is assumed:

$$\phi^{1-}_\omega(\boldsymbol{r}) = N_\omega e^{-\alpha_\omega r^2}\left[\frac{1}{2}\frac{\bar{1}}{2}\right]^{1M}_S\left[\frac{1}{2}\frac{\bar{1}}{2}\right]^\infty_F[(10)(01)]^\infty_C\,, \tag{6}$$

$$\phi^{0+}_\sigma = N_\sigma r e^{-\alpha_\sigma r^2}\left[Y_1(\hat{r})\left[\frac{1}{2}\frac{1}{2}\right]^1\right]^\infty_S\left[\frac{1}{2}\frac{1}{2}\right]^\infty_F[(10)(01)]^\infty_C\,, \tag{7}$$

for the omega and sigma as ${}^3S_1$ and ${}^3P_0$ states, respectively, with a typical size parameter $\alpha_{\sigma,\omega} = \frac{1}{2b^2}$; $b \simeq 0.6\,\mathrm{fm} \sim \sqrt{\frac{3}{8}\langle r^2_\lambda\rangle}$. Above the brackets in angular momentum, flavor and color space denote the standard coupling of the quarks to the (external) quantum numbers of the corresponding meson. The corresponding effective nonlinear coupling constants are then easily extracted in comparison with the corresponding overlap matrix elements, schematically, $g_{\sigma\lambda\lambda} = \langle[\phi_\lambda\phi_\lambda]^\infty|\sum L_{q\to q(q\bar{q})}|\phi_\sigma\rangle$ with $\lambda = \sigma, \omega$, where the sum includes pair creation from the quark and anti-quark of the σ-meson in the initial state.

Actually, only preliminary results can be reported: with current values of the strong quark-gluon or the instanton coupling constant, which enter as typical parameters into the calculation, we find in cubic order qualitatively a natural behaviour of the non-linearities within a factor 2; this trend is qualitatively confirmed to higher orders by just investigating the relative re-coupling strengths of the nonlinear vertices. However, in particular for the σ-meson, these findings have to take with care: in view of the highly unknown structure of the σ as the lightest scalar mesons with its (compared to the glue ball-scale) very low mass and its extremely strong coupling to the $\pi\pi$ channel (which suggests a dominant $(q\bar{q})(q\bar{q})$ 4-quark component), further detailed investigations are indispensable. Deferring details, we just mention an economical alternative to the problem above: the quark-meson coupling model QMC [9]. In this model the interaction of mesons as quasi-elementary objects is reduced by construction to a simple counting scheme. Different investigations of the baryon-meson and meson-meson interactions predict a natural ordering of the nonlinear couplings [10]. As a consistent generalization of the QMC to the meson-meson interactions is still an open problem, further investigations have to be awaited for.

We explore the consequences of natural expansions for dense hadronic matter. Of course, here still the problem of the continuation of the vertices to higher densities arises. In our present approach, we neglect as an exploratory step the density dependence both in the mean-field potential and the effective baryon masses

$$\begin{aligned}U_{\text{Hartree}} &\cong -\left(\frac{g^2_\sigma}{m^2_\sigma} - \frac{g^2_\omega}{m^2_\omega}\right)\rho(r); \\ M^* &= M - g_\sigma\sigma \cong M - \frac{g^2_\sigma}{m^2_\sigma}\rho(r).\end{aligned} \tag{8}$$

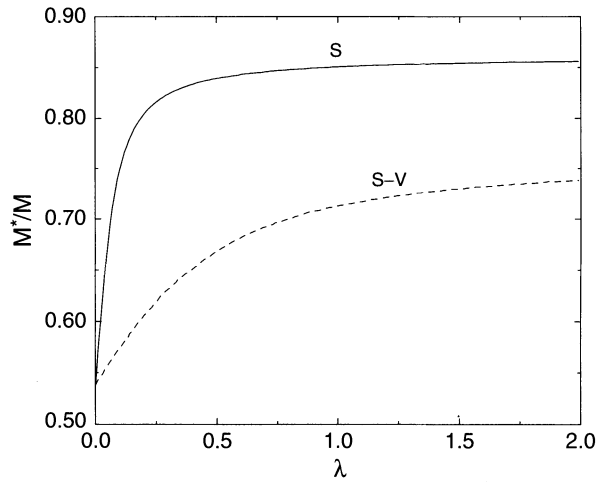

Fig. 1. Ratio M^*/M as a function of λ for cases S (variations of λ and $\alpha = \beta = 0$) (full line) and S-V ($\lambda = \alpha = \beta = 0$) (dashed line).

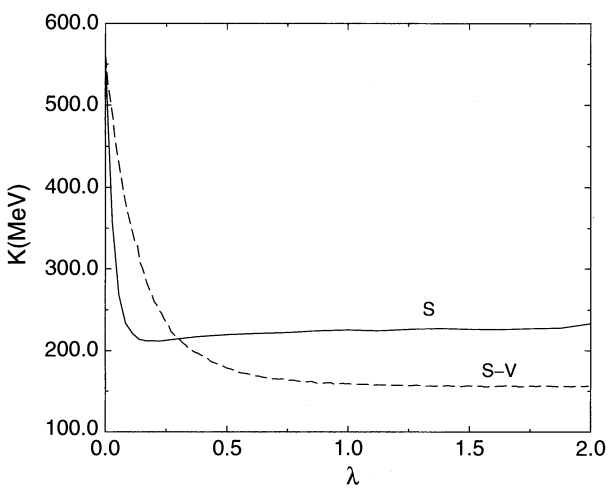

Fig. 2. Compression modulus of nuclear matter K as a function of λ for cases S (variations of λ and $\alpha = \beta = 0$) (full line) and S-V ($\lambda = \alpha = \beta = 0$) (dashed line).

Then applying the model to standard nuclear matter up to neutron stars we solve a system of transcendental equations taking into account chemical equilibrium, baryon number and electrical charge conservation, which determines the equation of state (EOS) for the system considered. The Lagrangian density of our approach includes the eight octet baryons coupled to three mesons (σ, ω, ϱ), and two free lepton species ($\ell = e^-, \mu^-$), with he scalar, vector and iso-vector coupling constants determined to reproduce bulk nuclear matter properties (see for example [4]). Typical results of our approach on the summation of the nonlinear couplings in eq. (5), are presented in figs. 1-3 for the effective nucleon mass in the medium, the compressibility and the

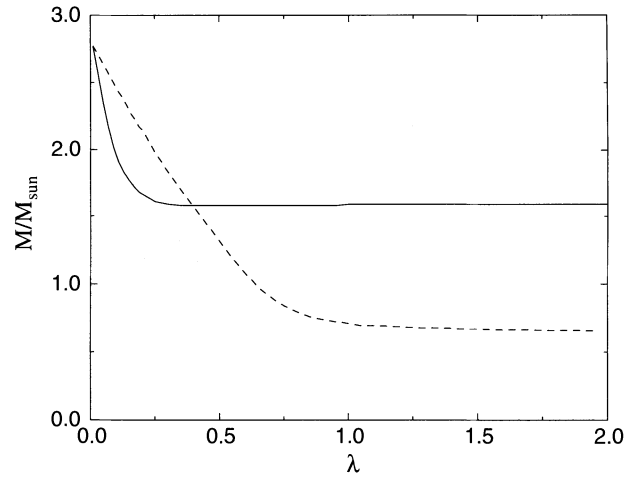

Fig. 3. Maximum neutron star mass as a function of the λ parameter (full line: S case; dashed line: S-V case).

maximum mass of a neutron star, showing a substantial sensitivity. In particular, our finding of maximum neutron star masses up to $1.8M_\odot$ in the S case seems to support recent observations of masses well above the typical masses of $1.4M_\odot$ (see references in [4,5]).

In summarizing our brief comment, we feel that the implementation of dimensional analysis in effective field theories is a promising strategy. Further detailed and extensive model calculations are however indispensable to establish a natural continuation of nonlinear expansions to hadronic densities as typical for new forms of nuclear matter.

This work was partly supported by the Forschungszentrum FZ Jüelich, Contract 41445386 (COSY-062) and CNPq.

References

1. B.D. Serot, J.D. Walecka, Adv. Nucl. Phys. **16**, 327 (1986); Int. J. Mod. Phys. E **6**, 515 (1997).
2. A. Manohar, H. Georgi, Nucl. Phys. B **234**, 189 (1984).
3. R.J. Furnstahl, B.D. Serot, H.-B. Tang, Nucl. Phys. A **598**, 539 (1996).
4. A.R. Taurines, C.A.Z. Vasconcellos, M. Malheiro, M. Chiapparini, Phys. Rev. C **63**, 065801 (2001).
5. G.F. Marranghello, C.A.Z. Vasconcellos, J.A. de Freitas Pacheco, M. Dillig, Int. J. Mod. Phys. E **11**, 83 (2002).
6. A. Szczepaniak, E.S. Swanson, Phys. Rev. D **65**, 025012 (2002).
7. O. Jahn, F. Lenz, J.W. Negele, M. Thies, Nucl. Phys. Proc. Suppl. **83**, 524 (2000).
8. B. Desplanques, A. Nicolet, L. Theussl, nucl-th/0204026.
9. P.A.M. Guichon, Nucl. Phys. A **680**, 229 (2000).
10. K. Saito, K. Tsushima, A.W. Thomas, Phys. Lett. B **406** 287 (1997).

Eur. Phys. J. A **18**, 487–490 (2003)
DOI 10.1140/epja/i2002-10266-6

THE EUROPEAN PHYSICAL JOURNAL A

Some recent results in baryon chiral perturbation theory

Ulf-G. Meißner[a]

IKP, FZ Jülich, D-52425 Jülich, Germany and ITP, Karl-Franzens-Universität Graz, A-8010 Graz, Austria

Received: 30 September 2002 /
Published online: 22 October 2003 – © Società Italiana di Fisica / Springer-Verlag 2003

Abstract. I present and discuss recent results on elastic pion-nucleon scattering and near-threshold neutral-pion electroproduction off deuterium obtained in the framework of chiral perturbation theory.

PACS. 13.75.Gx Pion-baryon interactions – 25.30.Rw Electroproduction reactions – 12.39.Fe Chiral Lagrangians

1 Introduction

Chiral perturbation theory (CHPT) is a well established and systematic tool to analyze in a model-independent manner the reactions between pions, nucleons and photons (or other external sources), based on a systematic power counting in terms of small external momenta and quark (pion) masses. In this paper I want to present new results on isospin violation in elastic pion-nucleon scattering and neutral pion electroproduction off deuterium. The latter study was partly motivated by the dramatic difference between the prediction for the S-wave cross-section in [1] and the recent MAMI experiment [2]. As it turns out, this puzzle has been resolved as explained below.

2 Isospin violation in pion-nucleon scattering

We first want to apply CHPT to one of the most studied processes, elastic pion-nucleon scattering. More precisely, we will consider systematically effects of isospin violation (IV) due to the light quark mass difference, $m_u \neq m_d$, and electromagnetism, $q_u \neq q_d$. Before discussing in some detail isospin violation in πN scattering, a few general remarks are in order. In QCD plus QED, we have *two* sources of isospin violation. In QCD, the light-quark mass difference leads to isovector terms, as reflected in the quark mass term (for two flavors)

$$\begin{aligned}\mathcal{H}_{\rm QCD}^{\rm mass} &= m_u \bar{u}u + m_d \bar{d}d \\ &= \frac{1}{2}(m_u+m_d)(\bar{u}u+\bar{d}d) + \frac{1}{2}(m_u-m_d)(\bar{u}u-\bar{d}d)\,,\end{aligned}$$

where the last term is clearly of isovector nature leading to strong IV. Naively, one could expect huge IV effects since $|(m_u - m_d)/(m_u + m_d)| \simeq 1/3$. However, the scale one should compare to is the hadronic one, so that one indeed anticipates very small effects, $(m_u - m_d)/\Lambda_\chi < 1\%$. Only in processes involving neutral pions one can expect much bigger effects [3]. The other source of IV is electromagnetism (em). Hadron mass shifts due to virtual photon exchange between quarks can be estimated as $\delta m \simeq \alpha_{\rm em} \cdot \Lambda_{\rm QCD} \cdot \mathcal{O}(1) \sim$ few MeV. In fact, typical em mass splittings in meson and baryon multiplets are of this order. Therefore, these two types of IV have to be considered *consistently*. This can be done by including virtual photons in the chiral effective Lagrangian of pions and nucleons, treating the electric charge e as another small parameter. This was done for the case of pion-nucleon scattering in the framework of heavy-baryon chiral perturbation theory to third order in ref. [4], leading to a new phase shift analysis (valid for pion lab momenta below 100 MeV as deduced from the isospin symmetric fourth-order calculation [5]). The resulting S- and P-wave phases for the three measured physical channels $\pi^\pm p \to \pi^\pm p$ and $\pi^- p \to \pi^0 n$ (charge exchange) are shown in fig. 1. CHPT does not leave any doubt about the correct definition of the *hadronic* masses of pions and nucleons and allows to extract the strong part of the scattering amplitude in a unique way. At this order, there is only one strong IV-violating operator whose strength can be fixed from the np mass difference. The em corrections are a bit more subtle. First, there are one- and two-photon exchanges, the latter amount to a few percent correction for the kinematics pertinent to the existing data. More precisely, for pion lab momenta $\boldsymbol{q}_\pi$, two-photon exchange is suppressed compared to one-photon exchange by a factor $e^2 M_\pi/(32|\boldsymbol{q}_\pi|) \leq 0.04$ for $|\boldsymbol{q}_\pi| \geq 10\,$MeV. Then there are soft photon contributions in terms of loops and external leg radiation. Only the sum of these is IR finite and their contribution depends of course on the detector resolution. We have used $\Delta E_\gamma = 10\,$MeV. In addition, there are hard photon contributions encoded in contact

[a] e-mail: u.meissner@fz-juelich.de

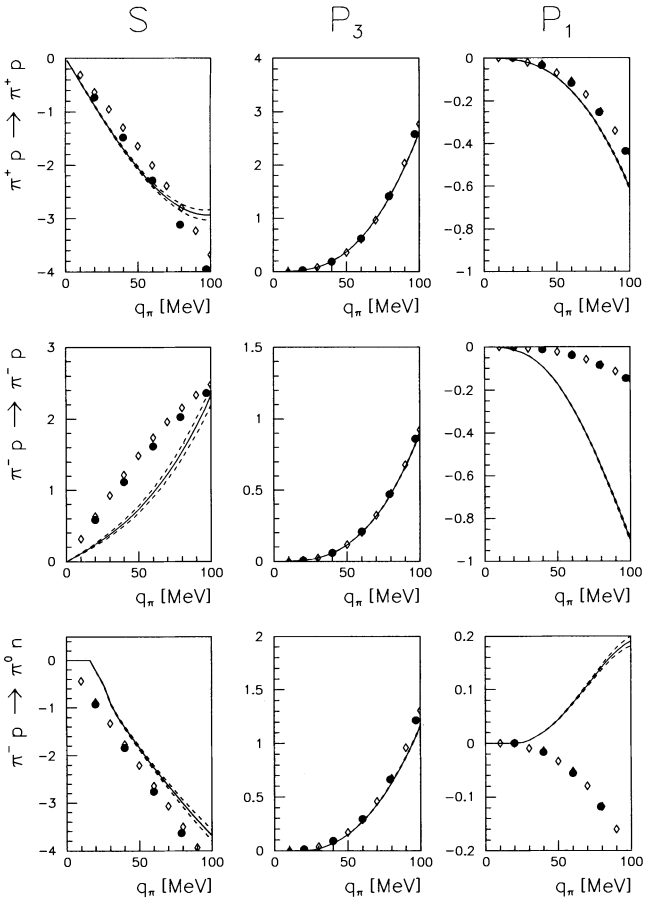

Fig. 1. Strong pion-nucleon phase shifts as a function of the pion laboratory momentum q_π for the three measured channels. Shown are the S-wave and the $j = 1/2$, $3/2$ P-waves. The solid line corresponds to the CHPT solution [4], the dashed one to the one-sigma uncertainty range. Also shown are the KA85 [6] (full dots) and the SP98 [8] (open diamonds) phases.

terms with undetermined low-energy constants (LECs). After determining the unknown LECs by a fit to experimental data, one can switch off all electromagnetic interactions and describe QCD with unequal up- and down-quark masses and $e^2 = 0$. The so-determined strong phase shifts (mostly) agree with those of previous works [6–9] in the P-waves, but one finds a sizeably different behavior in the S-waves (in particular for $\pi^- p$ elastic scattering), compare fig. 1. This difference can be traced back to the inclusion (in CHPT) or omission (in other approaches) of *non-linear* photon-pion-nucleon couplings, *i.e.* vertices of the type $\bar{N}N\pi\pi\gamma$. Such vertices are a consequence of chiral symmetry and thus must be included. One should investigate how such non-linear couplings can be included in the often used dispersion theoretical approaches to em corrections [10]. Given the hadronic amplitudes constructed in [4], one can address the question of isospin violation by studying the usual triangle relation involving elastic $\pi^\pm p$ scattering and the charge exchange reaction (for a general discussion of such triangle ratios, see [11] and references therein). An important advantage of the CHPT calculation lies in the fact that one can easily separate

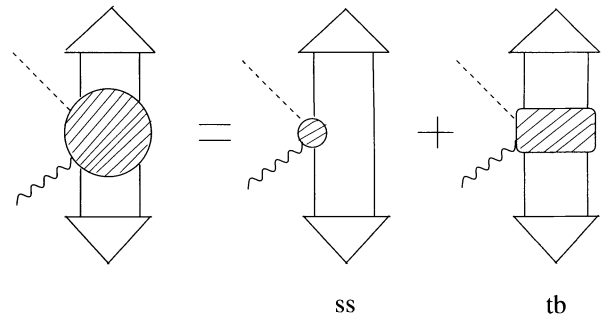

Fig. 2. Decomposition of the interaction kernel into the single-scattering (ss) and three-body (tb) contribution.

dynamical from static isospin breaking, the latter are due to hadron mass differences. Dynamical isospin breaking only occurs in the S-wave and is very small, $\sim 0.75\%$, in agreement with the estimate given above. Static effects do not increase the size of isospin violation in the S-wave significantly; by no means can one account for the reported 7 % isospin breaking [12,13]. These are presumably due to a mismatch between the models for the strong and the em interactions used in these works. Note also that one finds large error bars on the parameter values in the CHPT analysis. In order to improve this situation, one would like to fit to more experimental data. However, a third-order CHPT calculation allows to describe scattering data for pion laboratory momenta not much higher than 100 MeV, a region where the data situation is not yet as good as one would hope. A fourth-order calculation would certainly allow to fit to data higher in energy, but, on the other hand, would also introduce many more unknown coupling constants. Since isospin breaking effects are expected to be most prominent in the low-energy region, one might question the usefulness of extending the analysis to full one-loop (fourth) order. Additional data for pion-nucleon scattering at very low energies would be very helpful in this respect. Also a combined fit to several reactions involving nucleons, pions, and photons, *e.g.* pion electro- and photoproduction, as well as $\pi N \to \pi\pi N$, would help in pinning down the fundamental low-energy constants more precisely.

3 π^0 electroproduction off deuterium

In [14], we have studied neutral-pion electroproduction off deuterium in the framework of CHPT at and above threshold. For doing that, we have developed a general multipole decomposition for neutral-pion production off spin-1 particles that is particularly suited for the threshold region and formulated in close analogy to the standard CGLN amplitudes for pion production off nucleons (spin-1/2 particles). A similar work was previously published in [15]. The interaction kernel and the wave functions are based consistently on chiral effective field theory. The kernel decomposes into a single scattering and a three-body contribution, cf. fig. 2. We have chirally expanded the various contributions working to first non-trivial loop

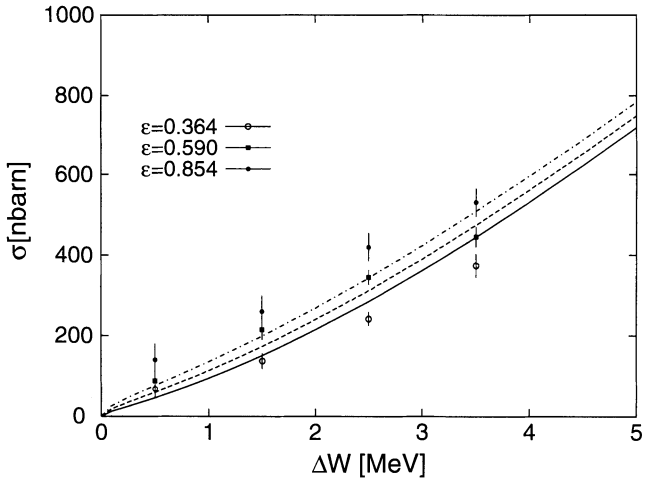

Fig. 3. Two-parameter fit of the near-threshold total cross-section in neutral-pion electroproduction off deuterium. The data are from MAMI [2].

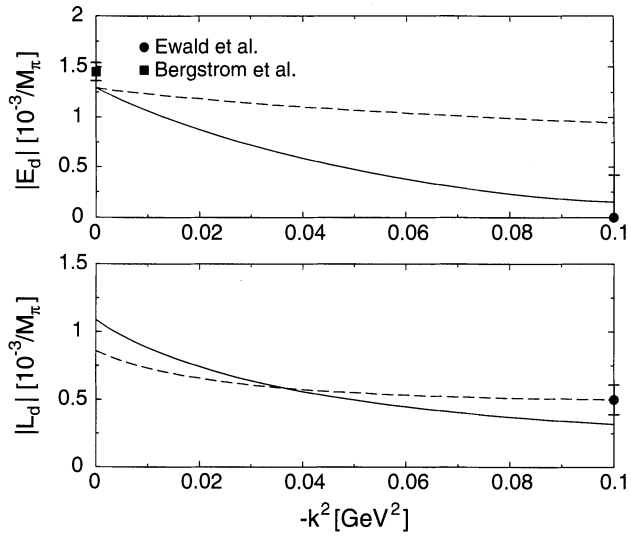

Fig. 4. Threshold multipoles E_d and L_d as a function of the photon virtuality in comparison to the photoproduction data from SAL [17] and the electroproduction data from MAMI [2].

order $\mathcal{O}(q^3)$, with the exception of the S-waves for the single-scattering contribution. These have to be included to fourth order with one additional fifth-order term [16]. All parameters for pion production off the proton and the ones appearing in the three-body terms are fixed. The longitudinal neutron S-wave amplitude contains effectively two parameters, which we have determined by two different procedures. In the fits of type 1 we have fitted the fifth-order parameter to the threshold multipole L_d from ref. [2] (and assuming resonance saturation to pin down the other LEC). The second procedure is based on a two-parameter fit to the total cross-section data from ref. [2], see fig. 3. All results are completely insensitive to the wave functions used, showing that this reaction is sensitive to the long-range pion exchange firmly rooted in the chiral symmetry of QCD. The predicted differential cross-sections are satisfactorily described for both fit procedures, although some systematic discrepancies for the higher values of the excess energy ΔW remain. In particular, for fit 1 the total cross-section rises too steeply with pion excess energy. The calculated S- and P-wave multipoles exhibit a more complex pion energy and photon virtuality dependence as assumed in the fits of ref. [2]. Within one standard deviation, the chiral predictions for the threshold multipoles $|E_d|$ and $|L_d|$ are consistent with the data at $k^2 = 0$ [17] and $k^2 = -0.1\,\mathrm{GeV}^2$ [2], cf. fig. 4. In [1], we had calculated these threshold multipoles to third order and performed a shift to the fourth-order predictions for the single-scattering contributions. This led to a too large longitudinal multipole L_d and thus a much too large S-wave cross-section. The properly calculated S-wave cross-section is consistent with the MAMI data, see table 3 in [14]. Clearly, the calculation presented here needs to be improved, in particular, the fourth order corrections to the P-waves and the three-body terms have to be included (note that similar work for the P-waves in neutral-pion photoproduction off protons has only appeared recently [18]). However, we have demonstrated that chiral perturbation theory can be used successfully to analyze pion electroproduction data off the deuteron which gives access to the elementary neutron amplitude. It would be very interesting to also have data at lower photon virtuality, which might also help to resolve the mystery surrounding the proton data at $k^2 = -0.05\,\mathrm{GeV}^2$.

I am grateful to Véronique Bernard, Nadia Fettes and Hermann Krebs for very pleasant collaborations on the topics reported here.

References

1. V. Bernard, H. Krebs, Ulf-G. Meißner, Phys. Rev. C **61**, 058201 (2000).
2. I. Ewald *et al.*, Phys. Lett. B **499**, 238 (2001).
3. S. Weinberg, Trans. N.Y. Acad. Sci. **38**, 185 (1977); Ulf-G. Meißner, S. Steininger, Phys. Lett. B **419**, 403 (1998); N. Fettes, Ulf-G. Meißner, S. Steininger, Phys. Lett. B **451**, 233 (1999).
4. N. Fettes, Ulf-G. Meißner, Nucl. Phys. A **693**, 693 (2001).
5. N. Fettes, Ulf-G. Meißner, Nucl. Phys. A **676**, 311 (2000).
6. R. Koch, Nucl. Phys. A **448**, 707 (1986).
7. E. Matsinos, arXiv:hep-ph/9807395.
8. SAID on-line program, R.A. Arndt *et al.*, see website `http://gwdac.phys.gwu.edu/`.
9. A. Gashi *et al.*, hep-ph/0009081.
10. J. Hamilton, B. Tromberg, I. Øverbrø, Nucl. Phys. B **60**, 443 (1973); B. Tromberg, J. Hamilton, Nucl. Phys. B **76**, 483 (1974); B. Tromberg, S. Waldenstrøm, I. Øverbrø, Phys. Rev. D **15**, 725 (1977).
11. N. Fettes, Ulf-G. Meißner, Phys. Rev. C **63**, 045201 (2001).
12. W.R. Gibbs, Li Ai, W.B. Kaufmann, Phys. Rev. Lett. **74**, 3740 (1995).

13. E. Matsinos, Phys. Rev. C **56**, 3014 (1997).
14. V. Bernard, H. Krebs, Ulf-G. Meißner, arXiv:nucl-th/0702072.
15. H. Arenhövel, Few-Body Syst. **25**, 127 (1998); **27**, 141 (1999).
16. V. Bernard, N. Kaiser, Ulf-G. Meißner, Nucl. Phys. A **607**, 379 (1996).
17. J.C. Bergstrom *et al.*, Phys. Rev. C **57**, 3203 (1998).
18. V. Bernard, N. Kaiser, Ulf-G. Meißner, Eur. Phys. J. A **11**, 209 (2001).

Eur. Phys. J. A **18**, 491–494 (2003)
DOI 10.1140/epja/i2002-10267-5

THE EUROPEAN PHYSICAL JOURNAL A

Including virtual photons in strong interactions

A. Rusetsky[a]

Institute for Theoretical Physics, University of Bern, Sidlerstrasse 5, 3012 Bern, Switzerland and High Energy Physics Institute, Tbilisi State University, University St. 9, 380086 Tbilisi, Georgia

Received: 30 September 2002 /
Published online: 22 October 2003 – © Società Italiana di Fisica / Springer-Verlag 2003

Abstract. In the perturbative field-theoretical models we investigate the inclusion of the electromagnetic interactions into the purely strong theory that describes hadronic processes. In particular, we study the convention for splitting electromagnetic and strong interactions and the ambiguity of such a splitting. The issue of the interpretation of the parameters of the low-energy effective field theory in the presence of electromagnetic interactions is addressed, as well as the scale and gauge dependence of the effective theory couplings. We hope, that the results of these studies are relevant for the electromagnetic sector of ChPT.

PACS. 13.40.Ks Electromagnetic corrections to strong- and weak-interaction processes – 13.40.Dk Electromagnetic mass differences – 11.30.Rd Chiral symmetries – 11.10.Hi Renormalization group evolution of parameters

1 Introduction

The systematic approach to take into account the electromagnetic corrections in the low-energy processes involving hadrons is based on the Chiral Perturbation Theory (ChPT) with virtual photons [1], which is the low-energy effective theory of the Standard Model in the hadron sector. Despite being widely used in the applications, the procedure of the construction of the effective chiral Lagrangian with virtual photons from QCD is not free from conceptual difficulties. In particular, we mention the following points:

i) The effective Lagrangian with virtual photons operates with quantities like the quark masses m_q, the parameter B which is related with the quark condensate, the pion decay constant in the chiral limit F, etc. It is usually not specified, to which underlying theory — QCD + photons, or pure QCD— do these quantities refer. Obviously, if one interprets m_q to be the running quark masses in the full theory (including virtual photons), then the quark mass ratio m_u/m_d in ChPT Lagrangian turns out to be QCD-scale dependent. One encounters similar problem in relating B to the quark condensate, since $\langle 0|\bar{u}u|0\rangle$ and $\langle 0|\bar{d}d|0\rangle$ run differently for $e \neq 0$.
ii) According to the commonly used terminology, in the effective theory the combined contribution of the explicit photon loops and the electromagnetic effective couplings is called "electromagnetic corrections", and the rest is referred to as "strong piece". This implies, that exactly the latter survives when electromagnetic interactions are switched off. The problem is, however, how to rigorously define the theory with electromagnetic interactions switched off, even for the underlying QCD. To be precise, note that the initial theory with photons had four parameters: strong-coupling constant g, fine-structure constant α, and the quark masses m_u and m_d. The theory without photons has only three parameters: the strong-coupling constant $\bar{g}$ which is obtained from g in the limit $\alpha \to 0$, and the quark masses $\bar{m}_u$, $\bar{m}_d$ to which m_u and m_d converge in the same limit. The question is, how to determine $\bar{g}$, $\bar{m}_u$ and $\bar{m}_d$ which define the theory in the limit $\alpha \to 0$? And, once this is done, how the above definition translates into the commonly used splitting of the low-energy effective theory?
iii) Although it has been pointed out [2,3], that some of the electromagnetic effective couplings do indeed contain scale- and gauge-dependence which is determined by the underlying QCD, a systematic study of this phenomenon is still lacking.

Although some of the issues mentioned here, have been already addressed and/or mentioned in the literature (see, *e.g.*, [2,3]), a focused discussion of the conceptual problems in ChPT with virtual photons, to the best of our knowledge, does not exist so far. The aim of our investigations, which are very briefly surveyed in this work, is to set up notions for creation of such a coherent framework. We would like to stress in addition, that such investigations are an important ingredient in carrying out

[a] e-mail: rusetsky@itp.unibe.ch

the consistent calculation of isospin-breaking corrections in the context of the hadronic atom problem [4]. In order to demonstrate the general procedure, we do not consider QCD here —rather, we restrict ourselves to the simple perturbative models, where one may include electromagnetic interactions in a crystal clear manner. We believe, that the lessons one learns from these models, provide the necessary clue in a much more complicated case of QCD. A detailed discussion of the issues raised in this work, is given in the forthcoming publication [5].

2 Convention for the splitting

In this section, the following question is addressed: suppose, that one has the field theory which describes both electromagnetic and non-electromagnetic (referred hereafter as to the "strong") interactions. How does one systematically split strong and electromagnetic contributions in the quantities which are calculated within this theory? In order to answer this question, we find it useful to consider a simple perturbative model —the Yukawa model. The splitting convention which is explained in this model, is general and can be applied in the context of any other field-theoretical model.

The Yukawa model considered in this work, describes the doublet of "colored" fermions $\bar{\Psi} = (\bar{u}^i, \bar{d}^i)$, where the "color" index $i = 1, 2$. The fermions interact with the triplet of boson fields through the usual Yukawa coupling $\mathcal{L}_{\rm str} = g\bar{\Psi}\boldsymbol{\tau}\boldsymbol{\phi}\Psi$, which is characterized by a "strong" constant g. Further, the fermions whose charge matrix is given by $eQ = e\,\mathrm{diag}(Q_u, Q_d)$, interact with the photon field in a standard manner, whereas the bosons described by the field $\boldsymbol{\phi}$, are neutral. For the renormalization, $\overline{\rm MS}$ scheme is used.

We demonstrate the idea of the splitting on the example of the physical mass of the fermion fields, given by the position of the pole in the propagator. Below, we restrict ourselves to the one-loop order. Denoting the masses by M_q where $q = u, d$, we find

$$M_q = m_q\left[1 + \frac{3}{16\pi^2}(3g_r^2 - 2e_r^2Q_q^2)\ln\frac{m_q}{\mu} + A_1 g_r^2 + \right.$$
$$\left. + A_2 Q_q^2 e_r^2\right] + O(g_r^4, e_r^2 g_r^2, e_r^4)\,, \qquad (1)$$

where g_r, e_r denote the renormalized couplings, μ is the scale of the dimensional regularization, m_q stands for the running fermion mass. Further, A_1 is a known function of the boson-fermion mass ratio which is independent of the scale μ at this order (the explicit expression for this quantity is not needed), and $A_2 = (16\pi^2)^{-1}$.

The physical masses become scale independent, provided that the masses m_q run properly with the scale,

$$\mu\frac{\mathrm{d}m_q}{\mathrm{d}\mu} = \frac{3}{16\pi^2}(3g_r^2 - 2e_r^2Q_q^2)m_q + O(g_r^4, e_r^2g_r^2, e_r^4)\,. \qquad (2)$$

The couplings g_r, e_r are scale independent at this order in the perturbative expansion. Once the running mass m_q is known at a some scale, the physical mass M_q is fixed in terms of the coupling constants g_r, e_r and of the running boson and fermion masses at this order in the perturbative expansion.

We now discuss the splitting of the physical masses into a strong and an electromagnetic part. This splitting should divide the mass into a piece that one would calculate in a theory with no electromagnetic interactions, and a part proportional to e_r^2: $M_q = \bar{M}_q + e_r^2 M_q^1 + O(e_r^4)$. Here and below, barred quantities refer to the theory at $e_r = 0$. The first term on the right-hand side is

$$\bar{M}_q = \bar{m}_q\left[1 + \frac{9\bar{g}_r^2}{16\pi^2}\ln\frac{\bar{m}_q}{\mu} + A_1\bar{g}_r^2\right] + O(\bar{g}_r^4)\,. \qquad (3)$$

This part is scale independent by itself, provided that the mass $\bar{m}_q$ runs according to renormalization group equation (2) for $e_r = 0$. On the other hand, $\bar{g}_r$ is scale independent in this approximation. We see, that one has to fix a boundary condition in order to determine unambiguously $\bar{M}_q$. As a natural condition, we choose the running mass $\bar{m}_q$ to coincide with the running mass m_q in the full theory at a some scale: $m_q(\mu) = \bar{m}_q(\mu;\mu_1)$ at $\mu = \mu_1$ (here, we have explicitly indicated the μ_1-dependence of the barred quantities). With the use of the above matching condition, we express $m_q(\mu)$ through $\bar{m}_q(\mu;\mu_1)$, and insert the result into the expression for the mass M_q. Identifying g_r with $\bar{g}_r$ at this order, we find that

$$\bar{M}_q = \bar{m}_q(\mu;\mu_1)\left[1 + \frac{9\bar{g}_r^2}{16\pi^2}\ln\frac{\bar{m}_q}{\mu} + \bar{g}_r^2 A_1\right] + O(\bar{g}_r^4)\,,$$
$$M_q^1 = -\bar{m}_q(\mu;\mu_1)\left[\frac{6}{16\pi^2}\ln\frac{\bar{m}_q}{\mu_1} - A_2\right]Q_q^2 + O(\bar{g}_r^2)\,. \qquad (4)$$

This splitting has the desired properties: Each term on the right-hand side is scale-independent. However, as is explicitly seen in the contribution proportional to e_r^2, the splitting does depend on the *matching scale* μ_1. Indeed, one has

$$\mu_1\frac{\mathrm{d}\bar{M}_q}{\mathrm{d}\mu_1} = -\mu_1\frac{\mathrm{d}[e_r^2M_q^1]}{\mathrm{d}\mu_1} = -\frac{6e_r^2Q_q^2}{16\pi^2}\bar{M}_q\,. \qquad (5)$$

In other words, both terms in the splitting depend on the scale μ_1. This scale dependence is of order e_r^2 in the approximation considered. The sum M_q is of course independent of the matching scale.

A similar splitting may be considered for the running masses themselves. Indeed, expressing $m_q(\mu)$ through the running mass in the purely strong theory $\bar{m}_q(\mu;\mu_1)$ gives

$$m_q(\mu) = \bar{m}_q(\mu;\mu_1)\left[1 - \frac{6e_r^2Q_q^2}{16\pi^2}\ln\frac{\mu}{\mu_1}\right]. \qquad (6)$$

This result is the analogue of the relation (4) for the physical masses. It shows that the splitting of the running masses into a part that runs with the strong interaction alone, and a piece proportional to e_r^2, depends on the matching scale.

The dependence of the splitting on the scale μ_1 originates in the different running of the masses in the full

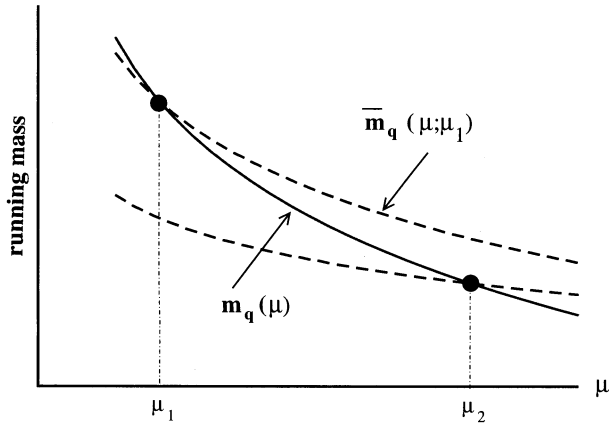

Fig. 1. The matching condition. The solid line represents the running of the mass m_q in the full theory according to (2), whereas the dashed lines display the running of $\bar{m}_q$.

theory and in the approximation when $e_r = 0$. This is illustrated in fig. 1. The solid line refers to the running of the mass m_q in the full theory, whereas the dashed lines represent the running of $\bar{m}_q$. Because, for a fixed value of the scale μ, the running mass $\bar{m}_q$ depends on the matching scale chosen, the mass $\bar{M}_q$ does so as well.

One may wonder whether there is a way to split the pole mass in a unique manner. The reason why this is not the case is the following. In the Yukawa model considered here, the pole mass is proportional to m_q, which itself depends on the scale μ. In order to compare this mass with the corresponding quantity at $e_r = 0$, one has to compare two quantities that run differently, $\bar{m}_q$ and m_q. This running is itself a one-loop effect. There is therefore no possibility to avoid the ambiguity.

Finally, we mention that the splitting of the parameters of the theory (masses and couplings) along the lines demonstrated above can be performed from a knowledge of the relevant beta-functions of the masses and of the coupling constants to any order in the perturbative expansion [5].

3 Splitting in the effective theory

On the example of the linear σ model (LσM) with electromagnetic interactions we illustrate, how the prescription for splitting of electromagnetic and strong interactions does translate to the language of the low-energy effective theory. The calculations are done at one loop. In the limit of the large σ mass, the model is equivalent to ChPT with the particular values of the couplings, expressed explicitly through the parameters of the initial model. This allows one to study the consequence of the splitting, performed in the LσM, for the couplings of the effective theory. The dependence of these couplings on the renormalization scale in the LσM, as well as on the gauge parameter, can be also studied. Below, we briefly list our conclusions obtained from these investigations. Detailed discussion is given in ref. [5].

i) The splitting which is carried out in the underlying theory, is directly translated to the level of the low-energy effective Lagrangian of this theory. The μ_1-ambiguity of the parameters (masses and coupling constants) of the underlying *purely strong* theory which is matched to the theory with virtual photons at a scale $\mu = \mu_1$, is lumped in the couplings of the effective Lagrangian. These couplings have to be expressed in terms of the parameters of the purely strong theory and, possibly, some additional parameters that have to be introduced when the electromagnetic interactions are turned on. The advantage of doing so is, that the different parts of the Lagrangian then exactly describe the low-energy limit of the purely strong theory, and what is called the electromagnetic corrections. The price for this is just the above-mentioned μ_1-dependence of the effective couplings.

ii) When the electromagnetic interactions are turned on, some quantities like, *e.g.* the matrix elements of the vector current, start to be scale- and gauge-dependent. At the level of the effective theory, this dependence is systematically transformed into the scale- and gauge-dependence of the couplings of the Lagrangian.

iii) Most of the above conclusions can be straightforwardly applied to QCD without any change. The splitting of the quark masses, condensates, etc proceeds along lines similar to those described in sect. 2. Further, the parameters of the low-energy effective Lagrangian of QCD in the strong sector refer to the pure QCD rather then to QCD + photons: *e.g.* the quark masses are the masses in pure QCD, etc. The price to pay is, that the couplings in ChPT depend on the matching scale μ_1. The (μ_1-dependent) results of calculations for any physical quantity, based only on the strong part of the effective Lagrangian, exactly reproduce the results that would be obtained for the same quantity in pure QCD matched to QCD + photons at $\mu = \mu_1$.

iv) It is important to note, that the μ_1-dependence puts natural limitations on the accuracy at which the couplings of the effective Lagrangian can be determined from the physical data which, of course, contains no μ_1 dependence. In principle, such a dependence should be observed if the couplings are theoretically derived from the underlying QCD, *e.g.*, via the lattice simulations.

The present work is based on the results obtained in collaboration with J. Gasser, I. Mgeladze and I. Scimemi [5]. We have profited from unpublished notes by H. Leutwyler, whom we thank in addition for informative discussions on the subject. We are thankful to G. Ecker, H. Neufeld, B. Moussallam and U. Wiese for interesting discussions. This work was supported in part by the Swiss National Science Foundation, and by TMR, BBW-Contract No. 97.0131 and EC-Contract No. ERBFMRX-CT980169 (EURODAΦNE), and by SCOPES Project No. 7UZPJ65677.

References

1. R. Urech, Nucl. Phys. B **433**, 234 (1995).
2. J. Bijnens, J. Prades, Nucl. Phys. B **490**, 239 (1997).
3. B. Moussallam, Nucl. Phys. B **504**, 381 (1997).
4. A. Gall, J. Gasser, V.E. Lyubovitskij, A. Rusetsky, Phys. Lett. B **462**, 335 (1999); Phys. Rev. D **64**, 016008 (2001); J. Gasser, V.E. Lyubovitskij, A. Rusetsky, Phys. Lett. B **471**, 244 (1999); V.E. Lyubovitskij, A. Rusetsky, Phys. Lett. B **494**, 9 (2000); J. Gasser *et al.*, Eur. Phys. J. C **26**, 13 (2002), arXiv:hep-ph/0206068.
5. J. Gasser, I. Mgeladze, A. Rusetsky, I. Scimemi, in preparation.

Eur. Phys. J. A **18**, 495–497 (2003)
DOI 10.1140/epja/i2002-10268-4

THE EUROPEAN PHYSICAL JOURNAL A

Electromagnetic corrections in the anomaly sector and the π^0 lifetime

B. Moussallam[a]

Groupe de Physique Théorique, IPN, Université Paris-Sud, F-91406 Orsay Cédex, France

Received: 30 September 2002 /
Published online: 22 October 2003 – © Società Italiana di Fisica / Springer-Verlag 2003

Abstract. The framework for computing radiative corrections in ChPT in the anomaly sector is set up. Application to the lifetime of the π^0 and the possibility to extract information on $m_d - m_u$ from precision data is discussed.

PACS. 11.30.Rd Chiral symmetries – 12.15.Ff Quark and lepton masses and mixing – 12.39.Fe Chiral Lagrangians

1 Introduction

In order to determine the masses of the light quarks from experimental data, it is necessary to consider isospin-breaking phenomena which are induced in part by the quark mass difference $m_u - m_d$. The second source of isospin violation, radiative effects, must then also be taken into account. In this paper I will present the formalism which allows one to take into account radiative corrections in ChPT in the anomaly sector, extending the work of Urech [1] who has shown how to do so in the ordinary sector (there as still some open theoretical questions in this field, see the contribution by A. Rusetsky [2] to this conference). As an application I will discuss the lifetime of the neutral pion in ChPT at next-to-leading order. In this problem, the corrections to the current algebra result are dominated by isospin breaking, and the precision of the experimental measurement now underway at CEBAF (Primex experiment [3]) allows one to probe these corrections. I will show that in this problem, it is possible to quantitatively estimate the contributions of electromagnetic origin. This presentation summarizes the work done in collaboration with B. Ananthanarayan which is described in more detail in ref. [4]

2 Formalism

Introducing the photon as a dynamical field in the chiral expansion induces new terms in the Lagrangian which parametrize the high-energy part of the photon loops. One must then solve the problem of classifying a minimal set of independent terms at each chiral order and the related problem of determining the divergence structure of the associated chiral coupling constants. In ref. [4] we have considered this problem for the case of the $SU(2)$ chiral expansion. Because of the limited space I will only mention the results here. At leading order (which is p^4) one has the WZW [5,6] action for which Kaiser [7] has recently derived a particularly simple form,

$$\mathcal{L}^W_{p^4} = \kappa\, \epsilon^{\mu\nu\alpha\beta}\Big(\langle U^\dagger r_\mu U l_\nu - r_\mu l_\nu + i\Sigma_\mu(U^\dagger r_\nu U + l_\nu)\rangle\langle v_{\alpha\beta}\rangle + \frac{2}{3}\langle \Sigma_\mu \Sigma_\nu \Sigma_\alpha\rangle\langle v_\beta\rangle\Big) \tag{1}$$

with $\kappa = -N_c/32\pi^2$. We will consider terms of order e^2p^4: according to the non-renormalization theorem [8] they must be non-anomalous and therefore may be constructed from standard chiral building blocks (see, *e.g.*, ref. [9]). We found that there are exactly eight independent terms at this order which may be chosen as follows:

$$\begin{aligned}\mathcal{L}^W_{e^2p^4} &= \epsilon^{\mu\nu\alpha\beta}\\ &\times\Big\{k_1^W i\langle Q_+\rangle\langle Q_- u_\mu\rangle\langle u_\nu u_\alpha u_\beta\rangle + k_2^W\langle [Q_+, Q_-]u_\alpha u_\beta\rangle\langle f_{+\mu\nu}\rangle\\ &+k_3^W\langle Q_+\rangle\langle [Q_-, f_{+\mu\nu}]u_\alpha u_\beta\rangle + k_4^W\langle Q_+^2 u_\alpha\rangle\langle f_{-\mu\nu}u_\beta\rangle\\ &+k_5^W i\langle [Q_+, f_{+\mu\nu}]Q_-\rangle\langle f_{+\alpha\beta}\rangle + k_6^W i\langle Q_+\rangle\langle [Q_+, f_{+\mu\nu}]f_{-\alpha\beta}\rangle\\ &+k_7^W i\langle [Q_{+\mu}, Q_+]u_\nu\rangle\langle f_{+\alpha\beta}\rangle + k_8^W i\langle [Q_{-\mu}, Q_-]u_\nu\rangle\langle f_{+\alpha\beta}\rangle\Big\}.\end{aligned} \tag{2}$$

As usual in ChPT, the couplings k_i^W are divergent. The divergence is generated from one-loop diagrams containing one vertex from the Lagrangian (1). As in the non-anomalous case, there are both diagrams with explicit photons and diagrams with pions in which the EM effects are induced from the π^+-π^0 mass difference. In the

[a] e-mail: moussall@inpno.in2p3.fr

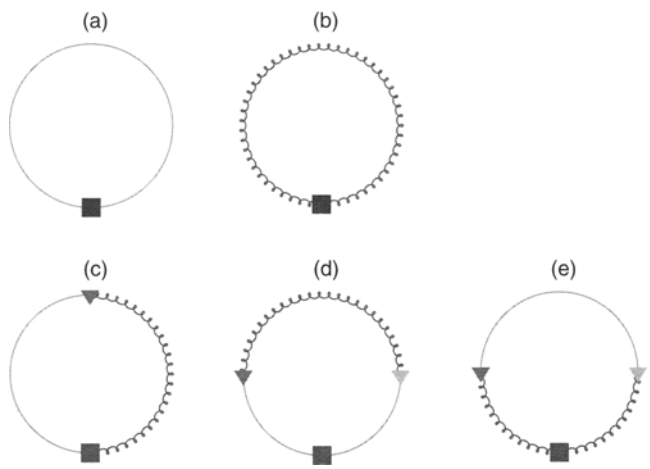

Fig. 1. One-particle-irreducible graphs which contribute to the $O(p^6)$ and the $O(e^2p^4)$ divergences in the anomalous sector: a triangle denotes an $O(p^2)$ vertex a box denotes an $O(p^4)$ vertex. The solid line represents the (full) pion propagator and the curly line the full photon propagator.

present case, because the chiral order is p^6, one must only be careful that there are contributions which are one particle reducible. The set of irreducible graphs that one must compute is shown in fig. 1. Putting all these contributions together and defining the relation between bare and renormalized couplings as follows:

$$k^W_{i,\text{bare}} = (c\mu)^{d-4}\left(\frac{1}{16\pi^2(d-4)}\beta_i + k^W_{i,r}(\mu)\right) , \qquad (3)$$

we find that the coefficients β_i have the following values in the Feynman gauge:

$$\beta_1 = \beta_6 = \beta_8 = 0 \qquad (4)$$

and

$$\begin{aligned} &\beta_2 = \left(\tfrac{1}{8} - \tfrac{1}{6}\tfrac{C}{F^4}\right)\kappa, \quad \beta_3 = -\tfrac{1}{8}\kappa, \ \beta_4 = -\tfrac{1}{4}\kappa, \\ &\beta_5 = \left(-\tfrac{1}{16} + \tfrac{1}{6}\tfrac{C}{F^4}\right)\kappa, \ \beta_7 = \tfrac{1}{4}\kappa\ . \end{aligned} \qquad (5)$$

C is the EM chiral parameter which induces π^+-π^0 mass splitting at leading order: $m^2_{\pi^+} - m^2_{\pi^0} = 2e^2C/F^2_\pi$. The divergence structure for other gauges is also discussed in ref. [4].

3 π^0 lifetime at NLO

We would like here to collect in a complete way the contributions to the π^0 lifetime beyond the current algebra prediction including, in particular, the electromagnetic contributions. One has in mind to match from the theoretical side a precision of the order of 1% which is the typical precision expected from the PrimEx experiment [3]. This involves three steps:

Step 1: One must be able to determine F_π, defined as the axial pion coupling *in the absence of QED* to high precision, as it is the basic coupling entering the chiral expansion.

Step 2: One must perform a ChPT calculation up to one loop (including the photon) and include the tree level contributions of the relevant chiral order (*i.e.* up to order six here, since the leading order is four). In this manner, one obtains an expression for the decay amplitude in terms of a (numerous) set of chiral couplings.

Step 3: One must evaluate the chiral couplings involved. The real interest of this enterprise is that this turns out to be actually possible. Let us now go through these steps in turn.

The problem involved in step 1 was solved by Marciano and Sirlin [10]. Making use of some improvements in the modelling of form factors performed in ref. [11] on obtains the value $F_\pi = 92.16 \pm 0.11$ MeV. We note that the precision matches the one that we are after and that, as defined, this coupling is exactly the same for charged or for neutral pions at this level of accuracy. Turning to step 2 now, we choose to perform the calculation in the framework of the $SU(3)$ expansion for, otherwise, we would not be able to successfully go through step 3. At leading order, the amplitude is determined from the WZW Lagrangian and also picks up a contribution from π^0-η mixing:

$$A_{p^4} = \frac{\alpha}{\pi F_\pi}\left(1 + \frac{m_d - m_u}{4(m_s - m)}\right), \quad m = \frac{1}{2}(m_u + m_d)\,. \qquad (6)$$

At NLO let us consider the one-particle *irreducible* contributions (the parametrization of the chiral field and of the fluctuations being the same as in ref. [12]) first: there are no photon loop contribution and the sum of pseudo-scalar loops vanish [13,14]. As for the tree level contributions, there are none coming from $\mathcal{L}^W_{e^2p^4}$ and the only contributions are from $\mathcal{L}^W_{p^6}$. Using the notations of ref. [15], they involve the two coupling-constants C^W_7, C^W_8. Next come the one-particle-*reducible* contributions. These can be encoded as a matrix of wave function renormalization and mixing. π^0-η mixing whose at the leading oder is described by one mixing parameter ϵ now involves two mixing parameters ϵ_1, ϵ_2, whose expressions can be found in ref. [12]. Only ϵ_2 occurs in our problem:

$$\begin{aligned} \epsilon_2 = &\frac{\sqrt{3}(m_d - m_u)}{4(m_s - m)} \\ &\times\left\{1 - \frac{32(m^2_K - m^2_\pi)}{F^2_0}(3L_7 + L_8) + \chi_{\text{logs}}\right\}. \end{aligned} \qquad (7)$$

At this level, electromagnetic contributions are present, which involve the chiral couplings K_i introduced by Urech. They can be collected in two terms:

$$\begin{aligned} \delta_2 = \frac{\sqrt{3}e^2 m}{m_s - m}\Big(&-(2K_3 - K_4) + \frac{2}{3}(K_5 + K_6) \\ &-\frac{2}{3}(K_9 + K_{10}) - \frac{2C}{F^4_0}\tilde{\nu}_K\Big) \end{aligned} \qquad (8)$$

and

$$\delta_\pi = e^2\Big\{ -\frac{4}{3}(K_1+K_2) + (2K_3-K_4) - \frac{10}{9}(K_5+K_6) + \frac{C}{F_0^4}(4\tilde{\nu}_\pi + \tilde{\nu}_K)\Big\}. \quad (9)$$

From this, we can write the $\pi^0 \to 2\gamma$ amplitude including all the contributions which are of chiral order p^6 or e^2p^4, *i.e.* linear in the quark masses m_u, m_d and the electric charge e^2

$$A_{\pi 2\gamma} = \frac{\alpha}{\pi F_\pi}\Big\{1 + \frac{\epsilon_2}{\sqrt{3}} + \frac{\delta_2}{\sqrt{3}} + \delta_\pi + \Big(1 - \frac{m_d - m_u}{m}\frac{4r-5}{4(r-1)}\Big)T_1 - \frac{3(m_d-m_u)}{4m}T_1'\Big\}, \quad (10)$$

where r is the mass ratio m_s/m and

$$T_1 = -\frac{256\pi^2}{3}m_\pi^2 C_7^W, \quad T_1' = -\frac{1024\pi^2}{3}m_\pi^2 C_8^W. \quad (11)$$

We note that all the contributions are isospin violating except for one term proportional to C_7^W. Let us now discuss the determination of the various couplings. Those appearing in ϵ_2: L_7 and L_8 have been discussed in ref. [12]. The couplings C_7^W, C_8^W can be estimated from resonance saturation models using methods proposed in ref. [16]. Equivalently, one can express both of them as convergent sum rules and then estimate the integrals using resonance saturation. C_8^W encodes the influence of π^0-η' mixing, while C_7^W has an analogous interpretation in terms of π^0-$\pi^0(1300)$ mixing. The experimentally observed suppression of the $\pi(1300)$ electromagnetic decay then leads to the fact that C_7^W is strongly suppressed compared to C_8^W. The latter parameter can then be determined more precisely using ChPT and input from η electromagnetic decay. There remains to estimate the combination of Urech couplings K_i which appear in δ_π and δ_2. This again, can be done using resonance saturation models. These models must be constrained by chiral symmetry and also by proper QCD asymptotic conditions. Assuming dominance of the vector meson resonances here a unique answer is found for the two combinations

$$\frac{4}{3}(K_1+K_2) - (2K_3-K_4) + \frac{10}{9}(K_5+K_6) = \frac{5g_1^2}{48\pi^2},$$
$$-\frac{2}{3}(2K_3-K_4) + \frac{4}{9}(K_5+K_6) = \frac{g_1^2}{24\pi^2}, \quad (12)$$

in terms of a vector meson coupling constant g_1 which can be precisely determined from the $\omega \to \pi\gamma$ decay width. Putting these results together one can express the pion decay amplitude as follows in terms of $m_u - m_d$:

$$A_{\pi 2\gamma} = \frac{\alpha}{\pi F_\pi}\Big\{1 - 0.3410^{-2} + \frac{m_d-m_u}{m_s-m}(0.93 \pm 0.12) \pm 0.1410^{-2}\Big\}. \quad (13)$$

The electromagnetic contributions are found to decrease the decay width by approximately 0.6%. The order of magnitude of the quark mass ratio involved is $1/R \equiv (m_d - m_u)/(m_s - m) \simeq 1/43$ (*e.g.* [17]). This generates a contribution which increases the pion decay width by approximatively 5%. Such a contribution can be probed at the qualitative level by the PrimEx experiment. Assuming the above value for R, the theoretical prediction for the pion decay width would be

$$\Gamma_{\pi 2\gamma} = 8.06 \pm 0.02 \pm 0.06 \text{ eV}, \quad (14)$$

where the first error originates from the determination of F_π and second collects the incertainties in the values of the coupling constants. A very similar result was obtained recently in ref. [18] using an expansion scheme which combines the chiral and the large-N_c expansions. One reason for the smallness of the NLO corrections is the suppression of the contributions which are not isospin breaking (other than those which can be absorbed into F_π). Such isospin-conserving contributions could be present at NNLO and it would be useful, in the future, to try to estimate their order of magnitudes.

This work is supported in part by the Indo-French collaboration contract IFCPAR-2504-1 and by the EEC-TMR contract ERBFMRXCT98-0169.

References

1. R. Urech, Nucl. Phys. B **433**, 234 (1995), hep-ph/9405341.
2. A. Rusetsky, this issue, p. 491, hep-ph/0209182.
3. A. Gasparian, *Proceedings of the 3rd Workshop on Chiral Dynamics - Chiral Dynamics 2000: Theory and Experiment, Newport News, Virginia, 17-22 July 2000*, hep-ph/0012024.
4. B. Ananthanarayan, B. Moussallam, JHEP **05**, 052 (2002), hep-ph/0205232.
5. J. Wess, B. Zumino, Phys. Lett. B **37**, 95 (1971).
6. E. Witten, Nucl. Phys. B **223**, 422 (1983).
7. R. Kaiser, Phys. Rev. D **63**, 076010 (2001), hep-ph/0011377.
8. S.L. Adler, W.A. Bardeen, Phys. Rev. D **182**, 1517 (1969).
9. J. Bijnens, G. Colangelo, G. Ecker, JHEP **02**, 020 (1999), hep-ph/9902437.
10. W.J. Marciano, A. Sirlin, Phys. Rev. Lett. **71**, 3629 (1993).
11. M. Finkemeier, Phys. Lett. B **387**, 391 (1996), hep-ph/9505434.
12. J. Gasser, H. Leutwyler, Nucl. Phys. B **250**, 465 (1985).
13. J.F. Donoghue, B.R. Holstein, Y.-C.R. Lin, Phys. Rev. Lett. **55**, 2766 (1985); **61**, 1527 (1988)(E).
14. J. Bijnens, A. Bramon, F. Cornet, Phys. Rev. Lett. **61**, 1453 (1988).
15. J. Bijnens, L. Girlanda, P. Talavera, Eur. Phys. J. C **23**, 539 (2002), hep-ph/0110400.
16. G. Ecker, J. Gasser, A. Pich, E. de Rafael, Nucl. Phys. B **321**, 311 (1989).
17. H. Leutwyler, Phys. Lett. B **378**, 313 (1996), hep-ph/9602366.
18. J.L. Goity, A.M. Bernstein, B.R. Holstein, Phys. Rev. D **66**, 076014(2002), hep-ph/0206007.

Eur. Phys. J. A **18**, 499–502 (2003)
DOI 10.1140/epja/i2002-10269-3

THE EUROPEAN PHYSICAL JOURNAL A

Quark mass dependence of the nuclear forces

E. Epelbaum[1,a], Ulf-G. Meißner[2,3], and W. Glöckle[1]

[1] Ruhr-Universität Bochum, Institut für Theoretische Physik II, D-44870 Bochum, Germany
[2] Karl-Franzens-Universität Graz, Institut für Theoretische Physik A-8010 Graz, Austria
[3] Forschungszentrum Jülich, Institut für Kernphysik (Theorie), D-52425 Jülich, Germany

Received: 30 September 2002 /
Published online: 22 October 2003 – © Società Italiana di Fisica / Springer-Verlag 2003

Abstract. We investigate the behavior of the nuclear force as a function of the light-quark masses m_q in the framework of chiral effective field theory at next-to-leading order. The unknown m_q-dependent short-range contribution is estimated by means of dimensional analysis. We calculate various observables for different values of m_q. We found no new bound states and a larger deuteron binding energy, $B_D^{\rm CL} = 9.6 \pm 1.9^{+1.8}_{-1.0}$ MeV, in the chiral limit.

PACS. 11.30.Rd Chiral symmetries – 13.75.Cs Nucleon-nucleon interactions (including antinucleons, deuterons, etc.) – 21.30.Cb Nuclear forces in vacuum – 21.30.Fe Forces in hadronic systems and effective interactions

1 Introduction

Chiral Perturbation Theory (CHPT) is a well-established model-independent and systematic tool for calculating low-energy properties of hadronic systems. It is based upon the approximate and spontaneously broken chiral symmetry of QCD. Starting from the most general chiral invariant effective Lagrangian for Goldstone bosons (pions in the two-flavor case of light up and down quarks) and matter fields (nucleons, Δ-excitations, ...) low-energy S-matrix elements can be calculated via simultaneous expansion in the low external momenta and quark mass (or, equivalently, pion mass[1]). If two and more nucleons are considered, the interaction becomes too strong to be treated perturbatively and an additional nonperturbative resummation of the amplitude is necessary. Since the absolute values of the running up and down quark masses at the scale 1 GeV [1] $m_u \simeq 5$ MeV, $m_d \simeq 9$ MeV are rather small, one expects that hadronic properties at low energy do not change strongly in the chiral limit of (CL) $M_\pi \to 0$. This feature is crucial for the chiral expansion to make sense and is certainly true for the π and πN systems, where the interaction becomes arbitrarily weak in the CL and for vanishing external momenta. The purpose of this work is to look at the NN system in the CL (and, in general, for values of the pion mass different from the physical one), which is much more complicated due to the nonperturbative aspect. We stress that the question about the M_π-dependence of the nuclear force is not only of academic interest, but also of practical use for interpolating results from the lattice gauge theory, see [2] for more discussion. For example, the S-wave scattering lengths have been calculated recently on the lattice using the quenched approximation [3]. Another interesting application is related to imposing bounds on the time-dependence of fundamental couplings from the two-nucleon sector, as discussed in [4].

2 M_π-dependence of the nuclear force

A convenient way of (nonperturbative) evaluation of the S-matrix elements for nucleon-nucleon (NN) interactions from the chiral effective Langangian suggested by Weinberg [5] is to apply CHPT methods to derive the effective NN potential. One can then calculate observables by solving the appropriate Lippmann-Schwinger equation. In [6] we have introduced a scheme, which leads to an energy-independent and Hermitian NN potential and is based upon the method of unitary transformation [7]. At leading order (LO) the potential is given by the (static) one-pion exchange (OPE) and two contact interactions without derivatives:

$$V^{\rm LO} = -\frac{1}{4}\frac{g_{\pi N}^2}{m_N^2}\boldsymbol{\tau}_1\cdot\boldsymbol{\tau}_2\frac{(\boldsymbol{\sigma}_1\cdot\boldsymbol{q})(\boldsymbol{\sigma}_2\cdot\boldsymbol{q})}{\boldsymbol{q}^2+M_\pi^2} + C_S + C_T\boldsymbol{\sigma}_1\cdot\boldsymbol{\sigma}_2, \quad (1)$$

where $g_{\pi N}$ is the pion-nucleon coupling constant, m_N the nucleon mass, $\boldsymbol{q}$ the nucleon momentum transfer, $\boldsymbol{\sigma}$ ($\boldsymbol{\tau}$)

[a] e-mail: Evgeni.Epelbaum@tp2.ruhr-uni-bochum.de

[1] In the isospin limit with the quark masses $m_u = m_d = \hat{m}$ one finds for the pion mass M_π: $M_\pi^2 = 2\hat{m}B(1+\mathcal{O}(\hat{m}))$, where B is a constant.

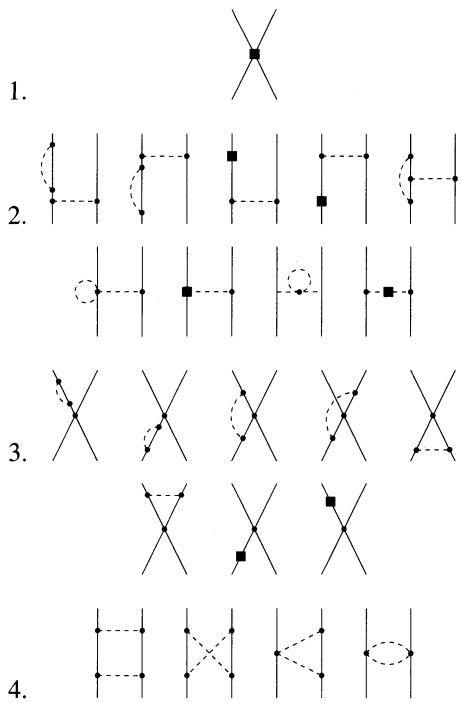

Fig. 1. NLO corrections to the NN potential. The solid (dashed) lines refer to nucleons (pions). The heavy dots denote the leading vertices, while the solid rectangles represent vertices of higher chiral dimension as defined in [6,8].

refer to spin (isospin) Pauli matrices and $C_{S,T}$ denote the low-energy constants (LECs). At next-to-leading order (NLO) the correction have to be taken into account from:

1. contact terms with two derivatives or one M_π^2-insertion,
2. renormalization of the OPE,
3. renormalization of the contact terms,
4. two-pion exchange (TPE).

The corresponding diagrams are depicted in fig. 1 in symbolic form, *i.e.* we only show the general topologies without indicating specific time orderings. The energy denominators and overall factors in each individual case can be read off from the operators given in [6]. For a detailed discussion of the NLO corrections the reader is referred to [8]. Apart from the explicit M_π-dependence of the OPE in eq. (1) an additional implicit dependence of the ratio $g_{\pi N}/m_N$ on the pion mass has to be taken into account at NLO. For an arbitrary value $\tilde{M}_\pi$ of the pion mass one has

$$\frac{g_{\pi N}}{m_N} = \frac{g_A}{F_\pi}\left(1 - \frac{g_A^2 \tilde{M}_\pi^2}{4\pi^2 F_\pi^2}\ln\frac{\tilde{M}_\pi}{M_\pi} - \frac{2\tilde{M}_\pi^2}{g_A}\bar{d}_{18} + \left(\frac{g_A^2}{16\pi^2 F_\pi^2} - \frac{4}{g_A}\bar{d}_{16} + \frac{1}{16\pi^2 F_\pi^2}\bar{l}_4\right)\left(M_\pi^2 - \tilde{M}_\pi^2\right)\right), \quad (2)$$

where $g_A = 1.26$, $F_\pi = 92.4\,\mathrm{MeV}$ and $M_\pi = 138\,\mathrm{MeV}$ denote the physical values of the nucleon axial vector coupling, pion decay constant and pion mass, respectively. Further, $\bar{l}_4$, $\bar{d}_{18}$ and $\bar{d}_{16}$ are LECs related to pion and pion-nucleon interactions. We use the following values for these LECs: $\bar{l}_4 = 4.3$ [9], $\bar{d}_{16} = -1.23^{+0.32}_{-0.53}\,\mathrm{GeV}^{-2}$ [10] and $\bar{d}_{18} = -0.97\,\mathrm{GeV}^{-2}$. The constant $\bar{d}_{18}$ is fixed from the observed value of the Golberger-Treiman discrepancy with $g_{\pi N} = 13.2$ [11]. Note further that for the LEC $\bar{d}_{16}$ we use an average of three values given in [10], which result from different fits. The shown uncertainty is defined in the way to cover the whole range of values from [10].

The remaining $\tilde{M}_\pi$-dependence of the nuclear force at NLO is given by the TPE [8] as well as by the short-range terms of the form

$$V_{\tilde{M}_\pi}^{\mathrm{cont}} = \tilde{M}_\pi^2\Big[\bar{D}_S + \bar{D}_T(\boldsymbol{\sigma}_1\cdot\boldsymbol{\sigma}_2) - \big(\beta_S + \beta_T(\boldsymbol{\sigma}_1\cdot\boldsymbol{\sigma}_2)\big)\ln\frac{\tilde{M}_\pi}{M_\pi}\Big], \quad (3)$$

where the constants $\beta_{S,T}$ are given in terms of g_A, F_π and C_T [8]. All other contact terms do not depend on the pion mass and the corresponding LECs $C_{1,\ldots,7}$ can be adopted from the analysis of [12], performed for the physical value of $\tilde{M}_\pi$. The essential difficulty in extrapolating the nuclear forces in the pion mass is due to the fact that one cannot disentangle the short-range contribution given in eq. (3) from the LO one in eq. (1) in the NN system and at the physical point $\tilde{M}_\pi = M_\pi$[2]. Thus, the LECs D_S and D_T are unknown. In order to proceed further we assume natural values for these constants, *i.e.*:

$$\bar{D}_{S,T} = \frac{\alpha_{S,T}}{F_\pi^2 \Lambda_\chi^2}, \quad \text{where } \alpha_{S,T} \sim 1, \quad (4)$$

and $\Lambda_\chi \simeq 1\,\mathrm{GeV}$. In [13] we have shown that *all values* of the dimensionless coefficients α related to the contact terms lie at NLO in the range $-2.1\ldots3.2$ for all cut-offs employed. In the following we will make a conservative estimation for $\alpha_{S,T}$:

$$-3.0 < \alpha_{S,T} < 3.0. \quad (5)$$

Certainly, the lack of information about the values of $D_{S,T}$ is the main source of uncertainty of our analysis. We have adopted the same procedure to regularize the LS equation as in [12], *i.e.* the potential $V(\boldsymbol{p}',\boldsymbol{p})$ is multiplied by the regulator functions $f_{\mathrm{R}}^{\mathrm{expon}}(|\boldsymbol{p}|)$, $f_{\mathrm{R}}^{\mathrm{expon}}(|\boldsymbol{p}'|)$, whose precise form is given in [12]. In the next section we will show how various observables behave with $\tilde{M}_\pi$.

3 Results

Having specified the NN interaction at arbitrary value of $\tilde{M}_\pi$ we are now in the position to calculate observables. Let us begin with the behavior of the NN phase shifts in

[2] This can be done in the processes including pions such as, *e.g.*, pion-deuteron scattering. Such an analysis is however not yet available.

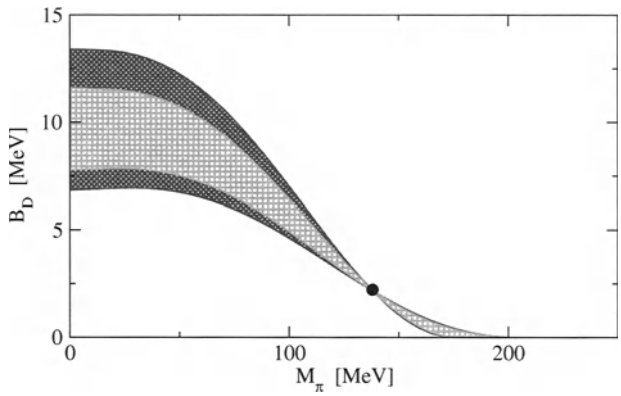

Fig. 2. Deuteron BE *versus* $\tilde{M}_\pi$. The shaded areas show allowed values. The light-shaded band corresponds to our main result with the uncertainty due to the unknown LECs $\bar{D}_{S,T}$. The dark-shaded band gives the additional uncertainty due to the uncertainty of $\bar{d}_{16}$. The heavy dot shows the BE for the physical case $\tilde{M}_\pi = M_\pi$.

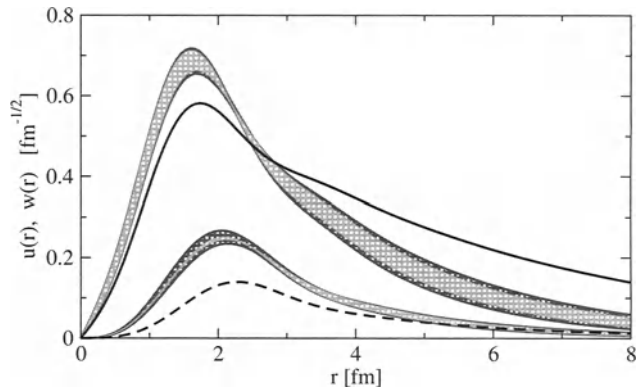

Fig. 3. Deuteron wave functions in the CL compared with the ones in the physical case. The upper and lower bands (solid and dashed lines) refer to the S- and D-wave functions $u(r)$ and $w(r)$ in the CL (in the physical case), respectively. For remaining notations see fig. 2.

the CL. First of all we would like to stress that the OPE in eq. (1) leads to a significant scattering even in higher partial waves due to the Coulomb-like pion propagator in the CL. Further, no effective range expansion of the form

$$k^{2l+1} \cot \delta_l(k) = -\frac{1}{a_l} + r_l \frac{k^2}{2} + v_l^2 k^4 + \cdots , \qquad (6)$$

exists due to the vanishing pion mass[3]. In eq. (6) k is the c.m. momentum and l the angular momentum. It is easy to derive the low-momentum behavior of $\delta_l(k)$ at least for large l, where the potential becomes weak and one can use the Born approximation for the T-matrix. It is then sufficient to look at on-the-energy shell matrix elements of the OPE in the CL $V_{\rm OPE}^{\rm CL}(k)$, which strongly dominantes the nuclear interaction at low momenta. We found that $V_{\rm OPE}^{\rm CL}(k) = 0$ in all spin-singlet ($s = 0$) and $V_{\rm OPE}^{\rm CL}(k) = \gamma$ in the spin-triplet ($s = 1$) channels, where the constant γ depends on the partial wave. As a consequence, we expect in the CL a strong reduction of $\delta_l(k)$ in the $s = 0$ channels and linear with k growth of $\delta_l(k)$ in the $s = 1$ channels. Numerical analysis performed in [8] confirms this estimation. It remains to stress that we have not found new bound states in the CL in agreement with the previous work by Bulgac *et al.* [14], although a strong enhancement of $\delta_l(k)$ is observed in many cases[4]. Last but not least, we found smaller (in magnitude) and more natural values for the two S-wave scattering lengths in the chiral limit $a_{\rm CL}(^1S_0) = -4.1 \pm 1.6^{+0.0}_{-0.4}$ fm and $a_{\rm CL}(^3S_1) = 1.5 \pm 0.4^{+0.2}_{-0.3}$ fm, where the first indicated error refers to the uncertainty in the value of $\bar{D}_{^3S_1}$ and $\bar{d}_{16}$ being set to the average value $\bar{d}_{16} = -1.23\,{\rm GeV}^{-2}$, while the second indicated error shows the additional uncertainty due to the uncertainty in the determination of $\bar{d}_{16}$ as described before.

We have also calculated the deuteron binding energy (BE) as a function of $\tilde{M}_\pi$. Our results for the cut-off $\Lambda = 560$ MeV are depicted in fig. 2. According to our *complete NLO analysis* deuteron is stronger bound in the chiral limit with the BE $B_{\rm D}^{\rm CL} = 9.6 \pm 1.9^{+1.8}_{-1.0}$ MeV. For the root-mean-square radius of the deuteron in the CL we found a smaller value $r_{\rm D}^{\rm CL} = 1.27 \pm 0.09 \pm 0.04$ fm to be compared with the observed one $r_{\rm D} = 1.97$ fm. A more short-range nature of the deuteron in the CL is also clearly visible in the deuteron wave function presented in fig. 3. It is interesting that the probability for the deuteron to be in the D-state is strongly enhanced in the CL (9.5% ... 11.8% compared to 3.5% for the NLO with the observed value of the pion mass). The detailed description of the deuteron properties will be published elsewhere.

4 Summary

To conclude, we did not find dramatic changes in the properties of the NN systems in the CL, such as the appearance of new bound states. Various observables like the deuteron binding energy and the S-wave scattering lengths are shown to be more natural in the CL.

References

1. J. Gasser, H. Leutwyler, Phys. Rep. C **87**, 77 (1982).
2. S.R. Beane *et al.*, Nucl. Phys. A **700**, 377 (2002).
3. M. Fukugita *et al.*, Phys. Rev. D **52**, 3003 (1995).
4. S.R. Beane, M.J. Savage, Nucl. Phys. A **720**, 399 (2003), hep-ph/0206113.
5. S. Weinberg, Nucl. Phys. B **363**, 3 (1991).

[3] The maximal radius of convergence of the effective range expansion is proportional to $\tilde{M}_\pi^2$ and goes to zero in the CL.

[4] For example, $\delta_l(k)$ in the $^3P_0$ partial wave reaches a maximum of $\sim 32°$ to be compared with $\sim 11°$ in the physical case.

6. E. Epelbaoum, W. Glöckle, Ulf-G. Meißner, Nucl. Phys. A **637**, 107 (1998).
7. S. Okubo, Prog. Theor. Phys. Jpn. **12**, 603 (1954).
8. E. Epelbaum, Ulf-G. Meißner, W. Glöckle, nucl-th/0207089.
9. J. Gasser, H. Leutwyler, Ann. Phys. (N.Y.) **158**, 142 (1984).
10. N. Fettes, doctoral thesis, published in *Berichte des Forschungszentrum Jülich*, **3814** (2000).
11. E. Matsinos, hep-ph/9807395.
12. E. Epelbaum, W. Glöckle, Ulf-G. Meißner, Nucl. Phys. A **671**, 295 (2000).
13. E. Epelbaum, Ulf-G. Meißner, W. Glöckle, Ch. Elster, Phys. Rev. C **65**, 044001 (2002).
14. A. Bulgac, G.A. Miller, M. Strikman, Phys. Rev. C **56**, 3307 (1997).

Eur. Phys. J. A **18**, 503–505 (2003)
DOI 10.1140/epja/i2002-10270-x

THE EUROPEAN PHYSICAL JOURNAL A

Moments of polarized parton distribution functions

V. Bernard[1], T:R. Hemmert[2,a], and U.-G. Meißner[3]

[1] U. L. Pasteur, LPT, Strasbourg, France
[2] Theoretische Physik T39, Physik Department, TU München, Garching, Germany
[3] FZ Jülich, IKP(Th), Jülich, Germany

Received: 30 September 2002 /
Published online: 22 October 2003 – © Società Italiana di Fisica / Springer-Verlag 2003

Abstract. We present novel results for the first moment of the spin-dependent structure function $g_1(x, Q^2)$ of the nucleon at "small" ($Q^2 < 0.3$ GeV^2) photon virtuality in the framework of a relativistic formulation of baryon chiral perturbation theory. We perform a next-to-leading order calculation and obtain significant differences to previously found results based on the heavy-baryon approach for the proton and neutron.

PACS. 12.39.Fe Chiral Lagrangians – 14.20.Dh Protons and neutrons

1 Introduction

The spin structure of the nucleon is under active theoretical and experimental investigation. Of particular interest is the transition from the perturbative regime at high momentum transfer to the non-perturbative low-energy region. Interestingly, systematic and controlled theoretical calculations are only available for very small or very large momentum transfer, while the intermediate region is accessible to resonance models or can be investigated using dispersion relations. Of special interest is the generalized Gerasimov-Drell-Hearn (GDH) sum rule [1] for virtual photons. It was pointed out in [2] that one can systematically investigate its momentum evolution at low energies in the framework of chiral perturbation theory (ChPT). In a series of papers, Ji *et al.* [3,4] proposed a formalism that is better suited for the direct connection with the spin-dependent structure functions measured in deep inelastic scattering. A leading-order calculation was presented in [4] for the first moment of the spin-dependent nucleon structure function $g_1(x, Q^2)$ and it was found that the Q^2 variation was much stronger than expected from naive dimensional analysis. Here we present the results of a recent next-to-leading order calculation [5] of the first moment $\Gamma_1(Q^2)$ for proton and neutron targets based on a relativistic formulation of ChPT [6].

2 The first moment of $g_1(x, Q^2)$

We start from the spin amplitude of forward doubly virtual Compton scattering (VVCS), which can be written in terms of two structure functions, called $S_1(\nu, Q^2)$ and $S_2(\nu, Q^2)$:

$$T^{[\mu\nu]}(p,q,s) = -i\,\epsilon^{\mu\nu\alpha\beta} q_\alpha \Big\{ m s_\beta S_1(\nu, Q^2) + [p\cdot q\, s_\beta - s\cdot q\, p_\beta]\, \frac{S_2(\nu, Q^2)}{m} \Big\}, \quad (1)$$

where s^μ denotes the spin-polarization four-vector of the nucleon, m is the nucleon mass, $\epsilon^{\mu\nu\alpha\beta}$ the totally antisymmetric Levi-Civita tensor with $\epsilon^{0123} = 1$, $Q^2 \geq 0$ (the negative of) the photon virtuality and $\nu = p\cdot q/m$ the energy transfer. In what follows, we will be concerned with the amplitudes $\bar{S}_i(0, Q^2) = S_i(0, Q^2) - S_i^{\rm el}(0, Q^2)$, *i.e.* the Compton amplitudes with the contribution from the elastic intermediate state subtracted. Here we are interested in the so-called "first-moment" sum rule $\Gamma_1(Q^2)$, which via the optical theorem is connected with the VVCS structure function $\bar{S}_1(\nu, Q^2)$ by

$$\frac{2}{Q^2}\int_0^{x_0} {\rm d}x\, g_1(x, Q^2) = \frac{1}{4e^2}\,\bar{S}_1(0, Q^2) = \frac{2}{Q^2}\,\Gamma_1(Q^2)\ , \quad (2)$$

with $g_1(x = Q^2/2m\nu, Q^2)$ denoting the spin-dependent structure function of the nucleon. Furthermore, x_0 denotes the inelastic threshold. The subtracted Compton amplitude $\bar{S}_1(\nu, Q^2)$ is normalized as $\bar{S}_1(0,0) = -e^2\kappa^2/m^2$, with κ the anomalous magnetic moment of the spin-1/2 particle. Equation (2) therefore constitutes one of the possible generalizations of the GDH sum rule to non-zero Q^2. At small photon virtualities, the subtracted Compton amplitudes $\bar{S}_i(0, Q^2)$ ($i = 1, 2$) can be calculated in ChPT and thus allow us to give predictions for $\Gamma_1(Q^2)$ via eq. (2).

[a] e-mail: themmert@physik.tu-muenchen.de

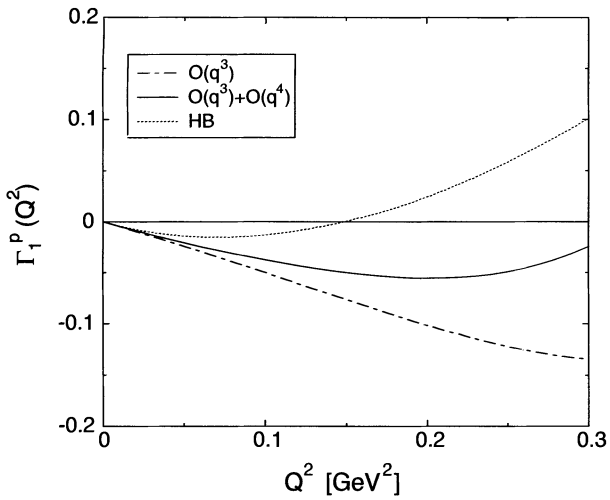

Fig. 1. Four-momentum dependence of the first moment $\Gamma_1(Q^2)$ for a proton target. The solid (dot-dashed) line gives the result of the present calculation to order q^3 (q^4) in comparison to the heavy-baryon result of [4] (dotted line).

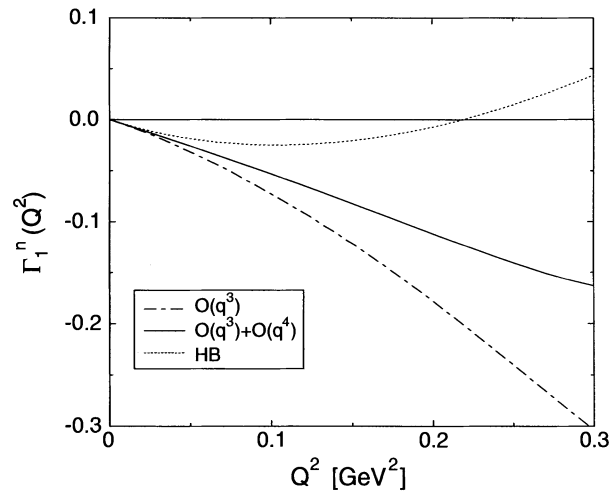

Fig. 2. Four-momentum dependence of the first moment $\Gamma_1(Q^2)$ for a neutron target. The plot symbols are explained in fig. 1.

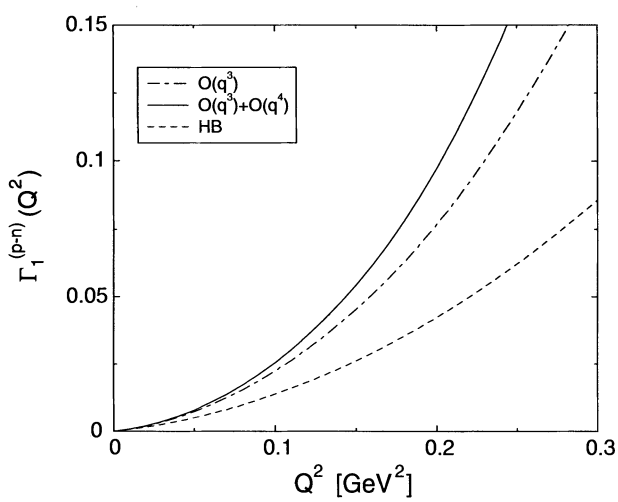

Fig. 3. Four-momentum dependence of the first moment $\Gamma_1(Q^2)$ for the isovector combination proton-neutron. The plot symbols are explained in fig. 1.

3 Results

In fig. 1 we show $\Gamma_1(Q^2)$ for a proton target. We note that in the heavy-baryon framework of ref. [4] the $\mathcal{O}(p^4)$ calculation shown as the dotted line constitutes the leading-order (LO) result for the four-momentum dependence of $\Gamma_1(Q^2)$, whereas in the relativistic framework [5] the leading-order contribution to $\Gamma_1(Q^2)$ already starts at $\mathcal{O}(p^3)$. We note that for $Q^2 < 0.2$ GeV^2 the next-to-leading order (NLO) result of the relativistic calculation represents a small correction to the leading-order one. However, comparing the NLO relativistic with the LO heavy-baryon result, one notices large differences (*e.g.*, the delayed zero crossing in the relativistic calculation). Given that the heavy-baryon results can be obtained from the relativistic calculation by taking the nucleon mass to infinity, one must conclude that the $1/m$ expansion of heavy-baryon ChPT converges very slowly for this spin-dependent observable.

In fig. 2 we show $\Gamma_1(Q^2)$ for a neutron target. Once more both the LO and NLO relativistic results compared to the LO heavy-baryon result are compared. As in the case of the proton, the relativistic chiral expansion seems under good control, whereas the heavy-baryon result is remarkably different, showing even a zero crossing in the low-Q^2 domain ! We note that as in the case of the proton all curves have the same slope near $Q^2 = 0$, as the (real-photon) GDH sum-rule is satisfied (by construction) in all these calculations.

Finally, in fig. 3 we show $\Gamma_1(Q^2)$ for the isovector difference proton-neutron. At very large Q^2 this moment is related to the well-known Bjorken sum rule. In the low-Q^2 resonance region this quantity is also of interest because it is free from $\Delta(1232)$ pole contributions. It has therefore been suggested [7] that the isovector channel at low Q^2 can be calculated quite reliably in ChPT, without the need of employing explicit delta degrees of freedom[1]. However, again comparing the NLO relativistic and the LO heavy baryon result, one must conclude that the isovector channel is not only plagued by a slowly converging $1/m$ expansion, but that additional physics beyond the one-loop pion-nucleon continuum seems to play an important role, as the NLO relativistic calculation rises far too quickly to smoothly meet the Bjorken limit at large Q^2. Clearly these issues need to be further investigated, necessitating investigations with (relativistic) Chiral Effective Field Theories that go beyond pions and nucleons as the only explicit degrees of freedom [8].

[1] We note that all the $\Gamma_1(Q^2)$ ChPT calculations for proton and neutron shown in figs. 1, 2 only contain the one-loop pion-nucleon continuum contribution. Possible contributions from nucleon or vector meson resonance are not shown.

References

1. S.B. Gerasimov, Yad. Fiz. **2**, 598 (1965); S.D. Drell, A.C. Hearn, Phys. Rev. Lett. **16**, 908 (1966).
2. V. Bernard, N. Kaiser, Ulf-G. Meißner, Phys. Rev. D **48**, 3062 (1993).
3. X.D. Ji, J. Osborne, J. Phys. G **27**, 127 (2001).
4. X.D. Ji, C.W. Kao, J. Osborne, Phys. Lett. B **472**, 1 (2000).
5. V. Bernard, T.R. Hemmert, U.-G. Meißner, Phys. Lett. B **545**, 105 (2002).
6. T. Becher, H. Leutwyler, Eur. Phys. J. C **9**, 643 (1999).
7. V.D. Burkert, Phys. Rev. D **63**, 097904 (2001).
8. V. Bernard, T.R. Hemmert, U.-G. Meißner, in preparation.

Eur. Phys. J. A **18**, 507–510 (2003)
DOI 10.1140/epja/i2002-10271-9

THE EUROPEAN PHYSICAL JOURNAL A

In-medium chiral perturbation theory

A. Wirzba[1,a], Ulf-G. Meißner[1], and J.A. Oller[2]

[1] Institut für Kernphysik (Theorie), Forschungszentrum Jülich, D-52425 Jülich, Germany
[2] Departamento de Física, Universidad de Murcia, E-30071 Murcia, Spain

Received: 30 September 2002 /
Published online: 22 October 2003 – © Società Italiana di Fisica / Springer-Verlag 2003

Abstract. We report on how to tackle the problem of establishing a chiral effective field theory in nuclear matter with explicit pion fields and in the presence of external sources (Ann. Phys. **297**, 27 (2002)). We have made use of the results of J.A. Oller (Phys. Rev. C **65**, 025204 (2002)) where the generating functional for the in-medium chiral $SU(2) \times SU(2)$ Lagrangian has been derived. Within this approach we develop the so-called standard power counting rules for the calculation of in-medium pion properties if the residual nucleon energies are of the order of the pion mass. In addition, for the case of vanishing residual nucleon energies, a modified scheme (non-standard counting) is introduced. For both schemes the pertinent scales where the chiral expansions have to break down are established as well. We have performed a systematic analysis of n-point in-medium Green functions up to and including next-to-leading order when the standard rules apply. These include the in-medium contributions to quark condensates, pion propagators, pion masses and couplings of the axial-vector, vector and pseudoscalar currents to pions.

PACS. 12.39.Fe Chiral Lagrangians – 11.30.Rd Chiral symmetries – 21.65.+f Nuclear matter

1 Introduction

In this paper we will report about a *systematic* study of the properties of pions and external sources in nuclear matter [1,2]. For typical nuclear densities, the interactions of the constituents of nuclear matter belong to the low-energy regime of strong interactions, such that one has to deal with phenomena in the non-perturbative sector of the underlying theory, QCD. Thus approximations are unavoidable. However, they should be controllable as in the methodology of effective field theories. Consequently, the aim is to create an in-medium QCD effective field theory that allows to estimate the errors when the pertinent perturbative expansion is truncated at some order.

The low-energy effective field theory of QCD in the vacuum is chiral perturbation theory (ChPT) [3,4]. It is believed that the approximate $SU(2)_{\rm L} \times SU(2)_{\rm R}$ chiral symmetry of QCD is spontaneously broken down to its vectorial subgroup, $SU(2)_{\rm L+R}$, with the appearance of three (Pseudo-)Goldstone bosons which can be identified with the three pion states, $\pi^{\pm}, \pi^0$. The unique order parameter signaling this symmetry violation is the finiteness of the square of the weak pion decay constant in the chiral limit, $f^2 \neq 0$; in fact, $f \simeq f_\pi = 92.4\,\mathrm{MeV}$. In addition, the chiral symmetry is also explicitly broken because the current up and down quarks have a small mass (small compared to a typical hadronic scale of 1 GeV). Due to Goldstone's theorem, the interactions of the pions with themselves or matter fields must vanish as the three-momentum and energy go to zero in the chiral limit. This in turn allows for a systematic treatment of such processes in the framework of an effective field theory, namely ChPT [3,4], in terms of a simultaneous expansion in external momenta and mass terms.

ChPT allows not only to tackle processes involving pions, but as well to consider nucleons (baryons). These massive states are included as matter fields chirally coupled to pions and external sources.

There are many articles [5–8] in the literature where ChPT Lagrangians, at most bilinear in the nucleon fields, are applied to the nuclear matter case in the mean-field approach, *i.e.* where the information contained in the vacuum ChPT Lagrangians is kept, but the baryon propagators in the medium are replaced by local densities in the mean-field approach. Proceeding in this way one looses the chiral counting in the medium, since the non-local nucleon correlations, due to the baryon propagators, are not considered. In fact, such contributions can be of the same or even of lower chiral order as those terms kept in the mean-field approach. Especially, they are the dominant contributions when the energy flowing through the baryon propagator is of the order of a nucleonic kinetic energy [1].

[a] e-mail: a.wirzba@fz-juelich.de

2 In-medium generating functional

Our starting point is the ChPT Lagrangian supplemented by external fields [4]. As in the mean-field approaches, multi-nucleon interactions will be left out here. Thus only the perturbative expansion of the chiral lagrangians $\mathcal{L}_{\pi\pi}$ and $\mathcal{L}_{\overline{\psi}\psi}$ (the latter is bilinear in the nucleon field) in powers of the external four-momenta of the pions, the external three-momenta of the nucleons and the quark masses will be taken into account. We apply the generating functional techniques of ref. [2]; *i.e.* the *in-medium* $SU(2)\times SU(2)$ generating functional is written as a path integral over the chiral field $U\equiv uu\equiv\exp[i\phi/f]$, where the ground states at asymptotic times have been replaced by the Fermi sea states of protons and neutrons and where secondly the nucleon fields have been integrated out:

$$
\begin{aligned}
e^{i\mathcal{Z}[v,a,s,p]} &= \int[\mathrm{d}U] \\
&\times\exp\Bigg\{i\int\mathrm{d}x\,\mathcal{L}_{\pi\pi}+\int\frac{\mathrm{d}\boldsymbol{p}}{2E(p)(2\pi)^3}\int\mathrm{d}x\mathrm{d}y \\
&\times e^{ip(x-y)}\mathrm{Tr}\left[-iA\left(I_4-D_0^{-1}A\right)^{-1}|_{(x,y)}(\not{p}+m_N)n(p)\right] \\
&-\frac{1}{2}\int\frac{\mathrm{d}\boldsymbol{p}}{2E(p)(2\pi)^3}\int\frac{\mathrm{d}\boldsymbol{q}}{2E(q)(2\pi)^3}\int\mathrm{d}x\mathrm{d}x'\mathrm{d}y\mathrm{d}y'\,e^{ip(x-y)} \\
&\times e^{-iq(x'-y')}\mathrm{Tr}\Big[-iA\left(I_4-D_0^{-1}A\right)^{-1}|_{(x,x')}(\not{q}+m_N)n(q) \\
&\times(-iA)\left(I_4-D_0^{-1}A\right)^{-1}|_{(y',y)}(\not{p}+m_N)n(p)\Big]+\cdots\Bigg\} \\
&\equiv\int[\mathrm{d}U]\,\exp\left\{i\int\mathrm{d}x\widetilde{\mathcal{L}}_{\pi\pi}[U;v,a,s,p]\right\}. \qquad (1)
\end{aligned}
$$

Here $A=D_0(x)-D(x)$ is the difference between the free Dirac operator $D_0=i\gamma^\mu\partial_\mu-m_N$ and the Dirac operator $D(x)$ of $\mathcal{L}_{\overline{\psi}\psi}\equiv\overline{\psi}(x)D(x)\psi(x)$, while I_4 is the unit operator in 4 dimensions. Thus $A(x)$ is a vertex operator in terms of pion legs and external (vector v, axial-vector a, scalar s, and pseudoscalar p) sources. The diagonal flavor matrix $n(p)=\mathrm{diag}[\theta(k_\mathrm{F}^{(p)}-|\boldsymbol{p}|),\theta(k_\mathrm{F}^{(n)}-|\boldsymbol{p}|)]$ parametrizes the upper cutoff for the three-momentum integrations, where $k_\mathrm{F}^{(p)}$ and $k_\mathrm{F}^{(n)}$ are the proton and neutron Fermi momenta, respectively. Finally, $E(p)=(\boldsymbol{p}^2+m_N^2)^{1/2}$ is the on-shell energy of the nucleon of mass m_N.

In this way the *in-medium* ChPT Lagrangian $\widetilde{\mathcal{L}}_{\pi\pi}$, is derived. The structure is the same as for vacuum ChPT, except for the important difference that the resulting Lagrangian is *non-covariant* as well as *non-local*. Especially, there appears now a non-local vacuum vertex $\Gamma\equiv-iA(I_4-D_0^{-1}A)^{-1}$ that generates a geometric series in terms of the local interaction operator A and the free Dirac propagator D_0^{-1}. The vertex-operator A in turn is subject to a chiral power expansion. The pertinent interaction operators of first and second order read

$$
\begin{aligned}
A^{(1)} &= -i\gamma^\mu\Gamma_\mu-ig_A^0\gamma^\mu\gamma_5\Delta_\mu\ , \\
A^{(2)} &= -c_1\langle\,\chi_+\,\rangle-2c_2\langle\Delta_\mu\Delta_\nu\rangle\frac{D^\mu}{m_N}\frac{D^\nu}{m_N} \\
&\quad+2c_3\langle\Delta_\mu\Delta^\mu\rangle-c_5\left(\chi_+-\tfrac{1}{2}\langle\chi_+\rangle\right)+\cdots\ ,
\end{aligned}
$$

$$
\text{with}\quad \chi_+\equiv u^\dagger\chi u^\dagger+u\chi^\dagger u\ ,\quad \chi\equiv-2\frac{\langle\bar{q}q\rangle}{f^2}(s+ip)\ ,
$$

$$
2\begin{Bmatrix}\Gamma_\mu\\ \Delta_\mu\end{Bmatrix}\equiv\left[u^\dagger,\partial_\mu u\right]_\mp-iu^\dagger(v_\mu+a_\mu)u\pm iu(v_\mu-a_\mu)u^\dagger.
$$

Here $D_\mu\equiv\partial_\mu+\Gamma_\mu$ and $\langle\cdots\rangle$ is defined as the trace in the flavor space. The c_i's are low-energy constants of $\mathcal{O}\left(p^2\right)$ terms and therefore finite, see ref. [9,10] for more details. $A^{(1)}$ includes the S-wave Weinberg-Tomozawa term and the derivative P-wave pion-nucleon coupling, while the sigma-term (proportional to c_1) and the so-called range terms (proportional to c_2 and c_3) appear in $A^{(2)}$. The generalized *in-medium* vertices consist of non-local vacuum vertices Γ connected through the exchange of on-shell Fermi-sea states with pertinent three-momenta smaller than $k_\mathrm{F}^{(p)}(k_\mathrm{F}^{(n)})$. These generalized vertices may still be linked to each other by pion legs from the local Lagrangian $\mathcal{L}_{\pi\pi}$. The lowest order *in-medium* vertices contain only $A^{(1)}$ operators; the next-to-leading order is obtained when one $A^{(2)}$ operator is involved. We refer to ref. [1] for the pertinent Feynman rules for the computation of connected in-medium graphs in momentum space.

3 Results

The novel results that we have obtained in ref. [1] can be summarized as follows:

i) In contrast to most previous works, which adopt the mean-field approach or many-body calculations, the in-medium chiral counting has been established including contributions from baryon propagators. The counting scheme depends on the energy flowing into the nucleon lines. This leads to a separate treatment of the standard and the non-standard case (*i.e.*, vanishing energy flow), respectively. In the standard case, the chiral expansion of pion properties in the medium starts with terms at $\mathcal{O}(p^4)$, and the next-to-leading order corrections appear at $\mathcal{O}(p^5)$, in the non-standard case (*e.g.*, in the in-medium $\pi\pi$ scattering) these orders are $\mathcal{O}(p^3)$ and $\mathcal{O}(p^4)$, respectively, whereas the in-vacuum power counting starts at $\mathcal{O}(p^2)$ with next-to-leading corrections of $\mathcal{O}(p^4)$.

ii) In the vacuum, the scale at which the chiral expansion is bound to break down is approximately $\Lambda_\chi\simeq 1\,\mathrm{GeV}\sim 4\pi f_\pi$. In the medium, there appear two further scales. These are $\sqrt{6}\pi f_\pi\simeq 0.7$ GeV and $6\pi^2 f_\pi^2/2m_N\simeq 0.27$ GeV for the standard or the non-standard counting rules, respectively. If there are P-wave interactions, the two in-medium scales have to be reduced by a factor of $1/g_A$ or $1/g_A^2$, respectively.

iii) We have re-derived, from the effective field theory point of view, the in-medium quark condensates in

symmetric nuclear matter [12,13] and have further extended them to the non-symmetric case:

$$\langle\Omega|\bar{q}q|\Omega\rangle = \langle\bar{q}q\rangle_{\rm vac}\left[1-\frac{2\sigma}{f^2M_\pi^2}\widehat{\rho}\pm\frac{4c_5}{f^2}\overline{\rho}\right].$$

Here the $\pm$ sign applies for the $\langle\bar{u}u\rangle$ and $\langle\bar{d}d\rangle$ condensate, respectively. $|\Omega\rangle$ is the nuclear matter background, while $\widehat{\rho}\equiv\frac{1}{2}(\rho_p+\rho_n)$ and $\overline{\rho}\equiv\frac{1}{2}(\rho_p-\rho_n)$ are defined as the isospin symmetric and asymmetric combinations of the proton and neutron density, ρ_p and ρ_n respectively. The quantity $\sigma=-4c_1M_\pi^2\approx 44\pm 8\pm 7\,\mathrm{MeV}$ is pion-nucleon sigma term [11,14] and M_π is the vacuum pion mass. The low-energy constant $c_5=-(0.09\pm 0.01)\,\mathrm{GeV}^{-1}$ parametrizes the strong isospin breaking [14]. It is very suppressed as compared to $2c_1=2(-0.81\pm 0.12)$ GeV^{-1} [15]. Hence the presence of a c_5 term does not induce a sizable change of the quark condensates at finite density, as studied in refs. [7,12,13] for the symmetric nuclear matter case. At normal nuclear matter density $\rho=\rho_0$, there is a 35% reduction of the condensates. This is compatible with a partial restoration of chiral symmetry.

iv) We have obtained the inverse pion propagator up to $\mathcal{O}(p^5)$. The corresponding dispersion relation between the energy ω and the three-momentum $\boldsymbol{q}$ of an in-medium pion π^a $(a=+,-,0)$ is given by

$$\begin{aligned}\omega^2-M_{\pi^a}^2\left(1+c_1\frac{8\widehat{\rho}}{f^2}\right)+\frac{4\widehat{\rho}}{f^2}\omega^2\left(c_2+c_3-\frac{g_A^2}{8m_N}\right)\\ -\boldsymbol{q}^2\left(1+\frac{4\widehat{\rho}}{f^2}c_3-\frac{g_A^2\widehat{\rho}}{m_Nf^2}\right)-\frac{g_A^2\widehat{\rho}}{2f^2m_N}\frac{(\boldsymbol{q}^2)^2}{\omega^2}\\ -\delta_{a0}\frac{4M_{\pi^a}^2\overline{\rho}}{f^2}\frac{m_u-m_d}{m_u+m_d}c_5\pm\delta_{a\pm}\left(\frac{g_A^2\boldsymbol{q}^2}{f^2\omega}-\frac{\omega}{f^2}\right)\overline{\rho}=0.\quad(2)\end{aligned}$$

Here M_{π^a} is the vacuum mass of pion π^a at $\mathcal{O}(p^4)$. For symmetric matter ($\overline{\rho}=0$) and in the chiral limit ($m_q=0$) the dispersion law simplifies to $\omega^2=\boldsymbol{q}^2\left(1-4\widehat{\rho}c_2/f^2\right)$. Thus the in-medium pion velocity $\widetilde{v}=\mathrm{d}\omega/\mathrm{d}|\boldsymbol{q}|=1-2\widehat{\rho}c_2/f^2$ is less than the vacuum speed of light ($c=1$) for the empirical value of the low-energy constant $c_2=(3.2\pm 0.25)\,\mathrm{GeV}^{-1}$ of ref. [9,10]. Inserting furthermore the value $c_3=(-4.70\pm 1.16)\,\mathrm{GeV}^{-1}$ from ref. [15], we have established from eq. (2) that chiral symmetry can account for the observed shift of the mass of the negative pion in deeply bound pionic states in ^{207}Pb [16,17], see also [18].

v) The wave function renormalizations of the in-medium pion fields, $\langle\Omega|\pi^\alpha(x)|\pi^\beta(p)\rangle\equiv Z_\alpha(\boldsymbol{q}^2)^{-1/2}\delta_{\alpha\beta}e^{-ipx}$, have been established from general principles via the equal-time commutation relations.

vi) With the help of the generating-functional formalism we can also study the coupling of pions with axial-vector and pseudoscalar sources [1]. In particular, we have shown that there is a splitting of the temporal and space-like component of the in-medium pion decays constants f_t and f_s, respectively [19,7,8]), which we have determined in the isospin-limit ($\overline{\rho}=m_u-m_d=0$) and at threshold as

$$f_{t/s}=f_\pi\left\{1\pm\frac{2\widehat{\rho}}{f^2}\left(c_2\pm c_3\mp\frac{g_A^2}{8m_N}\right)\right\}.\quad(3)$$

Moreover, we have confirmed that in-medium corrections up to $\mathcal{O}(p^5)$ do not spoil the validity of the Gell-Mann-Oakes-Renner relation, see ref. [7]. The decrease with increasing density for both, the quark condensates and the temporal component of the pion decay constant f_t seem to indicate a partial chiral symmetry restoration with increasing density. In addition, we have checked that the QCD Ward identities between the axial-vector currents and pseudoscalar (isovector and isoscalar) currents hold to $\mathcal{O}(p^5)$.

vii) Finally, the in-medium $\pi\pi$ scattering has been studied up to $\mathcal{O}(p^3)$ since in this case the non-standard counting occurs. Note that not only the in-medium corrections start at a lower order than in the standard case, namely already at $\mathcal{O}(p^3)$, but also the scale, below which the perturbative expansion is applicable, decreases. This leads to a rapid increase of the in-medium corrections with density. In fact, already at $k_{\rm F}\simeq 200$ MeV, or at a density of just $\sim 0.4\rho_0$, they are of the same size as the lowest order ChPT results.

4 Outlook

There are still open problems, *e.g.* the inclusion of multi-nucleon contact interactions remains a challenge, especially since the S-wave nucleon-nucleon interactions are enhanced because of the largeness of the S-wave scattering lengths related to the presence of shallow NN bound states. Moreover, this task has to be combined with simultaneous pion-loop calculation in order to guarantee that *all* in-medium $\mathcal{O}(p^6)$ contributions are taken into account. Finally, a search for a non-perturbative scheme that would allow to recover the scale $\sqrt{6}\pi f_\pi$, even in the case of the non-standard counting or even in the presence of multi-nucleon contact interactions, should be high on the list of future investigations in this field.

References

1. U.-G. Meißner, J.A. Oller, A. Wirzba, Ann. Phys. **297**, 27 (2002).
2. J.A. Oller, Phys. Rev. C **65**, 025204 (2002).
3. S. Weinberg, Physica A **96**, 327 (1979).
4. J. Gasser, H. Leutwyler, Ann. Phys. (N.Y.) **158**, 142 (1984).
5. D.B. Kaplan, A.E. Nelson, Phys. Lett. B **175**, 57 (1986).
6. G.E. Brown, K. Kubodera, M. Rho, V. Thorsson, Phys. Lett. B **291**, 355 (1992); T. Muto, R. Tamagaki, T. Tatsumi, Prog. Theor. Phys. Suppl. **112**, 159 (1993); V. Thorsson, M. Prakash, J.M. Lattimer, Nucl. Phys. A **572**, 693 (1994); (E) **574**, 851 (1994); G.E. Brown, C. Lee, M. Rho, V. Thorsson, Nucl. Phys. A **567**, 937 (1994); C. Lee, G.E. Brown, D. Min, M. Rho, Nucl. Phys. A **585**, 401 (1995).
7. V. Thorsson, A. Wirzba, Nucl. Phys. A **589**, 633 (1995); A. Wirzba, V. Thorsson, hep-ph/9502314.
8. M. Kirchbach, A. Wirzba, Nucl. Phys. A **604**, 395 (1996); **616**, 648 (1997).

9. N. Fettes, U.-G. Meißner, S. Steininger, Nucl. Phys. A **640**, 199 (1998).
10. N. Fettes, U.-G. Meißner, Nucl. Phys. A **676**, 311 (2000).
11. J. Gasser, M.E. Sainio, A. Svarc, Nucl. Phys. B **307**, 779 (1988).
12. E.G. Drukarev, E.M. Levin, Prog. Part. Nucl. Phys. **27**, 77 (1991).
13. T.D. Cohen, R.J. Furnstahl, D.K. Griegel, Phys. Rev. C **45**, 1881 (1992).
14. V. Bernard, N. Kaiser, U.-G. Meißner, Nucl. Phys. A **615**, 483 (1997).
15. P. Büttiker, U.-G. Meißner, Nucl. Phys. A **668**, 97 (2000).
16. H. Gilg *et al.*, Phys. Rev. C **62**, 025201 (2000).
17. K. Itahasi *et al.*, Phys. Rev. C **62**, 025202 (2000).
18. N. Kaiser, W. Weise, Phys. Lett. B **512**, 283 (2001).
19. M. Kirchbach, D.O. Riska, Nucl. Phys. A **578**, 511 (1994).

Eur. Phys. J. A **18**, 511–513 (2003)
DOI 10.1140/epja/i2002-10272-8

THE EUROPEAN PHYSICAL JOURNAL A

Chiral-symmetry restoration in clustered hadronic matter

G. Krein[a]

Instituto de Física Teórica, Universidade Estadual Paulista, Rua Pamplona, 145, 01405-900 São Paulo, SP, Brazil

Received: 30 September 2002 /
Published online: 22 October 2003 – © Società Italiana di Fisica / Springer-Verlag 2003

Abstract. Chiral-symmetry restoration is usually discussed in the context of quark matter, a system of deconfined quarks. However, many systems like stable nuclei and neutron stars have quarks confined within nucleons. In the present paper we use a Fermi sea of three-quark clusters instead of a Fermi sea of deconfined quarks to investigate the in-medium quark condensate. We find that an enhancement of the chiral breaking in clustered matter as claimed in the literature is not a consequence of the clustering but rather dependent on the microscopic model dynamics.

PACS. 21.65.+f Nuclear matter – 24.85.+p Quarks, gluons, and QCD in nuclei and nuclear processes – 12.39.-x Phenomenological quark models

1 Introduction

One of the key issues of contemporary nuclear physics is to understand how hadronic properties change in a hadronic medium at finite density and temperature. In general, low-energy hadronic properties, such as meson and baryon masses, are determined by the chiral condensate. In ultra-relativistic heavy-ion collisions it is possible to produce matter at temperatures that, much likely, lead to color deconfinement and to the chiral phase transition. The chiral phase transition is also related to the behavior of the condensate as a function of the temperature. Therefore, both at low- and high-energy nuclear physics, fundamental questions on the physics of strong interactions are related to the in-medium behavior of the quark condensate.

Chiral-symmetry restoration at finite baryon density is usually discussed in the context of quark matter, *i.e.* a system of deconfined quarks. For many systems like stable nuclei and neutron stars, quarks are confined within nucleons and are far from being free. The usual scenario for in-medium chiral restoration is Pauli blocking. That is, the quarks that occupy uniformly the Fermi sea contribute positively to the quark condensate and when this positive contribution is added to the negative contribution coming from the quarks in the Dirac sea, the absolute value of the condensate decreases. This decrease is the signal of the chiral restoration. The original model of Nambu and Jona-Lasinio [1] (NJL), reinterpreted in terms of quarks, has been the prototype model for such investigations [2,3].

In a recent publication [4] it was argued that once quarks are confined within nucleons, there is the possibility of an in-medium enhancement of the chiral breaking. This is because the momentum distribution of confined quarks is very different from that of free quarks and, depending on the dynamics of the constituent quarks, the Pauli blocking becomes less effective than in a Fermi sea of quarks. This is a very interesting result, with far reaching consequences for many experiments planned for the near future.

The author of ref. [4] substantiated his claim on the basis of a model inspired on Coulomb gauge QCD [5] (CgQCD). This model is basically a generalization of the NJL model in that instead of the point-like NJL interaction, it uses a confining potential. The wave functions of the clusters of three quarks were obtained using a variational approach [6]. In the present paper we reinvestigate this issue using the same ideas of ref. [4], but use a slightly different philosophy with respect to the dynamics. We employ the NJL model to generate the massive constituent quarks, and then confine them with a nonrelativistic potential in a way to obtain a nucleon cluster of three constituent quarks. Then we construct a Fermi sea of nucleon clusters and obtain the gap equation. In this way, one is able to investigate the differences in the Pauli blocking within the same basic underlying NJL model.

2 The model

We start considering chiral-symmetry restoration in quark matter in the context of the NJL model. For our purposes in the present paper it is sufficient to use the following two-flavor Lagrangian density [2,3]:

$$\mathcal{L} = i\bar{\psi}\gamma^\mu\partial_\mu\psi + G_S\left[(\bar{\psi}\psi)^2 - (\bar{\psi}\boldsymbol{\tau}\gamma_5\psi)^2\right], \qquad (1)$$

[a] e-mail: gkrein@ift.unesp.br

where ψ is the quark field operator (with color and flavor indices suppressed). For simplicity we have taken zero current quark masses. The energy density of quark matter,

$$\mathcal{E}_{\rm QM} = \frac{1}{V}\int {\rm d}^3x\, \langle QM|T^{00}(x)|QM\rangle, \tag{2}$$

where $|QM\rangle$ is the many-quark state and T^{00} is the zero-zero component of the energy-momentum stress-tensor

$$T^{\mu\nu}(x) = i\bar{\psi}\gamma^\mu\partial^\nu\psi(x) - g^{\mu\nu}\mathcal{L}. \tag{3}$$

In the mean-field approximation, the state $|QM\rangle$ can be written in a schematic way as

$$|QM\rangle = q^\dagger(\boldsymbol{k}_{\rm F})\cdots q^\dagger(\boldsymbol{k}_2)q^\dagger(\boldsymbol{k}_1)|\Omega\rangle, \tag{4}$$

where $q^\dagger(\boldsymbol{k})$ are constituent quark creation operators and $|\Omega\rangle$ is the vacuum of constituent quarks —we have suppressed color-flavor-spin indices. In this approximation, and not using the equations of motion of the quark field operator, $\mathcal{E}$ can be written as

$$\mathcal{E}_{\rm QM} = -(2N_fN_c)\int \frac{{\rm d}^3k}{(2\pi)^3}\frac{k^2}{E^*(k)}[1-n(k)] - G_S\,(2N_fN_c)^2\left\{\int\frac{{\rm d}^3k}{(2\pi)^3}\frac{M^*}{E^*(k)}[1-n(k)]\right\}^2, \tag{5}$$

where N_f and N_c are respectively the number of quark flavors and colors, $E^*(k) = (k^2+M^{*2})^{1/2}$, M^* is the in-medium constituent quark mass, and $n(k)$ is the quark density. For the state given in eq. (4), the quark density is simply

$$n(k) = \theta(k_{\rm F}-k), \tag{6}$$

with $k_{\rm F}$ being the quark Fermi momentum. The normalization of quark density is such that

$$\int_0^\infty {\rm d}^3k\, n(\boldsymbol{k}) = \frac{4\pi}{3}k_{\rm F}^3 \equiv \frac{\rho_q}{\gamma_q}, \tag{7}$$

where ρ_q and γ_q are respectively the quark density and degeneracy. The integrals in eq. (2) are ultraviolate divergent and a cutoff Λ has to be introduced. Since the model is nonrenormalizable, Λ is an additional parameter of the model.

The in-medium constituent quark mass M^* can be obtained by minimizing $\mathcal{E}_{\rm QM}$ with respect to M^*. The minimization leads to the usual gap equation [2,3]

$$M^* = 2\,G_S\,(2N_fN_c)\int^\Lambda \frac{{\rm d}^3k}{(2\pi)^3}\frac{M^*}{E^*(k)}[1-n(k)]. \tag{8}$$

Given the solution of this equation, one can calculate the in-medium quark condensate. The condensate of quark flavor $q(=u,d)$ is given by

$$\langle\bar{q}q\rangle = -2N_c\int^\Lambda \frac{{\rm d}^3k}{(2\pi)^3}\frac{M^*}{E^*(k)}[1-n(k)] = 2N_c\int^\Lambda\frac{{\rm d}^3k}{(2\pi)^3}\frac{M^*}{E^*_-(k)} + 2N_c\int_0^{k_{\rm F}}\frac{{\rm d}^3k}{(2\pi)^3}\frac{M^*}{E^*_+(k)}, \tag{9}$$

where $E^*_\pm(k) = \pm(k^2+M^{*2})^{1/2}$.

The last two lines in eq. (9) are written in a way to make clear the physical interpretation of the effect of the Fermi sea of constituent quarks: the positive-energy quarks of the Fermi sea add a positive contribution to the condensate and therefore cancel the contributions of the negative-energy quarks of the Dirac sea. The positive contribution of the Fermi sea is a monotonically increasing function of quark Fermi momentum $k_{\rm F}$, and leads to a partial restoration of chiral symmetry in a medium with a finite quark density. This is the basis of the common wisdom of the in-medium decrease of (the absolute value of) the condensate.

Next, we populate the positive-energy states with clusters of three constituent quarks confined by a potential. The Fermi sea is now is written as

$$|NM\rangle = N^\dagger(\boldsymbol{p}_{\rm F})\cdots N^\dagger(\boldsymbol{p}_2)N^\dagger(\boldsymbol{p}_1)|\Omega\rangle, \tag{10}$$

where the $N^\dagger(\boldsymbol{p})$ are nucleon creation operators. These are written in terms of the constituent quark creation operators as

$$N^\dagger(\boldsymbol{p}) = \int {\rm d}^3k_1{\rm d}^3k_2{\rm d}^3k_3\,\Psi_{\boldsymbol{p}}(\boldsymbol{k}_1,\boldsymbol{k}_2,\boldsymbol{k}_3) \times q^\dagger(\boldsymbol{k}_1)q^\dagger(\boldsymbol{k}_2)q^\dagger(\boldsymbol{k}_3), \tag{11}$$

where $\Psi_{\boldsymbol{p}}$ is the Fock-space amplitude for a nucleon with c.m. momentum $\boldsymbol{p}$. In the equations above we have suppressed nucleon spin-isospin indices and, as usual, quark color-spin-flavor indices.

In order to confine the constituent quarks, we add a nonrelativistic two-body harmonic-oscillator potential and write for $\Psi_{\boldsymbol{p}}$

$$\Psi_{\boldsymbol{p}}(\boldsymbol{k}_1\boldsymbol{k}_2\boldsymbol{k}_3) = \delta(\boldsymbol{p}-\boldsymbol{k}_1-\boldsymbol{k}_2-\boldsymbol{k}_3)\Phi_{\boldsymbol{p}}(\boldsymbol{k}_1\boldsymbol{k}_2\boldsymbol{k}_3), \tag{12}$$

and for Φ we make a Gaussian ansatz [6],

$$\Phi_{\boldsymbol{p}}(\boldsymbol{k}_1\boldsymbol{k}_2\boldsymbol{k}_3) = \left(\frac{3b^4}{\pi^2}\right)^{\frac{3}{4}}\exp\left[-\frac{b^2}{2}\sum_{i=1}^3\left(\boldsymbol{k}_i-\frac{\boldsymbol{p}}{3}\right)^2\right], \tag{13}$$

where b is the variational parameter. This leads to the following normalization for the amplitude Ψ:

$$\langle\Psi_{\boldsymbol{p}'}|\Psi_{\boldsymbol{p}}\rangle = \delta(\boldsymbol{p}'-\boldsymbol{p}). \tag{14}$$

In the mean-field approximation, and neglecting effects of quark-exchange between different nucleons [7], the energy density of nuclear matter,

$$\mathcal{E}_{NM} = \frac{1}{V}\int {\rm d}^3x\,\langle NM|T^{00}(x)|NM\rangle, \tag{15}$$

is given by precisely the same form as in eq. (5), but with a different quark momentum distribution $n(k)$. For the ansatz in eqs. (12) and (13), the quark momentum distribution in the state of clustered matter, eq. (10), is given by

$$n(\boldsymbol{k}) = \int_0^{p_{\rm F}} {\rm d}^3p\, n_{\boldsymbol{p}}(\boldsymbol{k}), \tag{16}$$

with

$$n_{\boldsymbol{p}}(\boldsymbol{k}) = \left(\frac{3b^2}{2\pi}\right)^{\frac{3}{2}} \exp\left[-\frac{3}{2}b^2\left(\boldsymbol{k} - \frac{1}{3}\boldsymbol{p}\right)\right]. \tag{17}$$

The quark distribution function is normalized as

$$\int_0^\infty \mathrm{d}^3k\, n(\boldsymbol{k}) = \frac{4\pi}{3}p_{\mathrm{F}}^3 \equiv \frac{\rho_N}{\gamma_N}. \tag{18}$$

For symmetrical nuclear matter,

$$\frac{\rho_N}{\gamma_N} = \frac{\rho_q}{\gamma_q}, \tag{19}$$

and therefore quarks and nucleons have the same Fermi momentum, $k_{\mathrm{F}} = p_{\mathrm{F}}$

The gap equation has the same form as in eq. (8), but now it is coupled with the equation for b, the variational parameter of the nucleon amplitude. Numerical results are presented in the next section.

3 Numerical results

Initially we fix the parameters to vacuum properties. Using $\Lambda = 0.7$ GeV and $G_S\Lambda^2 = 2.14$, we obtain for the constituent quark mass the value $M = 335$ MeV and for the condensate $\langle\bar{q}q\rangle = (-268\ \mathrm{MeV})^3$. We adjust the spring constant of the confining potential to obtain for the size parameter of the nucleon the value $b = 0.5$ fm. Then the nucleon mass can be fitted by adding a negative constant to the potential, as usually done in quark potential models.

Next, we solve the gap equation and minimize the nucleon mass with respect to the size parameter. The solutions will be M^* and b^*. We are interested in the behavior of the quark condensate as a function of the nucleon density. In fig. 1 we present the ratio of the in-medium to vacuum condensates, as a function of the ratio of the nucleon density to the saturation density of normal nuclear matter. The figure shows that the (absolute value of the) condensate in medium decreases monotonically with the density. In addition, clearly there is no sign of reversing this tendency.

The result shown in fig. 1 is easy to understand. The gap equation always gives a density dependence of the mass for the constituent quarks that is monotonically decreasing as the density increases. Therefore, the kinetic energy of the quarks in the nucleon bound state tends to increase, leading to the swelling of the nucleons. In order to obtain an increase of $|\langle\bar{q}q\rangle|$ in medium, the nucleon should shrink, as argued in ref. [4]. In the CgQCD model of ref. [4], there is a spin-spin force that induces a very strong attraction as the symmetry becomes restored. This attraction then leads to a shrinking of the nucleon. In the present model this is impossible, and the usual scenario of chiral symmetry restoration is maintained.

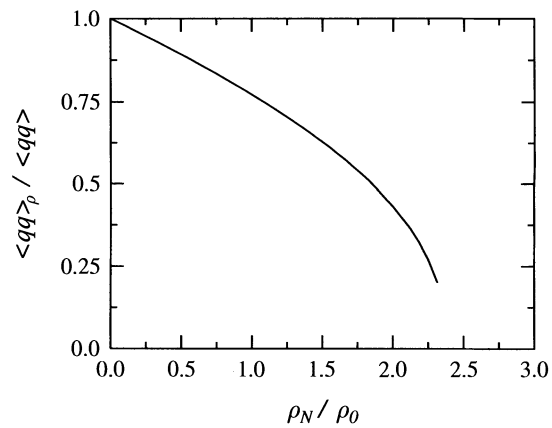

Fig. 1. The ratio of the in-medium to vacuum condensates as a function of the ratio of the nucleon density to the saturation density of normal nuclear matter.

4 Conclusions and perspectives

In the present paper we have shown that the question of an enhancement of the chiral breaking in hadronic matter as argued in ref. [4] seems to be model dependent. This is because the basic mechanism that could drive an enhancement depends crucially on a very attractive interaction that becomes stronger as the symmetry is restored. In ref. [4] the attraction comes from a spin-spin force that is a consequence of the very peculiar form of the confining potential used there. It would be interesting to investigate this question further with another spin-dependent interaction, such as transverse-gluon interactions that have been shown [5] to play an important role in the mechanism of dynamical chiral symmetry breaking.

Certainly the issue is very interesting and, in order to make progress, it is necessary to have a better understanding on the dynamics of the interaction that drives the symmetry breaking.

References

1. Y. Nambu, G. Jona-Lasinio, Phys. Rev. **122**, 345 (1961); **124**, 246 (1961).
2. T. Hatsuda, T. Kunihiro, Phys. Rev. Lett. **55**, 158 (1985).
3. V. Bernard, U.-G. Meissner, I. Zahed, Phys. Rev. D **36**, 819 (1987).
4. P.J.A. Bicudo, Phys. Rev. Lett. **72**, 1600 (1994).
5. A. Amer, A. Le Yaouanc, L. Oliver, O. Pene, J.C. Raynal, Phys. Rev. Lett. **50**, 87 (1983); Phys. Rev. D **28**, 1530 (1983); P.J.A Bicudo, J.E. Ribeiro, Phys. Rev. D **42**, 1611; 1625; 1635 (1990).
6. P.J.A Bicudo, G. Krein, J.E.F.T. Ribeiro, Phys. Rev. C **64**, 025202 (2001); Phys. Rev D **45**, 1673 (1992).
7. M.E. Bracco, G. Krein, M. Nielsen, Phys. Lett. B **432**, 258 (1998).

Eur. Phys. J. A **18**, 515–519 (2003)
DOI 10.1140/epja/i2002-10273-7

THE EUROPEAN PHYSICAL JOURNAL A

Exploring superdense matter at RHIC

B.V. Jacak[a]

Department of Physics, Stony Brook University, SUNY, Stony Brook, NY, 11794, USA

Received: 30 September 2002 /
Published online: 22 October 2003 – © Società Italiana di Fisica / Springer-Verlag 2003

Abstract. I report first results on Au + Au collisions at $\sqrt{s}$ = 130 GeV per nucleon pair from all four experiments at the Relativistic Heavy Ion Collider.

PACS. 25.75.Dw Particle and resonance production

1 Introduction

RHIC collides the heaviest possible ions at the highest possible energy to create matter at maximum temperature and density. These collisions should reproduce the conditions that existed in the first microseconds after big bang, where the distances among hadrons were much smaller than the size of the hadrons themselves. Such conditions probably still occur in the universe, at the core of neutron stars. Quantum chromodynamics indicates that under such extreme conditions quarks and gluons are no longer confined into hadrons, but rather exist as a plasma, with constituents free to roam over the entire volume of the hot matter. We seek to reproduce these conditions in the laboratory and study the properties of such matter. I will describe results from the first run of the Relativistic Heavy Ion Collider at Brookhaven National Laboratory. In 2000, gold ions were collided with each other at a center of mass energy of 130 GeV per nucleon pair. The 2001 run of RHIC reached 200 GeV per nucleon pair.

The QCD potential between quarks increases linearly in strength with the distance between quarks and confines them into hadrons. At high density and/or temperature, the color charges of the quarks are screened, decreasing the potential. At sufficiently high temperature/density, the potential at large distance vanishes altogether, and the system should undergo a phase transition to quark gluon plasma. It has been further proposed that the gluon density just after the nuclei collide could be so large that the gluon distribution is saturated.This happens if the wavefunctions of partons overlap sufficiently that the self-coupling gluons fuse. In effect, the gluons become weakly coupled and may be treated as a classical field. This would imply a different initial condition for the quark gluon plasma formation.

In the strongly coupled regime of the quark gluon plasma, QCD cannot be solved perturbatively, and calculations are carried out via simulation on a lattice. Recent progress in computational technology has allowed large-scale lattice simulations at high temperature. Karsch, Laermann and Peikert showed that the energy density of a 3 flavor system experiences a rapid rise when the temperature reaches 170 ± 10 MeV, characteristic of a phase transition [1]. The calculation indicates that experiments must achieve an energy density of 1–3 GeV/fm^3 to enter the quark gluon plasma regime.

Four complementary experiments have been carried out at the Relativistic Heavy Ion Collider at Brookhaven National Laboratory in Upton, NY. Beams start in a Tandem Van de Graaf accelerator, then enter the Booster, Alternating Gradient Synchrotron, and finally RHIC. After filling, RHIC accelerates each beam to 100 GeV per nucleon, and then brings the beams into collision in up to 6 intersection regions around the ring. The design of RHIC is for luminosities of $2 \times 10^{26}\,\mathrm{cm}^{-2}\mathrm{s}^{-1}$.

There are two large and two smaller experiments currently running at RHIC. BRAHMS, one of the small experiments, consists of a pair of movable small-acceptance spectrometers with good particle identification capability. BRAHMS is optimized to sample the particle distributions over a wide range of longitudinal velocity. The other small experiment is PHOBOS, which employs highly granular silicon detectors to count all charged particles and measure the particle spectra at low momentum near the rapidity of the center of mass of the collision. PHOBOS also has hadron identification by time-of-flight. It is optimized to search for large distance phenomena and fluctuations in particle production. PHENIX is a large experiment optimized to measure leptons and photons to probe the early time of the collision via electromagnetically interacting probes. PHENIX has high rate capability and selective triggers to measure rare processes, in both electromagnetic and hadronic observables. STAR is the other large experiment and consists primarily of a large time projection chamber. STAR is optimized to have large acceptance for

[a] e-mail: Barbara.Jacak@stonybrook.edu

hadrons to study particle production and event-by-event fluctuations.

When two nuclei collide at RHIC, they are highly Lorentz contracted and the initial nucleon-nucleon collisions all take place in less than 1 fm/c. Nucleons undergo multiple collisions that do not factorize well in time, making theoretical description of the low-momentum-transfer processes very challenging; models of the collisions are crucial tools. At $\sqrt{s}$ of 130 or 200 GeV per nucleon pair, the collisions can probe parton distributions near $x = 10^{-2}$. At such short distances, the interactions that take place are necessarily at the partonic, rather than hadronic level. Large Q^2 processes are in the weakly coupled regime and may be calculated by perturbative QCD, with the collision probability given by nuclear structure functions. The large number of individual collisions gives rise to copious secondary particle production and a parton cascade results. Around 10^4 gluons, quarks and antiquarks are produced, and it is these produced partons which are expected to thermalize and form a quark gluon plasma.

The cascade of parton interactions is modeled using a cutoff separating "hard" from "soft" processes, handling the former perturbatively and the latter via string models of particle production (such as the Lund model). Thermalization on the timescale of 1 fm/c is predicted [2]. Of course, the thermalized system expands into the vacuum, cooling and eventually re-hadronizing. Experimentally, the challenge is to deal with many thousands of particles in the final state and identify observables which illuminate the underlying physics. I separate the observables into two classes.

One class of observables reflects the collision dynamics and addresses the extent of equilibration. Measures of collective behavior and the pressure generated in the collision fall into this class, along with hadron spectra and correlations which map the space-time evolution of the hadronic part of the collision. The other class of observables consists of probes of the early, hot phase of the collision. Such probes are particles produced early in the collision, which either do not interact with the hot, dense medium at all (such as thermal radiation) or which interact with the medium differently than with normal nuclear matter. These include fast quarks which lose energy depending on the density of scattering centers in a colored medium, charm quarks and antiquarks created by gluon fusion, the $c\bar{c}$ bound state J/ψ which can be dissolved by screening in a colored medium, and strange quarks formed more easily by a hot medium.

2 Thermodynamics of dense matter

It is important to first ascertain that the initial conditions at RHIC are in fact sufficient for creation of quark gluon plasma. This is generally addressed by measuring the number of produced particles and the energy flow perpendicular to the direction of the beams. At RHIC, over 5000 charged particles are formed in collisions of two gold nuclei at small impact parameter, *i.e.* in central collisions [3]. Compared to p-p collisions at the same $\sqrt{s}$, the number of charged particles produced per interacting nucleon pair is considerably higher. All four experiments find more than 3 charged particles per nucleon pair in central Au + Au, rather than the 2 seen in p-p.

Measurement of the energy flow transverse to the beam allows estimation of the energy density attained in the early phase of the collision, prior to expansion and cooling. PHENIX measured the transverse energy,

$$E_{\mathrm{T}} = \sum_i E_i \sin\theta_i \,,$$

where the sum runs over produced particles at mid-rapidity [4]. For central collisions at $\sqrt{s} = 130$ GeV per nucleon pair, E_{T} per unit rapidity equals 503±2 GeV. This can be used to estimate the energy density assuming longitudinal expansion at the speed of light, using Bjorken's formula

$$\epsilon_{\mathrm{Bj}} = \frac{1}{\pi R^2}\frac{1}{2c\tau_0}(2\frac{\mathrm{d}E_{\mathrm{T}}}{\mathrm{d}y}) \,,$$

yielding $\epsilon \geq 4.6$ GeV/fm^3. This is 50% higher than previously observed and is comfortably above the threshold predicted by lattice QCD. The value has a significant uncertainty because the value of the parton formation time τ_0 is not well known. The value given here uses 1 fm/c, which is almost certainly an overestimate.

As many particles are produced in a rather small volume, one may expect that significant pressure is developed in the early stage of the collision. To quantify this experimentally, we need a "barometer" for heavy-ion collisions. Such a barometer is available by measuring collective "elliptic flow" of particles in each collision. The origin of the elliptic flow is the spatial anisotropy of the overlap region of two nuclei (this overlap region only approaches isotropy for the most central collisions). Extensive rescattering of the particles in the evolving system can translate the spatial anisotropy to a momentum space anisotropy as it is easier to emit particles in the thinner direction of the almond-shaped overlap region. The anisotropy is experimentally accessible by Fourier analysis of the azimuthal distribution of particles. One can identify in each event a preferred direction, which is aligned with the reaction plane, or direction of the impact parameter between the two nuclei. The second harmonic Fourier coefficient of the azimuthal distribution of particles with respect to the reaction plane, known as v_2 is used to quantify the collective elliptic flow. STAR showed that v_2 reaches 6% in semi-peripheral collisions of Au + Au [5], and the magnitude of v_2 is quite well reproduced by hydrodynamical models of the collision [6]. The other three experiments have confirmed this high value of v_2.

As hydrodynamics, by definition, treats the medium as fully equilibrated, its applicability to the early stage of the collision while the spatial anisotropy is still large implies early equilibration of the matter at RHIC. It should be noted that RHIC produces the highest-energy heavy-ion collisions so far, and this is the first time that hydrodynamics provides an accurate description of experimental observables.

Eventually the expansion cools the system below the critical temperature and the quark gluon plasma hadronizes. The thermodynamics of the hadron gas is studied via distributions of emitted hadrons in the final state. These reflect the temperature of the system when the hadrons cease to interact: the relative yields are fixed when the inelastic collisions stop (chemical freeze-out), and the spectra are determined later, at the time of kinetic freeze-out. The hydrodynamic flow affects the system during its entire thermal history. Hadrons are identified by time-of-flight (PHENIX, PHOBOS and BRAHMS) or energy loss in gas detectors (STAR and BRAHMS).

To evaluate the chemical freeze-out temperature, hadron yields from all four experiments are used. Braun-Munzinger, Magestro, Redlich and Stachel assumed emission of hadrons from a chemically and thermally equilibrated gas [7]. They fit the ratios of different hadron yields according to a Grand Canonical ensemble and extracted the temperature and baryo-chemical potential for central Au + Au collisions at RHIC. They found a baryo-chemical potential of 51 MeV, corresponding to a nearly, but not quite, *net* baryon-free gas at central rapidity. The observed antibaryon-to-baryon ratios near 1 at mid-rapidity confirm this [8]. The chemical freeze-out temperature of 175 MeV from their fit is surprisingly near that expected for the hadronization phase transition. This implies that the hadrons are created in chemical equilibrium from the plasma, and the expansion is so explosive that the hadrons decouple immediately, undergoing no inelastic collisions. This is in qualitative agreement with prediction of hydrodynamics, though the density at hadronization is predicted to be very large and one would naively expect *some* hadronic interactions to take place once the hadrons are formed.

The hydrodynamic models which reproduce the elliptic flow, v_2, indicate very rapid expansion [6,9], which should give rise to a collective radial expansion in addition to the observed elliptic flow. The radial expansion can be measured with spectra of hadron momenta transverse to the beam. In order to use hadrons of different masses, the spectra are plotted as a function of transverse mass, $m_{\mathrm{T}}^2 = p_{\mathrm{T}}^2 + m_0^2$. PHENIX [10], followed by BRHAMS, showed that the proton spectrum is flatter in m_{T} than the lighter mesons. Such a flattening would be expected if all particles receive a collective velocity boost, resulting in a larger momentum boost for the heavier hadrons. Fitting the observed pion, kaon, proton and antiproton spectra simultaneously, PHENIX found that they could be described by emission from a gas at 140–150 MeV temperature, expanding radially about the beam direction at a mean velocity of approximately half the speed of light. In peripheral collisions, the kinetic freeze-out temperature does not change much, but the radial flow is considerably less.

The large radial flow velocity causes the proton yield to nearly equal that of the pions at transverse momenta larger than approximately 2 GeV/c [10]. Such a "crossing" of the spectra has never been observed before, and impacts the interpretation of high-momentum particle production. It is noteworthy that the hydrodynamical calculations successfully reproduce the hadron spectra, including the cross of the baryon spectra over that of the mesons [6,9].

Another experimental observable sensitive to the expansion of the hadronic source is two-particle correlations. Identical pion pairs and identical kaon pairs, following Bose-Einstein statistics, experience final-state interactions that reflect the particle density and momentum distributions at freezeout. Thus the study of correlation functions of identical bosons is a further tool to understand the expansion dynamics. Both STAR [11] and PHENIX [12] have observed smaller apparent source radii and stronger dependence of the correlation on particle momentum than is expected from the above picture of an expanding hadron gas. It remains one of the mysteries at RHIC that hydrodynamics can explain single-hadron spectra and multi-hadron correlations, but fails to reproduce the observed two-hadron correlations.

3 Hard processes as early stage probes

We have already seen that there is copious production of particles and development of significant pressure early in the collision —these give rise to the observed radial and elliptic flows and indicate that high densities are achieved. There exists, however, a more direct probe of the early density and its effects on gluon transport by the medium. The probe is a high momentum quark or gluon, arising from hard scattering of partons in the initial nucleon collisions. These partons are scattered early, at a rate calculable by perturbative QCD, and traverse the hot, dense medium on their way out of the collision region. As they traverse the colored medium, these scattered partons radiate gluons, and the radiation rate is sensitive to the density of the medium [13,14]. There is a characteristic formation time, which depends on the transverse momentum of the radiated gluon. If the medium is sufficiently dense, the mean free path can be less than the distance the parton travels before the radiation is complete. In this case, the radiation becomes coherent, and the amount of energy radiated can change substantially. Radiation by partonic probes has observable effects as it decreases the production of high-p_{T} particles when the scattered parton fragments into a hadronic jet. The process is referred to as "jet quenching" and can be measured experimentally via the spectrum of leading high-p_{T} particles from jet fragmentation or by azimuthal correlations of the leading particle from each of the two hard-scattering partons.

Both PHENIX and STAR measured the hadron spectrum to large transverse momentum ($p_{\mathrm{T}} \approx 5$ GeV/c). PHENIX alone made three separate measurements of the spectrum of charged hadrons and of identified π^0's [15]. In all channels the observed spectra in peripheral collisions of Au + Au nuclei agree well with the spectrum predicted by folding individual p-p collisions by the number of binary nucleon-nucleon collisions corresponding to the selected centrality range. However, this is not the case in central collisions. The spectral shape is more exponential than the scaled p-p spectrum, and the observed yield is well below that expected by scaling individual p-p collisions by the

approximately 900 binary nucleon-nucleon collisions corresponding to the most central 10% of Au + Au collisions. The suppression is by a factor of 3–4 for π^0 and a factor of approximately 2 for charged hadrons.

Comparing the measurements at RHIC to those at lower energy at the SPS makes the observation even more striking. At the SPS, the yield in central Pb + Pb was not only not suppressed, it was actually *enhanced* due to multiple scattering of the incoming partons in the nuclear medium prior to the hard scattering which sends them to large p_{T}. This initial state scattering, referred to as the "Cronin effect" is well known from p + nucleus collisions and should occur at RHIC as well. If so, the actual suppression of high-p_{T} hadrons is even larger than that inferred by comparing to scaled p-p collisions! We have investigated the importance of another known nuclear effect upon the parton distributions, namely nuclear shadowing. This occurs at small momentum fraction, x, in large nuclei, due to recombination of nearby partons from the overlapping parton clouds in neighboring nucleons. Moderate to large Q^2 processes at RHIC reach $x \approx 2 \times 10^{-2}$. However, data and calculations show that quark and gluon shadowing have less than 10% effect at these modestly small x values. Thus nuclear shadowing cannot explain the suppression, supporting its interpretation as a first observation of jet quenching.

We can understand the difference in the suppression of charged hadrons and identified neutral pions recalling the momentum boost for protons from the collective radial flow. The near parity of baryon or antibaryon yields and pion yields at 2 GeV/c leads one to expect a smaller suppression factor for all hadrons compared to just pions. This is because the boost applies to particles produced by "soft" processes, rather than those arising from jet fragmentation. These soft particles should not be sensitive to the hard-scattered parton energy loss. It would appear from the existing data that this is so. An important corollary is that the large hydrodynamic boost extends the p_{T} region where non-perturbative processes contribute substantially to the particle yields. This seems to be the case in Au + Au collisions at RHIC for $p_{\mathrm{T}} \leq 3$ GeV/c.

The data suggest that there is substantial energy loss by partons traversing the dense medium created in central Au + Au collisions. This can be tested and quantified by comparison to model calculations. One such calculation has been made by X.N. Wang and co-workers, taking into account the expected nuclear shadowing and Cronin effects [16]. The data are best described by inclusion of an energy loss of 0.25 GeV/fm. This value seems rather low, and is in fact very close to that expected in cold nuclear matter. However, this is an average value over the lifetime of the medium, which is not at all static. Taking into account the rapid expansion of the medium, the data require an initial energy loss closer to 7 GeV/fm. This is large indeed.

Another probe of the medium is charmed quark production. The primary formation mechanism for charm and anti-charm quark pairs is gluon fusion. Thus the production rate should be sensitive to the gluon number and distribution and may be expected to increase in the presence of hot plasma with many gluons. Furthermore, spectroscopy of the bound $c\bar{c}$ states offers an excellent probe of the color screening capability of the medium.

By observation of single-electron production in Au + Au collisions, PHENIX can measure the rate of open charm (D-meson) production [17]. Unambiguous identification of the few electrons among the many charged particles produced is technically very challenging, but PHENIX accomplishes this by use of a Ring Imaging Čerenkov Counter with photomultiplier tube readout, in concert with a very granular electromagnetic calorimeter. Electrons produce Čerenkov light, and their energy in the calorimeter should match the measured momentum. Comparison to a calculation of hadronic decay sources of electrons along with photon conversions in the detector material of PHENIX provides a measure of the D-meson production cross-section. The background calculation is tuned using measured hadron yields. The result shows that the charm yield matches very well that expected from cross-sections measured in p-p and p-antiproton collisions. Thus, there appears to be no enhancement of charm production, nor energy loss as observed for the light quarks. It may, of course, be that Mother Nature is very sly and the two effects happen to cancel exactly. But this is not extremely likely.

4 Conclusions

First results from RHIC have shown that the final state in central Au + Au collisions consists of more than 5000 charged particles, and the energy density achieved early in the collision is well above the threshold predicted by Lattice QCD for deconfinement. High pressure is developed early in the collision, leading to a very significant collective elliptic flow. The fact that the system "remembers" the initial spatial asymmetry indicates that thermalization must occur rapidly. Chemical freeze-out of the hadrons from this system occurs near 170 MeV, which is also the temperature at which the transition back to hadrons is expected.

Hard processes with large momentum transfer at RHIC are important. They boost the number of produced particles and result in significant production of charmed quarks and scattered light quarks and gluons to probe the medium. A deficit of high-p_{T} particles from the fragmentation of these scattered partons is observed in central collisions, which may be the first indication of jet quenching. Charmed quarks are not suppressed, which could indicate that their larger mass suppresses collinear gluon radiation.

The second run at RHIC collected significantly more data, allowing measurements to higher transverse momenta, correlations among particles from jets, multi-strange baryon spectra, direct photon measurements and a first look at charmonium spectroscopy. Furthermore, the baseline physics in proton-proton collisions has been measured in the same detectors. Subsequent RHIC runs will provide proton-nucleus data to quantify nuclear effects

and will then allow study of the volume and energy dependence of the collision dynamics and probes of the hottest, densest phase.

So, is there quark gluon plasma being made at RHIC? At this point there is not yet an unambiguous answer. However, the evidence for early thermalization, high temperature achieved, and energy loss by fast quarks suggest that there is indeed quark gluon plasma at RHIC. Proton-nucleus reference data is absolutely essential to demonstrate that these are indeed the correct interpretations of the data.

References

1. F. Karsch, E. Laermann, A. Peikert, Phys. Lett. B **478**, 447 (2000).
2. K. Geiger, Phys. Rev. D **48**, 4129 (1993).
3. PHOBOS Collaboration (B.B. Back *et al.*), Phys. Rev. Lett. **87**, 102303 (2001).
4. PHENIX Collaboration (K. Adcox *et al.*), Phys. Rev. Lett. **87**, 052301 (2001).
5. STAR Collaboration (C. Adler *et al.*), Phys. Rev. Lett. **86**, 402 (2001).
6. P.F. Kolb, P. Huovinen, U. Heinz, H. Heiselberg, Phys. Lett. B **500**, 232 (2001).
7. P. Braun-Munzinger, D. Magestro, K. Redlich, J. Stachel, Phys. Lett. B **518**, 41 (2001).
8. STAR Collaboration (C. Adler *et al.*), Phys. Rev. Lett. **86**, 4778 (2001); PHOBOS Collaboration (B. Back *et al.*), Phys. Rev. Lett. **87**, 102301(2001); BRAHMS Collaboration (I.G. Bearden *et al.*), Phys. Rev. Lett. **87**, 112305 (2001).
9. D. Teaney, J. Lauret, E. Shuryak, Phys. Rev. Lett. **86**, 4783 (2001) and nucl-th/0110037.
10. PHENIX Collaboration (K. Adcox *et al.*), Phys. Rev. Lett. **88**, 242301 (2002).
11. STAR Collaboration (C. Adler *et al.*), Phys. Rev. Lett. **87**, 082301 (2001).
12. PHENIX Collaboration (K. Adcox *et al.*), Phys. Rev. Lett. **88**, 192302 (2002).
13. M. Gyulassy, M. Pluemer, Phys. Lett. B **243**, 432 (1990); X.N. Wang, M. Gyulassy, Phys. Rev. Lett. **68**, 1480 (1992).
14. R. Baier, Yu.L. Dokshitzer, A.H. Mueller, S. Peigne, D. Schiff, Nucl. Phys. B **483**, 291 (1997); **484**, 265 (1997).
15. PHENIX Collaboration (K. Adcox *et al.*), Phys. Rev. Lett. **88**, 022301 (2002).
16. X.N. Wang, E. Wang, Phys. Rev. Lett. **89**, 162301 (2002).
17. PHENIX Collaboration (K. Adcox *et al.*), Phys. Rev. Lett. **88**, 192303 (2002).

Eur. Phys. J. A **18**, 521–525 (2003)
DOI 10.1140/epja/i2002-10274-6

THE EUROPEAN PHYSICAL JOURNAL A

Electron-positron pairs as a probe for hadrons in dense matter

J.P. Wessels[a]

Gesellschaft für Schwerionenforschung, Planckstr. 1, D-64291 Darmstadt, Germany

Received: 30 September 2002 /
Published online: 22 October 2003 – © Società Italiana di Fisica / Springer-Verlag 2003

Abstract. In this paper the latest results from the analysis of e^+e^--pairs emitted in Pb + Au collisions at 40 AGeV/c and a combined analysis of all data available at 158 AGeV/c are presented. The enhancement of low-mass e^+e^--pairs ($m_{ee} > 0.2\,\mathrm{GeV}/c^2$) with respect to the expected yield from hadron decays first reported at 158 AGeV/c is also found at 40 AGeV/c and is even larger there. Comparing to various theoretical models based on $\pi^+\pi^-$ annihilation, the data can only be reproduced, if the properties of the intermediate ρ in the hot and dense medium are modified. Hadron data taken at the same beam energies sheds light on the dynamical evolution of the fireball and addresses the question whether the medium modification is linked to baryon density rather than temperature. In the future e^+e^--pairs emitted in heavy-ion collisions will be measured at the LHC with the ALICE Transition Radiation Detector (TRD). Here, special emphasis will be put on the production of heavy vector mesons (J/ψ, Υ).

PACS. 25.75.-q Relativistic heavy-ion collisions – 12.38.Mh Quark-gluon plasma – 13.85.Qk Inclusive production with identified leptons, photons, or other nonhadronic particles

1 Introduction

Along with the deconfinement phase transition to the quark gluon plasma (QGP), chiral symmetry is expected to be restored. The energy density at which the phase transition is predicted by two-flavor lattice calculations is $\epsilon \approx 0.7\,\mathrm{GeV/fm^3}$ [1] with large errors due to uncertainties in the critical temperature. Simple estimates employing the Bjorken expansion scenario [2] show that the initial energy density reached in central Pb + Pb collisions is about $3\,\mathrm{GeV/fm^3}$ at the full SPS energy. The totality of the observables has led to the announcement that a new state of matter is indeed formed in central heavy-ion collisions at the SPS [3]. The measurement of e^+e^--pairs is particularly well suited to study this matter since they are emitted throughout the entire collision and are themselves not subject to the strong final-state interaction. In this context, the decay of the ρ vector meson into e^+e^--pairs is of particular interest, due to its direct link to chiral-symmetry restoration. Because of the short lifetime (1.3 fm/c), e^+e^--pairs from ρ decays are dominated by decays within the hot and dense medium, directly mirroring its properties. Experimentally, however, the study of e^+e^--pairs is notoriously difficult, because of the small production cross-section as well as the large combinatorial background in heavy-ion collisions. This paper will be subdivided into two parts. The first part focuses on data taken at two different beam energies with the CERES-Experiment at the SPS. We briefly describe the experimental setup, followed by a description of the electron analysis procedure. We then present results from a combined analysis of all the data that were taken at the full SPS energy of 158 AGeV and the final results of the data taken at 40 AGeV are shown. A comparison of the data to models and a discussion of the fireball evolution concludes this part.

The second part will deal with future measurements of e^+e^--pairs with the ALICE Transition Radiation Detector (TRD) at the LHC with focus on the prospects of heavy vector mesons (J/ψ, Υ) measurements.

2 The CERES experimental setup

The CERES spectrometer is optimized to measure e^+e^--pairs in the mass range up to about $1\,\mathrm{GeV}/c^2$ in the range $2.1 < \eta < 2.65$ close to midrapidity. A cross-section through the azimuthally symmetric setup is shown in fig. 1.

A segmented micro target (8 disks of Au of 25 μm thickness and 600 μm diameter evenly spaced along 22 mm) is followed by a set of two Silicon Drift Detectors (SDD1/ SDD2) at a distance of 10 cm and 13 cm, respectively. The segmentation minimizes conversions of photons in the target. The set of silicon drift detectors provides precise determination of the angles of all charged particles, determination of the event vertex, and the total charged-particle multiplicity for each event. Along

[a] e-mail: j.wessels@gsi.de

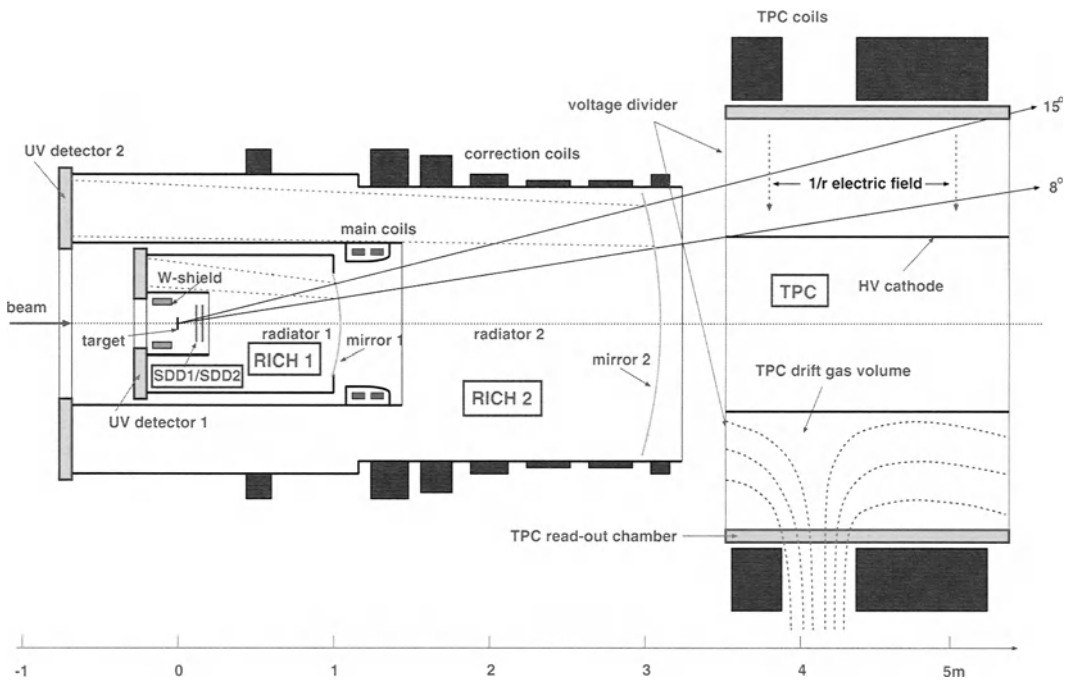

Fig. 1. The CERES experimental setup.

with the position measurement the specific energy loss is recorded for each charged particle.

Electrons are identified with two Ring Imaging Čerenkov counters (RICH1/2) which are operated at a threshold of $\gamma_{\rm th} = 32$ suppressing more than 99% of all charged hadrons. In 1995/96 the spectrometer was operated with a radial magnetic field provided by two air coils with counter-running current in between the two RICHes [4]. With this setup a mass resolution of about 6% was reached in the mass region of the ρ/ω.

For the runs in 1999/2000 the experiment was upgraded by the addition of a radial TPC [5] inside a separate radial magnetic field ($B_{\rm max} = 0.5\,{\rm T}$). Over the total length of 2 m a maximum of 20 hits are recorded for each charged-particle track. In the 1999 analysis a mass resolution of about 4.2% was achieved in the ρ/ω region, when tracks were fully reconstructed. For the 2000 data the goal is to reach with better calibration about 2%. For runs with the TPC the magnetic field between the RICHes was switched off and electrons were identified by combining the two RICHes, improving the electron efficiency to about 90% (as compared to about 70% in 1995/1996).

The data taken in 1995 and 1996 used the original CERES setup without the TPC. All data taken thereafter employed the upgraded setup shown in fig. 1. The new read-out of the experiment was only partially operational for the low-energy run at 40 AGeV/c in 1999 limiting both statistics and performance. The large data sample with about 36 million central events taken in 2000 at the full SPS energy is still being analyzed.

3 Electron analysis

While e^+e^--pairs are an attractive probe, they are notoriously hard to measure due to the small production cross-section and the enormous combinatorial background from unrecognized photon conversions and π^0 Dalitz decays. The analysis steps for the 1995/96 data are detailed in ref. [6]. Here, we only describe the analysis of data taken with the TPC and the field between the RICHes turned off. Electron candidates are selected when ten or more photon hits in RICH1 and RICH2 form a ring with asymptotic radius. To those candidates a transverse-momentum cut of 200 MeV/c is applied reducing contributions from π^0 Dalitz decays and conversions by about a factor of 10. Electron identification is further improved, removing high-$p_{\rm t}$ pions and accidental matches between the RICHes and the TPC, by a cut on specific energy loss in the TPC *vs.* momentum. Those conversions and Dalitz pairs with very small opening angles that do not lead to separate rings in the RICHes are efficiently removed by rejecting tracks with large specific energy loss in both silicon drift detectors. Further, electron candidates without a match in the TPC within 70 mrad of an electron track are also removed. The complete set of cuts employed in the analysis is shown in detail in ref. [7–9]. Finally, the invariant-mass spectrum of e^+e^--pairs is obtained by subtracting twice the geometric average of the remaining like-sign pairs from the remaining unlike-sign pairs ($N_{e^+e^-} - 2\sqrt{N_{e^+e^+} \cdot N_{e^-e^-}}$).

4 Invariant-mass spectrum of e^+e^--pairs: Pb + Au at 158 AGeV/c

Analyses of the invariant-mass spectra of e^+e^--pairs from the runs in 1995/1996 have been published [10–12]. In

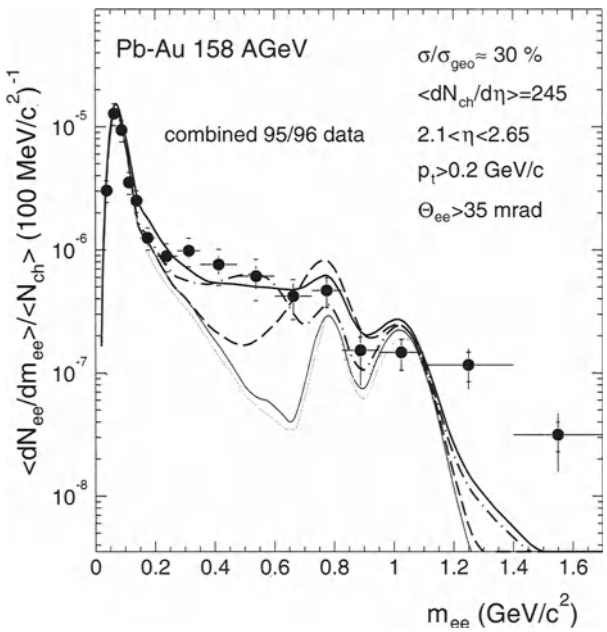

Fig. 2. Comparison of the experimental data to i) free hadron decays without ρ decays (thin solid line), ii) model calculations with a vacuum ρ spectral function (thick dashed line), iii) with dropping in-medium ρ mass (thick dash-dotted line), iv) with a medium-modified ρ spectral function (thick solid line). See text for a discussion of systematic errors.

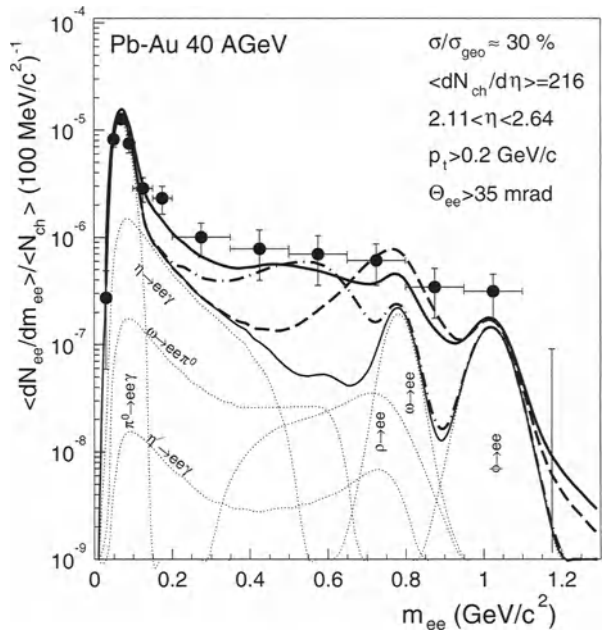

Fig. 3. e^+e^--pair mass spectrum from Pb + Au collisions at 40 AGeV/c compared to free hadron decays and various model calculations (line codes as in fig. 2). Errors shown are only statistical.

all cases cuts on the pair opening angle ($\Theta_{ee} > 35$ mrad) and the transverse momentum of the single-electron track ($p_t > 200\,\mathrm{MeV}/c^2$) have been applied, and the spectra were compatible within their respective statistical and systematic errors. Recently [6] the data of 1995 and 1996 were combined in a unified analysis approach. For the two runs the trigger cross-section was slightly different. The cross-section for the combined data corresponds to the 32% most central events. The average charged-particle multiplicity is $\langle N_{\mathrm{ch}}\rangle = \langle \mathrm{d}N_{\mathrm{ch}}/\mathrm{d}\eta\rangle \cdot \Delta\eta = 245 \cdot 0.55 = 135$ for the quoted rapidity interval. Since the efficiency for detecting e^+e^--pairs depends on multiplicity, an efficiency correction is applied on an event-by-event basis. In the combination, the data were averaged bin-by-bin with weights according to the inverse squares of the relative errors of the individual measurements.

The combined data along with comparisons to model calculations are shown in fig. 2. The yield of pairs with $m_{ee} > 0.2\,\mathrm{GeV}/c^2$ for the entire data sample is 2666 ± 260 with a signal-to-background ratio of 1/12. On top of the statistical errors, the spectrum has systematic errors of 20% for $m_{ee} < 0.2\,\mathrm{GeV}/c^2$ and 28% on average for $m_{ee} > 0.2\,\mathrm{GeV}/c^2$, larger here due to the background subtraction and smoothing procedure. The background smoothing procedure introduces an additional 7% uncertainty in the overall normalization of the spectrum for $m_{ee} > 0.2\,\mathrm{GeV}/c$. A detailed description of all errors can be found in ref. [9,6]. In the region $m_{ee} > 0.2\,\mathrm{GeV}/c^2$ the data exceed the expected yield from the *cocktail* of hadron decays fitted to statistical model calculations and measured rapidity and p_t-distributions by a factor of $2.3 \pm 0.2(\mathrm{stat}) \pm 0.6(\mathrm{syst})$. An additional systematic error of 0.7 is connected to the decay *cocktail* itself. This enhancement is not observed in proton-induced reactions [13].

The data are compared to the yield from various models based on $\pi^+\pi^-$ annihilation with an intermediate ρ vector meson. The hadron decay *cocktail* is added without any contribution from the ρ to avoid double counting (thin line). Using the vacuum ρ spectral function produces the thick dashed line. The other two model calculations both contain modifications of the ρ spectral function. They involve in-medium ρ spectral functions with either a dropping ρ mass [14] (thick dash-dotted line) or with a spread ρ width [15] (thick line). Clearly, a modification of the ρ properties in the medium is needed to reach agreement with the experimental data. Unfortunately, the data do not allow to discern between the two different scenarios.

5 Invariant-mass spectrum of e^+e^--pairs: Pb + Au at 40 AGeV/c

In 1999 the SPS delivered a 40 AGeV/c Pb-beam when the upgraded CERES spectrometer had just been commissioned. The data shown contain central events with an average multiplicity density at this energy of $\langle \mathrm{d}N_{\mathrm{ch}}/\mathrm{d}\eta\rangle = 216$. The analysis leading to the invariant-mass spectrum for the 40 AGeV/c data shown in fig. 3 has been outlined in sect. 3 and is described in detail in [9]. The resulting spectrum contains 249 ± 28 e^+e^--pairs in the mass range below $0.2\,\mathrm{GeV}/c^2$ at a signal-to-background ratio of 1/1. The integrated yield for high mass pairs above $0.2\,\mathrm{GeV}/c^2$

is 185 ± 48 pairs at a signal-to-background ratio of 1/6. The systematic errors are 16% and 20% for the low and high mass region, respectively.

For comparison to the hadron decay *cocktail* the particle ratios have again been taken from statistical model fits adjusted to measured ratios from Pb + Pb collisions at 40 AGeV/c. Also the rapidity distributions and transverse-momentum spectra follow the systematics of measurements at 40 AGeV/c. Again the cocktail has been folded with the experimental mass resolution.

In the low-mass region $m_{ee} < 0.2\,\mathrm{GeV}/c^2$ excellent agreement between the data and the *cocktail* is obtained. Here, the ratio of data/decays is $0.98 \pm 0.11(\mathrm{stat}) \pm 0.16(\mathrm{syst})$. In the high mass region $m_{ee} > 0.2\,\mathrm{GeV}/c^2$, however, the data exceeds the *cocktail* by a factor of $5.1 \pm 1.3(\mathrm{stat}) \pm 1.0(\mathrm{syst})$ with an additional systematic error of 1.5 from the *cocktail*. This enhancement is larger than that observed at full SPS energy as quoted above, while the yield itself is not much larger than at 158 AGeV/c. Note that in the comparison of the enhancement factors between the two energies the additional systematic uncertainty from the *cocktail* essentially drops out.

Along with the data, model *predictions* [16] are presented for this energy. Again, a treatment of the ρ unmodified by medium effects is clearly ruled out. However, once more the data do not allow to discern the two scenarios involving in-medium modifications of the ρ propagator with a shifted mass, *i.e. Brown/Rho scaling* [14,16], or with a spread width [16].

6 Discussion of results

We find, both at 158 AGeV/c as well as at 40 AGeV/c, that the production of e^+e^--pairs with $m_{ee} > 0.2\,\mathrm{GeV}/c^2$ is significantly enhanced as compared to expectations from hadron decays. Moreover, the enhancement seems to be larger at 40 AGeV/c compared to 158 AGeV/c. In both cases, theories based on $\pi^+\pi^-$ annihilation are only able to describe the data, if medium modifications of the ρ propagator are included [14–17].

Comparison of the two energies sheds light on the interesting question whether changes in the properties of the ρ propagator are more sensitive to changes in the temperature or changes of the baryon density as favored by theory [14–17]. In order to evaluate the e^+e^--rates one would need complete knowledge of the dynamical evolution of the fireball. There is no direct handle on the time spent in the various stages of the collision (with the exception of the emission duration of at most 2–3 fm/c and the thermal freeze-out time of 6–8 fm/c from HBT measurements [18,19]). The evolution in terms of temperature and baryochemical potential can, however, be determined at chemical and thermal freeze-out. At chemical freeze-out the total baryon density can be estimated from statistical model calculations fitted to measured particle ratios. It is found to be approximately 0.75 in units of normal nuclear matter density ρ_0 at associated temperatures of 168(145) MeV for 158(40) AGeV/c [20]. The baryon density at thermal freeze-out can be derived from the measured HBT-radii [18,21,19] and rapidity densities [22]. It is 0.34(0.53) at temperatures of 120(120) MeV for 158(40) AGeV/c.

Theoretical calculations which evolve the system through higher baryon densities at the lower beam energy are in agreement with the observed increased enhancement [16]. Taken together, these observations therefore lend support to the importance of coupling the ρ propagator in the medium to baryon density rather than temperature.

The TPC calibration for the 2000 data has been completed; the analysis of the large number of events taken at the full SPS energy is about to start. With this data it should also be possible to study the behavior of the ω and the ϕ. It would further be interesting to compare the invariant-mass spectrum of $\pi^+\pi^-$-pairs [23] to that from e^+e^--pairs, which may allow to discriminate between earlier and later stages of the collision.

7 e^+e^--Measurements at the LHC

ALICE [24] is the dedicated heavy-ion experiment at the Large Hadron Collider (LHC) which is currently under construction. At the LHC it will be possible to collide Pb-ions at a center-of-mass energy of $\sqrt{s} = 5.5\,\mathrm{TeV}$ per nucleon pair. At this energy a qualitatively new region for heavy-ion physics will be explored. The energy density will be high enough and the gluon density is large enough that rapid equilibration will be reached and the generated quark-gluon plasma can be treated as an ideal gas. Particle production will be governed by hard processes.

In general, the central barrel of ALICE ($|\eta| < 0.9$), which sits in a solenoidal field of 0.4 T, consists of an Inner Silicon Tracking System (ITS), a Time Projection Chamber (TPC), a Transition Radiation Detector (TRD), a Time-of-Flight detector (TOF). In a limited angular range the system is complemented by a Čerenkov detector (HMPID) and a Photon Spectrometer (PHOS). The combination of theses detectors yields good particle identification capabilities and it provides momentum resolution for ($0.1 < p < 100\,\mathrm{GeV}/c$). This will *e.g.* allow for the study of jet fragmentation functions up to well over 100 GeV/c jet-p_t.

With the Transition Radiation Detector (TRD) [25] shown in fig. 4 it will be possible to measure electrons and positrons in the central barrel in an environment which is designed to cope with a charged particle density of up to $\mathrm{d}N/\mathrm{d}y = 8000$. The detector consists of 540 individual detector modules. They are arranged in six layers with a five-fold segmentation in z-direction in a total of 18 super modules each subtending 20° in azimuth. Each detector module consists of a sandwich radiator of ROHACELL and polypropylene fibers followed by a gas detector with drift and amplification region operated with a $\mathrm{Xe/CO_2}(85:15)$-mixture. The induced signals are read out from segmented cathode pads, $1.2 \cdot 10^6$ in total. For good electron identification the total radiation

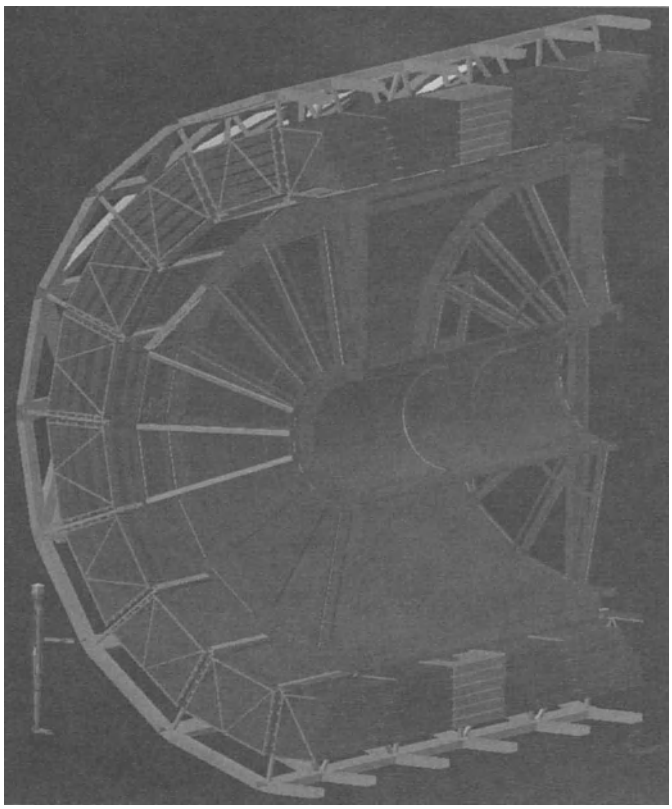

Fig. 4. Cut through the space frame of the ALICE central detectors with the TPC surrounded by six layers of TRDs arranged in five stacks in the z-direction.

thickness of the detector for all six layers is designed to be $X/X_0 < 15\%$. The readout is sampled over the entire drift of $2\,\mu$s. This allows for momentum determination and in conjunction with the fully on the detector integrated electronics fast ($6\,\mu$s) triggering on high-p_t particles. This triggering capability is essential for the study of rare probes like high-p_t J/ψ's and Υ's. Comprehensive test measurements on prototype detectors show that with the TRD a π-rejection of a factor 100 can be reached at 90% electron efficiency [26].

The electron measurement coupled with the vertexing capabilities of the ITS and TPC allow for the direct measurement of the yield of B and D mesons via their semileptonic decay. This provides the natural reference for the measurement of the *charmonium* (J/ψ) and *bottomium* (Υ) states which directly probe properties of the medium that they traverse [27]. The mass resolution for the Υ-states is of the order of 1%. In the absence of full calorimtetric coverage of the central barrel, the study of jets is facilitated by the triggering capability of the TRD, which allows for fast selection particles with high p_t, *i.e.* leading particles of jets.

Current planning foresees that about half of the TRD will be ready in 2006. This will be in time for the first heavy-ion collisions at LHC expected in 2007.

References

1. F. Karsch, Nucl. Phys. A **698**, 199c (2002).
2. J.D. Bjorken, Phys. Rev. D **17**, 140 (1983).
3. CERN Press Release, CERN 2000-02-07.
4. CERES Collaboration (G. Agakichiev *et al.*), Nucl. Instrum. Meth. A **371**, 16 (1996).
5. A. Marín *et al.*, Nucl. Phys. A **661**, 673c (1999).
6. CERES Collaboration (G. Agakichiev *et al.*), in preparation.
7. CERES Collaboration (H. Appelshäuser *et al.*), Nucl. Phys. A **698**, 253c (2002).
8. CERES Collaboration (K. Filimonov *et al.*), *Proceedings of the International Nuclear Physics Conference, Berkley 2001*, nucl-ex/0109017; CERES Collaboration (S. Damjanović, K. Filimonov *et al.*), *Proceedings of CHEP, Budapest 2001*, nucl-ex/0111009; CERES Collaboration (S. Damjanović *et al.*), *Proceedings of the 4th ICPAQGP, Jaipur 2001*, to be published in Pramana J. Phys.
9. S. Damjanović, Doctoral Thesis, University of Heidelberg (2002); CERES Collaboration (D. Adamová *et al.*), Phys. Rev. Lett. **91**, 042301 (2003), nucl-ex/0209024.
10. CERES Collaboration (G. Agakichiev *et al.*), Phys. Lett. B **422**, 405 (1998).
11. CERES Collaboration (G. Agakichiev *et al.*), Nucl. Phys. A **638**, 159c (1998).
12. CERES Collaboration (B. Lenkeit *et al.*), Nucl. Phys. A **661**, 23c (1999).
13. CERES Collaboration (G. Agakichiev *et al.*), Eur. Phys. J. C **4**, 231 (1998).
14. G. Brown, M. Rho, Phys. Rep. **363**, 85 (2002).
15. R. Rapp, J. Wambach, Eur. Phys. J. A **6**, 415 (1999).
16. R. Rapp, *Proceedings of the 4th ICPAQGP, Jaipur 2001*, to be published in Pramana J. Phys., hep-ph/0201101, and private communication (2001).
17. R. Rapp, J. Wambach, Adv. Nucl. Phys. **25**, 1 (2000); R. Rapp, G. Chanfray, J. Wambach, Phys. Rev. Lett. **76**, 368 (1996); Nucl. Phys. A **617**, 472 (1997); R. Rapp, this issue, p. 459.
18. CERES Collaboration (H. Tilsner, H. Appelshäuser *et al.*), *Proceedings of the QM2002*, Nucl. Phys. A **715**, 607c (2003).
19. CERES Collaboration (D. Adamová *et al.*), Nucl. Phys. A **714**, 124 (2003), nucl-ex/0207005.
20. P. Braun-Munzinger, J. Stachel, J. Phys. G **28**, 1971 (2002).
21. CERES Collaboration (D. Adamová *et al.*), Phys. Rev. Lett. **90**, 022301 (2003), nucl-ex/0207008.
22. NA44 Collaboration (I.G. Bearden *et al.*), submitted to Phys. Rev. C; nucl-ex/0202019; NA49 Collaboration (M. van Leeuwen *et al.*), *Proceedings of the QM2002*, Nucl. Phys. A **715**, 161 (2003).
23. STAR Collaboration (P. Facchini *et al.*), *Proceedings of the QM2002*, Nucl. Phys. A, **715**, 462c (2003).
24. ALICE, Technical Proposal, CERN/LHCC 95-71.
25. TRD Technical Design Report, CERN/LHCC 2001-021; `http://www.gsi.de/~alice/trdtdr/index.html`.
26. A. Andronic *et al.*, IEEE Trans. Nucl. Sci. **48**, 1259 (2001).
27. T. Matsui, H. Satz, Phys. Lett. B **178**, 416 (1986).

Eur. Phys. J. A **18**, 527–530 (2003)
DOI 10.1140/epja/i2002-10275-5

THE EUROPEAN PHYSICAL JOURNAL A

Saturation in small-x and heavy-ion physics

A.H. Mueller

Physics Department, Columbia University, New York, NY 10027, USA

Received: 30 September 2002 /
Published online: 22 October 2003 – © Società Italiana di Fisica / Springer-Verlag 2003

Abstract. The idea of parton saturation is reviewed. The use of saturation in describing HERA data is discussed in the context of the McLerran-Venugopalan and Golec-Biernat Wüsthoff models. Applications of saturation ideas to RHIC data are reviewed and a comparison between applications at HERA and at RHIC is given.

PACS. 11.10.-z Field theory

1 Introduction

Partons in hadrons and saturation

The partonic picture of hadrons and the saturation of partons are not easily seen in the same reference frame. We shall choose to describe deeply inelastic lepton-hadron scattering in two distinct frames. One of these frames will make the parton picture manifest while the other will make unitarity limits (saturation) manifest.

1.1 The Bjorken frame

In the Bjorken frame one choses the proton momentum to be large and along the z-axis while the momentum of the virtual photon is mainly in the transverse direction

$$P_\mu = (p + \frac{m^2}{2p}, 0, 0, p)\,, \tag{1}$$

$$q_\mu = (q_0, q_\perp, 0)\,. \tag{2}$$

As $p \to \infty$, $q_0 = \frac{q \cdot P}{p} \to 0$. The invariants usually chosen to describe the process are $-q_\mu q^\mu = Q^2 \simeq q_\perp^2$ and $x = \frac{Q^2}{2P \cdot q}$ and this latter variable serves to label the momentum fraction, of the original proton momentum P, carried by the struck quark. The process is illustrated in fig. 1.

The virtual photon is absorbed over a length scale $\Delta x_\perp \simeq 1/q_\perp = 1/Q$ and during a time $\Delta t = (E_k + E_q - E_{k+q})^{-1} \simeq 1/Q$. The time of absorption and the region of absorption in the proton are so small, for large Q, that the absorption must take place on single quarks or antiquarks in the wave function of the proton. This makes the following formula natural:

$$F_2(x, Q^2) = \sum_f e_f^2 [x q_f(x, Q^2) + x \bar{q}_f(x, Q^2)]\,, \tag{3}$$

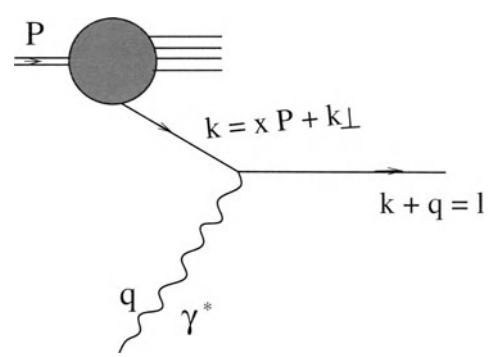

Fig. 1.

where q_f and $\bar{q}_f$ are the quark and antiquark number densities in the proton, and e_f is the quark charge as a fraction of the charge of the proton.

1.2 The dipole frame

The Bjorken frame shows deep inelastic scattering in terms of the quark components of the infinite-momentum wave function of the proton. There is an alternate view where one still gives the proton a large momentum but where now the γ^* also has a sufficiently large longitudinal momentum so that the process can be viewed as $\gamma^* \to q\bar{q}$ and then the $q\bar{q}$ dipole scatters on a highly developed wave function of the proton as illustrated in fig. 2. The momenta can be given as

$$P = (p + \frac{m^2}{2p}, 0, 0, p)\,, \tag{4}$$

$$q = (\sqrt{q^2 - Q^2}, 0, 0, q)\,, \tag{5}$$

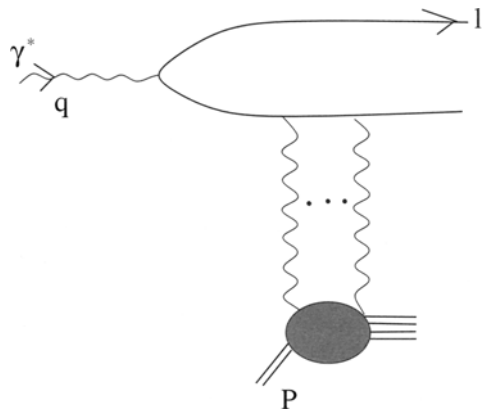

Fig. 2.

where $q/Q > 1$ but not too large. QCD evolution is still in the proton. We shall see below that parton scattering corresponds to the unitarity limit of dipole scattering on the proton.

2 Simple models of saturation in nuclei

It is simplest to illustrate saturation in deep inelastic scattering by using a large nucleus to create large quark and gluon number densities. Most of what occurs in a large nucleus can be taken over to protons where it is BFKL evolution which there creates large parton densities.

2.1 Quark saturation

We are going to calculate $\frac{\mathrm{d}x(q+\bar{q})}{\mathrm{d}^2b\mathrm{d}^2\ell_\perp}$, the sea quark distribution of light quarks per unit of transverse phase space in the nuclear wave function [1]. One can view the cross-section for producing a quark jet either as in fig. 1, where the partonic interpretation is clear, or as in fig. 2, where the scattering of the dipole on a large nucleus can be done in the multiple scattering approximation. In this latter picture one easily finds [1]

$$\begin{aligned}\frac{\mathrm{d}x(q_f+\bar{q}_f)}{\mathrm{d}^2b\mathrm{d}^2\ell_\perp} &= \int \mathrm{d}^2x_1\mathrm{d}^2x_2 e^{-i\ell_\perp\cdot(x_{1\perp}-x_{2\perp})} \\ &\times \int_0^1 \mathrm{d}z\Big\{\frac{Q^2N_c}{32\pi^6}\,[z^2+(1-z^2)] \\ &\times\nabla_{x_1}K_0\Big(\sqrt{Q^2x_{1\perp}^2z(1-z)}\,\Big) \\ &\times\nabla_{x_2}K_0\Big(\sqrt{Q^2x_{2\perp}^2z(1-z)}\,\Big)\Big\} \\ &\times\Big[1+e^{-(x_{1\perp}-x_{2\perp})^2\bar{Q}_s^2/4}-e^{-x_{1\perp}^2\bar{Q}_s^2/4} \\ &-e^{-x_{2\perp}^2\bar{Q}_s^2/4}\Big], \end{aligned} \tag{6}$$

where

$$\bar{Q}_s^2 = \frac{C_F}{C_A}\,Q_s^2 = 4/9Q_s^2 \tag{7}$$

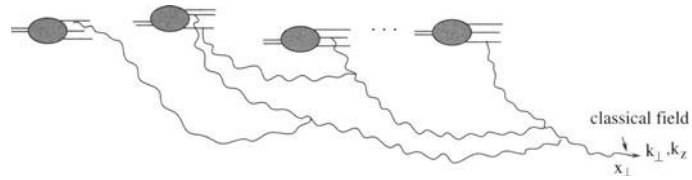

Fig. 3.

and

$$Q_s^2 = \frac{4\pi^2\alpha N_c}{N_c^2-1}\,2\sqrt{R^2-b^2}\,\rho xG. \tag{8}$$

In (6) $x_{1\perp}$ is the transverse coordinate of the measured quark in the amplitude and $x_{2\perp}$ is the corresponding coordinate in the complex conjugate amplitude. The term $\{\}$ in (6) is $\frac{1}{8\pi^2}\psi_\gamma^*(x_{2\perp})\psi_\gamma(x_{1\perp})$; ρ is the nuclear density; xG is the gluon density of a nucleon, and b is the impact parameter of the nucleus. The four terms in [ ] in (6) correspond to no interactions, an arbitrary number of interactions in the amplitude and in the complex conjugate amplitude, an arbitrary number of interactions in the amplitude with no interactions in the complex conjugate amplitude, and an arbitrary number of interactions in the complex conjugate amplitude with none in the amplitude, respectively. Thus, for example, the third term

$$S(x_{1\perp},b) = \bar{e}^{x_{1\perp}^2Q_s^2(b)/4} \tag{9}$$

is the S-matrix for the interaction of a dipole of size $x_{1\perp}$ with the nucleus at impact parameter b. Unitarity is imposed by the fact that $|S|\le 1$ and $S\to 0$ for large $x_{1\perp}^2$.

Saturation show up when $\ell_\perp^2/Q_s^2 \ll 1$ in which case (6) gives [1]

$$\frac{\mathrm{d}^2x(q_f+\bar{q}_f)}{\mathrm{d}^2b\mathrm{d}^2\ell_\perp} = \frac{N_c}{2\pi^4} \tag{10}$$

a remarkable result which says that the number of quarks in the nucleus cannot grow too big in a given region of phase space. This can be turned (approximately) into a 3-dimensional occupation number:

$$f_q = \frac{(2\pi)^3}{2\cdot 2\cdot N_c}\,\frac{\mathrm{d}x(q_f+\bar{q}_f)}{\mathrm{d}^2b\mathrm{d}^2\ell_\perp} = \frac{1}{\pi}, \tag{11}$$

where the two factors of 2 in the denominator count particle and antiparticle and spin factors.

2.2 Gluon saturation (McLerran-Venugopalan model) [2]

Quark saturation occurs at the one fermionic loop level and is purely a quantum phenomenon. Gluon saturation, on the other hand, occurs at the semiclassical level and for a large nucleus corresponds to graphs like those shown in fig. 3 in the Bjorken frame and in a particular light-cone gauge [3]. One finds [4,5]

$$\frac{\mathrm{d}xG}{\mathrm{d}^2b\mathrm{d}^2\ell_\perp} = \frac{N_c^2-1}{4\pi^4\alpha N_c}\int\frac{\mathrm{d}^2x_\perp}{x_\perp^2}e^{-i\ell_\perp\cdot x_\perp}\Big(1-e^{-x_\perp^2Q_s^2/4}\Big). \tag{12}$$

When $\ell_\perp^2/Q_s^2 \gg 1$ the additive result is recovered while for $\ell_\perp^2/Q_s^2 \ll 1$

$$\frac{\mathrm{d}xG}{\mathrm{d}^2b\mathrm{d}^2\ell_\perp} = \frac{N_c^2-1}{4\pi^3}\ln(Q_s^2/\ell_\perp^2) \tag{13}$$

or

$$f_g = \frac{(2\pi)^3}{2(N_c^2-1)}\frac{\mathrm{d}^2xG}{\mathrm{d}^2b\mathrm{d}^2\ell_\perp} = \frac{1}{\alpha N_c}\ln(Q_s^2/\ell_\perp^2). \tag{14}$$

Now occupation numbers are of order $1/\alpha$ which signals a strongly nonlinear classical field theory. Higher orders will likely modify the constants in (13), but the general form, including $\ln Q_s^2/\ell_\perp^2$, are expected to be general [1,6–8].

3 Application to HERA phenomenology

Refer back to (6) which can be written as

$$\begin{aligned}\frac{\mathrm{d}x(q_f+\bar{q}_f)}{\mathrm{d}^2b\mathrm{d}^2\ell_\perp} &= \frac{1}{8\pi^2}\int \mathrm{d}^2x,\mathrm{d}^2x_2\int_0^1 \mathrm{d}z e^{-i\underline{\ell}\cdot(\underline{x}_1-\underline{x}_2)}\\ &\times\psi_\gamma^*(x_{1\perp},z,Q)\psi_\gamma(x_2,z,Q)\\ &\times\left[1+e^{-(x_{1\perp}-x_{2\perp})^2\bar{Q}_s^2/4}-e^{-x_{1\perp}^2\bar{Q}_s^2/4}-e^{-x_{2\perp}^2\bar{Q}_s^2/4}\right],\end{aligned} \tag{15}$$

again for a large nucleus. If we integrate over $\mathrm{d}^2\ell_\perp$ and d^2b with the replacement $\mathrm{d}^2b \to \sigma_0$ on the right-hand side of (15), one obtains

$$\begin{aligned}F_2(x,Q^2) &= \sigma_0\int\sum_f e_f^2\mathrm{d}^2x_\perp\\ &\times\int_0^1 \mathrm{d}z|\psi_\gamma(x_\perp,z,Q)|^2\left(1-e^{-x_\perp^2Q_s^2/4}\right).\end{aligned} \tag{16}$$

Taking this form for a proton gives the Golec-Biernal–Wüsthoff model [9]. For diffractive scattering

$$\begin{aligned}F_2^D &= \sigma_0\int\sum_f e_f^2\mathrm{d}^2x_\perp\int_0^1 \mathrm{d}z|\psi_\gamma|^2\\ &\times\frac{1}{2}\left(1-e^{-x_\perp^2Q_s^2/4}\right)^2 + q\bar{q}g \text{ state.}\end{aligned} \tag{17}$$

The Golec-Biernat–Wüsthoff model has just three parameters

$$\sigma_0 = 23\,\mathrm{mb},\quad \bar{Q}_s^2 = (\frac{x_0}{x})^{0.3}\,\mathrm{GeV}^2,\quad x_0 = 3\times10^{-4}. \tag{18}$$

In general the exponential form for the S-matrix as given in (9) cannot be expected to work for protons in detail. However, the general characteristics $S \underset{x_\perp\to 0}{\to} 1$ and $S \underset{x_\perp\to\text{large}}{\to} 0$ as well as the fact that the corrections to $1-S$ are of order $x_\perp^2$ at small $x_\perp$ are general results which are nicely built into the Golec-Biernat–Wüsthoff model.

The Golec-Biernal–Wüsthoff model works surprisingly for fits to F_2 and F_2^D at HERA. There are also now many variations on the model [10–12] which try to reflect more precisely QCD constraints.

4 Application to heavy-ion phenomenology

Once densities of produced quarks and gluons in heavy-ion collisions are large enough to be in the quark-gluon phase it does not make sense to try and describe the collision in terms of hadrons. On the other hand, QCD perturbation theory may not give reliable numerical results, but it should be a reasonably accurate guide to the production and early stages of a heavy-ion collision.

4.1 The production of gluons

In a head-on heavy-ion collision production in the central rapidity region should be dominated by gluons [13]. It is convenient to view the collision as a right-moving collection of gluons, the wave function of the right-moving nucleus, colliding with a stationary nucleus. Then the primary effect of the collision is to free all the right-moving gluons whose transvese momentum is below the saturation momentum [13].

To try and get some reasonable estimates, we use the McLerran-Venugopalan model as a model for the gluons in the right-moving nucleus. This gives the gluons in the wave function according to (12) above. Just after the collision we suppose that a good fraction of the gluons having $\ell_\perp/Q_s < 1$ have been liberated. Thus we write for the initial gluon distribution produced in the collision

$$\frac{\mathrm{d}N_g}{\mathrm{d}^2b\mathrm{d}\eta} = c\frac{N_c^2-1}{4\pi^2\alpha N_c}Q_s^2, \tag{19}$$

where c accounts for the fact that not all gluons may be freed in the collision.

Krasnitz and Venugopalan [14] and Krasnitz, Nara and Venugopalan [15] calculate $\frac{\mathrm{d}N_g}{\mathrm{d}^2b\mathrm{d}\eta}$ numerically using classical Yang-Mills field equations starting from McLerran-Venugopalan wave functions for the colliding nuclei. They find

$$\frac{\mathrm{d}N_g}{\mathrm{d}^2b\mathrm{d}\eta} = \frac{1}{g^2}f_N\Lambda_s^2, \tag{20}$$

where $\frac{1}{4\pi}\Lambda_s^2\ln Q_s^2/\Lambda_{\mathrm{QCD}}^2 = Q_s^2$. One gets [16]

$$c = \frac{4\pi^2 f_N}{(N_c^2-1)\ln Q_s^2/\Lambda_{\mathrm{QCD}}^2} \simeq \frac{1}{2} \tag{21}$$

for the calculated value, $f_N \simeq 0.3$.

4.2 The production of charged hadrons

Now take (19), integrate over d^2b and include a factor of R to account for gluon inelasticity as the gluon system evolves toward equilibrium and also include a factor of 2/3 to account for the fraction of produced particles, mostly pions, which are charged. One gets

$$\frac{\mathrm{d}N_{\mathrm{ch}}}{\mathrm{d}\eta} = \frac{2}{3}Rc\frac{N_c^2-1}{4\pi^2\alpha N_c}\int \mathrm{d}^2bQ_s^2. \tag{22}$$

Using (8) along with $xG \simeq \frac{1}{2}\ln Q_s^2/\Lambda_{\rm QCD}^2$, one finds [17]

$$\frac{2}{N_{\rm part}}\frac{{\rm d}N_{\rm ch}}{{\rm d}\eta} = \frac{Rc}{3}\ln Q_s^2/\Lambda_{\rm QCD}^2\,, \tag{23}$$

where the number of participants in the reaction is

$$N_{\rm part} = 2A = 2\int {\rm d}^2b\rho 2\sqrt{R^2-b^2}. \tag{24}$$

We shall now use (23) to help summarize various, closely related, approaches to charged-particle production at RHIC.

4.2.1 Kharzeev, Nardi and Kharzeev, Levin, Nardi picture [17–19]

Here one supposes $R = 1$. Using the experimental value $\frac{2}{N_{\rm part}}\frac{{\rm d}N_{\rm ch}}{{\rm d}\eta} \simeq 3.8$ at $\sqrt{s} = 200$, one sees from (23) that one needs $c \simeq 2.5-3$ for $Q_s^2 = 1-2\,{\rm GeV}^2$. The centrality dependence and energy dependence come out well in this model as well as the η-dependence.

4.2.2 Krasnitz, Nara, Venugopalan model [14,15]

This model is close to that of Kharzeev *et al.* The authors take McLerran-Venugopalan initial conditions and solve classical Yang-Mills equations to determine the number of gluons radiated during an ion-ion collision. They determine as initial conditions for the freed gluons

$$\frac{{\rm d}N_g}{{\rm d}^2b{\rm d}\eta} = \frac{1}{g^2}f_N\Lambda_s^2 \quad \text{with} \quad f_N \simeq 0.3 \tag{25}$$

and

$$\langle E_T^g\rangle \simeq \frac{3}{2}\Lambda_s. \tag{26}$$

One gets (23) for $\Lambda_s \simeq 1.1-1.3\,{\rm GeV}$ and with $R \simeq 2$–2.5.

4.2.3 "Bottom-up" picture [16]

The "bottom-up" picture uses the Boltzman equation, and especially the inelastic collision term in the Boltzmnn equation, to follow the initially freed gluons, coming from a McLerran-Venugopalan distribution, to the time of equilibration. In this picture (23) also emerges. If $c \simeq 1$ and $R \simeq 3$, one finds that equilibration occurs at a time $\simeq 3.5$ fm and at a temperature $T_{\rm eq} \simeq 230\,{\rm MeV}$.

4.3 Problems with the models

Although saturation models give results which are generally compatible with the early RHIC results there are a few difficulties which particular versions of the model have.

i) Kharzeev *et al.* need a value of c which is much larger than the value obtained from numerical calculation.

ii) In order to fit the RHIC data Krasnitz, Nara and Venugopalan take $\Lambda_s^2 \simeq 1$–$1.5\ {\rm GeV}^2$, while the McLerran-Venugopalan model gives

$$\Lambda_s^2 \simeq \frac{1}{2}\,{\rm GeV}^2\,.$$

iii) Baier *et al.* need $c \simeq 1$, while the calculations give $c \leq 1/2$. Also analytic calculations are dangerous when Q_s^2 is as small as $1\,{\rm GeV}^2$.

iv) The Golec-Biernat–Wüsthoff model gives

$$Q_s^2 = \left(\frac{3x10^{-4}}{x}\right)^{0.3}\cdot\frac{N_c}{C_F} \tag{27}$$

for protons. At $x = 10^{-2}$ this gives $Q_s^2 \simeq 0.8\,{\rm GeV}^2$, while the McLerran-Venugopalan model gives about the same value for gold at $x = 10^{-2}$. The values of Q_s^2 do not match too well between RHIC and HERA.

This work has been supported in part by the Department of Energy, Columbia University, New York.

References

1. A.H. Mueller, Nucl. Phys. B **558**, 285 (1999).
2. L. McLerran, R. Venugopalan, Phys. Rev. D **49**, 2233; 3352 (1994); **50**, 2225 (1994).
3. Yu.V. Kovchegov, Phys. Rev. D **54**, 5463 (1996); **55**, 5445 (1997).
4. J. Jalilian-Marian, A. Kovner, L. McLerran, H. Weigert, Phys. Rev. D **55**, 5414 (1997).
5. Yu.V. Kovchegov, A.H. Mueller, Nucl. Phys. B **529**, 451 (1998).
6. E. Iancu, A. Leonidov, L. McLerran, hep-ph/0202270.
7. E. Iancu, A. Leonidov, L. McLerran, Nucl. Phys. A **692**, 583 (2001).
8. E. Ferreiro, E. Iancu, A. Leonidov, L. McLerran, Nucl. Phys. A **703**, 489 (2002), hep-ph/0109115.
9. K. Golec-Biernat, M. Wüsthoff, Phys. Rev. D **59**, 014017 (1999); **60**, 114023 (1999).
10. J. Bartels, R. Golec-Biernat, H. Kowalski, Phys. Rev. D. **66**, 014001 (2002), hep-ph/0203258.
11. J.R. Forshaw, G. Kerley, G. Shaw, Phys. Rev. D **60**, 074012 (1999); Nucl. Phys. A **675**, 80 (2000).
12. M. McDermott, L. Frankfurt, V. Guzey, M. Strikman, Eur. Phys. J. C **16**, 641 (2000).
13. J.-P. Blaizot, A.H. Mueller, Nucl. Phys. **289**, 747 (1987).
14. A. Krasnitz, R. Venugopalan, Nucl. Phys. B **557**, 537 (1999); Phys. Rev. Lett. **86**, 1717 (2001).
15. A. Krasnitz, Y. Nara, R. Venugopalan, Phys. Rev. Lett. **87**, 192302 (2001).
16. R. Baier, A.H. Mueller, D. Schiff, D.T. Son, Phys. Lett. B **502**, 51 (2001); **539**, 46 (2002), hep-ph/0204211.
17. D. Kharzeev, M. Nardi, Phys. Lett. B **507**, 121 (2001).
18. D. Kharzeev, E. Levin, Phys. Lett. B **523**, 79 (2001).
19. D. Kharzeev, E. Levin, M. Nardi, hep-ph/0111315.

Eur. Phys. J. A **18**, 531–536 (2003)
DOI 10.1140/epja/i2002-10276-4

THE EUROPEAN PHYSICAL JOURNAL A

Charmonium cross-sections and the QGP

T. Barnes[a]

Physics Division ORNL and Department of Physics and Astronomy, University of Tennessee, TN, USA

Received: 30 September 2002 /
Published online: 22 October 2003 – © Società Italiana di Fisica / Springer-Verlag 2003

Abstract. In this contribution we summarize experimental information and theoretical results for the dissociation cross-sections of charmonium by light hadrons, which are of great importance for the identification of a quark-gluon plasma (QGP). Recent theoretical predictions for these cross-sections differ by orders of magnitude over the physically relevant energy range. The methods discussed here include a color-dipole model, meson exchange models, a quark interchange model, and QCD sum rules.

PACS. 25.75.-q Relativistic heavy-ion collisions – 25.75.Dw Particle and resonance production

1 Introduction

A rather exotic process in hadron-hadron scattering, the dissociation of charmonia through collisions with light hadrons, has recently been identified as of great importance to the RHIC community. This interest has arisen from the suggestion by Matsui and Satz [1] that suppression of J/ψ production could be used as a signature for the formation of a quark-gluon plasma.

The suggested mechanism for QGP-suppression of charmonium is that a QGP will screen the linear confining interaction between quarks, so that a $c\bar{c}$-pair produced within a QGP is unlikely to form a bound $c\bar{c}$ charmonium resonance as in fig. 1, but will instead separate into open-charm mesons.

Even if this simple picture of $c\bar{c}$ production in a QGP is qualitatively correct, interpretation of this signature requires an understanding of the competing effects of direct charm production and scattering by the initial relativistic nucleons [2], as well as the effect of subsequent dissociation of charmonia through collisions with the many "co-moving" light hadrons produced in a heavy-ion collision. It is thus of great importance for QGP searches using the charmonium-suppression signature to establish the approximate scale of these low-energy $c\bar{c}$ + light-hadron co-mover dissociation cross-sections.

To summarize, if charmonium + light-hadron dissociation cross-sections are small (case 1, top of fig. 1) and the background of direct charm production from the initial nucleons is understood, one may have a useful signature for QGP formation. Conversely, if the co-mover dissociation cross-sections are large (case 2, bottom of fig. 1), one must distinguish between QGP-reduced charmonium production and subsequent dissociative scattering, and the interpretation of the J/ψ signal will be biased unless these dissociation cross-sections are included in the event simulations.

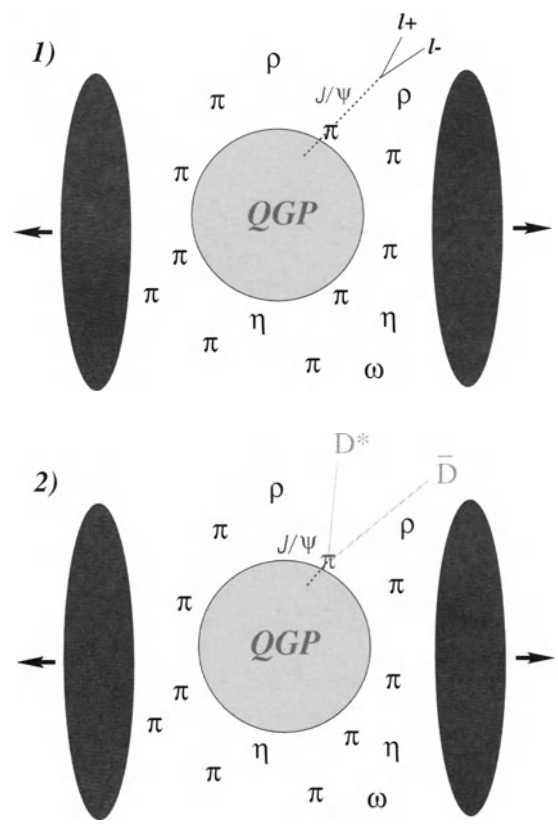

Fig. 1. Matsui and Satz speculated that J/ψ production would be strongly suppressed if a QGP has been formed. We address the subsequent effect of J/ψ absorption by light co-movers, which may be 1) weak, or 2) strong.

[a] e-mail: tbarnes@utk.edu

2 Experiment

Unfortunately we have no charmonium beams or targets, so experimental low-energy charmonium cross-sections must be inferred indirectly and are poorly known. The earliest estimates of charmonium cross-sections at moderate energies came from J/ψ photoproduction experiments in the mid 1970s, which were interpreted in terms of a $J/\psi + N$ total cross-section. Early Fermilab and SLAC photoproduction experiments gave rough estimates of $\sim 1\,\mathrm{mb}$ for $\sigma_{J/\psi+N}$, assuming vector dominance, for photon energies from $E_\gamma \approx 13$ to $200\,\mathrm{GeV}$ [3,4]. A subsequent SLAC photoproduction experiment in 1977 used the A-dependence of J/ψ absorption to infer a rather larger cross-section of $\sigma_{J/\psi+N} = 3.5 \pm 0.8\,\mathrm{mb}$ at $E_\gamma \approx 17\,\mathrm{GeV}$ ($\sqrt{s} \approx 6\,\mathrm{GeV}$) [5]. The vector dominance hypothesis may have led to an underestimate of the cross-section in the earlier references [6].

In heavy-ion collisions these cross-sections may be estimated from the ratio of lepton pairs produced in the J/ψ peak to "background" Drell-Yan pairs nearby in energy. Since the J/ψ must reach the exterior of the nuclear target to decay into a sharp mass peak, this ratio gives us an estimate of the absorption cross-section through the classical survival probability formula,

$$\sigma(J/\psi \longrightarrow \mu^+\mu^-)/\sigma(\text{Drell-Yan } \mu^+\mu^-) = \exp\left(-\rho\sigma^{abs}_{J/\psi+N} L\right), \quad (1)$$

where ρ is the mean nucleon density and L is the estimated mean path length in the experimental nuclear system. A "naive" interpretation of the J/ψ production data from collisions of various nuclear species using this formula gives $\sigma^{abs}_{J/\psi+N} \approx 6\,\mathrm{mb}$ at $\sqrt{s} \approx 10\,\mathrm{GeV}$ [7], with a numerically similar result for the ψ' (see fig. 2).

Of course one may raise many questions about the validity of this simple estimate, such as the importance of shadowing in Drell-Yan, the neglect of J/ψ scattering by other light hadrons formed in the collision (such as π and ρ), and the assumption of a single, constant $J/\psi+N$ cross-section in all circumstances.

Recently, concerns have been expressed that the J/ψ and ψ' wave functions have not had sufficient time to form within the nucleus in these collisions, so experiment may instead be measuring the cross-section for a small initial $c\bar{c}$ "premeson" on a nucleon. One can increase the time spent in the interior of the nuclear system by selecting small and even negative x_F events, as has been done by E866 at Fermilab. As discussed by He, Hüfner and Kopeliovich [8], this leads one to infer $\sigma^{abs}_{J/\psi+N} = 2.8 \pm 0.3\,\mathrm{mb}$ and $\sigma^{abs}_{\psi'+N} = 10.5 \pm 3.6\,\mathrm{mb}$ respectively, also at $\sqrt{s} \approx 10\,\mathrm{GeV}$. This is rather more satisfying to people who have an intuitive notion that the larger ψ' should have a larger reaction cross-section. Actually the connection between cross-section and physical extent is less direct (compare KN and $\bar{K}N$), and in any case the relative proximity of inelastic thresholds alone would suggest a larger ψ' cross-section. These experiments also suggest a preference for dissociation over elastic cross-sections at $\sqrt{s} \approx 10\,\mathrm{GeV}$ by roughly a factor of 30 [8].

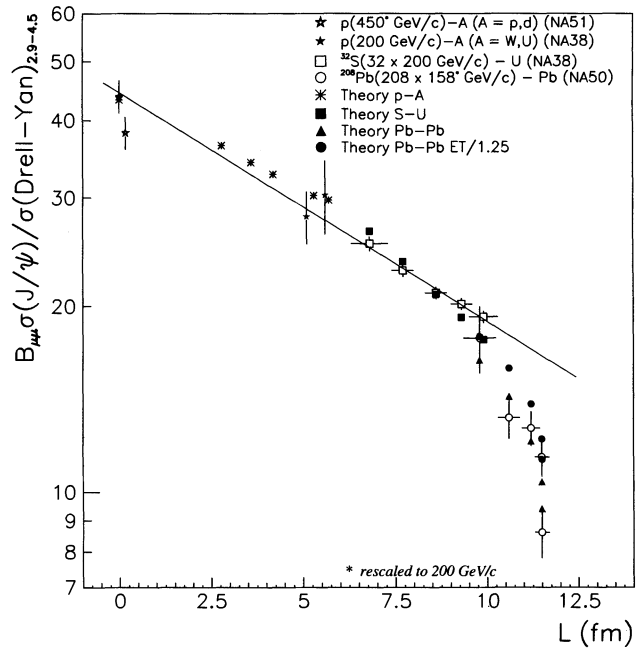

Fig. 2. A fit of eq. (1) to experimental J/ψ production *versus* path length [7]; the line corresponds to 6.2 mb.

3 Theory: introduction

To quote B. Müller, "...the state of the theory of interactions between J/ψ and light hadrons is embarrassing ... Only three serious calculations exist (after more than 10 years of intense discussions about this issue!) and their results differ by at least two orders of magnitude in the relevant energy range.... There is a lot to do for those who would like to make a serious contribution to an important topic." (*Quark Matter 99* Summary, ref. [9]).

The theoretical situation has improved considerably since these remarks. A partial list of recent $c\bar{c}$ + light-hadron cross-section calculations is given in table 1.

Table 1. A representative set of $c\bar{c}$ + light-hadron cross-section calculations.

Method	Init State	Reference
color-dipole	$J/\psi + N$	[10]
	$J/\psi + N$; $\psi' + N$; $\chi + N$	[11]
meson ex.	$J/\psi + \pi$	[12]
	$J/\psi + \pi, \rho$	[13]
	$J/\psi + \pi, \rho$	[14]
	$J/\psi + N$	[15,16]
	$J/\psi + \pi, K, \rho, N$	[17,18]
quark int.	$J/\psi + \pi$	[12,19]
	$J/\psi + \pi, \rho$; $\psi' + \pi, \rho$	[20]
	$(J/\psi, \psi', \chi) + (\pi, \rho, K)$	[21]
	$J/\psi + \pi, N$; $\psi' + \pi, N$	[22]
QCD sum rules	$J/\psi + \pi$	[23]

Approaches to calculating cross-sections of charmonia on light hadrons have to date usually employed one of three descriptions, which are a high-energy diffractive model originally due to Bhanot and Peskin [24], t-channel meson exchange as first discussed by Matinyan and Müller [13], and the quark interchange model discussed here. Unfortunately the space available does not allow a detailed discussion of the two earlier approaches; here we simply tabulate references that have used the various methods (table 1), and note that there are serious problems with all of these approaches (see, for example, the discussion in ref. [25]).

4 Theory: quark interchange

One may also calculate these cross-sections in the quark model, using nonrelativistic quark model wave functions and the quark interchange scattering mechanism, driven by the Born-order matrix element of the standard quark model Hamiltonian. This technique, which has no free parameters once quark model wave functions and the interquark Hamiltonian are specified, has been shown to compare reasonably well with experimental low-energy hadron scattering data near threshold for a wide range of no-annihilation reactions [26,27]. In meson-meson scattering there are four distinct diagrams (see fig. 3), each of which has an associated overlap integral of quark model meson wave functions convolved with the interquark Hamiltonian. Constituent interchange is forced at Born-order because $H_I \propto \lambda^a \cdot \lambda^a$ changes each initial color-singlet $q\bar{q}$ meson into a color-octet; these have a nonzero projection onto color-singlet final-state mesons after quark line interchange. The Feynman rules for these diagrams were given by Barnes and Swanson [26].

The first charmonium cross-section calculation using this approach was due to Martins, Blaschke and Quack [19], who considered the reactions $J/\psi + \pi \to D^*\bar{D}$+h.c. and $D^*\bar{D}^*$. (The amplitude for $J/\psi+\pi \to D\bar{D}$ is zero in the nonrelativistic quark model without spin-orbit forces, and has been found to be quite weak in a relativized calculation [12].) Martins *et al.* found that these exclusive final states have numerically rather similar cross-sections (except for their different thresholds), and gave a maximum total cross-section of about 7 mb at $\sqrt{s} \approx 4.1$ GeV. A quark interchange calculation of $J/\psi+N$ and $\psi' + N$ cross-sections using a simplified quark + diquark model of the nucleon [22] also found several-mb peak cross-sections not far above threshold.

Our collaboration recently carried out similar quark interchange model calculations (Wong *et al.* [20,21]). We used numerically determined Coulomb plus linear plus hyperfine quark potential model wave functions, and evaluated the Born-order meson-meson T-matrix represented by the diagrams of fig. 6. The parameters used for the examples shown here are $\alpha_s = 0.6$, b (string tension) $= 0.18\,\mathrm{GeV}^2$, $m_{u,d} = 0.33\,\mathrm{GeV}$, $m_c = 1.6\,\mathrm{GeV}$, and the OGE contact hyperfine smearing parameter was $\sigma = 0.8\,\mathrm{GeV}$; these are all reasonably well-established nonrelativistic quark model parameters. We generated wave functions

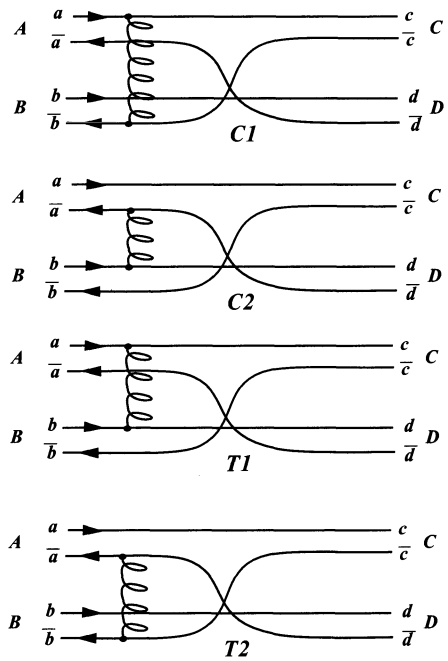

Fig. 3. The four quark interchange scattering diagrams evaluated in the $J/\psi + q\bar{q}$ cross-section calculation [19,20,22]. The "exchange" is the full quark model interaction Hamiltonian H_I.

for each meson by solving the radial Schrödinger equation with this interaction, and evaluated the scattering overlap integrals represented by each diagram in fig. 6 for each of the three interactions, using Monte Carlo methods. The full hadron scattering amplitudes were then evaluated in the CM frame given these overlap integrals by attaching color, flavor and spin matrix elements, and were projected onto L-moments to separate the different partial waves (here including $L = 0$ to $L = 4$). In converting the amplitude moments to physical cross-sections we assumed physical hadron masses, relativistic dispersion relations and relativistic phase space. Recovery of the known analytic results for scattering amplitudes and cross-sections given SHO wave functions and this quark model interaction provided a check of the programs.

There is a formal ambiguity as to whether we allow the interaction before quark interchange, as in fig. 6 (prior), or after (post). This "post-prior ambiguity" is well known from studies of exchange collisions in atomic physics, and one may show that the final scattering amplitudes are identical in a nonrelativistic Schrödinger formalism. Since we have relativistic particles, we do find a significant post-prior discrepancy in some cases, as discussed in ref. [20]. The numerical results shown here use the "prior" formalism.

In fig. 4 we show our results for the $J/\psi + \pi^+ \to \bar{D}^\circ D^{*+}$ and $\psi'+\pi^+ \to \bar{D}^\circ D^{*+}$ dissociation cross-sections. We find a somewhat smaller $J/\psi + \pi$ cross-section than Blaschke *et al.*; after summing over $\bar{D}D^*$, $\bar{D}^*D$ and $\bar{D}^*D^*$ final channels, our final result [20] has a maximum of only about 1 mb at $\sqrt{s} \approx 4.0\,\mathrm{GeV}$. The important difference between our work and Blaschke *et al.* is in the treatment

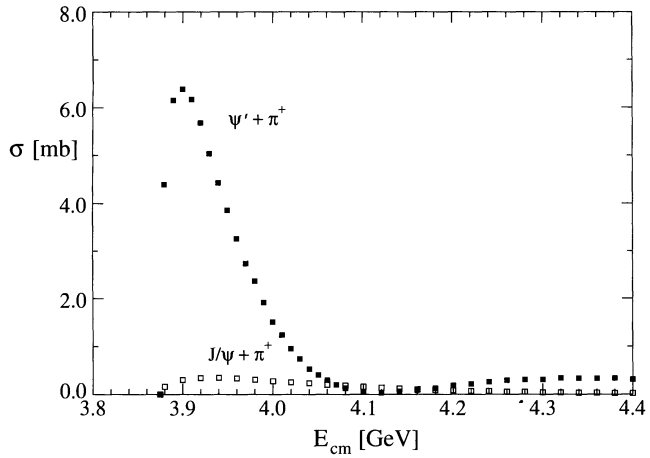

Fig. 4. Constituent interchange model predictions for the cross-sections $J/\psi + \pi^+ \to \bar{D}^\circ D^{*+}$ and $\psi' + \pi \to \bar{D}^\circ D^{*+}$.

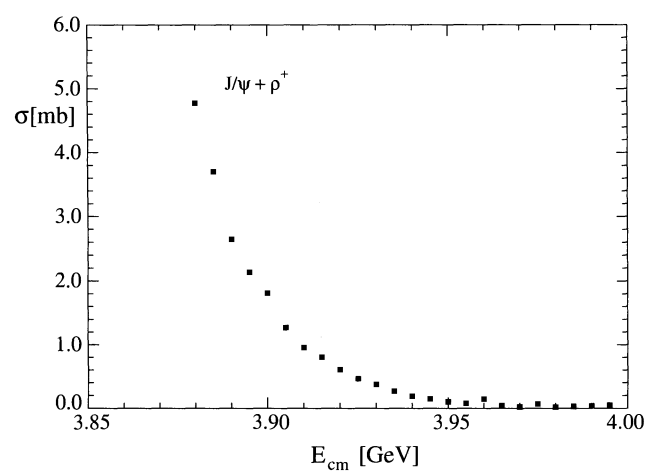

Fig. 5. Constituent interchange model prediction for exothermic reaction $J/\psi + \rho^+ \to \bar{D}^o D^+$. Some scatter of numerical results due to the Monte Carlo evaluation of overlap integrals is evident.

of the confining interaction; for simplicity, Blaschke *et al.* treated confinement as a color-independent Gaussian potential that acts only between quark and antiquark (hence they include only diagrams $C1$ and $C2$), whereas we assumed the standard $\lambda^a \cdot \lambda^a$ linear confining potential between all pairs of constituents. We find destructive interference between the C and T diagrams, leading to a much reduced $J/\psi + \pi$ peak cross-section relative to Blaschke *et al.*

Evaluation of the $\psi' + \pi^+$ cross-section involves a simple change to a $2S$ $c\bar{c}$ wave function and a change of phase space; this gave a rather large (ca. 12 mb) cross-section maximum (twice fig. 7 when we add $\bar{D}D^*$ and $\bar{D}^*D$), due mainly to the proximity of the initial $\psi' + \pi$ mass to the open-charm DD^* threshold. Our $c\bar{c} + q\bar{q}$ cross-sections typically have their strongest support just a few hundred MeV in $\sqrt{s}$ above threshold, since the overlap integrals are damped by the tails of the wave functions at higher energies.

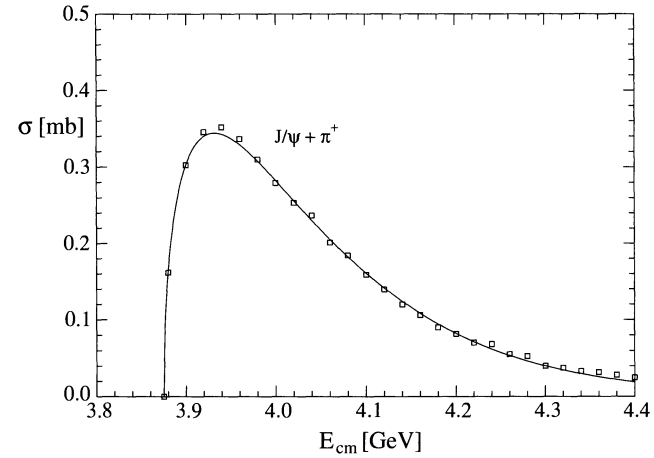

Fig. 6. A fit of eq. (2) to our numerical cross-section for the reaction $J/\psi + \pi^+ \to \bar{D}^\circ D^{*+}$.

The predicted $J/\psi + \rho$ cross-section is shown in fig. 5; this is very large near threshold for the simple reason that it is exothermic; there is a $1/v_i$ divergence in this cross-section (and those of most higher-mass initial mesons) as we approach threshold.

Although our scattering amplitudes and cross-sections are evaluated numerically and have no simple functional form given realistic quark model wave functions, it is nonetheless interesting that a simple function gives a useful parametrization of our cross-sections at low energies. This function is

$$\sigma(s) = \sigma_{\max}(\epsilon/\epsilon_{\max})^p e^{p(1-\epsilon/\epsilon_{\max})}, \qquad (2)$$

where $\epsilon = \sqrt{s} - M_C - M_D$ and $\sigma_{\max}$ is the maximum value of the cross-section, at $\epsilon_{\max}$. As an example, in fig. 6 we show our numerical results for the reaction $J/\psi + \pi^+ \to \bar{D}^o D^{*+}$ and a fit using the function in eq. (2). The fitted parameters are $\sigma_{\max} = 0.344$ mb, $\epsilon_{\max} = 57.1$ MeV and $p = 0.485$. Note that the fitted power is quite close to the $p = 1/2$ expected for an S-wave final state; the threshold exponent p is determined specified by the angular quantum numbers of the hadrons, and is $\pm 1/2 + L^{\rm CD}_{\min}$ (for endothermic/exothermic), where $L^{\rm CD}_{\min}$ is the lowest angular momentum allowed for the final meson pair CD. Our moment projection confirms that this cross-section is dominantly S-wave at low energies.

5 Theory: QCD sum rules

Finally, a very recent and exciting development is the application of QCD rum rules to the determination of low-energy charmonium cross-sections. This work has been carried out by Navarra *et al.* [23], who consider the processes $J/\psi + \pi \to DD, DD^*$ and D^*D^*. They find a ca. 1 mb dissociation cross-section to these final states at $\sqrt{s} \approx 4.1$ GeV (see fig. 7), similar in scale to the meson exchange and quark interchange results at this energy. Note however that the QCD sum rule calculation with current approximations predicts cross-sections that continue to rise with increasing $\sqrt{s}$.

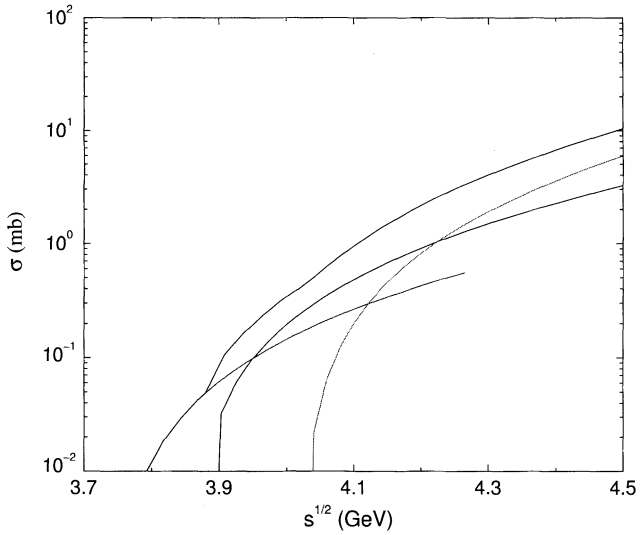

Fig. 7. QCD sum rule results for $J/\psi + \pi$ dissociation cross-sections [23]. With increasing $\sqrt{s}$ along the x-axis one encounters the cross-sections for $J/\psi + \pi \to DD$; DD^*; and D^*D^*. The total cross-section (the sum of these three) is also shown.

6 Conclusions

We have reviewed the experimental status and recent theoretical predictions for the cross-sections of $c\bar{c}$-mesons on light hadrons, which is a topic of great interest for the interpretation of heavy-ion collisions. Three scattering models are currently being investigated, which are color-dipole, t-channel meson exchange, and quark interchange. Theoretical cross-sections have also been estimated using QCD sum rules. The color-dipole approach gives very small cross-sections at low energies, whereas the other approaches typically find cross-sections of $\sim 1\,\mathrm{mb}$ for endothermic reactions within several hundred MeV of threshold. Most exothermic charm dissociation cross-sections (for example $J/\psi + \rho \to DD$) diverge as we approach threshold. The models predict very different energy dependences for these cross-sections at higher energies.

Should it be possible to determine these low-energy cross-sections experimentally, especially to exclusive final states, comparison with these theoretical results should lead to a much improved understanding of the mechanisms of low-energy hadron-hadron scattering.

We would like to acknowledge the kind invitation and support of the organisers of QNP 2002, which made it possible to attend the meeting and present these results. This research was supported in part by the DOE Division of Nuclear Physics, at ORNL, managed by UT-Battelle, LLC, under Contract No. DE-AC05-00OR 22725, Research Corp, and by the Deutsche Forschungsgemeinschaft DFG under contract Bo 56/ 153-1. We would also like to thank N. Black, D.B. Blaschke, B. Kopeliovich, M. Peskin, A. Sibirtsev, S. Sorensen, E.S. Swanson, C.Y. Wong and X.M. Xu for useful discussions and communications.

References

1. T. Matsui, H. Satz, Phys. Lett. B **178**, 416 (1986).
2. This issue is discussed, for example, by J. Hüfner, B.Z. Kopeliovich, Phys. Lett. B **445**, 223 (1998), hep-ph/9809300; Y.B. He, J. Hüfner, B. Kopeliovich, Eur. Phys. J. A **7**, 239 (2000), hep-ph/9908244; C.Y. Wong, Nucl. Phys. A **610**, 434c (1996).
3. B. Knapp *et al.*, Phys. Rev. Lett. **34**, 1040 (1975).
4. U. Camerini *et al.*, Phys. Rev. Lett. **35**, 4830 (1975).
5. R.L. Anderson *et al.*, Phys. Rev. Lett. **38**, 263 (1977).
6. J. Hüfner, B.Z. Kopeliovich, Phys. Lett. B **426**, 154 (1998), hep-ph/9712297.
7. This example is taken from A. Capella, A. Kaidalov, A. Kouider Akil, C. Gerschel, Phys. Lett. B **393**, 431 (1997), hep-ph/9607265.
8. J. Hüfner, B. Kopeliovich, Phys. Rev. Lett. **76**, 192 (1996); Y.B. He, J. Hüfner, B. Kopeliovich, Eur. Phys. J. A **7**, 239 (2000), hep-ph/9908243.
9. B. Müller, *Quark Matter 99*, Theory Summary Talk, nucl-th/9906029v3; Nucl. Phys. A **661**, 272 (1999).
10. D. Kharzeev, H. Satz, Phys. Lett. B **334**, 155 (1994), hep-ph/9405414.
11. J. Hüfner, Yu.P. Ivanov, B.Z. Kopeliovich, A.V. Tarasov, Phys. Rev. D **62**, 094022 (2000), hep-ph/0007111.
12. D.B. Blaschke, G.R.G. Burau, M.I. Ivanov, Yu.L. Kalinovsky, P.C. Tandy, hep-ph/0002047.
13. S.G. Matinyan, B. Müller, Phys. Rev. C **58**, 2994 (1998), nucl-th/9806027.
14. Z.W. Lin, C.M. Ko, Phys. Rev. C **62**, 034903 (2000), nucl-th/9912046.
15. A. Sibirtsev, K. Tsushima, A.W. Thomas, Phys. Rev. C **63**, 044906 (2001), nucl-th/0005041.
16. W. Liu, C.M. Ko, Z.W. Lin, Phys. Rev. C **65**, 015203 (2002), nucl-th/0107058.
17. K.L. Haglin, Phys. Rev. C **61**, 031902 (2000), nucl-th/9907034.
18. K.L. Haglin, C. Gale, nucl-th/0002029.
19. K. Martins, D. Blaschke, E. Quack, Phys. Rev. C **51**, 2723 (1995), hep-ph/9411302.
20. C.Y. Wong, E.S. Swanson, T. Barnes, Phys. Rev. C **62**, 045201 (2000), hep-ph/9912431.
21. C.Y. Wong, E.S. Swanson, T. Barnes, Phys. Rev. C **65**, 014903 (2002), nucl-th/0106067.
22. K. Martins, Prog. Part. Nucl. Phys. **36**, 409 (1996), hep-ph/9601314.
23. F.S. Navarra, M. Nielsen, R.S. Marques de Carvalho, G. Krein, Phys. Lett. B **529**, 87 (2002), nucl-th/0105058.
24. M. Peskin, Nucl. Phys. B **156**, 365 (1979); G. Bhanot, M. Peskin, Nucl. Phys. B **156**, 391 (1979); see also A.B. Kaidalov, P.E. Volkovitsky, Phys. Rev. Lett. **69**, 3155 (1992).
25. T. Barnes, *Charmonium + light hadron cross-sections*, invited contribution to *Heavy Quark Physics 5, Dubna, 6-8 April 2000*, nucl-th/0006012.
26. T. Barnes, E.S. Swanson, Phys. Rev. D **46**, 131 (1992).
27. E.S. Swanson, Ann. Phys. (N.Y.) **220**, 73 (1992); D. Hadjimichef, G. Krein, S. Szpigel, J.S. daVeiga, Ann. Phys. **268**, 105 (1998), hep-ph/9805459; Phys. Lett. B **367**, 317 (1996); hep-ph/9511423; for $\pi\pi$ see also G.-Q. Zhao, X.-G. Jing, J.-C. Su, Phys. Rev. D **58**, 117503 (1998); for $K\pi$, see T. Barnes, E.S. Swanson, J. Weinstein, Phys. Rev. D **46**, 4868 (1992); for NN, see T. Barnes, S. Capstick,

M.D. Kovarik, E.S. Swanson, Phys. Rev. C **48**, 539 (1993), nucl-th/9302007; for KN see T. Barnes, E.S. Swanson, Phys. Rev. C **49**, 1166 (1994), nucl-th/9212008; for BB see T. Barnes, N. Black, D.J. Dean, E.S. Swanson, Phys. Rev. C **60**, 045202 (1999), nucl-th/9902068; for VPs and spin-orbit forces see T. Barnes, N. Black, E.S. Swanson, Phys. Rev. C **63**, 025204 (2001), nucl-th/0007025.

Eur. Phys. J. A **18**, 537–539 (2003)
DOI 10.1140/epja/i2002-10277-3

THE EUROPEAN PHYSICAL JOURNAL A

Properties of hot residual nuclei produced in pA reactions

Z. Rudy[1,2,a], W. Cassing[3], B. Kamys[1], L. Jarczyk[1], and A. Kowalczyk[1]

[1] Institute of Physics, Jagellonian University, PL-30059 Kraków, Poland
[2] Institut für Kernphysik, Forschungszentrum Jülich, D-52425 Jülich, Germany
[3] Institut für Theoretische Physik, Justus Liebig Universität Giessen, D-35392 Giessen, Germany

Received: 30 September 2002 /
Published online: 22 October 2003 – © Società Italiana di Fisica / Springer-Verlag 2003

Abstract. The predictions for the production of nuclides and particles in proton-induced reactions are important *e.g.* for the detailed design of spallation neutron sources or accelerator-driven-systems. Computational tools are required that are able to describe quantitatively the two-stage process *i.e.* intra-nuclear cascade followed by evaporation-fission. The first stage is a highly non-equilibrated process in which incoming proton deposits in hot residual nucleus both excitation energy and angular momentum. The CBUU transport model calculation for few targets, for the proton energy range 0.4–2.0 GeV are presented, with the idea to find global parametrizations for the distributions of charge, mass, excitation energy, angular momentum of hot residual nuclei.

PACS. 24.10.-i Nuclear reaction models and methods – 24.10.Lx Monte Carlo simulations (including hadron and parton cascades and string breaking models)

Nowadays neutron beams are produced mainly by fission in nuclear reactors optimized for high neutron brightness. Reactors dedicated to the production of neutron *e.g.* for condensed matter research produce a lot of heat. Its dissipation in the core approached the limits set by up-to-date material technology ($\sim$ 190 MeV of energy dissipated for produced neutron). Future solutions are accelerator-based pulsed sources, see fig. 1. By bombarding heavy metal target with high-energy particles (*e.g.* protons) in a spallation process neutrons are produced with only $\sim$ 30 MeV of energy dissipated for generated neutron. During the last decade several spallation sources (IPNS [1], ISIS [1], LANSCE [2], SINQ [3] became operational. Technical study of 5 MW spallation neutron source is being completed in Germany [4] and its construction is under discussion now.

With the advent of spallation neutron sources there is a growing need for high-energy nuclear transport codes for incident proton energy in the GeV range. The main objective is to simulate what are the distributions of emitted particles (protons, alphas...) and residual nuclei. Two stages of the reaction have to be suitably described: a) high-energy intra nuclear cascade INC, followed by b) subsequent statistical evaporation-fission process. The second stage of the reaction (statistical evaporation in competition with fission) is rather nonexpensive computationally (many well-checked codes are available).

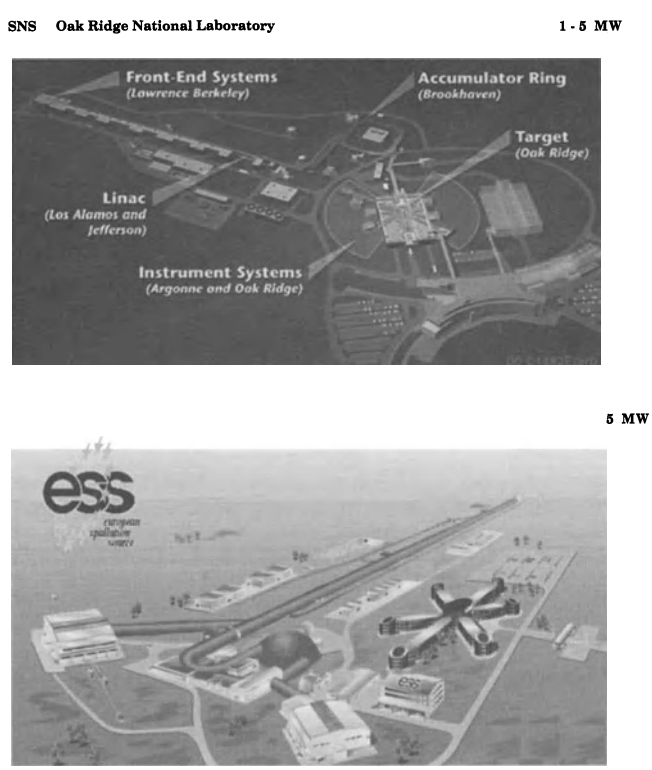

Fig. 1. Planned accelerator-driven neutron sources.

[a] e-mail: ufrudy@cyf-kr.edu.pl

However, the first stage it is a highly non-equilibrated process that has to be calculated using state-of-the-art sophisticated methods based, *e.g.*, on the CBUU approach [5, 6]. It would be useful to find a way to perform the first stage of the calculations "cheaply" while still sufficiently exactly. The solution may be to calculate the properties of hot residual nuclei produced during INC stage (*i.e.* the distributions of their mass, charge, excitation energy, angular distribution) for some chosen sample of impact proton energies and targets in order to have the possibility to interpolate for other energies and targets.

The CBUU model describes the propagation and mutual interaction of nucleons, Delta's, N^*-resonances as well as π- and η-mesons. It consists of a set of coupled equations of the one-body phase-space distributions [5,6] which can be solved by means of test particle method (every real particle is substituted by possibly large number of test particles).

In the CBUU calculations the four-momenta of all hadrons are propagated in time, therefore it is a straighforward task to evaluate the distributions of properties of the residual (hot) nuclei (mass, charge, angular momentum, excitation energy). For this purpose one computes, as a function of time, those particles (essentially nucleons) that have left the residual heavy fragment at position $\mathbf{R}$, *i.e.*

$$|\mathbf{r}_i - \mathbf{R}| \geq R_A + 2\,\mathrm{fm}, \tag{1}$$

where $R_A = 1.2\,\mathrm{fm}\ A_\mathrm{t}^{1/3}$ denotes the radius of the target with mass number A_t. Now let the number of particles emitted be $N_p(t)$. For each parallel ensemble one is able to evaluate then the fragment's average mass number, its excitation energy, three-momentum and angular momentum by exploring the conservation of total energy, mass number, momentum and angular momentum [7]:

$$\begin{aligned}
\langle E^* \rangle(t) &= E_\mathrm{tot} - \sum_{j=1}^{N_p(t)} \sqrt{p_j^2 + M_j^2} - M_\mathrm{res} - E_\mathrm{coul}, \\
\langle A_F \rangle(t) &= A_\mathrm{t} + 1 - N_p(t), \\
\langle \mathbf{p} \rangle(t) &= \mathbf{P}_\mathrm{tot} - \sum_{j=1}^{N_p(t)} \mathbf{p}_j(t), \\
\langle \mathbf{L} \rangle(t) &= \mathbf{L}_\mathrm{tot} - \sum_{j=1}^{N_p(t)} \mathbf{r}_j(t) \times \mathbf{p}_j(t).
\end{aligned} \tag{2}$$

In eq. (2) M_res denotes the mass of the "residual nucleus", E_coul stands for the Coulomb energy between the emitted particles and the "residual nucleus".

All quantities in (2) depend explicitly on time t due to the continuous evaporation of particles from the final compound system. Since the further decay chains will be followed by statistical model codes, the actual transition time for the connection of the CBUU and the statistical model calculation is of no significance as long as the system has left the *nonequilibrium phase* of the reaction and achieved *statistical equilibrium.* It has been checked that it is sufficient to trace the history of each ensemble of events within CBUU up to $150\,\mathrm{fm}/c$ ($5 \times 10^{-22}\,\mathrm{s}$).

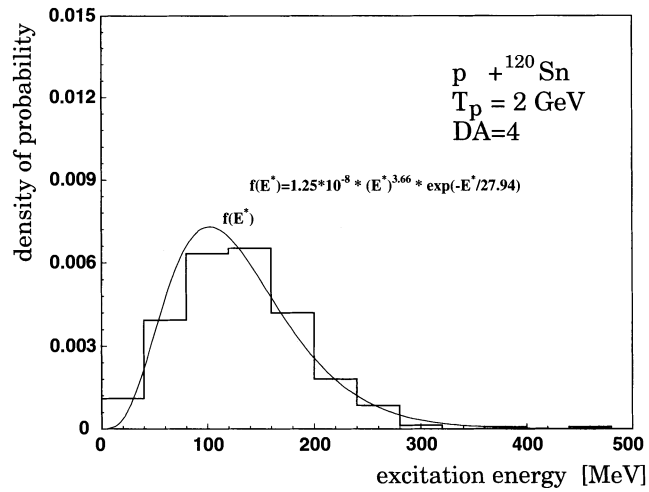

Fig. 2. An example of simulated distribution of excitation energy with imposed on it fitted gamma distribution (solid line).

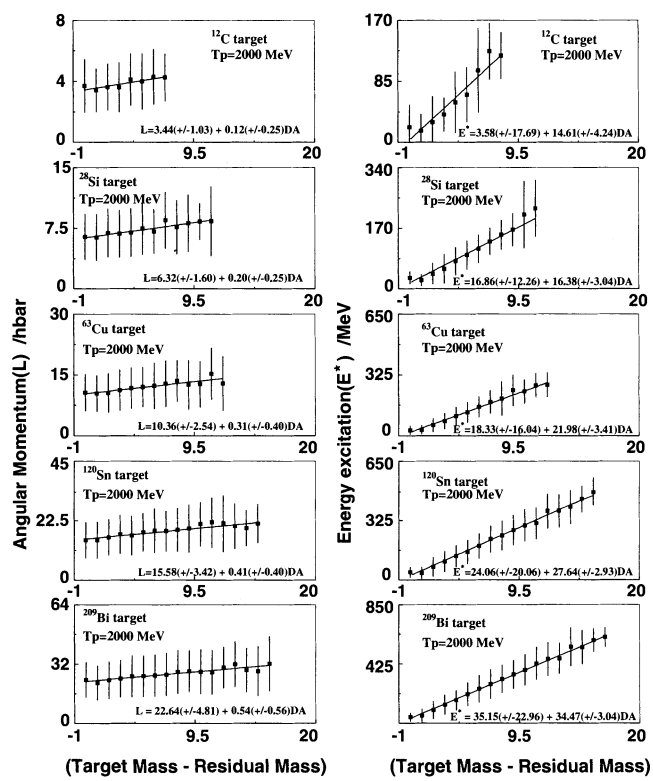

Fig. 3. Left side: calculated in the framework of the CBUU model angular momentum of created hot nuclei (*i.e.* after the INC stage of reaction), for proton incident energy $T_p = 2\,\mathrm{GeV}$, for the following targets: $^{12}\mathrm{C}$, $^{28}\mathrm{Si}$, $^{63}\mathrm{Cu}$, $^{120}\mathrm{Sn}$, $^{209}\mathrm{Bi}$. On the abscissa axis the difference DA = Target Mass − Residual Mass is indicated. The full squares denote the average values of angular momentum for a given value of DA, vertical bars show what is the σ parameter (standard deviation) of the distribution of angular momentum for given DA.

The CBUU calculations were performed for proton kinetic energiesin the range 0.4–2.0 GeV, for the following

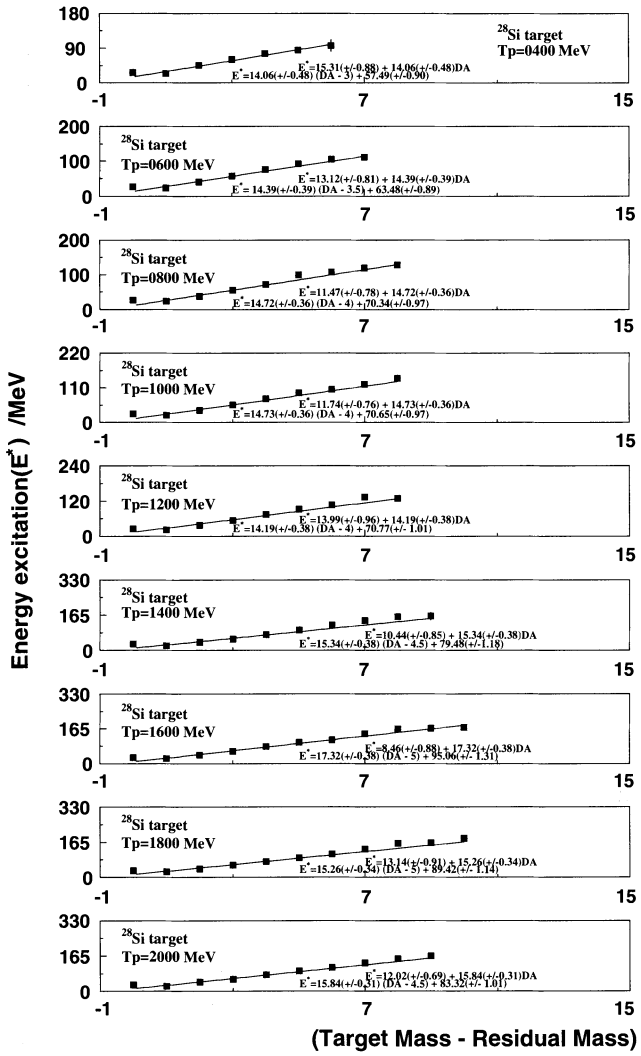

Fig. 4. Average values of excitation energy distributions are presented for proton incident energies $T_p = 0.4$–2.0 GeV (full squares), as a function of DA = Target Mass – Residual Mass.

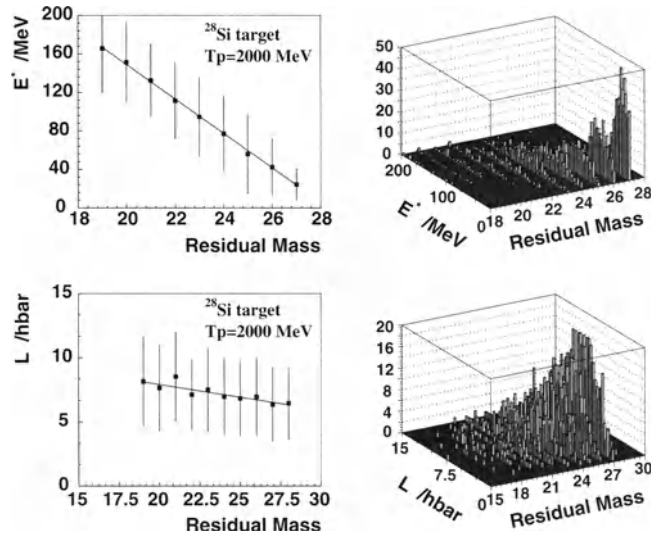

Fig. 5. Two-dimensional correlation plots of excitation energy *versus* residual mass and angular momentum *versus* residual mass, presented as: right, standard two-dimensional histograms; left, as function of regression with imposed vertical bars whose length is twice the standard deviation of the distribution for given value of residual mass.

targets: ^{12}C, ^{28}Si, ^{63}Cu, ^{120}Sn, ^{209}Bi. We have found that the distribution of angular momentum and excitation energy are quite well described by gamma distributions, *i.e.* $f(t) = \frac{1}{x_0^{s+1}\Gamma(s+1)}(t)^s \exp(-t/x_0)$; for $t > 0$; $x_0 = \frac{\sigma^2(t)}{\langle t\rangle}$; $s = \left[\frac{\langle t\rangle}{\sigma(t)}\right]^2 - 1$ (statistical inference tests were performed —fig. 2).

In figs. 3, 4 the results of CBUU simulations are shown. Only average values and standard deviations σ are presented for the distributions of angular momentum and excitation energy, because just these two parameters are needed to present the gamma distribution in an unambiguous way. One finds from the figures that if the number of ejected nucleon DA = Target Mass – Residual Mass increases, the average values of both excitation energy and angular momentum increases as well. There is a very intuitive way to explain it —when more nucleons are ejected, one should treat this as a signature that more nucleons were involved in INC. The more nucleon-nucleon collisions, the larger the part of the (introduced by incoming proton) energy and angular momentum deposited into the residual nucleus. What is more (as seen in figs. 3, 4) the dependency is smooth and linear as a function of DA.

In fig. 5 two-dimensional correlation plots are shown: excitation energy *versus* residual mass and angular momentum *versus* residual mass. One draws the conclusion that it is possible to parametrize the excitation energy and angular momentum taking the residual mass (or the introduced parameter DA = Target Mass – Residual Mass), as independent variable for given target and proton energy. We work now on the parametrization that involves also dependency on the target mass and proton impact energy.

References

1. B.S. Brown, A.D. Taylor, *ICANS XIII, 13th Meeting of the International Collaboration on Advanced Neutron Sources*, Report PSI-Proc. 95-02, November 1995, ISSN 1019-6447.
2. R. Pynn, *ICANS XI, 11th Meeting of the International Collaboration on Advanced Neutron Sources*, Report KEK 90-25.
3. G.S. Bauer, *ICANS XIV, 14th Meeting of the International Collaboration on Advanced Neutron Sources*, Report ANL-98/33, ISSN 1560-859X.
4. *The ESS Technical study*, ESS-96-53-M, ISBN 0902376659 (1996); `http://www.ess-europe.de`.
5. Gy. Wolf, W. Cassing, U. Mosel, Nucl. Phys. A **552**, 549 (1993).
6. W. Cassing, T. Demski, L. Jarczyk, B. Kamys, Z. Rudy, O.W.B. Schult, A. Strzalkowski, Z. Phys. A **349**, 77 (1994).
7. Z. Rudy, Report INP No. 1811/PH, Kraków 1998; (`http://mezon.if.uj.edu.pl/ kamys/COSY13/zrhab.pdf`).

Eur. Phys. J. A **18**, 541–542 (2003)
DOI 10.1140/epja/i2002-10278-2

THE EUROPEAN PHYSICAL JOURNAL A

Heavy-quark physics

Recent developments and old problems

M. Jeżabek[a]

The Henryk Niewodniczński Institute of Nuclear Physics, ul. Radzikowskiego 152, PL-31342 Kraków, Poland

Received: 30 September 2002 /
Published online: 22 October 2003 – © Società Italiana di Fisica / Springer-Verlag 2003

Abstract. Recent advances as well as some problems in physics of bottom and top quarks are discussed.

PACS. 12.39.-x Phenomenological quark models – 13.20.-v Leptonic, semileptonic, and radiative decays of mesons – 13.30.-a Decays of baryons – 13.60.Rj Baryon production

1 Introduction

There are multiple reasons for studying physics of heavy quarks: to probe our theoretical understanding of QCD, extract fundamental quantities like quark masses and CKM mixing matrix; search for New Physics. During last few years a tremendous progress in both experimental and theoretical studies of heavy-flavor dynamics has been achieved. B-meson physics is now the most intensively studied part of the high-energy particle physics. In particular the CKM paradigm has been successfully tested and nearly established; see, *e.g.*, [1]. This development is accompanied by an impressive progress in theoretical methods including applications of effective theories in heavy-flavor physics. In this short review some recent advances are briefly reviewed as well as some problems which still remain unsolved.

2 Old and new problems in B physics

B physics is an ideal place to check our understanding of QCD. Both exclusive and inclusive B decays have been studied. Recently CP violation and rare decays attract particular attention because theoretical predictions can soon be tested by experiments at B factories. Combining experimental input from different decay channels experimentalist can perform multidimensional fits and extract not only fundamental parameters like b-quark mass and the strong-coupling constant α_s but also phenomenological parameters of the Heavy Quark Effective Theory or Heavy Quark Expansion which describe non-perturbative aspects of QCD for inclusive and exclusive decays, respectively. An example of this strategy is presented in ref. [2] where by combining the information from $b \to s\gamma$ and inclusive semileptonic B decays a fairly precise determination of V_{ub} has been obtained. With higher statistics a further significant reduction of experimental errors is expected. At this point accuracy will be limited by perturbative QCD calculations which for differential distributions in semileptonic B decays have been done only at the lowest non-trivial order [3]. Moreover, there are also some data which cannot be explained by present-day theory in a convincing way: semileptonic branching ratios for B-mesons are smaller than expected, the ratio of the lifetimes for the $\Lambda_{\rm B}$-baryon and B-meson is much smaller than predicted, and the bottom production cross-section measured at Tevatron, HERA and LEP is about a factor of three larger than QCD calculations predict. It is possible that these problems reflect contributions of some New Physics. A light gluino and a $\tilde{b}$-squark may explain the high value of the bottom production cross-section [4]. However, much less spectacular options are also possible [5] implying that our present understanding of QCD is not as good as believed.

3 Top quark pair production

Studies of top quark pair production will be an important part of the physics program at future linear e^+e^- colliders [6,7]. A Linear Collider (LC) operating at energies close to the $t\bar{t}$ threshold is an ideal machine to study the properties of the top quark. Prospects that the LC will be built during this decade stimulate growing interest in the precise theoretical description of this reaction. The large top quark width $\Gamma_t \sim 1.5$ GeV [8] makes the threshold cross-section look quite different from those for charmonium and bottomium production. As first observed by Fadin and Khoze [9] the excitation curve for top pairs is smooth due to smearing of overlapping topponium resonances. They showed also that thanks to the large top

[a] e-mail: marek.jezabek@ifj.edu.pl

width this curve is not sensitive to large distance effects in QCD and allows for a precise determination of important short-distance parameters like the strong-coupling constant α_s, and top quark mass m_t and width Γ_t. This leading order (LO) results were extended to the next-to-leading order (NLO) in [10]. Furthermore in [11] and [12] some differential distributions, including the momentum distribution of top quarks, were calculated with NLO accuracy in momentum and position space, respectively. It should be mentioned that, although these numerical calculations are in perfect agreement, in QCD the transition between the momentum and the position space is highly non-trivial and in fact in higher orders it introduces renormalon ambiguities related to asymptotic characters of the corresponding series [13]. In the threshold region ($\sqrt{s} \approx 2m_t$) both t and $\bar{t}$ move with non-relativistic velocities $\beta \sim \alpha_s$. In this region an approach based on pure α_s expansion is not useful at all. Instead one considers the following expansion for the cross-section:

$$\sigma_{t\bar{t}} \sim \sum_k c_k \left(\frac{\alpha_s}{\beta}\right)^k \left[1 + \{\alpha_s, \beta\}\left\{\alpha_s^2, \alpha_s\beta, \beta^2\right\} + \dots\right]. \tag{1}$$

In the above expression the terms in the square bracket correspond to the LO and NLO approximations, respectively. At the end of the nineties even the next–to–next-to-leading order (NLLO) results were computed independently by a few groups, see [14] and the original papers cited therein. It was very disappointing when rather large uncertainties were observed at NNLO in the normalization of $\sigma_{t\bar{t}}$. However, recently an even more ambitious calculation has been accomplished by Hoang, Manohar, Stewart and Teubner, see [15,16] for recent reviews. Using renormalization group equations they have also performed additional resummation of terms proportional to $(\alpha_s \log\beta)^j$. In this way theoretical uncertainties in the normalization of the total cross-section $\sigma_{t\bar{t}}$ have been reduced to the level of few percent. This paves the way to precision studies of top quark pair production near threshold at a future linear collider [17]. It has been also shown that e^+e^- annihilation near the top quark production threshold is an ideal place for studies of top quark polarization and spin-dependent interactions [18]. Unfortunately, even at the NNLO level neither calculations of top quark polarization nor of its momentum distribution have been performed.

Top quark production and decay will be also studied at hadron colliders. High-statistic data samples from Run II of the Tevatron collider and the LHC will make possible detailed investigations of the electroweak and strong interactions of top quarks. On the theory side NLO QCD calculations for hadronic production and decay have been recently completed by Bernreuther *et al.*, see [19] and references therein.

This work is supported in part the European Community's Human Potential Programme under contract HPRN-CT-2000-00149 Physics at Colliders, and by the KBN grant 5P03B09320.

References

1. S. Laplace, arXiv:hep-ph/0209188.
2. CLEO Collaboration (H. Schwarthoff), arXiv:hep-ex/0205015.
3. M. Jezabek, J.H. Kuhn, Nucl. Phys. B **320**, 20 (1989); A. Czarnecki, M. Jezabek, Nucl. Phys. B **427**, 3 (1994).
4. E.L. Berger *et al.*, Phys. Rev. Lett. **86**, 4231 (2001).
5. M. Cacciari, P. Nason, Phys. Rev. Lett. **89**, 122003 (2002).
6. E. Accomando *et al.*, Phys. Rep. **299**, 1 (1998).
7. ECFA/DESY LC Physics Working Group Collaboration (J.A. Aguilar-Saavedra *et al.*) arXiv:hep-ph/0106315.
8. M. Jezabek, J.H. Kuhn, Nucl. Phys. B **314**, 1 (1989); Phys. Rev. D **48**, 1910 (1993).
9. V.S. Fadin, V.A. Khoze, JETP Lett. **46**, 525 (1987), (Pis'ma Zh. Eksp. Teor. Fiz. **46**, 417 (1987)).
10. M.J. Strassler, M.E. Peskin, Phys. Rev. D **43**, 1500 (1991).
11. M. Jezabek, J.H. Kuhn, T. Teubner, Z. Phys. C **56**, 653 (1992).
12. Y. Sumino, K. Fujii, K. Hagiwara, H. Murayama, C.K. Ng, Phys. Rev. D **47**, 56 (1993).
13. M. Jezabek, M. Peter, Y. Sumino, Phys. Lett. B **428**, 352 (1998); M. Jezabek, J.H. Kuhn, M. Peter, Y. Sumino, T. Teubner, Phys. Rev. D **58**, 014006 (1998).
14. A.H. Hoang *et al.*, Eur. Phys. J. Direct C **3**, 1 (2000).
15. A.H. Hoang, arXiv:hep-ph/0204299.
16. I.W. Stewart, AIP Conf. Proc. **618**, 395 (2002), arXiv:hep-ph/0201180.
17. M. Martinez, R. Miquel, Eur. Phys. J. C **27**, 49 (2003), arXiv:hep-ph/0207315.
18. R. Harlander, M. Jezabek, J.H. Kuhn, T. Teubner, Phys. Lett. B **346**, 137 (1995); R. Harlander, M. Jezabek, J.H. Kuhn, M. Peter, Z. Phys. C **73**, 477 (1997).
19. W. Bernreuther, A. Brandenburg, Z.G. Si, P. Uwer, arXiv:hep-ph/0209202.

Eur. Phys. J. A **18**, 543–545 (2003)
DOI 10.1140/epja/i2002-10279-1

THE EUROPEAN PHYSICAL JOURNAL A

Chiral dynamics and B $\to 3\pi$ decay

Ulf-G. Meißner[1,a] and S. Gardner[2]

[1] IKP, FZ Jülich, D-52425 Jülich, Germany and ITP, Karl-Franzens-Universität Graz, A-8010 Graz, Austria
[2] Department of Physics and Astronomy, University of KY, Lexington, Kentucky 40506-0055, USA

Received: 30 September 2002 /
Published online: 22 October 2003 – © Società Italiana di Fisica / Springer-Verlag 2003

Abstract. We discuss our knowledge of the scalar sector of QCD and how it impacts the determination of the CKM angle α from the isospin analysis of the $B \to \rho\pi$ decay.

PACS. 13.25.Hw Decays of bottom mesons – 11.30.Er Charge conjugation, parity, time reversal, and other discrete symmetries – 12.39.Fe Chiral Lagrangians – 14.40.Cs Other mesons with $S = C = 0$, mass < 2.5 GeV

1 Introduction

CP violation has been established experimentally in the K- and B-meson systems. In the standard model, this can be explained in terms of one single phase, which leads to complex entries in the CKM matrix. The unitarity of this matrix may be represented in terms of various triangles, one of them to be measured at the B factories. Any violation of unitarity would be a signal of physiscs beyond the Standard Model. However, to achieve the required accuracy to really test the relation $\alpha + \beta + \gamma = \pi$, where α, β, and γ are the three angles of the triangle, one has to be able to precisely calculate or eliminate the final-state interactions of the mesons generated in the various B decays. Here, we will be concerned with the decay $B \to 3\pi$, because the isospin analysis possible in $B \to \rho\pi$ decay allows to extract $\sin(2\alpha)$ [1,2]. Recent observations, however, have triggered the question about a possible "hadronic pollution" in the $\rho\pi$ phase space. In particular, the E791 Collaboration has found that half of the rate of $D^- \to \pi^-\pi^+\pi^-$ decay goes via the $D^- \to \pi^-\sigma(500) \to \pi^-\pi^+\pi^-$ doorway state [3]. This measurement was also considered as further evidence for a light scalar-isoscalar meson, the elusive σ. Furthermore, it was shown in ref. [4] that the inclusion of this channel can improve the theoretical description of the ratio

$$\mathcal{R} = \frac{\mathrm{Br}(\bar{B}^0 \to \rho^\mp\pi^\pm)}{\mathrm{Br}(B^- \to \rho^0\pi^-)} = 2.7 \pm 1.2 \ , \qquad (1)$$

measured at CLEO and BABAR. Note that $\mathcal{R} \simeq 6$ at the tree level in naive factorization. Since there is on-going debate about the nature of the σ, we will address here the following questions: What do we know about the scalar sector of QCD? What is its impact on $B \to \rho\pi$ decay?

[a] e-mail: u.meissner@fz-juelich.de

2 The scalar sector of QCD

The scalar-isoscalar sector of QCD is highly interesting because of its vacuum quantum numbers, and its direct relation to the quark mass terms (explicit chiral-symmetry breaking), the related σ-terms, and so on. Its most distinct characteristics are the very strong final-state interactions (FSI), signaled, *e.g.*, by the rapidly rising isospin zero, S-wave $\pi\pi$ phase shift $\delta_0^0(s)$ or the observation that the scalar pion radius, $\langle r_S^2\rangle_\pi \simeq 0.6\,\mathrm{fm}^2$, is sizeably bigger than the corresponding vector (charge) radius, $\langle r_V^2\rangle_\pi \simeq 0.4\,\mathrm{fm}^2$. Note also that there is no direct experimental probe with such quantum numbers. Therefore, theoretical investigations using different tools have been employed to deepen our understanding of this sector, these are Chiral Perturbation Theory (CHPT), resummation schemes consistent with CHPT, unitarity, analyticity, ... (like, *e.g.*, the chiral unitary approach [5]) and also dispersion relations. The following general results emerge: First, a *consistent* picture of the scalar (pion and kaon) form factors is obtained, and, second, all the light (non-strange and strange) scalar mesons are dynamically generated in a large class of resummation schemes (see, *e.g.*, ref. [6]), although this later topic is still vigorously debated[1]. For the impact on the $B \to \rho\pi$ decay, we fortunately only need the (non-strange) scalar form factor of the pion, $\Gamma_\pi(s)$ (or, equivalently, the $\sigma \to \pi\pi$ vertex function $\Gamma_{\sigma\pi\pi}(s)$), defined via

$$\begin{aligned}\langle 0|\hat{m}(\bar{u}u + \bar{d}d)|\pi^a(p)\pi^b(p')\rangle &= \delta^{ab} M_\pi^2\, \Gamma_\pi(s) \\ &= \mathcal{N}\, \Gamma_{\sigma\pi\pi}(s) \ , \ s = (p+p)^2 \ . \end{aligned} \qquad (2)$$

[1] Consequently, by "σ" we always mean a two-pion state with total isospin zero and in a relative S-wave state, $(\pi\pi)_S$, understanding its dynamical origin in the strong pionic FSI for these quantum numbers.

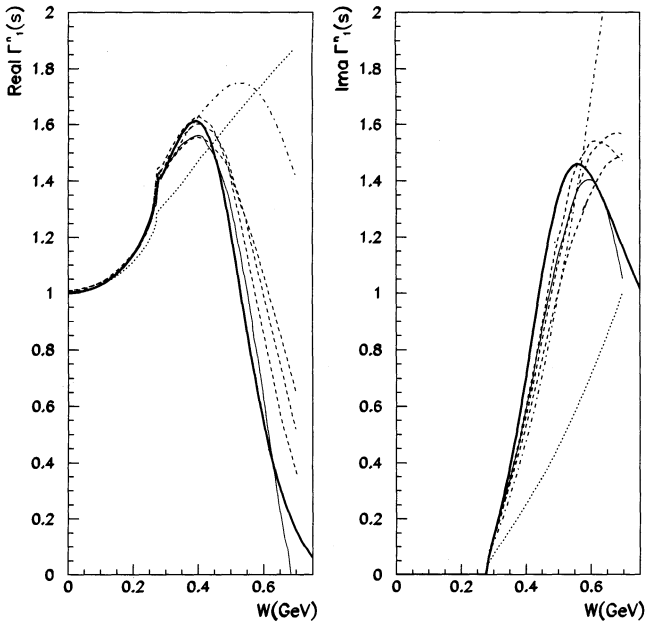

Fig. 1. Real (left) and imaginary part (right) of the non-strange scalar form factor of the pion. Solid line: chiral unitary approach as discussed in the text, dotted/dash-dotted line: CHPT to one/two loops, dashed lines: dispersive results based on different $\pi\pi$ phase shift analyses [7].

The scalar form factor is shown in fig. 1 for the various theoretical approaches mentioned above. We will use here the result of the chiral unitary approach [8], which was successfully tested, *e.g.*, in $J/\Psi \to \phi\pi\pi(\bar{K}K)$ decays. It is worth to point out that the scalar form factor constructed in [8] is systematically matched to the CHPT representation, and it embodies by construction the coupled channel $\pi\pi/\bar{K}K$ dynamics. It is also consistent with the dispersive results of ref. [7]. Most importantly for the later discussion, we remark that the form of the pion scalar form factor is very different from a Breit-Wigner (BW) form with a running width, as used, *e.g.*, in [3]. This apparent difference casts doubt on the recent conclusions of refs. [3, 4]. The situation is completely different for the pion vector form factor entering the $\rho\pi$ intermediate state — it can be described to good precision by a BW with running width. More generally, the vector form factor can be reconstructed from unitarity and analyticity and matched to CHPT. The resulting vertex function does not differ significantly from a BW with running width (see ref. [9] for a detailed discussion on this point and corresponding figures).

3 Evaluating B $\to \rho\pi$ in the presence of the $\sigma\pi$ channel

Our starting point is the effective $|\Delta B| = 1$ Hamiltonian for the $b \to dq\bar{q}'$ decay:

$$\mathcal{H}_{\rm eff} = \frac{G_{\rm F}}{\sqrt{2}} \left[\sum_{j=u,c} \lambda_j \left(C_1 O_1^j + C_2 O_2^j \right) - \lambda_t \sum_{i=3}^{10} C_i O_i \right] , \tag{3}$$

Table 1. Effective branching ratios (in units of 10^{-6}) for the $B \to \sigma\pi$ and the $B \to \rho\pi$ decay, computed at the tree level. The form factors (f.f.) are defined as: BW = Breit-Wigner, RW = BW with a running width, $*$ the form factors advocated here [9].

δ (f.f.) [MeV]	$B^- \to \sigma\pi^-$	$B^- \to (\rho^0+\sigma)\pi^-$	$\bar{B}^0 \to \sigma\pi^0$	$\bar{B}^0 \to (\rho^0+\sigma)\pi^0$
200 (BW)	2.97	6.16	0.0258	0.516
300 (BW)	5.17	8.61	0.0457	0.940
200 (RW)	2.97	6.19	0.0258	0.475
300 (RW)	5.17	8.62	0.0457	0.855
200 ($*$)	4.11	7.61	0.0396	0.508
300 ($*$)	7.01	10.7	0.0663	0.916

with $\lambda_q = V_{qb}V_{qq}^\star$, V_{ij} an element of the CKM matrix and the operators are ordered such that the Wilson coefficients obey $C_1 \sim O(1)$, $C_1 > C_2 \gg C_{3,\ldots,10}$. We evaluate the resonance contributions to the $B \to 3\pi$ decay by using a product ansatz. For the requisite amplitudes, this means

$$\begin{aligned} A_R(B \to \pi^+\pi^-\pi) &= \langle (R \to \pi^+\pi^-)\,\pi|\mathcal{H}_{\rm eff}|B\rangle \\ &= \underbrace{\langle R\pi\,|\mathcal{H}_{\rm eff}|B\rangle}_{\rm m.e.}\,\underbrace{\Gamma_{R\to\pi\pi}}_{\rm v.f.} , \end{aligned} \tag{4}$$

where we compute the matrix element (m.e.) in factorization (including penguins) in the same way it was done in refs. [4,10] for a crisp comparison (detailed formulae can be found in ref. [9]). To ascertain the impact of the $B \to \sigma\pi$ channel to $B \to \rho\pi$ decay, we combine the decay channels at the amplitude level, $\mathcal{M} = A_\sigma(B \to \pi^+\pi^-\pi) + A_\rho(B \to \pi^+\pi^-\pi)$, and then integrate over the relevant three-body phase space to compute the effective $B \to \rho\pi$ branching ratios. The main new ingredient is the vertex function (v.f.) for which we employ in the $\sigma\pi$ channel the scalar form factor discussed earlier and the for the $\rho\pi$ mode the vector form factor from ref. [11]. The effective branching ratios for the $B \to \rho\pi$ decay computed at the tree level (and also including penguins following ref. [10]) lead to $\mathcal{R}_{\rm T} \simeq 5.5$ ($\mathcal{R}_{\rm T+P} \simeq 5.1$). Neither this ratio nor the calculated branching ratios depend in any significant way on the various vector form factors employed. The $B \to \sigma\pi$ branching ratios are collected in table 1. The computed values of

$$\mathcal{R} \simeq 2.0 \ldots 2.6 \tag{5}$$

are consistent with the empirical value of $\mathcal{R}_{\rm exp} = 2.7 \pm 1.2$, albeit the errors are large. The reduction in $\mathcal{R}$ is mostly due to the effect of the $\sigma\pi$ channel on the B^- decay mode. Turning to the $B \to \sigma\pi^0$ decay, we see that the contribution of the σ-meson to the $B^0(\bar{B}^0) \to \rho\pi$ decay is *much* smaller — with the scalar form factor we advocate, the effect is some 10%. Interestingly the σ has a tremendous impact on the $B^- \to \rho^0\pi^-$ decay (very similar to the large effect in $D^- \to \pi^+\pi^-\pi^-$), and a relatively modest one on the $\bar{B}^0 \to \rho^0\pi^0$ decay. Let us emphasize that we have realized our numerical analysis at the tree level, so that the precise numbers but not the trends will change

when a more refined analysis is performed. It is the relative size of the penguin contributions in the $\bar{B}^0 \to \sigma\pi^0$ and the $\bar{B}^0 \to \rho^0\pi^0$ decay which is of relevance to the isospin analysis to extract α. The presence of the $\sigma\pi^0$ final state in the $\rho^0\pi^0$ phase space can break the assumed relationship between the penguin contributions in $\rho\pi$ and thus mimic the effect of isospin violation — alternatively we can expand the $\rho\pi$ analysis to include the $\sigma\pi$ channel. It is worth noting that the $\sigma\pi^0$ and $\rho^0\pi^0$ contributions can, to some measure, be distinguished. Certainly the $\sigma\pi^0$ and $\rho\pi^0$ contributions behave differently under the cut on the invariant mass of the $\pi^+\pi^-$ pair. Moreover, making a cut on the helicity angle θ, ought also be helpful in separating the ρ^0 and σ contributions. *E.g.* for $B^- \to \rho^0/\sigma\pi^-$, the $\rho^0\pi$ contributions roughly follow a $\cos^2(\theta)$ distribution, whereas the $\sigma\pi$ contributions are quite flat, save for the bump at backward angles resulting from the u-channel contribution $\sim \Gamma_{\sigma\pi\pi}(u)$. Cutting on the helicity angle θ should also help disentangle the contributions from some of the intermediate B^*- and B_0-resonances, discussed first in ref. [10]. The contributions of such non-resonant intermediate states to the $\rho\pi$ channels has recently been scrutinized in ref. [12], where it was shown that the energy dependence of the intermediate heavy-meson propagator can lead to a drastic suppression of such contributions and thus the lowering of the value for $\mathcal{R}$ due to the σ persists in such a refined analysis.

4 Summary and outlook

In this paper, we have scrutinized the role of the σ-meson in the $B \to \rho\pi \to 3\pi$ decay, understanding its dynamical origin in the strong pion-pion final-state interactions in the scalar-isoscalar channel. The presence of the $\sigma\pi^0$ contribution in the $\rho^0\pi^0$ phase space is important in that it can break the assumed relationship between the penguin amplitudes, consequent to an assumption of isospin symmetry. In this, then, its presence mimics the effect of isospin violation. The salient results of our investigation can be summarized as follows: i) We have considered how SM isospin violation can impact the analysis to extract α in the $B \to \rho\pi$ decay. Under the assumption that the $|\Delta I| = 3/2$ and $|\Delta I| = 5/2$ amplitudes share the same weak phase, the presence of an additional amplitude of $|\Delta I| = 5/2$ character, induced by isospin-violating effects, does not impact the $B \to \rho\pi$ analysis in any way. This is in contradistinction to the isospin analysis in $B \to \pi\pi$. Thus the isospin-violating effects of importance are those which can break the assumed relationship between the penguin contributions. ii) The scalar form factor can be determined to a good precision by combining the constraints of chiral symmetry, analyticity, and unitarity. The form factor we adopt describes the appearance of the $f_0(980)$ as well, so that the shape of the $f_0(980)$ contribution in $B \to f_0(980)\pi \to 3\pi$, *e.g.*, should serve as a test of our approach. We emphasize that the resulting scalar form factor is very different from the commonly used Breit-Wigner form with a running width. This is in stark contrast to the vector form factor, which is dominated by the ρ-resonance. In that case, one can construct simple forms that fit the theoretical and empirical constraints. iii) Remarkably, the impact of the $\sigma\pi$ channel on the ratio $\mathcal{R}$, cf. eq. (1), is huge. The numbers we find for $\mathcal{R}$ are in agreement with the empirical ones, given its sizeable experimental uncertainty. This underscores the suggestion made, as well as improves the calculations done, in ref. [4]. Our analysis is based on *consistent* scalar and vector form factors. This conclusion persists if one includes non-resonant B^*, B_0 intermediate states [12]. iv) On the other hand, the impact of the $\sigma\pi$ channel on the $B \to \rho\pi$ isospin analysis is merely significant. Varying the cuts on the $\pi\pi$ invariant mass and helicity angle θ should be helpful in disentangling the various contributions. v) We have shown that one can expand the isospin analysis to include the $\sigma\pi$ channel because it has definite properties under CP. This may be necessary if varying the cuts in the $\pi\pi$ invariant mass and helicity angle θ are not sufficiently effective in suppressing the contribution from the $\sigma\pi^0$ channel in the $\rho^0\pi^0$ phase space. This work is merely a first step in exploiting constraints from chiral symmetry, analyticity, and unitarity in the description of hadronic B decays. In particular, the contribution of the "doubly" OZI-violating strange scalar form factor and its phenomenological role in factorization breaking ought be investigated.

References

1. H.J. Lipkin, Y. Nir, H.R. Quinn, A. Snyder, Phys. Rev. D **44**, 1454 (1991).
2. A.E. Snyder, H.R. Quinn, Phys. Rev. D **48**, 2139 (1993).
3. E791 Collaboration (M. Aitala *et al.*), Phys. Rev. Lett. **86**, 770 (2001).
4. A. Deandrea, A.D. Polosa, Phys. Rev. Lett. **86**, 216 (2001).
5. J.A. Oller, E. Oset, A. Ramos, Prog. Part. Nucl. Phys. **45**, 157 (2000).
6. M. Jamin, J.A. Oller, A. Pich, Nucl. Phys. B **587**, 331 (2000).
7. J.F. Donoghue, J. Gasser, H. Leutwyler, Nucl. Phys. B **343**, 341 (1990).
8. U.-G. Meißner, J.A. Oller, Nucl. Phys. A **679**, 671 (2001).
9. S. Gardner, Ulf-G. Meißner, Phys. Rev. D **65**, 094004 (2002). **433**, 441(E) (1998).
10. A. Deandrea, R. Gatto, M. Ladisa, G. Nardulli, P. Santorelli, Phys. Rev. D **62**, 036001 (2000).
11. S. Gardner, H.B. O'Connell, Phys. Rev. D **57**, 2716 (1998); **62**, 019903(E) (1998).
12. J. Tandean, S. Gardner, Phys. Rev. D **66**, 034019 (2002).

Eur. Phys. J. A **18**, 547–549 (2003)
DOI 10.1140/epja/i2002-10280-8

THE EUROPEAN PHYSICAL JOURNAL A

Mott effect and J/ψ dissociation at the quark-hadron phase transition

D. Blaschke[1,2,a], G. Burau[1], Yu. Kalinovsky[3], and T. Barnes[4,5]

[1] Department of Physics University of Rostock, D-18051 Rostock, Germany
[2] Bogoliubov Laboratory for Theoretical Physics, JINR Dubna, 141980 Dubna, Russia
[3] Laboratory for Information Technologies, JINR Dubna, 141980 Dubna, Russia
[4] Oak Ridge National Laboratory, Oak Ridge, TN 37831-6373, USA
[5] Department of Physics and Astronomy, University of Tennessee, Knoxville, TN 37996-1501, USA

Received: 30 September 2002 /
Published online: 22 October 2003 – © Società Italiana di Fisica / Springer-Verlag 2003

Abstract. We investigate the in-medium modification of pseudoscalar and vector mesons in a QCD-motivated chiral quark model by solving the Dyson-Schwinger equations for quarks and mesons at finite temperature for a wide mass range of meson masses, from light (π, ρ) to open-charm (D, D^*) states. At the chiral/deconfinement phase transition, the quark-antiquark bound states enter the continuum of unbound states and become broad resonances (hadronic Mott effect). We calculate the in-medium cross-sections for charmonium dissociation due to collisions with light hadrons in a chiral Lagrangian approach, and show that the D- and D^*-meson spectral broadening lowers the threshold for charmonium dissociation by π- and ρ-mesons. This leads to a step-like enhancement in the reaction rate. We suggest that this mechanism for enhanced charmonium dissociation may be the physical mechanism underlying the anomalous J/ψ suppression observed by NA50.

PACS. 05.20.Dd Kinetic theory – 12.38.Mh Quark-gluon plasma – 14.40.-n Mesons – 25.75.Nq Quark deconfinement, quark-gluon plasma production, and phase transitions

1 Introduction

Charmonia, in particular the J/ψ-meson, play an important role in the experimental search for the quark-gluon plasma (QGP) in relativistic heavy-ion collisions. The anomalous suppression of J/ψ production found by the NA50 Collaboration at CERN SPS in 158 A GeV Pb-Pb collisions [1] is reminiscent of the signal for QGP formation suggested by Matsui and Satz [2], although one should also consider the competing, non-QGP mechanisms for J/ψ suppression such as charmonium dissociation through collisions with projectile and target nucleons [3] and by co-moving hadrons formed in the collision [4]. A combination of hadronic and quark/gluon processes appears to give a satisfactory parametrization of the NA50 data [5,6]. However, we should inquire as to whether we do now have a consistent picture of anomalous J/ψ suppression. In this contribution we consider a unified theoretical approach based on the quark (gluon) substructure of hadrons, which predicts a characteristic energy dependence of the J/ψ dissociation cross-sections through collisions with light hadrons, as well as the dissociative "Mott effect" at the chiral/deconfinement phase transition.

[a] e-mail: david.blaschke@physik.uni-rostock.de

2 The Mott effect and spectral function for D-mesons

Due to their strong couplings to two-body decay channels, light mesons such as the ρ and the controversial light σ can be modeled as quark-antiquark bound states or alternatively as meson-meson interactions in the corresponding channel. In the $I = 0$ $\pi\pi$ "*sigma*" channel, the total spectral width $\Gamma_\sigma(T)$ associated with a σ-meson shows a minimum that correlates with the chiral restoration phase transition in the phase diagram of strongly interacting matter [7], since the hadronic decay width $\Gamma_{\sigma\to 2\pi}$ is already negligible but the coupling $\Gamma_{\sigma\to q\bar{q}}$ is still small. The transition from a bound state with vanishing decay width (infinite lifetime) to a resonance in the continuum of unbound states is called the Mott transition [8], and can be described by the behavior of the spectral function

$$A_h(s;T) = \frac{1}{N}\frac{\Gamma_h(T)M_h(T)}{\left[s - M_h^2(T)\right]^2 + \Gamma_h^2(T)M_h^2(T)}\,, \quad (1)$$

where $M_h(T)$ and $\Gamma_h(T)$ are the temperature-dependent mass and width of the hadron h. Critical phenomena related to the Mott transition for mesons at the chiral transition have been discussed in the context of the NJL model

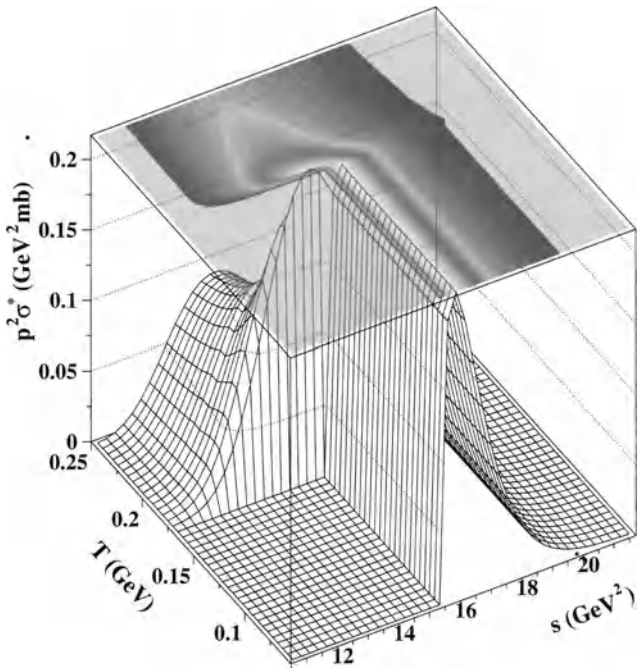

Fig. 1. In-medium cross-sections σ_h^* for $J/\psi + \pi \to D^* + \bar{D}$ as a function of s and T, using the spectral function of ref. [11].

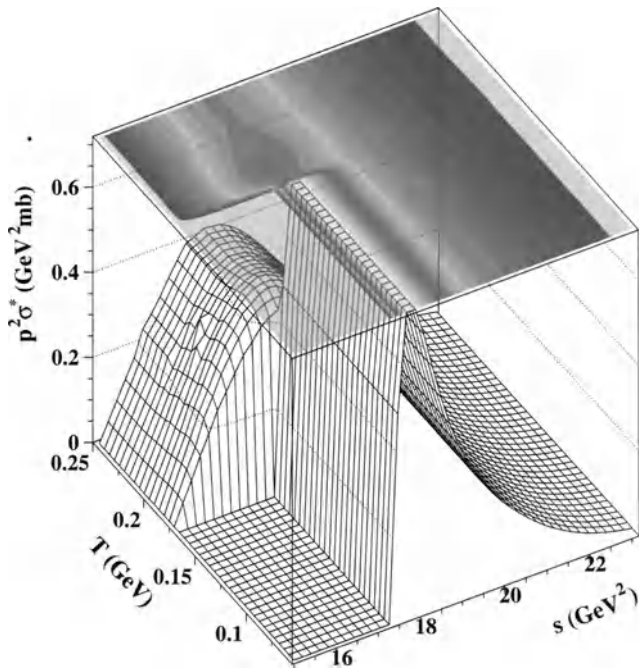

Fig. 2. Same as fig. 1 for the process $J/\psi + \rho \to D^* + \bar{D}^*$.

for quark matter in ref. [9]. In this model it was found that the Mott transition temperature for D-mesons is very close to that of the π- and K-mesons [10]. To estimate spectral function parameters (1) for the light and open-charm mesons, we use a modified NJL model in which unphysical quark production thresholds below the Mott temperature are excluded by an infrared cutoff [11]. In the following section we investigate the consequences of the meson Mott effect for charmonium dissociation processes.

3 In-medium J/ψ dissociation cross-section

The in-medium dissociation cross-section is defined in the Green function formalism by

$$\sigma_{\psi h}^*(s;T) = \int \mathrm{d}s_1 \int \mathrm{d}s_2 A_{D_1}(s_1;T) \times A_{D_2}(s_2;T)\sigma_{\psi h}^{\mathrm{vac}}(s;s_1,s_2). \quad (2)$$

(For details of this approach see ref. [12].) The cross-sections for the processes $J/\psi+\pi \to D^*+\bar{D}$ and $J/\psi+\rho \to D^* + \bar{D}^*$ are displayed in figs. 1 and 2, respectively. The vacuum cross-sections $\sigma_{\psi h}^{\mathrm{vac}}$ assumed here follow from the chiral Lagrangian approach of ref. [13].

In both cases the Mott effect ($T^{\mathrm{Mott}} \approx 172\,\mathrm{MeV}$) increases the spectral width in (1) of the D- and D^*-mesons, and hence effectively lowers the threshold for charmonium dissociation reactions. At temperatures above T^{Mott} these reactions become exothermic, whereas they were endothermic for $T < T^{\mathrm{Mott}}$. In addition to the lowered reaction thresholds, in figs. 1 and 2 one can also see a decrease in the maximum values of these exclusive cross-sections multiplied by the squared momentum p^2 of the incoming light particles. This behavior is slightly larger in $J/\psi + \pi$ than $J/\psi + \rho$ at high temperatures. In general, $J/\psi + \rho$ is the dominant dissociation process. In ref. [14] it was shown that this behavior of the in-medium cross-section leads to a strong enhancement in the thermal averaged dissociation cross-section, *i.e.* in the inverse lifetime of the J/ψ given by $\tau^{-1} = \tau_\pi^{-1} + \tau_\rho^{-1}$, with

$$\tau_h^{-1} = \langle \sigma_{\psi h}^* v \rangle n_h(T) = \int \frac{\mathrm{d}^3 p}{(2\pi)^3} \int \mathrm{d}s' A_h(s';T) f_h(p,s';T) j_h(p,s') \sigma_{\psi h}^*(s;T)\,, \quad (3)$$

where $f_h(p,s';T)$ is the Bose distribution function with the energy momentum $E(p,s') = (p^2+s')^{1/2}$ and $j_h(p,s')$ is the flux factor for the ψ-h collisions , $h = \{\pi,\rho\}$. The thermal average of this total J/ψ dissociation cross-section as a function of T, usinge the in-medium cross-sections shown in figs. 1 and 2, is displayed in fig. 3. This J/ψ dissociation rate due to impact by hadronic resonances shows a step-like enhancement by an order of magnitude above T^{Mott} for mesonic states due to their spectral broadening and thus the effective lowering of the breakup threshold. The effect is dominated by the ρ-meson subprocess shown in fig. 2 and its magnitude is quite sensitive to the detailed temperature dependence of the D- and D^*-meson spectral functions, as was discussed in [14].

The hadronic Mott effect scenario described here could be the dominant physical mechanism underlying the anomalous J/ψ suppression [1]. It could also contribute to an understanding of fast chemical equilibration [15] reported for the NA50 results on charm production. The role of the Mott effect on charmonium recombination ($D\bar{D}$ fusion) is an interesting topic for further investigation. It

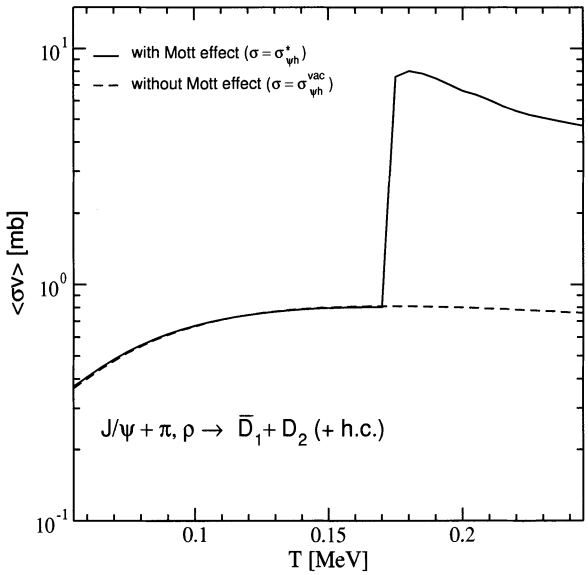

Fig. 3. Total thermal averaged J/ψ dissociation cross-section as a function of T without (dashed line) and with Mott effect for the π-, ρ- and D-mesons (solid line), using the spectral functions of ref. [11].

remains to be investigated which role dissociation processes by quark and gluon impact in the plasma phase have to play. A preliminary comparison with the NA50 data [16] shows that the bulk of the anomalous J/ψ suppression pattern can be explained by dissociation due to hadronic resonance impact, provided the dramatic changes of mesonic spectral functions obtained from the modified NJL model calculation [11] turn out to be realistic.

4 Conclusion

An understanding of the quark substructure of mesons is essential for determining meson-meson vacuum cross-sections as well as their modifications in hadronic matter. We have shown that the D-meson Mott effect at the QGP phase transition reduces the threshold for charmonium dissociation, which leads to a large increase in the J/ψ dissociation rate. A new finding reported here is that J/ψ dissociation is dominated by $J/\psi + \rho$ collisions, so that a direct connection to the in-medium ρ spectral function, as measured, for example, by NA45 (CERES), should be investigated. In subsequent research we plan to model the temperature-dependent meson spectral functions, using QCD Dyson-Schwinger equations as an improvement over the NJL model. Comparison with recent lattice QCD results for these spectral functions [17] is a promising approach for future studies of the hadronic Mott effect at the quark-hadron phase transition.

We are grateful to many colleagues for discussions, in particular to P.-B. Gossiaux, J. Hüfner, C.-M. Ko, S.H. Lee, Y. Oh, P. Petreczky, A. Polleri, R. Rapp and C.Y. Wong. Yu.K. acknowledges support from DFG grant No. 436 RUS 17/129/02, G.B. was supported by the DFG Graduiertenkolleg "Stark korrelierte Vielteilchensysteme", and D.B. and G.B. acknowledge support from the DAAD for their visits to the Oak Ridge National Laboratory and the University of Tennessee in Knoxville. T.B. acknowledges support from NSF grant No. INT-0004089.

References

1. NA50 Collaboration (M.C. Abreu *et al.*), Phys. Lett. B **477**, 28 (2000).
2. T. Matsui, H. Satz, Phys. Lett. B, **178**, 416 (1986).
3. C. Gerschel, J. Hüfner, Phys. Lett. B **207**, 253 (1988).
4. R. Vogt, M. Prakash, P. Koch, T.H. Hansson, Phys. Lett. B **207**, 263 (1988).
5. L. Grandchamp, R. Rapp, Nucl. Phys. A **709**, 415 (2002).
6. X.M. Xu, C.Y. Wong, T. Barnes, Phys. Res. C, **67**, 014907 (2003), arXiv:nucl-th/0207018.
7. E.A. Kuraev, M.K. Volkov, D. Blaschke, G. Röpke, S. Schmidt, Phys. Lett. B **424**, 235 (1998).
8. R. Redmer, Phys. Rep. **282**, 35 (1997).
9. J. Hüfner, S.P. Klevansky, P. Rehberg, Nucl. Phys. A **606**, 260 (1996).
10. F.O. Gottfried, S.P. Klevansky, Phys. Lett. B **286**, 221 (1992).
11. D. Blaschke, G. Burau, M.K. Volkov, V.L. Yudichev, Eur. Phys. J. A **11**, 319 (2001).
12. G. Burau, D. Blaschke, Yu. Kalinovsky, Phys. Lett. B **506**, 297 (2001).
13. V. Ivanov, Yu. Kalinovsky, D. Blaschke, G. Burau, *Chiral Lagrangian approach to the J/ψ breakup cross section*; [arXiv:hep-ph/0112354], and references therein.
14. D. Blaschke, G. Burau, T. Barnes, Yu. Kalinovsky, E. Swanson, in *Proceedings of the Budapest '02 Workshop on Quark & Hadron Dynamics* (2002) 261, arXiv:hep-ph/0210265.
15. P. Braun-Munzinger, J. Stachel, Phys. Lett. B **490**, 196 (2000).
16. G. Burau, *Charmonium Dissoziation am QCD Phasenübergang* PhD Thesis, Rostock (2002), unpublished.
17. F. Karsch, S. Datta, E. Laermann, P. Petreczky, S. Stickan, I. Wetzorke, Nucl. Phys. A **715**, 701 (2003), arXiv:hep-ph/0209028.

Eur. Phys. J. A **18**, 551–553 (2003)
DOI 10.1140/epja/i2002-10281-7

THE EUROPEAN PHYSICAL JOURNAL A

Gluonic penguin contribution to B $\rightarrow \pi\pi$ decays

P. Urban[a]

Institut für Theoretische Teilchenphysik, Universität Karlsruhe, D-76128 Karlsruhe, Germany and Henryk Niewodniczański Institute of Nuclear Physics, Kawiory 26a, 30-055 Kraków, Poland

Received: 30 September 2002 /
Published online: 22 October 2003 – © Società Italiana di Fisica / Springer-Verlag 2003

Abstract. We use the light-cone sum rule technique to calculate the contribution of the gluonic penguin operator O_{8g} to the decay of the B-meson to two pions. Leading-order perturbative and non-perturbative corrections are included, corresponding to hard and soft exchanged gluons, respectively. While the overall contribution of this operator to the decay is small as expected before, we find that the so-called soft-gluon part of this contribution is of the order of the hard-gluon one. This implies that the inclusion of soft gluons in the calculation of $B \rightarrow \pi\pi$ matrix elements may be important.

PACS. 13.25.Hw Hadronic decays of mesons: Decays of bottom mesons – 11.55.Hx Sum rules

1 Introduction

The hadronic decays of B-mesons are a source of information on CP violation and the parameters of the CKM mixing matrix, in particular the angles α and γ. Together with the present intensive experimental investigation of the B physics, this makes the $B \rightarrow \pi\pi$ decays interesting.

Hadronic decays of bottom mesons are not easily tractable within the framework of perturbation theory alone. One starts from an effective Hamiltonian and computes the Wilson coefficients and parametrizes the matrix elements of the relevant operators. The main difficulty lies in the accurate evaluation of the matrix elements, which are essentially non-perturbative. Recently QCD factorization has been suggested and applied [1] to the computation of these matrix elements. It is able to provide answers in the limit of infinite b-quark mass, but the question remains whether finite-mass effects affect the results significantly.

In this contribution, we present the results of a recent calculation [2] of the gluonic penguin operator matrix element contributing to the $B \rightarrow \pi\pi$ decay. Our approach to the problem relies on the QCD (light-cone) sum rules [3–6]. The framework for this calculation was introduced in [7]. This method allows the inclusion of both hard and soft gluons in a consistent manner, so that their respective contributions can be consistently compared to each other. Importantly enough, the soft gluons often evade other methods, like constituent quark models or factorization. On the other hand, our result shows that they cannot be neglected since at a finite value of the b-quark mass they are responsible for a large part of the matrix element of the gluonic penguin operator. Although the overall role of this particular operator in the description of the decay considered is not overwhelming, this fact is nevertheless an indication that similar sum rule analyses may be worthwhile for other operators. We have begun with O_{8g} due to its relative computational simplicity as compared to other terms of the effective Hamiltonian.

In the following, we present the method used to evaluate the matrix element $\langle B|O_{8g}|\pi\pi\rangle$ based on light-cone sum rules and define the appropriate correlation function. We then present the results and the various contributions appearing in the evaluation of this element, including the comparison between the hard- and soft-gluon part. Numerical predictions are also given. Finally, we present the conclusions.

2 Method

The $B \rightarrow \pi\pi$ decay is described by the effective Hamiltonian,

$$H_W = \frac{G_F}{\sqrt{2}}\left\{\lambda_u\left[\left(c_1(\mu)+\frac{c_2(\mu)}{3}\right)O_1(\mu)+2c_2(\mu)\widetilde{O}_1(\mu)\right] + \cdots + \lambda_t c_{8g}(\mu)O_{8g}(\mu)\right\}, \quad (1)$$

where $\lambda_u = V_{ub}V_{ud}^*$, $\lambda_t = V_{tb}V_{td}^*$ and we have displayed only the most important operators and the gluonic penguin operator O_{8g}, which is of our interest in this paper:

$$O_1 = (\bar{d}\Gamma_\mu u)(\bar{u}\Gamma^\mu b), \quad \widetilde{O}_1 = \left(\bar{d}\Gamma_\mu \frac{\lambda^a}{2}u\right)\left(\bar{u}\Gamma^\mu \frac{\lambda^a}{2}b\right), \quad (2)$$

$$O_{8g} = \frac{m_b}{8\pi^2}\bar{d}\sigma^{\mu\nu}(1+\gamma_5)\frac{\lambda^a}{2}g_s G^a_{\mu\nu}b, \quad (3)$$

[a] e-mail: urban@particle.physik.uni-karlsruhe.de

where $\Gamma_\mu = \gamma_\mu(1-\gamma_5)$ and m_b is the b-quark mass. In order to find the matrix element $\langle B|O_{8g}|\pi\pi\rangle$, we use the correlation function

$$F_\alpha(p,q,k) = -\int \mathrm{d}^4x\,\mathrm{d}^4y e^{-i(p-q)x+i(p-k)y} \times\langle 0|T\left\{j^{(\pi)}_{\alpha 5}(y)O_{8g}(0)j^{(B)}_5(x)\right\}|\pi^-(q)\rangle, \quad (4)$$

where the quark currents $j^{(\pi)}_{\alpha 5} = \bar{u}\gamma_\alpha\gamma_5 d$ and $j^{(B)}_5 = m_b\bar{b}i\gamma_5 d$ interpolate π- and B-mesons, respectively. This correlation function is evaluated in the spacelike region of the variables $s_1 = (p-k)^2$, $s_2 = (p-q)^2$, and $Q^2 = (p-q-k)^2$. Then the result is analytically continued and matched with the double dispersion relation to give a sum rule for the desired matrix element, see [2, 7] for details. After Borel transformations in the variables s_1 and s_2, the final formula for the matrix element is [7]

$$\langle\pi^-(p)\pi^+(-q)|O_{8g}|B(p-q)\rangle = \frac{-i}{\pi^2 f_\pi f_B m_B^2}\int_0^{s_0^\pi}\mathrm{d}s e^{-s_1/M_1^2}\int_{m_b^2}^{s_0^B}\mathrm{d}s_2 e^{(m_B^2-s_2)/M_2^2} \times \mathrm{Im}_{s_1}\mathrm{Im}_{s_2}F(s_1,s_2,m_B^2), \quad (5)$$

where F is the part of the correlation function F_α (4) proportional to the momentum $(p-k)$:

$$F_\alpha = (p-k)_\alpha F + q_\alpha\tilde{F}_1 + k_\alpha\tilde{F}_2 + \epsilon_{\alpha\beta\lambda\rho}q^\beta p^\lambda k^\rho\tilde{F}_3, \quad (6)$$

and the thresholds s_0^π and s_0^B are fitted from other sum rules, while f_π and f_B are the pion and B-meson decay constants, respectively and m_B stands for the B-meson mass. M_1 and M_2 are the Borel parameters.

3 Evaluation and results

The main task consists in computing the correlation function defined in eq. (4) in the spacelike region of the variables s_1, s_2, and Q^2. The details of this computation are described in [2]. It can be split into three parts: the hard, soft, and quark condensate contribution. This calculation includes the twist-2 and -3 hard-gluon effects as well as soft-gluon effects of twist 3 and 4. The latter are suppressed by the quark mass but not by α_s so that they become numerically of the same order as the hard gluonic ones. Also we include the quark condensate contribution as a check on the validity of the twist expansion. The calculation was done with the help of FORM [8].

The hard-gluon contribution gives one-loop diagrams whose ultraviolet divergencies are removed after subsequent Borel transformation. The soft-gluon contribution as well as the quark condensate are calculated at the tree level. The result for the matrix element is

$$A^{(O_{8g})}(\bar{B}^0_d\longrightarrow\pi^+\pi^-) \equiv \langle\pi^-(p)\pi^+(-q)|O_{8g}|B(p-q)\rangle = A^{(O_{8g})}_{\mathrm{hard}} + A^{(O_{8g})}_{\mathrm{soft}} + A^{(O_{8g})}_{\langle\bar{q}q\rangle}, \quad (7)$$

where

$$A^{(O_{8g})}_{\mathrm{hard}} = i\frac{\alpha_s C_F}{2\pi}m_b^2\left(\frac{1}{4\pi^2 f_\pi}\int_0^{s_0^\pi}\mathrm{d}s e^{-s/M_1^2}\right)\frac{m_b^2 f_\pi}{2m_B^2 f_B} \times\int_{u_0^B}^1\frac{\mathrm{d}u}{u}e^{m_B^2/M_2^2-m_b^2/uM_2^2}\left(\frac{\varphi_\pi(u)}{u}+\text{twist 3}\right), \quad (8)$$

$$A^{(O_{8g})}_{\mathrm{soft}} = -im_b^2\left(\frac{1}{4\pi^2 f_\pi}\int_0^{s_0^\pi}\mathrm{d}s e^{-s/M_1^2}\right)\left(\frac{20 f_\pi\delta_\pi^2}{m_B^2 f_B} \times\int_{u_0^B}^1\mathrm{d}u e^{m_B^2/M_2^2-m_b^2/uM_2^2}\bar{u}\left(u+\frac{m_b^2}{m_B^2}\right)\right), \quad (9)$$

$$A^{(O_{8g})}_{\langle\bar{q}q\rangle} = i\frac{\alpha_s C_F}{3\pi}m_b^2\left(\frac{-\langle\bar{q}q\rangle}{f_\pi m_b}\right)\left(\frac{m_b^2 f_\pi}{2m_B^2 f_B}\int_{u_0^B}^1\frac{\mathrm{d}u}{u} \times e^{m_B^2/M_2^2-m_b^2/uM_2^2}\left(\frac{\varphi_\pi(u)}{u}+\text{twist 3}\right)\right), \quad (10)$$

where $u_0^B = m_b^2/s_0^B$ and we have employed the asymptotic distribution amplitudes for the soft part. The twist-2 distribution amplitude φ_π as well as the omitted terms of higher twist can be found in [2]. The parameter δ_π^2 determines the normalization of the twist-4 quark-antiquark-gluon distribution amplitude and $\langle\bar{q}q\rangle$ is the quark condensate density.

From the formulae above, it is seen that although the soft contribution is suppressed by the second power of the heavy-quark mass with respect to the hard-gluon contribution, a factor of 20 invalidates neglecting this formally higher-order term. In fact, numerically the hard and soft contributions are of similar size.

Since we have at our disposal the exact sum rule for the matrix element, we can expand it in the heavy-quark mass. Such an analysis is interesting since it helps see the importance of finite-mass effects. The heavy-mass limit can be systematically performed once we make explicit the scaling of the different quantities with the b-quark mass:

$$m_B = m_b + \bar{\Lambda}, \qquad s_0^B = m_b^2 + 2m_b\omega_0,$$
$$M_2^2 = 2m_b\tau, \qquad f_B = \frac{\hat{f}_B}{\sqrt{m_b}}, \quad (11)$$

where $\bar{\Lambda}$, ω_0, τ, and $\hat{f}_B$ are the parameters independent of the heavy-mass scale. On substitution of these in the full result (7) and keeping only the leading terms of the each of the hard, soft, and quark condensate contributions we find that the three contributions scale as follows,

$$A^{(O_{8g})}_{\mathrm{hard}}\sim\sqrt{m_b}, \quad A^{(O_{8g})}_{\mathrm{soft}}\sim\frac{\delta_\pi^2}{m_b^{3/2}}, \quad A^{(O_{8g})}_{\langle\bar{q}q\rangle}\sim m_b^{-1/2}. \quad (12)$$

Rather than dealing with the matrix element $A^{(O_{8g})}$ itself, one can reduce the theoretical uncertainty by considering the ratio of this element to the factorizable amplitude for $B\to 2\pi$ decay, which comes from the O_1 operator, and is expressed as

$$A_E^{(O_1)} \equiv \langle\pi^-(p)\pi^+(-q)|O_1|B(p-q)\rangle_E = im_B^2 f_\pi f^+_{B\pi}(0). \quad (13)$$

The form factor $f^{+}_{B\pi}$ is found in the LCSR [9–11]. We thus define

$$r_{8g} = A^{(O_{8g})}/A^{(O_1)} \tag{14}$$

and give a numerical predicition for the ratio r_{8g} due to its smaller sensitivity to input parameters compared to the matrix element $A^{(O_{8g})}$. Doing the numerical analysis we use the asymptotic forms of the distribution amplitudes. The detailed formulae for these can be found in [2]. The inclusion of non-asymptotic corrections, however, does not lead to any significant modifications. The numerical input in the expression for the matrix element $A^{(O_{8g})}$ includes the Borel parameters M_1^2, M_2^2, the duality cutoffs s_0^π, s_0^B, the decay constants f_π and f_B, the quark pole mass m_b, the parameters of the distribution amplitudes, δ_π^2, μ_π, and the quark condensate $\langle\bar{q}q\rangle$.

The pion channel parameters fitted from the two-point SVZ sum rule [3] for $f_\pi = 132\,\mathrm{MeV}$ are $s_0^\pi = 0.7\,\mathrm{GeV}^2$ and $M_1^2 = 0.7\text{–}1.2\,\mathrm{GeV}^2$. The b-quark pole mass is taken at $m_b = 4.7 \pm 0.1\,\mathrm{GeV}$, consistent with the recent average of the $\overline{MS}$ mass $m_b(m_b) = 4.24 \pm 0.11\,\mathrm{GeV}$ [12] and then from the QCD sum rule for f_B we have $s_0^B = 35 \pm 2\,\mathrm{GeV}^2$. The renormalization scale is allowed to vary from $\mu_b/2$ to $2\mu_b$, where $\mu_b = \sqrt{m_B^2 - m_b^2} \simeq 2.4\,\mathrm{GeV}$. This range is chosen due to the two scales present in the problem, the Borel parameters $M_1^2 = 0.7\text{–}1.2\,\mathrm{GeV}^2$ and $M_2^2 = 10 \pm 2\,\mathrm{GeV}^2$. For the parameters of the distribution amplitudes, we take $\delta_\pi^2(\mu_b) = 0.13\,\mathrm{GeV}^2$ and $\mu_\pi(\mu_b) = 2\,\mathrm{GeV}$, and for the quark condensate $\langle\bar{q}q\rangle(\mu_b) = (-260\,\mathrm{MeV})^3$. With these ranges of the parameters, one obtains the following prediction for the ratio r_{8g}:

$$\begin{aligned} r_{8g} = 0.02 = 0.027\ (\text{hard}) - 0.015\ (\text{soft}) \\ + 0.008\ (\text{condensate}), \end{aligned} \tag{15}$$

see [2] for the discussion of the theoretical uncertainty on this number. In eq. (15) the contributions from the different parts of the amplitude are indicated. Evidently one cannot neglect the soft-gluon contribution.

Having at hand the expression for the matrix elements and for the ratio r_{8g} valid for a finite m_b, it is easy to see how important finite-mass effects are. For the ratio r_{8g}, the limit of an infinite heavy-quark mass gives

$$r_{8g}|_{m_b\to\infty} = 0.04. \tag{16}$$

Clearly, the infinite-mass limit is not very close to the exact value of the prediction. This is another incentive to study the hadronic B decays with the sum rule method, making it complementary to the factorization approach.

4 Conclusions

We have calculated the leading-order contribution to the matrix element of the chromomagnetic dipole operator O_{8g} relevant to the $B \to \pi\pi$ decay. The method used is based on the light-cone sum rules. Both hard and soft gluons contribute to this quantity and our method has allowed us to take these two effects into account in a systematic way. It has been found that the formally suppressed soft-gluon contribution is of the same order as the hard-gluon one. We have also computed the quark condensate contribution which is in fact small compared to the leading one. We give a numerical prediction for the ratio of the operator O_{8g} matrix element and the factorizable amplitude. It is pointed out that the finite-mass effects modify the infinite-mass limit rather substantially.

This work was supported by the DFG Forschergruppe "Quantenfeldtheorie, Computeralgebra und Monte Carlo Simulationen", by the German Ministry for Education and Research (BMBF), and by the KBN grant 5P03B09320. The author acknowledges support by the Humboldt Foundation.

References

1. M. Beneke, G. Buchalla, M. Neubert, C.T. Sachrajda, Phys. Rev. Lett. **83**, 1914 (1999); Nucl. Phys. B **606**, 245 (2001).
2. A. Khodjamirian, T. Mannel, P. Urban, Phys. Rev. D **67**, 054027 (2003), University of Karlsruhe preprint TTP02-16, hep-ph/0210378.
3. M.A. Shifman, A.I. Vainshtein, V.I. Zakharov, Nucl. Phys. B **147**, 385; 448 (1979).
4. I.I. Balitsky, V.M. Braun, A.V. Kolesnichenko, Nucl. Phys. B **312**, 509 (1989).
5. V.M. Braun, I.E. Filyanov, Z. Phys. C **44**, 157 (1989).
6. V.L. Chernyak, I.R. Zhitnitsky, Nucl. Phys. B **345**, 137 (1990).
7. A. Khodjamirian, Nucl. Phys. B **605**, 558 (2001).
8. J.A. Vermaseren, arXiv:math-ph/0010025.
9. A. Khodjamirian, R. Rückl, S. Weinzierl, O. Yakovlev, Phys. Lett. B **410**, 275 (1997).
10. E. Bagan, P. Ball, V.M. Braun, Phys. Lett. B **417**, 154 (1998).
11. P. Ball, R. Zwicky, JHEP **0110**, 019 (2001).
12. A.X. El-Khadra, M. Luke, Annu. Rev. Nucl. Part. Sci. **52**, 201, (2002), hep-ph/0208114.

Eur. Phys. J. A **18**, 555–558 (2003)
DOI 10.1140/epja/i2002-10282-6

THE EUROPEAN PHYSICAL JOURNAL A

Cross-sections and spin observables in proton-proton elastic scattering: Results from EDDA at COSY

H. Rohdjeß[1,a], F. Bauer[2], J. Bisplinghoff[1], K. Büßer[2], M. Busch[1], T. Colberg[2], L. Demirörs[2], C. Dahl[1], P.D. Eversheim[1], O. Eyser[2], O. Felden[3], R. Gebel[3], J. Greiff[2], F. Hinterberger[1], E. Jonas[2], H. Krause[2], C. Lehmann[2], J. Lindlein[2], R. Maier[3], A. Meinerzhagen[1], C. Pauly[2], D. Prasuhn[3], D. Rosendaal[1], P. von Rossen[3], N. Schirm[2], W. Scobel[2], K. Ulbrich[1], E. Weise[1], T. Wolf[2], and R. Ziegler[1]

[1] Helmholtz-Institut für Strahlen- und Kernphysik, Universität Bonn, D-53115 Bonn, Germany
[2] Institut für Experimentalphysik, Universität Hamburg, D-22761 Hamburg, Germany
[3] Institut für Kernphysik, Forschungszentrum Jülich, D-52425 Jülich, Germany

Received: 30 September 2002 /
Published online: 22 October 2003 – © Società Italiana di Fisica / Springer-Verlag 2003

Abstract. At the Cooler-Synchrotron COSY/Jülich polarized and unpolarized elastic proton-proton scattering has been investigated with the EDDA-Experiment in the energy range ($T_p \approx 0.5$–2.5 GeV). By taking scattering data during the acceleration of the beam with a large-acceptance ($\theta_{\mathrm{c.m.}} \approx 30°$–$90°$) detector, precise excitation functions for differential cross-section and analyzing power have been measured in small energy steps with consistent normalization with respect to luminosity and polarization. These data have helped to improve the determination of phase-shifts at higher energies and impose tight quantitative upper bounds on possible resonant contributions to pp elastic scattering, as they might arise from exotic 6-quark configurations. Recently, with polarized beam and target, the spin-correlation parameters A_{NN}, A_{SS}, and A_{SL} have been determined at 10 energies between 0.8 and 2.5 GeV. The observable A_{SS} has been measured the first time above 800 MeV and our results are in sharp contrast to phase-shift predictions at higher energies.

PACS. 24.70.+s Polarization phenomena in reactions – 25.40.Cm Elastic proton scattering – 11.80.Et Partial-wave analysis – 13.75.Cs Nucleon-nucleon interactions (including antinucleons, deuterons, etc.)

1 Introduction

The nucleon-nucleon (NN) interaction is fundamental to nuclear physics and has been studied over a broad energy range. The contribution of extensive experimental and theoretical efforts to our understanding of the strong interaction cannot be overestimated. NN elastic scattering data, parameterized by energy-dependent phase-shifts, are used as an important ingredient in theoretical calculations of inelastic processes, nucleon-nucleus and heavy-ion reactions. While below the pion production threshold at about 300 MeV elastic scattering is described to a high level of precision [1] by a number of models, *e.g.* phenomenological, meson exchange, and more recently chiral perturbation theory [2], only meson exchange models have been pushed further to roughly reproduce experimental data up to 0.8 GeV. However, at even higher energies, where details of the short-range interaction may become important, the limits of these models remains to be explored. On the experimental side, available data allow to do a Phase-Shift Analysis (PSA) unambiguously up to about 1 GeV [3–7]. At higher energies, the increased number of partial waves to be determined is not yet met by experimental data of sufficient quality and density, leading to serious discrepancies between phase-shift solutions of different groups [7,8] above about 1.2 GeV.

To this end, the EDDA-experiment has been conceived to provide highly accurate data between 0.5 and 2.5 GeV. Being internal to the COSY ring it takes advantage of this unique experimental environment: data acquisition during beam acceleration to measure quasi-continuous excitation function, first done at SATURNE [9], and the use of pure polarized hydrogen targets for fast and easy spin-manipulation to minimize systematic errors, a technique pioneered by the PINTEX [10,11] Collaboration at IUCF at lower energies.

EDDA uses the recirculating proton beam of COSY in conjunction with thin internal targets, CH_2-fibers for unpolarized and a hydrogen atomic beam target [12] for polarized measurements. Elastically scattered protons are detected in coincidence by a cylindrical double-layered

[a] e-mail: rohdjess@iskp.uni-bonn.de

scintillator hodoscope [13,14] for scattering angles ranging from 30° to 90° in the center of mass. Excitation functions of unpolarized differential cross-sections [15] and analyzing power [16] have been measured in the first phases of the experiment and helped to extend the PSA up to 2.5 GeV [7,17].

Such excitation functions with small energy steps are ideally suited to search for resonant contributions, as they might arise by coupling of dibaryonic states B_2 [18,19] to the elastic channel. Although these states have been proposed in many different models (*e.g.*, [20–22]) they have not been established experimentally [23].

Here, we report on two recent achievements: preliminary results on spin correlation parameters, where data taking with polarized beam and target has been recently completed, and upper limits on resonant contributions to elastic scattering in the mass range $\sqrt{s} = 2.2 \ldots 2.8$ GeV based on the previously published data.

2 Spin correlation parameters

With a vertically polarized (50–75%) COSY-beam and a polarized atomic beam, spin-aligned in the interaction region by a weak (1 mT) magnetic guiding field to one of the 6 possible directions $\pm x$, $\pm y$, and $\pm z$, we have access to the spin correlation parameters A_{NN}, A_{SS}, and A_{SL}. A_{BT} describe the deviation of the cross-section from the spin-averaged value for the spin of beam (B) and target (T) protons oriented longitudinal to the beam (L) or normal (N) to or sideways (S) in the scattering plane. With beam intensities ranging from $3 \cdot 10^9$ to $1.5 \cdot 10^{10}$ protons stored we achieved luminosities in the $(1\text{–}5) \cdot 10^{27}/(\mathrm{cm}^2\mathrm{s})$ range. We took data during acceleration and at the flat-top momentum, where 9 about evenly spaced beam momenta between 2.1 and 3.3 GeV/c were selected. This allows to cover the low (acceleration) and high (flat-top) energy region with sufficient statistical accuracy. Data analysis proceeds in two steps: First the elastic scattering rate for 5° wide bins in the c.m. polar angle $\theta_{\mathrm{c.m.}}$ is determined as a function of the azimuthal angle ϕ. A cut on the reconstructed vertex to select events from the beam-target overlap are applied as well as cuts selecting events which obey elastic scattering kinematics. Due to the analyzing power and the non-vanishing spin correlation coefficients, the scattering rate for each spin combination exhibits characteristic modulations with the azimuthal angle. Secondly, the spin correlation parameters as well as beam and target polarizations are extracted either by calculating certain asymmetries [25,26] which cancel the influence of detector efficiencies to first order, or by standard χ^2 minimization techniques. Both methods yield consistent results. The overall normalization of the target and beam polarizations is fixed with reference to the EDDA analyzing power data [16]. An example of a preliminary angular distribution obtained at 2572 MeV/c ($T_p = 1.8$ GeV) is shown in fig. 1. The data analysis is almost finalized.

Previous measurements of spin correlation parameters at these energies were done mainly at SATURNE [24] on A_{NN}, A_{LL}, and A_{SL}. In comparison, our new data on A_{NN}

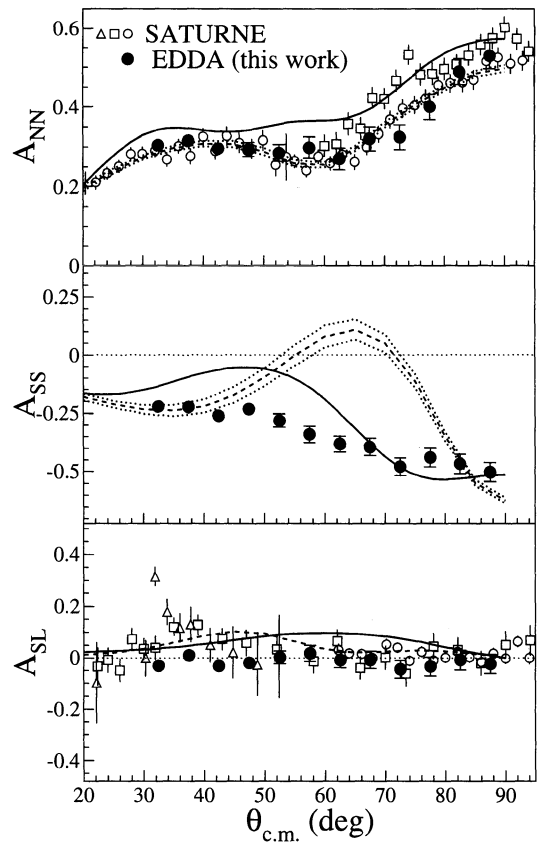

Fig. 1. Angular distribution of the spin correlation parameters A_{NN}, A_{SS}, and A_{SL} at $p = 2572$ MeV/c ($T_p = 1.8$ GeV) in comparison to phase shift predictions of SAID (SM00, solid line) [7] and the Saclay-Geneva (dashed line) analysis [8] and data from SATURNE [24]. The EDDA data are preliminary.

is consistent at all energies, however, we find values for A_{SL} more or less compatible with zero at all angles and do not confirm excursions in the angular distributions (see fig. 1) as evinced in the SATURNE data. In contrast the observable A_{SS} has not been measured before above 800 MeV. These data thus put the predictive power of existing parameterization by scattering phase shifts to a true test. In fig. 1 the new data are compared to different PSA variants. They disagree strikingly with our data on A_{SS} and with each other. This highlights that the world data base on proton-proton elastic scattering to date does not allow to unambiguously determine the scattering phase shifts or amplitudes at energies well above 1 GeV. It will be interesting to see to what extent the new spin correlation data on A_{SS} will be a remedy. As a first step we found [27] that the addition of our data to the world database removes some of the ambiguities in the reconstruction of the scattering amplitudes found in [8].

3 Upper limits on resonance contributions

The excitation functions of the differential cross-sections and analyzing powers have shown no apparent resonant

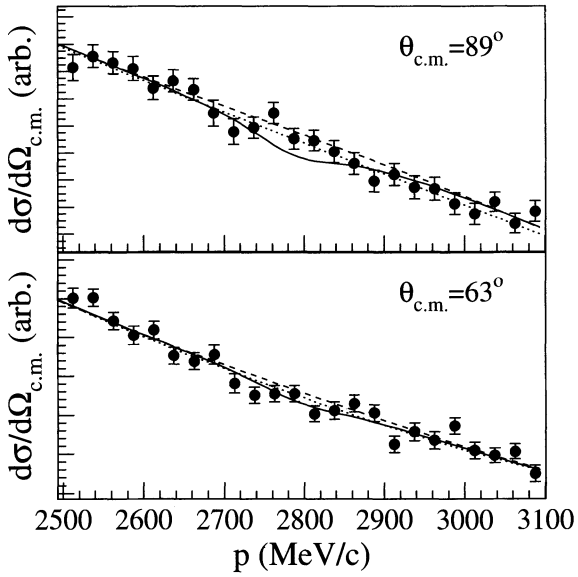

Fig. 2. Differential cross-sections at two out of 28 scattering angles in comparison to PSA solutions. The best fit, with (without) a $^1S_0$ resonance at $\sqrt{s}$ = 2.7 GeV, $\Gamma_{\rm tot}$= 50 MeV and $\eta_{\rm el}$= 0.043, excluded with 99% CL by the data is shown as the solid (dashed) line. The dotted line shows the nonresonant background as described by the PSA in the presence of the resonance.

Table 1. Typical values for the partial elastic width $\Gamma_{\rm el}$ of resonances for $\sqrt{s} = 2.2 \ldots 2.8$ GeV and $\Gamma_{\rm tot} = 10 \ldots 100$ MeV excluded with 99% CL.

$^{2S+1}L_J$	$\eta_{\rm el}= \Gamma_{\rm el}/\Gamma_{\rm tot}$
$^1S_0$	0.08
$^1D_2$	0.04
$^3P_0$	0.10
$^3P_1$	0.03
$^3F_3$	0.05

structure. By using the PSA analysis as a model for the non-resonant background [28], the compatibility of a narrow (10–100 MeV) resonance in a particular partial wave with the data can be tested quantitatively, as long as the energy dependence assumed in the PSA is slowly varying with energy as compared to the resonance width to be tested. The hypothesis of the existence of a resonance in a partial wave with energy $\sqrt{s}$, total width $\Gamma_{\rm tot}$ and partial elastic width $\Gamma_{\rm el}$ was tested by the following procedure: An energy dependent PSA along ref. [17] was done on a database tailored to give the best fit to the EDDA data by excluding all data from other experiments for this observable in the same energy range and served as the null-hypothesis for comparison. Then a Breit-Wigner term representing the resonance was added to the S-matrix and the PSA parameters adjusted to yield the best fit to the data in the presence of the resonance to be tested. The partial elastic width $\Gamma_{\rm el}$ was then gradually increased until the resonance was excluded with 99% confidence level (CL) by a χ^2-test based on the EDDA data. For the unknown phase between the resonant and non-resonant amplitudes the value giving the largest $\Gamma_{\rm el}$ excluded was chosen. An example —corresponding to a $^1S_0$ resonance predicted in ref. [29]— is shown in fig. 2, and typical minimal values in $\eta_{\rm el} = \Gamma_{\rm el}/\Gamma_{\rm tot}$ for the five lowest uncoupled partial waves are listed in table 1. The EDDA data, in particular those on differential cross-sections, therefore exclude a sizeable coupling of isovector resonances, like dibaryons, to the elastic channel in the parameter space covered.

The excellent beam support by the COSY accelerator team during all phases of the experimental program of EDDA is warmly acknowledged. We are indebted to Prof. R. Arndt for providing us and helping with the PSA software used in the analysis. This work was supported by the BMBF and FZ-Jülich.

References

1. R. Machleidt, I. Slaus, J. Phys. G **27**, R69 (2001), and references herein.
2. P.F. Bedaque, U. van Kolck, nucl-th/0203055, to be published in Annu. Rev. Nucl. Part. Sci. **53**, (2002) and references therein.
3. V.G.J. Stoks, R.A.M. Klomp, M.C.M. Rentmeester, J.J. de Swart, Phys. Rev. C **48**, 792 (1993).
4. J. Bystricky, C. Lechanoine-LeLuc, F. Lehar, J. Phys. (Paris) **48**, 199 (1987).
5. J. Bystricky, C. Lechanoine-LeLuc, F. Lehar, J. Phys. (Paris) **51**, 2747 (1990).
6. J. Nagata, H. Yoshino, M. Matsuda, Prog. Theor. Phys. **95**, 691 (1996).
7. R.A. Arndt, I.I. Strakovsky, R.L. Workman, Phys. Rev. C **62**, 34005 (2000).
8. J. Bystricky, F. Lehar, C. Lechanoine-LeLuc, Eur. Phys. J. C **4**, 607 (1998).
9. M. Garçon *et al.*, Nucl. Phys. A **445**, 669 (1985).
10. B. von Przewoski *et al.*, Phys. Rev. C **58**, 1897 (1998).
11. F. Rathmann *et al.*, Phys. Rev. C **58**, 658 (1998).
12. P.D. Eversheim *et al.*, Nucl. Phys. A **626**, 117 (1997)c.
13. J. Bisplinghoff *et al.*, Nucl. Instrum. Methods A **329**, 151 (1993).
14. M. Altmeier *et al.*, Nucl. Instrum. Methods A **431**, 428 (1999).
15. D. Albers *et al.*, Phys. Rev. Lett. **78**, 1652 (1997).
16. M. Altmeier *et al.*, Phys. Rev. Lett. **85**, 1819 (2000).
17. R.A. Arndt, Chang Heon Oh, I.I. Strakovsky, R.L. Workman, F. Dohrmann, Phys. Rev. C **56**, 3005 (1997).
18. R. Jaffe, Phys. Rev. Lett. **38**, 195 (1977).
19. P.J. Mulders, A.T. Aerts, J.J. De Swart, Phys. Rev. D **21**, 2653 (1980).
20. N. Konno, H. Nakamura, H. Noya, Phys. Rev. D **35**, 239 (1987).
21. A.P. Balachandran, F. Lizzi, V.G.J. Rodgers, A. Stern, Nucl. Phys. B **256**, 525 (1985).
22. C.W. Wong, Prog. Nucl. Part. Phys. **8**, 223 (1982).
23. K.K. Seth, *Proceedings of Baryon-Baryon Interaction and Dibaryonic Systems, Bad Honnef, 1988*, p. 41.
24. J. Ball *et al.*, CTU Reports **4**, 3 (2000).

25. G.G. Ohlsen, Nucl. Instrum. Methods **109**, 41 (1973).
26. F. Bauer, Ph.D. thesis, Universität Hamburg, 2001.
27. F. Bauer *et al.*, (2002), nucl-ex/0209006.
28. H. Rohdjess, Habilitationsschrift, Universität Bonn, 2000.
29. P. Gonzalez, P. LaFrance, E.L. Lomon, Phys. Rev. D **35**, 2142 (1987).

Eur. Phys. J. A **18**, 559–562 (2003)
DOI 10.1140/epja/i2002-10283-5

THE EUROPEAN PHYSICAL JOURNAL A

Flavor symmetry breaking and strangeness in the nucleon

H. Weigel[a]

Institute for Theoretical Physics, Tübingen University, D-72076 Tübingen, Germany

Received: 30 September 2002 /
Published online: 22 October 2003 – © Società Italiana di Fisica / Springer-Verlag 2003

Abstract. We suggest that breaking of $SU(3)$ flavor symmetry mainly resides in the baryon wave functions while the charge operators have no (or only small) explicit symmetry-breaking components. We utilize the collective coordinate approach to chiral soliton models to support this picture. In particular we compute the g_A/g_V ratios for hyperon beta-decay and the strangeness contribution to the nucleon axial current matrix elements and analyze their variation with increasing flavor symmetry breaking.

PACS. 12.39.Dc Skyrmions – 12.39.Fe Chiral Lagrangians – 13.30.Ce Leptonic, semileptonic, and radiative decays – 14.20.Jn Hyperons

1 Introduction and motivation

There has been much interest in the strangeness content of the nucleon ever since the analysis of the DIS data [1] suggested a large (negative) polarization of strange quarks in the nucleon [2,3], $\Delta S_N \approx -0.15$. This surprising result particularly relies on the assumption of flavor covariance for the axial current matrix elements of the $\frac{1}{2}^+$ baryons. This assumption originates from the feature that the Cabibbo scheme [4], that utilizes the $F\&D$ parameterization for the flavor changing axial charges, works unexpectedly well [5] as the comparison in table 1 shows.

Here we will investigate in how far this agreement justifies to carry over flavor covariance to strangeness-conserving axial current matrix elements in order to disentangle the various quark flavor components of the nucleon axial current matrix element. This investigation requires baryon axial current matrix elements as functions of the (effective) strength of flavor symmetry breaking. This can be achieved within the three-flavor version of the Skyrme model (and generalizations thereof) in which baryons emerge as solitons. In such models baryon states are constructed by quantizing the large amplitude fluctuations about the soliton and constructing exact eigenstates in the presence of symmetry breaking. We focus on a picture where symmetry breaking mainly resides in the baryon wave functions, including important contributions which would be missed in a first-order treatment. In contrast, we assume that the current operators, from which the charges are computed, are dominated by flavor covariant components. In a first step we do not specify the model Lagrangian but adjust the prefactors of the few possible flavor covariant components of the axial current operator to observables in hyperon beta-decay and analyze their matrix elements as functions of flavor symmetry breaking. We also present results obtained from a realistic vector meson soliton model that supports the suggested picture. Details omitted here may be traced from ref [8].

Table 1. The empirical values for the g_A/g_V ratios of hyperon beta-decays [6], see also [5]. For $\Sigma \to \Lambda$ only g_A is given. Also the flavor symmetric predictions are presented using $F = 0.459$ and $D = 0.799$. Analytic expressions which relate these parameters to the g_A/g_V ratios may *e.g.* be found in table I of [7].

	$\Lambda \to p$	$\Sigma \to n$	$\Xi \to \Lambda$
Empirical	0.718 ± 0.015	0.340 ± 0.017	0.25 ± 0.05
$F\&D$	0.725 ± 0.009	0.339 ± 0.026	0.19 ± 0.02
	$\Xi \to \Sigma$	$\Sigma \to \Lambda$	
Empirical	1.287 ± 0.158	0.61 ± 0.02	
$F\&D$	$1.258 = g_A$	0.65 ± 0.01	

2 Symmetry breaking in the baryon wave functions

The collective coordinates A that parameterize the large amplitude fluctuations off the soliton are introduced via

$$U(\boldsymbol{r},t) = A(t)U_0(\boldsymbol{r})A^\dagger(t)\,, \qquad A(t) \in SU(3)\,. \quad (1)$$

$U_0(\boldsymbol{r})$ describes the soliton embedded in the isospin subgroup. A prototype model Lagrangian for $U(\boldsymbol{r},t)$ consists of the Skyrme model supplemented by the Wess-Zumino-Witten term and suitable symmetry-breaking pieces. We

[a] *Heisenberg-Fellow*;
e-mail: herbert.weigel@uni-tuebingen.de

parameterize the collective coordinates by "Euler angles"

$$A = D_2(\hat{I})\, \mathrm{e}^{-i\nu\lambda_4} D_2(\hat{R})\, \mathrm{e}^{-i(\rho/\sqrt{3})\lambda_8} \,. \tag{2}$$

Here D_2 denote the rotation matrices for rotations in isospace ($\hat{I}$) and coordinate space ($\hat{R}$). Substituting (1) into the model Lagrangian yields upon canonical quantization the Hamiltonian for the collective coordinates A:

$$H = H_{\mathrm{s}} + \tfrac{3}{4}\gamma \sin^2\nu \,. \tag{3}$$

The symmetric piece of this collective Hamiltonian only contains Casimir operators and may be expressed in terms of the $SU(3)$-right generators R_a ($a = 1, \ldots, 8$):

$$H_{\mathrm{s}} = M_{\mathrm{cl}} + \frac{1}{2\alpha^2}\sum_{i=1}^{3} R_i^2 + \frac{1}{2\beta^2}\sum_{\alpha=4}^{7} R_\alpha^2 \,. \tag{4}$$

$M_{\mathrm{cl}}, \alpha^2, \beta^2$ and γ are functionals of the soliton, $U_0(\boldsymbol{r})$. The generators R_a can be expressed in terms of derivatives with respect to the "Euler angles". The essential feature of the parameterization (2) is that the flavor-symmetry-breaking part of the full Hamiltonian (3) only depends on the flavor-changing angle ν. Therefore the eigenvalue problem $H\Psi = \epsilon\Psi$ reduces to ordinary second-order differential equations for isoscalar functions which only depend on ν [9]. Solely the product $\omega^2 = \frac{3}{2}\gamma\beta^2$ appears in these differential equations as the effective strength of symmetry breaking on which the eigenfunctions of H depend parametrically. A value in the range $5 \lesssim \omega^2 \lesssim 8$ is required to obtain reasonable agreement with the empirical mass differences for the $\frac{1}{2}^+$ and $\frac{3}{2}^+$ baryons [10]. Such large a value for ω^2 is without reach of a perturbation expansion as the resulting baryon wave functions exhibit strong distortion from flavor covariance.

3 Charge operators

In the soliton description the effect of the derivative-type symmetry-breaking terms is mainly indirect. They provide the splitting between the various decay constants and thus increase γ since it is proportional to $f_K^2 m_K^2 - f_\pi^2 m_\pi^2 \approx 1.5 f_\pi^2 (m_K^2 - m_\pi^2)$. Otherwise, the derivative-type symmetry-breaking terms are negligible. Whence symmetry-breaking terms can be omitted in the current operators and the non-singlet axial charge operator is parameterized as ($a = 1, \ldots, 8$, $i = 1, 2, 3$)

$$\int \mathrm{d}^3 r A_i^{(a)} = c_1 D_{ai} - c_2 D_{a8} R_i + c_3 \sum_{\alpha,\beta=4}^{7} d_{i\alpha\beta} D_{a\alpha} R_\beta \,, \tag{5}$$

where $D_{ab} = \frac{1}{2}\mathrm{tr}\left(\lambda_a A \lambda_b A^\dagger\right)$. For $\omega^2 \to \infty$ (infinitely heavy *strange* degrees of freedom) the strangeness contribution to the nucleon axial charge should vanish. Noting that $\langle N|D_{83}|N\rangle \to 0$ and $\langle N|\sum_{\alpha,\beta=4}^{7} d_{3\alpha\beta} D_{8\alpha} R_\beta|N\rangle \to 0$ while $\langle N|D_{88}|N\rangle \to 1$ for $\omega^2 \to \infty$, we demand

$$\int \mathrm{d}^3 r A_i^{(0)} = -2\sqrt{3} c_2 R_i \,, \quad i = 1, 2, 3 \tag{6}$$

for the axial singlet current because it leads to the strangeness projection, $A_i^{(s)} = (A_i^{(0)} - 2\sqrt{3} A_i^{(8)})/3$ that vanishes for $\omega^2 \to \infty$. Actually all model calculations in the literature [11,12] are consistent with this relation between singlet and octet currents. The singlet current matrix element, $\Delta\Sigma_B = \sqrt{3} c_2$, is the quark spin contribution to the spin of the considered baryon, B. It is well known that the empirical value for the nucleon matrix element, $\Delta\Sigma_N \approx 0.20 \pm 0.10$ [3] is insensitive to the strength of flavor symmetry breaking [13]. This suggests to adjust c_2 accordingly. In order to completely describe the hyperon beta-decays we also demand matrix elements of the vector charges. These are obtained from the operator

$$\int \mathrm{d}^3 r V_0^{(a)} = \sum_{b=1}^{8} D_{ab} R_b = L_a \,, \tag{7}$$

which introduces the $SU(3)$-left generators L_a.

The values for g_A and g_V (only g_A for $\Sigma^+ \to \Lambda e^+ \nu_e$) are obtained from the matrix elements of the operators in eqs (5) and (7), respectively, sandwiched between the eigenstates of the full Hamiltonian (3). We still have to specify c_1 and c_3. We determine these two parameters such that nucleon axial charge, g_A and the g_A/g_V ratio for $\Lambda \to p e^- \bar{\nu}_e$ are reproduced[1] at a prescribed strength of flavor symmetry breaking, $\omega^2_{\mathrm{fix}} = 6.0$. Then we are not only left with predictions for the other decay parameters but we can in particular study the variation with symmetry breaking. This is shown in fig. 1. The dependence on flavor symmetry breaking is very moderate[2] and the results can be viewed as reasonably agreeing with the empirical data, cf. table 1. The observed independence of ω^2 shows that these predictions are not sensitive to the choice of ω^2_{fix}. The two transitions, $n \to p$ and $\Lambda \to p$, which are not shown in fig. 1, exhibit a similar negligible dependence on ω^2. We therefore have a two parameter (c_1 and c_3, c_2 is fixed from $\Delta\Sigma_N$) fit of the hyperon beta-decays. Comparing the results in fig. 1 with the data in table 1 we see that the present calculation using the strongly distorted wave functions agrees equally well with the empirical data as the flavor-symmetric $F\&D$ fit. On the other hand, the strangeness contribution to the nucleon axial current matrix element reduces from $\Delta S_N \approx -0.13$ in the symmetric treatment to $\Delta S_N \approx -0.07$ in the realistic case.

4 Model calculation

We consider a realistic soliton model containing pseudoscalar and vector meson fields. It has been established for two flavors in ref. [14] and been extended to three flavors in ref. [11] where it has been shown to fairly well describe the parameters of hyperon beta-decay (cf. table 4 in ref. [11]). The model Lagrangian contains terms which involve the

[1] In this section we will not address the problem of the too small model prediction for g_A.

[2] However, the individual matrix elements entering the ratios g_A/g_V vary strongly with ω^2 [8].

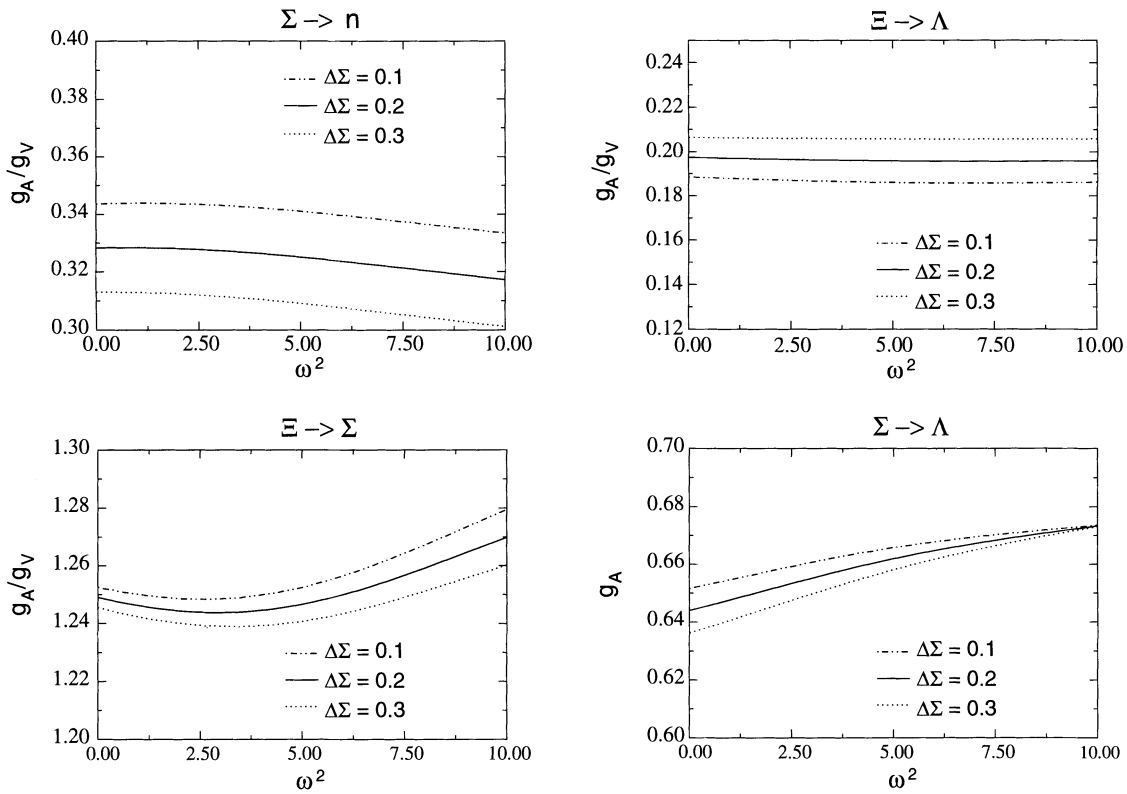

Fig. 1. The predicted decay parameters for the hyperon beta-decays using $\omega^2_{\rm fix} = 6.0$. The errors originating from those in $\Delta\Sigma_N$ are indicated.

Levi-Cevita tensor $\epsilon_{\mu\nu\rho\sigma}$, to accommodate processes like $\omega \to 3\pi$ [15]. Such terms contribute to c_2 and c_3. A minimal set of symmetry-breaking terms is included [16] to account for different masses and decay constants. They add symmetry-breaking pieces to the axial charge operator,

$$\delta A_i^{(a)} = c_4 D_{a8} D_{8i} + c_5 \sum_{\alpha,\beta=4}^{7} d_{i\alpha\beta} D_{a\alpha} D_{8\beta} + c_6 D_{ai}(D_{88} - 1)\,,$$

$$\delta A_i^{(0)} = 2\sqrt{3}\, c_4 D_{8i}\,.$$

Unfortunately the model parameters cannot be completely determined in the meson sector [14]. We use the remaining freedom to accommodate baryon properties in three different ways as shown in table 2. The set denoted by "b.f." refers to a best fit to the baryon spectrum. It predicts the axial charge somewhat on the low side, $g_A = 0.88$. The entry "mag. mom." labels parameters that yield magnetic moments close to the empirical data (with $g_A = 0.98$) and finally the set labeled "g_A" reproduces the axial charge of the nucleon [11]. We observe that in particular the strangeness projection of the nucleon axial current is very small and depends only mildly on the model parameters. This confirms the above conclusion from the general structure of the axial current matrix elements that the strangeness admixture in the nucleon is significantly smaller than an analysis based on flavor covariance suggests. Also the predictions for the axial properties of the Λ hyperon are quite insensitive to the model parameters. Sizable polarizations of the *up* and *down* quarks in the Λ are predicted; comparable to those obtained from the $SU(3)$ analysis [17] of the available data.

Table 2. Quark spin content of the nucleon and the Λ in the realistic vector meson model. Three sets of model parameters are considered, see text.

	N			
	ΔU	ΔD	ΔS	$\Delta\Sigma$
b.f.	0.603	−0.279	−0.034	0.291
mag. mom.	0.636	−0.341	−0.030	0.265
g_A	0.748	−0.476	−0.016	0.256
	Λ			
	$\Delta U = \Delta D$	ΔS	$\Delta\Sigma$	
b.f.	−0.155	0.567	0.256	
mag. mom.	−0.166	0.570	0.238	
g_A	−0.164	0.562	0.233	

5 Conclusions

We have suggested a picture for the axial charges of the low-lying $\frac{1}{2}^+$ baryons which manages to reasonably reproduce the empirical data without introducing (significant)

flavor-symmetry-breaking components in the corresponding operators. Rather, a sizable symmetry breaking, as demanded by the baryon spectrum, resides almost completely in the baryon wave functions. In this picture the empirical data for hyperon beta-decay are as reasonably reproduced as in the Cabibbo scheme. We emphasize that the present picture is not a re-application of the Cabibbo scheme since here the "octet" baryon wave functions have significant admixture of higher-dimensional representations. Especially, when compared with the flavor-covariant treatment, the present approach predicts a sizable suppression of strangeness in the nucleon.

This work is supported by the Deutsche Forschungsgemeinschaft (DFG) under contract We 1254/3-2.

References

1. European Muon Collaboration (J. Ashman *et al.*), Phys. Lett. B **206**, 364 (1988); for more recent references, see E143 Collaboration (K. Abe *et al.*), Phys. Rev. Lett. **76**, 587 (1996); SMC Collaboration (D. Adams *et al.*), Phys. Rev. D **56**, 5330 (1997).
2. S.J. Brodsky, J.R. Ellis, M. Karliner, Phys. Lett. B **206**, 309 (1988).
3. J.R. Ellis, M. Karliner, arXiv:hep-ph/9601280.
4. N. Cabibbo, Phys. Rev. Lett. **10**, 531 (1963).
5. R. Flores-Mendieta, E. Jenkins, A.V. Manohar, Phys. Rev. D **58**, 094028 (1998).
6. Particle Data Group (C. Caso *et al.*), Eur. Phys. J. C **3**, 1 (1998); M. Bourquin *et al.*, Z. Phys. C **12**, 307 (1982); C **21**, 1 (1983).
7. N.W. Park, J. Schechter, H. Weigel, Phys. Rev. D **41**, 2836 (1990).
8. H. Weigel, Nucl. Phys. A **690**, 595 (2001) and references therein.
9. H. Yabu, K. Ando, Nucl. Phys. B **301**, 601 (1988).
10. H. Weigel, Int. J. Mod. Phys. A **11**, 2419 (1996); J. Schechter, H. Weigel, hep-ph/9907554:
11. N.W. Park, H. Weigel, Nucl. Phys. A **541**, 453 (1992).
12. A. Blotz, M. Praszałowicz, K. Goeke, Phys. Lett. B **317**, 195 (1993).
13. R. Johnson *et al.*, Phys. Rev. D **42**, 2998 (1990).
14. P. Jain *et al.*, Phys. Rev. D **37**, 3252 (1988); Ulf-G. Meißner *et al.*, Phys. Rev. D **39**, 1956 (1989).
15. Ö. Kaymakcalan, S. Rajeev, J. Schechter, Phys. Rev. D **30**, 594 (1984).
16. P. Jain *et al.*, Phys. Rev. D **40**, 855 (1989).
17. R.L. Jaffe, Phys. Rev. D **54**, 6581 (1996).

Eur. Phys. J. A **18**, 563–565 (2003)
DOI 10.1140/epja/i2002-10284-4

THE EUROPEAN PHYSICAL JOURNAL A

Experimental review of charmonium spectroscopy

K.K. Seth[a]

Northwestern University, Evanston, IL 60208, USA

Received: 30 September 2002 /
Published online: 22 October 2003 – © Società Italiana di Fisica / Springer-Verlag 2003

Abstract. Charmonium spectroscopy is one of the best means of making precision study of QCD, the strong-interaction component of the Standard Model of particle physics. Recent progress in the study of charmonium, the need for additional precision data, and the opportunities that the new facilities offer, are discussed.

PACS. 12.38.Qk Quantum chromodynamics: Experimental tests – 12.39.Pn Potential models – 13.25.Gv Decays of J/ψ, Υ, and other quarkonia – 14.40.Gx Mesons with $S = C = B = 0$, mass > 2.5 GeV (including quarkonia)

1 Introduction

The strong interaction is manifest in Nature through the existence of nuclei, but its foundations lie in the interactions between quarks and gluons as described by the non-Abelian field theory of QCD (Quantum Chromodynamics). The basic properties and symmetries of the interaction are best studied not in the many-body systems that nuclei represent, but in the simplest structures to which it gives rise. Mesons, composed of a quark and an antiquark, constitute such "simple" two-body systems. Further simplification results in Quarkonia in which the quark and antiquark are of the same flavor. Because the masses of the light $SU(3)$ quarks, the up-, down-, and strange-quarks, are very similar (3.3(17) MeV, 7(2) MeV, and 118(38) MeV, respectively [1]), light quark mesons are invariably mixtures of all three flavors. This results in complicated structures and a high density of broad overlapping states. For example, in the 1000 MeV mass region, from 1500 MeV to 2500 MeV, as many as 77 mesons are expected [2] with typical widths of 200–400 MeV. Further, the small masses of the u-, d-, and s-quarks pose serious theoretical problems; the quarks are highly relativistic in these light mesons, and the strong interaction coupling constant is too large to allow the use of perturbation theory.

In contrast, the charm quark is much heavier (1260(240) MeV [1]), and relativistic and coupling constant problems in charmonium mesons are much less serious. Figure 1 illustrates the spectrum of charmonium states. Only eight well-isolated and narrow (all widths ≤ 20 MeV) bound states exist in the 800 MeV region from 2900 MeV to 3700 MeV. Thus, the charmonium system is obviously immensely "cleaner" and more tractable than light quark mesons. It offers the best opportunity to make precision spectroscopy of a quarkonium system, and to thus contribute to a deeper understanding of QCD and the phenomenological models based on QCD.

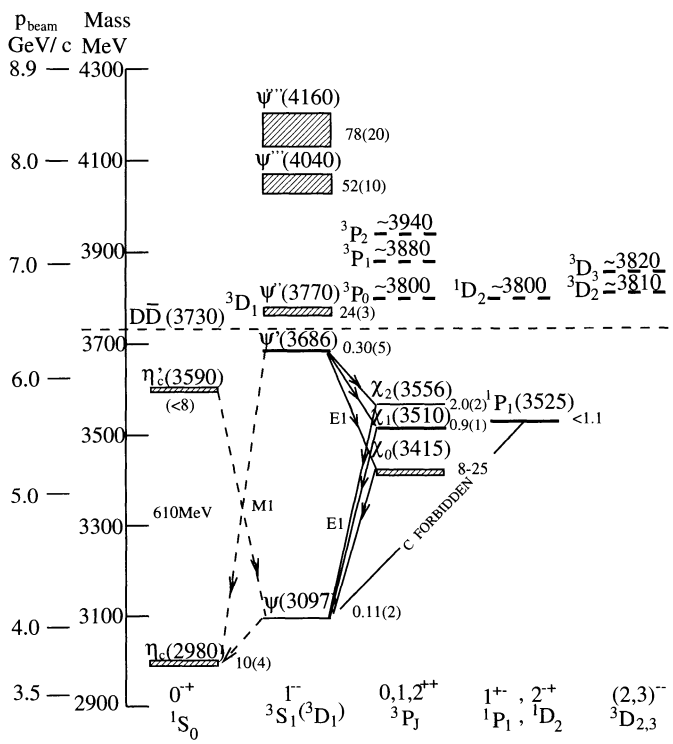

Fig. 1. The charmonium spectrum.

In my talk I reviewed the latest experimental data in charmonium spectroscopy, and the successes and failures

[a] e-mail: kseth@northwestern.edu

of the existing experiments, the applicability and limitations of pQCD, the future developments, both theoretical and experimental, which are needed, and the prospects of their realization at upcoming new facilities. It is not possible to present all that in the limited space here. So, the following presentation is essentially a summary of my talk.

2 The experimental developments

As is well known, extensive amount of charmonium spectroscopy was done during 1974-1985 at SLAC with its Mark I, II, III, and Crystal Ball detectors, at Orsay by the DM2 detector, and at DESY by the DASP detector. A large amount of discovery physics was done, but much of it lacked precision. The primary reason for the shortcomings of these experiments was the fact that in these e^+e^- annihilation experiments only the vector states, J/ψ and ψ' could be directly excited, and all other states had to be studied by their indirect excitation via the radiative decays of J/ψ and ψ'. This lead to serious limitations in the study of P-wave states (1^3P_J, χ_c states) and even the ground state of charmonium, the singlet S-wave state ($1^1S_0, \eta_c$). And then, there was the ultimate limitation imposed by the fact that further studies of charmonium stopped as all these facilities moved on to b-quark physics. Both limitations have been overcome by two recent developments. At Fermilab precision studies of charmonium spectroscopy were initiated by the novel technique of the direct formation of resonances of any J^{PC} in proton antiproton annihilation, and at the Beijing Electron Positron Collider (BEPC), the BES detector was commissioned uniquely for the renewed pursuit of charmonium spectroscopy in e^+e^- annihilation.

The BES detector is essentially identical to the Mark III detector at SLAC, and it needs no introduction. The Fermilab technique is unique, and a brief description is desirable. At the Fermilab antiproton source the circulating beam of stochastically cooled antiprotons (upto 8×10^{11} antiprotons) intersected a hydrogen gas-jet target (of density upto 3×10^{14} atom/cm^3). The annihilation products were detected in a detector of cylindrical geometry whose design was optimized for the detection and identification of electrons, positrons, and photons (unfortunately, with no facility for charged-particle tracking). Unprecedented mass resolution with half-width of 300–600 keV was achieved, and luminosities of $(1-5) \times 10^{31}$ cm^{-2}s^{-1} were routinely used. Excitation curves for individual charmonium resonances were measured by varying the antiproton energy across the resonance. The technique resulted in high precision measurements of resonance masses, and direct and precise measurements of total widths.

3 The new results

The new results obtained by the Fermilab E760/E835 experiments are presented in table 1, together with the earlier results of e^+e^- annihilation experiments, as summarized in the PDG(1990) compilation. We see that in the $p\bar{p}$ experiments many results were improved by upto an order of magnitude. Of special note is the nearly 50% increase in the width of the J/ψ-resonance which has the effect of increasing the earlier estimate of the gluon condensate by a similar amount. The large value of $B(p\bar{p})$ for χ_0 is found to be in dramatic violation of the Hadron Helicity Conservation rule of massless QCD, according to which spin-zero states cannot be populated in $p\bar{p}$ anihilation. For a recent review, see ref. [3].

Table 1. Total and partial widths of charmonium states, as measured by e^+e^- annihilation experiment (PDG 1990) and Fermilab $p\bar{p}$ annihilation experiments E760/E835.

State	$\Gamma_{\rm tot}$ (MeV)	$\Gamma_{\gamma\gamma}$ (keV)	$B(p\bar{p}) \times 10^{-4}$
η_c PDG	$10.3^{+3.8}_{-3.4}$	8^{+7}_{-5}	10.4 ± 1.9
E760	$23.9^{+12.6}_{-7.1}$	$6.7^{+3.3}_{-2.9}$	
E835	$20.4^{+8.0}_{-7.0}$	$3.8^{+2.2}_{-1.4}$	
J/ψ PDG	0.068 ± 0.010		21.6 ± 1.1
E760	0.099 ± 0.013		$18.2^{+3.1}_{-2.6}$
χ_0 PDG	13.5 ± 5.3	4.0 ± 2.8	< 9
E835	9.8 ± 1.0	< 2.0	$4.1^{+1.6}_{-0.9}$
χ_1 PDG	< 1.3		< 12
E760	0.88 ± 0.13		0.86 ± 0.12
χ_2 PDG	2.8 ± 2.1	2.8 ± 2.0	
E760	1.98 ± 0.18	0.321 ± 0.095	1.00 ± 0.11
E835		0.270 ± 0.059	
h_c E760	< 1.1		
η_c' PDG	< 8.0		
ψ' PDG	0.243 ± 0.043		1.9 ± 0.5
E760	0.306 ± 0.039		$2.61^{+0.39}_{-0.36}$

It is worth noticing that the Fermilab/E760/835 experiments did not succeed in providing very good results for the total width, or the two-photon width of the charmonium ground state, η_c. Neither did they succeed in identifying the singlet resonances η_c' (2^1S_0), and $h_c(1^1P_1)$. They also did not attempt to study charmonium above the $D\bar{D}$ threshold at 3.73 GeV, a region in which several interesting narrow resonances ($^1D_2$,$^3D_2$, 2^1P_1, etc.) are predicted to exist. The primary reason for most of these shortcomings was the limited amount of antiproton beam-time which could be made available at a facility whose primary objective was to do Tevatron physics. In addition, the design of the E760/E835 detector precluded the study of charged hadron decays of any of the charmonium resonances.

The BEPC/BES experiments have relatively poor photon detection, but have the advantage of being able to identify charged particles. The results from the first series of BES I experiments based on 8 million J/ψ and 3.7 million ψ', often suffered from inadequate statistics. The latest series of BES II measurements are based on 58 million J/ψ and 14 million ψ'. The results from these measurements are beginning to come out, and they supercede,

and in some cases contradict, the earlier results. Notable among these is the fact that in the BES II measurements no evidence is found for the narrow $\xi(2230)$ which was claimed to be a candidate for the 2^{++} tensor glueball on the basis of its "observation" in BES I measurements.

With its ability to study charged-particle decay channels, BES has rightly concentrated on measuring a large number of decay channels of both J/ψ and ψ'. A notable result of these measurements is the so called "ρ-π problem". pQCD predicts that the ratio $B(\psi' \to \text{hadrons})/B(J/\psi \to \text{hadrons})$ should be equal to the ratio $B(\psi' \to e^+e^-)/\ B(J/\psi \to e^+e^-) = 0.12$. It is found that for the decay to ρ-π, and to many other decay channels, the ratio is often orders of magnitude smaller. Although many theoretical speculations about this phenomenon have been offered, it is not clear to me why a prediction for the sum of all hadronic decay channels should be expected to be true for individual decay channels, anyway.

BES results for the indirectly populated charmonium resonances, η_c and the χ_J have been controversial in the past. It remains to be seen how these controversies resolve with the new data from BES II. The improvements due to seven times larger statistics are to be expected, but the dependence of width determinations on experimental energy resolution in the different decay channels will perhaps continue to present problems.

BES has also reported quite detailed measurements of the R-parameter ($\sigma(e^+e^- \to \text{hadrons})/\sigma(e^+e^- \to \mu^+\mu^-)$) in the energy region 2–5 GeV. These measurements have given rise to renewed doubt on the correctness of the present "knowledge" of the vector resonances ($\psi''', \psi'''', \psi'''''$, etc.) in the region above the $D\bar{D}$ threshold at 3.73 GeV.

4 Open problems and future prospects

There are many problems and unanswered questions in charmonium spectroscopy. The pursuit of these will require dedicated facilities both for e^+e^- annihilation and proton antiproton annihilation experiments. Fortunately, two such facilities are indeed planned for the near future. These are CESR-c/CLEO-c at Cornell, in Ithaca (USA), and the antiproton physics facilty at GSI, in Darmstadt (Germany).

The CESR-c/CLEO-c project consists of the conversion of the existing high-energy physics facility at Cornell (bottomonium and B-physics) to what has often been called a Tau-Charm Factory [4]. CESR-c will operate in the 2–5 GeV mass region with e^+e^- luminosities in the range of $(1.5\text{–}4.5) \times 10^{32}\,\text{cm}^{-2}\text{s}^{-1}$, essentially factors 30 to 100 more than what is currently available at BEPC, Beijing. The superb CLEO-c detector is being modified to do charmonium and D-physics in a dedicated fashion. Just to give an idea of what this facility is expected to do, let me mention that in about six months operation it is expected to produce one billion J/ψ, and one billion ψ'. With such prolific production one expects to successfully overcome all the disadvantages inherent in the indirect production of non-vector states of charmonium in e^+e^- annihilation, make precision measurements of the decay branching ratios of all charmonium states, and make extremely sensitive searches of hybrids and glueballs. The facility is expected to be in operation within the next year.

The GSI project [5], which has already passed the initial stages of review, and expects formal approval within the next year, will have an accelerator complex which can store upto 15 GeV/c of cooled antiprotons. With an internal target it will be able to improve and extend the high precision measurements done at Fermilab. An ambitious program of charmonium and open charm physics, and searches of exotic states, hybrids and glueballs, is planned. There are two clear advantages which this facilty will have over the Cornell program. The energy resolution available at GSI should be an order of magnitude better than that at Cornell, which should be a great advantage in the search of narrow states like $^1P_1$, the D-states, and the radial excitations of the P-states. Unlike the e^+e^- collider at Cornell, at the GSI facility one can also study charmonium and open charm in the nuclear environment by using nuclear targets. If approved, the project is expected to be operational in about 2008.

To summarize, recent developments at Fermilab and BEPC have made significant contributions to the precision spectroscopy of charmonium, but many important questions remain unanswered. Fortunately, the planned new facilities at Cornell and GSI promise to carry the baton forward, and make even more exciting contributions to this very important component of strong interaction physics.

This work was supported in part by the US Department of Energy

References

1. K. Hagiwara *et al.*, Phys. Rev. D **66**, 010001 (2002).
2. S. Godfrey, N. Isgur, Phys. Rev. D **32**, 189 (1985).
3. K.K. Seth, *Proceedings of the International Conference on Heavy Flavours, Southampton (England)*, JHEP (2001), on CD.
4. *CLEO-c and CESR-c: A New Frontier of Weak and Strong Interactions*, CLNS Report 01/1742, 2001.
5. *An International Accelerator Facility for Beams of Ions and Antiprotons*, GSI Conceptual Design Report, 2001.

Eur. Phys. J. A **18**, 567–569 (2003)
DOI 10.1140/epja/i2002-10285-3

THE EUROPEAN PHYSICAL JOURNAL A

Summary talk

R.G. Milner[a]

MIT-Bates Linear Accelerator Center, 21 Manning Avenue, Middleton, MA, 01949 USA

Received: 30 September 2002 /
Published online: 22 October 2003 – © Società Italiana di Fisica / Springer-Verlag 2003

Abstract. An overview of some of major physics themes covered at this conference is presented.

PACS. 12.38.-t Quantum chromodynamics – 12.39.-x Phenomenological quark models – 11.15.-q Gauge field theories – 24.85.+p Quarks, gluons, and QCD in nuclei and nuclear processes – 12.38.Mh Quark-gluon plasma – 25.20.-x Photonuclear reactions – 25.30.-c Lepton-induced reactions – 21.80.+a Hypernuclei – 25.40.-h Nucleon-induced reactions – 25.75.-q Relativistic heavy-ion collisions

1 Introduction

It is a pleasure to be asked to summarize what has been an outstanding Quark Nuclear Physics 2002 meeting here at Jülich. The focus of this meeting is the study of strongly interacting matter in terms of the fundamental constituents of Quantum Chromodynamics (QCD). Approximately 99.9% of the mass of the physical world around us is due to atomic nuclei. Approximately 98% of this mass is due to QCD. Thus, Quark Nuclear Physics is the study of the fundamental structure of matter and remains one of the core problems in Physics at the dawn of the 21st century.

The Jülich conference has continued the excellent series of QNP international meetings and has demonstrated the vigorous intellectual vitality and tremendous excitement in this field of physics. This past week we have heard of significant new advances in theoretical understanding of this complex, non-linear problem. We have also seen impressive new data in all experimental areas of investigation. Further, we have glimpsed into the future with presentations on exciting new initiatives underway worldwide. Here I will present a selection of QNP2002 highlights from the conference plenary sessions. My summary is influenced by available time and personal taste.

2 Theoretical highlights

The ability to carry out *ab initio* calculations in QCD is a much prized goal among physicists working in strong-interaction physics. This would allow definitive tests of QCD —an essential requirement to establish whether this is the corrrect theory of the strong interaction. Calculations using the world's most powerful computers and a discretization of space-time, lattice calculations, are the present technique which come closest to exact calculations.

A. Thomas presented a summary of recent developments in the field of lattice QCD. A major area of current activity is the use of extrapolations to low quark mass based on chiral-symmetry arguments. For a number of observables these new extrapolations provide a determination of the observable which is much closer to the experimental value. For example, lattice calculation of the moments of parton distributions provide determination of the Bjorken-x dependence which is in good agreement with experiment. This success demonstrates that chiral-symmetry considerations play a fundamental role in understanding hadron structure. Further, it demonstrates that present lattice QCD calculations, while still being far from exact, can provide important insight into hadron structure.

B. Holstein provided an overview of effective field theory (EFT), which provides a theoretical framework consistent with QCD for processes below the chiral-symmetry-breaking scale, a scale comparable with the nucleon mass. EFT organizes quantum field theories according to hierarchies of physical scale. The Standard Model of electroweak interactions is a beautuful example of an EFT, which describes observables at energies below the scale of electroweak symmetry breaking. To describe hadronic interactions, a dual expansion in the up- and down-quark masses, m_u and m_d, and in the momentum of external probes is required. This framework, known as chiral perturbation theory (χPT), provides a cornerstone in our understanding of QCD and is the only rigorous way in which to encode the entire body of QCD predictions at low energy. χPT has developed a very successful calculational scheme for pseudoscalar meson interactions. At present, a major focus is to extend this scheme to the baryonic realm and to multinucleon systems. A consistent and convergent power

[a] e-mail: milner@MITLNS.mit.edu

counting remains to be established for systems of pions and nucleons below the chiral-symmetry-breaking scale.

D. Riska presented a derivation of the major aspects of the phenomenological nucleon-nucleon interaction in terms of the $1/N_c$ expansion, in the large-N_c limit.The numerically significant components of a number of different modern realistic phenomenological interaction models are shown to admit very similar meson exchange interpretations in the large-N_c limit. The conclusion is that the ordering of nuclear inteactions and interaction current operators by their dependence on $1/N_c$ corresponds well with their significance ordering based on empirical evidence and phenomenological analysis.

A. Mueller described the current understanding of low-x parton distributions and diffractive processes in terms of some phenomenological models. Unitarity tells us that the rising gluon distribution at low-x must saturate. HERA data do not provide definitive evidence for saturation. Using nuclear targets, it should be possible to probe substantially lower-x values, because the Lorentz contraction boosts the gluon density by $A^{\frac{1}{3}}$. Such a search for saturation could be carried out at an electron-nuclear collider.

3 Cold QCD: hadronic physics

QNP2002 contained a number of excellent review talks which spanned the essential aspects of the worldwide program to understand and study the structure and properties of hadrons. I divide my summary into separate highlights from studies which use electromagnetic and hadronic probes, respectively.

3.1 Electromagnetic probe

K. Kumar presented a comprehensive review of the worldwide program in the study of hadron structure using parity-violating electron scattering. By measuring the interference between Z^0 and single-photon exchange, experiments can determine the strange-quark contribution to the charge and magnetism of the nucleon, the neutron matter distribution in ^{208}Pb and can test the Standard Model with a precise measurement of $\sin^2\theta_W$. Experiments are in progress at MIT-Bates, Mainz, Jefferson Laboratory and SLAC and the demonstrated experimental capabilities are truly impressive.

C. Papanicolas presented the latest information on a determination of the shape of the proton. This shape has been called the most fundamental in our universe as QCD tells us that the proton is constructed completely from the binding of pointlike constituents. By studying deformation in the transition of the proton to its first excited state, the $\Delta(1232)$, it is concluded (within model uncertainties) that the proton is cigar-shaped at the level of a few percent.

R. Schumacher presented new data from the CLAS detector at Jefferson Lab. Measurement of photoproduction of strangeness from the nucleon substantially extends in kinematic range and precision the data from previous experiments. Further, CLAS data show hints of strength at locations where missing resonances are sought. However, no definite conclusions are yet available. M. Garçon presented new data from CLAS on deeply virtual Compton scattering (DVCS) which can open up an entirely new vista into hadronic physics using generalized parton distributions (GPSDs).

G. van der Steenhoven presented the latest results from the HERMES experiment at DESY. These included the latest polarized quark distribution results. The u-quark polarization is measured to be positive; the d-quark polarization is found to be negative; and the sea polarization is consistent with zero. HERMES has also measured deeply virtual Compton scattering for the first time and the results are consistent with theoretical expectation. CLAS and HERMES should produce new data on GPDs over the next several years. In addition, the HERMES determination of parton energy loss in nuclei is used to constrain a successful theoretical caluclation which describes measured high-p_T meson production by PHENIX at RHIC.

3.2 Hadronic probe

T. Nagae presented an overview of some recent exciting work in hypernuclear physics. A bubble chamber sighting of a very rare ${}^{6}_{\Lambda\Lambda}$He was shown and the binding energy $\Delta B_{\Lambda\Lambda}=1.01\pm0.20^{+0.18}_{-0.11}$ determined. In addition, the Hyperball was cleverly used to study the spectroscopy of ${}^{7}_{\Lambda}$Li. The structure of ^{6}Li can be approximated by an α-particle orbited by a loosely bound proton and neutron. The addition of a Λ-particle to this system causes the ${}^{7}_{\Lambda}$Li to be significantly smaller in size than the ^{6}Li. Consequently, the spectroscopy of ${}^{7}_{\Lambda}$Li can be well described by a calculation using the ΛN interaction.

J.-C. Peng discussed the present understanding of the flavor structure of the quark sea of the nucleon. Drell-Yan data show that $\overline{d}>\overline{u}$, which can be understood in terms of a model based on the meson cloud picture of the nucleon. Upcoming experiments planned for RHIC using polarized protons should provide accurate determination of any flavor asymmetry in the polarized sea.

H. Ströher gave an overview of status and plans at the local COSY facility in Jülich. A central focus of the program is the study of strangeness production above 2 GeV/c using polarized beams and targets. First results include the ratio of Λ to Σ production as a function of incident proton energy and Λ polarization measurements. This promises to be a productive area of research in an almost virgin territory before COSY.

4 Hot QCD: the search for the quark gluon plasma

B. Jacak gave a comprehensive overview of one of the most important new areas of research, namely the search for the quark gluon plasma using the Relativistic Heavy Ion Collider (RHIC) at Brookhaven National

Laboratory. This machine has turned on and the four detectors have acquired and analyzed initial data in a most impressive fashion. The energy density at RHIC has been determined to be greater than 4.6 GeV/fm^3, which exceeds the calculated value of 3 GeV/fm^3 at which the phase transition occurs. The freeze-out temperature at RHIC has been determined to be about 175 MeV which is close to the phase transition temperature predicted by lattice QCD. Significant elliptic flow is observed for central collisions which supports the conclusion of early equilibrium and pressure buildup. Significant quenching of jets is observed in central collisions. While the general parameters observed at RHIC are consistent with formation of a quark gluon plasma, it is too early for a definitive conclusion. It is clear that RHIC data will be of great interest in the next several years as a detailed understanding of what is happening in these tremendously violent and energetic collisions becomes possible.

5 Summary

In closing, I would like to thank Prof. Speth for his leadership in the successful organization of QNP2002. I would like to acknowledge the hospitality of his Jülich colleagues for the very pleasant nature of the meeting, particularly the excellent banquet and social activities. Jülich has set a high standard for the next meeting of QNP in 2004 at Bloomington, Indiana, USA.

DOI 10.1140/epja/i2003-10143-x

The Publishing Policy of the European Physical Journal A

The publishing of scientific work has seen dramatic changes in the last decade through the invention of the World Wide Web. One such change is the establishment of electronic servers providing extremely fast and very accessible dissemination of papers. However, the price we pay for this change is the disappearance of peer reviewing for publications on electronic servers. This has the consequence of inflating the already immense volume of published material and leads to a division of physics into smaller and smaller communities who communicate their unreviewed work via the Web. Therefore, the role of the traditional peer-reviewed journals remains, and has even increased as a consequence of the Web revolution.

Of course, the Web has changed the way the traditional journals operate, for instance the production of a publication with the computer allows for electronic submission and handling of all aspects of the editorial and production process. In this Editorial, we want to update the publishing policy of the European Physical Journal A "Hadrons and Nuclei" (EPJ A), now that the changes associated with the Web have stabilised. This summary emphasises the advantages of publishing in EPJ A and describes what EPJ A can offer.

Since a few years EPJ A comprises two parts: the traditional printed one called simply EPJ A and an "electronic only" part called EPJ A direct incorporating essentially all aspects of an electronic server plus the advantages of peer reviewing. The basic concepts of both parts are the same. However, EPJ A direct uses solely the medium "electronic storage" providing all possibilities of the printed one plus several additional ones as will be outlined below. At the present time the two parts coexist and it is left to the taste of the author to choose. It is our conviction that in the long run the electronic publishing will prevail.

The common qualities of EPJ A and EPJ A direct are:

1. Peer review directed by personally known editors of outstanding international scientific stature. This review process can significantly improve the readability and reliability of published articles. The editors can also act as neutral mediators to resolve the occasional strong differences of opinion between authors and referees. Also, although referees usually operate anonymously, they may choose to reveal their identities.
2. Fast processing of the papers with an average delay of 10 weeks for the refereeing and editorial work due to the loyal relation between the editors and the referees of EPJ A. The subsequent appearance in print depends largely on the delay of the proofreading by the authors. In addition, all articles of both, EPJ A and EPJ A direct, can be accessed at Springer's Web server SpringerLink (URL: http://www.springerlink.com/journals/epja) within 10 days after submission of the final proofread paper to the publisher. From this moment on, all articles are citable using the Digital Object Identifier (DOI), an internationally agreed citation method uniquely identifying all published work worldwide and guaranteeing copyright protection for the article. This service is available via the "Online First" button of the EPJ A homepage.
3. All papers are published in the renowned compact and pleasant style of EPJ. A style file with convenient macros available to prepare papers with LaTeX can be downloaded from the EPJ A web site. But also papers in other formats are accepted and transposed into the EPJ style. This style provides economically dense printing, an aspect which is more and more appreciated in view of the ever increasing prices of some competing scientific journals.

Due to the new medium of electronic storage EPJ A direct offers some features which are still unfamiliar to many. The number of pages is within reasonable limits no constraint anymore. This allows, among other advantages, the inclusion of great volumes of data until now frequently lost or the publishing of detailed, extensive calculations that make their verification and understanding easier. Also, the full possibilities of electronic media as e.g. CAD drawings, coloured or animated figures or even sound and short movies are possible.

The subfields of "Hadrons and Nuclei" are given in the section "Aims & Scope", again accessible via the home page of EPJ A. The kind of articles EPJ A accepts are classified in the following subsections:

1. Letters
   "Letters" will in the future replace the "Short Notes" in order to make the actual intention of this section more obvious. Manuscripts submitted as Letters should comprise important topical results deserving fast publication. They will get special attention of the responsible editor and priority in the production, without proofreading if the authors consent. Their length will be limited to four pages, normally including all figures and tables.
2. Papers
   "Papers" are normally limited to about 20 pages. Exceeding this limit will need a special justification since we can now publish large volumes of experimental or calculational results in EPJ A direct with almost no limitations.

3. Topical Reports
   "Topical Reports" are review articles on a topical subject. They can be submitted as normal papers on one's own initiative, or are invited by the Editors.

The type of articles EPJ A direct accepts are the same as those of EPJ A plus the following:

4. Scientific Notes
   "Scientific Notes" are papers on intermediate results of simulations, detectors, analyses, etc. intended to help the communication of the progress of lengthy experiments and simulations needing long preparations or running time. This should help particularly young physicists to produce refereed and citable publications during the long phase of the realization of a major set-up or investigation. We should like to point out that excellent thesis (master, laurea, diploma, doctoral, etc.) may qualify for this section. But also appropriately prepared accounts of more technical nature may be published here. In special cases notes in other languages than English may be accepted for this section.
5. Topical Volumes
   The Proceedings of Conferences can be included in EPJ A direct as "Topical Volumes", if they meet the same quality standards as normal papers in EPJ A. They will be reviewed and revisions or rejection may be recommended. Depending on the negotiations with the publisher, the Conference Proceedings published in EPJ A direct can be accessed free of charge or can be ordered by the conference organisers in printed form. The printed volume may also contain conference contributions not accepted for publication in EPJ A direct.

All manuscripts for EPJ A and EPJ A direct have to be submitted following the procedure accessible via the EPJ A home page. The abstracts of all articles published in EPJ A direct appear also in EPJ A. This together with the fact that the very same editorial board handles both parts of EPJ A shows the close relationship between the traditional EPJ A and the electronic only EPJ A direct.

Heidelberg, June 2003

Th. Walcher
Editor-in-Chief
for the Editorial Board

W. Beiglböck
for the Publishers

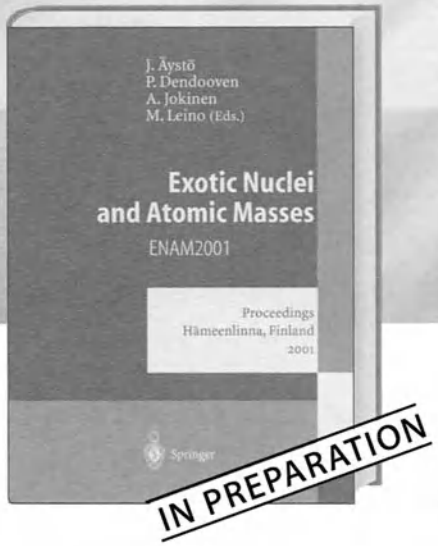

ENAM 2001
Proceedings

Juha **Äystö**,
Peter **Dendooven**,
Ari **Jokinen**,
Matti **Leino** (Eds.)

Exotic Nuclei and Atomic Masses

Proceedings of the Third International Conference on Exotic Nuclei and Atomic Masses. ENAM2001 Hämeenlinna, Finland, 2-7 July 2001

2003. Approx. 500 p.
Hard cover **€ 149,95**; £ 105,00; sFr 242,50
ISBN 3-540-00101-8

The proceedings of this major nuclear physics conference report the state of the art in the field of exotic nuclei and nuclear masses. This includes the measurement of fundamental constants, the structure of nuclear matter, radioactivity and the synthesis of heaviest elements. A special session is devoted to the "laboratories" for nuclear reaction naturally provided by stars and other astronomical objects. Of special interest for the experts is the last section giving an outlook on future experimental and theoretical research.

From the Contents: Atomic Masses and Fundamental Constants.- Moments and Radii.- Nuclear Astrophysics.- Forms of Radioactivity.- Direct Reactions and Nuclear Spectroscopy.- Nuclei at the Drip Lines.- Cluster Phenomena.- Nuclear Structure and Shapes.- Fission and Heaviest Elements.- Fundamental Symmetries and Interactions.- Traps for Radioactive Isotopes.- Experimental Developments and Applications.- Closing Session.

For more information on Springer books see our
Physics Online Library:
http://www.springer.de/phys/

Free table of contents and abstracts of our journals at:
http://link.springer.de

Complete Landolt-Börnstein now available online at
http://www.landolt-boernstein.com

Please order from
Springer · Customer Service
Haberstr. 7
69126 Heidelberg, Germany
Tel.: +49 (0) 6221 - 345 - 0
Fax: +49 (0) 6221 - 345 - 4229
e-mail: orders@springer.de
or through your bookseller

Springer

All Euro and GBP prices are net-prices subject to local VAT, e.g. in Germany 7% VAT for books and 16% VAT for electronic products. Prices and other details are subject to change without notice. d&p · 009030_001x_1c

Computing and Visualization in Science

Online First
Immediately Online
http://link.springer.de
link.springer-ny.com
Faster publication!

- Read journal articles online before they appear in print.
- Papers are published online shortly after they are accepted.
- Each **Online First**™ article is fully retrievable, searchable and citable by the DOI (Digital Object Identifier), which is linked to the article.

Devoted to computational sciences - a field of a major and continually growing importance for both research and applications, this journal provides the ideal platform for scientists eager to cooperate in solving scientific and technological challenges. The aim is to link professionals from the diverse fields of

- **mathematics**
- **physics**
- **environmental sciences**
- **engineering**
- **computer science**
- **chemistry**
- **biosciences**

The rapid development of computer technology has opened up new perspectives, increased the importance of mathematical models and created an urgent need for efficient algorithms. Reflecting these trends, the journal has set itself the goal of publishing pioneering methods and applications which precipitate the solution of complex problems - or even make such solutions possible at all.

Since visualization has become an important scientific tool, especially in the analysis of complex situations, it is treated in close connection with the other areas covered by the journal. These areas include: mathematical modeling and analysis of model systems, numerical methods and algorithms, development of simulation software, optimization and control, parallel computing, visualization and image analysis, computational physics and chemistry, structural mechanics, fluid dynamics, environmental sciences, computation in biosciences and medicine, modeling and computation in engineering.

As well as publishing this exciting material in print form, **Computing and Visualization in Science** also makes the documents available to subscribers electonically via a server.

Managing Editor:

Gabriel Wittum, Heidelberg

Editorial Board

R.E. Bank, La Jolla, CA; **P. Bastian**, Heidelberg; **P. Deuflhard**, Berlin; **M. Espedal**, Bergen ; **R.E. Ewing**, College Station, TX; **C. Farhat**, Boulder, CO; **M. Feistauer**, Prague; **R. Helmig**, Stuttgart; **W. Jäger**, Heidelberg; **R. Jeltsch**, Zürich; **C. R. Johnson**, Salt Lake City, UT; **U. Langer**, Linz; **B. Lesyng**, Warsaw; **U. Maas**, Stuttgart; **O. Pironneau**, Paris; **A. Quarteroni**, Lausanne; **M. Rumpf**, Duisburg; **H.D. Simon**, Berkeley, CA; **A. Tveito**, Lysaker

Subscription information 2003:

Volume 6, 4 issues, incl. basic SpringerLink licence
€ 279.00, plus carriage charges

ISSN 1432-9360 (print edition)
ISSN 1433-036 (electronic edition)
Title No. 00791

free electronic sample copy available

http://link.springer.de/journals/CVS

Please order from:
Springer · Customer Service
Haberstr. 7 · 69126 Heidelberg, Germany
Tel.: +49 (0) 6221 - 345 - 0
Fax: +49 (0) 6221 - 345 - 4229
e-mail: subscriptions@springer.de
or through your bookseller

All prices are net-prices subject to local VAT, e.g. in Germany 7%. All prices exclusive of carriage charges.
Prices and other details are subject to change without notice. d&p · 009212x

Springer